

Postclosure Safety Assessment of a Used Fuel Repository in Sedimentary Rock



NWMO-TR-2018-08
December 2018



nwmo

NUCLEAR WASTE
MANAGEMENT
ORGANIZATION

SOCIÉTÉ DE GESTION
DES DÉCHETS
NUCLÉAIRES

Nuclear Waste Management Organization

22 St. Clair Avenue East, 6th Floor

Toronto, Ontario

M4T 2S3

Canada

Tel: 416-934-9814

Web: www.nwmo.ca

EXECUTIVE SUMMARY

For decades Canadians have been using electricity generated by nuclear power reactors in Ontario, Quebec and New Brunswick. The used nuclear fuel removed from these reactors is a highly radioactive waste product requiring careful short and long-term management. Although its radioactivity decreases with time, the used fuel will remain a potential health risk for many hundreds of thousands of years. Canada's used nuclear fuel is currently safely stored on an interim basis at licensed facilities located where it is produced.

The Nuclear Waste Management Organization (NWMO) is responsible for the implementation of Adaptive Phased Management (APM), the federally-approved plan for safe long-term management of Canada's used nuclear fuel. Under the APM plan, used nuclear fuel will ultimately be placed within a deep geological repository in a suitable rock formation.

A deep geological repository is a multi-barrier system designed to protect people and the environment in the long term. The barriers are the durable wasteform, long-lived corrosion resistant containers, engineered sealing materials and the surrounding geosphere.

A site selection process is currently underway to identify a safe site for a deep geological repository in an informed and willing host community. The process of site selection will take several years. As potentially suitable sites are identified with interested communities, detailed field studies and geoscientific site characterization activities will be conducted to assess whether the APM multi-barrier repository concept could be safely implemented in accordance with rigorous regulatory requirements.

At this early stage in the process, before specific sites have been identified for detailed examination, generic studies have been conducted to understand and illustrate the long-term performance and safety of the multi-barrier repository system within various geological settings.

This report provides an illustrative case study of postclosure safety for a deep geological repository in a hypothetical sedimentary rock setting in Southern Ontario. Its purpose is to illustrate a postclosure safety assessment consistent with the Canadian Nuclear Safety Commission (CNSC) Regulatory Document REGDOC-2.11.1, Volume III: Assessing the Long-Term Safety of Radioactive Waste Management (CNSC 2018). For a licence application for an actual candidate site, a full safety case would be prepared that would include the results of site-specific geoscience investigations, a site specific deep geological repository design, and a more comprehensive safety assessment than described in this document.

Design Concept

The current conceptual design for sedimentary rock consists of a repository constructed at a nominal depth of 500 m. The repository contains a network of placement rooms for the estimated inventory of about 5.2 million used fuel bundles encapsulated in approximately 109,000 long-lived used fuel containers. The container design consists of an outer corrosion-resistant material (copper) and an inner supporting material (steel). The copper provides resistance to container corrosion under deep geological conditions, while the steel provides strength for the container to withstand expected hydraulic and mechanical loads, including those arising from glaciation.

Within each placement room, used fuel containers, encased in bentonite clay buffer boxes, are placed and separated from adjacent containers by bentonite clay spacer blocks. Containers will

be staggered and stacked in two rows in a retreating manner, and empty spaces will be backfilled with bentonite based gap fill.

Bentonite is a durable natural clay material that swells on contact with water, resulting in a self-sealing property that renders it essentially impervious to flowing water.

Geosphere

A reference geosphere has been derived for this report, in part, from historic experience gained in the Canadian program. It is not based on any specific site, and it represents one example of a possible sedimentary rock setting. In combination with the other Canadian case studies for alternative geologic settings, this work illustrates a basis for the long-term safety of a deep geologic repository under a range of settings.

The geosphere is an important part of the multi-barrier system. It provides a natural barrier that is hydrogeologically, geomechanically and geochemically stable on timeframes relevant to repository safety. The geosphere isolates the repository from surface conditions and provides an environment conducive to long container life.

Postclosure Safety Assessment

The primary safety objective of a deep geological repository is the long-term containment and isolation of used nuclear fuel. The safety of the repository is based on a combination of the geology, properties of the waste material, the engineered design, careful operations, and quality assurance processes including review and monitoring.

The purpose of a postclosure safety assessment is to determine the potential effects of the repository on the health and safety of people and the environment during the postclosure period. The assessment timeframe is one million years based on the time period needed for the radioactivity of the used fuel to decay to essentially the same level as that in an equivalent amount of natural uranium. This timeframe is also within a reasonable extrapolation of the geological stability of the surrounding rocks.

The postclosure safety assessment adopts scientifically informed, physically realistic assumptions for processes and data that are understood and can be justified on the basis of the results of research and/or future site investigations. Where there are high levels of uncertainty associated with processes and data, conservative assumptions are adopted and documented to allow the impacts of uncertainties to be bounded.

Scope of the Postclosure Safety Assessment

The scope of the assessment is developed to illustrate the effectiveness of the deep geological concept in this rock setting, consistent with regulatory requirements documented in CNSC REGDOC-2.11.1, Volume III, Assessing the Long-Term Safety of Radioactive Waste Management (CNSC 2018). As such, analysis cases are limited to those needed to provide a demonstration of the overall approach and to those needed to reach possible conclusions for the hypothetical site. Items excluded from the scope but which might be included in a licence submission as part of a more comprehensive assessment are also discussed.

Repository safety is judged by whether or not results meet interim acceptance criteria defined for the protection of people and the environment from the radiological and non-radiological hazards associated with the repository.

Consistent with CNSC REGDOC-2.11.1, Volume III (CNSC 2018), both Normal Evolution and Disruptive Event Scenarios are considered.

The Normal Evolution Scenario

The Normal Evolution Scenario is based on a reasonable extrapolation of present day site features and receptor lifestyles. It includes the expected evolution of the site and expected degradation of the repository system. Its purpose is to illustrate the anticipated effects of the repository on people and on the environment.

In this report, the Normal Evolution Scenario is described in terms of a “Reference Case”, a “Base Case” sensitivity study and a series of additional sensitivity studies around the “Base Case”.

Reference Case

The Reference Case represents the situation in which all repository components meet their design specification and function as anticipated. As such, the used fuel containers remain intact essentially indefinitely and no contaminant releases occur in the one million year time period of interest. Radiological doses to the public and the environment are therefore zero.

Base Case

Sensitivity studies illustrate repository performance for a range of reasonably foreseeable deviations from key Reference Case assumptions. These deviations arise as a result of components placed in the repository that either (a) do not meet their design specification or (b) do not fully function as anticipated.

The likelihood of such deviations will be very low. Care is being taken to design, develop and test a robust fabrication and placement technology which will ultimately be implemented under a comprehensive quality assurance program. A key element of the quality assurance program will be an inspection process designed to ensure all placed components meet design specification. Similarly, component performance is supported by an extensive research and testing program, such that the behaviour of all materials placed in the repository will also be well understood.

Nevertheless, given the large number of containers, it is not unreasonable to anticipate that some failures may occur. To illustrate repository performance in the presence of failed containers, the “Base Case” sensitivity study assumes a small number of containers are fabricated with sizeable defects in their copper coating, and that a smaller number of these off-specification containers escape detection by the quality assurance program and are unknowingly placed in the repository.

Studies are underway to determine the likelihood and number of off-specification containers that could potentially be present; however, the results of this work are not currently available. In the meantime, 10 containers with large undetected defects in the copper coating are assumed present. Postclosure studies assuming 10 defective containers are sufficient to illustrate repository performance and to provide a measure of the consequences that could be expected should such an event (or a similar one) actually occur.

The defects are assumed sufficiently large to cause each of the 10 containers to fail within one million years. As the actual nature (size, location) of each defect will vary, it is highly unlikely that 10 containers would all fail simultaneously. The failure times are assumed to be evenly spread over the one million year time period of interest, with the first failure occurring at 1000 years and subsequent failures occurring every 100,000 years.

In addition, failures in the fabrication, placement and quality assurance systems could also affect other repository components. For example, off-specification material could unknowingly be used in the fabrication of buffer box bentonite, placement room spacer blocks or bentonite pellets. Off-specification material could also unknowingly be used in the construction of repository tunnel seals and repository shaft seals. Placement rooms and access tunnels could exceed their design dimensions because blasting removes too much rock in some places leading to the use of more bentonite pellets and potentially establishing conditions that are more conducive to microbial growth.

The principal end result of such failures would be either (a) nothing adverse happens, or (b) early container failure(s). Studies are underway to determine the likelihood and number of repository components that could potentially be out of compliance with their design requirements; however, the results of this work are also presently not available. In the meantime, for this postclosure safety assessment, other fabrication and quality assurance system failures that lead to container failure are assumed to be covered by the Base Case and associated sensitivity cases.

A number of uncertainties are addressed through bounding assumptions. These are assumptions that result in a greater consequence than the entire range of the uncertainty. To illustrate, the Base Case replaces the uncertainty associated with the location and lifestyle of people living in the vicinity of the repository in the future with an assumption that instead has people unknowingly living on top of the repository and obtaining all of their drinking and crop irrigation water from a deep well, with the well positioned in the location that maximizes the uptake of any potential contaminant release.

The adoption of bounding assumptions is a common technique in safety assessment. It allows for complex problems to be reduced to much simpler ones, with the downside being that the resulting case is no longer the most realistic. While this is acceptable from a licensing viewpoint (provided results meet acceptance criteria), it can make repository performance appear to be much worse than it really is. To provide context, the Scope section of Chapter 7 includes a discussion of key assumptions and compares them to what is most likely to occur in reality.

Sensitivity Studies for the Base Case

A deep geological repository is a multi-barrier system. The following deterministic sensitivity cases are examined to illustrate the effect of deviations in barrier performance on the Base Case results:

Fuel Barrier:

- Fuel dissolution rate increased by a factor of 10; and
- Instant release fractions set to 0.10 for all contaminants (i.e., 10% of the entire inventory is instantly released).

Zircaloy Sheath Barrier:

No credit is taken in the postclosure safety assessment for the presence of the Zircaloy fuel sheath as a barrier to contaminant release from the fuel. However, because the sheath itself contains contaminants and because the screening analysis identifies some of these contaminants as potentially important, the following Zircaloy specific sensitivity cases are simulated:

- Zircaloy dissolution rate increased by a factor of 10; and
- Instant release fractions set to 0.10 for all contaminants.

Container Barrier:

- All 10 containers fail at 1000 years;
- 50 containers fail at 1000 years;
- 50 and 1000 containers fail at 10,000 years;
- Low sorption in the engineered barrier materials with coincident high solubility limits in the container; and
- No solubility limits in the container.

Buffer and Backfill and Seals Barrier:

- Hydraulic conductivities of all engineered barrier sealing materials in the repository and shaft increased by a factor of 10;
- Low sorption in the engineered barrier sealing materials with coincident high solubility limits in the container;
- Bentonite and geosphere diffusivities increased by a factor of 10 and by a factor of 100;
- I-129 sorption credited in the bentonite and geosphere; and
- No sorption in the engineered sealing materials.

Geosphere Barrier:

- Hydraulic conductivities increased by a factor of 10;
- Hydraulic conductivity in the excavation damaged zones (EDZ) increased by a factor of 10;
- Bentonite and geosphere diffusivities increased by a factor of 10 and by a factor of 100;
- 100 m of surface erosion in one million years;
- I-129 sorption credited in the bentonite and geosphere;
- 150 m overpressure in the Shadow Lake formation; and
- Sorption parameters set to two standard deviations below the mean.

Additional cases (not listed here but described in the Scope section of Chapter 7) are also examined to illustrate the effect of well assumptions (in particular, “no well” with water obtained from surface waters) and the effect of modelling parameter assumptions (i.e., time-step and mesh size).

To provide an indication of repository response allowing for uncertainty in multiple parameters, two types of probabilistic sensitivity studies are also performed. In these simulations, random sampling is used to simultaneously vary input parameters for which probability distribution functions are available. Radionuclide release and transport parameters are varied within the fixed reference geosphere.

The specific probabilistic cases are:

- Number, locations and failure times for defective containers fixed at their Base Case values, with all other available parameters varied; and
- All parameters with probability distributions varied, including the number, locations and failure times for the defective containers.

Dose rate to people is an important indicator of repository performance; however, the relevance of dose rate tends to decrease with time as assumptions concerning the biosphere (e.g., climate), human lifestyles (i.e., critical group characteristics) and water flows in the near-surface environment become increasingly uncertain. Consequently, two complementary long-term indicators using system characteristics that are much less sensitive to such assumptions are also assessed. The indicators are:

- Radiotoxicity concentration in a water body, for medium time scales; and
- Radiotoxicity transport from the geosphere, for longer time scales.

Finally, all sensitivity cases assume a constant temperate climate; however, during the past one million years, much of Canada has been covered by kilometre-thick ice sheets. The main factors that initiated these cycles (i.e., solar insolation variation due to Earth orbital dynamics and the location and size of the continents) are still present. Current levels of greenhouse gases in the atmosphere may delay the onset of the next glaciation, however, glacial cycles are expected to reassert themselves in the time period of interest to this postclosure safety assessment. To address the effects of glaciation, a discussion is presented which is based on the analysis of a glaciation scenario carried out as part of earlier work for the same geosphere but with a different repository design. The important features of this glaciation study are described and its applicability to the current study is also discussed in Chapter 7.

Disruptive Event Scenarios

Disruptive Event Scenarios postulate the occurrence of unlikely events leading to possible penetration of barriers and abnormal loss of containment.

The following Disruptive Event Scenarios are applicable to the conceptual design and hypothetical geosphere in this study. These are identified in Chapter 6 through consideration of the features, events and processes that are important to the repository system, and through consideration of the key barriers:

- Inadvertent Human Intrusion;
- All Containers Fail;
- Repository Seals Failure;
- Undetected Fault;

- Severe Erosion;
- Poorly Sealed Borehole;
- Container Failure; and
- Partially Sealed Repository.

The first four scenarios are analyzed in this illustrative safety assessment. It is recognized that for an actual site, the full set of scenarios would need to be evaluated.

The ***Inadvertent Human Intrusion Scenario*** considers the possibility of a future deep borehole drilled at the site. This scenario is a special case, as recognized in CNSC REGDOC-2.11.1, Volume III, since it bypasses the multiple barrier system. The likelihood of this event occurring is very small due to institutional controls and markers that would be placed on the site, and because the used fuel containers are placed deep underground in a location with no currently economically viable mineral resources or potable groundwater resources. Furthermore, normal deep drilling practices (e.g., control of drilling fluids, use of gamma logging, etc.) would reduce consequences relative to those estimated here.

The ***All Containers Fail Scenario*** considers the very unlikely and hypothetical case in which all the containers simultaneously fail (i.e., water enters all containers and contacts the fuel) at 60,000 years. This timeframe corresponds to the assumed time scale for glacial cycles to resume and an ice sheet to cover the site. A sensitivity case in which all containers fail at 10,000 years is also assessed.

The ***Repository Seals Failure Scenario*** considers the consequences of the tunnel and shaft seals being less effective than designed.

For the ***Undetected Fault Scenario***, it is anticipated that any large fractures intercepting the repository not identified during site characterization would be discovered during construction such that appropriate mitigating measures could be taken. These measures could include possible redesign of the repository layout to avoid large transmissive features. This scenario, however, assumes a fault in the nearby rock is not identified.

Regarding the excluded scenarios:

- The ***Severe Erosion Scenario*** considers the impact of severe glacial erosion on the performance of the used fuel repository.
- The ***Poorly Sealed Borehole Scenario*** is also a Disruptive Event Scenario because it creates a pathway that bypasses the low-permeability geosphere. However, as long as the boreholes are kept sufficiently far from the repository underground structures, they are unlikely to be important due to their small size and the limits of diffusive transport. This scenario would be analyzed as part of a real site, when the borehole distances are known; however, the consequences are expected to be low.
- The ***Container Failure Scenario*** considers failure of some containers due to unexpected in-situ conditions. It is different from the Base Case of the Normal Evolution Scenario which considers a defect unknowingly present in some containers as the initiating event. Although a detailed analysis of the Container Failure Scenario is not included in this study, the dose arising from this event is anticipated to be significantly less than that associated with the All Containers Fail Scenario due to the much reduced number of affected containers.

- The ***Partially Sealed Repository Scenario*** considers the consequences if the repository is abandoned and the shafts are not sealed, thereby implying a near-future loss-of-society.

All Disruptive Event Scenarios are analysed with deterministic methods since the basic parameters defining the scenarios are chosen conservatively.

Results for the Normal Evolution Scenario

The results for cases measured against the interim acceptance criteria for the radiological protection of persons are presented below, with additional details being included in Chapter 7.

Deterministic Results

The dose rate is zero for the Reference Case.

For all other cases, transport rates are extremely low due to the very low hydraulic conductivity of the host rock, the absence of fractures, and the dominance of diffusive transport. As such, the dose rates at one million years for all cases, except the case with diffusivities increased by a factor of 100, are below 0.000001 mSv/a, or more than a factor of 300,000 times less than the interim dose rate acceptance criterion. These dose rates are so low that they can be considered zero.

The case with diffusivities increased by a factor of 100 is an extreme case, but considers the importance of the diffusive rock barrier. In this case, the peak value essentially occurs within the one-million-year time period of interest. The dose rate is 0.00004 mSv/a, or a factor of 7,500 times less than the interim dose rate criterion.

Results show that I-129 is the only dose contributor of note. This is because I-129 has a sizeable initial inventory, a non-zero instant release fraction, a very long half-life, no solubility limit, is non-sorbing in the buffer, backfill and geosphere and has a radiological impact on humans. All other fission products and actinides either decay away, or are released very slowly as the fuel dissolves and are thereafter sorbed in the engineered barriers and geosphere.

The actual dose rate could be even lower, depending on the location of the defective containers, whether or not a well is present, and where the well is located with respect to the defective containers. Results indicating this are presented in Chapter 7.

The Glaciation Sensitivity shows that a potential dose increase of 100 times could occur if a deep well were drilled over repository after ice retreat. This is caused by the accumulation of radionuclides during the glacial period if there is no groundwater movement in relevant aquifers due to permafrost. However the resulting doses still would be below the dose criterion.

Probabilistic Results

Probabilistic cases examine the effect of simultaneous variation in multiple parameters.

The first case, in which the number, location and failure times of the 10 defective containers are fixed at the same values as in the Base Case while all other available parameters are varied, gives a measure of the overall uncertainty in the Base Case. The 95th percentile 1 Ma dose rate

arising from 100,000 simulations is 1.3×10^{-7} mSv/a. This is a factor of about 2,300,000 times less than the interim dose rate criterion of 0.3 mSv/a. Extending the simulation beyond one million years results in a peak value of 3.4×10^{-5} mSv/a, which is well below the interim dose rate criterion.

The second probabilistic case, in which all parameters are varied including the number, location and failure times of the defective containers has a 95th percentile 1 Ma dose rate of 9.3×10^{-8} mSv/a, which is a factor of 3,200,000 times less than the interim dose rate criterion. This is less than the previous case because there is a large number of probabilistic cases in which zero container failures occur. Extending the simulation beyond one million years results in a peak value of 1.45×10^{-5} mSv/a, which is well below the interim dose rate criterion.

Results for the Disruptive Event Scenarios

Key features arising from the analysis of the All Containers Fail, the Repository Seals Failure and the Undetected Fault Disruptive Event Scenarios are:

- Both the All Containers Fail at 60,000 Years and the All Containers Fail at 10,000 Years cases result in a peak dose rate of 0.01 mSv/a. These results are below the interim dose rate criterion.
- The Repository Seals Failure scenario has a small effect (increase of about 1.4 times) on the peak impact for I-129 transport as compared to the Base Case, and the inferred dose consequence would remain well below the interim dose rate criterion.
- The peak impact for the Undetected Fault Scenarios increases, with I-129 transport for the 100 m offset case being about 22 times higher than that for the Base Case. Even with this increase, the inferred dose consequence would still be well below the interim dose rate acceptance criterion. In reality, this would depend on the location of the fault with respect to the well (if any) and the number and location of the defective containers (if any).

In the Inadvertent Human Intrusion Scenario, all barriers are bypassed and used fuel material is brought directly to surface via a borehole. The consequences for the case where the intrusion is promptly recognized is a dose to the drill crew of 90 mSv, and no dose to public as the site would be remediated. If the intrusion is not recognized, and if used fuel material is left on the site at surface, and if a person were to live on the site, then that person could receive a dose of several hundred mSv per year until the activity has substantially decayed. However the repository is placed deep in the bedrock away from natural resources which, along with land use controls or markers, makes the probability of this occurring very low.

Other Potential Impacts

Gas Behaviour

Gas is of special interest in this study because the extremely low hydraulic conductivity of the host rock is not conducive to significant gas transport away from the repository. As such, gas can be retained leading to high repository pressure.

Detailed studies of gas behaviour are presented in Chapter 8 for the Base Case and for the All Containers Fail at 10,000 years Disruptive Event Scenario. The assessment adopts extremely

conservative assumptions in which no credit is taken for the copper barrier and no credit is taken for carbonate limited corrosion.

For the Base Case, results show there are no adverse consequences; the possibility of gas pressures leading to fracturing can be excluded and gas-borne radionuclides are not able to reach the surface.

For the All Containers Fail Scenario, extremely conservative assumptions lead to sufficient corrosion-generated gas for transport controlled by dilational flow. Limited modelling shows pore pressures within the intact rock remain low while repository gases dissipate through bentonite-based sealing materials by dilational flow. Corrosion-generated gas from the All Containers Fail Scenario could carry volatile radionuclides (notably C-14) through the repository. In the unlikely event of corrosion-generated gas reaching the repository shafts, any gas-borne radioactivity would be dispersed within the Guelph formation. A conservative dose assessment shows any hypothetical dose consequence would be well below natural background radioactivity.

Other Protection Criteria

Results for cases examining the protection of persons from hazardous substances, the radiological protection of the environment, and the protection of the environment from hazardous substances are also all within their associated interim acceptance criteria. These results are presented in Chapter 7.

Conclusion

This report describes the reference design for a deep geological repository in sedimentary rock and provides an illustrative postclosure safety assessment approach which is structured, systematic and consistent with CNSC REGDOC-2.11.1, Volume III (CNSC 2018). The illustrative assessment includes a description of the repository system, systematically identifies scenarios, models and methods for evaluating safety, uses different assessment strategies, addresses uncertainty, and compares the results of the assessment with interim acceptance criteria.

The postclosure safety assessment shows, for the Normal Evolution Scenario and associated sensitivity cases, that all radiological and non-radiological interim acceptance criteria are met with substantial margins during the postclosure period. This result is consistent with previous assessments of a deep geological repository in Canada, as well as with safety assessment studies by other national radioactive waste management organizations.

TABLE OF CONTENTS

	<u>Page</u>
EXECUTIVE SUMMARY	i
1. INTRODUCTION.....	1
1.1 Purpose and Scope	1
1.2 Background and Project Overview	1
1.3 APM Project Phases	3
1.3.1 Site Selection	3
1.3.2 Site Preparation and Construction	3
1.3.3 Operation	3
1.3.4 Extended Monitoring	4
1.3.5 Decommissioning	5
1.4 Repository Timeframes	5
1.4.1 Preclosure Period.....	5
1.4.2 Postclosure Period	5
1.5 Relevant Legislation	8
1.5.1 CNSC Regulatory Requirements	8
1.5.2 Transportation of Used Nuclear Fuel	10
1.5.3 Canadian Codes and Standards	11
1.5.4 Safeguards.....	11
1.5.5 Indigenous Knowledge.....	11
1.5.6 International Guidance	12
1.6 Safety Case	12
1.6.1 Safety Case Context	13
1.6.2 Safety Strategy.....	15
1.6.3 Repository System	15
1.6.3.1 Geology.....	15
1.6.3.2 Waste Characteristics	16
1.6.3.3 Design	16
1.6.4 Safety Assessment	17
1.6.5 Management of Uncertainties	17
1.6.6 Iterative Approach	17

1.6.7	Integration of Safety Arguments.....	18
1.6.8	Stakeholder and Regulatory Involvement	18
1.6.9	Management System	19
1.7	International Status of Deep Geological Repositories	21
1.8	Report Structure and Content	22
1.9	References for Chapter 1	23
2.	DESCRIPTION OF THE HYPOTHETICAL SITE.....	25
2.1	Introduction.....	25
2.1.1	Site Attributes.....	25
2.1.2	Modelling Strategy	26
2.2	Conceptual Model for Hypothetical Site.....	26
2.2.1	Descriptive Geological Model.....	26
2.2.1.1	Geologic Description.....	26
2.2.1.1.1	Basement Geology.....	28
2.2.1.1.2	Sedimentary Bedrock Geology.....	28
2.2.1.2	Surface Features	29
2.2.1.2.1	Topography	29
2.2.1.2.2	Surface Hydrology.....	30
2.2.2	Descriptive Hydrogeologic Model.....	31
2.2.2.1	Groundwater Systems	31
2.2.2.2	Hydraulic Parameters	31
2.2.2.3	Paleohydrogeology Boundary Conditions.....	35
2.2.2.4	Abnormal Pressure Distributions	36
2.2.2.5	Saturated Conditions	36
2.2.3	Descriptive Geochemical Model.....	40
2.2.3.1	Microbial Conditions in Sedimentary Environments.....	44
2.2.3.2	Sorption.....	45
2.2.3.3	Gas Characterization	46
2.2.4	Descriptive Geomechanical Model.....	46
2.2.4.1	Rock Mass Strength.....	46
2.2.4.2	Ground Stresses	50
2.2.4.3	Seismicity.....	52
2.3	Regional Scale Hydrogeologic Modelling	53
2.3.1	Computational Models	53
2.3.2	System Performance Measures.....	53

2.3.3	Regional Scale Conceptual Model	54
2.3.3.1	Model Domain and Spatial Discretization	54
2.3.3.2	Model Parameters.....	57
2.3.3.2.1	Hydraulic Conductivity of Permafrost	57
2.3.3.2.2	Precambrian Hydraulic Conductivity	58
2.3.3.2.3	Groundwater Transport Parameters.....	58
2.3.3.3	Flow Boundary Conditions	60
2.3.3.4	Initial Conditions and Solution of Density-Dependent Flow	61
2.3.3.5	Model Uncertainties and Sensitivities	64
2.3.4	Regional Scale Analyses	65
2.3.4.1	Reference Case Simulation	65
2.3.4.2	Temperate Transient Sensitivity Cases	71
2.3.4.3	Paleohydrogeologic Sensitivity Cases	77
2.3.4.4	Groundwater System Behaviour	92
2.3.4.4.1	Glaciation	92
2.3.4.4.2	Permafrost.....	92
2.3.4.4.3	Depth of Surficial Recharge and Pathways.....	95
2.3.4.4.4	The Role of Density.....	95
2.3.4.4.5	Anomalous Heads.....	96
2.3.5	Additional Temperate Transient Sensitivity Analyses	98
2.4	Summary and Conclusions	104
2.5	References for Chapter 2.....	105
3.	USED FUEL CHARACTERISTICS.....	113
3.1	Used Fuel Description.....	113
3.1.1	Used Fuel Type and Amount	113
3.1.2	Geometry	114
3.1.3	Discharge Burnup and Linear Power	115
3.1.4	Effect of Irradiation	118
3.1.5	Reference Used Fuel Parameters.....	123
3.2	Radionuclide and Chemical Element Inventories and Uncertainties.....	123
3.2.1	Potentially Hazardous Radionuclides and Elements.....	123
3.2.2	Inventories of Potentially Hazardous Radionuclides and Elements	125
3.2.3	Uncertainties in Isotope Inventories	128
3.3	References for Chapter 3.....	130
4.	REPOSITORY FACILITY – CONCEPTUAL DESIGN.....	133

4.1	General Description	133
4.2	Design Requirements	134
4.2.1	Canadian Acts, Regulations and Codes	134
4.2.2	Safeguards.....	135
4.2.3	Facility Requirements.....	135
4.2.4	Engineered Barrier Requirements.....	136
4.2.4.1	Used Fuel Container Requirements.....	136
4.2.4.2	Room and Tunnel Sealing Requirements	137
4.2.4.3	Shaft Sealing Requirements	137
4.3	Description of Engineered Barriers	137
4.3.1	Used Fuel Container	138
4.3.2	Room, Tunnel and Shaft Sealing Materials.....	141
4.3.2.1	Highly Compacted Bentonite	141
4.3.2.2	Dense Backfill	143
4.3.2.3	Gap Fill.....	143
4.3.2.4	Shaft Backfill	144
4.3.2.5	Asphalt.....	144
4.3.2.6	Concrete	144
4.3.2.7	Grout	145
4.4	Surface Facilities	146
4.5	Used Fuel Packaging Plant	150
4.5.1	Used Fuel Transport Package Receipt and Unloading	153
4.5.2	Used Fuel Container Loading and Sealing	155
4.5.3	Used Fuel Container Intra-Plant Transfer System	157
4.6	Sealing Materials Production Facilities	158
4.6.1	Sealing Materials Compaction Plant	158
4.6.2	Concrete Batch Plant	159
4.6.3	Aggregate Supply.....	159
4.7	Shafts and Hoists	160
4.8	Underground Facility Design	160
4.8.1	Underground Layout	161
4.8.2	Placement Room Geometry and Spacing	164
4.8.3	Placement Room Closure	166

4.8.4	Ventilation System	167
4.9	Site Preparation and Construction of the Repository	168
4.9.1	Site Preparation	168
4.9.2	Shaft Sinking	168
4.9.3	Underground Demonstration Facility.....	168
4.9.4	Lateral Development	169
4.9.5	DGR Facility Commissioning	169
4.10	Repository Operation	169
4.10.1	Preparation of Placement Room	170
4.10.2	Buffer Box Placement	170
4.10.3	Description of Placement Equipment.....	171
4.10.4	Storyboard Description of Preparation and Placement Operations	172
4.10.5	Environmental Monitoring Programs.....	182
4.11	Extended Monitoring	183
4.12	Decommissioning and Closure	183
4.12.1	Sealing of Underground Horizontal Openings.....	183
4.12.2	Sealing of Hydraulically Active Zones	184
4.12.3	Sealing of Shafts	185
4.12.4	Sealing of Boreholes	187
4.12.5	End State	187
4.13	References for Chapter 4	187
5.	LONG-TERM EVOLUTION OF THE MULTIPLE-BARRIER SYSTEM	189
5.1	Long-Term Evolution of the Geosphere	194
5.1.1	Seismicity	194
5.1.2	Glaciation	194
5.1.2.1	Glacial Loading	195
5.1.2.2	Permafrost Formation	196
5.1.2.3	Glacial Erosion.....	196
5.1.2.4	Groundwater System Evolution	198
5.1.3	Confidence in Geosphere Evolution.....	199
5.2	Long-Term Evolution of the Repository Environment	200
5.2.1	Temperature.....	200
5.2.2	Repository Saturation.....	201

5.2.3	Near-Field Chemistry	202
5.2.4	Steel Corrosion and Gas Generation	203
5.2.5	Excavation-Damaged Zone.....	207
5.2.6	Geomechanical Evolution of the Placement Room	207
5.2.6.1	Impact of Time-Dependent Strength Degradation	208
5.2.6.2	Impact of Glaciation	210
5.2.6.3	Impact of Seismic Ground Shaking.....	211
5.2.7	Confidence in Repository Evolution	212
5.3	Long-Term Evolution of Used Fuel	213
5.3.1	Radioactive Decay	213
5.3.2	Changes in Temperature	215
5.3.3	Changes in the UO ₂	216
5.3.3.1	Alpha Radiation Damage	216
5.3.3.2	Radionuclide Diffusion	216
5.3.3.3	Oxidation State of Fuel	217
5.3.4	Zircaloy Cladding	217
5.3.5	Build-Up of Helium Gas.....	217
5.3.6	Criticality.....	218
5.3.7	Mechanical Integrity	218
5.3.8	Biological Processes	218
5.3.9	Confidence	219
5.4	Long-Term Evolution of a Used Fuel Container	219
5.4.1	Irradiation of Container Materials	220
5.4.2	Container Temperature	220
5.4.3	Mechanical Integrity	220
5.4.3.1	Effects of Hydrostatic and Buffer Swelling Pressures.....	221
5.4.3.1.1	Effects of Glacial Loading.....	221
5.4.3.1.2	Effect of Seismic Stresses.....	222
5.4.3.1.3	Effect of Creep	223
5.4.3.2	Effect of Chemical Processes inside the Container	223
5.4.3.3	Effect of Chemical Processes outside the Container.....	224
5.4.3.3.1	Uniform Copper Corrosion	225
5.4.3.3.2	Uniform Copper Corrosion Modelling	229

5.4.3.3.3	Localized Corrosion.....	231
5.4.3.3.4	Stress Corrosion Cracking	231
5.4.3.3.5	Microbially Influenced Corrosion	232
5.4.3.4	Summary.....	234
5.4.4	Effects of the Environment on Containers with Defects in the Copper Coating.....	235
5.4.4.1	Impacts of Coating Defects.....	235
5.4.4.2	Impacts of Through-Copper Defects.....	237
5.4.4.2.1	Oxic Galvanic Corrosion.....	237
5.4.4.2.2	Anoxic Galvanic Corrosion	238
5.4.4.2.3	Anaerobic Corrosion of the Steel Vessel through a Defect in the Coating.....	238
5.4.4.3	Modelling Steel Corrosion beneath a Through-Copper Defect.....	238
5.4.4.4	Stresses in the Copper Defect As a Result of Corrosion.....	243
5.4.4.5	Failure of the Steel Vessel during Corrosion at a Defect in Copper Coating.....	244
5.4.4.6	Corrosion and Deformation of the Zircaloy Cladding	244
5.4.4.7	Dissolution of the Used Fuel Matrix	245
5.4.4.8	Radionuclide Release from the Fuel Pellets and Cladding.....	247
5.4.4.9	Fate of Released Radionuclides	247
5.4.4.10	Summary.....	248
5.4.5	Confidence	248
5.5	Long-Term Evolution of Buffer, Backfill and Seals	250
5.5.1	Changes during Saturation	250
5.5.2	Temperature Changes	253
5.5.3	Chemical Changes.....	254
5.5.4	Changes due to Biological Processes.....	254
5.5.5	Radiation.....	257
5.5.6	Sorption.....	257
5.5.7	Vertical Movement of Containers.....	257
5.5.8	Buffer Erosion and Colloid Formation	257
5.5.9	Confidence	258
5.6	Summary	259
5.7	References for Chapter 5	259

6.	SCENARIO IDENTIFICATION AND DESCRIPTION	269
6.1	The Normal Evolution Scenario	271
6.1.1	External FEPs	271
6.1.2	Internal FEPs	280
6.1.3	Description of the Normal Evolution of the Repository System.....	280
6.1.3.1	Events Occurring for Intact Containers	281
6.1.3.2	Events Occurring for Defective Containers	284
6.2	Disruptive Event Scenarios	289
6.2.1	Identification of Disruptive Event Scenarios	286
6.2.2	Description of Disruptive Event Scenarios	312
6.2.2.1	Inadvertent Human Intrusion Scenario	312
6.2.2.2	Repository Seals Failure Scenario.....	313
6.2.2.3	Partially Sealed Repository Scenario.....	313
6.2.2.4	Poorly Sealed Borehole Scenario	313
6.2.2.5	Undetected Fault Scenario	313
6.2.2.6	Severe Erosion Scenario	314
6.2.2.7	All Containers Fail Scenario.....	314
6.2.2.8	Container Failure	314
6.3	References for Chapter 6	315
7.	POSTCLOSURE SAFETY ASSESSMENT – CONTAMINANT TRANSPORT	317
7.1	Interim Acceptance Criteria	318
7.1.1	Interim Acceptance Criteria for the Radiological Protection of Persons.....	318
7.1.2	Interim Acceptance Criteria for the Protection of Persons from Hazardous Substances	319
7.1.3	Interim Acceptance Criteria for the Radiological Protection of the Environment	322
7.1.4	Interim Acceptance Criteria for the Protection of the Environment from Hazardous Substances	324
7.2	Scope	324
7.2.1	The Normal Evolution Scenario	327
7.2.1.1	Reference Case	327
7.2.1.2	The Base Case	327
7.2.1.3	Sensitivity Studies to Illustrate the Effects of Well Assumptions.....	333
7.2.1.4	Sensitivity Studies to Illustrate the Effect of Deviations in Anticipated Barrier Performance for the Base Case	334

7.2.1.5	Sensitivity Studies to Illustrate the Effect of Modelling Attributes and Numeric Parameters on the Base Case	347
7.2.1.6	Sensitivity Study to Illustrate the Effect of Glaciation.....	347
7.2.2	Disruptive Event Scenarios	348
7.2.3	Analysis Exclusions.....	351
7.3	Conceptual Model.....	351
7.3.1	Used Fuel Containers	353
7.3.2	Engineered Barrier System	356
7.3.3	Geosphere	357
7.3.4	Biosphere.....	359
7.4	Computer Codes.....	363
7.5	Overall Analysis Approach and Selected Data for Groundwater Flow and Radionuclide Transport	370
7.5.1	Overall Approach	370
7.5.2	Data for Selected Parameters.....	373
7.5.2.1	Initial Inventory.....	373
7.5.2.2	Instant Release Fractions and Fuel Dissolution Rate.....	373
7.5.2.3	Radionuclide Source Terms.....	376
7.5.2.4	Reference Groundwater Composition.....	379
7.5.2.5	Element Solubilities.....	380
7.5.2.6	Effective Diffusion Coefficients	382
7.5.2.7	Sorption Parameters	383
7.6	Modelling and Results for Radionuclide and Chemical Hazard Screening	388
7.6.1	Methods	388
7.6.1.1	Radionuclide Screening.....	389
7.6.1.2	Chemical Element Screening.....	390
7.6.2	Results	391
7.7	Modelling and Results for 3D Groundwater Flow and Radionuclide Transport.....	395
7.7.1	Methods	396
7.7.1.1	Subregional Flow Model	396
7.7.1.2	Main and Detailed Transport Models.....	400
7.7.1.3	Container Transport Model	416
7.7.2	Results	422

7.7.2.1	Subregional Flow Model Results	423
7.7.2.1.1	Base Case – No Well Flow Results.....	423
7.7.2.2	Main and Detailed Transport Models Flow Results	426
7.7.2.2.1	Base Case – No Well Flow Results.....	427
7.7.2.2.2	Base Case Flow Results	431
7.7.2.3	Main and Detailed Transport Model Radionuclide Transport Results	433
7.7.2.3.1	Comparison of Different Transport Models	433
7.7.2.3.2	Location of the Well and Defective Containers	436
7.7.2.3.3	Base Case Results.....	438
7.7.2.3.4	Well Assumption Sensitivity Cases	448
7.7.2.3.5	Barrier Sensitivity Cases	449
7.7.2.3.6	Numeric Parameter Sensitivity Cases	451
7.7.2.4	Container Transport Model Flow Results.....	452
7.7.2.5	Container Transport Model Radionuclide Transport Results	454
7.7.2.6	Effect of Barriers on Radionuclide Transport.....	464
7.7.2.7	Summary of Results for 3D Modelling	467
7.8	Modelling and Results for the System Model	469
7.8.1	Methods	469
7.8.1.1	Repository Submodel.....	469
7.8.1.2	Geosphere Submodel.....	470
7.8.1.3	Biosphere Submodel.....	474
7.8.1.4	Verification of the System Model	479
7.8.2	Results	484
7.8.2.1	Base Case	486
7.8.2.2	Well Assumption Sensitivity Cases.....	487
7.8.2.3	Barrier Performance Sensitivity Cases	487
7.8.2.3.1	Fuel Barrier Sensitivity	487
7.8.2.3.2	Zircaloy Sheath Barrier Sensitivity	490
7.8.2.3.3	Container Barrier Sensitivity.....	492
7.8.2.3.4	Buffer, Backfill, and Seals Barrier Sensitivity	496
7.8.2.3.5	Geosphere Barrier Sensitivity.....	499
7.8.2.4	Glaciation Sensitivity.....	500
7.8.2.4.1	Glacial Cycles.....	501

7.8.2.4.2	Hydrogeological Modelling	502
7.8.2.4.3	Transport Modelling.....	505
7.8.2.4.4	Dose Results for Glaciation Scenario.....	512
7.8.2.4.5	Applicability to the Current Study	512
7.8.2.5	Probabilistic Analysis	513
7.8.2.5.1	Results for Container Failure Assumptions Fixed	514
7.8.2.5.2	Results for All Parameters Varying	518
7.8.2.6	Summary of Results for System Modelling	523
7.9	Modelling and Results for Disruptive Event Scenarios	525
7.9.1	Inadvertent Human Intrusion.....	526
7.9.1.1	Description	527
7.9.1.2	Model and Assumptions.....	529
7.9.1.3	Dose Results.....	533
7.9.2	All Containers Fail	538
7.9.2.1	3D Model Methods and Results.....	538
7.9.2.2	System Model Methods and Results	541
7.9.3	Repository Seal Failure.....	543
7.9.4	Undetected Fault.....	545
7.9.4.1	Model and Assumptions.....	545
7.9.4.2	Transport Results.....	546
7.10	Modelling and Results for the Radiological Protection of the Environment.....	548
7.10.1	Method	548
7.10.2	Results	550
7.11	Modelling and Results for the Protection of Persons and the Environment from Hazardous Substances	552
7.11.1	Used Fuel Chemical Hazard Assessment.....	553
7.11.2	Copper Container Chemical Hazard Assessment.....	557
7.12	Modelling and Results for Complementary Indicators.....	559
7.12.1	Reference Values.....	560
7.12.2	Results for Complementary Indicators	564
7.13	Summary and Conclusions	567
7.13.1	Scope Overview	567
7.13.2	Result Summary.....	571

7.13.2.1	Radiological Protection of Persons	571
7.13.2.1.1	Normal Evolution Scenario	571
7.13.2.1.2	Disruptive Event Scenarios	575
7.13.2.2	Radiological Protection of the Environment	577
7.13.2.3	Protection of Persons and the Environment from Hazardous Substances	577
7.13.2.4	Complementary Indicators	578
7.13.3	Conclusion	578
7.14	References for Chapter 7	579
8.	POSTCLOSURE SAFETY ASSESSMENT – GAS GENERATION AND TRANSPORT	587
8.1	Interim Acceptance Criteria	587
8.2	Scope	588
8.3	Conceptual Model	588
8.3.1	Gas Generation	589
8.3.2	Gas Migration and Transport	589
8.4	Computer Code	591
8.5	Overall Approach and Selected Data for Gas Transport and Migration	597
8.6	Analysis Methods and Key Assumptions	598
8.6.1	Room-Scale Model	598
8.6.2	Repository-Scale Model	603
8.7	Results of Gas Generation and Transport Modelling	607
8.7.1	Room-Scale Model	608
8.7.1.1	Resaturation Period	609
8.7.1.2	Base Case	609
8.7.1.3	All Containers Fail Disruptive Event Scenario	618
8.7.2	Repository-Scale Model	622
8.7.2.1	Resaturation Period	623
8.7.2.2	Base Case	629
8.7.2.3	All Containers Fail Disruptive Event Scenario	634
8.7.3	Gas Flow and Gas Mass Allocation	639
8.7.3.1	Resaturation Period	639
8.7.3.2	Base Case	640
8.7.3.3	All Containers Fail Disruptive Event Scenario	642

8.8	Dose Consequences	645
8.8.1	Conventional Two-Phase Flow	645
8.8.2	Dilational Flow	646
8.9	Summary and Conclusions	647
8.10	References for Chapter 8	648
9.	TREATMENT OF UNCERTAINTIES	651
9.1	Approach	651
9.2	Key Uncertainties	656
9.3	References for Chapter 9	657
10.	NATURAL ANALOGUES	659
10.1	Analogues for Used Nuclear Fuel	659
10.1.1	Natural Uranium Deposits	659
10.1.2	Natural Fissioned Uranium.....	661
10.1.3	Fractured Uranium Deposits	663
10.2	Analogues for Barriers	664
10.2.1	Copper	664
10.2.2	Iron	665
10.2.3	Clays	666
10.2.4	Concrete.....	670
10.2.5	Asphalt	671
10.3	Analogue for Geosphere	671
10.4	Natural Analogue Summary.....	672
10.5	References for Chapter 10	672
11.	QUALITY ASSURANCE.....	677
11.1	Introduction.....	677
11.2	APM Safety Case Project Quality Plan	677
11.3	Examples of Peer Review and Quality Assurance	678
11.4	Future Safety Case Quality Assurance.....	679
11.5	References for Chapter 11	679
12.	SUMMARY AND CONCLUSIONS	681
12.1	Safety Case	681
12.2	Repository System	684
12.2.1	Geologic Description of the Hypothetical Site	684

12.2.2	Used Fuel.....	685
12.2.3	Design Concept.....	685
12.3	Safety Assessment.....	685
12.3.1	Assessment Strategies	687
12.3.2	Modelling Tools and Computer Codes.....	687
12.3.2.1	Key Assumptions and Conservatisms in Modelling	689
12.3.3	Normal Evolution Scenario.....	690
12.3.3.1	Results from Sensitivity Analyses and Bounding Assessments	692
12.3.3.2	Results from the Probabilistic Analysis	694
12.3.3.3	Results from Complementary Indicators.....	696
12.3.4	Disruptive Event Scenarios	696
12.4	Future Work.....	698
12.5	Conclusion	698
12.6	References for Chapter 12	698
13.	SPECIAL TERMS	699
13.1	Units.....	699
13.2	Abbreviations and Acronyms.....	700

LIST OF TABLES

	<u>Page</u>
Table 1-1: CNSC Regulatory Documents Applicable to the APM Project	9
Table 1-2: International Guidance Applicable to Safety Assessment	12
Table 1-3: Status of National Plans for High-Level Waste	21
Table 1-4: Case Study Report Content Mapped to CNSC REGDOC-2.11.1 Volume III.....	23
Table 2-1: Formation Thicknesses at the Hypothetical Site.....	27
Table 2-2: Regional Hydrogeologic Parameters	32
Table 2-3: Average TDS Values for Sedimentary Formation Groundwaters and Porewaters.....	43
Table 2-4: Reference SR-270-PW Composition	44
Table 2-5: Geological Profile Near Repository Horizon with Formation Thicknesses.....	47
Table 2-6: Intact Rock and Rock Mass Mechanical Properties (Itasca 2015).....	48
Table 2-7: Thermal Properties for the Units in the Sedimentary Setting.....	50
Table 2-8: Summary of Seismic Hazard Analysis Results	53
Table 2-9: Sub-divisions of Geologic Formations	55
Table 2-10: Loading Efficiency (ζ) and Specific Storage (S_s) for Scenario (fr-base-paleo-biot05) with a Biot Coefficient of 0.5.....	59
Table 2-11: Groundwater Transport Parameters	60
Table 2-12: Table of Regional Scale Simulations for this Study	72
Table 2-13: Computed MLE Values at the Repository Footprint for Alternate Temperate Scenarios.....	100
Table 3-1: Discharge Burnup Percentiles on a Per Station Basis.....	116
Table 3-2: Reference Used Fuel Parameters	123
Table 3-3: Potentially Significant Radionuclides Included in the Assessment	124
Table 3-4: Potentially Hazardous Elements Included in the Assessment.....	125
Table 3-5: Inventories of Potentially Hazardous Radionuclides in UO ₂ Fuel for 30 Year Decay Time.....	126
Table 3-6: Inventories of Potentially Hazardous Radionuclides of Interest in Zircaloy for 30 Years Decay Time	127
Table 3-7: Inventories of Potentially Hazardous Elements for 30 Year Decay Time	128
Table 3-8: ORIGEN-S: Pickering Fuel Measure and Calculated Inventory Comparison	130
Table 4-1: Reference Used Fuel Container and Copper Coating Parameters.....	140
Table 4-2: Physical Composition and As-Placed Properties of Clay-Based and Asphalt Materials for Room, Tunnel and Shaft Sealing	143

Postclosure Safety Assessment of a Used Fuel Repository in Sedimentary Rock

Document Number: NWMO-TR-2018-08

Revision: 000

Class: Public

Page: xxvi

Table 4-3:	Expected Annual Concrete Requirements for the Repository	145
Table 4-4:	APM Facility Number and Description	149
Table 4-5:	Key Data for Average UFPP Throughput	152
Table 4-6:	Proposed Sealing System for Shafts	185
Table 5-1:	Main Safety Attributes.....	190
Table 5-2:	General Parameters of Key Repository Features	192
Table 5-3:	Summary of Seismic Hazard Analysis Result (AMEC Geomatrix 2011)	194
Table 5-4:	Time to Exposed Steel beneath Defects in a Nominal 3 mm Copper Coating ..	237
Table 5-5:	Time for Steel Corrosion to Perforate the Container Wall.....	243
Table 6-1:	FEP List Showing FEPs Down to Level 2.....	270
Table 6-2:	Status of External FEPs for the Normal Evolution of the Repository System....	272
Table 6-3:	External FEPs Potentially Compromising Safety Attributes Relating to Long-Term Safety	288
Table 6-4:	Internal FEPs Potentially Compromising Safety Attributes Relating to Long-Term Safety	301
Table 6-5:	Potential Failure Mechanisms and Associated Scenarios	307
Table 6-6:	Additional Scenarios Considered in Other Safety Assessments	311
Table 7-1:	Interim Acceptance Criteria for the Protection of Persons and the Environment from Non-Radiological Impacts	320
Table 7-2:	Interim Acceptance Criteria for the Radiological Protection of the Environment.....	324
Table 7-3:	Conservatisms in Base Case Assumptions	329
Table 7-4:	Sensitivity Cases to Illustrate the Effects of Well Assumptions	334
Table 7-5:	Sensitivity Cases to Illustrate the Effect of Deviations in Anticipated Barrier Performance for the Base Case	337
Table 7-6:	Modelling Attributes and Numeric Parameter Sensitivity Cases.....	347
Table 7-7:	Analysis Cases for Disruptive Event Scenarios.....	349
Table 7-8:	RSM, Version 1.1.....	366
Table 7-9:	SYVAC3-CC4, Version SCC4.09.3	367
Table 7-10:	FRAC3DVS-OPG, Version 1.3	368
Table 7-11:	HIMv2.1	369
Table 7-12:	NHBv1.0	369
Table 7-13:	Fuel Instant Release Fractions	374
Table 7-14:	Zircaloy Instant Release Fractions	376
Table 7-15:	Reference Groundwater Composition at Repository Depth.....	380

Table 7-16:	Element Solubilities	381
Table 7-17:	Effective Diffusion Coefficients, Base Case Values.....	382
Table 7-18:	Effective Diffusion Coefficients, Base Case Values.....	383
Table 7-19:	Bentonite Sorption Coefficients (K_d), Base Case Values.....	384
Table 7-20:	Geosphere Sorption Coefficients K_d for Shale, Base Case Values	385
Table 7-21:	Geosphere Sorption Coefficients K_d for Limestone, Base Case Values	386
Table 7-22:	Values of $[\rho_s(1-\epsilon_{\text{expt}})/\epsilon_{\text{expt}}]$ for Several Geological Materials	387
Table 7-23:	Screening Model Geosphere Zone Properties	388
Table 7-24:	RSM Cases Considered for the Screening Assessment	389
Table 7-25:	Chemical Elements Excluded from Chemical Hazard Assessment.....	391
Table 7-26:	Erosion based Screening of Some Excluded Chemical Elements.....	391
Table 7-27:	Ratio of the RSM results and Chemical Acceptance Criteria.....	392
Table 7-28:	Superset of Screened in Radionuclides and Chemically Hazardous Elements.....	394
Table 7-29:	List of Potentially Significant Radionuclides	395
Table 7-30:	List of Potentially Significant Chemically Hazardous Elements	395
Table 7-31:	Formation Depths, Thicknesses, and Hydraulic Conductivities	398
Table 7-32:	Main and Detailed Transport Model Engineered Barrier Hydraulic Properties ..	403
Table 7-33:	Summary of Results for I-129 3D Modelling	468
Table 7-34:	System Model - Biosphere Submodel, Surface Water Discharge Areas.....	475
Table 7-35:	System Model - Biosphere Submodel, Soil Properties	476
Table 7-36:	System Model - Biosphere Submodel, Climate and Atmosphere Parameters ..	477
Table 7-37:	System Model - Biosphere Submodel, Human Lifestyle Data	478
Table 7-38:	Statistical Information for the 1Ma Dose Rate Histogram with Container Assumptions Fixed	515
Table 7-39:	Probabilistic Assessment: Individual Radionuclides Dose Contributions for Container Assumptions Fixed.....	516
Table 7-40:	Probabilistic Assessment: Results for Top 5 High-Dose Simulations with Container Assumptions Fixed.....	517
Table 7-41:	Probabilistic Assessment: I-129 Pathway.....	518
Table 7-42:	Statistical Information for the 1 Ma Dose Rate Histogram with All Assumptions Varying	521
Table 7-43:	Individual Radionuclide Dose Rates with All Assumptions Varying.....	521
Table 7-44:	Probabilistic Assessment: Results for Top 5 High Dose Simulations with All Assumptions Varying	523

Table 7-45:	Summary of Dose Results for System Model	524
Table 7-46:	Human Intrusion Pathways Considered in Recent Safety Assessments.....	528
Table 7-47:	Parameters for Human Intrusion Scenario	532
Table 7-48:	1 Ma Dose Rates to Non-Human Biota	550
Table 7-49:	System Model: Concentration Quotients for the Base Case.....	554
Table 7-50:	System Model: Concentration Quotients for the All Containers Fail Case.....	554
Table 7-51:	Concentration Impurity Levels in Copper and Estimated Element Concentration Quotients	559
Table 7-52:	Background Concentration of Radionuclides in Surface Waters	561
Table 7-53:	Radioactive Element Concentrations in Rocks	562
Table 7-54:	Radiotoxicity Concentration in Rocks	563
Table 7-55:	Reference Values for Indicators	564
Table 7-56:	Results for Complementary Indicators.....	567
Table 7-57:	Normal Evolution Result Summary.....	572
Table 7-58:	Disruptive Event Scenarios Result Summary	576
Table 7-59:	Inadvertent Human Intrusion Dose Summary for Intrusion at 300 years.....	577
Table 8-1:	Two-Phase Flow Properties.....	592
Table 8-2:	T2GGM Version 3.2.1	596
Table 8-3:	Comparison of Volatile, Long-Lived Radionuclides	645
Table 9-1:	Base Case Sensitivity Study Assumptions	654
Table 12-1:	Summary of Key Safety Attributes	682

LIST OF FIGURES

	<u>Page</u>	
Figure 1-1:	Illustration of Deep Geological Repository Concept	4
Figure 1-2:	Perspective of Past Events and Expected Future Events in Earth’s History Including Repository Events	7
Figure 1-3:	Components of the Safety Case.....	14
Figure 1-4:	Iterative Process for Developing the Safety Case	20
Figure 2-1:	Regional Scale Topography	30
Figure 2-2:	nn9930 GSM Model Outputs for the Grid Block Containing the Repository Footprint for this Study.....	37

Figure 2-3:	nn9921 GSM Model Outputs for the Grid Block Containing the Repository Footprint for this Study.....	38
Figure 2-4:	gsm2015 GSM Model Outputs for the Grid Block Containing the Repository Footprint for this Study.....	39
Figure 2-5:	Unconfined Compressive Strength and Elastic Modulus of Cobourg Formation from DGR 1 to 6.....	48
Figure 2-6:	Static-fatigue and Creep Testing on Cobourg and Jura Limestones to verify Long-term Strength Assumptions	49
Figure 2-7:	Distribution of (1) Crack Initiation Stresses and (2) Crack Damage Stresses for the Cobourg and Sherman Fall Formations	49
Figure 2-8:	Comparison of Calculated Maximum Horizontal In Situ Stress Profiles at the Bruce Site	51
Figure 2-9:	Seismicity in the Bruce Region to December 2016	52
Figure 2-10:	Block Cut View of HGS Zone Identifiers for Regional Scale Domain	56
Figure 2-11:	Block Cut View Showing Spatial Extent of the Bedrock Units	57
Figure 2-12:	Precambrian Horizontal and Vertical Matrix Permeabilities as a Function of Depth	60
Figure 2-13:	Plot of TDS versus Depth for Groundwater from the Canadian Shield.....	63
Figure 2-14:	Block Cut View of Initial Total Dissolved Solids Concentration Distribution.....	63
Figure 2-15:	Block Cut View of Steady-State Density-Independent Freshwater Heads	66
Figure 2-16:	Block Cut View of Freshwater Heads at Pseudo Equilibrium Time with Temporally Varying TDS Distribution.....	66
Figure 2-17:	Block Cut View of Total Dissolved Solids Concentration at Pseudo Equilibrium Time with Temporally Varying TDS Distribution.....	67
Figure 2-18:	Total Dissolved Solids Concentration at Pseudo Equilibrium Time at East-West Cross-Section through the Hypothetical Repository Footprint	67
Figure 2-19:	Block Cut View of Reference Case Porewater Velocity Magnitude at Pseudo Equilibrium Time	68
Figure 2-20:	Block Cut View of Reference Case Ratio of Vertical Velocity to Velocity Magnitude at Pseudo Equilibrium Time	69
Figure 2-21:	Block Cut View of Base Case Mean Life Expectancy at Pseudo Equilibrium Time	70
Figure 2-22:	Reference Case Mean Life Expectancy at Pseudo Equilibrium Time at East-West Cross-Section through the Hypothetical Repository Footprint	70
Figure 2-23:	Ratio of Velocity Magnitudes of Steady-State Groundwater Flow to Density-Dependent Flow Reference Case	73
Figure 2-24:	Ratio of MLEs of Steady-State Groundwater Flow to Density-Dependent Flow Reference Case.....	73

Figure 2-25:	Total Dissolved Solids Concentrations at Pseudo Equilibrium Time for an Increased Rock Mass Hydraulic Conductivity.....	75
Figure 2-26:	Difference in Freshwater Heads between a Simulation Using an Increased Rock Mass Hydraulic Conductivity and Reference Case	75
Figure 2-27:	Ratio of Pore Velocity Magnitudes of Sensitivity Case using an Increased Rock Mass Hydraulic Conductivity to Reference Case	76
Figure 2-28:	MLE Ratio of Increased Rock Mass Hydraulic Conductivities Simulation to Reference Case Simulation	76
Figure 2-29:	Block View Showing the Depth of Penetration of a Tracer after 120,000 Years for a Reference Case Paleohydrogeologic Scenario	78
Figure 2-30:	Vertical Profile Plots of Tracer Concentrations for the Paleohydrogeologic Simulations at the Location of the Hypothetical Repository Footprint at 120,000 Years	79
Figure 2-31:	Block View Showing the Depth of Penetration of a Tracer after 120,000 Years for the nn9921 Paleoclimate Boundary Conditions (fr-base-paleo-cold)...	80
Figure 2-32:	Block View Showing the Depth of Penetration of a Tracer after 120,000 Years for the gsm2015 Paleoclimate Boundary Conditions (fr-base-paleo-gsm2015)	81
Figure 2-33:	Block View Showing the Depth of Penetration of a Tracer after 120,000 Years for the nn9930 Paleoclimate Boundary Conditions and a Loading Efficiency of 1 (fr-base-paleo-le1).....	83
Figure 2-34:	Block View Showing the Depth of Penetration of a Tracer after 120,000 Years for the nn9930 Paleoclimate Boundary Conditions and a Loading Efficiency of 0 (fr-base-paleo-le0).....	83
Figure 2-35:	Block View Showing the Depth of Penetration of a Tracer after 120,000 Years for the nn9930 Paleoclimate Boundary Conditions, a Loading Efficiency of 1, and a 0% of Ice-Sheet Thickness Equivalent Freshwater Head for the Surface Hydraulic Boundary Condition (fr-base-paleo-0-le1)	84
Figure 2-36:	Péclet Number of Molecular Diffusion versus Time at the Hypothetical Repository Footprint for the Reference Paleohydrogeological Scenario (fr-base-paleo)	85
Figure 2-37:	Péclet Number of Molecular Diffusion versus Time at the Hypothetical Repository Footprint for the Paleohydrogeological Scenario with Increased Rock Mass Hydraulic Conductivity (fr-base-paleo-sens)	87
Figure 2-38:	Footprint for nn9930 Paleoclimate Boundary Conditions and a Loading Efficiency of 0 (fr-base-paleo-le0).....	88
Figure 2-39:	Péclet Number of Molecular Diffusion versus Time at the Hypothetical Repository Footprint for nn9930 Paleoclimate Boundary Conditions, a Loading Efficiency of 1, and a 0% of Ice-Sheet Thickness Equivalent Freshwater Head for the Surface Hydraulic Boundary Condition (fr-base-paleo-0-le1)	89

Figure 2-40:	Environmental Head versus Time for the Reference Paleohydrogeological Scenario (fr-base-paleo)	90
Figure 2-41:	Environmental Head versus Time for nn9930 Paleoclimate Boundary Conditions and a Loading Efficiency of 0 (fr-base-paleo-le0)	91
Figure 2-42:	Environmental Head versus Time for nn9930 Paleoclimate Boundary Conditions, a Loading Efficiency of 1, and a 0% of Ice-Sheet Thickness Equivalent Freshwater Head for the Surface Hydraulic Boundary Condition (fr-base-paleo-0-le1)	91
Figure 2-43:	Vertical Profile Plots of TDS Concentrations for the Paleohydrogeologic Simulations at 120,000 Years at the Location of Hypothetical Repository Footprint.....	94
Figure 2-44:	Environmental Head versus Time for the Paleohydrogeological Scenario without Salinity (fr-base-paleo-nobrine)	96
Figure 2-45:	Vertical Profile Plots of Freshwater Heads for the Paleohydrogeologic Simulations at 120,000 Years at the Location of Hypothetical Repository Footprint.....	97
Figure 2-46:	Vertical Profile Plots of Mean Life Expectancies at One Million Years for the Reference Case and Additional Sensitivity Scenarios	101
Figure 2-47:	Vertical Profile Plots of Total Dissolved Solids Concentrations at One Million Years for the Reference Case and Additional Sensitivity Scenarios	102
Figure 2-48:	Total Dissolved Solids Concentrations at One Million Years for a Three Order of Magnitude Enhancement in Hydraulic Conductivities	103
Figure 2-49:	Porewater Velocity Magnitude for a Three Order of Magnitude Enhancement in Hydraulic Conductivities	103
Figure 3-1:	Typical CANDU Fuel Bundle	114
Figure 3-2:	Used Fuel Discharge Burnup.....	115
Figure 3-3:	Maximum Fuel Bundle Linear Power	117
Figure 3-4:	Typical Microstructure of Unirradiated and Irradiated UO ₂ Fuel	119
Figure 3-5:	Grain Growth in Irradiated UO ₂ Fuel.....	120
Figure 3-6:	Segregation of Metallic Fission Products from UO ₂ Fuel.....	120
Figure 3-7:	Illustrative Distribution of Some Fission Products and Actinides within a Used-Fuel Element	122
Figure 4-1:	Illustration of APM Facility in Sedimentary Rock	134
Figure 4-2:	Used Fuel Container Manufacturing Process	139
Figure 4-3:	Copper Coated Used Fuel Container with an Open Section	140
Figure 4-4:	Buffer Box	141
Figure 4-5:	APM Surface Facilities Illustration	147

Figure 4-6:	APM Surface Facilities Layout.....	148
Figure 4-7:	Overview of the UFPP Layout	151
Figure 4-8:	UFTP Receiving and Fuel Module Handling.....	154
Figure 4-9:	Fuel Transfer into Used Fuel Container.....	155
Figure 4-10:	Automated Work Tables inside Processing Cell.....	156
Figure 4-11:	Weld Worktable and Non-Destructive Examination Worktable.....	156
Figure 4-12:	Copper Cold Spray and Copper Annealing Worktable	157
Figure 4-13:	Example of a Closed-Die Forging Press (Uniaxial Compaction)	158
Figure 4-14:	Cold Isostatic Press for Production of Highly Compacted Bentonite Blocks.....	159
Figure 4-15:	Underground Layout for 5.224 Million Bundles.....	162
Figure 4-16:	Plan View and Longitudinal Section of Placement Room	163
Figure 4-17:	Placement Room Section Views.....	165
Figure 4-18:	Room Seal	167
Figure 4-19:	Shielding Canopy.....	171
Figure 4-20:	Floor Plate with Built-in Ventilation Duct.....	172
Figure 4-21:	Legend for Container Placement Equipment.....	173
Figure 4-22:	Preparation of Placement Room & Shielding Canopy	174
Figure 4-23:	Container/Buffer Box Placement	176
Figure 4-24:	Illustrative Tunnel Plug in a Hydraulically Active Region	184
Figure 5-1:	Three Ice Sheet and Permafrost Thickness Time Series	197
Figure 5-2:	Block View Showing the Depth of Penetration of a Tracer after 120,000 Years for the gsm2015 Paleoclimate Boundary Conditions (fr-base-paleo-gsm2015)	199
Figure 5-3:	Illustrative Example of the Range of Temperature Variation over Time in a Placement Room	201
Figure 5-4:	Evolution of the Repository Environment from an Initial Warm, Oxidizing Period to a Prolonged Cool, Anoxic Phase.....	203
Figure 5-5:	Evolution of Damage up to One million years.....	210
Figure 5-6:	Calculated Glacially Induced Rebound Stress Histories (BP = before present); S11, S22 & S33 are the Normal Stress Components; S12, S13 & S23 are the Shear Stress Components (Itasca 2018).....	211
Figure 5-7:	Radioactivity of Used CANDU Fuel (220 MWh/kgU burnup).....	214
Figure 5-8:	Amounts of Key Long-Lived Radionuclides in Used Fuel (220 MWh/kg U burnup)	215
Figure 5-9:	Temperature inside Container after Placement (Guo 2015).....	216
Figure 5-10:	Evolution of Pressure on UFC over a Glacial Cycle	222

Figure 5-11:	Reaction Scheme for the Uniform Corrosion of Copper in Compacted Bentonite Saturated with O ₂ -Containing Chloride Solution.....	230
Figure 5-12:	Normalized Diffusive Sulphide Flux Ratio for UFCs in Placement Room for a Uniform Background Concentration of Sulphide in the Host Rock	233
Figure 5-13:	Reduction in Thickness of Copper Due to Reaction with Groundwater Sulphide.....	234
Figure 5-14:	Hypothetical Defects in the Copper Coating	236
Figure 5-15:	Time to Exposed Steel beneath Defects in a Nominal 3 mm Copper Coating ..	236
Figure 5-16:	Minimum Corrosion Depth for Through-Wall Perforation of Steel Container.....	239
Figure 5-17:	Evolution of Steel Corrosion Rates	240
Figure 5-18:	Illustration of Defect Corrosion	241
Figure 5-19:	Adaption of Open-Surface Corrosion Models for Defect Corrosion.....	242
Figure 5-20:	Evolution of Steel Corrosion Depth.....	243
Figure 5-21:	Radiation Dose Rate in Water at the Fuel Surface (220 MWh/kgU burnup).....	246
Figure 5-22:	Hydraulic Conductivity and Swelling Pressure under Various Water Conditions: Variation with Effective Montmorillonite Dry Density.....	252
Figure 5-23:	Thermal Conductivity of 50:50 wt% Bentonite-Sand Buffer (BSB) and of 100 wt% MX-80 Bentonite (HCB)	253
Figure 5-24:	Effect of Water Activity on Aerobic Culturability in Compacted Bentonite	256
Figure 6-1:	Total Thermal Power of the Repository (Average 220 MWh/kgU Burnup)	282
Figure 7-1:	Illustration showing Normal Evolution Scenario and Sensitivity Studies, and Disruptive Event Scenarios.....	326
Figure 7-2:	General Conceptual Model for Defective Containers	352
Figure 7-3:	Conceptual Model for the Waste Form and Container	353
Figure 7-4:	Radiation Dose Rate in Water at the Fuel Surface (220 MWh/kgU and 280 MWh/kgU Burnup)	355
Figure 7-5:	Conceptual Model for the Geosphere.....	358
Figure 7-6:	Conceptual Model for the Constant Biosphere	360
Figure 7-7:	Environmental Transfer Model Showing Critical Group Exposure Pathways	363
Figure 7-8:	Main Computer Codes	364
Figure 7-9:	3D Subregional Flow, Main Transport, Detailed Transport and Container Transport Model Domains	372
Figure 7-10:	Fuel Dissolution Rate.....	375
Figure 7-11:	I-129 Source Term.....	377
Figure 7-12:	Cl-36 Source Term	377
Figure 7-13:	Cs-135 Source Term	378

Figure 7-14:	U-238 Source Term	378
Figure 7-15:	I-129 Individual Container Source Term for the All Containers Fail Disruptive Event Scenarios.....	379
Figure 7-16:	Subregional Flow Model: Plan view discretization	396
Figure 7-17:	Subregional Flow Model: Vertically Exaggerated to show Discretization	399
Figure 7-18:	Main and Detailed Transport Model Setting	401
Figure 7-19:	Distance from Top and Bottom of Cobourg Formation to Repository	402
Figure 7-20:	Subregional Flow Model: Relative Tracer Concentration at Surface	404
Figure 7-21:	Main Transport Model: Relative Tracer Concentration at Surface.....	405
Figure 7-22:	Main and Detailed Transport Models: Plan Discretization	406
Figure 7-23:	Main Transport Model: Vertical Discretization	407
Figure 7-24:	Main and Detailed Transport Models: Detailed Vertical Discretization	408
Figure 7-25:	Detailed Transport Model: Plan View of Repository Property Assignment.....	410
Figure 7-26:	Detailed Transport Model: Detailed Plan Discretization Showing Seal Implementation	411
Figure 7-27:	Main and Detailed Transport: Source Node Locations and Discretization.....	412
Figure 7-28:	Main and Detailed Transport: 3D View of Example Source Nodes	413
Figure 7-29:	Detailed Transport Model: Vertical Slice Showing Shaft and Seals	414
Figure 7-30:	Main and Detailed Transport Models: Three Dimensional View of Repository Features.....	415
Figure 7-31:	Container Transport Model: Location in Repository	417
Figure 7-32:	Container Transport Model: Plan Property Assignment through the Source Placement Room	418
Figure 7-33:	Container Transport Model: Vertical Property Assignment Parallel to the Source Placement Room.....	418
Figure 7-34:	Container Transport Model: Vertical Property Assignment Perpendicular to the Source Placement Room.....	419
Figure 7-35:	Container Transport Model: 3D View of EBS and EDZ near Source Containers	420
Figure 7-36:	Container Transport Model: 3D View of EBS and EDZ	420
Figure 7-37:	Container Transport Model: 3D View of Base Case Head Boundary Conditions.....	421
Figure 7-38:	Subregional Flow Model: Base Case (No Well) - Advective Velocity	423
Figure 7-39:	Subregional Flow Model: Base Case (No Well) - Advective Velocity and Hydraulic Head over a Horizontal Slice through the Cobourg Formation	424
Figure 7-40:	Subregional Flow Model: Base Case (No Well) - Mean Life Expectancy (a).....	425

Figure 7-41: Subregional Flow Model: Base Case (No Well) - Mean Life Expectancy on a Vertical Slice through the Grid Origin 426

Figure 7-42: Detailed Transport Model: No Well Comparison of Hydraulic Heads and Advective Velocities With Subregional Flow Model at Repository Elevation 427

Figure 7-43: Main and Detailed Transport Models: No Well Comparison of Hydraulic Heads and Advective Velocities at Repository Elevation 428

Figure 7-44: Subregional Flow and Main Transport Model: No Well Mean Life Expectancy on Vertical Slice through Repository..... 429

Figure 7-45: Main Transport Model: Watershed Boundaries 430

Figure 7-46: Main Transport Model: With Well Mean Life Expectancy on Vertical Slice through Repository 431

Figure 7-47: Main Transport Model: No Well and Base Case Hydraulic Head and Mean Life Expectancy Ratio on Vertical Slice through Repository 432

Figure 7-48: Main Transport Model: No Well and Base Case Hydraulic Head and Mean Life Expectancy Ratio on Plan through Repository 432

Figure 7-49: Main and Detailed Transport Models: Base Case Comparison of Container Source Term and the Combined Source Term for I-129 Transport to the Well..... 434

Figure 7-50: Main and Detailed Transport Models: Base Case Comparison of Container Source Term and the Combined Source Term for Cs-135 Transport into the Georgian Bay Formation..... 435

Figure 7-51: Main Transport Model: Effective Diffusion Coefficient on Vertical Slice through Repository 436

Figure 7-52: Well / Source Location Pairs..... 437

Figure 7-53: Main Transport Model: Well Transport for All Tested Well and Source Locations using Pulse Source Term 438

Figure 7-54: Main Transport Model: Base Case I-129 Transport to the Well and Surface 439

Figure 7-55: Main Transport Model: Base Case I-129 Integrated Activity Allocation 440

Figure 7-56: Detailed and Main Transport Model: Base Case I-129 Concentration at 10 k Years 441

Figure 7-57: Detailed and Main Transport Model: Base Case I-129 Concentration at 100 k Years..... 442

Figure 7-58: Detailed and Main Transport Model: Base Case I-129 Concentration at 1 Ma Years 443

Figure 7-59: Detailed Transport Model: Base Case I-129 Concentration in 3D at 1 Ma 444

Figure 7-60: Main Transport Model: Base Case Cl-36 Transport to the Well and Surface 445

Figure 7-61: Main Transport Model: Base Case Cl-36 Concentration in 3D at 1 Ma 445

Figure 7-62: Main Transport Model: Base Case Cs-135 Integrated Activity Allocation..... 446

Figure 7-63:	Main Transport Model: Base Case U-238 Integrated Activity Allocation	447
Figure 7-64:	Rooms-Only Repository-Scale Model: Intermittent Well Sensitivity – I-129 Comparison to Base Case	449
Figure 7-65:	Main Transport Model: I-129 Transport to the Water-Supply Well for Geosphere Sensitivity Cases.....	450
Figure 7-66:	Main Transport Model: I-129 Time Step Sensitivity – Time Steps.....	452
Figure 7-67:	Main Transport Model: I-129 Time Step Sensitivity – Comparison of Well Transport	452
Figure 7-68:	Container Model: Hydraulic Head and Advective Velocity on Horizontal Plane through Repository (top) and Vertical Plane through Source Room (bottom) ...	453
Figure 7-69:	Container Model: 3D View of Advective Velocity Magnitudes in EBS and EDZ.....	454
Figure 7-70:	Container Transport Model: I-129 Concentration at 10 ka and 50 ka (top Horizontal, bottom Vertical)	455
Figure 7-71:	Container Transport Model: I-129 Concentration at 100.5 ka and 500.5 ka (top Horizontal, bottom Vertical)	456
Figure 7-72:	Container Transport Model: I-129 Concentration at 750 ka and 1 Ma (top Horizontal, bottom Vertical)	457
Figure 7-73:	Container Transport Model: 3D View of I-129 Concentration at 1500 a	458
Figure 7-74:	Container Transport Model: 3D View of I-129 Concentration at 10000 a	458
Figure 7-75:	Main Container Transport Model: 3D View of I-129 Concentration at 500 ka....	459
Figure 7-76:	Container Transport Model: 3D View of I-129 Concentration at 1 Ma	459
Figure 7-77:	Container Transport Model: Cs-135 Concentration at 100 and 500 ka	460
Figure 7-78:	Container Transport Model: Cs-135 Concentration at 750 ka and 1 Ma	461
Figure 7-79:	Main Container Transport Model: 3D View of Cs-135 Concentration at 1 Ma ...	462
Figure 7-80:	Container Transport Model: U-238 Concentration at 500.5 and 1 Ma.....	463
Figure 7-81:	Main Container Transport Model: 3D View of U-238 Concentration at 1 Ma.....	464
Figure 7-82:	Main Transport and Container Models: Base Case I-129 Transport through Barriers	465
Figure 7-83:	Main Transport and Container Transport Models: Base Case Cs-135 Transport through Barriers.....	466
Figure 7-84:	Main Transport and Container Transport Models: Base Case U-238 Transport through Barriers.....	466
Figure 7-85:	Container Transport Model: Transport Surface for the Bentonite and Repository Release	467
Figure 7-86:	System Model, Repository Submodel.....	469
Figure 7-87:	System Model, Geosphere Submodel: Transport Network Connectivity	473

Figure 7-88: Transport Comparison for I-129 for the Base Case 480

Figure 7-89: Transport Comparison for Cs-135 for the Base Case 480

Figure 7-90: Transport Comparison for Cl-36 for the Base Case 481

Figure 7-91: Transport Comparison for I-129 for the All Containers Fail Case 482

Figure 7-92: Transport Comparison for Cs-135 for the All Containers Fail Case 482

Figure 7-93: Transport Comparison for Cl-36 for the All Containers Fail Case 483

Figure 7-94: System Model: Base Case Total Dose Rate 486

Figure 7-95: System Model: Sensitivity to a Factor of 10 Increase in Fuel Dissolution Rate 488

Figure 7-96: System Model: Sensitivity to Fuel Instant Release Fractions Set to 10%..... 489

Figure 7-97: System Model: Sensitivity to a Factor of 10 Increase in Zircaloy Corrosion Rate 491

Figure 7-98: System Model: Sensitivity to Zircaloy Instant Release Fractions Set to 10% 492

Figure 7-99: System Model: Sensitivity to 10 Containers Fail at 1000 years 493

Figure 7-100: System Model: Sensitivity to Low Sorption in the EBS Materials with Coincident High Solubility Limits in the Container 495

Figure 7-101: System Model: Sensitivity to No Solubility Limits 496

Figure 7-102: System Model: Sensitivity to No Sorption in the Near Field..... 497

Figure 7-103: System Model: Sensitivity to 10 and 100 Time Higher Bentonite and Geosphere Diffusivity Coefficients 498

Figure 7-104: System Model: Sensitivity to I-129 Sorption 499

Figure 7-105: System Model: Sensitivity to Two Standard Deviations (Low) Sorption in the Geosphere 500

Figure 7-106: Simulated Ice Thickness, Permafrost Depth, and Well Operation at the Repository Site over One Full Glacial Cycle 501

Figure 7-107: Glaciation Subregional Model Property Assignments (after Avis and Calder, 2015) 503

Figure 7-108: Glacial Cycle Simulations: Hydraulic Head at the Repository Location within Selected Formations (Avis and Calder, 2015) 504

Figure 7-109: Glacial Cycle Simulations: Hydraulic Head at Times of Maximum Well Transport for Each Glacial Cycle (Avis and Calder, 2015) 504

Figure 7-110: Glacial Cycle Simulations: Advective Velocity within Selected Formations (Avis and Calder, 2015) 505

Figure 7-111: Glacial Cycle Simulations: Assumed Container Release of I-129 506

Figure 7-112: Glaciation Site Model: Vertical Discretization (Avis and Calder, 2015)..... 507

Figure 7-113: Glaciation Site Model: Vertical Property Assignment (Avis and Calder, 2015) 507

Figure 7-114: Comparison of I-129 Concentration between Glaciation and Constant
 Climates (Avis and Calder, 2015) 509

Figure 7-115: Transport of I-129 for Constant-Climate Conditions vs. Glacial Cycling
 (Avis and Calder, 2015) 510

Figure 7-116: No-Well Site Glaciation Model: I-129 Transport into the Guelph Formation
 (Avis and Calder, 2015) 511

Figure 7-117: Probabilistic Assessment: 1 Ma Dose Rate Histogram with Container
 Assumptions Fixed 515

Figure 7-118: Probabilistic Assessment: Time Dependence of Percentile Values with
 Container Assumptions Fixed 516

Figure 7-119: Probabilistic Assessment: Distribution of Container Failures with All
 Assumptions Varying 519

Figure 7-120: Probabilistic Assessment: 1 Ma Dose Rate Histogram with All Assumptions
 Varying 520

Figure 7-121: Probabilistic Assessment: Time Dependence of Percentile Values with All
 Assumptions Varying 522

Figure 7-122: General Sequence of Events for Inadvertent Human Intrusion 527

Figure 7-123: Inadvertent Human Intrusion - General Conceptual Model 530

Figure 7-124: Inadvertent Human Intrusion: Exposure Pathways to the Drill Crew - Hazard
 Identified and Site Remediated 534

Figure 7-125: Inadvertent Human Intrusion: Summary of Exposures - Hazard Not Identified
 and No Remediation 535

Figure 7-126: Inadvertent Human Intrusion: Effect of Leaching on Exposure to the
 Resident - Hazard Not Identified and No Remediation 536

Figure 7-127: Inadvertent Human Intrusion: Pathways for Drill Crew Exposure - Hazard
 Identified and Site Remediated, Higher Burnup Fuel 537

Figure 7-128: 3D Model: All Containers Fail at 60,000 Years - Evaluated and Final Well
 Locations 539

Figure 7-129: 3D Model: All Containers Fail at 60,000 Years - I-129 Transport 540

Figure 7-130: System Model: All Containers Fail at 60,000 Years: Dose Rate 542

Figure 7-131: All Containers Fail at 10,000 Years: Sensitivity Case Dose Rate 543

Figure 7-132: Main Transport Model: Repository Seal Failure - I-129 Transport to the Well
 for Each Well/Source Location 545

Figure 7-133: Main Transport Model: Assumed Vertical Fault Locations 546

Figure 7-134: Main Transport Model: Vertical Fault Cases - I-129 Transport to the Well 547

Figure 7-135: Main Transport Model: Vertical Fault Cases - I-129 Transport to Surface for
 Each Fracture Location 547

Figure 7-136: Non-Human Biota Dose Assessment Flow Chart 549

Figure 7-137: Tier 1 Quotients in the All Containers Fail Disruptive Event Scenario 552

Figure 7-138: Non-Radiological Hazard: Base Case Groundwater Results 555

Figure 7-139: Non-Radiological Hazard: Base Case Surface Water Results 555

Figure 7-140: Non-Radiological Hazard: Base Case Soil Results 556

Figure 7-141: Non-Radiological Hazard: Base Case Sediment Results 556

Figure 7-142: Non-Radiological Hazard: Base Case Air Results 557

Figure 7-143: Main Transport Model: Copper Transport to the Well 558

Figure 7-144: System Model: Base Case - Results for Indicators 565

Figure 7-145: System Model: All Containers Fail at 60,000 Years - Results for Indicators 566

Figure 7-146: Dose Rate Result Summary 579

Figure 8-1: Capillary Pressure Curves for Placement Room Bentonite (Homogenized Bentonite), Repository Inner EDZ, and the Cobourg Formation 593

Figure 8-2: Relative Gas Permeability Curves for Placement Room Bentonite (Homogenized Bentonite), Repository Inner EDZ, and the Cobourg Formation 593

Figure 8-3: Relative Liquid Permeability Curves for Placement Room Bentonite (Homogenized Bentonite), Repository Inner EDZ, and the Cobourg Formation 594

Figure 8-4: Main Computer Code 595

Figure 8-5: Room-Scale Model: Illustration 599

Figure 8-6: Room-Scale Model: Tunnel End of Room 599

Figure 8-7: Room-Scale Model: Plan-Section through Middle of Placement Room 600

Figure 8-8: Room-Scale Model: Cross-Section through Container 600

Figure 8-9: Geothermal Gradient 601

Figure 8-10: Room-Scale Model: Plan-Section View showing GGM Node for the Base Case 602

Figure 8-11: Room-Scale Model: Plan- and Cross-Section View showing GGM Nodes for the All Containers Fail Scenario 603

Figure 8-12: Repository-Scale Model: Illustration 604

Figure 8-13: Repository-Scale Model: Plan-Section View showing the Link Node for the Base Case 604

Figure 8-14: Repository-Scale Model: Plan-Section View showing the Link Nodes for the All Containers Fail Scenario 605

Figure 8-15: Repository-Scale Model: Cross-Section Discretization 606

Figure 8-16: Repository-Scale and Room-Scale Model: 3D Relationship of Linked Model Domains 607

Figure 8-17: Room-Scale Model: Locations of Time-Series Plot Points 608

Figure 8-18: Room-Scale Model: Gas Saturation and Pore Pressure at Closure (0 Years) .. 610

Figure 8-19: Room-Scale Model: Temperature and Gas Saturation Conditions prior to Container Failures 610

Figure 8-20: Room-Scale Model: Nodal and Average Pore Pressure prior to Container Failures 611

Figure 8-21: Room-Scale Model: Base Case - Gas Saturation and Pore Pressure at 1000 Years 612

Figure 8-22: Room-Scale Model: Base Case - Steel Consumption and Corrosion Processes for First Container Failure 612

Figure 8-23: Room-Scale Model: Base Case - Nodal and Average Temperature and Gas Saturation Conditions after First Container Failure..... 613

Figure 8-24: Room-Scale Model: Base Case – Nodal and Average Pore Pressure after First Container Failure 613

Figure 8-25: Room-Scale Model: Base Case - Gas Saturation and Pore Pressure at Time of Peak Pressure after First Container Failure (7400 Years)..... 614

Figure 8-26: Room-Scale Model: Base Case - Gas Saturation and Pore Pressure at Time of Second Container Failure (100,000 Years) 614

Figure 8-27: Room-Scale Model: Base Case - Steel Consumption and Corrosion Processes for Second Container Failure 615

Figure 8-28: Room-Scale Model: Base Case - Nodal and Average Pore Pressure after Second Container Failure 616

Figure 8-29: Room-Scale Model: Base Case - Gas Saturation and Pore Pressure at Time of Peak Pore Pressure for Second Container Failure (120,500 Years).... 616

Figure 8-30: Room-Scale Model: Base Case - Comparison of Gas Saturation Profiles for Container 2, 3, and 4 Failures 617

Figure 8-31: Room-Scale Model: Base Case - Gas Saturation and Pore Pressure at Time of Peak Pore Pressure for Third Container Failure (221,000 Years)..... 618

Figure 8-32: Room-Scale Model – All Containers Fail Scenario – Gas Saturation and Pore Pressure at 10,000 Years 619

Figure 8-33: Room-Scale Model: All Containers Fail Scenario - Steel Consumption and Corrosion Processes 620

Figure 8-34: Room-Scale Model: All Containers Fail Scenario - Nodal and Average Temperature and Gas Saturation Conditions after Container Failures..... 620

Figure 8-35: Room-Scale Model: All Containers Fail Scenario - Gas Saturation and Pore Pressure at 10,500 Years 621

Figure 8-36: Repository-Scale Model: Locations of Time-Series Plot Points in the Tunnels 622

Figure 8-37: Repository-Scale Model: Locations of Time-Series Plot Points in the Model Shaft 623

Figure 8-38: Repository-Scale Model: Gas Saturation prior to Container Failures 624

Figure 8-39: Repository-Scale Model: Tunnel Pore Pressure prior to Container Failures 625

Figure 8-40: Repository-Scale Model: Nodal and Average Shaft Pore Pressure prior to Container Failures 626

Figure 8-41: Repository-Scale Model: Gas Saturation and Pore Pressure in the Repository Tunnels at 1000 Years 627

Figure 8-42: Repository-Scale Model: Gas Saturation and Pore Pressure in the Repository Shaft at 1000 Years 627

Figure 8-43: Repository-Scale Model: Gas Saturation and Pore Pressure in the Repository Tunnels at 10,000 Years 628

Figure 8-44: Repository-Scale Model: Gas Saturation and Pore Pressure in the Repository Shaft at 10,000 Years 628

Figure 8-45: Repository-Scale Model: Locations of Time-Series Plot Points in the Model Tunnels for the Base Case 629

Figure 8-46: Repository-Scale Model: Base Case - Gas Saturation in the Tunnels and Shaft 630

Figure 8-47: Repository-Scale Model: Base Case - Gas Saturation and Pore Pressure in a Vertical Section through the Tunnel at the Room-Scale/Repository-Scale Linking Point at 1000 Years 631

Figure 8-48: Repository-Scale Model: Base Case - Gas Saturation and Pore Pressure in a Vertical Section through the Tunnel at the Room-Scale/Repository-Scale Linking Point at the Time of Peak Room Pressure after First Container Failure (7400 Years) 631

Figure 8-49: Repository-Scale Model: Base Case - Gas Saturation and Pore Pressure in a Vertical Section through the Tunnel at the Room-Scale/Repository-Scale Linking Point at the Time of Peak Room Pressure after Second Container Failure (120,500 Years) 632

Figure 8-50: Repository-Scale Model: Base Case - Gas Saturation and Pore Pressure in a Vertical Section through the Tunnel at the Room-Scale/Repository-Scale Linking Point at the Time of Peak Room Pressure after Third Container Failure (221,500 Years) 632

Figure 8-51: Repository-Scale Model: Base Case - Nodal and Average Tunnel Pore Pressure after Container Failures 633

Figure 8-52: Repository-Scale Model: Base Case - Nodal and Average Shaft Pore Pressure after Container Failures 634

Figure 8-53: Repository-Scale Model: All Containers Fail Scenario - Gas Saturation in the Tunnels and Shaft after Container Failures 635

Figure 8-54: Repository-Scale Model: All Containers Fail Scenario - Gas Saturation and Pore Pressure on a Plan Section in the Tunnels at 10,500 Years 637

Figure 8-55: Repository-Scale Model: All Containers Fail Scenario - Gas Saturation and Pore Pressure on a Vertical Section in a Single Tunnel at 10,500 Years 638

Figure 8-56: Repository-Scale Model: All Containers Fail Scenario - Gas Saturation and Pore Pressure in the Shaft at 14,000 Years 638

Figure 8-57: Gas Mass in Room and Repository prior to Container Failures 639

Figure 8-58: Base Case: Gas Mass Distribution after Container Failures..... 640

Figure 8-59: Base Case: Gas Flow out the Top of the Model 641

Figure 8-60: Base Case: Dissolved Gas Flow out the Top of the Model..... 641

Figure 8-61: All Containers Fail Scenario: Gas Mass Distribution after Container Failures... 643

Figure 8-62: All Containers Fail Scenario: Gas Flow out the Top of the Model 644

Figure 8-63: All Containers Fail Scenario: Dissolved Gas Flow out the Top of the Model..... 644

Figure 8-64: Rate at which C-14 enters the Guelph Formation 647

Figure 10-1: Cigar Lake Ore Deposit 660

Figure 10-2: Naturally Occurring Fission Reactor 663

Figure 10-3: Copper Plate and Mudstone Covering..... 665

Figure 10-4: Bentonite Clay 667

Figure 10-5: 1.5 Ma Sequoia-like Tree Stumps at Dunarobba, Italy 668

Figure 10-6: Swelling Performance of Various Bentonites (Cyprus is circled in red)..... 669

Figure 12-1: Illustration Showing Normal Evolution Scenario, Sensitivity Studies, and Disruptive Event Scenarios..... 693

Figure 12-2: Key Results from Sensitivity Analyses and Bounding Assessments 695

1. INTRODUCTION

1.1 Purpose and Scope

The Nuclear Waste Management Organization (NWMO) is responsible for the implementation of Adaptive Phased Management (APM), the federally-approved plan for the safe long-term management of Canada's used nuclear fuel (GC 2007). Under the APM plan, used nuclear fuel will ultimately be placed within a deep geological repository in a suitable rock formation. The repository and its surroundings comprise a multiple-barrier system that is designed to protect people and the environment.

This report provides an illustrative postclosure safety assessment for a conceptual deep geological repository in a hypothetical sedimentary rock setting.

The APM facility is a self-contained complex with a combination of surface and underground engineered structures designed to provide multiple isolation barriers and passive safety to provide long-term containment and isolation. It consists of the surface facilities and the Deep Geological Repository (DGR).

A licence application to prepare the site and to construct a used fuel repository will be supported by a safety case. A safety case is defined as the integration of arguments and evidence that describe, quantify and substantiate the safety, and the level of confidence in the safety, of the deep geological repository and associated facilities. It includes the collection of scientific and technical arguments and evidence covering the site characterization and geosynthesis, the design, construction and operation of the facility, the assessment of radiation risk during operation and postclosure, and quality assurance of all safety-related work.

This definition is consistent with the Canadian Nuclear Safety Commission (CNSC) Regulatory Document REGDOC-2.11.1 Volume III as well as international guidance. The International Atomic Energy Agency (IAEA) also provides guidance in SSG-23 – The Safety Case and Safety Assessment for the Disposal of Radioactive Waste (IAEA 2012), where it notes that the primary objective of a safety case is to allow for informed decisions to be made that are commensurate with the lifecycle phase of the project.

The level of detail in the current study is consistent with the pre-licensing stage of the APM facility and is not a full safety case. It considers a hypothetical site for a deep geological repository in sedimentary rock. It identifies and analyzes key scenarios sufficient to understand and illustrate postclosure safety.

For an actual licence application, site-specific information would be used. Further environmental impacts and preclosure safety, including transportation safety, and conventional safety, would be assessed. However, at this pre-licensing stage and in place of site-specific information, data representing a sedimentary setting are used to illustrate how the postclosure safety assessment can be carried out consistent with Canadian regulatory requirements.

1.2 Background and Project Overview

Investigations into the long-term management of used nuclear fuel have a long history in Canada. In 1977, a task force commissioned by Energy, Mines and Resources Canada recommended burial in geological formations with a preference for crystalline rock of the

Canadian Shield, but noted that other rock types such as sedimentary rock and salt should also be studied (Hare et al. 1977). Also in 1978, the Porter Commission for Electricity Planning in Ontario recommended that an independent committee be established to report on progress on waste disposal research and demonstration. Subsequently, the governments of Canada and Ontario initiated the Canadian Nuclear Fuel Waste Management Program in 1980.

From this Canadian program and parallel international work, the concept for a deep geological repository was developed by Atomic Energy of Canada Limited (AECL). The work included an underground research laboratory in Manitoba, in which approaches and materials were tested. The AECL concept was then submitted for review by a federal environmental assessment panel. For this review, AECL completed two case studies illustrating the deep geological repository concept in crystalline Canadian Shield settings. AECL submitted its Environmental Impact Statement to the federal review panel in 1994. In 1998, the panel made a number of recommendations and identified the following key conclusions (CEAA 1998):

- *“From a technical perspective, safety of the AECL concept has been on balance adequately demonstrated for a conceptual stage of development, but from a social perspective, it has not.*
- *As it stands, the AECL concept for deep geological disposal has not been demonstrated to have broad public support. The concept in its current form does not have the required level of acceptability to be adopted as Canada’s approach for managing nuclear fuel wastes.”*

In 2002, the NWMO was created by Canada’s nuclear energy generators as a requirement of the *Nuclear Fuel Waste Act*, which largely incorporates recommendations from the earlier federal review panel. The Act required the NWMO to study possible approaches, recommend an approach, and then implement the approved plan for the long-term management of Canada’s used nuclear fuel.

In 2005, based on extensive discussions across Canada, the NWMO recommended the APM approach, which consists of both a technical method and a management system. Its key attributes include:

- Ultimate centralized containment and isolation of used nuclear fuel in an appropriate geological formation;
- Phased and adaptive decision-making; and
- Citizen engagement throughout all phases of implementation.

In 2007, the Government of Canada accepted APM as the recommended approach (GC 2007). The NWMO is implementing the approach in a manner that is consistent with Canadian federal government policy and with international best practice.

APM includes the development of a deep geological repository, associated surface facilities and a used fuel transportation system. The repository system is a multiple-barrier concept designed to safely contain and isolate used nuclear fuel over the long term.

An extensive study of options was later conducted to update and optimize the repository design and engineered barriers. The new reference design concept assessed in this study consists of a repository constructed for an inventory of about 5.2 million used CANadian Deuterium-

Uranium (CANDU) fuel bundles at a depth of approximately 500 metres (see Figure 1-1). The actual depth of the repository will depend on geologic characteristics at the specific site.

1.3 APM Project Phases

This section briefly describes the phases of APM, along with the milestones and the assumed associated timeline. The legal framework that governs these activities is described in Section 1.5.

1.3.1 Site Selection

The site selection process was launched by the NWMO in 2010. It has been designed to identify an informed and willing host community for the APM facility and to ensure that the site selected to host the facility will safely contain and isolate the used nuclear fuel. Site selection is a multi-step process based on social and technical considerations, with screening criteria established to ensure safety is considered from the very beginning of the siting process. Section 1.6.3 of this report highlights the evaluation factors used.

After a site has been selected, further detailed site characterization would be undertaken. This information would ultimately be used to develop a licence application for the selected site. Licences are issued under the *Nuclear Safety and Control Act* as described in Section 1.5.

1.3.2 Site Preparation and Construction

The site will be prepared by clearing, grading, installing fencing, installing temporary construction services, and establishing a stormwater management system. The first part of site preparation and construction will be to excavate the shafts, the central service areas and main tunnels, and the Underground Demonstration Facility. The detailed design will also be completed, taking into account information learned during this excavation.

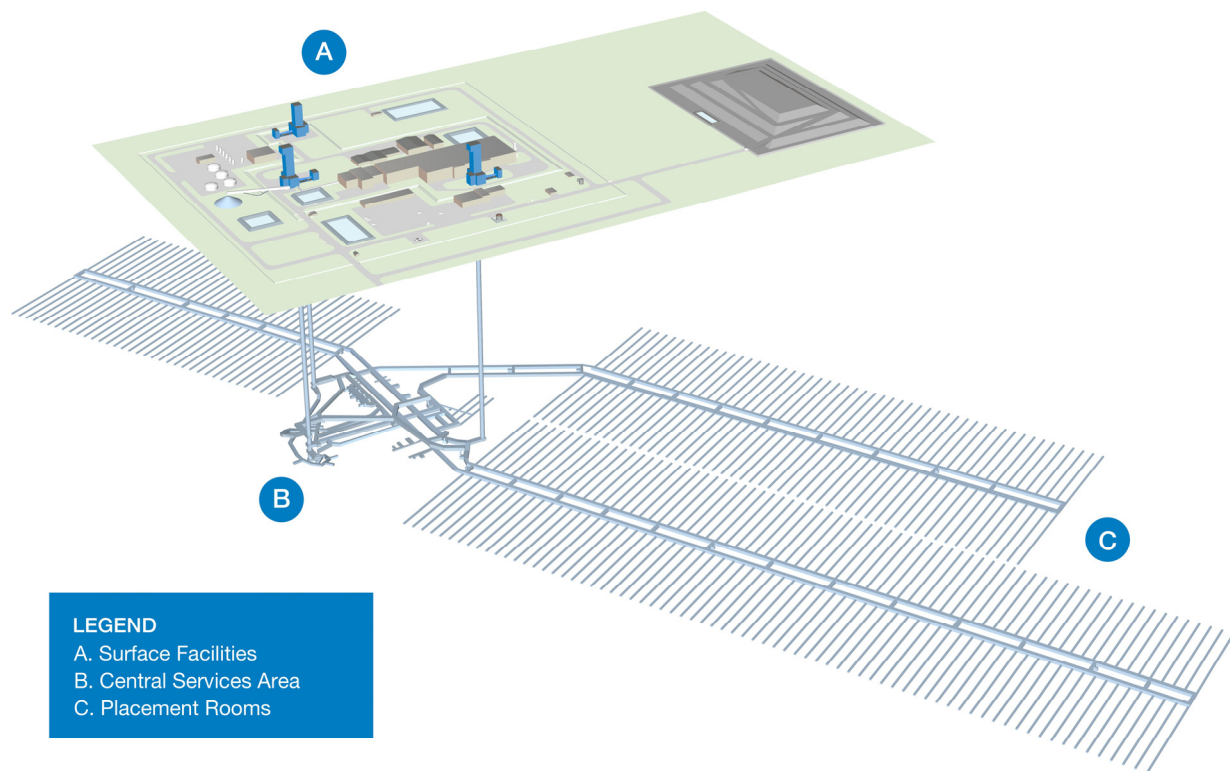
The second part is to excavate and erect all of the facilities necessary for the nuclear operation of the repository. The safety case will be updated to support the operating licence application.

The total time required for the site preparation and construction phase could be about 10 years.

1.3.3 Operation

Operation will consist of receiving used nuclear fuel transported to the site, repackaging the fuel into long-lived used fuel containers, placing the containers deep underground in the repository, and continuing underground development.

For a reference used fuel inventory of about 5.2 million used CANDU fuel bundles, these operational activities are expected to last about 40 years or more assuming a throughput of 120,000 bundles per year. The actual duration of repository operation will depend on the total inventory of used fuel to be managed at the site and the timing of its production, transportation and other operational factors.



Note: This figure is not to scale

Figure 1-1: Illustration of Deep Geological Repository Concept

1.3.4 Extended Monitoring

Following placement of used fuel in the repository, a period of monitoring is assumed to continue for an extended period of time. The duration of extended monitoring will be decided in collaboration with a future society. For planning purposes, the period of extended monitoring is assumed to be up to 70 years.

Towards the end of the extended monitoring period (i.e., during the final five years), a detailed decommissioning plan will be prepared and the detailed design of the shaft sealing system will be finalized.

1.3.5 Decommissioning

Decommissioning consists of sealing access tunnels and shafts, and removal of surface facilities. The site will be restored to a defined end-state that will depend largely on future plans for the site (e.g., industrial, park). For planning purposes, the period of decommissioning is assumed to be 30 years.

It is anticipated that appropriate institutional controls and postclosure monitoring will be put in place at that time.

1.4 Repository Timeframes

The evolution of conditions within and around the repository can be considered as a sequence of different periods during which certain events or processes dominate. These are discussed below.

1.4.1 Preclosure Period

The preclosure period covers the activities described in Section 1.3.1 to Section 1.3.5 and is assumed to last up to about 150 years.

During this time, the reference inventory of about 5.2 million used nuclear fuel bundles will be transported to the APM facility, repackaged into approximately 109,000 long-lived used fuel containers, transferred to the underground repository and surrounded by clay-based sealing materials. The total radioactivity will increase as more used fuel is placed in the repository, and then start to decrease due to radioactive decay.

1.4.2 Postclosure Period

The postclosure period starts at the end of decommissioning, after the shafts have been sealed and the surface facilities have been dismantled.

In the postclosure period, the site is assumed to remain under institutional controls for a period of time. Institutional controls can be defined as, “the control of residual risks at a site (by a designated Institution or Authority) after it has been decommissioned” (CNSC 2018). These controls can include both active measures (requiring activities on the site such as monitoring and maintenance) and passive measures (that do not require activities on the site, such as land use restrictions, as well as measures taken to support societal memory). Such measures should prevent inappropriate land use, including drilling, deep excavation, or disruption of the shaft seals.

Although institutional controls and societal memory of the site could last indefinitely, it is assumed for safety assessment purposes that these institutional controls and societal memory are effective for about 300 years.

The postclosure period is discussed in the following four timeframes. To provide context, Figure 1-2 highlights timescales for relevant past events and expected future events in Earth’s history.

Up to 1,000 years

At the beginning of this time, the facility is decommissioned. Distinct physical and chemical gradients exist between the various components of the repository, and between the repository and the geosphere. The containers reach their peak temperature. Slow saturation of the repository by groundwater occurs, which is accompanied by swelling of bentonite sealing materials. Especially during the first 500 years, radioactivity and heat in the used fuel decrease significantly due to the decay of most of the fission products.

1,000 - 60,000 years

This represents conditions with no glaciation coverage of the site. During this period, the initial sharp physical and chemical gradients around the repository slowly diminish. The surrounding sedimentary rock reaches its peak temperature and largely cools back down to natural ambient temperatures. Surface conditions are likely to change reflecting human activities and natural evolution, possibly in response to climate change. Although the overall climate is likely to remain temperate, climate change could include global warming in the near term, and the advent of cooler climate in the long term.

60,000 - 1,000,000 years

Over this period, the main perturbations in the system cease to be repository-driven. Instead, there are regional-scale changes in the geosphere that in turn may be transmitted to the repository. In particular, climate change initiated by long-term changes in solar insolation patterns may occur, leading to initiation of a new glaciation cycle. Based on past history, several cycles of glaciation are likely to occur over the next million years.

1,000,000 years and beyond

At these times, the repository will be a relatively passive feature of the geosphere, in quasi-equilibrium with the surrounding rock. The dominant processes will be regional perturbations to the geosphere that in turn affect the repository. Over this period, changes will mainly be due to the result of slow-acting tectonic forces, and cumulative erosion or deposition processes.

In the safety assessment presented in this report, the discussion of repository evolution focuses on the interval covered by the first three postclosure timeframes (i.e., up to one million years). It will be during this period that the differences between the natural environment and an engineered repository are noticeable. Beyond one million years, radioactivity in the used fuel bundles becomes similar to that in an equivalent amount of natural uranium (see Chapter 5).

As part of the safety case prepared for an actual candidate site, geoscientific arguments and evidence supporting the long-term stability and resilience to change of a sedimentary rock environment would also be presented.

Postclosure Safety Assessment of a Used Fuel Repository in Sedimentary Rock

Document Number: NWMO-TR-2018-08

Revision: 000

Class: Public

Page: 7

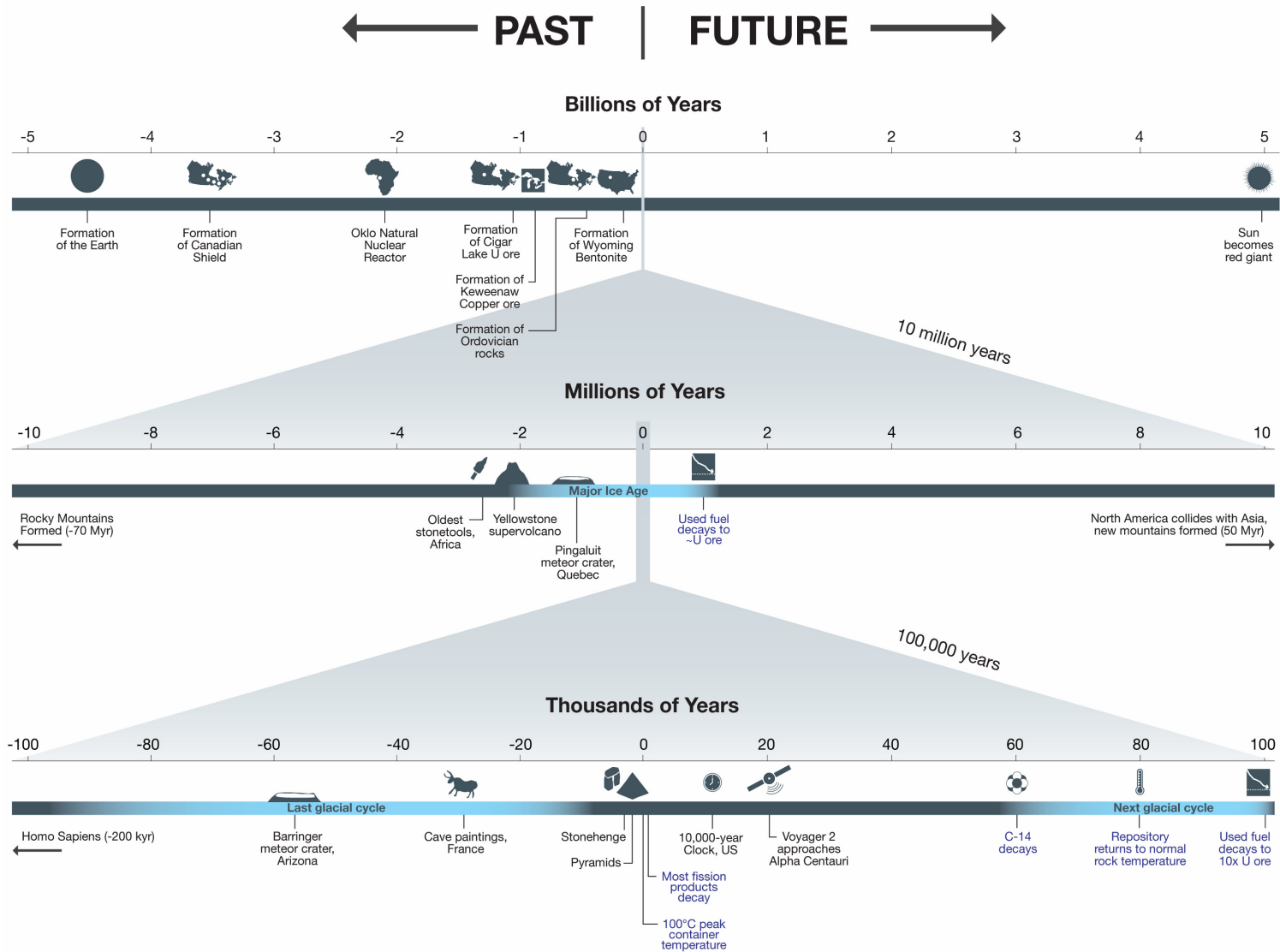


Figure 1-2: Perspective of Past Events and Expected Future Events in Earth's History Including Repository Events

1.5 Relevant Legislation

The intention is for the deep geological repository to meet or exceed all Canadian regulatory requirements, and to be consistent with international practices during site preparation, construction, operation, and beyond.

The primary legislation is the *Canadian Environmental Assessment Act* (CEAA) and the *Nuclear Safety and Control Act*. CEAA is under federal review; however, it currently requires an Environmental Impact Statement (EIS) and other supporting documents.

1.5.1 CNSC Regulatory Requirements

In accordance with paragraph 2(g) of *Nuclear Safety and Control Act* and paragraph 1(e) of the Class I Nuclear Facilities Regulations, the repository is a Class 1B nuclear facility.

Paragraph 26(e) of the Act states that, “subject to the Regulations, no person shall, except in accordance with a licence...prepare a site for, construct, operate, modify, decommission or abandon a nuclear facility”. The following licences are required over the life of the repository:

- Site Preparation Licence;
- Construction Licence;
- Operating Licence;
- Decommissioning Licence; and
- Abandonment Licence.

The detailed requirements to obtain a licence are described in Section 3 of the General Nuclear Safety and Control Regulations and in the Class I Nuclear Facilities Regulations. Other applicable regulations include the Nuclear Security Regulations, Radiation Protection Regulations, Packaging and Transport of Nuclear Substances Regulations, which apply to all nuclear facilities, and the Uranium Mines and Mills Regulations – due to similarities of some aspects of the APM facility (i.e., deep geological repository) to a mining project.

In addition to the regulations, a number of CNSC regulatory documents in the following categories are also applicable:

- Regulatory Policies – describe general principles applied by the CNSC in their review;
- Regulatory Documents and Standards – establish regulatory standards; and
- Regulatory Guides – set out regulatory expectations.

In Canada, the primary regulatory requirements and expectations for the assessment of long-term safety of radioactive waste management are given in REGDOC-2.11.1 Volume III. More generally, the regulatory framework for a licence is organized into 14 Safety and Control Areas. These areas, and examples of regulatory documents that will apply to the APM project, are listed in Table 1-1.

Table 1-1: CNSC Regulatory Documents Applicable to the APM Project

Document Number	Topic
Key references related to safety assessment	
REGDOC-2.11.1	Volume III: Assessing the Long Term Safety of Radioactive Waste Management (CNSC 2018)
Other areas relevant to a licence application	
REGDOC-2.2.1	Human Factors
P-211	Compliance
REGDOC-3.5.3	Regulatory Fundamentals
R-72	Geological Considerations in Siting a Repository for Underground Disposal of High-Level Radioactive Waste
REGDOC-2.3.1	Conduct of Licensed Activities: Construction and Commissioning Programs
REGDOC-2.9.1	Environmental Protection: Environmental Principles, Assessments and Protection Measures
G-129 Rev.1	Keeping Radiation Exposures and Doses "As Low as Reasonably Achievable (ALARA)"
REGDOC-2.10.1	Nuclear Emergency Preparedness and Response, version 2
REGDOC-2.12.2	Site Access Security Clearance
REGDOC-3.1.2	Reporting Requirements for Non-Power Reactor Class I Facilities and Uranium Mines and Mills
G-206	Financial Guarantees for the Decommissioning of Licensed Activities
REGDOC-2.12.3	Security of Nuclear Substances: Sealed Sources and Category I, II or III Nuclear Material, Version 2
G-219	Decommissioning Planning for Licensed Activities
REGDOC-2.5.4	Design of Uranium Mines and Mills: Ventilation Systems
REGDOC-2.5.1	General Design Considerations: Human Factors
REGDOC-3.2.1	Public Information and Disclosure
REGDOC-3.2.2	Aboriginal Engagement
REGDOC-2.4.3	Nuclear Criticality Safety
REGDOC-2.13.1	Safeguards and Nuclear Material Accountancy
REGDOC-2.2.4	Fitness for Duty, Volume III: Nuclear Security Officer Medical, Physical, and Psychological Fitness

Note: Current versions of the CNSC regulatory documents can be found on the CNSC website (www.cnsccsn.gc.ca)

REGDOC-2.11.1 Volume III identifies the need for long-term management of radioactive waste and hazardous waste arising from licensed activities. The principles that relate to long-term management are:

- The management of radioactive waste is commensurate with its radiological, chemical, and biological hazard to the health and safety of persons and the environment, and to national security;
- The assessment of future impacts of radioactive waste on the health and safety of persons and the environment encompasses the period of time when the maximum impact is predicted to occur; and
- The predicted impact on the health and safety of persons and the environment from the management of radioactive waste is no greater than the impact that is permissible in Canada at the time of the regulatory decision.

Key objectives for long-term management are *containment* and *isolation* of the waste. The REGDOC further states that:

“...containment can be achieved through a robust design based on multiple barriers providing defence-in-depth. Isolation is achieved through proper site selection and, when necessary, institutional controls to limit access and land use”.

Expectations are also identified for *“developing a long term safety case that includes a safety assessment complemented by various additional arguments based on:*

1. *Appropriate selection and application of assessment strategies;*
2. *Demonstration of system robustness;*
3. *The use of complementary indicators of safety; and*
4. *Any other evidence that is available to provide confidence in the long term safety of radioactive waste management.”*

Guidance is also provided for defining acceptance criteria and performing long-term assessments that includes considerations for: selection of methodology, assessment context, system description, assessment timeframes, assessment scenarios, assessment models, and the interpretation of results.

A mapping that shows how the content of this report is consistent with aspects of REGDOC-2.11.1 Volume III is shown at the end of this chapter and described in more detail in Chapter 12.

1.5.2 Transportation of Used Nuclear Fuel

The safe and secure transportation of used nuclear fuel is regulated through a comprehensive multi-agency framework of regulations, oversight, and inspections. The process builds on the roles of federal, provincial, and local agencies.

The regulatory oversight of safe transportation of used nuclear fuel in Canada is jointly shared by the CNSC and Transport Canada. Transport Canada’s *Transportation of Dangerous Goods Regulations*, and the *Transportation of Dangerous Goods Act*, and CNSC’s *Packaging and Transport of Nuclear Substances Regulations*, associated with *Nuclear Safety and Control Act*, and the *Nuclear Security Regulations* apply to all persons who handle, offer for transport, transport or receive nuclear substances.

Transport Canada and CNSC regulations follow IAEA regulations (SSR-6) for the safe transport of radioactive materials and cover certification of the package used to transport the used fuel, the licence to transport, the security planning, training requirements for the shipper and the transporter, emergency response planning, and communications. These are in addition to the normal commercial vehicle and rail operating regulations and are similar to those used internationally. Packages designed for the transport of used nuclear fuel require certification by the CNSC before they can be used in Canada.

The provinces are responsible for developing, maintaining, and operating the highway infrastructure and for inspecting the commercial vehicles and their drivers. Local governments provide law enforcement and emergency response to incidents. The interaction and cooperation between these agencies facilitates comprehensive regulation and oversight of all transportation of used nuclear fuel.

1.5.3 Canadian Codes and Standards

A number of Canadian codes and standards apply to a deep geological repository project. Compliance with these will be demonstrated in the future in support of a licence application. For example, requirements exist in the following areas:

- Civil structures will comply with the National Building Code of Canada and the National Fire Code of Canada;
- Electrical installations and components will be in accordance with the Canadian Electrical Code and associated Canadian Standards Association (CSA) standards;
- The management system will comply with the CSA N286 series of standards as well as International Standards Organization (ISO) 9001;
- The environmental management and monitoring programs will comply with the CSA N288 series of standards as well as ISO 14001; and
- The occupational health and safety management programs will comply with the CSA Z1000 standard.

Some regulatory requirements from the provincial jurisdiction will also be applicable. For example, the health and safety program will comply with provincial Occupational Health and Safety Requirements. Although there is presently no specific site, relevant Ontario provincial standards have been used, such as the Ontario Water Quality Objectives (MoEE 1994) and the Soil, Groundwater and Sediment Standards (MoE 2011).

1.5.4 Safeguards

Canada's international safeguards obligations are the result of treaty commitments (IAEA 1970, IAEA 1972, and IAEA 2000). The specific legal requirements to implement these commitments come in the form of licence conditions that are included in a CNSC licence. Compliance with these requirements will be demonstrated in support of a future licence application.

1.5.5 Indigenous Knowledge

NWMO respects the status and rights of First Nations and understands that interweaving of Indigenous Knowledge in the implementation of APM benefits the long-term management of

used nuclear fuel. Early in the project this includes recognizing the importance of water, the relationships between various aspects of the environment, as well as the health, trade and spiritual needs of people. The NWMO’s Site Selection Process looks to Indigenous peoples as practitioners of Indigenous Knowledge to be active participants in the process, and to share that knowledge with the NWMO to the extent they wish in order to help guide the decisions involved in site selection and ensure safety and the long-term well-being of the community.

1.5.6 International Guidance

A number of technical documents are available that provide guidance on best international practices with respect both to achieving safety, and on the demonstration of safety. Particular international documents relevant to development and safety for a repository are listed in Table 1-2.

Table 1-2: International Guidance Applicable to Safety Assessment

Document Number	Title
IAEA SSR-5	Disposal of Radioactive Waste (IAEA 2011)
IAEA SSG-23	The Safety Case and Safety Assessment for Radioactive Waste Disposal (IAEA 2012)
ICRP 103	The 2007 Recommendations of the International Commission on Radiological Protection (ICRP 2007)

Note: The latest version of international guidance can be found on the associated agency’s website (www.iaea.org, www.icrp.org).

1.6 Safety Case

REGDOC-2.11.1 Volume III states *“Demonstrating long term safety consists of providing reasonable assurance that waste management will be conducted in a manner that protects human health and the environment. This is achieved through the development of a safety case, which includes a safety assessment complemented by various additional arguments”*.

Section 1.1 defines the safety case as: “the integration of arguments and evidence that describe, quantify and substantiate the safety, and the level of confidence in the safety, of the deep geological repository and associated facilities. It includes the collection of scientific and technical arguments and evidence in support of the safety of the APM facility covering the site characterization and geosynthesis, the design, construction and operation of the facility, the assessment of radiation risk during operation and postclosure, and quality assurance of all safety-related work associated with the facility”.

This report documents components of a safety case (specifically the postclosure safety assessment), but is not in itself a full safety case.

REGDOC-2.11.1 Volume III recommends following a structured approach for preparing a safety case and safety assessment. The safety assessment is defined as: the process of systematically analyzing the hazards associated with the facility, and the ability of the site and design to provide the safety functions and meet technical requirements.

The most recent international guidance is included in the IAEA's SSG-23 (IAEA 2012). This guidance is used to present the safety case components for this study. The guidance also acknowledges applying the concept of defence in depth to disposal facilities by stating that: *"the host environment shall be selected, the engineered barriers of the disposal facility shall be designed... to ensure that safety is provided by means of multiple safety functions. Containment and isolation of the waste shall be provided by means of a number of physical barriers of the disposal system. The performance of these physical barriers shall be achieved by means of diverse physical and chemical processes...The capability of the individual barriers...shall be demonstrated. The overall performance of the disposal system shall not be unduly dependent on a single safety function."* It further recommends that the number and extent of required barriers depends on the type of waste and should be commensurate with the hazard potential of the waste, in accordance with the graded approach.

Figure 1-3 is largely consistent with the IAEA's components of a safety case (IAEA 2012). This figure illustrates the current work and identifies additional work that will be included as part of a licensing project at the selected site. Key elements pertinent to this study are discussed below.

1.6.1 Safety Case Context

The primary *safety objective* of the deep geological repository is to provide safe long-term management of used fuel without posing unreasonable risk to the environment or health and safety of humans.

This objective is consistent with the CNSC *Nuclear Safety and Control Act* (subparagraph 9(a) (i)) and IAEA guidance in SSR-5 (IAEA 2011), which notes that geological disposal of radioactive waste is focused on:

- Containing the waste until most of the radioactivity, and especially that associated with shorter-lived radionuclides, has decayed;
- Isolating the waste from the biosphere and substantially reducing the likelihood of inadvertent human intrusion into the waste;
- Delaying any significant migration of radionuclides to the biosphere until a time in the far future when much of the radioactivity will have decayed; and
- Ensuring that any levels of radionuclides eventually reaching the biosphere are such that possible radiological impacts in the future are acceptably low.

As described in Section 1.1, this study presents a conceptual design and illustrative safety assessment for a deep geological repository at a hypothetical site. The level of detail is consistent with the pre-project stage (i.e., before a final site has been selected). It is not a full safety case. It considers a hypothetical site, and therefore does not include a geosynthesis. It identifies and analyzes key scenarios, but does not assess all relevant scenarios.

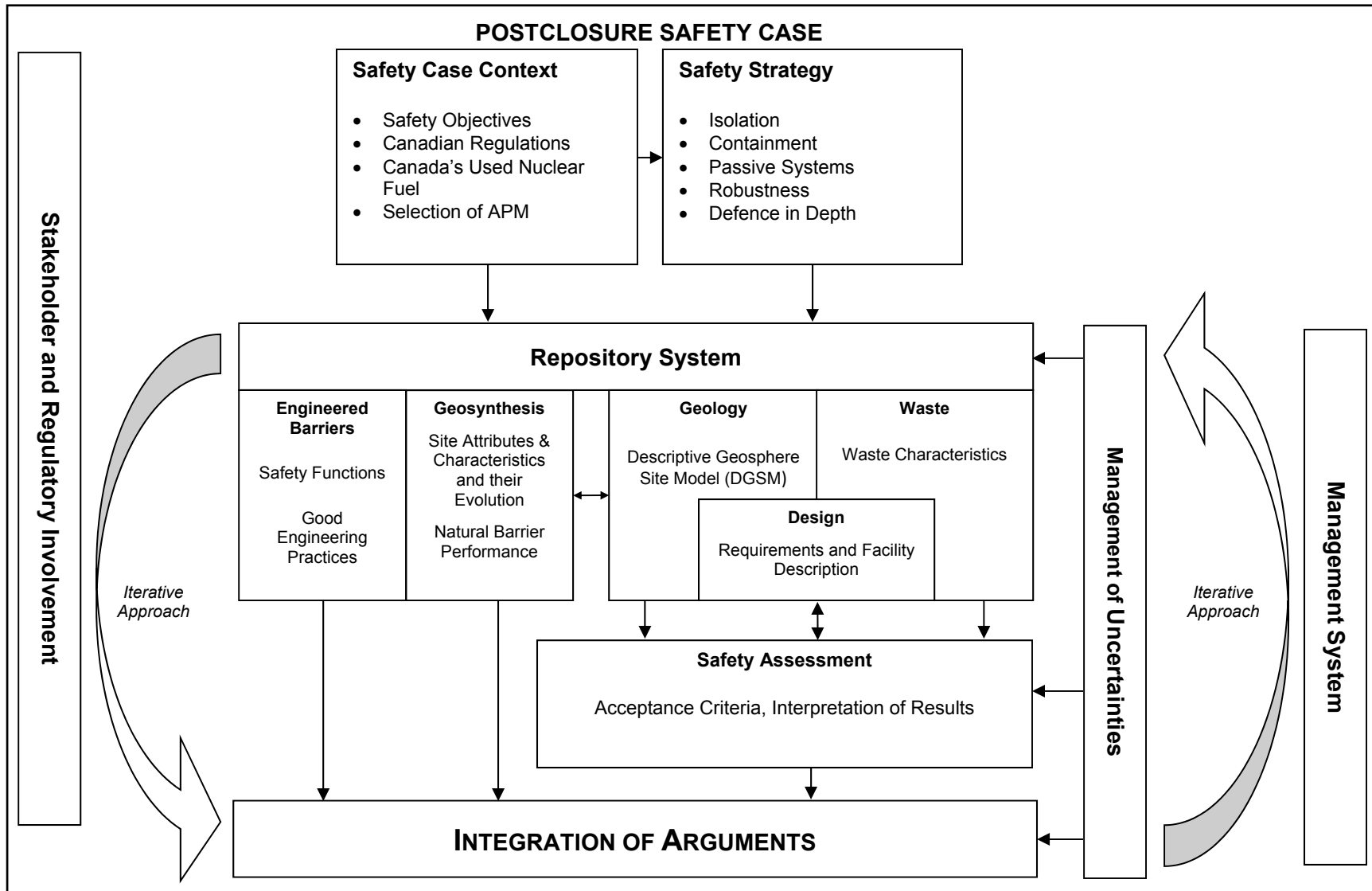


Figure 1-3: Components of the Safety Case

1.6.2 Safety Strategy

Used nuclear fuel is hazardous. Initially, the radioactivity in the fission products and other radionuclides dominate the hazard, while in the long term the hazard is from uranium and its decay chain. The uranium content of the APM repository is similar to that of a large uranium ore body such as the Cigar Lake or McArthur River sites in Saskatchewan. These ore bodies existed for over one billion years, and were isolated from their surface environments.

The safety strategy is to provide long-term containment and isolation while the radioactivity decays, and to position the repository to be ultimately similar to large ore bodies confined within a stable geosphere. The strategy relies on the use of multiple barriers and passive systems to achieve this containment and isolation over the relevant timeframes.

The geological characteristics and the engineered barrier's safety attributes are consistent with the concept of defence in depth and are further described in the following section.

1.6.3 Repository System

The DGR system includes the DGR facility, its geological setting, and the surrounding surface environment. The system includes the engineered and the natural barriers that provide containment and isolation of the waste. The repository system includes the waste, containers, sealing systems and the near-field geosphere around the repository.

Figure 1-1 represents the system across three main areas for which safety arguments are presented: 1) geology, 2) waste characteristics, and 3) design.

In this study for a hypothetical site, no specific description of communities is considered, although that will be important for any candidate site.

1.6.3.1 Geology

A key part of the safety case is the geosphere.

The NWMO's siting process (NWMO 2010) includes technical evaluations of a candidate site. The factors affecting safety that are addressed in this process are:

- The containment and isolation characteristics of the host rock;
- The long-term stability of the site;
- The ability of the site to support repository construction, operation and closure;
- The likelihood of future human intrusion;
- The confidence in the site characteristics; and
- The ability to safely transport used fuel to the site.

Site characterization activities for an actual site in sedimentary rock would include a thorough and systematic assessment of the site with respect to the above factors. This would be documented in:

- A Descriptive Geosphere Site Model (DGSM) that provides a description of the present day

three-dimensional physical and chemical characteristics of a specific site as related to implementation of the repository; and

- A Geosynthesis that provides a geoscientific explanation of the overall understanding of site characteristics, attributes and evolution as they relate to demonstrating long-term performance and safety.

For the purpose of conducting the illustrative safety assessment, this type of information is presented in Chapter 2. The key attributes assumed for the hypothetical site are:

- The repository is located at a depth of 500 m in a sufficient volume of competent, low-permeability rock;
- The repository is located in an area of low seismic hazard;
- The repository location is not associated with potable groundwater resources;
- The repository location is not associated with economically viable natural resources;
- The groundwater system at repository depth is electrochemically reducing;
- The host rock formation can withstand transient thermal and mechanical stresses; and
- The rates of site uplift and erosion are sufficiently small so as not to influence repository safety.

1.6.3.2 Waste Characteristics

The waste characteristics guide the design of the DGR facility and are a key input to the safety assessment. The waste form also has safety features that contribute to the safety case. In particular, used CANDU fuel is a barrier which contributes the following:

- Most radionuclides are immobile within the uranium oxide (UO₂) grains of the used fuel;
- The used fuel grains are mechanically durable and not significantly affected by radiation;
- The used fuel has low solubility under conditions of a failed container in contact with groundwater;
- The Zircaloy cladding provides a barrier to contact between groundwater and the used fuel in a failed container; and
- The Zircaloy cladding corrodes slowly under conditions of a failed container in contact with groundwater.

The waste characteristics are further described in Chapter 3 and the evolution of used fuel is described in Chapter 5.

1.6.3.3 Design

The design is guided by the geological characteristics and features of a candidate site and by the characteristics of the waste that will be placed in the repository. For this study, a hypothetical sedimentary site in the Southern Ontario is considered. Representative characteristics of the site are used to guide specific repository design requirements which include engineered barriers to fulfill specific safety functions. Design requirements are used as an input to the safety assessment.

The safety strategy acknowledges that properties of the engineered barriers are selected to fulfill safety functions. Passive engineered barriers of the used fuel container, buffer and sealing systems contribute to the isolation and containment of contaminants as follows:

- The used fuel container is a barrier for the underground conditions at timeframes relevant to repository safety;
- Inspection methods would ensure the container is built consistent with design specifications;
- The in-room buffer system holds and protects the containers;
- Engineered seals isolate the placement room from the access tunnels; and
- Shaft backfill and seals isolate the repository from the surface.

The repository design is described in Chapter 4 at a conceptual level of detail. The description includes the underground portions relevant to postclosure safety.

1.6.4 Safety Assessment

The safety assessment is defined as: “the process of systematically analyzing the hazards associated with the facility, and the ability of the site and design to provide the safety functions and meet technical requirements”.

The postclosure scenarios, assessment tools, methods and results are presented in Chapters 6, 7 and 8. Both radiological and non-radiological impacts are assessed and the safety assessment results are compared against acceptance criteria.

1.6.5 Management of Uncertainties

This report describes the assessment of uncertainties associated with numerical analyses at a level that is reasonable for a conceptual design at a hypothetical site. The discussion is consistent with the CNSC guidance for analyzing uncertainties and addresses degree of conservatism, conceptual model uncertainty, parameter value uncertainty, and scenario uncertainty.

For a candidate site, the postclosure safety assessment would be supported by a DGSM and Geosynthesis developed in the site characterization program. The site characterization program will allow for the iterative development, testing and refinement of a site-specific model that will contribute to managing uncertainties in scientific understanding, data or models supporting the geoscience basis for the repository.

1.6.6 Iterative Approach

Consistent with international guidance, the NWMO plans to use an iterative approach in the strategies for management, site characterization, design and assessment of a candidate site. The documentation process to support this iterative approach is included in Figure 1-4.

Once a site has been selected, Figure 1-4 illustrates that characterization and engineered design programs will go through iterations based on increased knowledge of site characteristics and safety assessment input. A few iterations are expected during the phase of detailed investigation.

Some of the key activities in this approach include:

- Peer reviews;
- Using site characterization results as an input to repository design and safety assessment, and in building the safety case;
- Conducting complementary geoscience analogue studies to enhance confidence in the understanding of long-term repository safety;
- Using proven technology in the design;
- Use of a range of safety and performance indicators in safety analyses;
- Assessing associated uncertainties and identification of any significant deficiencies in scientific understanding, data or analysis that might affect the analysis results that are presented; and
- Using the results of safety assessment, in particular the preclosure safety assessment and occupational radiation dose ALARA¹ assessment and conventional safety considerations in the design.

1.6.7 Integration of Safety Arguments

The safety arguments will be integrated as part of a complete safety case. These arguments will be supported by evidence and multiple lines of reasoning gathered in the site characterization work program and documented in a Geosynthesis for a candidate site.

For the purpose of this report, a number of safety arguments have been assumed as noted in Section 1.6.3. These assumptions are made to show how site characteristics or attributes and safety functions are used to illustrate the robustness of a multi-barrier system.

The assessment results presented in Chapter 7 and 8 will be used to support safety arguments resulting from the postclosure assessment.

1.6.8 Stakeholder and Regulatory Involvement

As noted earlier, the purpose of this report is to present an illustrative postclosure safety assessment of a deep geological repository in a representative sedimentary rock setting.

This report considers a hypothetical site and is not being prepared for a licensing process, so there are no direct stakeholders. However, it will be publicly available as a basis for discussion with interested communities on NWMO's approach to safety assessment and on the potential performance of its current design concept in the context of a repository system. It will also be available to CNSC to provide background information to support any planned technical reviews.

¹ ALARA: As low as reasonably achievable, social and economic factors taken into account.

1.6.9 Management System

A project quality plan describes how APM design and technical work activities are conducted under an appropriate management system framework. The plan covers the following elements:

- The project organization and responsibilities;
- NWMO and project-specific governance;
- Quality requirements;
- Verification requirements;
- Requirements for consultant or contractor quality management system;
- Records requirements;
- Program's periodic assessment activities; and
- Annual assessment activities.

Chapter 11 describes the elements of the project quality plan in more detail.

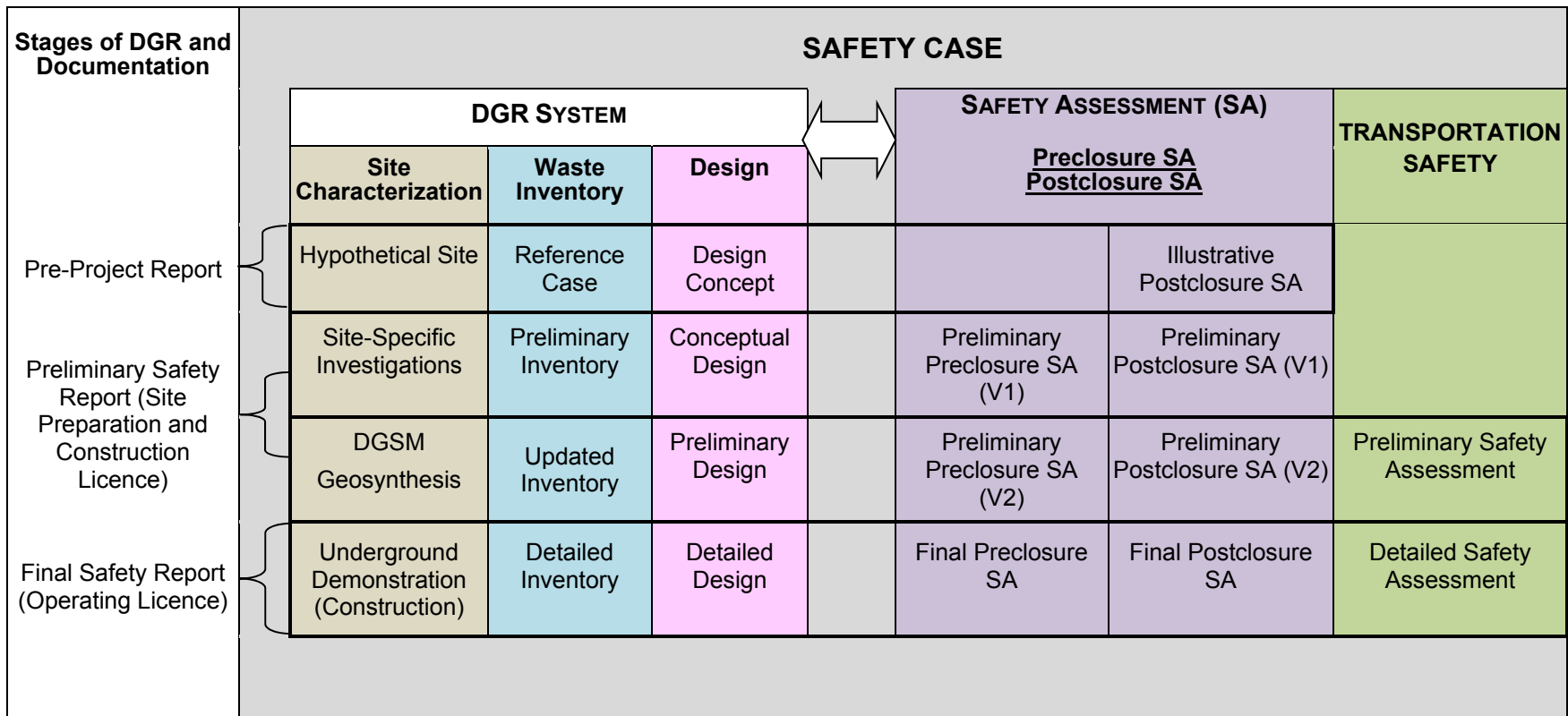


Figure 1-4: Iterative Process for Developing the Safety Case

1.7 International Status of Deep Geological Repositories

The concept of using a deep geological repository for long-term management of used nuclear fuel is consistent with other national plans for high-level waste as summarized in Table 1-3.

Table 1-3: Status of National Plans for High-Level Waste

Country	National Plan for High-Level Waste	Potential Rock Type	Repository Status
Finland	Geological Repository	Crystalline Rock	- Willing host community selected - Underground demonstration facility at site - 2015: construction licence received - 2020s: plan in-service date
Sweden	Geological Repository	Crystalline Rock	- Willing host community selected - Underground demonstration facility operating at nearby site - 2011: construction licence application - 2025: plan in-service date
France	Geological Repository	Sedimentary Rock	- General geological region identified - Underground demonstration facility operating at nearby site - 2025: plan in-service date
Switzerland	Geological Repository	Sedimentary Rock	- Underground demonstration facilities operating at generic sites - General geological regions identified - 2050: plan in-service date
China	Geological Repository	Crystalline Rock	- 2050: plan in-service date
Germany	Geological Repository	Salt, Crystalline, and Sedimentary Rock	- 2050: earliest in-service date
South Korea	Geological Repository	To be decided	- 2053: plan in-service date
United Kingdom	Geological Repository	Crystalline Rock	- 2075: plan in-service date
Japan	Geological Repository	Crystalline and Sedimentary Rock	- Underground research facilities operating at generic sites - No official date
USA	Geological Repository	To be decided	- No official date

1.8 Report Structure and Content

The structure of this postclosure safety assessment report is as follows:

- Chapter 1 Introduction: An overview of the APM project and the context for the report.
- Chapter 2 Description of a Hypothetical Site: Information related to a hypothetical site is presented.
- Chapter 3 Used Fuel Characteristics: Information is provided on the reference fuel bundle adopted in the postclosure safety assessment.
- Chapter 4 Repository Facility – Conceptual Design: Description of conceptual design for a deep geological repository.
- Chapter 5 Long-Term Evolution of the Multiple Barrier System: Description of the deep geological repository system, including the interaction of different components of the system.
- Chapter 6 Scenario Identification and Description: Description of the systematic scenario identification process used to identify Normal Evolution and Disruptive Event Scenarios.
- Chapter 7 Postclosure Safety Assessment – Contaminant Transport: Provides an evaluation of potential impacts during Normal Evolution and Disruptive Event Scenarios for water-borne transport.
- Chapter 8 Postclosure Safety Assessment – Gas Generation and Transport: Provides an evaluation of potential impacts for gas-borne transport.
- Chapter 9 Treatment of Uncertainties: Description of scenario, model and data uncertainties.
- Chapter 10 Natural Analogues: Description of natural analogues that illustrate material integrity and identification of the role of site-specific analogues.
- Chapter 11 Quality Assurance: Description of the APM quality assurance plan.
- Chapter 12 Summary and Conclusions: Summary of information presented in the pre-project report and overall conclusion on meeting the pre-project report objective.
- Chapter 13 Special Terms: Includes units, abbreviations and acronyms.

To illustrate how the content of REGDOC-2.11.1 is captured in this report, a mapping of the report sections to the content of the REGDOC is provided in Table 1-4.

Table 1-4: Case Study Report Content Mapped to CNSC REGDOC-2.11.1 Volume III

REGDOC-2.11.1 Content	Relevant Section(s) in Report
Developing a Long-Term Safety Case	
Safety Assessment	Chapters 7 and 8
Use of Different Assessment Strategies	Sections 7.2 and 8.2
Robustness and Natural Analogues	Chapters 7, 8 and 10
Use of Complementary Indicators to Safety	Section 7.12
Defining Acceptance Criteria	
Overview	Sections 7.1 and 8.1
Criteria for Protection of Persons and the Environment	Section 7.1
Performing Long-Term Assessments	
Selection of Appropriate Methodology	Sections 7.3-7.5 and 8.3-8.5
Assessment Context	Sections 1.6.1, 7 and 8
System Description	Chapters 2 to 5
Assessment Time Frame	Sections 1.4 and 6.1.3
Assessment Scenarios	Sections 6.1 and 7.2
Developing and Using Assessment Models	Chapters 7 and 8
Interpretation of Results	
Comparing Assessment Results with Acceptance Criteria	Sections 7.13, 8.7 and 8.8
Analyzing Uncertainties	Chapter 9

1.9 References for Chapter 1

- CEAA. 1998. Nuclear Fuel Waste Management and Disposal Concept: Report of the Nuclear Fuel Waste Management and Disposal Concept Environmental Assessment Panel. Canadian Environmental Assessment Agency. Ottawa, Canada.
- CNSC. 2018. Regulatory Document REGDOC-2.11.1 Volume III: Assessing the Long-Term Safety of Radioactive Waste Management. Canadian Nuclear Safety Commission. Ottawa, Canada.
- GC. 2007. Government Approval of APM, Order-in-Council, Part 11, Vol. 141, No. 13 of the Canada Gazette, SI/TR/2007-63. Government of Canada.

- Hare, F.K., A.M. Aikin and J.M. Harrison. 1977. The Management of Canada's Nuclear Wastes. Report of a Study Prepared under Contract for the Minister of Energy, Mines and Resources Canada. Report EP 77-6. Energy, Mines and Resources Canada. Ottawa, Canada.
- IAEA. 1970. Treaty on the Non-Proliferation of Nuclear Weapons. International Atomic Energy Agency INFCIRC/140. Vienna, Austria.
- IAEA. 1972. Agreement Between the Government of Canada and the International Atomic Energy Agency for the Application of Safeguards in Connection with the Treaty on the Non-Proliferation of Nuclear Weapons. International Atomic Energy Agency INFCIRC/164. Vienna, Austria.
- IAEA. 2000. Protocol Additional to the Agreement between Canada and the International Atomic Energy Agency for the Application of Safeguards in Connection with the Treaty on the Non-Proliferation of Nuclear Weapons. International Atomic Energy Agency INFCIRC/164/Add.1. Vienna, Austria.
- IAEA. 2011. IAEA Safety Standards: Disposal of Radioactive Waste. International Atomic Energy Agency. Specific Safety Requirements IAEA SSR-5. Vienna, Austria.
- IAEA. 2012. IAEA Safety Standards: The Safety Case and Safety Assessment for the Disposal of Radioactive Waste. International Atomic Energy Agency. Specific Safety Guide IAEA SSG-23. Vienna, Austria.
- ICRP. 2007. The 2007 Recommendations of the International Commission on Radiological Protection. ICRP Publication 103. Ann. ICRP 37 (2-4).
- MoEE. 1994. Water Management Policies Guidelines Provincial Water Quality Objectives of the Ministry of Environment and Energy. Ministry of Environment and Energy. Ontario, Canada.
- MoE. 2011. Soil, Ground Water and Sediment Standards for Use under Part XV.1 of the Environmental Protection Act. Ontario Ministry of Environment. Ontario, Canada.
- NWMO. 2010. Moving Forward Together: Process for Selecting a Site for Canada's Deep Geological Repository for Used Nuclear Fuel. Nuclear Waste Management Organization. Toronto, Canada.

2. DESCRIPTION OF THE HYPOTHETICAL SITE

2.1 Introduction

The purpose of this chapter is to describe the characteristics of a hypothetical sedimentary rock site in southern Ontario. The description is provided in-lieu of geoscientific information that would be derived through site-specific surface and sub-surface investigations. The intent is to provide the information necessary to illustrate the postclosure safety of a deep geological repository for Canada's used nuclear fuel in a sedimentary rock geosphere at an approximate depth of 500 metres below ground surface (mBGS).

Although the data represent a hypothetical sedimentary basin site, the information is consistent with values for the sedimentary rocks of southern Ontario, in particular as obtained from both regional and site-specific investigations for Ontario Power Generation's Deep Geological Repository for Low and Intermediate Level Waste (Intera 2011, Sykes et al. 2011).

The following sections describe typical site features through the presentation of descriptive geologic (Section 2.2.1), hydrogeologic (Section 2.2.2), geochemical (Section 2.2.3) and geomechanical (Section 2.2.4) site models. Numerical groundwater simulations are presented in Section 2.3.

2.1.1 Site Attributes

There are several key site attributes that relate to demonstrating the geoscientific suitability of the hypothetical sedimentary site. These are:

- Site Predictability – near-horizontally layered, undeformed sedimentary shale and limestone formations of large lateral extent;
- Multiple Natural Barriers – multiple low permeability bedrock formations enclose and overlie the repository site;
- Low rates of Contaminant Transport – the deep groundwater flow system is stagnant, with long travel times and no indication of perturbations from glaciation;
- Shallow Groundwater Resources are Isolated – near-surface groundwater aquifers are isolated from the deep saline groundwater system;
- Rock Strength – the host rock should be capable of withstanding mechanical and thermal perturbations induced by the repository without significant structural deformation or fracturing that could compromise the containment and isolation functions of the repository;
- Rock Volume – the volume of available competent rock at repository depth should be sufficient to host the repository and to provide sufficient distance from active geological features such as zones of deformation or faults and unfavourable heterogeneities; and
- Seismically quiet - comparable to a Canadian Shield setting.

These attributes would be tested through a site characterization and Geosynthesis program at a real candidate site.

2.1.2 Modelling Strategy

The behaviour and stability of the geosphere at repository depth are illustrated through the use of a Reference Case, contrasted with comparative sensitivity cases, based upon the conceptual model described in Section 2.2. The Reference Case simulates current site conditions at the regional scale and includes groundwater salinity distributions to allow simulation of density-dependent flow. The Reference Case is described in Section 2.3.

Sensitivity cases examine the role of spatially variable groundwater density (salinity) distributions in governing groundwater system stability and dominant mass transport processes. The permeability of the rock mass is also varied to illustrate the sensitivity of the groundwater performance measures.

Paleohydrogeologic scenarios are also analyzed to assess the influence of a glacial event on groundwater system stability. The boundary conditions are varied to include cold and warm based glaciers, and the effect of hydromechanical coupling during glacial scenarios is also investigated.

2.2 Conceptual Model for Hypothetical Site

The following section describes the geosphere model for the hypothetical sedimentary site, including information on the site and regional scale geology, surface features, hydrogeological and geochemical conditions, and natural resource potential.

2.2.1 Descriptive Geological Model

The geologic site model describes the geologic composition and structural features of the geosphere, and provides the basis for geoscientific understanding of the current conditions as well as its past evolution.

2.2.1.1 Geologic Description

The geology of the site is comprised of a layer of Quaternary-aged glacial drift, overlying thick sequences of Paleozoic-aged sedimentary rock, which sit upon basement bedrock of Precambrian-aged granitic gneiss. Fractures within the regional study area are expected to be sparse and infrequent, and will not penetrate Paleozoic sedimentary rocks younger than Ordovician in age (NWMO, 2011). The stratigraphic column for the sedimentary rock found at the centre of the hypothetical repository site is shown in Table 2-1. Table 2-1 also includes geologic formations that are not present at the repository site, but are found within the regional modelling area (described in Section 2.3). Formation thicknesses will vary across the regional modelling area, and a total of 15 formations pinch-out within 10 km of the repository site.

Table 2-1: Formation Thicknesses at the Hypothetical Site

Period	Geological Unit	Unit Top Depth (mBGS)	Thickness (m)
Quaternary	Drift	0.0	29.4
Devonian	Hamilton Group	-	-
	Dundee	-	-
	Detroit River Group	-	-
	Bois Blanc	-	-
Silurian	Bass Islands	-	-
	Unit G	-	-
	Unit F	-	-
	Unit F Salt	-	-
	Unit E	-	-
	Unit D	-	-
	Unit B and C	29.4	52.3
	Unit B Anhydrite	-	-
	Unit A-2 Carbonate	81.7	27.0
	Unit A-1 Upper Carbonate	108.7	3.0
	Unit A-1 Carbonate	111.7	22.1
	Unit A-1 Evaporite	133.8	2.0
	Unit A0	135.8	2.3
	Guelph	138.1	71.4
	Goat Island	-	-
	Gasport	-	-
	Lions Head	-	-
	Reynales/Fossil Hill	209.5	6.8
	Cabot Head	216.3	15.8
	Manitoulin	232.1	15.6
Ordovician	Queenston	247.7	77.6
	Georgian Bay/Blue Mountain	325.3	154.3
	Cobourg	479.6	46.4
	Sherman Fall	526.0	47.3
	Kirkfield	573.3	39.5
	Coboconk	612.8	8.0
	Gull River	620.8	53.4
	Shadow Lake	674.2	7.6
Cambrian	Cambrian	-	-
Precambrian	Upper Precambrian	681.8	20.0
	Precambrian	701.8	-

Note: Repository location at the hypothetical site is in the Cobourg Formation. Dash (-) indicates that formation is not present at the repository location.

2.2.1.1.1 Basement Geology

The basement geology at the repository site is found at a depth of 682 mBGS. The Precambrian bedrock beneath the repository site is composed of metamorphic gneiss.

2.2.1.1.2 Sedimentary Bedrock Geology

The sedimentary rock overlying the Precambrian basement at the hypothetical repository site has a thickness of 682 m and comprises a thick sequence of limestones and dolostones, as well as shales and evaporites. The formation descriptions in the following sections are derived from Armstrong & Carter (2006, 2010), as well as Armstrong & Goodman (1990) and Armstrong & Dodge (2007).

Cambrian

The Cambrian lithologies include fine- to medium-grained crystalline dolostones, sandy dolostone, argillaceous dolostone, as well as fine and coarse sandstone. The Cambrian pinches-out against the Precambrian surface and is assumed not to be present at the repository site.

Ordovician

The Ordovician rocks beneath the repository site are composed of a thick sequence of shales overlying carbonates. The Ordovician shales include the Queenston and the Georgian Bay/Blue Mountain Formations, and have a total thickness 232 m. The Ordovician carbonates include the argillaceous limestone of the Cobourg Formation, as well as the limestones of the Sherman Fall and Kirkfield formations. At the base of the Ordovician sequence is the Black River Group, which is comprised of the Shadow Lake, Gull River and Coboconk formations.

The Shadow Lake Formation is made up of poorly sorted shales, sandstones and argillaceous dolostones, with rare conglomerates. The overlying Gull River Formation is composed of limestone. At the top of the Black River Group, the Coboconk is composed of bioclastic limestone.

Overlying the Black River Group is the Trenton Group, which is comprised of the Kirkfield, Sherman Fall and Cobourg formations. The Kirkfield Formation is composed of limestone with thin shale interbeds. The overlying Sherman Fall Formation ranges from argillaceous limestone at its base to fossiliferous limestone in its upper section.

The Cobourg Formation is composed of fine-grained to argillaceous limestone. The Cobourg Formation is the proposed host rock for the repository discussed herein.

The upper part of the Ordovician sequence at the repository site is made up of a thick sequence of shale, and is comprised of the Blue Mountain, Georgian Bay and Queenston formations. The Blue Mountain Formation is composed of non-calcareous shale. The Georgian Bay Formation is composed of shale with intermittent siltstone and limestone interbeds. The Queenston Formation is composed of shale and minor amounts of siltstone, sandstone and limestone.

Silurian

The Silurian lithologies can be grouped into three sets of formations, the Lower, Middle and Upper Silurian. The Lower Silurian rocks unconformably overlie the Queenston Formation and are comprised of the Manitoulin and Cabot Head formations. The Manitoulin Formation is composed of argillaceous dolostone with minor shale. The overlying Cabot Head Formation is composed of noncalcareous shale with minor sandstone and carbonate interbeds.

The Middle Silurian rocks are composed of the Fossil Hill, Lions Head, Gasport, Goat Island and Guelph formations. The Fossil Hill Formation is composed of a fossiliferous dolostone. The Lions Head, Gasport, Goat Island and Guelph formations overlie the Fossil Hill to form the Niagaran Group, which is included within the regional geologic framework model but only the Guelph Formation is present at the site (Section 2.3.3.2). The Lions Head is a sparsely fossiliferous dolostone with minor chert nodules. The Gasport Formation is composed of dolostone. The Goat Island is lithologically similar to the Gasport, but is more argillaceous. The Guelph Formation is composed of reefal to inter-reefal dolostones. Reefal facies represent pinnacle, patch and barrier reefs.

The Upper Silurian rocks are composed of the Salina Group, which include a thick sequence of carbonates and evaporites. The Salina Group at the repository site includes the following units: Unit A0 (carbonate), Unit A1-Evaporite, Unit A1-Carbonate, Unit A1-Upper Carbonate, Unit A2 Carbonate and Unit B and C (carbonate). In addition to the Salina units described above, the following units are found regionally: Unit D (carbonate and evaporite), Unit E (carbonate and shale), Unit F (carbonate, shale and evaporite), and Unit G (carbonite, shale, evaporite).

Lying on top of the Salina Group, and at the top of the Silurian lithologies, the Bass Island Formation is composed of microcrystalline dolostone.

Devonian

Overlying the Silurian strata are the Devonian formations and groups, which include the Bois Blanc Formation, the Detroit River Group, the Dundee Formation and the Hamilton Group. These strata are found regionally, but are not present at the hypothetical repository site. The Bois Blanc Formation is composed of cherty dolostone. The Amherstburg and the Lucas formations comprise the Detroit River Group, which is made up of mixed limestones and dolostones. Overlying the Detroit River Group is the Dundee Formation, which is composed of fossiliferous limestones with minor dolostones.

Quaternary

The Quaternary cover found at the repository site is composed of a thick sequence of glacial till, glaciofluvial sands and gravels, and glaciolacustrine clays and silts.

2.2.1.2 Surface Features

2.2.1.2.1 Topography

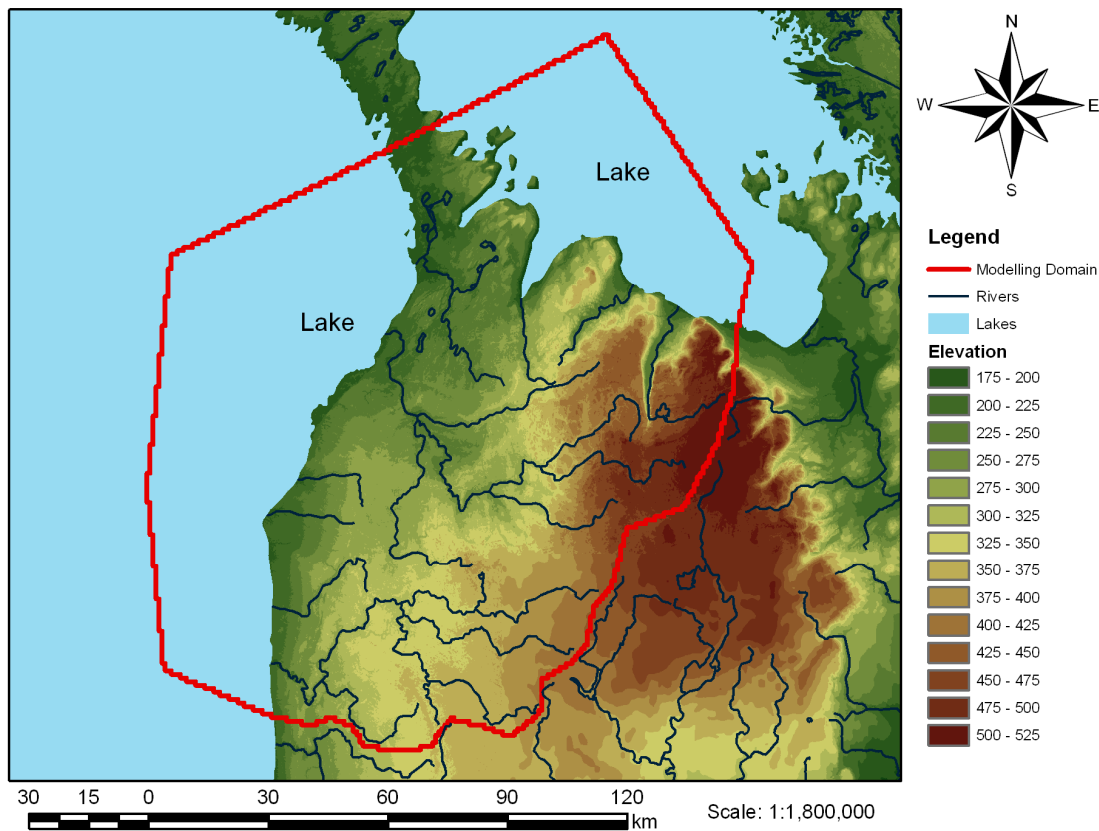
A representative regional area encompassing a watershed was selected for this postclosure safety assessment, and is shown in Figure 2-1 with an area of 18,000 km². The lateral boundaries for the regional domain have been selected to correspond with surface and groundwater divides, which represent planes across which groundwater flow is not expected.

The top surface of the domain was defined by a Digital Elevation Model (DEM) from the Shuttle Radar Topography Mission (SRTM) and a river network in ArcGIS. Based on the assumption that the water table is a subdued reflection of surface topography, the topographic divides representing no-flow boundaries are a reasonable choice for the upper flow regime (Section 2.2.2.1). The higher permeability Niagaran Group, within the intermediate flow regime, subcrops within the modelling domain, while the western boundary occurs at a groundwater divide beneath Lake Huron. The modelling domain includes the local topographic high in southern Ontario and the domain extends to the deepest portions of both Lake Huron and Georgian Bay. The bathymetric data of both water bodies, provided by National Oceanic and Atmospheric Administration (NOAA), was combined with the DEM to provide a continuous surface for the top of the Earth's solid surface.

The regional watershed and hydrogeologic conditions are described in Section 2.3.

2.2.1.2.2 Surface Hydrology

The regional domain contains two major lakes and is located in the western and northern portions of the regional area, as shown in Figure 2-1. Smaller rivers flowing into the two major lakes can also be found in Figure 2-1.



Note: Elevation is measured in metres above sea level (mASL). The elevation for the lakes shown is 176 mASL.

Figure 2-1: Regional Scale Topography

2.2.2 Descriptive Hydrogeologic Model

2.2.2.1 Groundwater Systems

Three groundwater systems are considered for the site. The groundwater systems are identified, in part, by the regional distribution of hydraulic conductivities, as well as groundwater total dissolved solids (TDS) concentrations and redox conditions (a detailed geochemical conceptual model is presented in Section 2.2.3). The primary characteristics of the three groundwater systems are described below.

Shallow Groundwater System (0 - 215 mBGS)

The shallow groundwater system, located near surface, is predominately driven by local- and sub-regional scale topographic changes. Meteoric water, in the form of rain or snowmelt, initially recharges the groundwater system by infiltration in near surface weathered zones, and flows from topographic highs near the surface before discharging into streams, rivers, lakes or swamps and bogs associated with local topographic lows. The average travel time for groundwater to recharge, and then subsequently discharge, in the shallow groundwater zone is typical less than 1,000 years. The groundwater in the shallow groundwater zone is fresh and oxygen-rich, with low TDS concentrations (further discussion can be found in Section 2.2.3).

Intermediate Groundwater System (215 - 250 mBGS)

The groundwater in the intermediate groundwater system transitions from fresh and oxygen-rich, to more mineralized and chemically reducing with depth. At the hypothetical site, the shift from oxidizing to reducing conditions occurs within this system. In the intermediate groundwater system, larger domains of low permeability rock tend to decrease mass transport rates.

Deep Groundwater System (> 250 mBGS)

In contrast to the shallow and intermediate groundwater zones, groundwaters in the deep system have higher total dissolved solids concentrations and consequently, higher fluid densities. The geochemical redox potential is reducing. The increased fluid density will influence both energy gradients within the groundwater regime and vertical upward movement of groundwater between the shallow/intermediate and deep groundwater zones (Park et al. 2009).

2.2.2.2 Hydraulic Parameters

The key hydraulic parameters, including the horizontal and vertical hydraulic conductivities (K_H , and K_V respectively), anisotropy ratio for the hydraulic conductivity ($K_H : K_V$), porosity, specific storage (S_s), tortuosity (τ), fluid density, and loading efficiencies (ζ) for the hypothetical site are shown in Table 2-2 (unless otherwise noted, the hydrogeologic parameters are derived from Table 4.2 in Sykes et al. 2011).

Postclosure Safety Assessment of a Used Fuel Repository in Sedimentary Rock

Document Number: NWMO-TR-2018-08

Revision: 000

Class: Public

Page: 32

Table 2-2: Regional Hydrogeologic Parameters

Formation	Unit Top Depth (mBGS)	Thickness (m)	K_H (m/s)	K_V (m/s)	$K_H : K_V$	Porosity	Fluid Density (kg/m ³)	Initial TDS (g/L)	$S_s^{(1)}$ (m ⁻¹)	$\zeta^{(1)}$	$\tau^{(2)}$
Drift	0	29.4	1×10^{-7}	5×10^{-8}	2:1	0.2	1,000	0	1×10^{-4}	0.99	4.00×10^{-1}
Hamilton Group	-	-	2×10^{-11}	2×10^{-12}	10:1	0.1	1,008	12	2×10^{-6}	0.8	1.19×10^{-1}
Dundee	-	-	8×10^{-8}	8×10^{-9}	10:1	0.1	1,005	8	2×10^{-6}	0.8	1.19×10^{-1}
Detroit River Group	-	-	6×10^{-7}	2×10^{-8}	30:1	0.077	1,001	1.4	1×10^{-6}	0.84	1.56×10^{-1}
Bois Blanc	-	-	1×10^{-7}	1×10^{-8}	10:1	0.077	1,002	3.2	1×10^{-6}	0.84	1.56×10^{-1}
Bass Islands	-	-	5×10^{-5}	2×10^{-6}	25:1	0.056	1,004	6	2×10^{-6}	0.92	1.07×10^{-1}
Unit G	-	-	1×10^{-11}	1×10^{-12}	10:1	0.172	1,010	14.8	1×10^{-6}	0.55	3.01×10^{-3}
Unit F	-	-	5×10^{-14}	5×10^{-15}	10:1	0.1	1,040	59.6	1×10^{-6}	0.68	4.93×10^{-2}
Unit F Salt	-	-	5×10^{-14}	5×10^{-15}	10:1	0.1	1,040	59.6	1×10^{-6}	0.68	4.93×10^{-2}
Unit E	-	-	2×10^{-13}	2×10^{-14}	10:1	0.1	1,083	124	7×10^{-7}	0.51	5.66×10^{-2}
Unit D	-	-	2×10^{-13}	2×10^{-14}	10:1	0.089	1,133	200	6×10^{-7}	0.53	6.35×10^{-2}
Unit B and C	29.4	52.3	4×10^{-13}	4×10^{-14}	10:1	0.165	1,198	296.7	1×10^{-6}	0.38	8.75×10^{-2}
Unit B Anhydrite	-	-	3×10^{-13}	3×10^{-14}	10:1	0.089	1,214	321	7×10^{-7}	0.53	1.04×10^{-3}
Unit A-2 Carbonate	81.7	27	3×10^{-10}	3×10^{-11}	10:1	0.12	1,091	136	7×10^{-7}	0.46	1.20×10^{-2}

Postclosure Safety Assessment of a Used Fuel Repository in Sedimentary Rock

Document Number: NWMO-TR-2018-08

Revision: 000

Class: Public

Page: 33

Formation	Unit Top Depth (mBGS)	Thickness (m)	K_H (m/s)	K_V (m/s)	$K_H : K_V$	Porosity	Fluid Density (kg/m ³)	Initial TDS (g/L)	$S_s^{(1)}$ (m ⁻¹)	$\zeta^{(1)}$	$\tau^{(2)}$
Unit A-2 Evaporite	-	-	3×10^{-13}	3×10^{-14}	10:1	0.089	1,030	45.6	6×10^{-7}	0.53	1.04×10^{-3}
Unit A-1 Upper Carbonate	108.7	3	2×10^{-7}	2×10^{-7}	1:1	0.07	1,019	28.6	5×10^{-7}	0.59	1.17×10^{-1}
Unit A-1 Carbonate	111.7	22.1	9×10^{-12}	9×10^{-13}	10:1	0.019	1,128	192	4×10^{-7}	0.84	1.14×10^{-2}
Unit A-1 Evaporite	133.8	2	3×10^{-13}	3×10^{-14}	10:1	0.007	1,217	325	4×10^{-7}	0.94	5.16×10^{-3}
Unit A0	135.8	2.3	3×10^{-13}	3×10^{-14}	10:1	0.032	1,240	360	5×10^{-7}	0.76	1.13×10^{-3}
Guelph	138.1	71.4	3×10^{-8}	3×10^{-8}	1:1	0.057	1,247	370	4×10^{-7}	0.47	6.12×10^{-1}
Goat Island	-	-	2×10^{-12}	2×10^{-13}	10:1	0.02	1,200	300	3×10^{-7}	0.72	9.03×10^{-3}
Gasport	-	-	2×10^{-12}	2×10^{-13}	10:1	0.02	1,200	300	3×10^{-7}	0.72	9.03×10^{-3}
Lions Head	-	-	5×10^{-12}	5×10^{-13}	10:1	0.031	1,200	300	3×10^{-7}	0.62	4.66×10^{-1}
Rochester	-	-	5×10^{-12}	5×10^{-13}	10:1	0.031	1,200	300	3×10^{-7}	0.62	4.66×10^{-1}
Reynales/Fossil Hill	209.5	6.8	5×10^{-12}	5×10^{-13}	10:1	0.031	1,200	300	3×10^{-7}	0.62	1.67×10^{-3}
Cabot Head	216.3	15.8	9×10^{-14}	9×10^{-15}	10:1	0.116	1,204	306	1×10^{-6}	0.6	3.22×10^{-2}
Manitoulin	232.1	15.6	9×10^{-14}	9×10^{-15}	10:1	0.028	1,233	350	8×10^{-7}	0.86	6.45×10^{-3}

Postclosure Safety Assessment of a Used Fuel Repository in Sedimentary Rock

Document Number: NWMO-TR-2018-08

Revision: 000

Class: Public

Page: 34

Formation	Unit Top Depth (mBGS)	Thickness (m)	K_H (m/s)	K_V (m/s)	$K_H : K_V$	Porosity	Fluid Density (kg/m ³)	Initial TDS (g/L)	$S_s^{(1)}$ (m ⁻¹)	$\zeta^{(1)}$	$\tau^{(2)}$
Queenston	247.7	77.6	2×10^{-14}	2×10^{-15}	10:1	0.073	1,207	310	9×10^{-7}	0.71	1.65×10^{-2}
Georgian Bay/ Blue Mountain	325.3	154.3	4×10^{-14}	3×10^{-15}	13:1	0.07	1,200	299.4	1×10^{-6}	0.79	1.41×10^{-2}
Cobourg	479.6	46.4	2×10^{-14}	2×10^{-15}	10:1	0.015	1,181	272	3×10^{-7}	0.8	2.97×10^{-2}
Sherman Fall	526	47.3	1×10^{-14}	1×10^{-15}	10:1	0.016	1,180	270	5×10^{-7}	0.88	1.65×10^{-2}
Kirkfield	573.3	39.5	8×10^{-15}	8×10^{-16}	10:1	0.021	1,156	234	5×10^{-7}	0.85	2.41×10^{-2}
Coboconk	612.8	8	4×10^{-12}	4×10^{-15}	1,000:1	0.009	1,170	255	5×10^{-7}	0.93	3.61×10^{-2}
Gull River	620.8	53.4	7×10^{-13}	7×10^{-16}	1,000:1	0.022	1,135	203	5×10^{-7}	0.85	1.42×10^{-2}
Shadow Lake	674.2	7.6	1×10^{-9}	1×10^{-12}	1,000:1	0.097	1,133	200	7×10^{-7}	0.56	1.61×10^{-2}
Cambrian	-	-	3×10^{-6}	3×10^{-6}	1:1	0.071	1,157	235	4×10^{-7}	0.34	2.88×10^{-1}
Upper Precambrian	681.8	20	1×10^{-10}	1×10^{-10}	1:1	0.038	1,200	300	3×10^{-7}	0.49	9.50×10^{-3}
Precambrian	701.8	-	1×10^{-12}	1×10^{-12}	1:1	0.005	1,200	300	2×10^{-7}	0.88	7.22×10^{-2}

Notes: For this study, the permeability of the upper 50 m of the domain is set to 1.0×10^{-7} m/s in order to reflect weathering of the geologic units near surface.

(1) S_s represents specific storage and ζ represents loading efficiencies.

(2) The estimated tortuosities for formations below the drift are based upon a free solution diffusion coefficient for NaI of 1.662×10^{-9} m²/s (Weast 1983), porosity values specified above, the effective diffusion coefficients ($D_{e,v}$) for NaI in Table 1 of APM-REF-01900-29841, assuming a diffusion accessible porosity factor of 0.5 for NaI (Intera 2011). The tortuosity for the drift was adopted from Sykes et al. (2011).

2.2.2.3 Paleohydrogeology Boundary Conditions

Paleohydrogeological simulations are used to illustrate the long-term evolution and stability of the geosphere to external perturbations. Glaciation is expected to be the largest external perturbation to which the repository would be subjected.

Over the last one million years, the sedimentary rocks in southern Ontario at the hypothetical site have been subjected to nine glacial cycles, each lasting for a period of approximately 100,000 years (Peltier 2002). During the last glacial advance and retreat, up to three kilometres of ice was present. In assessing the long-term stability and evolution of groundwater systems at depth in sedimentary rock, the loading and unloading of the geosphere by the glacier will represent one of the most significant perturbations from the current conditions.

The University of Toronto (UofT) Glacial Systems Model (GSM) provides the hydraulic and mechanical paleoclimate boundary conditions and permafrost depths for the paleohydrogeologic simulations (Peltier 2011). Peltier (2011) describes eight models that “span the apparent range of model characteristics that provide acceptable fits to the totality of the observational constraints.” Of these eight models, nn9921 and nn9930 are two of the best models based on aggregate misfit, and both include high-resolution permafrost development. Paleoclimate simulation nn9930 represents a single realization of a glacial cycle, as predicted by the GSM. A plot of various nn9930 GSM outputs for the grid cell containing the sub-regional modelling domain is shown in Figure 2-2. These outputs include ice thickness, meltwater production rate, lake depth, permafrost depth, and ice-sheet basal temperature relative to the pressure melting point of ice. Only the ice thickness, lake depth, and permafrost depth outputs are applied to the paleohydrogeologic groundwater simulations. The isostatic movement of the ground surface due to ice loading is not considered; applied hydraulic boundary conditions are stated in terms of elevation, assuming the grid does not move vertically. The application of lake depth is also a relative term independent of isostatic movement, although isostatic depression is required for a proglacial lake to form. Although lake depth could be interpolated across the TIN (Triangulated Irregular Network) in a similar manner to permafrost depth and vertical stress due to ice, large gradients could be created across the domain which would not exist in the presence of a large proglacial body of water because isostatic movement is not considered. Due to this, lake depth is added to the existing lake elevation and the hydraulic boundary conditions are adjusted accordingly.

The alternate paleoclimate simulation, nn9921, GSM model outputs for the grid cell containing the sub-regional modelling domain are shown in Figure 2-3. The paleoclimate simulation nn9921 represents a cold-based ice sheet, whereas paleoclimate simulation nn9930 represents a warm-based ice sheet. The main difference between the two glaciation scenarios is the duration of permafrost during the 121,000 years GSM simulation; the length of time nn9930 is subject to permafrost and glaciated conditions is less than that of nn9921. In addition, more frequent glacial advances and retreats occur in paleoclimate simulation nn9921. The paleoclimate boundary conditions presented in Figure 2-2 and Figure 2-3 are applied to the paleoclimate simulations described in Section 2.3.4.3. Permafrost hydraulic conductivity is discussed in Section 2.3.3.2.1.

A third paleoclimate simulation, gsm2015 (Stuhne and Peltier 2015), is produced using the latest version of the University of Toronto GSM allowing for better representations of basal pro

cesses, ice-shelves, temperate ice-water mixtures and other physics. A nudging technique is also employed which offers a more practical approach to leading-order data assimilation and error estimation than the Bayesian calibration used in earlier paleoclimate models. Model outputs are shown in Figure 2-4. In contrast to nn9930, gsm2015 shows only one cycle of ice-sheet advance and retreat lasting approximately 60 ka with meltwater production occurring concurrent with ice coverage. Permafrost is simulated to extend to nearly 200 m depth, significantly more than either nn9930 or nn9921 and continuous over a period of nearly 100 ka.

2.2.2.4 Abnormal Pressure Distributions

Within the Michigan Basin in Southern Ontario, abnormal pressure distributions have been observed. Where the Cambrian Formation is present within the regional area, overpressures with respect to ground elevation have been observed in the formation. Overpressures in the Cambrian Formation, partnered with underpressures in the Ordovician shales and carbonates, have been observed at the Bruce site (NWMO 2011). However, the Cambrian Formation is not present at the hypothetical site. For the purpose of this study, hydrostatic pressure with depth is assumed.

2.2.2.5 Saturated Conditions

Although there is evidence of residual gas phases in some formations in the Michigan Basin, the geoscience scenarios investigated for this study only consider fully-saturated conditions.

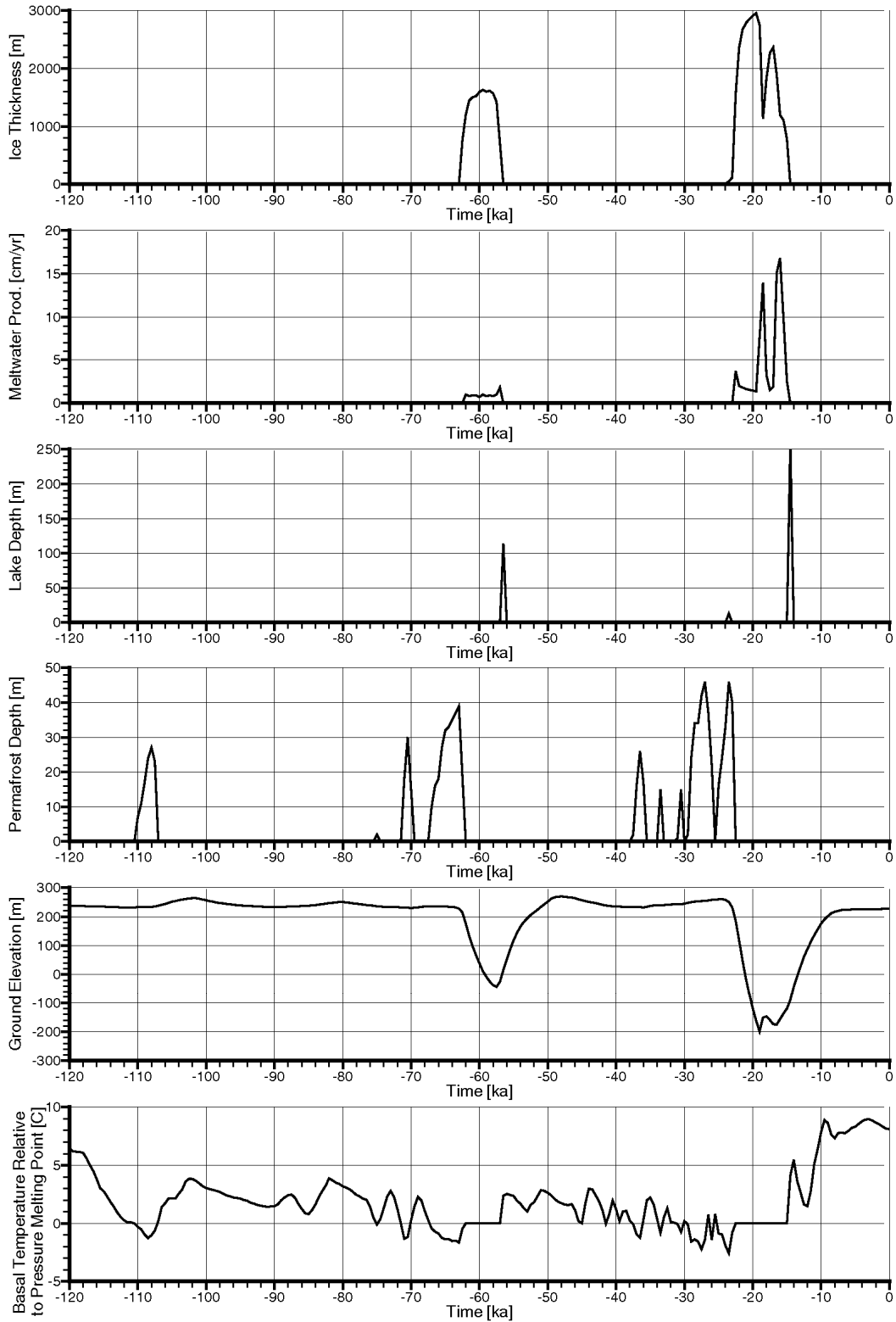


Figure 2-2: nn9930 GSM Model Outputs for the Grid Block Containing the Repository Footprint for this Study

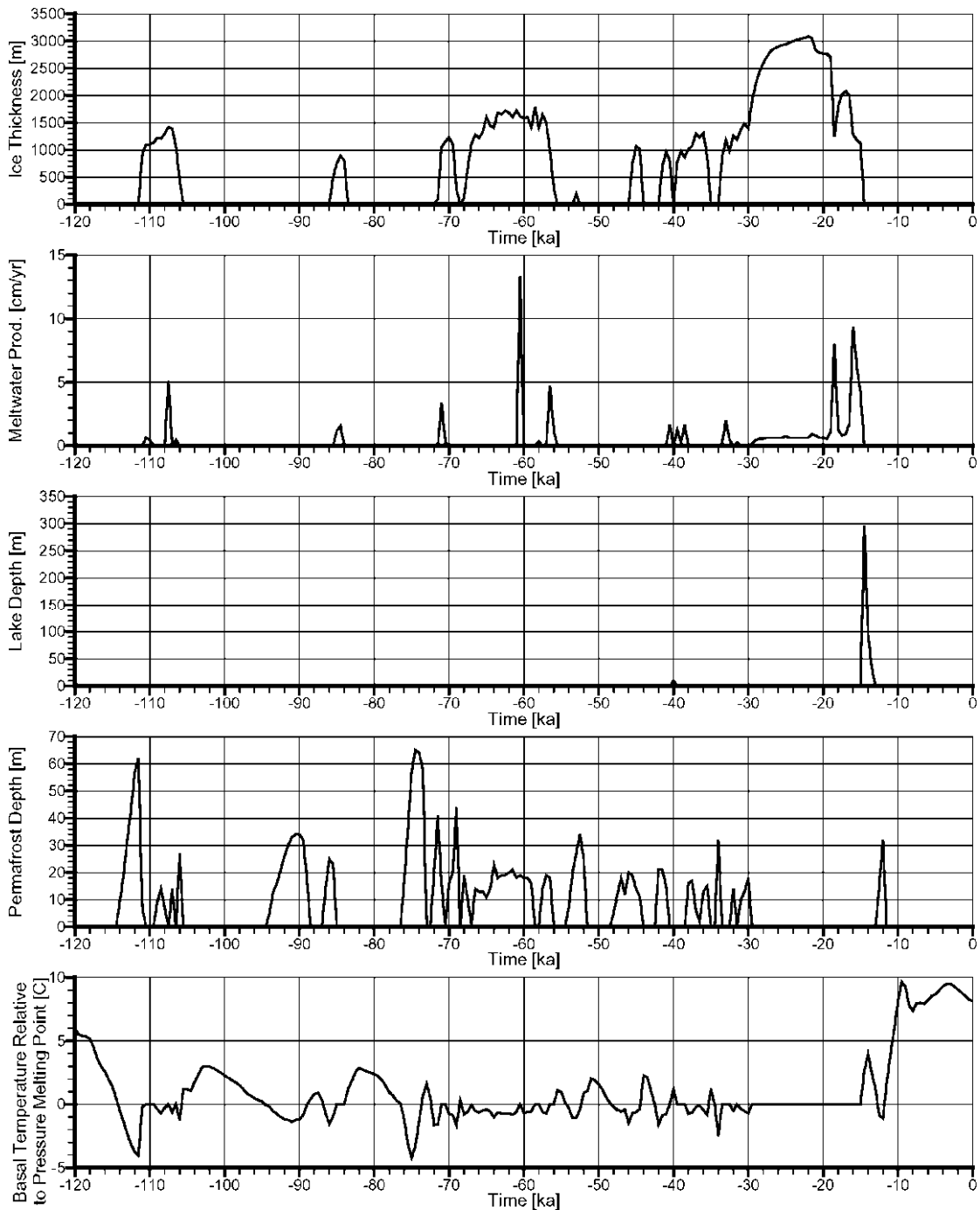


Figure 2-3: nn9921 GSM Model Outputs for the Grid Block Containing the Repository Footprint for this Study

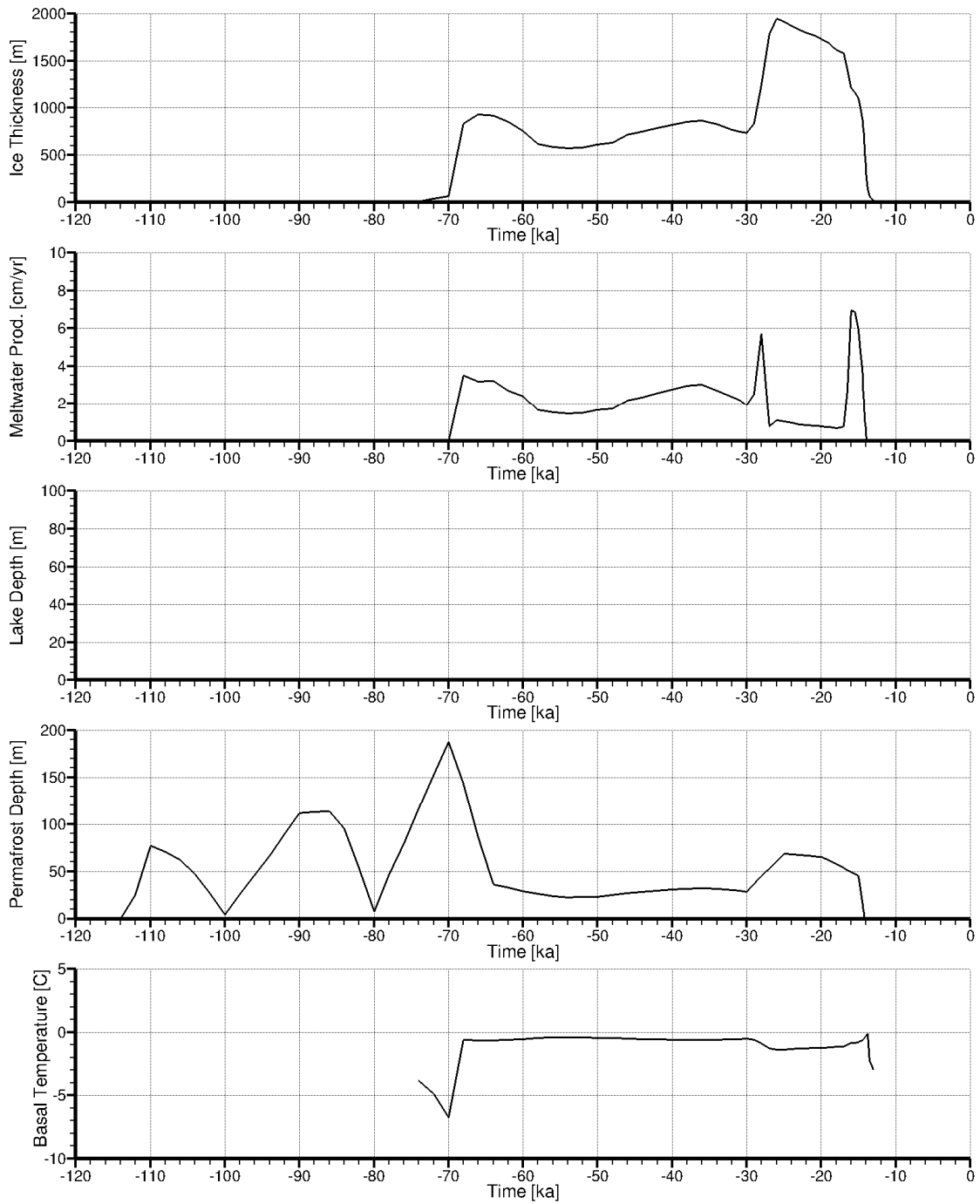


Figure 2-4: gsm2015 GSM Model Outputs for the Grid Block Containing the Repository Footprint for this Study

2.2.3 Descriptive Geochemical Model

Groundwaters and porewaters in sedimentary basin environments can often be typified by the following characteristics.

- $\delta^{18}\text{O}$ and $\delta^2\text{H}$ signatures are enriched relative to the Global Meteoric Water Line (GMWL), typically plotting to the right and below the GMWL on a plot of $\delta^{18}\text{O}$ versus $\delta^2\text{H}$.
- Formation waters are attributed to an ancient seawater or evaporated seawater origin, with relatively high concentrations of sodium (Na), calcium (Ca) and chloride (Cl).
- Variations in formation water chemistry from a seawater or evaporated seawater signature are often attributed to a variety of natural processes, such as water-rock interaction, mixing with other waters, dilution, and microbially-mediated reactions. Groundwater and porewater geochemistry is modified over both time and space by such processes.
- High total dissolved solids (TDS) concentrations which are typical of sedimentary formations as a result of the aforementioned processes.

The regional hydrogeochemical data (presented in Hobbs et al. 2011) generally indicates elevated, and often increasing salinity with depth below ground surface in southwestern Ontario. A vertical salinity profile, between ground surface and a depth of 865 m, collected at the Bruce site (presented as Figure 4.6 in NWMO 2011), located near Tiverton, Ontario, is consistent with the regional trend of elevated salinity at depth (i.e. TDS values in excess of 150 g/L).

Numerous geochemical processes have been proposed to account for the high salinity of sedimentary brines. In the context of southern Ontario, processes that are considered possible include:

1. the evaporation of seawater (e.g., Carpenter 1978, Kharaka et al. 1987);
2. the dissolution of halite or other evaporites (e.g., Rittenhouse 1967, Land and Prezbindowski 1981);
3. membrane filtration (e.g., Bredehoeft et al. 1963, Berry 1969, Kharaka and Berry 1973, Graf 1982); and/or
4. ingress of concentrated brines from crystalline shield-type rocks (e.g., Land 1997).

It is generally agreed that most chloride in sedimentary basin brines has been derived from some combination of entrapped and/or infiltrated evaporated seawater and dissolved, subsurface evaporites (e.g., Kharaka and Hanor 2005, Hanor 2001). Data and interpretations from the Bruce site (e.g. Clark et al. 2013; Al et al. 2015) are consistent with these earlier observations.

Sedimentary formation waters typically have chemistries that vary considerably from what would be expected of evaporated meteoric water or seawater. During the diagenetic evolution of the brines, calcium and strontium concentrations can increase by up to an order of magnitude compared to evaporated seawater, whereas magnesium and potassium concentrations may decrease by as much as an order of magnitude (Kharaka and Hanor 2005). Variations in the chemistry of brines from that expected for evaporated seawater are often explained using water-rock reaction processes, including:

1. dissolution or precipitation of evaporite minerals, including halite and gypsum and/or anhydrite;
2. calcite precipitation or dissolution;
3. dolomitization;
4. dissolution or precipitation of aluminosilicates; and
5. ion exchange reactions with clays (e.g., McIntosh and Walter 2006).

Dolomitization is the most extensive diagenetic process to have influenced the sedimentary sequence underlying southern Ontario (Hobbs et al. 2011). The occurrence of dolomitization within the sedimentary sequence was also confirmed in research conducted on rock core from the Bruce site (Al-Aasm and Crowe, 2018). The research suggests that dolomitization in the Ordovician rocks of the sedimentary sequence is likely associated with moderate to-temperature (>65-125°C) fluid mobilization diagenesis that occurred over several periods during the Paleozoic (Haeri-Ardakani et al. 2013).

Information on the geochemical conditions collected as part of detailed site characterization activities would be combined with available regional information to define site-specific conditions. The geochemical conditions in the shallow, intermediate and deep groundwater systems assumed for the hypothetical site are described below. Microbiology, sorption, and the anticipated gas species in groundwaters within the sedimentary setting at the proposed repository horizon are also described in Sections 2.2.3.1 to 2.2.3.3, respectively.

For the site, a hypothetical TDS profile (presented in Section 2.3.4.1; Figure 2-22), suggests the presence of three distinct groundwater systems within the sedimentary package: a shallow system (0-215 m), consisting of relatively fresh water, with a typical TDS of ≤ 5 g/L; an intermediate system (215-250 m); and, a deep system (>250 m) with significantly elevated groundwater and porewater salinities (200-300 g/L TDS). The transition zone between the shallow and deep systems is loosely termed the intermediate system, which is marked by a change in salinity from ~ 5 g/L TDS to ~ 275 g/L over a vertical distance of approximately 35 m.

Table 2-3 shows the average TDS (g/L) values, which are based on the modelled salinity profile presented in Section 2.3.4.1. The groundwaters and porewaters in the sedimentary formations at the site show the following general salinity distribution trends with depth. The TDS values are indicative of relatively fresh water (< 5 g/L) in the shallow system between ground surface and 215 m depth. The TDS values begin to increase at the base of the Fossil Hill Formation (215 m). Between the base of the Fossil Hill Formation and the top of the Manitoulin Formation, TDS values increase from ~ 5 g/L to ~ 260 g/L. Maximum salinity (~ 290 g/L) is projected to occur near the contact between the Queenston Formation and the Georgian Bay/Blue Mountain Formation at a depth of approximately 330 m. Salinity values are relatively consistent with depth through the remainder of the shales until just above the Georgian Bay/Blue Mountain-Cobourg Formation contact, where TDS values begin to decrease steadily with depth to a value of 200 g/L in the Shadow Lake Formation (680 m).

The geochemical conditions described below pertain to the overall properties of both the groundwaters and porewaters present within the shallow, intermediate and deep groundwater systems at the hypothetical site.

Shallow Groundwater System (0 - 215 mBGS)

The shallow groundwater system extends from ground surface to approximately 215 m depth. The shallow groundwater system is characterized by relatively fresh waters (<5 g/L TDS) and includes the Quaternary, Late Silurian and Middle Silurian groundwaters and porewaters. Based on regional observations, as well as data collected at the Bruce site, the shallow groundwater system is expected to be oxidizing.

Intermediate Groundwater System (215 - 250 mBGS)

The intermediate groundwater system is characterized by a transition in salinity from approximately 5 g/L TDS at the top of the Cabot Head Formation to a salinity of approximately 275 g/L TDS at the base of the Manitoulin Formation, over a vertical distance of ~35 m. The intermediate groundwater system represents a transition zone from oxidizing to reducing conditions as well (NWMO 2011). Although no site-specific data exists, similar conditions are anticipated for the hypothetical site. Such conditions would be verified during site characterization activities.

Deep Groundwater System (>250 mBGS)

The deep groundwater system is characterized by high salinity, ranging between 200 and 300 g/L TDS. Based on regional data, as well as data collected at the Bruce site, reducing conditions are expected at all depths below 250 m.

Saline groundwater conditions are expected at the depth of the hypothetical repository (500 mBGS). Groundwater chemistry at this depth in sedimentary formations of southern Ontario is typically Na-Ca-Cl or Ca-Na-Cl water under reducing conditions (Hobbs et al. 2011; Al et al. 2015). A reference composition has been defined for the porewaters anticipated to be found within the proposed repository horizon. The composition known as the SR-270 groundwater (sedimentary rock with a total dissolved solids of approximately 270 g/L) is presented in Table 2-4.

Based on diffusion experiments performed on core collected during characterization activities at the Bruce site, effective diffusion coefficients (D_e) for iodide and tritiated water (HTO) were estimated for the proposed host rock, and for the surrounding Silurian and Ordovician shale and carbonate rocks. The D_e values obtained with HTO are on average 1.9 times greater than the D_e values obtained with an iodide tracer. The D_e values at the hypothetical site are anticipated to be similar to those measured for the Bruce site (see below), but would have to be verified during site characterization activities:

Silurian carbonate: 10^{-13} to 10^{-10} m²/s, and

Ordovician shale and carbonate: 10^{-13} to 10^{-11} m²/s (Intera 2011).

More recently, research was performed to investigate the impact of confining pressure on diffusion coefficients using core samples from the Bruce site (Xiang et al. 2016). The results suggest that in situ diffusion coefficients for iodine and HTO may be up to 35% and 55% lower, respectively, than those determined in the laboratory under unconfined conditions. This

suggests that the reference values above, which represent unconfined conditions, will likely be conservative estimates for diffusion coefficients at the hypothetical site.

Table 2-3: Average TDS Values for Sedimentary Formation Groundwaters and Porewaters

Formation	Average TDS (g/L)
Drift	0.1
Unit B and C	0.3
Unit A-2 Carbonate	0.6
Unit A-1 Upper Carbonate	0.8
Unit A-1 Carbonate	2
Unit A-1 Evaporite	3
Unit A-0	3
Guelph	3
Reynales/Fossil Hill	4
Cabot Head	12
Manitoulin	142
Queenston	294
Georgian Bay/Blue Mountain	298
Cobourg	279
Sherman Fall	260
Kirkfield	244
Coboconk	235
Gull River	219
Shadow Lake	204
Upper Precambrian	203
Precambrian	250

Table 2-4: Reference SR-270-PW Composition

Composition	SR-270-PW
Water Type	Na-Ca-Cl
pH	5.8
Environment Type	Reducing
Eh	-200 mV
Density	1,181
Solutes (mg/L)	
Na	50,100
K	12,500
Ca	32,000
Mg	8,200
HCO ₃	110
SO ₄	440
Cl	168,500
Br	1,700
Sr	1,200
Li	5
F	1
I	3
B	80
Si	4
Fe	30
NO ₃	<5
PO ₄	-
TDS	275,000

2.2.3.1 Microbial Conditions in Sedimentary Environments

Microorganisms are likely to be present in the deep geological repository (DGR) environment. Concentrations of microorganisms found in different deep subsurface environments appear to vary with location, ranging from none detected in high salt, low-permeability rock formations (e.g., 750 m salt deposits at Asse, Germany) to diverse and abundant microbial communities living in fractures of crystalline rock (West and McKinley 2002). The prevalent geochemistry largely dictates the physiological potential of the resident microbes, as well as the biogeochemical reactions that they catalyze (Fredrickson and Balkwill 2006) since microbial metabolism requires a carbon source, terminal electron donor and terminal electron acceptor. Over time, metabolic activity of the microorganisms could alter the geochemistry of the repository environment. The dominant species in a given environment tend to be those microorganisms that extract the most energy from the available nutrient sources.

Some of the most extensive work on microbial activity in low permeability sedimentary systems has been performed on the Opalinus Clay Formation at the Mont Terri Rock Laboratory in Switzerland (Wersin et al. 2011, Stroes-Gascoyne et al. 2011). Due to the low salinity of the waters at Mont Terri, application of the results of such studies to the present hypothetical Canadian sedimentary rock site is somewhat limited. However, aspects of the Mont Terri work are relevant. A key result of the work indicated that contamination during drilling could promote anaerobic microbial activity (in particular, NO_3^- , Fe- and SO_4^- reducers and methanogens; Wersin et al. 2011, Stroes-Gascoyne et al. 2011) and that the effects of drilling and excavation disturbances are both temporary and spatially limited. In a state of science review documenting the role of microorganisms in relation to the design and performance of a DGR, Sherwood Lollar (2011) concluded that hydrology, geochemistry, and resident microbial populations may be sensitive to changes (i.e., perturbations) in any given system, but that many systems possess a geochemical buffering capacity to counter the effects of perturbations. In the context of the hypothetical site, properties of the deep system, such as low porosity and very high salinity, are anticipated to provide a natural buffering capacity to microbial activity within the proposed host and surrounding rock.

Microbial analyses have been performed on samples of Queenston Formation shale and Cobourg Formation limestone from drill core collected during site characterization activities at the Bruce nuclear site (Stroes-Gascoyne and Hamon 2008, Slater et al. 2013). Based on the results of both studies of Canadian low-permeability sedimentary rocks, it is anticipated that very low microbial biomass will exist at the hypothetical site at the proposed repository depth of 500 m. In addition, it is anticipated that similar conditions – i.e., low water activity, high salinity – would occur at the hypothetical site and restrict growth and activity of microorganisms.

2.2.3.2 Sorption

The sorption of radionuclides onto mineral surfaces within the geosphere is a potential mechanism for slowing the transport of some radionuclides from the repository to the surface environment. There are many factors that impact radionuclide sorption processes in the geosphere, such as rock type, mineral surface area, temperature, groundwater salinity, pH, redox conditions and the presence or absence of complexing ligands.

Sorption of radionuclides is generally reduced in groundwaters with high salinity, but the extent of reduction varies, depending on the element and how it interacts with the sedimentary rock surfaces (Vilks 2009). Measurements of sorption processes in Na-Ca-Cl brine solutions within Canadian sedimentary rocks have been underway in the Canadian program for a range of elements. Sorption of a number of elements (Ni, Cu, As, Se, Zr, Tc, Pd, Sn, Cs, Pb, Eu, Th, U, Np and Pu) on shale and limestone was tested in the SR-270-PW reference brine (ionic strength of 6.0 M) (Vilks et al. 2011; Vilks and Miller 2014; Bertetti 2016; Nagasaki 2018; Nagasaki et al. 2017; Nagasaki et al. 2016; Riddoch and Nagasaki 2016). Experiments to investigate sorption of redox sensitive elements (Se, Zr, Tc, U, Np and Pu) were conducted under reducing conditions (Bertetti 2016; Nagasaki 2018; Nagasaki et al. 2017).

These results, along with relevant literature data and modelling, have been combined into a reference sorption database that was used to support sorption values used in this study (Vilks and Yang, 2018).

2.2.3.3 Gas Characterization

Natural gases commonly encountered in deep sedimentary formations include methane, helium and carbon dioxide. Both concentrations and isotopes of methane, helium and carbon dioxide can be helpful in assessing fluid origin and solute transport.

Sherwood Lollar et al. (1994) examined natural gases from within Ordovician and Cambrian reservoirs in southwestern Ontario, and characterized the gases using isotopic and compositional indicators. Consistent with the findings of Barker and Pollock (1984), gases from the Cambrian and Ordovician reservoirs are composed predominantly of CH₄. The Cambrian and Ordovician gases were found to be thermogenic in origin, with no evidence of bacterial CH₄ contributions. Where the sedimentary rocks were in direct contact with the Precambrian basement, the gases sampled had elevated helium concentrations (Sherwood Lollar et al. 1994). The elevated helium concentrations, and associated high ³He/⁴He ratios, may reflect mixing between gases generated in-situ (in the Cambrian and Ordovician strata) and an end-member enriched in helium. Possible sources for the helium-rich end-member include gas deep within the Precambrian basement rock or an external helium-enriched fluid that migrated from deeper within the sedimentary system along pathways controlled by basement-structures (Sherwood Lollar et al. 1994).

Data collected at the Bruce site are generally consistent with regional scale findings. Thermogenic methane has been identified in the Ordovician Trenton and Black River Groups, while the overlying shales and Cobourg Formation are characterized by the presence of biogenic methane (NWMO 2011; Section 4.4.3.1). There is little evidence of mixing between the biogenic and thermogenic gas, and it is hypothesized that the thermogenic methane may have been generated in-situ in association with peak burial and/or has been transported from a deep basin or Precambrian source. ³He/⁴He ratios in the Trenton and Black River groups are observed to be elevated relative to the overlying Ordovician shales, and also relative to values estimated for in-situ formation due to natural decay processes in the rock, which suggests an enriched end-member for mixing, possibly of deep basin or Precambrian origin. Carbon dioxide was also analyzed for both concentration and isotopic composition, but only the isotopic data is considered to be reliable for interpretation purposes. The isotopic composition ($\delta^{13}\text{C}$ and $\delta^{18}\text{O}$ of CO₂) of the carbon dioxide is consistent with the assessment of biogenic gas formation in the Ordovician shales and thermogenic (non-biotic) gas formation in the Trenton and Black River groups.

At the hypothetical site, which is located in Southern Ontario, it is anticipated that similar gas distributions and signatures would be observed, indicative of very low permeability formations containing ancient gases. These characteristic would require verification during site characterization activities.

2.2.4 Descriptive Geomechanical Model

2.2.4.1 Rock Mass Strength

The proposed repository horizon is at a nominal depth of 500 mBGS, in the competent, low porosity limestone of the Cobourg Formation. In Table 2-5, the Cobourg Formation at the hypothetical site is further subdivided into upper and lower units, from the formation sequence provided in Table 2-1 and Table 2-2. The mechanical properties used for long-term stability

analyses were based mainly on laboratory testing of rock samples taken from the site investigation boreholes at the Bruce site (Gorski et al. 2009a, 2009b, 2010a, 2010b and Golder 2013).

Table 2-5: Geological Profile Near Repository Horizon with Formation Thicknesses

Geological Unit	Top of Rock Unit (mBGS)	Thickness (m)
Georgian Bay	325.3	96.2
Blue Mountain	421.5	49.5
Collingwood ⁽¹⁾	471	8.6
Cobourg ⁽²⁾	479.6	38.4
Cobourg – Lower ⁽²⁾	518	8
Sherman Fall	526	47.3

Notes: From Itasca (2015).

(1) a part of Georgian Bay/Blue Mountain formations

(2) a part of Cobourg Formation

Various laboratory geotechnical tests, such as unconfined (uniaxial) compressive strength (UCS) and triaxial compression strength tests, Brazilian or indirect tension tests, direct shear tests, and long-term strength degradation tests, were carried out on samples from the representative units throughout the geological profile (Gorski et al. 2009a, 2009b, 2010a, 2010b and Golder 2013). In particular, over 80 uniaxial compression tests were conducted on the samples from the Cobourg limestone host rock. These tests provide the basic stress-strain parameters for intact rock, such as the UCS, modulus of elasticity and Poisson’s ratio. They also allow an examination of the damage development of the limestone and the selection of the long-term rock strength.

Figure 2-5 shows the histograms of the compressive strength and elastic modulus of the Cobourg limestone. The mechanical properties (e.g., Hoek Brown and Mohr Coulomb parameters) of the five geological units included in the numerical modelling of the placement room stability analysis (Table 2-5) are tabulated in Table 2-6 (Itasca 2015). To predict the long-term strength degradation of the rock around the placement rooms, the long-term rock mass strength was taken as 40% of UCS, which is equivalent to that of crack initiation stress (Itasca 2015). The methodology on simulating time-dependent processes is detailed in Itasca (2015). Data from static fatigue tests of Lac du Bonnet granite (with relatively fast strength decay) were originally adopted for the modelling of the long-term strength degradation of the host rock (Itasca 2011, 2015). The degradation curve used for the rock was later verified by static-fatigue and creep testing on the Cobourg limestone retrieved from the Bowmansville Quarry, Ontario and the Jura Limestone from Switzerland (Paraskevopoulou et al. 2017). These tests reveal that the degradation rate of the Cobourg Limestone is lower than the granite and no failure was observed below 60% of UCS (Figure 2-6; Paraskevopoulou et al. 2017).

Figure 2-7 shows the distributions of the crack initiation and damage thresholds of rock units at and around the repository horizon at the Bruce nuclear site (NWMO 2011).

Table 2-6: Intact Rock and Rock Mass Mechanical Properties (Itasca 2015)

Unit	Intact Lab			Hoek Brown Parameters			Rock Mass			Mohr Coulomb			Bedding Kn (GPa/m)
	UCS (MPa)	E _i (GPa)	GSI	m _i	m _b	S	a	E _{rm} (GPa)	σ _{cm} (MPa)	σ ₃ (MPa)	C (MPa)	φ (deg)	
Georgian Bay	34	9.04	76	10.1	4.3	0.069	0.501	7.51	11.4	10.1	3.04	37	-
Blue Mountain	34	9.64	77	6.0	2.6	0.078	0.501	8.14	10.1	12.1	3.16	31	-
Collingwood	117	36.9	76	10.0	4.2	0.070	0.501	30.7	39.2	12.8	6.66	44	1157
Cobourg ⁽¹⁾	121	43.5	89	11.4	7.7	0.295	0.5	41.4	67.3	9.4	11.1	49	1157
Cobourg – Lower ⁽¹⁾	101	39.1	89	7.2	4.8	0.295	0.5	37.2	52.4	14.1	11.4	42	1157
Sherman Fall	76	38.8	87	11.0	6.9	0.236	0.5	36.5	38.7	14.8	7.76	44	-

Notes: -UCS & E_i are uniaxial compressive strength and elastic modulus of intact rock

-GSI is Geological Strength Index

-m_i, m_b, S and a are Hoek-Brown parameters

-σ_{cm} and E_{rm} are strength and modulus of rock mass

-C and φ are cohesion and friction angles

-Kn depicts bedding plane stiffness

(1) a part of Cobourg Formation

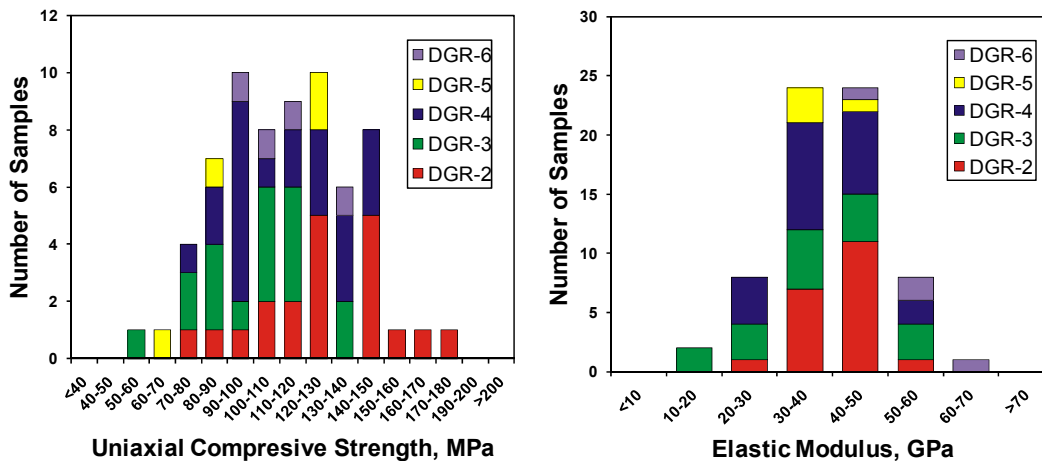
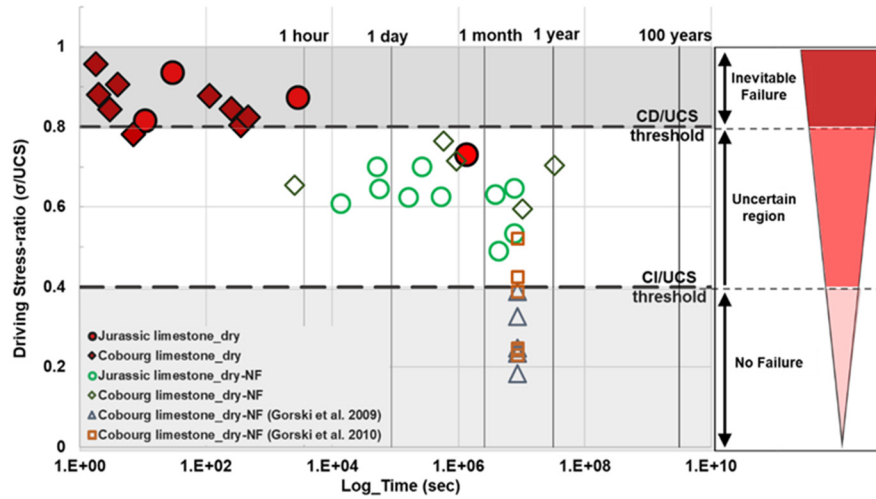


Figure 2-5: Unconfined Compressive Strength and Elastic Modulus of Cobourg Formation from DGR 1 to 6

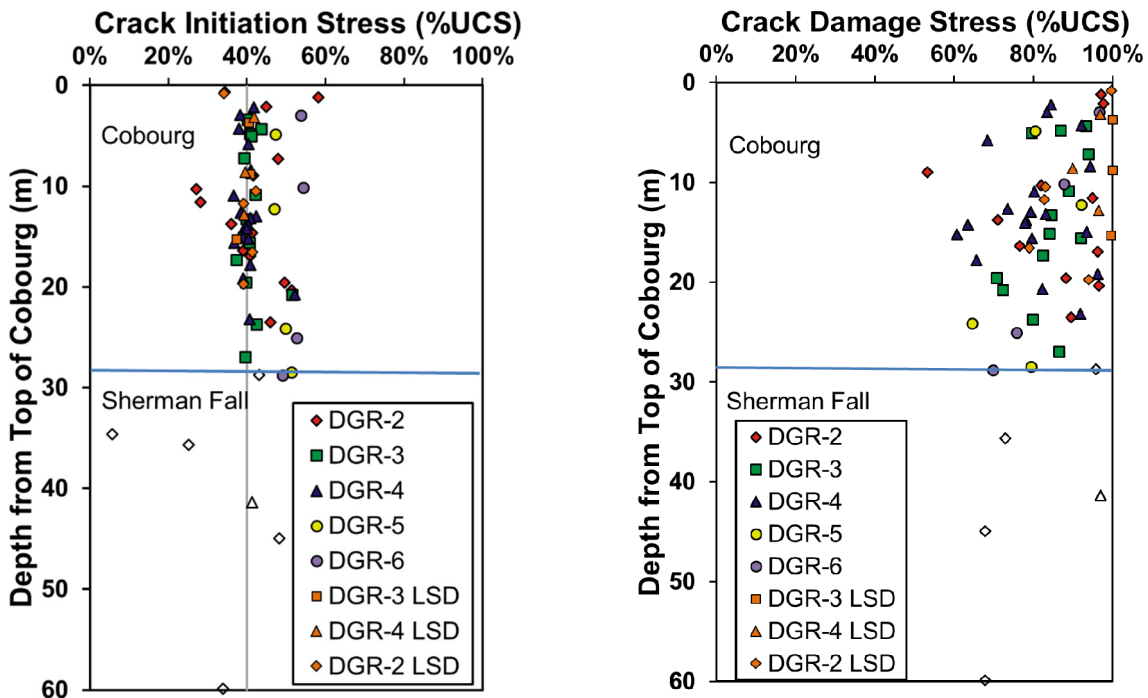


Note: Open marker indicates no failure.

Figure 2-6: Static-fatigue and Creep Testing on Cobourg and Jura Limestones to verify Long-term Strength Assumptions

(1)

(2)



Notes: LSD = Long-term Strength Degradation Results determined from Intact DGR core.

Figure 2-7: Distribution of (1) Crack Initiation Stresses and (2) Crack Damage Stresses for the Cobourg and Sherman Fall Formations

The thermal properties for these geological units are listed in Table 2-7 (Golder 2013). The average values in the table are calculated based on the test results of core samples from DGR boreholes. In the thermal models, some of the units with relatively small thickness or unavailable thermal properties were lumped together (Itasca 2015). Also, the units of same rock types (e.g., carbonate, sandstone or shale) were lumped together where possible. Linear coefficients of thermal expansion of $2.0 \times 10^{-6} \text{ 1/}^\circ\text{K}$ and $6.7 \times 10^{-6} \text{ 1/}^\circ\text{K}$ were used in the analysis for shales and carbonates, respectively (Baumgartner 2005). The data for carbonates is consistent with the testing results on Cobourg Limestone at Darlington, Ontario, reported by Lo and Wai (1982).

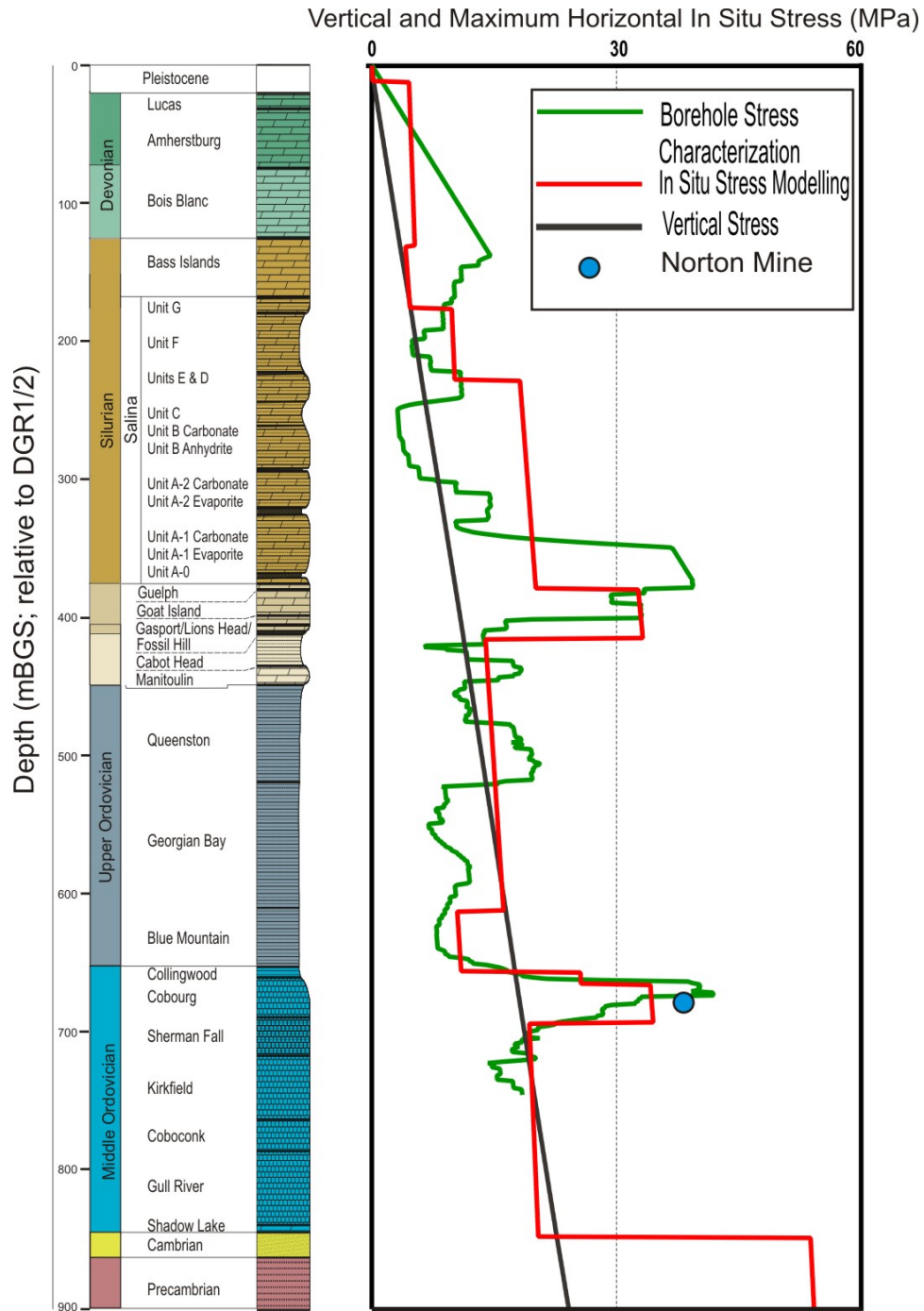
Table 2-7: Thermal Properties for the Units in the Sedimentary Setting

Geological unit	Unit Top Depth (mBGS)	Thickness (m)	Thermal Conductivity (W/m ^{°K})		Specific Heat (MJ/m ³ °K)	
			Average Measured Value	Model Values	Average Measured Value	Model Values
Queenston	247.7	77.6	1.89	1.89	1.79	1.79
Georgian Bay/Blue Mountain	325.3	154.3	1.89	1.89	1.27	1.27
Cobourg	479.6	46.4	2.27	2.27	1.63	1.69
Sherman Fall	526	47.3	1.90	1.90	1.61	1.61

2.2.4.2 Ground Stresses

The stress tensor at the depth of the repository was constrained using a bounding analysis. A simple three-dimensional model of the stratigraphy at the Bruce site was used to evaluate the effect of tectonic strains on the distribution of stresses in the different stratigraphic units (Cartwright 1997). The stresses developed in the model were then verified by comparison with limiting stress conditions estimated from borehole breakout observations and other data from the literature. A comparison between the estimated maximum horizontal in situ stress from the modelling and the constraints deduced from the analysis based on the observed lack of borehole breakouts at the Bruce nuclear site is given in Figure 2-8 (NWMO 2011).

For the sedimentary geological setting in this postclosure safety assessment, the vertical stress is gravitational. However, horizontal stresses are calculated for each layer using the elastic relation between stresses and strains based on calibrated tectonic strains, as was done for the Bruce DGR site (Itasca 2011). Because the same tectonic strains calibrated at the Bruce DGR site and same rock stiffness are used, the in situ horizontal stresses in the Cobourg host rock at the repository horizon are anticipated to be in the same order of magnitude as those predicted for the DGR (Itasca 2011).



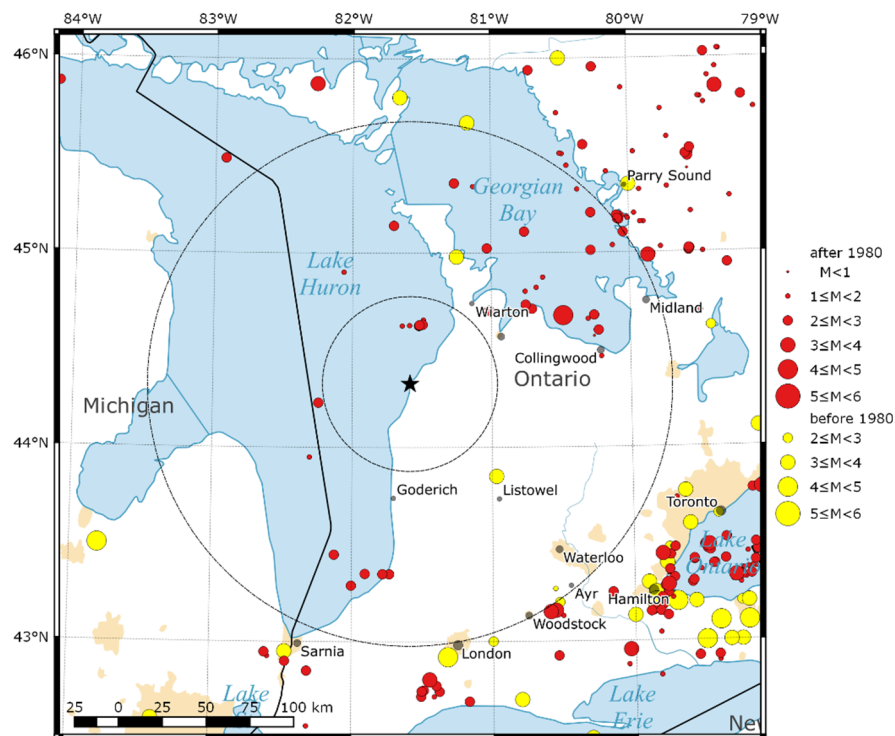
Notes: Numerical modelling results (red line) plotted against vertical stress profile (black line) and the absence of borehole failure constraint based on borehole wall strength of 100 % UCS (green line). Figure is based on data from Itasca (2011) and Valley and Maloney (2010).

Figure 2-8: Comparison of Calculated Maximum Horizontal In Situ Stress Profiles at the Bruce Site

2.2.4.3 Seismicity

Southwestern Ontario and the Bruce region lie within the tectonically stable interior of the North American continent which is characterized by low rates of seismicity. Figure 2-9 shows all known earthquakes in the region up to December 2016 (Ackerley et al. 2018). This figure shows that seismic activity in the Bruce region is sparse, indicating a lack of regional seismogenic features or active faults. Since 1952, 34 events have been detected in this region. Most recorded events have magnitude less than M3. The maximum magnitude of 4.3 was measured approximately 50 km northwest of Collingwood. The low seismicity in the region is comparable with that of the stable Canadian Shield.

As part of detailed site characterization for a deep geologic repository for low and intermediate level waste proposed by Ontario Power Generation, a borehole seismograph array was established around the Bruce nuclear facility in 2007. This array was intended to detect very low or microseismic events in addition to large events. The purpose of this array was to increase understanding of the seismicity of the area in general, and also to be able to delineate seismogenic features deep in the bedrock. The monitoring area of this network encompasses the study site described in this report, and supports the basic representation of this area as low seismicity.



Note: Circles around Bruce Site represent 50 km and 150 km radius

Figure 2-9: Seismicity in the Bruce Region to December 2016

Based on the lack of both seismic activity and appreciable concentrations of activity that might indicate regional seismogenic features or active faults, an assessment of earthquake ground shaking hazards was conducted (AMEC GEOMATRIX 2011). The estimated surface bedrock peak ground accelerations are expected to be about 0.6g for probabilities of 10^{-6} per annum (1/1,000,000 year). A summary of seismic hazard is tabulated in Table 2-8.

Table 2-8: Summary of Seismic Hazard Analysis Results

Event (Prob. Of exceed per annum)	Peak Ground Acceleration (% g)
10^{-3}	1.7
4×10^{-4} (CCBFC 2010)	2.7
10^{-5}	18.7
10^{-6}	60.6

2.3 Regional Scale Hydrogeologic Modelling

The primary objective of the analyses described in this section is to investigate the role of key geosphere parameters and processes, such as sedimentary rock permeabilities and groundwater salinity, on geosphere stability at repository depth. The following sections describe the suite of regional scale numerical groundwater models that were developed.

2.3.1 Computational Models

The numerical groundwater modelling was performed using HydroGeoSphere (HGS) revision 1553_1554 (Aquanty 2013). This is a computational model capable of solving three-dimensional variably-saturated groundwater flow and solute transport in discretely-fractured media. The model includes a dual porosity formulation, whereas discrete fractures can be represented as idealized two-dimensional parallel plates, or as fracture zones defined by hydraulic conductivity and width. HGS couples fluid flow with salinity transport through fluid density, which is dependent on the total dissolved solids concentration. Details of the HGS model that are pertinent to the study are described in Aquanty (2013). HGS is a successor to FRAC3DVS-OPG. Additionally, HGS includes algorithms to estimate performance measures of groundwater age and life expectancy for the domain groundwater (Cornaton and Perrochet 2006a, 2006b; Park et al. 2008).

2.3.2 System Performance Measures

The safety case for a potential deep geologic repository relies, in part, on the ability of the geosphere to provide a long-term barrier to solute transport. The behaviour and stability of the groundwater flow and transport regimes found at repository depth can be illustrated by determining the impact, if any, that the variability of model parameters will have upon the model results.

Common measures of the performance of a groundwater system include the flow state variables of equivalent freshwater head or environmental head, the derived porewater velocity, the solute concentration for a conservative tracer, the Péclet number of molecular diffusion (Bear 1988,

Huysmans and Dassargues 2005) and, as shown in Normani et al. (2007), mean lifetime expectancy (MLE). Lifetime expectancy can be estimated by determining the Probability Density Function (PDF) for the time required for water particles at a spatial position in a groundwater system to reach potential outflow points. Particles can migrate to the outflow points by advection and hydrodynamic dispersion. In this case study, the first moment of the PDF for lifetime expectancy is estimated with the value being expressed as the MLE. MLE correctly replicates the transport processes, but is subject to the classical limitations of numerical instability. For a model with large grid blocks and, hence, a large numerical dispersivity that meets grid or cell Péclet number stability criteria, MLE tends to underestimate the average time for particles to reach discharge points.

2.3.3 Regional Scale Conceptual Model

2.3.3.1 Model Domain and Spatial Discretization

The reference case data set for the conceptual model consists of 32 stratigraphic units, as defined by the 3-dimensional geologic framework (3DGF) model (Table 2-2 from Itasca Canada and AECOM 2011), and the regional scale modelling domain boundary was chosen by Sykes (2007). In this postclosure safety assessment, the Niagaran Group in the 3DGF model was divided into the Guelph, Goat Island, Gasport, and Lions Head (Rochester) formations; the A-1 Carbonate unit in the 3DGF was divided into the A1-Upper Carbonate and the A1-Carbonate. Some stratigraphic units are sub-divided into multiple model layers, as shown in Table 2-9. In total, 102 model layers were developed for the regional scale domain.

Table 2-9: Sub-divisions of Geologic Formations

Period	Formation	Model Layers
Quaternary	Drift	1
Devonian	Hamilton Group	1
	Dundee	2
	Detroit River Group	6
	Bois Blanc	1
Silurian	Bass Islands	2
	Unit G	1
	Unit F	1
	Unit F Salt	1
	Unit E	1
	Unit D	1
	Units B and C	4
	Unit B Anhydrite	2
	Unit A-2 Carbonate	6
	Unit A-2 Evaporite	6
	Unit A-1 Upper Carbonate	6
	Unit A-1 Carbonate	6
	Unit A-1 Evaporite	4
	Unit A0	4
	Guelph	6
	Goat Island	2
	Gasport	2
	Lions Head/Rochester	2
	Reynales/Fossil Hill	1
	Cabot Head	1
Manitoulin	1	
Ordovician	Queenston	2
	Georgian Bay/Blue Mtn.	3
	Cobourg	1
	Sherman Fall	1
	Kirkfield	1
	Coboconk	1
	Gull River	1
	Shadow Lake	4
Cambrian	Cambrian	6
Precambrian	Upper Precambrian	4
	Precambrian	6

A two-dimensional square grid (1 km × 1 km) was developed to fit within the regional model boundary. The grid has an east-west extent of 152 km, a north-south extent of 179 km, and covers an area of 18,887 km². The two-dimensional grid forms a horizontal template to develop the three-dimensional grid by interpolating the vertical position of each node from the 32 interfaces provided by Itasca Canada and AECOM (2011). Four additional interfaces are generated by the refinement of both the Niagaran Group and the A-1 Carbonate.

A block-cut view of the assigned HGS geologic layer zone identifiers within the model domain is shown in Figure 2-10. Each zone identifier is associated with a specific geologic layer or geologic grouping. Note that the vertical exaggeration is 40:1 in this and other figures showing the regional scale spatial domain (152 km × 179 km). A view of all geologic units and the spatial variation in their thickness is shown in Figure 2-11. The inset block in the Cobourg represents a 20 km x 20 km area around the hypothetical site.

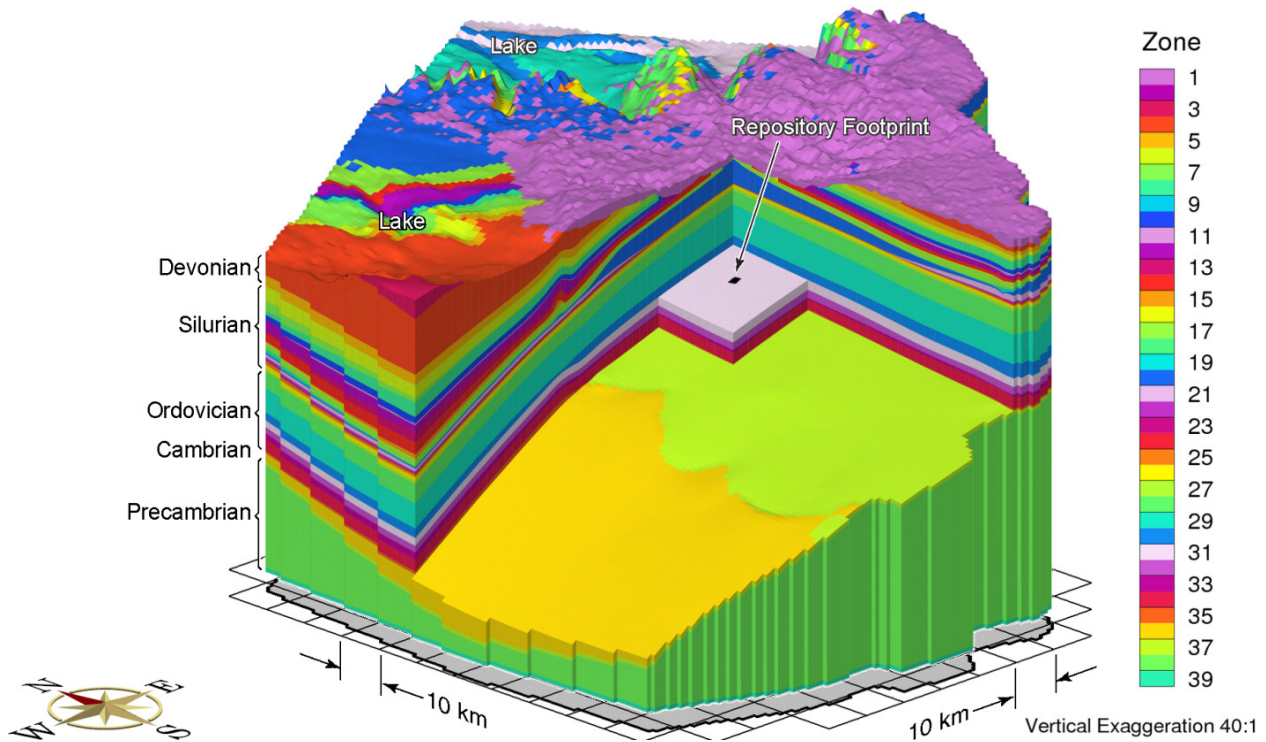


Figure 2-10: Block Cut View of HGS Zone Identifiers for Regional Scale Domain

2.3.3.2 Model Parameters

The physical hydrogeological parameters defined in this section are applied to the regional scale numerical models. All groundwater flow parameters summarized in Table 2-2 are consistent with parameters used for regional modelling for the OPG Low and Intermediate Level Waste Deep Geologic Repository (Sykes et al. 2011). For the scenario with a Biot coefficient of 0.5, alternate computed loading efficiency and specific storage values for each geologic unit are listed in Table 2-10.

2.3.3.2.1 Hydraulic Conductivity of Permafrost

For paleohydrogeologic simulations, the interpolated permafrost depths from the Glacial Systems Model (GSM) simulations (Peltier 2011, Stuhne and Peltier 2015) were used to select any HGS grid block whose top face was within the permafrost zone for each time step. A detailed description of selected paleoclimate simulations is discussed in Section 2.3.4.3. A permafrost hydraulic conductivity of 5×10^{-11} m/s is applied (McCauley et al. 2002). Permafrost within a grid block would limit vertical flow in and out of the groundwater system due to its very low effective hydraulic conductivity.

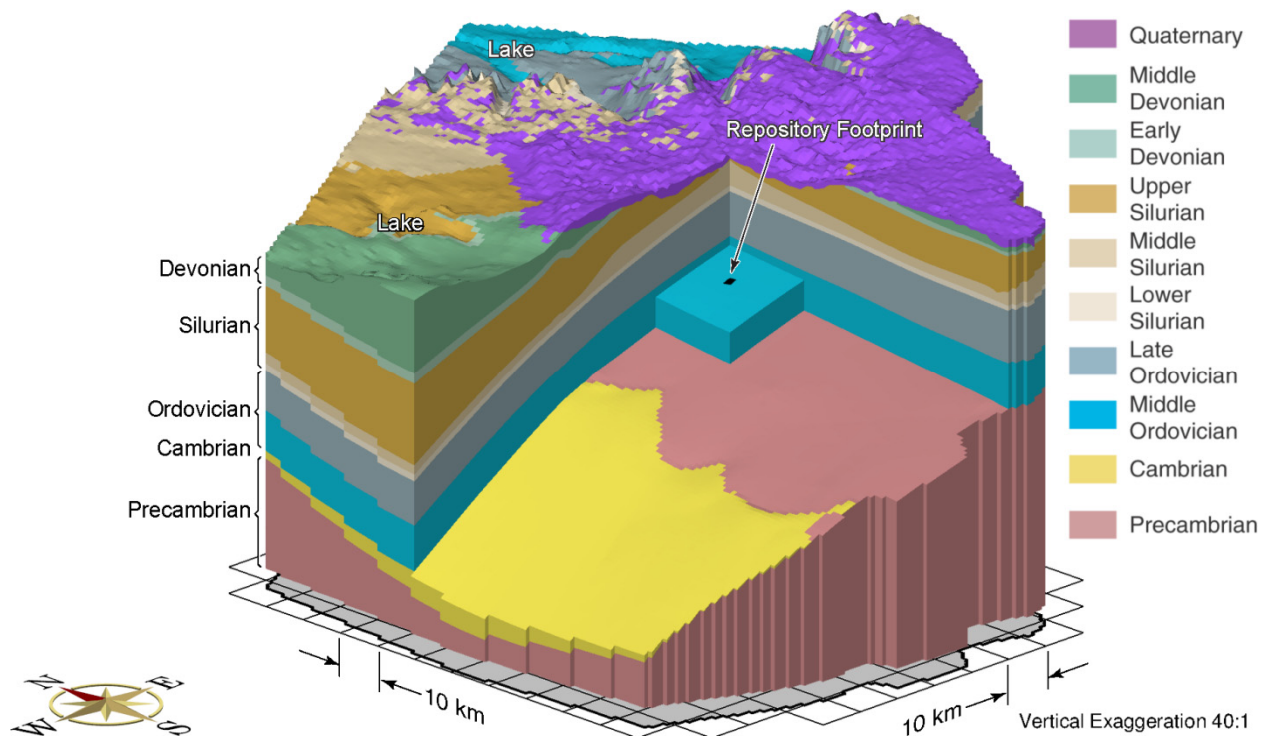


Figure 2-11: Block Cut View Showing Spatial Extent of the Bedrock Units

2.3.3.2.2 Precambrian Hydraulic Conductivity

Horizontal and vertical permeabilities for the Precambrian units, as a function of depth, are expressed following Normani (2009), as determined for data from various Canadian field studies at the Whiteshell Research Area (WRA):

$$k_H = 10^{-14.5-4.5(1-e^{-0.002469d})} \quad (2-1)$$

$$k_V = \begin{cases} 10k_H, & \text{for } d \leq 300 \text{ m;} \\ [0.09(400 - d) + 1]k_H, & \text{for } 300 < d \leq 400 \text{ m;} \\ k_H, & \text{for } d > 400 \text{ m.} \end{cases} \quad (2-2)$$

where k_H is the horizontal permeability (L^2);
 k_V is the vertical permeability (L^2); and
 d is the depth relative to a constant reference elevation of 176 m for the top of the Precambrian (L).

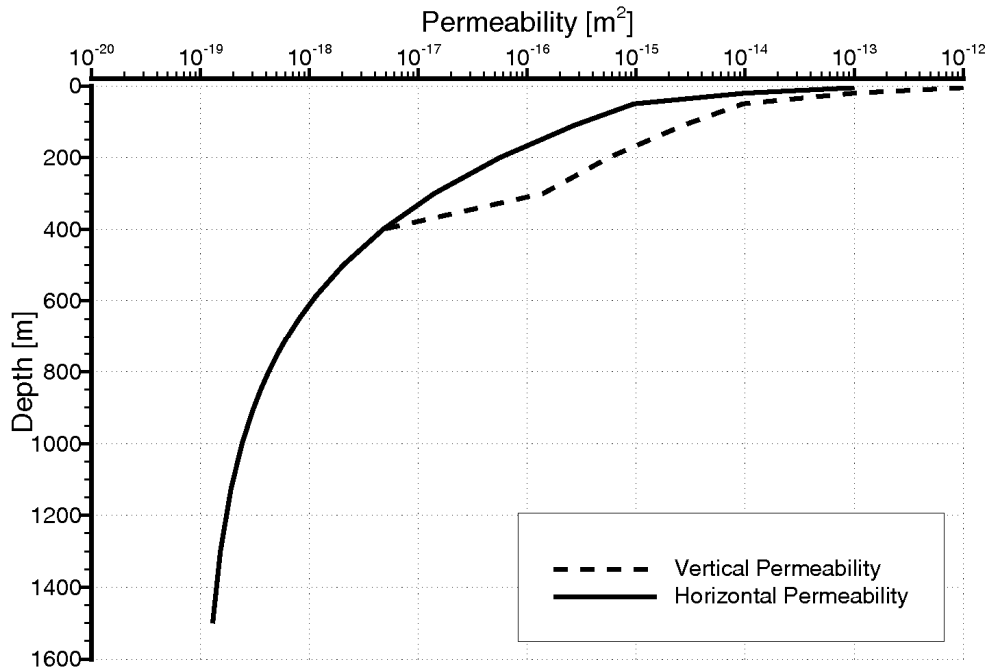
As shown in Figure 2-12, the matrix permeabilities decrease exponentially with increasing depth.

2.3.3.2.3 Groundwater Transport Parameters

Table 2-2 lists various transport parameters that are used to simulate the movement of variably dense pore fluids, for tracer movement to determine the depth of recharge water penetration, and for mean life expectancy calculations. The large grid spacing used for the regional scale domain necessitates relatively large dispersivity values employed in the modelling phase of this study to maintain numerically stable results. The impact of increasing dispersivity values is discussed in Section 2.3.3.5. The dispersivity values used for MLE calculations are triple the values listed in Table 2-11.

Table 2-10: Loading Efficiency (ζ) and Specific Storage (S_s) for Scenario (fr-base-paleo-biot05) with a Biot Coefficient of 0.5

Formation	S_s (m^{-1})	ζ
Drift	9.9×10^{-5}	0.99
Hamilton Group	1.1×10^{-6}	0.54
Dundee	1.1×10^{-6}	0.54
Detroit River Group	1.0×10^{-6}	0.56
Bois Blanc	1.0×10^{-6}	0.56
Bass Islands	1.3×10^{-6}	0.71
Unit G	8.7×10^{-7}	0.36
Unit F	7.2×10^{-7}	0.45
Unit F Salt	7.2×10^{-7}	0.45
Unit E	5.1×10^{-7}	0.32
Unit D	4.9×10^{-7}	0.35
Unit B and C	7.7×10^{-7}	0.24
Unit B Anhydrite	5.3×10^{-7}	0.35
Unit A-2 Carbonate	5.7×10^{-7}	0.29
Unit A-2 Evaporite	4.5×10^{-7}	0.35
Unit A-1 Upper Carbonate	3.9×10^{-7}	0.39
Unit A-1 Carbonate	2.8×10^{-7}	0.62
Unit A-1 Evaporite	2.6×10^{-7}	0.71
Unit A0	3.5×10^{-7}	0.54
Guelph	3.1×10^{-7}	0.30
Goat Island	1.8×10^{-7}	0.51
Gasport	1.8×10^{-7}	0.51
Lions Head	2.1×10^{-7}	0.42
Rochester	2.1×10^{-7}	0.42
Reynales/Fossil Hill	2.1×10^{-7}	0.42
Cabot Head	7.7×10^{-7}	0.41
Manitoulin	5.1×10^{-7}	0.63
Queenston	6.4×10^{-7}	0.50
Georgian Bay/Blue Mountain	8.0×10^{-7}	0.58
Cobourg	1.8×10^{-7}	0.58
Sherman Fall	3.7×10^{-7}	0.59
Kirkfield	3.8×10^{-7}	0.56
Coboconk	3.4×10^{-7}	0.62
Gull River	3.7×10^{-7}	0.56
Shadow Lake	5.9×10^{-7}	0.35
Cambrian	3.2×10^{-7}	0.19
Upper Precambrian	2.2×10^{-7}	0.29
Precambrian	1.1×10^{-7}	0.60



Note: Figure from Normani (2009). Depth is relative to a constant reference elevation of 176 m (elevation of Lake Huron) for the top of the Precambrian.

Figure 2-12: Precambrian Horizontal and Vertical Matrix Permeabilities as a Function of Depth

Table 2-11: Groundwater Transport Parameters

Parameter	Value	Reference
Brine diffusion coefficient	1.484×10 ⁻⁹ m ² /s	Weast (1983, p. F-46)
Tracer diffusion coefficient	2.66×10 ⁻⁹ m ² /s	Singh and Kumar (2005, p. 37)
Longitudinal dispersivity	500 m	
Horizontal transverse dispersivity	50 m	
Vertical transverse dispersivity	5 m	

2.3.3.3 Flow Boundary Conditions

For the solution of the groundwater flow equation, a specified head (Dirichlet) boundary condition is applied to all surface nodes to set the water table 3 m below ground surface, regardless of streams or other inland water bodies such as lakes or wetlands, but not less than the elevation of the larger lakes which were set to a mean water elevation of 176 m. Zero flux boundary conditions are applied to both the lateral and bottom boundaries of the modelling domain. Based on results of sensitivity analyses conducted by Sykes et al. (2011) for a regional modelling domain of similar lateral extent, the assigned lateral and bottom boundary conditions

are not expected to affect rates of mass transport at the location of the proposed repository. For simulations involving coupled density-dependent flow and transport of brine, a Dirichlet boundary condition equal to the TDS value at the bottom of the modelling domain is applied to all bottom nodes and a mixed (Cauchy) boundary condition with zero concentration for recharging waters is applied to all surface nodes.

A tracer representing recharge waters is used in the paleohydrogeologic simulations and its boundary conditions are set to zero concentration for all bottom nodes and a concentration of unity using a Cauchy boundary condition for all surface nodes. Lateral boundary conditions for both brine and tracer transport are zero-gradient.

2.3.3.4 Initial Conditions and Solution of Density-Dependent Flow

Salinity plays an important role with regard to fluid flow at depth. An increase in the concentration of TDS with depth results in an increase in the fluid density with depth, which will then act as an inhibitor of active flow at depth (Park et al. 2009).

While the HGS code is capable of solving flow and transport in variably-dense systems, an important modelling question is the initial salinity profile in the model. This is not a trivial question, as the geosphere is essentially in a slow but nonetheless transient situation with respect to salinity so there is not an obvious steady-state initial condition. And there is not sufficient data to fully characterize the current conditions as model input. The method for developing the initial model solution for density-dependent flow analyses is described in the following paragraphs.

Essentially, a transient analysis is required to determine a self-consistent quasi-equilibrium solution that represents an initial state for subsequent analysis. The analysis requires the specification of an initial approximate distribution throughout the spatial domain for both freshwater heads and total dissolved solids concentrations. In the transient analysis, the initial prescribed salinity distribution is allowed to equilibrate to a new self-consistent state that reflects the boundary conditions, hydraulic properties and transport properties of the regional scale domain. For the coupled density-dependent flow and transport system, fresh water can recharge at the surface, reducing the TDS concentration in the shallow groundwater system. For low-permeability regions with a relatively high total dissolved solids concentration, the time to flush the region or displace the fluids can be very long (i.e., millions of years). With this approach, as time progresses, the dissolved solids will gradually decrease as the groundwater discharges from the system. However this is a slow process, and the transient analysis yields a quasi-equilibrium state that represents current conditions.

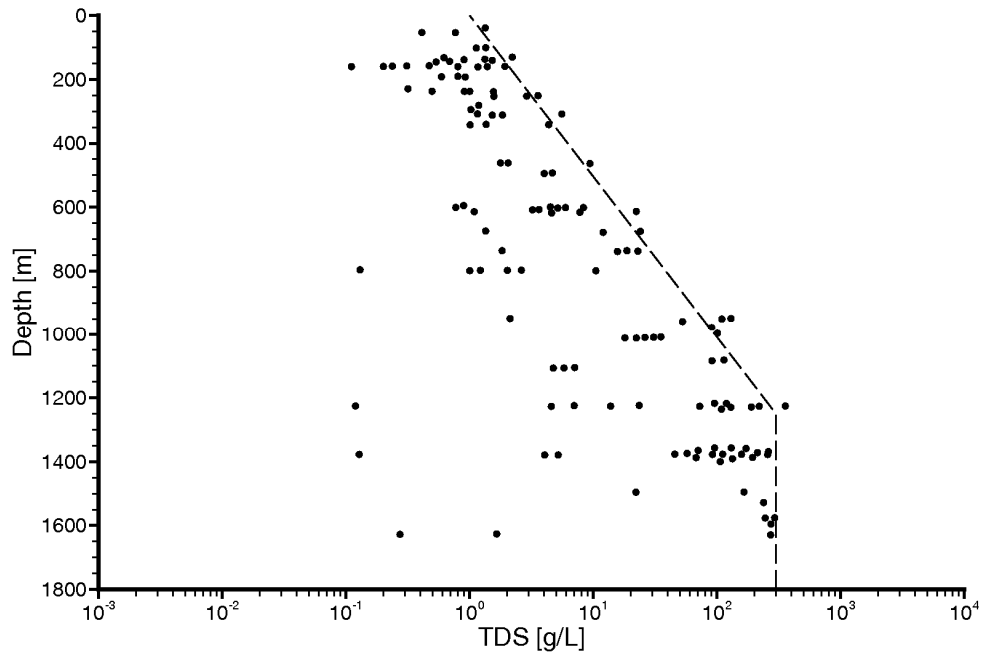
The initial condition for total dissolved solids must specify concentrations for all lithologies at all locations in the regional scale domain. Field data are not available for the spatial distribution of TDS in the shallow low permeability units, such as the Queenston shale where it outcrops, or for the spatial distribution in the deeper units. The values from Table 2-2 for a given lithology were assigned to all areas of the spatial domain assigned to that zone. For the model zones representing the Precambrian, a depth-dependent initial TDS distribution was determined using the data described by the dashed line in Figure 2-13, and represented by Equation 2-3, where *TDS* is in units of g/L.

$$TDS = \begin{cases} 10^{0.001981697d}, & \text{for } d \leq 1250 \text{ m;} \\ 300, & \text{for } d > 1250 \text{ m.} \end{cases} \quad (2-3)$$

The depth, d , is the depth relative to a constant reference elevation of 176 m for the top of the Precambrian; there is no Precambrian above this elevation in the regional scale domain. If the concentration from the dashed line in Figure 2-13 at a given depth was lower than that assigned to the lowest sedimentary rock at the location (Shadow Lake or Cambrian sandstone, where present), the higher zone TDS concentration was assigned. The initial TDS distribution developed for this study is shown in block-cut view in Figure 2-14. A linear relationship is assumed between fluid density and TDS such that a fluid density of 1200 kg/m³ is equal to 300 g/L. Further discussion of the linear relationship between fluid density and TDS can be found in Normani et al. (2007).

For this study, the final freshwater head distribution for the reference case analysis was calculated using the following three-step process:

1. The steady-state solution was calculated for a density-independent groundwater flow system;
2. The total dissolved solids concentration distribution in Figure 2-14 was assigned throughout the domain as an initial condition using the procedure described in the preceding paragraph. The density-independent freshwater heads were allowed to equilibrate to the assigned TDS distribution in a transient analysis, while fixing the TDS distribution;
3. A further transient analysis was performed to allow evolution of the TDS distribution over a one million year time interval.



Note: Figure adapted from Figure 2b in Frappe and Fritz (1987). Depth is relative to a constant reference elevation of 176 m (elevation of Lake Huron) for the top of the Precambrian.

Figure 2-13: Plot of TDS versus Depth for Groundwater from the Canadian Shield

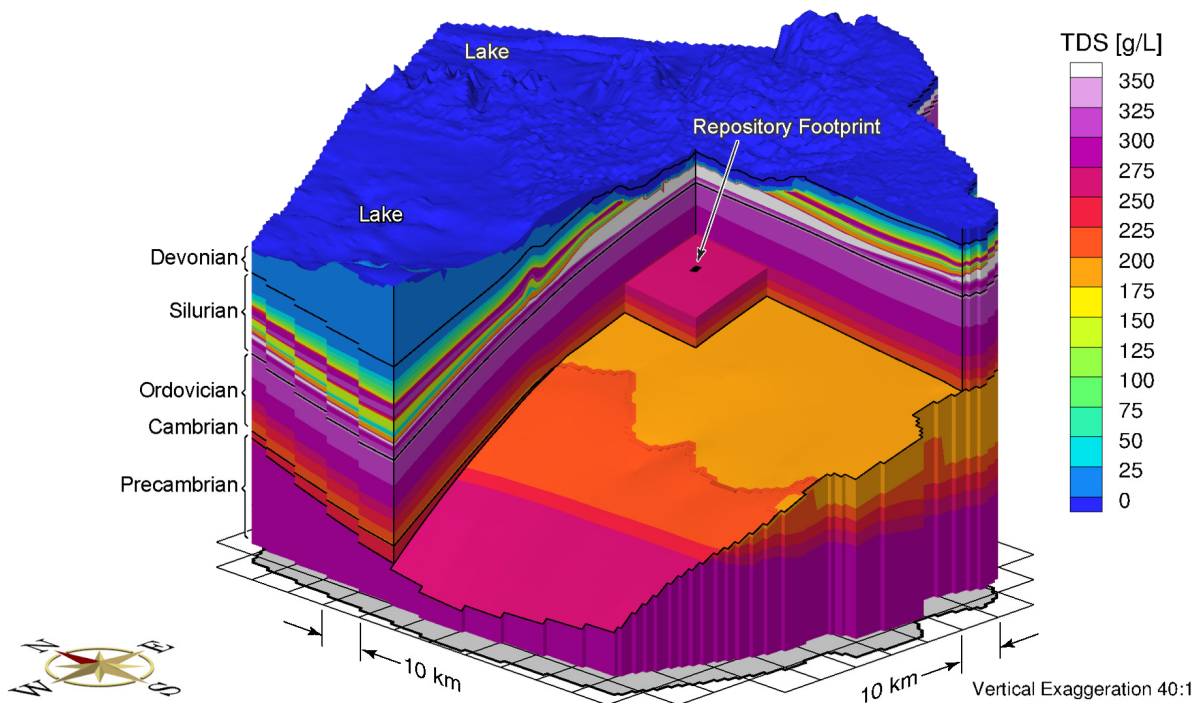


Figure 2-14: Block Cut View of Initial Total Dissolved Solids Concentration Distribution

After one million years, the model, having been allowed to reach pseudo-equilibrium between freshwater heads and TDS distribution, produces a salinity distribution that is compatible with the boundary conditions, geochemical framework and, hence, the flow domain. Generally, pseudo-equilibrium is reached when the model TDS reasonably matches field measurements (for detailed discussion, see Normani 2009). Note that in this study, no field data were available for comparison. In recharge areas, brine will be flushed because of a combination of the absence of a source term for brine and the effect of meteoric recharge. This is contrasted with discharge locations, which tend to transport higher concentration brines from deeper in the groundwater system. Both the freshwater heads and brine concentrations at one million years are used as the initial conditions for the paleohydrogeologic simulations.

2.3.3.5 Model Uncertainties and Sensitivities

Uncertainty is unavoidable and inherent to groundwater models, due to uncertain estimates of model parameter values. System performance measures, such as mean life expectancies, porewater velocities, Péclet number, and recharge water tracer migration, are related to model parameters through the governing equations describing groundwater flow and solute transport. As such, model parameter bounding scenarios are used in this study to investigate groundwater system behaviour.

In addition to the regional scale reference case analysis, two temperate sensitivity cases were developed. An increase in fluid density by salinity tends to retard groundwater flow at depth (Park et al. 2009). The regional scale reference scenario accounts for pore fluid density effects by assuming a linear relationship between fluid density and salinity, expressed as TDS. A conservative bounding case regarding pore fluid density is represented by a steady-state freshwater groundwater flow simulation. The second sensitivity case included enhanced hydraulic conductivities of one order of magnitude to evaluate the impact of enhanced advection on the system performance measures. Additionally, a conservative bounding case was simulated by increasing hydraulic conductivities by three orders of magnitude (see Section 2.3.5).

In terms of paleohydrogeologic simulations, additional uncertain model parameters include alternative paleoclimate simulations, surface boundary conditions, one-dimensional loading efficiencies and Biot coefficients. In addition to the warm-based paleoclimate simulation used for the paleohydrogeologic Reference Case, an alternative cold-based paleoclimate simulation includes greater permafrost extent and more frequent glacial episodes. A third paleoclimate simulation provides for nearly continuous ice-sheet coverage. The bounding scenarios for surface hydraulic boundary conditions are either 100% of ice-sheet thickness expressed as equivalent freshwater head or a free draining surface boundary condition. The impacts of no hydro-mechanical coupling and full hydro-mechanical coupling were investigated by setting the one-dimensional loading efficiencies to zero and unity, respectively. Incompressible mineral grains are assumed for the reference paleohydrogeologic scenario, resulting in a Biot coefficient of 1.0. To investigate the effects of compressible mineral grains, an alternative Biot coefficient of 0.5 is assumed for all lithologic layers. The resulting changes to both specific storage and loading efficiency are listed in Table 2-10.

2.3.4 Regional Scale Analyses

2.3.4.1 Reference Case Simulation

As described in Section 2.3.3.4, the Reference Case is comprised of a three-step simulation procedure: steady-state freshwater groundwater flow, transient groundwater flow equilibrated to a static TDS distribution, and a transient groundwater and salinity simulation for one million years. The pseudo-equilibrium result at one million years is taken to represent the present day state of the density-dependent groundwater flow system, i.e. the Reference Case initial condition.

The steady-state freshwater head distribution, as a block-cut view, is shown in Figure 2-15. The freshwater steady-state heads shown are calculated without the influence of density. The freshwater heads for the shallow groundwater regime above the Salina Formation (within the Silurian) are dominated by the prescribed Dirichlet boundary condition representing local topography. Beneath the shallow groundwater zone, the heads are not controlled to the same extent by local topography.

The equivalent freshwater heads at the pseudo-equilibrium time are shown in Figure 2-16. For a density-dependent flow system, freshwater heads increase with an increase in fluid density and include the effects of both topographic and density gradients. However, the plot of freshwater heads can only be used to interpret horizontal head gradients, not vertical gradients. The main control for the horizontal head gradients at depth is the elevation difference between the lakes and the topographic high at the escarpment.

The distribution of total dissolved solids at the pseudo-equilibrium time is shown in Figure 2-17. Meteoric water recharging into the shallow groundwater zone above the Salina will dilute any salinity that diffuses upward through the Silurian or Ordovician formations, resulting in relatively fresh groundwater within the shallow groundwater regime. High TDS concentrations for the deep groundwater zone, including the Ordovician formations and below, are attributed to the initial high TDS concentration and the low permeability layers. The TDS transitional zone occurs in the Silurian, specifically where most of the Salina units pinch out. A TDS distribution plot shown as an east-west cross-section through the hypothetical repository in Figure 2-18 clearly displays the sharp transition of TDS concentrations in the vicinity of the hypothetical repository footprint due to significantly varying lithology. Within 10 km of the hypothetical repository footprint, a total of 15 units pinch out, based on the three-dimensional regional geologic framework model (see Section 2.3.3.2). In addition, a total of 7 units pinch out west of the 20 km by 20 km inset block shown in Figure 2-11.

The Reference Case porewater velocity magnitudes at the pseudo-equilibrium time are presented in Figure 2-19. Relatively high velocities occur in the shallow groundwater zone and permeable geologic units, including the Guelph and Cambrian formations. The reduction of velocities beneath the lake in the northeastern part of the domain are the result of the absence of a horizontal gradient. The low velocities in the Salina units and the Ordovician result from the low permeability of each unit. Within the Ordovician in the vicinity of the hypothetical repository footprint, the majority of porewater velocity magnitudes are less than 1×10^{-6} m/a. For a brine diffusion coefficient of 1.484×10^{-9} m²/s and a characteristic length of 1 m, the Péclet number of molecular diffusion (Bear 1988) is less than 2.13×10^{-5} , indicating solute transport in the Ordovician is diffusion dominated.

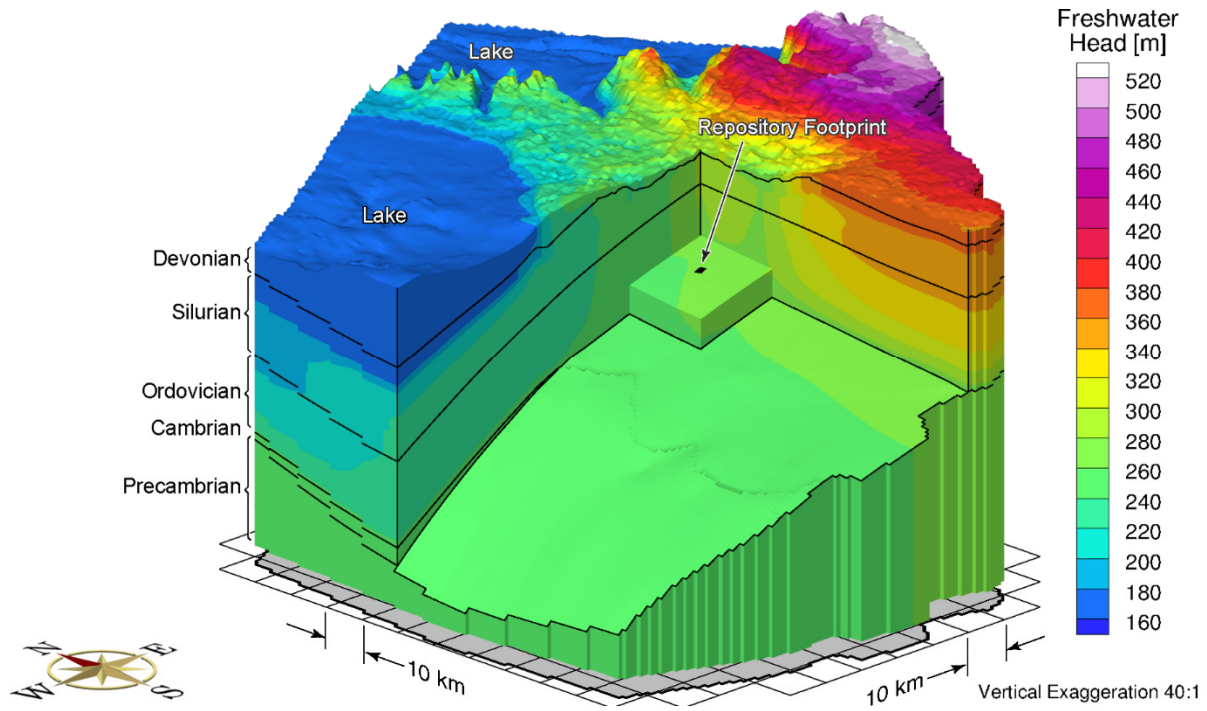


Figure 2-15: Block Cut View of Steady-State Density-Independent Freshwater Heads

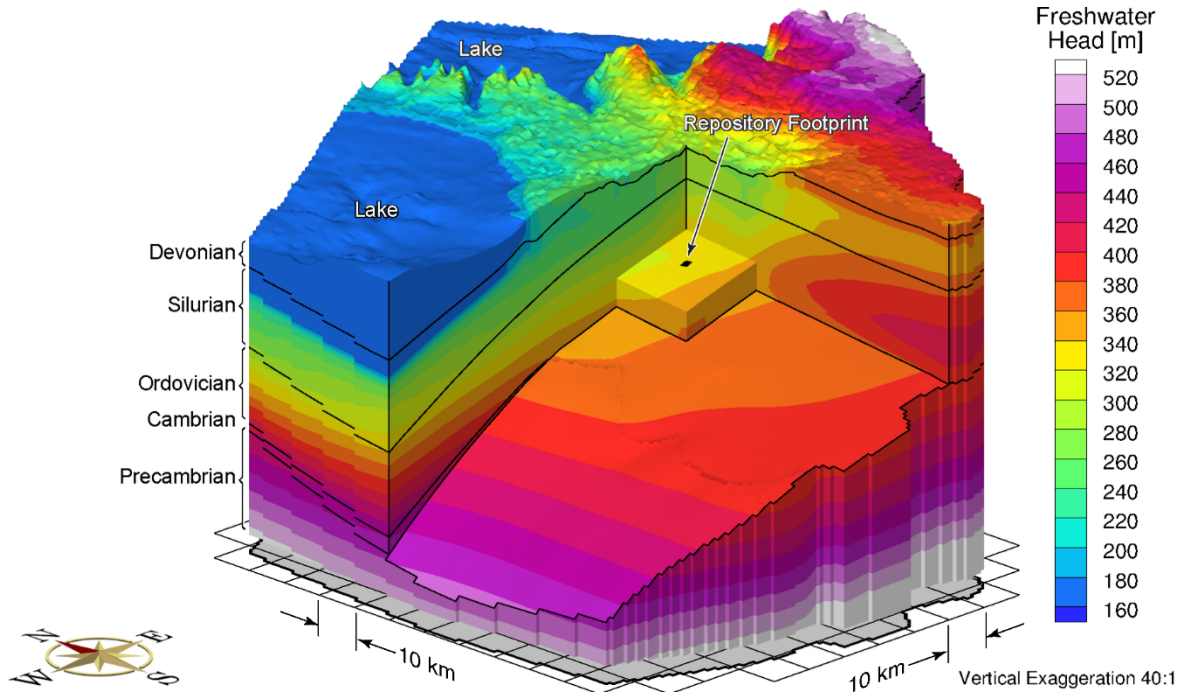


Figure 2-16: Block Cut View of Freshwater Heads at Pseudo Equilibrium Time with Temporally Varying TDS Distribution

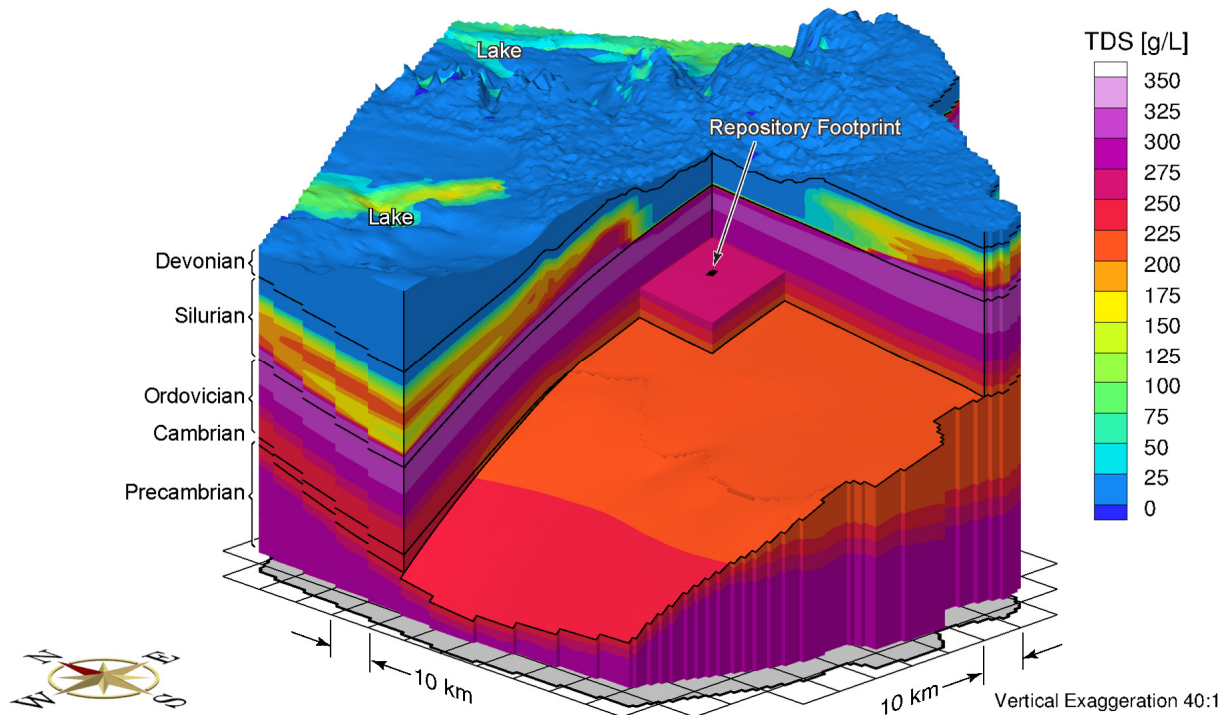


Figure 2-17: Block Cut View of Total Dissolved Solids Concentration at Pseudo Equilibrium Time with Temporally Varying TDS Distribution

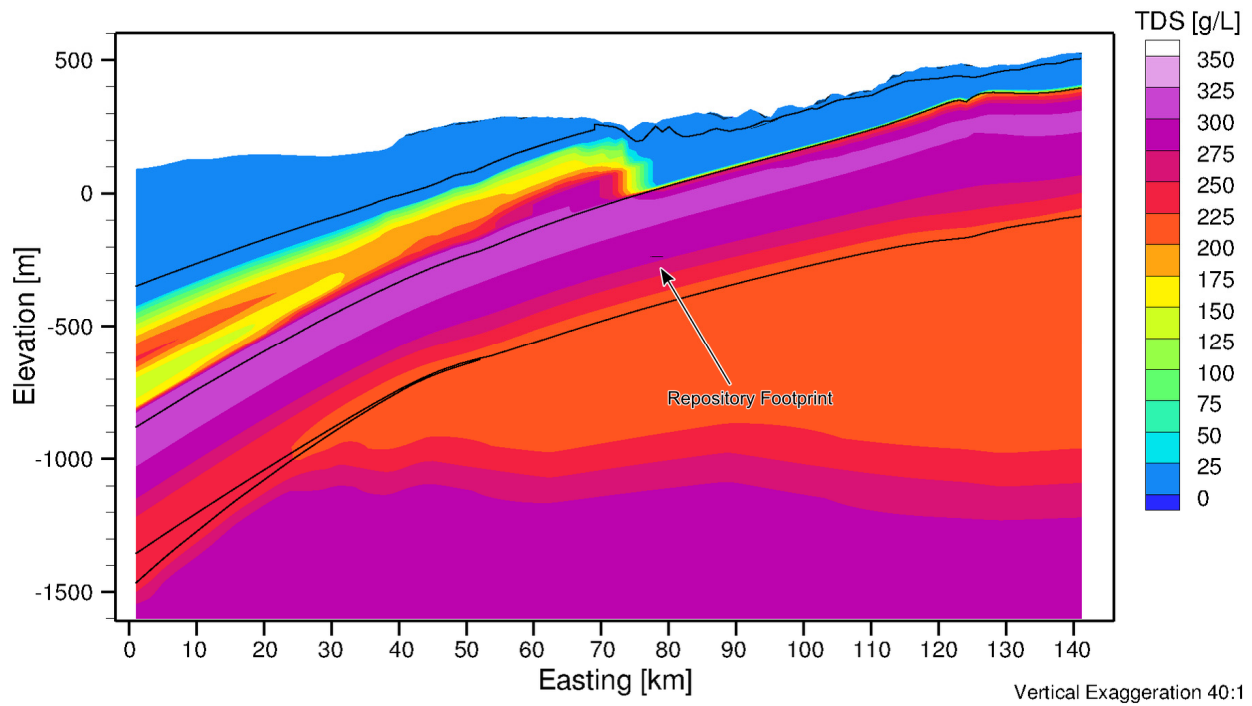


Figure 2-18: Total Dissolved Solids Concentration at Pseudo Equilibrium Time at East-West Cross-Section through the Hypothetical Repository Footprint

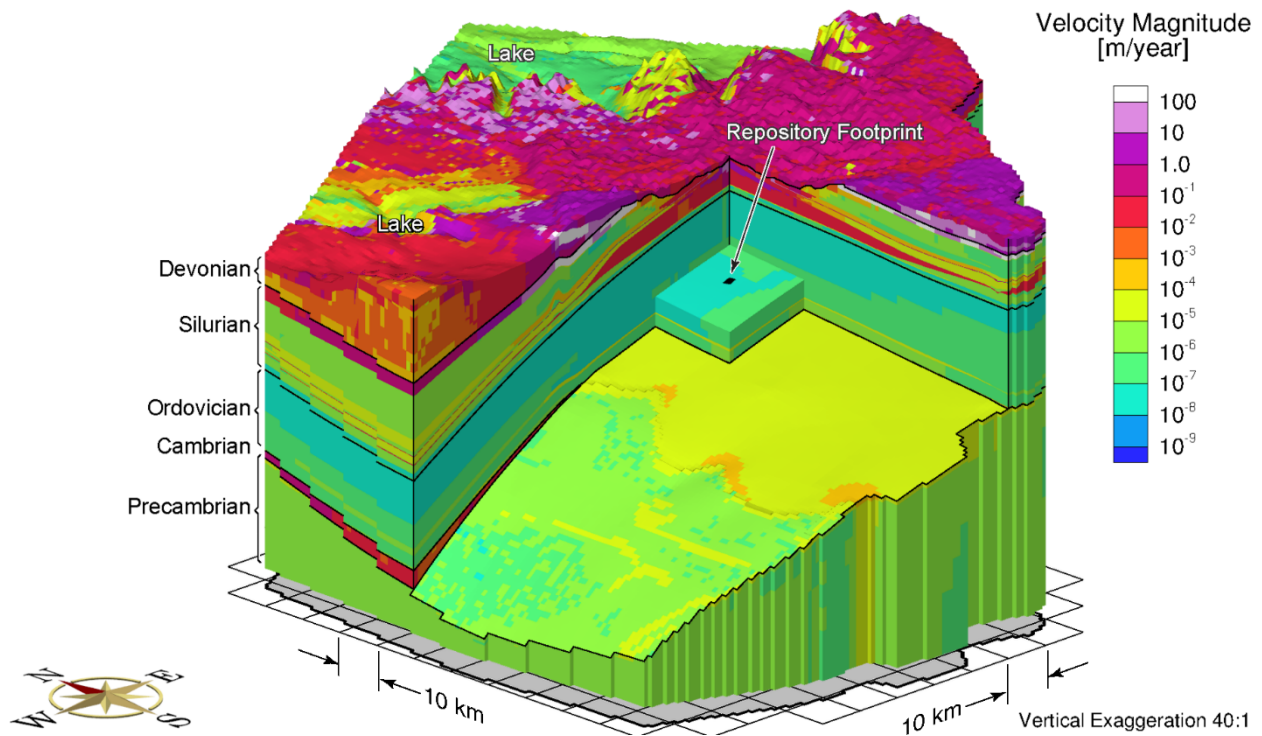


Figure 2-19: Block Cut View of Reference Case Porewater Velocity Magnitude at Pseudo Equilibrium Time

The ratio of the vertical component of velocity to velocity magnitude for the regional scale domain is shown in Figure 2-20. The figure can be used to determine the predominant direction of the calculated velocity vectors in the hydrostratigraphic units of the regional scale model. The vertical component of the velocity vector will equal the velocity magnitude only when there are no horizontal components to the velocity vector; the ratio of the vertical component of the velocity vector to the velocity magnitude will be positive 1.0 for solely upward velocity and negative 1.0 for solely downward velocity. In the figure, blue corresponds to zones where the vertically downward velocity component dominates the velocity vector, white to zones where horizontal velocity components dominate the velocity vector, and red to zones where the velocity vectors are dominated by the vertically upward component. Transition zones are evident in the figure. It is important to note that the figures cannot be used to interpret velocity magnitude; they can only be used to interpret the direction of the calculated velocity vectors at a given location. This figure should be referred to in conjunction with Figure 2-19, which shows the porewater velocity magnitudes. In the upper Precambrian, sharp transitions in flow direction over relatively short distances, in combination with low velocity magnitude, indicate stagnant flow where subtle changes in topography and total dissolved solids concentration affect the direction of the velocity vectors.

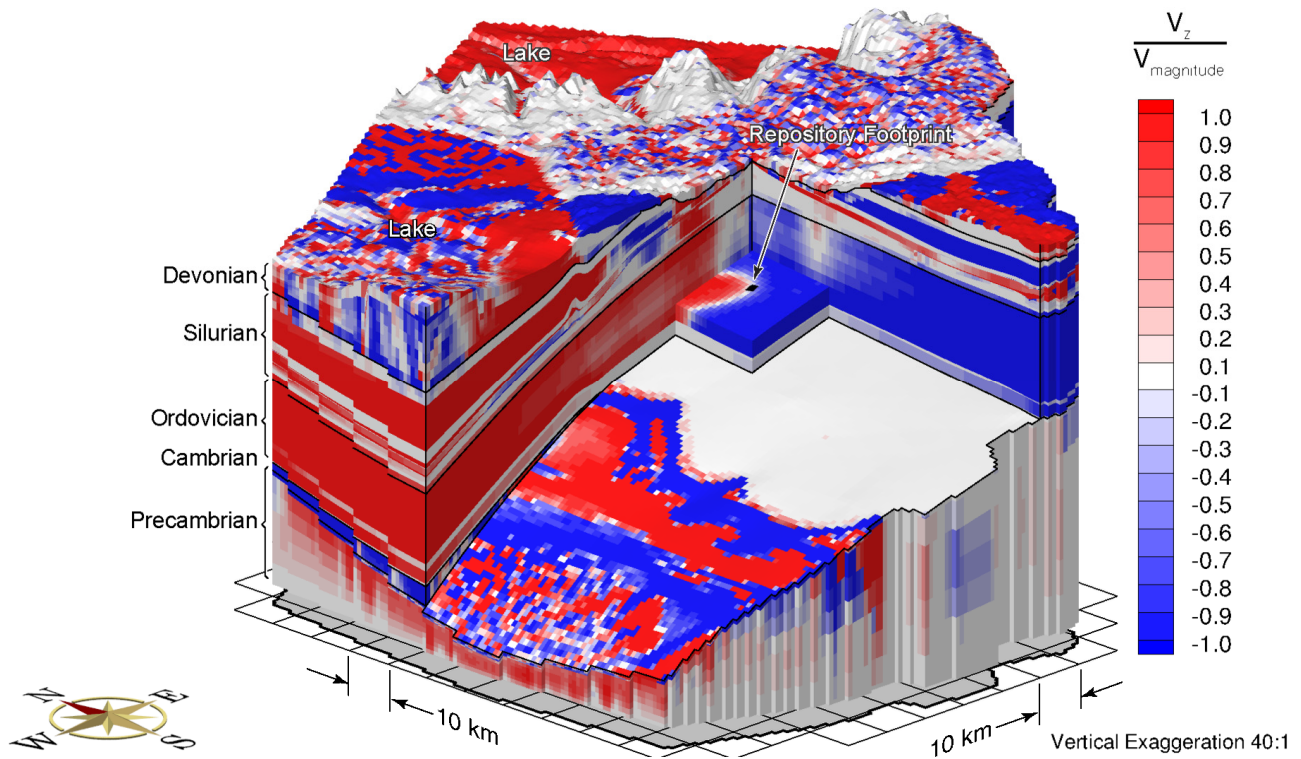


Figure 2-20: Block Cut View of Reference Case Ratio of Vertical Velocity to Velocity Magnitude at Pseudo Equilibrium Time

The performance measure selected for the evaluation of the groundwater system is mean life expectancy (MLE), as shown in Figure 2-21. The shallow groundwater zone has significantly shorter mean life expectancies compared to the deep groundwater system. The areas of recharge versus discharge can be noted in the figure as the recharge areas have high MLEs while the discharge areas have low MLEs. As a result of many geologic units pinching out, the sharp MLE transition zones in the Silurian, as shown in Figure 2-22, correspond with the behavior of the TDS distribution shown in Figure 2-18.

The MLEs in the vicinity of the hypothetical repository footprint are greater than 100 Ma for the Reference Case simulation.

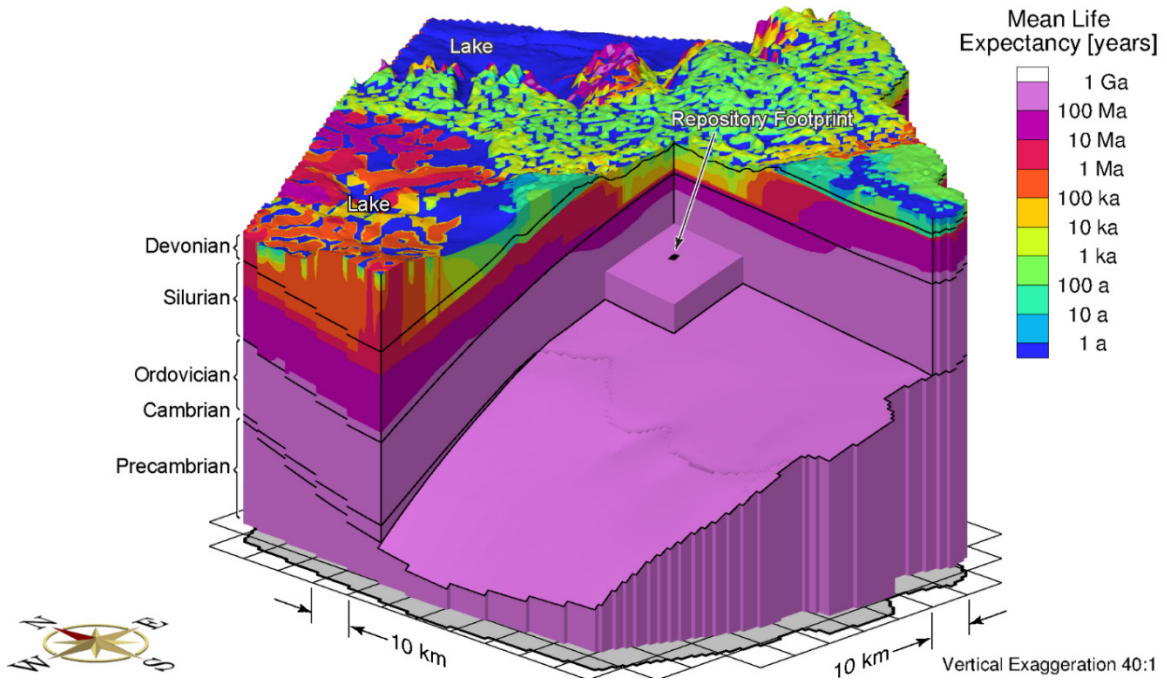


Figure 2-21: Block Cut View of Base Case Mean Life Expectancy at Pseudo Equilibrium Time

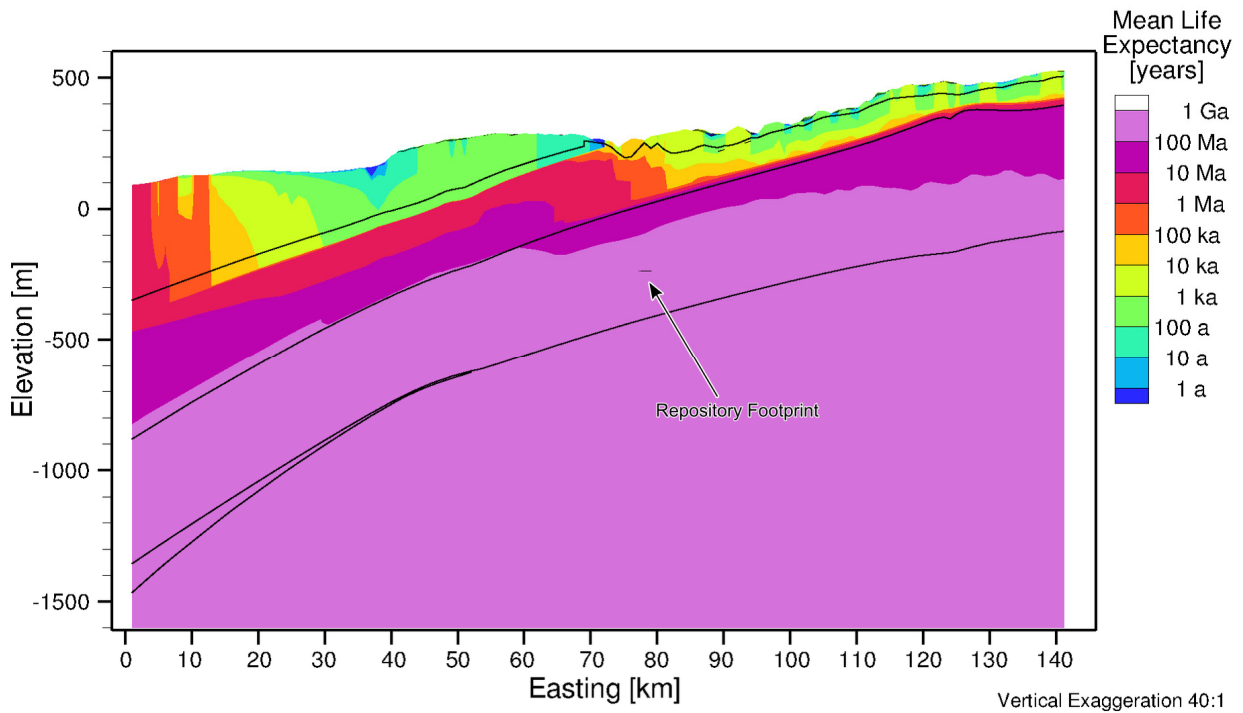


Figure 2-22: Reference Case Mean Life Expectancy at Pseudo Equilibrium Time at East-West Cross-Section through the Hypothetical Repository Footprint

2.3.4.2 Temperate Transient Sensitivity Cases

The attributes of the sensitivity cases investigated in this study are summarized in Table 2-12.

This section provides a comparison of two temperate sensitivity cases to the Reference Case. The first comparison investigates the role of fluid density between a steady-state freshwater simulation and the density-dependent Reference Case. The second comparison investigates the effects relative to the Reference Case of enhanced hydraulic conductivity on porewater velocities, TDS and MLE for all geologic units, excluding the upper 50 m of bedrock.

The effect of assuming groundwater flow is independent of density is shown by comparing porewater velocity magnitudes and mean life expectancies between a steady-state groundwater flow simulation (fr-base-nobrine) and the reference transient density-dependent flow simulation (fr-base). Figure 2-23 shows the ratio or quotient of porewater velocity magnitudes between scenarios fr-base-nobrine and fr-base on a logarithmic scale. In the figure, blue corresponds to zones where the density-independent groundwater flow from the steady-state simulation has lower velocity magnitudes than those of the Reference Case. Red zones indicate porewater velocities in the steady-state model are greater than in the density-dependent Reference Case model.

Porewater velocities are generally about the same or less without brine present; in some portions of the domain, the velocities can be slightly greater, for instance, in the close vicinity of the hypothetical repository footprint. The reduced velocities in the density-independent case are caused by the attainment of an equilibrium state, while the groundwater flow system of the Reference Case with salinity is experiencing slow evolution even after one million years of simulated time. A slight change in TDS distribution will have an impact on the magnitude and direction of porewater velocities, especially in the high permeability units.

Within the Ordovician formation containing the hypothetical repository footprint, the velocity magnitude ratio is close to unity due to the dominance of diffusive solute transport. Calculating the ratio of MLE between a steady-state freshwater system without brine and the pseudo-equilibrium transient brine simulation, as shown in Figure 2-24, shows order-of-magnitude changes across the domain. The mean life expectancies are generally similar or greater in the freshwater simulation, except for the portion beneath the lake, where the MLEs are reduced by one order of magnitude. At the location of the hypothetical repository footprint, a MLE of 183 Ma was estimated for the case of density-independent flow when compared to a MLE of 179 Ma for the Reference Case including salinity. It is non-intuitive that MLE is less in the density-independent system, as density usually retards active groundwater flow at depth and results in a smaller value of MLE. The reason lies in the fact that the groundwater movement attained in the freshwater simulation is steady-state and purely driven by topography.

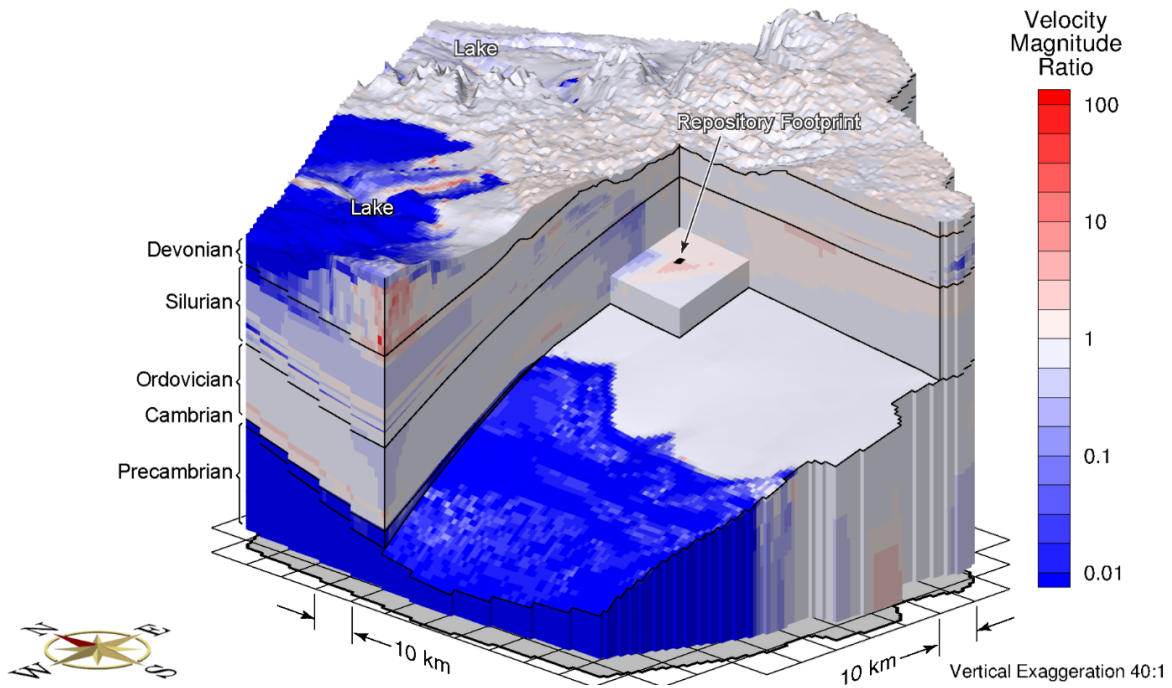


Figure 2-23: Ratio of Velocity Magnitudes of Steady-State Groundwater Flow to Density-Dependent Flow Reference Case

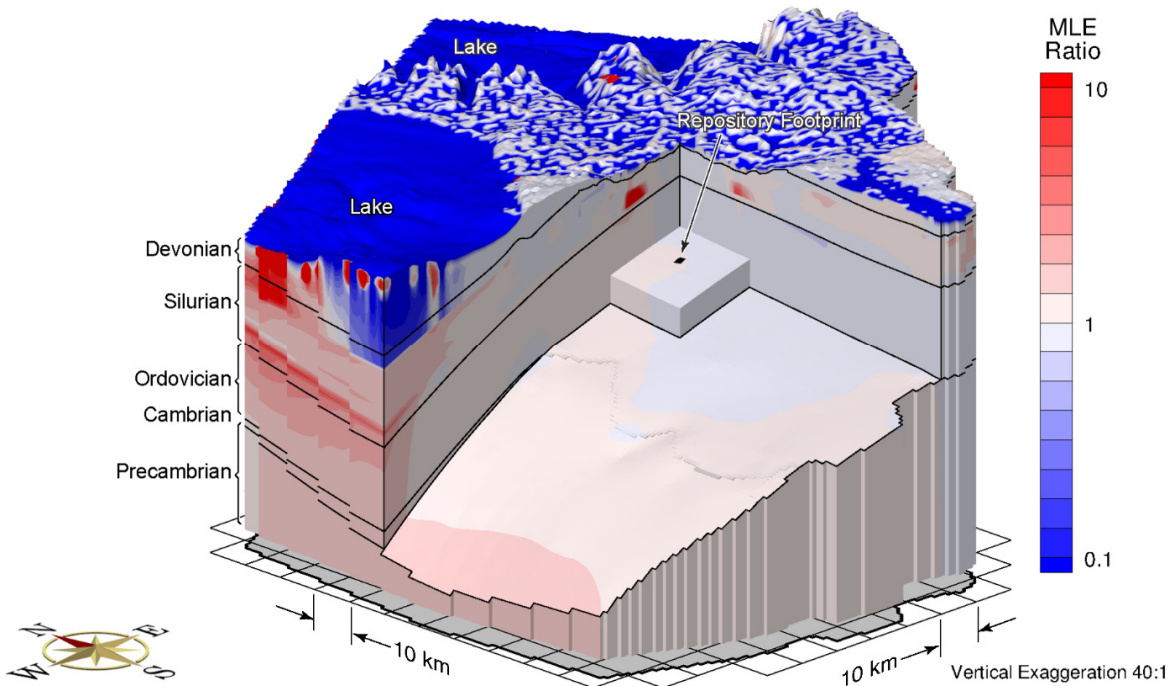


Figure 2-24: Ratio of MLEs of Steady-State Groundwater Flow to Density-Dependent Flow Reference Case

In contrast, the density-dependent solution is also affected by the evolving TDS distribution even at one million years of simulation time. In this study, the groundwater flow induced by non-equilibrated TDS gradients is more significant than the inhibition of the groundwater flow system by the density effect, which leads to a lower MLE. The relative difference in the MLE for the two cases is considered to be trivial. For a system dominated by low permeability units, the MLE is not sensitive to fluid density effects.

To investigate the effect of enhanced hydraulic conductivities on the groundwater flow system, the permeability profiles for all geologic units were increased by one order-of-magnitude, except for the upper 50 m of bedrock scenario (fr-sens). Higher hydraulic conductivities allow the groundwater system to transport TDS from the Salina group to the shallow groundwater system and then to flush the TDS from the system in a shorter period of time. Figure 2-25 shows the total dissolved solids at one million years for the sensitivity case. A comparison of the results to those of the Reference Case (fr-base), shown in Figure 2-17, reveals that the TDS concentrations in the Salina group are now much lower. The difference in freshwater heads between the sensitivity case and the Reference Case are shown in Figure 2-26. In the Silurian and below, freshwater heads are generally decreased as a result of lower TDS when compared to TDS values in the Reference Case.

The ratio of porewater velocities between the sensitivity case and the Reference Case is shown in Figure 2-27. Due to the enhancement of hydraulic conductivities, the porewater velocities are consistently greater throughout the modelling domain, excluding portions of upper layers beneath the lake. Higher hydraulic conductivities allow the groundwater system to equilibrate to a more stable state more quickly than for the Reference Case at one million years. Therefore, an increase in hydraulic conductivity by a given factor under similar hydraulic gradients will result in an increase in porewater velocities and a decrease in travel times by a similar factor. The MLE ratios shown in Figure 2-28 generally indicate a decrease in the MLE values for the sensitivity case, resulting in an MLE for the hypothetical repository of 113 Ma. At the location of the hypothetical repository footprint, the corresponding mean life expectancy for the sensitivity case decreases by a factor of 1.6, significantly less than the one order-of-magnitude increase in the hydraulic conductivities. This highly nonlinear relationship between MLE and hydraulic conductivities indicates the dominance of molecular diffusion in the transport mechanism.

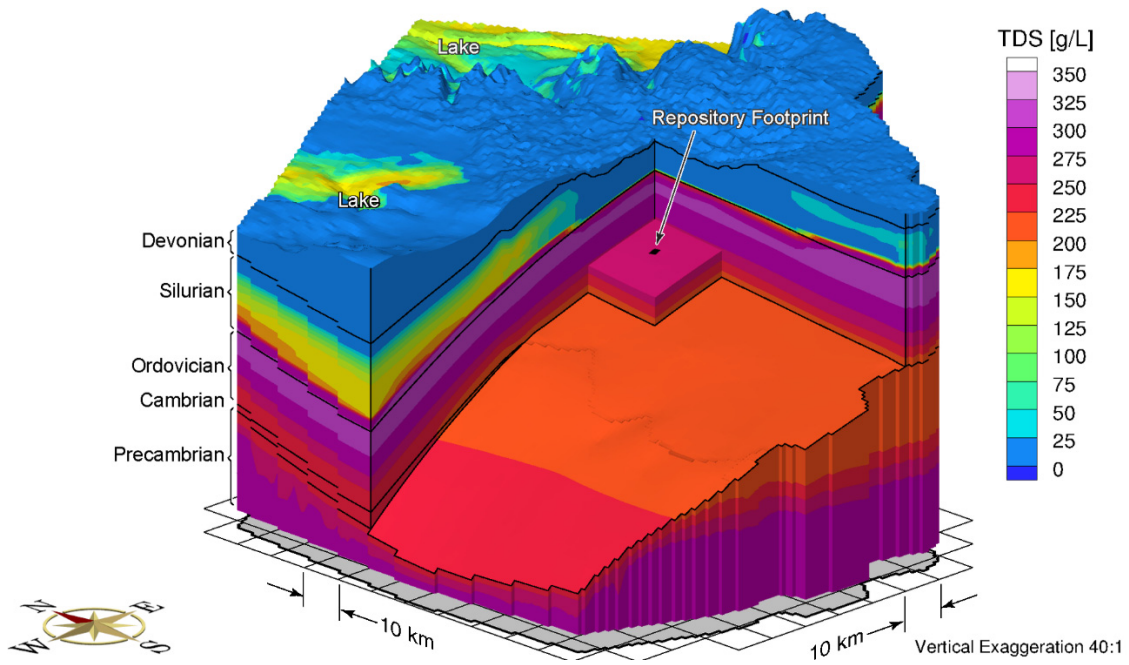


Figure 2-25: Total Dissolved Solids Concentrations at Pseudo Equilibrium Time for an Increased Rock Mass Hydraulic Conductivity

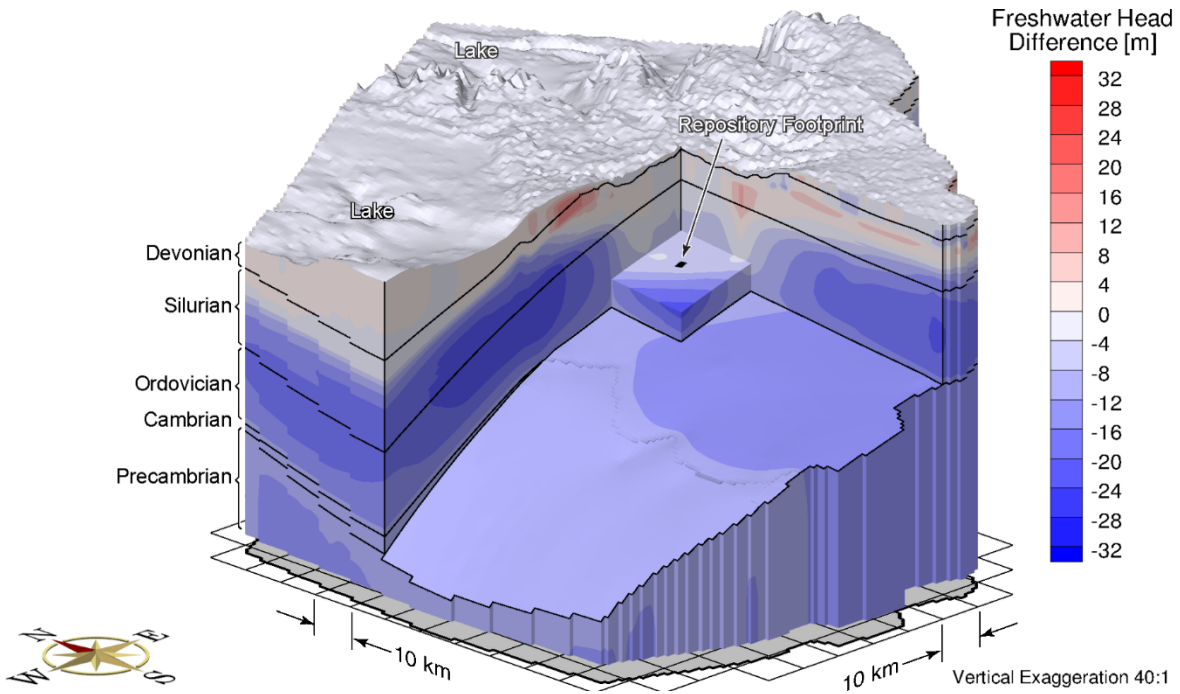


Figure 2-26: Difference in Freshwater Heads between a Simulation Using an Increased Rock Mass Hydraulic Conductivity and Reference Case

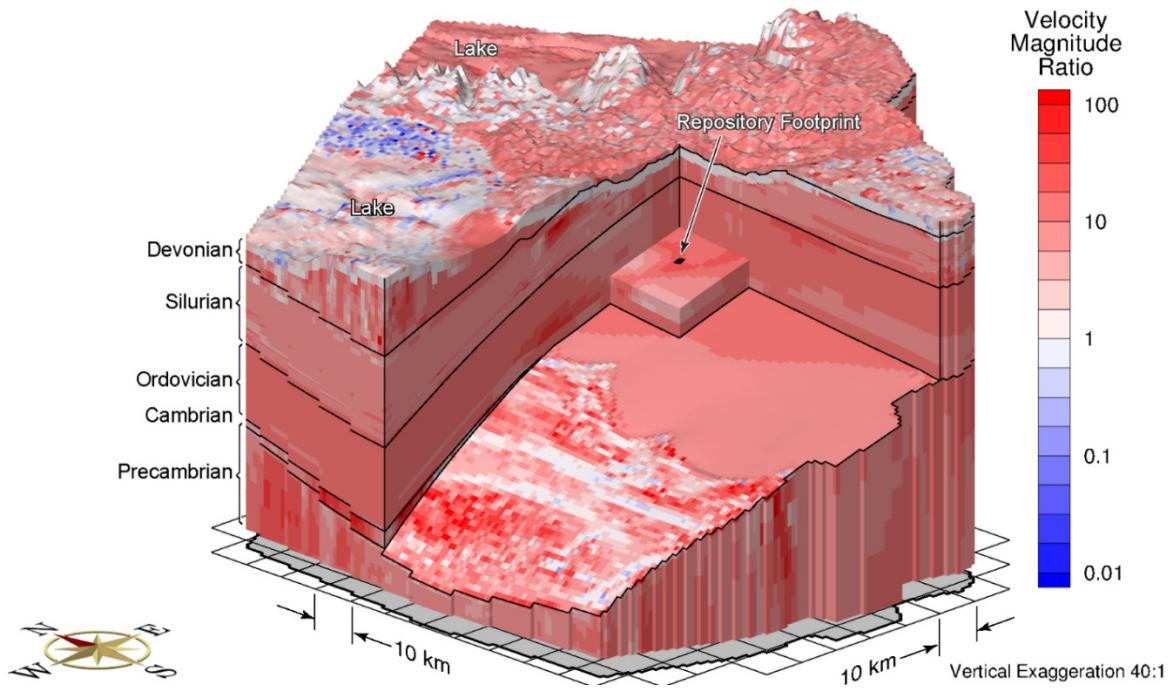


Figure 2-27: Ratio of Pore Velocity Magnitudes of Sensitivity Case using an Increased Rock Mass Hydraulic Conductivity to Reference Case

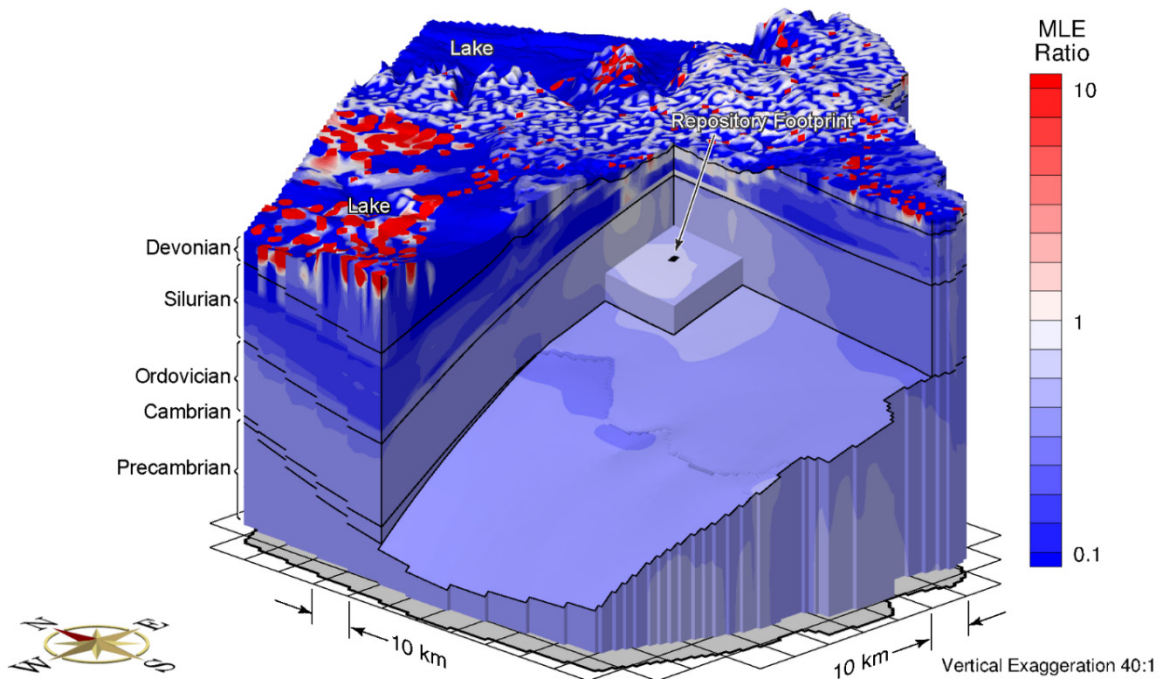


Figure 2-28: MLE Ratio of Increased Rock Mass Hydraulic Conductivities Simulation to Reference Case Simulation

2.3.4.3 Paleohydrogeologic Sensitivity Cases

A total of twelve paleohydrogeologic simulations were performed to investigate the role of varying paleoclimate boundary conditions and the characterization of hydro-mechanical coupling. These simulations are summarized in Table 2-12.

The Reference Case model (fr-base) is used as the basis for all simulations and the initial conditions for both freshwater heads and brine distribution come from the transient brine simulation at one million years, as described in Section 2.3.3.4 (the pseudo-equilibrium time).

A conservative tracer of unit concentration is applied as a Cauchy boundary condition at the top surface of the model domain. This tracer represents the migration of recharge water, including glacial meltwater, which occurs during a paleohydrogeologic simulation. The tracer migration at 120,000 years for the Reference Case simulation (fr-base-paleo) is shown in Figure 2-29. The 5% isochlor is considered conservative because it represents a pore fluid containing 5% recharge water and provides an indication of recharge water migration into the subsurface. For the Reference Case, the 5% isochlor migrates to the top of the Ordovician in the vicinity of the hypothetical repository footprint. The model units in the Salina and the Ordovician are of comparatively low hydraulic conductivity and tend to retard the downward advective migration of the tracer, which indicates that diffusion is the dominant transport mechanism. Furthermore, Figure 2-30 shows the tracer concentration with depth at the location of the hypothetical repository footprint. Tracer penetration depth can be determined by the intersection of tracer concentration with a vertical line representing the 5% isochlor concentration. All paleohydrogeologic simulations are plotted on the same figure for comparison. The tracer concentrations do not reach formations below the Queenston in any of the paleoclimate scenarios.

To apply the same logic as the temperate transient sensitivity cases, the analysis of a no density scenario (fr-base-paleo-nobrine) in Table 2-12 investigates the impact of assuming that groundwater flow is independent of density. Additionally, the impact of enhanced hydraulic conductivities on the groundwater flow system (fr-base-paleo-sens) is investigated by increasing the permeability profiles for all the geologic units by one order-of-magnitude, except for the upper 50 m of bedrock. The initial conditions for these two simulations are from the density-independent steady-state and enhanced hydraulic conductivities sensitivity case simulations, respectively. The importance of fluid density and enhanced hydraulic conductivities in affecting the groundwater flow system is revealed in a comparison of the results obtained from these scenarios with the Reference Case (see Figure 2-30). The increase in density of the deeper fluids will act as an inhibitor of active flow at depth (Park et al. 2009); higher hydraulic conductivity leads to deeper tracer migration, as confirmed by Figure 2-30 which shows slightly higher tracer concentration profiles than does the Reference Case.

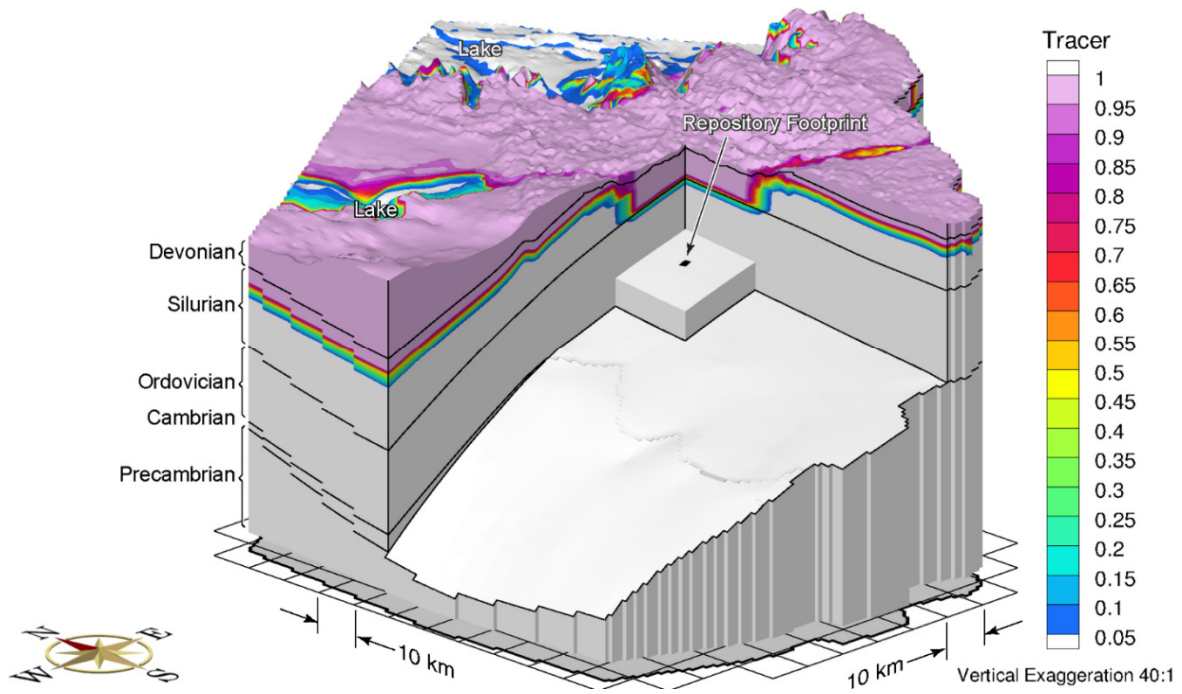


Figure 2-29: Block View Showing the Depth of Penetration of a Tracer after 120,000 Years for a Reference Case Paleohydrogeologic Scenario

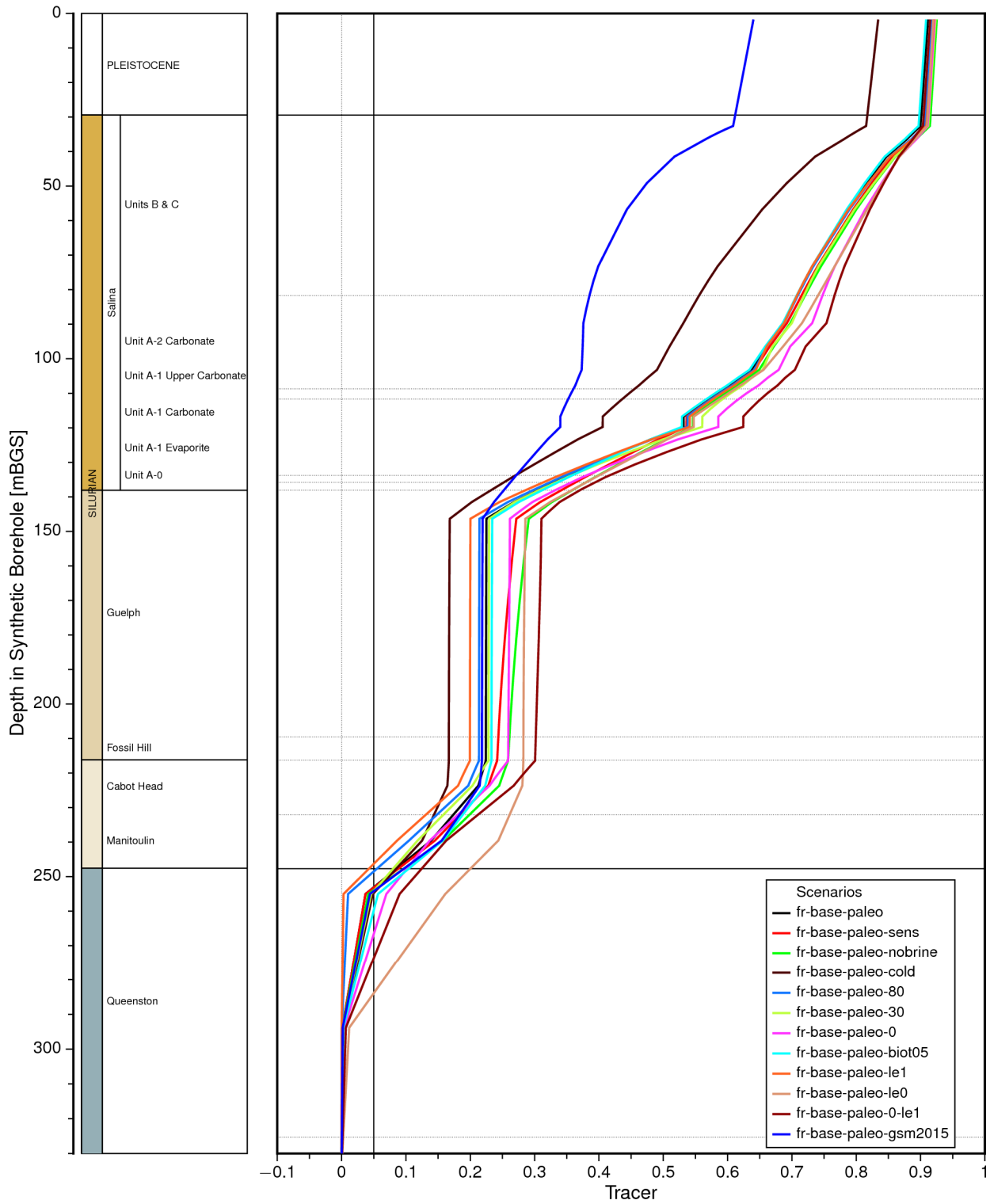


Figure 2-30: Vertical Profile Plots of Tracer Concentrations for the Paleohydrogeologic Simulations at the Location of the Hypothetical Repository Footprint at 120,000 Years

Peltier (2011) reconstructs eight paleoclimate glacial systems models (GSM). The Reference Case paleohydrogeologic simulation (fr-base-paleo) uses paleoclimate simulation nn9930, representing a warm-based ice-sheet condition. An alternative paleoclimate simulation, nn9921 (fr-base-paleo-cold), represents much more extensive permafrost over the 120,000 year paleoclimate time span and more ice-sheet advance/retreat cycles than nn9930. A third paleoclimate simulation gsm2015 (Stuhne and Peltier 2015) provides for a longer duration of ice coverage. All GSM models provide ice thickness, lake depth and permafrost depth over the 120,000 year simulation period, as shown in Figure 2-2, Figure 2-3, and Figure 2-4. These outputs are applied to the paleohydrogeologic groundwater flow simulations.

Figure 2-31 shows the tracer migration at 120,000 years for the alternative nn9921 paleoclimate boundary conditions. In comparison to the Reference Case, there is a significant decrease of tracer concentrations in the Silurian formations, as shown in Figure 2-30. Decreased tracer migration is a result of the longer duration of permafrost conditions. Figure 2-32 shows the tracer migration for the gsm2015 paleoclimate boundary conditions. In comparison to the Reference Case and the fr-base-paleo-cold case, there is a further decrease of tracer concentrations in the Silurian formations, as shown in Figure 2-30, due to permafrost duration in the gsm2015 paleoclimate simulation.

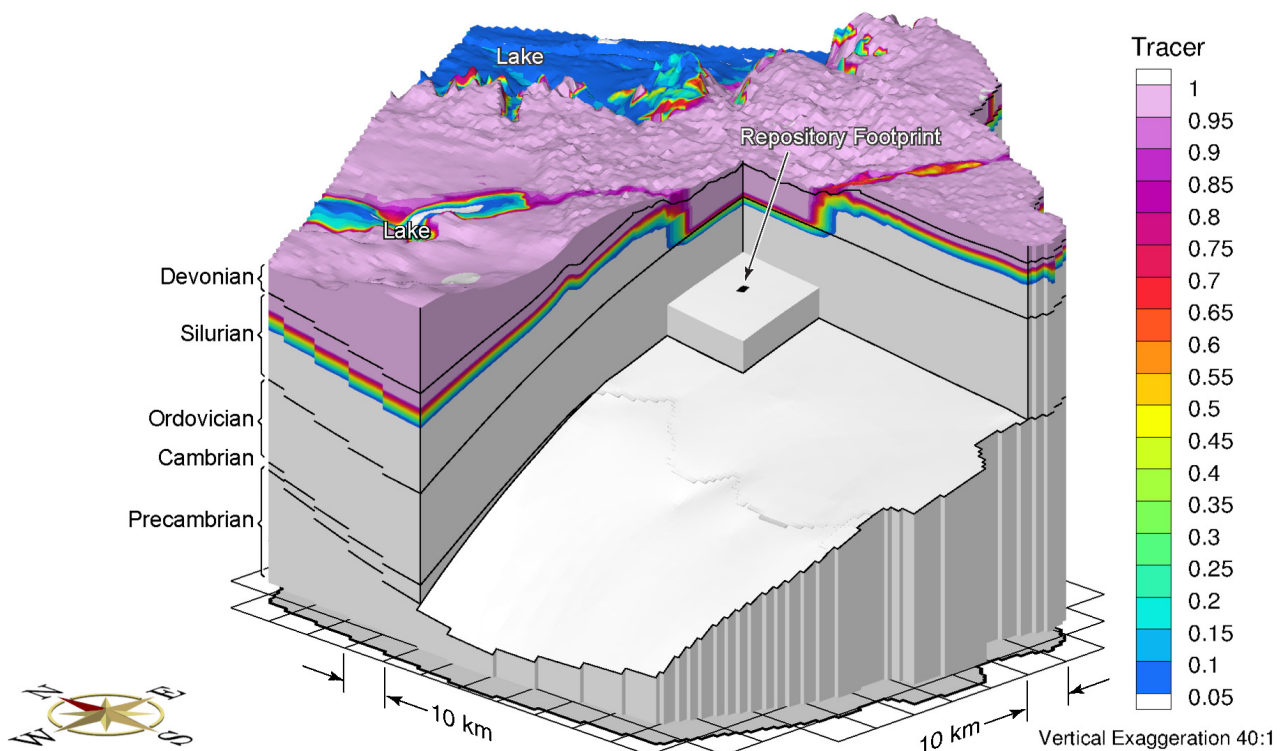


Figure 2-31: Block View Showing the Depth of Penetration of a Tracer after 120,000 Years for the nn9921 Paleoclimate Boundary Conditions (fr-base-paleo-cold)

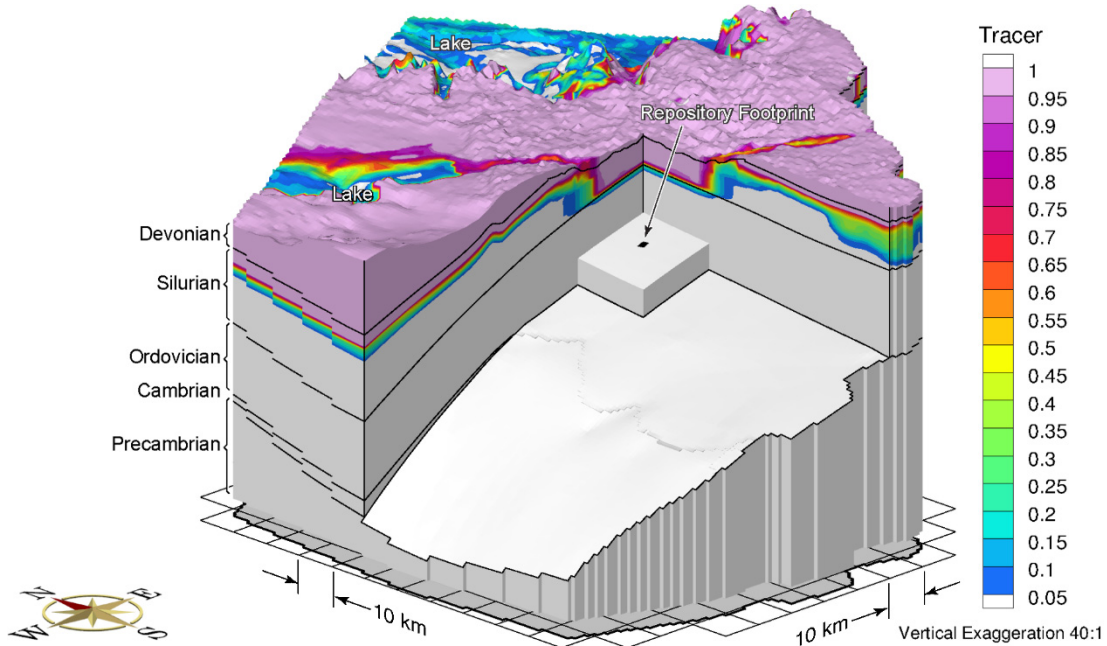


Figure 2-32: Block View Showing the Depth of Penetration of a Tracer after 120,000 Years for the gsm2015 Paleoclimate Boundary Conditions (fr-base-paleo-gsm2015)

The top surface hydraulic boundary condition can be varied using different percentages of ice-sheet thickness. The Reference Case uses 100% of ice-sheet thickness in calculating the equivalent freshwater head. The Reference Case equivalent freshwater head hydraulic boundary condition is consistent with observations made as a part of the Greenland Analogue Project (Claesson-Liljedahl et al. 2016). Paleohydrogeologic scenarios with equivalent freshwater heads of 0%, 30%, and 80% (named fr-base-paleo-0, fr-base-paleo-30, and fr-base-paleo-80, respectively) of ice-sheet thickness were assessed to allow for some reduction in heads beneath the ice-sheet. The 30% and 80% cases result in a tracer concentration profiles that are very similar to the Reference Case. For the 0% case, representing zero fluid pressure at the top surface, upward flow occurs during glacial loading, and downward flow occurs during glacial unloading due to in situ pore fluid pressure changes resulting from hydromechanical coupling. Higher tracer concentrations occur for the fr-base-paleo-0 case than for the Reference Case.

In addition to the surface hydraulic boundary condition, an equally important parameter is the one-dimensional loading efficiency. The loading efficiency is calculated based on the pore fluid and rock matrix compressibilities. In the Reference Case simulation, the one-dimensional loading efficiencies use this computed value for each geologic unit in Table 2-9. In two paleohydrogeologic sensitivity scenarios, the one-dimensional loading efficiencies are set to zero (fr-base-paleo-le0) to investigate the role of neglecting hydro-mechanical coupling, and

unity (fr-base-paleo-le1) to evaluate the impact of full hydro-mechanical coupling on the groundwater flow system at depth. Both the loading efficiency and specific storage values are affected by the choice of Biot¹ coefficient.

An additional sensitivity case investigates the role of the Biot coefficient on hydro-mechanical coupling. For a Biot coefficient of 0.5 (fr-base-paleo-biot05), alternative one-dimensional loading efficiencies and specific storages for each unit are listed in Table 2-10.

The final simulation (fr-base-paleo-0-le1) uses a loading efficiency of unity and 0% of ice-sheet thickness equivalent freshwater head for the surface hydraulic boundary condition. Of the paleohydrogeologic simulations with nn9930 paleoclimate boundary conditions, two extreme scenarios are represented by fr-base-paleo-le0 (having the most downward flow) and fr-base-paleo-0-le1 (having the most upward flow) during the loading portion of ice-sheet advance.

For the nn9930 paleoclimate boundary conditions, fr-base-paleo-le1 (Figure 2-33) represents the shallowest predicted tracer depth, while fr-base-paleo-le0 (Figure 2-34) represents the deepest penetration tracer depth. As the one-dimensional loading efficiency is decreased, vertical gradients increase because in situ pore pressures are reduced during ice-sheet loading for the same 100% of ice-sheet thickness equivalent freshwater head surface hydraulic boundary condition. Similar to the comparison between fr-base-paleo-0 and fr-base-paleo, higher tracer concentrations occur in the fr-base-paleo-0-le1 (Figure 2-35) simulation as compared to fr-base-paleo-le1, as shown in Figure 2-30. Deeper tracer migration is attributed to larger downward vertical gradients resulting from the combination of a zero pressure hydraulic surface boundary condition with full hydromechanical coupling and a loading efficiency of unity.

¹ According to Wang (2000), "The Biot-Willis parameter α is the ratio of increment of fluid content to change in bulk volume when the pore fluid remains at constant pressure [...]. It would be exactly one if all of the bulk strain were due to pore volume change (i.e., the solid phase is incompressible). It is less than one for a compressible solid phase because the change in bulk volume is greater than the change in pore volume by the amount of the change in the solid volume."

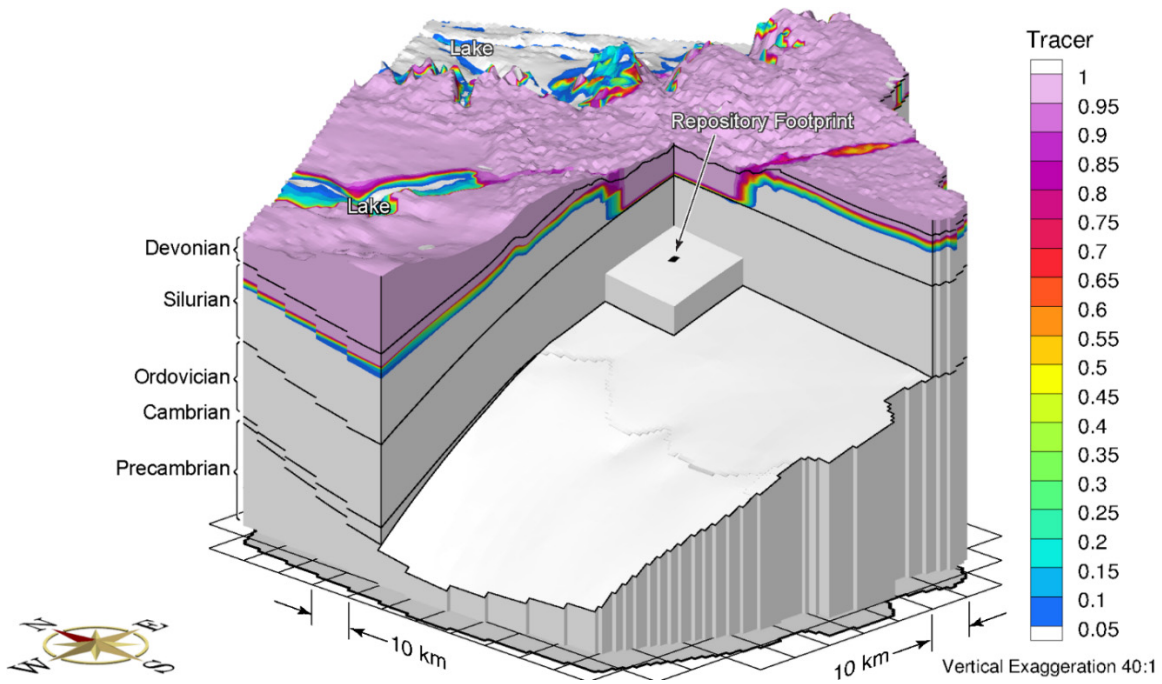


Figure 2-33: Block View Showing the Depth of Penetration of a Tracer after 120,000 Years for the nn9930 Paleoclimate Boundary Conditions and a Loading Efficiency of 1 (fr-base-paleo-le1)

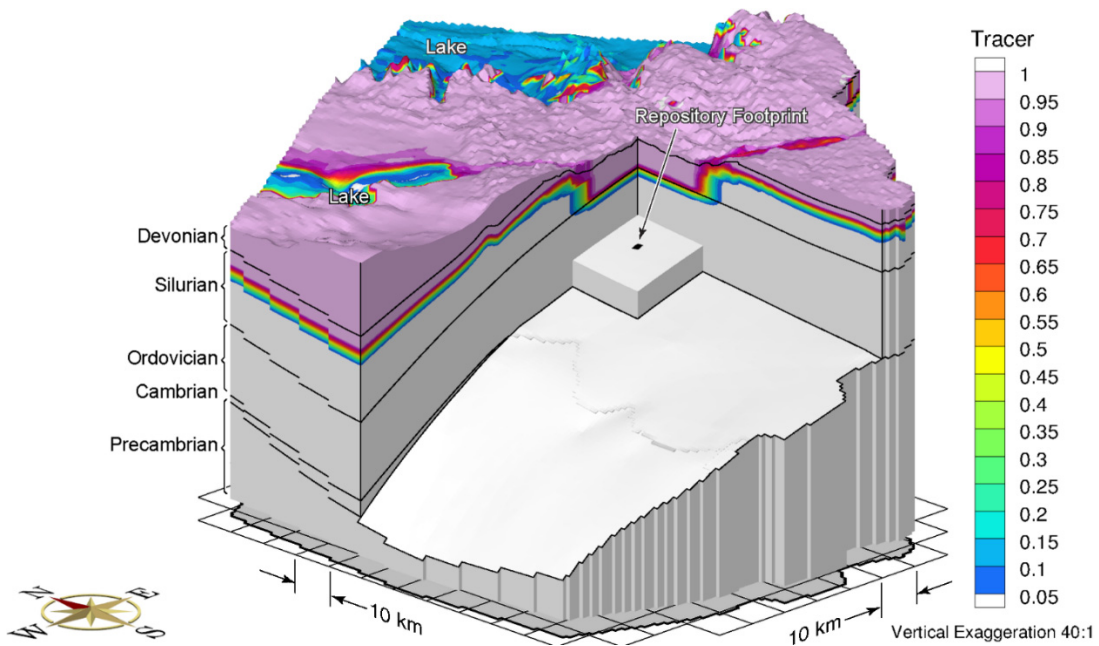


Figure 2-34: Block View Showing the Depth of Penetration of a Tracer after 120,000 Years for the nn9930 Paleoclimate Boundary Conditions and a Loading Efficiency of 0 (fr-base-paleo-le0)

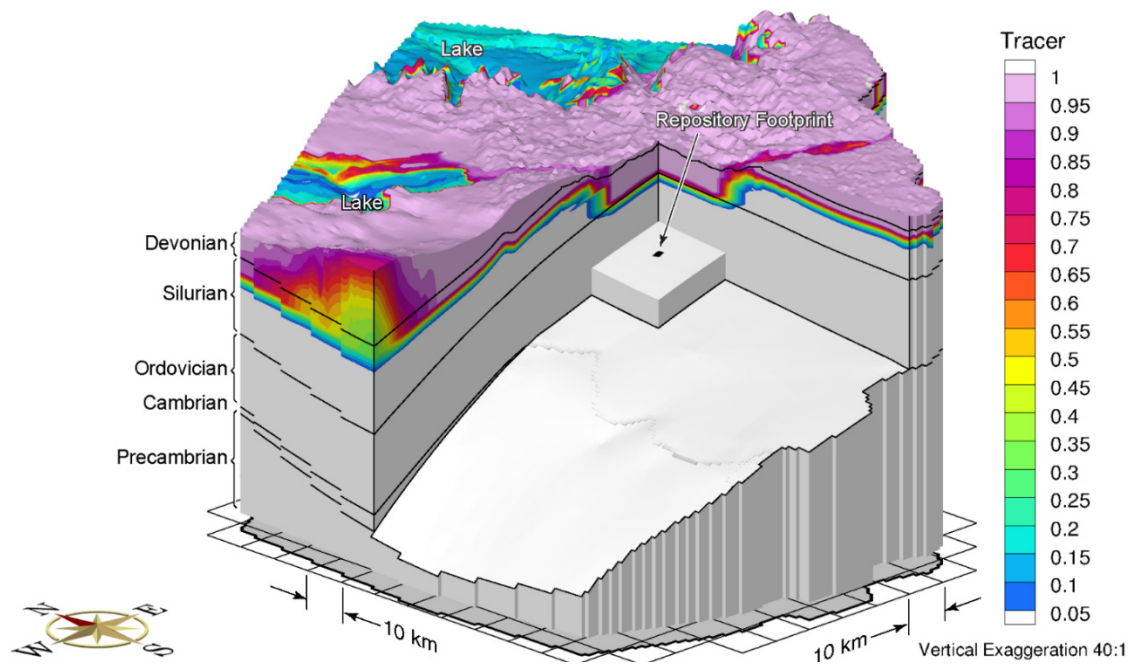
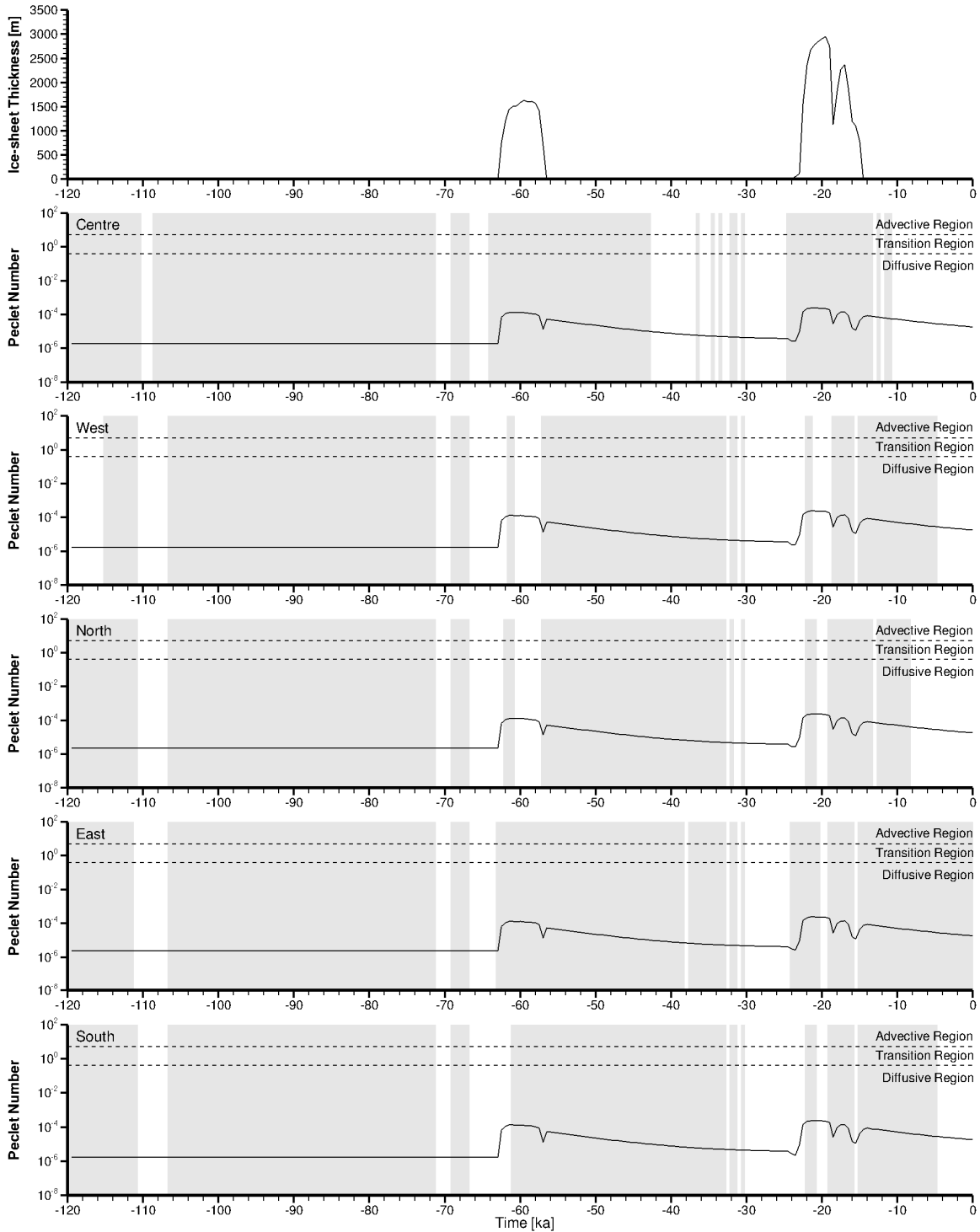


Figure 2-35: Block View Showing the Depth of Penetration of a Tracer after 120,000 Years for the nn9930 Paleoclimate Boundary Conditions, a Loading Efficiency of 1, and a 0% of Ice-Sheet Thickness Equivalent Freshwater Head for the Surface Hydraulic Boundary Condition (fr-base-paleo-0-le1)

The Péclet number, calculated as a ratio of the product of the porewater velocity and a characteristic length to the effective diffusion coefficient (Bear 1988), serves as an indicator for the dominance of advection or diffusion in mass transport processes. A plot of the Péclet number of molecular diffusion versus time for the Reference Case paleohydrogeologic scenario (fr-base-paleo), with a characteristic length of unity, is shown in Figure 2-36, and illustrates the stability of the geosphere during glacial advances and retreats. Five time series curves of the Péclet number are extracted at the center, west corner, north corner, east corner, and south corner of the hypothetical repository footprint, respectively. The grey regions in the figure represent upward groundwater movement, while the white regions represent downward groundwater movement. Through the duration of the glacial cycle, the Péclet number is well below the transition region, which indicates diffusion as the dominant transport mechanism for the Reference Case.



Note: Grey regions represent upward flow and white regions represent downward flow.

Figure 2-36: Péclet Number of Molecular Diffusion versus Time at the Hypothetical Repository Footprint for the Reference Paleohydrogeological Scenario (fr-base-paleo)

Select sensitivity cases illustrating the Péclet numbers versus time for scenarios fr-base-paleo-sens, fr-base-paleo-le0 and fr-base-paleo-0-le1 are shown in Figure 2-37, Figure 2-38, and Figure 2-39. These scenarios were chosen based upon porewater velocities, which are governed by hydraulic conductivities and head gradients. The Péclet numbers for the scenario with enhanced rock mass hydraulic conductivities (fr-base-paleo-sens), as illustrated in Figure 2-37, are slightly greater than for the Reference Case, but are still far below the transition zone. Thus, diffusion remains the dominant transport mechanism for the duration of the glacial cycles.

Scenarios fr-base-paleo-le0 and fr-base-paleo-0-le1 have the greatest downward and upward hydraulic gradients during glacial loading, however, their Péclet numbers versus time curves show less variation than the Reference Case. This can be explained as follows: firstly, the uniform loading efficiencies for these two cases means that inter-formational vertical gradients will not be generated during the glacial cycles. Secondly, the hydraulic conductivities of the Salina and Ordovician sediments are so low that the hydraulic boundary conditions at the top surface will not propagate into the deep groundwater flow system at the hypothetical repository footprint level. Both of the scenarios have Péclet numbers consistently far less than 0.4, which indicates that solute transport is dominated by molecular diffusion (Bear 1988).

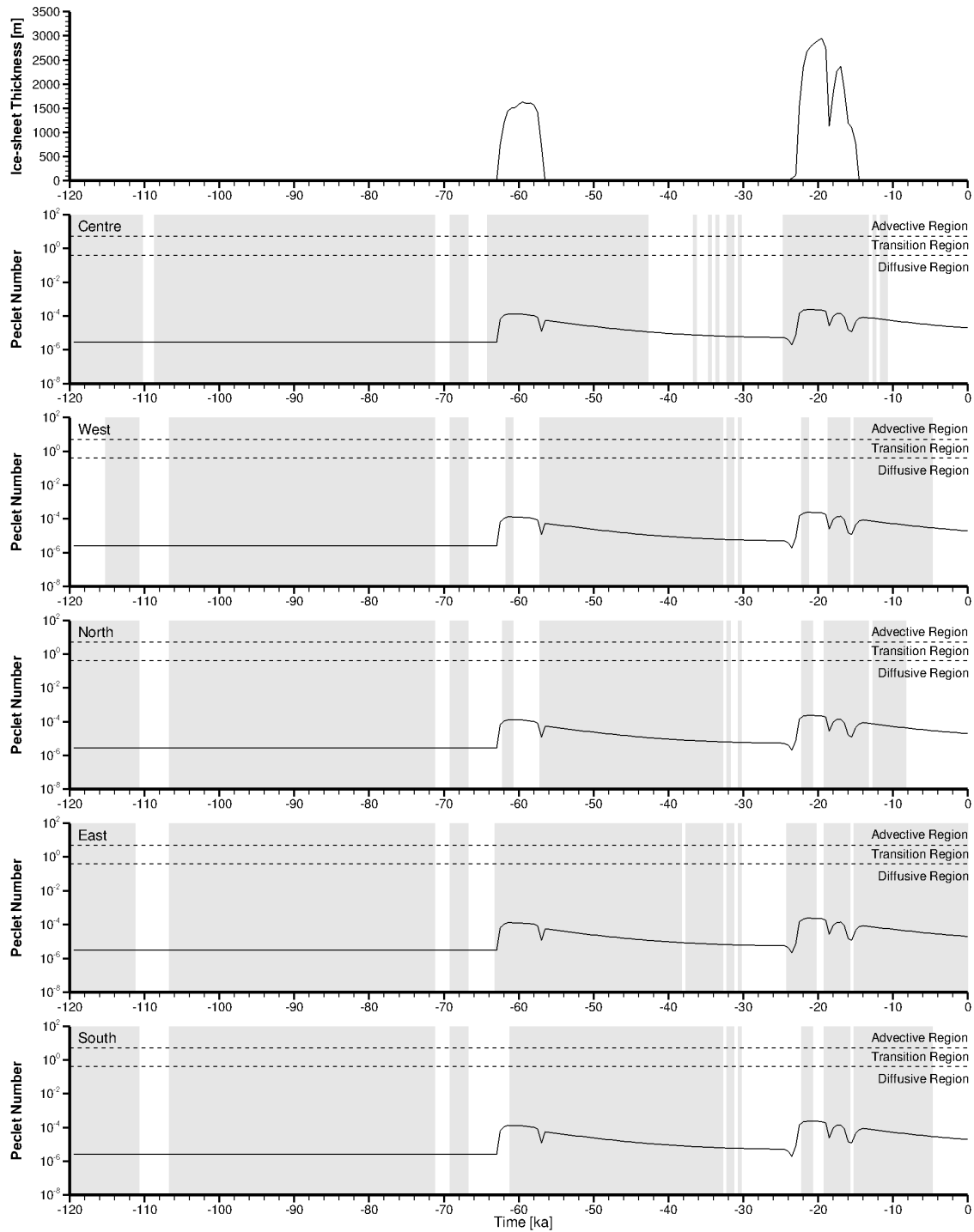


Figure 2-37: Péclet Number of Molecular Diffusion versus Time at the Hypothetical Repository Footprint for the Paleohydrogeological Scenario with Increased Rock Mass Hydraulic Conductivity (fr-base-paleo-sens)

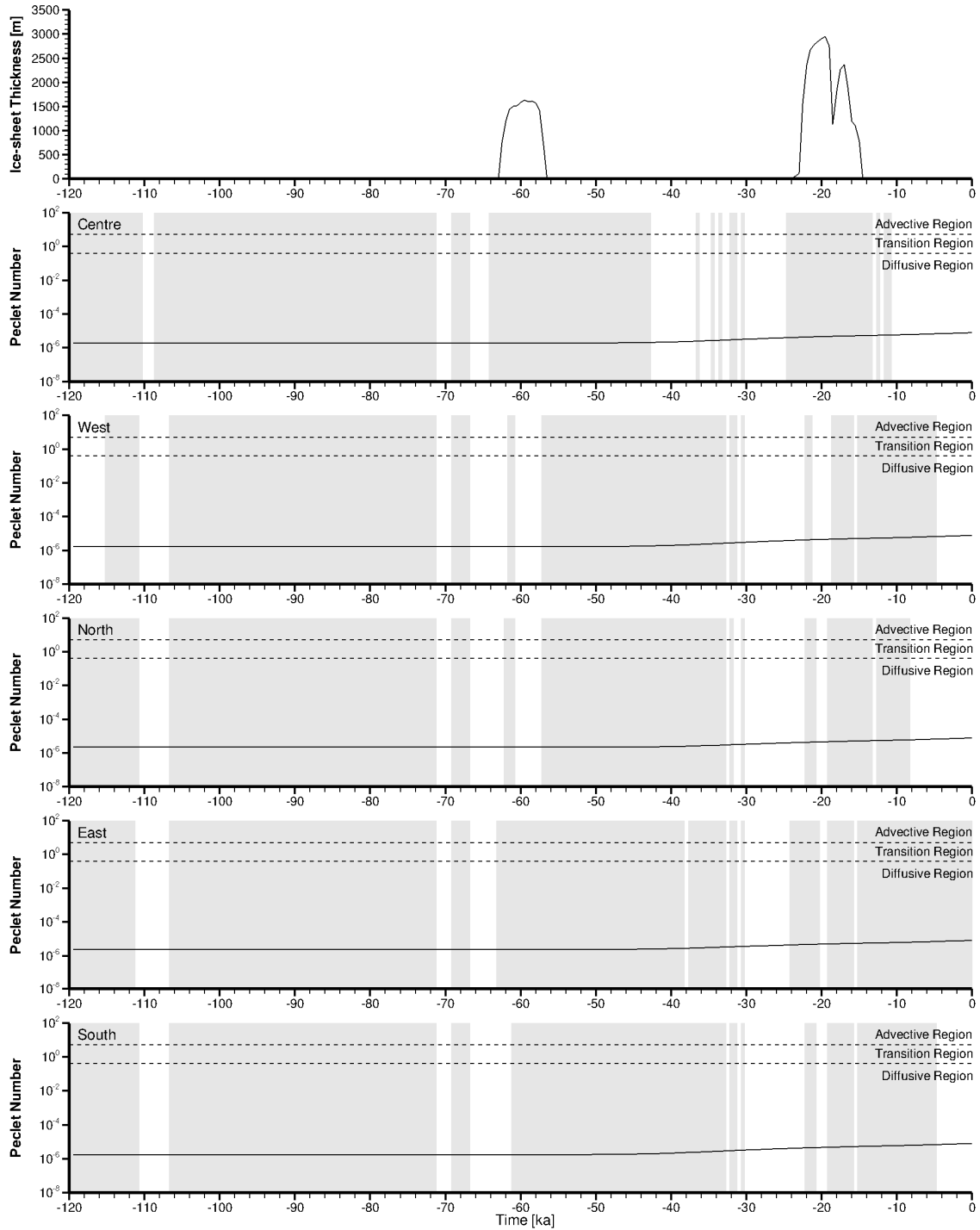


Figure 2-38: Péclét Number of Molecular Diffusion versus Time at the Hypothetical Repository Footprint for nn9930 Paleoclimate Boundary Conditions and a Loading Efficiency of 0 (fr-base-paleo-le0)

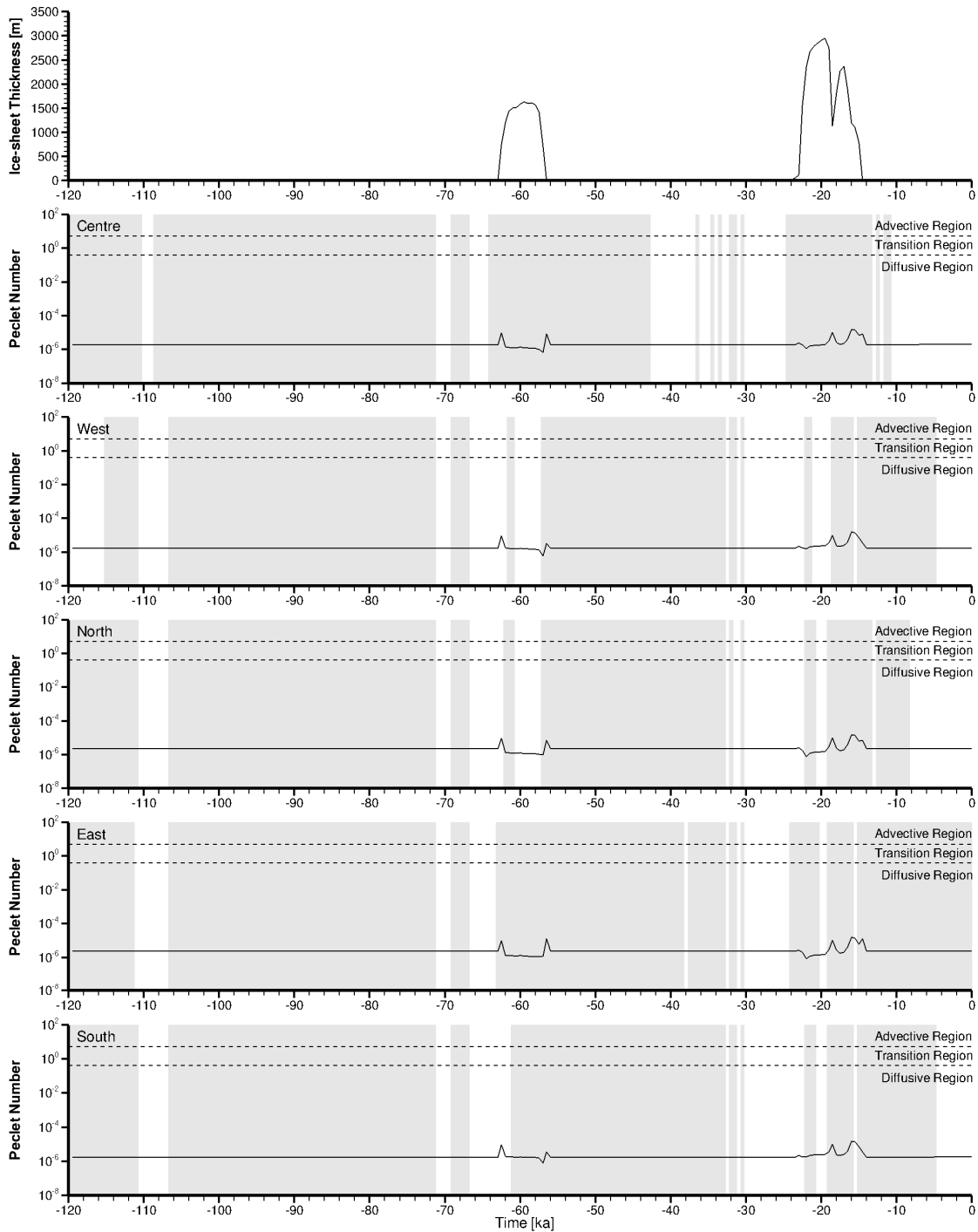


Figure 2-39: Péclet Number of Molecular Diffusion versus Time at the Hypothetical Repository Footprint for nn9930 Paleoclimate Boundary Conditions, a Loading Efficiency of 1, and a 0% of Ice-Sheet Thickness Equivalent Freshwater Head for the Surface Hydraulic Boundary Condition (fr-base-paleo-0-le1)

In a density-dependent groundwater flow system, freshwater head can only be used to determine hydraulic gradients along a horizontal plane; and environmental heads define hydraulic gradients along a vertical line (Luszczynski 1961). For the Reference Case paleohydrogeologic scenario (fr-base-paleo), a plot of environmental head versus time for various formations (Figure 2-40) indicates vertical gradients due to head differences across formations at the hypothetical repository footprint during the nn9930 glacial cycle. A large portion of the hydraulically conductive Guelph Formation is exposed to the Quaternary drift layer, which creates a hydraulic connection between the Guelph Formation and the top surface of the model. Therefore, Figure 2-40 shows that minimal vertical hydraulic gradients exist between the top surface and Guelph Formation throughout the 120,000 years paleohydrogeologic simulation. The very low hydraulic conductivities in the Salina units and Ordovician sediments ensure the deep groundwater flow system is not hydraulically connected to the surface boundary conditions, even during ice-sheet advance and retreat. The variations of heads over time are caused by one-dimensional hydro-mechanical coupling. The vertical hydraulic gradients at depth are mainly determined by the relative magnitude of loading efficiency for each formation. The Queenston Formation has the smallest loading efficiency and the value for the Precambrian is the largest. The resulting vertical hydraulic gradients from the Queenston to the Precambrian are mostly upward during the loading and unloading intervals. Figure 2-41 and Figure 2-42 show the time series plots of environmental heads for fr-base-paleo-le0 and fr-base-paleo-0-le1.

The same conclusion can be drawn (as for the preceding section) that uniform loading efficiencies result in zero vertical hydraulic gradients in this case. Additionally, it is worth noting that the environmental heads in the Queenston Formation behave differently. At the location of hypothetical repository footprint, most of the Salina units pinch out west of the site such that the heads above the Ordovician sediments will be affected by the surface boundary conditions during the glacial cycles to some degree.

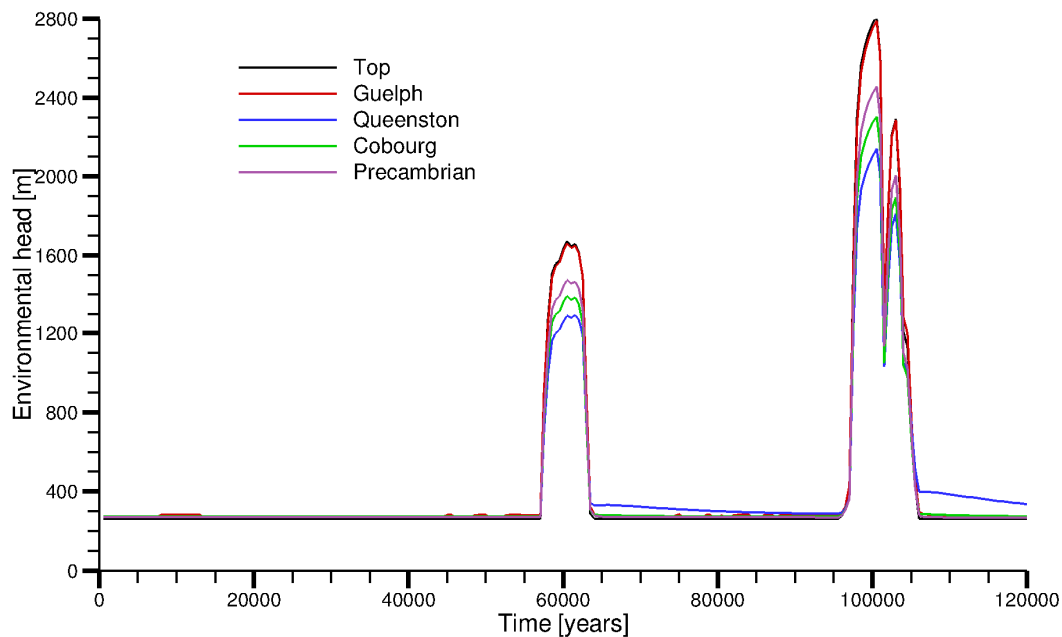


Figure 2-40: Environmental Head versus Time for the Reference Paleohydrogeological Scenario (fr-base-paleo)

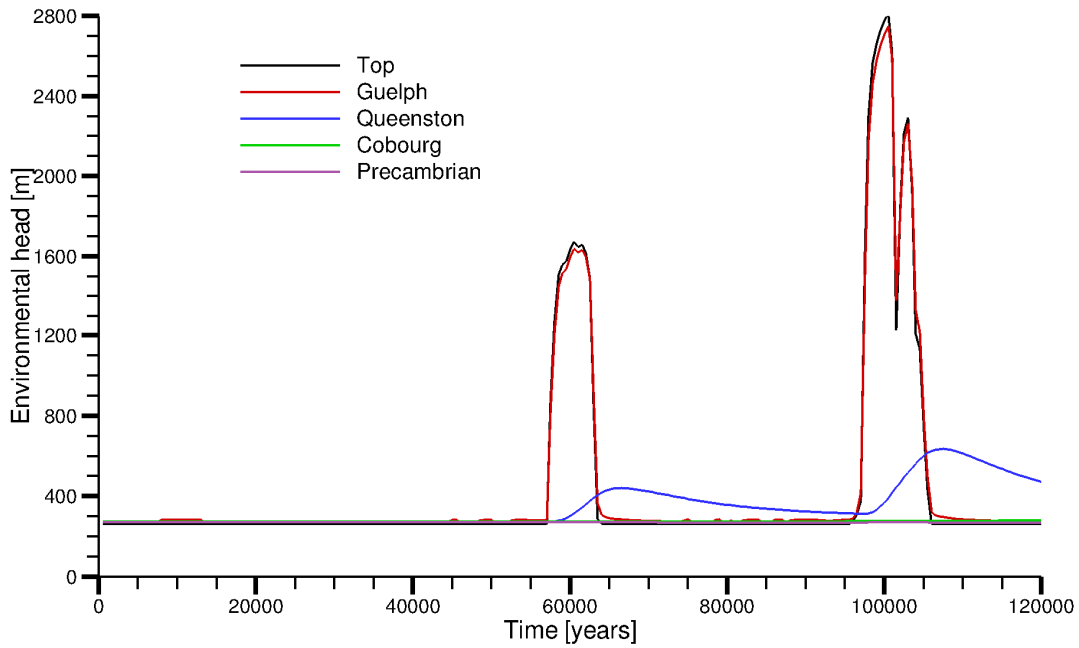


Figure 2-41: Environmental Head versus Time for nn9930 Paleoclimate Boundary Conditions and a Loading Efficiency of 0 (fr-base-paleo-le0)

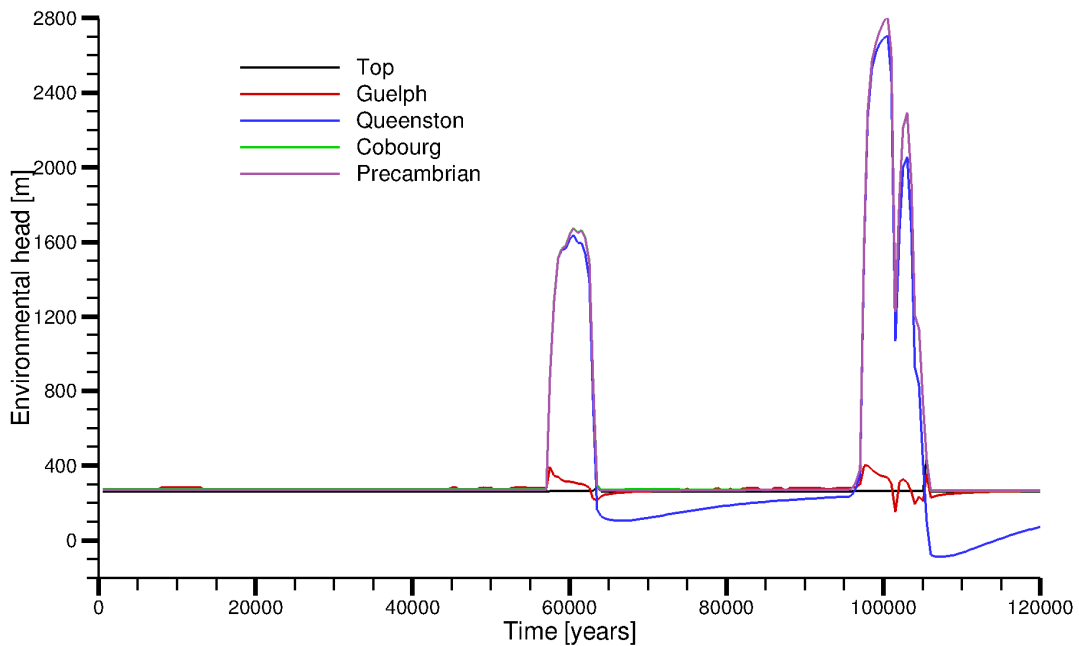


Figure 2-42: Environmental Head versus Time for nn9930 Paleoclimate Boundary Conditions, a Loading Efficiency of 1, and a 0% of Ice-Sheet Thickness Equivalent Freshwater Head for the Surface Hydraulic Boundary Condition (fr-base-paleo-0-le1)

2.3.4.4 Groundwater System Behaviour

2.3.4.4.1 Glaciation

The effect of using a different paleoclimate model was investigated by scenario fr-base-paleo-cold using the nn9921 paleoclimate simulation and scenario fr-base-paleo-gsm2015. Through a comparison of Figure 2-31 to Figure 2-33, nn9921 includes more glaciation episodes, and longer glacial duration and permafrost presence at the hypothetical repository footprint within a 120,000 years period than does paleoclimate model nn9930. Paleoclimate model gsm2015 demonstrates greater permafrost presence than either nn9930 or nn9921. Glacial presence tends to induce downward tracer migration and groundwater dilution by recharge water. Permafrost presence, on the contrary, tends to retard these processes by reducing the effective hydraulic conductivity of the layer. Figure 2-30 shows that the tracer migration for model nn9921 is still largely contained within the Silurian, and tracer concentrations are largely less than the tracer profile of the Reference Case. Figure 2-43 indicates that TDS concentrations in the Silurian are consistently greater for model nn9921 (fr-base-paleo-cold) than TDS concentrations in the reference scenario, with TDS concentrations for gsm2015 in between those of nn9930 and nn9921. Therefore, the impact of permafrost presence on the tracer migration outweighs the role of glaciation.

The Reference Case uses 100% of ice-sheet thickness in calculating the equivalent freshwater head. Alternative hydraulic boundary conditions applied to the surface of the modelling domain are analyzed in this study. These hydraulic boundary conditions are set to 80%, 30%, and 0% of the ice thickness equivalent freshwater head. For the reference scenario, glaciation generally results in downward flow during the loading phase and upward groundwater flow during the unloading phase. In the shallow units, the tracer migrates from surface and is then flushed out within one glacial episode. For the 0% case, representing zero fluid pressure at the top surface, upward flow occurs during glacial loading, and downward flow occurs during glacial unloading, primarily due to increased pore fluid pressures resulting from hydromechanical coupling. Thus, slightly deeper tracer migration occurs when compared to the reference case (as shown in Figure 2-30). The 30% case results in the tracer profiles situated between the reference case (100%) and the 0% case. The 80% case demonstrates a lower tracer concentration than the reference case, primarily due to loading efficiencies in the upper formations close to a value of 0.8 (see Table 2-2); a loading efficiency of 0.8 would result in no vertical gradients from glacial loading or unloading. The different TDS distributions in Figure 2-43 for these four scenarios are attributed to the relative magnitude of ice-sheet loading and unloading rates, in addition to the relative proportion of the surface hydraulic boundary condition to the one-dimensional loading efficiency for various formations.

2.3.4.4.2 Permafrost

Permafrost develops in advance of the ice-sheet because the ground surface is directly exposed to climate variations, whereas ice-sheets thermally insulate the underlying geosphere from climate influences (Peltier 2002). Permafrost with very low permeability often acts as the inhibitor of surface water migration downward and groundwater discharge. By a comparison of tracer migration in Figure 2-30 and TDS distribution at 120,000 years in Figure 2-43 (between the Reference Case with the nn9930 paleoclimate condition and fr-base-paleo-cold with the nn9921 paleoclimate condition), it is found that the cold-based paleohydrogeologic simulation has higher TDS concentrations in the shallow regime and less penetration depth of recharge

water. In fact, Figure 2-33 demonstrates that the more frequent glacial cycles and longer permafrost presence in the nn9921 model, as compared to the nn9930 model, will inhibit both surface recharge water migration downward and the dilution of brines with fresh water. For the gsm2015 paleoclimate model (fr-base-paleo-gsm2015), tracer migration, as shown in Figure 2-30, is less compared to the fr-base-paleo-cold simulation due to a longer period of permafrost duration and deeper permafrost formation. Similarly, TDS concentrations (Figure 2-43) in the shallow regime are less for fr-base-paleo-gsm2015 as compared to fr-base-paleo-cold also due to the greater spatial and temporal extent of permafrost in the gsm2015 paleoclimate simulation.

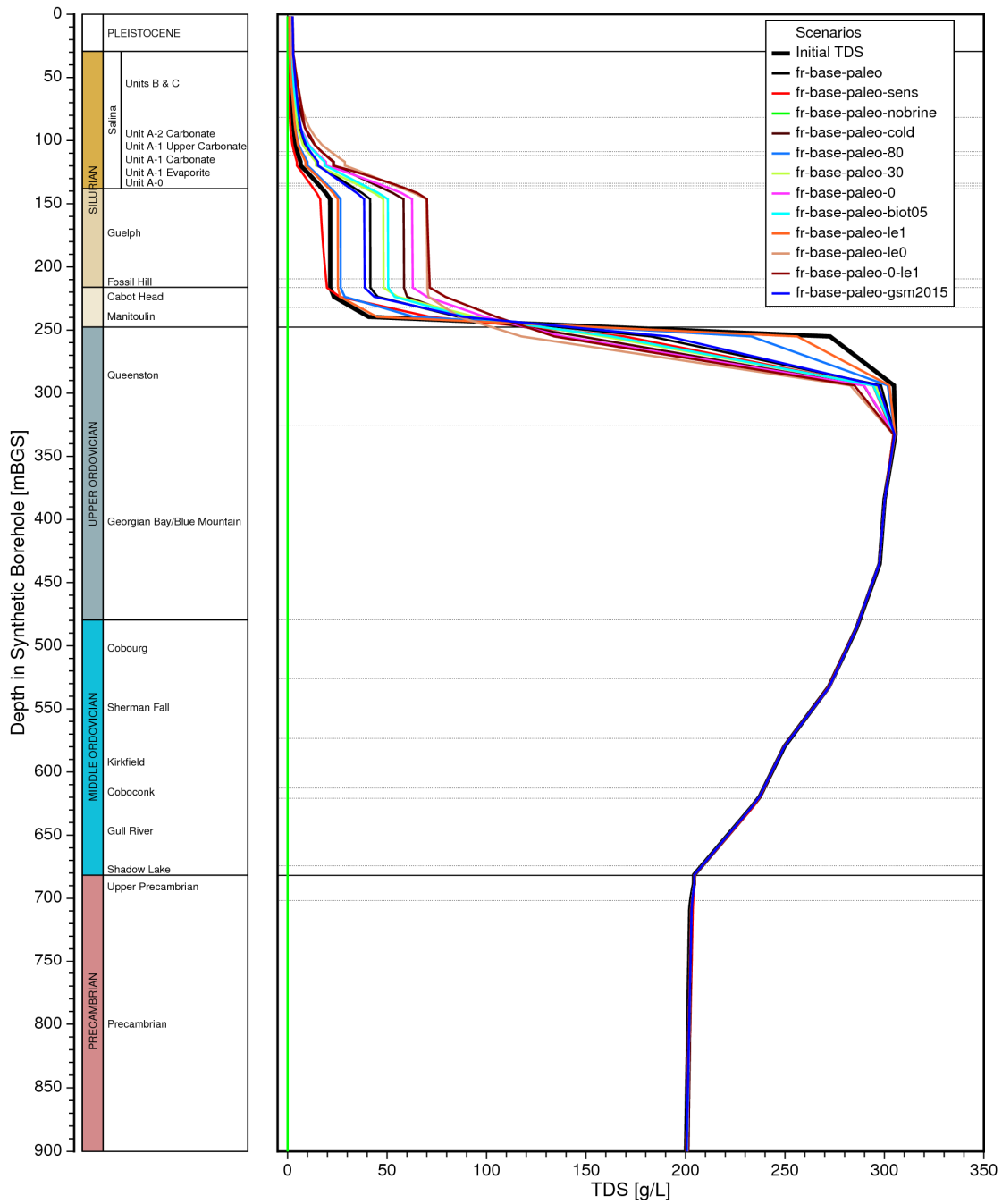


Figure 2-43: Vertical Profile Plots of TDS Concentrations for the Paleohydrogeologic Simulations at 120,000 Years at the Location of Hypothetical Repository Footprint

2.3.4.4.3 Depth of Surficial Recharge and Pathways

A tracer summary plot at 120,000 years for all paleohydrogeologic simulations is shown in Figure 2-30. The penetration depths of surficial recharge are represented by the intercepts between a straight line at a concentration of 0.05 and tracer concentration profiles at the hypothetical repository footprint at 120,000 years. The tracer for all the simulations only migrates into the bottom of the Silurian or the top of the Queenston Formation at 120,000 years. Thus, the downward migration of tracer is largely retarded by the low permeable Ordovician formations, which indicates the dominance of diffusion as a transport mechanism in the Ordovician. The greatest downward tracer migration occurs for the scenario fr-base-paleo-le0 with zero loading efficiency and 100% of ice-sheet thickness equivalent freshwater head for the surface hydraulic boundary condition. This tends to induce the greatest downward hydraulic gradient during the glacial loading phase. Scenario fr-base-paleo-le1 has the shallowest penetration depth, as the additional in-situ head induced by the mechanical coupling always equilibrates to the hydraulic surface boundary conditions with 100% of ice-sheet thickness equivalent freshwater head. Thus, for this scenario, negligible vertical hydraulic gradients exist throughout the paleohydrogeologic simulation period, including during glaciation cycles. The tracer in this case migrates downward mostly by diffusion.

2.3.4.4.4 The Role of Density

The increase in density of fluids at depth tends to slow down active flow in the deep groundwater system because resistance to driving forces increases with denser groundwater at depth (Park et al. 2009). However, the comparison of porewater velocities between steady-state and density-dependent simulation results in Figure 2-23 show that the velocity magnitude at depth in the steady-state model without brine (fr-base-nobrine) is slightly less than that in the reference model (fr-base). This can also be verified by the MLE comparison plot in Figure 2-24. Except for the portion beneath the lake, the mean life expectancies are generally higher in the freshwater simulation, which indicates a more stagnant groundwater system. The apparent contradiction can be explained by factors that influence fluid movement. A steady-state solution can be derived from the freshwater model, where the groundwater flow is purely driven by topography. The groundwater flow system of the Reference Case (with salinity) is still experiencing slow evolution at one million years of simulation time. Groundwater movement is not only driven by topography, but also is affected by the evolving TDS distribution.

For the paleohydrogeologic simulations, Figure 2-30 shows that no major difference in tracer profiles is observed between the Reference Case and the sensitivity case without salinity (fr-base-paleo-nobrine). Tracer only migrates into the shallow groundwater regime, which has low TDS concentrations in Figure 2-43. The groundwater system with high salinity at depth is diffusion dominant. The impact of density on the tracer migration cannot be evaluated based on these two paleohydrogeologic simulations. A plot of environmental head versus time for the paleohydrogeologic scenario without brine (in Figure 2-44) shows the vertical gradients at the hypothetical repository footprint. The direction and magnitude of the vertical gradients at depth are almost identical throughout the simulation period, as in the Reference Case shown in Figure 2-40.

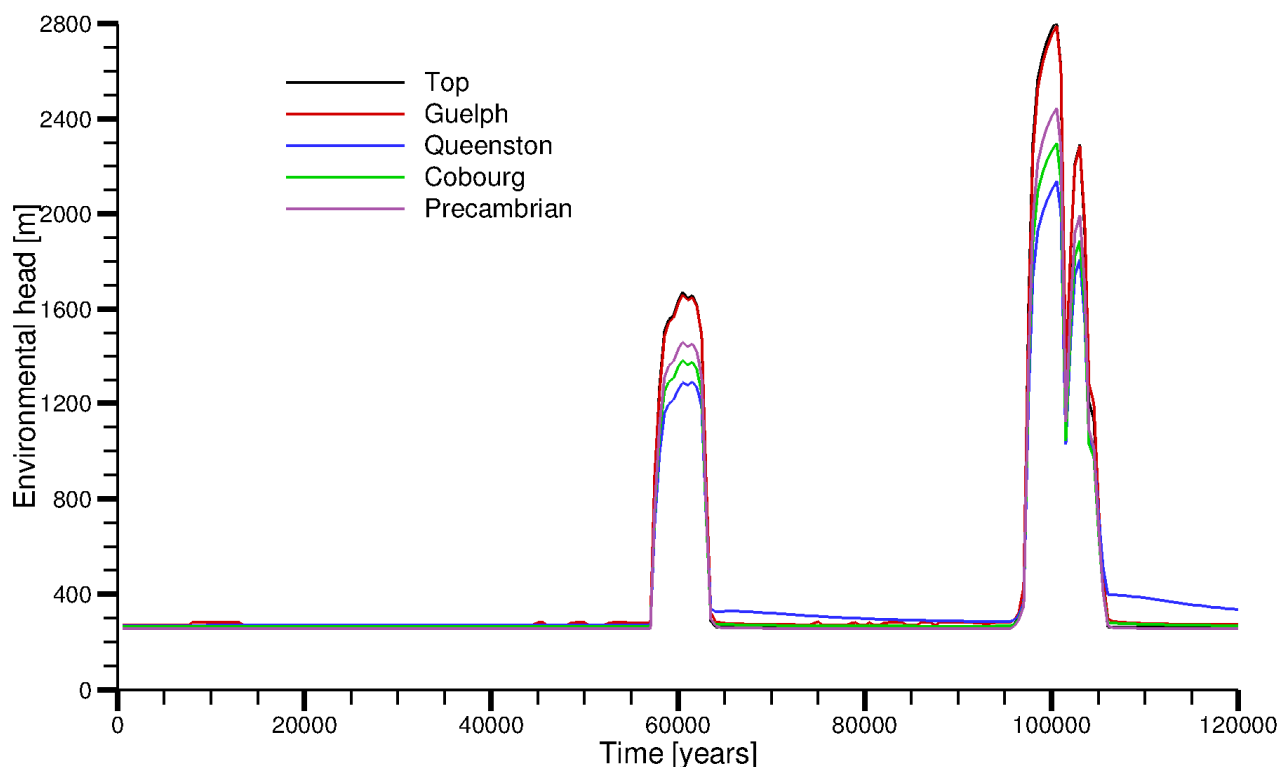


Figure 2-44: Environmental Head versus Time for the Paleohydrogeological Scenario without Salinity (fr-base-paleo-nobrine)

2.3.4.4.5 Anomalous Heads

A summary plot of freshwater heads versus depth at 120,000 years for all paleohydrogeologic simulations is shown in Figure 2-45. At the Upper Ordovician, including the Queenston and Georgian Bay/Blue Mountain formations, no under or over-pressures are simulated for the scenario (fr-base-paleo-le1) with a loading efficiency of unity and a 100% ice-sheet thickness as equivalent freshwater head for the surface hydraulic boundary condition. The increase or decrease of hydraulic heads, due to hydro-mechanical coupling, always equilibrates to the surface hydraulic boundary condition; no vertical gradients are imposed by glacial loading and unloading.

Three scenarios (fr-base-paleo-0, fr-base-paleo-30, and fr-base-paleo-0-le1) result in under-pressured head distributions, owing to the reduced surface boundary heads. Among them, fr-base-paleo-0-le1 has the greatest under-pressures in the Upper Ordovician, as the loading efficiency of unity, combined with a free surface boundary condition, causes the largest upward hydraulic gradient during glacial loading. Discharge of groundwater during glacial loading leads to a deficit of water and the formation of under-pressures during glacial unloading. As compared to the Reference Case with a slight over-pressure, a reduction of surface boundary heads can shift the head distribution in the Upper Ordovician from over-pressured to under-pressured. Simulations with 80%, 30%, and 0% of ice-sheet thickness as equivalent freshwater heads result in less over-pressure than the Reference Case, slight under-pressure and more under-pressure in the Upper Ordovician, respectively.

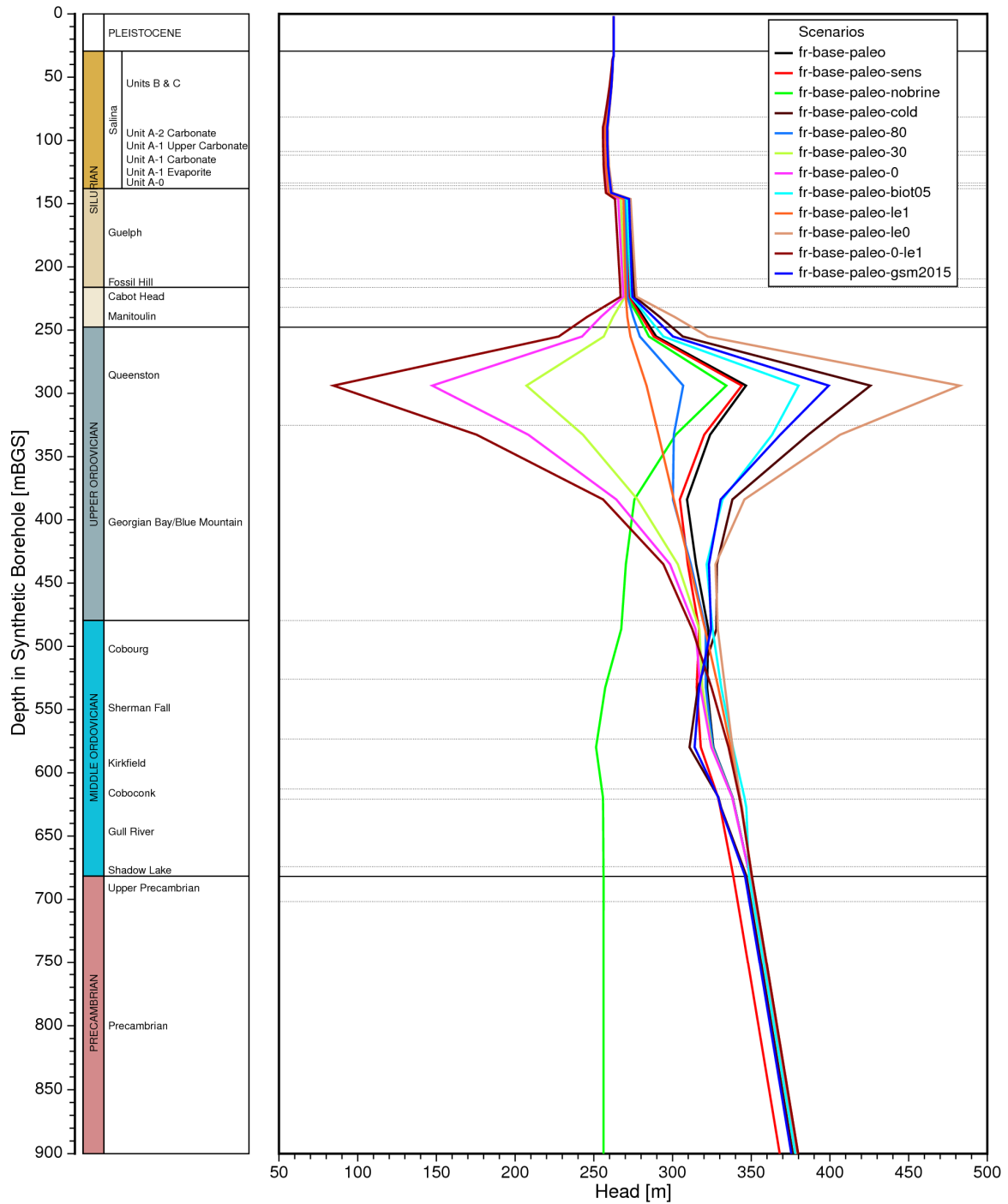


Figure 2-45: Vertical Profile Plots of Freshwater Heads for the Paleohydrogeologic Simulations at 120,000 Years at the Location of Hypothetical Repository Footprint

Scenario fr-base-paleo-le0 has the greatest over-pressures due to the lack of hydro-mechanical coupling, which does not allow for an increase in in-situ pore pressures throughout the domain as a result of glacially induced hydro-mechanical coupling. The increase in pore pressure tends to diminish the vertical hydraulic gradient from the surface boundary condition for a non-zero loading efficiency. The increased downward gradients lead to the greatest residual heads of all the paleohydrogeologic simulations.

2.3.5 Additional Temperate Transient Sensitivity Analyses

Additional temperate scenarios were developed to determine the sensitivity of system performance to parameters including diffusion coefficients, dispersivities and hydraulic conductivities. Generally, an increase in diffusion or dispersion leads to mean life expectancy (MLE) spreading and overall reductions in MLE values. Similarly, total dissolved solids (TDS) are more uniformly distributed. At pseudo-equilibrium times of one million years, the groundwater system state is closer to equilibrium and can result in higher MLE values. The sensitivity of MLE to parameter changes is represented using dimensionless or normalized local sensitivities.

The base case (fr-base) MLE value at the repository footprint is 179 Ma. Table 2-13 lists MLE values at the center of the repository footprint for the Reference Case and for the additional temperate scenarios. Free solution diffusion coefficients for both brine and mean life expectancy were increased by one order of magnitude, resulting in an MLE value of 19.0 Ma at the repository footprint, nearly one-tenth the MLE of the base case. The local sensitivity was determined by perturbing the diffusion coefficients by 1%; the normalized local sensitivity (the percentage change in computed MLE divided by the percentage change in diffusion coefficients) is -1.99 at the repository footprint. In this case, MLEs are considered sensitive and negatively related to diffusion coefficients; increasing diffusion coefficients will yield lower MLEs.

Increasing the free solution diffusion coefficients affects both brine and MLE transport. In coupled density-dependent groundwater systems, a change to TDS distributions throughout the domain also affects the flow system and porewater velocities; changes to the flow system affect MLE transport. To separate the combined effects of changes to both MLE and to the flow system, resulting from modified transport parameters, further simulations were performed using the base case velocity fields to compute MLE, and are listed in Table 2-13. MLE values at the repository footprint for scenarios with diffusion coefficients increased by 1% and increased by one order of magnitude are 177 Ma and 19.0 Ma, respectively. These values are slightly higher than their counterpart MLE values because the base case velocity fields are closer to equilibrium. By comparing the differences in MLE values, it can be concluded that the direct impact of MLE diffusion coefficients on MLE values is more important than the brine diffusion coefficients, which have an indirect influence on MLEs through a more evenly distributed TDS field and a more equilibrated velocity field.

Figure 2-46 and Figure 2-47 show the vertical MLE and TDS profiles, respectively, at the repository footprint for the Reference Case and the additional scenarios. TDS and MLE profiles for scenarios with a 1% increase in diffusion coefficients (fr-de1p) are almost indistinguishable from the Reference Case. A one order of magnitude increase (fr-de10) in diffusion coefficients significantly increases solute transport by diffusion, forcing high initial TDS in the upper Ordovician to dissipate upward to the Silurian and downward to the lower Ordovician much

faster than in the Reference Case. The resulting MLE profiles are well below the Reference Case.

The second set of analyses increased dispersivity values by 1%, 10%, and 100% and are identified as scenarios fr-disp1p, fr-disp10p, and fr-disp2. The local sensitivity analysis of dispersivities, determined by perturbing dispersivities by 1%, indicates that MLEs are positively related to dispersivities with a coefficient of 0.22 and an increase in MLE values relative to the base case. Further increases in dispersivity tend to yield similar MLE values within 5% of the base case (see Table 2-13); MLEs at the repository footprint are, therefore, not deemed to be sensitive to changes in dispersivity, and are largely attributed to the diffusion dominant transport regime below the Guelph Formation. Figure 2-46 and Figure 2-47 demonstrate that TDS and MLE profiles for scenarios with alternate dispersivities are either very close to or almost indistinguishable from the Reference Case. In doubling dispersivities (100% increase) for both brine and MLE, the MLE value at the repository footprint decreases to 170.9 Ma with a normalized sensitivity of -0.045.

Scenarios using the Reference Case porewater velocity field (fr-base prefix) and enhanced dispersivities for MLE were performed for two purposes: to evaluate the direct impact of MLE dispersivities on performance measures; and separately, to evaluate the indirect influence of brine dispersivities. Increasing MLE dispersivities always contributes to lower MLEs at the repository footprint, as shown in Table 2-13. Brine dispersivity enhancement leads to greater equilibration in TDS distribution and the groundwater flow field, leading to greater MLEs. For the 1% and 100% alternate dispersivity scenarios, brine dispersivities contribute to increased MLE, while the 10% cases result in decreased MLE at the repository footprint.

For the third sensitivity analysis, hydraulic conductivities were enhanced by three orders-of-magnitude for the low permeability units between the Guelph and the Cambrian formations. The substantial increase in hydraulic conductivities results in more brine and TDS being flushed from the groundwater system, as shown in Figure 2-48.

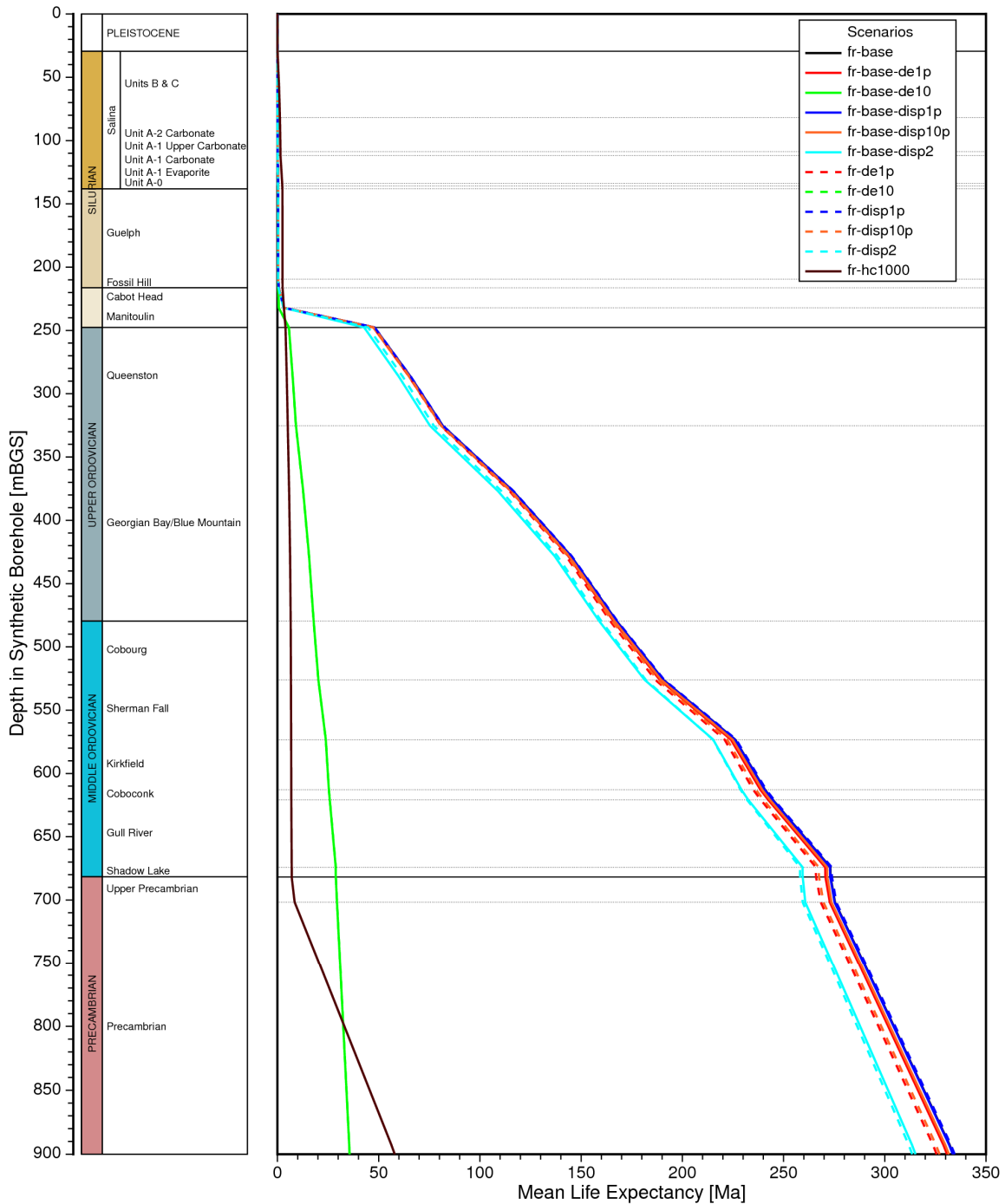
Compared to the Reference Case (Figure 2-19), Figure 2-49 shows that the velocity magnitude in those units with enhanced hydraulic conductivities is approximately increased by three orders-of-magnitude. The solute transport at the repository footprint is still dominated by diffusion; the Peclet number of molecular diffusion of 0.05 for a characteristic length of unity is well below 0.4 (Bear 1988). The mean life expectancy at the repository footprint is 6.6 Ma. Solute transport, by both advection and diffusion, from the upper Ordovician, with high initial TDS upward to the Silurian and downward to the lower Ordovician, is greatly enhanced during the one million year pseudo-equilibrium simulation. This results in lower TDS in the upper Ordovician shales and higher TDS in the Silurian formations and in the Ordovician carbonate formations, due to advective transport, than are observed in the Reference Case (Figure 2-47). Figure 2-46 and Figure 2-47 demonstrate that higher TDS concentrations in the shallow groundwater flow regime within the Silurian formations contributes to lower groundwater flow velocity magnitude and larger MLEs than in the Reference Case. As noted by Park et al. (2009), the increase in pore fluid density often acts to retard active flow. The MLEs in the Ordovician are significantly less than in the Reference Case due to higher velocity magnitudes caused by the increase of hydraulic conductivities in these units. In the Precambrian, the same profiles of MLE versus depth are observed, as the properties of this portion of the model domain remain unchanged.

Table 2-13: Computed MLE Values at the Repository Footprint for Alternate Temperate Scenarios

Scenario	Transport Parameter Application	
	Brine and MLE ⁽¹⁾	MLE ⁽²⁾
Base case (fr-base)	179.0 Ma	179.0 Ma
Increase diffusion coefficient by 1% (prefix-de1p)	175.5 Ma	177.4 Ma
Increase diffusion coefficient by 1 order of magnitude (prefix-de10)	19.02 Ma	19.05 Ma
Increase dispersivities by 1% (prefix-disp1p)	179.4 Ma	178.9 Ma
Increase dispersivities by 10% (prefix-disp10p)	176.5 Ma	178.0 Ma
Increase dispersivities by 100% (prefix-disp2)	170.9 Ma	170.1 Ma
Increase hydraulic conductivity by 3 orders of magnitude (fr-hc1000)	6.60 Ma	N/A

Notes: (1) prefix = 'fr' in Column 1

(2) prefix = 'fr-base' in Column 1



Notes: Solid lines represent scenarios which use the base case porewater velocity field. Scenarios fr-base-de10 and fr-de-10 overlap.

Figure 2-46: Vertical Profile Plots of Mean Life Expectancies at One Million Years for the Reference Case and Additional Sensitivity Scenarios

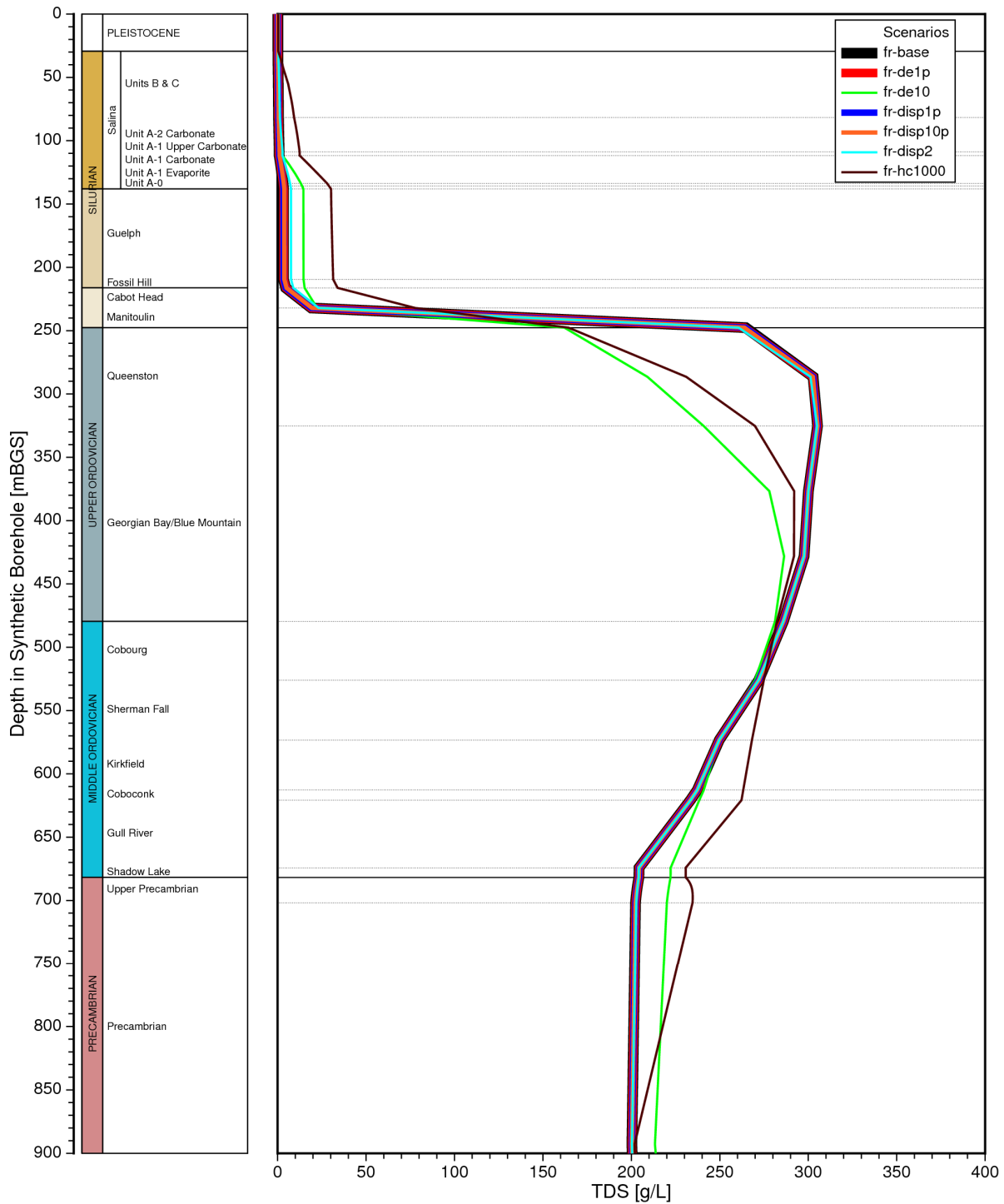


Figure 2-47: Vertical Profile Plots of Total Dissolved Solids Concentrations at One Million Years for the Reference Case and Additional Sensitivity Scenarios

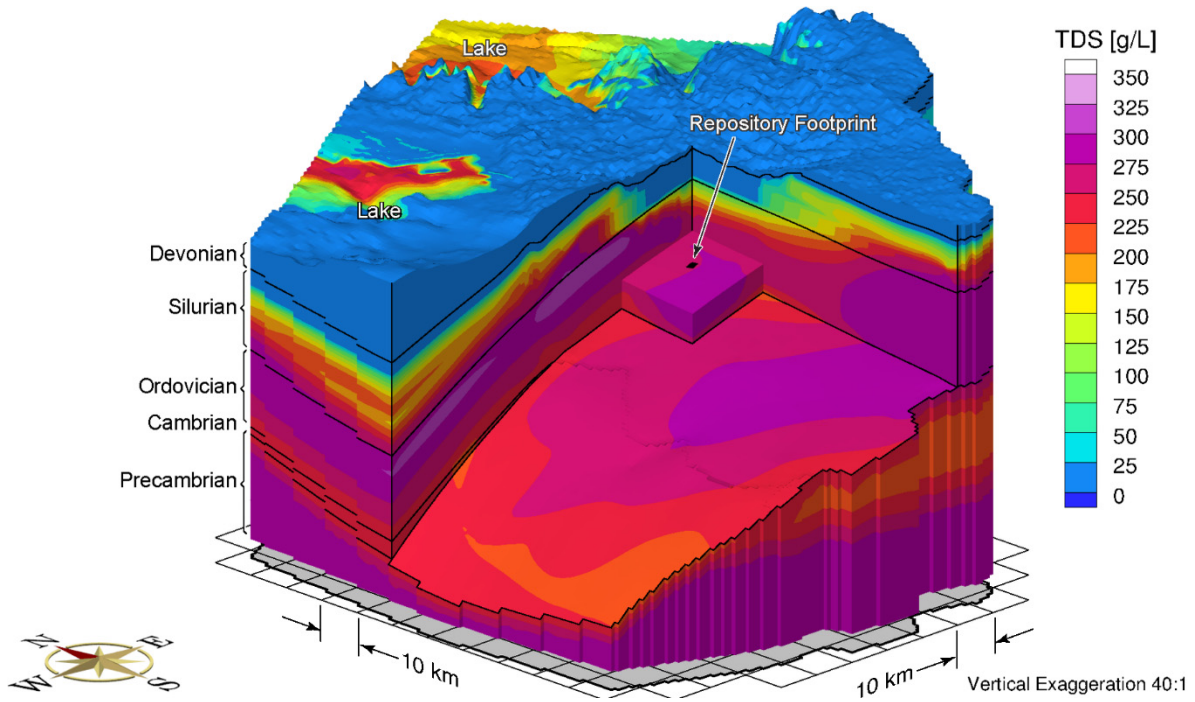


Figure 2-48: Total Dissolved Solids Concentrations at One Million Years for a Three Order of Magnitude Enhancement in Hydraulic Conductivities

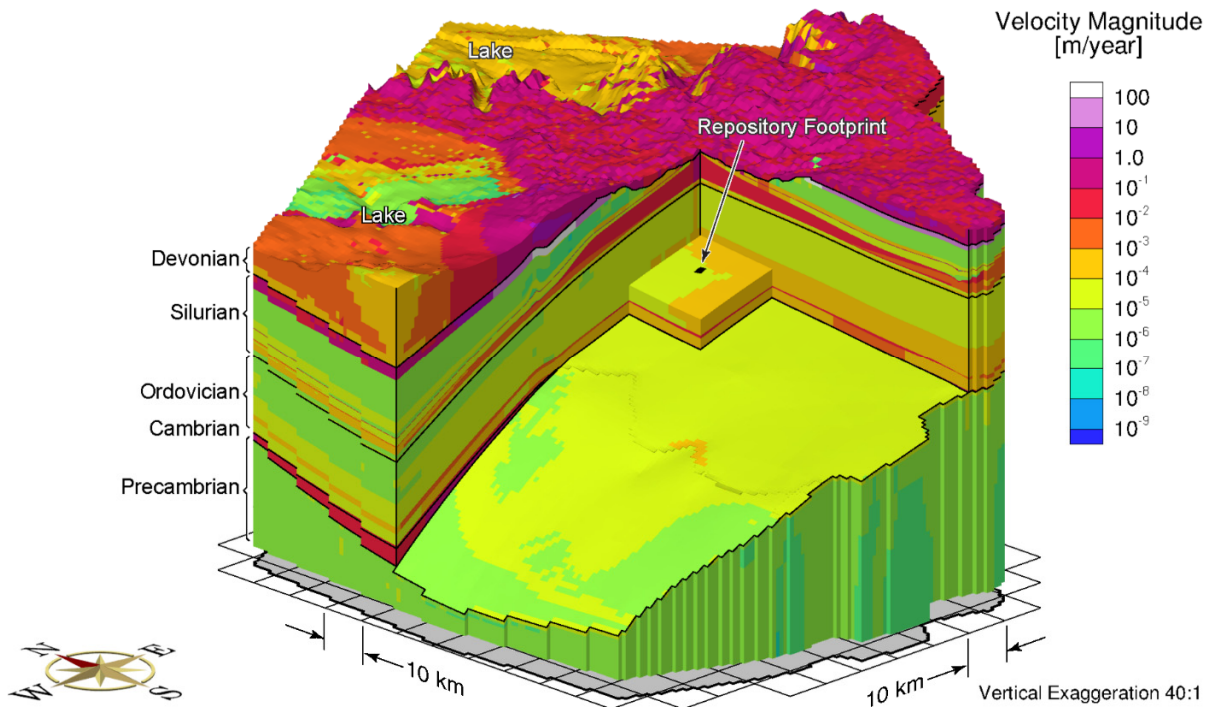


Figure 2-49: Porewater Velocity Magnitude for a Three Order of Magnitude Enhancement in Hydraulic Conductivities

2.4 Summary and Conclusions

This chapter describes a geosphere dataset for a hypothetical sedimentary rock site. The geosphere data set described in this chapter is provided for the purpose of performing an illustrative postclosure safety assessment. Three groundwater systems are considered: shallow, intermediate and deep. The behaviour of the groundwater systems during temperate and glacial conditions was explored through a suite of sensitivity cases.

The sedimentary rock overlying the hypothetical repository contains a thick sequence of low permeability limestones and shales. Temperate hydrogeologic modelling illustrates the role played by the low permeability limestones and shales as natural barriers to groundwater movement and contaminant transport.

The hydrogeological domain for the geosphere described in this chapter is divided into three groundwater systems: shallow (0- 215 mBGS), intermediate (215-250 mBGS) and deep (>250 mBGS). These systems are identified, in part, by rock mass hydraulic conductivities, as well as groundwater total dissolved solids (TDS) concentrations and redox conditions. The shallow groundwater zone occurs in the upper 215 m and comprises glacial sediment overlying a relatively permeable sequence of limestone and dolostone. In the shallow system, groundwater is considered to be fresh, oxygen-rich and isolated from the deeper groundwater systems. The intermediate groundwater system is a transition zone in which the groundwater becomes progressively more mineralized and reducing with depth. Within the deep groundwater system, groundwater conditions are saline and reducing. With increasing depth, the general increase in salinity and decreased rock mass hydraulic conductivities leads to improved groundwater system stability at time frames relevant to repository safety.

Péclet numbers and MLEs were used as illustrative performance measures to gain insight into the processes most influencing mass transport. For an assumed Reference Case, the shallow groundwater system is advective, whereas at greater depths, the low permeability rock mass results in low rates for mass transport. Further groundwater system stability occurs as a result of salinity gradients within the intermediate and deep groundwater systems.

Paleohydrogeological simulations were used to illustrate the long-term evolution and stability of the geosphere and groundwater systems to external perturbations. The distribution and duration of permafrost above the repository location play a role in governing the depth to which meltwater penetrates. Paleohydrogeologic simulations suggest that glacial meltwaters will not reach the repository horizon, due to the low hydraulic conductivity of the overlying Ordovician shales dolostones and evaporites of the Salina Group. Glacial recharge penetrating below the shallow groundwater system is not expected to be oxygenated or to influence redox conditions at the repository horizon. For the sensitivity cases assessed, the glacial perturbations did not materially change mass transport rates at repository depth and mass transport remained diffusion dominated throughout the glacial cycle.

2.5 References for Chapter 2

Ackerley, N., J. Adams, V. Peci, S. Halchuk and P. Street. 2018. OPG's L &ILW DGR Seismic Monitoring - Annual Report 2016, NWMO DGR-TR-2018-01. Toronto, Ontario, Canada.

Al, T.A., I.D. Clark, L. Kennell, M. Jensen and K.G. Raven. 2015. Geochemical evolution and residence time of porewater in low-permeability rocks of the Michigan Basin, Southwest Ontario. *Chemical Geology* 404, 1-17.

Al-Aasm, I. S. and R. Crowe. 2018. Fluid compartmentalization and dolomitization in the Cambrian and Ordovician successions of the Huron Domain, Michigan Basin. *Marine and Petroleum Geology* 92, 160-178. <https://doi.org/10.1016/j.marpetgeo.2018.02.011>

AMEC Geomatrix, Inc. 2011. OPG's L &ILW DGR Seismic Hazard Assessment. NWMO DGR-TR-2011-20. Toronto, Ontario, Canada.

Aquanty. 2013. HGS 2013: HydroGeoSphere User Manual, Release 1.0. Waterloo, Ontario, Canada.

Armstrong, D.K. and T.R. Carter. 2006. An Updated Guide to the Subsurface Paleozoic Stratigraphy of Southern Ontario. Ontario Geological Survey, Open File Report 6191. Ottawa, Ontario, Canada.

Armstrong, D.K. and T.R. Carter. 2010. The Subsurface Paleozoic Stratigraphy of Southern Ontario. Ontario Geological Survey, Special Volume 7.

Armstrong, D.K. and J.E.P. Dodge. 2007. Paleozoic geology of southern Ontario. Ontario Geological Survey, Miscellaneous Release-Data 219.

Armstrong, D.K. and W.R. Goodman. 1990. Stratigraphy and depositional environments of Niagaran carbonates, Bruce Peninsula, Ontario. Field Trip No. 4 Guidebook. American Association of Petroleum Geologists, 1990 Eastern Section Meeting, hosted by the Ontario Petroleum Institute. London, Ontario, Canada.

Barker, J.F. and S.J. Pollock. 1984. The Geochemistry and Origin of Natural Gases in Southern Ontario. *Bulletin of Canadian Petroleum Geology* 32, 313-326.

Baumgartner, P. 2005. Scoping Analyses for the Design of a Deep Geologic Repository in Sedimentary Rock. Atomic Energy of Canada Limited, Report number: 06819-REP-01300-10093-R00. Pinawa, Manitoba, Canada.

Bear, J. 1988. *Dynamics of Fluids in Porous Media*. Dover Publications Inc., New York, USA.

Berry, F.A.F. 1969. Relative factors influencing membrane filtration effects in geologic environments. *Chemical Geology* 4, 293-301.

Bertetti, F.P. 2016. Determination of Sorption Properties for Sedimentary Rocks under Saline, Reducing Conditions – Key Radionuclides. Nuclear Waste Management Organization Report NWMO-TR-2016-08. Toronto, Ontario, Canada.

Bredehoeft, J.D., C.R. Blyth, W.A. White and G.G. Maxey. 1963. Possible mechanism for concentration of brines in subsurface formations. *American Association of Petroleum Geologists Bulletin* 47, 257-269.

CCBFC. 2010. National Building Code of Canada, 13th Edition. Canadian Commission on Building and Fire Codes. Ottawa, Ontario, Canada.

Carpenter, A.B. 1978. Origin and chemical evolution of brines in sedimentary basins. *Oklahoma Geological Survey Circular* 79, 60-77.

Cartwright, P.B. 1997. A review of recent in situ stress measurements in United Kingdom coal measures strata. *In: Sugawara K, Y. Obara (Eds.). Proceedings International Symposium on Rock Stress, Kumamoto. A. A. Balkema, Rotterdam.*

Claesson-Liljedahl, L., A. Lehtinen, J. Harper, J-O Näslund, J-O Selroos, P. Pitkänen, I. Puigdomenech, M. Hobbs, S. Follin, S. Hirschorn, P. Jansson, H. Järvinen, L. Kennell, N. Marcos, T. Ruskeeniemi, E-L Tullborg and P. Vidstrand. 2016. Greenland Analogue Project: Final Report. Nuclear Waste Management Organization Report NWMO-TR-2016-12. Toronto, Ontario, Canada.

Clark, I.D., T.A. Al, M. Jensen, L. Kennell, M. Mazurek, and R. Mohapatra. 2013. Paleozoic-aged Brine and Authigenic Helium Preserved in an Ordovician Shale Aquiclude. *Geology* 41(9), 951–954.

Cornaton, F. and P. Perrochet. 2006a. Groundwater age, life expectancy and transit time distributions in advective–dispersive systems: 1. Generalized reservoir theory. *Advances in Water Resources* 29(9), 1267–1291.

Cornaton, F. and P. Perrochet. 2006b. Groundwater age, life expectancy and transit time distributions in advective–dispersive systems: 2. Reservoir theory for sub-drainage basins. *Advances in Water Resources* 29(9), 1292–1305.

Frape, S.K. and P. Fritz. 1987. Geochemical trends for groundwaters from the Canadian Shield. *In: Saline Water and Gases in Crystalline Rocks (P. Fritz and S.K. Frape, Eds.). Number 33 in Geological Association of Canada Special Paper, 19–38.*

Fredrickson, J.K. and Balkwill, D.L. 2006. Geomicrobial processes and biodiversity in the deep terrestrial subsurface. *Geomicrobiology Journal* 23, 345–356.

Golder (Golder Associates Ltd.). 2013. OPG's Deep Geological Repository for Low & Intermediate Level Waste, Factual Report – Borehole DGR-7 and DGR-8 Geotechnical Logging. OPG 1011170042-REP-G2040-0004-01.

Gorski, B., T. Anderson and B. Conlon. 2009a. Laboratory Geomechanical Strength Testing of DGR-1 & DGR-2 Core. Intera Engineering Ltd. Report TR-07-03 Rev.3. CANMET Mining and Mineral Sciences Laboratories. Ottawa, Ontario, Canada.

- Gorski, B., T. Anderson and B. Conlon. 2009b. DGR-2 Long-term strength degradation testing of DGR-2 Core. TR-08-11, Revision 0. Canada Centre for Mineral and Energy Technology – Mining and Mineral Sciences Laboratories. Ottawa, Ontario, Canada.
- Gorski, B., T. Anderson and B. Conlon. 2010a. Laboratory Geomechanical Strength Testing of DGR-3 & DGR-4 Core. Intera Engineering Ltd. Report TR-08-24 Rev.1. CANMET Mining and Mineral Sciences Laboratories. Ottawa, Ontario, Canada.
- Gorski, B., T. Anderson and B. Conlon. 2010b. Long-term strength testing of DGR-3 and DGR-4 Core TR-08-36, Revision 1. Canada Centre for Mineral and Energy Technology – Mining and Mineral Sciences Laboratories. Ottawa, Ontario, Canada.
- Graf, D.L. 1982. Chemical osmosis, reverse chemical osmosis, and the origin of subsurface brines. *Geochimica et Cosmochimica Acta* 46, 1431-1448.
- Haeri-Ardakani, O., I.S. Al-Aasm and M. Coniglio. 2013. Petrologic and geochemical attributes of fracture-related dolomitization in Ordovician carbonates and their spatial distribution in southwestern Ontario, Canada. *Marine and Petroleum Geology* (2013). DOI: 10.1016/.
- Hanor, J.S. 2001. Reactive transport involving rock-buffered fluids of varying salinity. *Geochimica et Cosmochimica Acta* 65(21), 3721-3732.
- Hobbs, M.Y., S.K. Frape, O. Shouakar-Stash and L.R. Kennell. 2011. Regional Hydrogeochemistry – Southern Ontario. Nuclear Waste Management Organization Report DGR-TR-2011-12. Toronto, Ontario, Canada.
- Huysmans, M. and A. Dassargues. 2005. Review of the use of Péclet numbers to determine the relative importance of advection and diffusion in low permeability environments. *Hydrogeology Journal* 13, 895–904.
- Intera (Intera Engineering Ltd.). 2011. Descriptive Geosphere Site Model. Intera Engineering Ltd. report for the Nuclear Waste Management Organization Report NWMO DGR-TR-2011-24. Toronto, Ontario, Canada
- Itasca (Itasca Consulting Group Inc.). 2011. Long Term Geomechanical Stability Analysis. Nuclear Waste Management Organization Report NWMO DGR-TR-2011-17. Toronto, Ontario, Canada.
- Itasca Canada and AECOM. 2011. Three-Dimensional Geological Framework Model. Nuclear Waste Management Organization Report NWMO DGR-TR-2011-42. Toronto, Ontario, Canada.
- Itasca. 2015. Long-Term Stability Analysis of APM Mark II Conceptual Design in Sedimentary and Crystalline Rock Settings. Nuclear Waste Management Organization Report NWMO-TR-2015-27. Toronto, Ontario, Canada.
- Kharaka, Y.K. and J.S. Hanor. 2003. Deep fluids in the Continents: 1. Sedimentary Basins. *In*: J.I. Drever (Ed.). *Treatise on Geochemistry, Surface and Groundwater, Weathering, and Soils* 5, 499-540.

- Kharaka, Y.K., A.S. Maest, W.W. Carothers, L.M. Law, P.J. Lamothe and T.L. Fries. 1987. Geochemistry of metal-rich brines from central Mississippi Salt Dome Basin, U.S.A. *Applied Geochemistry* 2, 543-561.
- Kharaka Y.K. and F.A.F. Berry. 1973. Simultaneous flow of water and solutes through geological membranes I: Experimental investigation. *Geochimica et Cosmochimica Acta* 37, 2577-2603.
- Land, L.S. 1997. Mass transfer during burial diagenesis in the Gulf of Mexico sedimentary basin: an overview. *Society for Sedimentary Geology* 57, 29-39.
- Land, L.S. and D.R. Prezbindowski. 1981. The origin and evolution of saline formation water, Lower Cretaceous carbonates, south-central Texas, U.S.A. *Journal of Hydrology* 54, 51-74.
- Lo, K.Y. and R.S.C. Wai. 1982. Thermal expansion, diffusivity, and cracking of rock cores from Darlington, Ontario. *Canadian Geotechnical Journal* 19, 154-166.
- Luszczynski, N.J. 1961. Head and flow of ground water of variable density. *Journal of Geophysical Research* 66(12), 4247-4256.
- McCauley, C.A., D.M. White, M.R. Lilly and D.M. Nyman. 2002. A comparison of hydraulic conductivities, permeabilities and infiltration rates in frozen and unfrozen soils. *Cold Regions Science and Technology* 34(2), 117-125.
- McIntosh, J.C. and L.M. Walter. 2006. Paleowaters in Silurian-Devonian carbonate aquifers: Geochemical evolution of groundwater in the Great Lakes region since the late Pleistocene. *Geochimica et Cosmochimica Acta* 70, 2454-2479.
- Nagasaki, S., T. Saito and T. Yang. 2016. Sorption Behavior of Np(V) on Illite, Shale and MX-80 in High Ionic Strength Solutions. *Journal of Radioanalytical and Nuclear Chemistry* 308 (1), 143-153.
- Nagasaki, S., J. Riddoch, T. Saito, J. Goguen, A. Walker and T. Yang. 2017. Sorption behavior of Np(IV) on illite, shale and MX-80 in high ionic strength solutions. *Journal of Radioanalytical and Nuclear Chemistry* 313(1), 1-11.
- Nagasaki, S. 2018. Sorption Properties of Np on Shale, Illite and Bentonite Under Saline, Oxidizing and Reducing Conditions. Nuclear Waste Management Organization Report NWMO-TR-2018-02. Toronto, Ontario, Canada.
- NWMO. 2011. Geosynthesis. Nuclear Waste Management Organization Report NWMO DGR-TR-2011-11. Toronto, Ontario, Canada.
- Normani, S.D. 2009. Paleoevolution of Pore Fluids in Glaciated Geologic Settings. Ph.D. thesis, University of Waterloo. Waterloo, Ontario, Canada.

- Normani, S.D., Y.J. Park, J.F. Sykes, and E.A. Sudicky. 2007. Sub-regional Modelling Case Study 2005-2006 Status Report. Nuclear Waste Management Organization Report NWMO TR-2007-07. Toronto, Ontario, Canada.
- Park, Y.-J., E.A. Sudicky and J.F. Sykes. 2009. Effects of shield brine on the safe disposal of waste in deep geologic environments. *Advances in Water Resources* 32, 1352–1358.
- Park, Y.-J., E.A. Sudicky, S. Panday, J.F. Sykes, and V. Guvanasen. 2008. Application of implicit sub-time stepping to simulate flow and transport in fractured porous media. *Advances in Water Resources* 31(7), 995-1003.
- Paraskevopoulou, C., M. Perras, M. Diederichs, F. Amann, S. Loew, T. Lam and M. Jensen. 2017. The three stages of stress relaxation-Observations for the time-dependent behaviour of brittle rocks based on laboratory testing. *Engineering Geology* 216, 56-75.
- Peltier, W.R. 2002. A design basis glacier scenario. Ontario Power Generation Report 06819-REP-01200-10069-R00. Toronto, Ontario, Canada.
- Peltier, W.R. 2011. Long-Term Climate Change. Nuclear Waste Management Organization Report NWMO DGR-TR-2011-14. Toronto, Ontario, Canada.
- Rittenhouse, G. 1967. Bromine in oil-field waters and its use in determining possibilities of origin of these waters. *American Association of Petroleum Geology Bulletin* 51(12), 2430-2440.
- Riddoch, J. and S. Nagasaki. 2016. Sorption and Speciation of Palladium under High Ionic Strength Conditions. Proceedings of 3rd Canadian Conference on Nuclear Waste Management, Decommissioning and Environmental Restoration, Ottawa, Canada, September 11-14, 2016.
- Sherwood Lollar, B. 2011. Far-field Microbiology Considerations Relevant to a Deep Geological Repository – State of Science Review. Nuclear Waste Management Organization Report NWMO TR-2011-09. Toronto, Ontario, Canada.
- Sherwood Lollar B., S.M. Weise, S.K. Frape and J.F. Barker. 1994. Isotopic constraints on the migration of hydrocarbon and helium gases of southwestern Ontario. *Bulletin of Canadian Petroleum Geology* 42, 283-295.
- Singh, B.P. and B. Kumar. 2005. *Isotopes in Hydrology, Hydrogeology, and Water Resources*. Narosa Publishing House Pvt. Ltd., New Delhi, India.
- Slater, G.F., D.P. Moser and B. Sherwood Lollar. 2013. Development of Microbial Characterization Techniques for Low-Permeability Sedimentary Rocks. Nuclear Waste Management Organization Report TR-2013-17. Toronto, Ontario, Canada.
- Stroes-Gascoyne, S. and C.J. Hamon. 2008. Preliminary Microbial Analysis of Limestone and Shale Rock Samples. Nuclear Waste Management Organization Report NWMO TR-2008-09. Toronto, Canada.

- Stroes-Gascoyne, S., C. Sergeant, A. Schippers, C.J. Hamon, S. Nèble, M.-H. Vesvres, V. Barsotti, S. Poulain and C. Le Marre. 2011. Biogeochemical processes in a clay formation *in situ* experiment: Part D - Microbial analyses - Synthesis of results. Applied Geochemistry 26, 980-989.
- Stuhne, G. and W.R. Peltier. 2015. Surface Boundary Conditions During Long-Term Climate Change. Nuclear Waste Management Organization Report NWMO-TR-2015-16. Toronto, Ontario, Canada.
- Stuhne, G. and W.R. Peltier. 2016. Sensitivity Analyses of Surface Boundary Conditions During Long-Term Climate Change. Nuclear Waste Management Organization Report NWMO-TR-2016-19. Toronto, Ontario, Canada.
- Sykes, J.F., S.D. Normani and Y. Yin. 2011. Hydrogeologic Modelling. Nuclear Waste Management Organization Report NWMO DGR-TR-2011-16. Toronto, Ontario, Canada.
- Sykes, E.A. 2007. Hydrogeologic modelling to assess conditions related to OPG's proposed Deep Geologic Repository in Tiverton, Ontario. Master's thesis, University of Waterloo. Waterloo, Ontario, Canada.
- Valley, B. and S. Maloney. 2010. Analysis of DGR-1, DGR-2, DGR-3 and DGR-4 Borehole Images for Stress Characterization. MIRARCO/Geomechanics Research Centre, Laurentian University, Sudbury. Nuclear Waste Management Organization Report NWMO DGR-TR-08-35. Toronto, Ontario, Canada.
- Vilks, P. 2009. Sorption in Highly Saline Solutions – State of the Science Review. Nuclear Waste Management Organization Report NWMO TR-2009-18. Toronto, Ontario, Canada.
- Vilks, P., N.H. Miller and K. Felushko. 2011. Sorption Experiments in Brine Solution with Sedimentary Rock and Bentonite. Nuclear Waste Management Organization Report NWMO TR-2011-11. Toronto, Ontario, Canada.
- Vilks, P. and N.H. Miller. 2014. Sorption Studies with Sedimentary Rock under Saline Conditions. Nuclear Waste Management Organization Report NWMO TR-2013-22. Toronto, Ontario, Canada.
- Vilks, P. and T. Yang. 2018. Sorption of Selected Radionuclides on Sedimentary Rocks in Saline Conditions – Updated Sorption Values. Nuclear Waste Management Organization Report NWMO-TR-2018-03. Toronto, Canada.
- Wang, H.F. 2000. Theory of Linear Poroelasticity with Applications to Geomechanics and Hydrogeology. Princeton University Press, Princeton, USA.
- Weast, R.C. (Ed.). 1983. CRC Handbook of Chemistry and Physics. 64th edition. CRC Press, Inc., Boca Raton, Florida, USA.
- Wersin, P., S. Stroes-Gascoyne, F.J. Pearson, C. Tournassat, O.X. Leupin and B. Schwyn. 2011. Biogeochemical processes in a clay formation *in situ* experiment: Part G - key

interpretations and conclusions. Implications for repository safety. *Applied Geochemistry* 26, 1023-1034.

West, J.M. and I.G. McKinley. 2002. The geomicrobiology of radioactive waste disposal. In: Bitton G (ed) *The encyclopedia of environmental microbiology*. Wiley, New York, pp 2661–2674.

Xiang, Y., T. Al and M. Mazurek. 2016. Effect of confining pressure on diffusion coefficients in clay-rich, low-permeability sedimentary rocks. *Journal of Contaminant Hydrology* 195, 1-10.

THIS PAGE HAS BEEN LEFT BLANK INTENTIONALLY

3. USED FUEL CHARACTERISTICS

3.1 Used Fuel Description

3.1.1 Used Fuel Type and Amount

The inventory of used fuel in interim storage in Canada consists primarily of 28-element and 37-element natural uranium CANDU fuel bundles and their variants. Variants include the 37-element long length bundle and the 37m bundle¹, while additionally there are some older bundles that do not have the CANLUB coating (i.e., a thin graphite layer between the fuel pellet and the fuel sheath). Other fuel bundles in storage include small quantities of 18-element bundles², 19-element bundles³, and 43-element bundles⁴.

The storage inventory also includes very small quantities of experimental fuel types and research reactor fuels (including some enriched in U-235) stored by AECL.

Given the overwhelming predominance of CANDU fuel in interim storage, the used fuel waste form evaluated in this assessment is a natural uranium UO₂ CANDU fuel bundle. The AECL experimental fuel types mentioned above are not included due to their small amount and limited data on fuel characteristics.

The conceptual repository is assumed to contain 5,224,000 used bundles (Garamszeghy 2016). This number of fuel bundles is based on the announced life plans for the reactor fleet (i.e. refurbishment or not). Under this scenario, refurbishment of Darlington, Bruce A Units 3 and 4 and Bruce B is assumed, while refurbishment of Bruce A Units 1 and 2, and Point Lepreau has already been completed. Pickering reactors are assumed to run until 2020 with no refurbishment⁵, and refurbished reactors are assumed to operate until the new pressure tubes have accumulated 25 effective full power years.

Because the inventory projections indicate there will be 4.4×10^6 37-element bundles, 7.8×10^5 28-element bundles, and 3.3×10^4 other bundle types (e.g. 18 or 19 element bundles), the standard 37-element fuel bundle is selected as the reference fuel bundle for this assessment. Sensitivity studies in Tait et al. (2000) show the differences in radionuclide inventories on unit mass basis between the 28-element and 37-element designs are small enough to be ignored. Specifically:

- Radionuclide inventories calculated for a discharge burnup of 250 MWh/kgU differ by less than 3%, with the most significant differences occurring for Ra-225, Ac-225, Ra-225, Th- 229, U-233, Np-237, Pu-239, Pu-242, and Cm-244.
- The difference between standard and long 37 element bundles was small on a unit mass basis, with (integrated) thermal and gamma powers agreeing within 0.02% at 10 years.

¹ A modified 37-element bundle (37m) with slightly smaller center pin diameter; it has entered service at Bruce and Darlington stations.

² Used in Gentilly 1.

³ Used in NPD and Douglas Point.

⁴ 43-element CANFLEX LVRFB bundle with a central dysprosium element; used in a limited run at Bruce B.

⁵ Pickering 5-8 licences were renewed in 2018 for continued operation to 2024.

Note that the age of the fuel when placed in the repository will vary. Because the earliest bundles date back to 1970 and because the repository is unlikely to open before 2040, some fuel will be over 70 years old at the time of placement. For this assessment, all fuel bundles are assumed to have an out-of-reactor decay time of 30 years.

3.1.2 Geometry

Fuel pellets formed from natural uranium UO_2 are placed inside a fuel sheath made of a zirconium-tin alloy (Zircaloy-4) with a thin CANLUB graphite coating on the inside. The ends of the sheath are closed by a welded zirconium alloy plug to produce a sealed fuel element. Fuel elements are welded to zirconium alloy end plates to form a fuel bundle as shown in Figure 3-1.

The number of pellets in a fuel element, and the number and dimensions of the fuel elements in a fuel bundle depend on the particular CANDU reactor. As noted previously, the most common bundle contains 37 fuel elements, each of which is 13.1 mm diameter and 486 mm long. This fuel bundle weighs 23.9 kg, of which 21.7 kg is UO_2 and 2.2 kg is Zircaloy (Tait et al. 2000). This is the bundle that has been selected as the reference bundle for this assessment.

Upon discharge, less than 0.015% of the bundles are expected to have minor damage or defects (such as pinhole failures in the fuel sheaths) based on statistics from 1994 to 2006 (IAEA 2010), although pre-1994 bundle defect rates were approximately 0.1% (Tait et al. 2000). Analysis of the integrity of used fuel bundles indicates that they are unlikely to fail during storage (Freire-Canosa 2011). A small percentage may have increased susceptibility to integrity failure during subsequent transport to permanent storage. While the specific value may be relevant to the packaging plant design, the postclosure safety assessment is not sensitive to this value since no credit is taken for fuel integrity.

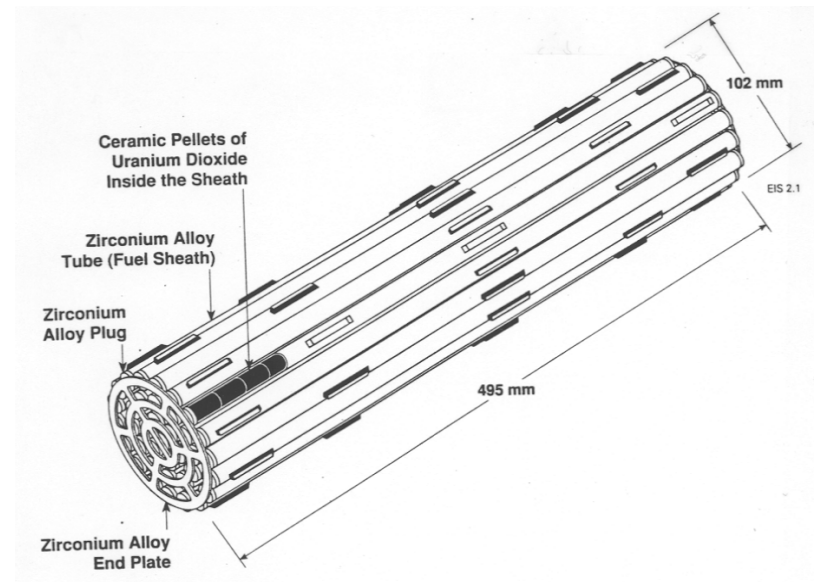


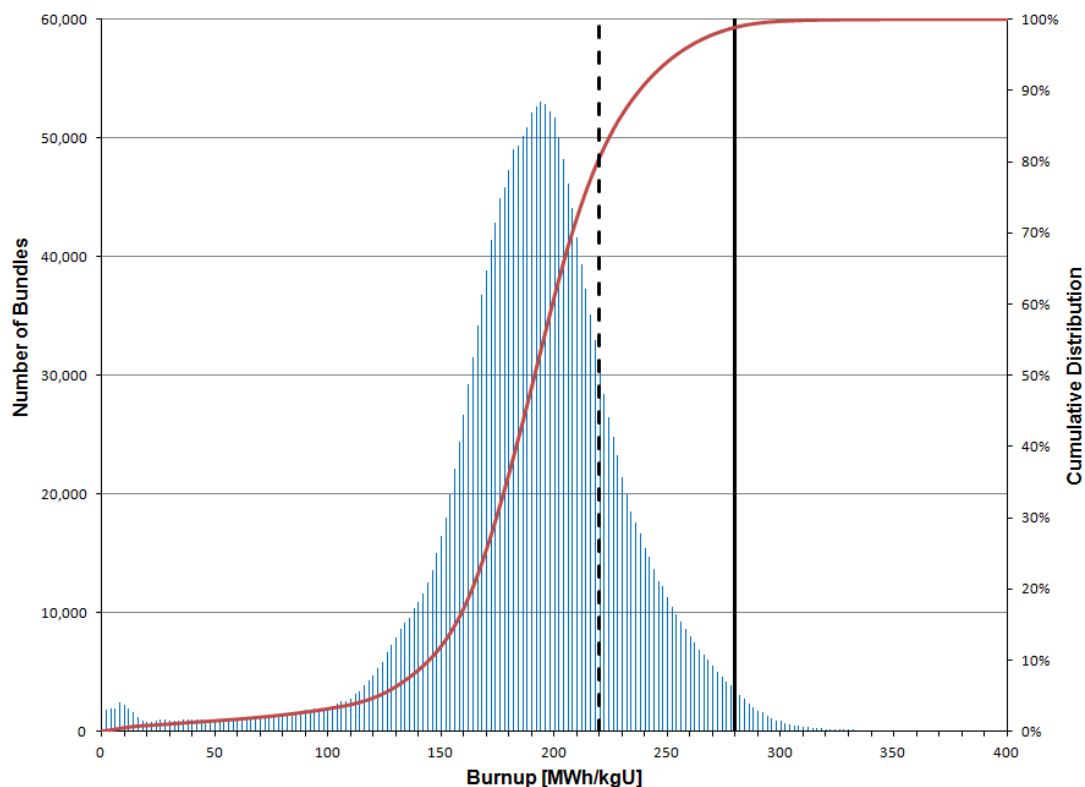
Figure 3-1: Typical CANDU Fuel Bundle

3.1.3 Discharge Burnup and Linear Power

Discharge Burnup:

Discharge burnup is a measure of the total energy produced by the used fuel bundle while it is still in the reactor. The radioactivity level, heat generation rate, and radionuclide composition all depend on this value. The discharge burnup itself depends on many factors including the type of reactor, the location of the bundle in the core, the bundle residence time, and bundle shifts that occur during fuelling operations. Although each bundle has a unique irradiation history, used fuel from all CANDU reactors is similar enough that it is not necessary to know individual detailed characteristics to assess the overall behaviour of the used fuel assemblies in the repository.

Figure 3-2 shows the distribution of discharge burnup for all CANDU used fuel bundles in interim storage for the time period up to and including 2012 (Wilk 2013). The aggregate 95th percentile value is 254 MWh/kgU, with some exceptional fuel elements experiencing burnups as high as 706 MWh/kgU. The median value is 192 MWh/kgU. At this burnup level, about 2% of the initial uranium is converted into other elements.



Note: The vertical dashed and solid black lines correspond to burnup values of 220 MWh/kgU and 280 MWh/kgU, while the red line represents the cumulative distribution. The figure is based on data in Wilk (2013).

Figure 3-2: Used Fuel Discharge Burnup

Table 3-1 shows the corresponding discharge burnup percentiles using lifetime aggregate values on a per station basis for burnup values of 220 MWh/kgU and 280 MWh/kgU (Wilk 2013).

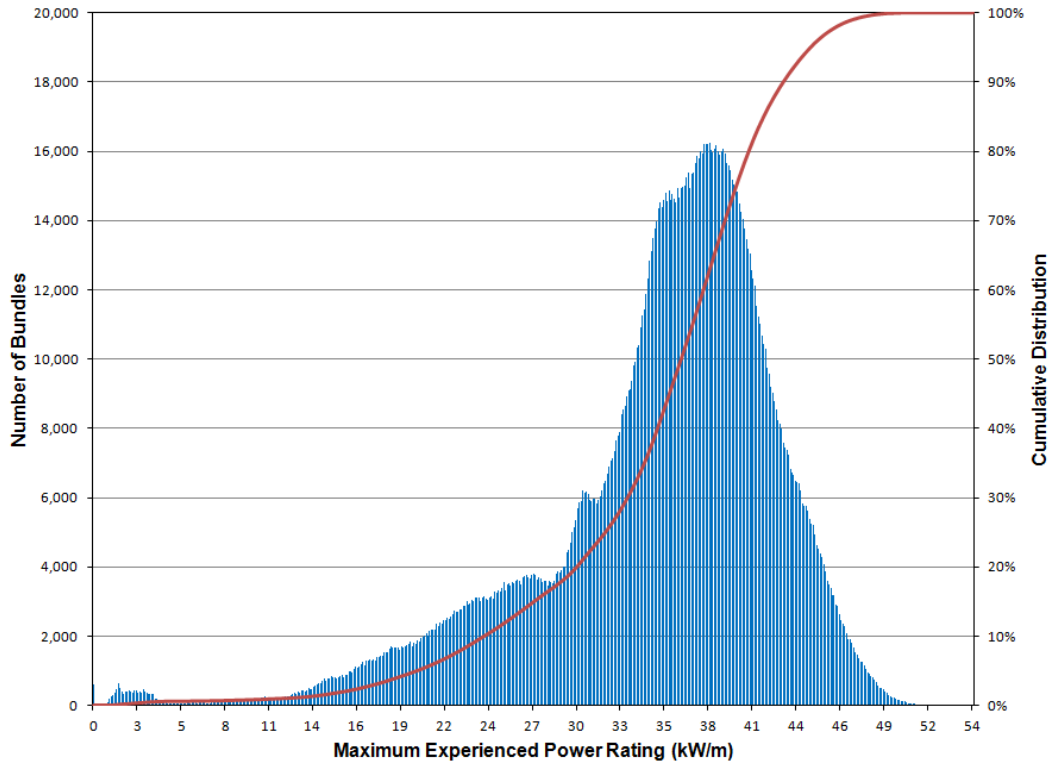
Table 3-1: Discharge Burnup Percentiles on a Per Station Basis

Reactor	Burnup Percentile for 220 MWh/kgU	Burnup Percentile for 280 MWh/kgU
Bruce A	62.9	96.7
Bruce B	92.3	99.7
Darlington A	75.3	99.7
Gentilly-2	93.3	99.9
Point Lepreau	93.0	99.9
Pickering A	71.5	95.0
Pickering B	87.3	99.8
Aggregate	80.7	98.8

Linear Power:

Linear power is a measure of the energy production rate per unit length of the fuel. Linear power primarily affects the operating temperatures, which typically range from around 400°C on the outside of the fuel sheath to between 800°C and 1700°C at the fuel centreline, well below the UO₂ melting temperature of 2865°C.

Figure 3-3 shows the distribution of maximum linear power for all CANDU used fuel bundles in interim storage for the time period up to and including 2012 (Wilk 2013). Tait et al. (2000) show that the differences in radionuclide inventories between typical minimum and maximum power levels (200 kW/bundle and 900 kW/bundle) are generally less than about 2% for the same burnup. Tait et al. (2000) therefore adopted a mid-range value of 455 kW/bundle for reference inventory calculations.



Note: The standard deviation of the distribution is approximately 7.4 kW/m or 140 kW/bundle.
The figure is based on data in Wilk (2013).

Figure 3-3: Maximum Fuel Bundle Linear Power

Given these burnup and linear power data, the following values are adopted in this assessment:

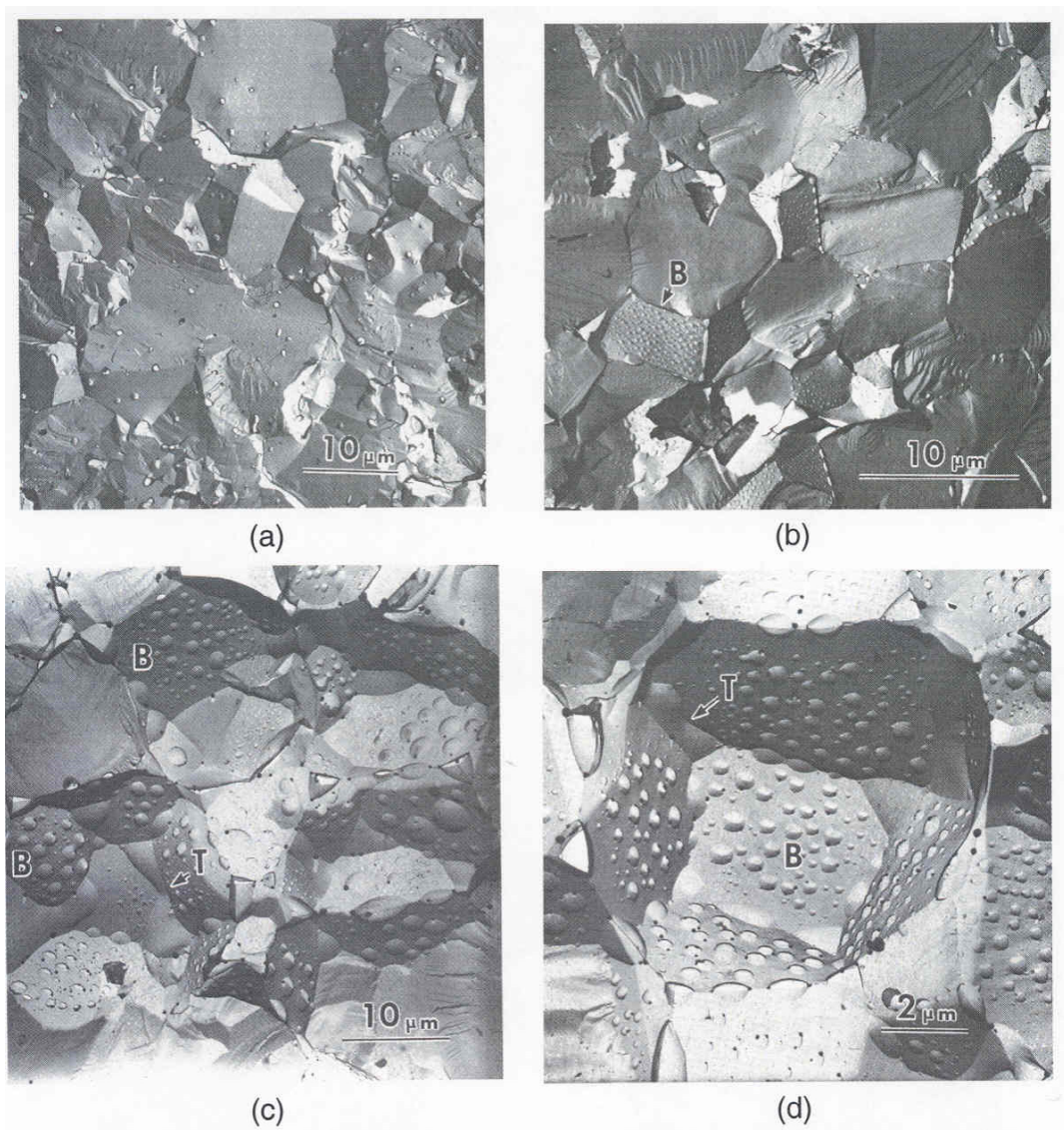
- For scenarios involving a small number of used fuel containers (such as the Normal Evolution Scenario – see Chapter 6), the discharge burnup is 280 MWh/kgU and the maximum linear power level is 455 kW/bundle. Table 3-1 shows this burnup value corresponds to at least the 95th (and up to 99.9th) percentile discharge burnup, depending on the station.
- For scenarios involving a large number of used fuel containers (such as the All Containers Fail Scenario – see Chapter 6), the discharge burnup is 220 MWh/kgU and the maximum linear power level is 455 kW/bundle. Table 3-1 shows this burnup value corresponds to the 80th percentile discharge burnup across the entire inventory, with values for individual stations both above and below this percentile.

The higher value is adopted for events involving a small number of containers to address the potential situation in which the container is fully loaded with high burnup fuel bundles. This is conservative, in part because it is unlikely that all the bundles in a given load are high burnup, but also because such a container could have a high heat load, and would be deliberately monitored to avoid this situation during the container filling stage. For events involving a large number of containers, it is not physically possible for all containers to be fully loaded with 95th percentile burnup bundles and therefore a lower (yet still conservative) value is adopted.

3.1.4 Effect of Irradiation

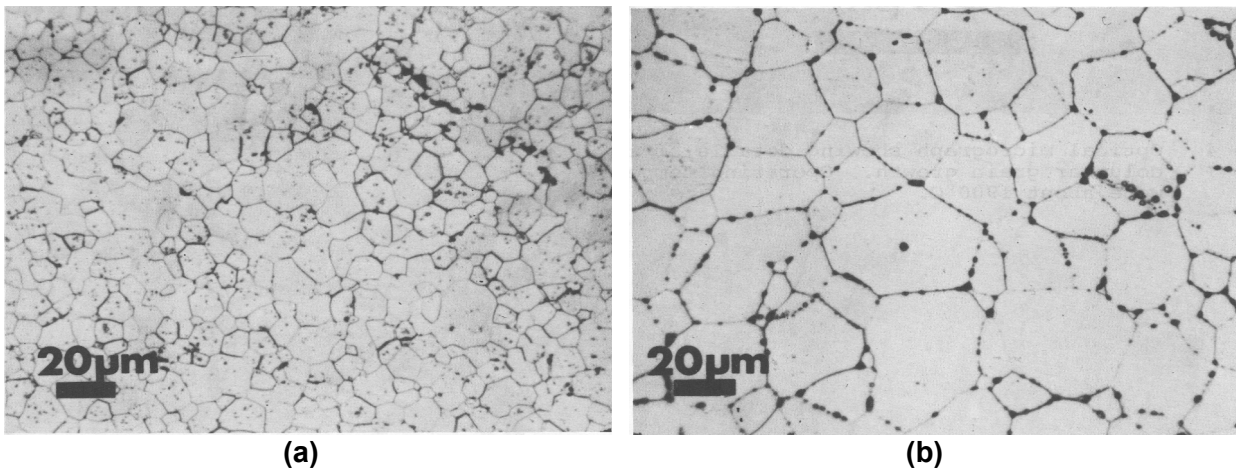
The fuel undergoes a number of microstructural changes during irradiation, as illustrated by the sequence of photographs in Figure 3-4. Unirradiated fuel has a cohesive, interlocking microstructure and many grains have some internal sintering porosity from the fuel fabrication process. During irradiation, the sintering porosity is largely eliminated, boundaries between individual grains become more distinct, and some volatile elements diffuse out of the fuel grains to form fission gas bubbles at the interfaces between grains. At linear power ratings higher than approximately 50 kW/m (equivalent to about 900 kW/37-element bundle, i.e., higher than achieved in most CANDU bundles), the fission gas bubbles enlarge and begin to coalesce, leading in some cases to the formation of gas tunnels along grain boundaries.

Unirradiated fuel pellets are very fine-grained, but at linear power ratings higher than approximately 50 kW/m equiaxial grain growth occurs in the pellet interior where temperatures are highest (Figure 3-5). Grain growth is typically accompanied by the diffusion and segregation of non-volatile fission products, some of which form small metallic particles at grain boundaries as shown in Figure 3-6.



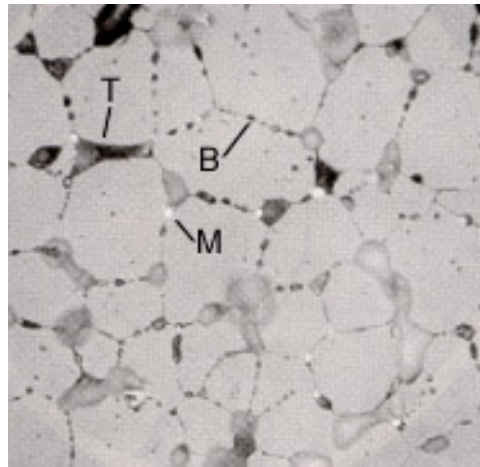
- Notes: (a) Typical microstructure of unirradiated UO_2 . Small inclusions = sintering porosity.
 (b) Irradiated at low power ($< 45 \text{ kW/m}$). Note loss of sintering porosity and development of small intergranular fission gas bubbles (B).
 (c) Irradiated at higher power ($\geq 50 \text{ kW/m}$), showing growth of fission gas bubbles (B) and initiation of tunnels (T).
 (d) Magnified view of irradiated higher power fuel. Note the grain-edge tunnels (T) and the development of fission gas bubbles (B) on all faces of the "pull-out" of a single grain.
 Ref.: Hastings (1982).

Figure 3-4: Typical Microstructure of Unirradiated and Irradiated UO_2 Fuel



- Notes:
- (1) Unirradiated UO_2 . Note sintering porosity in grain interiors.
 - (2) Irradiated UO_2 at low burnup and high power (20 MWh/kgU at 50 kW/m). Note increase in grain size, loss of sintering porosity, and formation of fission gas bubbles and tunnels along boundaries. Ref.: Hastings (1982).

Figure 3-5: Grain Growth in Irradiated UO_2 Fuel



- Notes: Optical micrograph of polished and etched UO_2 fuel irradiated to very high burnup (770 MWh/kgU at 52 kW/m), showing small white particles at grain boundaries (M) that are formed from incompatible metals such as Mo, Ru, and Pd that have diffused out of the UO_2 grains. Well-developed fission gas bubbles (B) and tunnels (T) are also present at grain boundaries. Scale is approximately same as shown for Figure 3-5. Ref.: Novak and Hastings (1991).

Figure 3-6: Segregation of Metallic Fission Products from UO_2 Fuel

Compared to fresh bundles, used bundles contain new elements (approximately 2% by mass), including fission products, activation products and actinides other than uranium. Of these, more than 95% remain within the UO_2 grains very close to the location of their formation (Gobien et al. 2018, and references therein).

As indicated in Figure 3-7, the species produced can be grouped according to their chemical behaviour into the following categories (Kleykamp 1985):

1. Species such as He, Kr, Ar, Cs and I that are gaseous or somewhat volatile at fuel operating temperatures (i.e., 400-1700°C). Due to their relatively high diffusion coefficients, during reactor operation a small fraction of each species migrates out of the fuel grains and into fuel element void spaces (i.e., into the fuel sheath gap and into cracks in the fuel pellets). At the same time, another small fraction moves to the grain boundaries within the fuel pellets and forms fission gas bubbles. The remainder (roughly 95%) of the fission gases are held in the UO_2 crystal lattice.
2. Species such as the metals Mo, Ru, and Pd that are non-volatile but have a low solubility in UO_2 . At high in-reactor temperatures, small quantities of these species can diffuse from the fuel grains and segregate as metallic alloy phases at grain boundaries, particularly in areas of UO_2 grain growth. The majority of incompatible species remain trapped within the fuel grains due to their low diffusion coefficients in UO_2 at fuel operating temperatures.
3. Species that are compatible with UO_2 , including the lanthanide elements and actinides such as Pu, Am, Np. These elements can substitute chemically for uranium in UO_2 , and the atoms are then structurally bound as trace elements in the UO_2 crystal lattice.

The Zircaloy-4 fuel sheath consists of approximately 98 wt% Zr and 1.5 wt% Sn, with a number of other elements present at trace levels or as impurities (Tait et al. 2000). During irradiation, the cladding receives a neutron fluence of around 10^{25} n/m² (Truant 1983). The irradiated metal cladding is a fine-grained material (grain size typically 10 μm , thickness typically 0.4 mm) with neutron activation products, such as C-14, Ni-59 and Ni-63, present at concentrations less than 1 mg/kg Zr. Due to the low temperature of the cladding material during irradiation (< 400°C), activation products in the Zircaloy cannot diffuse any significant distance from the site of their formation, and they are therefore likely to be distributed uniformly throughout the metal. While in-reactor, coolant pressure causes the fuel cladding to collapse onto the fuel pellets, the heat generated in the fuel causes the pellets to expand slightly into an hourglass shape, which leads to the formation of minor cylindrical ridges in the cladding. This effect is more pronounced at high linear power and when fuel is in the reactor for long times.

Corrosion products formed within the primary coolant circuit of a reactor can deposit on the surfaces of fuel bundles in the reactor core. Neutron activation of some of these corrosion products can generate radioactive isotopes. In addition, fission products and uranium released from defective fuel bundles can also deposit on fuel bundle surfaces. In the context of a geological repository for used fuel, these surface deposits provide a small additional source of radionuclides. Information on radionuclide concentrations on the external surfaces of fuel bundles (Chen et al. 1986, Gobien et al. 2018) indicates that the fission product, uranium and transuranium inventories in these surface deposits are very low (< 0.001%) compared to the corresponding inventories within the fuel bundle itself and they can therefore be neglected in postclosure safety assessment calculations. The compilation also indicates that the inventories of Fe, Ni, Cu, and Cr on the outside surfaces of the fuel bundles are approximately 1.5%, 1%, 2.5% and 1% of the corresponding inventories in the fuel itself.

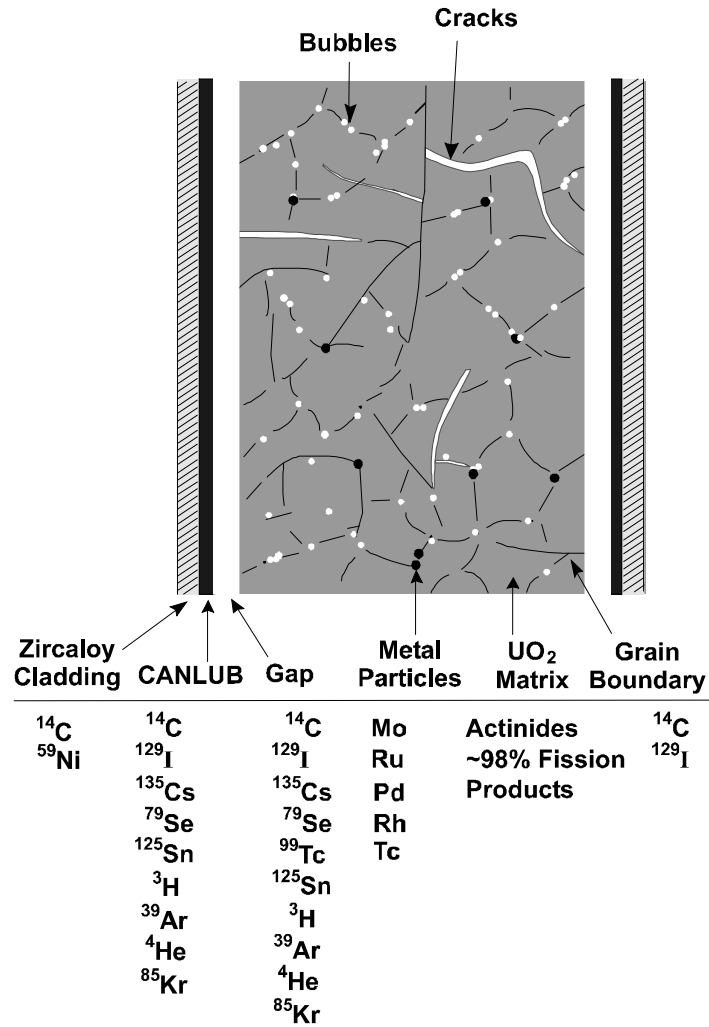


Figure 3-7: Illustrative Distribution of Some Fission Products and Actinides within a Used-Fuel Element

3.1.5 Reference Used Fuel Parameters

Table 3-2 summarizes the characteristics of the reference used fuel bundle adopted in this assessment.

Table 3-2: Reference Used Fuel Parameters

Parameter	Value	Comment
Waste Form	37-element UO ₂ fuel bundle	Standard fuel bundle from Bruce and Darlington stations
Mass U/bundle	19.25 kg	Initial mass (before irradiation)
Mass Zircaloy/ bundle	2.2 kg	Includes cladding, spacers, end plates
Initial U-235	0.72 wt% U	Natural uranium is used in all CANDU fuel, except a small number of research or test bundles.
Burnup	220 MWh/kgU	For events affecting a large number of containers (such as the All Containers Fail Disruptive Event Scenario – see Chapter 6)
	280 MWh/kgU	For events affecting a small number of containers (such as the Base Case of the Normal Evolution Scenario – see Chapter 6)
Power Rating	455 kW/bundle	Nominal mid-range value
Fuel Age (when placed in repository)	30 years	e.g., 10 years in pools, 20 years in dry storage
Fuel Pellet Geometric Surface Area	8.47 cm ²	Surface area of undamaged pellet (37 element design)

Note: Fuel data from Tait et al. (2000), burnup data from Wilk (2013).

3.2 Radionuclide and Chemical Element Inventories and Uncertainties

3.2.1 Potentially Hazardous Radionuclides and Elements

When discharged from the reactor, the used fuel bundle initially contains hundreds of different radionuclides; however, many of these decay quickly and/or are present at very low levels. Following placement in a deep geological repository, only a small fraction of these pose a potential radiological hazard to humans or the environment. The subset of radionuclides of potential concern for safety is identified via a screening analysis.

The screening analysis, described in Chapter 7, identifies 31 radionuclides from the UO₂ fuel and 1 radionuclide from the Zircaloy sheath as potentially important. C-14 in the fuel and the Zircaloy sheath were not identified in the screening analysis but are included in this assessment due to their potential radiological significance in gas pathways. Six additional radionuclides are included to ensure ingrowth is properly accounted for so that a total of 40 radionuclides are included in the detailed safety assessment calculations described in Chapter 7.

Table 3-3 shows the included radionuclides and their associated decay chains.

Table 3-3: Potentially Significant Radionuclides Included in the Assessment

Radionuclides	
Fuel	
Single Nuclides	I-129, Cl-36, Cs-135, Pd-107, Se-79, Sm-147, Tc-99, C-14
Chain Nuclides	Pu-239 → U-235 = Th-231 → Pa-231 = Ac-227 = Th-227 = Ra-223
	Pu-240 → U-236 → Th-232 = Ra-228 = Th-228 = Ra-224
	Pu-242 → U-238 = Th-234 → U-234 → Th-230 → Ra-226 = Rn-222 = Pb-210 = Bi-210 = Po-210
	Am-241 → Np-237 = Pa-233 → U-233 → Th-229 = Ra-225 = Ac-225
Zircaloy	
Single Nuclides	Cl-36, C-14

Note: Red shows the screened-in radionuclides. The '→' indicates decay is modelled while the '=' indicates the species is modelled in secular equilibrium with the parent. Radionuclides in black are added to account for ingrowth.

At the time of discharge the used fuel also contains essentially the full set of elements ranging from hydrogen to californium; however, only a small fraction of these could potentially pose a non-radiological hazard to humans or to the environment. The subset of chemical elements of potential concern is identified via a screening analysis.

This screening analysis is also described in Chapter 7. The analysis identifies 7 elements of potential concern arising from the fuel, where multiple isotopes of an element are considered as one element. No elements of potential concern from the Zircaloy sheath were identified. To ensure that ingrowth is properly accounted for (leading to formation of these elements within the repository), an additional 3 radionuclides are also included in the chemical hazard analysis.

Table 3-4 shows the included chemical elements and their associated decay chains.

Table 3-4: Potentially Hazardous Elements Included in the Assessment

Chemically Hazardous Elements	
Fuel	
Elements	Hg, Mo, Nd, Pd, Rh, Ru
Ingrowth Path	Pd-107 → Ag Sm-147 → Nd Sm-148 → Nd

Note: Red shows the screened-in elements. The '→' indicates decay is modelled. Radionuclides in black are added to account for ingrowth.

3.2.2 Inventories of Potentially Hazardous Radionuclides and Elements

Table 3-5 and Table 3-6 list all the radionuclides shown in either Table 3-3 or Table 3-4 together with their half lives, their inventories at the assumed time of placement in the repository, and various uncertainties associated with the inventories (discussed in next section). The inventories are taken from Tait and Hanna (2001).

Tait and Hanna (2001) and Tait et al. (2000) calculated radionuclide inventories using an average burnup calculation (i.e., all fuel elements in the bundle are assumed to experience the same average neutron flux and, hence, the same average burnup). However, since elements in each ring of the bundle will see a different neutron flux because of shielding by the surrounding elements, the actual burnup in each ring will be different.

A more accurate but computationally more difficult calculation can be done by performing an inventory calculation for each bundle ring and summing the results to derive an average bundle inventory. Tait et al. (2000) carried out such a sensitivity study to determine the differences between radionuclide inventories calculated using an average fuel bundle burnup and by summing inventories produced in individual bundle rings. For this postclosure safety assessment, corrections have been made to the inventories calculated by Tait and Hanna (2001) to account for the difference in the bundle average and “ring sum”⁶ inventories wherever those differences exceed +1%, as described in Gobien et al. (2018).

⁶ “Ring sum” refers to a radionuclide inventory calculation performed with different neutron fluxes and, hence, different burnup assumptions in the individual fuel bundle ‘rings’ (Tait et al. 2000)

Table 3-5: Inventories of Potentially Hazardous Radionuclides in UO₂ Fuel for 30 Year Decay Time

Nuclide	Half-life ⁽⁴⁾ (a)	280 MWh/kgU Inventory (moles/kgU initial)	220 MWh/kgU Inventory (moles/kgU initial)	σ _{OR} (%)	σ _{PR} (%)	σ _{Total} (%)
Ac-225	2.7380E-02	1.856E-14	1.662E-14	-	-	(1)
Ac-227	2.1770E+01	1.872E-11	1.573E-11	3	-	3
Am-241	4.3260E+02	1.544E-03 ⁽⁵⁾	1.155E-03 ⁽⁵⁾	15	-	15
Bi-210	1.3720E-02	5.225E-18	5.296E-18	-	-	(1)
C-14	5.7000E+03	6.725E-06	5.207E-06	-	-	(2)
Cl-36	3.0100E+05	6.886E-06	5.422E-06	-	-	(3)
Cs-135	2.3000E+06	3.455E-04	2.675E-04	7	7.9	10.6
I-129	1.5700E+07	5.486E-04	4.228E-04	7	-	7
Np-237	2.1440E+06	2.218E-04	1.708E-04	20	-	20
Pa-231	3.2760E+04	4.473E-08	3.820E-08	3	-	3
Pa-233	7.3850E-02	7.662E-12	5.901E-12	-	-	(1)
Pb-210	2.2200E+01	8.488E-15	8.604E-15	55	-	55
Pd-107	6.5000E+06	9.866E-04	6.901E-04	7	-	7
Po-210	3.7890E-01	1.443E-16	1.463E-16	-	-	(1)
Pu-239	2.4110E+04	1.152E-02	1.123E-02	3	-	3
Pu-240	6.5610E+03	6.788E-03	5.339E-03	4	-	4
Pu-242	3.7350E+05	7.773E-04	4.257E-04	7	-	7
Ra-223	3.1290E-02	2.669E-14	2.243E-14	-	-	(1)
Ra-224	1.002E-02	1.656E-12	1.099E-12	-	-	(1)
Ra-225	4.0790E-02	2.747E-14	2.460E-14	-	-	(1)
Ra-226	1.6000E+03	2.282E-12	2.354E-12	55	-	55
Ra-228	5.7500E+00	8.309E-13	8.370E-13	-	-	(1)
Rn-222	1.0470E-02	1.493E-17	1.541E-17	-	-	(1)
Se-79	2.9500E+05	2.216E-05	1.762E-05	7	-	7
Sm-147	1.060E+11	7.699E-04	6.551E-04	7	-	7
Sm-148	7.000E+15	1.507E-04	9.633E-05	7	-	7
Tc-99	2.1110E+05	3.021E-03	2.409E-03	10	-	10
Th-227	5.1140E-02	4.308E-14	3.620E-14	-	-	(1)
Th-228	1.912E+00	3.162E-10	2.097E-10	-	-	(1)
Th-229	7.3400E+03	5.341E-09	4.783E-09	20	-	20

Postclosure Safety Assessment of a Used Fuel Repository in Sedimentary Rock

Document Number: NWMO-TR-2018-08

Revision: 000

Class: Public

Page: 127

Nuclide	Half-life ⁽⁴⁾ (a)	280 MWh/kgU Inventory (moles/kgU initial)	220 MWh/kgU Inventory (moles/kgU initial)	σ_{OR} (%)	σ_{PR} (%)	σ_{Total} (%)
Th-230	7.5380E+04	1.571E-08	1.636E-08	55	-	55
Th-231	2.9110E-03	1.932E-14	2.944E-14	-	-	(a)
Th-232	1.4050E+10	2.078E-03	2.095E-03	4	-	4
Th-234	6.5980E-02	6.074E-11	6.091E-11	-	-	(a)
U-233	1.5920E+05	4.004E-05	3.608E-05	20	-	20
U-234	2.4550E+05	2.166E-04 ⁽⁵⁾	2.089E-04 ⁽⁵⁾	50	-	50
U-235	7.0380E+08	4.748E-03	7.238E-03	3	-	3
U-236	2.3420E+07	3.845E-03	3.501E-03	4	-	4
U-238	4.4680E+09	4.114E+00	4.125E+00	0	-	0

Notes: (1) Nuclide assigned a constant inventory because it has a short half-life.

(2) Nuclide inventory calculated by ORIGEN-S software is based on a N impurity level of 15 µg/gU. Inventory is assigned a uniform distribution with maximum value 1.25x the ORIGEN-S predicted values and minimum value equal to 0.45x the ORIGEN-S predicted inventory. Limits are based on measured C-14 values from Stroes-Gascoyne et al. 1994.

(3) Nuclide inventory is assigned a uniform distribution with maximum value equal to ORIGEN-S software predicted value based on the CI impurity level of 5 µg/gU from Tait et al. (2000). The minimum value is set equal to maximum/10. Table shows the median value.

(4) Half-life from ENDF/B VII.1 (Chadwick et al. 2011) and converted as required using 365.25 days = 1 year.

(5) Incl. inventory of short-lived precursor: Am-241 (Pu-241, 2.737E-4 mol/kgU) and U-234 (Pu-238, 2.259E-5 mol/kgU).

Table 3-6: Inventories of Potentially Hazardous Radionuclides of Interest in Zircaloy for 30 Years Decay Time

Nuclide	Half-life ⁽²⁾ (a)	280 MWh/kgU Inventory (moles/kgZr initial)	220 MWh/kgU Inventory (moles/kgZr initial)	σ_{OR} (%)	σ_{PR} (%)	σ_{Total} (%)
C-14	5.7000E+03	2.457E-05	2.180E-06	-	-	(1)
Cl-36	3.0100E+05	1.489E-05	9.860E-06	-	-	(2)

Notes: (1) Nuclide assigned a constant inventory because it is formed by activation of impurity in the fuel, and impurity levels were assigned high values in Tait et al. (2000).

(2) Half-life from ENDF/B VII.1 (Chadwick et al. 2011) and converted as required using 365.25 days = 1 year.

Table 3-7 lists the chemical elements included in Table 3-4, their inventories at the assumed time of placement in the repository, and the various associated uncertainties. The inventory of an element shown in Table 3-7 excludes the concentration of all short-lived isotopes of the element.

The inventories are from Tait and Hanna (2001) with corrections applied to account for the difference in the bundle average and “ring sum” inventories if differences exceed +1%, as described in Gobien et al. (2018).

Table 3-7: Inventories of Potentially Hazardous Elements for 30 Year Decay Time

Nuclide	Main Source ⁽²⁾	280 MWh/kgU Inventory (moles/kgU initial)	220 MWh/kgU Inventory (moles/kgU initial)	σ_{OR} (%)	σ_{PR} (%)	σ_{Total} (%)
Ag	FP	4.628E-04	3.348E-04	7	-	7
Hg	IMP	7.105E-06	6.719E-06	-	-	(1)
Mo	FP	1.195E-02	9.488E-03	7	-	7
Nd	FP	9.481E-03	7.562E-03	7	-	7
Pd	FP	5.421E-03	3.775E-03	7	-	7
Rh	FP	2.143E-03	1.707E-03	7	-	7
Ru	FP	7.804E-03	5.956E-03	7	-	7

Notes: (1) Nuclide assigned a constant inventory because it is formed by activation of impurity in the fuel, and impurity levels were assigned high values in Tait et al. (2000).

(2) Source of chemical element in fuel is either fission product (FP) or impurity in fuel (Imp).

3.2.3 Uncertainties in Isotope Inventories

Uncertainty in the isotope inventories may occur due to the following factors:

- Uncertainties in the ORIGEN-S inventory calculations due to uncertainties in the software’s input data (e.g., nuclear cross-sections), model approximations, initial impurity levels, and the reference bundle;
- Variation in the burnup and power rating of the fuel from reference value; and
- Variation in the age of the fuel from reference value.

Validation studies (Tait et al. 1995) indicate that ORIGEN-S calculations generally agree with measured actinide and fission product inventories. A comparison of measured and predicted values for several relevant radionuclides in a Pickering fuel bundle is shown in Table 3-8. The larger differences are associated with nuclides with greater experimental difficulty (e.g. loss of I-129 due to volatility). Other comparisons are presented in Gobien et al (2018).

Overall, the results show that the calculated value is either larger than measured, or within measurement uncertainty. Therefore, the calculated inventories are adopted here, with the indicated measurement uncertainties (σ_{OR}).

The inventory of some radionuclides or elements may be dependent on the trace impurity amounts in the initial materials; however these were selected conservatively so there is no need to further account for that as an uncertainty.

Similarly, inventory variation due to differences with the reference fuel are less than a few percent. And the effect of the average-burnup approximation versus the ring-sum value was accounted for as described in the previous section.

There is also no need to account for the distribution or uncertainty in burnup of the fuel bundles in a given container because the reference burnups of 280 MWh/kgU or 220 MWh/kgU are already conservative as described in Section 0. Since inventories generally increase with relevant burnups (Tait et al. 2000), the resulting calculated inventories are conservative.

Uncertainty due to the distribution of maximum power ratings compared with the adopted reference value (σ_{PR}) is small for the radionuclides of interest except for Cs-135 (Gobien et al. 2018).

All fuel is presently assumed to be 30 years post-discharge. As noted earlier, the range of fuel ages will be up to 70 years at DGR start. As the fuel age within a given container must be managed to bound the thermal and gamma loading of each container, this is considered an appropriate value for inventory purposes.

Table 3-5 to Table 3-7 summarize the uncertainty considered for each radionuclide inventory, in the context of total inventory within a container and also considering conservatism in deriving these inventories as noted above.

Further information on the derivation of the uncertainties is available in Appendix A of Gobien et al. (2018).

Table 3-8: ORIGEN-S: Pickering Fuel Measure and Calculated Inventory Comparison

Isotope	Measured ^{(1),(2)} (g/kg U)	ORIGEN-S (g/kg U)	Ratio (calc/meas)
Cm-244	7.12E+08 ± 15%	7.44E+08	1.05
Am-241	1.86E+10 ± 20%	1.92E+10	1.03
Np-237	1.00E+06 ± 20%	8.51E+05	0.85
H-3	2.07E+09 ± 7%	2.23E+09	1.08
Sr-90	4.86E+11 ± 4%	5.03E+11	1.03
Tc-99	1.08E+08 ± 10%	1.50E+08	1.39
Ru-106	8.72E+07 ± 5%	2.52E+08	2.89
Sb-125	2.20E+09 ± 18%	2.56E+09	1.16
I-129	2.44E+05	3.62E+05	1.48
Cs-134	4.16E+09 ± 7%	4.03E+09	0.97
Cs-137	8.05E+11 ± 5%	7.88E+11	0.98
Eu-154	8.14E+09 ± 5%	9.07E+09	1.11
Eu-155	3.35E+09 ± 8%	3.13E+09	0.93
U-233	< 0.01	2.22E-07	--
U-234	0.0339 ± 55%	0.0423	1.25
U-235	1.64 ± 2.4%	1.64	1.00
U-236	0.802 ± 3.7%	0.813	1.01
U-238	983.5 ± 0.01%	983.5	1.00
Pu-238	0.0058 ± 5.6%	0.0053	0.91
Pu-239	2.69 ± 2.5%	2.72	1.01
Pu-240	1.22 ± 37%	1.25	1.03
Pu-241	0.134 ± 9%	0.142	1.06
Pu-242	0.094 ± 6.8%	0.0972	1.03

Notes : (1) Data from Tait et al. (1995)

(2) Analytical or measurement uncertainty, σ_{meas} , expressed as a percentage.

3.3 References for Chapter 3

Chadwick, M.B., M. Herman, P. Obložinský, M.E. Dunn, Y. Danon, A.C. Kahler, D.L. Smith, B. Pritychenko, G. Arbanas, R. Arcilla, R. Brewer, D.A. Brown, R. Capote, A.D. Carlson, Y.S. Cho, H. Derrien, K. Guber, G.M. Hale, S. Hoblit, S. Holloway, T.D. Johnson, T. Kawano, B.C. Kiedrowski, H. Kim, S. Kunieda, N.M. Larson, L. Leal, J.P. Lestone, R.C. Little, E.A. McCutchan, R.E. MacFarlane, M. MacInnes, C.M. Mattoon, R.D. McKnight, S.F. Mughabghab, G.P.A. Nobre, G. Palmiotti, A. Palumbo, M.T. Pigni, V.G. Pronyaev, R.O. Sayer, A.A. Sonzogni, N.C. Summers, P. Talou, I.J. Thompson, A. Trkov, R.L. Vogt, S.C. van der Marck, A. Wallner, M.C. White, D. Wiarda, P.G. Young. 2011.

- ENDF/B-VII.1 Nuclear data for science and technology: Cross section, covariances, fission product yields, and decay data. *Nuclear Data Sheets*: 112-12, 2887-2996 (2011).
- Chen, J.D., P.A. Seeley, R. Taylor, D.C. Hartrick, N.L. Pshhyshlak, K.H. Wasywich, A. Rochon and K.I. Burns. 1986. Characterization of corrosion deposits and the assessment of fission products released from used CANDU fuel. Proceedings 2nd International Conference on Radioactive Waste Management. Winnipeg, Canada, 7-11 September 1986. Canadian Nuclear Society, Canada.
- Freire-Canosa, J. 2011. Used Fuel Integrity Program: Summary Report. Nuclear Waste Management Organization Report NWMO TR-2011-04. Toronto, Canada.
- Garamszeghy, M. 2016. Nuclear Fuel Waste Projections in Canada - 2016 Update. Nuclear Waste Management Organization Report NWMO-TR-2016-09. Toronto, Canada.
- Gobien, M., F. Garisto, E. Kremer and C. Medri. 2018. Seventh Case Study: Reference Data and Codes. Nuclear Waste Management Organization Report NWMO-TR-2018-10. Toronto, Canada.
- Hastings, I.J. 1982. Structures in Irradiated UO₂ Fuel from Canadian Reactors. Atomic Energy of Canada Limited Report AECL-MISC-249. Chalk River, Canada.
- IAEA. 2010. Review of Fuel Failures in Water Cooled Reactors. International Atomic Energy Agency. IAEA Nuclear Energy Series No. NF-T-2.1. Vienna, Austria.
- Kleykamp, H. 1985. The chemical state of the fission products in oxide fuels. *Journal of Nuclear Materials* 131, 221-246.
- Novak, J. and I.J. Hastings. 1991. Ontario Hydro Experience with Extended Burnup Power Reactor Fuel. Atomic Energy of Canada Limited Report AECL-10388. Chalk River, Canada.
- Tait, J.C., I.C. Gauld and A.H. Kerr. 1995. Validation of the ORIGEN-S code for predicting radionuclide inventories in used CANDU fuel. *Journal of Nuclear Materials* 223, 109-121.
- Tait, J.C. and S. Hanna. 2001. Characteristics and radionuclide inventories of used fuel from OPG nuclear generating stations, Volume 3 - Radionuclide inventory data. Ontario Power Generation Report 06819-REP-01200-10029-R00. Toronto, Canada.
- Tait, J.C., H. Roman and C.A. Morrison. 2000. Characteristics and Radionuclide Inventories of Used Fuel from OPG Nuclear Generating Stations, Volumes 1 and 2. Ontario Power Generation Report 06819-REP-01200-10029. Toronto, Canada.
- Truant, P.T. 1983. CANDU Fuel Performance: Power Reactor Experience. Atomic Energy of Canada Limited Report AECL-MISC-250, Rev. 1. Chalk River, Canada.
- Wilk, L. 2013. CANDU Fuel Burnup and Power Rating – 2012 Update. Nuclear Waste Management Organization Report NWMO TR-2013-02. Toronto, Canada.

THIS PAGE HAS BEEN LEFT BLANK INTENTIONALLY

4. REPOSITORY FACILITY – CONCEPTUAL DESIGN

4.1 General Description

The Adaptive Phased Management (APM) facility includes an underground repository for used fuel and a number of surface facilities designed to support the construction and operation of the repository (Noronha 2016). The primary function of the surface facilities is to receive used fuel that is shipped from reactor-site storage facilities, to place fuel in durable containers and prepare used fuel containers (UFC) for transfer to the underground repository. The underground repository consists of several panels of used fuel containers in placement rooms which are connected to the surface via a series of access tunnels and three vertical shafts. An illustration of the APM facility in sedimentary rock is shown in Figure 4-1.

The used fuel container is designed with a corrosion-resistant copper barrier and an inner supporting steel vessel to provide long-term containment of the fuel in the repository. Before transfer underground, each container is placed inside a number of highly compacted bentonite blocks creating an assembly called a “buffer box”. Each fully assembled buffer box is then transferred inside a shielded transfer cask to a placement room where the buffer box is unloaded and stacked underground.

For the purpose of this study, the repository is assumed constructed at a depth of 500 m in the sedimentary rock of Southern Ontario. The used fuel container, the sealing systems surrounding the container and the rock mass in which the repository is constructed provide protective barriers that are capable of containing and isolating the used fuel indefinitely. In the repository, the used fuel containers will be surrounded by engineered, highly compacted bentonite (HCB) blocks that will provide protection against possible mechanical, chemical and biological agents that could cause container damage. The repository engineered barriers will also create a chemical and physical environment that would limit the mobility of contaminants during postulated long-term disruptive scenarios that deviate from the expected, normal evolution of the repository.

Monitoring systems for verification of safety performance are provided as part of the repository system design. Retrievability of the fuel containers is another design feature of the APM repository.

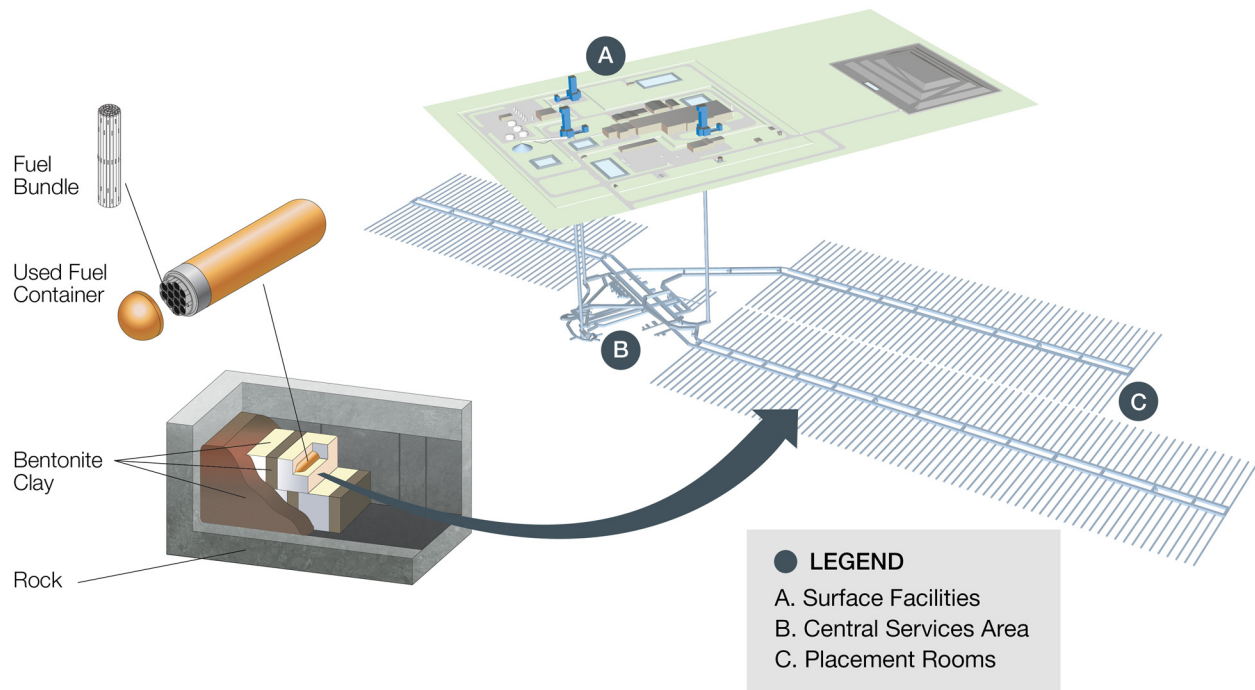


Figure 4-1: Illustration of APM Facility in Sedimentary Rock

4.2 Design Requirements

4.2.1 Canadian Acts, Regulations and Codes

The DGR facility falls under federal jurisdiction. Thus, Canadian federal acts, regulations and codes apply to all aspects of the DGR facility. Under the Nuclear Safety and Control Act (NSCA) and its associated Regulations, Class 1 Nuclear Facility Regulations apply, and the DGR facility is classified as a Class 1B nuclear facility under these regulations as described in Chapter 1.

The following Canadian acts, regulations and codes apply to a deep geological repository project. Compliance with these will be demonstrated in the future in support of a licence application:

1. Above-ground civil structures will comply with the National Building Code of Canada and the National Fire Code of Canada;
2. Nuclear aspects of the facility will be designed to comply with the Nuclear Safety and Control Act and its associated regulations;
3. Electrical installations and components will be in accordance with the Canadian Electrical Code and associated Canadian Standards Association (CSA) standards;
4. The management system will comply with the CSA N286 series of standards as well as ISO 9001;
5. The environmental management and monitoring programs will comply with the CSA N288 series of standards as well as ISO 14001; and
6. The occupational health and safety management programs will comply with the CSA Z1000 standard.

By Canadian Federal Regulation 98-180, responsibility for workplace health and safety at all nuclear facilities in Ontario (including nuclear waste management facilities) has been delegated to the Province of Ontario. It is expected that workplace health and safety during the construction and operation of the DGR facility will also be regulated under the Ontario Occupational Health and Safety Act (OHSA) and its associated regulations. In particular, it is assumed that underground aspects (e.g. shafts, tunnels and placement rooms) will comply with relevant requirements in Ontario Regulation 854/90, Mines and Mining Plants, which is a regulation under OHSA.

4.2.2 Safeguards

Canada's international safeguards obligations are the result of treaty commitments (IAEA 1970, IAEA 1972, and IAEA 2000). The specific legal requirements to implement these commitments come in the form of licence conditions that are included in a Canadian Nuclear Safety Commission (CNSC) licence. Compliance with these requirements will be demonstrated in support of a future licence application.

4.2.3 Facility Requirements

1. The deep geological repository shall accommodate the intact, damaged and defective used fuel bundles arising from the nuclear reactors currently operating or previously operated in Canada.
2. The deep geological repository shall be sized to contain the used fuel, plus a contingency allowance (to be determined). This contingency shall consider the possibility of additional Canadian non-standard fuel and high-level radioactive waste. For the purpose of conceptual facility design updates, the reference inventory is 5.224 million used fuel bundles.
3. It shall also be assumed that the placement rate for the used fuel in the deep geological repository will be 120,000 used fuel bundles per year. This allows the reference inventory of 5.224 million bundles to be placed within approximately 40 years or more.

4. The deep geological repository shall be sited and designed to provide passive containment and isolation of used fuel using the multiple-barrier concept.
5. The deep geological repository shall be constructed at a depth within the host geological media that will provide a stable environment for excavation and operation, provide environmental conditions that contribute to used fuel isolation, and contribute to the safety. The depth of the placement rooms will be established based on the analyses of actual site information. For conceptual facility design updates, the preliminary requirement is that the depth of the used-fuel placement rooms is a nominal 500 m below ground surface.
6. The deep geological repository shall be designed to allow for an extended period of personnel access to the major underground service areas and access tunnels for continued monitoring after the placement of all used fuel containers is completed and before decommissioning and closure is initiated. Such access will be provided without compromising the long-term postclosure safety performance of the sealed repository.
7. The deep geological repository facility shall be designed to allow the safe construction of placement rooms to occur concurrently with placement of used fuel containers.
8. The deep geological repository shall be designed to allow retrieval of some or all placed used fuel containers prior to the decommissioning of the repository. Design of the deep geological repository shall consider measures to assist postclosure retrieval insofar as these measures do not compromise safe repository performance and nuclear material safeguard measures.
9. Following closure of the deep geological repository, monitoring to observe the performance of the repository and to verify the non-diversion of used fuel, by deterrence and detection as required by nuclear material safeguards agreements, shall be possible without compromising the long-term postclosure safety of the repository.
10. The repository layout will be designed to maintain the surface temperature of the used fuel container below 100°C to ensure that the properties of the surrounding bentonite and the copper are not adversely affected.

4.2.4 Engineered Barrier Requirements

4.2.4.1 Used Fuel Container Requirements

The high level design requirements of the used fuel container are given as follows:

1. The used fuel container shall provide containment for used fuel (as well as other high level radioactive waste deemed acceptable for the repository) from the time of loading through handling, transfer operations, placement in the repository, potential retrieval operations, and during the postclosure period as required to ensure postclosure safety.
2. The used fuel container shall be designed with sufficient mechanical stability and strength to withstand mechanical loads during handling and in the repository after emplacement, and maintain mechanical integrity to provide containment.
3. The used fuel container shall be designed with sufficient corrosion allowance for corrosion processes (internal and external to the UFC) to maintain mechanical stability and strength and to prevent through-wall corrosion penetration.

4.2.4.2 Room and Tunnel Sealing Requirements

1. Each used fuel container shall be completely surrounded by a buffer material. The buffer material shall restrict groundwater flow around the container, create a stable chemical environment that minimizes corrosion of the container and act as a mechanical buffer to dampen external loading (e.g. due to rock movements).
2. Each placement room in the deep geological repository shall be filled with a placement room sealing system as the used fuel containers are placed and the entrance closed with a bulkhead sealing system after the room is filled. The placement room sealing system shall act to minimize the movement of groundwater within the placement room. The bulkhead sealing system will include a cut-off trench through the excavation damage zone EDZ to impede the migration of groundwater from the placement room, provide shielding to mitigate the radiation fields in adjacent unsealed areas, contribute to maintaining the integrity of the buffer materials surrounding each used-fuel container within the room and provide access control to filled and sealed rooms.

4.2.4.3 Shaft Sealing Requirements

1. The shaft sealing materials and design shall be compatible with chemical and mechanical conditions within the host rock surrounding the shafts and the chemical conditions of the pore fluid in the host rock and repository sealing system components.
2. The sealing system applied in a shaft shall maintain its function during the postclosure period without need for maintenance or replacement.
3. Each shaft shall be completely filled by the sealing system in order to minimize subsidence of sealing materials that have been placed in the shaft and to reduce likelihood of future inadvertent intrusion.
4. The sealing systems applied in a shaft shall be designed to prevent flow and mixing of groundwater between permeable bedrock formations connected via the vertical shaft(s).

4.3 Description of Engineered Barriers

Within the deep geological repository, a series of engineered and natural barriers will work together to safely contain and isolate used nuclear fuel from people and the environment. This chapter describes the characteristics of the engineered barriers.

Used fuel bundles will be placed into large, very durable containers. In 2014, the NWMO refined its container design to one that is optimized for the used CANDU fuel produced by Canadian nuclear power reactors. Together with the bentonite clay buffer box, the container is a key part of the engineered barrier system. The container isolates and contains the used nuclear fuel from the underground environment, leaving most of the radionuclide inventory fixed in the ceramic matrix of the fuel and preventing radionuclides in the fuel from being released into the underground environment. Each container holds 48 used fuel bundles in a steel basket within a carbon steel pipe. This steel pipe has the mechanical strength to withstand pressures of the overlying rock and loading from glaciers much higher than those evidenced in Canada's glacial history. The container is protected by a corrosion-resistant copper coating. The container has spherical heads that are welded to the core of the container. This hemispherical shape can withstand significant pressure.

Each used fuel container will be encased in a highly compacted bentonite clay buffer box before placement in the repository. Bentonite clay is a natural material evolved from volcanic ash. Compacted bentonite is proven to be a powerful barrier to water flow. It swells when exposed to water, making it an excellent sealing material. Bentonite is also very stable, as seen in natural deposits formed millions to hundreds of millions of years ago. In the repository, the chemical properties of the bentonite clay, backfill, and sealing materials would also help to trap any radionuclides in the unlikely event they were released from the container. Each buffer box will be placed and separated from horizontally adjacent boxes with spacer blocks. Containers will be stacked in two layers. After the used nuclear fuel containers are placed in the repository, all open spaces in each placement room will be filled with bentonite clay. A 6-m-thick highly compacted bentonite clay seal and a 10-m-thick concrete bulkhead will be used to seal the entrance to each placement room.

Before closing the repository, all tunnels and shafts will be filled with backfill and sealing materials, isolating the repository from the environment. The performance of the repository will be monitored during placement operations and during an extended monitoring period.

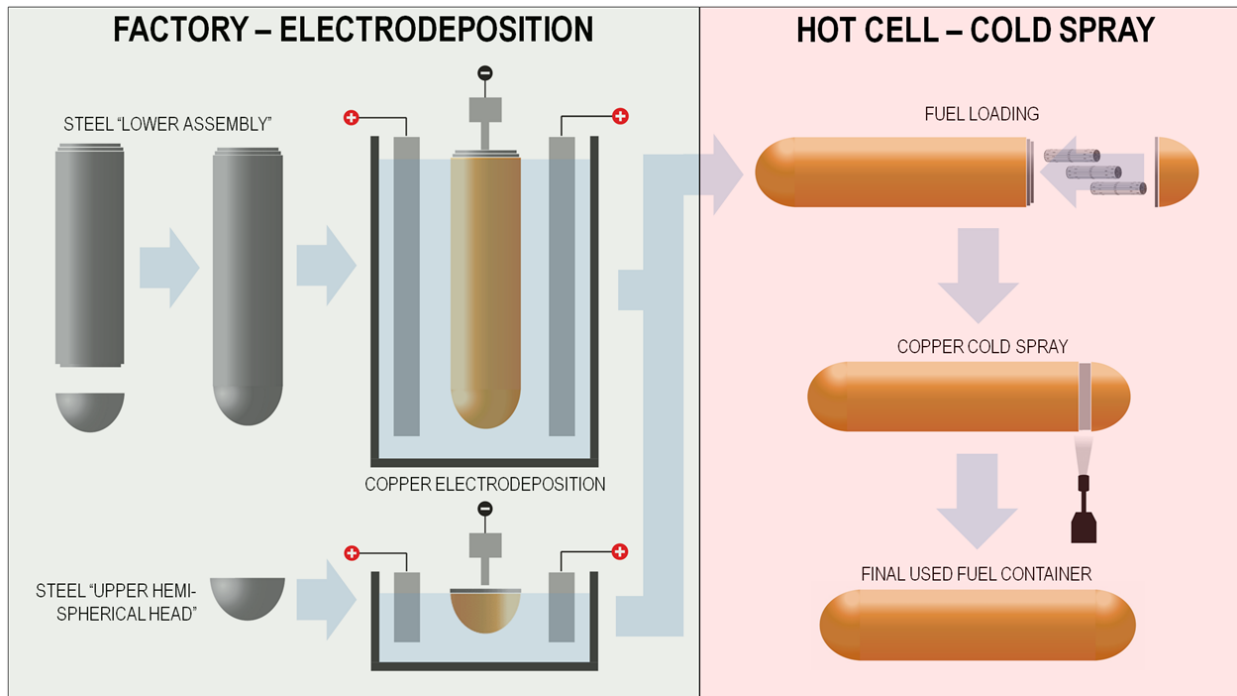
4.3.1 Used Fuel Container

The used fuel container incorporates a steel core for structural strength and an exterior copper coating for corrosion protection. The capacity of the UFC is 48 used CANDU fuel bundles for a fuel mass of about 1.2 metric tonne, based on a typical fuel bundle mass of 24 kg (Garamszeghy 2016). The inner vessel wall thickness is about 46 mm and it is designed to sustain a maximum external hydrostatic pressure of 45 MPa which is a conservative estimate of maximum loads the container might experience in the repository during a glaciation cycle as described in Chapter 5 of this report. To ensure best practices consistent with the principles of CSA N285.0-12, the components of the UFC will be designed and manufactured following the intent of ASME BPVC (Boiler Pressure Vessel Code), Section III, Division 3, Subsection WC: Class SC Storage Containments, except those identified as exempt and/or modified.

The UFC has been designed with a 3-mm-thick outer copper coating for corrosion resistance. Under repository conditions, corrosion of the copper barrier is predicted to be much less than 2 mm over a period of one million years (Kwong 2011), which is approximately the time required for the radioactivity of the used CANDU fuel to decay to levels comparable to those of an equivalent amount of natural uranium. The fabrication materials selected for the manufacturing of the UFC structural vessel will have a suitable corrosion performance for the anticipated facility environment to ensure penetration of the corrosion barrier will not occur with the expected ground water chemistry as described in Chapter 5. The UFC structural vessel will be designed with sufficient corrosion allowance for all postulated corrosion processes (internal and external to the UFC).

The UFCs will be fabricated at qualified vendor sites in accordance with pre-approved manufacturing processes and procedures, many of which are being developed under the NWMO proof testing program. An example is the factory copper coating, which will be accomplished by electrodeposition, and is illustrated on the left-hand side of Figure 4-2. The UFCs will be fabricated and inspected to meet the requirements listed in pre-approved technical specification and will employ standard commercially available components, materials and manufacturing techniques to the extent practical.

In contrast, some manufacturing operations will be conducted in a hot cell at the site, during fuel repackaging. This includes fuel loading, welding, welding inspection, cold spray application over the weld zone with copper, coating inspection, and all relevant heat treatments. The right side of Figure 4-2 illustrates a simplified scheme of hot cell operations.



Note: This figure shows the two processes used for copper-coating the container: 1) the lower assembly and the upper hemispherical head are electroplated in a factory environment; and 2) the final steel zone is welded after the used fuel is loaded in the hot cell and then cold-sprayed with copper.

Figure 4-2: Used Fuel Container Manufacturing Process

Copper coating and base material inspections, weld inspections and hydrostatic pressure testing are examples of things being tested under NWMO's proof testing program. Various Non-destructive Examination (NDE) techniques like Eddy Current, Ultrasonic Examination and Liquid Penetrant Examination are being developed for quality assurance testing of coatings, base materials and weld inspections, for future manufacturing.

The containers will be inspected at various stages of fabrication to ensure minimal defects in the final product. Inspections will be performed systematically in accordance with pre-approved written procedures or applicable industry standards. Where required, fabrication hold points will be imposed to allow witnessing of tests/inspections. The tests and inspection results will be recorded in the Inspection and Test Plan document, which will be archived for future reference.

The design parameters of the copper coating and the inner steel vessel are given in Table 4-1. Figure 4-3 is an illustration of the used fuel container. The total mass of a loaded used fuel container is about 2800 kg.

Table 4-1: Reference Used Fuel Container and Copper Coating Parameters

Used Fuel Container – Design Parameters		
Assembled Used Fuel Container	Container capacity	48 CANDU fuel bundles
	Overall container diameter	564 mm (nominal)
	Overall container length	2514 mm (apex head-to-head)
	Loaded container mass	2815 kg (with fuel)
Steel Vessel	Outer diameter	556 mm
	Shell length	1950 mm
	Shell thickness	46.2 mm (nominal)
	Hemispherical head thickness	30 mm (nominal)
	Overall length	2506 mm (apex head-to-head)
	Mass	1343 kg
	Material	A/SA-106 Gr. C (shell), A/SA-516 Gr. 70 (hemispherical head)
Copper Coating	Thickness	3 mm (minimum)
	Mass	157 kg (nominal)
	Material	Low oxygen, high purity copper
Insert for Used Fuel Bundles	Mass	115 kg (estimated, prototype)
	Material	Low carbon steel

Note: The values presented here are from the data clearance process used to conduct this safety assessment.

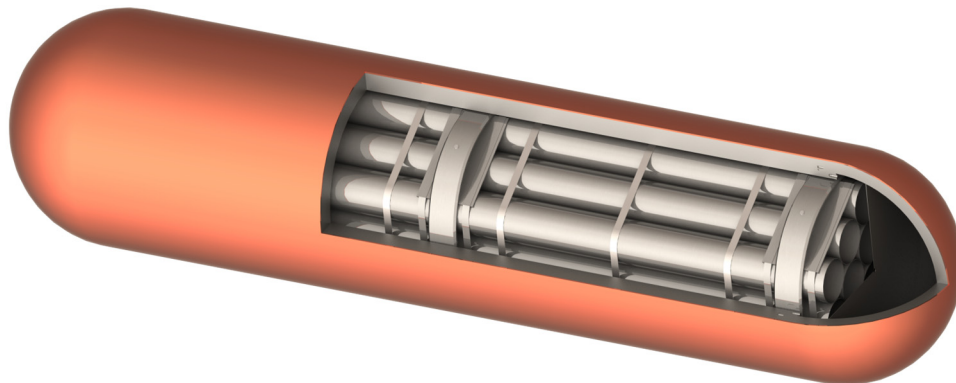


Figure 4-3: Copper Coated Used Fuel Container with an Open Section

4.3.2 Room, Tunnel and Shaft Sealing Materials

The key functions for various components of the repository sealing system are to:

- Fill the entire excavated volume of each area being sealed;
- Resist physical and chemical deterioration by the local environment, which includes the preclosure and postclosure geochemical conditions;
- Limit the rate of groundwater flow to and from the sealed placement rooms; and
- Limit the rate of potential radionuclide migration from the sealed placement rooms and, if released from the rooms, radionuclide migration along various underground tunnels and within the shafts.

Clay-based materials will be used to backfill most of the underground space. At the entrance to each placement room and at strategic locations in the tunnels, seals comprising highly compacted bentonite blocks would be keyed through the EDZ. These seals will be held in place by a concrete bulkhead.

Each shaft will be backfilled with a bentonite/sand mixture. At strategic locations in each shaft, concrete bulkheads will be constructed. In addition, asphalt may be used as a component in the shaft sealing system.

The following sections describe the various materials that will be used to seal the underground repository. Additional information about the configuration of sealing materials in the placement rooms is presented in Section 4.8.1. The possible arrangement of sealing materials to be placed in the tunnels and shafts during decommissioning and closure is described in Section 4.12.

4.3.2.1 Highly Compacted Bentonite

Highly compacted bentonite will be used to create buffer boxes, machined to accept the cylindrical UFCs, and spacer blocks. The HCB buffer boxes will completely surround each UFC (see Figure 4-4). HCB will also be used as a component in the construction of room and tunnel seals. Dimensions of various HCB products will vary depending on the application.

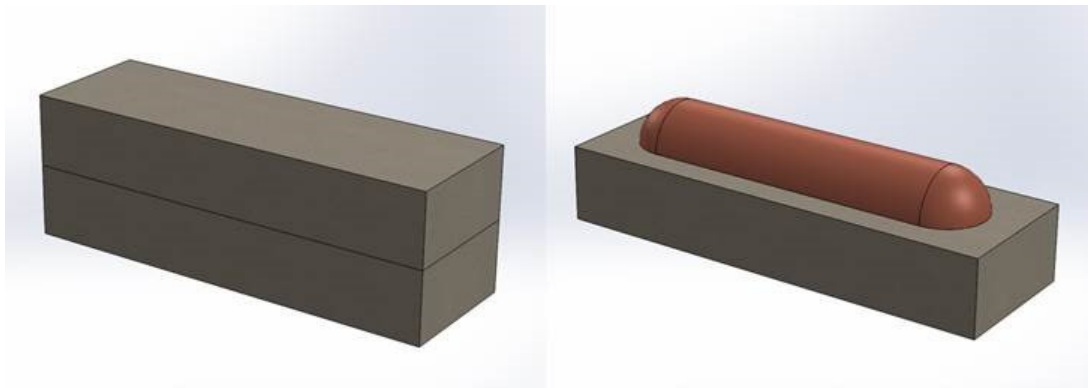


Figure 4-4: Buffer Box

HCB contains only bentonite, the commercial name given to a naturally occurring clay-rich sediment that evolves from volcanic ash. The main mineral phase in bentonite is montmorillonite, a smectitic clay mineral that has expandable layers and a high cation-exchange capacity. Montmorillonite is responsible for the most distinctive property of bentonite, which is that it can swell to many times its original volume when placed in fresh water. In a confined space, swelling of compacted bentonite during resaturation can apply a substantial swelling pressure on its confinement, producing tight surface contacts and providing very effective sealing of fractures. Bentonite-based materials also have the advantage of very low permeability, reducing mass transport in the vicinity of the container and, at high density, providing an unfavourable environment for microbial activity.

Bentonite deposits in many parts of the world (e.g., Wyoming, Saskatchewan, Greece, India, China, Korea, Japan) have been assessed for their potential use as buffer material in a deep geological repository. The proportion and composition of montmorillonite varies with the source of the bentonite, with corresponding differences in swelling and mass transport properties. Bentonite that contains a high proportion of montmorillonite and whose main exchangeable cation is sodium (Na) (i.e., Na-bentonite) generally has the greatest swelling and sealing properties. Depending on its source, bentonite also contains some non-expandable clays, such as illite, and other minerals such as quartz, feldspars, calcite and gypsum, which generally are inert filler materials that do not actively affect buffer behaviour. Some bentonites are not chemically dominated by Na⁺ (e.g., Ca, Mg, Fe). These non-Na clays generally have a lower swelling capacity, higher hydraulic conductivity and some (e.g., Fe varieties) have the potential to interact adversely with their surroundings. It is also anticipated that ultimately Na-bentonites will evolve towards a calcium bentonite (Ca-bentonite) as ion exchange occurs with calcium-rich groundwater. However for the critical period immediately following container placement, the buffer behaviour will be that of a Na-bentonite. Like Na-bentonites, Ca-bentonites exhibit a swelling capacity (< Na-varieties) and low permeability, making them suitable for use as buffer materials.

Important functions of the highly compacted bentonite that surrounds the used fuel containers are:

- The buffer prevents damage to the UFCs by acting as mechanical protection against stresses;
- The buffer controls groundwater flow in the area around the UFC and furthermore, controls the chemistry of the groundwater and other substances in the vicinity of the UFC;
- The buffer controls microbial activity in the vicinity of the UFC, therefore reducing the potential for microbial-induced corrosion of the container; and
- The buffer keeps the container in place.

In the case of a breach of the container, the buffer system provides a hydraulic and chemical environment which would limit the mobility of contaminants in defective UFCs.

Properties of the highly compacted bentonite are shown in Table 4-2.

Table 4-2: Physical Composition and As-Placed Properties of Clay-Based and Asphalt Materials for Room, Tunnel and Shaft Sealing

Material ⁽¹⁾	Nominal Dry density (kg/m ³)	Saturation (%)	Porosity (%)	Bulk density (kg/m ³)	Water content (kg/kg) ⁽²⁾	Effective montmorillonite dry density (kg/m ³) ⁽³⁾
Highly compacted bentonite (100% bentonite; MX-80 or equivalent)	1700	67	38.2	1955	0.15	1550
Dense backfill (5:25:70 bentonite:clay:aggregate)	2120	80	19.4	2276	0.074	376
Gap fill (100% bentonite; MX-80 or equivalent)	1410	6	48.6	1439	0.021	1261
Shaft backfill (70:30 bentonite:granitic sand)	1700	73	37.5	1972	0.161	1325
Asphalt	--	--	2	1960	--	n/a

Notes: (1) Actual backfill compositions and their engineered physical properties will depend on the site-specific design requirements for a repository.

(2) Water content calculated by using the formula $(\text{Bulk Density} - \text{Dry Density}) / (\text{Dry Density})$.

(3) The effective montmorillonite dry density (EMDD) normalizes different clay mixtures in terms of their active component, montmorillonite clay. EMDD is determined using calculations illustrated in Baumgartner (2006).

4.3.2.2 Dense Backfill

Dense backfill, as currently formulated, is a mixture of bentonite, naturally-occurring glacial lake clay and crushed rock, formed into blocks. Dense backfill blocks and gap fill will be used to fill the various horizontal access tunnels at the time of repository decommissioning and closure.

Properties of the dense backfill are shown in Table 4-2.

4.3.2.3 Gap Fill

The gap fill's sole constituent is bentonite. The gap fill will be used to fill the nominal 100-mm-thick gap that will exist between the stacks of buffer boxes, with their accompanying HCB spacer blocks, and the surrounding rock walls. Gap fill material will also be placed on the floor of each room before buffer boxes are stacked in the room. Gap fill would be used during closure of various tunnels and other horizontal openings. It will be used to fill the sides and upper (crown) regions of tunnels where it would not be possible to place dense backfill due to geometric or other constraints. The bentonite gap fill will swell when saturated with water and seal the gap.

Properties of the gap fill are shown in Table 4-2.

4.3.2.4 Shaft Backfill

Shaft backfill is a mixture of bentonite and sand that will be delivered in bulk to each shaft at the time of repository closure. It will be placed in layers and each layer will be compacted in-situ to the required density. Once saturated, the compacted bentonite/sand materials will act as a low permeability barrier to minimize groundwater flow and resist the movement of radionuclides out of the repository. Compacted clays or clay/sand mixtures are the most commonly proposed sealing materials for nuclear waste repositories. Sand will be added to the bentonite to improve workability during placement, ease compaction and improve dust control. The amount of sand will not compromise the low hydraulic conductivity and swelling potential of the bentonite-dominant material. As the compacted bentonite/sand materials saturate with groundwater from the surrounding rock, they will generate swelling pressures, which will aid in the development of a tight seal against the shaft wall and provide a confining pressure to the rock surface.

Properties of the shaft backfill are shown in Table 4-2.

4.3.2.5 Asphalt

Asphalt may be used as one component in the shaft sealing system. Asphalt has been selected because it has the ability to flow and make good contact with host rock. Immediately upon placement, the asphalt will create an effective barrier to water flow. Furthermore, the use of another low permeability sealing material provides an additional level of redundancy to the sealing system against upward or downward fluid flow.

Properties of the asphalt are shown in Table 4-2.

4.3.2.6 Concrete

During operations concrete is used to construct shaft liners and tunnel floors, and to construct bulkheads at the entrance to each placement room. During closure of the repository concrete will also be used to create bulkheads in the tunnels and shafts, and to create a concrete monolith at the base of each shaft. The concrete would be mass-poured. The shaft liners would be constructed using standard high performance concrete, which will be removed during decommissioning and closure of the repository. The bulkheads will be constructed using low-heat high-performance concrete and these bulkheads will remain in place after repository closure.

Table 4-3 shows expected annual concrete requirements that could be used during the operations phase of the repository.

Table 4-3: Expected Annual Concrete Requirements for the Repository

Material	Low-Heat High-Perf. Concrete Batch Plant (tonnes/a)
Concrete Stone	484
Concrete Sand	416
Cement T50	45
Silica Fume	45
Silica Flour	90
Superplasticizer	5
Water	60
Total	1,145

Note: Table from Noronha (2016).

Because interactions between concrete and water in a repository have the potential over the long term to produce alkaline chemical conditions that are detrimental to the swelling properties of bentonite, a special low-heat, high-performance concrete has been developed for use in the concrete bulkheads. Such a concrete has much lower lime content than regular concrete, giving it a lower pH in reactions with water. This lower alkalinity would limit the potential for adverse chemical reactions within the repository. In addition, the low-heat, high-performance concrete generates less heat during curing than regular concrete. The poured concrete would be less likely to crack due to thermal expansion and subsequent contraction during cooling.

4.3.2.7 Grout

Grouting is a short-term expedient that allows excavation and construction to be carried out in localized regions where groundwater inflow would otherwise be unacceptably high, or to limit seepage around or into engineered structures. Clay-based grouting materials may be an option under some conditions in a repository, but silica-based grouts are more likely to be used. Low-viscosity grouts having a low cement content and silica rather than lime bases have been developed for use in conditions anticipated to be encountered in a repository environment.

4.4 Surface Facilities

The surface facilities require a dedicated surface area of about 700 m by 625 m.

The site layout is shown in Figure 4-5 & Figure 4-6 and individual buildings and other surface facilities are listed in Table 4-4. The site is surrounded by a perimeter fence, with the facilities within the perimeter arranged in two areas:

- a) the Protected Area, which is a high-security zone; and
- b) the Balance of Site, a zone which includes facilities that do not require high security.

The main facilities included in the Protected Area are the Used Fuel Packaging Plant (UFPP), the main shaft, service shaft and ventilation shaft buildings as well as the auxiliary building, quality control offices, laboratory, radioactive waste handling facilities, switchyard, transformer area and emergency generators. All activities pertaining to handling and storage of used fuel are conducted in the UFPP. A description of the UFPP and its operation is given in Section 4.5.

The Balance of Site zone includes the administration building, the fire hall, and ancillary facilities such as the cafeteria, garage, warehouse, water and sewage treatment plants, and helicopter pad. Fuel and water storage tanks and an air compressor building are also found in this zone.

Balance of Site also includes the concrete batch plant and the sealing materials compaction plant. The concrete batch plant will produce the concrete mixes that are required in the repository, including the low-heat, high-performance (LHHP) concrete required for the bulkheads to be placed at entrance of the container-filled placement rooms. At the sealing materials compaction plant, externally sourced materials will be mixed to produce compacted bentonite blocks and gap-fill material required for sealing the used fuel containers inside the placement rooms.

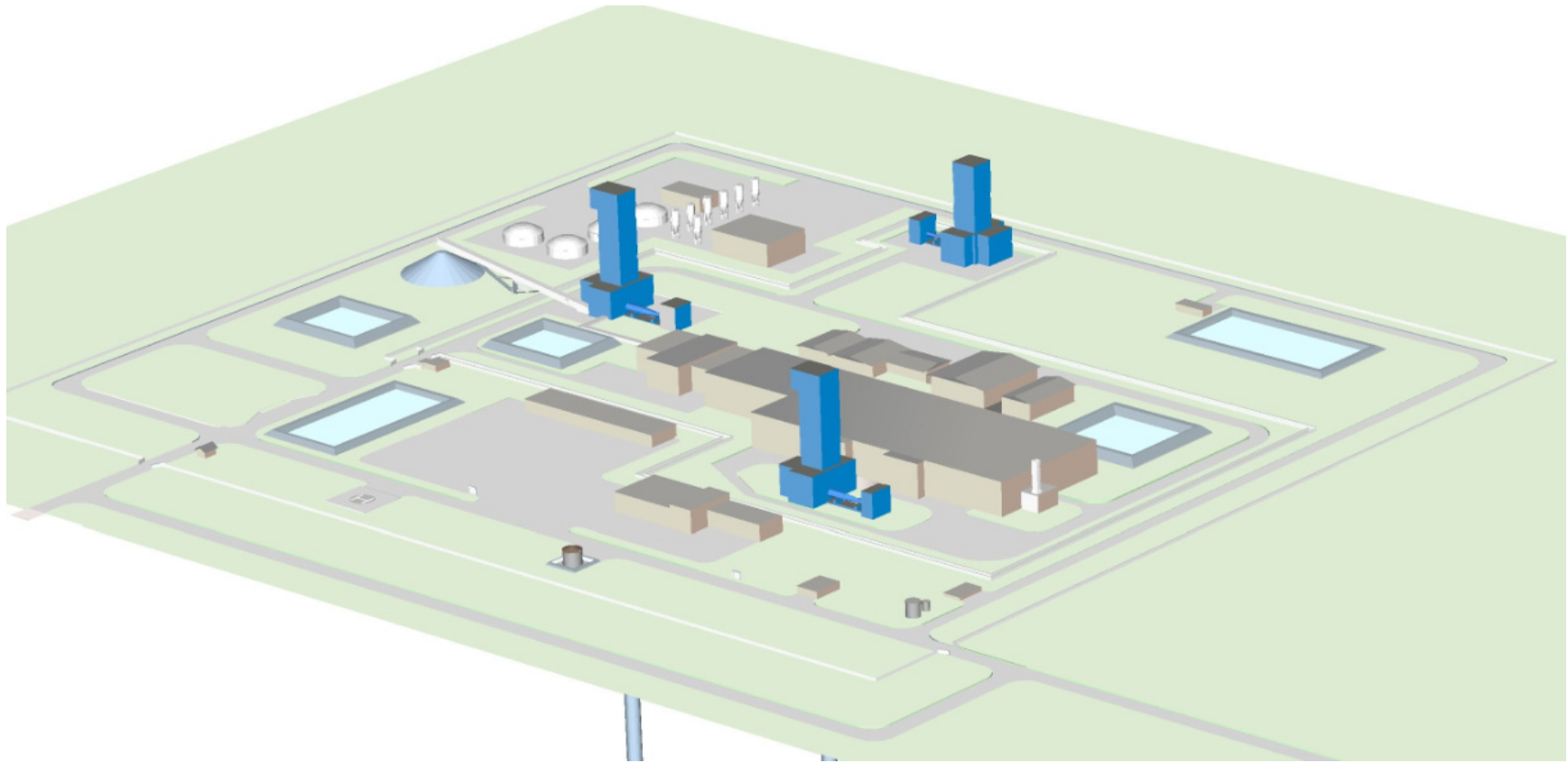


Figure 4-5: APM Surface Facilities Illustration

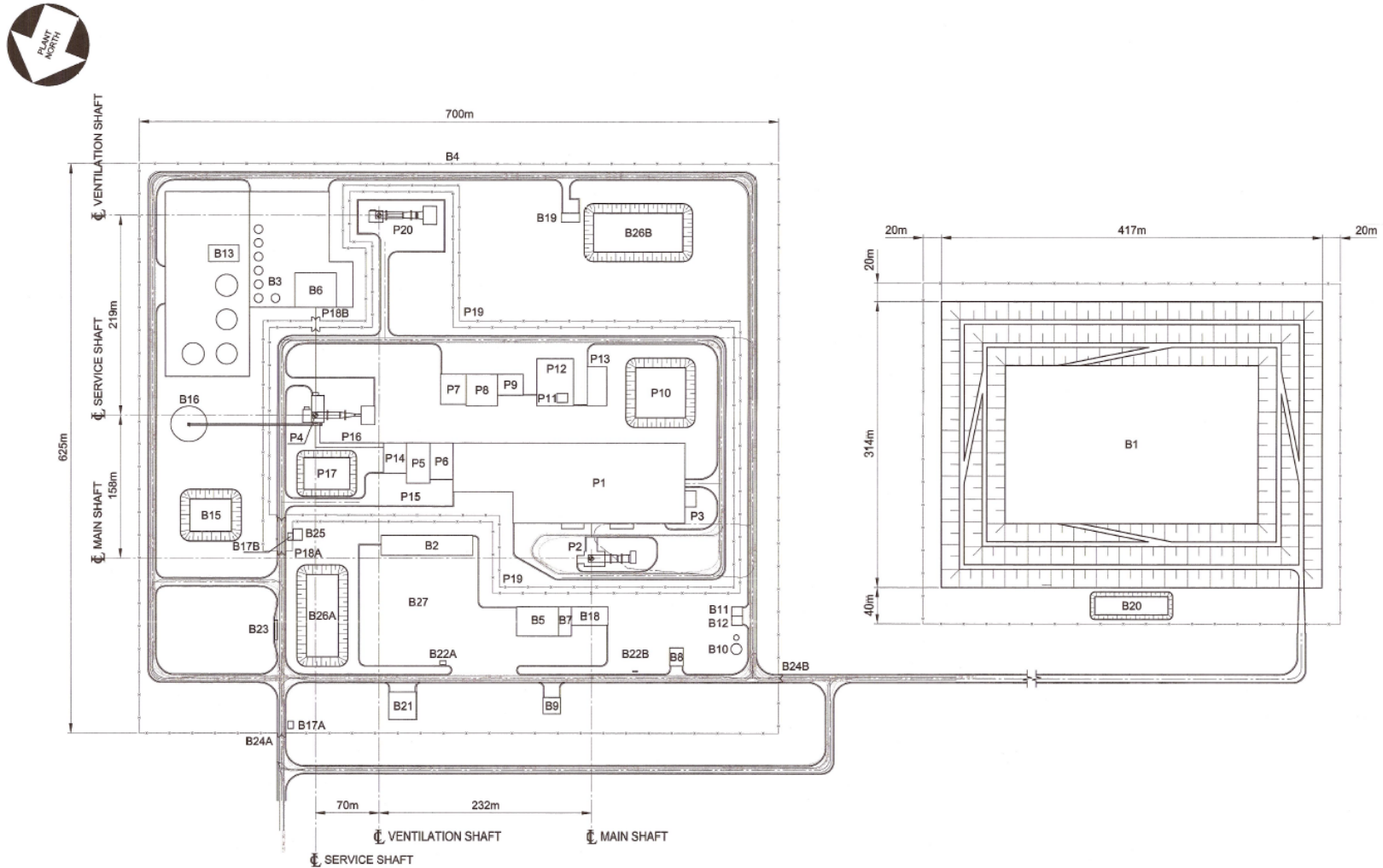


Figure 4-6: APM Surface Facilities Layout

Table 4-4: APM Facility Number and Description

Area	Protected Area	Area	Balance of Site
P1	Used Fuel Packaging Plant	B1	Excavated Rock Management Area ⁽¹⁾
P2	Main Shaft Complex	B2	Administration Building including Fire hall and Cafeteria
P3	Stack	B3	Sealing Material Storage Bins
P4	Service Shaft Complex	B4	Perimeter Fence
P5	Auxiliary Building	B5	Garage
P6	Active Solid Waste Handling Facility	B6	Sealing Materials Compaction Plant
P7	Waste Management Area	B7	Warehouse and Hazardous Materials Storage Building
P8	Active Liquid Waste Treatment Building	B8	Air Compressor Building
P9	Low-Level Liquid Waste Storage Area	B9	Fuel Storage Tanks
P10	Storm Water Management Pond	B10	Water Storage Tanks
P11	Switchyard	B11	Water Treatment Plant
P12	Transformer Area	B12	Pump House
P13	Emergency Generators	B13	Concrete Batch Plant
P14	Quality Control Offices and Laboratory	B14	Not Used
P15	Parking Area	B15	Process Water Settling Pond
P16	Covered Corridor / Pedestrian Routes	B16	Excavated Rock Stockpile (working)
P17	Mine Dewatering Settling Pond	B17	Guardhouse (A, B)
P18	Security Checkpoint	B18	Storage Yard
P19	Double Security Fence	B19	Sewage Treatment Plant
P20	Ventilation Shaft Complex	B20	Storm Water Management Pond*
		B21	Helicopter Pad
		B22	Bus Shelters (A, B)
		B23	Weigh Scale
		B24	Security Checkpoints
		B25	Security Monitoring Room
		B26	Storm water Management Ponds (A, B)
		B27	Parking Area

Notes: (1) Refers to off-site facilities

The APM facility will also require a storage area of about 0.18 km² for the excavated rock (Area B1). Its location would be selected in consultation with the community and surrounding region. The area will initially be prepared using dumped crusher wastes to directly fill any low-lying depressions. Additional excavated rock will then be placed in layers on the prepared ground surface. Access routes and paths will be prepared for loaders, dumpers and trucks to move around and up the piles easily.

The excavated rock management area will include a storm water management pond (Area B20) to collect and monitor the run-off water before being released to the receiving water body. The potential contaminants of concern in the run-off will likely be various chemical constituents due to leaching of minerals in the excavated rock and nitrogen compounds from residual explosives on the excavated rock. The surface water run-off from the excavated rock pile will be monitored and appropriate effluent control procedures will be implemented based on the monitoring results.

4.5 Used Fuel Packaging Plant

The UFPP is identified as Area P1 on Figure 4-6 and the layout is shown in Figure 4-7. This single storey building is a reinforced concrete structure with a basement. It will include all necessary provisions for receiving used fuel bundles in Used Fuel Transportation Packages (UFTPs), and for transferring used fuel bundles from the UFTPs to the UFCs. The UFPP has equipment for sealing, inspecting and assembly of UFCs into buffer boxes, and for dispatching buffer boxes for placement in the underground repository. Any defective UFCs would require repacking into a new container. Figure 4-7 also shows preliminary radiological zones for the movement of staff and materials, including required maintenance activities, to keep doses As Low As Reasonably Achievable (ALARA).

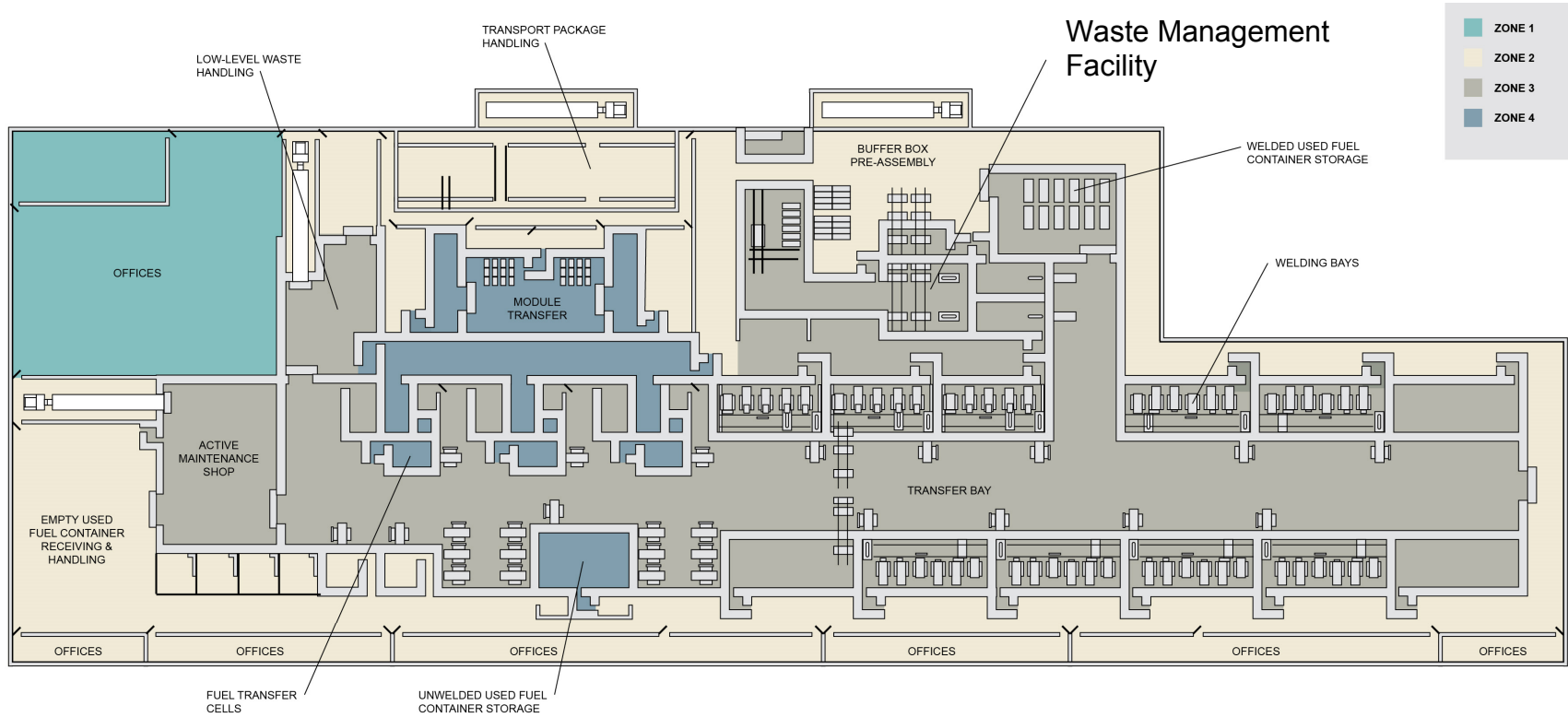


Figure 4-7: Overview of the UFPF Layout

There are processing lines for receiving and unloading UFTPs and handling the UFCs. The processing line for UFCs is designed so that several containers can be in process simultaneously. Key data for the UFPP throughput is provided in Table 4-5.

The UFPP also includes auxiliary systems, such as ventilation, electrical power systems, a central control room, waste management facility, and facilities for personnel and visitors.

Table 4-5: Key Data for Average UFPP Throughput

	Bundles per Unit	Throughput		
		Base Case Total	Annual	Daily ⁽¹⁾
Bundles	1	5.224 million	120,000	480
Modules	96	54417	1,250	5.0
UFTP	192	27208	625	2.5
UFC	48	108,833	2500	10

Note: (1) Based on assumption of 250 working days per year.

Most steps in the packaging process are remotely operated. However, after removal of the radiation source and decontamination by remote-controlled processes, all areas can be accessed by maintenance personnel. Areas and equipment for handling used fuel bundles and filled UFCs are radiation shielded. The fuel receiving and transfer area will be kept at a negative pressure to prevent the spread of airborne contamination.

4.5.1 Used Fuel Transport Package Receipt and Unloading

To achieve the specified daily throughput, an average of three UFTPs will need to be processed each day. To achieve this throughput, the system will incorporate two parallel and independent processing lines. Each line will process between one and two UFTPs per day. Fuel-filled modules will be placed into temporary dry storage, as required, until modules can be accepted for processing inside the UFPP. It is assumed that wet storage is not required because all fuel received at the UFPP will be sufficiently cool for dry storage.

Used fuel inside a UFTP arrives at the UFPP from the interim storage facilities at reactor sites via the ground transportation system and is transferred to one of two parallel UFTP handling cells which are located on the basement level of the plant (see Figure 4-8). After the impact limiter is removed, the UFTP loaded with modules is raised and connected to an opening in the ground-level floor. The UFTP lid is removed and modules are lifted out of the package and transferred to the respective module handling cell on the ground level. There will be a process in place to clearly distinguish and track the empty and filled transportation packages, and to keep these packages in separate locations.

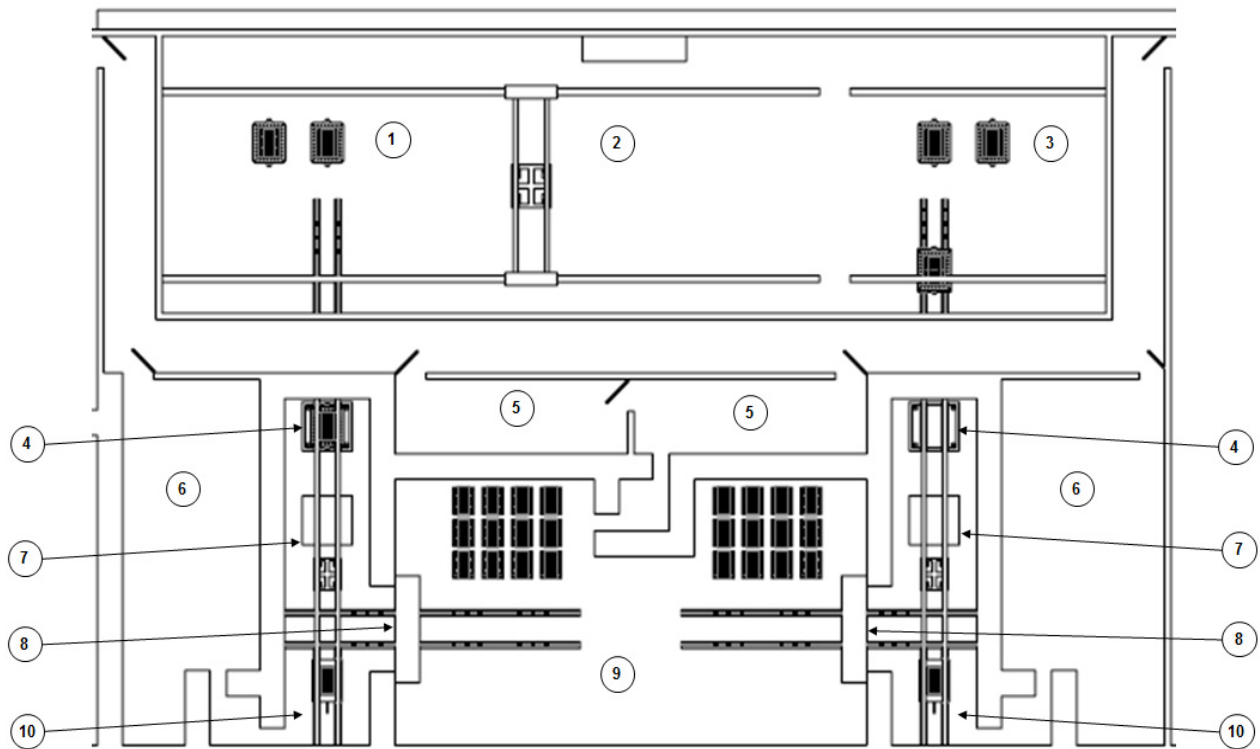


Figure 4-8: UFTP Receiving and Fuel Module Handling

The UFTP Handling Cells illustrated in Figure 4-8 consist of the following areas or components (numbers refer to locations in the figure):

1. UFTP Storage area
2. UFTP Shipping and Receiving Hall
3. Impact Limiter Removal area
4. UFTP Lid Removal
5. Control Room
6. Operator Room
7. Module Transfer Cell
8. Module Transfer to Dry Storage
9. Dry Storage area
10. Module Transfer to Distribution Hall

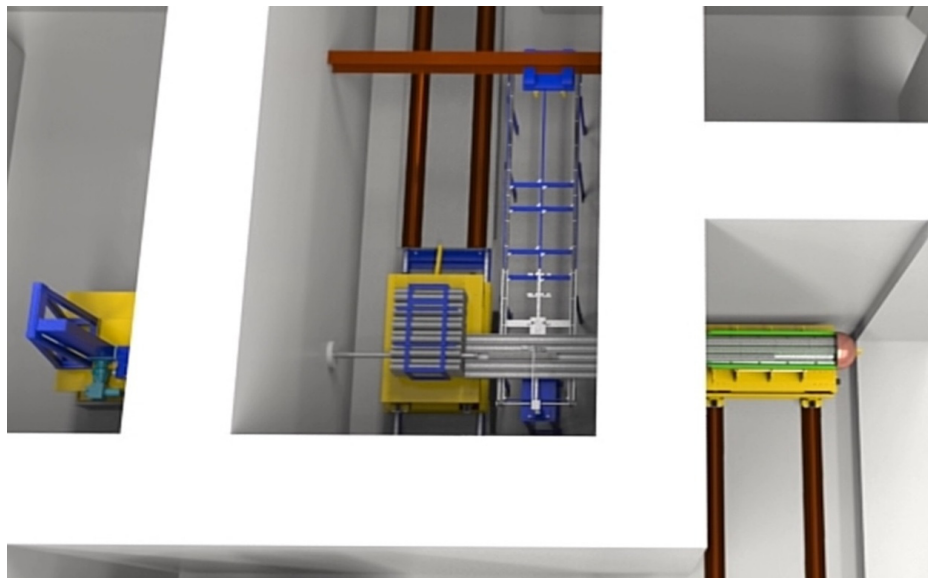
4.5.2 Used Fuel Container Loading and Sealing

To ensure the daily throughput listed in Table 4-5 is achieved, a total of 12 UFCs are planned to be loaded per day, which corresponds to six fuel modules. To accomplish this, the system will utilize three parallel and independent processing lines, each processing an average of two modules and four UFCs per day (Figure 4-9).

The three processing lines will be isolated from one another with airlocks and concrete shielding walls to create “hot cells”. The ‘hot cell’ areas will have lead glass windows and will be equipped with closed circuit cameras for remote viewing.

Empty containers will be produced off-site at a dedicated factory and delivered to the UFPP. Fuel will be received, unloaded and transferred into used fuel containers in a hot cell process. Once the fuel is loaded into the used fuel container, the top hemispherical head will be temporarily installed and the assembly transferred to the used fuel container processing cell. The UFC is welded, examined, copper-cold-sprayed and annealed prior to being placed inside a buffer box in the UFPP. The buffer box is placed inside a shielded cask for transfer underground.

Figure 4-9 to Figure 4-12 illustrate the key steps in the process to load and seal the UFC.



Notes:

1. Room at left of figure houses the equipment to operate the push rod that penetrates the hot cell shield wall.
2. Module loaded with fuel bundles is located in hot cell at center of figure.
3. Bundles are pushed by the rod into the UFC located in hot cell at right of figure. The UFC is shown in a cut-away view with top half of the UFC removed for the purpose of this illustration.

Figure 4-9: Fuel Transfer into Used Fuel Container

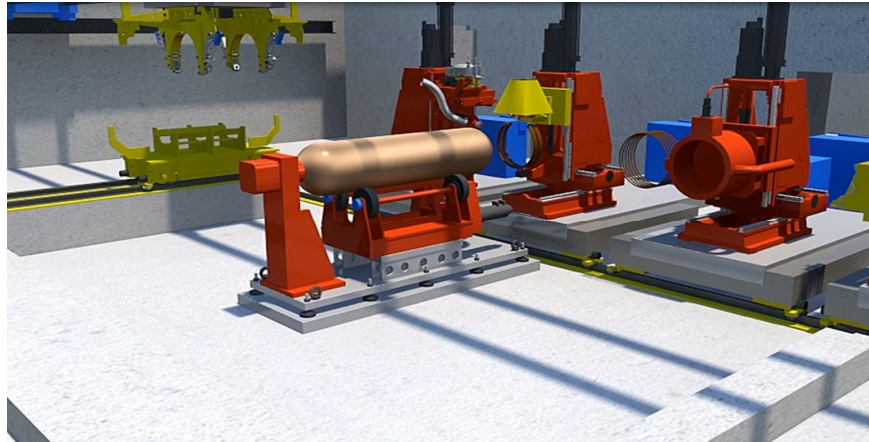


Figure 4-10: Automated Work Tables inside Processing Cell

Inside the processing cell shown in Figure 4-10, automated work tables are responsible for:

1. Welding the hemispherical head to the shell (Figure 4-11)
2. Clean-up machining of the weld (if required)
3. Non-destructive examination of the weld (Figure 4-11)
4. Copper cold spray over weld area (Figure 4-12)
5. Clean-up machining of the copper cold spray (if required)
6. Annealing of copper cold spray (Figure 4-12)
7. Non-destructive examination of the copper cold spray

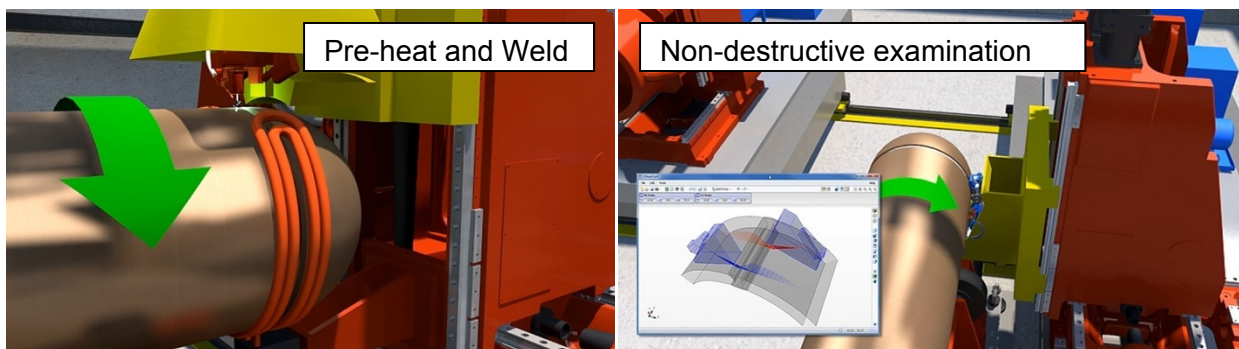


Figure 4-11: Weld Worktable and Non-Destructive Examination Worktable

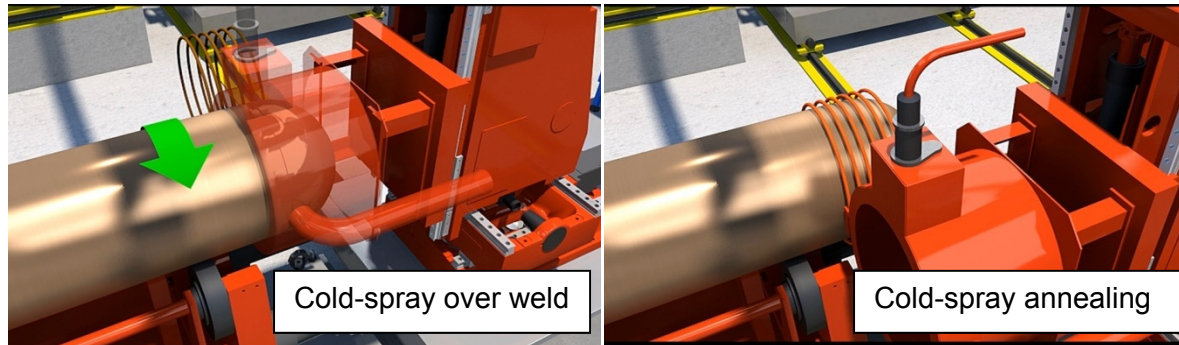


Figure 4-12: Copper Cold Spray and Copper Annealing Worktable

4.5.3 Used Fuel Container Intra-Plant Transfer System

The UFC intra-plant transfer system is comprised primarily of an Automated Guided Vehicle (AGV) system and the UFC transfer hall where four AGVs will operate. The transfer hall contains three Work in Progress (WIP) storage areas:

- WIP Storage Area #1 for loaded UFCs – UFCs loaded with used fuel;
- WIP Storage Area #2 for post-weld UFCs - UFCs that have just completed the welding operation; and
- WIP Storage Area #3 for completed UFCs – UFCs that have successfully been coated with copper and are ready for dispatch to buffer box assembly area.

The hall allows AGVs to access the active maintenance shop, waste management facility, fuel loading cells, process contingency manual work cell, UFC weld cell, UFC copper application cell and the UFC final decontamination cells.

All areas of the transfer hall will be shielded from radiation fields given off by the UFC using concrete shielding walls between processing areas, or by the use of a shielded UFC transfer flask. The main transfer hall is expected to be classed as Zone 2; however, because there is risk that contamination could spread from the unsealed UFCs, this area may have to be designated Zone 3. Hot cells in this facility can be considered as Zone 4 for control purposes.

The used fuel packaging plant illustrated in Figure 4-7 consists of the following areas or components:

1. UFC Transfer Hall
2. Fuel Handling Cell Docking
3. UFC Weld Cell Docking
4. UFC Copper Application Cell Docking
5. WIP Storage Area #1 - Loaded UFCs
6. WIP Storage Area #2 – Post-Weld UFCs
7. WIP Storage Area #3 - Completed UFCs
8. UFC Decontamination Cell Docking
9. Process Contingency Manual Work Cell Docking

4.6 Sealing Materials Production Facilities

The sealing materials are produced in the sealing materials compaction plant (Area B6 in Figure 4-6) and the concrete batch plant (Area B13 in Figure 4-6). For logistics reasons the sealing materials facilities are situated outside the Protected Area but as close as possible to the service shaft.

4.6.1 Sealing Materials Compaction Plant

During repository operations the sealing materials compaction plant will be used to manufacture the following materials:

- HCB blocks, spacers and bricks; and
- Gap fill.

The presses used to produce the HCB material are a specialized item that will need to be designed to suit this purpose. Two compaction options exist for the very large HCB blocks (a uniaxial compaction approach and an isostatic compaction approach).

Examples of the large presses that would be required for production of some of the bentonite components are shown in Figure 4-13 and Figure 4-14.

All raw materials used in the sealing materials compaction plant will be externally sourced.



Figure 4-13: Example of a Closed-Die Forging Press (Uniaxial Compaction)



Figure 4-14: Cold Isostatic Press for Production of Highly Compacted Bentonite Blocks

During closure of the underground repository, the sealing materials compaction plant will be reconfigured, as required, to produce different categories of clay based sealing materials:

- Dense backfill blocks,
- Gap fill,
- Highly Compacted Bentonite blocks, and
- Bentonite/sand mixture.

Additional information about tunnel and shaft sealing is presented in Section 4.12.

4.6.2 Concrete Batch Plant

The concrete batch plant will produce two different qualities of high-performance concrete mixes, one used for the shaft liners and the other for tunnel floors, placement room bulkheads and shaft seals. Externally sourced raw materials will be used to produce the concrete including aggregate and binders. The concrete batch plant will also be used during closure of the underground repository.

4.6.3 Aggregate Supply

Due the relatively small quantity of aggregate required by the sealing materials compaction plant and concrete batch plant during repository operations, an on-site rock crushing plant is not required and all aggregate will be imported to the site. Modified granular A (a graded crushed stone) and fine sand will also be delivered and used to produce aforementioned sealing materials in the sealing material compaction plant. Aggregate (sand and stone) will be delivered to the site for use in the concrete batch plant.

4.7 Shafts and Hoists

Access to the repository is via shafts serviced by hoisting facilities. Three shafts will be constructed, the main shaft, the service shaft, and the ventilation shaft (Figure 4-15) each serving specific functions during construction and operations of the repository facility. Their primary functions are the transport of materials and personnel, and providing ventilation to the repository. The shafts will be constructed using techniques that minimize host rock damage, to enhance the effectiveness of postclosure shaft seals.

All shaft finished diameters are 7 m.

The headframes for the three shafts will be of slip-formed concrete construction for durable and easily maintainable structures. All the shafts will be concrete lined and the lining will be removed during sealing of the shafts following the end of operations.

The three shaft structures (including head frames and hoisting plants) provide a number of support functions during construction and operation of the underground repository:

- The main shaft serves as the exclusive means for transfer of used fuel containers from the surface to the underground repository. Conversely, it could also be used for transfer of a retrieved used fuel container from the repository to the surface, if this was required. Finally, the main shaft will have a minimal exhaust flow to surface;
- The service shaft serves as the principal conveyance for personnel, materials, fresh air and equipment to the underground as well as for transport of excavated rock to the surface; and
- The exhaust ventilation shaft is the primary route to exhaust underground air and also serves as a second emergency exit from the repository.

4.8 Underground Facility Design

For the purpose of this postclosure safety assessment, the used fuel repository is assumed to be developed on a single level, at a depth of 500 m, in a setting capable of withstanding mechanical and thermal stresses. The actual layout for a selected repository site will be adapted to suit the specific site conditions.

The geology of the hypothetical site used in this study is described in Chapter 2. The volume of available competent rock in this hypothetical geosphere allows sufficient distance from unfavourable geological features. A possible layout for a repository designed to accommodate a reference inventory of 5.224 million used fuel bundles is shown in Figure 4-15.

Other countries, such as Finland and Sweden, have identified their hosting locations. This has allowed them to start developing site-specific layouts which are adaptive (flexible) layouts in that the layouts can be adjusted to suit the conditions encountered underground. NWMO has recognized the necessity for this flexibility in the layouts, and has started the process of identifying the challenges and options to be faced in achieving this design flexibility.

4.8.1 Underground Layout

The placement rooms are a series of parallel tunnels arranged in panels, as shown in Figure 4-15. Within each panel, the placement rooms have a centre-to-centre spacing of 25 m to satisfy thermal constraints, and each room has a single access from the corresponding panel access tunnel. The length of the rooms in the reference design is specified as 341.6 m where the useable length in each room is 324.6 m. The used fuel container density is designed to minimize the repository underground footprint while, at the same time, satisfying thermal design requirements. The placement room design is shown in Figure 4-16 and described in further detail in Section 4.8.2.

The repository includes provision for an underground demonstration facility located near the main and service shafts. This facility will be used to support long-term testing and demonstration of repository technology.

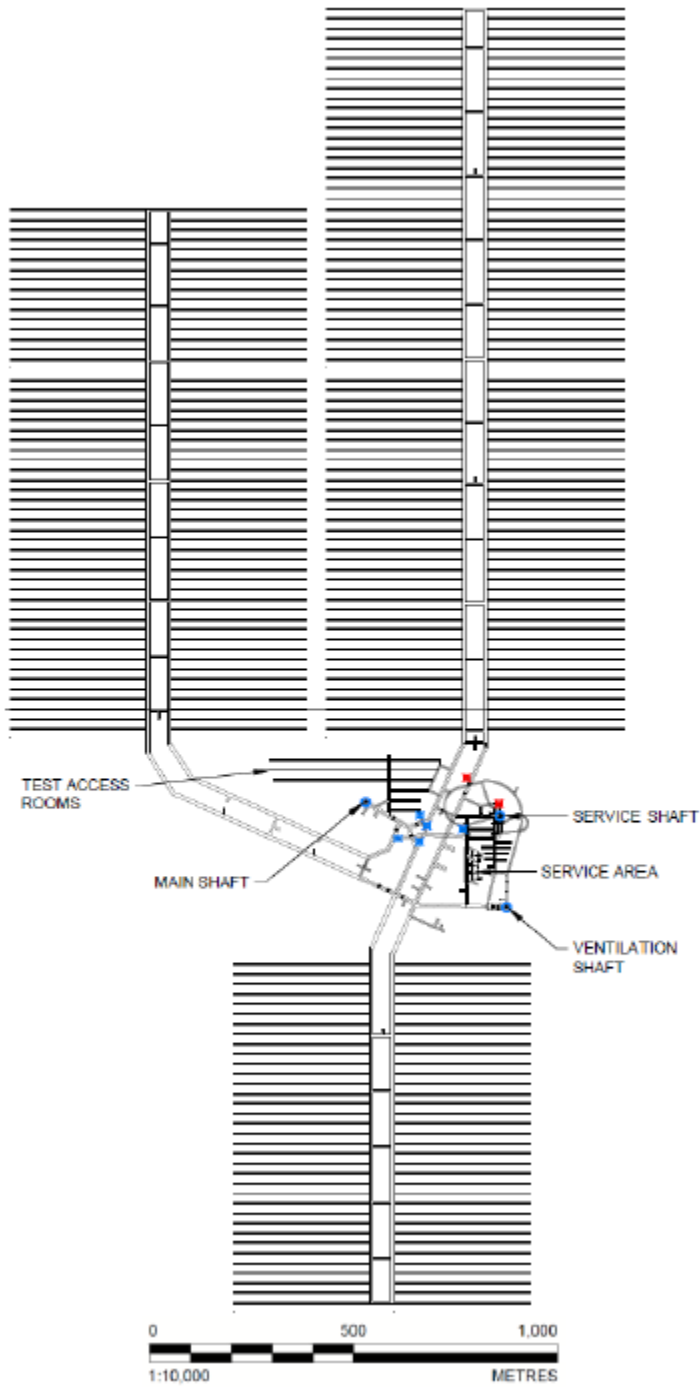


Figure 4-15: Underground Layout for 5.224 Million Bundles

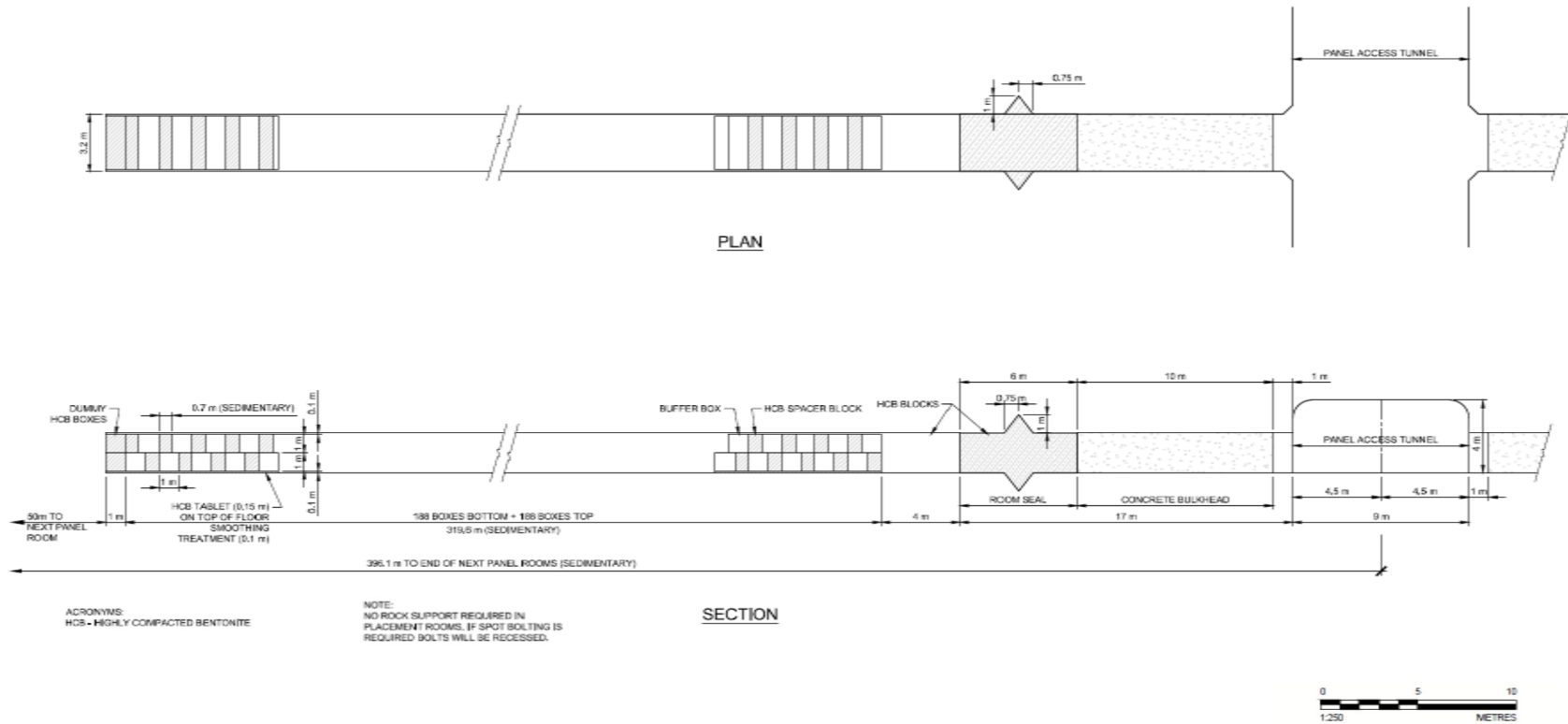


Figure 4-16: Plan View and Longitudinal Section of Placement Room

4.8.2 Placement Room Geometry and Spacing

The size of the buffer box and the placement equipment determines the placement room dimensions and profile. These factors and the need to minimize stresses (to maximize rock stability) were addressed by using room cross-section geometry with a height of 2.4 m and a width of 3.2 m (Figure 4-17).

The sealing materials used in placement rooms are:

- HCB blocks which surround the used fuel containers inside the buffer boxes;
- HCB blocks which act as 0.7-m-thick spacers between the buffer boxes; and
- Gap fill which is placed on the floor before start of placement activities and in the nominal 150-mm-thick gap between stacks of buffer boxes and spacer blocks and the rock wall and roof.

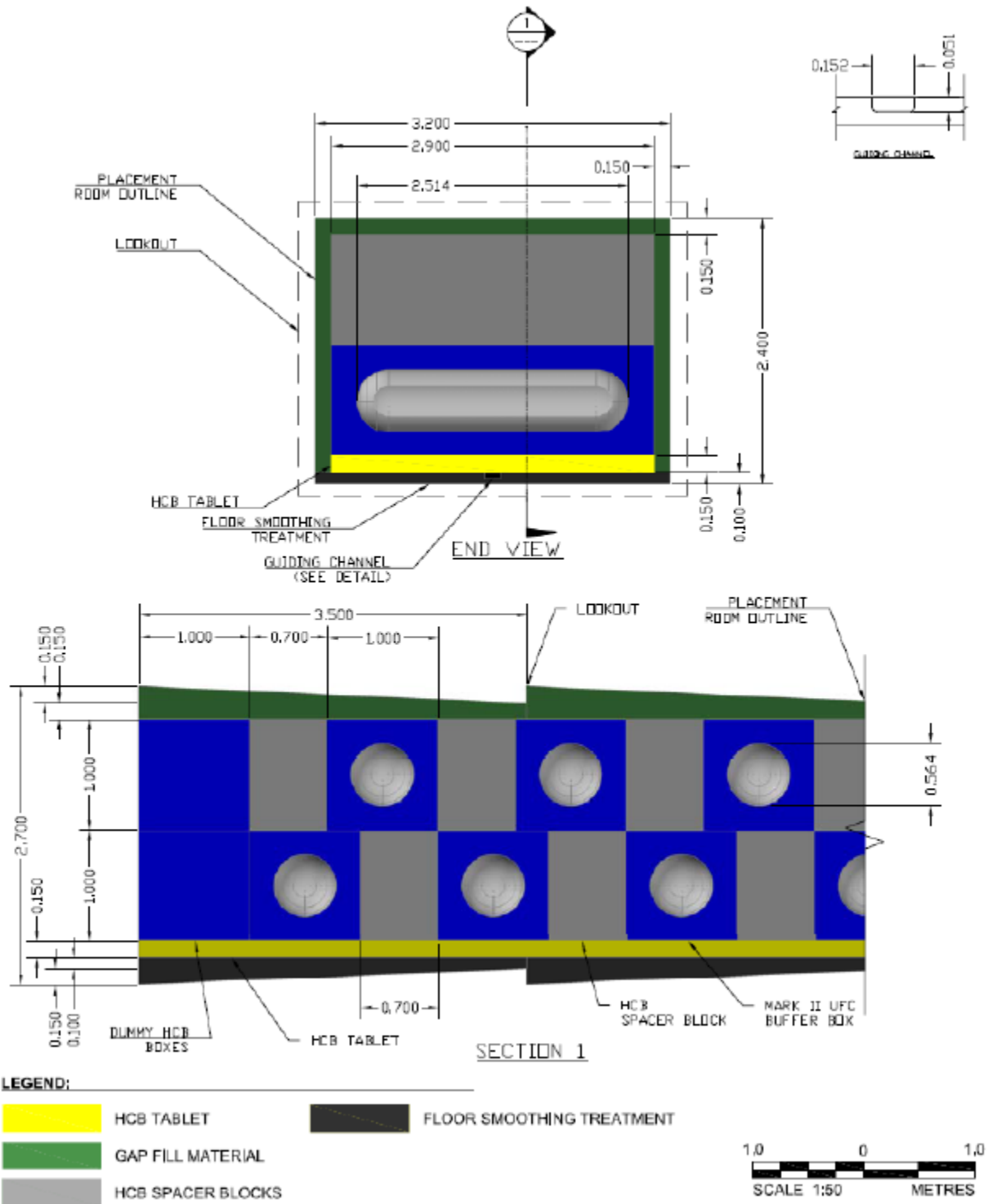


Figure 4-17: Placement Room Section Views

Thermal analyses were conducted to establish the temperature regimes for both the engineered barriers and the geosphere. The thermal analysis results were used to optimize both room spacing and container spacing. These parameters were chosen to ensure that the temperature at the container surface will not exceed 100°C at any time. To meet this requirement, the centre-to-centre spacing of placement rooms was set at 25 m and the centre-to-centre spacing of buffer boxes was set at 1.7 m.

Regardless of the room geometry and spacing, some excavation damage is expected to occur in the rock around placement rooms. However, the maximum depth of the damaged zone is not expected to exceed a few tens of centimeters.

Although it is expected that rock support will not be required inside the placement rooms, there may be minor amounts of metal rock bolts and screens used to stabilize excavated walls and ceilings for worker safety.

4.8.3 Placement Room Closure

Once the placement room has been filled with buffer boxes, the room will be closed with a bentonite room seal and concrete bulkhead. This room closure would permit physical isolation of the regions where container placement has been completed, improving security and permitting the continued use of the tunnels and access ways for ongoing repository operations in adjacent rooms. The major components of the placement room sealing system are illustrated in Figure 4-18.

Before the room seal is constructed a 4 m length of room between the last stack of buffer boxes and the start of the room seal will be filled with HCB spacer blocks. The void space around the 0.5-m-thick HCB blocks will be filled with gap fill material similar to the process used during buffer box placement.

Upon completion of these activities, a 6-m-thick bentonite room seal will be constructed at the entrance of the placement room. The seal will be constructed with HCB blocks and bricks, as illustrated in Figure 4-18 (HCB blocks in red, HCB bricks in green). The HCB bricks will be placed to create a wedge-shaped ring designed to interrupt the continuity of the excavation damage zone. The void space around the HCB blocks will be filled with gap fill material in parallel with the block placement process.

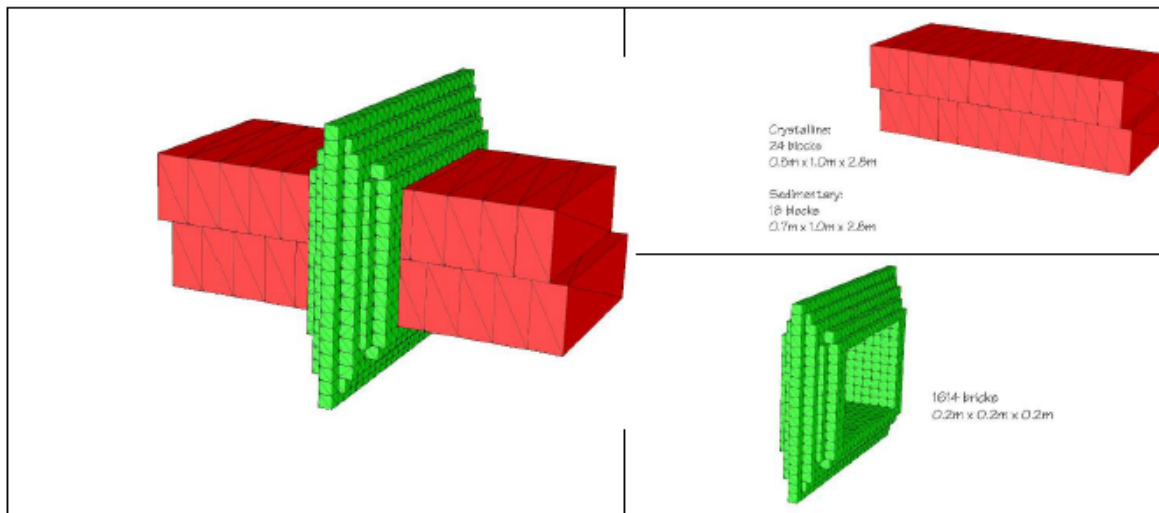


Figure 4-18: Room Seal

After HCB blocks and bricks have been placed, a thick bulkhead of low-heat, high-performance concrete (see Figure 4-16) will be constructed. The purpose of the bulkhead is to provide mechanical restraint against the forces exerted by swelling clay sealing materials. The bulkhead will thereby act to keep the sealing materials isolated in their intended positions while the access tunnels remain unfilled.

4.8.4 Ventilation System

The repository ventilation system utilizes the three shafts and a combination of parallel airways for intake and exhaust. Underground booster fans, ventilation doors and dampers are used to control the airflow distribution. Since the primary repository ventilation system consists of relatively large airways, the overall circuit can be described as having relatively low resistance characteristics in a push-pull type network. Air is heated as required during winter months. The fresh air supply reaches the repository level at the service shaft level and is split to the underground services area and the panels of placement rooms.

The majority of the exhaust air from the repository area is routed to the ventilation shaft. A small portion of the exhaust air flow is routed to the main shaft.

Air distribution in the repository is promoted through the use of fans and regulators. The system will be operated to ensure that the underground work is performed in a fresh air supply stream with the exhaust being directed through unoccupied areas, going generally from clean areas towards operation areas.

During development of individual placement rooms, auxiliary fans will be installed near room entrances to deliver air via ducting to the working face in the rooms. The fans will provide approximately 6 m³/s of air to the room face and the air will exhaust via cross-section of the room.

For the purpose of this conceptual design, stand-by HEPA filtration systems are assumed to be installed underground.

4.9 Site Preparation and Construction of the Repository

Implementation of a deep geological repository falls under federal jurisdiction. It will be regulated under the NSCA and its associated regulations as described in Chapter 1. The following sections describe the site preparation and construction work to be performed at the DGR site.

4.9.1 Site Preparation

Initial site preparation activities, which include clearing and grading, establishing access roads and the installation of basic infrastructure systems would be conducted. The site infrastructure required to support excavation, including electrical delivery systems, headframes, ventilation and excavated rock management systems would also be established.

4.9.2 Shaft Sinking

Controlled construction methods will be used to minimize disturbances to the area surrounding the facility. The three shafts will be developed using a controlled drill and blast shaft sinking approach specifically designed to minimize the excavation damage zone. The shaft sinking process will involve the following steps:

- Collaring or starting the shaft;
- Setting up the equipment needed to sink the shaft;
- Sinking the shaft to its full depth using the drill and blast method; and
- Dismantling the equipment used for sinking.

Conventional blasting operations include drilling blast holes in a converging pattern designed to minimize the quantity of detonated explosive per volume of rock. In order to reduce damage to the perimeter of the opening, a larger number of blast holes with smaller individual explosive charges are used in the outer region of the shaft. This is usually referred to as contour wall blasting, and it will be used to minimize the thickness of the excavation damage zone. Between the blasting cycles, fumes are vented, scaling is done to remove loose rock and ground support is applied as required. This excavation method is expected to result in a rate of advance in the range of 2.6 m per day for each shaft. This rate excludes the delays associated with geoscientific verification testing.

4.9.3 Underground Demonstration Facility

An Underground Demonstration Facility (UDF) will be constructed at the DGR site. Studies that would be conducted as part of the UDF include verification of geological conditions, demonstration of applicable procedures for management of used fuel containers and sealing materials, long-term studies of engineered barrier materials, monitoring instrumentation and ground support system and/or monitoring of specially instrumented containers.

The UDF is a stand-alone testing location near the Main and Service Shafts. The UDF will be constructed as soon as possible after the Service Shaft reaches the shaft station and a rock

handling system is installed. The UDF would operate on a stand-alone basis for about five years prior to start of operations and would continue to operate over the complete life of the repository.

The UDF will be designed to integrate with the overall underground repository but will be located so as to be separate from the placement rooms with respect to the test room activities. This will ensure that facilities common to both the UDF and the repository are centrally located to both operations.

The test room excavation work in the UDF will provide an opportunity to demonstrate and refine drilling and blasting techniques intended for the placement rooms. To minimize potential pathways for groundwater movement after closure, and to reduce the use of ground support in the placement rooms and tunnels, the blasting damage in the rock surrounding the created openings needs to be minimized. This EDZ can be controlled through the use of careful excavation techniques. Detailed mapping of the rock after excavation, and correlation of the EDZ thickness to the blast-hole pattern and blasting techniques (for example) will ensure that the methods adopted meet all requirements. Excavation methodologies for the various underground openings can therefore be optimized.

Geoscience verification activities will be carried out in the UDF and at other locations in the underground repository for the purpose of verifying assumptions and geoscience data used in the safety case. In particular, data will be gathered to confirm that the host rock formation will be able to act as a long-term barrier and will be able to contain and isolate the used fuel. The results of these geoscience investigations and monitoring activities will be used in the application seeking approval for full construction of the repository, and eventually in the application for an operating licence.

The UDF would support the long-term demonstration and monitoring of container placement and sealing systems, and will provide a training area for DGR employees. The test placement rooms would be available for prototype equipment testing five years before the repository is operational.

4.9.4 Lateral Development

The remaining underground excavations, like access tunnels and panels, will be constructed by controlled drilling and blasting after the UDF.

4.9.5 DGR Facility Commissioning

The DGR facility will be commissioned once initial construction of the underground repository is complete.

4.10 Repository Operation

During repository operations, panel development and used fuel placement operations will be performed concurrently in separate arms. The repository development/operation strategy will optimize efficiency while considering both safety and operating factors (e.g., vehicle traffic and ventilation) as well as the potential interactions between repository development and operations.

The repository operations will continue until all used fuel has been repackaged in used fuel containers and buffer boxes, all buffer boxes placed into rooms and all placement rooms sealed. This is expected to take approximately 45 years for a used fuel inventory of 5.224 million bundles.

The following sections describe the preparation of placement rooms to receive buffer boxes (with UFCs), equipment to be used for placement of buffer boxes and the sequence of placement operations.

4.10.1 Preparation of Placement Room

After excavation work is complete, and prior to the start of buffer box placement operations, the room will be prepared by first placing a 100-mm-thick levelling layer of bentonite pellets on the room floor. Temporary metal plates will be installed on top of the bentonite layer to facilitate equipment access to the work face. The metal plates will be placed over the full length of the room to the near end of the room. The temporary metal plates will have a metal ventilation duct integrated into the design of the plate. Fresh air is delivered into the placement room via the room cross-section. The air is then exhausted (“pulled”) from the room via ventilation ducts which remove heat and dust from the room. As placement operations retreat from the end of the room toward the room entrance, the floor plates will be removed to allow stacking of buffer boxes directly on top of the bentonite layer.

4.10.2 Buffer Box Placement

The UFCs will be assembled into buffer boxes inside the UFPP. Fully assembled buffer boxes will be staged inside the UFPP awaiting transfer to the main shaft. After final inspection, each buffer box will be loaded into a shielded transfer cask and then the cask will be loaded onto a rubber-tired trolley. Using a tow vehicle, the trolley with transfer cask will be moved into and secured within the main shaft cage. Upon arrival at the repository level, the trolley with transfer cask will be removed from the cage by another tow vehicle and taken to the shielding canopy at the entrance of a placement room.

Once the transfer cask is mated to the access window of the shielding canopy, an ejection ram will push the buffer box out of the cask onto the placement vehicle waiting inside the shielding canopy. The unmanned and remote-controlled placement vehicle will travel the length of the placement room to the final placement location. Radiation protection controls will be in-place to deny workers entry to the room to protect them from the radiation fields emitted from the UFCs. After two buffer boxes have been stacked, two spacer blocks will be stacked by procedures similar to those used to place the buffer boxes. After two buffer boxes and two spacer blocks are placed, then placement operations will be temporarily stopped to allow placement of gap fill (bentonite pellets).

The placement vehicle will exit the placement room through the shielding canopy. The bentonite pellet placement equipment will enter the placement room and perform the pellet placement operation – injecting loose bentonite pellets in the void spaces between the stacked buffer boxes and dense backfill blocks, and the rock wall. Due to presence of radiation fields, the bentonite pellet placement operation must also be remotely-controlled.

After the bentonite pellet placement equipment has exited the placement room, the placement vehicle, equipped with a magnetic floor plate removal system, would enter the placement room through the shielding canopy, and remove a floor plate segment and then exit the room. It is expected that the entire buffer box placement process will take approximately four hours per box. Further, it is anticipated that each phase of the process will take four operators to complete (connecting and operating equipment, etc.). Placement operations must be performed concurrently within three rooms in order to achieve a throughput of 2,500 buffer box per year.

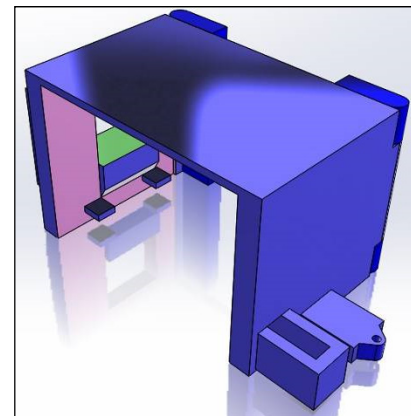
4.10.3 Description of Placement Equipment

The key equipment to be used in the placement operations is described in this section.

Buffer Box Placement Vehicle: This remotely-controlled underground vehicle is based on a highly customized commercial electric forklift with various enhancements including built-in remote operation sensing, lighting, and camera equipment as well as a customized lifting attachment to accommodate the buffer boxes and spacer blocks. It will also have an attachment for removal of the floor plates.

Shielding Canopy: The mobile shielding canopy will permit shielded activities to take place inside rooms, while also allowing use of the panel access tunnel by passing vehicles and personnel. The small void space around the canopy perimeter can be covered by manually placed lead shielding packs to ensure radiation does not escape through the gap between the shield and rock.

The canopy has shielded hinged access doors for vehicle access. It also includes a shielded access window which, when opened, allows passage of buffer boxes and dense backfill spacer blocks.



The canopy is illustrated in Figure 4-19.

Figure 4-19: Shielding Canopy

Bentonite Pellet Injection System: After two buffer boxes and two spacer blocks are placed, all void spaces around the boxes and blocks will be filled with loosely-placed bentonite pellets (gap fill). The bentonite placement system will be mounted on a vehicle that is similar to the placement vehicle and it will use a pneumatic or auger insertion system for placing loose bentonite.

Floor Plates with Ventilation Ducts: The floor plates will be installed before the start of buffer box placement activities. As placement activities progress towards the room entrance, segments of floor plates will be removed. A magnetic attachment on the placement vehicle would be used to pick up the plate segments and bring them out of the placement room.

The floor plate is illustrated in Figure 4-20.

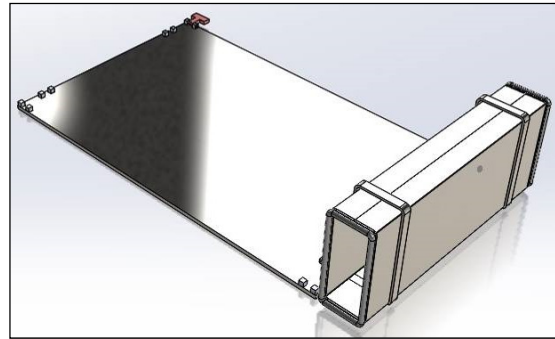


Figure 4-20: Floor Plate with Built-in Ventilation Duct

4.10.4 Storyboard Description of Preparation and Placement Operations

Graphical storyboards showing key steps in room preparation, and the transfer and placement of the buffer boxes are provided in the following figures. Figure 4-21 provides a summary of the placement equipment. Figure 4-22 illustrates, step-by-step, all activities that are required to prepare each room for the receipt of buffer boxes. Figure 4-23 illustrates the steps that would be taken to place the buffer boxes inside a placement room.

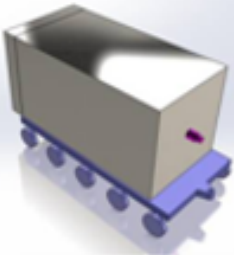
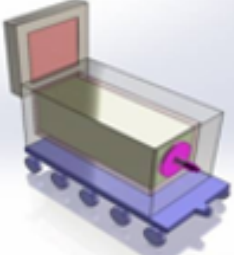


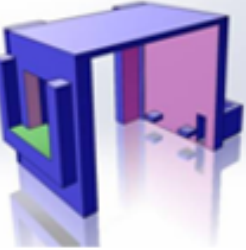
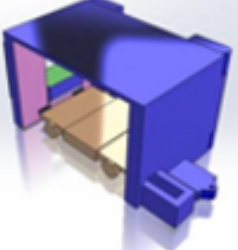


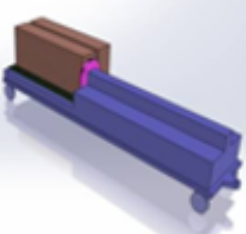

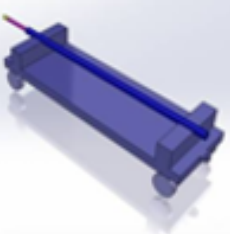
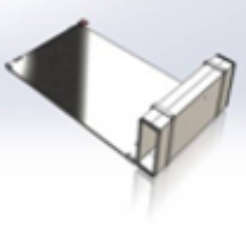
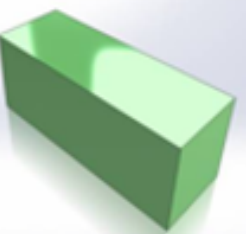
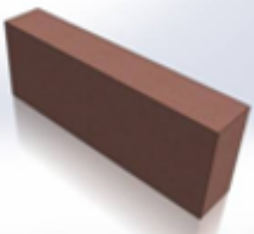

			
UFC Transfer Cask & Trolley	UFC Transfer Cask Door Open with UFC	Tow Vehicle	Tow Vehicle with UFC Transfer Cask
			
Shielding Canopy	Shielding Canopy with Trolley	Placement Machine	Floor Plate Handling System
			
Trolley for Bentonite Blocks	Bentonite Pellet Blowing System	Hydraulic Cylinder Cart	25-mm-thick Floor Plate with Ventilation Duct
			
Buffer Box	HCB Spacer Block	UFC	

Figure 4-21: Legend for Container Placement Equipment

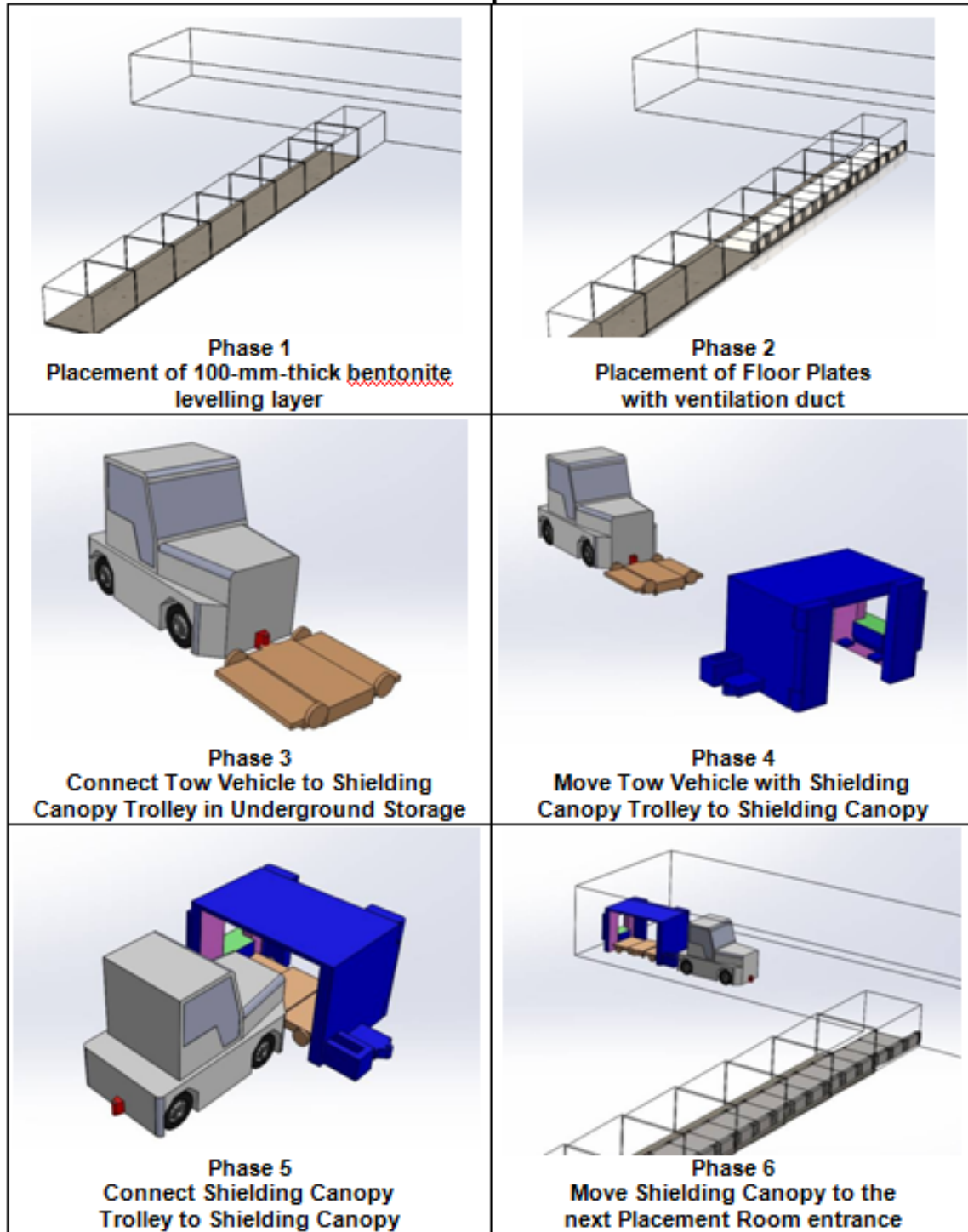


Figure 4-22: Preparation of Placement Room & Shielding Canopy

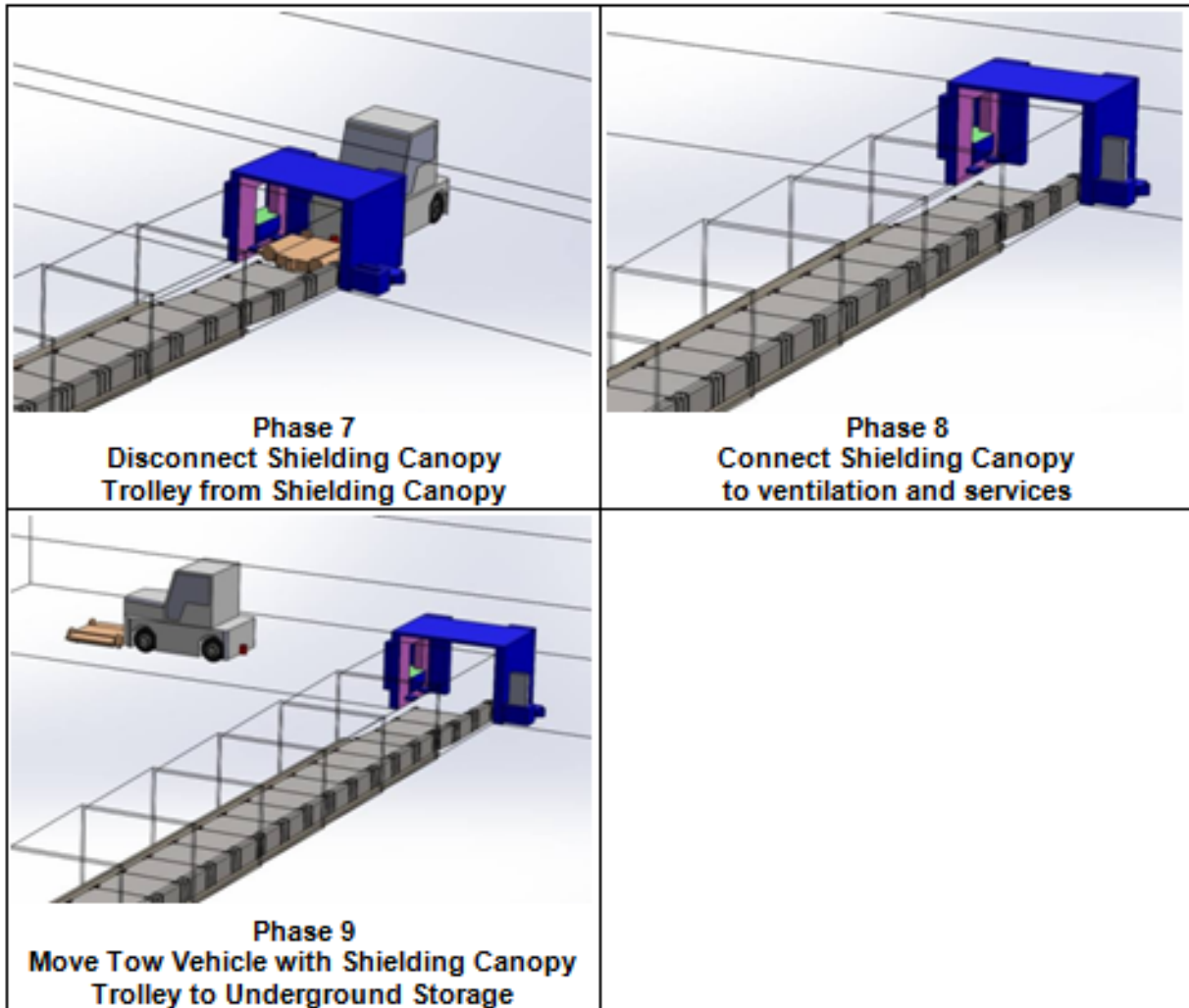


Figure 4-22: Preparation of Placement Room & Shielding Canopy (concluded)

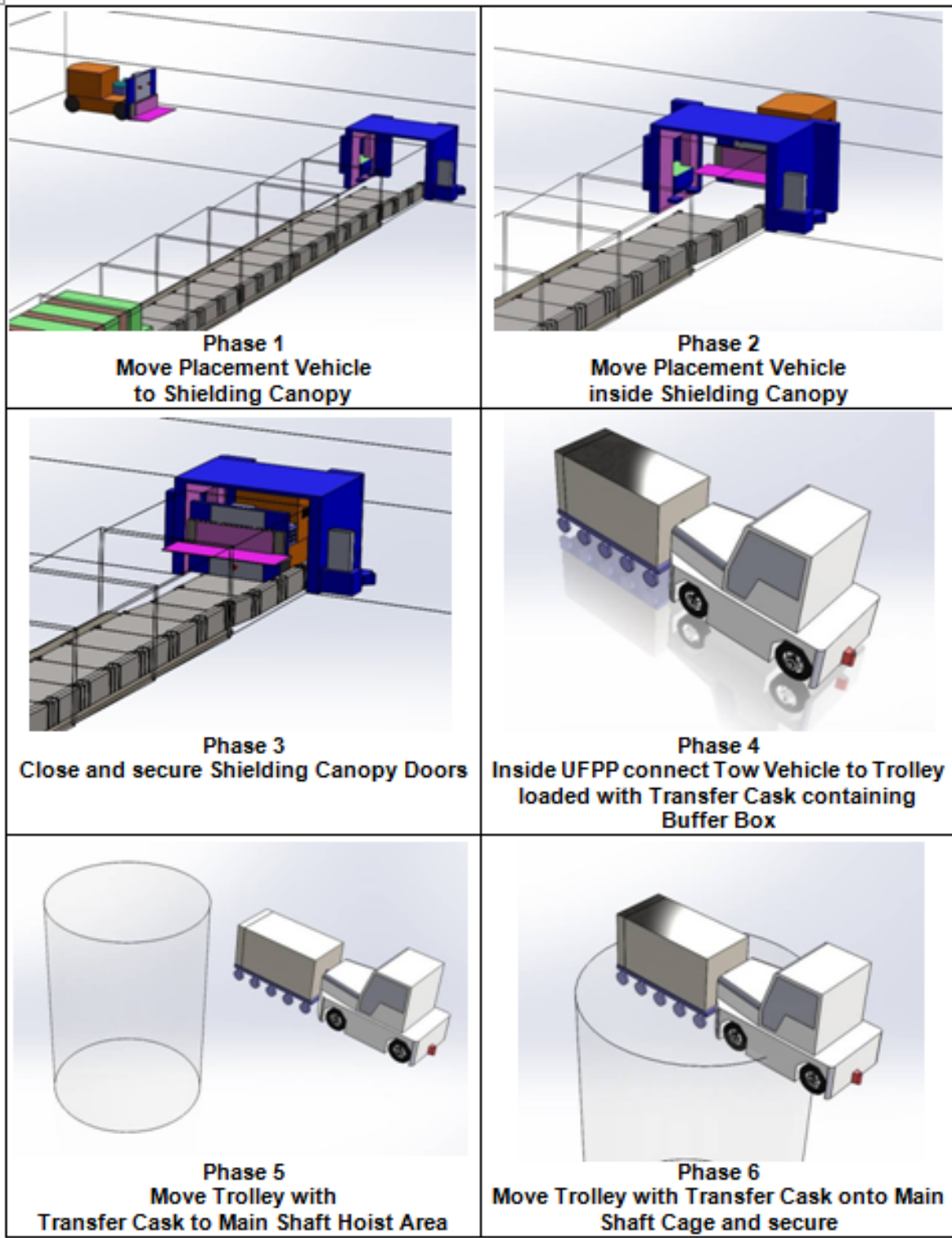


Figure 4-23: Container/Buffer Box Placement

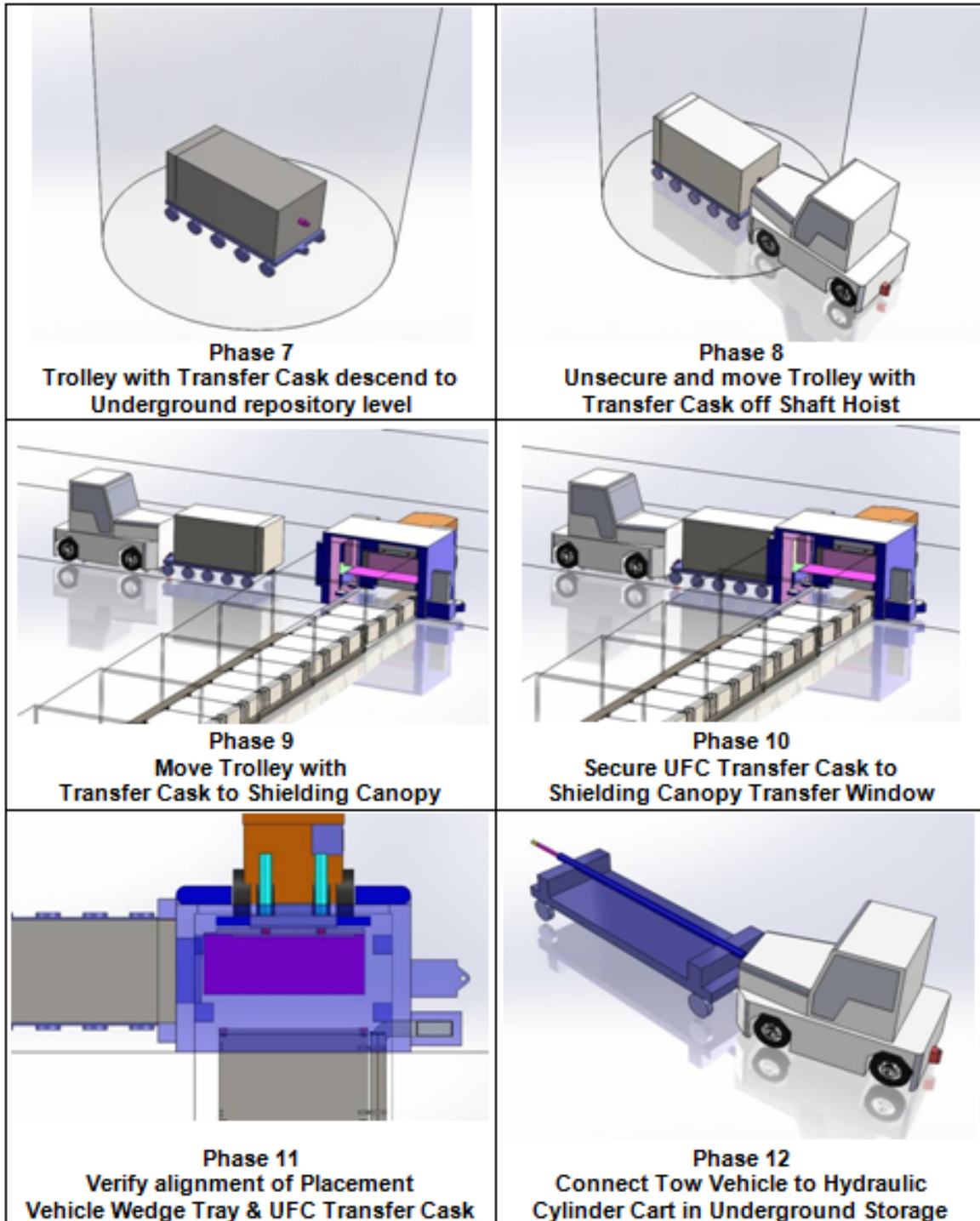


Figure 4-23: Container/Buffer Box Placement (continued)

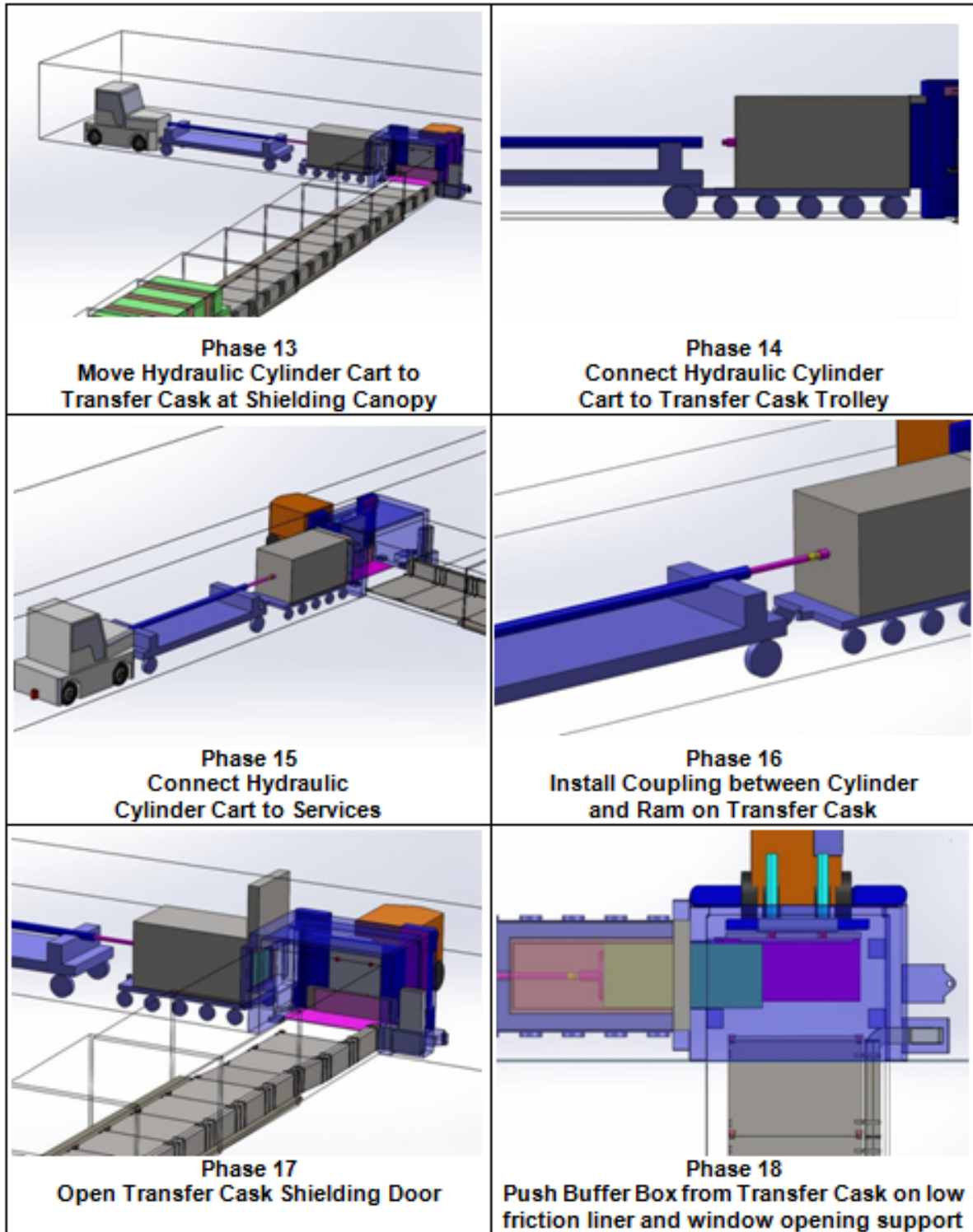


Figure 4-23: Container/Buffer Box Placement (continued)

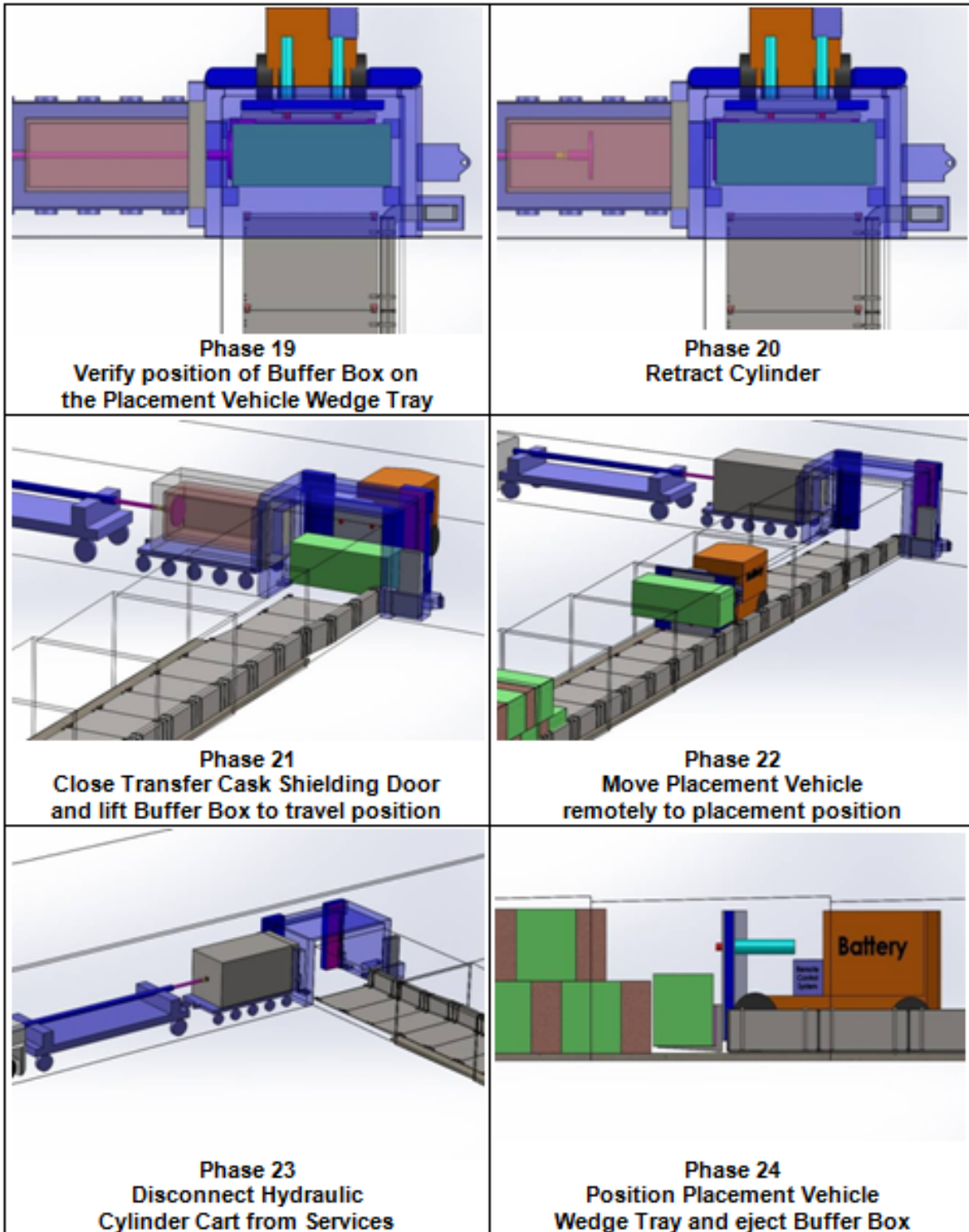


Figure 4-23: Container/Buffer Box Placement (continued)

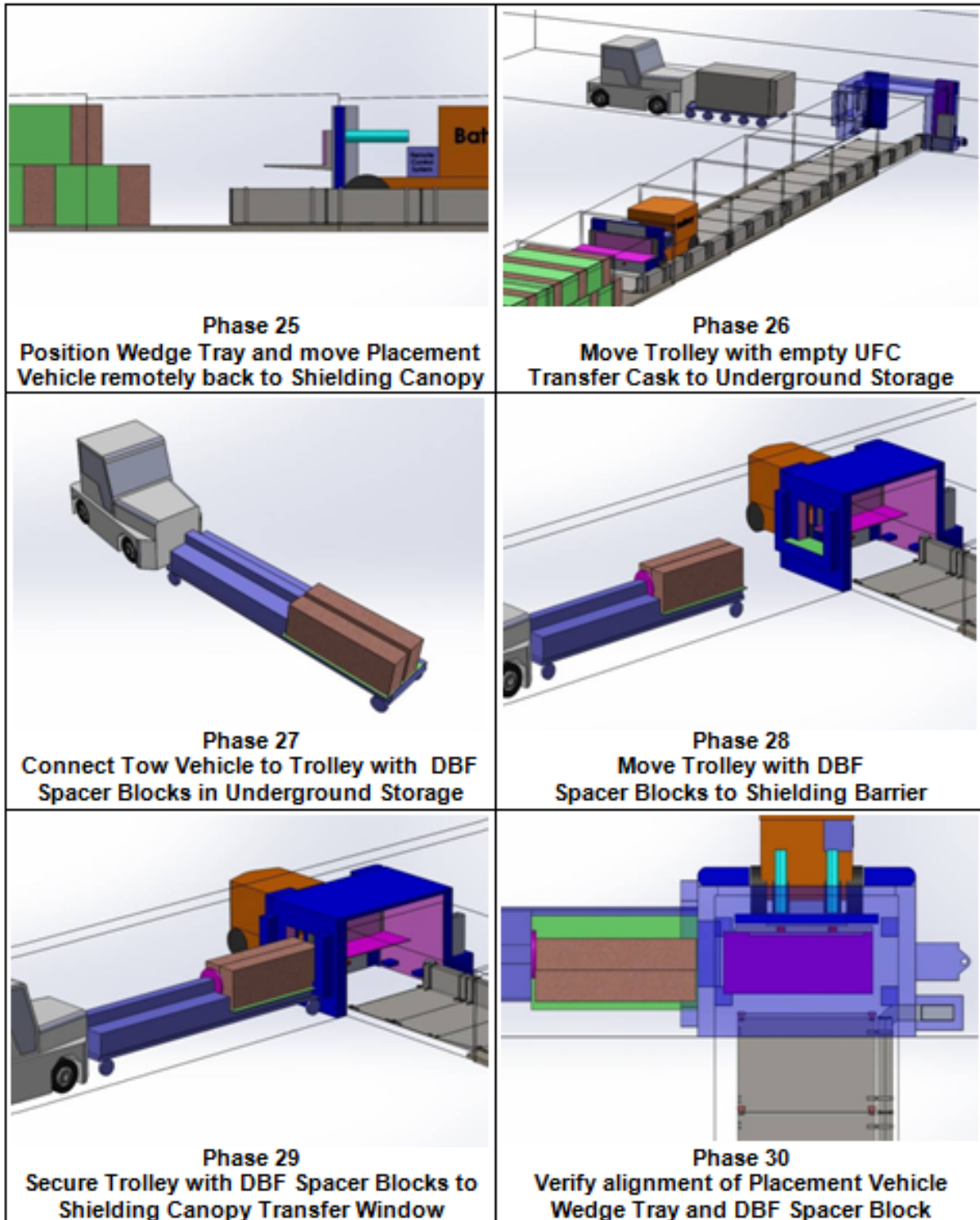


Figure 4-23: Container/Buffer Box Placement (continued)

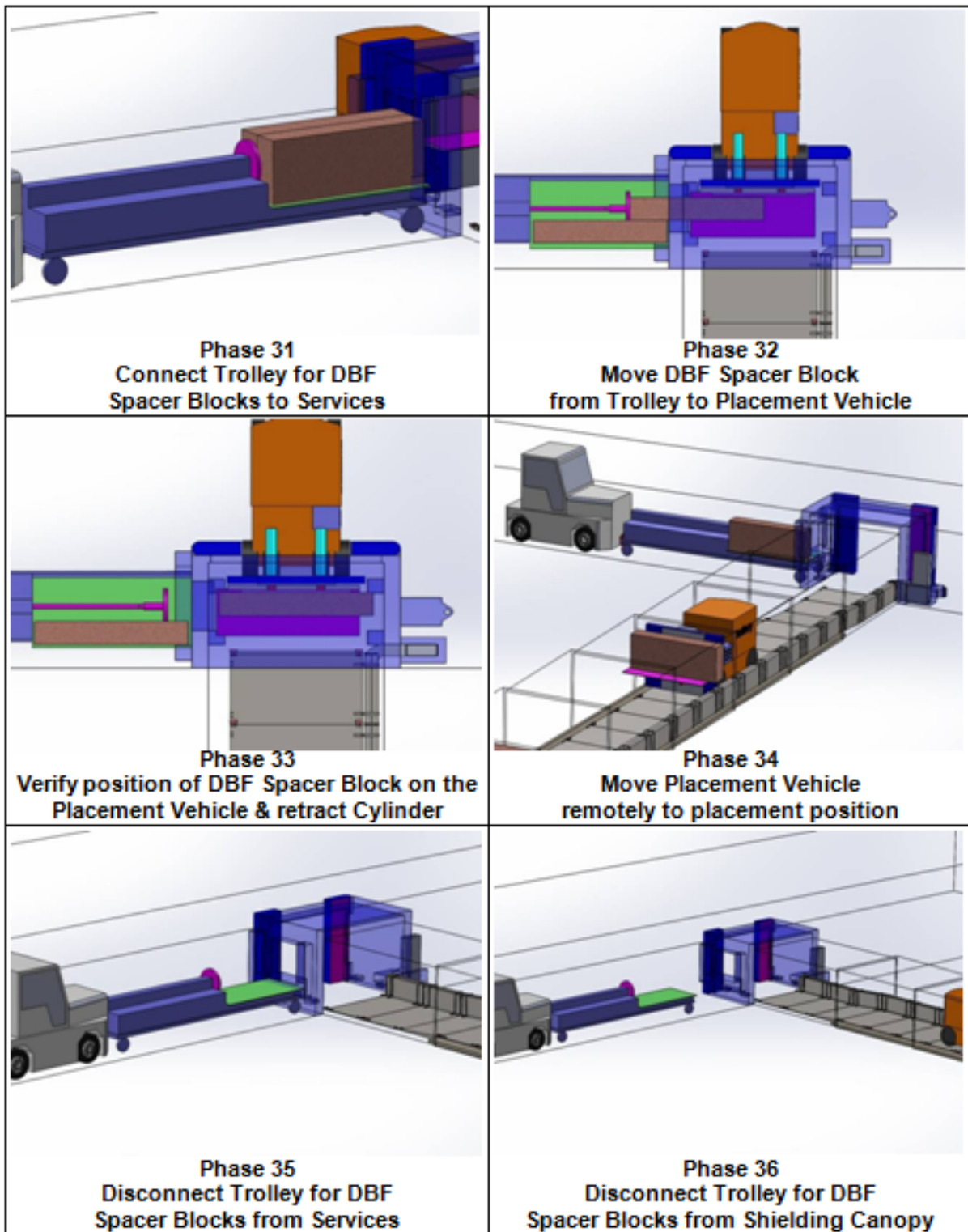


Figure 4-23: Container/Buffer Box Placement (continued)

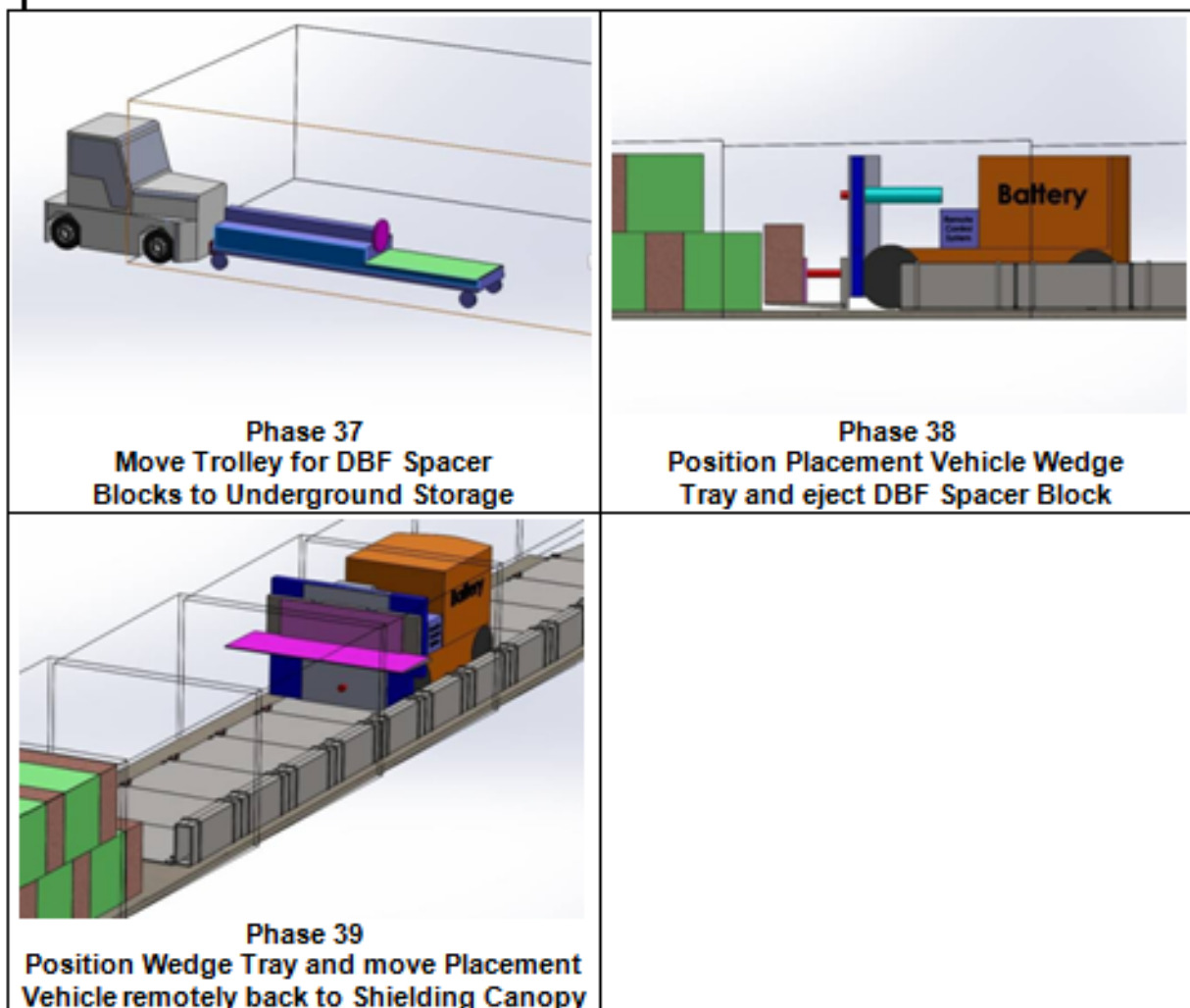


Figure 4-23: Container/Buffer Box Placement (concluded)

4.10.5 Environmental Monitoring Programs

Prior to start of construction the environmental monitoring program will collect data to establish baseline conditions. Thereafter, the program will monitor for any changes that may be imposed on the environment due to construction activities and ultimately the operation of the DGR facility. Monitoring requirements for the postclosure period will need to be re-examined as part of the final plan for decommissioning and closing the site.

The environmental monitoring program will be comprised of the following components:

- Radiological monitoring;
- Groundwater quality and levels monitoring;
- Monitoring of surface water and storm water;
- Air quality monitoring; and
- Meteorological monitoring

The final elements will be developed as part of the formal licensing process for the DGR. The expectation is that the program will provide reliable, accurate and timely data in a fashion that is easily audited.

4.11 Extended Monitoring

Upon completion of used fuel container placement activities all placement rooms will be sealed and closed, but the access tunnels and shafts will remain open. The facility will be placed in an extended care and maintenance program during which monitoring of the repository and surrounding geosphere will continue to confirm the performance of the repository system. The extended monitoring period could have a duration of several decades.

4.12 Decommissioning and Closure

Following the receipt of regulatory approval and the licence to decommission and close the DGR facility, underground facilities are expected to be removed first, in parallel with those surface facilities not required to support the remaining underground decommissioning and closure activities.

Decommissioning of underground facilities involves the removal of operational systems and furnishings, the interim installation of temporary services and furnishings, and the repair and preparation of exposed rock surfaces for sealing. As currently envisaged, the decommissioning and closure activities will be carried out in several stages and will include activities related to removal of material handling systems, the sealing of underground horizontal openings, and the sealing of shafts and boreholes.

As the repository saturates, the sealing materials will swell, forming dense, low-permeability seals throughout the underground repository and in the shafts. These seals will isolate and contain the used fuel located in the placement rooms. The following sections describe the decommissioning and closure of various underground horizontal openings and the three shafts. Descriptions of the sealing materials to be used for the closure of the underground repository are presented in Section 4.3.2.

4.12.1 Sealing of Underground Horizontal Openings

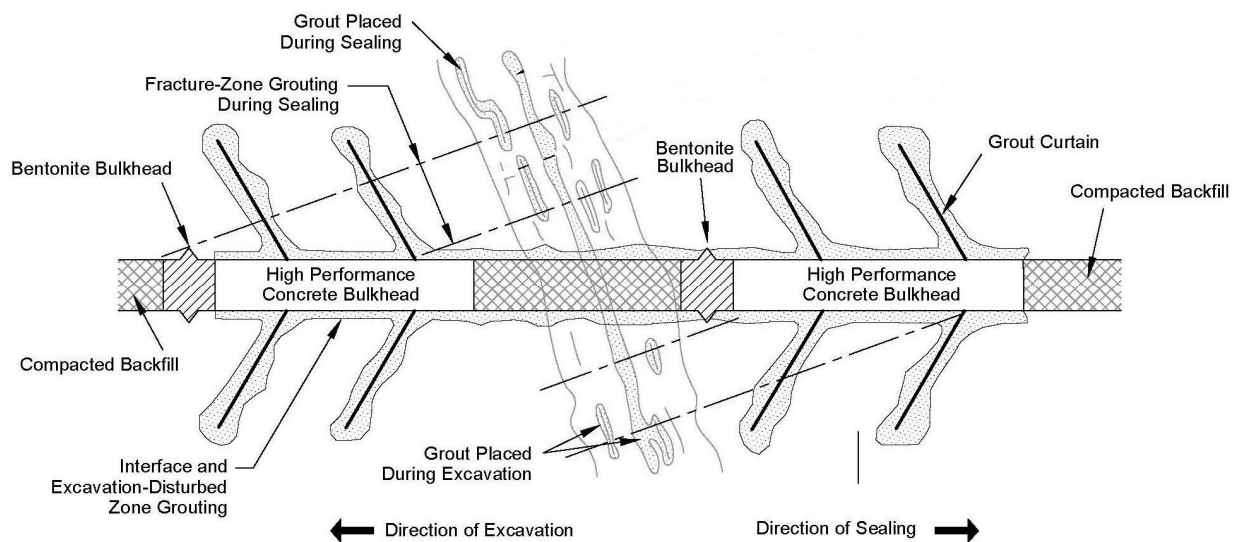
The sealing of underground horizontal openings consists of closing off access tunnels and ancillary facilities. Such activities would commence with the removal of instrumentation and sealing of associated boreholes, followed by the preparation of exposed rock surfaces and removing loose rock before backfilling and sealing. The access tunnels would then be backfilled with dense backfill blocks and light backfill, and tunnel bentonite seals with associated concrete

bulkheads would be installed at strategic locations. All sealing materials would be created in the sealing materials compaction plant and concrete batch plant.

The bentonite tunnel seals and associated concrete bulkheads would be located at strategic locations through the network of underground access tunnels. The tunnels seals and bulkheads would be designed similar to room seals and associated concrete bulkhead. The primary function of tunnel seals would be to limit fluid flow along the access tunnels.

4.12.2 Sealing of Hydraulically Active Zones

The most robust sealing arrangements in access tunnels would be required at locations where tunnels intersect hydraulically active regions in the rock. A possible seal arrangement including grouting is shown in Figure 4-24. The seals and bulkheads would be required to withstand rapidly developing hydraulic pressures. The properties of clay-based seals and the concrete are presented in Table 4-2 and Table 4-3.



Note: Figure is not to scale.

Figure 4-24: Illustrative Tunnel Plug in a Hydraulically Active Region

4.12.3 Sealing of Shafts

Sealing of the shafts is the last step in the closure of the underground repository. This activity starts after sealing of underground tunnels and ancillary areas is complete, and when the concrete monolith has been constructed in underground openings around the base of each shaft. At that time, the following activities will take place:

- Removal of shaft services including compressed air lines, water lines, power supply, lighting and communication cables;
- Removal of instruments and sealing of any impacted geological investigation boreholes;
- Removal of furnishings including all of the shaft guides and sets, steel support brackets, brattice and lower crash beam assemblies from bottom to top while backfilling;
- Reaming of the shafts (as required) to remove the concrete linings and any degraded wall rock. It is assumed that approximately 0.5 m of rock will be removed from the shaft walls to expose the sound rock; and
- After each shaft is re-equipped with services and staging, placement of sealing materials in each shaft will be initiated.

The proposed design for a shaft seal system is described in Table 4-6. The final design for the shaft seals will depend on the geological conditions of the site. The approach for the shaft seal design focuses on the use of simple, relatively well understood and durable materials, and use of proven methodologies for placement. The shaft seal system consists primarily of a column of compacted bentonite/sand. Sand and bentonite are durable natural materials. An asphalt or HCB column may be placed above the first bentonite/sand layer to provide a redundant low permeability sealing material against upward or downward fluid flow. Concrete bulkheads could be used to provide structural components to the column and provide additional (early) sealing capability.

Table 4-6: Proposed Sealing System for Shafts

Depth from Surface	Material
0 – 20 m	Low-heat high-performance concrete– concrete cap at surface
20 – 150 m	Shaft backfill - 70/30 bentonite/sand mixture compacted in-situ
150 – 170 m	Low-heat high-performance concrete for concrete bulkhead keyed into rock / overburden to a distance of 0.5 times the original radius of the shaft
170 – 330 m	Shaft backfill - 70/30 bentonite / sand mixture compacted in-situ
330 – 380 m	Asphalt or highly-compacted bentonite seal
380 – 480 m	Shaft backfill - 70/30 bentonite / sand mixture compacted in-situ
480 – 500 m	Concrete monolith – Low-heat high-performance concrete

The shaft sealing system presented in Table 4-6 is based on the assumption that all shafts will intersect low permeability rock over the full depth of the shafts. However it is possible that the DGR shafts will intersect relatively permeable rock near ground surface. If so, then engineered fill material based on rock excavated during shaft sinking or some other suitable material will be used in the upper portion of each shaft. This engineered fill would likely be placed from surface to a depth where low permeability rock is first encountered.

The shaft seal design concept in Table 4-6 has focused on the use of simple, relatively well understood and durable materials, and use of proven methodologies for placement. Concrete, bentonite/sand mixture and asphalt will be the sealing materials used in each shaft. All shaft sealing materials, except asphalt, would be created in the sealing materials compaction plant (Section 4.6.1) or the concrete batch plant (Section 4.6.2). Asphalt material would be imported to the site. Additional information about each major component of the shaft seal system is presented below.

Concrete Monolith: A concrete monolith will be placed at the base of the seal system. The LHHP concrete will provide a stable foundation for the overlying seal materials. The monolith will be constructed in stages beneath each shaft. Each monolith will form a contiguous mass concrete structure with no structural reinforcement within the concrete. All services and utilities will be stripped out of the excavations to be filled by the monolith.

Shaft Backfill: The column of sealing materials in each shaft is largely composed of a compacted bentonite/sand mixture (see Table 4-6 for properties). The mixture will be created in the sealing materials compaction plant and then delivered to shaft as a bulk material. The mixture will be placed in layers and each layer will be compacted to achieve required density. As the compacted bentonite/sand materials saturate with groundwater from the surrounding rock, they will generate swelling pressures, which will aid in the development of a tight seal against the shaft wall and provide a confining pressure to the rock surface.

Asphalt Seal: An asphalt column may be placed above the lowermost bentonite/sand column. Immediately upon placement, the asphalt will create an effective barrier to water flow. Furthermore, the use of another low permeability sealing material provides an additional level of redundancy to the sealing system against upward or downward fluid flow.

Highly Compacted Bentonite Seal: As an alternative to the aforementioned asphalt seal, a seal comprised of HCB blocks would be constructed above the lowermost bentonite/sand column. Once saturated and the swelling is complete, this seal would create an additional level of redundancy to the sealing system against upward or downward fluid flow.

Concrete Bulkhead: The primary function of the LHHP concrete bulkhead will be to provide structural support in the column of sealing materials (see Section 4.3.2 for properties). In the short-term the concrete will act as an additional seal and over the long-term the ability to act as a seal will diminish as concrete degrades. As with the monolith, concrete for the bulkhead will be placed in mass and with no reinforcing steel, and using measures to control heat build-up. Contact/seal grouting will be applied around the bulkheads to minimize the potential impacts of shrinkage at the interface with the host rock formation. Concrete will be poured directly onto the bentonite/sand columns located below each bulkhead.

Concrete Cap: A surficial concrete cap will be installed on each shaft to minimize risk of human intrusion into the underground repository via shafts. The cap will be constructed using LHHP concrete (see Section 4.3.2 for properties). Air entrainment within the concrete is required to minimize adverse effects of freeze/thaw action on the concrete cap.

4.12.4 Sealing of Boreholes

Siting, construction, and operation of a repository would require the drilling of numerous exploration and monitoring boreholes, including those drilled from the ground surface in the vicinity of the repository and boreholes drilled from within the repository into the adjacent rock. As part of the final closure of the repository, all boreholes would be sealed to ensure that there are no direct paths for water movement between the repository and the surface environment. The borehole seals would be composite seals made of bentonite, sand and concrete. The borehole seal design would be adjusted, as needed, to compensate for hydraulically active regions in the adjacent rock.

The purpose of removing monitoring wells and then sealing the geological borehole is to inhibit groundwater movement and contaminant transport. A combination of cement-based materials and clay-based materials with low permeability and a high swelling potential will be installed as required to prevent the boreholes from becoming preferential transport pathways.

4.12.5 End State

A minimized administration area will be maintained during the end of decommissioning to support the post-decommissioning monitoring systems. If at that time it is felt that permanent facilities are no longer required, the monitoring systems could be supported by small enclosures for the electrical equipment, and all other remaining facilities could be removed and the site essentially fully returned to greenfield conditions.

The facility's environmental monitoring carried out during the operational and extended monitoring periods as well as throughout the decommissioning stage may be continued following decommissioning and closure. The scope and duration of such tasks will be decided at the appropriate time by both regulatory entities and society at large.

4.13 References for Chapter 4

Baumgartner, P. 2006. Generic Thermal-Mechanical-Hydraulic (THM) Data for Sealing Materials – Volume 1: Soil-water Relationships. Ontario Power Generation Report 06819-REP-01300-10122-R00. Toronto, Canada.

Garamszeghey, M. 2016. Nuclear Fuel Waste Projections in Canada – 2016 Update. Nuclear Waste Management Organization Report NWMO-TR-2016-09. Toronto, Canada.

IAEA. 1970. Treaty on the Non-Proliferation of Nuclear Weapons. International Atomic Energy Agency INFCIRC/140. Vienna, Austria.

IAEA. 1972. Agreement Between the Government of Canada and the International Atomic Energy Agency for the Application of Safeguards in Connection with the Treaty on the

Non-Proliferation of Nuclear Weapons. International Atomic Energy Agency INFCIRC/164. Vienna, Austria.

IAEA. 2000. Protocol Additional to the Agreement between Canada and IAEA for the Application of Safeguards in Connection with the Treaty on the Non-Proliferation of Nuclear Weapons. International Atomic Energy Agency INFCIRC/164/Add. 1. Vienna, Austria.

Kwong, G. 2011. Status of Corrosion Studies for Copper Used Fuel Containers under Low Salinity Conditions. Nuclear Waste Management Organization Report NWMO TR-2011-14. Toronto, Canada.

Noronha, J. 2016. Deep Geological Repository Conceptual Design Report Crystalline / Sedimentary Rock Environment. Nuclear Waste Management Organization Report APM-REP-00440-0015 R001. Toronto, Canada.

5. LONG-TERM EVOLUTION OF THE MULTIPLE-BARRIER SYSTEM

The repository will be sited, designed and constructed in order to provide long-term containment and isolation of the used fuel. It will do so through a multiple-barrier approach, with a combination of natural and engineered barriers. Table 5-1 summarizes the main safety attributes of the repository.

Some of these attributes are important to safety in the preclosure period during construction and operation. This report is focused on the postclosure period, and therefore on those safety attributes relevant in the long term (i.e., one million years).

Chapters 2, 3, and 4 of this report describe the site, the used fuel waste form and the repository design. Table 5-2 presents a summary of the key repository components.

This chapter describes how these components of the repository are expected to evolve and interact with their environment during the postclosure period. This includes both their expected behavior as well as a range of unlikely but plausible circumstances.

Additional features, events and processes (FEPs) were assessed and excluded for the reasons outlined in the FEPs report (Garisto 2018), and therefore are not included in the repository evolution described in this chapter.

Table 5-1: Main Safety Attributes

1. The geologic setting provides isolation and containment.
1.1. The repository depth isolates the waste and repository components from surface changes created by human activities or natural events.
1.2. The repository is enclosed by stable, competent and low permeability rock.
1.3. The hydrogeologic setting that encloses the repository restricts groundwater and radionuclide movement.
1.4. The mineralogy of the host rock, and the composition of the ground/porewater, are compatible with the engineered barriers.
1.5. The host rock mineralogy and the composition of the ground/porewater are favourable for mitigating radionuclide movement.
1.6. Natural resource potential is low within the repository geologic setting.
1.7. Seismic hazard is low.
1.8. The host rock is predictable and amenable to characterization.
2. The site geology has long-term stability.
2.1. The hydrogeologic conditions at repository depth are stable and resilient to internal and external perturbations, including glaciation.
2.2. The host rock is capable of withstanding thermal and mechanical stresses induced by internal and external perturbations, including glaciation.
2.3. The repository conditions including chemistry and physical condition important for safety are not influenced by internal and external perturbations, including glaciation.
2.4. Rate of erosion is low.
2.5. Repository safety is not influenced by strong ground motions associated with rare earthquakes.
3. The site supports robust construction and operation.
3.1. Repository host rock conditions allow safe construction and operation.
3.2. Safe transportation route to site.
3.3. Frequency of severe natural events at site during construction and operation is low.
3.4. Robust facility design for safe construction and operation.
3.5. The site is not located in a sensitive ecological environment.
4. The used fuel wasteform is a barrier which contributes to the containment of radionuclides.
4.1. Most radionuclides are immobile within the uranium oxide grains of the used CANDU fuel.
4.2. The used CANDU fuel grains are mechanically durable and not materially impacted by radiation damage or helium gas buildup.
4.3. The used fuel has low solubility under conditions of a failed container with contact with ground/porewater.

4.4. The Zircaloy cladding provides a barrier to contact between ground/porewater and used fuel in a failed container.

4.5. The Zircaloy cladding corrodes slowly under conditions of a failed container in contact with ground/porewater.

5. Container and sealing systems are barriers which contribute to the isolation and containment of radionuclides.

5.1. The container is designed for the underground conditions at timeframes relevant to repository safety.

5.2. Inspection methods would ensure the container is built consistent with design specifications.

5.3. The in-room buffer system holds and protects the containers.

5.4. Engineered seals isolate the placement rooms from the access tunnels.

5.5. Shaft backfill and seals isolate the repository from the surface.

6. Repository construction, operation and closure supports the long-term repository performance objective.

6.1. Repository layout and spacing are designed for long-term structural stability.

6.2. Repository design and construction methods minimize the excavation damaged zone.

6.3. Materials used in repository construction and operation will not compromise long-term performance.

6.4. Institutional controls and monitoring will verify performance.

7. The repository is robust to accidents and unexpected events.

7.1. Credible accident during operations would have low effects on public and environment.

7.2. Postclosure analyses show low effect from normal or expected scenarios, with large safety margin to regulatory criteria.

7.3. Postclosure analyses show risk from disruptive scenarios to be acceptable.

Table 5-2: General Parameters of Key Repository Features

PROPERTY	REFERENCE VALUE
Used Fuel	
Waste form	Used CANDU fuel bundles
Bundle	37-element standard bundle
Initial mass U	19.25 kg/bundle
Initial mass Zircaloy	2.2 kg/bundle
Burnup (nominal value)	220 MWh/kgU
Power rating (nominal value)	455 kW/bundle
Minimum fuel age at placement	30 years (out of reactor)
Used Fuel Container	
Design	Steel load-bearing vessel coated with high purity copper, fuel bundles held in steel sleeves
Coating material	High-purity copper applied by a combination of electroplating and cold spray
Container material	A106 Grade C cylinder body welded to hemispherical heads fabricated from A516 grade 70 carbon steel
Container fill gas	Ambient air installed at atmospheric pressure
Container capacity	48 bundles
Container dimensions	0.564 m outer diameter x 2.514 m long
Coating thickness	3 mm
Container mass	2815 kg loaded
Thermal output	170 W based on 30 year old, 220 MWh/kgU used fuel
Temperature (outer surface)	Up to 100°C
Buffer/Backfill	
Buffer design	Container is placed between two 1.0 x 0.7 x 2.9 m Highly Compacted Bentonite buffer blocks. The remainder of the placement tunnel is backfilled with 100% bentonite gap fill
Buffer material	100% bentonite clay, MX-80 or equivalent
Buffer density	1,700 kg/m ³ dry density
Gap fill density	1,410 kg/m ³ dry density
Buffer temperature	<100°C
Backfill design	Backfill is used to fill access drifts and perimeter drifts. Primarily a dense backfill material, with 50:50 bentonite:sand gap fill
Concrete	Low-heat, high-performance concrete

Postclosure Safety Assessment of a Used Fuel Repository in Sedimentary Rock

Document Number: NWMO-TR-2018-08

Revision: 000

Class: Public

Page: 193

PROPERTY	REFERENCE VALUE
Placement Rooms	Horizontal rooms, buffer boxes stacked in two rows Rooms aligned taking account of principal stresses Rooms sealed with end plugs from access tunnels
Repository	
Depth	500 m (nominal)
Footprint	~5 km ²
Total number of bundles	5.224 million
Total number containers	108,833
Operation phase	40 years
Extended monitoring phase	Nominally 70 years (following placement of all containers)
Geosphere at repository depth	
Predominant rock type	Sedimentary
Rock structure at depth	Limestone / Shale
Geothermal gradient	14°C/km
Temperature	~17°C
Rock Mass hydraulic conductivity	2×10 ⁻¹⁴ m/s horizontally and 2×10 ⁻¹⁵ m/s vertically at repository horizon
Rock mass porosity fraction	0.015
Porewater Total Dissolved Solids	275 g/L
Surface/Biosphere	
Land surface temperature	+10°C annual average (present)
Air surface temperature	+10°C annual average (present)
Ecosystem	Temperate deciduous (present)

5.1 Long-Term Evolution of the Geosphere

Within a Canadian sedimentary rock environment, natural processes that could potentially affect the geosphere at repository level over one million years are primarily seismicity and glaciation.

Volcanism is not present on the margin of Southern Ontario and neither is it likely to occur on relevant timescales. This and other potential Features, Events and Processes (FEPs) were assessed and excluded, based on the rationale provided in the FEPs report (Garisto 2018), and therefore are not a part of the expected evolution described in this section.

The influence and likelihood of seismicity and glaciation are described in the following sections, in support of the geologic site attributes listed below (see also Section 1.6.3.1):

- The repository depth isolates the waste and components from surface disturbances, as well as from changes induced by human activities and natural events; and
- The site geology provides long-term stability to the repository.

5.1.1 Seismicity

Seismicity within southwestern Ontario is described in Section 2.2.4.3. A probability seismic hazard analysis was performed to estimate bedrock ground motions that are expected for probabilities of up to 10^{-6} (1/1,000,000) per annum (p.a) (AMEC Geomatrix 2011). The peak ground accelerations site obtained from the seismic hazard analysis are summarized in Table 5-1. The table also presents the results of a 4×10^{-3} probability (1/2500 p.a.) event determined from this study as defined in 2010 National Building Code of Canada.

Table 5-3: Summary of Seismic Hazard Analysis Result (AMEC Geomatrix 2011)

Event (per annum)	Peak Ground Acceleration (%g)
1/1000	1.7
1/2500 (NBCC 2010)	2.7
1/100,000	18.7
1/1,000,000	60.6

5.1.2 Glaciation

The last million years of Earth's history has been marked by periods of glaciation (Peltier 2002, 2006). Ice coverage was marked by many cycles of glacial ice sheet advance and retreat, separated by ice-free periods of warmer climate (interglacials), lasting from thousands to hundreds of thousands of years. Nine glacial cycles occurred over the past million years. During the last glaciation, starting approximately 120,000 years before present, over 97% of Canada was covered by ice. The final retreat of the ice sheet occurred between 9000 and 6500 years ago. Numerical realization of this glaciation, as well as discussion of processes that

cause glaciations, can be found in Peltier (2002, 2003, 2006, 2011) and Stuhne and Peltier (2015, 2016).

Conditions suitable for the reglaciation of the Canadian land mass will likely occur ~60,000 years from present, and again ~125,000 years from present (Stuhne and Peltier 2015). However, if at that time the concentration of carbon dioxide and other greenhouse gases in the atmosphere are similar to present levels, it is unlikely that a renewed episode of glaciation would occur. As the ability to predict the atmospheric CO₂ level so far into the future is limited, the possibility of a renewed glacial event cannot be discounted and, therefore, glacial processes must be taken into account when developing the safety case for a used fuel repository in a Canadian Shield environment.

The characteristics of the glaciation process that are relevant to the understanding of repository performance include:

- Groundwater system stability, including deep groundwater chemical conditions, which has the potential to impact rates of mass transport at repository depth;
- Geomechanical stability of the repository system and geosphere, as impacted by the increased ground stresses due to the ice-thickness;
- Erosion, related to the movement of the ice sheet and meltwater across the land surface; and
- Permafrost formation, which will affect groundwater movement, and potentially the repository if it extends to that depth.

The phenomena associated with glaciation are described in detail in Chapter 2 in the context of this site, but are summarized below in four broad categories: glacial loading, glacial erosion, permafrost formation and groundwater system stability.

5.1.2.1 Glacial Loading

As noted in Chapter 2, climate modelling of the late Quaternary indicates that the last glacial episode had a duration of approximately 120,000 years and involved a prolonged glacial advance and retreat. The model predicts ice thicknesses were up to 3 km over northern Canada, and approaching 2 km in southern Ontario (Stuhne and Peltier 2015, 2016). These predictions of ice-thickness are constrained by observations of relative sea-level and isostatic uplift.

The weight of the thick ice sheet acts to depress the Earth's crust over a large area. Stuhne and Peltier (2015) predicted that the maximum crustal depression from the equilibrium level occurred at the Last Glacial Maximum and reached approximately 500 m. Removal of the ice load by melting leads to slow crustal rebound, a process that continues today in the Canadian Shield from the last glaciation.

The University of Toronto Glacial Systems Model (UofT GSM), which is a model of continental-scale glaciation events, was used by Stuhne and Peltier (2015, 2016) to develop a description of past glaciation of the Canadian landmass. A time series of ice sheet thickness for the past 120,000 years was developed, as shown in Figure 5-1 (as SP15). The ice thickness time series from previous model results, representing two different glacial potential basal conditions, are also shown in the plot for comparison (nn9921 and nn9930). Ensemble results for sensitivity analyses for SP15 are also shown (Stuhne and Peltier 2016), which give an estimate of the range in variability of the ice thickness and permafrost depths as a result of

model parameter sensitivity. In particular, the variability arising from the GSM model parameter sensitivity result in ice-thickness variability at the Last Glacial Maximum of approximately 50 m for the SP15 simulation.

5.1.2.2 Permafrost Formation

Future glacial conditions at the hypothetical repository site would be accompanied by an extended period with widespread formation of permafrost. The range of permafrost thickness time series applicable to this site is shown in Figure 5-1.

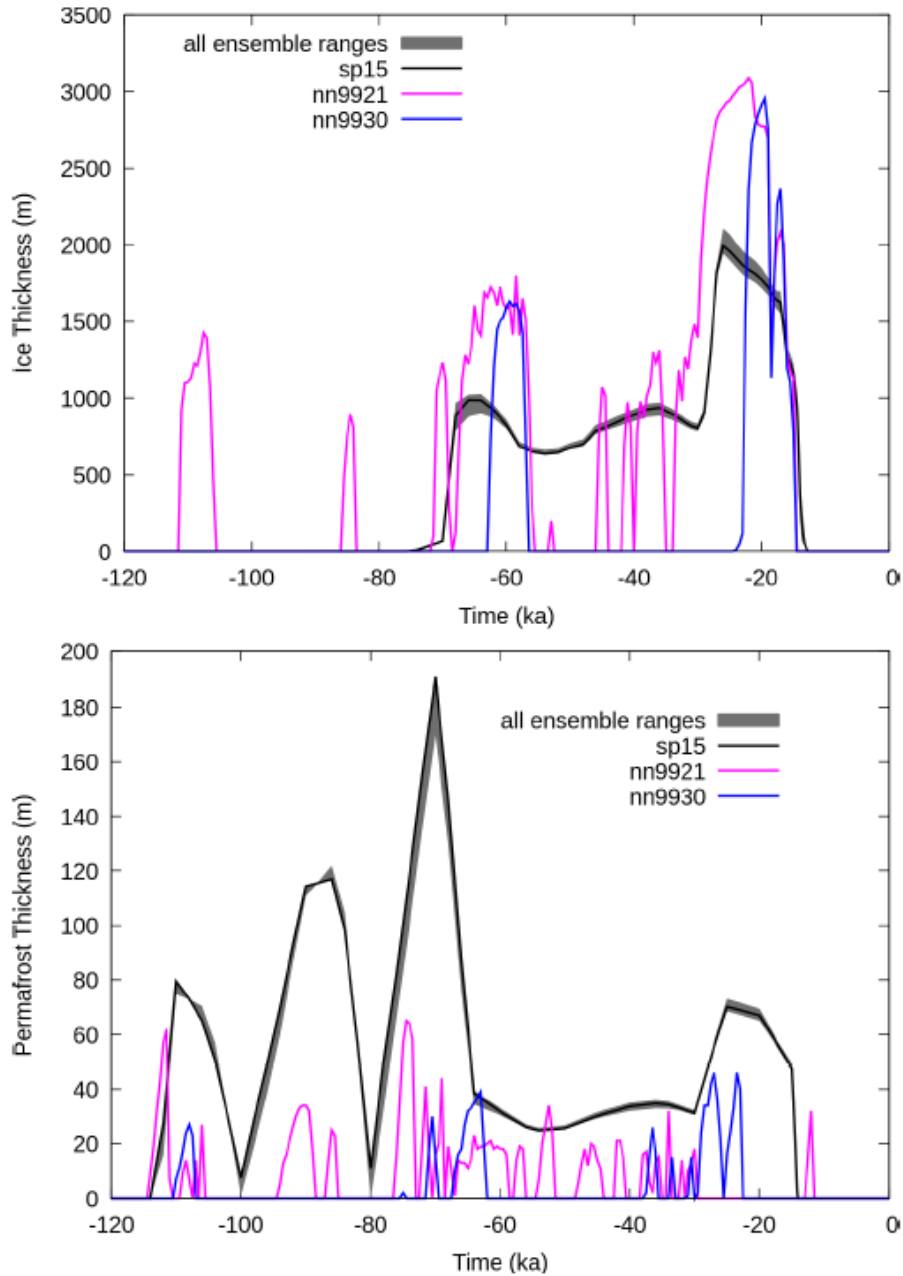
The repository itself at 500 m would be below the depth of permafrost, so not directly affected. However the presence of permafrost in the geosphere will act to reduce the hydraulic conductivity, thereby limiting recharge from the surface during glaciation. The effects of this permafrost is considered in the next section as part of the analysis of groundwater system evolution.

In regions of permafrost, taliks are regions of perennially unfrozen ground that exist within otherwise continuous permafrost environments. The formation of taliks is dependent on site-specific conditions, and for example may exist under large water bodies. At the repository site, the heat load from the used fuel is expected to have sufficiently dissipated by the time glaciation occurs, so this heat load is not expected to significantly influence the permafrost at the site.

5.1.2.3 Glacial Erosion

The predominant geosphere process that will result in erosion over the next million years is glaciation. Glacial meltwater can erode sediment and rock by abrasion, quarrying, and mechanical erosion. Regardless of the mechanism, the rate of surface erosion can be limited by the ability of the meltwater to remove debris (e.g., due either to an insufficient hydraulic head gradient to carry debris-laden subglacial water out of the basin, or the lack of adequate subglacial pathways for water). In terms of erosion at a local level, the basal sliding velocity is the primary factor controlling the rate of erosion. However, rapid basal sliding velocity does not necessarily correlate with rapid erosion at the base of the glacier, as the glacier may be decoupled from the bedrock surface by a thin layer of basal melt water, or by a layer of deformable sediment.

Hallet (2011) conducted a glacial erosion assessment in which several independent types of geological evidence were examined to assess the magnitude of erosion which would likely occur over one glacial cycle at different scales, from regional to local. In total, thirteen estimates (eleven of which are independent of one another) were presented which support the conclusion that erosion would not exceed many tens of metres in southern Ontario over one glacial cycle; no erosion and net deposition of sediments in the region is also possible. For the hypothetical site considered in this study, it is assumed that net erosion is likely on the order of tens of metres over one million years. This assumption is supported by the local erosion estimates reported by Hallet (2011) for the Bruce nuclear site. As part of site characterization activities, an investigation would be conducted of topographic features or other known factors that might tend to localize erosion at a potential site.



Note: Glaciation scenario nn9921 represents cold based glacial conditions, scenario nn9930 represents warm based glacial conditions, and scenario SP15 represents best estimate conditions (variability in SP15 ensemble shown as shaded area).

Figure 5-1: Three Ice Sheet and Permafrost Thickness Time Series

5.1.2.4 Groundwater System Evolution

Glaciation, as the strongest single external perturbation to the geosphere, will impact the long-term evolution and stability of groundwater systems at depth, including:

- Depth of penetration of glacial meltwater,
- Changes to rates of mass transport, and
- Redox stability.

The impact of glaciation on the deep groundwater system at the hypothetical sedimentary rock site was considered in this study. Paleohydrogeological modelling was completed for the Laurentide glacial episode (120,000 to 10,000 years before present) and is presented in detail in Chapter 2 (Section 2.3.4.3). The key insights from the illustrative modelling are summarized below.

Eleven simulations were performed to investigate the role of varying paleoclimate boundary conditions. Details of the paleoclimate modelling scenario can be found in Section 2.3.5.3. The performance measure used to compare these simulations is the movement of a conservative unit tracer applied with a Cauchy boundary condition at the top surface of the model domain. This tracer represents the predicted migration of recharge waters into the groundwater system over the course of a 120,000 year simulation. The depth of the tracer is determined by the 5% isochlor, which represents a pore fluid containing 5% recharge water. The 5% isochlor provides an indication of recharge water migration into the subsurface, which can be used to compare alternative paleohydrogeologic scenarios. The simulations do not consider reactive transport; therefore, although the 5% isochlor provides an indication of the percentage of meltwater, it does not take into account the consumption of oxygen within this meltwater as it penetrates.

The depth of penetration of the tracer is shown in Figure 5-2 for the best estimate glacial systems model boundary conditions (Stuhne and Peltier 2015). The tracer concentrations in Figure 5-2 are shown after 120,000 year simulation time. The low hydraulic conductivity of the Ordovician formations limits the depth of penetration of surficial recharge during glaciation.

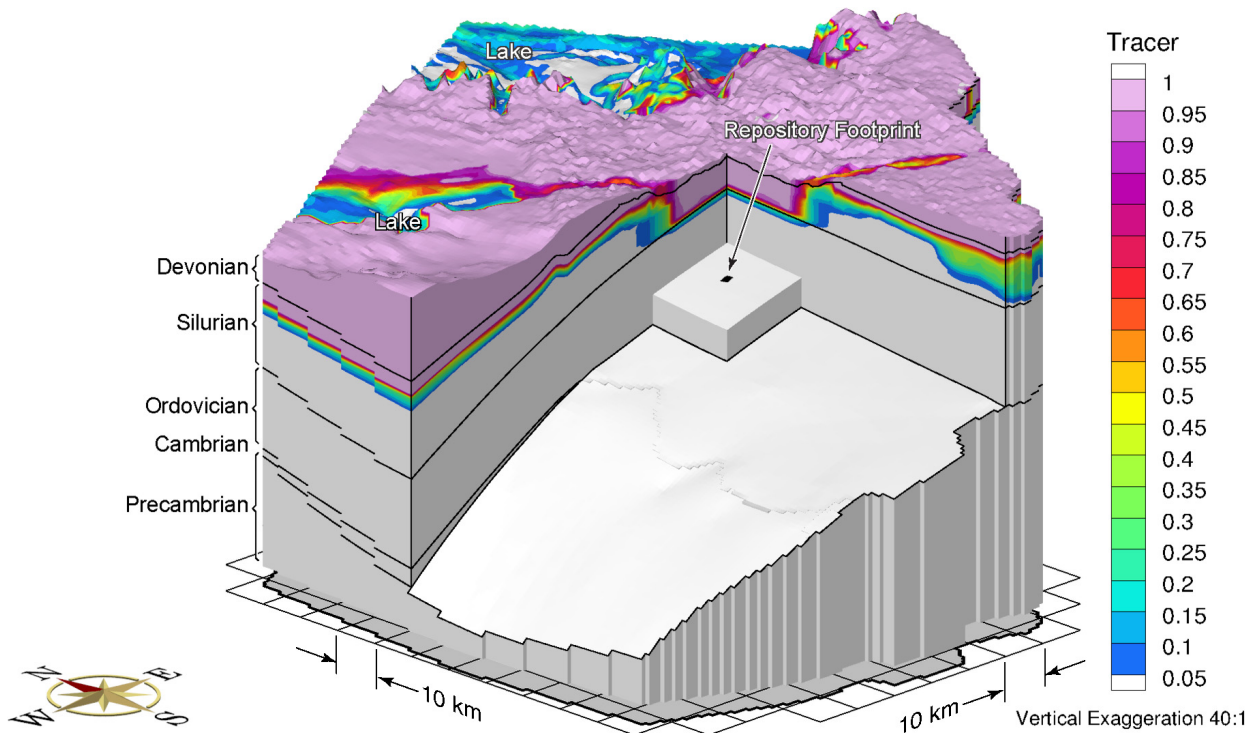


Figure 5-2: Block View Showing the Depth of Penetration of a Tracer after 120,000 Years for the gsm2015 Paleoclimate Boundary Conditions (fr-base-paleo-gsm2015)

5.1.3 Confidence in Geosphere Evolution

The geosciences program for a candidate site will be designed to support the safety case. A site model and geosynthesis will be developed during a phased site characterization work program. The work program will allow for the iterative development, testing and refinement of a site-specific model that will contribute to managing uncertainties in scientific understanding, data and models.

Seismicity: The host rock would be demonstrably resilient to earthquakes based on its history. The actual repository room location would be chosen to avoid fracture zones or faults where future fracture movement is more likely.

Glaciation: Peltier (2011) provides a review of what is known concerning the geologically recent history of long-term climate change, as background to the detailed analysis of the conditions that would be expected to develop at and below the surface of the Earth if the Canadian land mass were to be reglaciated. Results from an appropriately-calibrated model of the most recent glaciation events that occurred in the Late Quaternary period are used as a proxy for a future reglaciation event (Stuhne and Peltier 2015, 2016). The method, additionally, has been validated using recreations of existing ice sheets in Greenland and Antarctica.

Groundwater System Evolution: Evidence gathered during site characterisation activities would minimize uncertainties through a synthesis of geologic, structural geologic, hydrogeochemical and physical hydrogeologic data to assess long-term groundwater system evolution and

stability. Such efforts would be aided through the application of numerical methods that provide a systematic framework to integrate independent data sets (such as those described in Chapter 2). Such techniques, as supported by field data, can provide insight (i.e., time rates of change and magnitude) into groundwater system response to external events and can constrain uncertainty with regard to geosphere performance.

Uncertainties in the future evolution of groundwater compositions are coupled to uncertainties about the movement of groundwater. Similarly, impacts of glaciation at repository depth will be dependent on site-specific conditions. The age of, and potential influence of glaciation on, groundwaters and porewaters cannot be determined directly; instead, they are inferred from paleohydrogeological evidence, such as fluid inclusion data and stable water isotope ratios. Together with numerical tools, such as reactive transport modelling, this information can be used to illustrate the potential evolution of geochemical conditions at repository depths.

5.2 Long-Term Evolution of the Repository Environment

Although the construction, operation and closure will be conducted so as to avoid compromising the long-term safety of the repository, the repository will be a change in the geosphere setting. Potential disturbances to the geosphere include those induced by excavation itself (e.g. damage to surrounding rock, introduction of blast residue) and those due to placement of the waste and engineered systems (e.g., changes in temperature, saturation, near-field chemistry, gas generation). The relevant changes with respect to long-term safety are described below. Additional Features, Events and Processes (FEPs) were assessed and excluded for the reasons outlined in the FEPs report (Garisto 2018) and thus are not part of the expected evolution described in this section.

5.2.1 Temperature

Among the first changes to occur in a repository after container placement is an increase in temperature of the sealing materials around the containers. Figure 5-3 shows the thermal profiles for select locations within the engineered barrier system of a placement room: the exterior surface of a container, the midpoint between upper-row containers, and the interface between the buffer and the host rock above an upper-row container (adapted from Guo 2018).

Key points to note in Figure 5-3 are:

- The temperature of sealing materials adjacent to the surface of the container increases rapidly at first, within days to weeks after placement.
- The maximum temperature of the buffer occurs after 47 years and remains below the targeted maximum of 100°C (note that the calculated peak of 92°C in this simulation is sensitive to the specific conditions of a site and optimizations to the repository layout).
- Within about one hundred years, reflecting in part the decay of the heat source, there is clear reduction in peak temperatures.
- After several thousand years, the thermal evolution is marked by a slow, steady cooling. Temperatures return to near-ambient conditions within 100,000 years.

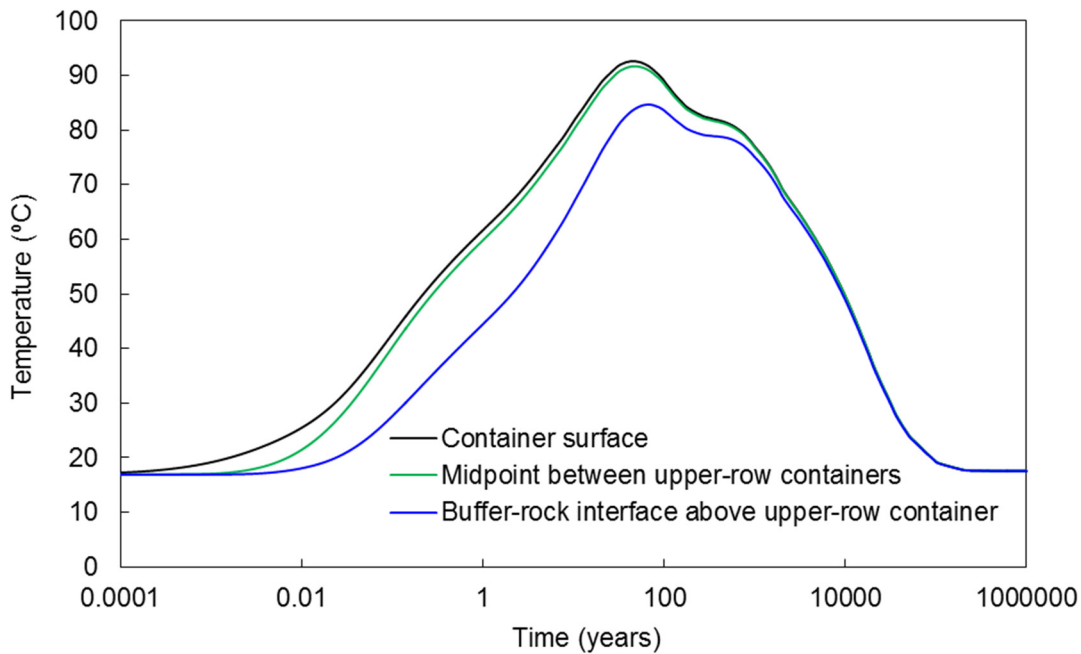


Figure 5-3: Illustrative Example of the Range of Temperature Variation over Time in a Placement Room

5.2.2 Repository Saturation

During the construction and operational phases, groundwater entering the excavations will be removed by pumping. At a depth of 500 m below the surface, the hydrostatic pressure within a water-saturated rock mass is about 6 MPa. A sharply defined hydraulic gradient would exist between the geosphere at repository depth and the excavated openings (rooms, cross-cuts and drifts), which would be at atmospheric pressure. This difference would tend to draw groundwater through the rock into the open spaces of the repository. The movement of fluids would occur slowly through the low-permeability rock, but faster through any transmissive fractures. Groundwater seeping into the repository from the surrounding rock will be pumped away to maintain dry conditions within excavated openings, and may also result in drawdown of the groundwater level above the repository. Evaporation would tend to keep the rock surfaces in the excavated openings dry, and may induce partial desaturation of the rock immediately adjacent to the openings (i.e., within the excavation damaged zone and host rock near the repository).

Any dewatering during construction and operation of the repository will be of relatively short duration and will result in groundwater movement toward the repository until pumping activities cease following repository closure. In the postclosure phase, water will move towards the repository and the near-field will resaturate.

The process of saturation may take a long time, as ingress of water will be restricted because of low host-rock permeabilities and the use of grouting and seals. In saturated rock, increases in

near-field porewater pressures as a result of repository warming could also change the flow field and affect resaturation time.

The time elapsed before full saturation will vary in different areas of the repository, affected by the local temperature, chemistry, stress states (including buffer swelling) and groundwater flow rates. The bentonite buffer and backfill are initially partially saturated. They will uptake water during repository saturation, resulting in swelling of these materials. Swelling in response to the addition of water is a natural property of bentonite, resulting in the development of its self-sealing capabilities (low hydraulic conductivity and high swelling pressure). At the same time, heat from the container would cause the nearby bentonite to dry out, and condensation of the water vapour would occur in cooler portions of the sealing materials.

Overall, this “pre-saturated period” covers the time period from when the containers are first placed in a repository until their exterior surface is in contact with saturated sealing materials. In low-permeability sedimentary rock, this pre-saturated period is estimated to last approximately 1000 years (see Chapter 8).

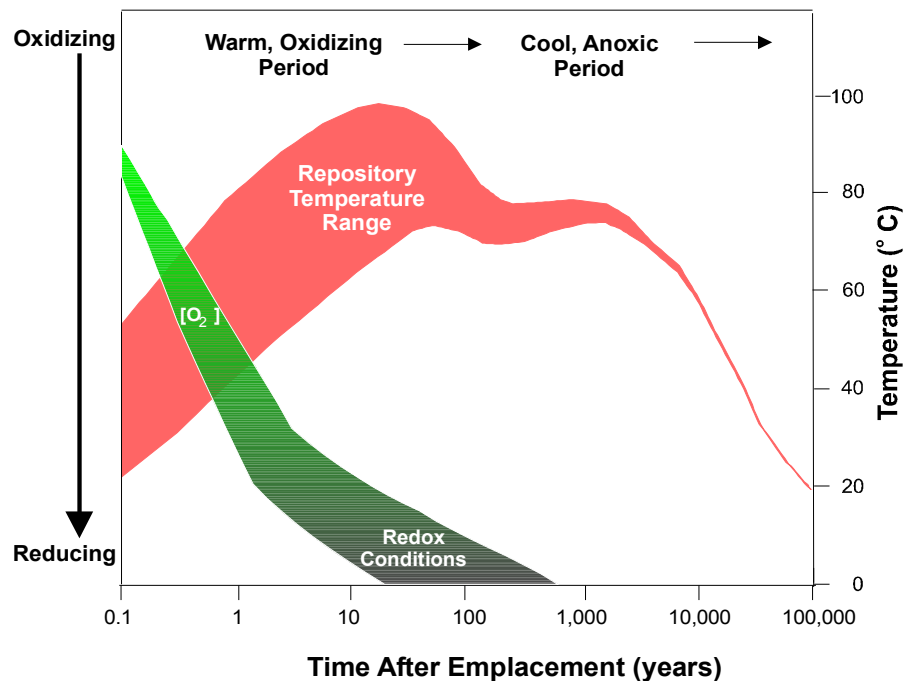
5.2.3 Near-Field Chemistry

During repository excavation and operations, oxidizing conditions would develop in the porewaters of the adjacent rock due to exposure to the air in the repository.

However, after the rooms are closed and sealed, the redox conditions within the near-field will evolve back to an anaerobic state. Oxygen is consumed by a number of reactions, including reactions with residual iron in the rooms (e.g., rock bolts) and with copper on the containers (i.e., some combination of Reaction (5-1) and Reaction (5-2)), as well as by reactions with microbes and with redox-sensitive materials throughout the buffer.



Figure 5-4 illustrates the evolution of environmental conditions over time, from warm and oxidizing initially from construction, to cool and anoxic eventually once the oxygen is consumed and the fuel has cooled.



Note: Figure from McMurry et al. (2003).

Figure 5-4: Evolution of the Repository Environment from an Initial Warm, Oxidizing Period to a Prolonged Cool, Anoxic Phase

Most of the repository-related changes in groundwater chemistry would occur at or near the interface between the geosphere and the sealing materials. The diffusion of porewater components, or the mixing of fluids at the repository-geosphere interface, may result in the precipitation of secondary mineral phases at the interface or in nearby fractures in the geosphere. A broader effect would be due to heat from the repository, which would raise the temperature of water in the geosphere. This could result in a slightly greater dissolution rate for some minerals. Later, as the waters cool, the precipitation of secondary phases, such as amorphous silica and calcite, would occur. The extent and significance of the precipitation would depend on site-specific characteristics, such as the distribution and dimensions of the fractures.

In the long term, the geosphere, as a whole, would act as a strong buffer in response to chemical and thermal perturbations from a repository. As the pore fluids in the repository evolve to a composition more similar to that of the surrounding groundwater, and as temperatures in the geosphere gradually return to ambient levels, the chemical conditions in the geosphere would be diminishingly affected by the presence of a repository.

5.2.4 Steel Corrosion and Gas Generation

Small amounts of steel (primarily carbon steel) will be used in construction of the underground facilities. A larger amount is present in the used fuel containers, but this is only exposed in the

case of failed containers (see Section 5.4.4.3). This steel will corrode, and relevant effects of steel corrosion are summarized below.

- Dissolved ferrous species, produced as a result of corrosion reactions, can interact with bentonite and convert swelling smectite clays to non-swelling illitic forms, resulting in a partial loss of swelling capacity (Lanson et al. 2015; Osacký et al. 2013; Wersin et al. 2007) near the steel components.
- Anaerobic corrosion will result in the generation of hydrogen (Senior et al. 2017); although it is unlikely that the modest amounts of steel proposed for construction will produce a gaseous H₂ phase in the repository.
- Hydrogen may impact the viability of some microbial species, favouring anaerobic species that can use hydrogen as an energy source.

For the placement rooms, only small amounts of steel are expected to be present, generally as rock bolts. This volume of steel is sufficiently small that the quantity of hydrogen gas produced does not have the potential to alter the repository characteristics. However, because of the use of carbon steel as a container material, the impact of hydrogen generation on the repository due to postulated failed containers is considered in Chapter 8.

The corrosion behaviour of the steel components will change with time as the environment in the repository evolves (Necib et al. 2017). From a corrosion perspective, the most important environmental factors are the temperature, the redox conditions, the degree of saturation of the repository material, and the composition of the porewater in contact with the steel components. Saturation of the repository could take a very long time so this transient has led to the conceptual definition of four phases in the evolution of the environment, as described below (see King 2013).

Phase 1

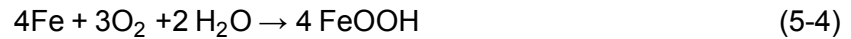
Phase 1 represents an early aerobic period prior to the onset of aqueous corrosion. Immediately following closure of the repository, saturation of the Engineered Barrier System (EBS) has not yet occurred, so no liquid water is available for corrosion, and the EBS near the UFCs remains unsaturated. Oxygen is initially present in the unsaturated pore space when the EBS is emplaced. If relative humidity is also low, corrosion will be limited to slow air oxidation. This unsaturated aerobic corrosion is modelled as follows:



Aqueous corrosion is possible above a critical or threshold relative humidity (RH) that is determined by the nature of the surface and the presence of surface contaminants. As RH increases above a lower threshold value, the consumption of carbon steel by Phase 1 corrosion will decrease until an upper RH threshold is reached, upon which Phase 1 corrosion stops (King 2013).

Phase 2

Phase 2 represents an unsaturated aerobic phase, following the condensation of liquid water on the steel surface. During Phase 1, if relative humidity rises above 60-80%, aerobic aqueous corrosion may instead proceed according to the following relationships:



Note that Phase 1 and Phase 2 corrosion overlap as the relative humidity increases from 60% to 80%.

Phase 3

Phase 3 represents an unsaturated anaerobic phase that will occur following the consumption of the oxygen and prior to the full resaturation of the repository; the gaseous phase will be predominantly N₂, H₂ and H₂O vapour. Corrosion during this period is supported by the cathodic reduction of water accompanied by the evolution of hydrogen. Detailed surface analysis indicates that corrosion under unsaturated anaerobic conditions forms magnetite as the predominant corrosion product, as follows:

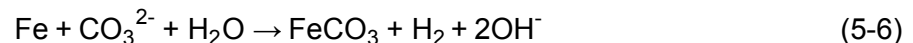


The rate of reaction is affected by relative humidity (RH) where the values are dependent on the cationic content of the buffer system, but may be as low as 0.1 and 0.2, respectively, for highly saline systems. Thus, for RHs as low as 20%, the reaction could proceed at its maximum rate.

Phase 4

Phase 4 represents a long-term saturated anaerobic phase, once the EBS material has become completely saturated by groundwater. As in Phase 3, corrosion during Phase 4 is supported by the cathodic reduction of water accompanied by the evolution of hydrogen. In the presence of compacted bentonite under saturated conditions, in addition to the reaction shown in (5-5), where magnetite (Fe₃O₄) is the corrosion product, carbon steel corrodes with the formation of a carbonate-containing corrosion product. The source of carbonate is calcite and other carbonate minerals assumed to be present in the EBS material. Iron carbonate, or some form of FeCO₃ incorporating cations from the pore solution, will predominate until such time that all carbonate minerals in the clay have been consumed; after which the predominant corrosion reaction is then likely to be the formation of Fe₃O₄ according to the reaction shown in (5-5).

The overall stoichiometry of the corrosion reaction for Phase 4 is:



It is important to note that these four phases do not necessarily occur sequentially. Phases 1 and 2 both occur under aerobic conditions and the degree to which the Phase 1 and Phase 2 corrosion processes are active depends on the relative humidity. The Phase 3 and 4 corrosion processes proceed under anaerobic conditions after Phase 1 and Phase 2. The degree to which the Phase 3 and Phase 4 corrosion processes are active depends on whether or not liquid water is in contact with the steel components or not. As noted above, the Phase 3 process also depends on relative humidity.

The vast majority of H₂ that will be produced in the repository will result from the uniform corrosion of carbon steel during the (unsaturated and saturated) anaerobic phase. Hydrogen can be produced under aerobic conditions due to the reduction of H⁺ in acidic environments in pits, crevices, or in porous corrosion products formed as a result of the hydrolysis of Fe(III)

species (Akiyama et al. 2010; Tsuru et al. 2005). Local reduction of H⁺ may lead to enhanced hydrogen absorption and environmentally assisted cracking (King 2009a), but will not lead to the generation of significant H₂ and is not considered further here.

Hydrogen generated by corrosion can undergo a number of subsequent processes. The H₂ that is evolved could be consumed by microbes (Pedersen 2000) in those parts of the near- and far-fields in which the environment is conducive to microbial activity (namely a water activity greater than 0.96; Stroes-Gascoyne et al. 2006, Stroes-Gascoyne and Hamon 2008). Another fraction of the hydrogen will be absorbed by the carbon steel as atomic H, either from adsorbed H atoms prior to their evolution as H₂, or via the dissociative absorption of gaseous H₂; however, eventually this hydrogen will be released as the steel continues to corrode.

In addition to the evolution of the redox conditions and the degree of saturation, the temperature will also change during these different phases. In general, Phases 1 and 2 will be warmer than Phases 3 and 4, with Phases 3 and 4 encompassing the period of long-term ambient conditions.

The rate of oxidation of carbon steel in dry air (Phase 1) is low at the temperatures of interest (maximum of approximately 120°C) and will result in only a few microns of corrosion. Although the rate of aerobic corrosion in the presence of moisture under unsaturated conditions (Phase 2) is higher, the extent of corrosion is limited by the initial inventory of trapped oxygen in the repository. Therefore, upon the establishment of high humidity Phase 2 conditions, the duration of aerobic corrosion is predicted to be less than 1 year.

Of most interest is the rate of anaerobic corrosion under first unsaturated (Phase 3) and subsequently saturated (Phase 4) conditions. Based on published corrosion studies, these rates are temperature dependent; the corrosion rate decreases with time as the container cools.

A number of other environmental parameters, in addition to the temperature, relative humidity, and redox conditions, also affect the uniform corrosion behaviour, including:

- Porewater chemistry: Under saturated conditions, the steel will be in contact with EBS porewater. At least initially, the composition of the porewater may differ from that of the groundwater. Eventually, however, the porewater will equilibrate with the ground water.
- pH: Calcite minerals in the bentonite may effectively buffer the pH in the range pH 7-8.
- Mass transport: During the aerobic phase, the rate of corrosion may be limited by the rate of transport of O₂ to the steel surface through low-permeability EBS materials.
- Radiation: Gamma radiolysis of water will produce oxidizing and reducing radiolysis products. However, the maximum surface absorbed dose rate for a UFC will be <2.3 Gy/h (Morco et al. 2017), for which there is no significant effect on the corrosion rate (Shoesmith and King 1999). Steel components more distant from the UFC will certainly see no effect of radiation/radiolysis.
- Microbial activity: Microbial activity is suppressed by the low water activity within the compacted bentonite (Stroes-Gascoyne et al. 2006, Stroes-Gascoyne and Hamon 2008). However, because rock bolts and other steel

components will reside outside the UFC engineered barrier system, it is possible that microbial species may accelerate steel corrosion versus a non-microbially active region of the engineered barrier system.

Stress: Applied and residual stresses affect the environmentally assisted cracking behaviour of the steel but have no effect on uniform corrosion.

Mineral impurities: Mineral impurities in the host rock (e.g., pyrite) will have an insignificant effect on the uniform corrosion behaviour of the container.

5.2.5 Excavation-Damaged Zone

The zones of rock immediately surrounding the placement rooms, tunnels, shafts, and other underground openings are disturbed during excavation which, in turn, disturbs the natural geosphere system and could potentially affect the performance of the repository (Fracture Systems 2011). For this conceptual repository, it is assumed that the drill-and-blast-technique will be used for repository development. Careful control of the drill-and-blast design and execution will be used to minimize damage created by the excavation technique.

Based on the coupled thermo-hydro-mechanical (THM) modelling using a discontinuum modelling approach (Itasca 2018), the excavation-damaged zone (EDZ) around placement rooms is not expected to be significant, given that backfill will be placed inside the rooms and will prevent its growth (i.e., spalling failure and opening of fractures). The damage that will develop around the placement rooms is limited to approximately 1.3 m – 1.6 m around the peripheral of the opening.

Due to the confining pressure of the backfill materials, perturbations to the geosphere (e.g., glaciations and earthquakes) are not expected to have any major structural effects on the long-term behaviour of the EDZ and, thus, the integrity of the placement rooms.

5.2.6 Geomechanical Evolution of the Placement Room

The reference geosphere for this case study is assumed to be the argillaceous limestone of the Cobourg Formation, with characteristics similar to that encountered at the Bruce nuclear facility and described in Chapter 2. This section describes the expected evolution of a placement room over time.

The rock mass at the repository depth of 500 m would be good quality as described in detail in Chapter 2 and by Itasca (2015, 2018).

An analysis was undertaken to study the impact of both repository-induced and natural perturbations. The analysis consists of THM modelling of a typical single placement room of the repository using commercially-available codes: FLAC3D, 3DEC and UDEC. To optimize numerical simulations, a one-way coupled approach was performed to identify the worst loading scenarios (Itasca 2015) following by fully coupled analyses (Itasca 2018). A detailed description of the numerical modelling process is presented by Itasca (2015 and 2018). These simulations were used to demonstrate the evolution of a placement room under different types of natural- and repository-induced perturbation scenarios. Data were selected based on the sedimentary geosphere information presented in Chapter 2. Previous knowledge from work within crystalline rock environments was used in parameter selection, when geological data on relevant material

properties and geosphere conditions were unavailable. The following plausible conditions were considered for model simulations of a repository placement room for a timeframe of over 1 Ma:

1. Time-dependent strength degradation;
2. Glaciations;
3. Low-probability seismic ground shaking; and
4. Effects of combinations of loads and perturbations were considered in all cases.

A number of key conservative assumptions regarding geotechnical conditions were introduced in these analyses in order to provide bounding solutions for the various scenarios, including those listed below.

1. Hydrostatic groundwater pressures: The repository is situated at a depth of 500 m within a water saturated rock mass. Hydrostatic (fresh water) groundwater pressures are considered (i.e., 5 MPa).
2. Time-dependent strength degradation / geological stress corrosion: Data from static fatigue tests of Lac du Bonnet granite (with fast strength decay) were adopted for long-term strength degradation of the granite. The long-term rock mass strength was assumed to be 40% of UCS, which is equivalent to that of crack initiation stress. (Subsequent tests with Cobourg Limestone showed that this was conservative (see Section 2.2.4.1).
3. Discontinuity properties: Rock fractures were assumed to be cohesionless with a relatively low friction angle.
4. Repository temperature evolution: The repository layout and design are based on maintaining a used fuel canister outer-surface temperature of less than 100°C. Estimated near- and far-field temperature histories, based on UFC heat fluxes, are merged to yield bounding thermal stresses in the enclosing rock mass.
5. Long-term climate change: Estimates of long-term climate change include prediction of glacial ice-sheet advance and retreat. At the Last Glacial Maximum, which is considered in the analysis, ice-sheet thickness above the repository site is about 2.6 km.
6. Seismic loading: Rare and extreme (i.e., 10^{-6} per annum; 0.5 PGA) seismic ground motions were assumed to occur at times of greatest repository vulnerability (i.e., maximum repository temperature and maximum glacial ice-sheet loading).

Conservative loading combinations were used to create overstressed bounding conditions within the rock mass around placement rooms, an extreme seismic event during peak glacial loading and during peak rock temperature. The former scenario is not credible; however, it does create a bounding overstress condition for the analysis.

5.2.6.1 Impact of Time-Dependent Strength Degradation

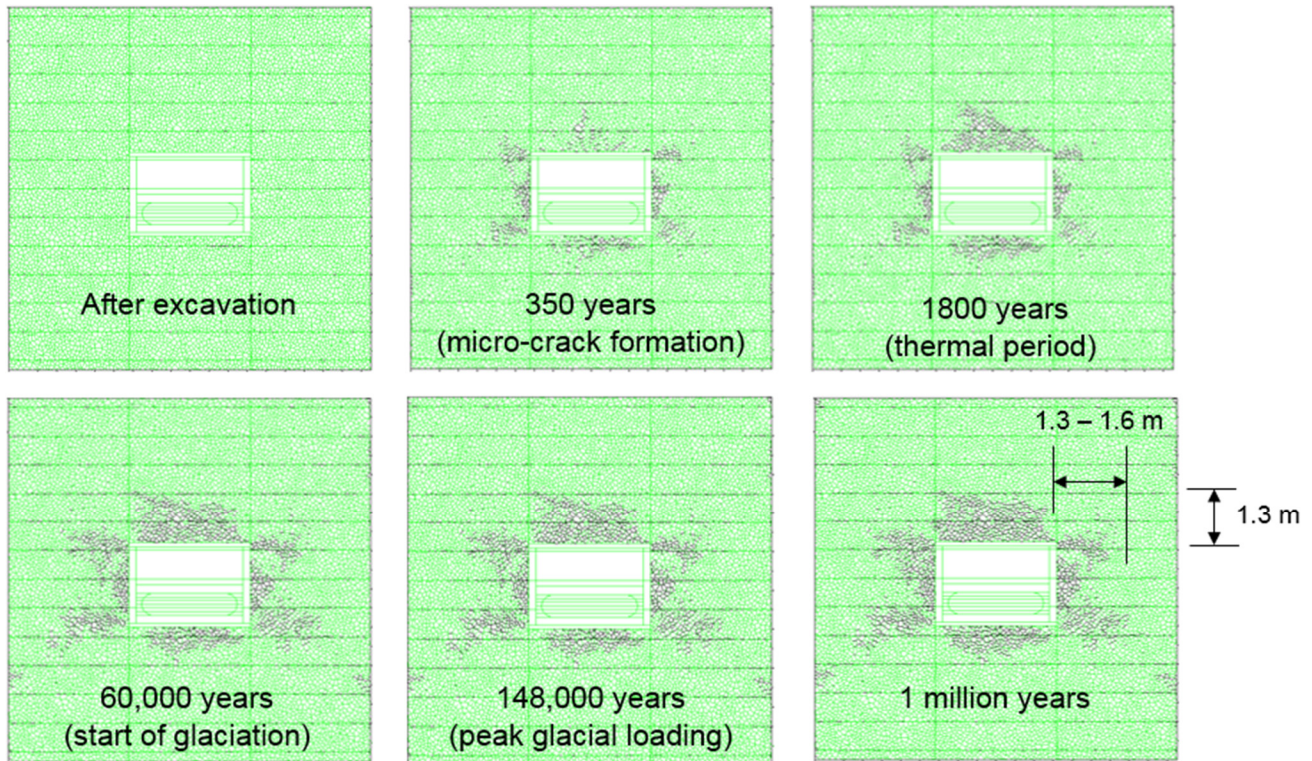
The long-term safety and performance of a used fuel repository will depend in part on the surrounding geosphere and the perturbation effects imposed on it. Fully coupled thermal-hydromechanical (THM) analyses were performed taking into account the influence of pore pressure evolution on damage of the rock mass (Itasca 2018).

Figure 5-5 shows the evolution of the placement room over a one million year time-frame, providing insight into the geomechanical stability of the repository concept. The response of the rock mass around the placement room opening subjected to different perturbation effects are described individually in the following subsections. The study focused primarily on the emplacement panels, which represent the most extensive development in a repository. The details of the THM study are presented in Itasca (2018).

After excavation of the placement room and its subsequent filling with UFCs and backfill materials, damage around the room is minimal. The first two panels of Figure 5-5 shows the early evolution of the EDZ around the room, in cross-section, after excavation and for several centuries afterwards (Itasca 2018).

The analyses address time-dependent strength degradation of the rock and thermal stresses induced by UFCs. The modelled temperature is a combination of the temperatures calculated by near- and far-field thermal models. The peak temperature occurs at approximately 47 years. A detailed description of the thermal analysis is documented by Itasca (2018).

The THM analysis (Itasca 2018) shows that the extent of damage is confined to the vicinity of the opening. Before approximately 10,000 years, the EDZ is limited to damage created during the thermal loading period. Beyond that, there is no noticeable change in the EDZ (see Figure 5-5). In the analysis, conservative assumptions on the long-term strength (40% of the rock mass UCS) were also assumed. The long-term reduction in strength of Cobourg Limestone rock mass has an insignificant effect on room stability (i.e., resulting in relatively small incremental damage). The main reason for overall good performance of the placement rooms, and the relatively small effect of low long-term strength, is due to backfilling of the room. The backfill provides the confining pressure which prevents spalling of the rock and opening of the fractures, and significantly slows the time-dependent strength degradation/stress corrosion processes.

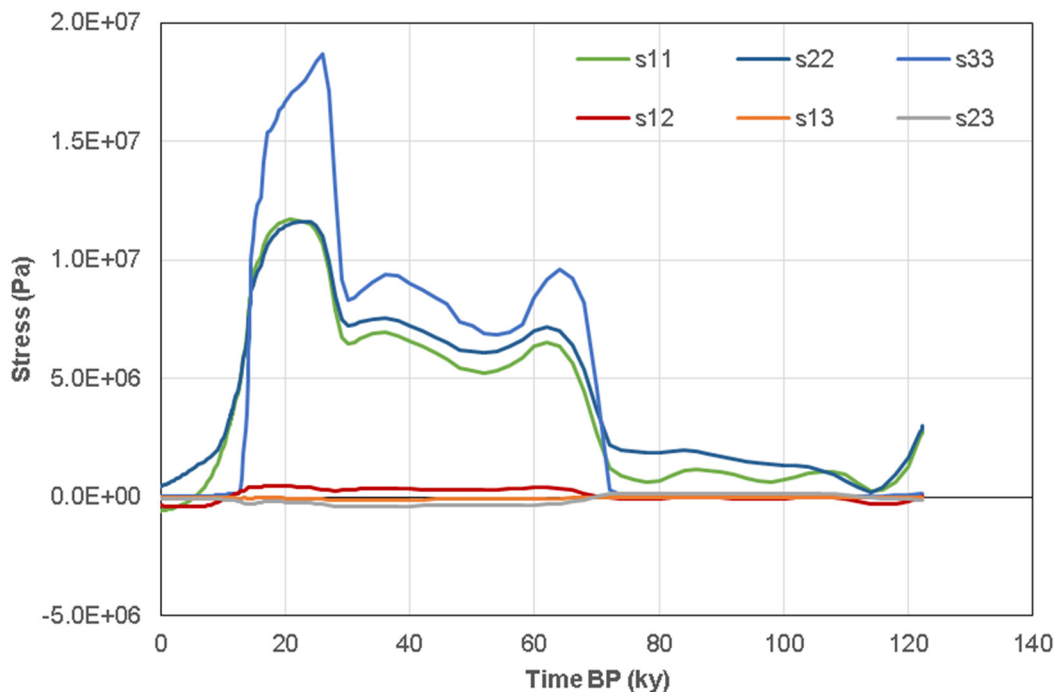


Note: (1) Black markings indicate micro-crack damage; (2) placement room dimensions: 3.2 m (W) x 2.2 m (H)

Figure 5-5: Evolution of Damage up to One million years

5.2.6.2 Impact of Glaciation

The assessed site is located in a region of southwestern Ontario that has been subjected to numerous glacial episodes over the past million years. A simulation was conducted assuming that a sequence of glacial events and corresponding histories of rebound stress (Itasca 2018) occurs in the future, starting at about 60,000 years after present (Figure 5-6). An ice thickness of 2.6 km may be expected at the site (Stuhne and Peltier 2015). Figure 5-5 shows that glacial loading does not significantly affect the damage zones around the placement room during and after the event. The lack of damage development around the opening is also attributed mainly to the confinement provided by the backfill in the placement room. The placement room and pillars between rooms remain stable throughout the glacial cycles.



Note: '1' denotes the vertical direction and '2' and '3' denote horizontal directions

Figure 5-6: Calculated Glacially Induced Rebound Stress Histories (BP = before present); S11, S22 & S33 are the Normal Stress Components; S12, S13 & S23 are the Shear Stress Components (Itasca 2018)

5.2.6.3 Impact of Seismic Ground Shaking

The impact of seismic ground motions was not studied in the analyses performed by Itasca (2018). However, in Itasca's earlier study (Itasca 2015), three very low-probability seismic events (with contemporary 10^{-6} per annum probability level) were simulated to evaluate their impact on repository stability. The analysis considered a magnitude 5.5 (M5.5) event at a distance of 20 km, a M6.5 event at a distance of 100 km, and a M7.4 event at a distance of 300 km, covering the high, medium and low frequency ranges of the uniform hazard spectrum from the probabilistic seismic hazard analysis (PSHA), respectively, similar to that for the Bruce nuclear site (AMEC Geomatrix 2011).

To evaluate the worst-case scenario, the 10^{-6} per annum seismic loading was applied to the model at two critical instances in time: when peak temperature is reached in the rock, and when maximum glacial loading occurs (Itasca 2015). This provides a bounding loading combination to ensure that the maximum stress increase in the surrounding rock mass is considered in the analysis. The damage level in the model for the three seismic time histories is first applied at the peak temperature state. The additional damage resulting from seismic loading is insignificant. A similar observation was noted at the time of maximum glacial loading (Peltier 2011). Thus, it is concluded that the simulations do not show any appreciable rock damage for the 10^{-6} per annum probability level extreme seismic shaking.

5.2.7 Confidence in Repository Evolution

Temperature: The thermal conductivity of sedimentary rock is primarily influenced by the rock composition and matrix. Many of the uncertainties associated with estimates of heat transport properties of the geosphere would be resolved during site characterization. Temperature distributions in the geosphere would vary on a local scale as a result of repository layout.

However, there is good confidence in results obtained from thermal models over long periods of time, and in conservative estimates at shorter time. Some uncertainties exist in temperature predictions for pre-saturation conditions due to varying physical parameters (such as shrinkage or cracks) and moisture content (affecting thermal conductivity) of the material surrounding the container.

Repository Saturation: The resaturation rate depends on properties of the host rock and engineered barrier materials, temperature, hydraulic gradients, and gas or vapour transport, thus requiring coupled models. The modelling would be supported in part through engineering demonstration tests or monitoring of early placement rooms. While there is some inherent uncertainty, long-term repository performance is not particularly sensitive to the actual time of full saturation.

Near-Field Chemistry: The time at which reducing conditions will be re-established following repository closure is uncertain due to the complex interactions between groundwater, repository components and microbial processes.

Regardless of the amount of time required, the total amount of oxygen is limited and it can confidently be assured that reducing conditions will be re-established. Conservative assumptions can be applied in the repository design and analysis process that bound the associated uncertainties, to ensure that appropriate conclusions concerning repository performance are made.

Steel Corrosion and Gas Generation: Gas generation and migration depends upon host rock properties, the rate at which water enters the repository, the quantity of organic material present, the number and distribution of rock bolts, the degree to which radiolysis of water occurs, the postulated number and timing of hypothetical container failures, and corrosion rates.

Chapter 8 discusses the potential for corrosion-generated gases to impact the performance of the repository system.

Excavation-Damaged Zone: Estimates of the extent and permeability of the EDZ should be based on site-specific findings for the sedimentary rock site, for which data, such as ground stresses and mechanical properties of the host rock, become available during site characterization. Once available, these data will be incorporated into the various assessments, together with appropriate allowances for residual uncertainties.

EDZ predictions were based on bounding simulations that consider combinations of loading resulting from extreme geological and repository perturbations. Sensitivity studies to-date indicate that long-term repository stability and performance is not especially sensitive to variations in long-term EDZ development processes.

5.3 Long-Term Evolution of Used Fuel

A description of the used fuel waste form as placed in the repository is provided in Chapter 3. The used fuel assemblies remain isolated and dry within the container. The main long-term process is radioactive decay, including heating, as long as there is no container failure. The processes in a failed container are described in Section 5.4.4. Additional FEPs were assessed and excluded for the reasons outlined in the FEPs report (Garisto 2018) and thus are not part of the expected evolution described in this section.

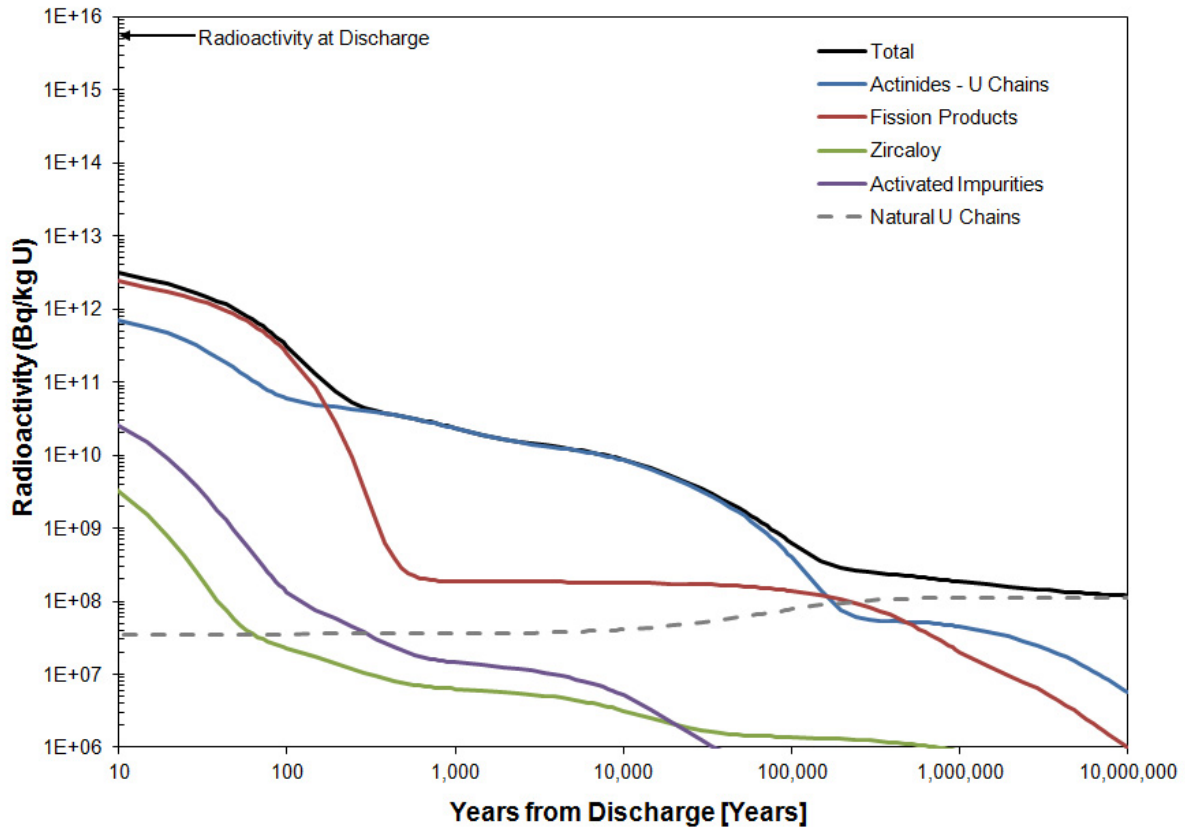
5.3.1 Radioactive Decay

When used fuel is first removed from the reactor it is highly radioactive. This activity decreases rapidly over the first year, and more slowly thereafter, as shown in Figure 5-7.

During the first year out of the reactor, the overall radioactivity decreases to about 1% of its initial value, and after about 100 years it decreases to 0.01% of its initial value. For the first 500 years, the total radioactivity of the fuel will be dominated by numerous short-lived fission products, most of which are gamma emitters; thereafter, it will be dominated by long-lived actinides, including uranium, many of which decay by emission of alpha particles.

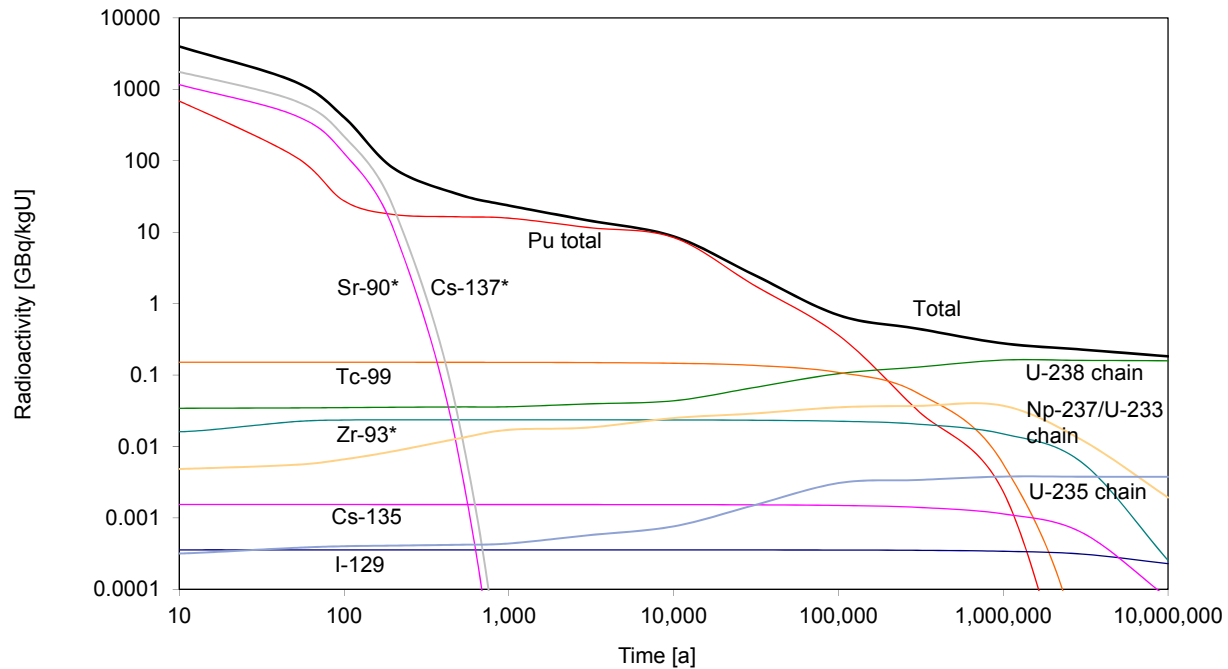
After about a million years, the total radioactivity in the fuel will have declined to levels that are equivalent to those found in naturally-occurring uranium ore bodies with similar amounts of total uranium. In particular, the repository with 5.2 million fuel bundles will hold about 100,000 Mg of uranium. The Cigar Lake and McArthur River ore bodies in Saskatchewan held about 90,000 Mg U and 130,000 Mg U, respectively, at an average ore grade of 20%.

Radioactive decay will gradually change the radionuclide composition of the used fuel. The radionuclide inventory, radiation output and heat output can be calculated as a function of time, as illustrated in Figure 5-8 for the radionuclide inventory. The greatest change in the composition of the used fuel is a pronounced decrease in fission products after about 500 years. Nevertheless, over a million-year timeframe all of the changes resulting from radioactive decay will represent only a modest change in the composition of the fuel, of which about 98% would persist as uranium and oxygen.



Note: U Chains represent radioactivity from uranium in fuel, including all progeny.

Figure 5-7: Radioactivity of Used CANDU Fuel (220 MWh/kgU burnup)



Note: Figure based on data from Tait et al. (2000). * Includes short-lived daughter.

Figure 5-8: Amounts of Key Long-Lived Radionuclides in Used Fuel (220 MWh/kg U burnup)

5.3.2 Changes in Temperature

Radioactive decay of the fuel is accompanied by alpha, beta and gamma radiation that is largely absorbed by the fuel itself and converted to heat. Immediately after being removed from a power reactor, a reference used fuel bundle would release about 27,000 watts of heat. This heat output rapidly decreases. After 10 years, the thermal output has decreased to 5.4 watts and after 30 years about 3.5 watts. In this study, the used fuel age at the time of placement is 30 years out of reactor. For fuel that is 10 years or older, passive cooling is sufficient.

Around 80 years after placement (as 30-year old fuel), the heat output of the entire 48-bundle container will be less than 60 watts.

The temperature of the container's outer surface will initially increase after placement (see Section 5.2.1). The temperature inside the reference container, loaded with 30-year-cooled used CANDU fuel, is expected to remain below 125°C (Guo 2015). The maximum temperature of the used fuel bundles will be attained within about 15 years after placement in the repository (see Figure 5-9).

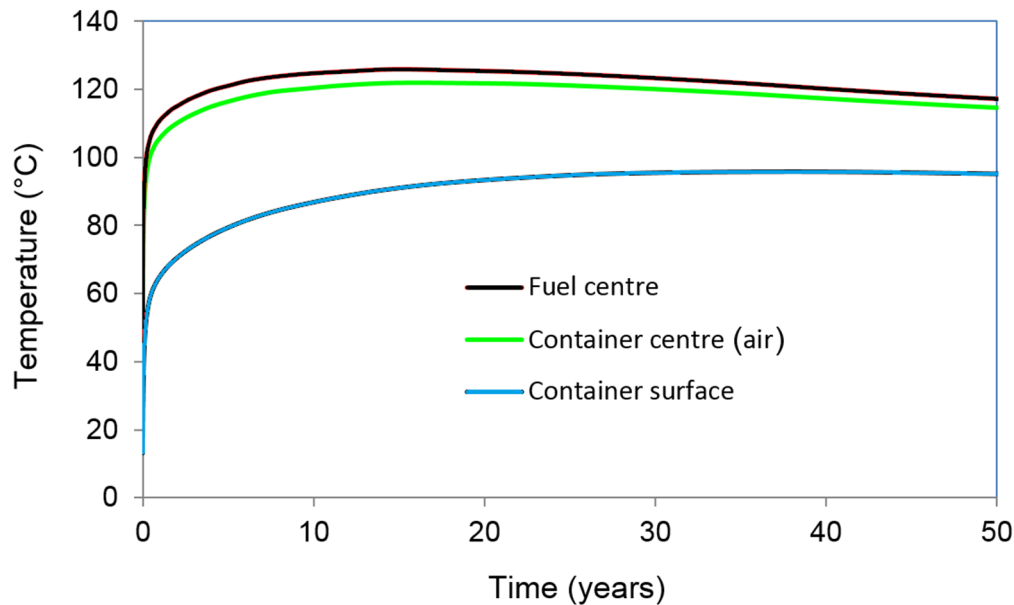


Figure 5-9: Temperature inside Container after Placement (Guo 2015)

5.3.3 Changes in the UO_2

Inside the sealed containers, processes and changes occurring over long timeframes will not materially impact relevant UO_2 properties (i.e., UO_2 grain size, distribution of radionuclides). This is described below.

5.3.3.1 Alpha Radiation Damage

During radioactive decay, the crystalline matrix of the used fuel will experience localized damage to the crystal lattice from the emission of alpha particles, which travel only short distances from the nucleus. The amount of accumulated damage in CANDU fuel is not expected to be significant given its generally low burnup.

Natural analogue evidence suggests that alpha irradiation damage would not cause used fuel to crumble, even after extremely long times. At Oklo in western Africa, uraninite (UO_2) ore deposits underwent spontaneous nuclear fission reactions more than two billion years ago. Although affected by brecciation during fission and by subsequent hydrothermal alteration in some cases, the uraninite is still granular and massive (Jensen and Ewing 2001).

5.3.3.2 Radionuclide Diffusion

Under repository conditions, the relatively low fuel temperature means that radionuclide movement within the grains towards a grain boundary or fuel element void is slow. This is important because for the bulk of the radionuclides, their release in the case of damaged container then depends on the corrosion of the UO_2 itself.

Radiation damage has the potential to accelerate diffusion beyond normal thermal processes. However, theoretical and experimental assessments (Ferry et al. 2008) indicate that this effect

is small, and in particular there is little redistribution of radionuclides within the fuel under repository conditions.

5.3.3.3 Oxidation State of Fuel

In some cases, radioactive decay results in the formation of an element with a higher oxidation valence than that of the parent radionuclide. In principle this could modify the oxygen potential and oxidation state of the UO_2 matrix, in turn affecting diffusion coefficients for radionuclides. Thermal diffusion coefficients of radionuclides are small at repository temperatures, but increase as the oxygen/metal (O/M) ratio of the fuel increases. However, any changes in CANDU fuel are expected to be quite small, from O/M ~ 2.001 to 2.010 or less, and this would not significantly affect thermal diffusion coefficients.

The oxidation state of the fuel potentially could be changed by the reaction of UO_2 and Zr to produce ZrO_2 , which is more stable thermodynamically than UO_2 . Where the cladding and UO_2 are in direct contact, the Zr eventually would reduce UO_2 to U by solid-state diffusion of oxygen atoms. This process is unlikely to be significant for used fuel due to the small amount of Zr present (10% of UO_2) and very slow solid-state diffusion rates at repository temperatures (Cox 1999). Consequently, the effects of possible galvanic couples are extremely small.

Within the intact container, the fuel cladding will be exposed to ambient air conditions within the container. However, zirconium forms a thin durable oxide layer, which will limit further oxidation of the cladding. And given that oxygen reactivity with the other container internal metals (i.e., steel) is much greater, as well as the limited amount of air present, this will not affect the fuel and cladding.

5.3.4 Zircaloy Cladding

The Zircaloy cladding is a resilient alloy (Freire-Canosa 2011) with a low corrosion rate (Shoesmith and Zagidulin 2010), and therefore can provide a barrier to prevent water from contacting the fuel or to inhibit radionuclide release in a failed container. However this Zircaloy cladding could fail due to processes such as creep, embrittlement and delayed hydride cracking. As the cladding is thin, it is conservatively given no credit within this safety assessment.

5.3.5 Build-Up of Helium Gas

Alpha decay results in the formation of helium (He) atoms in the used fuel. The total amount of helium in the fuel elements will increase over time. Calculations for high-burnup CANDU fuel (320 MWh/kgU) indicate that the helium content from alpha decay increases from 8×10^{-6} mol/kgU at discharge, to 0.01 mol/kgU at 10 thousand years, to 0.031 mol/kgU at one million years, and 0.091 mol/kgU at 10 million years (Tait et al. 2000). This is in addition to the 0.018 mol/kgU of other inert gas fission products present at discharge and largely unchanged with time (Tait et al. 2000).

The post-discharge helium would be largely formed within the grains since that is where the radionuclides reside. The helium would tend to move towards grain boundaries and vacancies due to the low solubility of helium in the lattice. Helium bubble formation has been observed for concentrations above 5×10^{18} He atoms/g, and it has been conservatively assumed that this level would lead to fuel cracking (Pencer et al. 2017). This amount of helium from alpha decay

would be reached in median burnup CANDU fuel in a few tens of thousands of years. However in used fuel this helium is accumulating under relatively low temperatures, and the time for diffusion to grain boundaries will be long; furthermore, fuel lattice swelling associated with helium bubble formation is not expected to occur during the first million years of aging (Pencer et al. 2017). Therefore, for low burnup fuel like CANDU fuel, the quantity of He produced is not expected to be sufficient to induce micro-cracking of grains (Ferry et al. 2008). Nonetheless, for safety assessment purposes it is assumed that the fuel is fragmented into small pieces, although not grain-sized.

While much of this inert gas could remain within the UO_2 grains, even if all this gas would be released into the container, then after one million years the container pressure would be less than 0.6 MPa even if fully loaded with high-burnup fuel.¹ (As noted above in Sec 5.3.4, the fuel element cladding is not credited as a barrier at long times.)

5.3.6 Criticality

Criticality is not an issue since CANDU fuel cannot become critical without the presence of heavy water, regardless of the density or age of the fuel (Garisto et al. 2014). Ordinary water cannot support criticality of used CANDU fuel even if embedded in ordinary water. Furthermore, water would not have access to the used fuel in intact containers anyway.

5.3.7 Mechanical Integrity

The fuel bundles are expected to be largely intact at the time of loading, although some of the cladding or cladding/endplate welds may be cracked due to creep, hydride embrittlement and vibration during transport and handling. The fuel itself will be cracked as is typical after irradiation.

As the fuel bundles are supported by steel baskets, they are not subjected to significant stresses after emplacement. Further damage to the cladding will likely occur due to creep and embrittlement, and the fuel may be further fractured due to buildup of helium gas. Vibrations from significant earthquakes could also cause this damage.

It is assumed for safety assessment purposes that the cladding does not provide a long-term barrier to radionuclide release, and that the fuel is fractured into small pieces immediately on placement.

5.3.8 Biological Processes

No changes arising from biological processes are expected because the combination of high temperatures, significant radiation fields, and the absence of water and organic carbon will exclude any biological reactions inside a container.

¹ 48 bundles × 19.7 kgU/bundle × (0.031+0.018) mol gas/kgU at 1 Ma ~ 46 mol gas in 0.27 m³ at 60°C ~ 0.47 MPa

5.3.9 Confidence

At the time of placement in a deep geological repository, the physical properties of the used fuel and the inventory of radionuclides will be well characterized. Radionuclide decay constants are well defined, and so the changes in the inventory and the related changes in decay heat over time can be calculated with a high degree of confidence.

UO₂ is expected to be a durable material. This is supported by the existence of very old natural uranium deposits, many of which are a form of UO₂. The rates of several processes within the fuel, such as the diffusion of helium in UO₂, are influenced by temperature. These rates would be low because the temperature inside the container will be, at most, about 125°C, and will decrease to ambient host rock temperatures on a 100,000 year timeframe.

In the closed-system environment provided by an intact container, the physical condition of the fuel is not expected to change significantly over long periods of time.

5.4 Long-Term Evolution of a Used Fuel Container

The used fuel container (UFC) is designed to provide long-term containment of the used fuel, preventing contact with groundwater. As described in Section 4.3, the reference container design includes a steel structural vessel that is protected from corrosion with a copper coating. Also, as described in earlier sections, the repository environment will transition from hot (~100°C), dry and aerobic, to cool, water-saturated and anaerobic conditions. Within this environment, specific effects have been examined as they pertain to the evolution of the used fuel container. These are summarized here and described below:

- The copper coating of the UFC will resist external corrosion mechanisms including:
 - Corrosion attributable to oxygen trapped in the repository from placement activities;
 - Corrosion from chloride or other groundwater species that may be present or diffuse into the repository;
 - Corrosion from sulphide that (1) may be present or produced in the undisturbed rock that is capable of migrating to the UFC, (2) may be present in the buffer, and (3) may be produced in the near field, including the EDZ, by sulphate-reducing bacteria;
 - Corrosion due to radiation effects (including radiolysis);
 - Galvanic corrosion; and
 - Stress corrosion cracking.
- Internal degradation mechanisms and processes will not affect the integrity of UFCs over long timeframes.
- The container is designed to withstand an external isotropic pressure of 45 MPa at 50°C. This value would accommodate the normal loads plus the hydrostatic load exerted at repository depth by a glacier above the repository.

Additional FEPs were assessed and excluded for the reasons outlined in the FEPs report (Garisto 2018) and thus are not part of the expected evolution described in this section.

5.4.1 Irradiation of Container Materials

The radioactivity inside the container is at its maximum value when the fuel is first loaded. The radiation field around the container is dominated by the gamma emission from short-lived fission products, which decay almost completely within the first 500 years after placement (see Figure 5-7). Thereafter, the residual radiation field would be very low because most of the remaining radioactivity will be from the alpha emission of long-lived actinides. Alpha particles do not penetrate beyond the fuel cladding.

High levels of neutron radiation, as found in nuclear reactors, can lead to hardening and embrittlement of reactor parts. The neutron flux inside a reactor is on the order of 4×10^{13} n/cm²·s (neutron per centimetre squared, per second). In comparison, the neutron flux from used fuel is much smaller, about 10^2 - 10^3 n/cm²·s initially in a UFC. Over a million-year timeframe, the total neutron fluence experienced by the container would be less than 10^{15} n/cm² (based on Tait et al. 2000). A neutron fluence greater than 10^{22} n/cm² would be required to produce measurable displacement effects in metal. Furthermore, a thermal neutron fluence of 10^{19} - 10^{21} n/cm² would be needed for defect formation and significant hardening in copper and iron at 70 - 80°C. Consequently, the container metals will not be significantly affected by radiation over a million year exposure to used fuel.

Radiation would be more likely to have an indirect influence on container properties, in terms of changes to the chemical environment that will result from the decomposition (radiolysis) of air and water in the vicinity of the container; this topic is discussed in Section 5.4.3.3.1.

5.4.2 Container Temperature

The repository layout described in Section 4.8.1 is designed to ensure that the exterior surface temperature of the UFCs after placement remain below 100°C (see Figure 5-3), considering the reference horizontal placement concept at a depth of 500 m in sedimentary rock.

In practice, only a fraction of the containers in a repository (those with the youngest fuel and / or the highest burnup values) would approach this maximum temperature. In the case of containers that otherwise are identical, those near the edges of a repository would have lower maximum temperatures than those in the centre of a repository because they would be less affected by heat from adjacent containers.

The repository layout is designed based in part on thermal analyses that limit the UFC temperature (Guo 2018). The models used for this analysis have been benchmarked against various heated field experiments (e.g., the full-scale Canister Retrieval Test at the Äspö Hard Rock Laboratory in Sweden; Guo 2009).

5.4.3 Mechanical Integrity

Containers would experience a range of stress conditions over time. The structural design of the container is determined largely by the requirement to provide adequate mechanical strength throughout its design life.

5.4.3.1 Effects of Hydrostatic and Buffer Swelling Pressures

After placement, the external load on the containers initially would consist of little more than the weight of the overlying sealing materials. The load would gradually increase during saturation of the repository. The swelling of the bentonite in the sealing materials is likely to occur unevenly on a local scale because the swelling would be controlled by the supply of water from the rock, by the shape of the room, and by the pathway of water along interfaces. The heterogeneous development of swelling pressures would result initially in non-uniform external loads on the containers, an effect that is expected to diminish as full saturation is achieved. The container design is robust enough to account for this.

By the time a repository is fully saturated, the hydrostatic pressure will have increased up to about 5 MPa at the repository depth of 500 m. As heating progresses, the pressure gradually increases, reaching the peak of 6.6 MPa at about 1000 years. Subsequently, the cooling period begins and the pressure reduces. Buffer swelling pressures could contribute up to 7 MPa to the load on the containers, depending on groundwater salinity and buffer density (Baumgartner 2006). The resulting loads are within the container design pressure of 15 MPa under the normal evolution conditions; the container is designed also to withstand the full added load of glaciers 3 km in thickness.

5.4.3.1.1 Effects of Glacial Loading

Additional compressive stresses would be applied to the container by glaciation. It is unlikely that an ice sheet would develop over the repository until at least several tens of thousands of years have elapsed (Peltier 2011). By this time, the buffer saturation-related pressure loads would be fully applied. The loads on the UFC shown in Figure 5-10 are total loads due to effective stresses and pore pressures. In order to obtain the total pressure, the swelling pressure of bentonite backfill of 7 MPa, has been conservatively added.

Major increases in the pressure on the UFC arise during the glaciation period. As a bounding limit, a 3 km ice sheet could potentially add a pure hydrostatic load at the repository equivalent to almost a 3 km column of water (a little less allowing for density difference between water and ice), or about 30 MPa.

However, the loading is more complicated in reality, in part because the ice sheet is solid and much of its weight is carried through the rock structure. Analysis conducted by Itasca (2015) indicated that at the peak glacial load, the mean pressure exerted on the container reaches 17.6 MPa (without fluid migration). This is further mitigated at the container in part, by “stress arching” created when the lower modulus backfill carries less load than the stiffer enclosing rock mass.

The exerted pressure on the UFC is the sum of the initial hydrostatic groundwater pressure (5 MPa), and the change in porewater pressure created by ice sheet loading – representing the resultant total stress change in the far-field. Using a conservative Skempton coefficient of 0.7 to estimate the excess pore pressure, an upper bound pressure on UFC could be 23 MPa with fluid migration (Itasca 2015). The pressure will further increase to 30 MPa if the swelling pressure of the bentonite backfill is included (Figure 5-10). This estimated value represents a conservative assumption that considers maximum porewater pressure increases allowing for anticipated fluid migration and porewater pressure dissipation. The estimated UFC loading

value in this analysis is based on an ice thickness of 3 km. The transient loading on the UFC throughout a glacial cycle is shown in Figure 5-10.

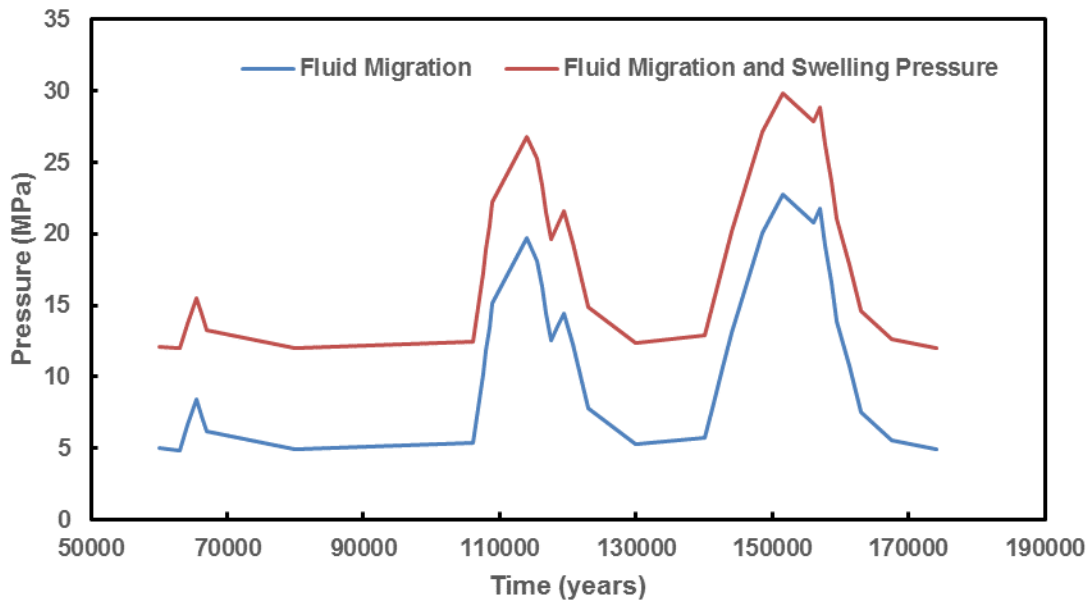


Figure 5-10: Evolution of Pressure on UFC over a Glacial Cycle

5.4.3.1.2 Effect of Seismic Stresses

Southern Ontario is characterized, in general, by low levels of seismic activity as it is within the tectonically stable interior of the North American continent (see Section 2.2.4.3). Large earthquakes would therefore be very unlikely, although an increase in the number and intensity of earthquakes is likely in response to the reduction in loading as ice sheets retreat.

Earthquakes typically are less destructive at depth than at the surface, diminishing the impact of any seismic activity on a deep geological repository (Bäckblom and Munier 2002), and postglacial faulting is more likely to reactivate an existing zone of weakness in the rock than it is to develop new fractures (see Section 5.1.1).

The present repository site is assumed to be a low seismicity area. The repository is placed away from large fractures, and containers are only placed in rooms without significant local fractures. Normal small earthquakes are unlikely to have significant effect on the site, repository or containers. Large earthquakes could affect the existing fractures, and are considered through the assumption of a high permeability for the existing fractures, which likely is much higher than the in-situ permeability of deep fractures at a real site. Other effects of a very large earthquake are considered within the Disruptive Event Scenarios.

5.4.3.1.3 Effect of Creep

Creep is the slow deformation of a material under an applied stress that results in a permanent change in shape. For a copper coated vessel, no gap exists between the integrally bonded steel and copper components; thus, the mechanism does not impact either copper or steel independently of each other. For both cylindrical body and hemispherical head components of the UFC, creep is determined by the performance of the steel. As the copper is bonded to the steel, creep rupture of the copper coating is not an issue.

Steel is designed to remain load-bearing over the design lifetime of a container (Werme 1998, Saiedfar and Maak 2002). For example, the maximum stresses developed in the reference steel vessel are only about 30% of its yield strength under normal saturation-related pressures, and approaches the yield strength under peak design-basis glaciation pressures. The creep rate of steel under the anticipated loading conditions (20% of its ultimate tensile strength under saturation-related pressures) and temperature (about 100°C or less) is insignificant. The exact rate is uncertain, but it is expected that it would take at least 100,000 years for any appreciable amount of creep deformation to develop in the steel vessel (Dutton 2006).

5.4.3.2 Effect of Chemical Processes inside the Container

The containers are expected to remain intact throughout the timeframe of the safety assessment. Chemical changes over time involving those processes that affect the interior of the container (a closed system) may therefore be considered separately from those that affect its exterior surface.

At the time of packaging, which will be conducted in ambient conditions, the container interior is dry, as are the used fuel bundles. It is expected that air and water vapour trapped during the closure of the container will subsequently react with the metals in the container interior (SKB 2011).

The zirconium alloy in the fuel bundles described in Section 5.3.4 will already have a surface film of ZrO_2 that formed at high temperatures in a reactor. This resistant ZrO_2 surface layer on the cladding will inhibit any further reaction with the small amount of air initially available inside the container. This is in contrast to the more porous and reactive air-formed iron oxide layer on steel that is not expected to prevent further oxidation. Thermodynamic and kinetic arguments predict that reaction between the iron and oxygen will occur, even at a very low oxygen partial pressure. Therefore, the steel inner vessel and the steel baskets holding the fuel bundles would tend to react rapidly with any available oxygen, forming iron oxides/hydroxides as corrosion products. This would remove any gaseous oxygen and water from the interior of the container, so that conditions in the interior will become dry and anoxic. Using conservative assumptions with respect to high amounts of water being trapped (e.g., damaged fuel bundles), approximately 1 μm of iron oxide is expected to form from these internal reactions.

In addition, irradiation of air will produce small quantities of oxidized nitrogen by radiolysis. Owing to the limited quantities of oxygen and water, and the reactivity of these species with the carbon steel inside the container, no significant quantities of species such as nitric acid are anticipated. Studies are being directed at localized corrosion within the container, either at welded zones or as a result of radiation/radiolysis processes; no significant issues have been identified (Guo et al. 2016, Morco et al. 2017, Turnbull et al. 2017, Wu et al. 2017).

Fuel elements with defective cladding would also release some fission gases to the container interior, particularly if the cladding fails after the container is sealed. Iodine, which assists stress corrosion cracking of metals under some conditions, is the most noteworthy of these gases. However, the partial pressure and total quantities of any released gases would be small (e.g., $<10^{-7}$ MPa for iodine). Most of the other released gases would be adsorbed onto the internal surfaces of the steel structure, or they would be distributed among the exposed iron, zirconium and copper surfaces, yielding no significant changes to the interior of the container (McMurry et al. 2003).

In summary, the interior of the container would quickly develop a dry, reducing chemical environment that would persist as long as the container remains intact.

5.4.3.3 Effect of Chemical Processes outside the Container

This section summarizes the current understanding of the corrosion behaviour of copper used fuel containers in a deep geological repository. This understanding has been developed based on an extensive experimental program carried out in Canada, and other parts of the world, over the past 30 years, and on the results of mechanistically-based modelling of various corrosion processes.

The corrosion behaviour of copper depends on the nature of the environmental conditions. For this discussion, the following attributes of the container and reference repository design are important.

- The container corrosion barrier is manufactured from high purity copper.
- The container is placed in the room within clay blocks, capable of sealing the system when in contact with water.
- The containers are surrounded by buffer material comprising dense bentonite block and gap fill, with an average dry density of at least 1.6 Mg/m^3 .
- The groundwater is a Ca-Na-Cl solution, with small amounts of sulphate and low levels of carbonate.
- The available O_2 is limited to that trapped initially in the pores of the buffer and backfill materials, and the groundwater itself is O_2 -free.
- The container has an inner steel vessel, resulting in a surface dose rate of less than 2 Gy/h .
- The container surface temperature does not exceed 100°C .
- There is a period of unsaturated conditions immediately following container placement and prior to saturation of the repository.
- There is little or no sulphide (HS^-) present in the groundwater.
- The container is subject to external loading from a combination of the hydrostatic load and bentonite swelling pressure.

Experimental research and modelling has considered uniform corrosion, pitting corrosion, stress corrosion cracking (SCC) and microbially influenced corrosion (MIC). A list of studies conducted in the Canadian copper corrosion program is tabulated in Kwong (2011) and reviewed in Scully and Edwards (2013). A more recent review has been performed of all copper corrosion mechanisms, particularly for active research topics, which further supports the conclusions below (Scully et al. 2016).

Overall, these studies conclude that a used fuel container with an external barrier of copper, placed in a deep geological repository, will be primarily subject to general corrosion, regardless of copper form (i.e. manufacturing method, Standish et al. 2016). The degree of localized attack (pitting), microbial-influenced corrosion and stress corrosion cracking will be negligible, and can be controlled using standard engineering design. All forms of corrosion will be stifled as the repository environment becomes anoxic. The various corrosion mechanisms are discussed in more detail in the following sections.

The important characteristics of the corrosion of copper containers in a deep geological repository are as follows.

- The corrosion behaviour changes with time, largely as a result of the evolution of the repository environment (King and Shoosmith 2010). This environment evolves from an initial period of warm, aerobic conditions to an indefinite period of cool, anoxic conditions. From a corrosion perspective, this environmental evolution means that localized corrosion processes are limited to the early period, with corrosion becoming more uniform in nature as time progresses.
- The nature of the environment at the container surface determines the corrosion behaviour. The surface environment can be different from that in the host rock as a result of the chemical conditioning of the groundwater by the bentonite clay and the slow mass transport of reactants to, and of corrosion products away from, the container surface due to the presence of the bentonite.
- A limited period of time of a few hundred years is available during which gamma radiation from within the container can interact with water in the surrounding media (i.e., buffer) and produce trace amounts of reactive species, such as hydrogen peroxide, that may interact with the container surface.
- In general, groundwater chloride promotes the uniform dissolution of copper and suppresses localized corrosion and SCC (King et al. 2010, 2011a).
- The dense bentonite clay buffer and high groundwater salinity around the container suppress microbial activity.

Specific corrosion processes are described below.

5.4.3.3.1 Uniform Copper Corrosion

The uniform corrosion of copper in the environment expected in a deep geological repository has been extensively studied, and the corrosion mechanism is well understood and summarized in Kwong (2011). Figure 5-11 illustrates the mechanism developed to describe the uniform corrosion of copper in compacted bentonite saturated with oxygen (O₂) and containing chloride (Cl⁻) porewaters. The mechanism couples the interfacial electrochemical reactions that occur

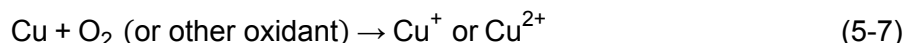
on the container surface to various processes occurring at or within the bentonite. These processes include: the diffusive mass-transport of species to and from the corroding interface (denoted by the wavy arrows in Figure 5-11); the adsorption and desorption of Cu(II) on the clay; redox reactions involving dissolved O₂, Fe(II), and Cu(I) and Cu(II) species; the dissolution and precipitation of various solid mineral phases and corrosion products; the partitioning of O₂ between the gaseous and aqueous phases; and, in a simplistic manner, the microbial consumption of dissolved O₂. This reaction scheme applies equally to both the buffer and backfill materials, as well as the host rock, and further details are included below.

Copper can react in dry air as shown in Reaction (5-6). The rate of copper oxidation in dry air at temperatures below 150°C is of the order of nm/a, and, therefore, is effectively negligible.

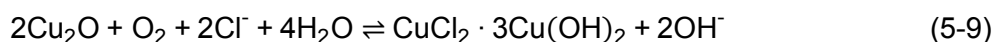
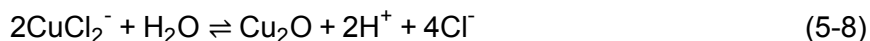


Copper will corrode in solutions containing O₂ under atmospheric conditions, providing the relative humidity is above that required to form a thin surface water film, i.e., approximately 50 to 70% relative humidity. The rate of corrosion may also depend on the presence of atmospheric contaminants, such as SO₂, NO₂, and CO₂. The ion-containing water film acts as an electrolyte to support electrochemical reactions and the dissolved impurities will further enhance the corrosion process. For instance, in water, SO₂ forms H⁺ and HSO₃⁻; the latter species can be oxidized to sulphate by oxidants in the air to produce local quantities of sulphuric acid. Similarly NO₂ can be absorbed in the water film as HNO₃, nitric acid. Either of these acidic media can enhance corrosion and copper dissolution; although the effect is very limited in this case, as oxygen is very limited. The corrosion behaviour of copper in O₂-containing Cl⁻ solution has also been well studied. A detailed reaction mechanism exists that accounts for the various electrochemical, chemical, redox, adsorption/desorption, precipitation/dissolution, and mass transport processes involved in the corrosion process in compacted bentonite. The behaviour of copper over a range of chloride concentrations has also been experimentally evaluated. Kinetic rate constants, equilibrium constants and other thermodynamic parameters required for modelling are available, as summarized in Kwong (2011).

During corrosion, the anodic reaction is coupled to the cathodic reduction of an oxidant such as dissolved O₂; however, it may also be supported by the presence of another oxidizing species such as Cu²⁺, Fe³⁺, Pb⁴⁺, etc.



Both Cu⁺ and Cu²⁺ can precipitate as species such as Cu₂O and CuCl₂·3Cu(OH)₂, respectively (Reactions (5-8) and (5-9)). Such a duplex corrosion product layer could comprise an inner layer of Cu₂O and an outer layer of basic Cu(II) salts, such as CuCl₂·3Cu(OH)₂ or Cu₂CO₃(OH)₂, depending on the specific composition of the porewater.

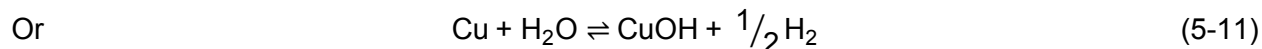


While a precipitated surface film of this nature could block surface electrochemical reactions and prevent the permanent separation of anodic and cathodic reactions required for localized

corrosion to occur, it is notable that Cu^+ dissolves readily in Cl-containing solutions. This feature is likely to ensure that the metallic copper will be continuously exposed to the solution, which will enhance general corrosion. In addition, as the repository environment becomes anaerobic, residual $\text{CuCl}_2 \cdot 3\text{Cu}(\text{OH})_2$ layers will also dissolve owing to the disproportionation of Cu^{2+} with metallic copper (Cu^0) to produce 2Cu^+ , the stable and soluble species.

The radiation field, which begins at < 2.3 Gy/h (Morco et al. 2017) and diminishes over several hundred years, is significantly below the value expected to cause alterations to the copper (i.e., at dose rates >100 Gy/h, see SKB 2010). However, since water radiolysis is known to produce oxidants such as oxygen, there is significant research ongoing to validate this assessment. When high gamma fields are used in experiments designed to accelerate the effect (i.e., 3 kGy/h for 72 h in air), copper oxidation takes the form of deposits that spread laterally (Ibrahim 2015). Despite the absence of evidence for radiolytic-related corrosion, an allowance of 0.1 mm of general corrosion has been assumed for this process.

In the absence of oxygen, corrosion would require a reaction with water to produce hydrogen gas (H_2):



Known thermodynamic relationships (Puigdomenech and Taxén 2000) indicate that the equilibrium shown in Reaction (5-10) is very strongly biased towards the reactants: metallic copper and water. Accordingly, upon formation of a very small amount of Cu_2O (i.e., a single monolayer), only a very small amount of hydrogen, with a partial pressure on the order of 10^{-11} mbar, is necessary to suppress the corrosion reaction (i.e., Reaction (5-10) becomes unfavourable in the forward direction). In addition, the corrosion product in Reaction (5-11) has not been shown to be stable. Therefore, Reactions (5-10) and (5-11) are considered very improbable in water.

Under anaerobic conditions, copper corrosion accompanied by the evolution of H_2 does occur in the presence of sulphide, as per Reaction (5-12).



Sulphide is not widely found in groundwaters in sedimentary rock in Canada (King et al. 2017). However, owing to the possibility of remote microbial reactions that produce sulphide (see Section 5.4.3.3.5), and the very small dissolution of sulphide from pyrite in the rock and bentonite, a reference value of $1 \mu\text{mol/L}$ (0.034 mg/L or 34 ppb) has been considered in the absence of site-specific data. This value is less than those projected for Sweden and Finland, where deep groundwaters do contain small amounts of HS^- (typically <1 mg/L; King et al. 2010, 2011a). In all cases, these concentrations result in corrosion rates of well below one nm/a due to the slow transport of sulphide to the container surface through the compacted bentonite buffer (SKB 2011).

Researchers from the Royal Institute of Technology (Sweden) have published experimental results indicating that copper can corrode in pure, oxygen-free water. Their research claims that water is reduced in the anaerobic corrosion process to form hydrogen atoms (Szakálos et al.

2007, Hultquist et al. 2009, 2011), and that a hydroxyl-containing copper corrosion product may be produced. Subsequent expert review (Swedish National Council 2010) concluded that it was necessary to demonstrate that the proposed corrosion product was thermodynamically stable before it could be justifiably claimed that copper could corrode in oxygen and sulphide-free water. An SKB review also concluded that there were possible errors in the original experiments (SKB 2010).

Further studies have been conducted in Sweden, as well as by NWMO. Preliminary results were reported in SSM (2011a) and Hultquist et al. (2013). These have found extremely small quantities of hydrogen in similar experiments, although the tests were not definitive. In addition, careful analysis of the thermodynamics of the reactions between copper, pure water, and sulphide (SSM 2011b) has indicated that copper-water interactions, as described by (5-10) and (5-11), are theoretically possible but would only produce very small quantities of hydrogen, and that reactions with sulphide species are much more important (SSM 2011b). More recent experimentation has focused on preparation and cleaning of copper samples and the effects on measured hydrogen (Johansson et al. 2015), and some truly definitive work by Ottosson et al. (2016) has demonstrated very clear evidence that as-produced/purchased copper contains significant amounts of hydrogen prior to its immersion in water. In this latter work, it was demonstrated that pretreatment of copper prior to experiments can completely remove hydrogen and suppress all hydrogen production during very long-term immersion in ultrapure water.

In addition, while this topic is still being studied, it appears that the hydrogen produced from a copper-water interaction would be self-limiting, and not a significant corrosion mechanism within a repository. If the corrosion mechanism via reaction (5-11) does occur, for example, hydrogen partial pressures of ~1 mbar (Szakálos et al. 2007) and 0.5 mbar (Hultquist et al. 2009) are all that is required at temperatures of 73°C and 45°C, respectively, to suppress the corrosion reaction. In a DGR, sufficient hydrogen could be present from many sources: the copper-water reaction, if it occurs; anaerobic corrosion of steel components; reactions between copper or steel with trace levels of sulphides; and/or native hydrogen levels.

The rate-controlling process for the overall uniform corrosion of copper changes as the environmental conditions evolve. Under aerobic conditions, there is evidence that the transport of dissolved Cu away from the corroding interface can be rate controlling (King et al. 2010, 2011a) (i.e., the corrosion reaction is anodically transport limited). As the repository environment becomes anoxic, the corrosion rate must eventually become cathodically transport limited as a result of the slow diffusion of oxidant to the container surface. In the presence of sulphide, if such species were to be found in Canadian groundwaters or produced from sulphates by microbes, then the corrosion rate is limited by the rate of transport of HS⁻ to the container surface (Chen et al. 2011, King et al. 2011b).

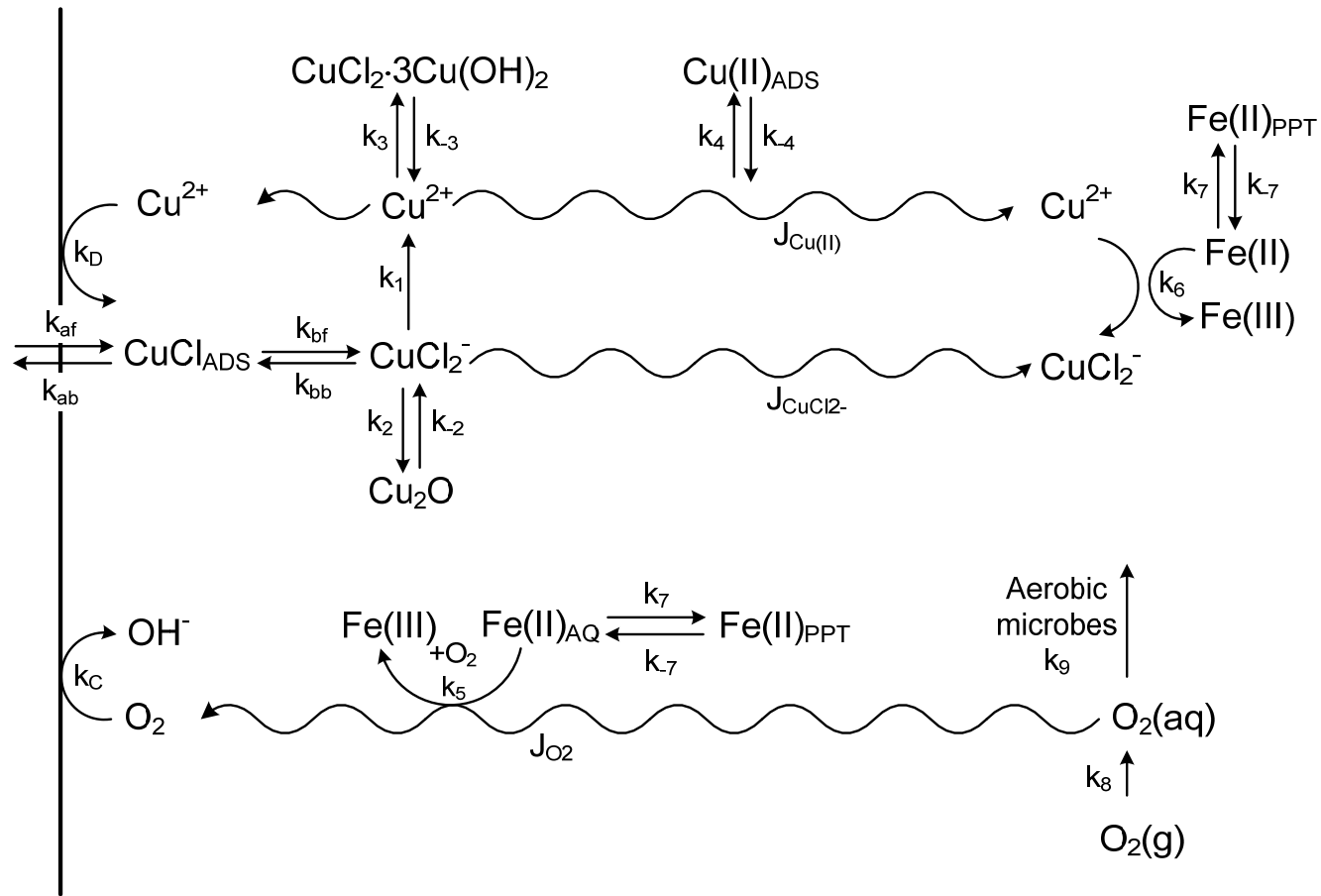
Overall, the uniform corrosion behaviour of copper in conditions expected for a deep geological repository in sedimentary rock is well understood. Both the mechanism of copper corrosion in oxygen-containing chloride solution and kinetic and thermodynamic parameters required for modelling are available.

5.4.3.3.2 Uniform Copper Corrosion Modelling

To complement the extensive experimental studies on which the mechanism in Figure 5-11 is based, a detailed reactive-transport model has been developed to predict the long-term uniform corrosion behaviour of copper containers in the repository. The model, referred to as the Copper Corrosion Model for Uniform Corrosion (CCM-UC), is based on the mechanism in Figure 5-11 and couples the corrosion behaviour of the container to the various processes occurring in the near- and far-fields of the repository, specifically the evolution of the environmental conditions. The corrosion behaviour is modelled using electrochemical mixed-potential principles. As a result, the model not only predicts the time-dependent corrosion rate (as a corrosion current density), but also the time-dependent corrosion potential (E_{CORR}). E_{CORR} is a useful parameter for assessing the probability of localized corrosion and stress corrosion cracking, as well as providing information about uniform corrosion.

Various methods have been developed to predict the rate or extent of the uniform corrosion of copper containers. Because uniform corrosion is limited by the availability of oxidant, the rate of corrosion is of less importance than the extent of corrosion. The maximum depth of corrosion can be assessed based on mass-balance principles (SKB 2011) or using the detailed mechanistically-based CCM-UC model (King et al. 2008).

The exact amount of O_2 trapped in a repository placement room during its closure depends on the buffer and backfill material porosity, volume (relative to the total UFC surface area in the room), and, crucially, degree of saturation at the time of closure (the majority of the trapped O_2 is present as gaseous O_2 in the air-filled pores of the buffer and backfill). If all trapped oxygen in the reference placement room, corresponding to $2.6 \text{ mol}_{\text{O}_2}/\text{m}^2_{\text{Cu}}$, is consumed by copper corrosion, then the maximum wall penetration of the UFCs in the present design would be $75 \mu\text{m}$ (0.075 mm). In reality, nearly all of the O_2 will be consumed by aerobic microbial activity in the backfill material and the oxidation of ferrous species, so that the actual depth of uniform copper corrosion will be much lower. Depending upon the relative rates of the different microbial and redox reactions, the model predictions suggest that more than 50% of the trapped O_2 could be consumed by processes other than corrosion. A consequence of the limited availability of oxidant is that, once all of the O_2 (or the Cu^{2+} produced by the oxidation of CuCl_2 by O_2) has been consumed, and there is sufficient generation of H_2 , corrosion of the container ceases.



Notes: From King and Kolář (2000) and King et al. (2008, 2010, 2011a). The k 's denote rate constants for the various interfacial electrochemical and homogeneous reactions and the J 's denote diffusive fluxes.

Figure 5-11: Reaction Scheme for the Uniform Corrosion of Copper in Compacted Bentonite Saturated with O₂-Containing Chloride Solution

5.4.3.3.3 Localized Corrosion

Kwong (2011) and Scully and Edwards (2013) identify that studies designed to specifically examine the surface profile of copper corroded in groundwater-saturated, compacted buffer materials have been completed. Experimental results showed that the copper will only undergo a form of surface roughening as a result of the non-permanent separation of anodic and cathodic processes. A mechanism to account for the observed surface profile, which involved the periodic separation of anodic and cathodic processes through the formation of temporary occluded cells, has since been proposed (King and Kolář 2000). Conceptually, these conditions could exist where there are differences in the flux of O₂ to different parts of the container surface, i.e., where bentonite blocks of different density might be used around the container.

Experimentally and through thermodynamic analysis, it has been shown that any localized corrosion rates would decrease with decreasing oxygen concentration and decreasing container surface temperature. The resultant corroded copper surfaces showed only general corrosion with minor surface roughening and no distinct pitting, and it was concluded that the rate and extent of localized corrosion in a deep geological repository will be very small because there will be a limited supply of oxygen.

More recent work (Qin et al. 2017) has focused on the environmental and surface conditions of copper within a DGR during the early oxidizing period, as coverage by a surface passive film is required for classical pitting. Experimental conditions have included expected groundwater constituents, such as chloride, sulphate and carbonate, over a range of pH and temperature values. Broadly speaking, passive films can be produced on copper in the absence of chloride and low temperatures (i.e., 25°C) for pH < 9. As temperature or chloride are increased, or as pH or carbonate are reduced, passive conditions are lost, and active, general corrosion is favoured. At expected repository conditions, where groundwater is dominated by chloride and temperatures exceed 75°C (i.e., during the oxic period), there is a significant safety margin of at least 2.5 pH units between expected repository pH and the conditions under which passive films can be formed. Work is ongoing to enhance the statistical significance of these data sets.

The long-term localized corrosion behaviour of copper has also been extensively studied in the Swedish / Finnish nuclear waste management programs. They predicted the depth of localized corrosion based on pitting factors and an analysis of empirical pitting data from archaeological artifacts subject to long-term burial in natural environments. Extreme-value statistics have also been applied to estimate the maximum pit depth on a container as a function of exposure time in the repository (King 2006). A pit propagation model was developed for reducing conditions, assuming the pit growth was limited by the transport of HS⁻ to the copper surface.

Based on the various measurements and models summarized above, it is clear that a copper corrosion barrier in a deep geological repository will not undergo classical pitting corrosion, but only a surface roughening. This process may necessitate provision for a maximum of 0.1 mm of additional copper wall thickness to account for any wall loss due to general oxic corrosion.

5.4.3.3.4 Stress Corrosion Cracking

Considerations for stress corrosion cracking (SCC) of the copper shell have been extensively explored in Kwong (2011). The occurrence of SCC requires a susceptible metal to be exposed to sufficient tensile stress and an active SCC agent. Copper is known to be susceptible to SCC in environments containing ammonia, nitrite ions, acetate, or, possibly, high concentrations of

sulphide. Studies focused on SCC have concluded that the SCC of copper requires the prior formation of a thin oxide or tarnish film. When this film does not form, SCC is not observed.

While SCC agents are not normally found in natural groundwater, they can be introduced by either mining or microbial activities. Numerous tests have, therefore, been performed to assess the SCC behaviour of copper in nitrite-, ammonia- and acetate-containing environments. Results indicate that copper SCC susceptibility would decrease with decreasing concentrations of the SCC agents. These studies also suggest a threshold concentration level for each agent below which SCC would not occur. Also observed in these studies is the inhibiting effect of chloride on copper SCC in nitrite, ammonia and acetate environments; the SCC susceptibility decreases with increasing chloride concentration. The ability of chloride to inhibit SCC also appears to be enhanced by elevated temperatures, as exhibited in tests conducted at 100 to 130°C (in nitrite only and nitrite/chloride solutions). This effect can be attributed to the ability of chloride ions to promote general dissolution of copper, which results in more uniform corrosion (see Section 5.4.3.3.3).

Furthermore, tensile stress is needed on a material to initiate SCC. However, the UFC design has been optimized to ensure that stress patterns are predominantly compressive. This design is significantly improved over UFCs that utilize flat heads, as the latter contains regions with tensile stress that result during loading to conservative glacial conditions (i.e., > 40 MPa).

In summary, research results have suggested SCC under aerobic conditions in a deep geological repository is unlikely, as the pre-requisite conditions of corrosion potential, interfacial pH, tensile stress and concentration of SCC agents do not exist simultaneously at the container surface. According to mechanistic arguments, there is also no evidence to indicate that SCC of copper is possible under anaerobic conditions at the sulphide levels expected at the container surface. Based on the nature of the repository environment, SCC does not appear to be a threat to the integrity of a copper used fuel container. Despite the low risk of SCC on copper, suitable engineering procedures can be effectively applied to further minimize the probability of SCC. This will include ensuring that the level of airborne ammonia and nitrite formed during blasting operations are controlled (i.e., below the threshold concentration) in order to preclude the possibility of cracking.

5.4.3.3.5 Microbially Influenced Corrosion

The historical microbially influenced corrosion (MIC) program is summarized in Kwong (2011). Similar to other engineering materials, copper is susceptible to this type of corrosion should the environment be hospitable to microbes that produce corrosion-causing species. MIC is largely mitigated within the DGR by ensuring that the water activity of the system is ≤ 0.96 near the container (i.e., within the bentonite buffer). During the evolution of the repository, the water activity will remain low, from the early dry period through to the saturated period, largely owing to the very high average compaction of the bentonite material (> 1,600 kg/m³) and the nature of the bentonite. As placed, bentonite contains no available water, owing to the modest amounts used in manufacturing and the high suction potential of the material (King et al. 2010). Subsequently, incoming water is tightly bound by the confined material as it swells against the host rock. Section 5.5 describes buffer performance comprehensively, including the rationale for excluding near-field microbial growth as a corrosion mechanism.

In principle, far-field microbial metabolic by-products may affect the SCC behaviour of copper, as microbial activity may form SCC agents, ammonia, nitrite, and acetate ions that traverse the buffer toward the UFC. These species are not likely to be produced in sufficient quantity to affect SCC (see Section 5.4.3.3.4), and the UFC is not under sufficient stress. With respect to MIC, another species often considered is HS^- produced by the reduction of sulphate by sulphate-reducing bacteria. This reaction occurs under anaerobic conditions and requires the presence of simple organic molecules or H_2 as electron donors. Without the formation of biofilms on the container surface, which are prevented via the highly-compacted bentonite material, the only form of MIC possible is that due to the diffusion of remotely-produced metabolic by-products through the bentonite to the container surface. Sulphide ions produced at a location away from the container surface must diffuse through the bentonite sealing materials to have any effect on container corrosion. The maximum corrosion rate is, therefore, limited by the rate of diffusion of sulphide (HS^-) to the container surface, a continued supply of which is required to sustain MIC.

To assess potential damage from sulphide ingress toward the UFCs, the NWMO has modelled the diffusion-based flow for a continuously produced source of sulphide in the far field (Briggs et al. 2017a). Sensitivity studies have been completed for values ranging from the reference groundwater value of $1 \mu\text{mol/L}$ (0.034 mg/L or 34 ppb) to beyond $300 \mu\text{mol/L}$ (10 mg/L or 10 ppm), and the relationship between concentration and corrosion rate has proven to be linear, owing to the Fickian diffusion. However, because of the complex shape of the UFC and buffer box, MIC is not uniform; rather, it tends to concentrate its effects on the ends of the UFCs. This result is readily visible in Figure 5-12, which normalizes low flux areas against the highest region (on the end cap, from Briggs et al. 2017b).

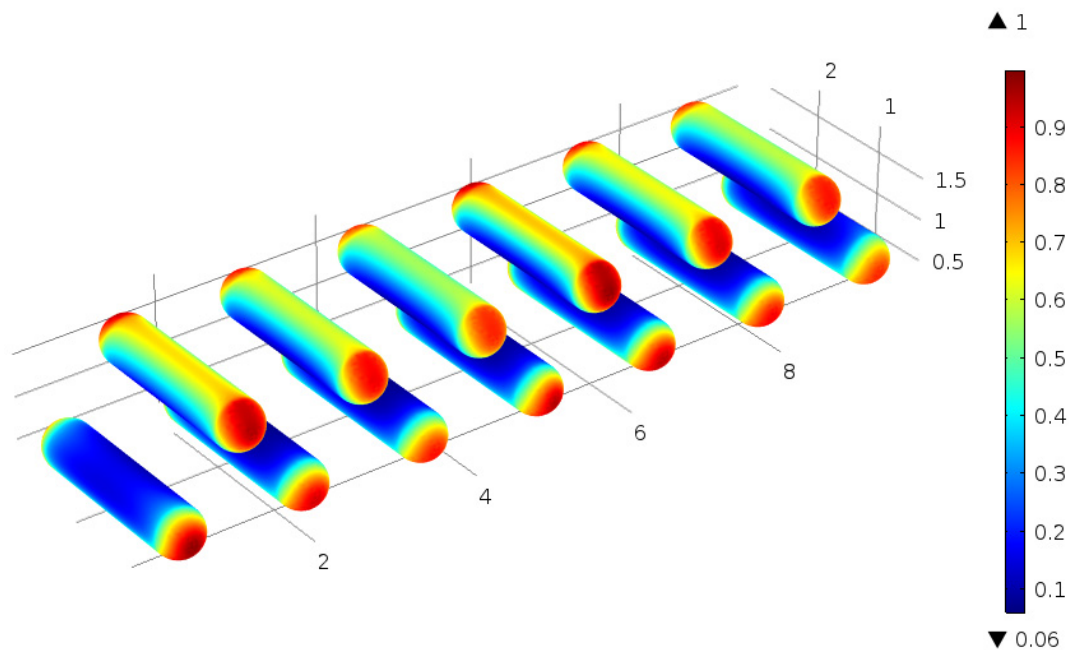


Figure 5-12: Normalized Diffusive Sulphide Flux Ratio for UFCs in Placement Room for a Uniform Background Concentration of Sulphide in the Host Rock

From these results, a simplified equation can be derived for the maximum corrosion rate observed in a placement room:

$$CR_{MAX}, \text{ nm/a} = 0.8[\text{HS}^-], \text{ mg/L} \quad (5-13)$$

Thus, for a groundwater sulphide concentration of 1 $\mu\text{mol/L}$ (i.e., 0.034 mg/L or 34 ppb), the maximum corrosion rate from sulphide diffusion would be 0.026 nm/a, while values of 340 ppb or 3400 ppb produce 0.26 nm/a and 2.6 nm/a, respectively. Over one million years, the wall loss from sulphide corrosion from the scenario of 1 $\mu\text{mol/L}$ sulphide will be just 0.026 mm, a value hardly discernable from the wall loss assumed due to oxic corrosion/localized corrosion of 0.27 mm. This feature can be seen in Figure 5-13, which presents the remaining copper thickness after corrosion as a function of time for a period up to one hundred million years.

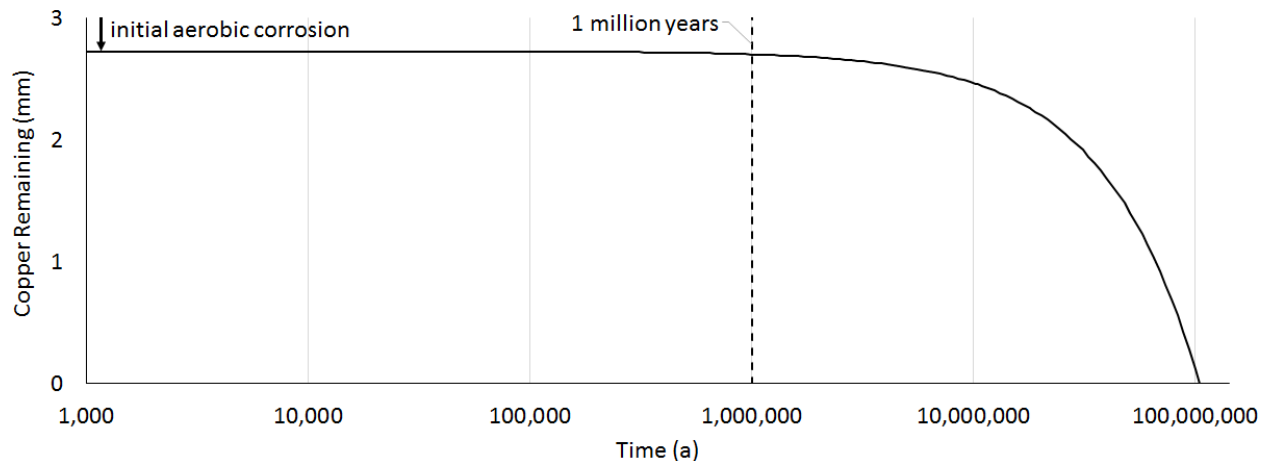


Figure 5-13: Reduction in Thickness of Copper Due to Reaction with Groundwater Sulphide

5.4.3.4 Summary

Research work over the past 30 years has established a good understanding of the long-term performance of copper used fuel containers in a deep geological repository.

In the environments anticipated in sedimentary rock, copper will begin to corrode under early atmospheric conditions, provided the relative humidity is above 50-70%. The rate and mechanism of corrosion will be affected by the presence of atmospheric contaminants, such as SO_2 and NO_2 , as these species potentially acidify the surface. Maximum damage from these processes is expected to be 70 μm ; an additional factor of 100 μm may also be conservatively considered to account for the minor roughening that may occur concurrent with this process. An additional 100 μm allowance is included for radiolysis-related corrosion.

Stress corrosion cracking is highly unlikely, owing to the lack of the pre-requisite conditions for SCC (the required threshold concentration of SCC agents, a suitable interfacial pH, tensile stress and the required corrosion potential on the copper surface).

Microbially influenced corrosion of copper will be controlled by the use of compacted bentonite around the copper container (and, in some rock types, the high salinity of native groundwater) to suppress microbial activity in the near field and to limit the migration of any corrosive agents produced by microbial activity in the far field. Nonetheless, trace sulphide concentrations of 1 $\mu\text{mol/L}$ account for far-field microbial activity that may impact the UFC.

Although there have been measurements of water acting as an oxidant for copper, the available evidence is not entirely reproducible. Regardless of such uncertainty, there is significant evidence that the hydrogen produced from a copper-water interaction, or steel corrosion, within the repository would compel any such mechanism to be self-limiting, and thus would not be a significant corrosion mechanism within a repository. In addition, any early effects of water corroding copper would be overwhelmed by the interaction of copper and microbiologically-produced sulphide over the long term. Nonetheless, the low rate of this reaction will provide for an extremely long-lived container.

5.4.4 Effects of the Environment on Containers with Defects in the Copper Coating

Containers for a repository will be manufactured according to a process that includes careful fabrication and a series of inspections to preclude significant defects, as described in Section 4.3.1. Failures during manufacturing or quality-assurance practices, while unlikely, present the risk for undetected defects within copper coatings. In addition, although strict protocols and procedures for handling the UFCs will be in place, there is a non-zero probability that a UFC may be damaged during placement, resulting in a copper-coating defect.

Coating defects include the subset of through-copper defects, where the defect extends across the full thickness of the copper coating, exposing the underlying steel to the environment. Probability and consequences of defects are described in the following sections.

5.4.4.1 Impacts of Coating Defects

In general, defects within the coating that do not expose the steel do not significantly impact the performance of the UFC. From a corrosion processes perspective, very little wall loss is expected over 100,000 or even 1,000,000 years (i.e., well below <0.5 mm, see Section 5.4.3.3), which is similar to the conservative Non-Destructive Examination (NDE) detection estimate of 0.8 mm. Accordingly, very long-lived containers can be expected where coating damage does not expose the underlying steel.

In terms of quantifying damage, the impact of an undetected defect on the local corrosion rate will depend partly on the size and shape of the defect. Figure 5-14 proposes some examples of hypothetical defects in a nominal 3 mm copper coating. If a defect results in a locally thinner copper coating, then the steel beneath a defect may be exposed to groundwater earlier than Figure 5-13 suggests. Figure 5-15 and Table 5-4 present the time to exposed steel beneath a defect as a function of the defect size. Calculations assume that defects are oriented for maximum reduction in the local coating thickness.

These results show that any defects passing a quality inspection undetected would lead to exposed steel only after a period greater than 10 million years. Exposed steel upon placement in the repository would require a through-copper defect to pass quality inspection undetected.

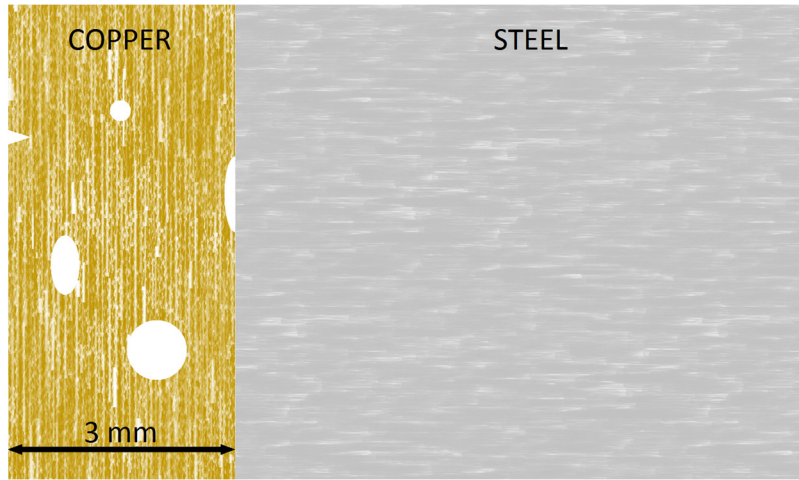


Figure 5-14: Hypothetical Defects in the Copper Coating

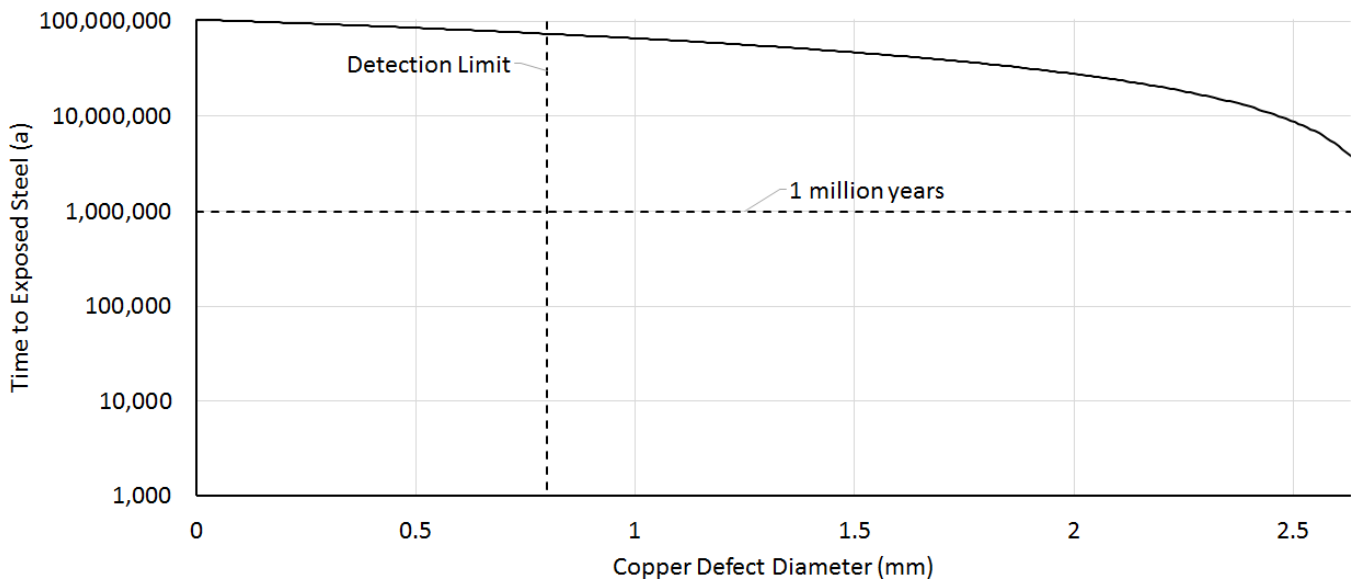


Figure 5-15: Time to Exposed Steel beneath Defects in a Nominal 3 mm Copper Coating

Table 5-4: Time to Exposed Steel beneath Defects in a Nominal 3 mm Copper Coating

Microbially Influenced Corrosion	0.026 nm/a
Corrosion = 3 mm	105 Ma
Time to Expose Steel, Defect = 0.8 mm	74 Ma
Time to Expose Steel, Defect = 2 mm	28 Ma

5.4.4.2 Impacts of Through-Copper Defects

Exposure of steel to the environment due to a through-copper defect would leave a (small) region of the container surface without protection from corrosion. As noted in Section 5.2.4, exposed steel can corrode throughout the entire life of the DGR, through a range of mechanisms. The very slow rate at which this process occurs in a DGR has led many countries, such as France and Switzerland, to select steel as their used container material, without any other corrosion barrier. Through a narrow defect in the copper coating, the steel corrosion processes are likely to be further slowed, as steel corrosion products are likely to plug the defect and inhibit contact with water (or oxygen). However, owing to the presence of copper directly on the steel (i.e., electrically connected), galvanic corrosion processes must also be considered for the oxic and anoxic periods (e.g. Standish et al. 2017).

5.4.4.2.1 Oxic Galvanic Corrosion

For galvanic corrosion to occur, one metal performs/catalyzes the cathodic electrochemical reactions, while the other metal performs/catalyzes anodic reactions. In the case of steel (iron) coupled to copper, oxidation of iron at the container breach would be enhanced if the very large intact copper surface could sufficiently support reduction reactions: either oxygen reduction during the aerobic period, or hydrogen reduction during the long anaerobic period.

Experiments conducted by Smart et al. (2004, 2005) have examined both conditions and measured galvanic currents – with the copper behaving as a cathode and the iron behaving as an anode. In aerated conditions, galvanic corrosion rates of iron (coupled to copper) are as high as 100 $\mu\text{m/a}$. Other research has revealed that copper-steel couples in aerated seawater can cause an enhancement in corrosion of steel (Chen et al. 2007). However, the actual depth of corrosion from this process would be significantly limited by the volume of oxygen available in the repository.

Competing with the galvanic couple during the oxic period is the copper oxidation mechanism (Section 5.4.3.3). While this reaction is not as energetically favourable as the galvanic couple that sees steel oxidized and oxygen reduced on copper, it does not require energy to transfer electrons between the metals or ionic species through the solution. As a result of these energy losses, galvanic couples typically have a small range over which they affect the system – for the UFC described above, this would imply that corrosion damage to the steel from the oxic galvanic couple would be very small compared to the anoxic corrosion of steel that would follow once oxygen is depleted from the system.

5.4.4.2.2 Anoxic Galvanic Corrosion

Smart et al. (2005) measured galvanic coupling currents in a deaerated system and values were much lower: typically $0.1 \mu\text{m/a}$ at 30°C and $1 \mu\text{m/a}$ at 50°C . These values are no different from those measured for iron corroding in deaerated groundwater, where water is reduced at the same steel interface at which steel is oxidized. In effect, the copper couple does not alter the corrosion properties of iron in this medium. The interpretation of this result is that the couple between iron and copper does not sufficiently polarize the copper negatively to support enhanced water reduction (King et al. 2010). Accordingly, the copper would be largely inactive in the context of the iron corrosion process.

The low importance of galvanic corrosion is also supported by results from the SKB Minican experiment. Post-test examination (of the first experiment after 4 years in-situ) has indicated extensive corrosion by sulphide present in the groundwater, but no evidence of galvanic corrosion (Smart et al. 2012).

5.4.4.2.3 Anaerobic Corrosion of the Steel Vessel through a Defect in the Coating

Where water is in contact with the steel, Reaction (5-4) will occur forming an iron corrosion product and, in the absence of oxygen, hydrogen. An amorphous or poorly crystalline solid would be likely to form first, which would gradually transform into a more crystalline phase, likely magnetite, and possibly siderite should sufficient carbonate be carried into the defect, as discussed in Section 5.4.4.3.

Initially, iron corrosion products would form only on the outside surface of the steel (within the coating defect). Literature values for the anaerobic corrosion rate of steel vary over a wide range, between 0.1 and $50 \mu\text{m/a}$. The corrosion rate in the defect likely would be at the lower end of the range, given that the water would be chemically buffered by clay, and given that the water would be supplied at a limited rate to the steel; this same limitation would likely mitigate any radiolysis reactions that could potentially impact corrosion. Among other factors, the water ingress would be restricted by 1) low permeability of the bentonite clay around the container, 2) the small aperture of the defect in the copper coating, which may be blocked by swelling bentonite, and 3) slow transport through the porosity of the corrosion products filling the through-copper defect.

5.4.4.3 Modelling Steel Corrosion beneath a Through-Copper Defect

If defects in the copper coating lead to exposed steel, then groundwater will begin to corrode the exposed steel and may eventually perforate the wall of the container. The time required for groundwater to perforate a container will depend on the thickness of the steel wall (Figure 5-16) and on the steel corrosion rate.

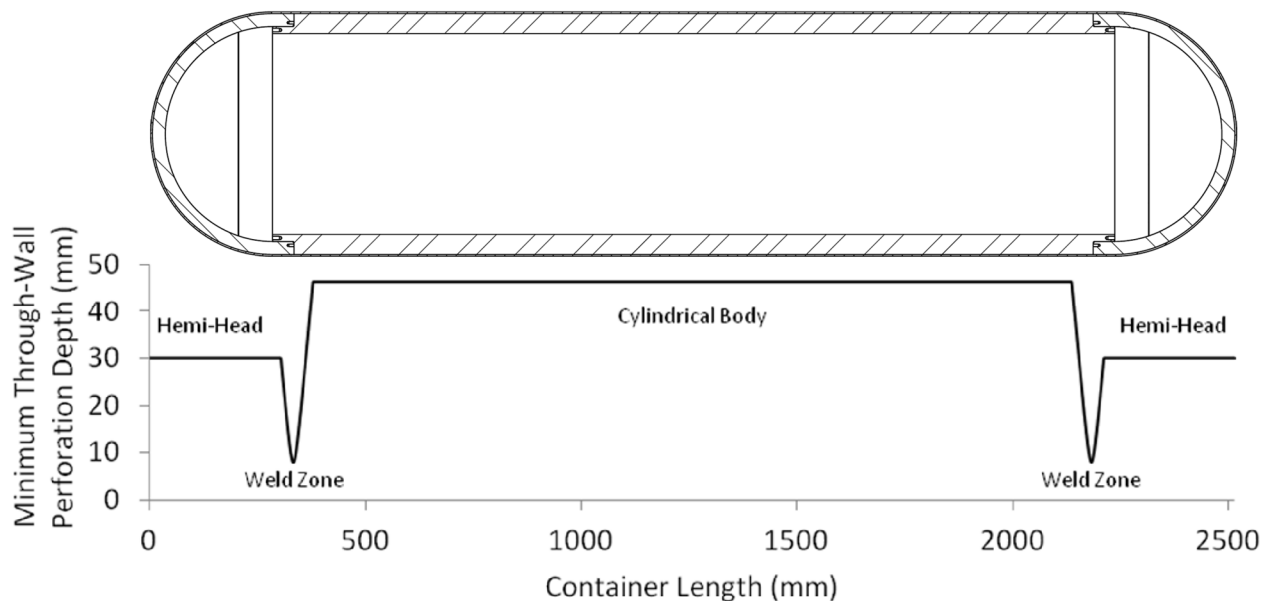


Figure 5-16: Minimum Corrosion Depth for Through-Wall Perforation of Steel Container

As described above, the UFC is protected by a continuous layer of copper. Although the container manufacturing and inspection processes are under development, presently there is no basis to assume there are any locations across the container surface where an undetected copper defect is more or less likely to occur.

Sections of the container wall have different thicknesses. From the information provided in Figure 5-16:

- 70% of the container surface, corresponding to the container body, requires 46.2 mm of corrosion to perforate the steel;
- 25.4% of the container surface, corresponding to the heads, requires 30 mm of corrosion to perforate the steel; and
- 4.6% of the container surface, corresponding to the weld region or zone within a few mm of the weld, requires something less than 30 mm of corrosion to perforate the steel (the partial-penetration weld itself presents the minimum wall thickness of at least 8 mm and accounts for less than 1% of the container surface).

The steel corrosion models used by the NWMO were developed by King (2013). Corrosion rates are temperature-dependent, and the calculations discussed here use the container surface temperatures determined by Guo (2018).

As noted above, the postclosure repository environment will become anoxic within a relatively short time. Under these conditions, magnetite is the likely corrosion product, particularly if the system is carbonate-limited or only partially saturated. The rate of magnetite-generating corrosion is based primarily on work by Newman et al. (2010) and passivation of the steel is

implicit. Siderite may be the primary corrosion product if the system has sufficient carbonate available and is fully saturated. The rate of siderite-generating corrosion is based on literature values (King 2013) and passivation is implicit. Rates for both forms of corrosion are shown in Figure 5-17, based on the container temperatures provided in Figure 5-3. Siderite-generating corrosion is much faster than magnetite-generating corrosion – more than 10 times faster if temperatures are below $\sim 40^{\circ}\text{C}$. As per Figure 5-3, the temperature becomes less than 40°C around 14,000 years postclosure.

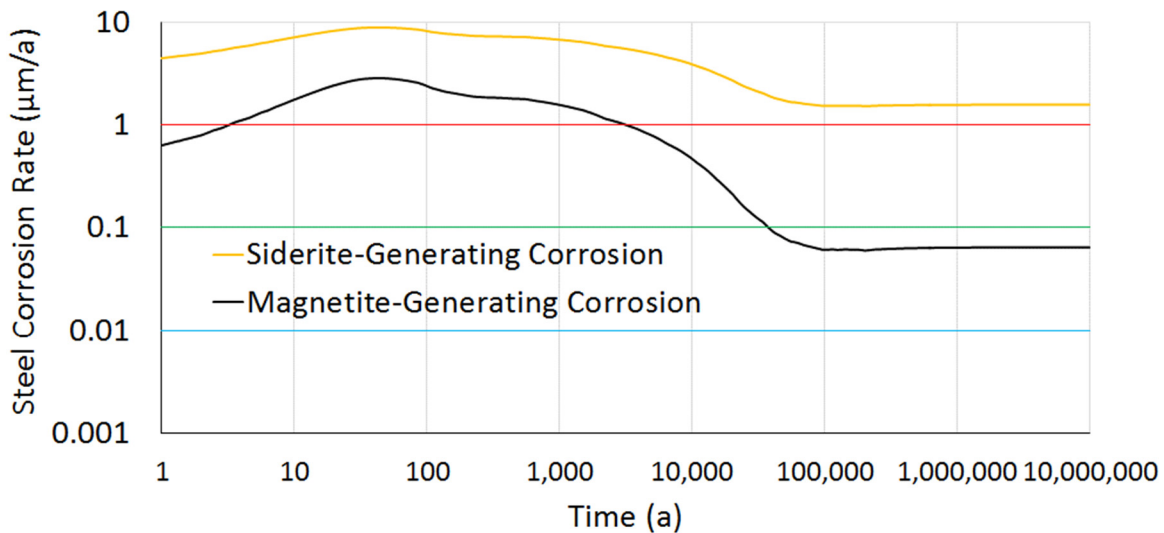
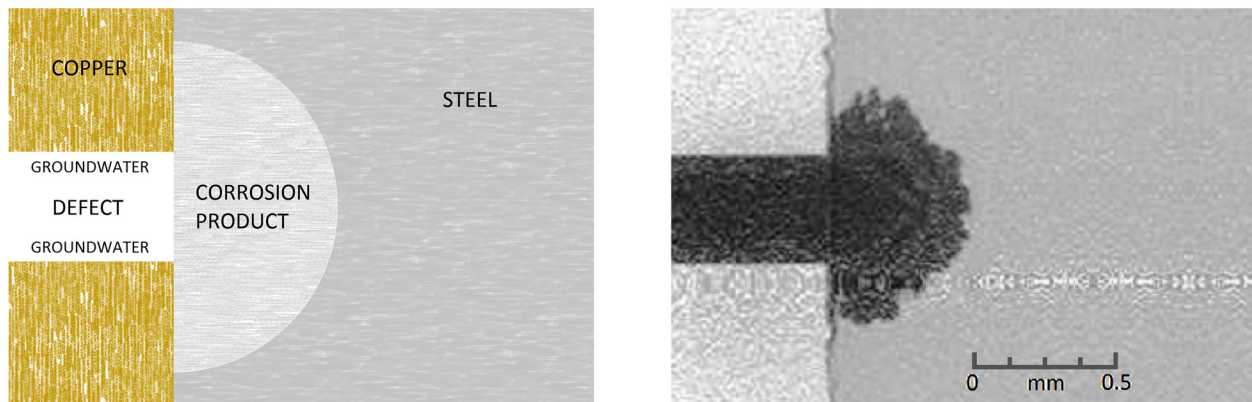


Figure 5-17: Evolution of Steel Corrosion Rates

The steel corrosion models developed by King (2013) apply to an open surface with no protective copper coating, referred to here as open-surface corrosion. The models consider a corrosion front advancing uniformly through steel, where the corrosion product steadily suppresses the corrosion rate. These models may be adapted to reflect corrosion through a defect in the copper coating, referred to here as defect corrosion. Figure 5-18 illustrates how open-surface corrosion differs geometrically from defect corrosion: the corrosion front is expected to advance radially from the defect, resulting in an expanding hemisphere of corroded steel. This is supported by the micrograph included in Figure 5-18, presenting early results from laboratory experiments assessing defect corrosion of copper-coated steel.



Note: The left panel represents a conceptual illustration and the right micrograph shows early results from laboratory experiments that have been accelerated by utilizing a free-flowing solution, purged with oxygen.

Figure 5-18: Illustration of Defect Corrosion

Assuming the material properties of the corrosion product (bulk porosity, ion diffusivity, etc.) are the same under open-surface and defect corrosion, it is then reasonable to infer that transport of the components of the corrosion reaction becomes dependent on the size of the defect. In this case, the rate of defect corrosion can be shown to relate to open-surface corrosion according to the following equation (Kremer 2017):

$$\frac{\text{Defect Corrosion}}{\text{Open-Surface Corrosion}} = \frac{r_0}{(r - r_0)} \quad (5-14)$$

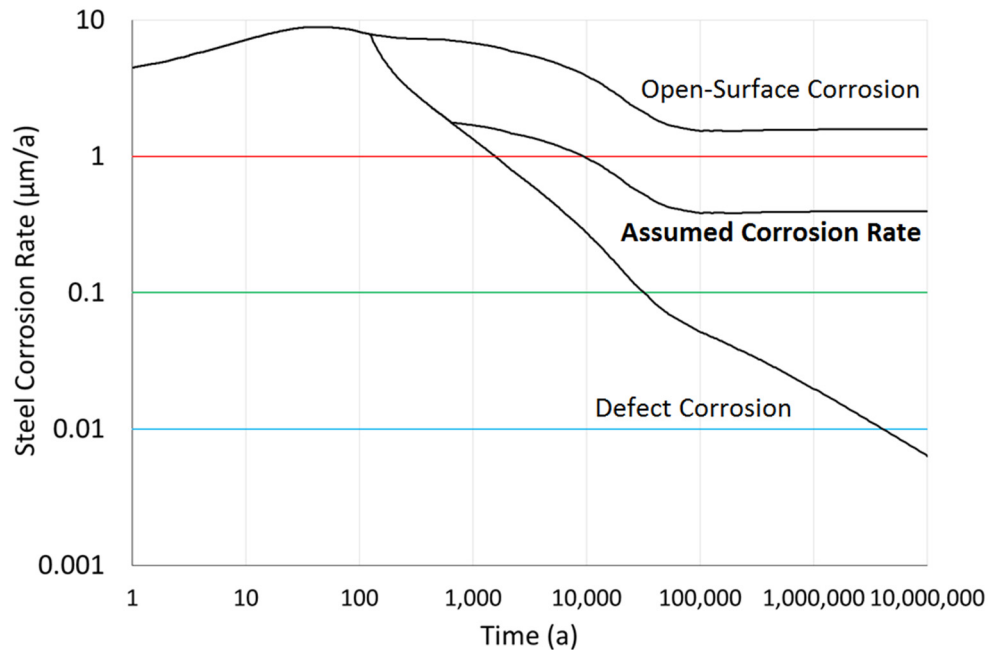
where r_0 is the radius of the defect and r is the radius of steel lost to corrosion.

This relationship includes several conservatisms:

- For $r \leq r_0$, calculations assume open-surface corrosion;
- Corrosion products grown within the protected environment of the defect may be more homogeneous and, consequently, more resistant to transport of reaction components;
- Expansion of corrosion product relative to corroded steel, confined and compressed between steel and copper boundaries, may increase corrosion-product density and further limit transport; and
- Even if sufficient carbonate is available, this configuration may inhibit siderite-generating corrosion.

In addition, the calculations for defect corrosion presented here respect the lower bounds imposed on the open-surface corrosion models (King 2013); that is, where defect corrosion predicts lower corrosion rates, the assumed corrosion rate is never lower than the lower bound for open-surface corrosion. This addresses the uncertainty implicit in modelled defect corrosion rates not yet confirmed experimentally. Corrosion model calculations for siderite-generating corrosion are shown in Figure 5-19, comparing open-surface corrosion and defect corrosion

with the (conservative) assumed corrosion rate used here. Calculations assume a 1 mm diameter through-copper defect.



Note: This figure illustrates siderite-generating corrosion.

Figure 5-19: Adaption of Open-Surface Corrosion Models for Defect Corrosion

Figure 5-20 presents the time required to perforate the different thicknesses of steel along the length of the container wall (see Figure 5-16). Table 5-5 provides a summary of perforation times. Depending on the modelled steel corrosion rate and the thickness of the steel wall, the time required for groundwater to perforate a container varies from as short as 1,100 years to well over 10 million years.

It should be noted that these calculations include corrosion rates driven by elevated temperatures associated with the first few thousands of years postclosure. As discussed above, for exposure of steel beneath a defect in the copper coating to occur within one million years, a fairly large defect, greater than 2 mm, as well as elevated groundwater sulphide concentrations, would be required. The steel corrosion calculations presented here assume exposed steel upon placement of containers in the repository. This would require a through-copper defect in the copper coating to pass a quality inspection undetected, which may be unrealistic.

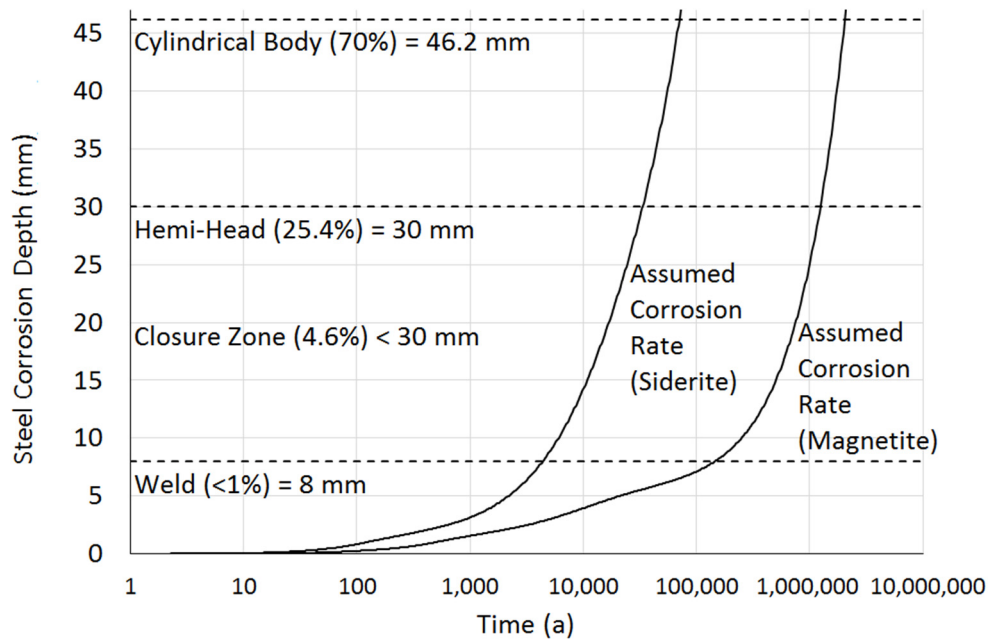


Figure 5-20: Evolution of Steel Corrosion Depth

Table 5-5: Time for Steel Corrosion to Perforate the Container Wall

	Cylindrical Body (46.2 mm) 70% Container Surface Magnetite- / Siderite- Generating Corrosion	Hemi-Head (30 mm) 25.4% Container Surface Magnetite- / Siderite- Generating Corrosion	Weld (8 mm) < 1% Container Surface Magnetite- / Siderite- Generating Corrosion
Open-Surface Corrosion	530 ka / 8.6 ka	280 ka / 5 ka	7.8 ka / 1.1 ka
Defect Corrosion	>10 Ma / 1.3 Ma	>10 Ma / 510 ka	700 ka / 11 ka
Assumed Corrosion Rate	2 Ma / 71 ka	1.3 Ma / 33 ka	140 ka / 4.4 ka

5.4.4.4 Stresses in the Copper Defect As a Result of Corrosion

As the iron that is exposed through the copper defect is corroded, it will form corrosion products. Iron corrosion products are less dense than the metal itself and therefore take up more volume. As a result, the formation of corrosion products in a confined space has the potential to exert a force on the adjacent solids. This effect can be important in the case of rebar rusting in concrete structures. However in this case the resultant stresses would have little effect on the steel vessel, due to its high mechanical strength. Similarly, while it has less mechanical

strength, the copper coating is integrally bonded to the steel; thus it is likely that the surrounding clay buffer would deform more easily if there is a volumetric expansion from corrosion products.

However, there are compelling reasons for the conclusion that there will not be a volumetric expansion as a result of the formation of iron corrosion products, as there is experimental evidence to that effect (Smart et al. 2003, 2006). Specifically, during analysis of stresses produced during anaerobic corrosion over a two-year period, no detectable expansion was observed for bentonite-equilibrated groundwaters under compressive loads (Smart et al. 2006). In addition, the anaerobic corrosion products were easily deformable and were incapable of producing expansion under simulated repository conditions. Only for aerobic conditions, and low applied loads, were expansions measureable due to corrosion products.

Similarly, after 4 years in-situ, observations from the first MiniCan experiment indicate no expansion in the SKB outer-copper shell due to corrosion of the cast iron insert, and there is apparent extrusion of iron corrosion products through the defect (Smart et al. 2012). As a result, it is likely that copper coating deformation at a defect would occur very slowly, if at all.

5.4.4.5 Failure of the Steel Vessel during Corrosion at a Defect in Copper Coating

During corrosion of steel below a coating defect, it is expected that there will be a gradually increasing volume of wall loss of steel. Should the defect be a narrow cylindrical pore, the damage would likely resemble a growing hemispherical region, as per Figure 5-18. Because the narrow pore would act as a bottleneck, limiting the amount of water reaching the hemisphere, overall corrosion would be slow, but the result would be a gradual widening of the defect in the steel vs. the initial defect in the copper. Eventually, the steel below the copper coating defect will sufficiently deplete via corrosion, or fail mechanically, and allow water to enter the container.

Owing to the slow rate of steel corrosion, this process may take many thousands of years. Once through-wall penetration occurs, it will permit corrosion to begin on the inside of the container on all of the steel components. This process will gradually thin the container wall, which will weaken it to mechanical loading; however, the incoming water will also equilibrate the interior and exterior pressure of the container. As a result, mechanical requirements for the container will be virtually eliminated, other than those associated with anisotropic loading. Regardless, interactions between the incoming water and the materials inside the “breached” container need to be considered for all scenarios considering hypothetical container breaches.

5.4.4.6 Corrosion and Deformation of the Zircaloy Cladding

At the time of placement in a repository, virtually all of the used fuel elements will have intact Zircaloy cladding. A few of the cladding sheaths would have become defective during their use in a reactor. Historical estimates of this number ranged from approximately 0.001 to 0.01% of fuel elements (Frescura and Wight 1979). More recent statistics from 1994 to 2006 indicate that upon discharge, less than 0.015% of CANDU fuel bundles have minor damage or defects such as pinhole failures in the fuel sheaths (IAEA 2010). Some others may have developed defects during post-reactor storage, transportation, or packaging into containers. In a breached container, one of the most significant changes in the used fuel bundles over time will be mechanical failure of the cladding, mainly in association with corrosion of the steel vessel. In

addition, the cladding will be subjected to hydrogen embrittlement, corrosion, and creep, as described below.

Over time, hydrogen gas would be produced inside a breached container by two separate processes: the anaerobic corrosion of steel and the radiolysis of water. Hydrogen-induced cracking is a potential failure mechanism for Zircaloy cladding. Studies of the durability of used fuel bundles in dry or moist air have found no evidence of cladding failures (Lovazic and Gierszewski 2005). Given that significant partial pressures of hydrogen gas would not develop in a container until saturation of the repository had occurred, lifetimes of the Zircaloy cladding in a breached container could exceed thousands of years.

On observable time scales, the uniform corrosion of Zircaloy cladding is negligible (likely between 1 and 5 nm/a, with an upper limit of 20 nm/a), even in contact with water, which is due largely to the corrosion resistance of a passive oxide film on the Zircaloy surface (Shoesmith and Zagidulin 2010).

In a breached container, pitting and crevice corrosion of cladding would be inhibited by the rapid consumption of oxidizing agents (residual oxygen and radiolysis products) by the iron and copper container materials. In addition, iodine-induced stress corrosion cracking would be inhibited because most of the iodine in the fuel gap in CANDU fuel exists as cesium iodide, preventing it from forming the zirconium iodides that are thought to be the chemical precursors to stress corrosion cracking in Zircaloy.

Using the above values, a general corrosion lifetime for a 0.5 mm cladding is calculated to exceed 25,000 years when presuming the highest corrosion rate of 20 nm/a; a more realistic value of >100,000 years is calculated for expected corrosion rates (i.e., those at or below 5 nm/a).

5.4.4.7 Dissolution of the Used Fuel Matrix

After the cladding is breached and the fuel pellets exposed to water, the next barrier against radionuclide release is the UO_2 fuel matrix, which contains most of the radionuclides and has a very low solubility. Dissolution of the UO_2 matrix of the used fuel would progress according to two general methods: oxidative dissolution (i.e., corrosion) and chemical dissolution. Radiolysis of water in contact with the fuel pellets would produce oxidizing conditions at or near the used fuel surface, contributing initially to oxidative dissolution of the UO_2 . If water is able to contact the fuel while radiation fields are high, this process would tend to promote the dissolution of the used fuel at a higher rate than would be expected solely on the basis of the chemical solubility of UO_2 in the near-field porewater. The production rate of oxidants by radiolysis would decrease with time as the strength of the radiation field decreases (Gobien et al. 2018).

At the fuel-water interface, the alpha dose rate exceeds the gamma and beta dose rates for most of the fuel history (Figure 5-21) and is the main contributor to radiolysis, producing molecular oxidants such as H_2O_2 . Other potential sources of oxidants, such as any O_2 trapped inside the container when it was sealed, would already have been consumed by Fe and Cu corrosion processes before the fuel cladding was breached, because these corrosion reactions are much faster than the reaction with UO_2 . In principle, the radiolytically produced oxidants would be consumed by reaction with container materials, rather than by reaction with used fuel; however, for alpha radiolysis, the oxidants would only be produced within

20 μm of the fuel-water interface and would have difficulty diffusing through openings in the cladding to react with container materials.

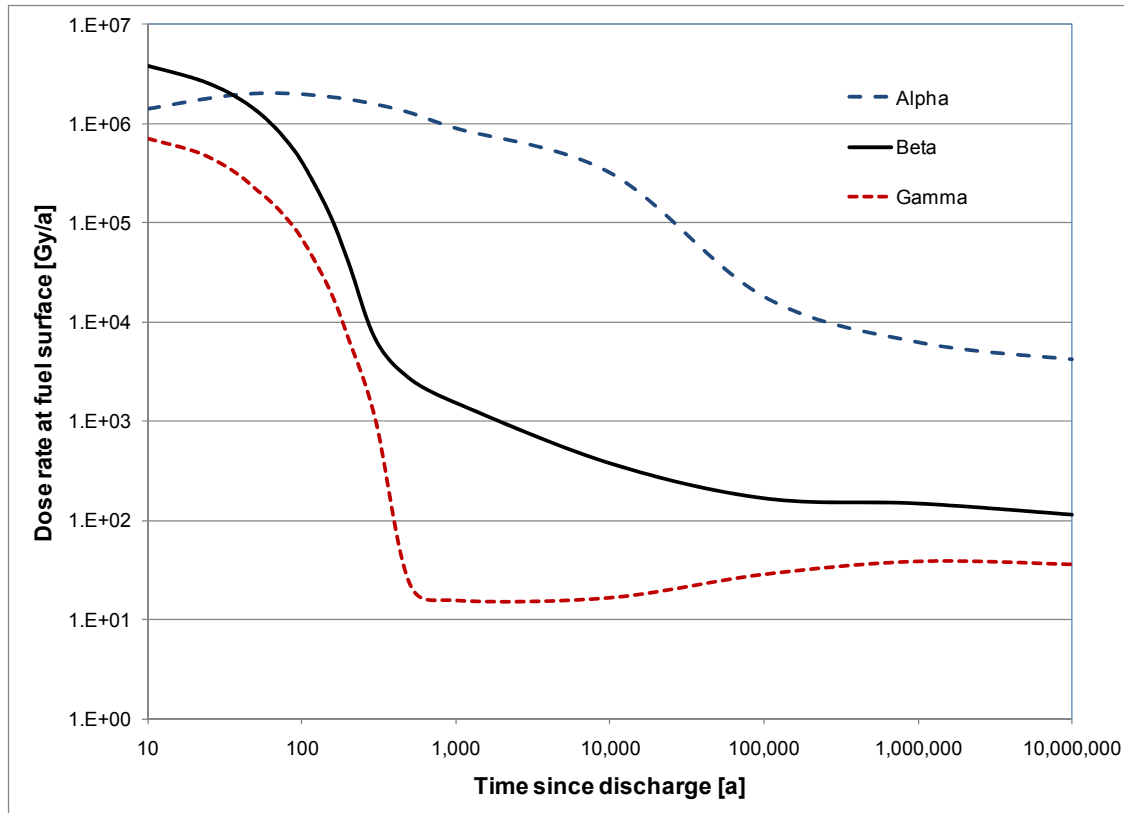


Figure 5-21: Radiation Dose Rate in Water at the Fuel Surface (220 MWh/kgU burnup)

Oxidative dissolution of the fuel continues as long as the alpha radiation field is sufficiently high. However, the actual dissolution rate of the fuel decreases over time, as the alpha radiation field decreases due to decay. Experiments and mechanistic models have been developed to describe this corrosion rate, and results indicate that the dissolution of the used fuel would take more than one million years (Gobien et al. 2018).

Furthermore, in UO_2 and used fuel dissolution experiments, the dissolution rate decreases by several orders of magnitude in the presence of even modest hydrogen gas pressures (Shoesmith 2008), which would certainly be present due to corrosion of the iron vessel. A number of mechanisms have been either demonstrated or proposed to explain these effects, all of which involve the activation of hydrogen to produce the strongly reducing $H\cdot$ radical – which scavenges radiolytic oxidants and suppresses fuel oxidation and corrosion (Shoesmith 2008).

After the alpha radiation field has decreased substantially after many thousands of years, chemical dissolution of the fuel proceeds according to the reaction,



under the anaerobic conditions expected in the repository. This reaction occurs very slowly, as illustrated by the age of uraninite ore (largely UO_2) deposits, such as those in northern Saskatchewan (Alexandre et al 2009).

5.4.4.8 Radionuclide Release from the Fuel Pellets and Cladding

Extensive studies of the interactions between used fuel and groundwater have established that radionuclide release from the used fuel occurs by two main processes. Instant release refers to the initial and comparatively rapid release of a small fraction (typically a few percent) of the inventory of a selected group of radionuclides that are either very soluble (such as ^{137}Cs , ^{129}I , ^{14}C and ^{36}Cl) or gaseous (such as Xe), and that are residing in the fuel sheath gap or at grain boundaries which are relatively quickly accessed by water. The second and slower release process comprises release of radionuclides from the UO_2 fuel matrix as the matrix itself corrodes or dissolves, and is referred to as congruent dissolution.

The instant release fractions for various important radionuclides in used CANDU fuel are given in Gobien et al. (2018). Note that the use of the term “instant release” with reference to the gap and grain boundary inventories is a simplification. In reality, it would take a finite time for water to penetrate into the grain boundaries and for the radionuclides located there to diffuse out. However, compared to the much longer time required for dissolution of the UO_2 matrix itself, grain boundary releases are so much faster that they can be considered “instantaneous”. Therefore, in conceptual models of radionuclide release, both locations – the gap and grain boundary inventories – are considered to contribute to the instant release fraction. Ferry et al. (2008) have shown that the instant release fractions do not change with time, with processes such as athermal diffusion of radionuclides induced by alpha-particle recoil displacements having negligible effects.

In addition to the bulk of the radionuclides in the used fuel pellets, there would be a small quantity of radionuclides present in the irradiated Zircaloy from neutron activation. These radionuclides are generally distributed uniformly through the cladding and would only be released as the cladding itself dissolves (C-14 may be concentrated within the zirconium oxide film, Gobien et al. 2018). Zircaloy is corrosion-resistant in water due to the stability of its oxide coating, and thus would corrode at a slow rate (as described in Section 5.4.4.6).

5.4.4.9 Fate of Released Radionuclides

As radionuclides are released to solution, some would become oversaturated and secondary radionuclide-bearing phases would precipitate on the fuel surface (e.g., ThO_2) or on other surfaces nearby, such as those provided by metal corrosion products. Aside from the low overall amount of such nuclides in a container, it is expected that their concentration in a precipitate would be diluted by the co-precipitation of other elements. Precipitation of a large mass of fissile nuclides, in particular, would be hindered by the intergrowth of such mixed-isotope precipitates along with iron corrosion products or buffer clays.

The radionuclides that remained in solution as aqueous species, and solids suspended in colloidal form, would diffuse through the various metal corrosion products inside the container. The corrosion products would also provide a surface for sorption of many of the radionuclides. In some cases, the sorption would be irreversible because the radionuclides would be incorporated into the crystal lattice of the corrosion product (i.e., if it undergoes a transformation to a more stable solid phase).

Dissolved radionuclides would diffuse by a tortuous path through what was left of the container, through the low-permeability sealing materials, and finally enter the host rock surrounding the repository. Migration of radionuclides away from the repository, and their transport rate through the geosphere as a whole, would be controlled by the local hydrogeological conditions. For the current hypothetical geosphere, groundwater velocities are low and transport is diffusion controlled. Radionuclides in colloid form or sorbed to colloids would be filtered by the buffer and would not reach the geosphere.

5.4.4.10 Summary

The postclosure safety assessment presented in Chapter 7 will consider a failure in the copper coating and inspection process that could lead to containers placed in the repository with small defects. Corrosion modelling results presented here suggest it may be reasonable and conservative to assume that defects passing a quality inspection undetected would lead to exposed steel only after more than 10 million years. Once steel is exposed to groundwater, corrosion model calculations find that the additional time required for groundwater to perforate a container may vary from as little as 1,100 years to well over 10 million years.

From these results, used fuel containers are expected to remain intact essentially indefinitely, with no releases (and no dose consequences) within the one million year timeframe of the postclosure safety assessment.

5.4.5 Confidence

Extensive corrosion experiments have been carried out to improve the confidence in the ability to predict the corrosion behaviour and lifetime of copper-coated used fuel containers in a deep geological repository in Canada.

Container Corrosion: Because of the extensive experimental database on the corrosion of copper, and the level of mechanistic understanding that has been developed over the past 30 years, in addition to the existence of natural and archaeological analogues, there is significant confidence in the prediction of the long-term corrosion behaviour of copper containers. Both the predictive models for corrosion processes that are expected to occur, such as uniform corrosion and localized surface roughening, and the reasoned arguments against those that are not thought to be possible, such as stress corrosion cracking, are robust. Where uncertainty exists, such as the mechanism and exact corrosion rate that describe copper corrosion in anaerobic water or brine solutions, these uncertainties do not compromise arguments for container integrity since the total corrosion possible from these processes is very small over the container design life.

The evidence from natural and man-made analogues builds confidence in the conclusions drawn from experimental and modelling studies. Man-made analogues, such as Bronze Age artifacts or more-recent anthropogenic objects (discussed in Chapter 9), also provide useful supporting evidence that copper corrodes slowly, even in near-surface aerobic environments. The existence of native metallic copper deposits indicates that, under certain environmental conditions, metallic copper is stable over geological time scales. The fact that the majority of copper deposits in the Earth's crust are in the form of sulphide minerals is also evidence of the potential role of HS⁻ species in the corrosion of copper containers. Although it is not a pre-requisite that the groundwater at repository depth be free of sulphide, as the programs in

Sweden and Finland demonstrate, there are clear advantages to selecting a site with little or no sulphide in groundwater, as appears to be the case in Canadian sedimentary rock.

Confidence in long-term predictions is supported by the robustness of those predictions and on the underlying information on which they are based. This confidence arises, for example, from achieving the same result from different modelling approaches. For example, the conclusion that the maximum depth of uniform corrosion is of the order of a few hundred micrometres is predicted by both simple mass-balance models (SKB 2011) and from detailed mechanistically-based reactive-transport modelling (King et al. 2008). These detailed reactive-transport models have been validated against experimental data and evidence from archaeological analogues (King et al. 2001).

Confidence also results from having a sound mechanistic understanding of corrosion processes. For example, the proposed mechanism to explain observations of local corrosion (Section 5.4.3.3.3) provides strong evidence that under repository conditions the localized corrosion of copper containers will take the form of surface roughening rather than pitting. This understanding is equally important for processes that are not considered likely to occur, such as stress corrosion cracking. The approach for stress corrosion cracking provides multiple lines of argument against this behaviour, and it is not considered feasible that all of the pre-requisite conditions for stress corrosion cracking would exist in the repository at the same time.

There are also multiple lines of argument for why MIC will have a minimal impact on the container (King 2009b, Sherwood Lollar 2011 and Wolfaardt and Korber 2012). However, uncertainties regarding the potential for microbial growth and activity under unsaturated conditions, and at component interfaces, requires further investigation. Because the possibility of remote microbial activity cannot be excluded, a corrosion allowance is made for this in lifetime assessments (Kwong 2011, Scully and Edwards 2013).

The multi-barrier repository system represents a robust system that is capable of withstanding upset or unexpected conditions whilst still maintaining a high degree of containment. For example, the predicted container lifetimes are insensitive to the groundwater salinity and, in fact, higher Cl⁻ concentrations promote uniform rather than localized corrosion (King et al. 2010, 2011a). Information from site investigations in sedimentary rock in Canada suggest that there is little or no sulphide in deep groundwaters (INTERA 2011). Experience from the Swedish and Finnish programs demonstrates that the combination of a copper container and dense bentonite buffer provides long-term containment even if sulphide were to be present at low concentrations. Similarly, there is no geological evidence that O₂-containing water has reached repository depths in the low permeability host rock formation in southern Ontario, even under glacial conditions (see Section 5.1.2.4).

Container Temperature: The container surface temperature is affected by the container power, placement method, chemical composition, water content and thickness of sealing materials, distance between containers, distance between the placement rooms and tunnels, etc. The thermal responses were successfully modelled and there is good confidence that the evolution of temperatures of the container surface and surrounding bentonite buffer materials can be well estimated by existing computer models.

Container Structural Integrity: To maintain long-term structural integrity during its design life, the UFC is designed to withstand an external isotropic pressure during the interglacial period, which

accounts for the 5 MPa hydrostatic pressure up to a 500 m depth, together with bentonite swelling. The container could also withstand an external pressure load during the glaciation period (which corresponds to a 3000 m thick ice sheet) with full load applied as hydrostatic head (i.e., no load carried by the rock matrix). These are conservative assumptions. While glaciation will be a significant load, the earliest site coverage due to an ice sheet would be thousands of years in the future (i.e., at least another 60,000 years from present).

The container would be subjected to uneven bentonite swelling loads during the transient period, before full water saturation, and also, possibly, after saturation (though to a reduced extent) because of density differences that do not entirely homogenize because of internal friction. It is expected that any such uneven swelling pressure loads would not cause container failure, based on the results of analyses for similar SKB and Posiva containers (Werme 1998, Raiko 2005). This will be verified by engineering analyses.

5.5 Long-Term Evolution of Buffer, Backfill and Seals

Each used fuel container will be placed within a buffer box, which will be surrounded by gap fill, other buffer boxes and spacer blocks. Bentonite is a type of clay that swells on contact with water, providing a natural self-sealing ability, and is widely available including as the commercial brand MX-80. Bentonite is a durable natural material that is expected to maintain its properties over the long term. Within the repository, bentonite will: 1) prevent damage to the repository system by acting as mechanical protection against stresses; 2) control groundwater in the area around the UFC and the chemistry of the groundwater and other substances in the vicinity of the UFC; and 3) control microbial activity in the vicinity of the UFC, therefore reducing the potential for microbially influenced corrosion of the container.

Within ongoing work, there are several programs that are relevant for bentonite. These include: 1) characterization of bentonite from a range of sources for a range of conditions (i.e., temperature, moisture, etc.); 2) interaction of bentonite and other repository components (i.e., container, concrete/grout); as well as a range of other works that explore corrosion and biological processes relevant to bentonite.

The main processes with potential influence on the evolution of the sealing systems are discussed in the succeeding sections.

Additional Features, Events and Processes (FEPs) were assessed and excluded for the reasons outlined in the FEPs report (Garisto 2018) and thus are not part of the expected evolution described in this section.

5.5.1 Changes during Saturation

After the gap fill material is installed, the water seeping into the repository will begin to wet this material and the HCB blocks and the bentonite in the buffer will expand. As this expansion progresses, it will fill the space between the granular particles and restrict water movement. Moreover, the swelling pressure will, in due course, provide mechanical resistance to the local effects of large-scale flexing and crustal rebound processes associated with glacial loading, reducing the severity of damage to the near-field rock surrounding the backfilled openings of the repository. The swelling capacity of the bentonite

decreases at high salinity, but the performance requirements for hydraulic conductivity and swelling pressures are met for high salinities, exceeding those expected at 500 m depth, (i.e., a total dissolved solids content of up to 275 g/L).

Figure 5-22 A illustrates the resultant swelling pressures for a range of salinities:

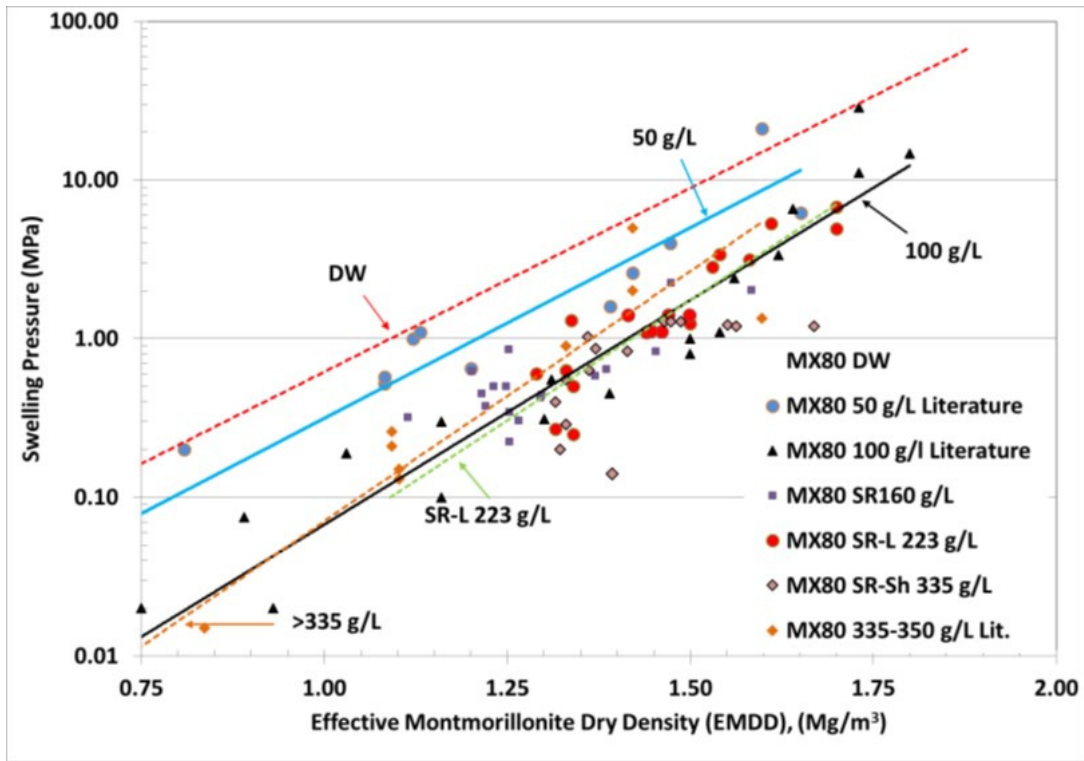
- no salinity (deionized water, DW);
- 50, 100 and 335 g/L of sodium chloride; and
- simulated groundwaters SR160, SR223 and SR335, which correspond to 160, 223 and 335 g/L of salinity, respectively..

Figure 5-22 B illustrates the effect of these same salinities on hydraulic conductivity, as well as the design limit of 10^{-10} m/s.

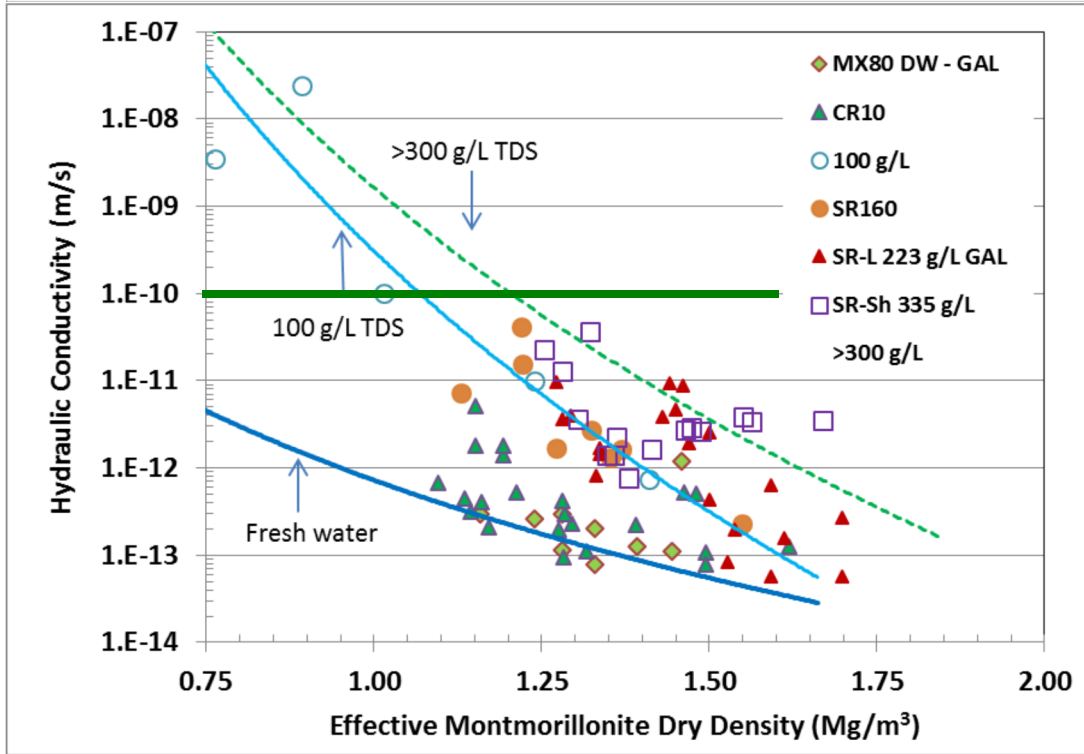
The Effective Montmorillonite Dry Density (EMDD) is a parameter that allows a comparison of the behaviour of different types and densities of clay-based materials (Man and Martino 2009, Dixon et al. 2011) (see Table 4-2). For the reference gap-fill material, using dense pellets of MX-80 clay and emplaced at an effective dry density of 1410 kg/m^3 , the EMDD will be around 1260 kg/m^3 .

The timing and rate of saturation of a repository depends on a number of site-specific conditions, as described in Section 5.2.2.

A



B



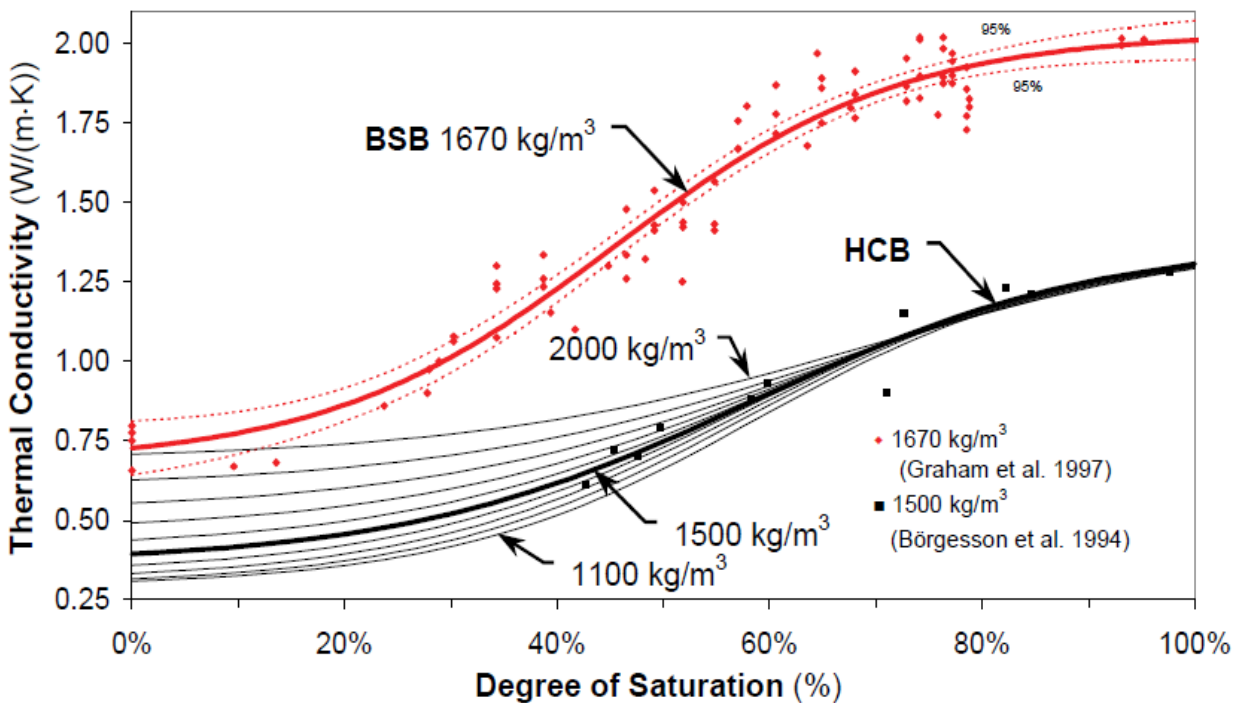
Note: Figures are taken from Dixon et al. (2016)

Figure 5-22: Hydraulic Conductivity and Swelling Pressure under Various Water Conditions: Variation with Effective Montmorillonite Dry Density

5.5.2 Temperature Changes

The thermal conductivity of the various clay-based sealing-system components changes with their degree of water saturation. Figure 5-23 illustrates this relationship for bentonite-only and bentonite-sand compositions. This figure illustrates the effects of sealing material composition and water content on its heat-transfer characteristics. Initially considered for use as the buffer material in the repository concept developed by AECL, a mixture of equal dry weight proportions of sand and bentonite was defined as the reference bentonite-sand buffer for use in filling the region between the container and the surrounding rock. Subsequent review identified bentonite-only clay as the preferred buffer material, such as the 100% bentonite gap-fill material with a dry density of 1410 kg/m³.

From Figure 5-23, it can be seen that in the region nearest the containers, the thermal conductivity of the buffer will decrease as heat from the containers drives moisture away. In contrast, buffer thermal conductivity will gradually increase as the degree of saturation increases. Good agreement is obtained in modelling of thermal profiles in field experiments, such as the SKB Container Retrieval Test, when the thermal conductivity characteristics provided in Figure 5-23 are used (Guo 2009).



Notes: From Man and Martino (2009). Label units are dry densities.

Figure 5-23: Thermal Conductivity of 50:50 wt% Bentonite-Sand Buffer (BSB) and of 100 wt% MX-80 Bentonite (HCB)

The maximum near-field temperature is predicted to occur within the first 30 years following placement as shown in Figure 5-3, when the buffer will be unsaturated. The main sealing material that would potentially be affected by thermal expansion is the concrete bulkheads at

the ends of placement rooms (Figure 4-15), which could also be affected by heat released during their curing process. These would be installed using low-heat concrete and in a manner that minimized contraction during the concrete-curing process.

Later, as the temperature of the repository declines (Figure 5-3), thermal contraction of the concrete bulkhead is likely to cause some rejuvenation of cracks or the production of new cracks at the rock-concrete interface. This process was observed in the concrete seal portion of the AECL URL Tunnel Sealing Experiment (Chandler et al. 2002). The concept of using a composite HCB-concrete structure in a repository anticipates that, by the time temperatures decrease significantly in this region, the clay gasket that was installed as part of the composite seal should be fully saturated. The clay would expand, providing a tight contact with the concrete and rock, and if water flow is occurring from the backfilled tunnel past the concrete, it is expected that the clay will seal the open interface and reduce mass-transport from any open features.

5.5.3 Chemical Changes

An important function of the buffer is to produce/maintain a chemical environment in the repository that will inhibit corrosion of the containers and, in the case of a breach in a container, would limit the solubility of the used fuel and the subsequent migration of radionuclides. Conversely, the composition of porewater in the repository will affect the mechanical and hydraulic properties of the buffer. The evolution of porewater chemistry in the sealing materials is complex, as it is influenced by many parameters: the compositions and proportions of minerals in the buffer and backfill, the composition of the saturating groundwater, the repository temperature, the relative rates of movement through the clay, the initial proportions of exchangeable cations in the clay minerals, and the composition of the water used during wetting and compaction of the sealing materials. Eventually the porewater in the buffer will resemble the groundwater entering the repository, and the Na in the bentonite will have exchanged with Ca in the groundwater, potentially causing a reduction in the swelling pressure and an increase in the hydraulic conductivity of the buffer. However, such potential effects are accounted for in the design of the repository.

5.5.4 Changes due to Biological Processes

Aerobic biodegradation of concrete is a well-known microbial process (Humphreys et al. 2010). Initially, conditions in the vicinity of the concrete seals and floors in the deep geological repository may be moist and aerobic enough that pyrite or other sulphide minerals present in the sealing materials (as part of the concrete aggregate or as minor components in buffer or backfill) could be converted to sulphuric acid (i.e. H_2SO_4) by sulphate-producing bacteria. The extent of the resulting corrosion would be minor, however, given the relatively short duration of oxidizing conditions in the repository and the likely low abundances of sulphide accessory minerals in the sealing materials.

Clay-based materials have been shown to contain indigenous aerobic and anaerobic microorganisms. Microorganisms could also enter the sealing materials during the operating phase of a repository from the air and human activities in the short term, and from the host rock in the long term. The current understanding of microbiology in the context of a repository is summarized by Wolfaardt and Korber (2012).

Specific biogeochemical processes in the buffer, backfill and seals pertain to:

- Consumption of oxygen and creation of an anaerobic environment;
- Gas production and consumption; and
- Microbially influenced corrosion (MIC).

As the geosphere of a deep geological repository is nutrient-poor, microbial activity at depth is limited compared to the near-surface environment.

During the time that a repository is open, the engineered barrier system and adjacent rock will be exposed to air, which will facilitate the growth of aerobic bacteria. After the repository is closed, the aerobic bacteria in this zone are expected to actively promote reducing conditions by consuming the remaining oxygen. Anaerobic bacteria, which were likely to have been the main forms of life in the deep subsurface environment prior to repository excavation, will eventually dominate again, and reducing groundwater conditions will be maintained far into the future. Upon establishment of anaerobic repository conditions, a variety of organisms with the capabilities to utilize alternate electron acceptors have the potential to become active. Anaerobic bacteria can both produce and consume gases, which have limited potential to impact both the physical and chemical aspects of the repository. Of particular interest is the potential for microbial activity to cause MIC, as discussed in Section 5.4.3.3.5. As a result, a substantial amount of research has been conducted on the ability of clay buffer materials to inhibit microbial activity (e.g., Stroes-Gascoyne 2010).

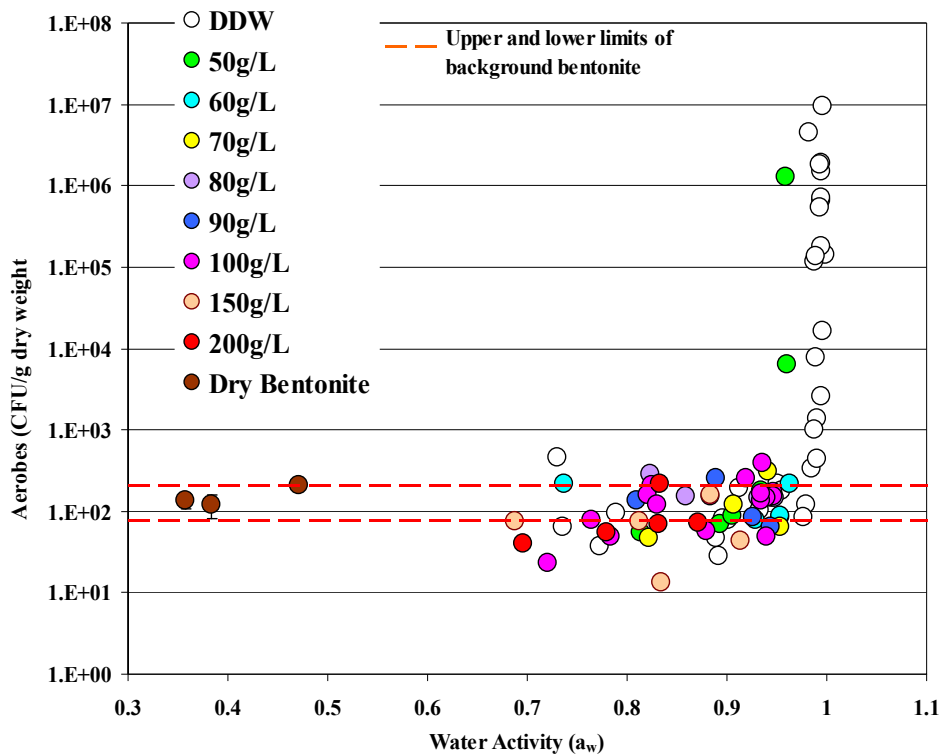
In the current EBS design, 100% HCB buffer material surrounding the waste containers is proposed to prevent or minimize potential negative consequences of microbial activity, such as damage to the container or barrier integrity. Numerous studies have evaluated the survival and activity of microorganisms in clay-based sealing materials under relevant environmental conditions, as summarized in Wolfaardt and Korber (2012). The activity and abundance of microbes in a repository are affected by three main factors: 1) the supply of usable nutrients and energy sources, 2) the availability of water, and 3) elevated temperatures. Radiation fields are not expected to be significant due to the shielding provided by the thick-walled containers.

Sources of nutrients in the sealing materials would include organic matter associated with the clays, nitrates and fuel oil from blasting residues, and hydrocarbons from diesel oils and exhaust gases, all potentially introduced during repository excavation and operation activities, but minimized to the extent possible. As the organic matter in such clays has already persisted in the presence of indigenous microbial assemblages for thousands to millions of years, it is probably unrealistic to assume that all of the organic carbon would be accessible to microbes. It is likely, therefore, that "available" organic carbon would be the limiting nutrient for microbial activity in a repository.

Microbiologists generally use a thermodynamic parameter, water activity (a_w), to express water availability in a quantitative sense. This term corresponds to the ratio of a solution's vapour pressure to that of pure water at a given temperature. The activity of porewater in sealing materials is affected, in particular, by the salinity of the water, as well as by the affinity of the clay for water. For example, while the water activity in pure water is 1.0, the water activity in a 2 mol/kg solution of CaCl_2 is about 0.85 within the buffer material (King and Stroes-Gascoyne 1997). Bacteria must expend extra effort to grow in a habitat with a low a_w because they must maintain a high internal solute concentration to retain water within their cells. Most bacteria

flourish only at or above an a_w of approximately 0.98, the a_w for seawater (see Figure 5-24). In order for the buffer to inhibit bacterial growth, the following criteria have been established: 1) the water activity to be less than or equal to 0.96; and 2) a bentonite dry density of at least 1600 kg/m³ or a porewater salinity of greater than 60 g NaCl/L (Stroes-Gascoyne et al. 2006, 2007a, 2007b).

Temperatures within the repository are anticipated to range from ambient (10 - 20°C) to ~100°C (i.e., adjacent to a container). Temperatures within this range would have some impact on the viability of most microbes indigenous to the sealing materials. The bacteria in buffer material closest to the container would be subjected to the most intense heat and related buffer desiccation. Experiments assessing the effect of temperature suggest that microbes were not particularly sensitive to a temperatures of 60°C, and some culturability remained after exposure to 80°C at all dry buffer densities studied (0.8 to 2.0 Mg/m³), but at temperatures ≥ 121°C, culturability was reduced (Stroes-Gascoyne and Hamon 2010). Importantly, the effect of temperature on culturability in low-dry-density bentonite was reversible once the heat source was removed and re-saturation was allowed to occur, highlighting the importance of maintaining high dry density to inhibit/minimize microbial activity (Stroes-Gascoyne and Hamon 2010).



Notes: Stroes-Gascoyne and Hamon (2008). CFU – Colony Forming Units.

Figure 5-24: Effect of Water Activity on Aerobic Culturability in Compacted Bentonite

In summary, experimental evidence indicates that in a low-salinity repository environment, a highly compacted bentonite with a dry density of 1600 kg/m³ will suppress microbial aerobic culturability to below background levels (Stroes-Gascoyne et al. 2010b). In contrast, in a high-salinity repository environment, with porewater salinities ≥ 50 g/L, salinity will suppress microbial activity over a wider range of bentonite dry densities (~ 800 to 1800 kg/m³) (Stroes-Gascoyne et al. 2010a, 2011). These studies further indicate that 100% highly-compacted bentonite, when directly in contact with the used fuel containers, will reduce microbial activity to insignificant levels.

5.5.5 Radiation

Radiation will have little effect on the sealing materials, even near the container surfaces. It was estimated that for the reference container, the initial external surface dose rate for 30-year fuel would be ~ 1 Gy/hr (Morco et al. 2017). The dose rate drops by over four orders of magnitude after 500 years and beyond. Radiation may restrict biological processes in the immediate vicinity of the container, and it may result in minor chemical changes in gas and porewater composition due to radiolysis, but none of these effects are expected to be significant (McMurry et al. 2003).

5.5.6 Sorption

The buffer system provides a chemical environment which will limit the mobility of contaminants in defective UFCs. Sorption is a general term for surface-related processes that involve the transfer of ions from a solution in which they have freedom of movement, to a fixed position on a surface. In addition to ion exchange, sorption includes surface complexation (in which ions form a strong chemical bond with a reactive surface group at the mineral surface without the displacement of any other ions) and surface precipitation (in which a chemical reaction occurs on the surface because conditions there differ from those in solution).

5.5.7 Vertical Movement of Containers

In the horizontal placement concept, used fuel containers are contained within the HCB box and the remaining void space is filled with gap-fill material. One of the design requirements of this buffer is to prevent containers from shifting from their respective as-placed locations within the placement room, which would reduce the buffer thickness.

Upon closure, water is expected to slowly enter the placement rooms, wetting, swelling and compressing the blocks and gap-fill material. The rate of resaturation will depend on the rate and location of water inflow, as well as the actual evolution of the saturation and homogenisation of the buffer. Variability in resaturation is expected to lead to an uneven distribution of swelling pressures within the placement rooms. However, the system will gradually move toward equilibrium very slowly (Kim and Priyanto 2011 and Chandler 2008). In addition, some upward swelling is expected because the gap-fill material has a lower swelling pressure and a certain degree of compressibility. Such small movements of the containers would not affect repository evolution.

5.5.8 Buffer Erosion and Colloid Formation

Colloids are small solid particles between 1 nm and 1 μ m in diameter that are suspended and dispersed in groundwater. Colloids may form by microbial activity, or as precipitates, or as eroded parts of the buffer clay. Colloids are of interest in a repository primarily because they have the

potential to sorb radionuclides (if containers have failed), at which point the transport of the contaminant is controlled by the mobility of the colloid, rather than by the chemical speciation of the radionuclide. This can be important for actinides as it can bypass their tendency to sorb onto mineral surfaces. Colloids and colloid transport is not expected to be important due to the low permeability of the sedimentary host rock, such that transport is by diffusion and not advection.

Buffer erosion is also a more general concern, particularly during emplacement, if there is potential for water inflow into an emplacement room or in such a manner that the water erodes and removes buffer material. In the low permeability sedimentary rock, this is not anticipated to be an issue.

5.5.9 Confidence

The engineered sealing-system components would be installed subject to design, manufacturing and construction specifications, and so their properties would be known with a high degree of confidence. Nevertheless, there are uncertainties about the long-term behaviour of the materials and the processes that would affect them.

Temperature: There is confidence in the results of thermal models over long timeframes. Temperatures in the near-field are generally well predicted in modelling of prototype repository-design experiments over a range of repository saturation levels. Uncertainties would tend to be localized and due to spatial variability in properties.

Repository Saturation: Considerable confidence exists in the ability to describe repository performance in a saturated state, but there would exist a period of potentially tens to hundreds of years in which saturation will not be fully achieved. During this pre-saturation stage of repository evolution, many interactions between repository components will occur, and resaturation of a repository involves coupling of thermal-hydraulic-mechanical processes. Current numerical models are sufficiently able to broadly explain the evolution of saturation conditions.

Swelling Pressures and Stresses: The swelling pressures generated by the buffer will depend on the buffer composition, buffer density, and groundwater conditions. The swelling characteristics of a wide range of bentonite-based sealing materials have been determined through testing, but would need to be confirmed for site-specific conditions. The manner in which stresses develop within a repository would also influence the swelling pressure. Strains within one component of the repository sealing system may affect the density and, hence, the swelling pressure development of another component. The development of thermal stresses, in conjunction with the hydraulic and swelling stresses, within a multi-component system is complex. Although numerical simulations have been conducted to evaluate the near-field stress in the buffer system, further effort is required to refine the results based on the site-specific data and the advanced understanding of the buffer materials. However, the UFC is designed to withstand significant buffer swelling load. The refinement in the near-field stress calculation is not expected to impact the UFC integrity.

Evolution of Material Properties: The properties of light and dense backfill used to close the repository are not yet thoroughly characterized with respect to their performance under repository conditions. Further studies on the long-term evolution of these materials and their interaction with adjacent materials and groundwater are warranted.

Mineralogical Stability of Montmorillonite: Under the expected repository conditions (temperatures less than 100°C, moderate pH levels, moderate potassium concentrations in groundwater), it is

very unlikely that substantial conversion of montmorillonite to illite would occur over a million-year timeframe.

Microbiological Processes: Although microbes would initially inhabit at least some portions of a deep geological repository, there are a number of uncertainties associated with their viability and effects. For example, experimental data indicate it is unlikely that bacteria would become active in saturated, highly compacted buffer material, but their behaviour in lower density gap-fill material needs to be better demonstrated.

Redox Conditions: There is some uncertainty about when reducing conditions would be established in the sealing materials. It has also been noted that estimates of the time required to reach anaerobic conditions vary from a few weeks/months to a few hundred years, depending on assumptions made in the calculations. Regardless of the amount of time required for oxygen in the repository to be consumed, the total amount of oxygen available for reaction is limited. There are no processes (including radiolysis) that are likely to introduce significant additional quantities of oxygen or other oxidizing species after closure.

Interactions between Sealing System Components: The interfaces between materials might provide preferential pathways for the migration of water, contaminants or microbes within a repository. Examples of such interfaces include: installation assembly gaps (e.g., between blocks of compacted buffer), shrinkage cracks during the desaturation phase, and the formation of an open space along the top of the room if there is insufficient backfill swelling.

5.6 Summary

The discussion in this chapter describes changes that would occur in the multi-barrier repository system during its lifetime. The discussion is based on reasonable expectations for conditions that are likely to be encountered in sedimentary rock.

Many properties of the repository components, and the processes that would affect them, are well characterized. The system is based on durable materials and passive natural processes. Natural and archaeological analogues help to support the descriptions of system behaviour into the future. Of the uncertainties that remain, some questions would be resolved during site characterization activities. Other uncertainties about the future evolution of the system arise from the recognition that simplifying assumptions and simple models may not, in all cases, adequately represent the complexity or heterogeneity of an actual repository over long periods of time. These uncertainties would be addressed by further analyses, by additional experimental or field studies (including extended monitoring in the repository itself), and by using conservative or bounding assumptions in the safety assessment models.

5.7 References for Chapter 5

AMEC GEOMATRIX. 2011. Seismic Hazard Assessment. AMEC Geomatrix, Inc. report for the Nuclear Waste Management Organization, NWMO DGR-TR-2011-20 R000. Toronto, Canada.

Akiyama, E., K. Matsukado, M. Wang and K. Tsuzaki. 2010. Evaluation of hydrogen entry into high strength steel under atmospheric corrosion. *Corrosion Science* 52, 2758-2765.

- Alexandre, P., Kyser, K., Thomas, D. P. Polito, J. Marlat, 2009. Geochronology of unconformity-related uranium deposits in the Athabasca Basin, Saskatchewan, Canada and their integration in the evolution of the basin. *Mineralium Deposita* 44, 41.
- Bäckblom, G. and R. Munier. 2002. Effects of Earthquakes on the Deep Repository for Spent Fuel in Sweden based on Case Studies and Preliminary Model Results. Swedish Nuclear Fuel and Waste Management Company Report TR-02-24. Stockholm, Sweden.
- Baumgartner, P. 2006. Generic Thermal-Mechanical-Hydraulic (THM) Data for Sealing Materials – Volume 1: Soil-water Relationships. Ontario Power Generation Report 06819-REP-01300-10122-R00. Toronto, Canada.
- Briggs, S.A., J. McKelvie, P. Keech, B. Sleep, and M. Krol. 2017a. Transient Modelling of Sulphide Diffusion under Conditions Typical of a Deep Geological Repository. *Corrosion Engineering, Science and Technology*, 52, 200-203.
- Briggs, S., J. McKelvie, B. Sleep and M. Krol. 2017b. Multi-dimensional transport modelling of corrosive agents through a bentonite buffer in a Canadian deep geological repository. *Science of the Total Environment*. 599, 348-354.
- Chandler, N.A, A. Cournut, D.A. Dixon, C. Fairhurst, F. Hansen, M. Gray, K. Hara, Y. Ishijima, E. Kozak, J. Martino, K. Masumoto, G. McCrank, Y. Sugita, P. Thompson, J. Tillerson and B. Vignal. 2002. The Five-year Report of the Tunnel Sealing Experiment: An International Project of AECL, JNC, ANDRA and WIPP. Atomic Energy of Canada Limited Report AECL-12727. Pinawa, Canada.
- Chandler, N. 2008. Modelling the Compliance of Swelling Clay Sealing Systems: In-Floor Borehole and Horizontal Borehole Numerical Simulations. Nuclear Waste Management Organization Report NWMO TR-2008-13. Toronto, Canada.
- Chen, Y., X.H. Wang, J. Li, J.L. Lu, F.S. Wang. 2007. Polyaniline for corrosion prevention of mild steel coupled with copper. *Electrochimica Acta* 52, 5392-5399.
- Chen, J., Z. Qin and D.W. Shoesmith. 2011. Rate controlling reactions for copper corrosion in anaerobic aqueous sulphide solutions. *Corrosion Engineering, Science and Technology* 46, 138-141.
- Cox, B. 1999. Corrosion and hydriding of zircaloy fuel cladding - the inside (and outside) story. Proceedings 6th International Conference on CANDU fuel, Niagara Falls, Canada, 338.
- Dixon D., T. Sandén, E. Jonsson and J. Hansen. 2011. Backfilling of Deposition Tunnels: Use of Bentonite Pellets. Swedish Nuclear Fuel and Waste Management Company Report SKB P-11-44. Stockholm, Sweden.
- Dixon, D.A. A. Man, J. Stone, S. Rimal, G. Siemens, P. Abootalebi and K. Birch. 2016. Backfilling and Sealing Materials for a Deep Geological Repository. 3rd Canadian Conference on Nuclear Waste Management, Decommissioning and Environmental Restoration, Ottawa, Canada, Session T3.

- Dutton, D. 2006. Preliminary Evaluation of the Creep Behaviour of the Inner Steel Vessel of a Used-fuel Container. Ontario Power Generation Report 06819-REP-01300-10108-R00. Toronto, Canada.
- Ferry, C., J.-P. Piron, A. Poulesquen and C. Poinssot. 2008. Radionuclides release from the spent fuel under disposal conditions: Re-evaluation of the instant release fraction. Materials Research Society Symposium Proceedings 1107, 447-454.
- Fracture Systems. 2011. Excavation Damaged Zones Assessment. Nuclear Waste Management Organization Report NWMO DGR-TR-2011-21. Toronto, Canada.
- Freire-Canosa, J. 2011. Used Fuel Integrity Program: Summary Report. Nuclear Waste Management Organization Report NWMO TR-2011-04. Toronto, Canada.
- Frescura, G.M. and A.L. Wight. 1979. Fuel Management & Reactor Operation Review of Operating Experience. From Canteach Website at: <https://canteach.candu.org/Content%20Library/20042116.pdf>.
- Garisto, F. 2018. Seventh Case Study: Features, Events and Processes. Nuclear Waste Management Organization Report NWMO-TR-2018-15. Toronto, Canada.
- Garisto, N.C., W. Newmyer and A. Ho. 2014. Criticality Safety Computations for Spent CANDU Fuel in a Deep Geologic Repository. Nuclear Waste Management Organization Report NWMO TR-2014-08. Toronto, Canada.
- Gobien, M., F. Garisto, E. Kremer and C. Medri. 2018. Seventh Case Study: Reference Data and Codes. Nuclear Waste Management Organization Report NWMO-TR-2018-10. Toronto, Canada.
- Guo, R. 2009. Coupled Thermal-Hydraulic-Mechanical Modelling of the Canister Retrieval Test. Nuclear Waste Management Organization Report NWMO TR-2009-31. Toronto, Canada.
- Guo, R. 2015. Thermal Modelling of a Mark II Container. Nuclear Waste Management Organization Report NWMO-TR-2015-06. Toronto, Canada.
- Guo, R. 2018. Thermal Response of a Conceptual Deep Geological Repository in Sedimentary Rock. Nuclear Waste Management Organization Report NWMO-TR-2018-09.
- Guo, D., L. Wu, A. Chin, J. J. Noel, and J. C. Wren. 2016. Localized Corrosion of Carbon Steel Nuclear Waste Containers Near Weld Regions in the Presence of γ -Radiation., Corrosion 2016, NACE International, Vancouver, Canada.
- Hallet, B. 2011. Glacial Erosion Assessment. Nuclear Waste Management Organization Report NWMO DGR-TR-2011-18. Toronto, Canada.
- Hultquist G., P. Szakálos, M.J. Graham, A.B. Belonoshko, G.I. Sproule, L. Gråsjö, P. Dorogokupets, B. Danilov, T. AAstrup, G. Wikmark, G.-K. Chuah, J.-C. Eriksson and A. Rosengren. 2009. Water corrodes copper. Catalysis Letters 132, 311-316.

- Hultquist G., M.J. Graham, P. Szakálos, G.I. Sproule, A. Rosengren and L. Gråsjö. 2011. Hydrogen gas production during corrosion of copper by water. *Corrosion Science* 53, 310-319.
- Hultquist, G., M.J. Graham, O. Kodra, S. Moisa, R. Liu, U. Bexell and J.L. Smialek. 2013. Corrosion of Copper in Distilled Water without Molecular Oxygen and the Detection of Produced Hydrogen. SSM Technical Note 2013:07. Stockholm, Sweden.
- Humphreys, P.N., J.M. West and R. Metcalfe. 2010. Microbial Effects on Repository Performance. Prepared by Quintessa Limited for the Nuclear Decommissioning Authority Report No. QRS-1378Q-1. Oxfordshire, United Kingdom.
- IAEA (International Atomic Energy Agency). 2010. Review of Fuel Failures in Water Cooled Reactors. IAEA Nuclear Energy Series No. NF-T-2.1. Vienna, Austria.
- Ibrahim, B. 2015. The Corrosion Behaviour of Cu in Irradiated and Non-Irradiated Humid Air. University of Western Ontario, Canada. Electronic Thesis and Dissertation Repository, #3315, <http://ir.lib.uwo.ca/etd/3315>.
- INTERA. 2011. Descriptive Geosphere Site Model. Nuclear Waste Management Organization Report NWMO DGR-TR-2011-24. Toronto, Canada.
- Itasca Consulting Group. 2015. Long-term Stability Analysis of APM Mark II Conceptual Design in Sedimentary and Crystalline Rocks. Nuclear Waste Management Organization Report NWMO-TR-2015-27. Toronto, Canada.
- Itasca Consulting Group. 2018. Sensitivity Analyses of Long-term Stability of APM Conceptual Repository Designs in Crystalline and Sedimentary Rock Setting. Nuclear Waste Management Organization Report NWMO-TR-2018-21. Toronto, Canada.
- Jensen, K.A. and R.C. Ewing. 2001. The Okélobondo natural fission reactor, southeast Gabon: Geology, mineralogy, and retardation of nuclear-reaction products. *Geological Society of America Bulletin* 113, 32-62.
- Johansson, J., A. Blom, A. Chukharkina, and K. Pedersen. 2015. Study of H₂ gas emission in sealed compartments containing copper immersed in O₂-free water. SKB Report, SKB TR-15-03. Stockholm, Sweden.
- Kim, C-S. and D. Priyanto. 2011. Two-Component Swelling Tests Operated for Three, Nine and Twenty-Seven Months. Nuclear Waste Management Organization Report NWMO TR-2011-15. Toronto, Canada.
- King, F. 2006. Review and Gap Analysis of the Corrosion of Copper Containers under Unsaturated Conditions. Ontario Power Generation Report 06819-REP-01300-10124-R00. Toronto, Canada.
- King, F. 2009a. Hydrogen Effects on Carbon Steel Used Fuel Containers. Nuclear Waste Management Organization Report NWMO TR-2009-29. Toronto, Canada.

- King, F. 2009b. Microbiologically influenced corrosion of nuclear waste container. *Corrosion* 65, 233-251.
- King, F. 2013. Consequences of the General Corrosion of Carbon Steel Used Fuel Containers for Gas Generation in a DGR. Nuclear Waste Management Organization Report NWMO TR-2013-16. Toronto, Canada.
- King, F. and S. Stroes-Gascoyne. 1997. Predicting the effects of microbial activity on the corrosion of copper nuclear waste disposal containers. Eds. J.H. Wolfram, R.D. Rogers and L.G. Gazso in *Microbial Degradation Processes in Radioactive Waste Repository and in Nuclear Fuel Storage Areas*. Volume 11 of NATO ASI Series. Kluwer Academic Publishers, Netherlands. 149-162.
- King, F. and M. Kolář. 2000. The Copper Container Corrosion Model Used in AECL's Second Case Study. Ontario Power Generation Report 06819-REP-01200-10041-R00. Toronto, Canada.
- King, F., L. Ahonen, C. Taxén, U. Vuorinen and L. Werme. 2001. Copper Corrosion under Expected Conditions in a Deep Geologic Repository. Swedish Nuclear Fuel and Waste Management Company Report SKB TR-01-23. Stockholm, Sweden.
- King, F., M. Kolář and P. Maak. 2008. Reactive-transport model for the prediction of the uniform corrosion behaviour of copper used fuel containers. *Journal of Nuclear Materials* 379, 133-141.
- King, F. and D. Shoesmith. 2010. Nuclear waste canister materials, corrosion behaviour and long-term performance in geological repository systems. Eds. J. Ahn and M.J. Apter in *Geological Repository Systems for Safe Disposal of Spent Nuclear Fuel and Radioactive Waste*. Woodhead Publishing, Cambridge, United Kingdom.
- King, F., C. Lilja, K. Pedersen, P. Pitkänen and M. Vähänen. 2010. An Update of the State-of-the-Art Report on the Corrosion of Copper under Expected Conditions in a Deep Geologic Repository. Swedish Nuclear Fuel and Waste Management Company Report SKB TR-10-67. Stockholm, Sweden.
- King, F., C. Lilja, K. Pedersen, P. Pitkänen and M. Vähänen. 2011a. An Update of the State-of-the-art Report on the Corrosion of Copper under Expected Conditions in a Deep Geologic Repository. Posiva Oy Report POSIVA 2011-01. Oikiluoto, Finland.
- King, F., M. Kolář, M. Vähänen and C. Lilja. 2011b. Modelling long term corrosion behaviour of copper canisters in KBS-3 repository. *Corrosion Engineering, Science and Technology* 46, 217-222.
- King, F., D.S. Hall and P.G. Keech. 2017. Nature of the near-field environment in a deep geological repository and the implications for the corrosion behaviour of the container. *Corrosion Engineering, Science and Technology* 52, 25-30.
- Kremer, E.P. 2017. Durability of the Canadian Used Fuel Container. *Corrosion Engineering, Science and Technology* 52, 173-177.

- Kwong, G.M. 2011. Status of Corrosion Studies for Copper Used Fuel Containers Under Low Salinity Conditions. Nuclear Waste Management Organization Report NWMO TR-2011-14. Toronto, Canada.
- Lanson, B., S. Lantenois, P. A. van Aken, A. Bauer, and A. Plançon. 2015. Experimental investigation of smectite interaction with metal iron at 80 °C: Structural characterization of newly formed Fe-rich phyllosilicates. *American Mineralogist*, 97, 864–871..
- Lovasic, Z. and P. Gierszewski. 2005. CANDU Fuel Long-Term Storage and Used Fuel Integrity. Paper at 9th International Conference on CANDU Fuel. Canadian Nuclear Society Bulletin Vol. 26, No. 4.
- Man, A. and J.B. Martino. 2009. Thermal, Hydraulic and Mechanical Properties of Sealing Materials. Nuclear Waste Management Organization Report NWMO TR-2009-20. Toronto, Canada.
- McMurry, J., D.A. Dixon, J.D. Garroni, B.M. Ikeda, S. Stroes-Gascoyne, P. Baumgartner and T.W. Melnyk. 2003. Evolution of a Canadian Deep Geologic Repository: Base Scenario. Ontario Power Generation Report 06819-REP-01200-10092-R00. Toronto, Canada.
- Morco, R.P., J. M. Joseph, C. Medri, D. S. Hall, and J. C. Wren. 2017. Model Calculations of Radiolytic Production of Oxidants Anticipated under Deep Geologic Repository Environments. *Corrosion Engineering Science and Technology*, In Press.
- Necib, S., Y. Linard, D. Crusset, M. Schlegel, S. Daumas, N. Michau. 2017. Corrosion processes of C-steel in long term repository conditions. *Corros. Eng. Sci. Techn.*, In Press.
- Newman, R.C., S. Wang and G. Kwong. 2010. Anaerobic Corrosion Studies of Carbon Steel Used Fuel Containers. Nuclear Waste Management Organization Report NWMO TR-2010-07. Toronto, Canada.
- Osacký, M., V. Šucha, A. Czímerová, M. Pentrák, and J. Madejová. 2013. Reaction of smectites with iron in aerobic conditions at 75 °C. *Applied Clay Science*, 72, 26–36.
- Ottosson, M., M. Boman, P. Berastegui, Y. Andersson, M. Hahlin, M. Korvela and R. Berger. 2016. Copper in ultrapure water. SKB Report, SKB TR-16-01. Stockholm, Sweden.
- Pedersen K. 2000. Microbial Processes in Radioactive Waste Disposal. Swedish Nuclear Fuel and Waste Management Company Report SKB TR 00-04. Stockholm, Sweden.
- Peltier, W.R. 2002. A Design Basis Glacier Scenario. Ontario Power Generation Report 06819-REP-01200-10069-R00. Toronto, Canada.
- Peltier, W.R. 2003. Long-Term Climate Change – Glaciation. Ontario Power Generation Report 06819-REP-01200-10113-R00. Toronto, Canada.
- Peltier, W.R. 2004. Permafrost Influences upon the Subsurface. Ontario Power Generation Report 06819-REP-01200-10134-R00. Toronto, Canada.

- Peltier, W.R. 2006. Boundary Conditions Data Set for Spent Fuel Repository Performance Assessment. Ontario Power Generation Report 06819-REP-01200-10154-R00. Toronto, Canada.
- Peltier, W.R. 2011. Long-term Climate Change. Nuclear Waste Management Organization Report NWMO DGR-TR-2011-14 R000. Toronto, Canada.
- Pencer, J, M. McDonald, D. Roubtsov and G. Edwards. 2017. Implications of alpha-decay for long term storage of advanced heavy water reactor fuels. *Annals of Nuclear Energy* 110, p.400-405.
- Puigdomenech, I. and C. Taxén. 2000. Thermodynamic Data for Copper: Implications for the Corrosion of Copper under Repository Conditions. Swedish Nuclear Fuel and Waste Management Company Report SKB TR 00-13. Stockholm, Sweden.
- Qin, Z., R. Deljeet, M. Ai, N. Farhangi, J.J. Noel, S. Ramamurthy, D.W. Shoesmith, F. King, and P.G. Keech. 2017. The active/passive conditions for copper corrosion under nuclear waste repository environment. *Corrosion Engineering, Science and Technology*, 52, 45-49.
- Raiko, H. 2005. Disposal Canister for Spent Nuclear Fuel – Design Report. Posiva Oy Report POSIVA 2005-02. Olkiluoto, Finland.
- Saiedfar, M. and P. Maak. 2002. Preliminary Assessment of the Deformation and Stresses of Copper Used-fuel Containers in a Hypothetical Deep Geologic Repository. Ontario Power Generation Report, 06819-REP-01300-10049-R00. Toronto, Canada.
- Scully, J. and M. Edwards. 2013. Review of the NWMO Copper Corrosion Allowance. Nuclear Waste Management Report NWMO TR-2013-04. Toronto, Canada.
- Scully, J.R., D. Féron, and H. Hänninen. 2016. Peer review of the NWMO copper corrosion program. Nuclear Waste Management Organization Report, NWMO-TR-2016-11. Toronto, Canada.
- Senior, N., R. Newman, S. Wang, and N. Diomidis. 2017. Understanding and Quantifying the Anoxic Corrosion of Carbon Steel in a Swiss L/ILW Repository Environment. *Corrosion Engineering Science and Technology*, In Press.
- Sherwood Lollar, B. 2011. Far-Field Microbiological Considerations Relevant to a Deep Geological Repository – State of Science Review. Nuclear Waste Management Organization Report NWMO TR-2011-09. Toronto, Canada.
- Shoesmith, D.W. 2008. The Role of Dissolved Hydrogen on the Corrosion/Dissolution of Spent Nuclear Fuel. Nuclear Waste Management Organization Report NWMO TR-2008-19. Toronto, Canada.
- Shoesmith, D.W. and F. King. 1999. The Effects of Gamma Radiation on the Corrosion of Candidate Materials for the Fabrication of Nuclear Waste Packages. Atomic Energy of Canada Limited Report AECL-11999. Pinawa, Canada.

- Shoesmith, D.W. and D. Zagidulin. 2010. The Corrosion of Zirconium under Deep Geological Repository Conditions. Nuclear Waste Management Organization Report NWMO TR-2010-19. Toronto, Canada.
- SKB. 2010. Critical Review of the Literature on the Corrosion of Copper by Water. Swedish Nuclear Fuel and Waste Management Company Report SKB TR-10-69. Stockholm, Sweden.
- SKB. 2011. Long-term Safety for the Final Repository for Spent Nuclear Fuel at Forsmark. Main Report of the SR-Site Project. Volume I. Swedish Nuclear Fuel and Waste Management Company Report SKB TR-11-01. Stockholm, Sweden.
- Smart N., A. Rance, P. Fennell and L. Werme. 2003. Expansion due to anaerobic corrosion of steel and cast iron: experimental and natural analogue studies. Eds. D. Féron and D.D. Macdonald in Prediction of Long Term Corrosion Behaviour in Nuclear Waste Systems: Proceedings of the International Workshop. Cadarache, France. London: Maney Pub. (European Federation of Corrosion Publications 36), paper 19, pp 280–294.
- Smart N., P. Fennell, A. Rance and L. Werme. 2004. Galvanic corrosion of copper-cast iron couples in relation to the Swedish radioactive waste canister concept. Ed. D. Féron in Prediction of Long Term Corrosion Behaviour in Nuclear Waste Systems: Proceedings of the 2nd International Workshop. European Federation of Corrosion, pp 52–60. Nice, France.
- Smart N.R., A.P. Rance and P.A.H. Fennell. 2005. Galvanic Corrosion of Copper-Cast Iron Couples. Swedish Nuclear Fuel and Waste Management Company Report SKB TR-05-06. Stockholm, Sweden.
- Smart N.R., A.P. Rance and P.A.H. Fennell. 2006. Expansion due to the Anaerobic Corrosion of Iron. Swedish Nuclear Fuel and Waste Management Company Report SKB TR-06-41. Stockholm, Sweden.
- Smart N., A. Rance, B. Reddy, P. Fennell and R. Winsley. 2012. Analysis of SKB MiniCan Experiment 3. Swedish Nuclear Fuel and Waste Management Company Report SKB TR-12-09. Stockholm, Sweden.
- SSM. 2011a. Evolution of Hydrogen by Copper in Ultrapure Water without Dissolved Oxygen. Strål Säkerhets Myndigheten Report 2011:34. Stockholm, Sweden.
- SSM. 2011b. Is Copper Immune to Corrosion when in Contact with Water and Aqueous Solutions? Strål Säkerhets Myndigheten Report 2011:09. Stockholm, Sweden.
- Standish, T., J. Chen, R. Jacklin, P. Jakupi, S. Ramamurthy, D. Zagidulin, P. Keech and D.W. Shoesmith. 2016. Corrosion of Copper-Coated Steel High Level Nuclear Waste Containers Under Permanent Disposal Conditions. *Electrochimica Acta*, 211, 331–342.
- Standish, T.E., D. Zagidulin, S. Ramamurthy, P. Keech, J. Noel and D. Shoesmith. 2017. Galvanic corrosion of copper-coated carbon steel for used nuclear fuel containers. *Corrosion Engineering Science and Technology*, 52(S1), 65-69.

- Stroes-Gascoyne, S. 2010. Microbial occurrence in bentonite-based buffer, backfill and sealing materials from large-scale experiments at AECL's Underground Research Laboratory. *Applied Clay Science* 47, 36-42.
- Stroes-Gascoyne, S., C.J. Hamon, C. Kohle and D.A. Dixon. 2006. The Effects of Dry Density and Porewater Salinity on the Physical and Microbiological Characteristics of Highly Compacted Bentonite. Ontario Power Generation Report 06819-REP-01200-10016 R00. Toronto, Canada.
- Stroes-Gascoyne, S., C.J. Hamon, D.A. Dixon and J.B. Martino. 2007a. Microbial analysis of samples from the tunnel sealing experiments at AECL's Underground Research Laboratory. *Physics and Chemistry of the Earth: Parts A/B/C* 32, 219-231.
- Stroes-Gascoyne, S., P. Maak, C.J. Hamon, and C. Kohle. 2007b. Potential Implications of Microbes and Salinity on the Design of Repository Sealing System Components. Nuclear Waste Management Organization Report NWMO TR-2007-10. Toronto, Canada.
- Stroes-Gascoyne, S. and C.J. Hamon. 2008. The Effect of Intermediate Dry Densities (1.1-1.5 g/cm³) and Intermediate Porewater Salinities (60-90 g NaCl/L) on the Culturability of Heterotrophic Aerobic Bacteria in Compacted 100% Bentonite. Nuclear Waste Management Organization Report NWMO TR-2008-11. Toronto, Canada.
- Stroes-Gascoyne, S. and C.J. Hamon. 2010. The Effects of Elevated Temperatures on the Viability and Culturability of Bacteria Indigenous to Wyoming MX-80 Bentonite. Nuclear Waste Management Organization Report NWMO TR-2010-08. Toronto, Canada.
- Stroes-Gascoyne, S., C.J. Hamon, D.A. Dixon and D.G. Priyanto. 2010a. The Effect of CaCl₂ Porewater Salinity (50-100 g/L) on the Culturability of Heterotrophic Aerobic Bacteria in Compacted 100% Bentonite with Dry Densities of 0.8 and 1.3 g/cm³. Nuclear Waste Management Organization Report NWMO TR-2010-06. Toronto, Canada.
- Stroes-Gascoyne, S., C.J. Hamon, P. Maak and S. Russell. 2010b. The effects of the physical properties of highly compacted smectitic clay (bentonite) on the culturability of indigenous microorganisms. *Applied Clay Science* 47, 155-162.
- Stroes-Gascoyne, S., C.J. Hamon and P. Maak. 2011. Limits to the Use of Highly Compacted Bentonite as a Deterrent for Microbiologically Influenced Corrosion in a Nuclear Fuel Waste Repository. *Physics and Chemistry of the Earth* 36(17-18), 1630-1638.
- Stuhne, G. and W.R. Peltier. 2015. Surface Boundary Conditions During Long-Term Climate Change. Nuclear Waste Management Organization Report NWMO-TR-2015-16. Toronto, Canada.
- Stuhne, G. and W.R. Peltier. 2016. Sensitivity Analyses of Surface Boundary Conditions During Long-Term Climate Change. Nuclear Waste Management Organization Report NWMO-TR-2016-19. Toronto, Canada.

Swedish National Council. 2010. Nuclear Waste State-of-the-Art Report 2010 – Challenges for the Final Repository Programme. Swedish Government Official Reports SOU 2010:6. Stockholm, Sweden.

Szakálos P., Hultquist G., Wikmark G. 2007. Corrosion of copper by water. *Electrochemical and Solid-State Letters* 10, C63–C67.

Tait, J.C., H. Roman and C.A. Morrison. 2000. Characteristics and Radionuclide Inventories of Used Fuel from OPG Nuclear Generating Stations. Ontario Power Generation Report 06819-REP-01200-10029-R00. Toronto, Canada.

Tsuru, T., Y. Huang, Md. R. Ali and A. Nishikata. 2005. Hydrogen entry into steel during atmospheric corrosion process. *Corrosion Science* 47, 2431-2440.

Turnbull, J., R. Szukalo, M. Behazin, D. Zagidulin, S. Ramamurthy, J.C. Wren and D.W. Shoesmith. 2017. Exploring the Effects of Cathodic Reagent Concentration and Small Solution Volumes on the Corrosion of Copper in Dilute Nitric Acid Solutions. *Corrosion*, <https://doi.org/10.5006/2655>

Werme, L. 1998. Design Premises for Canister for Spent Nuclear Fuel. Swedish Nuclear Fuel Waste Management Company Report SKB TR-98-08. Stockholm, Sweden.

Wersin, P., M. Birgersson, S. Olsson, O. Karnland and M. Snellman. 2007. Impact of Corrosion-Derived Iron on the Bentonite Buffer within the KBS-3H Disposal Concept – the Olkiluoto Site as Case Study. Posiva Oy Report POSIVA 2007-11. Olkiluoto, Finland.

Wheeler, R.L. 1995. Earthquakes and the cratonward limit of lapetan faulting in eastern North America. *Geology* 23, 105-108.

Wolfaardt, G.M. and D.R. Korber. 2012. Near-Field Microbiological Considerations Relevant to a Deep Geological Repository for Used Nuclear Fuel – State of Science Review. Nuclear Waste Management Organization Report NWMO TR-2012-02. Toronto, Canada.

Wu, L., D. Guo, M. Li, J.M. Joseph, J.J. Noël, P.G. Keech, J.C. Wren. 2017. Inverse Crevice Corrosion of Carbon Steel: Effect of Solution Volume to Surface Area, *J. Electrochem. Soc.*, 164, C539.

6. SCENARIO IDENTIFICATION AND DESCRIPTION

Postclosure safety is assessed through consideration of a set of potential future scenarios, where scenarios are descriptions of alternative possible evolutions of the repository system. Scenarios can also be designed with the aim of illustrating the properties of natural or engineered barriers (IAEA 2012). For that purpose, it can be instructive to assign parameter values such that the barrier under consideration is influenced in an exaggerated way so that the robustness of the barriers can be more clearly exhibited. Scenarios of this sort are often called “what-if” scenarios to distinguish them from realistic scenarios.

The purpose of scenario identification is to develop a comprehensive range of possible future evolutions against which the performance of the system can be assessed. Consistent with Regulatory Document REGDOC-2.11.1, Volume III (CNSC 2018), both Normal Evolution and Disruptive Event Scenarios are considered. The Normal Evolution Scenario represents the normal (or expected) evolution of the site and facility, while Disruptive Event Scenarios examine the effects of unlikely events that might lead to penetration of barriers and abnormal degradation and loss of containment.

Scenarios of interest are identified through consideration of the various factors (see Table 6-1) that could affect the repository system and its evolution (IAEA 2012). These factors can be further categorized into Features, Events and Processes (FEPs) as shown in Table 6-1. To provide a method for ensuring that all relevant factors are considered, FEPs are organized in a hierarchical structure with up to 4 levels. The finest discretization of the FEPs occurs at the lowest level. This is illustrated in Table 6-2 where the FEPs are listed down to level 3, the lowest level for these FEPs. This hierarchical structure used here, although reorganized, includes all FEPs listed in the FEPs database of the OECD Nuclear Energy Agency (NEA 2000, 2012), an intergovernmental agency that facilitates cooperation among countries with advanced nuclear technology infrastructures.

FEPs can be characterized as either “external” or “internal”, depending on whether they are outside or inside the spatial and temporal boundaries of the repository system domain, which here includes the repository, the geosphere and the affected biosphere. The external factors originate outside these boundaries; whereas, waste package, repository, geosphere, biosphere and contaminant factors can be considered as “internal” factors. Hence, the waste package, repository, geosphere, biosphere and contaminant factors and FEPs will be referred to as Internal FEPs and the external factors and FEPs will be referred to as External FEPs.

The External FEPs provide the system with boundary conditions and include influences originating outside the repository system that might cause change. Included in this group are decisions related to repository design, operation and closure since these are outside the temporal boundary of the postclosure behaviour of the repository system. If these External FEPs can significantly affect the evolution of the system and / or its safety functions of isolation and containment, they are considered scenario-generating FEPs in the sense that whether or not they occur (or the extent to which they occur or the form that they take) could define a particular future scenario that should be considered.

The External FEPs are listed in Table 6-2. Those that are likely to affect the repository system and its evolution are discussed in Section 6.1. The effects of less likely External FEPs and

certain Internal FEPs that might lead to abnormal degradation and loss of containment are discussed in Section 6.2.

Table 6-1: FEP List Showing FEPs Down to Level 2

FEP Number and Title	
1.	EXTERNAL FACTORS
1.1	Repository Factors
1.2	Geological Factors
1.3	Climatic Factors
1.4	Future Human Actions
1.5	Other External Factors
2.	WASTE PACKAGE FACTORS
2.1	Waste Package Characteristics
2.2	Waste Form Processes
2.3	Waste Container Processes
2.4	Contaminant Release and Transport (Waste Package)
3.	REPOSITORY FACTORS
3.1	Repository Characteristics
3.2	Repository Processes
3.3	Contaminant Release and Transport (Repository)
4.	GEOSPHERE FACTORS
4.1	Geosphere Characteristics
4.2	Geosphere Processes
4.3	Contaminant Release and Transport (Geosphere)
5.	BIOSPHERE FACTORS
5.1	Surface Environment
5.2	Human Behaviour
5.3	Contaminant Release and Transport (Biosphere)
5.4	Exposure Factors
6.	CONTAMINANT FACTORS
6.1	Contaminant Characteristics

Note: From Garisto (2018).

6.1 The Normal Evolution Scenario

The Normal Evolution Scenario is based on a reasonable extrapolation of present day site features and receptor¹ lifestyle. It includes the expected evolution of the site and expected degradation of the repository system.

6.1.1 External FEPs

The External FEPs shown in Table 6-2 have been reviewed to identify those that are likely to occur and could potentially affect the repository and, therefore, should be included in the Normal Evolution Scenario. The included / excluded items are also shown in Table 6-2 together with a brief justification for their inclusion / exclusion. Further details are provided in Garisto (2018).

Table 6-2 shows that the repository is largely unaffected by many External FEPs. The main External FEPs that are likely to have an impact are:

- Placement of some containers with undetected defects (FEP 1.1.03);
- Glaciation and its effects (FEPs 1.2.02, 1.2.03, 1.2.07, 1.3.01, 1.3.02, 1.3.04, 1.3.05, 1.3.08 and 1.3.09);
- Earthquakes (FEP 1.2.03);
- Human influence on global climate (FEP 1.4.01) delaying onset of the next glaciation; and
- Social and institutional developments leading to changes of land use at the repository site (FEP 1.4.02), and associated drilling, site development and water management (FEPs 1.4.04, 1.4.08 and 1.4.10).

With respect to undetected defects (FEP 1.1.03), the containers are robust and there are multiple inspection steps to ensure they are fabricated and placed correctly (Chapter 4). However, with the large number of containers (about 109,000), it is possible that some containers could unknowingly be placed in the repository with defects. Consequently, for the Normal Evolution Scenario, it is assumed that some containers with undetected defects are present in the repository.

An important external influence is glaciation (FEP 1.2.02 and others). Although glaciation will cause major changes in the surface and near-surface environment, the repository itself is intentionally isolated by its depth from these changes.

Glaciation erosion at the hypothetical repository site, although slow, could progressively remove rock overlying the repository. Hence, glacial erosion is considered in the Normal Evolution Scenario. Deep erosion is assumed not likely within this time frame for this hypothetical site and repository depth as this would be a factor considered in siting.

For the hypothetical site, the hydrogeologic simulations described in Chapter 2 indicate that glacial meltwaters will not reach the repository horizon. This is due to the low hydraulic conductivity of the overlying rock formations. Furthermore, for the sensitivity cases performed, the glacial perturbations did not materially change mass transport rates at the repository depth (i.e., diffusion remains the dominant transport mechanism). These characteristics of the repository system are used in the course of scenario identification.

¹ The receptor is a person (or persons) who may be exposed to contaminants potentially released from the repository.

Table 6-2: Status of External FEPs for the Normal Evolution of the Repository System

External FEP		Status ⁽¹⁾	Remark	
1.1	<i>Repository Factors</i>			
	1.1.01	Site investigation	Included	The repository site is hypothetical. The topography, stratigraphy and hydrological properties are typical of those found in Southern Ontario. The hypothetical site is described in Chapter 2. It is assumed there are no fractures or faults at or near the repository site, there are no undetected geological features at the site, and there are no identified commercially viable mineral resources at the site.
	1.1.02	Excavation and construction	Included	The repository is built consistent with the design basis, as described in Chapter 4. Controlled drill and blast excavation is used, which reduces but does not avoid formation of an excavation damaged zone (EDZ).
	1.1.03	Placement of wastes and backfill	Included	The in-room container placement method is used. Rooms are backfilled as containers are placed, as described in Chapter 4. It is assumed that a small fraction of the containers are placed with initial defects that are not detected during the fabrication, inspection and placement processes.
	1.1.04	Closure and repository sealing	Included	The repository is closed and sealed as described in Chapter 4. This includes sealing of the shafts.
	1.1.05	Repository records and markers	Included	Repository records and markers (and passive societal memory) are assumed sufficient to ensure that inadvertent intrusion would not occur for at least 300 hundred years.
	1.1.06	Waste allocation	Included	The repository holds about 5.2 million CANDU fuel bundles. There is no placement of other radioactive or chemically hazardous material at the site.
	1.1.07	As-built repository	Included	The repository design concept is described in Chapter 4.

Postclosure Safety Assessment of a Used Fuel Repository in Sedimentary Rock

Document Number: NWMO-TR-2018-08

Revision: 000

Class: Public

Page: 273

External FEP			Status ⁽¹⁾	Remark
	1.1.08	Quality control	Included	Construction, operation, monitoring and closure of the repository are all undertaken under a project quality plan that ensures that the design and safety basis is met (see Chapter 11). However, due to the large number of containers, it is assumed that some containers are placed with initial defects that are not detected during the fabrication, inspection and placement processes.
	1.1.09	Schedule and planning	Included	The assumed schedule is ~40 years of operation, 70 years of extended monitoring and 30 years for decommissioning and closure.
	1.1.10	Repository administrative control	Included	Administrative controls ensure proper operation and closure of the repository. Institutional controls (e.g., land use restrictions) will be implemented on closure, which, while they remain effective, will prevent inadvertent human intrusion and the drilling of wells.
	1.1.11	Monitoring	Included	The preclosure monitoring period is accounted for in all scenarios. The postclosure monitoring program will be designed to preserve the safety of the repository and is excluded from the assessment.
	1.1.12	Accidents and unplanned events	Excluded	The likelihood of preclosure accidents or unplanned events that could affect the long-term safety of the repository will be minimized by good engineering practice and quality control; and the effects of any that do occur will be mitigated before the repository is closed.
	1.1.13	Retrieval of wastes	Excluded	The repository schedule includes an extended period of monitoring after rooms have been filled but before the access tunnels and shaft are sealed, which would facilitate retrieval if required. However, retrieval after closure is not expected and is not included in this safety assessment.

Postclosure Safety Assessment of a Used Fuel Repository in Sedimentary Rock

Document Number: NWMO-TR-2018-08

Revision: 000

Class: Public

Page: 274

1.2		Geological Factors		
	1.2.01	Tectonic movement and orogeny	Excluded	The hypothetical site is in a tectonically stable region away from plate margins, with no tectonic activity over the time scale of interest (i.e., one million years).
	1.2.02	Deformation (elastic, plastic or brittle)	Included	<p>The repository site is assumed to be tectonically stable; hence, deformation due to tectonic movement and orogeny is unlikely over the timescales of interest. Thus, over the next million years, the only significant deformation force is that due to ice sheet advance over the site. This could cause crustal depression in excess of 500 m, but would occur on a continental scale (Peltier 2011).</p> <p>Ice sheet weight could also cause local movement along existing faults or fractures zones but would not lead to creation of new fractures. As per Chapter 2, it is assumed there are no fractures or faults intersecting the repository.</p>
	1.2.03	Seismicity (earthquakes)	Included	<p>Earthquakes will occur over the time scale of interest; however, since the site is assumed to be located in a seismically inactive region, the likely magnitude, frequency and distance of earthquakes would limit their impact at the repository location.</p> <p>Earthquakes are in general less destructive at depth than at the surface, diminishing the impact of any seismic activity on a deep repository. Furthermore, the repository is backfilled, preventing rock fall.</p> <p>Larger earthquakes which are more likely during retreat of ice sheets could, in theory, reactive an existing fracture or fault, potentially providing a groundwater pathway to the surface. However, it is assumed for the Normal Evolution Scenario that, consistent with Chapter 2, there are no fracture zones or faults at or near the site and that there are no undetected geological features at the repository site.</p>
	1.2.04	Volcanic and magmatic activity	Excluded	No volcanic or magmatic activity over the time scale of interest due to the site location.

Postclosure Safety Assessment of a Used Fuel Repository in Sedimentary Rock

Document Number: NWMO-TR-2018-08

Revision: 000

Class: Public

Page: 275

	1.2.05	Metamorphism	Excluded	No processes occur over the time scale of interest that will cause metamorphism.
	1.2.06	Hydrothermal activity	Excluded	The hypothetical repository is located in a geologically stable sedimentary basin in Ontario with a low geothermal flux. Hydrothermal processes therefore act too slowly to be of concern over the time scale of interest.
	1.2.07	Regional erosion and sedimentation	Included	The area is topographically relatively flat and not high above sea level so there is limited potential for large-scale denudation. However, over the past million years, ice-sheet erosion and deposition has shaped the topography and could continue to do so in the future. Erosion is accounted for in the definition of the Normal Evolution Scenario.
	1.2.08	Diagenesis	Excluded	Would have negligible effect on repository safety over the timescale of interest (one million years).
	1.2.09	Salt diapirism and dissolution	Excluded	No significant salt deposits are assumed to be located in the vicinity of the site. Historically, there could have been salt deposits but these have already been dissolved in the distant past.
	1.2.10	Hydrological response to geological changes	Excluded	A severe seismic event could potentially change the permeability of fractures or activate a closed fault, thereby changing the local hydrology. However, it is assumed for the Normal Evolution Scenario that site characterization has not identified any fractures or faults at or near the hypothetical repository site. At the hypothetical site, it is assumed that the hydraulic pressure is hydrostatic - there is no pattern of over- and under-pressures in the different rock formations (see Chapter 2). Also, none of the other included geologic processes identified above are able to cause significant hydraulic changes on relevant timescales.

Postclosure Safety Assessment of a Used Fuel Repository in Sedimentary Rock

Document Number: NWMO-TR-2018-08

Revision: 000

Class: Public

Page: 276

1.3		<i>Climatic Factors</i>		
	1.3.01	Global climate change	Included	After a period of global warming, it is assumed that glacial / interglacial cycling will eventually resume since the solar insolation variation driving this cycling will continue.
	1.3.02	Regional and local climate change	Included	In the near term, global warming is likely to cause temperature and precipitation changes, although the local / regional climate is likely to remain generally temperate due to the northerly latitude of the repository site. In the long term, the local / regional climate will respond to global climate change and will cool or warm with the glacial cycle.
	1.3.03	Sea level change	Excluded	Changes in sea level do not affect the site due to its assumed mid-continental location.
	1.3.04	Periglacial effects	Included	Periglacial effects will occur during the colder climate periods of the glacial cycles that are likely to occur at the site over a one million year timeframe. In particular, this would include permafrost development (see Chapter 2).
	1.3.05	Local glacial effects	Included	Ice sheets will cause a range of local effects, including changes in rock stress (FEP 1.2.02), earthquake initiation (FEP 1.2.03), changes in surface and near-surface hydrology (FEP 1.3.07), penetration of glacial waters to depth, and changes to ecosystems (FEP 1.3.08) and human behaviour (FEP 1.3.09).
	1.3.06	Warm climate effects (tropical and desert)	Excluded	Climate change is unlikely to result in development of tropical or hot desert conditions at the site due to its northerly latitude. An initial period of human-induced global warming is not expected to result in extreme temperature rise resulting in tropical or desert conditions in this region.

Postclosure Safety Assessment of a Used Fuel Repository in Sedimentary Rock

Document Number: NWMO-TR-2018-08

Revision: 000

Class: Public

Page: 277

	1.3.07	Hydrological response to near-term climate change	Excluded	<p>Surface and near-surface groundwater systems could be altered by a climatic change to wetter or drier conditions. However, the deep groundwater system at the site would not be significantly altered by climatic change to wetter or drier conditions (within expected variation, see FEP 1.3.06), due to its low-permeability and depth (see Chapter 2).</p> <p>Changes in hydrology due to glaciation are discussed separately under periglacial effects (1.3.04) and local glacial effects (1.3.05).</p>
	1.3.08	Ecological response to climate changes	Included	Flora and fauna at the site change in response to glacial / interglacial cycling.
	1.3.09	Human behavioural response to climate changes	Included	Human behaviour changes in response to glacial / interglacial cycling.
1.4	<i>Future Human Actions</i>			
	1.4.01	Human influences on climate	Included	Human actions are a possible cause of global climate change, which is included in the expected evolution of the repository system (see FEP 1.3.01, global climate change).
	1.4.02	Deliberate human intrusion	Excluded	<p>Deliberate human intrusion into the repository is not considered. It is assumed that any future society choosing to recover materials from the repository would have the technology to understand and manage the hazards.</p> <p>Note that unauthorized deliberate intrusion is unlikely due to the infrastructure needed to excavate to repository depth.</p>
	1.4.03	Non-intrusive site investigation	Excluded	Non-intrusive site investigations would not have any effect because of the repository depth.
	1.4.04	Drilling activities (human intrusion)	Excluded	<p>The drilling of deep exploration boreholes that penetrate to the repository is excluded from the expected evolution due to the repository depth (around 500 m), the relatively small repository footprint ~5 km², and the assumed lack of commercially viable natural resources at the site.</p> <p>Note that this FEP does not include drilling of shallow wells which are considered under FEP 1.4.07.</p>

Postclosure Safety Assessment of a Used Fuel Repository in Sedimentary Rock

Document Number: NWMO-TR-2018-08

Revision: 000

Class: Public

Page: 278

	1.4.05	Mining (human intrusion)	Excluded	It is assumed that there are no commercially viable mineral resources present at the site (see Chapter 1).
	1.4.06	Surface environment, human activities	Excluded	Surface activities are unlikely to have any direct impact on the repository due to the repository depth.
	1.4.07	Water management (wells, reservoirs, dams)	Included	<p>The drilling of shallow water wells in the area is considered once institutional controls are no longer effective (see FEP 1.1.10). Wells in the deeper groundwater zones are excluded since the groundwater in these zones is not potable. This is consistent with present-day practice in Ontario for extraction of water from shallow groundwater systems.</p> <p>Construction of dams and reservoirs is unlikely to have significant effects on the deep groundwater system due to the generally low topography around the site and the low permeability of the rock.</p>
	1.4.08	Social and institutional developments	Included	Institutional controls ensure appropriate use and control of the site in the near term, but it is assumed that this institutional control is eventually lost. Thereafter, the site is assumed to return to land use typical of the region and the site is occupied, including drilling of wells (see FEP 1.4.07).
	1.4.09	Technological developments	Excluded	It is assumed that the capabilities of future humans will largely resemble present-day capabilities, consistent with the International Commission on Radiological Protection's (ICRP 1998) recommendations and CNSC (2018). Thus, there is no credit taken for advances that might reduce the risk from the repository.
	1.4.10	Remedial actions	Excluded	Remedial actions are not expected following closure of the repository.
	1.4.11	Explosions and crashes	Excluded	Most surface explosions and crashes would have no direct impact on the repository due to its depth. Explosions large enough to affect repository depth would likely have large direct consequences that would be much more significant than any additional harm caused by damage to the repository.

Postclosure Safety Assessment of a Used Fuel Repository in Sedimentary Rock

Document Number: NWMO-TR-2018-08

Revision: 000

Class: Public

Page: 279

1.5		<i>Other External Factors</i>		
	1.5.01	Meteorite impact	Excluded	Excluded due to low probability (due to relatively small repository footprint) and / or low consequence (due to depth of repository). See FEP 1.5.01 in Garisto (2018). Furthermore, meteorites large enough to affect the repository would likely have large direct consequences that would be much more significant than any additional harm caused by damage to the repository.
	1.5.02	Species evolution	Excluded	No evolution of humans is assumed, consistent with the ICRP recommendation to apply the concept of (present-day) Reference Man to the management of long-lived solid radioactive waste (ICRP 1998). Similarly, no significant evolution of non-human biota is assumed – the general characteristics of biota are assumed to remain similar to current biota.
	1.5.03	Earth tides, reversal of earth's magnetic poles, polar wander and other unusual FEPs	Excluded	Consideration of unusual FEPs such as earth tides, reversal of earth's magnetic poles, polar wander, etc. are excluded because of their low probability or because they have no significant effect on the repository.

Note: (1) Status – *Included* means this factor is considered in the Normal Evolution Scenario. *Excluded* means this factor is not considered in the Normal Evolution Scenario.

6.1.2 Internal FEPs

Internal FEPs are important aids in defining the expected evolution of the repository. They assist in determining which features and processes are important to include in the conceptual model and related computer codes.

The significant FEPs are accounted for in the description of the Normal Evolution Scenario which appears in the following section.

The Internal FEPs are reviewed in Garisto (2018).

Internal FEPs are not usually scenario generating; however, they are considered with respect to Disruptive Event Scenarios in Section 6.2.1.

6.1.3 Description of the Normal Evolution of the Repository System

From consideration of the External FEPs and the Internal FEPs, the following high-level narrative of the expected evolution of the repository system can be developed. This understanding is based on many years of study, including laboratory studies, underground research studies, and observations of analogous natural and long-lived human-made structures and materials. This narrative is used to guide both the subsequent development of the conceptual model for the safety assessment and the variations to this model considered in alternative calculation cases.

The narrative summarizes the main events in the evolution of the repository in broad terms, including the long-term changes in the geosphere and biosphere due to glaciation. It is based on the reference design concept where used fuel is placed in the repository in long-lived copper-and-steel containers. These containers are designed not to fail and will be carefully fabricated and inspected. Most of these containers do not fail in the relevant time scale; however, as noted earlier there could be some containers with undetected defects in the copper shell, potentially leading to early releases of radioactivity. Since defective containers behave differently from intact containers, they are described separately in the following sections.

Most of the processes identified are well understood as discussed in Chapter 5. Key points are that the geosphere isolates the repository from the surface, that the groundwater around the repository level remains within its natural chemistry range and low oxygen state, and that the load-bearing capacity of the containers is sufficient to withstand the effects of glaciation and earthquakes at repository depth.

6.1.3.1 Events Occurring for Intact Containers

0-100 years

The repository is assumed to be open and actively monitored for a period of at least 100 years. The 100 year period consists of the reference design assumption of ~40 years of operation and up to 70 years of monitoring during which access tunnels are kept open. Decommissioning and closure will take a further 30 years. In the operation period, 108,833 containers (containing about 5.2 million used fuel bundles, or about 102,000 Mg of uranium) are placed in the repository with the placement rooms backfilled with clay-based sealing materials. The initial radioactivity in a full repository (assuming 30 year old fuel on average) is about 10^{20} Bq and the initial thermal load is about 18MW (Figure 6-1).

During the first 100 years after placement:

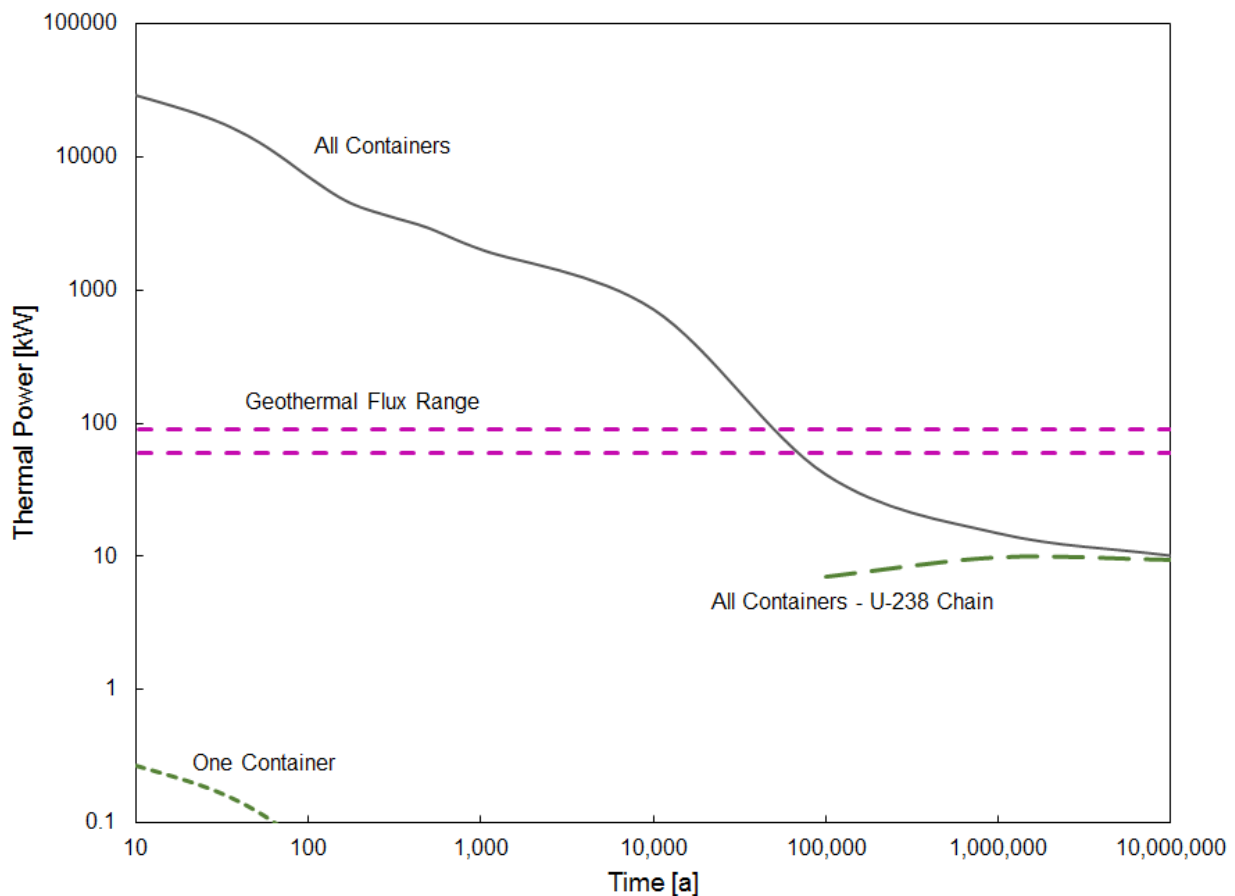
- Radioactivity drops by a factor of 10 and the thermal output drops by a factor of four. Radionuclides with short half-lives such as tritium (H-3) and Co-60 decay to negligible levels.
- Peak temperatures are reached within the repository, with values less than 100°C at the container outer surface.
- The copper container reacts with oxygen from the buffer to form a very thin corrosion layer.
- Any hydrogen gas generated at the copper surface from corrosion, if it occurs, suppresses further corrosion (see Chapter 5).
- Thermal expansion and contraction of the rock and concrete combine to create near-field stresses within the low-permeability rock and the concrete bulkhead at the end of the placement rooms, and a limited amount of microcracking occurs.
- In the rock around the repository, groundwater flow and heads are influenced by the presence of the open tunnels and the high-suction clay, which draw water towards the repository. This is countered by the container thermal power, which redistributes water away from the containers.
- Microbes in the buffer material near the containers die or become dormant because of heat, desiccation, lack of nutrients, or lack of space.

100–1,000 years

Around the beginning of this time period, all access tunnels and shafts are backfilled and sealed, with particular attention paid to sealing the shafts. All intrusive monitoring systems and deep boreholes are removed or closed. For several hundred years thereafter, distinct physical and chemical gradients (e.g., temperature, porewater composition) will exist between the various components of the repository, and between the repository and the geosphere. Many of the changes that occur within this timeframe are driven by these gradients. During this period:

- Radioactivity drops by a factor of 30. Most fission products decay to insignificant levels, including Sr-90 and Cs-137.
- Container thermal power drops to around 19 W per container. Residual heat comes from decay of the remaining actinides.
- Temperatures in the buffer material around the container are less than 93 °C and decreasing.
- The oxygen initially present in the sealing materials (as trapped air) is consumed.

- Groundwater from the geosphere continues to enter the repository. As the clay materials take up water, they swell and exert pressure on adjacent materials, including the container. The swelling process proceeds slowly and perhaps non-uniformly. The swelling clay fills cracks and voids. The EDZ properties are assumed unaffected by swelling of the clay-based seals.
- Climate change may have occurred. Global warming with higher average temperatures could lead to more or less precipitation at the site. This would affect the surface waters (lakes and rivers) and shallow groundwaters, and also the local ecosystem around the site, but deep groundwaters are unaffected.



Notes: The thermal power is similar to the natural geothermal flux range (based on lower and upper bound geothermal flux values from Perry et al. (2010) and an assumed repository footprint of 5 km²) after about 50,000 years. After about one million years, the residual power is due to radioactive decay of the decay products of uranium

Figure 6-1: Total Thermal Power of the Repository (Average 220 MWh/kgU Burnup)

1,000-60,000 years

- Radionuclides like C-14 have decayed.
- Thermal power drops to 1 W per container. Temperatures in the host rock in the horizontal direction surrounding the repository drop to less than 5°C above ambient, while temperatures above the centre of the repository decrease to about 20°C above ambient.
- By the end of this time, the repository is likely saturated and anaerobic, conditions typical of deep rock environments. Peak swelling loads of clay-based seals are 0.6 to 0.7 MPa under the high salinity conditions in the repository. The swelling clay fills cracks and voids. The EDZ properties are assumed unaffected by swelling of the clay-based seals.
- Hydrostatic loads and some of the rock mechanical loads are transmitted through the clays onto the container.
- The highly compacted bentonite and gap fill in the placement rooms become partially homogenized.
- The repository components gradually achieve equilibrium with the surrounding geosphere.
- Corrosion of the container has essentially stopped since the lack of oxygen prevents both uniform and localized corrosion.
- A fraction (< 5%) of the montmorillonite in the buffer is converted to illite due to the high potassium concentration (0.32 mol/L) present in groundwater and the slightly elevated temperatures experienced by the buffer over this period.
- The main microbial activity occurring in the repository is due to anaerobic bacteria, including sulphate-reducing bacteria, located mainly at the interfaces with the rock and in the backfill. The buffer remains largely inhospitable because of the high salinity, high clay density and pressure, which create adverse conditions of low water activity and small pore size.
- Locally near concrete surfaces, a more alkaline porewater develops in the clay-based sealing materials, resulting in an altered layer of clay, several centimetres thick, with a reduced swelling capacity near the interface.
- Changes continue to occur in the surface environment. Climate change due to natural or human influences would likely occur. In particular, the climate might start to cool as part of a long-term glacial cycle with possible formation of permafrost and initiation of glaciation at the site.

60,000-1,000,000 years

- Over this timeframe, the perturbations to the system are driven by external events. The most important events are glaciation cycles, which are likely to repeat on a period of roughly every 120,000 years, based on historical trends.
- The residual radioactivity is dominated by the decay of actinides. By the end of this period, all plutonium has decayed.
- The onset of a glaciation cycle starts with a cooling period, with mean surface temperatures over the sedimentary basin (in Ontario) dropping to approximately 0°C. Permafrost develops, disrupting groundwater flow down to about 190 m (see Chapter 2).
- Eventually, an ice sheet forms and extends across the site. The hydrological conditions at the edge of the glacier cause major perturbations to the near-surface groundwater flow system. The hydraulic heads at depth also change, but groundwater response is muted due to the low permeability of the deep rock.
- In some areas, glacially driven recharge may penetrate deeper, but reactions with minerals and microbes along the flow path of recharging meltwaters consume dissolved oxygen. Conditions at repository depth remain reducing.

- At its maximum development, the glacial ice sheet could be two to three kilometres thick above the repository, potentially increasing the hydrostatic pressure at repository depth by 20 to 30 MPa (possibly much less, depending on the rock properties and the nature of the ice sheet). This value is within the design tolerance of the containers.
- During glaciation, the land mass flexes vertically in excess of 500 m in response to the weight of the ice sheets. During glacial retreat, earthquakes may occur. Existing fracture zones may be reactivated in these locations although there is little change in terms of new fracture development.
- The advancing and retreating ice sheets and their associated meltwater both erode and deposit rock and till. Since the site has already experienced multiple glaciations in the past one million years, the amount of additional bedrock erosion could be up to tens of metres over a one million year timeframe. This would not adversely impact the isolation of the repository due to the low permeability of the intermediate and deep rock formations.
- The chemistry of the porewater within the sealing materials slowly changes to resemble that of the groundwater.
- Along with the porewater chemistry change, the montmorillonite component of the bentonite has lost Na and gained Ca, Mg, and Fe but has still retained its swelling capacity. Due to the lower temperatures, very little additional montmorillonite has converted to illite.
- Microbial activity in the repository is limited in general by the salinity of the groundwater (see Chapter 5). It is limited in terms of mobility by the impermeable dense buffer around the containers on one side and the low permeability rock on the other; and it is also limited metabolically by the low rate of anaerobic reactions at the ambient temperatures and by the requirement for nutrients to diffuse through the clay-based sealing materials.

Beyond 1,000,000 years

Virtually all the reactor-generated radioactivity has decayed, and most of the residual radioactivity in the used fuel comes from its natural uranium content. The amount of uranium in the repository is comparable to the large uranium ore bodies in north-central Canada. These natural deposits of uranium oxide have been stable for billions of years. Similarly, many ore deposits of metallic copper and sedimentary deposits of bentonite are known that range in age from millions to hundreds of millions of years. The ultimate fate of the repository and the materials it contains will be largely indistinguishable from these natural analogues.

6.1.3.2 Events Occurring for Defective Containers

The evolution of any defective containers will be different from that of intact containers. This evolution is summarized below (see Chapter 5 for a more detailed description).

Only the additional events that may occur in the evolution of these containers are summarized here, since most of the events occurring for the intact containers (e.g., radiation-related changes, thermal changes, etc.) also occur for defective containers. For the purposes of this discussion, it is assumed that (1) some containers are placed in the repository with undetected voids in the copper coating, larger than the expected detection limit of the inspection equipment, that are sufficiently large to cause these containers to be breached within the first one million years; and (2) a pathway through the copper coating to the underlying steel vessel is formed within the first 10,000 years, exposing the underlying steel to groundwater. The time frame for formation of a pathway through the copper coating is expected to be much longer than 10,000

years (see Chapters 5 and 7); in this case, the steel container would be breached at a much later time than described below.

0-100 years

Over this period the repository is not fully saturated. Atmospheric corrosion of the copper coating may occur but only to a very limited extent because the relative humidity near the copper container is low and oxygen is consumed by other processes.

100-1,000 years

The buffer swells and groundwater contacts the copper shell. Corrosion of copper is slow under the expected anaerobic conditions. The major corrosion mechanism is reaction with sulphide in the groundwater, which reaches the container surface from the surrounding geosphere by diffusion.

1,000-10,000 years

During this period, it is assumed that the corrosion of the copper coating is sufficiently fast and / or the void in the copper coating is sufficiently large that a pathway through the copper coating to the underlying steel vessel is formed. The buffer may swell into the defect and groundwater contacts the steel inner vessel. Anaerobic corrosion of the steel vessel begins, generating iron corrosion products and hydrogen gas. The most likely iron corrosion products are siderite and magnetite, depending on the carbonate groundwater concentration (see Chapter 5). For the discussion below, it is assumed that the steel corrosion rate is not limited by the availability of carbonate.

10,000-60,000 years

- During this period the steel below the defect continues to corrode and the depth of steel corrosion increases with time. If the steel corrosion rate is not carbonate limited, there may be penetration of the steel vessel if the defect occurs in the copper coating covering either the weld region (penetration in 4400 years) or the hemispherical heads (penetration in 33,000 years) of the steel vessel, which are thinner than the main cylindrical body of the steel vessel (see Section 5.4). If the defect is over the thicker parts of the steel vessel, then penetration occurs approximately 70,000 years after repository closure. (Penetration of the steel vessel would take much longer if the steel corrosion rate is carbonate limited, i.e., 140,000 years to 2 million years, depending on the location of the defect.)
- After penetration of the steel vessel, water (and bentonite) move into the interior of the vessel and the inside of the steel vessel also starts to corrode.
- Corrosion of the steel vessel continues and the hydrogen gas pressure increases near the breached container. The timing of events depends on the behaviour of the hydrogen.
- Hydrogen gas generated by steel corrosion forms a bubble or blanket that may inhibit water contact with the container and may inhibit ingress of liquid water into the container. Once the hydrogen pressure is high enough (on the order of the hydrostatic pressure plus swelling pressure), the gas will create a channel through the buffer, and move to the interface with the rock and into the EDZ. The pathway through the buffer re-seals after the gas passes so the effectiveness of the buffer is not impaired. The gas reaching the EDZ would move along the buffer-rock interface until the gas pressure decreases sufficiently that there is no driving force for advective gas movement.

- Water in the steel vessel contacts the fuel bundles. Local failure or corrosion of the Zircaloy cladding allows water to contact the used fuel in some fuel elements. The more soluble radionuclides (typically a few percent) in the fuel / cladding gap and grain boundaries are released into the water inside the steel vessel.
- A small amount of the used fuel dissolves, releasing other radionuclides into the water. The presence of hydrogen gas from corrosion of the steel container sustains conditions that significantly decrease the rate of fuel dissolution.
- Most radionuclides have decayed, or are trapped within the used fuel. Dissolved radionuclides diffuse out of the container and into the buffer surrounding the container.

60,000-1,000,000 years

- The steel vessel continues to corrode until all of the steel is consumed.
- Corrosion of the copper vessel continues but only a small fraction of the copper corrodes over this time period.
- Hydrogen gas from steel corrosion present within the EDZ slowly dissolves in groundwater and slowly diffuses away from the repository. Hydrogen gas remaining in the container also slowly dissolves allowing full saturation of the container.
- At some point, the steel vessel is sufficiently weakened by corrosion that it is no longer load bearing and could collapse, due to the external buffer swelling pressure (i.e., assuming infiltration of mainly water rather than bentonite into the breached container). Any remaining intact fuel bundles are damaged and exposed to water.
- Most of the UO₂ is fractured but intact. About 20% of the fuel has dissolved by the end of this period.
- Some radionuclides migrate out of the container, through the buffer, and into the nearby rock. Most radionuclides decay within or near the repository and surrounding rock. Slow migration of the more mobile, soluble and long-lived species (such as I-129) through the geosphere and into the shallow groundwater system and the biosphere can occur.

6.2 Disruptive Event Scenarios

Disruptive Event Scenarios postulate the occurrence of unlikely events leading to possible penetration of barriers and abnormal loss of containment.

6.2.1 Identification of Disruptive Event Scenarios

A set of Disruptive Event Scenarios has been identified by evaluating the potential for the External FEPs listed in Table 6-2 to compromise the isolation and containment function of the repository system. Specifically, relevant main safety attributes of the repository identified in Table 5-1 of Chapter 5 were checked to see if they could be significantly compromised by any of the External FEPs. This involved brainstorming sessions, and review of Disruptive Event Scenarios identified in previous Canadian and international safety assessments of a geological repository. The results of this assessment are summarized in Table 6-3.

As a further check, the potential for the Internal FEPs to compromise the relevant safety attributes is also considered, and summarized in Table 6-4. Note that the FEPs considered under the “Biosphere Factors” and “Contaminant Factors” categories are not capable on their own of modifying the repository system to an extent that results in a fundamentally different evolution to that considered in the Normal Evolution Scenario. These are therefore not scenario

generating and their effects can be evaluated through different calculation cases for the Normal Evolution Scenario rather than through the development of Disruptive Event Scenarios.

The failure mechanisms identified in Table 6-3 and Table 6-4 can be grouped into eight Disruptive Event Scenarios as discussed below and summarized in Table 6-5. Since the long-term safety of the repository is based on the strength of the geosphere and engineered barriers (including the container and shaft seals), the scenarios focus on events in which these can be degraded or bypassed.

Table 6-3: External FEPs Potentially Compromising Safety Attributes Relating to Long-Term Safety

Safety Attribute	Potentially Compromised by	Consider as Failure Mechanism
<p>1.1. The repository depth isolates the waste and repository components from surface changes created by human activities or natural events.</p>	<p>Meteorite impact (FEP 1.5.01).</p>	<p>No, due to low probability of meteor impact capable of compromising safety due to the relatively small repository footprint (~ 5 km²) and depth of repository (~500 m). See Garisto (2018) for further discussion of probabilities.</p>
	<p>Exploration borehole penetrates into repository providing enhanced permeability pathway to surface environment and potential for direct exposure to waste (FEP 1.4.04).</p>	<p>Yes, although the absence of economically exploitable resources, and the depth (~500 m) and relatively small repository footprint (~ 5 km²) mean that the likelihood of such a borehole intruding into the repository would be very low during the period of greatest potential hazard.</p>
	<p>Mining and other underground activities resulting in excavation in the vicinity of the repository (FEP 1.4.05).</p>	<p>No, due to assumption of the absence of commercially viable mineral resources near or below repository level. Shallow quarrying or tunnelling activities are unlikely to affect the repository because of repository depth (~500m). Also, most underground activities would likely be preceded by exploration boreholes, as addressed above.</p>
	<p>Deliberate human intrusion into repository (FEP 1.4.02).</p>	<p>No, exclude deliberate human intrusion since it is expected that the intruders would take appropriate precautions.</p> <p>Note that unauthorized deliberate intrusion is unlikely due to the infrastructure needed to excavate to repository depth.</p>

Postclosure Safety Assessment of a Used Fuel Repository in Sedimentary Rock

Document Number: NWMO-TR-2018-08

Revision: 000

Class: Public

Page: 289

Safety Attribute	Potentially Compromised by	Consider as Failure Mechanism
	<p>Could discover resources that were not identified during site investigations (FEP 1.1.01) or exploit existing rocks that have become a commercially viable resource. These new resources are exploited by drilling or mining at or below repository level (FEP 1.4.04 and FEP 1.4.05).</p>	<p>No, the lack of resources at the site is assumed to be consistent with regional information. Even if the existing rocks became commercially viable, the repository site is unlikely to become a mine site because of the uniformity and large lateral extent of the host rocks that extend to shallower depths elsewhere.</p> <p>Also, deep mining activities would likely be preceded by an exploration borehole, which is considered under FEP 1.4.04.</p>
	<p>Repository and shafts are not properly sealed providing an enhanced permeability pathway to the surface environment (FEP 1.1.04).</p>	<p>No, shaft seals are large structures consisting of composite materials that would take months or years to install under NWMO quality control and regulatory oversight. A highly improbable failure of the quality control system, lasting many months would be needed for these seals to perform poorly due to improper installation.</p>
	<p>Shaft seals perform poorly due to unexpected chemical interactions with groundwater and / or glacial meltwater, providing an enhanced permeability pathway to the surface environment (FEP 1.1.04).</p>	<p>Yes, although sealing materials will be chosen to be compatible with existing conditions at the repository site, unforeseen chemical interactions could unduly affect performance of seals.</p>
	<p>Repository and shafts not sealed, providing an enhanced permeability pathway to the surface environment (FEP 1.1.04).</p>	<p>Yes, due to some severe societal disruption, the repository is not closed as planned but remains open and unsealed, and not maintained.</p>

Postclosure Safety Assessment of a Used Fuel Repository in Sedimentary Rock

Document Number: NWMO-TR-2018-08

Revision: 000

Class: Public

Page: 290

Safety Attribute	Potentially Compromised by	Consider as Failure Mechanism
	Site investigation / monitoring borehole not properly sealed providing an enhanced permeability pathway to the surface environment (FEP 1.1.01 and FEP 1.1.11).	No , the boreholes are long and the seals would consist of composite materials that would be installed under enhanced NWMO quality control and regulatory oversight. Given the relatively small number of boreholes to be sealed, a highly improbable failure of the quality control system would be needed for borehole seals to perform poorly due to improper installation.
	Site investigation / monitoring borehole seals perform poorly due to unexpected chemical interactions with groundwater or glacial meltwater, providing an enhanced permeability pathway to the surface environment (FEP 1.1.01 and FEP 1.1.11).	Yes , although sealing materials will be chosen to be compatible with existing conditions at the repository site, unforeseen chemical interactions could unduly affect performance of seals.
	Site investigation / monitoring borehole not sealed, providing an enhanced permeability pathway to the surface environment (FEP 1.1.01 and FEP 1.1.11).	Yes , due to some severe societal disruption, the repository is not closed as planned but remains open and unsealed but not maintained.
	Poor construction techniques affect the performance of the repository and shaft excavation disturbed zones providing an enhanced permeability pathway to the surface environment (FEP 1.1.02).	Yes , although NWMO quality control and regulatory oversight will ensure that poor sealing is very unlikely.
	Site investigations do not identify a permeable fracture zone or fault that provides a connection between the repository horizon and shallow groundwater system (FEP 1.1.01).	Yes , although very unlikely, such a feature cannot be categorically ruled out due to the limits of current technologies to identify all fracture zones, and so is considered in a Disruptive Event Scenario.

Postclosure Safety Assessment of a Used Fuel Repository in Sedimentary Rock

Document Number: NWMO-TR-2018-08

Revision: 000

Class: Public

Page: 291

Safety Attribute	Potentially Compromised by	Consider as Failure Mechanism
	High magnitude seismic event results in reactivation of undetected existing structural discontinuity which provides an enhanced permeability pathway to higher horizons (FEP 1.2.03).	Yes , the assessment time scales are such that a significant seismic event may occur even though the annual probability is low. Also, the probability of seismic events increases during periods of glacial retreat. However, the probability that an earthquake could actually reactivate a nearby fracture is very small since it would take a significant amount of energy.
	High magnitude seismic event affects performance of repository and shaft excavation disturbed zones, and / or shaft seals, providing an enhanced permeability pathway to higher horizons (FEP 1.2.03).	Yes , the assessment time scales are such that a significant seismic event may occur even though the annual probability is low. Also, the probability of seismic events increases during periods of glacial retreat.
	Ice sheet erosion removes a significant thickness of rock above repository (FEPs 1.2.07, 1.3.01, 1.3.02, and 1.3.05).	Yes , the impact of realistic rates of glacial erosion is addressed as part of the Normal Evolution Scenario; whereas, severe erosion is considered as a Disruptive Event Scenario.
	Advance / retreat of ice sheets generate large hydraulic gradients which affect groundwater flow velocities in the deep groundwater zone (FEP 1.3.05).	No , the changing hydraulic head due to ice sheet advance and retreat over the repository site may affect groundwater flow at the repository level, but advective flows will remain low due to the low permeability of the deep rock (see Chapter 2, particularly the discussion of the paleohydrogeologic sensitivity cases). Since glaciation is included in the Normal Evolution Scenario, the normal changes caused by glaciation do not generate additional Disruptive Events.

Postclosure Safety Assessment of a Used Fuel Repository in Sedimentary Rock

Document Number: NWMO-TR-2018-08

Revision: 000

Class: Public

Page: 292

Safety Attribute	Potentially Compromised by	Consider as Failure Mechanism
	Other external geological processes disrupt the repository system, i.e., Tectonic movement and orogeny (FEP 1.2.01), Volcanic and magmatic activity (FEP 1.2.04), Metamorphism (FEP 1.2.05), Hydrothermal activity (FEP 1.2.06), Diagenesis (FEP 1.2.08) and Salt diapirism and dissolution (FEP 1.2.09).	No , since precluded by site's location and assessment time scales.
1.2. The repository is enclosed by stable, competent and low permeability rock.	Site investigations do not identify a permeable fracture zone or fault that provides a connection between the repository horizon and shallow groundwater system (FEP 1.1.01).	Yes , although very unlikely, such a feature cannot be categorically ruled out due to the limits of current technologies to identify all fracture zones, and so is considered in a Disruptive Event Scenario.
	High magnitude seismic event results in reactivation of undetected existing structural discontinuity which provides an enhanced permeability pathway to higher horizons (FEP 1.2.03).	Yes , the assessment time scales are such that a significant seismic event may occur even though the annual probability is low. However, the probability that an earthquake could actually reactivate a nearby fracture is very small since it would take a significant amount of energy.
	High magnitude seismic event affects performance of repository and shaft excavation disturbed zones, and / or shaft seals, providing an enhanced permeability pathway to higher horizons (FEP 1.2.03).	Yes , the assessment time scales are such that a significant seismic event may occur even though the annual probability is low.
	Other external geological processes disrupt the repository system, i.e., Tectonic movement and orogeny (FEP 1.2.01), Volcanic and magmatic activity (FEP 1.2.04), Metamorphism (FEP 1.2.05), Hydrothermal activity (FEP 1.2.06), Diagenesis (FEP 1.2.08) and Salt diapirism and dissolution (FEP 1.2.09).	No , since precluded by site's location and assessment time scales.

Postclosure Safety Assessment of a Used Fuel Repository in Sedimentary Rock

Document Number: NWMO-TR-2018-08

Revision: 000

Class: Public

Page: 293

Safety Attribute	Potentially Compromised by	Consider as Failure Mechanism
<p>1.3. The hydrogeologic setting that encloses the repository restricts groundwater and radionuclide movement.</p>	<p>High magnitude seismic event results in reactivation of undetected existing structural discontinuity which provides an enhanced permeability pathway to higher horizons (FEP 1.2.03).</p>	<p>Yes, the assessment time scales are such that a significant seismic event may occur even though the annual probability is low. However, the probability that an earthquake could actually reactivate a nearby fracture is very small since it would take a significant amount of energy.</p>
	<p>High magnitude seismic event affects performance of repository and shaft excavation disturbed zones, and /or failure of shaft seals, providing an enhanced permeability pathway to higher horizons (FEP 1.2.03).</p>	<p>Yes, the assessment time scales are such that a significant seismic event may occur even though the annual probability is low.</p>
	<p>Advance / retreat of ice sheets generate large hydraulic gradients which affect groundwater flow velocities in the deep groundwater zone (FEP 1.3.05).</p>	<p>No, for the paleohydrogeologic sensitivity cases examined in Chapter 2, the glacial perturbations did not materially change groundwater flow rates at repository depth and diffusion remains the dominant transport mechanism in the host rock zone.</p> <p>Note that it is assumed that there are no fracture zones or faults at or near the site, which is consistent with Chapter 2, and, furthermore, there are no undetected geological features at the repository site.</p>
	<p>Other external geological processes disrupt the repository system, i.e., Tectonic movement and orogeny (FEP 1.2.01), Volcanic and magmatic activity (FEP 1.2.04), Metamorphism (FEP 1.2.05), Hydrothermal activity (FEP 1.2.06), Diagenesis (FEP 1.2.08) and Salt diapirism and dissolution (FEP 1.2.09).</p>	<p>No, since precluded by site's location and assessment time scales.</p>

Postclosure Safety Assessment of a Used Fuel Repository in Sedimentary Rock

Document Number: NWMO-TR-2018-08

Revision: 000

Class: Public

Page: 294

Safety Attribute	Potentially Compromised by	Consider as Failure Mechanism
<p>1.4. The mineralogy of the host rock, and the composition of the ground/porewater, are compatible with the engineered barriers.</p> <p>1.5. The host rock mineralogy and the composition of the ground/porewater are favourable for mitigating radionuclide movement.</p> <p>2.3. The repository conditions including chemistry and physical condition important for safety are not influenced by internal and external perturbations, including glaciation.</p>	<p>Infiltration of glacial meltwater (without oxygen) into the repository modifies the hydrogeochemical conditions, affecting, for example, the stability of the buffer and backfill materials (i.e., leads to erosion of these materials due to colloid formation) (FEP 1.3.05).</p> <p>Infiltration of oxygenated glacial meltwater into the repository leads to oxidizing conditions in the repository, causing relatively rapid corrosion of copper containers, rapid corrosion of used fuel in any defective containers, and enhanced mobility of redox sensitive nuclides such as U and Tc.</p> <p>Other external geological processes disrupt the repository system, i.e., Tectonic movement and orogeny (FEP 1.2.01), Volcanic and magmatic activity (FEP 1.2.04), Metamorphism (FEP 1.2.05), Hydrothermal activity (FEP 1.2.06), Diagenesis (FEP 1.2.08) and Salt diapirism and dissolution (FEP 1.2.09).</p>	<p>No, the paleohydrogeologic simulations described in Chapter 2 suggest that glacial meltwaters will not reach the repository horizon. This is due to the low hydraulic conductivity of the overlying shales, dolostones and Salina Group evaporites.</p> <p>Note that, consistent with Chapter 2, it is assumed that there are no fracture zones (or faults) at the repository site.</p> <p>No, glacial recharge penetrating below the shallow groundwater system (i.e., depths greater than 215 m) is not expected to be oxygenated or influence redox conditions at the repository horizon (see Chapter 2).</p> <p>No, since precluded by site's location and assessment time scales.</p>

Postclosure Safety Assessment of a Used Fuel Repository in Sedimentary Rock

Document Number: NWMO-TR-2018-08

Revision: 000

Class: Public

Page: 295

Safety Attribute	Potentially Compromised by	Consider as Failure Mechanism
<p>2.1. The hydrogeologic conditions at repository depth are stable and resilient to internal and external perturbations, including glaciation.</p> <p>2.2. The host rock is capable of withstanding thermal and mechanical stresses induced by internal and external perturbations, including glaciation.</p>	<p>Presence of repository weakens rock near repository, potentially making it susceptible to fracturing during earthquakes which could be caused by ice sheet loading / unloading (FEP 1.2.02).</p>	<p>Yes, an unknown fault or fracture zone could be reactivated due to seismic activity.</p>
<p>1.7 Seismic hazard is low.</p> <p>2.5. Repository safety is not influenced by strong ground motions associated with rare earthquakes.</p>	<p>High magnitude seismic event results in reactivation of undetected existing structural discontinuity which provides an enhanced permeability pathway to higher horizons (FEP 1.2.03).</p> <p>High magnitude seismic event affects performance of repository and shaft excavation disturbed zones, and /or shaft seals, providing an enhanced permeability pathway to higher horizons (FEP 1.2.03).</p>	<p>Yes, the assessment time scales are such that a significant seismic event may occur even though the annual probability is low. However, the probability that an earthquake could actually reactivate a nearby fracture is very small since it would take a significant amount of energy.</p> <p>Yes, the assessment time scales are such that a significant seismic event may occur even though the annual probability is low.</p>

Postclosure Safety Assessment of a Used Fuel Repository in Sedimentary Rock

Document Number: NWMO-TR-2018-08

Revision: 000

Class: Public

Page: 296

Safety Attribute	Potentially Compromised by	Consider as Failure Mechanism
	<p>Large seismic event results in shearing along an existing fracture zone that passes through a placement room of the repository. The shearing load causes failure of a used fuel container.</p>	<p>Yes, the assessment time scales are such that a significant seismic event may occur even though the annual probability is low. However, the probability that an earthquake would cause failure of a container in a placement room due to a shear load is very small due to the low seismicity at the site, as assumed in Chapter 1; the lack of fractures in the host rock at the repository site, which is consistent with Chapter 2; and the tolerance of the design to some extent of shearing.</p>
<p>2.4. Rate of erosion is low.</p>	<p>Ice sheet erosion removes a significant thickness of rock above repository (FEPs 1.2.07, 1.3.01, 1.3.02, and 1.3.05).</p>	<p>Yes, the impact of realistic rates of glacial erosion is addressed as part of the Normal Evolution Scenario; whereas, severe erosion is considered as a Disruptive Event Scenario.</p>
	<p>Land uplift decreases depth of repository.</p>	<p>No, land uplift occurs on a continental scale so relative depth of repository does not change. Land uplift and large-scale erosion are also not significant factors in affecting repository depth on assessment time scale.</p>

Postclosure Safety Assessment of a Used Fuel Repository in Sedimentary Rock

Document Number: NWMO-TR-2018-08

Revision: 000

Class: Public

Page: 297

Safety Attribute	Potentially Compromised by	Consider as Failure Mechanism
<p>1.6. Natural resource potential is low within the repository geologic setting.</p>	<p>Mining and other underground activities resulting in excavation in the vicinity of the repository (FEP 1.4.05).</p>	<p>No, due to the assumption of the absence of commercially viable resources near or below repository level. Other underground activities are unlikely to affect the repository (e.g., rock quarry) because of repository depth (~500 m). Also, such activities would likely be preceded by exploration boreholes, as addressed above.</p> <p>Even if the host rock itself became commercially viable, the repository site is unlikely to become a mine site because of the uniformity and large lateral extent of the host rock that extends to shallower depths elsewhere.</p>
	<p>Deliberate human intrusion into repository (FEP 1.4.02).</p>	<p>No, exclude deliberate human intrusion since it is expected that the intruders would take appropriate precaution.</p>
	<p>Could discover resources that were not identified during site investigations (FEP 1.1.01) or exploit existing rocks that have become a commercially viable resource. These new resources are exploited by drilling or mining at or below repository level (FEP 1.4.04 and FEP 1.4.05).</p>	<p>No, the lack of resources at the site is assumed to be consistent with regional information.</p> <p>Even if the host rock itself became commercially viable, the repository site is unlikely to become a mine site because of the uniformity and large lateral extent of the host rock that extends to shallower depths elsewhere.</p> <p>Also, the impact of drilling is already considered under exploration borehole (FEP 1.4.04).</p>

Postclosure Safety Assessment of a Used Fuel Repository in Sedimentary Rock

Document Number: NWMO-TR-2018-08

Revision: 000

Class: Public

Page: 298

Safety Attribute	Potentially Compromised by	Consider as Failure Mechanism
<p>4.1 Most radionuclides are immobile within the uranium oxide grains of the used CANDU fuel.</p> <p>4.2 The used CANDU fuel grains are mechanically durable and not materially impacted by radiation damage or helium gas buildup.</p> <p>4.3 The used fuel has low solubility under conditions of a failed container with contact with ground/porewater.</p> <p>4.4 The Zircaloy cladding provides a barrier to contact between ground/porewater and used fuel in a failed container.</p> <p>4.5 The Zircaloy cladding corrodes slowly under conditions of a failed container in contact with ground/porewater.</p>	<p>Infiltration of oxygenated glacial meltwater into the repository leads to oxidizing conditions in the repository, causing relatively rapid corrosion of copper containers, rapid dissolution of used fuel in any defective containers, and enhanced mobility of redox sensitive nuclides such as U and Tc.</p>	<p>No, glacial recharge penetrating below the shallow groundwater system (i.e., depths greater than 215 m) is not expected to be oxygenated or influence the redox conditions at the repository horizon (see Chapter 2).</p>
<p>5.1. The container is designed for the underground conditions at timeframes relevant to repository safety.</p>	<p>Defects in the copper coating of some containers are not detected by the quality inspection program, impacting the durability and expected lifetime of these containers (FEP 1.1.03, 1.1.08).</p>	<p>Yes, although NWMO's quality control measures will make it very likely that poorly manufactured containers would be discovered and not used, some defective containers may somehow escape detection by the inspection program, given the large number of containers in the repository.</p>

Postclosure Safety Assessment of a Used Fuel Repository in Sedimentary Rock

Document Number: NWMO-TR-2018-08

Revision: 000

Class: Public

Page: 299

Safety Attribute	Potentially Compromised by	Consider as Failure Mechanism
<p>5.2. Inspection methods would ensure the container is built consistent with design specifications.</p>	<p>Unanticipated interactions of the containers with groundwater impact the durability of the used fuel containers (FEP 1.1.03, 1.1.08), significantly reducing their expected lifetime.</p>	<p>Yes, although the repository site would be selected to ensure the long-term durability of the containers, unexpected chemical interactions (e.g., due to the presence of sulphides) could impact the lifetime of the containers.</p>
	<p>Used fuel containers fail due to increase in the isostatic load caused by a thick ice sheet passing over the repository site.</p>	<p>Yes, although the containers are designed to withstand the total isostatic load from buffer swelling, the current hydrostatic load, and the additional hydrostatic load from a design-basis ice sheet passing over the repository site, the possibility that the design load of the container could be exceeded due to the passage of a beyond design-basis ice sheet needs to be considered.</p>
	<p>Infiltration of oxygenated glacial meltwater into the repository leads to oxidizing conditions in the repository, leading to relatively rapid corrosion of the copper containers (FEP 1.3.05).</p>	<p>No, glacial recharge penetrating below the shallow groundwater system (i.e., depths greater 215 m) is not expected to be oxygenated or influence the redox conditions at the repository horizon (see Chapter 2).</p>
<p>5.3. The in-room buffer system holds and protects the containers.</p> <p>5.4. Engineered seals isolate the placement rooms from the access tunnels.</p> <p>5.5. Shaft backfill and seals isolate the repository from the surface.</p>	<p>Bentonite buffer layer around some containers not properly installed and, therefore, the density of the buffer around these container is lower than the design requirement.</p> <p>Infiltration of glacial meltwater (without oxygen) into the repository modifies the hydrogeochemical conditions in the repository, affecting, for example, the stability of the buffer and backfill materials (i.e., leads to erosion of these materials due to colloid formation) (FEP 1.3.05).</p>	<p>Yes, although use of a buffer box and application of NWMO's quality control measures make it very unlikely that the bentonite layer would have substandard properties.</p> <p>No, the paleohydrogeologic simulations described in Chapter 2 suggest that glacial meltwaters will not reach the repository horizon. This is due to the low hydraulic conductivity of the overlying shales, dolostones and Salina Group evaporites.</p>

Postclosure Safety Assessment of a Used Fuel Repository in Sedimentary Rock

Document Number: NWMO-TR-2018-08

Revision: 000

Class: Public

Page: 300

Safety Attribute	Potentially Compromised by	Consider as Failure Mechanism
	<p>A large seismic event causes rock shear along an undetected fracture intersecting the repository at a container location, reducing the buffer thickness between the container surface and the rock.</p>	<p>Yes, the assessment time scales are such that a significant seismic event may occur even though the annual probability is low. Even then, the probability that the earthquake could actually reactivate a nearby fracture is very small since it would take a significant amount of energy.</p>
<p>6.4. Institutional controls and monitoring will verify performance.</p>	<p>Institutional controls on the development of the site are ineffective (FEP 1.4.08). This allows development of the site (FEP 1.4.06) and human intrusion into the repository to occur by drilling (FEP 1.4.04) and / or mining (FEP 1.4.05)</p>	<p>No, measures are assumed to be taken in the near term to ensure that information regarding the purpose, location, design and contents of the repository is preserved so that future generations are made aware of the consequences of any actions they may choose to take. With these institutional measures as well as general societal memory, and with the absence of commercially viable natural resources at depth, inadvertent intrusion in the near term after closure is not considered. However, Human Intrusion is considered in the long term.</p>

Table 6-4: Internal FEPs Potentially Compromising Safety Attributes Relating to Long-Term Safety

Safety Attribute	Potentially Compromised by	Consider as Failure Mechanism
1.1. The repository depth isolates the waste and repository components from surface changes created by human activities or natural events.	No Internal FEP could result in a significant change in the depth of the repository. Note that FEP 5.1.10 relates to the erosion of surficial deposits and not bedrock.	No.
1.2. The repository is enclosed by stable, competent and low permeability rock.	An undetected feature (e.g., a fracture zone) in the geosphere provides a relatively high permeability connection between the repository horizon and higher horizons (FEP 4.1.02 and FEP 4.1.03).	Yes , a nearby fracture zone or other feature could be missed during site investigation due to the limits of current technologies to identify such features.
1.3. The hydrogeologic setting that encloses the repository restricts groundwater and radionuclide movement.	An undetected feature (e.g., a fracture) in the geosphere provides a relatively high permeability connection between the repository horizon and higher horizons (FEP 4.1.02 and FEP 4.1.03).	Yes , a nearby fracture zone or other feature could be missed due to the limits of current technologies to identify such features.
	The failure of most of the containers in the repository, due to an unexpected mechanism, leads to generation of a significant amount of hydrogen gas due to corrosion of the iron inner vessel. The hydrogen pressure could, in theory, exceed the lithostatic pressure leading to rock fracture.	Yes , mechanisms have been identified by which most of the containers in the repository fail (see Table 6-3). For such a scenario, it will be necessary to determine the magnitude of the peak hydrogen pressure and its impact on the repository and host rock.

Postclosure Safety Assessment of a Used Fuel Repository in Sedimentary Rock

Document Number: NWMO-TR-2018-08

Revision: 000

Class: Public

Page: 302

Safety Attribute	Potentially Compromised by	Consider as Failure Mechanism
	<p>A pattern of over- and under-pressure in the groundwater and porewater hydraulic heads at the site is observed during site investigation or forms in the future due to, for example, glaciation. Such pressures would represent a state of disequilibrium.</p>	<p>Yes, such patterns have been observed at some sites in Southern Ontario. However, the hypothetical site is assumed to not include any significant over- or underpressure, and this would be readily detected during site characterization. No future geological mechanisms are identified that would cause this behavior on relevant timescales. Glaciation would cause pressure changes, but these are evaluated in Chapter 2 and are temporary and not significant. Nonetheless, the possibility of an overpressure forming at the boundary with the Precambrian basement is considered as a conservative sensitivity case for the Normal Evolution Scenario, even though the low hydraulic conductivity of the rock means advective flows would remain low for realistic overpressures.</p>
<p>1.4. The mineralogy of the host rock, and the composition of the ground/porewater, are compatible with the engineered barriers.</p> <p>1.5. The host rock mineralogy and the composition of the ground/porewater are favourable for mitigating radionuclide movement.</p>	<p>Various repository FEPs (e.g., FEPs 3.1.02, 3.2.01 to 3.2.05), such as temperature rise in the repository, groundwater salinity and groundwater-buffer interactions, and geosphere FEPs (e.g., FEPs 4.2.01 to 4.2.05), such as geothermal gradient and karst formation, have the potential to modify the hydrological, mechanical and chemical conditions at repository depth, affecting seal properties and / or radionuclide movement.</p>	<p>No, the effects are likely to be localized to the immediate vicinity of the repository and these FEPs can be evaluated through considering different calculation cases for the Normal Evolution Scenario (e.g., low sorption and high solubility sensitivity cases) rather than through the development of alternative Disruptive Event Scenarios. For conservatism, concrete seals are assumed degraded from the time of repository closure.</p>
<p>2.3. The repository conditions including chemistry and physical condition important for safety are not influenced</p>	<p>Various waste package FEPs (e.g., FEPs 2.3.01 to 2.3.04) can influence the durability of the used fuel containers, potentially leading to container failures.</p>	<p>Yes, poor local conditions (e.g., low buffer density) might cause a limited number of container failures due to, for example, biofilm formation on the copper surface leading to microbial corrosion.</p> <p>Note that the Normal Evolution Scenario already includes a number of containers with pre-existing defects in the copper coating which lead to container failures.</p>

Postclosure Safety Assessment of a Used Fuel Repository in Sedimentary Rock

Document Number: NWMO-TR-2018-08

Revision: 000

Class: Public

Page: 303

Safety Attribute	Potentially Compromised by	Consider as Failure Mechanism
<p>by internal and external perturbations, including glaciation.</p>	<p>Various repository FEPs (e.g., FEPs 3.2.01 to 3.2.05), such as temperature rise and groundwater interactions, and geosphere FEPs (e.g., FEPs 4.3.01 to 4.3.08), such as sorption and diffusion, can affect the rate at which contaminants are released from the repository and migrate through the shafts and geosphere.</p>	<p>No, the effects of these FEPs can be evaluated through considering different calculation cases for the Normal Evolution Scenario rather than through the development of alternative Disruptive Event Scenarios (e.g., no sorption and high solubility sensitivity cases). The repository and shaft excavation damaged zones (EDZs) are considered in the Normal Evolution Scenario. Also, concrete seals are assumed degraded from the time of repository closure.</p>
	<p>Changes in porewater chemistry in the repository due to, for example, temperature rise in the repository and presence of concrete adversely affects clay seals (FEP 3.1.02 and FEP3.2.04).</p>	<p>No, use of low-temperature, low pH concrete in the repository minimizes interactions with clay seals. Also, the amount of concrete in the repository is small compared to the amount of clay sealing materials.</p>
<p>2.1. The hydrogeologic conditions at repository depth are stable and resilient to internal and external perturbations, including glaciation.</p> <p>2.2. The host rock is capable of withstanding thermal and mechanical stresses induced by internal and external perturbations, including glaciation.</p>	<p>Mechanical and thermal stresses induced by presence of the repository are underestimated and cause greater than expected fracturing within the repository, the host rock and shaft EDZs, providing an enhanced permeability pathway to the surface environment (e.g., FEP 3.2.01 and FEP 3.2.03).</p>	<p>Yes, although application of NWMO's quality control measures and engineering safety factors would make it unlikely that stresses are underestimated.</p>

Postclosure Safety Assessment of a Used Fuel Repository in Sedimentary Rock

Document Number: NWMO-TR-2018-08

Revision: 000

Class: Public

Page: 304

Safety Attribute	Potentially Compromised by	Consider as Failure Mechanism
<p>1.7 Seismic hazard is low.</p> <p>2.5. Repository safety is not influenced by strong ground motions associated with rare earthquakes.</p>	<p>Relates to External FEPs only (see Table 6-3).</p>	
<p>2.4. Rate of erosion is low.</p>	<p>Relates to External FEPs only (see Table 6-3).</p>	
<p>1.6. Natural resource potential is low within the repository geologic setting.</p>	<p>Relates to External FEPs only (see Table 6-3).</p>	
<p>4.1 Most radionuclides are immobile within the uranium oxide grains of the used CANDU fuel.</p> <p>4.2 The used CANDU fuel grains are mechanically</p>	<p>Various waste package FEPs (e.g., FEP 2.1.02, and FEP 2.2), such as radiation and temperature effects, and rates of used fuel dissolution in groundwater, can affect the rate at which contaminants are released from the used fuel.</p>	<p>No, the effects of these FEPs can be evaluated through considering different calculation cases for the Normal Evolution Scenario rather than through the development of alternative Disruptive Event Scenarios (e.g., sensitivity cases with a faster fuel dissolution rate or larger instant release fractions).</p>

Postclosure Safety Assessment of a Used Fuel Repository in Sedimentary Rock

Document Number: NWMO-TR-2018-08

Revision: 000

Class: Public

Page: 305

Safety Attribute	Potentially Compromised by	Consider as Failure Mechanism
<p>durable and not materially impacted by radiation damage or helium gas buildup.</p> <p>4.3 The used fuel has low solubility under conditions of a failed container with contact with ground/porewater.</p> <p>4.4 The Zircaloy cladding provides a barrier to contact between ground/porewater and used fuel in a failed container.</p> <p>4.5 The Zircaloy cladding corrodes slowly under conditions of a failed container in contact with ground/porewater.</p>	<p>Release due to criticality accident.</p>	<p>No, the used fuel is natural uranium based. The fissile content of the used fuel is too low.</p>
<p>5.1. The container is designed for the underground conditions at timeframes relevant to repository safety.</p> <p>5.2. Inspection methods would ensure the container is built consistent with design specifications.</p>	<p>Containers are not fabricated to specifications and so are placed in the repository with defects (FEPs 2.3.01 to 2.3.04).</p>	<p>Yes, although the fabrication method is designed to be robust and there would be multiple methods of inspection, there is statistically some probability of some defective containers not being detected (given the large number of containers) such that a few containers are placed in the repository with defects.</p> <p>The Normal Evolution Scenario assumes some containers with undetected defects are present in the repository at the time of closure, leading to container failures.</p>

Postclosure Safety Assessment of a Used Fuel Repository in Sedimentary Rock

Document Number: NWMO-TR-2018-08

Revision: 000

Class: Public

Page: 306

Safety Attribute	Potentially Compromised by	Consider as Failure Mechanism
	<p>Various waste package and repository FEPs (e.g., FEPs 2.3.03, 2.3.04, 3.1.02, 3.2.01 to 3.2.05), such as uniform corrosion, buffer properties, temperature, and groundwater chemistry, can influence the durability of the used fuel containers, potentially leading to container failures.</p>	<p>Yes, although evidence suggests that the copper container would be thermodynamically stable under the reducing conditions expected in the repository, poor local conditions might cause a limited number of container failures.</p> <p>The Normal Evolution Scenario assumes some containers with undetected defects are present in the repository at the time of closure, leading to container failures.</p>
<p>5.3. The in-room buffer system holds and protects the containers.</p> <p>5.4. Engineered seals isolate the placement rooms from the access tunnels.</p> <p>5.5. Shaft backfill and seals isolate the repository from the surface.</p>	<p>Various repository FEPs (e.g., FEPs 3.1.02, 3.2.01 to 3.2.05), buffer properties, temperature, and groundwater chemistry, can influence the durability of the used fuel containers, potentially leading to container failures.</p> <p>Various repository FEPs (e.g., FEPs 3.1.02, 3.1.03, 3.2.01 to 3.2.05), such as temperature, hydrothermal alteration of the buffer, and buffer-groundwater interactions, have the potential to modify the hydrological, mechanical and chemical conditions at the repository depth, affecting properties of clay-based materials.</p>	<p>Yes, although evidence suggests that the copper container would be thermodynamically stable under the reducing conditions expected in the repository, poor local conditions might cause a limited number of container failures.</p> <p>The Normal Evolution Scenario assumes some containers with undetected defects are present in the repository at the time of closure, leading to container failures.</p> <p>No, the effects are likely to be localized to the immediate vicinity of the container and these FEPs can be evaluated through considering different calculation cases for the Normal Evolution Scenario (i.e., low sorption and high solubility sensitivity cases) rather than through the development of alternative Disruptive Event Scenarios.</p>
<p>6.4. Institutional controls and monitoring will verify performance.</p>	<p>Affected by External FEPs relating to Future Human Actions (see Table 6-3) rather than the Internal FEPs relating to human behaviour that responds to the Future Human Actions.</p>	

Note: (1) The Internal FEPs are shown in Garisto (2018).

Table 6-5: Potential Failure Mechanisms and Associated Scenarios

Failure Mechanism	Associated Disruptive Event Scenario
Exploration borehole penetrates into the repository providing an enhanced permeability pathway to the surface environment and potential for direct exposure to used fuel	Inadvertent Human Intrusion
Poor construction techniques affect the performance of repository and shaft EDZs, providing an enhanced permeability pathway to the surface environment	Repository Seals Failure
Repository and shaft seals perform poorly due to unexpected chemical interactions with groundwater or glacial meltwater, providing an enhanced permeability pathway to the surface environment	Repository Seals Failure
Site investigation / monitoring borehole seals perform poorly due to unexpected chemical interactions with groundwater or glacial meltwater, providing an enhanced permeability pathway to the surface environment	Poorly Sealed Borehole
The repository is not closed as planned after the monitoring period and tunnels, shafts and monitoring boreholes remain open	Partially Sealed Repository
Site investigations do not identify a permeable fracture zone or fault that provides a connection between the repository horizon and shallow groundwater system	Undetected Fault
Seismic event results in reactivation of an undetected existing fracture zone which provides an enhanced permeability pathway to higher horizons	Undetected Fault
Seismic event affects performance of repository and shaft EDZs, and /or shaft seals, providing an enhanced permeability pathway to higher horizons	Repository Seals Failure
Glacial erosion is much more extensive than expected at the repository site over a one million year period.	Severe Erosion
Seismic event results in shearing along an existing fracture zone passing through a placement room, resulting in failure of some container(s) due to the shear load	Container Failure
Mechanical and thermal stresses induced by the presence of the repository cause greater than expected fracturing within the repository and shaft EDZs, providing an enhanced permeability pathway to surface environment	Repository Seals Failure
Unexpected chemical interactions of the copper coating with groundwater, e.g., due to higher than anticipated sulphide concentrations, affect the durability of a significant number of containers	All Containers Fail
Passage of thicker than design-basis ice sheet over repository site causes isostatic load on all containers to exceed their design load, resulting in failure of all containers	All Containers Fail

The repository siting process will ensure that there are no known commercially viable natural resources near or below repository depth. Also, the repository has a relatively small footprint (~5 km²) and the repository is at a depth of around 500 m. These factors limit the range of human activities that could directly affect the closed repository to a borehole unintentionally drilled into the repository as part of a future geological exploration program². Even this situation has a low probability of occurrence. Nevertheless, the possibility of inadvertent human intrusion by this method cannot be ruled out over long time scales³. Such a borehole could provide an enhanced permeability pathway to the surface environment and potential for direct exposure to waste. This scenario is referred to as the **Inadvertent Human Intrusion Scenario**.

A second scenario by which the geosphere barrier can be bypassed is via the shafts (main, service and ventilation shafts). The shafts (with diameters of 9 m) penetrate the geosphere, and are centrally located but away from the waste panels. The shafts are carefully sealed during repository closure. The **Repository Seals Failure Scenario** considers the possibility that the long-term performance of the shaft seals or their surrounding EDZs is poor due to unexpected physical, chemical and / or biological processes, or that these seals and / or adjacent EDZs are somehow damaged by a seismic event. While these situations could result in an enhanced permeability pathway from the repository to the surface, they are very unlikely due to the quality control measures that will be applied during the selection of the seal materials (i.e., to ensure they are compatible with groundwater at the site), due to the low likelihood of major seismic events and due to the use of durable composite seals.

In the Repository Seals Failure Scenario, it is assumed that the other repository engineered barriers (i.e., the tunnel and room seals, and the backfill and buffer), are not degraded relative to their design properties except for the concrete component of the seals, for which degraded properties are used throughout the simulations, as in the Normal Evolution Scenario. The effects of degradation of these other engineered barriers would be investigated as sensitivity cases of the Repository Seals Failure Scenario.

The geosphere barrier is also bypassed via the shafts in the **Partially Sealed Repository Scenario** in which the repository is assumed not to be sealed following the monitoring period (i.e., after all containers are placed in the repository and all placement rooms are sealed). In this scenario, the access tunnels and shafts remain open and are not maintained at least for an extended period. Since closing the repository is clearly important and funds would have been set aside for this purpose, this scenario would require a societal collapse or abandonment of the site for other unknown reasons. The likelihood of such a scenario is unknown but is low.

Another way in which the geosphere barrier can be bypassed is through the site characterization / monitoring boreholes. These boreholes are located in the vicinity of the repository down to and below repository depth. These boreholes will be appropriately sealed on completion of site investigation / monitoring activities so they will have no effect on repository

²The assessment excludes deliberate human intrusion since it is expected that the intruders would take appropriate precaution.

³The repository might appear as an anomaly in a surface / air-borne survey of the area, and this could encourage drilling at the site if all records had been lost. However, the absence of interesting minerals or geologic features in the area would argue against deliberate surveys of the area. Furthermore, a cautious approach to drilling might be used if such unexpected anomalies were identified that would minimize the consequences of any intrusion into the repository.

performance. However, if the borehole seals were to degrade extensively due to, for example, unexpected chemical interactions with groundwater and / or glacial meltwater, then the borehole would provide a small but relatively permeable pathway for the migration of contaminants from the repository horizon to the environment. The scenario is termed the **Poorly Sealed Borehole Scenario**. Like the Repository Seals Failure Scenario, such a situation is very unlikely due to the adoption of good engineering practices and quality control measures, including the appropriate selection of sealing materials, and the use of durable composite seals.

For the Normal Evolution Scenario, it is assumed that site investigation would detect the occurrence of transmissive vertical faults / fracture zones which could provide an enhanced permeability pathway from the repository horizon to the overlying aquifer within the footprint or vicinity of the repository. However, it is possible that site characterization may not identify all significant fractures at the site and, therefore, a scenario is defined to investigate the safety implications of a hypothetical transmissive fault that is either undetected or formed by the extension of an existing structural discontinuity. The hypothetical fault is assumed to be in close proximity to the repository and to extend from below the repository level to the shallow groundwater system. This scenario is termed the **Undetected Fault Scenario**.

Glacial erosion is considered in the Normal Evolution Scenario. At this hypothetical site, a realistic amount of glacial erosion over a one million year time frame is considered as part of the Normal Evolution Scenario. However, a more severe glacial erosion rate is assessed in the **Severe Erosion Scenario**. Such a scenario is considered highly unlikely because of the absence of topographic features or other known factors that would tend to localize erosion by ice or water in Southern Ontario (Hallet 2011). Furthermore, future glaciations would tend to repeat the actions of their predecessors, by funneling into lake basins and deepening them, and maintaining the topographic highs where the ice flow velocities and erosion rates are relatively low and where sediments tend to accumulate.

The copper coated used fuel containers are expected to last considerably more than one million years based on thermodynamic, experimental and natural analogue evidence that copper is stable for very long periods under deep geological repository conditions (see Chapter 5). Nevertheless, there are several mechanisms by which a container could fail sometime after it is installed in the repository. These container failures are in addition to the failures that occur in the Normal Evolution Scenario due to the presence of undetected defects (e.g., voids) in the copper coating. Container failure mechanisms include, but are not limited to, the following:

- After the repository attains reducing conditions, the copper container should be immune to further corrosion. However, unexpected interactions between the groundwater and copper container (e.g., due to higher than expected sulphide concentrations) could damage the copper coating sufficiently over the time frame of interest that the steel vessel would be exposed to water, leading to weakening of the vessel due to corrosion and / or seepage of water into the container.
- A container could be damaged by a sufficiently large shear load. A large seismic event that causes the rock to slip along an undetected fracture zone intersecting a placement room could produce such a shear load. The probability of such an event depends on the likelihood of an earthquake of a sufficient magnitude; the likelihood that a placement room is intersected by an undetected fracture zone and the fracture zone is near a container; and, finally, how the shear load is transmitted through the buffer material, which depends on the

buffer thickness and density. The analysis in SKB (2011) indicates that, for their repository, less than 0.2 containers would fail due to shear load over one-million years.

The specific failure mode is not defined here, but the consequences are evaluated in the **Container Failure Scenario**. The key characteristics of this scenario are that only a few containers are affected, that the container damage is significant, but also that the failure occurs long after repository closure.

The containers are designed to be corrosion resistant and to be robust. As noted in Chapter 4, the inner steel vessel is able to sustain an external isostatic load of at least 45 MPa at 100°C. Thus, the containers are expected to have a long lifetime. However, it is possible that some unexpected event or process may occur in the future such that there are multiple container failures in the repository. For example, the copper coating of the container could fail at long times due to higher than expected sulphide concentrations in groundwater; or, the passage of a beyond design-basis ice-sheet over the site causes the load on the containers to exceed their design load. Consequently, an **All Containers Fail Scenario** is considered in which all the containers in the repository fail at 60,000 years, the time of the assumed first passage of an ice sheet over the site (see Chapter 2). The probability of such a scenario is likely low since site characterization would ensure the absence of groundwater species detrimental to the long life of the container and because the container can withstand beyond-design basis glacial loads before failure. Furthermore, there is no evidence from past glaciations for ice sheets thick enough to exert a load on the containers sufficient to cause failure, even if it is pessimistically assumed that the additional hydrostatic load on the container is equivalent to the height of the ice sheet.

Other potential Disruptive Event Scenarios were considered but ruled out on various grounds as discussed further in the FEPs report (Garisto 2018). No volcanic activity is anticipated in the area over the next one million years. The probability of a large meteor strike, capable of damaging the repository, is remote and the consequences of the impact itself would likely be more significant than those from the repository. Seismic activity is possible, and likely earthquakes are included in the Normal Evolution Scenario. Such seismic activity will not cause rockfall because the repository is backfilled. Large earthquakes are unlikely since it is assumed that the hypothetical site is located in a low-seismicity area. The main effects of an earthquake on the repository are represented by the Repository Seals Failure, the Undetected Fault and the Container Failure Scenarios, so there is no need to consider an additional earthquake scenario. Glaciation, which could affect the repository system, is considered within the Normal Evolution Scenario and is the potential cause of the All Containers Fail Scenario (if the glacial load exceeds the repository design basis.)

Further confidence that an appropriate set of Disruptive Event Scenarios has been identified can be obtained by examining the scenarios (or sensitivity cases) considered in the postclosure safety assessments of deep repositories in other countries. The results of such an examination, summarized in Table 6-6, show that most assessments have identified a limited number of additional scenarios that consider the degradation/failure of engineered and natural barriers by natural processes (e.g., earthquakes, climate change) and human actions (e.g., drilling, poor quality control). Although there are some scenarios that are not considered in the current study, these are either not relevant for the hypothetical site (e.g., volcanic activity, sea-level rise, mining of resources) or have been included in the Normal Evolution Scenario (e.g., climate change, container failure).

Table 6-6: Additional Scenarios Considered in Other Safety Assessments

Assessment	Reference	Additional Scenarios Considered
SR-Site (Sweden)	SKB (2011)	<ul style="list-style-type: none"> • Canister failure due to corrosion or shear load • Disrupted buffer (due to erosion, advection) • Extended greenhouse effects • Exploratory drilling • Rock facility (e.g., quarry) • Incompletely sealed (or abandoned) repository
Olkiluoto (Finland)	POSIVA (2012)	<ul style="list-style-type: none"> • Defective canister (early and delayed penetration) • Earthquake/rock shear • Disrupted buffer • Exploratory drilling
Dossier Argile (France)	ANDRA (2005)	<ul style="list-style-type: none"> • Seal failure and defective plug • Defective waste and spent fuel containers • Borehole penetrating repository • Functioning of repository greatly degraded
H12 (Japan) ⁽¹⁾	JNC (2000)	<ul style="list-style-type: none"> • Climate and sea-level change • Exploitation drilling (water well) • Engineering defects, including poorly sealed repository
Opalinus (Switzerland)	NAGRA (2002)	<ul style="list-style-type: none"> • Gas pathways • Exploratory drilling • Poorly sealed repository
GPA (UK)	NIREX (2003)	<ul style="list-style-type: none"> • Exploratory drilling
WIPP (USA)	DOE (2004)	<ul style="list-style-type: none"> • Mining • Exploratory drilling
Yucca Mountain (USA) ⁽²⁾	DOE (2002)	<ul style="list-style-type: none"> • Exploratory drilling • Seismicity • Volcanic event
SAFIR 2 (Belgium)	ONDRAF/NIRAS (2001)	<ul style="list-style-type: none"> • Exploratory drilling • Greenhouse effect • Poor sealing of repository • Fault activation • Severe glacial period • Failure of engineered barriers • Gas-driven transport

Notes: (1) Isolation Failure Scenarios that involve penetration of the repository (including magma intrusion, human intrusion and meteorite impact) were also considered but screened out on the grounds that they are extremely unlikely to occur. Some 'what if' calculations were carried out instead.

(2) The term 'scenario' is used in a way that differs from the other assessments reviewed. Three Thermal Load Scenarios are discussed that are design variants, while two No-action Scenarios refer to futures in which the Yucca Mountain facility does not go ahead.

6.2.2 Description of Disruptive Event Scenarios

The identified Disruptive Event Scenarios are described below. These scenarios are evaluated separately rather than in combination since they have low probability and independent causes, and so the likelihood of simultaneous occurrence is even lower.

6.2.2.1 Inadvertent Human Intrusion Scenario

The Inadvertent Human Intrusion Scenario considers the impact of human intrusion sometime in the future. In this scenario, an exploration borehole is drilled through the geosphere and into the repository with the drill bit intersecting a used fuel container.

It is assumed that the drill crew is unaware of the facility (i.e., the intrusion occurs after institutional controls are no longer effective and societal memory of the site is lost). The investigators will most likely collect samples or conduct measurements at the repository level, due to the unusual nature of the materials. This would identify significant residual radioactivity (e.g., gamma logging is a standard borehole measurement) and the investigators would likely take precautions to prevent further exposure, including appropriate management of any materials released at the surface and sealing of the borehole. Therefore, under normal drilling, there would be little impact after the initial drill crew exposure.

Nevertheless, the reference Inadvertent Human Intrusion Scenario assumes:

- It is not recognized that the drill has intercepted a waste repository so no safety restrictions are applied; and
- The borehole and drill site are not managed and closed to current standards, and material from the borehole is released onto the surface around the drill site.

Contaminants can be released and humans and biota exposed via:

- Retrieval and examination of drill core contaminated with waste; and
- Uncontrolled dispersal of contaminated drill core debris on the site.

This could result in the exposure of the drill crew or other people at the time of intrusion, and people who might occupy the site subsequent to the intrusion event.

A variant of the Inadvertent Human Intrusion Scenario can also be defined in which the drill crew recognizes that the borehole has intercepted a waste repository, immediately ceases operations and vacates the site. The site is then completely remediated by qualified experts. In this case only the drill crew is exposed to a radiation dose.

If the borehole is not properly sealed, it could provide an enhanced permeability pathway to the surface environment or even be used as a well by a future site resident. The impact of this open borehole on future residents of the site can, in theory, be examined as part of the Inadvertent Human Intrusion Scenario.

6.2.2.2 Repository Seals Failure Scenario

The shafts through the repository footprint represent potentially important pathways for contaminant release and, therefore, the repository design includes specific measures to provide good shaft seals, taking into account the characteristics of the geosphere. The Repository Seals Failure Scenario considers the consequences of extensive degradation of the shaft seals and / or their corresponding EDZs. This scenario, like the other Disruptive Event Scenarios, is a bounding scenario designed to investigate the robustness of the repository system.

The radionuclide exposure pathways (e.g., ingestion, inhalation, etc.) to which the critical group and non-human biota are exposed are the same as those considered in the Normal Evolution Scenario.

6.2.2.3 Partially Sealed Repository Scenario

Another scenario by which the geosphere barrier can be bypassed via the shafts is the Partially Sealed Repository Scenario. The basic assumption in the Partially Sealed Repository Scenario is that the repository is abandoned during the monitoring phase (i.e., after all containers are placed in the repository and all placement rooms are backfilled and sealed), but the main access tunnels and the shafts are still open. This is consistent with normal operations, in which the placement rooms are successively filled with containers and backfilled, and sealed as soon as they are filled.

Abandonment of the repository would require a significant societal breakdown because of the known importance of properly closing the repository.

The radionuclide exposure pathways (e.g., ingestion, inhalation, etc.) to which the critical group and non-human biota are exposed are the same as those considered in the Normal Evolution Scenario.

6.2.2.4 Poorly Sealed Borehole Scenario

Multiple deep site investigation / monitoring boreholes will be drilled in the vicinity of the repository during the site investigation phase. The Poorly Sealed Borehole Scenario considers the consequences of unexpected extensive degradation of the borehole seals. The poorly sealed borehole provides an enhanced permeability connection between the repository level and the overlying groundwater zones and biosphere, bypassing some of the natural geological barriers to contaminant migration from the repository.

The radionuclide exposure pathways (e.g., ingestion, inhalation, etc.) to which the critical group and non-human biota are exposed are the same as those considered in the Normal Evolution Scenario.

6.2.2.5 Undetected Fault Scenario

The Undetected Fault Scenario considers the impact of an undetected or seismically activated transmissive fault in close proximity to the repository that extends from about the repository level up into the shallow groundwater system. Such a fault could provide an enhanced permeability pathway that bypasses the natural geological barrier.

The radionuclide exposure pathways (e.g., ingestion, inhalation, etc.) to which the critical group and non-human biota are exposed are the same as those considered in the Normal Evolution Scenario.

6.2.2.6 Severe Erosion Scenario

The Severe Erosion Scenario considers the impact of severe glacial erosion on the performance of the used fuel repository.

The radionuclide exposure pathways (e.g., ingestion, inhalation, etc.) to which the critical group and non-human biota are exposed are the same as those considered in the Normal Evolution Scenario.

6.2.2.7 All Containers Fail Scenario

The long-lived used fuel containers are an important feature of the multi-barrier repository concept in this conceptual design. The copper containers are expected to last for a long time because copper is stable under anticipated conditions in a deep geological repository; however, the All Containers Fail Scenario considers the very unlikely and hypothetical case in which all the containers simultaneously fail (i.e., water enters all containers and contacts the fuel) at 60,000 years. This timeframe corresponds to the assumed time scale for glacial cycles to resume and an ice sheet to first cover the site (see Chapter 2). Such an ice sheet could be assumed to cause multiple container failures if the design load of the containers is exceeded or if the containers have been weakened due to penetration of the copper coating and subsequent corrosion of the steel vessel. For simplicity, in this scenario, it is assumed that there are no initially defected containers as in the Normal Evolution Scenario.

A variant case in which all containers are assumed to fail at 10,000 years is also investigated to determine the sensitivity to the assumed failure time.

The radionuclide exposure pathways (e.g., ingestion, inhalation, etc.) to which the critical group and non-human biota are exposed are the same as those considered in the Normal Evolution Scenario. However, the failure of all containers also leads to the generation of significant amounts of hydrogen gas due to corrosion of the inner steel vessel. Consequently, the impact of gas generation on the performance of the repository and the transport of gaseous contaminants is also addressed.

6.2.2.8 Container Failure

The Container Failure Scenario considers the impact of container failure due to several possible mechanisms:

- Corrosion of the copper coating on the container due to, for example, unexpectedly high sulphide concentrations near a small number of containers, allowing eventual corrosion and breach of the steel container; and
- A large seismic event (earthquake) in the vicinity of the repository that causes slip along an undetected fracture zone that intersects a placement room. The rock slip along the fracture zone is assumed to be sufficiently large that it causes complete failure of a container. The shearing action could also increase the transmissivity of the fracture. Although the shear

movement should not affect the buffer properties, the amount of buffer between the container and the shearing fracture zone would likely be reduced.

The radionuclide exposure pathways (e.g., ingestion, inhalation, etc.) to which the critical group and non-human biota are exposed are the same as those considered in the Normal Evolution Scenario.

6.3 References for Chapter 6

ANDRA. 2005. Dossier 2005 Argile Tome Safety evaluation of a geological repository. Paris, France.

CNSC. 2018. Regulatory Document REGDOC-2.11.1 Volume III: Assessing the Long-Term Safety of Radioactive Waste Management. Canadian Nuclear Safety Commission. Ottawa, Canada.

DOE. 2002. Final Environmental Impact Statement for a Geologic Repository for the Disposal of Spent Nuclear Fuel and High-level Radioactive Waste at Yucca Mountain, Nye County, Nevada. United States Department of Energy, Office of Civilian Radioactive Waste Management, DOE/EIS-0250. Nevada, USA.

DOE. 2004. 2004 WIPP Compliance Recertification Application (CRA) - Main Volume. US Department of Energy Report DOE/WIPP 04-3231. Available at: http://www.wipp.energy.gov/library/CRA/CRA_Index.htm. Accessed January 2011.

Garisto, F. 2018. Seventh Case Study: Features, Events and Processes. Nuclear Waste Management Organization Report NWMO-TR-2018-15. Toronto, Canada.

Hallet, B. 2011. Glacial Erosion Assessment. Nuclear Waste Management Organization Report NWMO DGR-TR-2011-18 R000. Toronto, Canada.

IAEA. 2012. The Safety Case and Safety Assessment for the Disposal of Radioactive Waste. IAEA Safety Standards. Specific Safety Guide No. SSG-23. International Atomic Energy Agency. Vienna, Austria.

ICRP. 1998. Radiation Protection Recommendations as Applied to the Disposal of Long-lived Solid Radioactive Waste. International Commission on Radiological Protection Publication No. 81, Annals of the ICRP 28(4).

JNC. 2000. H12: Project to Establish the Scientific and Technical Basis for HLW in Japan. Supporting Report 3: Safety Assessment of the Geological Disposal System. Japan Nuclear Cycle Development Institute Report JNC TN1410 2000-004. Tokai, Japan.

Nagra. 2002. Project Opalinus Clay: Safety Report, Demonstration of Disposal Feasibility for Spent Fuel, Vitrified High-level Waste and Long-lived Intermediate-level Waste (Entsorgungsnachweis). Nagra Technical Report 02-05. Wetztingen, Switzerland.

NEA. 2000. Features, Events and Processes (FEPs) for Geologic Disposal of Radioactive Waste, An International Database. OECD Nuclear Energy Agency Report. Paris, France.

- NEA. 2012. Radioactive Waste Management Committee, Updating the NEA International FEP List: An IGSC Technical Note, Technical Note 2: Proposed Revisions to the NEA International FEP List, OECD Nuclear Energy Agency Report. Paris, France.
- NIREX. 2003. Generic Repository Studies: Generic Post-closure Performance Assessment. Nirex Report N/080. Harwell, United Kingdom.
- ONDRAF/NIRAS. 2001. SAFIR 2: Safety Assessment and Feasibility Interim Report 2. ONDRAF/NIRAS Report NIROND 2001-06E. Brussels, Belgium.
- Perry, C., C. Rosieanu, J.-C. Mareschal and C. Jaupart. 2010. Thermal Regime of the Lithosphere in the Canadian Shield, Canadian Journal of Earth Sciences 47, 389-408.
- Peltier, W.R. 2011. Long-Term Climate Change. Nuclear Waste Management Organization Technical Report NWMO DGR-TR-2011-14 R000. Toronto, Canada.
- POSIVA. 2012. Safety Case for the Disposal of Spent Nuclear Fuel at Olkiluoto – Synthesis 2012. Posiva Report 2012-12. Olkiluoto, Finland.
- SKB. 2011. Long-term Safety for the Final Repository for Spent Nuclear Fuel at Forsmark, Main Report of the SR-Site Project. Swedish Nuclear Fuel and Waste Management Report SKB TR-11-01. Stockholm, Sweden.

7. POSTCLOSURE SAFETY ASSESSMENT – CONTAMINANT TRANSPORT

This chapter, together with Chapter 8, presents an illustrative postclosure safety assessment for a conceptual used fuel repository located in the sedimentary rock of Southern Ontario. This chapter addresses water-borne contaminant transport, where 'contaminant' includes both radionuclides and potentially hazardous chemical elements. Gas transport is addressed in Chapter 8.

The purpose of a postclosure safety assessment is to determine the potential effects of the repository on the health and safety of persons and the environment during the postclosure period. The assessment timeframe is one million years based on the time period needed for the radioactivity of the used fuel to decay to essentially the same level as that in an equivalent amount of natural uranium. This timeframe is within a reasonable extrapolation of the geological stability of these rocks; however, due to the very good retention properties of the sedimentary rock, the peak impacts often occur beyond one million years. Analyses presented here have therefore been extended beyond one million years to demonstrate that the peak impacts remain well below the interim acceptance criteria. These extensions are for illustration and to allow for case-by-case comparison of results.

The assessment is conducted by applying computer models to a range of analysis cases. The analysis cases here consider the Normal Evolution Scenario and some of the Disruptive Event Scenarios identified in Chapter 6, together with a series of sensitivity studies performed to examine the importance of various model features and assumptions. The discussion is arranged as follows:

- Section 7.1 – Interim Acceptance Criteria;
- Section 7.2 – Scope, a detailed description of the analysis cases and sensitivity studies;
- Section 7.3 – Conceptual Model of the repository evolution;
- Section 7.4 – Computer Codes;
- Section 7.5 – Overall Analysis Approach and Selected Data for Groundwater Flow and Radionuclide Transport;
- Section 7.6 – Modelling and Results for Radionuclide and Chemical Hazard Screening;
- Section 7.7 – Modelling and Results for 3D Groundwater Flow and Radionuclide Transport;
- Section 7.8 – Modelling and Results for the System Model, including discussion of the effects of glaciation;
- Section 7.9 – Modelling and Results for Disruptive Event Scenarios;
- Section 7.10 – Modelling and Results for Radiological Protection of the Environment;
- Section 7.11 – Modelling and Results for Protection of Persons and the Environment from Hazardous Substances;
- Section 7.12 – Modelling and Results for Complementary Indicators; and
- Section 7.13 – Summary and Conclusions.

7.1 Interim Acceptance Criteria

This section presents interim acceptance criteria applicable to the postclosure safety assessment. These criteria are used to judge the acceptability of analysis results.

The Canadian Nuclear Safety Commission (CNSC) REGDOC-2.11.1, Volume III (CNSC 2018) document identifies the following to be addressed in a postclosure safety assessment:

1. Radiological protection of persons;
2. Protection of persons from hazardous substances;
3. Radiological protection of the environment; and
4. Protection of the environment from hazardous substances.

Interim acceptance criteria are defined for each of the above and discussed in the following sections. These criteria are consistent with current Canadian and international practice; however, these are *interim* criteria because the criteria used in a licence application will need to be accepted by the CNSC at that time.

7.1.1 Interim Acceptance Criteria for the Radiological Protection of Persons

The fundamental regulatory radiological dose limit for public exposure is 1 mSv/a.

However for postclosure safety, in order to account for the possibility of exposure to multiple sources in the future, a dose constraint below the regulatory limit is adopted. Specifically, for the Normal Evolution Scenario, the interim dose rate acceptance criterion is:

- An annual individual effective dose rate of 0.3 mSv/a, with the calculation performed to encompass the time of maximum predicted impact to the average adult member of the critical group.

The 0.3 mSv/a dose constraint is consistent with recommendations of the International Commission on Radiation Protection (ICRP) and the International Atomic Energy Agency (IAEA) (ICRP 2007, ICRP 2013, IAEA 2006) and is significantly less than the average Canadian individual dose rate of 1.8 mSv/a received from background radiation (Grasty and LaMarre 2004).

At this dose rate, there is no clear evidence for adverse health effects (NRC 2006, CNSC 2011). However, the Linear-No-Threshold model recommended by international agencies (ICRP 2013) and adopted by Canadian regulator (CNSC 2013) assumes, for radiation protection purposes, that any dose exposure results in some increase in health risk, notably cancer. This dose constraint is therefore sufficiently low to ensure that the health risks are small in comparison to the risk from natural background radiation, and to the risk of cancer from all causes.

The criterion is also based on an adult. Calculating the exposure of an adult member of the critical group is consistent with ICRP recommendations which recognize that exposures are expected to occur in the distant future, that exposure would be associated with levels of radionuclides in the environment that change slowly over the time scale of a human lifetime, and that calculated exposures at long times have inherent uncertainties (ICRP 2013).

Futhermore, effective dose rates from ingestion and inhalation of radionuclides are calculated using the dose coefficients from ICRP 72 (ICRP 1995), which are based on a human model that includes male and female organs to ensure that it includes all radionuclide sensitivities and ICRP 60 recommendations (ICRP 1991). Effective dose coefficients for adult ground exposure, air immersion, water immersion and building exposure are also calculated based on ICRP 60 recommendations (Eckerman and Leggett 1996).

For Disruptive Event Scenarios, the interim acceptance criteria are:

- An annual individual effective dose rate target of 1 mSv/a for chronic¹ release scenarios with the calculation performed for the average adult member of the critical group; and
- Acceptability of any scenario with the calculated annual individual effective dose rate for chronic releases exceeding 1 mSv/a to be examined on a case-by-case basis taking into account the likelihood and nature of the exposure, the uncertainty in the assessment and the conservatism in the dose criterion. Where the probability of exposure can be quantified without excessive uncertainty, a measure of risk will be calculated based on the probability of exposure and the consequent health effects. This is compared with a reference risk value of $10^{-5}/a$ (ICRP 2013).

A dose rate of 1 mSv/a corresponds to the current regulatory limit for exposure of the public. This is below the 1.8 mSv/a average natural background dose rate for Canadians.

The reference health risk value of $10^{-5}/a$ is consistent with ICRP (2013), Health Canada (2010) and IAEA (2006). Based on the ICRP probability coefficient of 0.057 per Sv for stochastic effects (e.g., cancers or hereditary effects) (ICRP 2007), this corresponds to a health risk about a factor of 10 lower than the risk from the natural background dose rate.

Regulatory document REGDOC-2.11.1, Volume III (CNSC 2018) and ICRP (2013) recognize that inadvertent human intrusion into a repository could result in doses greater than 1 mSv/a because intrusion by definition bypasses the repository barriers. The risk from human intrusion is made low by the site selection criteria which require the facility to be located deep underground in an area known not to have economically exploitable natural resources or potable groundwater resources at repository depth. Institutional controls will also reduce risk in the short-term, when the hazard is greatest.

7.1.2 Interim Acceptance Criteria for the Protection of Persons from Hazardous Substances

Interim acceptance criteria for the protection of persons from hazardous substances are based on Canadian Federal and Provincial guidelines (principally from the Canadian Council of Ministers of the Environment (CCME) and the Ontario Ministry of the Environment (MOE)) for concentrations in environmental media relevant to human health and environmental protection, supplemented as needed by internationally developed guidelines. They have been assembled taking into account the direction of REGDOC-2.11.1, Volume III (CNSC 2018). The basis for the proposed interim acceptance criteria is discussed in detail in Medri (2015b).

¹ Chronic refers to a release that is sustained over many years.

Criteria for non-radiological contaminants in five different environmental media are protective of the following:

- Surface water:** Drinking water, aquatic life, agricultural water uses (irrigation and livestock), recreational water uses and aesthetic features.
- Groundwater:** Drinking water, agricultural water uses (irrigation and livestock) and surface water bodies from groundwater flow.
- Soil:** Ecological receptors and human health for soils for various land uses (agricultural, residential/parkland, commercial and industrial).
- Sediment:** Aquatic life, human health and the environment.
- Air:** Human health, the environment and nuisance effects (like odour).

The criteria are intended to be cautiously realistic; that is, they ensure the protection of all forms of life (animals, plants and humans) without being excessively conservative. They are intended for postclosure conditions in that they are selected for chronic exposure conditions, and that they are relevant for chemical species that could credibly exist in these media due to release of contaminants from the repository.

Interim acceptance criteria for environmental contaminants given in Table 7-1. Criteria are not available for all elements in all media but at least one criterion is available for each listed element. For some elements, the interim acceptance criteria are based on internal values, which have been adopted based on literature review and are subject to further confirmation.

Exceedance of a criterion does not necessarily indicate unacceptable risk. As appropriate, consideration may be given to assessing the conservatism of the criterion through reference to the original sources, to the use of less conservative release and exposure models, to the likelihood and nature of the exposure and to mitigation measures. Additive, synergistic or antagonistic effects from chemical species in mixtures are not considered in this stage.

Table 7-1: Interim Acceptance Criteria for the Protection of Persons and the Environment from Non-Radiological Impacts

Element	Surface Water (µg/L)	Groundwater (µg/L)	Soil (µg/g)	Sediment (µg/g)	Air (µg/m ³)
Ag	0.1	1.2	0.5	0.5	1
Al	=5 if pH<6.5 =100 if pH is ≥6.5	100	50	-	53
As	5	10	11	5.9	0.3
Au	6	60	0.1	0.6	2.5
B	200	500	1.5	-	5.8
Ba	1,000	1,000	210	-	10
Be	=11 if CaCO ₃ < 75 mg/L =1100 if CaCO ₃ >75 mg/L	4	2.5	-	0.01
Bi	140	1,400	20	65,000	100
Br	2	20	10	20	20
Ca	1,000,000	1,000,000	-	-	200
Cd	0.09	2.1	1	0.6	0.005

Postclosure Safety Assessment of a Used Fuel Repository in Sedimentary Rock

Document Number: NWMO-TR-2018-08

Revision: 000

Class: Public

Page: 321

Element	Surface Water (µg/L)	Groundwater (µg/L)	Soil (µg/g)	Sediment (µg/g)	Air (µg/m ³)
Ce	22	-	53	19,000	200
Cl	100,000	100,000	-	-	10
Co	0.6	3.8	22	50	0.1
Cr	1	4.9	0.66	26	10
Cu	=1 CaCO ₃ ≤ 20 mg/L =5 CaCO ₃ > 20 mg/L	69	62	12	50
Dy	9.3	-	-	2,200	200
Eu	-	-	-	-	200
F	120	1,000	200	-	17
Fe	300	300	200	21,000	4
Gd	7.1	-	-	1,800	340
Hf	-	-	-	-	10
Hg	0.004	0.12	0.2	0.17	0.5
Ho	-	-	-	-	40
I	100	100	4	4	0.67
In	10	100	1	1	0.1
Ir	0.068	0.68	0.012	0.27	0.002
K	53,000	-	-	-	15
La	10	-	50	4,700	200
Li	2,500	2,500	2	-	20
Lu	-	-	-	-	8
Mg	82,000	-	-	-	0.11
Mn	50	50	100	460	0.1
Mo	10	10	2	8.3	100
Na	200,000	200,000	-	-	87
Nb	600	-	9	-	200
Nd	1.8	-	-	7,500	200
Ni	= 25 if CaCO ₃ ≤ 60 mg/L = e ^{(0.76 ln(hardness)+1.06)} if CaCO ₃ > 60 and ≤ 180 mg/L = 150 if CaCO ₃ > 180 mg/L	100	37	16	0.02
Os	0.067	0.67	0.012	0.27	0.002
P	4	-	-	-	-
Pb	=1 if CaCO ₃ < 30 mg/L =3 if CaCO ₃ ≥ 30 but ≤ 80 mg/L =5 if CaCO ₃ > 80 mg/L	10	45	28	0.2
Pd	0.068	0.68	0.012	0.27	5
Pr	9.1	-	-	5,800	8
Pt	0.61	6.1	0.012	0.27	0.2
Rh	0.068	0.68	0.012	0.27	0.1
Ru	0.068	0.68	0.012	0.27	3
S	= 170 000 if sulphate = 1.9 if any other form	= 170 000 if sulphate	500	-	7

Element	Surface Water (µg/L)	Groundwater (µg/L)	Soil (µg/g)	Sediment (µg/g)	Air (µg/m ³)
		= 50 if any other form			
Sb	6	6	1	3	25
Sc	-	-	-	-	200
Se	1	10	1.2	0.9	10
Sm	8.2	-	-	2,500	200
Sn	73	-	5	-	10
Sr	1,500	-	33,000	-	100
Ta	-	-	-	-	67
Tb	-	-	-	-	8
Tc	-	-	0.2	-	-
Te	5.8	58	250	31	10
Ti	-	-	1,000	-	20
Tl	0.3	2	1	-	0.4
Tm	-	-	-	-	200
U	5	20	1.9	32	0.03
V	7	6.2	86	27	2
W	30	16	400	960	67
Y	6.4	-	-	1,400	20
Zn	=1000 if soil pH ≤6.5 =5000 if soil pH > 6.5	890	290	120	100
Zr	4	-	97	-	67

Notes: '-' indicates that there are no defined criteria for that element in the given medium.

7.1.3 Interim Acceptance Criteria for the Radiological Protection of the Environment

Protection policies for non-human biota are not as mature as those for humans. There are no internationally agreed upon environmental benchmarks or dose rate criteria against which to assess radiological effects to non-human biota. This stems from the fact that there is a relative lack of data compared to the breadth of parameters involved, such as animal species, type of effect (morbidity, mortality, reproductive success, etc.), type of exposure (internal, external, gamma, alpha, etc.), rate of exposure (chronic or acute) and type of experiment (field or lab). Also, the statistical analysis requires many samples of each data type to achieve statistical relevance. However, while ICRP (2008) notes that “dose limits” of the form used in human radiological protection would be inappropriate, some form of numerical guidance is required.

As such, ICRP (2008) recommends the use of the lower end of their Derived Consideration Reference Level (DCRL) bands as points of reference to optimize the level of effort expended on environmental protection. DCRLs are bands of dose rates for each type of reference animal or plant within which there is likely to be some chance of deleterious effects from ionizing radiation. Below the lower end of the DCRL bands, the risks to non-human biota are negligible. Similarly, ERICA (Garnier-Laplace et al. 2006) and PROTECT (Andersson et al. 2008) propose a generic screening criterion for chronic exposures of 10 µGy/h for all biota,

which is well accepted and widely used, especially in Europe. The generic screening criterion is typically used in tiered assessments, where exceeding the criterion would highlight the need to consider the level of potential impact in more detail.

In this assessment, a two-tiered approach is adopted as a risk-based method of demonstrating the protection of non-human biota. This is consistent with the approach proposed by BIOPROTA, an international forum which seeks to address key uncertainties in the assessment of radiation doses in the long term arising from releases of radionuclides as a result of radioactive waste management (Jackson et al. 2014).

The Tier 1 criteria are taken to be the lower of the generic ERICA screening criterion of 10 $\mu\text{Gy/h}$ and the bottom end of the ICRP DCRL band for each reference non-human biota. Calculated dose rates that fall below the Tier 1 criteria are considered to be of no radiological concern. The second tier criteria are delimited by the upper end of the DCRL band, which are taken to be realistic levels at which some effects to individual non-human biota could be observed, but that would be unlikely to produce significant effects at the population level. Acceptability of dose rates that fall between the first and second tier criteria will be judged within the context of the likelihood of the exposure situation, the conservatism in the dose rate estimate and the intended protection endpoint. Dose rates that exceed the second tier criteria would need to be investigated in more detail. Taken as a whole, this approach defines the acceptance criteria for this assessment, which is illustrated in Table 7-2.

Table 7-2: Interim Acceptance Criteria for the Radiological Protection of the Environment

Biota	First Tier Acceptance Criteria ($\mu\text{Gy/h}$)	Second Tier Acceptance Criteria ($\mu\text{Gy/h}$)
Amphibian	10	400
Aquatic Bird	4	40
Aquatic Mammal	4	40
Aquatic Plants	10	4,000
Benthic Invertebrates	10	4,000
Fish	10	400
Reptile	10	400
Terrestrial Bird	4	40
Terrestrial Invertebrates	10	4,000
Terrestrial Mammals	4	40
Terrestrial Plants (Grasses)	10	400
Terrestrial Plants (Trees)	4	40

7.1.4 Interim Acceptance Criteria for the Protection of the Environment from Hazardous Substances

For this category, the criteria defined in Section 7.1.2 also apply because the values selected in Table 7-1 are the lowest values relevant to either human health or to the environment.

7.2 Scope

This section presents the scope of work addressed in this postclosure safety assessment.

The scope is defined by taking into account the discussion of the Normal Evolution Scenario and the Disruptive Event Scenarios in Chapter 6 together with experience gained from previous postclosure studies performed for other hypothetical sites and conceptual designs.

The scope is intended to illustrate key aspects of a potential postclosure safety assessment for a sedimentary rock site, based on a hypothetical location. It also demonstrates methods and techniques as applied to the most recent container and placement room design. Analysis cases are limited to those needed to provide a demonstration of the overall approach and to those needed to reach possible conclusions for the hypothetical site.

Section 7.2.1 describes the Normal Evolution Scenario and associated sensitivity cases, and Section 7.2.2 summarizes the scope for Disruptive Event Scenarios. Items excluded from the scope but which might be included in a licence submission as part of a more comprehensive assessment are discussed in Section 7.2.3.

Results for all cases are measured against the interim acceptance criteria for the radiological protection of persons (Section 7.1.1).

Results for the Base Case (see below) of the Normal Evolution Scenario and for the Disruptive Event Scenario with the highest dose consequence (i.e., All Containers Fail) are measured against criteria for the protection of persons from hazardous substances (Section 7.1.2), criteria for the radiological protection of the environment (Section 7.1.3), and criteria for the protection of the environment from hazardous substances (Section 7.1.4).

Results are also developed for two complementary radiological indicators (i.e., radionuclide concentrations in the biosphere and radionuclide transport to the biosphere).

Figure 7-1 illustrates all deterministic cases considered. The figure shows the cases analyzed, ranging from likely through to highly unlikely. These cases are described in detail in subsequent sections.

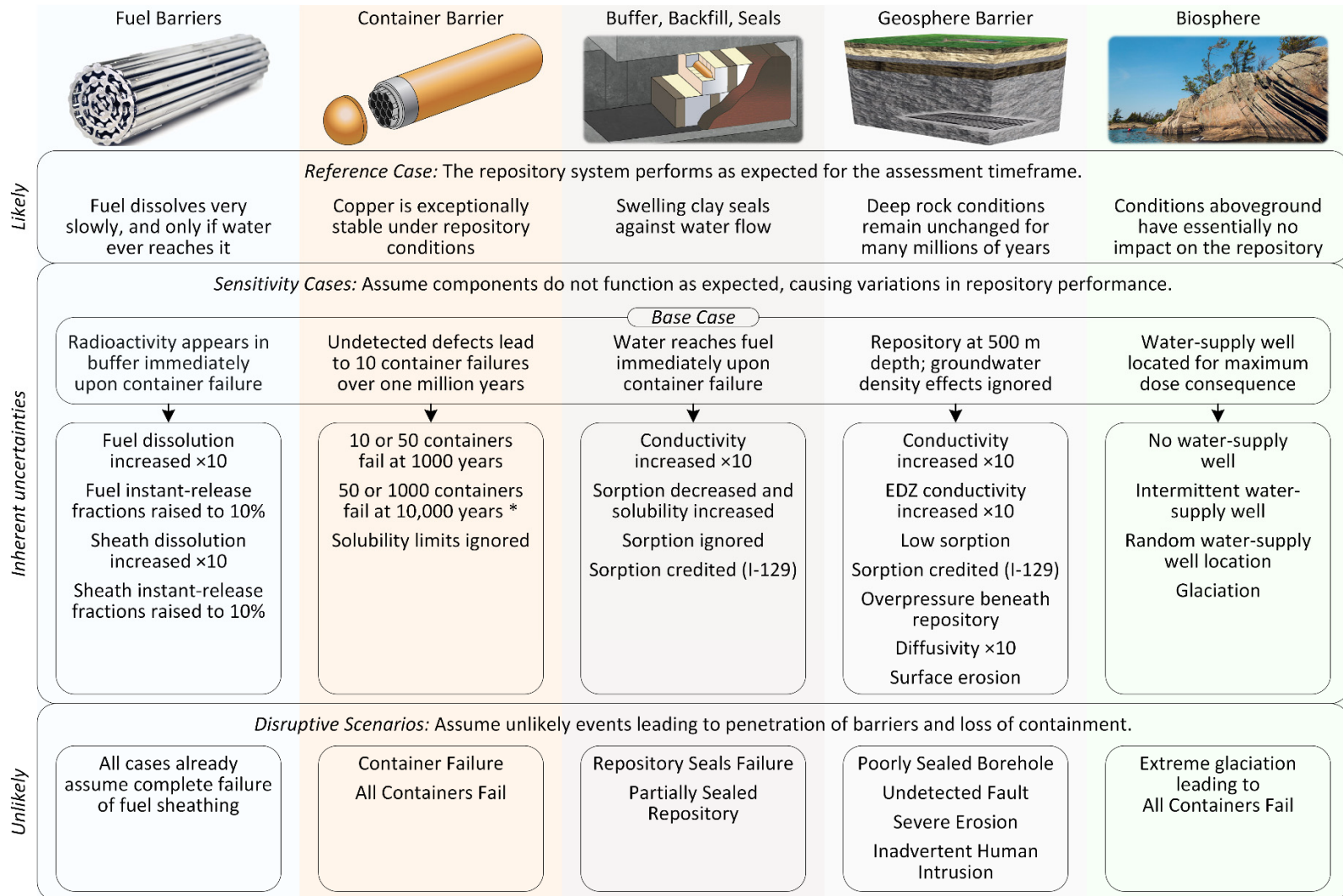
Postclosure Safety Assessment of a Used Fuel Repository in Sedimentary Rock

Document Number: NWMO-TR-2018-08

Revision: 000

Class: Public

Page: 326



Note: Hypothetical container failures all occur in the one location that would yield the largest dose consequence. The case marked '*' is an exception, where hypothetical container failures are equally likely to occur at all locations across the repository.

Figure 7-1: Illustration showing Normal Evolution Scenario and Sensitivity Studies, and Disruptive Event Scenarios

7.2.1 The Normal Evolution Scenario

The Normal Evolution Scenario is based on a reasonable extrapolation of present day site features and receptor lifestyles. It includes the expected evolution of the site and expected degradation of the repository system. Its purpose is to illustrate the anticipated effects of the repository on people and on the environment.

The Normal Evolution Scenario is described in terms of a “Reference Case” and a series of sensitivity studies.

The sensitivity studies illustrate repository performance for a range of reasonably foreseeable deviations from key Reference Case assumptions. These deviations arise as a result of components unknowingly placed in the repository that either (a) do not meet their design specification or (b) do not fully function as anticipated.

The likelihood of such deviations will be very low. Care is being taken to design, develop and proof test a robust placement technology which will ultimately be implemented under a comprehensive quality assurance program. A key element of the quality assurance program will be an inspection process designed to ensure all components cleared for placement meet design specification. Similarly, component performance is supported by an extensive research and testing program, such that the behaviour of all materials placed in the repository will also be well understood.

7.2.1.1 Reference Case

The Reference Case represents the situation in which all repository components meet their design specification and function as anticipated. As such, the used fuel containers remain intact essentially indefinitely (see Chapter 5) and no contaminant releases occur in the one million year time period of interest to the safety assessment.

7.2.1.2 The Base Case

The “Base Case” assumes a small number of containers are fabricated with sizeable defects in their copper coating, and that a smaller number of these off-specification containers escape detection by the quality assurance program and are unknowingly placed in the repository.

Studies are underway to determine the likelihood and number of off-specification containers that could potentially be present; however, the results of this work are currently not available. In the meantime, 10 containers with large undetected defects in the copper coating are assumed to be in the repository. Postclosure studies assuming 10 defective containers are sufficient to illustrate repository performance and to provide a measure of the consequences that could be expected should such an event (or a similar one) actually occur.

The defects are assumed sufficiently large to cause each of the 10 containers to fail within one million years. As the actual nature (i.e., size, location) of each defect will vary, it is highly unlikely that 10 containers would all fail simultaneously. The failure times are assumed to be evenly spread over the one million year time period of interest, with the first failure occurring at 1000 years and subsequent failures occurring sequentially every 100,000 years. Table 7-3

shows that 1000 years is a very conservative value for the time of first container failure and even more conservative as the assumed time of first radionuclide release.

To further define the Base Case, a number of bounding assumptions are made to account for uncertainties affecting case definition. A “bounding assumption” is an assumption that results in a greater consequence than the entire range of uncertainty, usually at the expense of realism. To illustrate, a bounding assumption is created if the uncertainty associated with the location and lifestyle of people unknowingly living in the vicinity of the repository in the future is replaced by an assumption that instead has people unknowingly living on top of the repository and obtaining all of their drinking and crop irrigation water from a deep well, with the well positioned in the location that maximizes the uptake of any potential contaminant release.

The adoption of bounding assumptions is a common technique in safety assessment. It allows for complex problems to be reduced to much simpler ones, with the downside being that the resulting case is no longer the most realistic. While this is acceptable from a licensing viewpoint (provided results meet acceptance criteria), it can make repository performance appear to be much worse than it really is.

To illustrate the degree to which conservatism (and departure from reality) is incorporated in the Base Case, Table 7-3 compares key Base Case assumptions with what might actually occur in reality. For simplicity, the table is focussed on only the 10 defective containers, with separate sections shown for defect, container and dose related assumptions. A discussion of the key parameters in each section is included below the table.

Table 7-3: Conservatisms in Base Case Assumptions

Parameter	Realistic Assumption	Base Case Assumption
When can contaminants escape the container?	After the container is breached and large amounts of water contact the fuel	After the container is breached
Defect Parameters		
What is the defect of concern?	Undetected defect in the copper corrosion barrier	Undetected defect in the copper corrosion barrier
What is smallest size of defect that can be reliably detected?	0.8 mm (Detection Threshold)	0.8 mm (Detection Threshold)
How large is the defect in the copper corrosion barrier?	Random sizes below the Detection Threshold	Large enough to cause container failure at the assumed times (>>0.8 mm depth)
Where is the defect located?	Random location <ul style="list-style-type: none"> • < 1% chance over 8 mm weld • ~5% chance over weld area (8-30 mm steel) • ~25% chance over container head (30 mm steel) • ~70% chance over container body (46 mm steel) 	Not applicable Complete container failure occurs at the assumed times independent of defect location
How long does a copper barrier with a defect remain effective?	> 74 million years for defects below the 0.8 mm Detection Threshold (see Chapter 5) <i>Based on an assumed groundwater sulphide concentration of 1 µM</i>	1000 years for the first container One additional container fails every 100,000 years
How many containers are breached prior to one million years?	0	10
Container Parameters		
Once the copper barrier is penetrated, how long before the steel inner shell is penetrated due to corrosion?	140,000 years for 8 mm 1,300,000 years for 30 mm 2,000,000 years for 46 mm <i>Based on 1 mm diameter hole in the copper barrier</i> <i>It is anticipated that there will be insufficient amounts of carbonate to promote siderite-</i>	0 years

Postclosure Safety Assessment of a Used Fuel Repository in Sedimentary Rock

Document Number: NWMO-TR-2018-08

Revision: 000

Class: Public

Page: 330

Parameter	Realistic Assumption	Base Case Assumption
	<i>producing corrosion reactions (see Chapter 5)</i>	
Once the steel barrier is penetrated, how long before large amounts of water enter the container?	It could take many tens of thousands of years for the container to fill with water	0 years
Do the Zr fuel sheaths prevent water from contacting fuel elements?	Possibly Some fuel sheaths may still be intact when water enters the container	No
For fuel elements that are contacted by water, how large is the instant release source term?	Depends on the power experienced while in the reactor and on the physical condition of each fuel pellet	Conservative Value
Does H ₂ released during steel corrosion and radiolysis inhibit the fuel dissolution rate (and thereby inhibit the contaminant release rate)?	Most likely Yes	No
Do corrosion products accumulate in the defect and obstruct the migration of contaminants?	Yes	No
After the steel barrier is penetrated, how long before the container wall corrodes away and no longer presents any resistance to contaminant release	120,000 years for 8 mm 460,000 years for 30 mm 710,000 years for 46 mm <i>It is anticipated that there will be insufficient amounts of carbonate to promote siderite-producing corrosion reactions (see Chapter 5)</i>	0 years
Dose Parameters		
Are people living close to the facility?	Unknown The repository footprint is small and the location may be far from populated areas	Yes Living on top of the repository
Are the nearby people using a deep well to obtain their drinking water?	Unlikely Surface water sources or a shallow well are more likely	Yes A greater than 200 m depth is assumed
If used, where is the well located in relation to the defective containers?	Random	Worst location The location that maximizes contaminant uptake
Where are the hypothetical defective containers located in the repository?	Random	Clustered In the location that maximizes uptake to the well

The following discussion provides contextual information on the contents of Table 7-3.

Defect Assumptions:

The concern is an undetected defect in the copper corrosion barrier.

In the Base Case, 10 containers with defects much greater than the assumed 0.8 mm detection threshold of the inspection equipment are assumed to be unknowingly placed in the repository. These defects are of sufficient size that the copper coating is fully penetrated by corrosion within 1000 years to 1,000,000 years.

In reality, defects of size greater than the detection threshold are not expected to be present. Copper defects (voids) smaller than this could exist however, and these would be randomly located anywhere in the copper coating. As noted in Chapter 5, containers with a design copper thickness of 3 mm could survive in excess of 74 million years in the type of groundwater conditions anticipated to be present at the hypothetical site, even if a defect in the copper coating of 0.8 mm is assumed.

Container Assumptions:

Table 7-3 compares Base Case assumptions for container performance following penetration of the copper barrier with what is likely to occur in reality.

Specifically:

- The steel inner container is assumed to be breached immediately upon penetration of the copper barrier. In reality, it could take a minimum of 140,000 additional years (and more likely more than one million years) before corrosion sufficient to breach the inner container occurs. The actual length of time would depend on the thickness of the steel barrier at the location of the copper defect and on the steel corrosion rate. The steel corrosion rate in turn depends on the availability of carbonate in the groundwater (see Chapter 5).
- The interior of the container is assumed to fill with water immediately upon penetration of the copper barrier. In reality, it could take many tens of thousands of years before significant quantities of water could pass through the bentonite buffer and enter the container once the steel barrier is penetrated. There could be a further delay due to the generation of gas within the container that could also inhibit water ingress. This is in addition to the time taken to penetrate the steel container discussed above.
- The zirconium fuel sheaths are assumed to not prevent water from coming into contact with the fuel. In reality, many fuel sheaths are expected to be intact when the fuel bundles are placed in the repository, as Zircaloy is a durable metal. As long as the fuel sheaths remain intact, there will be no contaminant release from fuel elements even if the container fills with water. As such, the fuel sheaths may further delay the time at which water contacts the fuel pellets; however, the likelihood of local hydride related cracking at longer times cannot be easily quantified so no credit is taken for the fuel sheath as a barrier.
- The entire instant release source term (Section 7.5.2.2) released immediately upon water contacting the fuel, which is assumed to occur as soon as the container is breached, which in turn is assumed to occur immediately after penetration of the copper barrier. In reality, there will be no instant release until the steel inner shell and Zr fuel sheaths are penetrated

and significant amounts of water contact the fuel. Even then, the instant release would depend on the number of fuel elements exposed to water, the power history of those elements, the fraction of contaminants that have migrated to cracks and grain boundaries, and the fraction of those cracks and grain boundaries that are initially exposed to water. Due to these variables, a conservative value is adopted in the Base Case.

- A radiolysis-driven fuel dissolution rate is assumed, which allows congruent release of the remaining radionuclides over time. In reality, there is emerging evidence that shows small amounts of dissolved hydrogen can slow down, and even stop the fuel matrix from undergoing radiolysis driven dissolution. If such dissolution does not occur, the long-term contaminant release from the fuel matrix decreases substantially.
- It is assumed there are no corrosion products present. In reality, corrosion products would accumulate in the penetration and inside the container, thereby providing additional resistance to water and contaminant migration. This will slow down the rate at which contaminants can escape the container; however, because this is difficult to quantify no credit for this behaviour is taken in the Base Case.
- The container itself is assumed to present no resistance to contaminant migration immediately upon penetration of the copper barrier. In reality, even though the container is assumed penetrated, the size of the penetration will be small compared to the size of the container. It could take at least another 120,000 years after the steel shell is breached (and potentially much longer) for the container walls to corrode from the inside to the extent that the container itself no longer presents a resistance to contaminant transport.

Dose Related Assumptions:

Base Case assumptions are defined to ensure the highest potential dose rate is calculated, with the intention being that the dose rate to people exhibiting more realistic behaviours or in alternate exposure situations will always be substantially less.

Specifically:

- A family is unknowingly living and growing their own food on top of the repository. In reality, given the small footprint and the potential for the site to be remote from population centres, it is possible that no-one will be living in exactly this location. A greater distance means more opportunity for dilution and dispersion of contaminants leading to lower doses.
- The family uses a deep well to obtain their drinking water. Given that there may be surface water bodies nearby, it is possible that a well would not be used. Contaminant concentrations in streams and lakes would be much lower than in the well due to greater dilution.
- The drinking water well is assumed to be fairly deep, about 219 m. In reality, it is unlikely that a family would use such a deep well. Current practice is to use more shallow wells for drinking water. Shallow wells allow for lengthier contaminant transport times with associated increased dispersion and dilution in the geosphere.
- The drinking water well is assumed to be in the location that maximizes the uptake of contaminants escaping the repository. In reality, the well would be in a random location with respect to the hypothetical defective containers. Depending on where the well is located, it is possible that no contaminants would be captured by the well.

- The defective containers are assumed to all be clustered in the location that results in the greatest possible contaminant transport to the well. While the defective containers are likely to be randomly distributed, clustering may occur following a temporary lapse of quality control. Even if the containers were clustered, the likelihood that they would be in the location that results in the greatest transport to the well would be low.

Many other assumptions not listed in Table 7-3 are also required before the entire Base Case can be fully defined. For example, values for such things as fuel burnup, radionuclide inventories, fuel dissolution rate, material and transport properties, the geology, the location of surface features, human characteristics and so on, are all required. Most of these assumptions are described in other sections of this report, with more detailed information available in Gobien et al. (2018). The key assumptions for the Base Case are:

- Geosphere properties as per Chapter 2;
- Used fuel inventories as per Chapter 3;
- Repository design as per Chapter 4;
- 10 containers with large defects in the copper coating are present in the repository. The copper coating is penetrated in the first container at 1000 years, with one additional container failing every 100,000 years;
- No other container failures occur;
- Constant temperate climate and steady-state groundwater flow;
- A self-sufficient farming family is unknowingly living on top of the repository, growing crops and raising livestock;
- Drinking and irrigation water for the family is obtained from a 219 m deep well that penetrates the entire thickness of the Guelph formation. The well / defective container locations are such that contaminant release to the well is maximized;
- The well is pumped at a rate of 1261 m³/a. This is sufficient for drinking water and irrigation of household crops;
- Input parameters with uncertainty and variability represented by probability distributions are set to either the most probable value (when there is one) or to the median value otherwise.

7.2.1.3 Sensitivity Studies to Illustrate the Effects of Well Assumptions

The Base Case described above in Section 7.2.1.2 assumes the presence of a continuously operating well pumping at a rate of 1261 m³/a from the permeable formation closest to the repository throughout the entire one million year period of interest. The sensitivity cases described below are selected to illustrate the sensitivity of Base Case results to some of the well assumptions. The cases considered are:

- No well;
- Intermittent well operation; and
- Random well location.

These cases are further described in Table 7-4.

Table 7-4: Sensitivity Cases to Illustrate the Effects of Well Assumptions

	Base Case Assumption ⁽¹⁾	Sensitivity Case Assumption	Rationale
Illustrative Cases	Deep well in the location that maximizes uptake of contaminants. The well intersects the Guelph formation and pumps continuously at a rate of 1261 m ³ /a throughout the entire one million year period of interest.	No well. The defective containers are in the same location as in the Base Case.	If there are adequate surface sources of water, it is unlikely that a deep well will be used.
		Intermittent well operation. The defective containers are in the same location as in the Base Case.	If a well is used, it will not be pumped continuously over a one million year period.
		Random well location. The defective containers are in the same location as in the Base Case.	If a well is used, it is not likely to be in the location that maximizes contaminant uptake from all for the defective containers in the repository.

Note: (1) A detailed description of the input data is available in Gobien et al. (2018).

7.2.1.4 Sensitivity Studies to Illustrate the Effect of Deviations in Anticipated Barrier Performance for the Base Case

The Base Case assumes fabrication failures with coincident quality assurance system failures leading to a small number of containers that do not meet design specification being unknowingly placed in the repository.

Coincident failures of this type could also affect other repository components. For example, off-specification material could unknowingly be used in the fabrication of buffer box bentonite, placement room spacer blocks or bentonite pellets. Placement rooms and access tunnels could exceed their design dimensions because blasting removes too much rock in some places. Off-specification material could unknowingly be used in the construction of repository tunnel seals and repository shaft seals.

The principal end result of such failures would be either (a) nothing adverse happens, or (b) the off-specification component eventually leads to early container failure(s). Studies are underway to determine the likelihood and number of repository components that could potentially be out of compliance with their design requirements; however, the results of this work are not presently available. In the meantime, for this postclosure safety assessment, fabrication and quality assurance system failures that lead to container failure are assumed to be covered by the Base Case. The Base Case assumes 10 containers fail at various times in the first one million years following repository closure.

Quality assurance failures leading to extreme events such as degraded / ineffective repository seals or degraded / ineffective shaft seals are deemed not credible for the Normal Evolution Scenario. While the sheer number of some repository components (e.g., almost 109,000

containers) creates opportunity for unknowingly placing associated non-compliant material in the repository, this opportunity does not exist to the same extent for components present in much reduced numbers, such as for the repository seals and shaft seals. Enhanced vigilance is also anticipated when fabricating and installing these seals to ensure they meet specification. For this reason, degraded repository seals are considered Disruptive Events and described in Section 7.2.2.

The following sensitivity cases are examined to illustrate the effect of deviations in barrier performance on the Base Case:

Fuel Barrier:

- Fuel dissolution rate increased by a factor of 10; and
- Instant release fractions set to 0.10 for all contaminants (i.e., 10% of the entire inventory is instantly released).

Zircaloy Sheath Barrier:

No credit is taken in the postclosure safety assessment for the presence of the Zircaloy fuel sheath as a barrier to contaminant release from the fuel. However, because the sheath itself contains contaminants and because the screening analysis (Section 7.6) identifies some of these contaminants as potentially important, the following Zircaloy specific sensitivity cases are simulated:

- Zircaloy dissolution rate increased by a factor of 10; and
- Instant release fractions set to 0.10 for all contaminants.

Container Barrier:

- All 10 containers fail at 1000 years;
- 50 containers fail at 1000 years;
- 50 and 1000 containers fail at 10,000 years;
- Low sorption in the engineered barrier materials with coincident high solubility limits in the container; and
- No solubility limits in the container.

Buffer and Backfill and Seals Barrier:

- Hydraulic conductivities of all engineered barrier sealing materials in the repository and shaft increased by a factor of 10;
- Low sorption in the engineered barrier sealing materials with coincident high solubility limits in the container;
- Bentonite and geosphere diffusivities increased by a factor of 10 and by a factor of 100;
- I-129 sorption credited in the bentonite and geosphere; and
- No sorption in the engineered sealing materials.

Geosphere Barrier:

- Hydraulic conductivities increased by a factor of 10;
- Hydraulic conductivity in the excavation damaged zones (EDZ) increased by a factor of 10;
- Bentonite and geosphere diffusivities increased by a factor of 10 and by a factor of 100;
- 100 m of surface erosion in one million years;
- I-129 sorption credited in the bentonite and geosphere;
- 150 m overpressure in the Shadow Lake formation; and
- Sorption parameters set to two standard deviations below the mean.

These sensitivity cases are shown in Table 7-5. The table includes a description of the variation from the Base Case assumptions for each case together with a brief rationale for the case selection.

To provide an indication of repository response allowing for uncertainty in multiple parameters, two types of probabilistic sensitivity studies are also performed. In these simulations, random sampling is used to simultaneously vary input parameters for which probability distribution functions are available. Radionuclide release and transport parameters are varied with the fixed reference geosphere adopted in the System Model (Section 7.8).

The specific probabilistic cases are:

- Number, locations and failure times for defective containers fixed at their Base Case values, with all other available parameters varied; and
- All parameters with probability distributions varied, including the number, locations and failure times for the defective containers.

These cases are also described in Table 7-5.

Table 7-5: Sensitivity Cases to Illustrate the Effect of Deviations in Anticipated Barrier Performance for the Base Case

Parameter	Base Case Assumption ⁽¹⁾	Sensitivity Case Assumption	Rationale
<i>Fuel Barrier</i>			
Fuel Dissolution Rate	<p>Generated via a model that takes into account radiolysis and chemical dissolution. No credit is taken for the effect of H₂ gas on suppressing dissolution.</p> <p>With this model, ~19% of the fuel dissolves in the first one million years for a burnup of 220 MWh/kgU, and ~21% dissolves for a burnup of 280 MWh/kgU.</p>	<p>The dissolution rate is increased by a factor of 10.</p> <p>With this increase, all of the used fuel dissolves in the first one million years in an early failed container.</p>	<p>The fuel is an important barrier to the release of radionuclides because most radionuclides are contained within the fuel matrix. As the fuel dissolves in the long term these radionuclides become available for transport.</p> <p>The factor of 10 increase roughly corresponds to the 95th percentile value.</p>
Fuel Instant Release Fractions	<p>Instant release fractions are as described in Section 7.5.2.2.</p> <p>Most radionuclides have no instant release. Instant release fractions for selected radionuclides are:</p> <p>C = 0.027 Cl = 0.06 Cs = 0.04 I = 0.04 Se = 0.006 Np, Pu, Th, U = 0.00</p>	<p>Instant release fractions for all fuel contaminants are set to 0.10.</p>	<p>Some radionuclides in the used fuel are present initially in the fuel sheath gap and grain boundaries and are therefore available for release early after contact with water. This fraction of the inventory is referred to as the instant release fraction.</p> <p>Assigning a high instant release fraction to all radionuclides (including actinides) ensures the results are bounding as well as providing information on the importance of this term to the overall dose consequence.</p>
<i>Fuel Sheath Barrier</i>			
Zircaloy Dissolution Rate	<p>Zircaloy dissolution is determined from the corrosion rate of Zr in water (~5 nm/a) and the surface area of Zr in contact with water.</p>	<p>The dissolution rate of the Zircaloy fuel sheath is increased by a factor of 10.</p>	<p>This is a companion to the fuel dissolution case described above; however, the focus of this case is on radiological contaminants in the Zircaloy fuel sheath (notably C-14 and Cl-36).</p>

Postclosure Safety Assessment of a Used Fuel Repository in Sedimentary Rock

Document Number: NWMO-TR-2018-08

Revision: 000

Class: Public

Page: 338

Parameter	Base Case Assumption ⁽¹⁾	Sensitivity Case Assumption	Rationale
Zircaloy Instant Release Fractions	C = 0.021 CI = 0 Other are set to zero.	Instant release fractions for all Zircaloy contaminants are set to 0.10.	This is a companion to the fuel instant release case described above; however, the focus of this case is on radiological contaminants in the Zircaloy fuel sheath.
Container Barrier			
Container Failure Times	The first container fails after 1000 years, with subsequent containers failing sequentially every 100,000 years.	All 10 containers fail at 1000 years.	This case illustrates repository performance if multiple container failures occur early and all at the same time. At early times, the fuel dissolution rate and the amount of radionuclides present are both higher than for later times. As per the information in Table 7-3, a container failure time of 1000 years is conservative.
Number of Failed Containers	10 containers fail, with the first container failing after 1000 years and subsequent containers failing sequentially every 100,000 years. All failed containers are clustered in the location that yields the highest dose consequence.	50 containers fail at 1000 years. All failed containers are clustered in the location that yields the highest dose consequence.	Because the container manufacturing and inspection processes are still being developed, there is uncertainty in the number of defective containers that could unknowingly be placed in the repository. This case illustrates repository performance for a greater number of defective containers than assumed in the Base Case. For conservatism, and to allow scaling of results from other cases, all 50 containers are assumed to fail early and to be located in

Postclosure Safety Assessment of a Used Fuel Repository in Sedimentary Rock

Document Number: NWMO-TR-2018-08

Revision: 000

Class: Public

Page: 339

Parameter	Base Case Assumption ⁽¹⁾	Sensitivity Case Assumption	Rationale
			<p>the position that yields the highest dose consequence.</p> <p>As per the information in Table 7-3, a container failure time of 1000 years is conservative.</p>
<p>Location and Number of Failed Containers</p>	<p>10 containers fail, with the first container failing after 1000 years and subsequent containers failing sequentially every 100,000 years.</p> <p>All failed containers are clustered in the location that yields the greatest dose consequence.</p>	<p>i) 50 containers fail at 10,000 years, with the containers uniformly distributed across the repository.</p> <p>ii) 1000 containers fail at 10,000 years, with the containers uniformly distributed across the repository.</p>	<p>If there are larger numbers of defective containers, it is highly unlikely that they will all be located in the position that yields the highest dose consequence.</p> <p>These cases illustrate repository behaviour for larger numbers of defective containers, but with the defective containers assumed to be uniformly distributed across the repository. For simplicity, a 10,000 year failure time is assumed to allow scaling of results from other cases.</p> <p>As per the information in Table 7-3, a container failure time of 10,000 years is conservative.</p>
<p>Low Sorption in the EBS and Shaft Seal Materials with Coincident High Solubility Limits in the Container</p>	<p>Sorption values for engineered barrier materials are described in Section 7.5.2.7.</p> <p>Solubility limits are as described in Section 7.5.2.5.</p>	<p>“Low” / “High” means the sorption values are set to their respective lower bounds and the solubility limits are set to two standard deviations in the conservative direction.</p>	<p>This case determines the effect of simultaneous pessimistic assumptions affecting the solubility in the container interior and retention in the clay based engineered barriers.</p> <p>This case is identical to that discussed in the Buffer, Backfill and Seals Barrier section of this table. It is included here because this case examines both container assumptions and near-field assumptions.</p>

Postclosure Safety Assessment of a Used Fuel Repository in Sedimentary Rock

Document Number: NWMO-TR-2018-08

Revision: 000

Class: Public

Page: 340

Parameter	Base Case Assumption ⁽¹⁾	Sensitivity Case Assumption	Rationale
Solubility Limits	<p>Solubility limits are determined externally from thermodynamic data and specified as input. Solubility limits are as described in Section 7.5.2.5.</p> <p>Solubility limits (mol/kg) for selected radionuclides are:</p> <p>C = 2.2×10^{-2} Se = 3.4×10^{-8} Np = 1.7×10^{-8} Th = 1.4×10^{-6} U = 4.5×10^{-8} Ca, Cl, Cs, I = no limit</p> <p>The solubility limits are calculated at 25°C and increased in the Base Case by a factor of 10 above the values listed here to account for the effects of temperature, and uncertainties in groundwater chemistry and thermodynamic data.</p>	<p>Solubility limits for all radionuclides are set to 2.0 mol/kg. This is equivalent to having no solubility limit since the limit is never reached.</p>	<p>The concentration of a dissolved radionuclide is one of the parameters that can affect the rate of radionuclide release from the defective container. While some radionuclides are highly soluble (e.g., I and Cl), others are not (e.g., Pu and U).</p> <p>Some side species such as organics or colloids may make some radionuclides more soluble than would be expected from straight thermodynamics.</p> <p>Removal of all solubility limits provides information on the importance of this parameter to the overall dose consequence.</p>
Buffer, Backfill and Seals Barrier			
Hydraulic Conductivity of EBS and Shaft Seal Materials Increased	<p>1×10^{-10} m/s for dense backfill 1×10^{-10} m/s for concrete 4×10^{-11} m/s for bentonite/sand shaft seal 1×10^{-12} m/s for asphalt shaft seal 2×10^{-12} m/s for HCB 5×10^{-11} m/s for gap fill</p> <p>These are the reference values at 20°C. Values are temperature corrected to 85°C.</p>	<p>Hydraulic conductivities increased by a factor of 10 for all EBS materials. For placement room bentonite, this is roughly equivalent to the upper bound of the measured variations.</p>	<p>EBS materials, especially the HCB bentonite that forms the buffer box, is an important barrier to advective flow.</p> <p>The case illustrates the effect of variation in hydraulic conductivity on barrier performance.</p>

Postclosure Safety Assessment of a Used Fuel Repository in Sedimentary Rock

Document Number: NWMO-TR-2018-08

Revision: 000

Class: Public

Page: 341

Parameter	Base Case Assumption ⁽¹⁾	Sensitivity Case Assumption	Rationale
Low Sorption in the EBS and Shaft Seal Materials with Coincident High Solubility Limits in the Container	<p>Sorption values for engineered barrier materials are described in Section 7.5.2.7.</p> <p>Solubility limits are as described in Section 7.5.2.5.</p>	<p>“Low” / “High” means the sorption values are set to their respective lower bounds and the solubility limits are set to two sigma values in the conservative direction.</p>	<p>This case determines the effect of simultaneous pessimistic assumptions affecting the solubility in the container interior and retention in the clay based engineered barriers.</p> <p>This case is identical to that discussed in the Container Barrier section of this table. It is included here because this case examines both container assumptions and near-field assumptions.</p>
Bentonite and Geosphere Diffusivity	<p>Effective diffusion coefficients vary from layer to layer.</p> <p>Anion and neutral species are assumed to have the same diffusion coefficients. This conservatively ignores anion exclusion.</p> <p>Cations are assumed to have an effective diffusion coefficient three times greater than neutral and anions due to surface diffusion.</p>	<p>Effective diffusion coefficients increased by a factor of 10.</p> <p>Effective diffusion coefficients increased by a factor of 100.</p>	<p>Diffusivity is an important parameter controlling radionuclide transport in low hydraulic conductivity sedimentary rock formations.</p> <p>The first sensitivity case examines the effect of higher diffusion coefficients on radionuclide transport. The second case represents an unrealistically large variation, the purpose of which is to ensure the peak dose consequence occurs with the one million year time frame of interest.</p> <p>This case is identical to that discussed in the Geosphere Barrier section of this table. It is included here because this case examines both bentonite assumptions and geosphere assumptions.</p>
I-129 Sorption in the Bentonite and Geosphere	<p>I-129 is non-sorbing.</p>	<p>The geometric mean of measured values for crushed rock / bentonite tests are (in m³/kg):</p> <p>Bentonite: 0.0013</p> <p>Shale: 1.3x10⁻⁴</p>	<p>There is some evidence in the literature of small sorption coefficients for iodide. This case examines the effect if credit is taken for these small values.</p>

Postclosure Safety Assessment of a Used Fuel Repository in Sedimentary Rock

Document Number: NWMO-TR-2018-08

Revision: 000

Class: Public

Page: 342

Parameter	Base Case Assumption ⁽¹⁾	Sensitivity Case Assumption	Rationale
		<p>Limestone: 1.08×10^{-4}</p> <p>The basis for these values is described in Vilks and Yang (2018). The values are adjusted when input to the models as described in Gobien et al. (2018). This adjustment accounts for the in-situ material not being crushed rock / bentonite.</p>	<p>The focus is on I-129 because, as the results will later show, this is the only radionuclide of importance to the long-term dose assessment.</p> <p>This case is identical to that discussed in the Geosphere Barrier section of this table. It is included here because this case examines both bentonite assumptions and geosphere assumptions.</p>
Sorption in the EBS and Shaft Seal Materials	<p>Use of linear equilibrium sorption model.</p> <p>Some elements are non-sorbing (e.g., Cl and I) while others are highly sorbing in the reducing environment (e.g., Np, Pu, Th, and U). Sorption values for engineered barrier materials are described in Section 7.5.2.7.</p>	<p>Sorption coefficients for all near field barrier components including the shafts are set to zero.</p> <p>Sorption coefficients in the geosphere are maintained at their Base Case values.</p>	<p>The clay-based seals have a high surface area and can sorb radionuclides released into the groundwater from the containers.</p> <p>Colloid transport within the dense clay seals is not expected, so it is not included in the Base Case values. Sorption on iron oxides, from corrosion of the steel inner vessel of the container is conservatively neglected.</p> <p>Setting the sorption coefficients to zero results in an unrealistic, yet conservative, case that provides information on the relative importance of sorption in the EBS.</p>
Geosphere Barrier			
Hydraulic Conductivity	Base Case hydraulic conductivity profile as defined in Chapter 2.	A factor of 10 increase relative to the Base Case.	<p>Geosphere hydraulic conductivity is an important parameter controlling groundwater flow and advective radionuclide transport.</p> <p>The sensitivity case examines the effect of higher hydraulic conductivity on the advective component of radionuclide transport.</p>

Postclosure Safety Assessment of a Used Fuel Repository in Sedimentary Rock

Document Number: NWMO-TR-2018-08

Revision: 000

Class: Public

Page: 343

Parameter	Base Case Assumption ⁽¹⁾	Sensitivity Case Assumption	Rationale
<p>Hydraulic Conductivity of EDZ</p>	<p>The excavation damaged zones are defined with higher hydraulic conductivity than the surrounding rock. Hydraulic conductivity (K/K_{rock}) for selected areas are: <i>Placement Rooms, Central Access, Panel Access and Perimeter Tunnels:</i> Inner EDZ = 1000 Seal EDZ = 1000 Outer EDZ = 100 <i>Shafts:</i> Inner EDZ = 100 Outer EDZ = 10 (See Chapter 5)</p>	<p>Hydraulic conductivity of all excavation damaged zones increased by a factor of 10.</p>	<p>The excavation damaged zone is a region of rock damaged during the construction process; potential thermal damage is also taken into account. The EDZ has higher hydraulic conductivity than the surrounding intact rock and could be a pathway for radionuclide transport.</p> <p>EDZ values reflect the likelihood of connected damage paths aligned with bedding planes. There is a possibility of some self-sealing due to shale swelling or salt precipitation.</p> <p>Increasing the hydraulic conductivity provides information on the importance of these damage zones to the transport and subsequent release of radionuclides to the surface.</p>
<p>Bentonite and Geosphere Diffusivity</p>	<p>Effective diffusion coefficients vary from layer to layer.</p> <p>Anion and neutral species are assumed to have the same diffusion coefficients. This conservatively ignores anion exclusion.</p> <p>Cations are assumed to have an effective diffusion coefficient three times greater than neutral and anions due to surface diffusion.</p>	<p>Effective diffusion coefficients increased by a factor of 10.</p> <p>Effective diffusion coefficients increased by a factor of 100.</p>	<p>Diffusivity is an important parameter controlling radionuclide transport in low hydraulic conductivity sedimentary rock formations.</p> <p>The first sensitivity case examines the effect of higher diffusion coefficients on radionuclide transport. The second case represents an unrealistically large variation, the purpose of which is to ensure the peak dose consequence occurs with the one million year time frame of interest.</p> <p>This case is identical to that discussed in the Buffer, Backfill and Seals Barrier section of this table.</p>

Postclosure Safety Assessment of a Used Fuel Repository in Sedimentary Rock

Document Number: NWMO-TR-2018-08

Revision: 000

Class: Public

Page: 344

Parameter	Base Case Assumption ⁽¹⁾	Sensitivity Case Assumption	Rationale
			It is included here because this case examines both bentonite assumptions and geosphere assumptions.
I-129 Sorption in the Bentonite and Geosphere	I-129 is non-sorbing.	The geometric mean of measured values for crushed rock / bentonite tests are (in m ³ /kg): Bentonite: 0.0013 Shale: 1.3x10 ⁻⁴ Limestone: 1.08x10 ⁻⁴ The basis for these values is described in Vilks and Yang (2018). The values are adjusted when input to the models as described in Gobien et al. (2018). This adjustment accounts for the in-situ material not being crushed rock / bentonite.	There is some evidence in the literature of small sorption coefficients for iodide. This case examines the effect if credit is taken for these small values. The focus is on I-129 because, as the results will later show, this is the only radionuclide of importance to the long-term dose assessment. This case is identical to that discussed in the Buffer, Backfill and Seals Barrier section of this table. It is included here because this case examines both bentonite assumptions and geosphere assumptions
Erosion	Tens of metres of erosion in the first one million years. This is neglected in the Base Case due to its anticipated negligible effect.	100 m erosion in the first one million years.	Repeated glaciations over one million years could remove a significant amount of the formations closest to the surface.
Overpressure in the Shadow Lake Formation	No overpressure.	150 m above hydrostatic conditions.	Overpressure in formations below the repository could result in increased advective flow to the surface. This case examines the significance of this effect.

Postclosure Safety Assessment of a Used Fuel Repository in Sedimentary Rock

Document Number: NWMO-TR-2018-08

Revision: 000

Class: Public

Page: 345

Parameter	Base Case Assumption ⁽¹⁾	Sensitivity Case Assumption	Rationale
Sorption in the Geosphere	<p>Sorption values are described in Section 7.5.2.7.</p> <p>Some elements are non-sorbing (e.g., Cl and I) while others are highly sorbing in the saline reducing environment (e.g., Np, Th, and U).</p> <p>Colloid transport is not important under diffusion-dominant and highly saline transport conditions, so it is not included.</p>	<p>The geosphere sorption coefficients for all elements are set to two standard deviations below the mean.</p> <p>All other near field sorption coefficients (i.e., buffer, backfill and seals) are maintained at their Base Case values.</p>	<p>Radionuclides can be sorbed onto the surfaces of the host rock minerals, thereby retarding their transport to the surface.</p> <p>Setting the sorption coefficients to low values provides information on the relative importance of sorption in the geosphere.</p>
<i>Probabilistic Assessment of Uncertainty</i>			
Container Parameters Fixed	<p>There are 10 defective containers all clustered in the location that maximizes contaminant uptake to the well. The containers have defects in their copper coating such that breaching of the first container occurs after 1000 years with breaching of the remaining containers occurring sequentially every 100,000 years.</p> <p>The well is in the location that maximizes contaminant uptake from the clustered containers.</p> <p>Input parameters represented by probability distributions are set to either the most probable value (when there is one) or to the median value.</p>	<p>The number, location and failure times of the 10 defective containers are identical to those in Base Case.</p> <p>All other available input parameters represented by probability distributions are varied.</p> <p>An important caveat is that these probabilistic simulations are performed in the fixed geosphere of the System Model.</p>	<p>Many of the modelling parameters are uncertain or have a natural degree of variability and as such are more generally characterized by a range or distribution of values.</p> <p>Varying all parameters simultaneously while maintaining the container locations and failure times provides information on the overall uncertainty in the Base Case.</p>
All Parameters Vary	<p>There are 10 defective containers all clustered in the location that maximizes contaminant uptake to the well. The containers have defects in their copper coating such that</p>	<p>The number, location, and failure times of the containers are varied.</p> <p>All other parameters for which distributions are available are also varied.</p>	<p>Varying all parameters, including the number, location and failure times of the containers provides information on how</p>

Parameter	Base Case Assumption ⁽¹⁾	Sensitivity Case Assumption	Rationale
	<p>breaching of the first container occurs after 1000 years with breaching of the remaining containers occurring sequentially every 100,000 years.</p> <p>The well is in the location that maximizes contaminant uptake from the clustered containers.</p> <p>Input parameters represented by probability distributions are set to either the most probable value (when there is one) or to the median value otherwise.</p>	<p>The number of failed containers is determined from a binomial distribution, with inputs being the probability of container failure and the number of containers (108,833). The probability of failure is defined using a lognormal distribution with a geometric mean of 1/108,833 and a standard deviation of 4.9. The lower bound is set to 1/108,833 and the upper bound is 1. This distribution was selected such that approximately one simulation in 100,000 would result in 1000 failed containers. This is then consistent with the Normal Evolution Scenario sensitivity case in which 1,000 containers fail.</p> <p>An important caveat is that these probabilistic simulations are performed in the fixed geosphere of the System Model.</p>	<p>such variations could affect the Base Case results.</p>

Note: (1) A detailed description of the input data is available in Gobien et al. (2018).

7.2.1.5 Sensitivity Studies to Illustrate the Effect of Modelling Attributes and Numeric Parameters on the Base Case

Some additional sensitivity cases have been simulated to illustrate the effect of differing modelling approaches and numeric parameters on the Base Case results. These cases are discussed in Table 7-6 and listed below:

- Increased spatial resolution to confirm convergence for the 3D Groundwater Flow and Transport Models; and
- Increased and decreased number of time steps to confirm model results are not sensitive to temporal resolution.

Table 7-6: Modelling Attributes and Numeric Parameter Sensitivity Cases

Modelling Attribute or Parameter	Base Case Assumption	Sensitivity Case Assumption	Rationale
Spatial Resolution	User defined in the Base Case.	Different levels of model resolution are compared.	Increasing the spatial resolution provides information on whether the model results are numerically accurate.
Time Step Size	User defined in the Base Case.	Time step control in the finite element model is adjusted to both increase and decrease the number of timesteps.	Changing the number of time steps provides information on whether the model results are numerically converged.

7.2.1.6 Sensitivity Study to Illustrate the Effect of Glaciation

During past 2.6 million years (i.e., the Quaternary period), much of Canada has been periodically covered by kilometre-thick ice sheets. The main factors that likely initiated these glacial cycles (i.e., solar insolation variation due to Earth orbital dynamics and the location and size of the continents and their influence on ocean currents) are still present. Current levels of greenhouse gases in the atmosphere may delay the onset of the next glaciation (Berger and Loutre 2002); however, glacial cycles are expected to reassert themselves in the time period of interest to this postclosure safety assessment.

The scenario identification discussion in Chapter 6 identifies glaciation as an important external factor influencing the behaviour of the Normal Evolution Scenario. However, for this postclosure safety assessment, the primary dose assessment is performed for a constant temperate climate. The purpose of this sensitivity study is to discuss the likely effects of glaciation on the calculated dose rates.

The effect of glaciation is discussed quantitatively based on the analyses by Avis and Calder (2015) and Chen et al. (2017). The important features of these glaciation studies are described and their applicability to the current study is discussed in Section 7.8.2.4.

7.2.2 Disruptive Event Scenarios

Disruptive Event Scenarios postulate the occurrence of unlikely events leading to possible penetration of barriers and abnormal loss of containment.

Chapter 6 describes the set of Disruptive Event Scenarios applicable to the conceptual design and hypothetical geosphere in this study. These have been identified through consideration of the features, events and processes that are important to the repository system, and through consideration of the key barriers. The scenarios are:

- Inadvertent Human Intrusion;
- All Containers Fail;
- Repository Seals Failure;
- Undetected Fault;
- Severe Erosion;
- Poorly Sealed Borehole;
- Container Failure¹; and
- Partially Sealed Repository.

The first four scenarios are within the scope of this illustrative safety assessment. Table 7-7 describes each of these four scenarios and includes a description of the parameters changed from the Base Case and the rationale for the scenario selection. It is recognized that for an actual site, the full set of relevant scenarios would need to be evaluated.

The consequences of gas generation caused by decomposition of organics and by corrosion of steel is assessed for the All Containers Fail Scenario. The gas assessment is described in Chapter 8.

The Poorly Sealed Borehole scenario is a Disruptive Event Scenario because it creates a pathway that bypasses the low-permeability geosphere. However, as long as the boreholes are sufficiently far from the repository underground structures, they are unlikely to be important due to the small size of the borehole and the limits of diffusive transport. This would be analyzed as part of a real site, when the borehole distances are known; however, the consequences are expected to be low.

Although a detailed analysis of the Container Failure Scenario is outside the scope of this study, the dose arising from this event is anticipated to be significantly less than that associated with the All Containers Fail Scenario due to the much reduced number of affected containers. The Partially Sealed Repository scenario considers the consequences if the repository is abandoned and the shafts are not sealed. This implies a near-future loss-of-society. All scenarios are analysed with deterministic methods since the basic parameters defining the scenarios are chosen conservatively.

¹ This considers delayed but substantive failure of a few containers due to unexpected in-situ conditions, and is different from the Normal Evolution Scenario which considers a defect unknowingly present in some containers as the initiating event.

Table 7-7: Analysis Cases for Disruptive Event Scenarios

Disruptive	Normal Evolution Scenario Base Case Assumption ⁽¹⁾	Disruptive Case Assumption	Rationale
Inadvertent Human Intrusion	No intrusion.	<p>The engineered and natural barriers are bypassed via the drilling of a borehole into the repository. The borehole intersects a used fuel container with 220 MWh/kgU burnup fuel and used fuel material is brought to the surface.</p> <p>Two stylized events are considered:</p> <ul style="list-style-type: none"> • The hazard is identified and the site is vacated (and subsequently mitigated) after two days; and • The hazard is not identified and the site is vacated after 14 days. <p>The effects of damaging a container with higher (280 MWh/kgU) burnup fuel on the first event are also addressed.</p> <p>The variant case, in which the borehole thereafter remains open, is not considered.</p>	<p>Institutional controls and knowledge of the repository can be lost in the future.</p> <p>This scenario examines the potential consequences to the drill crew and a future resident on the site.</p>
All Containers Fail	There are 10 defective containers all clustered in the location that maximizes contaminant uptake to the well. The containers have defects in their copper coating such that breaching of the first container occurs after 1000 years with the remaining containers failing at a rate of one additional container every 100,000 years.	<p><i>Baseline Case</i> All containers fail 60,000 years after repository closure and no containers fail prior to this time.</p> <p><i>Extreme Case</i> Identical to the above, except the time of container failure is 10,000 years.</p>	<p>The containers are anticipated to last for well in excess of one million years, based on the copper corrosion barrier, sturdy mechanical design and favourable site attributes, including geochemical stability (see Chapter 5).</p> <p>This scenario considers common cause failure of all containers. The Baseline Case corresponds to the likely earliest timeframe for an ice sheet to cover the site, and it is assumed that some unanticipated effect of</p>

Postclosure Safety Assessment of a Used Fuel Repository in Sedimentary Rock

Document Number: NWMO-TR-2018-08

Revision: 000

Class: Public

Page: 350

Disruptive	Normal Evolution Scenario Base Case Assumption ⁽¹⁾	Disruptive Case Assumption	Rationale
	The well is in the location that maximizes contaminant uptake from the clustered containers.	The well is repositioned to ensure the maximum contaminant uptake.	the ice sheet might cause failure, such as beyond-design ice thickness and mechanical loading or unexpected changes in groundwater chemistry. The Extreme Case with failure at 10,000 years provides information on the sensitivity of results to the assumed failure time.
Repository Seals Failure	The shaft is filled with a combination of bentonite / sand (70:30), concrete and asphalt with the following hydraulic conductivities (m/s): Bentonite / Sand = 4.0×10^{-11} Concrete = 1.0×10^{-10} Asphalt = 1.0×10^{-12}	The hydraulic conductivity of shaft seal materials is set to 10^{-7} m/s from the time of repository closure. Shaft EDZ hydraulic conductivities are increased by a factor of 100. The analysis redefines the locations for the defective containers and well to ensure the worst combination is identified for this event.	This scenario examines the effects of significant degradation in shaft seals. For conservatism, this degradation is assumed to occur at the time of repository closure.
Undetected Vertical Fault	There are no faults within the vicinity of the repository	An undetected vertical fault is located near and downgradient from the repository. The fault extends from the Precambrian basement up to the Guelph formation. It is characterized as one metre wide with a conductivity of 10^{-8} m/s. Two sensitivity cases are defined with the fault located at 100 m and 500 m downgradient from the repository. The well is repositioned to ensure the limiting consequences are determined.	Deep bedrock faults may be difficult to detect with available geophysical techniques, particularly if there are no associated formation offsets.

Note: (1) A detailed description of the input data is available in Gobien et al. (2018).

7.2.3 Analysis Exclusions

Consistent with the scope of work described in Section 7.2, the analysis cases are limited to those needed to reach preliminary conclusions for the hypothetical site and to those needed to provide a demonstration of the overall approach.

This section lists scope items that do not appear in this report but which might otherwise be included in a postclosure safety assessment for a licence submission. These are:

- Variable Climate Analysis. The effects of permafrost and glaciation are not explicitly determined in this assessment. Instead, these effects are discussed quantitatively based on the analyses by Avis and Calder (2015) and Chen et al. (2017). The important features of these glaciation studies are described and their applicability to the current study is discussed in Section 7.8.2.4.
- Additional Disruptive Event Scenarios. As described in Section 7.2.2, a reduced number of Disruptive Event Scenarios is evaluated here. However, the full list of Disruptive Event Scenarios anticipated for a licence submission is identified.
- Alternative Critical Groups. Other potential critical groups may be considered for a candidate site depending on communities nearby that could be interested in potential impacts - for example, downstream communities and / or First Nation lifestyles. This would be discussed with people in the area.

7.3 Conceptual Model

This section describes the conceptual model (and therefore the computer models) associated with key processes occurring in the repository. The presence of defective containers leads to releases of contaminants that eventually enter the biosphere. These biosphere releases have potential impacts on humans and on non-human biota living nearby.

Figure 7-2 illustrates the general conceptual model. There are four main elements:

- The used fuel containers;
- The engineered barrier system;
- The geosphere; and
- The biosphere.

Each of these elements is discussed below. The discussion is aligned for consistency with the Base Case of the Normal Evolution Scenario which, as noted in Section 7.2.1.2, assumes a constant temperate climate.

For simplicity, the descriptions of conceptual models are given in terms of radionuclides but the models are also applied to simulate the behaviour of potentially hazardous chemical elements, except that for chemical elements there is no radioactive decay and in the biosphere there is no food chain or dose rate calculations. Instead, protection of the environment is ascertained by comparison of calculated chemical element concentrations in various biosphere media to the criteria in Table 7-1.

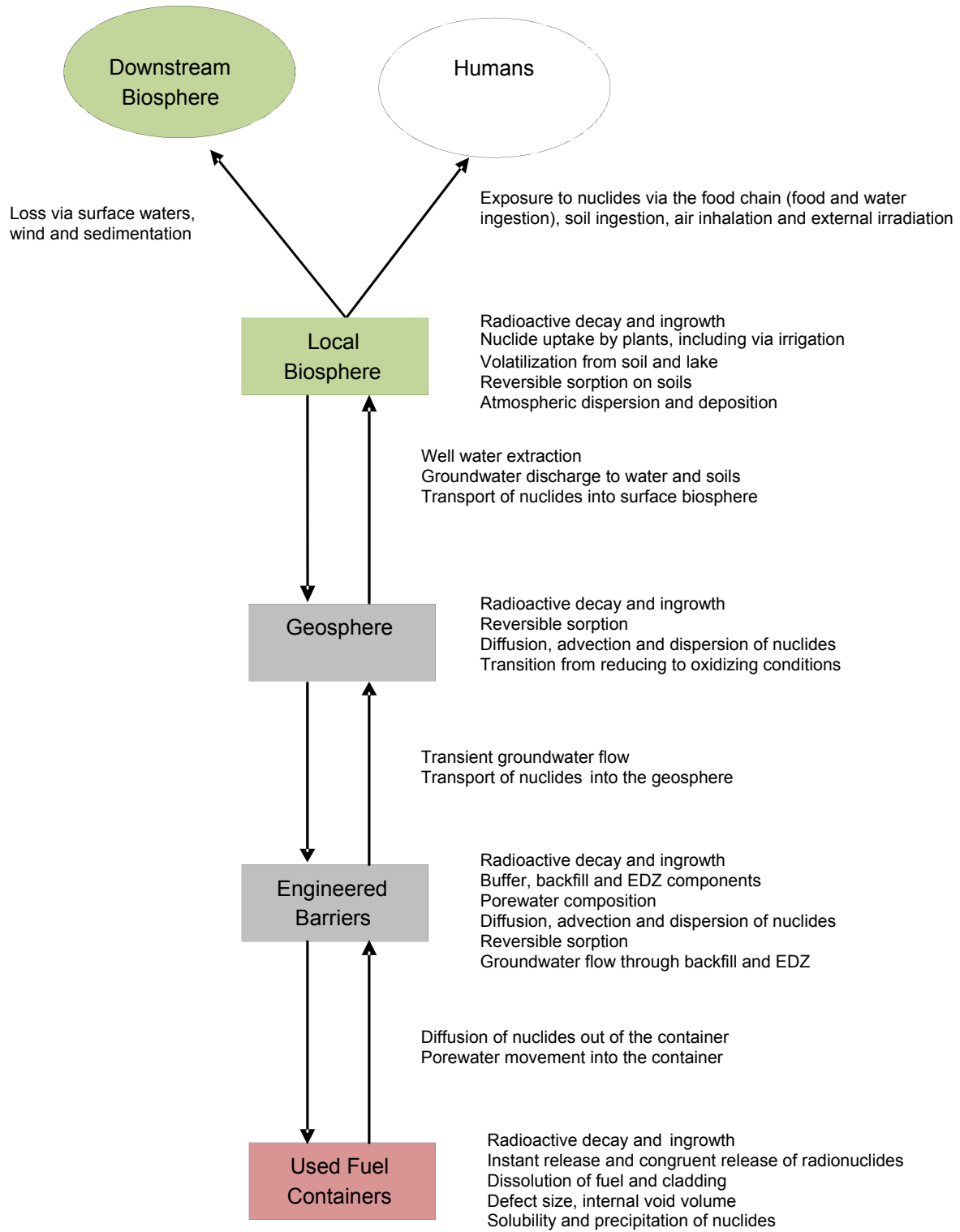


Figure 7-2: General Conceptual Model for Defective Containers

7.3.1 Used Fuel Containers

The principal fuel components and processes for the used fuel containers and waste form are shown in Figure 7-3.

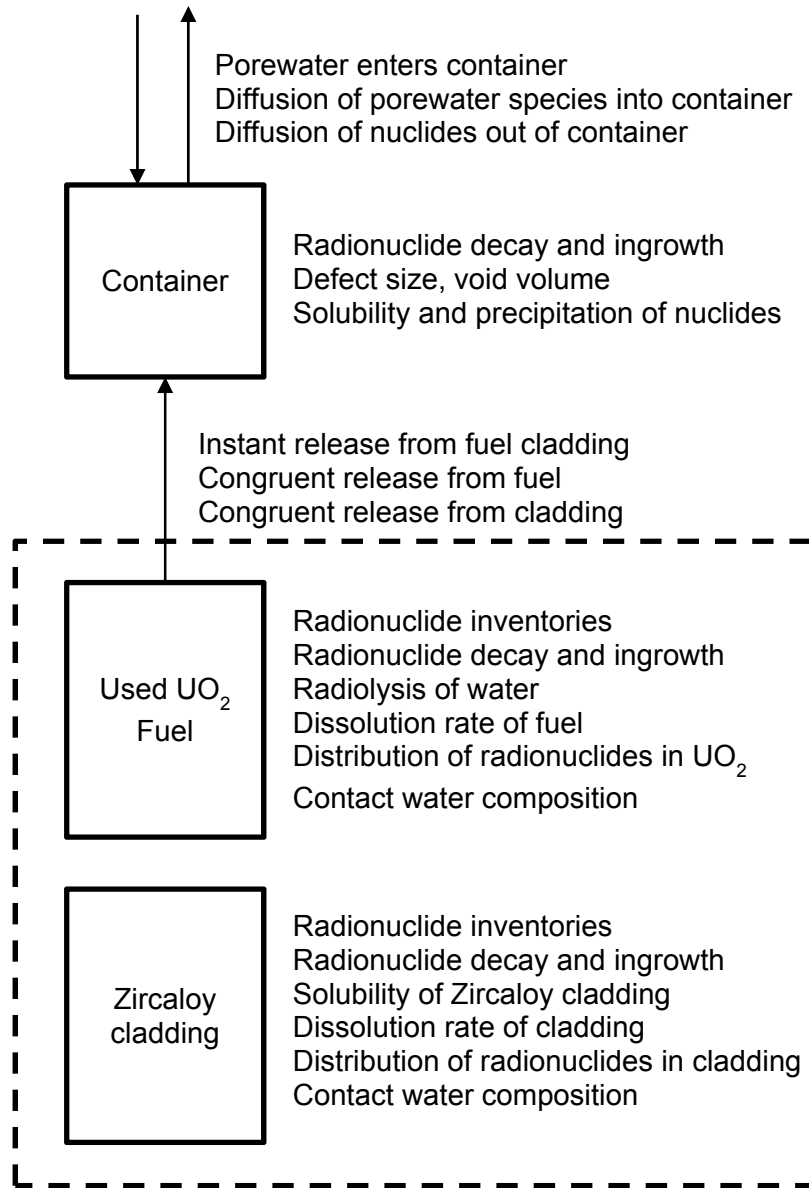


Figure 7-3: Conceptual Model for the Waste Form and Container

The container has a copper outer coating for corrosion protection and a steel inner vessel for structural support.

The inner steel vessel is not specifically included in the conceptual model, except that it is assumed to define the void volume inside the container. In practice, the steel components in any breached container would corrode, producing H_2 gas and iron oxides. The gas could delay

water ingress into the container, and also substantially reduce the dissolution rate of the UO_2 fuel; however, this effect is conservatively ignored. Similarly, formation of iron oxides would provide a high surface area for adsorption of some of the radionuclides released from the fuel, and these effects are also ignored.

For this conceptual repository and hypothetical geosphere, the temperature at the container surface reaches a peak value of about 93°C 47 years after container placement, decreases to about 81°C after 600 years, decreases slowly to 50°C after 10,000 years and reaches ambient conditions at around 200,000 years (Guo 2018). The temperature inside the container peaks at about 129°C within 47 years after placement and then decreases with time (Guo 2015). For a real site, with a different repository design and a different geosphere, the temperatures could be different, but the loading of the container and / or repository design would be adjusted such that container surface temperature would not exceed 100°C .

The reference waste form is a standard CANDU 37-element fuel bundle with a burnup of either 220 MWh/kgU (for scenarios involving a large number of bundles) or 280 MWh/kgU (for scenarios involving a small number of bundles) and an average fuel power during operation of 455 kW, as discussed in Chapter 3. The repository holds approximately 5.2 million bundles.

The waste form has two distinct components: the UO_2 fuel and the Zircaloy cladding. Releases of contaminants from these two waste forms are modelled separately.

After water enters the container, the Zircaloy cladding may prevent the water from contacting the fuel for some time. However, the cladding is neglected in the fuel dissolution model and it is assumed that water contacts all the fuel as soon as the container fills with water. The container is conservatively assumed to fill with water immediately after the container fails.

Contaminants within the UO_2 fuel are released by two mechanisms which operate on very different time scales (Grambow et al. 2010), as discussed below.

Instant Release from Fuel

Initially, there will be a comparatively rapid release of a small fraction (typically a few percent) of the inventory of a selected group of radionuclides that are either very soluble (such as C-14, Cl-35, Cs-137 and I-129) or gaseous, and that are residing in the fuel sheath gap or at grain boundaries which are easily and quickly accessed by water. This release process is referred to as "instant release" and is modelled assuming a certain fraction of the radionuclide inventory in the fuel is released at the same time that water contacts the fuel.

Ferry et al. (2008) have shown that the instant release fractions do not change with time due to, for example, athermal diffusion of radionuclides induced by alpha-particle recoil displacements.

The instant release fractions used in this assessment are given in Section 7.5.2.2.

Fuel Dissolution

The second and slower release process comprises release of radionuclides from the UO_2 fuel matrix as the matrix itself corrodes or dissolves (called "congruent dissolution").

The alpha dose rate at the fuel-water interface, which exceeds the gamma and beta dose rates for most of the fuel history (Figure 7-4), is the main contributor to radiolysis, producing molecular oxidants such as H₂O₂. Other potential sources of oxidants, such as any O₂ trapped in the porewater, will already have been consumed by corrosion processes (e.g., corrosion of the Cu shell) before the fuel cladding is breached because these corrosion reactions are relatively fast (see Chapter 5). In principle, the radiolytically produced oxidants will also be consumed by reaction with container materials rather than by reaction with used fuel, however, for alpha radiolysis, the oxidants (e.g., H₂O₂) are only produced within 20 μm of the fuel-water interface (Garisto 1989), so they are much closer to the fuel than to the container and thus more likely to react with the fuel.

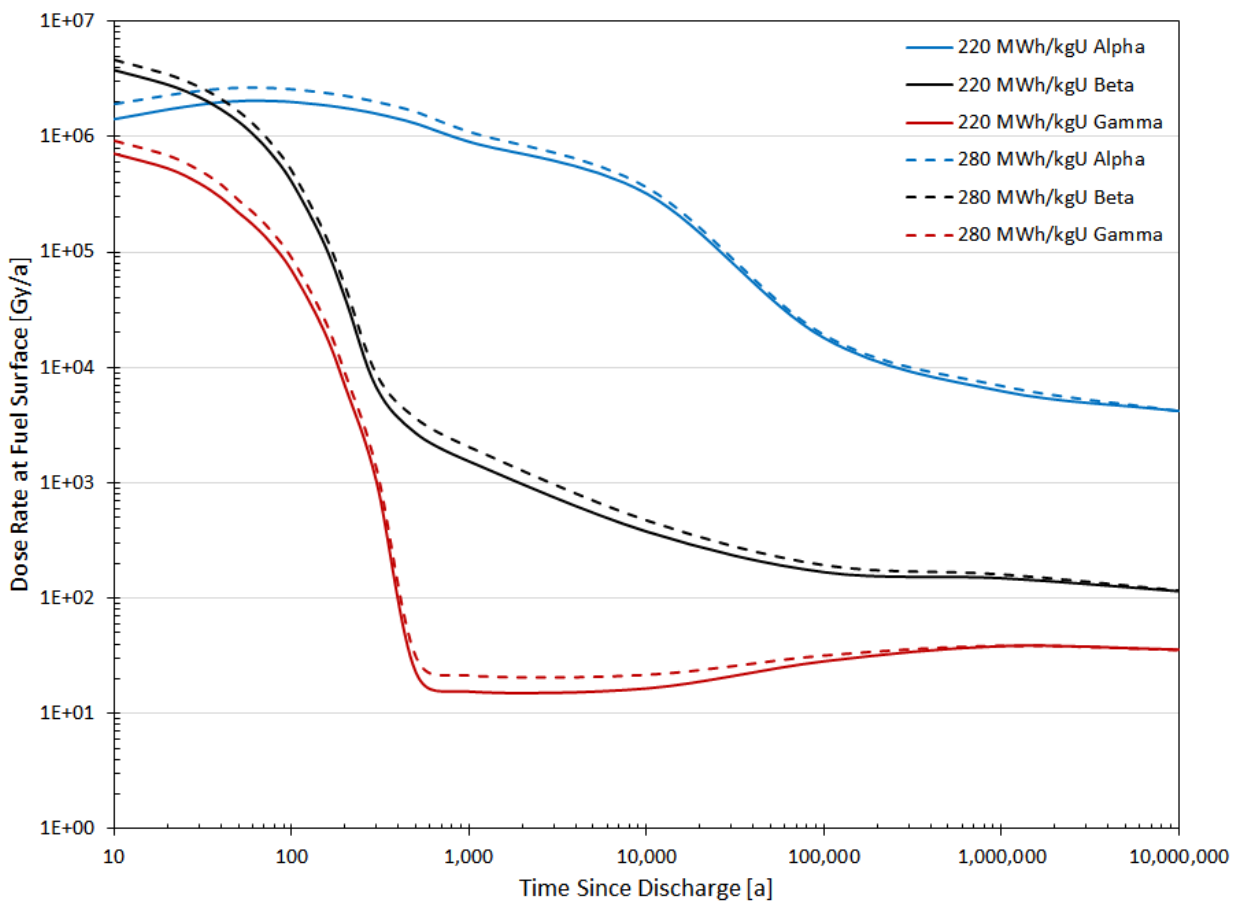


Figure 7-4: Radiation Dose Rate in Water at the Fuel Surface (220 MWh/kgU and 280 MWh/kgU Burnup)

Oxidative dissolution of the fuel continues as long as the alpha radiation field is sufficiently high. Eventually, after about 10 million years (Gobien et al. 2018), chemical dissolution of the fuel dominates according to the reaction:



This is a very slow process, as illustrated by the existence of uranium ore bodies that are millions or billions of years old.

The UO_2 dissolution rate would be affected by buildup of hydrogen gas inside the steel vessel generated by anaerobic corrosion of the steel. Experimental and theoretical evidence shows that the dissolution rate drops by several orders of magnitude in the presence of even modest pressures of hydrogen gas (Razdan and Shoemith 2015, Rollin et al. 2001, Carbol et al. 2005, Wu et al. 2014). This is likely due to the activation of hydrogen by various mechanisms to produce the strongly reducing H^\cdot radical, which in turn scavenges radiolytic oxidants and suppresses fuel corrosion (Liu et al. 2016). While this hydrogen effect will suppress fuel dissolution, it is conservatively ignored in the current assessment.

The fuel dissolution rate used in this assessment is shown in Section 7.5.2.2.

Radionuclide Releases from Zircaloy

The Zircaloy sheath surrounding the fuel pellets in a CANDU fuel bundle naturally forms a thin layer of protective ZrO_2 on its surface when in contact with air or water. This oxide layer greatly inhibits the Zircaloy dissolution rate in the postclosure period should water gain access to the used fuel container (Shoemith and Zagidulin 2010). Because the inventory of certain isotopes such as Cl-36 and C-14 within the fuel sheath is not insignificant relative to the amount present in the fuel, dissolution of the Zircaloy is modelled in the postclosure safety assessment. A kinetic dissolution model is used in which the zirconium dissolves at a rate proportional to the corrosion rate of Zircaloy in water and the surface area of the Zircaloy in contact with water. During corrosion, species trapped in the Zircaloy matrix are released congruently with Zircaloy dissolution.

Certain radionuclides (i.e., C-14), may be more concentrated in the zirconium oxide layer on the Zircaloy sheath. Radionuclides in the oxide layer may be released on a faster time scale than those trapped within the cladding. This is included in the Zircaloy release model by introducing an instant release fraction for Zircaloy radionuclides.

7.3.2 Engineered Barrier System

Chapter 4 provides a detailed description of the conceptual repository and engineered barriers assumed in this study.

A dense 100% bentonite layer surrounds the container. The purpose of this layer is to:

- Mechanically support the container;
- Prevent groundwater flow near the container;
- Prevent microbial activity that could cause corrosion of the copper shell; and
- Sorb and delay release of radionuclides from a breached container.

This buffer material has a sufficiently low hydraulic conductivity that transport through it is diffusion dominant (i.e., the advective velocity is negligible).

The excavation damaged zone (or EDZ) extends around the perimeter of excavated spaces and is modelled as a uniform porous medium with higher hydraulic conductivity than the surrounding

intact bedrock. Conceptually, the EDZ is divided into two zones, these being an Inner EDZ and Outer EDZ. The Inner EDZ exhibits more damage and has a higher conductivity than the Outer EDZ. Excavation damaged zones along placement rooms, which are narrower, may be less permeable than damage zones along the larger drifts and cross-cuts.

The design includes seals at the entrance of each placement room and seals spaced throughout the access tunnels. These seals are composed of concrete and clay bulkheads that interrupt the placement room and tunnel Inner EDZs. An additional smaller EDZ associated with excavation of the seals is also assigned the same hydraulic conductivity as the tunnel EDZ.

Groundwater contacting the container, and contacting the fuel in a breached container, must pass through the buffer. The composition of this contact water is strongly influenced by the buffer composition and in particular its minor mineral components, notably calcite and gypsum (Muurinen and Lehtikoinen 1999, Curti and Wersin 2002). In the long term, these minor mineral components would all dissolve and the contact water composition would resemble the geosphere porewater composition.

The time evolution in contact water composition is not explicitly taken into account; rather, two contact water compositions are defined. The first composition is geosphere porewater equilibrated with buffer minerals, and the second composition is geosphere porewater equilibrated with buffer minerals and the steel insert of the container. These compositions are used for the calculation of chemical element solubilities and the highest calculated solubility is used in the safety assessment calculations.

The maximum temperature at the interface between the engineered sealing materials and the host rock is about 85°C, occurring after 68 years, and about 93°C at the interface between the buffer and the container (Guo 2018). Temperature in the placement rooms would be about 50°C after 10,000 years, with ambient rock temperatures returning after 200,000 years. Given this, a temperature of 85°C is selected for the engineered barrier materials as a conservative reflection of the impact of the relatively brief thermal transient on mass transport. Use of a high temperature promotes increased diffusion.

7.3.3 Geosphere

Chapter 2 provides a description of the hypothetical geosphere assumed in this study.

The principal components of the conceptual model are shown in Figure 7-5.

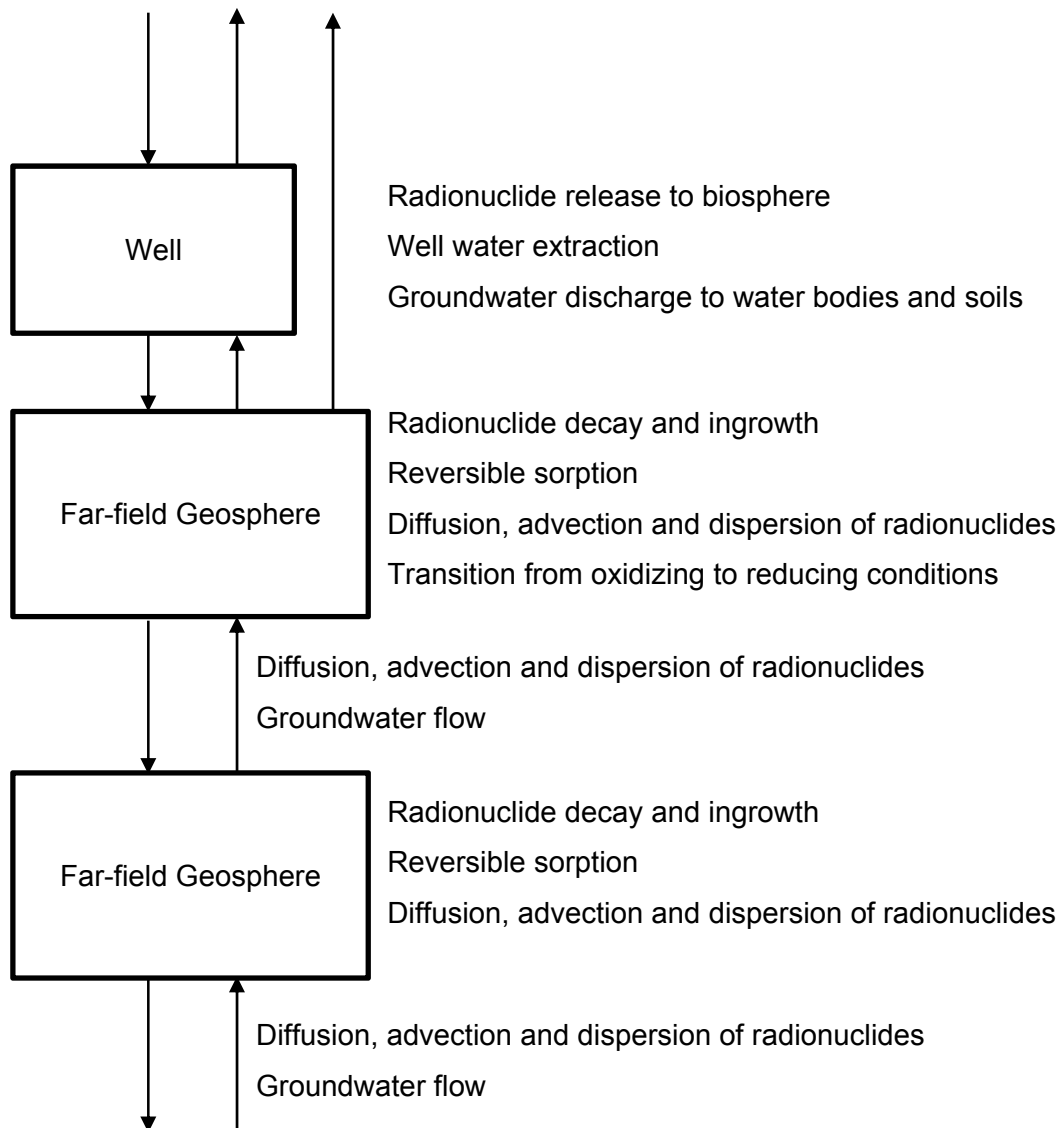


Figure 7-5: Conceptual Model for the Geosphere

The groundwater flow field is calculated assuming constant head boundary conditions at the surface, with the water table following the surface topography and no-flow boundary conditions at the boundaries of the watershed. This is reasonable for this hypothetical site where there is limited topographic relief and the water table is relatively close to the surface.

The hydrogeological model includes a 219 m deep well spanning the entire thickness of the Guelph formation, supplying water at the specified rate of 1261 m³/a (i.e., the rate required to meet the needs of the critical group). At this rate, the influence of the well on the overall groundwater flow field is small, although the flow field near the well is affected by well drawdown. Groundwater in the Guelph formation is slightly saline and less likely to be used, so assuming a deep well in this formation, rather than the shallower permeable formations, is therefore conservative with respect to contaminant uptake at the well.

In the near-field geosphere (i.e., around the repository), chemically reducing conditions prevail.

The ambient rock temperature at repository level is about 17°C. The temperature in the repository will initially be warmer than in the surrounding geosphere due to heat input from the used fuel bundles (caused by radioactive decay). The maximum temperature at the interface between the engineered sealing materials and the host rock is about 85°C, occurring after 68 years (Guo 2018). Temperature in the placement rooms would be about 49°C after 10,000 years, with rock temperatures after 10,000 years in the area within about 140 m and 230 m of the plane of the repository being above 25°C (and decreasing). In the vertical direction (i.e., towards the surface), at 10,000 years rock temperatures above 25°C could exist about 260 m above the repository plane, with ambient conditions returning after about 200,000 years. For the contaminant transport times estimated in this study, the bulk of the transport occurs under close to ambient conditions. Therefore 20°C values are adopted for geosphere transport parameters.

The physical properties of the rock are described in Chapter 2. The diffusion and sorption coefficients assumed for the rock at repository level are given in Section 7.5.2.6 and Section 7.5.2.7.

7.3.4 Biosphere

The main features of the biosphere model are illustrated in Figure 7-6. The model:

- Describes the movement of contaminants through soil, plants and animals, and the atmosphere in the surface environment near the repository;
- Calculates the concentrations of contaminants in water and air in the local habitat of the critical group; and
- Calculates radiological dose rates to an individual in the critical group due to ingestion and inhalation of radionuclides and by external exposure to radiation from radionuclides in the environment (air immersion, water immersion, building materials and groundshine).

Radionuclides are lost from the local biosphere by outflow with water, by radioactive decay, by atmospheric dispersion and by leaching into deep soil or sediments.

The local biosphere has the characteristics of a temperate climate region of Southern Ontario. As noted in Section 7.2.1.2, a constant temperate climate is assumed. While the properties of the biosphere could vary with time due to global warming in the near term, or due to other natural or human-induced changes, the assumption of a constant biosphere provides a convenient and clear measure of the potential impacts, which can be readily related to what is currently acceptable.

In the long term, it is assumed that glaciation will resume with consequent significant effects as a result of the glaciation itself and the related climate change. The anticipated effects of glaciation on the dose assessment for the Normal Evolution Scenario are discussed in Section 7.8.2.4.

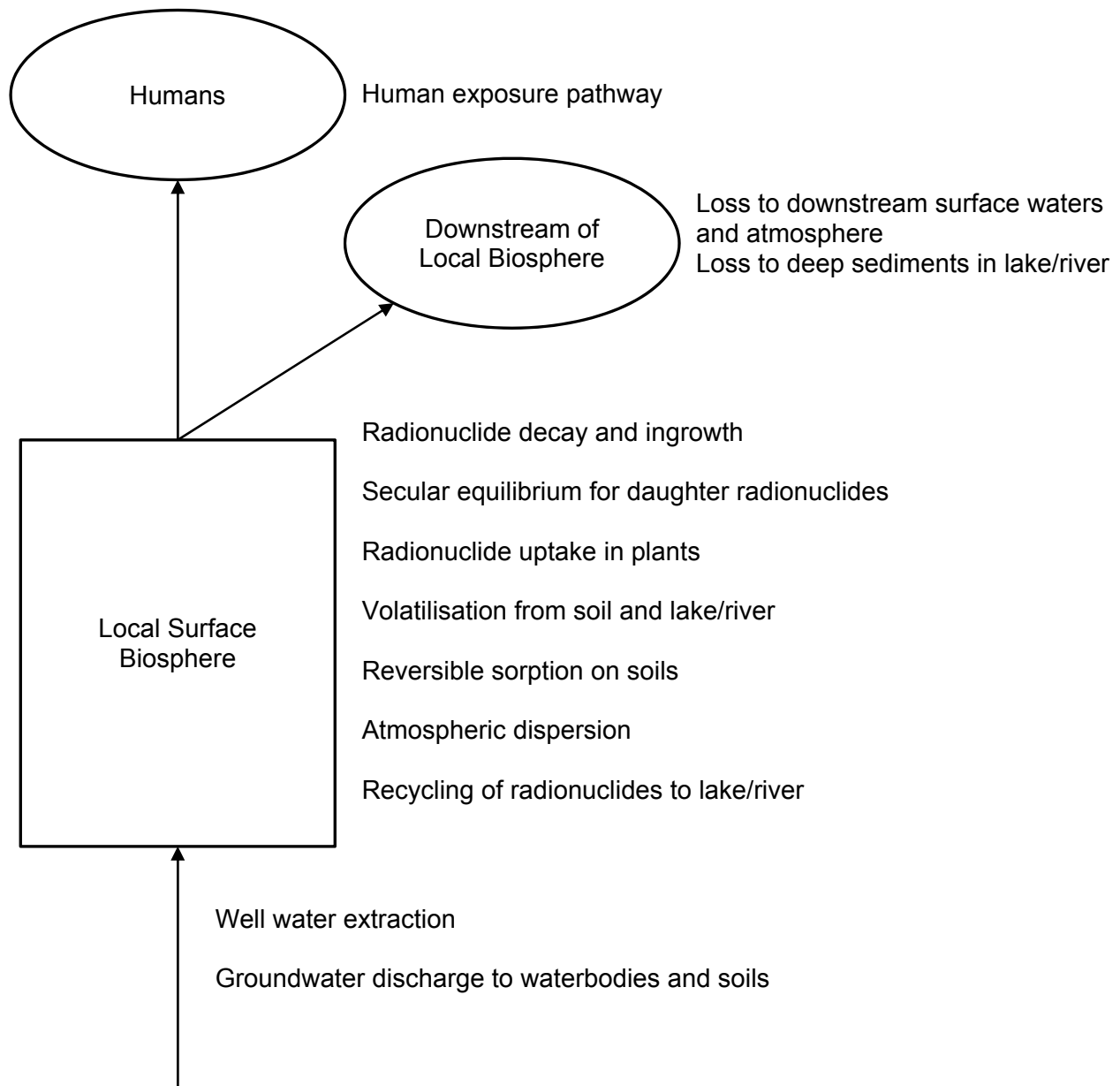


Figure 7-6: Conceptual Model for the Constant Biosphere

Following international practice, the site is assumed occupied by a group of people (i.e., the "critical group") that behaves in a plausible manner but with lifestyle characteristics that maximize their exposure to any radionuclides entering the biosphere. Members of the critical group are assumed to spend all their lives in the local biosphere and obtain all their food, water, fuel and building materials from the local vicinity.

The characteristics of the critical group will change with climate; however, since a constant temperate climate is assumed, a self-sufficient farming family is selected as the critical group. This group uses a well that intercepts any contaminant plume that might originate in the

repository, and grows its own crops and raises animals. Their food includes plants grown in a garden, domesticated animals and local fish. Their lifestyle is more self-sufficient than typical Canadian habits and, because this leads to higher exposure, it is therefore a useful basis for assessing potential repository impacts. Future safety assessments may consider additional lifestyles.

In this safety assessment, the groundwater well is conservatively placed in depth and location to intercept the radionuclide plume, such that the uptake of any radionuclides released from the repository is maximized. Any contaminants not captured by the well would diffuse or move with the groundwater flow until they naturally reach surface discharge locations, or would decay away before reaching the biosphere. The use of a well is conservative basis for maximizing dose as it results in exposing persons to higher concentration of contaminants than does surface discharge alone (i.e., surface discharge allows more time for decay and dispersion).

In the model, all radionuclide releases from the geosphere are assumed to enter the primary water body discharge point. In particular, radionuclides captured by the well or directly discharged into soils are not removed from the amount entering the water body. In effect, this assumes the holdup in these paths is relatively short, and the radionuclides eventually do transfer to the water body. This conservatively overestimates the amount of radionuclides in the biosphere, but simplifies the modelling because many processes that recycle radionuclides are accounted for implicitly, such as surface runoff into the water body.

The dose model uses the concentration of radionuclides in the various biosphere compartments (well, soil, plants, animals and air) to calculate the annual dose to a member of the critical group. The critical group is also exposed to sediments from the lake when these sediments are used for soil. In this case, the sediment exposure pathways are the same as those for the soil exposure pathways.

The internal exposure pathways considered are:

- Soil-to-man;
- Soil-to-plant-to-man;
- Soil-to-plant-to-animal-to-man;
- Soil-to-animal-to-man;

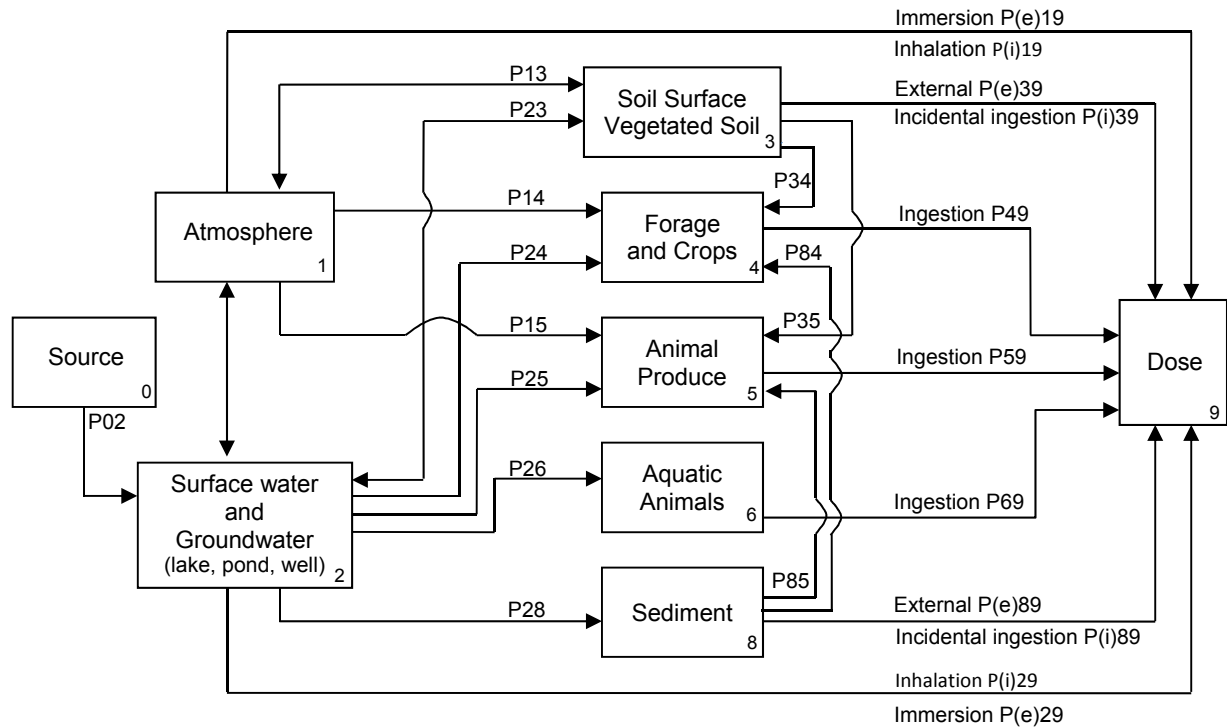
- Air-to-man;
- Air-to-plant-to-man;
- Air-to-plant-to-animal-to-man;
- Air-to-animal-to-man;

- Water-to-man;
- Water-to-plant-to-man;
- Water-to-animal (including fish)-to-man; and
- Water-to-plant-to-animal-to-man.

The external exposure pathways considered are:

- Air immersion;
- Water immersion (bathing or swimming if a suitable water body is nearby);
- Groundshine (exposure to radiation from contaminated soil); and
- Building materials (exposure to radiation from building materials).

These exposure pathways are similar to those considered in the guidelines used to calculate derived release limits for normal operation of a nuclear facility (CSA 2014) as shown in Figure 7-7.



Notes: From CSA (2014), where the P_{ij} represent transfer parameters from compartment i to compartment j . The building material exposure pathway is not shown here since it is not included in the CSA (2014) dose model.

Figure 7-7: Environmental Transfer Model Showing Critical Group Exposure Pathways

7.4 Computer Codes

The conceptual model for contaminant transport is numerically represented in a suite of computer codes used in postclosure safety assessment calculations.

Figure 7-8 identifies the codes used and their interrelationship. Information from used fuel characteristics, engineering design and site characterization is used to develop site-specific input parameters.

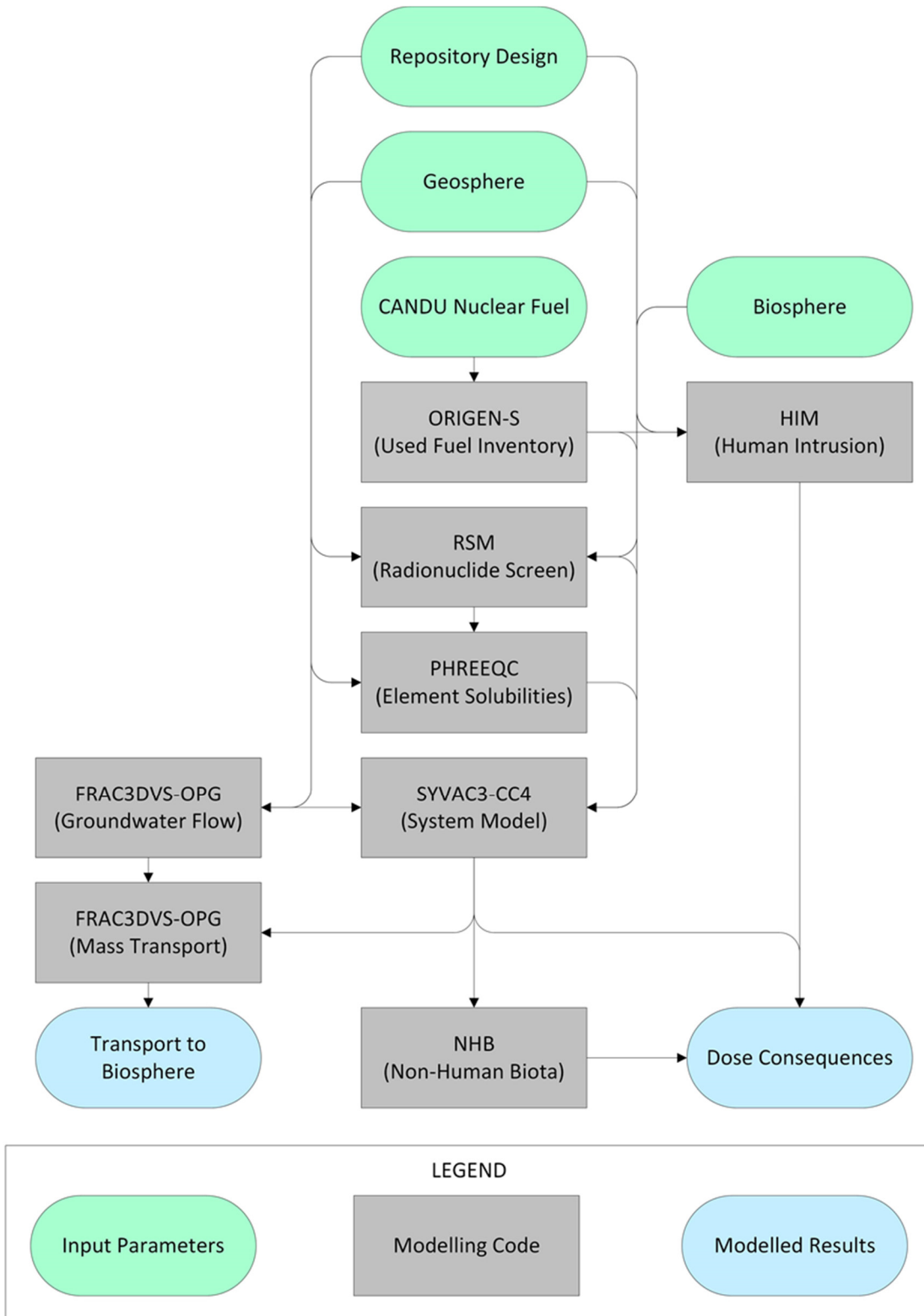


Figure 7-8: Main Computer Codes

ORIGEN-S is a CANDU-industry standard code used to calculate radionuclide inventories in the fuel and Zircaloy cladding at the time of placement, based on a defined reactor exposure scenario (Hermann and Westfall 1995, Tait et al. 1995).

ORIGEN-S was used to derive the used fuel inventories used in this study (see Chapter 3).

PHREEQC is a widely used and tested open source computer program developed by the United States Geological Survey (Parkhurst and Appelo 1999). PHREEQC is based on an ion-association aqueous model and is designed to perform a wide variety of aqueous geochemical calculations.

In this assessment, PHREEQC Version 2.17 has been used for solubility and speciation calculations. The ThermoChimie v.7.b thermodynamic dataset has been used, as described in Gobien et al. (2018).

RSM (Radionuclide Screening Model) is a project-specific simple model of groundwater transport of radionuclides from container to humans via a well. Through a conservative choice of input parameters, a large input set of radionuclides can be screened so as to objectively identify which should be considered further using more detailed models. RSM incorporates data for all radionuclides with half-lives longer than 0.1 years as well as radionuclides with half-lives longer than one day if they have a parent with a half-life longer than 0.1 years.

Table 7-8 provides more information on RSM.

SYVAC3-CC4 is the reference System Model for the assessment of radionuclide release, transport, decay, biosphere transfer and dose assessment. It has been developed for a deep geological repository concept based on used fuel placed in durable containers, surrounded by engineered barrier materials and located deep underground. The code can perform both deterministic and probabilistic calculations.

Table 7-9 provides more information on SYVAC3-CC4.

FRAC3DVS-OPG is the reference Groundwater Flow and Transport code. This is a commercially available 3D finite-element / finite-difference code (Therrien et al. 2010). FRAC3DVS-OPG supports both equivalent porous medium and dual porosity representations of the geologic media.

Table 7-10 provides more information on FRAC3DVS-OPG.

HIMv2.1 is a project-specific code that assesses the consequences of the Inadvertent Human Intrusion Scenario. The model considers a scenario in which a used fuel container is unknowingly intersected by a drilled borehole, resulting in used fuel being brought directly to surface. Dose consequences are estimated for the drill crew and for a resident subsequently using the contaminated area.

Table 7-11 provides more information on HIMv2.1.

NHBv1.0 is a project-specific code that uses as a basis the calculated environmental media concentrations as a function of time from the System Model to calculate dose rates to non-human biota.

Table 7-12 provides more information on NHBv1.0.

Table 7-8: RSM, Version 1.1

Parameter	Comments
Components:	
SYVAC3	Executive module, Version 3.10.1
RSM	System model, Version 1.1
Main	<i>RSM Version 1.1 - Theory</i> (Goodwin et al. 2001)
Documents	<i>RSM Version 1.1 Verification and Validation</i> (Garisto 2001)
Main Features	<ul style="list-style-type: none"> - Linear decay chains - Radionuclide release by instant release and by congruent dissolution - UO₂ dissolution calculated from user-supplied time-dependent data - Precipitation in container when user-supplied solubility limits exceeded - Durable containers, some fail with small defects - 1D buffer and backfill layer that surrounds the container and inhibits groundwater flow and radionuclide transport - Repository model based on one room containing failed container(s) - Linear sequence of 1D transport segments that connect the repository to a well. Transport segments are user-supplied; transport is solved considering diffusion, advection/dispersion and sorption - Dose impacts to a self-sufficient human household that uses well water, based on conservative model for drinking, immersion, inhalation and ground exposure. Effect of other ingestion pathways is included through a user-input multiplier - Ability to represent all input parameters with a probability density function (PDF) and to run Monte-Carlo type simulations - Time-independent material properties and biosphere characteristics - Database of all radionuclides with half-lives longer than 0.1 years as well as radionuclides with half-lives longer than one day if they have a parent with a half-life longer than 0.1 years

Table 7-9: SYVAC3-CC4, Version SCC4.09.3

Parameter	Comments
Components:	
SYVAC3	Executive module, Version 3.12.1
CC4	System model, Version 4.09.2
ML3	SYVAC3 math library, Version ML3.03
SLATEC	SLATEC Common Mathematical Library, Version 4.1
Main	<i>SYVAC3-CC4 Theory Manual (NWMO 2012)</i>
Documents	<i>SYVAC3-CC4 User Manual (Kitson et al. 2012)</i>
	<i>SYVAC3-CC4 Verification and Validation Summary (Garisto and Gobien 2013)</i>
Main Features	<ul style="list-style-type: none"> - Linear decay chains - Radionuclide release by instant release and by congruent dissolution - UO₂ dissolution rate calculated using radiation dose-rate based model - Precipitation in container when user-supplied solubility limits exceeded - Durable container, but some fail due to small defects - Cylindrical buffer and backfill layer that surrounds the container and inhibits groundwater flow and radionuclide transport - Multiple sector repository connected to the geosphere at sector-specific nodes chosen considering the local groundwater flow - Geosphere network of 1D transport segments that connect the repository to various surface discharge locations, including a well - Transport considers diffusion, advection / dispersion and sorption - Biosphere model that calculates field soil concentrations, well water concentrations, and uses a surface water body as a final collection point - Dose impacts to a self-sufficient human household that uses water body or well water, locally grown crops and food animals, local building materials and heating fuel - Dose impacts to generic non-human biota - Flow-based models in repository and geosphere, concentration-based models in biosphere - Generally time-independent material properties and characteristics for the biosphere and geosphere model. Transitions from one geosphere (or biosphere) state to another at specific times can be accommodated - Ability to represent all input parameters with a probability density function and to run Monte-Carlo type simulations

Table 7-10: FRAC3DVS-OPG, Version 1.3

Parameter	Comments
Components:	
FRAC3DVS-OPG	Main code, Version 1.3
Main Documents	<i>A Three-dimensional Numerical Model Describing Subsurface Flow and Solute Transport</i> (Therrien et al. 2010)
Main Features	<ul style="list-style-type: none"> - Linear decay chains - 3 D groundwater flow and solute transport in saturated and unsaturated media - Variable density (salinity) fluid - 1D hydromechanical coupling - Equivalent porous medium or dual-continuum model; fractures may be represented as discrete 2D elements - Finite-element and finite-difference numerical solutions - Mixed element types suitable for simulating flow and transport in fractures (2D rectangular or triangular elements) and pumping / injection wells, streams or tile drains (1D line elements) - External flow boundary conditions can include specified rainfall, hydraulic head and flux, infiltration and evapotranspiration, drains, wells, streams and seepage faces - External transport boundary conditions can include specified concentration and mass flux and the dissolution of immiscible substances - Options for adaptive time-stepping and sub-gridding

Table 7-11: HIMv2.1

Parameter	Comments
Components:	
AMBER	Executive Code, Version 5.5
HIMv2.1	Main Model Version
Main Documents	<i>Human Intrusion Model for the Mark II Container in Crystalline and Sedimentary Rock Environments: HIMv2.1 (Medri 2015a)</i>
Main Features	<ul style="list-style-type: none"> - Linear decay chains - Dose consequences by external, inhalation and ingestion pathways to drill crew and site resident - Surface contamination decreases with time due to radioactive decay and soil leaching - Constant material properties and biosphere characteristics - Includes data for potentially relevant radionuclides

Table 7-12: NHBv1.0

Parameter	Comments
Components:	
AMBER	Executive Code, Version 5.7.1
NHBv1.0	Main Model Version
Main Documents	<i>Non-Human Biota Dose Assessment Equations and Data (Medri and Bird 2015)</i>
Main Features	<ul style="list-style-type: none"> - Calculates dose rates to non-human biota from input environmental media concentrations as a function of time - Uses both transfer factor and concentration ratio approach - Media considered are: surface water, groundwater, soil, sediment and air - Considers non-human biota appropriate to the Southern Canadian Deciduous Forest, the Boreal Forest and the Inland Tundra ecosystems. - Constant material properties and biosphere characteristics - Includes data for potentially relevant radionuclides

7.5 Overall Analysis Approach and Selected Data for Groundwater Flow and Radionuclide Transport

This section describes the overall analysis approach and the manner in which the 3D Groundwater Flow and Transport Models and the System Model are used.

Data for selected parameters are also given to provide context. Additional data are available in Gobien et al. (2018).

7.5.1 Overall Approach

The general approach for conducting the postclosure safety assessment is as follows:

1. Perform Radionuclide and Chemical Hazard Screening

Used nuclear fuel initially contains hundreds of radionuclides and chemically hazardous stable elements; however, most are short lived and / or present in very small amounts. Following placement in a deep geological repository, only a small subset poses a potential risk to humans and the environment. The RSM code is used to identify this subset for more detailed assessment.

The methods used for performing the screening analysis are described in Section 7.6.

2. Perform 3D Groundwater Flow and Radionuclide Transport Modelling

Detailed 3D hydrogeological modelling is performed with the FRAC3DVS-OPG code to determine the groundwater flow field from the vicinity of the repository to surface water discharge locations.

Once the flow field is modelled, detailed 3D diffusive and advective / dispersive radionuclide transport calculations are performed for I-129, Cl-36, Cs-135, and U-238. These long-lived radionuclides are typically the most important in terms of potential radiological impact and also represent a range of low-sorption to high-sorption species. Radionuclide releases from the defective containers are obtained from the System Model (implemented in the SYVAC3-CC4 code) and input as a source term to the 3D transport calculation.

Dose consequences cannot be determined in this step because the FRAC3DVS-OPG code does not have biosphere and dose models.

Due to the large size of the modelled environment, different scales of nested models are used. These are:

- Subregional Flow Model – a reduced scale version of the regional model described in Chapter 2, this model includes the geosphere within a 40 km by 40 km area centred on the repository. This is sufficiently large that boundary effects at the model extremities will not affect the flow field near the repository. The model is oriented coincident with the repository, along the assumed directions of minimum and maximum horizontal stress. Vertically, the model extends from ground surface down to the top of the Pre-Cambrian basement rock, the depth of which varies over the domain from a minimum of 550 mBGS to a maximum of 880 mBGS.

Repository features are not incorporated at this scale of resolution, although the discretization is refined over the repository footprint to ensure accurate head representation in this area.

This model is used primarily to describe the larger scale flow field and to determine the external head boundary conditions that are applied in the Main and Detailed Transport Models.

- Main Transport Model – the model domain includes the repository and a section of the surrounding geosphere large enough to capture all transport from the repository to surface discharge. The model includes all rooms, main tunnels, and shafts with a simplified representation of the room and tunnel EDZ. The central services area is also simplified with all tunnel intersections set at right angles, coincident with the finite difference discretization. Individual containers are not represented.

This model is used for assessments determining the well and source locations, and for most radionuclide transport simulations. In comparison to the Detailed Model described below, this model takes considerably less time to run.

- Detailed Transport Model – the model domain is reduced compared to the Main Transport Model and does not include all potential surface discharge zones. The model includes all rooms, main and cross tunnels, and shafts with a full representation of the EDZ on source zone placement rooms, all tunnels and the shafts. The central services area is simplified as for the Main Transport Model.

This model is used to confirm that Main Transport Model results are not significantly affected by discretization simplifications. It is also used to supply head boundary conditions to the Container Transport Model.

- Container Transport Model - the model domain consists of a small section of the repository surrounding the defective containers together with the adjacent geosphere. The model incorporates a high level of detail and individual containers are represented at the source location.

The model is used to calculate radionuclide transport from defective containers into the surrounding rock. The output is used as source term input to the Main and Detailed Transport Models. Simulations are also performed to corroborate results of the Main and Detailed Transport Models and to provide a more complete understanding of repository component functions.

The groundwater flow field obtained using the Main Transport Model is also used to guide subsequent development of the SYVAC3-CC4 System Model. Radionuclide transport calculations performed for I-129, CI-36 and Cs-135 are used for comparison purposes to verify the System Model. U-238 is not included in this comparison because there is very little movement of U-238 within the repository and surrounding rock. All 3D radionuclide transport simulations are performed for a 10 million year simulation time frame, with selected cases extended beyond this time to illustrate peak transport values.

Figure 7-9 shows the spatial relationships for the different models.

The methods and results used in this phase of the assessment are described in Section 7.7.

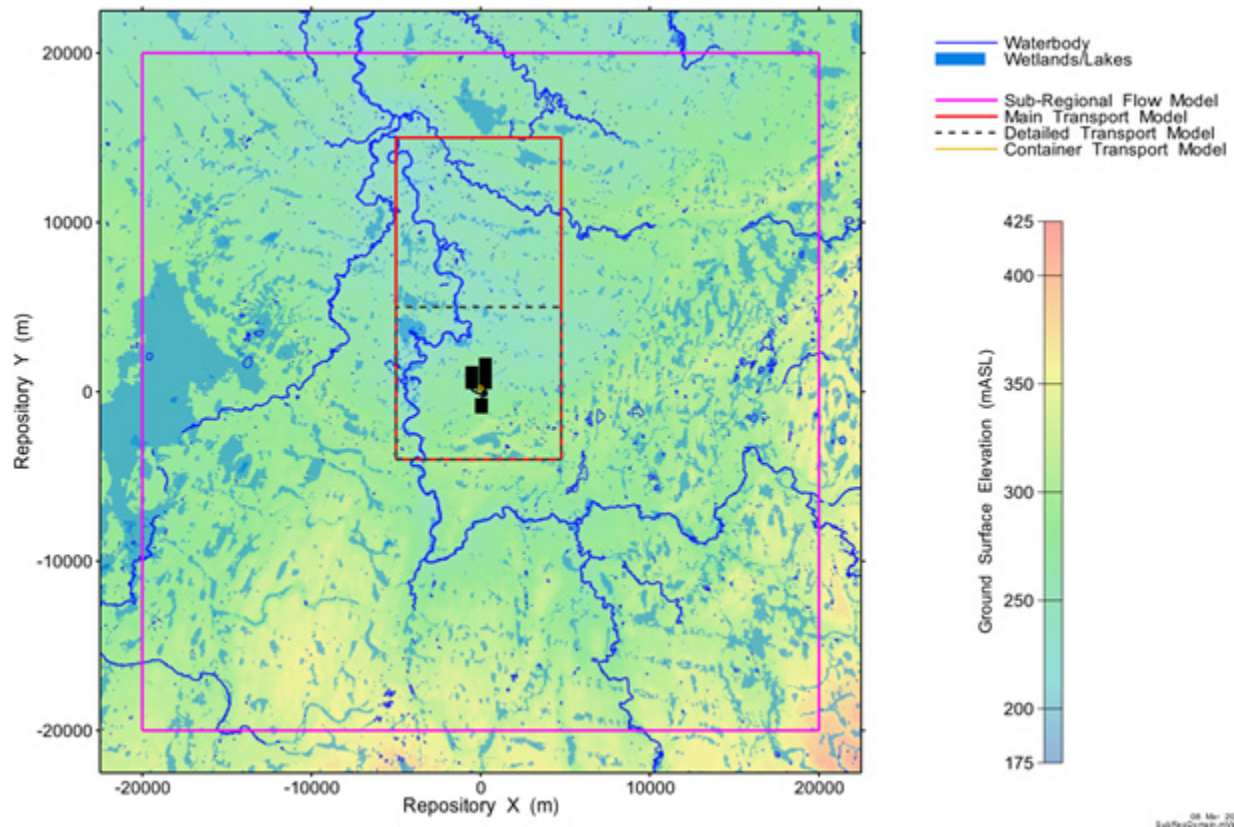


Figure 7-9: 3D Subregional Flow, Main Transport, Detailed Transport and Container Transport Model Domains

3. Perform System Modelling

The System Model includes representations for all aspects of the repository – used fuel, container, engineered barrier materials, geosphere, and biosphere. It is implemented in the SYVAC3-CC4 code.

The 3D groundwater advective flow field generated with FRAC3DVS-OPG is normally used to guide development of the geosphere submodel of the System Model. However, due to the very low hydraulic conductivity of the Southern Ontario host rock, much of the transport is by diffusion and therefore there is little reliance on the advective flow field when creating the submodel.

The geosphere submodel is verified by comparing radionuclide transport results with similar results from the 3D model. These comparisons are performed for I-129, Cl-36 and Cs-135, as

these represent the key radionuclides for groundwater transport, as well as providing comparison data for species that cover a wide range of sorption data.

Other aspects of the System Model - used fuel, container, near-field and biosphere are defined by the case and by input data.

The System Model includes the full suite of contaminants of interest (as identified from the radionuclide and chemical element screening assessment described in Step 1 above).

The System Model is also used for the probabilistic safety assessment, assuming a fixed geosphere. The radionuclide inventory, release and transport properties are varied about the Base Case values, as are the characteristics of the biosphere and dose receptor.

The methods used in this phase of the assessment are described in Section 7.8.

7.5.2 Data for Selected Parameters

This section presents data for a variety of parameters important to the postclosure safety assessment. A full description of the input parameters is available in Gobien et al. (2018).

7.5.2.1 Initial Inventory

The reference waste form is a standard CANDU 37-element fuel bundle with a discharge burnup of either 220 MWh/kgU (for scenarios involving releases from a large number of bundles) or 280 MWh/kgU (for scenarios involving releases from a small number of bundles), and an average fuel power during operation of 455 kW. Chapter 3 identifies the inventories for the radionuclides of interest, and provides additional information regarding the two discharge burnup values.

7.5.2.2 Instant Release Fractions and Fuel Dissolution Rate

Fuel

Section 7.3.1 describes that radionuclides within the UO₂ fuel are released by two distinct mechanisms which operate on very different time scales. These mechanisms are referred to as “instant release” and “congruent release”.

Table 7-13 shows the instant release fractions used in this study.

Table 7-13: Fuel Instant Release Fractions

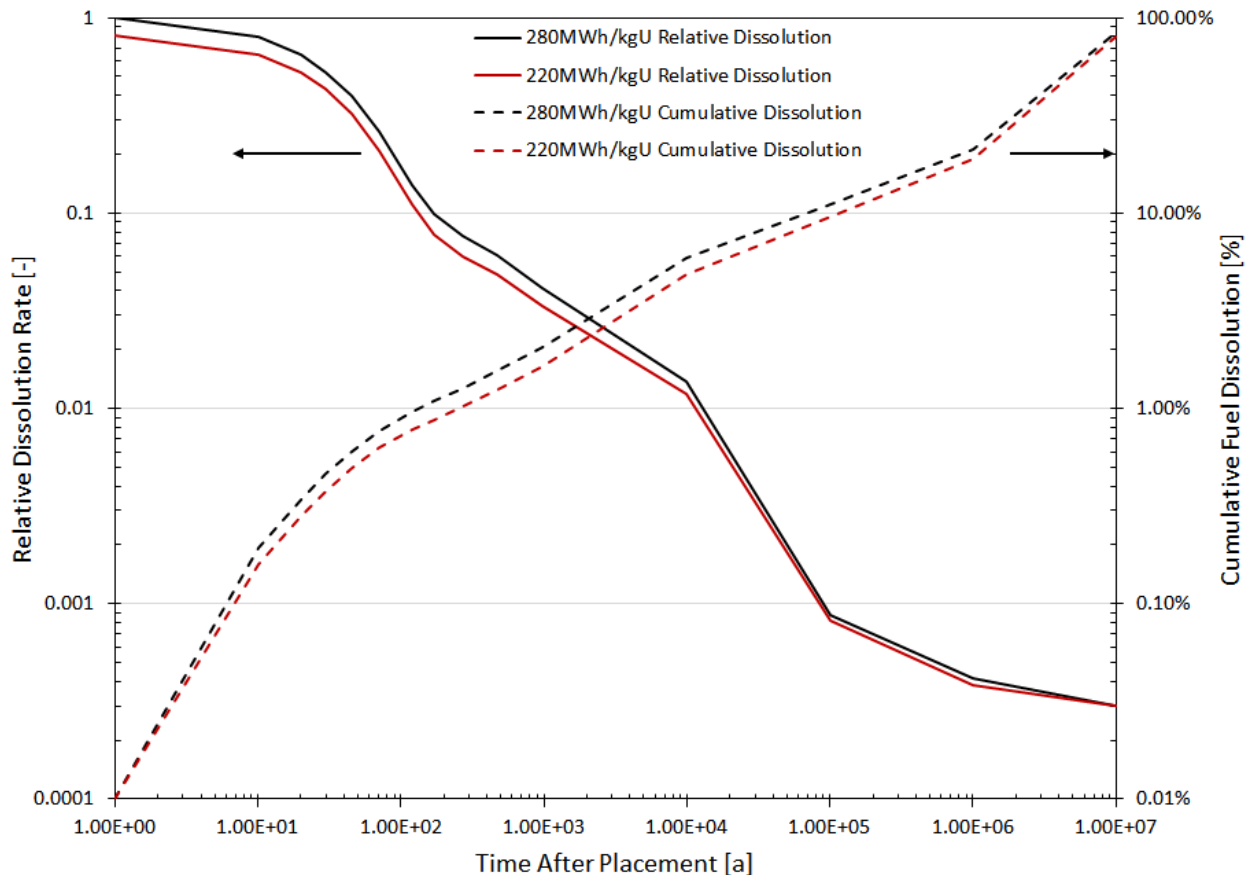
Element	PDF Type	PDF Attributes ⁽¹⁾	Lower Limit	Upper Limit
Ac	constant	0	-	-
Ag	uniform	-	0	0.001
Am	constant	0	-	-
Bi	normal	(0.006, 0.0015)	0.0023	0.03
C	normal	(0.027, 0.016)	0.0005	0.075
Cl	normal	(0.06, 0.01)	0.01	0.2
Cs	normal	(0.04, 0.01)	0.015	0.20
Hg	normal	(0.04, 0.01)	0.015	0.20
I	normal	(0.04, 0.01)	0.015	0.20
Mo	lognormal	(0.01, 2)	0.0005	0.05
Nd	constant	0	-	-
Np	constant	0	-	-
Pa	constant	0	-	-
Pb	normal	(0.006, 0.0015)	0.0023	0.03
Pd	lognormal	(0.01, 2)	0.0005	0.05
Po	normal	(0.04, 0.01)	0.015	0.20
Pu	constant	0	-	-
Ra	normal	(0.025, 0.008)	0.001	0.05
Rh	lognormal	(0.01, 2)	0.0005	0.05
Rn	normal	(0.04, 0.01)	0.015	0.20
Ru	lognormal	(0.01, 2)	0.0005	0.05
Se	normal	(0.006, 0.0015)	0.0023	0.03
Sm	constant	0	-	-
Tc	lognormal	(0.01, 2)	0.0005	0.05
Th	constant	0	-	-
U	constant	0	-	-

Notes: (1) PDF attributes are (mean, standard deviation) for the Normal PDF, and (geometric mean, geometric standard deviation) for the Lognormal PDF.

From Gobien et al. (2018)

A radiolysis-based UO_2 corrosion model is used based on alpha, beta and gamma dose rates near the fuel.

Figure 7-10 presents the calculated fractional and cumulative information for dissolution of the fuel. Information for both the 220 MWh/kgU and the 280 MWh/kgU burnup values is shown.



Notes: Relative Dissolution Rate is the ratio of the time-dependent fuel dissolution rate to the maximum fuel dissolution rate. The maximum dissolution rates are 3.12×10^{-3} [mol/m²/a] for 220 MWh/kgU burnup and 3.84×10^{-3} (mol/m²/a) for 280 MWh/kgU burnup, where the area is the surface area of the fuel in contact with water. A contact area of 209 m² per container is used in this study which assumes the fuel is highly fragmented and the container is full of water.

Figure 7-10: Fuel Dissolution Rate

Zircaloy

Since the Zircaloy cladding is thin, the composition and the activation products in the irradiated Zircaloy are expected to be uniformly distributed. There may be a small amount of surface deposits from coolant.

Leaching experiments indicate that the C-14 within the oxide film on the Zircaloy is released relatively rapidly compared to the C-14 within the metal itself (Gras 2014, Yamaguchi et al.

1999, Smith and Baldwin 1993). Consequently, the fraction of the C-14 within the oxide layer is assumed to be instantly released after water enters the container and contacts the Zircaloy.

Table 7-14 shows the Zircaloy instant release fractions used in this study.

Table 7-14: Zircaloy Instant Release Fractions

Element	PDF Type	Value
C	Constant	0.021
Other Elements	Constant	0

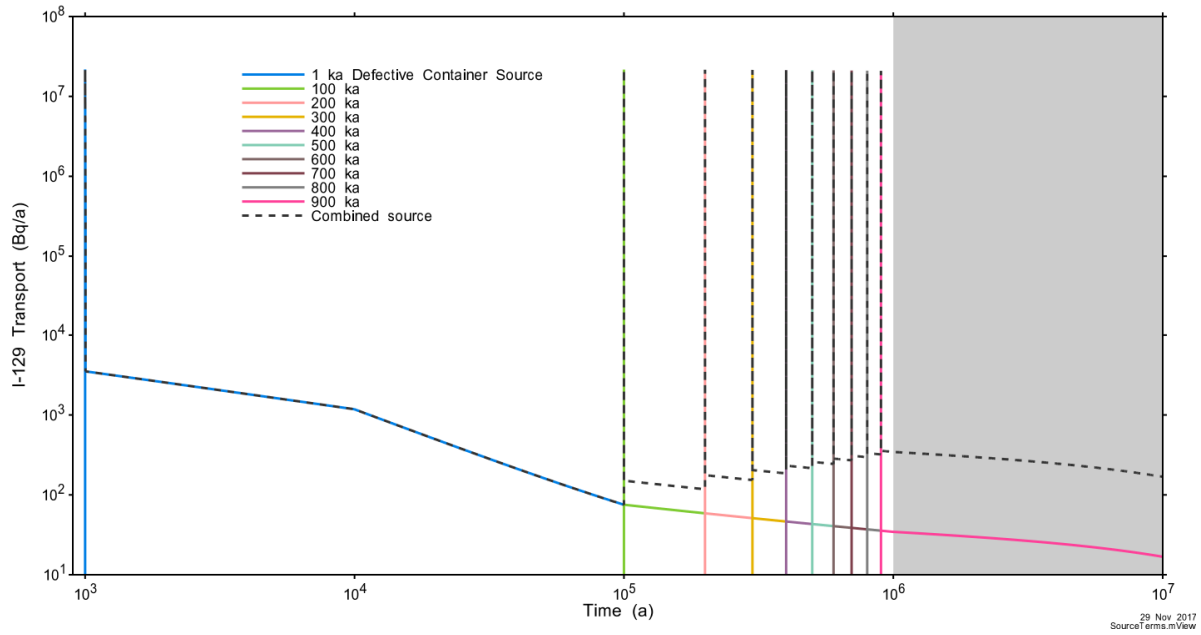
A kinetic dissolution model is used in which the Zircaloy dissolves based on its corrosion rate in water and its surface area. During this corrosion, species within the Zircaloy matrix are released proportional to the zirconium dissolution.

7.5.2.3 Radionuclide Source Terms

Figure 7-11 illustrates the Base Case source term for I-129, where this represents the source at the interface between the container and the surrounding buffer material. As noted in Table 7-3, this is calculated assuming the container volume is still present but the container walls are not (i.e., the container itself is not a barrier to release from container).

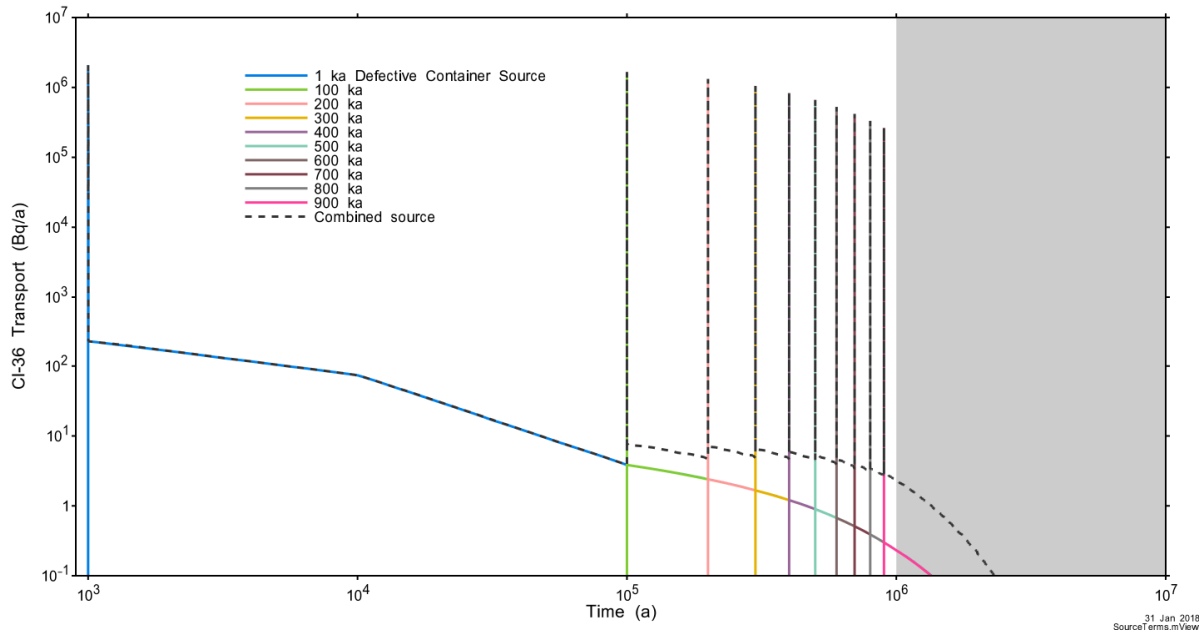
The coloured lines are the individual container source terms, while the dashed line is the combined total. The 10 spikes are due to the instant release term from each the 10 containers assumed to fail in the Base Case.

Three-dimensional transport calculations are also performed for Cl-36, Cs-135 and U-238. Combined and individual container source terms for these radionuclides are shown in Figure 7-12 through Figure 7-14.



29 Nov 2017
SourceTerms.mView

Figure 7-11: I-129 Source Term



31 Jan 2018
SourceTerms.mView

Figure 7-12: Cl-36 Source Term

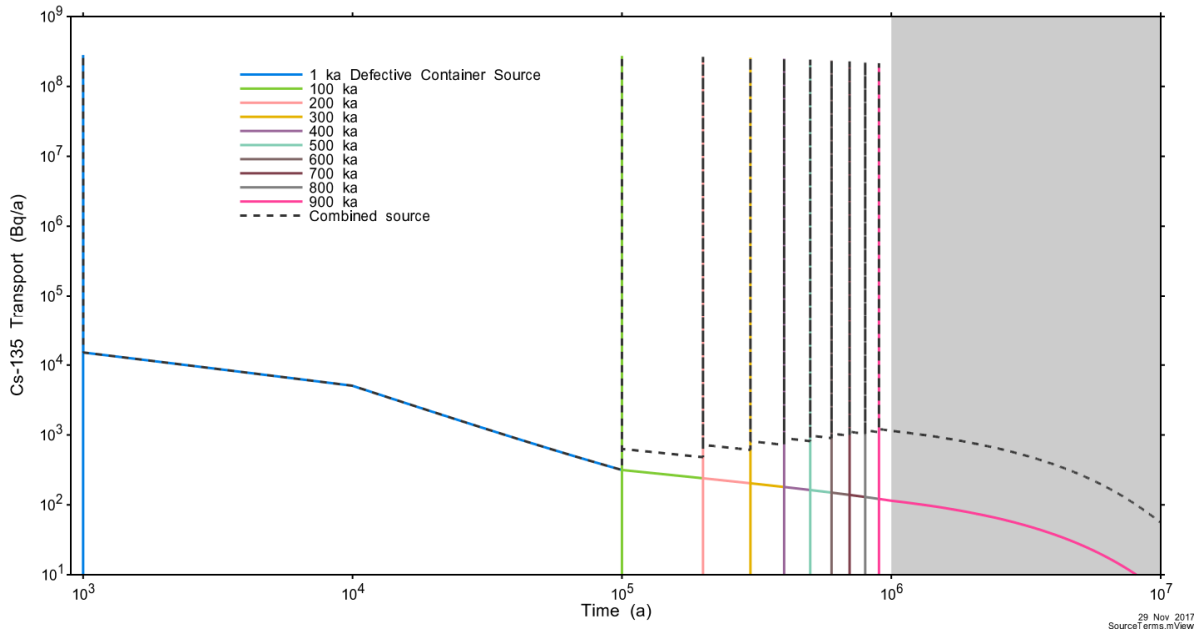


Figure 7-13: Cs-135 Source Term

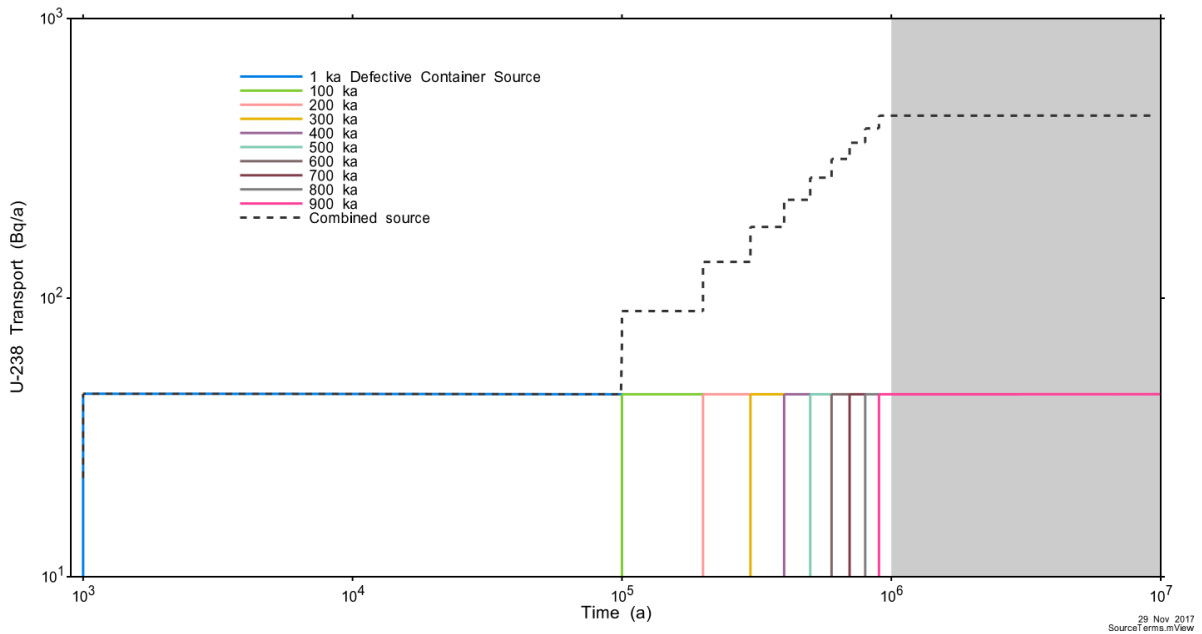


Figure 7-14: U-238 Source Term

Figure 7-15 shows the individual container I-129 source term used for the All Containers Fail Disruptive Event Scenarios.

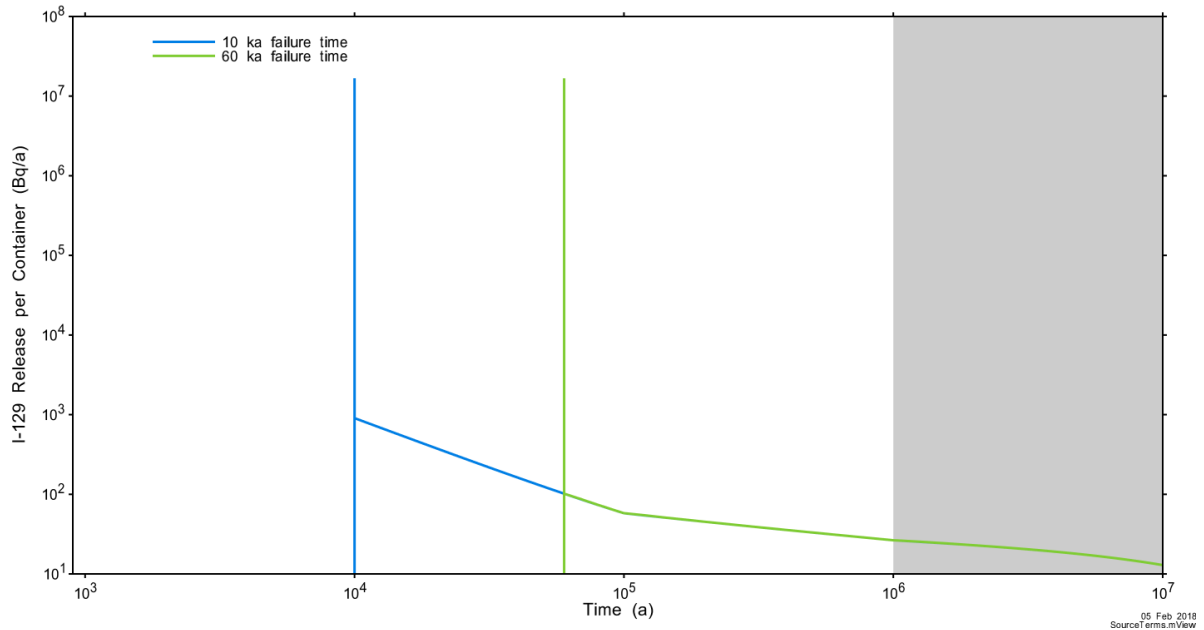


Figure 7-15: I-129 Individual Container Source Term for the All Containers Fail Disruptive Event Scenarios

7.5.2.4 Reference Groundwater Composition

The groundwater around the repository is highly saline (see Chapter 2). Table 7-15 shows the reference groundwater composition at repository depth. There are two compositions, one with rock porewater equilibrated with the host rock, and one with rock porewater equilibrated with the buffer and steel, representing the water that could be seen by the container and used fuel.

Table 7-15: Reference Groundwater Composition at Repository Depth

Composition	Rock Porewater Equilibrated with Host Rock	Rock Porewater Equilibrated with Buffer and Steel
pH	6.3	8.7
Environment	Reducing	Reducing
Eh (mV)	-200	-535
Ionic Strength (mol/kgw)	5.78	5.88
Density	1.192	1.192
Element	Solutes (mg/L)	
Na	50,025	48,673
K	12,486	3,482
Ca	32,494	37,285
Mg	8,173	9,940
HCO ₃	135	3
SO ₄	1,784	1,813
Cl	168,058	168,744
Br	1,698	1,703
Sr	1,198	1,200
Li	5	5
F	1	1
I	3	3
B	80	80
Si	4	10
Fe	30	579
NO ₃	10	10
PO ₄	-	-
Total Dissolved Solids	276,184	273,531

Note: From Gobien et al. (2018)

7.5.2.5 Element Solubilities

Element solubilities for all contaminants emerging from the screening assessment (Section 7.6) are shown in Table 7-16. These have been calculated at 25°C for the two groundwater compositions shown above, with the higher of the resulting values selected. To account for the higher temperatures in the near field and for uncertainties in the conditions near the container (e.g., pH, salinity, minor species), the solubility values shown in Table 7-16 are 10 times higher than the calculated solubilities.

Any elements not listed are assigned a high solubility value of 2.0 mol/kg to ensure they are treated as a fully soluble species.

Table 7-16: Element Solubilities

Element	Value (mol/kg)	GSD	Distribution Type
Ac	2.0	-	Constant
Ag	2.0	-	Constant
Am	2.0	-	Constant
Bi	2.0	-	Constant
C	2.2×10^{-2}	3.2	Lognormal
Cl	2.0	-	Constant
Cs	2.0	-	Constant
Hg	2.0	-	Constant
I	2.0	-	Constant
Mo	2.3×10^{-12}	3.2	Lognormal
Nd	2.0	-	Constant
Np	1.7×10^{-8}	3.2	Lognormal
Pa	3.2×10^{-7}	10	Lognormal
Pb	2.0	-	Constant
Pd	2.0	-	Constant
Po	2.0	-	Constant
Pu	2.0	-	Constant
Ra	1.7×10^{-4}	3.2	Lognormal
Rh	2.0	-	Constant
Rn	2.0	-	Constant
Ru	2.0	-	Constant
Se	3.4×10^{-8}	3.2	Lognormal
Sm	2.0	-	Constant
Tc	4.4×10^{-8}	3.2	Lognormal
Th	1.4×10^{-6}	3.2	Lognormal
U	4.5×10^{-8}	3.2	Lognormal

Note: From Gobien et al. (2018)

GSD = Geometric Standard Deviation

The values shown are 10 times higher than those in the original references

7.5.2.6 Effective Diffusion Coefficients

Effective diffusion coefficients for all EBS materials and geological units are shown in Table 7-17 and Table 7-18. The EBS materials are homogenous and isotropic, while sedimentary rocks have differences in vertical and horizontal directions.

Table 7-17: Effective Diffusion Coefficients, Base Case Values

Formation	D_e Anions / Neutral Species (m^2/a)	D_e Cationic Species (m^2/a)
High Compacted Bentonite (100% bentonite)	4.4×10^{-3}	1.3×10^{-2}
Gap Fill (100% Bentonite)	4.4×10^{-3}	1.3×10^{-2}
70% Bentonite (70:30 bentonite:silica sand)	9.46×10^{-3}	9.46×10^{-3}
Dense Backfill (5:25:70 bentonite:glacial clay:crushed granite)	1.6×10^{-3}	4.1×10^{-2}
Concrete	3.9×10^{-3}	3.9×10^{-3}
Asphalt	3.16×10^{-6}	3.16×10^{-6}

Note: From Gobien et al. (2018), the effective diffusion coefficients for engineered sealing materials are directionally homogeneous.

Table 7-18: Effective Diffusion Coefficients, Base Case Values

Formation	$D_{e,v}$ Anions / Neutral Species (m ² /a)	$D_{e,H}$ Anions / Neutral Species (m ² /a)	$D_{e,v}$ Cationic Species (m ² /a)	$D_{e,H}$ Cationic Species (m ² /a)
100% Bentonite	4.4x10 ⁻³	4.4x10 ⁻³	1.3x10 ⁻²	1.3x10 ⁻²
Backfill	1.6x10 ⁻³	1.6x10 ⁻³	4.1x10 ⁻²	4.1x10 ⁻²
Overburden	7.0x10 ⁻¹⁰	7.0x10 ⁻¹⁰	1.4x10 ⁻⁹	1.4x10 ⁻⁹
Sediment	6.2x10 ⁻¹⁰	6.2x10 ⁻¹⁰	1.2x10 ⁻⁹	1.2x10 ⁻⁹
Drift	6.0x10 ⁻¹⁰	6.0x10 ⁻¹⁰	1.2x10 ⁻⁹	1.2x10 ⁻⁹
Unit B and C	1.2x10 ⁻¹¹	2.4x10 ⁻¹¹	2.4x10 ⁻¹¹	4.8x10 ⁻¹¹
Unit A-2 Carbonate	1.2x10 ⁻¹²	2.4x10 ⁻¹²	2.4x10 ⁻¹²	4.8x10 ⁻¹²
Unit A-1 Upper Carbonate	6.8x10 ⁻¹²	6.8x10 ⁻¹²	1.4x10 ⁻¹¹	1.4x10 ⁻¹¹
Unit A-1 Carbonate	1.8x10 ⁻¹³	3.6x10 ⁻¹³	3.6x10 ⁻¹³	7.2x10 ⁻¹³
Unit A-1 Evaporite	3.0x10 ⁻¹⁴	6.0x10 ⁻¹⁴	6.0x10 ⁻¹⁴	1.2x10 ⁻¹³
Unit A0	3.0x10 ⁻¹⁴	6.0x10 ⁻¹⁴	6.0x10 ⁻¹⁴	1.2x10 ⁻¹³
Guelph	2.9x10 ⁻¹¹	2.9x10 ⁻¹¹	5.8x10 ⁻¹¹	5.8x10 ⁻¹¹
Reynales / Fossil Hill	4.3x10 ⁻¹⁴	8.6x10 ⁻¹⁴	8.6x10 ⁻¹⁴	1.7x10 ⁻¹³
Cabot Head	3.1x10 ⁻¹²	6.2x10 ⁻¹²	6.2x10 ⁻¹²	1.2x10 ⁻¹¹
Manitoulin	1.5x10 ⁻¹³	3.0x10 ⁻¹³	3.0x10 ⁻¹³	6.0x10 ⁻¹³
Queenston	1.0x10 ⁻¹²	2.0x10 ⁻¹²	2.0x10 ⁻¹²	4.0x10 ⁻¹²
Georgian Bay / Blue Mountain	8.2x10 ⁻¹³	1.6x10 ⁻¹²	1.6x10 ⁻¹²	3.2x10 ⁻¹²
Cobourg	3.7x10 ⁻¹³	7.4x10 ⁻¹³	7.4x10 ⁻¹³	1.5x10 ⁻¹²
Sherman Fall	2.2x10 ⁻¹³	4.4x10 ⁻¹³	4.4x10 ⁻¹³	8.8x10 ⁻¹³
Kirkfield	4.2x10 ⁻¹³	8.4x10 ⁻¹³	8.4x10 ⁻¹³	1.7x10 ⁻¹²
Cobokonk	2.7x10 ⁻¹³	5.4x10 ⁻¹³	5.4x10 ⁻¹³	1.1x10 ⁻¹²
Gull River	2.6x10 ⁻¹³	5.2x10 ⁻¹³	5.2x10 ⁻¹³	1.0x10 ⁻¹²
Shadow Lake	1.3x10 ⁻¹²	2.6x10 ⁻¹²	2.6x10 ⁻¹²	5.2x10 ⁻¹²

Note: From Gobien et al. (2018)

7.5.2.7 Sorption Parameters

Data for sorption coefficients for 100% bentonite under saline conditions are shown in Table 7-19. Sorption coefficients for dense backfill and shaft backfill are the same, except with the K_d scaled according to the bentonite content (i.e., 5% for dense backfill and 70% for shaft backfill).

Sorption coefficients for concrete are conservatively assumed to be zero given the high salinity groundwater and absence of sorption data applicable to these conditions. Similarly, due to a lack of data, and due to the small porosity and limited physical extent of this material, sorption coefficients for the asphalt shaft seal are also conservatively set to zero.

Table 7-19: Bentonite Sorption Coefficients (K_d), Base Case Values

Element	GM (m^3/kg)	GSD (m^3/kg)	Lower Bound (m^3/kg)	Upper Bound (m^3/kg)
Ac	6.8	6.6	0.23	78
Ag	0	-	-	-
Am	6.8	6.6	0.23	78
Bi	4.4	7.1	1.1	18
C	0	-	-	-
Cl	0	-	-	-
Cs	0.43	3.3	0.14	1.43
Hg	0	-	-	-
I	0	-	-	-
Mo	0	-	-	-
Nd	0	-	-	-
Np	48.1	4.1	17.8	130
Pa	4	-	-	-
Pb	0.003	5	0	0.011
Pd	0.68	9.1	0.03	14.5
Po	0.1	-	-	-
Pu	3.91	2.6	1.5	10
Ra	0.00009	-	-	-
Rh	0	-	-	-
Rn	0	-	-	-
Ru	0	-	-	-
Se	0.099	1.1	0.09	0.11
Sm	1.3	4.6	0.10	6.7
Tc	5	-	-	-
Th	8.9	1.8	3.4	15.9
U	8.9	1.8	3.4	15.9

Note: From Gobien et al. (2018).

Sorption in the geosphere is partly based on the information shown in Table 7-20 and Table 7-21. These tables show experimentally measured element specific K_d values for crushed shale and limestone units pertinent to Southern Ontario. These K_d data are combined with information in Table 7-22 to generate radionuclide and geological unit specific retardation factors for use in the advective diffusion equation describing contaminant transport.

More information concerning these values is available in Gobien et al. (2018).

Table 7-20: Geosphere Sorption Coefficients K_d for Shale, Base Case Values

Element	GM ⁽¹⁾ (m ³ /kg)	GSD ⁽²⁾ (m ³ /kg)	Lower Bound (m ³ /kg)	Upper Bound (m ³ /kg)
Ac	2.4	13	0.20	53
Ag	0	-	-	-
Am	2.4	13	0.20	53
Bi	2.9	5.8	0.84	10
C	0	-	-	-
Cl	0	-	-	-
Cs	0.2	2.8	0.069	0.63
Hg	0	-	-	-
I	0	-	-	-
Mo	0	-	-	-
Nd	0	-	-	-
Np (IV)	32.8	4.6	11	98
Np (V)	0.038	2.2	0.0078	0.12
Pa	2	-	-	-
Pb	0.0016	10	0	0.009
Pd	2.2	11	0.04	14.3
Po	0.05	-	-	-
Pu (III)	2.45	2.0	1.5	4.0
Pu (IV, V)	2.2	1.5	1.4	3.2
Ra	0	-	-	-
Rh	0	-	-	-
Rn	0	-	-	-
Ru	0	-	-	-
Se (-II)	0.021	4.8	0.003	0.1
Se (IV, VI)	0.010	1.2	0.008	0.011
Sm	0.16	1.6	0.11	0.22
Tc (IV)	0.02	-	-	-
Tc (VI)	0.0024	140	7.3×10^{-5}	0.079
Th	4.6	1.8	1.7	6.8
U (IV)	4.6	1.8	1.7	6.8
U (VI)	0.027	2.0	0.016	0.044

Notes: (1) GM= Geometric Mean

(2) GSD = Geometric Standard Deviation

From Gobien et al. (2018)

Table 7-21: Geosphere Sorption Coefficients K_d for Limestone, Base Case Values

Element	GM ⁽¹⁾ (m ³ /kg)	GSD ⁽²⁾ (m ³ /kg)	Lower Bound (m ³ /kg)	Upper Bound (m ³ /kg)
Ac	0.16	1.6	0.09	0.29
Ag	0	-	-	-
Am	0.16	1.6	0.09	0.29
Bi	0.16	1.6	0.09	0.29
C	0	-	-	-
Cl	0	-	-	-
Cs	0.14	4	0.032	0.69
Hg	0	-	-	-
I	0	-	-	-
Mo	0	-	-	-
Nd	0	-	-	-
Np (IV)	2.1	1.9	0.6	2.7
Np (V)	0.014	42	0.001	0.2
Pa	0.09	-	-	-
Pb	0.0004	14	0	0.004
Pd	1.94	5.7	0.1	22
Po	0	-	-	-
Pu (III)	2.45	2.0	1.5	4.0
Pu (IV, V)	0.49	7.3	0.069	3.7
Ra	0	-	-	-
Rh	0	-	-	-
Rn	0	-	-	-
Ru	0	-	-	-
Se (-II)	0.013	5.8	0.0037	0.1
Se (IV, VI)	0.0013	-	-	-
Sm	0.16	1.6	0.09	0.29
Tc (IV)	10	-	-	-
Tc (VI)	0.015	9.7	0.003	0.075
Th	2.1	1.9	0.6	2.7
U (IV)	2.1	1.9	0.6	2.7
U (VI)	0.011	1.6	0.008	0.015

Notes: (1) GM= Geometric Mean

(2) GSD = Geometric Standard Deviation

From Gobien et al. (2018)

Table 7-22: Values of $[\rho_s(1-\epsilon_{\text{expt}})/\epsilon_{\text{expt}}]$ for Several Geological Materials

Geological Material	$\rho_s(1-\epsilon_{\text{expt}})/\epsilon_{\text{expt}}$ (kg/m ³)	Rock Type
Sand	3660	Overburden ⁽¹⁾
Silt / loam	3660	
Clay	3660	
Sediment	2500	Sediment ⁽²⁾
Drift	2840	Limestone
Unit B and C	2810	Limestone
Unit A-2 Carbonate	2860	Limestone
Unit A-1 Upper Carbonate	2930	Limestone
Unit A-1 Carbonate	2730	Limestone
Unit A-1 Evaporite	2930	Limestone
Unit A0	2790	Limestone
Guelph	2810	Limestone
Reynales / Fossil Hill	2730	Limestone
Cabot Head	2790	Shale
Manitoulin	2720	Limestone
Queenston	2770	Shale
Georgian Bay / Blue Mountain	2760	Shale
Cobourg	2710	Limestone
Sherman Fall	2720	Limestone
Kirkfield	2710	Limestone
Coboconk	2690	Limestone
Gull River	2730	Limestone
Shadow Lake	2760	Limestone

Notes: (1) Mineral composition of the overburden is assumed to be 70% clay, 20% silt/loam and 10% sand. The mineral fractions are normally distributed with standard deviation of 0.28, 0.3, and 0.5 for the clay, silt/loam and sand respectively. Distribution bounds range from 0 to 1.

(2) Sediment mineral fraction is assumed to be composed of 100% organics.

Sorption values for other geosphere materials (e.g., soil, sediment, and overburden) can be found in Gobien et al. (2018).

7.6 Modelling and Results for Radionuclide and Chemical Hazard Screening

This section presents results for the radionuclide and chemical hazard screening assessment.

As noted in Section 7.5.1, this screening identifies the set of potentially important radionuclides and hazardous chemical elements for detailed assessment in this study.

Note that because the Inadvertent Human Intrusion Disruptive Scenario bypasses the geosphere barrier, the screening assessment described here does not apply and a separate scenario-specific screening assessment is completed, as described in Section 7.9.1.

7.6.1 Methods

The Screening Model resembles the System Model used to perform the primary dose assessment; however, a more stylized and conservative representation is adopted and implemented in the RSM code. The following discusses the Screening Model in terms of its key features and compares them to those in the System Model:

- Solubility limits, diffusion coefficients, sorption coefficients and decay constants are the same;
- The fuel contaminant source term is the same;
- The container release model is the same;
- The EDZ is represented but in a simplified form;
- The near field (the engineered barriers) is represented by a one dimensional pathway consisting of a 0.318 m thick layer of homogenized bentonite buffer and gapfill; and
- The geosphere is based on a one-dimensional diffusion-dispersion-advection transport model representing a single direct transport pathway. This pathway is composed of five zones, these being segments of the Cobourg, Georgian Bay, Queenston, Manitoulin and Cabot Head geological units. The Cabot Head segment is connected to a well in the biosphere.

The properties used to represent the five geosphere zones are shown in Table 7-23. These properties are selected to ensure a fast transport time to the surface. The transport in the rock mass is diffusion dominant and therefore the advective velocity is effectively zero.

Table 7-23: Screening Model Geosphere Zone Properties

Geosphere Zone	Material Type	Length (m)	Velocity (m/a)	Porosity (-)	Tortuosity (-)
1	Cobourg	25.24	0	0.015	5.7
2	Georgian Bay	153.65	0	0.070	10.5
3	Queenston	77.92	0	0.073	7.1
4	Manitoulin	15.5	0	0.028	12.9
5	Cabot Head	15.9	0	0.116	5.7

The biosphere includes the key set of exposure pathways. The model calculates doses from water ingestion, groundshine, air immersion and air inhalation. The plant ingestion dose rate is estimated from the drinking water dose rate using an ingestion multiplication factor.

The following assumptions are also incorporated in the biosphere model to ensure conservative results:

- The well demand is set to that corresponding to a single person, excluding irrigation. This ensures the minimum amount of dilution;
- The surface soil is a small irrigated garden large enough to support only a single person. This maximizes the soil concentrations; and
- Contaminant concentrations in any surface water present are set equal to those in the well. This maximizes the surface water concentrations.

7.6.1.1 Radionuclide Screening

The Screening Model is applied to all radionuclides with half-lives longer than 0.1 years, and all radionuclides with half-lives longer than one day if they have a parent with a half-life longer than 0.1 years.¹ This results in a total of 251 distinct radionuclides and 84 stable elements in the used fuel and zirconium fuel sheath requiring consideration.

The Screening Model (i.e., the RSM code) is then run for the analysis cases shown in Table 7-24. A wide range of cases is considered to encompass the full suite of Normal Evolution sensitivity cases introduced in Section 7.2.1 and to provide confidence that the set of potentially significant radionuclides has been identified. The All Containers Fail Disruptive Event Scenario is also included because this is the event most likely to have the greatest consequence.

All screening cases are run for a 10 million year simulation time. All cases use a solubility limited Zircaloy model except Case 6.

Table 7-24: RSM Cases Considered for the Screening Assessment

Case	Case ID
1	Median Case
2	All Parameters set to 3 Sigma Conservative Values
3	All Instant Release Fraction set to 10% and Fuel Dissolution Rate Increased by a Factor of 10
4	High Diffusivity (10 times Base Case values everywhere)
5	No Solubility Limits and No Geosphere Sorption
6	Zircaloy Degradation Rate Increased by a Factor of 10
7	All Containers Fail

¹ Radionuclides with longer-lived parent but half-life shorter than 0.1 years are assumed to be present in equilibrium with the parent and are directly included in the dose coefficient for the parent.

The set of radionuclides that together contribute 0.1% or less of the total peak dose rate for each case are screened out, and the remaining superset of radionuclides identified over all cases is then carried forward into the postclosure safety assessment.

The results of the radionuclide screening assessment are described in Section 7.6.2.

7.6.1.2 Chemical Element Screening

For chemical element screening, the release rates of elements from the repository to the biosphere are determined with the Screening Model for the set of cases shown in Table 7-24. As for radionuclide screening, a wide range of cases is considered to encompass the full suite of Normal Evolution sensitivity cases and to provide confidence that the set of potentially significant elements is complete. The All Containers Fail Disruptive Event Scenario is also included because this is the event most likely to have the greatest consequence.

In the RSM screening model, sediment concentrations are estimated by multiplying groundwater concentrations by the appropriate sediment sorption coefficient. Sediment K_d values are taken from either CSA (2014) where available, or estimated as 10 times the sandy soil K_d values in Gobien and Garisto (2012) otherwise.

All screening cases are run for a 10 million year simulation time. All cases use the solubility limited Zircaloy model except Case 6.

All elements with interim acceptance criteria in Table 7-1 are considered, with those exceeding 1% of their interim acceptance values screened in.

Elements not considered (due to the absence of interim acceptance criteria) are listed in Table 7-25 together with the rationale as to why their exclusion is not significant. Most of the exclusions are justified on the basis that the element is essential to life (and considered non-toxic at repository concentrations), or inert, or considered more radiotoxic than chemically toxic, or not relevant for used nuclear fuel. For the few remaining elements (i.e., Cs, Er, Ga, Ge, In, Re, Rb, and Yb), their significance can be assessed by comparing the rates at which they enter the environment due to repository sources with the rates at which they enter the environment due to natural erosion. This is done in Table 7-26.

Table 7-26 shows the maximum transport values (for a 10 million year simulation) over all cases considered in Table 7-24. Results show transport rates to the biosphere are orders of magnitude less than transport rates due to natural erosion. It is therefore reasonable to exclude Cs, Er, Ga, Ge, In, Re, Rb, and Yb from further consideration.

Table 7-25: Chemical Elements Excluded from Chemical Hazard Assessment

Category	Reason	Chemical Elements
Common or Essential Elements	Essential to life and abundant	C, H, N, O, Si
Inert Gases	Do not react chemically	Ar, He, Kr, Ne, Rn, and Xe
Radioactive, Actinide, or Lanthanide Elements ⁽¹⁾	All isotopes of each of these elements are radioactive and they are addressed through radiotoxicity	Ac, Am, At, Bk, Cf, Cm, Es, Fm, Fr, Lr, Md, No, Np, Pa, Pm, Po, Pu, Ra Th
Synthetic Elements	Very short lived man-made radionuclides	Bh, Cn, Db, Ds, Fl, Hs, Lv, Mc, Mt, Nh, Og, Rf, Rg, Sg, Ts
No Criteria	To be considered in the screening assessment	Cs, Er, Ga, Ge, In, Re, Rb, Yb

Note: (1) Uranium is included in the assessment because it is a special actinide for which the chemotoxicity exceeds the radiotoxicity. Thus, it does not appear in the list of excluded chemical elements.

Table 7-26: Erosion based Screening of Some Excluded Chemical Elements

Element	Crust Composition (µg/g)	Erosion Rate ⁽¹⁾ (mol/a)	Rate to Well ⁽²⁾ (mol/a)	Ratio (-)
Cs	4.9	51	4.53x10 ⁻⁴	8.94x10 ⁻⁶
Er	2.3	19	2.94x10 ⁻⁷	1.55x10 ⁻⁸
Ga	17.5	345	4.99x10 ⁻⁶	1.45x10 ⁻⁸
Ge	1.4	27	5.11x10 ⁻⁶	1.93x10 ⁻⁷
Re	0.000198	0.0015	7.16x10 ⁻⁷	4.90x10 ⁻⁴
Rb	84	1350	1.65x10 ⁻⁴	1.22x10 ⁻⁷
Yb	1.96	16	6.81x10 ⁻⁷	4.38x10 ⁻⁸

Notes: (1) Erosion Rate based on erosion of rate of 1x10⁻⁴ m/a from Hallet (2011), a rock density of 2750 kg/m³, an assumed repository footprint area of 5 km², and a crust composition from Rudnick and Gao (2014).

(2) As calculated by the radionuclide screening model run out to 10 Ma.

7.6.2 Results

This section presents results of the screening analysis.

Table 7-27 shows the results (over all cases listed in Table 7-24) of the chemical hazard screening assessment by expressing RSM results as a percentage of the interim acceptance criteria defined in Section 7.1.2. The water column is based on the minimum of the surface and ground water interim acceptance criteria.

The results show that Ag, Hg, Mo, Nd, Pd, Rh and Ru exceed 1% of the acceptance criteria and are therefore screened in.

Table 7-27: Ratio of the RSM results and Chemical Acceptance Criteria

Element	Water (%)	Soil (%)	Air (%)	Sediment (%)	Exceeds 1% of Criteria
Ag	12.33	1.17	0.00	234.22	Ag
Al	0.65	0.03	0.00	0.00	-
As	0.01	0.00	0.00	0.00	-
Au	0.00	0.03	0.00	0.00	-
B	0.00	0.00	0.00	0.00	-
Ba	0.01	0.02	0.00	0.00	-
Be	0.00	0.00	0.00	0.00	-
Bi	0.02	0.08	0.00	0.00	-
Br	0.08	0.01	0.00	0.00	-
Ca	0.00	0.00	0.00	0.00	-
Cd	0.00	0.00	0.00	0.00	-
Ce	0.35	0.07	0.00	0.09	-
Cl	0.00	0.00	0.00	0.00	-
Co	0.28	0.00	0.00	0.15	-
Cr	0.47	0.34	0.00	0.00	-
Cu	0.00	0.00	0.00	0.00	-
Dy	0.00	0.00	0.00	0.00	-
Eu	0.00	0.00	0.00	0.00	-
F	0.00	0.00	0.00	0.00	-
Fe	0.01	0.01	0.00	0.06	-
Gd	0.05	0.00	0.00	0.00	-
Hf	0.00	0.00	0.00	0.00	-
Hg	3.63	0.03	0.00	0.01	Hg
Ho	0.00	0.00	0.00	0.00	-
I	0.01	0.10	0.00	0.97	-
In	0.00	0.01	0.00	0.05	-
Ir	0.05	0.14	0.00	0.01	-
K	0.00	0.00	0.00	0.00	-
La	0.40	0.04	0.00	0.00	-
Li	0.00	0.00	0.00	0.00	-
Lu	0.00	0.00	0.00	0.00	-
Mg	0.00	0.00	0.00	0.00	-
Mn	0.00	0.00	0.00	0.05	-
Mo	1.09	2.59	0.00	0.13	Mo
Na	0.00	0.00	0.00	0.00	-
Nb	0.00	0.00	0.00	0.00	-
Nd	7.06	0.00	0.00	0.00	Nd
Ni	0.02	0.01	0.00	0.05	-
Os	0.19	0.51	0.00	0.09	-
P	0.14	0.00	0.00	0.00	-
Pb	0.00	0.00	0.00	0.00	-

Postclosure Safety Assessment of a Used Fuel Repository in Sedimentary Rock

Document Number: NWMO-TR-2018-08

Revision: 000

Class: Public

Page: 393

Element	Water (%)	Soil (%)	Air (%)	Sediment (%)	Exceeds 1% of Criteria
Pd	79	213	0.00	11	Pd
Pr	0.39	0.00	0.00	0.00	-
Pt	0.02	0.60	0.00	0.39	-
Rh	31	83	0.00	3	Rh
Ru	194	524	0.00	1569	Ru
S	0.10	0.00	0.00	0.00	-
Sb	0.01	0.02	0.00	0.07	-
Sc	0.00	0.00	0.00	0.00	-
Se	0.34	0.13	0.00	0.21	-
Sm	0.37	0.00	0.00	0.00	-
Sn	0.00	0.00	0.00	0.00	-
Sr	0.00	0.00	0.00	0.00	-
Ta	0.00	0.00	0.00	0.00	-
Tb	0.00	0.00	0.00	0.00	-
Tc	0.00	0.00	0.00	0.00	-
Te	0.31	0.00	0.00	0.00	-
Ti	0.00	0.00	0.00	0.00	-
Tl	0.00	0.00	0.00	0.00	-
Tm	0.00	0.00	0.00	0.00	-
U	0.17	0.21	0.00	0.00	-
V	0.03	0.00	0.00	0.02	-
W	0.01	0.00	0.00	0.00	-
Y	0.20	0.00	0.00	0.00	-
Zn	0.00	0.00	0.00	0.00	-
Zr	0.00	0.00	0.00	0.00	-

Table 7-28 shows the radionuclides that emerged from the radionuclide screening assessment. For completeness, chemical elements identified above are also shown. Altogether there are 32 radionuclides from the fuel and two from the Zircaloy, and seven chemically hazardous elements from the fuel and none from the Zircaloy.

Table 7-28: Superset of Screened in Radionuclides and Chemically Hazardous Elements

Radionuclides	Chemically Hazardous Elements
<p>Fuel</p> <p>I-129, C-14, Cl-36, Cs-135, Pd-107, Se-79, Sm-147, Tc-99, Np-237, Pa-233, U-233, Th-229, Ra-225, Ac-225, U-238, Th-234, U-234, Th-230, Ra-226, Rn-222, Pb-210, Po-210, U-235, Pa-231, Ac-227, Th-227, Ra-223, U-236, Th-232, Ra-228, Th-228, Ra-224</p> <p>Zircaloy</p> <p>C-14, Cl-36</p>	<p>Fuel</p> <p>Ag, Hg, Mo, Nd, Pd, Rh, and Ru</p>

Table 7-29 and Table 7-30 show the complete sets of potentially significant radionuclides and potentially significant chemically hazardous elements that are carried through into the System Model assessments. Items in red have been identified directly in the screening assessment (i.e., Table 7-28) while items in black have been added to account for in-growth. This results in three additional radionuclides being included for the radiological hazard and no additional radionuclides being included for the non-radiological hazard.

Table 7-29: List of Potentially Significant Radionuclides

Radionuclides ⁽¹⁾	
Fuel	
Single Nuclides	I-129, C-14 ⁽²⁾ , Cl-36, Cs-135, Pd-107, Se-79, Sm-147, Tc-99,
Chain Nuclides	Am-241 → Np-237 = Pa-233 → U-233 → Th-229 = Ra-225 = Ac-225
	Pu-242 → U-238 = Th-234 → U-234 → Th-230 → Ra-226 = Rn-222 = Pb-210 = Bi-210 = Po-210
	Pu-239 → U-235 = Th-231 → Pa-231 = Ac-227 = Th-227 = Ra-223
	Pu-240 → U-236 → Th-232 = Ra-228 = Th-228 = Ra-224
Zircaloy	
Single Nuclides	C-14 ⁽²⁾ , Cl-36

Notes: (1) Screened-in radionuclides are red
(2) Included for gas phase dose consequences
“=” signifies the radionuclides are in secular equilibrium

Table 7-30: List of Potentially Significant Chemically Hazardous Elements

Chemically Hazardous Elements ⁽¹⁾	
Fuel	
Elements	Hg, Mo, Nd, Pd, Rh, Ru
Misc	Pd-107 → Ag
	Sm-147 → Nd
	Sm-148 → Nd

Note: (1) Screened-in elements are red

7.7 Modelling and Results for 3D Groundwater Flow and Radionuclide Transport

This section describes the detailed 3D groundwater flow and transport models illustrated in Figure 7-9 and implemented using FRAC3DVS-OPG. Section 7.5.1 describes how these models fit into the overall assessment approach.

All flow modelling is steady-state, which is consistent with the Base Case Normal Evolution Scenario assumption of constant climate. Small changes in climate may affect the shallow groundwater system, but would not affect the deep groundwater system. The effects of large changes in climate associated with glacial cycles are discussed separately in Section 7.8.2.4.

The Subregional Flow Model, the Main Transport Model and the Detailed Transport Model are defined with reference to a common model coordinate system with an origin located at the main shaft. The X and Y axes follow the rooms and main access tunnels respectively. This allows natural finite-difference discretization of the generally orthogonal repository features. This coordinate system is used for most spatial figures presenting model results.

7.7.1 Methods

7.7.1.1 Subregional Flow Model

The Subregional Flow Model simulates flow through the geosphere surrounding the repository. The model provides head boundary conditions to the Main and Detailed Transport Models to ensure the flow system within those models is an accurate representation of that in the larger domain.

Regional-scale groundwater flow modelling is described in Chapter 2. The Subregional Flow Model extracts a 40 km by 40 km square section of the regional model domain centred on the repository and oriented coincident with repository features.

Domain Discretization and Permeability Profile

Horizontally, the Subregional Flow Model domain is discretized in variably sized elements. Discretization ranges from 1000 m to 100 m outside the repository footprint, with a constant 100 m within the footprint. There are 135 nodes in the X and Y directions, for a total of 18,225 elements in each model layer. The complete grid consists of 79 layers for a total of 1.44 million elements and is shown in Figure 7-16. Although the repository footprint is shown in most plan-section figures in this section, there are no repository features or properties specified within the model grid. The repository representation in the figures is only provided to add context.

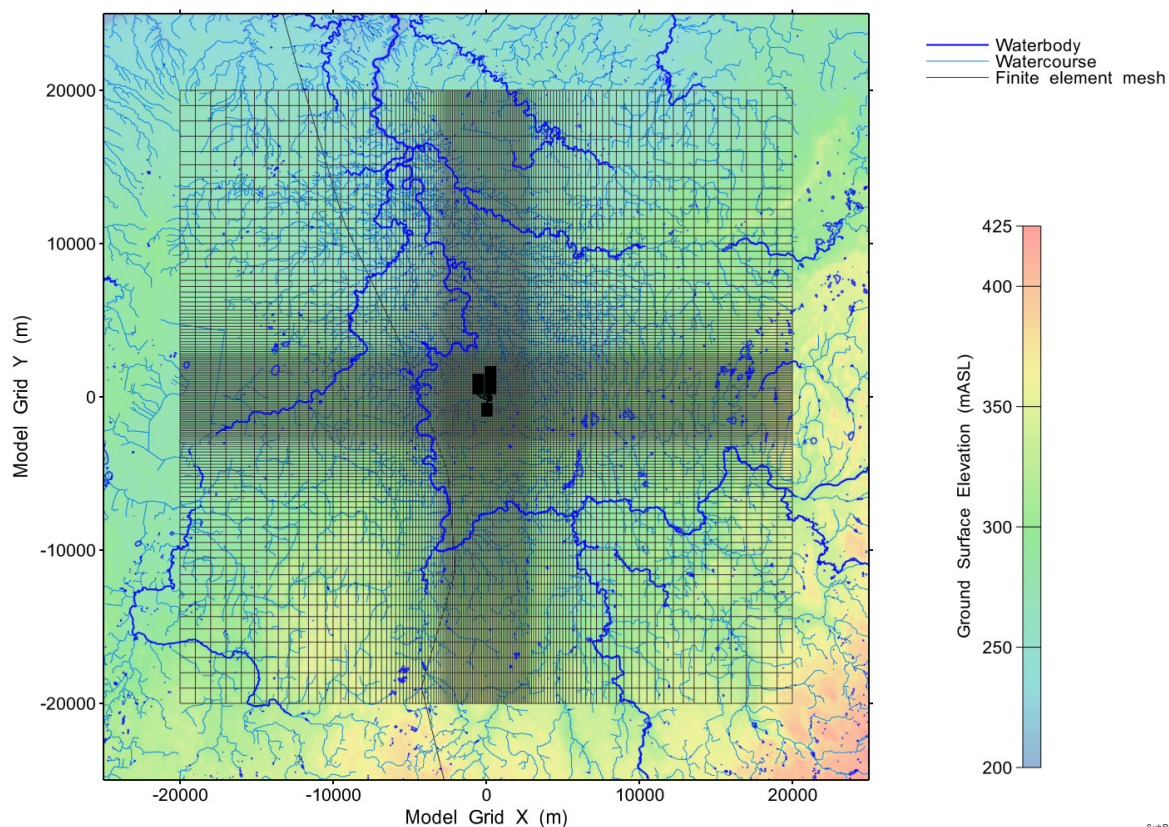


Figure 7-16: Subregional Flow Model: Plan view discretization

Vertical discretization was developed from geologic surfaces describing the tops of each formation described in Chapter 2 and illustrated in Figure 7-17. Not all formation tops are indicated in the figures; however, all were used in the discretization. Upper layers were modified so that a minimum of 50 m thickness weathered bedrock/overburden zone could be assigned. A minimum grid layer thickness of 0.1 m was enforced in the eastern end of the grid where sub-cropping layers were merged into the drift / weathered bedrock zone, as shown in the upper right of Figure 7-17. Formation hydraulic conductivities are shown on the figures and are assigned as specified in Table 7-31.

The formation dip shown in Figure 7-17 is significantly accentuated by the vertical exaggeration of the figure.

Table 7-31: Formation Depths, Thicknesses, and Hydraulic Conductivities

Formation	Formation-Top Depth (mBGS)	Formation Thickness (m)	Hydraulic Conductivity (m/s)		
			Reference Case (K_{Hori})	Sensitivity Case (K_{Hori})	Anisotropy $K_{Hori}:K_{Vert}$
Drift	0	45.2	1×10^{-7}	1×10^{-6}	2:1
Detroit River Group	-	-	6×10^{-7}	6×10^{-6}	30:1
Bois Blanc	-	-	1×10^{-7}	1×10^{-6}	10:1
Bass Islands	-	-	5×10^{-5}	5×10^{-4}	25:1
Unit G	-	-	1×10^{-11}	1×10^{-10}	10:1
Unit F	-	-	5×10^{-14}	5×10^{-13}	10:1
Unit E	-	-	2×10^{-13}	2×10^{-12}	10:1
Unit D	-	-	2×10^{-13}	2×10^{-12}	10:1
Unit B and C	45.2	31.3	4×10^{-13}	4×10^{-12}	10:1
Unit B Anhydrite	-	-	3×10^{-13}	3×10^{-12}	10:1
Unit A-2 Carbonate	76.5	27.4	3×10^{-10}	3×10^{-9}	10:1
Unit A-2 Evaporite	-	-	3×10^{-13}	3×10^{-12}	10:1
Unit A-1 Upper Carbonate	104.0	6.2	2×10^{-7}	2×10^{-6}	1:1
Unit A-1 Carbonate	110.1	18.6	9×10^{-12}	9×10^{-11}	10:1
Unit A-1 Evaporite	128.7	2.5	3×10^{-13}	3×10^{-12}	10:1
Guelph	131.2	73.0	3×10^{-8}	3×10^{-7}	1:1
Fossil Hill	204.1	6.9	5×10^{-12}	5×10^{-11}	10:1
Cabot Head	211.0	15.7	9×10^{-14}	9×10^{-13}	10:1
Manitoulin	226.7	15.6	9×10^{-14}	9×10^{-13}	10:1
Queenston	242.3	77.0	2×10^{-14}	2×10^{-13}	10:1
Georgian Bay/Blue Mountain	319.2	154.5	4×10^{-14}	4×10^{-13}	13:1
Cobourg	473.7	46.5	2×10^{-14}	2×10^{-13}	10:1
Sherman Fall	520.3	47.3	1×10^{-14}	1×10^{-13}	10:1
Kirkfield	567.5	39.9	8×10^{-15}	8×10^{-14}	10:1
Coboconk	607.5	7.9	4×10^{-12}	4×10^{-11}	1,000:1
Gull River	615.3	53.9	7×10^{-13}	7×10^{-12}	1,000:1
Shadow Lake	669.2	7.0	1×10^{-9}	1×10^{-8}	1,000:1
Pre-Cambrian	676.3				

Notes: The formations listed here are those that are present within the region of the repository, all of which are represented in the Subregional Flow Model.

The formation depths and thicknesses vary across the repository region; the values presented here are from the Central Services Area.

The Sensitivity Case examines the effect of a 10-fold increase in geosphere hydraulic conductivity. This is discussed further in Section 7.2.1.4 and Table 7-5.

Hydraulic conductivity data are from Gobien et al. (2018).

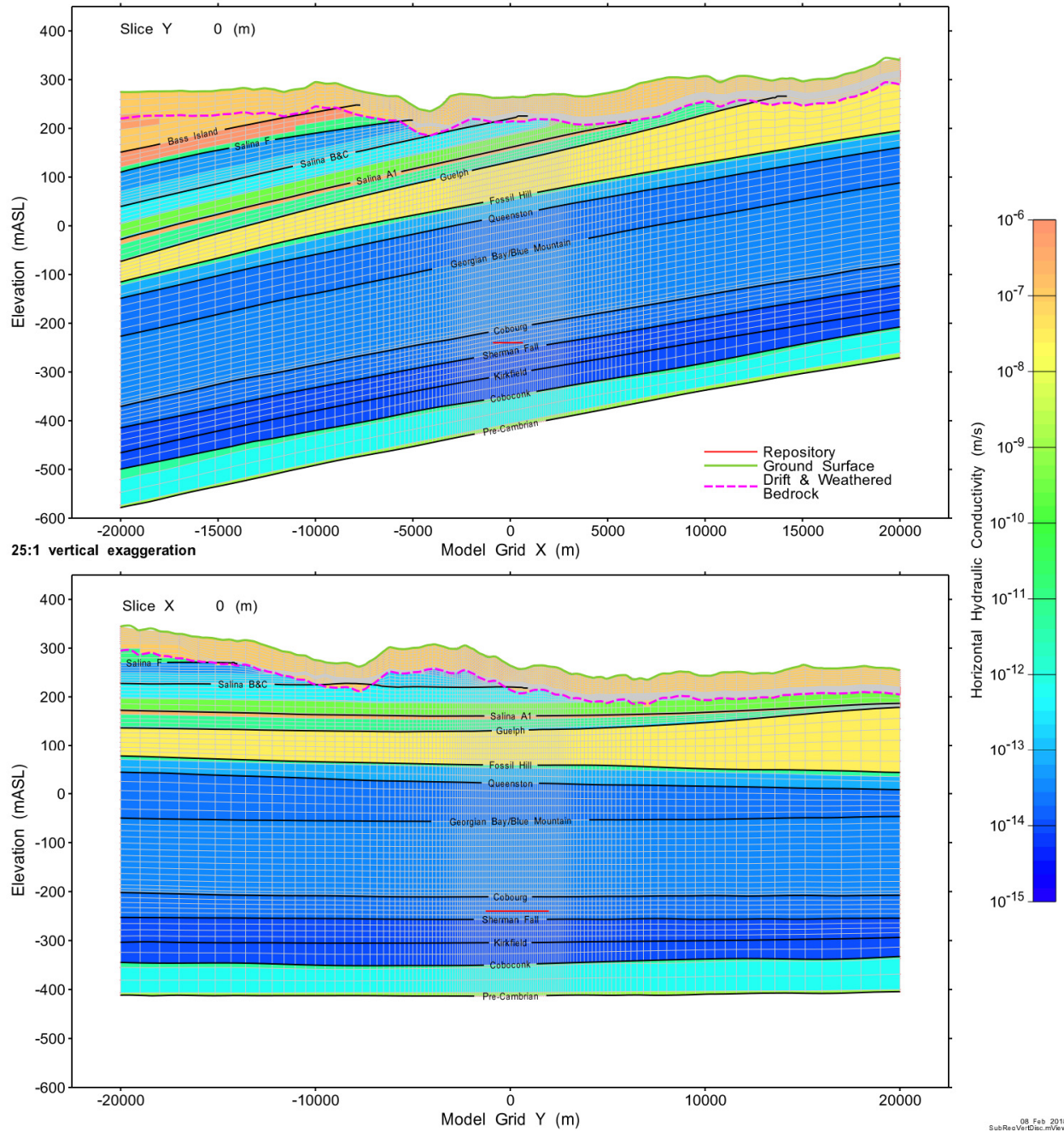


Figure 7-17: Subregional Flow Model: Vertically Exaggerated to show Discretization

Boundary Conditions

Zero-flow boundary conditions are specified on all external vertical faces and at the lower boundary of the model for the Base Case. The model extents are sufficiently large that any boundary influences will not affect the flow system in the vicinity of the repository. Fixed head

elevation boundary conditions are specified for the top surface of the model, representing a water table close to surface and reflecting the generally low topographic relief.

The lower boundary condition of the model is modified for the Overpressure Sensitivity case. For this case, the simulated head at the model origin for the Base Case is taken as the reference head, to which 150 m is added for the specified overpressure. This constant value is then applied as a fixed head boundary on the bottom of the model.

7.7.1.2 Main and Detailed Transport Models

The Main and Detailed Transport Models are used to investigate transport to the well and surface environment for contaminants released from various locations in the repository. The two models are distinguished by the level of detail given to repository features and by the extent of the model domain.

The Main Transport Model includes all placement rooms, a simplified tunnel network, and all shafts. The rooms and tunnels use a simplified approach to represent the EDZ. Inner and Outer EDZ are applied to the top and bottom of rooms and tunnels rather than to all sides. Conductivity and porosity values are scaled to ensure equivalent hydraulic and transport impact. Additionally, EDZ intercepting room seals are represented with blended properties. Finally, the domain of the Main Transport Model extends to surface water discharge locations a significant distance (5 to 15 km) from the repository.

The Detailed Transport Model is discretized for all repository and EBS features except containers. Tunnels, cross-tunnels, and placement rooms adjacent to source containers include a detailed representation of the EBS. The inner and outer EDZ are present on all sides of the tunnels and source rooms. Placement rooms removed from the anticipated transport path have a simplified EDZ with blended properties assigned to the EDZ region above and below the rooms. EDZ is not incorporated on the sides of these reduced complexity rooms. Room seals are explicitly included in a geometrically correct fashion. The domain of the Detailed Transport model is limited to the immediate vicinity of the repository.

The Main Transport Model is used for all cases, including: Base Case radionuclide transport, all container fail simulations, all sensitivity studies, disruptive events, determining high consequence well / container location pairs, and for providing advective transport pathway information for development of the System Model. The Main Transport Model is used preferentially because: a) it includes the full groundwater pathway to surface discharge, and b) the Detailed Transport Model is computationally very demanding, requiring both significantly more memory to execute and significantly more time to simulate the 10 Ma simulation period. A comparison of the models presented in Section 7.7.2.3.1 shows that the Main Transport Model results are very similar to the Detailed Transport Model results.

The Detailed Transport Model is used to replicate a limited number of cases including the Base Case.

The repository is located approximately 500 m below ground surface (mBGS) within the Cobourg formation. Repository rooms and tunnels are sloped at a 1% grade to promote drainage towards the central services area. Consequently, the depth of the repository varies across the footprint. The average ground surface elevation within the repository footprint is

267.4 mASL. Repository feature elevations have a 24 m range in repository floor depths (i.e., from 512 mBGS to 488 mBGS).

Figure 7-18 illustrates the surface topography in the region of the repository footprint.

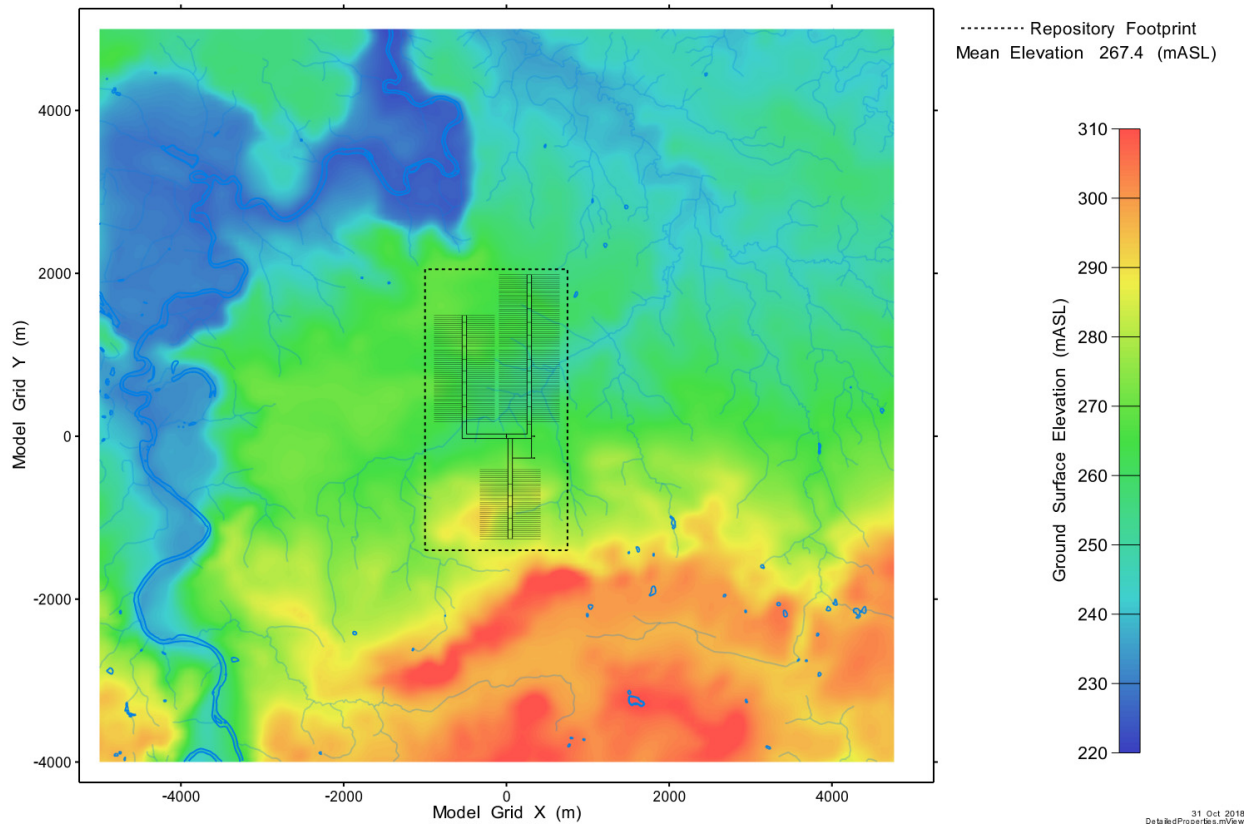
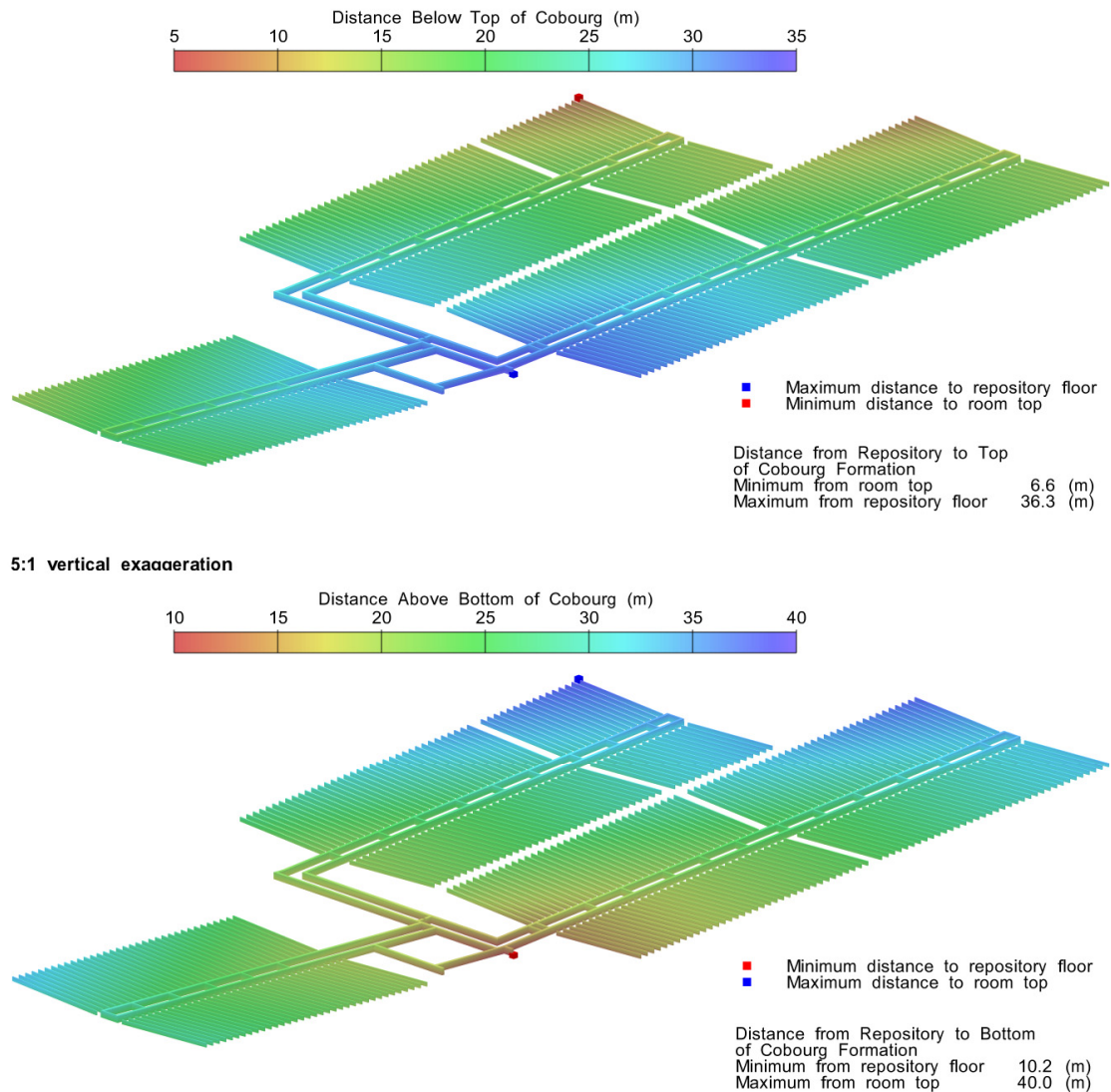


Figure 7-18: Main and Detailed Transport Model Setting

With the exception of shafts and shaft access ramps, the repository is located entirely within the Cobourg formation. The Cobourg formation dip is oriented roughly perpendicular to the main access tunnels and parallel to the placement rooms. Distances from the repository room and tunnel openings to the top and bottom of the Cobourg formation are shown in Figure 7-19.



08 Feb 2018
DetailedProperties.mView

Figure 7-19: Distance from Top and Bottom of Cobourg Formation to Repository

Properties of the engineered barrier system are shown in Table 7-32. Within the repository, EDZ properties are taken as multiples of the properties of the host rock. All repository tunnels and placement rooms have an Inner EDZ with hydraulic conductivity 100 times higher than the host rock, and porosity twice that of the host rock. Outer EDZ is assigned hydraulic conductivities 10 times greater than the host rock, while porosity is set equal to the host rock.

An Inner and Outer EDZ is defined for the shafts as well, with Inner EDZ having hydraulic conductivity 100 times greater than that of the host rock and Outer EDZ conductivity increased by a factor of 10 relative to the host rock. Inner EDZ porosity is doubled compared to the host rock. Shaft Inner and Outer EDZ are specified for all formations with shaft presence except for the overburden / drift. All other EDZ parameters are set equal to those of the host rock.

Table 7-32: Main and Detailed Transport Model Engineered Barrier Hydraulic Properties

Property Identifier	Description	Hydraulic Conductivity (m/s)	Porosity
Tunnel Dense Backfill	Used to backfill repository tunnels	1.0×10^{-10}	0.195
Tunnel Seal Bentonite (Compacted Bentonite)	Used for room seals	5.0×10^{-12}	0.416
Placement Room Bentonite (Homogenized Buffer)	Homogenized mixture of gap fill, buffer box, and spacer blocks in placement rooms at 85C	1.5×10^{-11}	0.416
Concrete, degraded	Low Heat High Performance Concrete (LHHP) used for room closure and shaft bulkheads	1.0×10^{-10}	0.1
Shaft Bentonite/Sand	Primary Shaft Seal material, 70:30 bentonite to sand	4.0×10^{-11}	0.375
Shaft Asphalt	Additional shaft sealing material	1.0×10^{-12}	0.02

Domain

Tracer simulations were performed for 10 Ma with all nodes within the repository volume at the repository elevation set to a constant unitless value of 1.0. Results at 10 Ma, shown in Figure 7-20, indicate that 99% of surface discharge (by flux) occurs within the interval between the repository and 15 km to the north. The lateral extents are exaggerated by the high dispersivity (750 m to 1000 m) required in the permeable formations for numeric stability of transport simulations using the large discretization of the Subregional Flow Model. It should be noted that Figure 7-20 is for a steady source concentration and non-decaying tracer for the purpose of defining model boundaries only.

These tracer results were used to define the Main Transport Model domain, which is set to the limits shown in Figure 7-20.

The Detailed Transport model domain is approximately 9.8 km x 9 km, roughly centred on the main shaft grid origin.

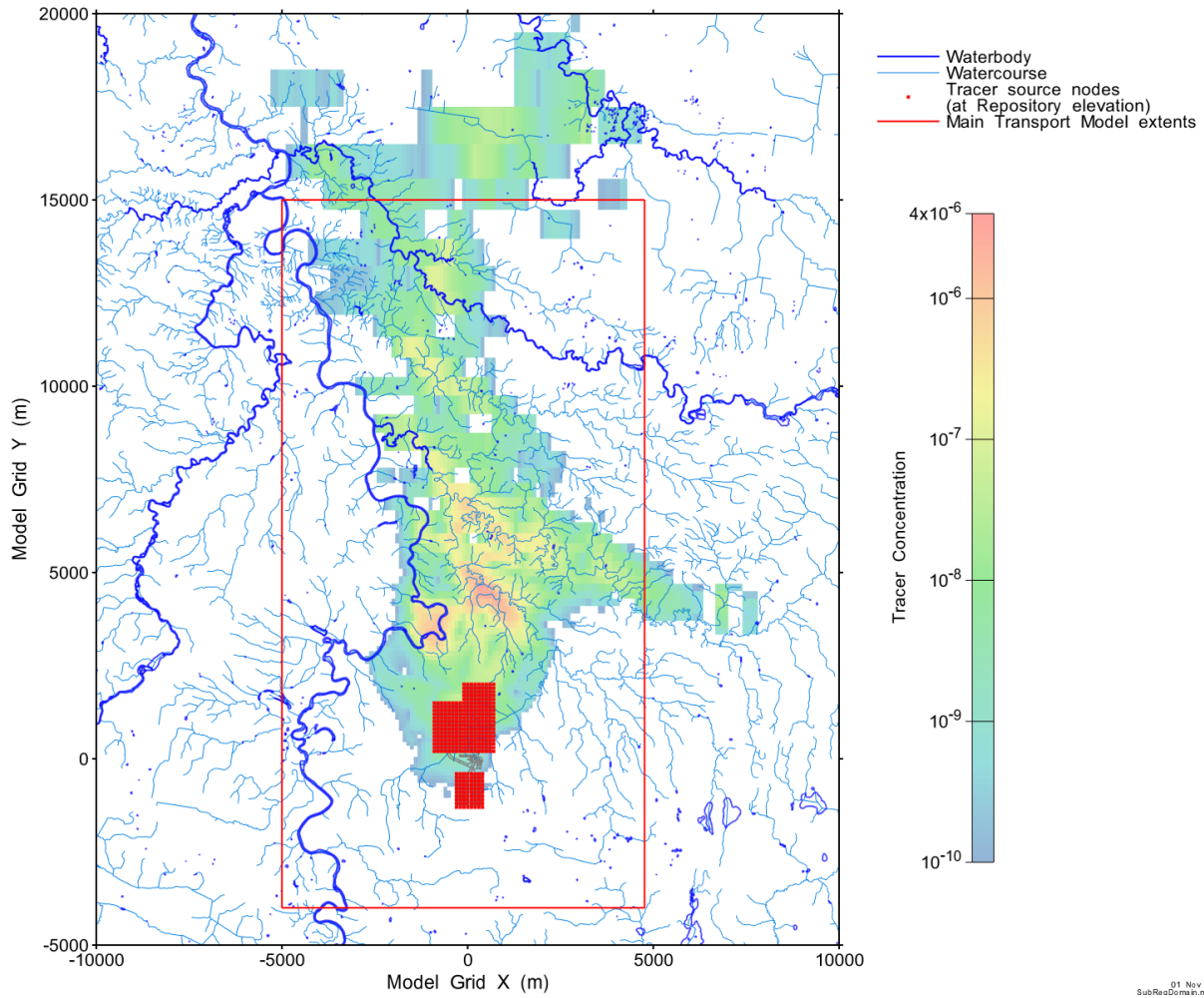


Figure 7-20: Subregional Flow Model: Relative Tracer Concentration at Surface

Tracer simulations were also run with the Main Transport Model to confirm the domain. As shown in Figure 7-21, results were spatially consistent with the Subregional Flow Model results, with discharge focussed on surface water features. Tracer concentrations at surface are significantly lower than those for the Subregional Flow Model, likely due to the reduced dispersivities (100 m in permeable formations) possible with the more refined grid.

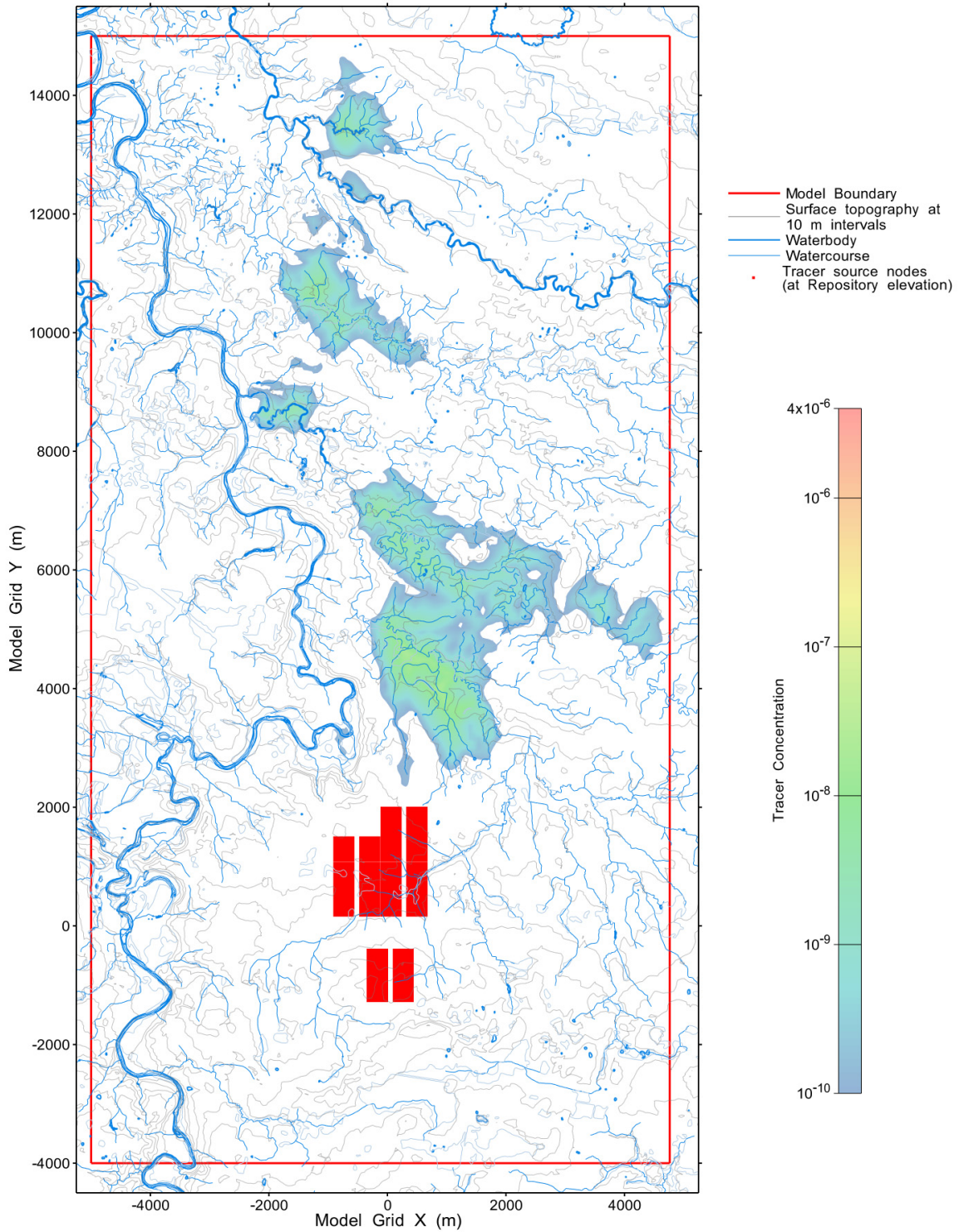


Figure 7-21: Main Transport Model: Relative Tracer Concentration at Surface

Discretization

In addition to the differences in domain extents, there are significant differences in horizontal discretization between the Main and Detailed Transport Models (Figure 7-22) which reflect the different features included in each model. The Main Transport Model has 147,250 elements in each layer (251 X nodes, 590 Y nodes), while the Detailed Transport Model contains 412,224 elements (457 X nodes, 905 Y nodes) per layer.

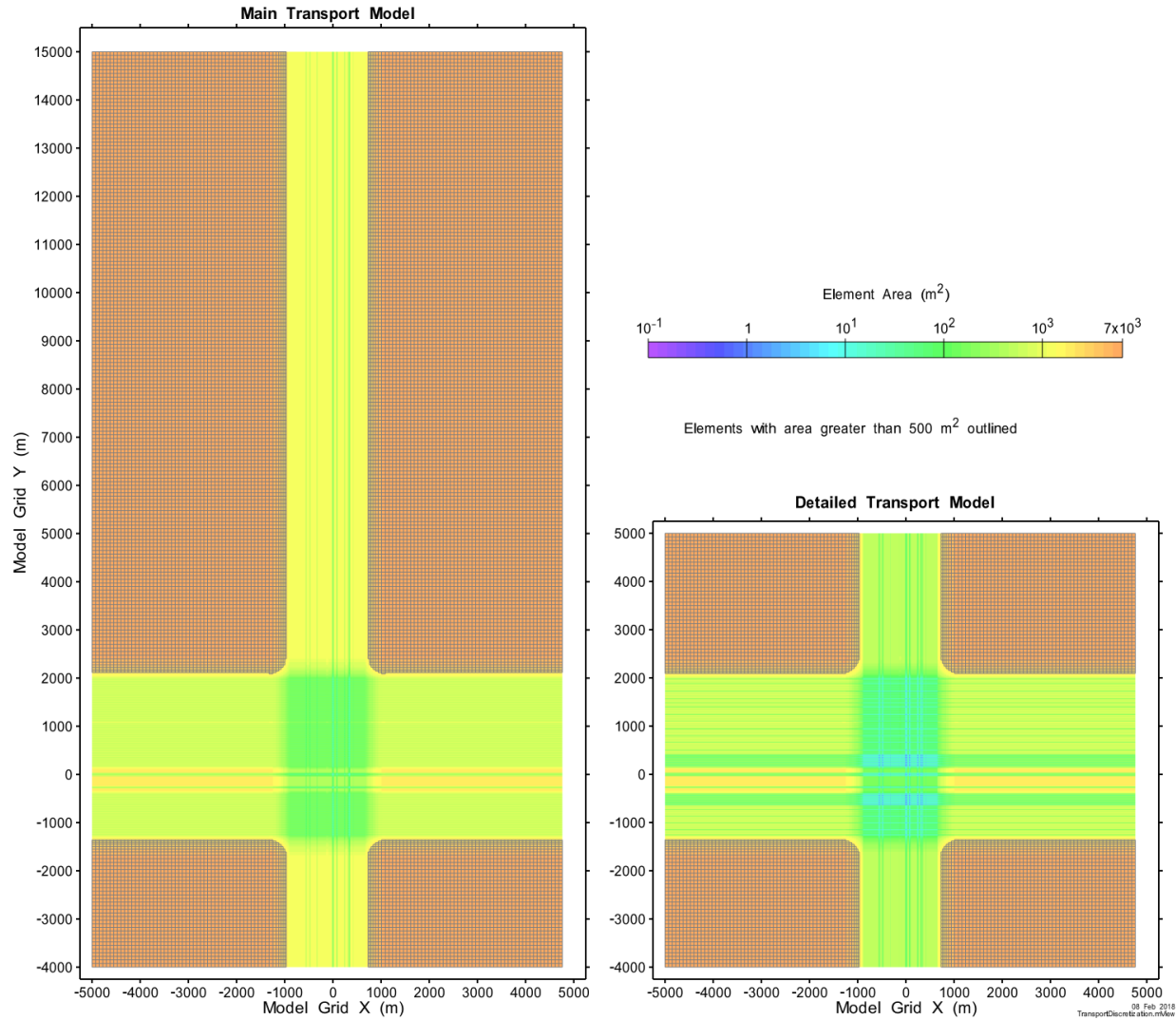


Figure 7-22: Main and Detailed Transport Models: Plan Discretization

The vertical discretization of the two models is similar except in the immediate vicinity of the repository, where the Detailed Transport Model has additional layers to incorporate the heights for seal features not included in the Main Transport Model. Figure 7-23 illustrates overall vertical discretization, while Figure 7-24 shows property assignments including repository

features, over the full three dimensional domain. There are 87 layers in the Main Transport Model and 93 layers in the Detailed Transport Model, yielding 12.88M elements for the Main Transport Model and 37.92 M elements for the Detailed Transport Model.

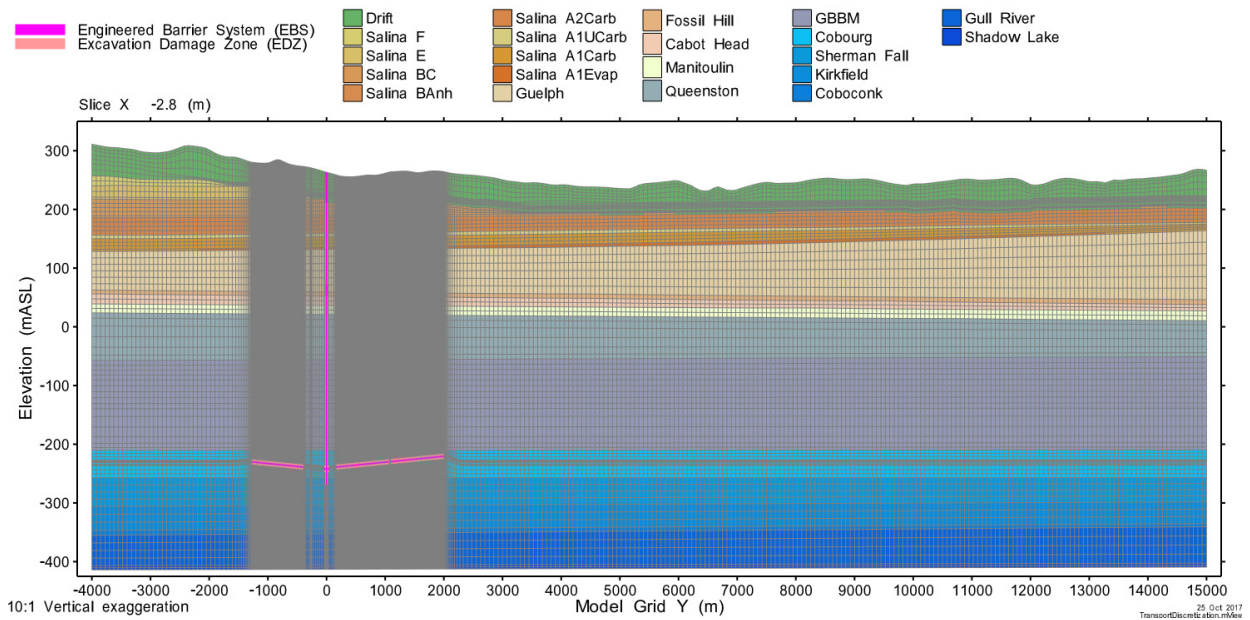


Figure 7-23: Main Transport Model: Vertical Discretization

Figure 7-24 shows property assignment details on a vertical slice through a placement room and connecting tunnel for the Main and Detailed Transport Models. The room seal in the Detailed Transport Model intercepts the Inner EDZ and has a 0.1 metre thick Inner EDZ over the seal. The Inner and Outer EDZ for the Detailed Transport Model have the same properties assignments for both rooms and tunnels. For the Main Transport Model, each EDZ assignment is different to reflect differences in property scaling required to approximate the full EDZ (surrounding the opening) with EDZ implemented only at the top and bottom of each opening. The simplification of the EDZ is largely responsible for the decreased number of elements in the Main Transport Model, compared to the Detailed Transport Model.

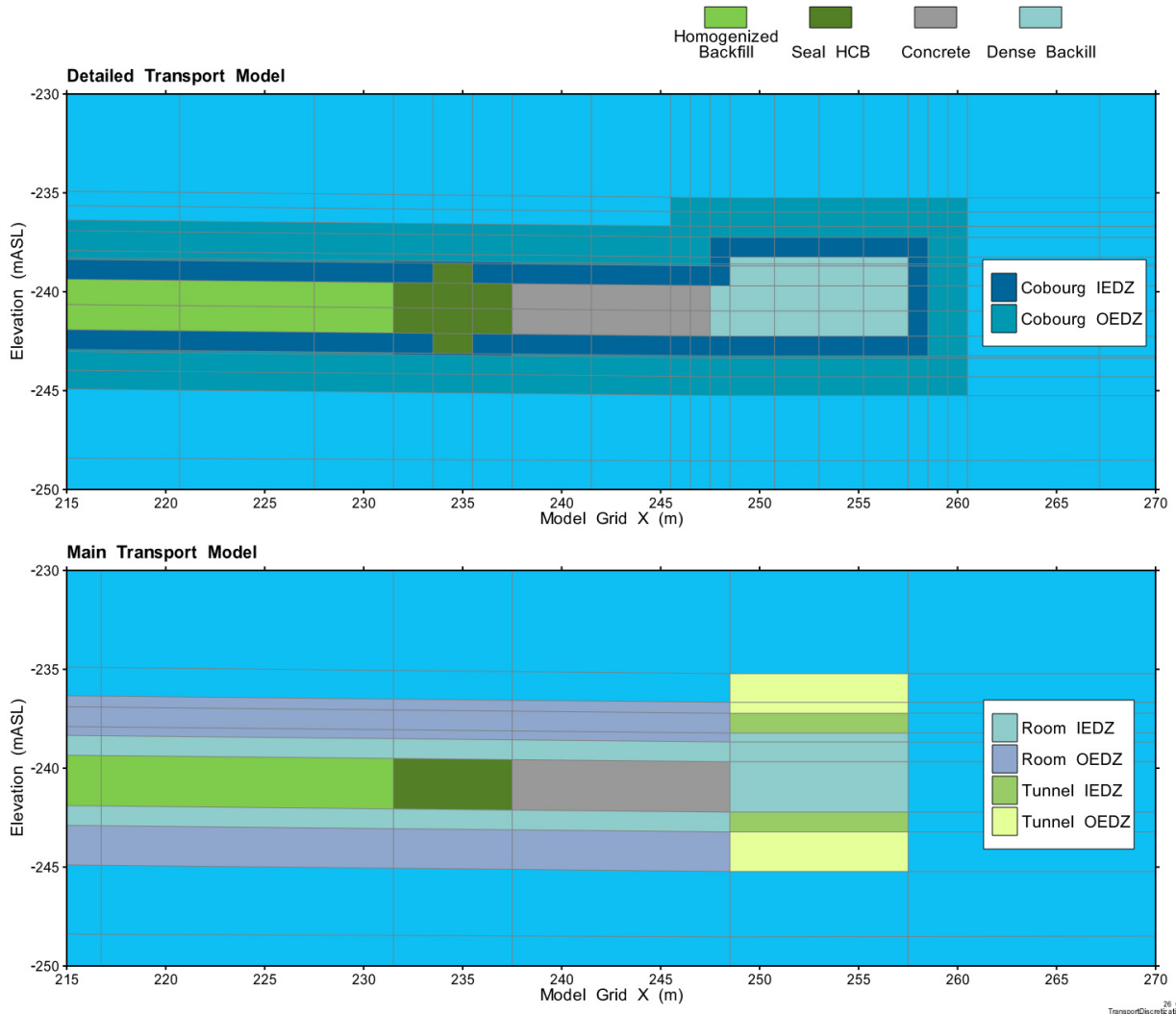


Figure 7-24: Main and Detailed Transport Models: Detailed Vertical Discretization

Detailed Transport Model discretization and property assignments are further described in Figure 7-25 and Figure 7-26. Figure 7-25 also shows the repository design layout to indicate the simplification in modelled tunnel location and orientation applied to the central services area. Note that all shafts are modelled at their design locations. As seen in the figures, only a limited number of placement rooms include both Inner and Outer EDZ on all sides of the room. These rooms include all rooms where defective container sources will be placed, and rooms adjacent to the selected source rooms. All other placement rooms do not have Inner and Outer EDZ on the vertical sides of the room. Instead, Inner and Outer EDZ above and below the rooms are implemented with modified hydraulic conductivity properties to provide the same conductivity x area term as would be present for fully discretized rooms, similar to the approach used by the Main Transport Model for all placement rooms.

The Detailed Transport Model discretization was finalized and refined subsequent to the well and source location simulations described in Section 7.7.2.3.2.

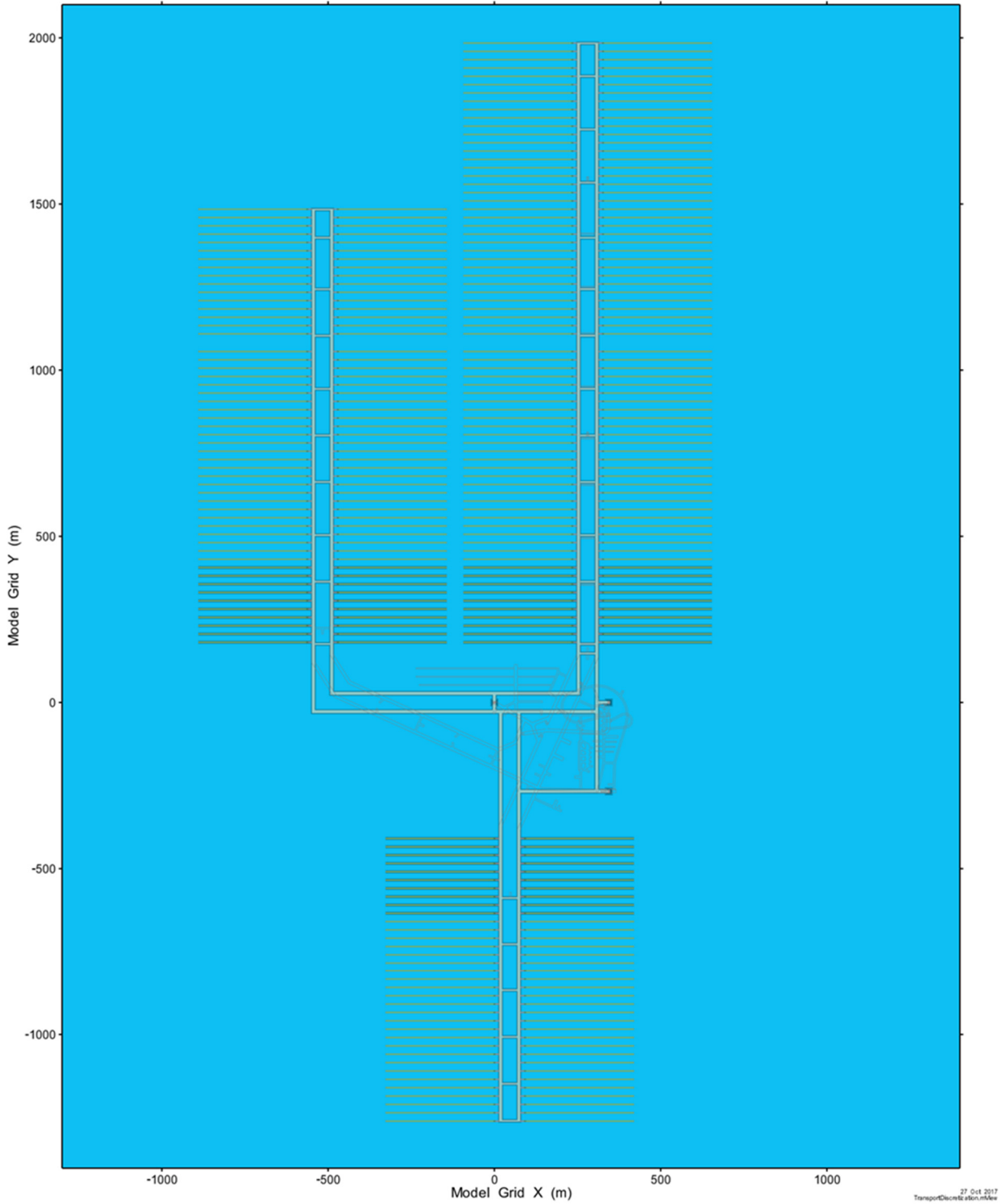


Figure 7-25: Detailed Transport Model: Plan View of Repository Property Assignment

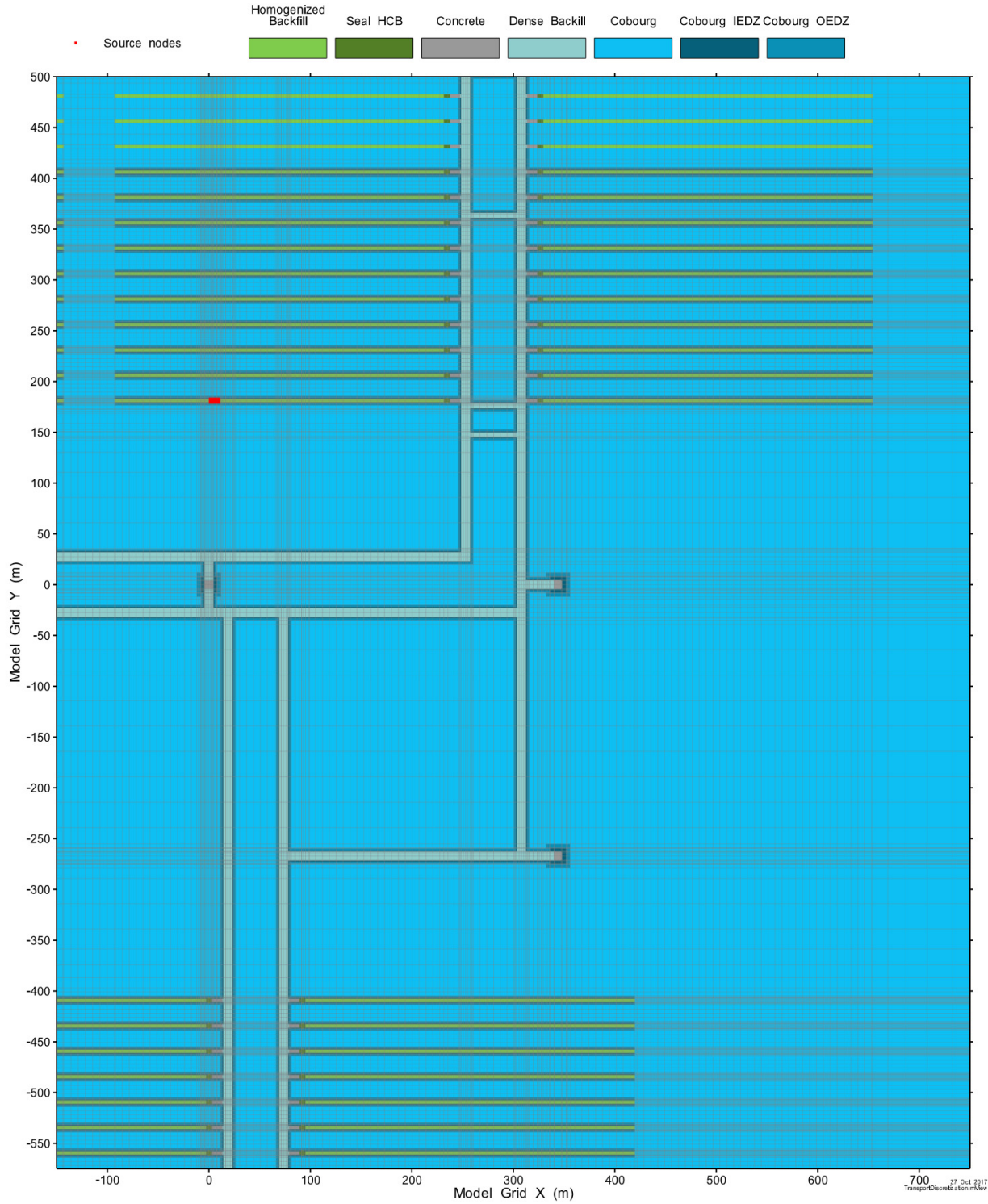


Figure 7-26: Detailed Transport Model: Detailed Plan Discretization Showing Seal Implementation

Figure 7-26 (above), Figure 7-27 and Figure 7-28 show example source nodes where radionuclides are injected for transport simulations. The source location shown is for the Base Case where the source nodes are at the room location close to the main shaft. Source nodes are placed at the interface between the EBS and Inner EDZ, and have a horizontal extent approximately equal to 10 adjacent containers. For the Detailed Transport Model, the source term is equally divided across 56 nodes at each source location, while there are eight source nodes at each source location in the Main Transport Model due to its coarser horizontal discretization.

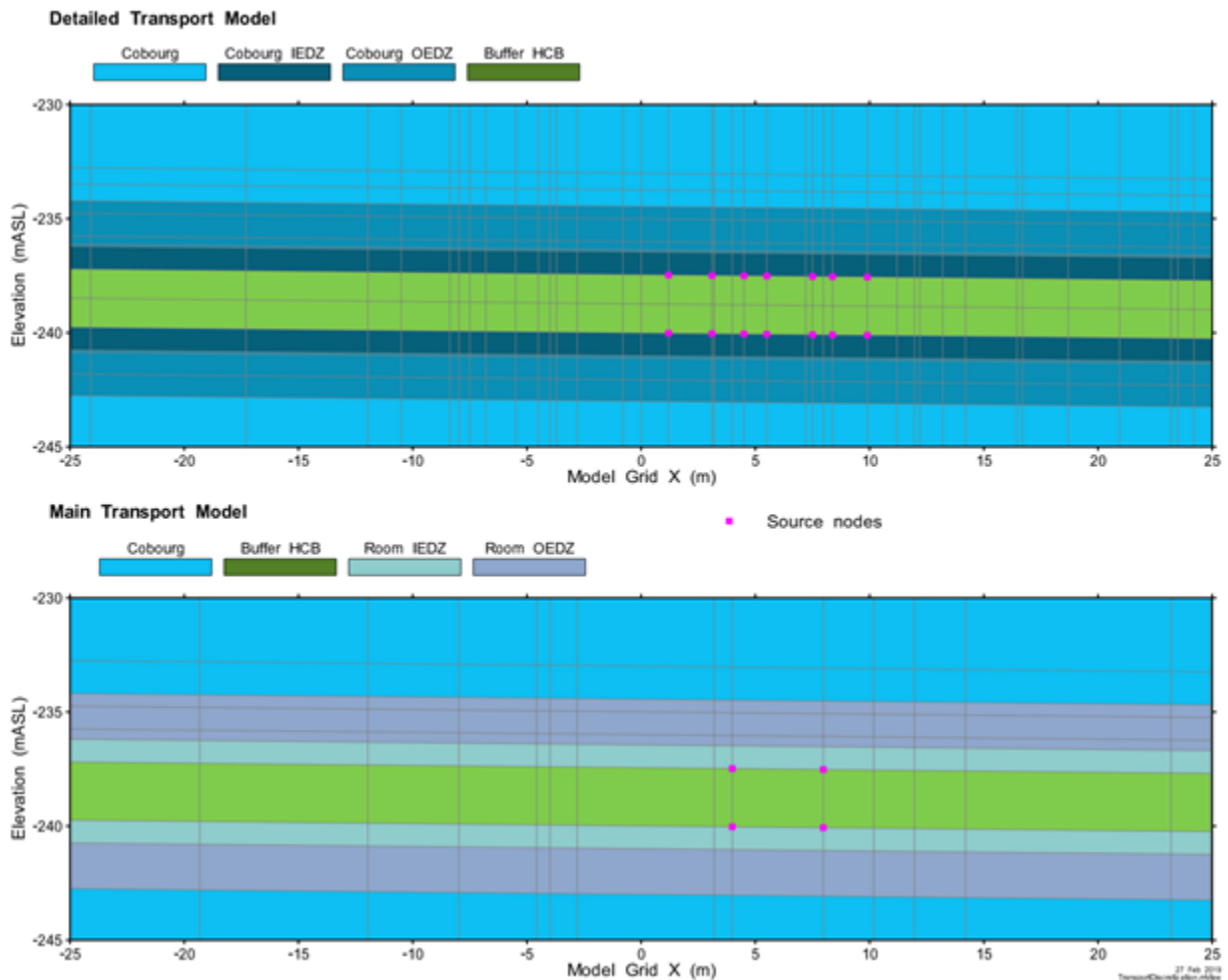


Figure 7-27: Main and Detailed Transport: Source Node Locations and Discretization

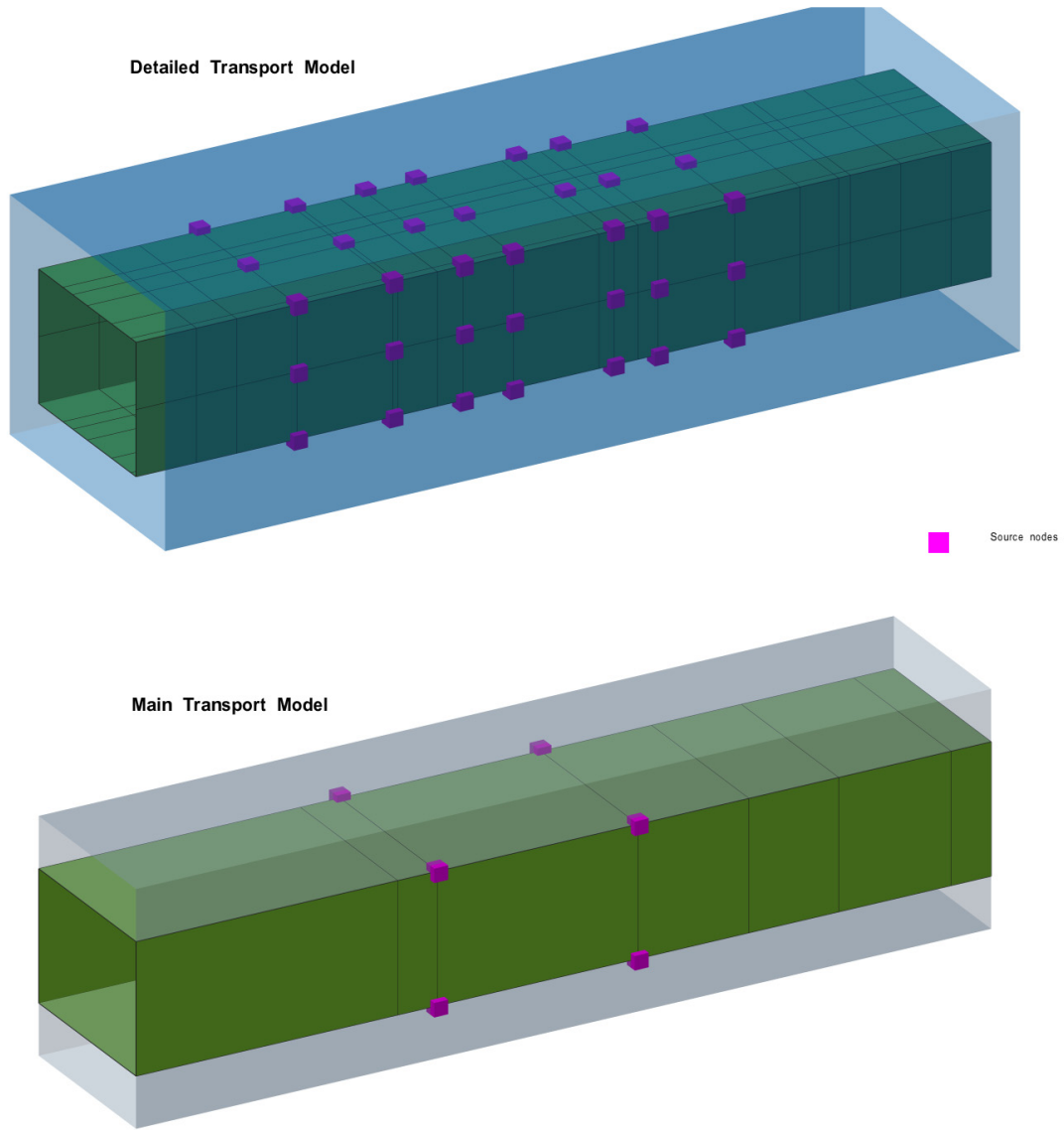


Figure 7-28: Main and Detailed Transport: 3D View of Example Source Nodes

Figure 7-29 shows the main shaft and seals for the Detailed Transport Model.

Both models use a similar property assignment, although the Main Transport Model discretization is less refined.

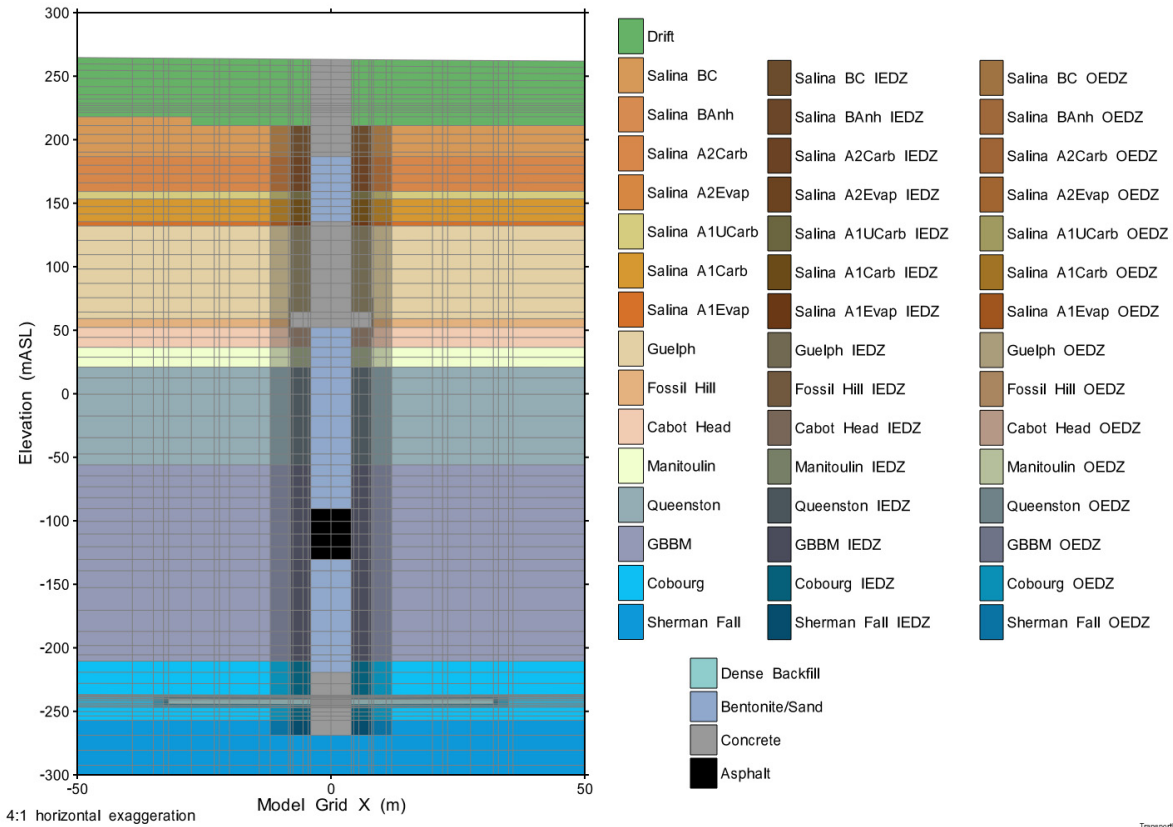
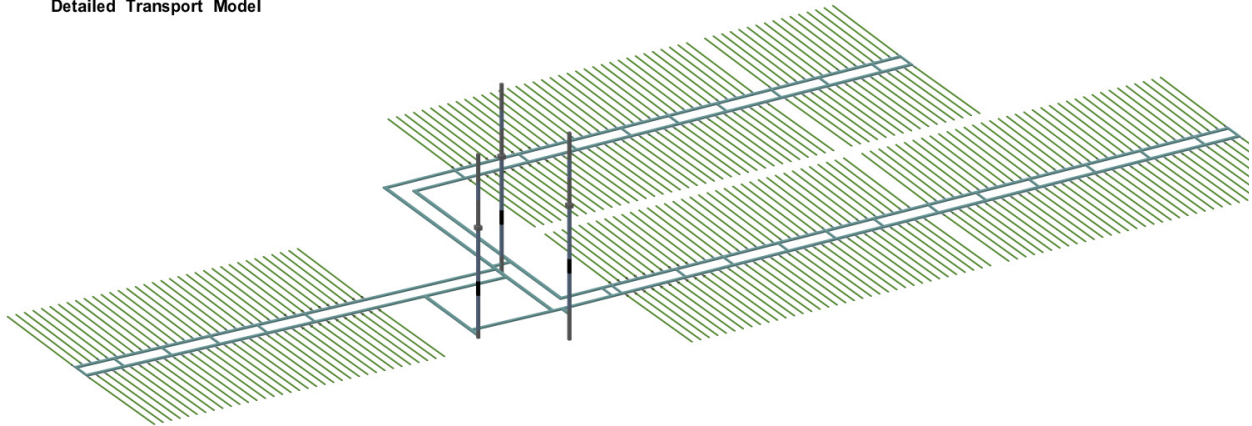


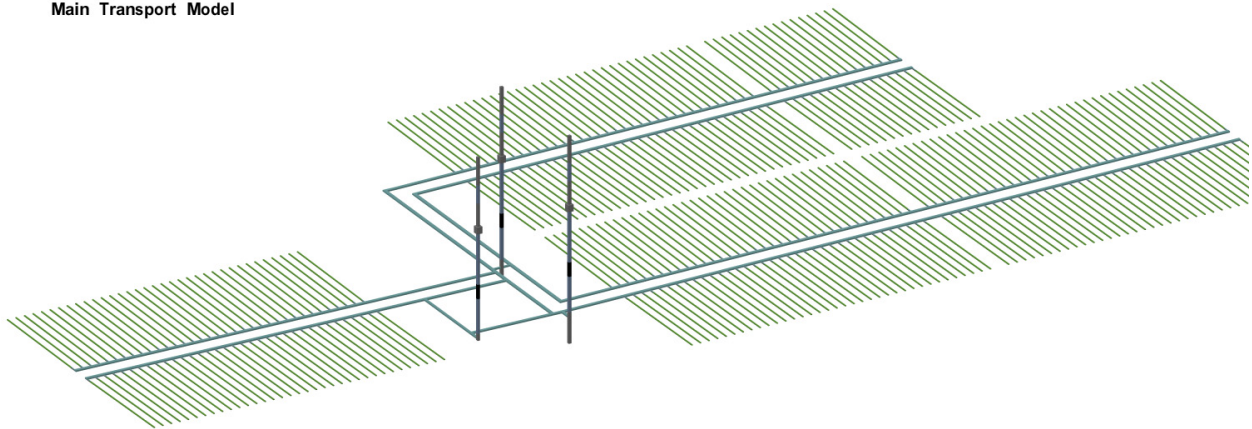
Figure 7-29: Detailed Transport Model: Vertical Slice Showing Shaft and Seals

As shown in Figure 7-30, both Main and Detailed Transport models offer a fairly complete representation of the repository, with the primary difference in layout being the inclusion of cross tunnels in the Detailed model.

Detailed Transport Model



Main Transport Model



28 Oct 2017
Transportation

Figure 7-30: Main and Detailed Transport Models: Three Dimensional View of Repository Features

Water Supply Well

The location of the water supply well is determined concurrently with the location of the defective containers and is described in detail in Section 7.7.2.3.2. Wells are screened over the entirety of the Guelph formation at a depth of approximately 130 to 200 mBGS.

The well is a 2D line element forming a segment, or edge, of a 3D element. Properties consistent with a nominal 6" diameter well are assigned to the segment to specify the hydraulic conductivity of the well. The lowest node on the segment is defined as the withdrawal node from which water is abstracted.

Hydraulic Head Boundary Conditions

All model top surface nodes are assigned fixed head boundary conditions at topographic elevations. With the exception of the Overpressure sensitivity case, model bottom boundary conditions are set to zero flow. Fixed head boundary conditions at vertical model sides (and the bottom for the Overpressure case) are interpolated from head fields calculated with the Subregional Flow Model. Boundary conditions are calculated separately for each well demand and for each high consequence well location.

7.7.1.3 Container Transport Model

The Container Transport Model encompasses a small section of the repository surrounding the defective container location and the immediately adjacent geosphere. The model incorporates significant detail and individual containers are represented. The model is used to generate source terms that include the effects of the EBS for input to the Main and Detailed Transport Models.

The location of the model with respect to the overall repository domain is shown in Figure 7-31.

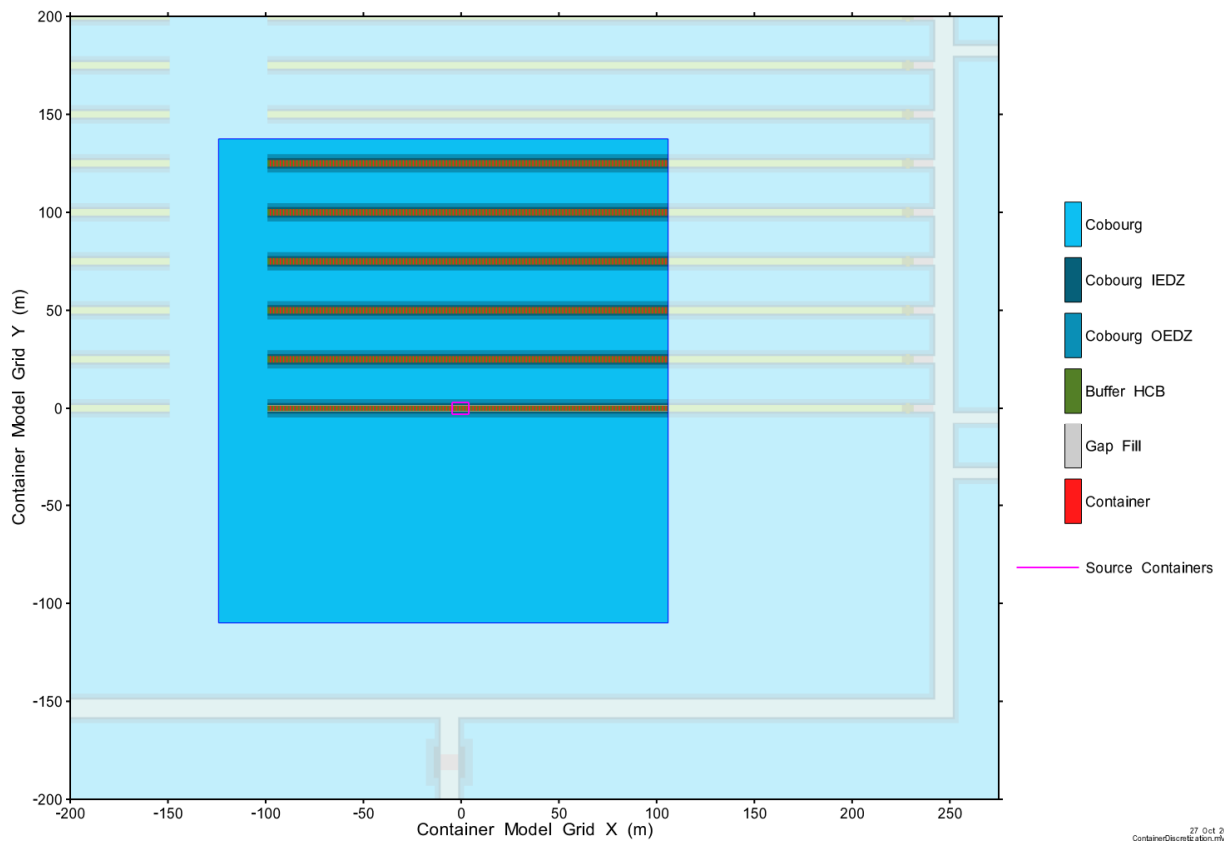


Figure 7-31: Container Transport Model: Location in Repository

Domain Discretization and Property Assignment

The model has a plan area of approximately 230 m by 250 m. The domain includes the specified defective container location and any adjacent repository features that may affect the flow system around the defective containers.

Vertically, the model domains extends from 120 m below the repository (-360 mASL) to 150 m above the repository (-94 mASL). The domain is entirely within the Ordovician formations with the lower boundary in the Gull River formation and the upper boundary within the Georgian Bay / Blue Mountain formation.

The placement rooms and engineered barrier system are discretized at differing levels of detail. The room containing the radionuclide source is discretized at the highest level and contains representations of the containers in the room. Detailed property assignments for plan and vertical slices along the room centre line and vertical slices perpendicular to the room are presented in Figure 7-32 through Figure 7-34. The discretization includes a basic representation of the room cross-section and associated EDZ with in-room EBS components (container, gap fill, buffer box) individually discretized. The 1% drainage slope is incorporated in the discretization. The property assignments used in simulations replace individual bentonite-based room EBS components with homogenized buffer material properties. Variations in room

width and height due to construction methods are not incorporated and defined average room widths and heights are used.

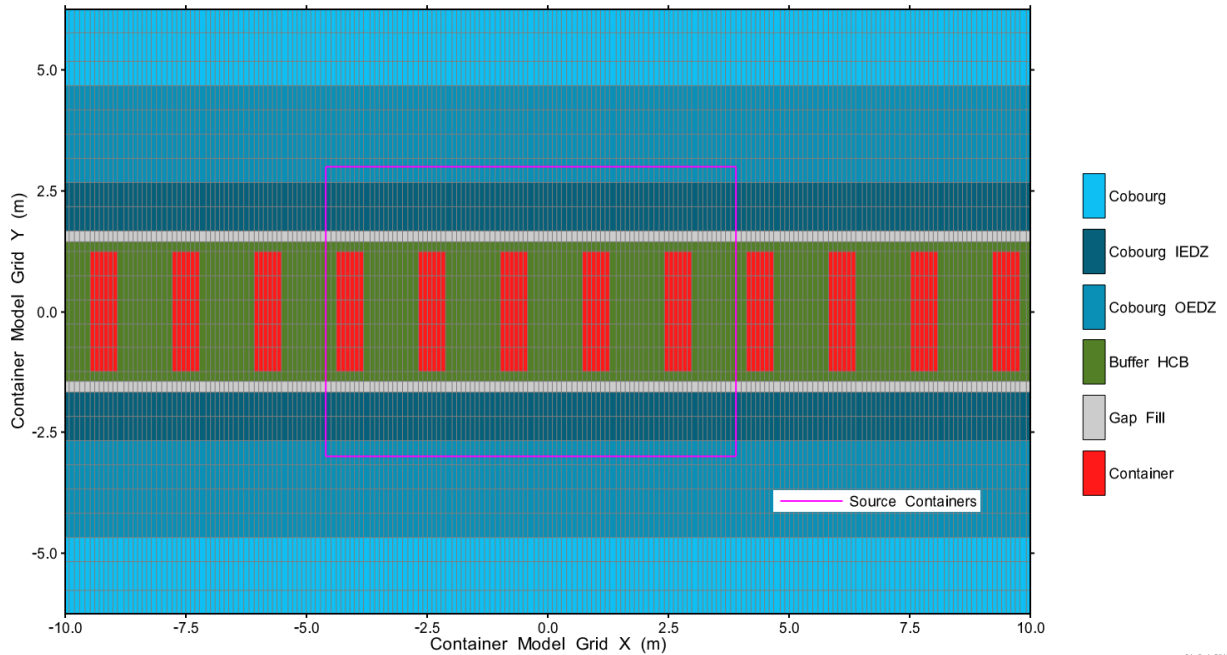


Figure 7-32: Container Transport Model: Plan Property Assignment through the Source Placement Room

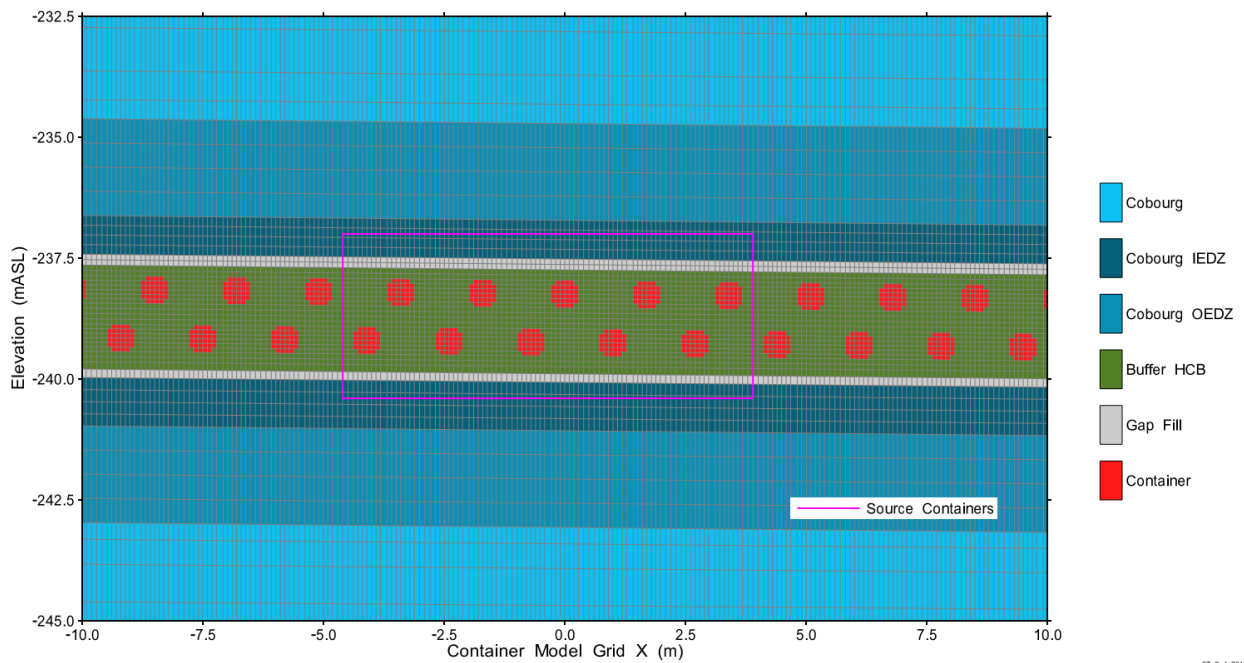


Figure 7-33: Container Transport Model: Vertical Property Assignment Parallel to the Source Placement Room

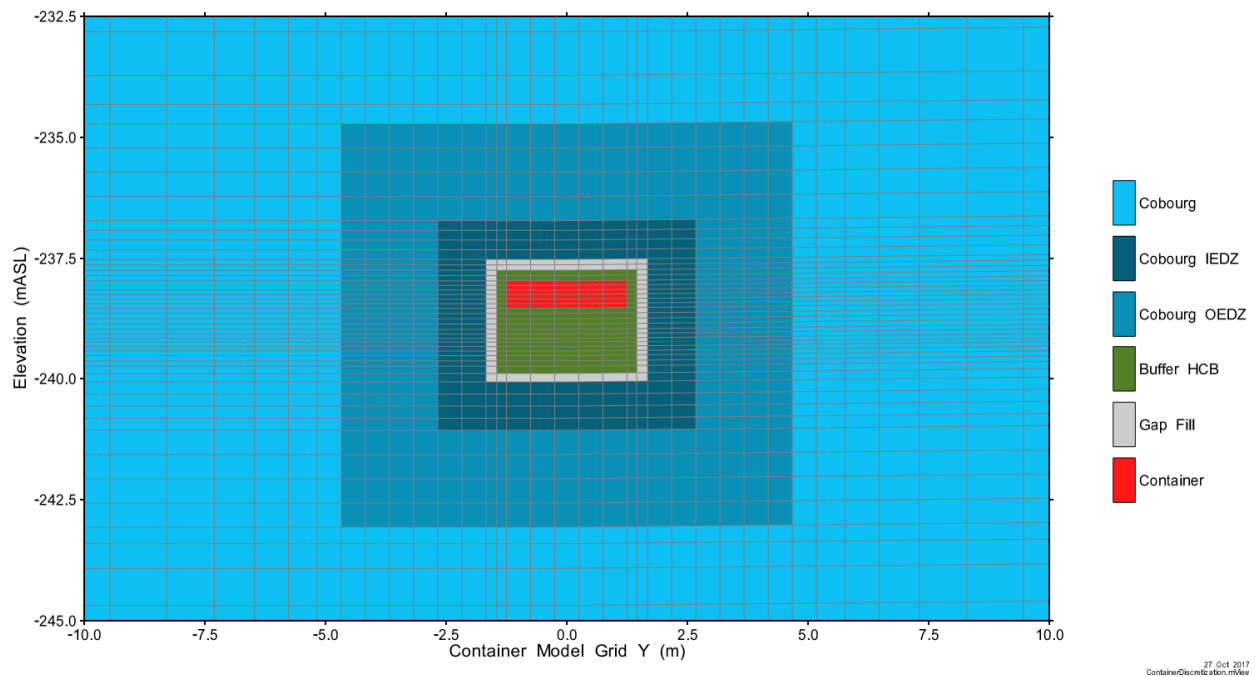


Figure 7-34: Container Transport Model: Vertical Property Assignment Perpendicular to the Source Placement Room

Figure 7-35 illustrates a section in the middle of a placement room assumed to contain defective containers. There are 144 source nodes allocated over the surface of each container. The figure also shows the transport boundary over which the release from 10 containers is integrated, for use as a source term in the Main and Detailed Transport Models. EBS and EDZ elements are shown in Figure 7-36.

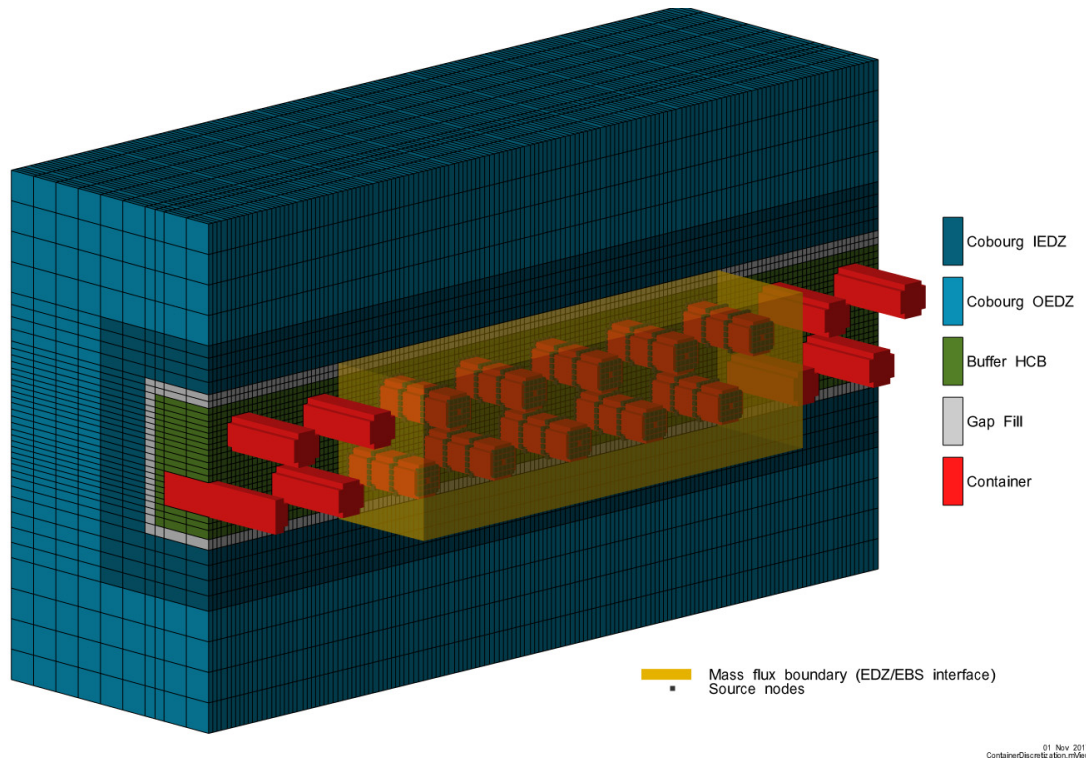
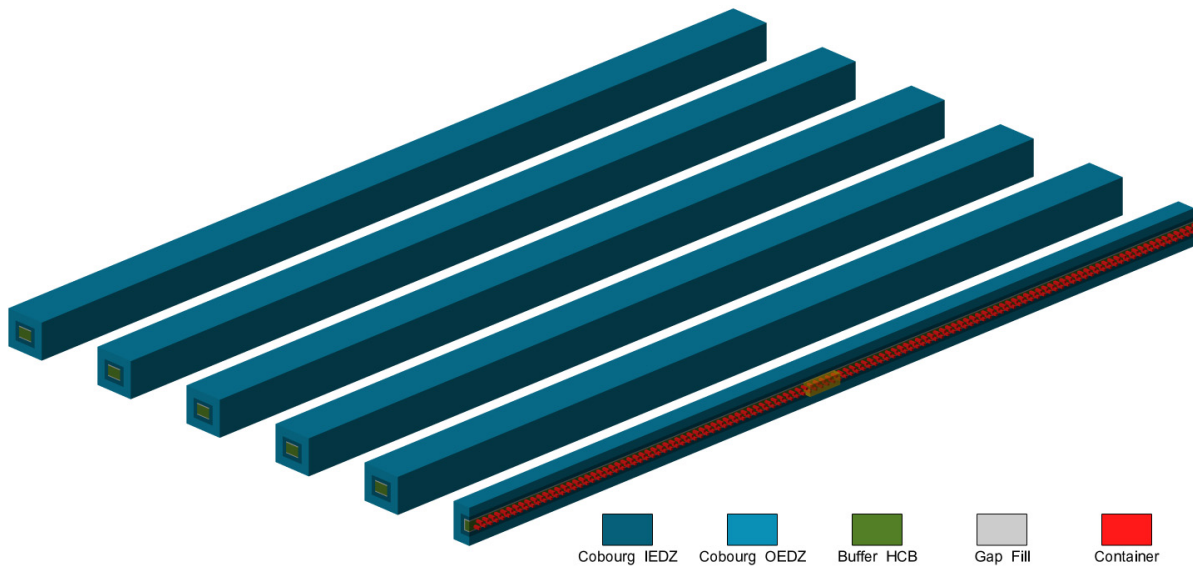


Figure 7-35: Container Transport Model: 3D View of EBS and EDZ near Source Containers

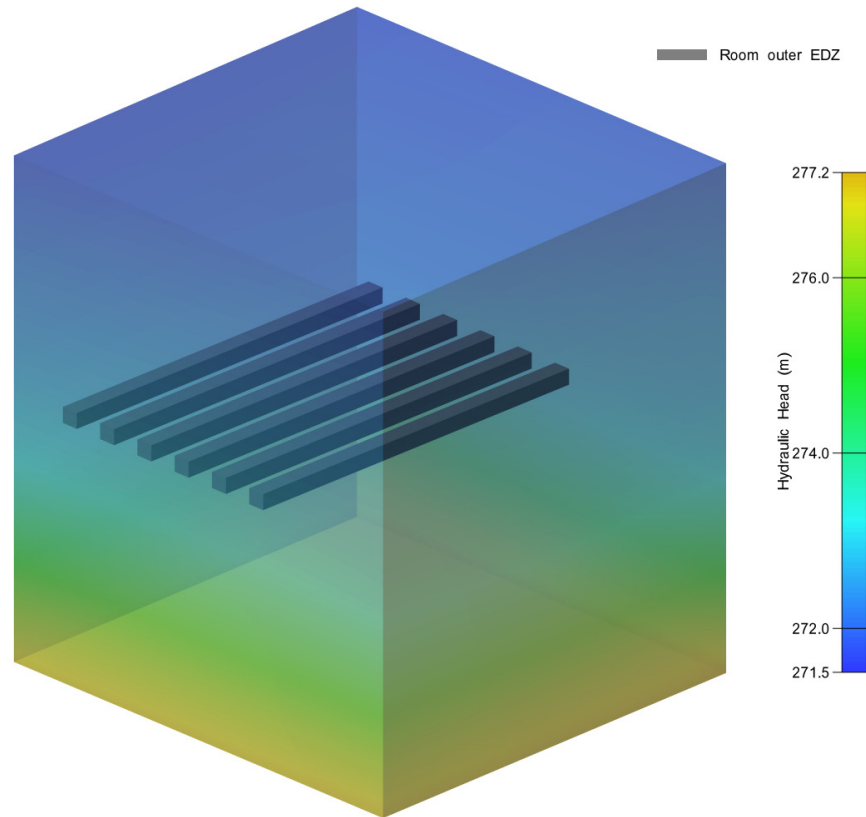


Source room cutaway to illustrate containers

Figure 7-36: Container Transport Model: 3D View of EBS and EDZ

Hydraulic Head Boundary Conditions

Head boundary conditions are extracted from the Detailed Transport Model and values are specified for all external model nodes. Base Case boundary conditions for the Container Transport Model are shown in Figure 7-37.



05 Feb 2018
ContainerDiscretization.mxd

Figure 7-37: Container Transport Model: 3D View of Base Case Head Boundary Conditions

7.7.2 Results

This section presents results of the detailed 3D groundwater flow and radionuclide transport analysis performed for the Base Case of the Normal Evolution Scenario and selected sensitivity studies.

Radionuclide transport is calculated for the Base Case for I-129, Cl-36, Cs-135, and U-238. These radionuclides are typically the most important in terms of potential radiological impact or in representing a range of low-sorption to high-sorption species. Radionuclide transport for most of the other sensitivity cases is calculated for I-129 only. This is because, as will be seen later in Section 7.8.2.1, I-129 is the overwhelmingly dominant contributor to dose.

Section 7.2.1.3 and Table 7-4 present the list of sensitivity cases developed to illustrate the effect of well assumptions and Section 7.2.1.4 and Table 7-5 present the list of sensitivity cases developed to illustrate the effect of deviations in barrier performance. Of these, a number of cases have the potential to affect the groundwater flow field and are therefore not amenable to modelling with the System Model (i.e., the System Model is based on the constant groundwater flow field associated with the Base Case). As a consequence, the following cases are simulated with the 3D Groundwater and Radionuclide Transport code:

- Hydraulic conductivities of the engineered barrier system (EBS), increased by a factor of 10;
- Hydraulic conductivities of the host rock increased by a factor of 10;
- Hydraulic conductivity in the excavation damaged zones (EDZ) increased by a factor of 10;
- 100 m of surface erosion;
- 150 m overpressure in the Shadow Lake Formation;
- Intermittent well operation; and
- Random well operation.

Section 7.2.1.5 and Table 7-6 also present a list of sensitivity cases developed to illustrate the effect of various modelling attributes and parameters on the Base Case results. These cases, listed below, are also discussed in this section.

- Increased spatial resolution; and
- Increased and decreased number of time steps.

Figures show vectors describing the magnitude and direction of velocity of groundwater movement, or advective² velocity, only in locations where velocities are greater than 10^{-4} m/a.

A description of the various 3D models is provided in Section 7.7.1.

² Advective velocity is the Darcy velocity (i.e., the volumetric flow rate of water passing through a planar surface divided by the area of that surface) divided by the material porosity. The advective velocity therefore represents the velocity of the fluid within the pore spaces in the rock.

7.7.2.1 Subregional Flow Model Results

The Subregional Flow Model is used to determine:

- The groundwater flow field in the vicinity of the repository; and
- The boundary conditions for the Main and Detailed Transport Models.

No repository features are incorporated at this scale of resolution. The repository representation in the figures is provided solely to add context. The water supply well is also not represented.

Radionuclide transport calculations are not performed with this model.

7.7.2.1.1 Base Case – No Well Flow Results

Groundwater flow in the deep sedimentary geosphere is essentially stagnant. The extremely low permeability Ordovician shale and limestone show advective velocities of less than one micron per year (10^{-6} m/a). Figure 7-38 shows groundwater velocity magnitudes over the model domain. Within the immediate vicinity of the repository and the Cobourg formation (the repository volume shown in the figure), the maximum advective velocity is 9×10^{-8} m/a, or 90 cm in 10 Ma.

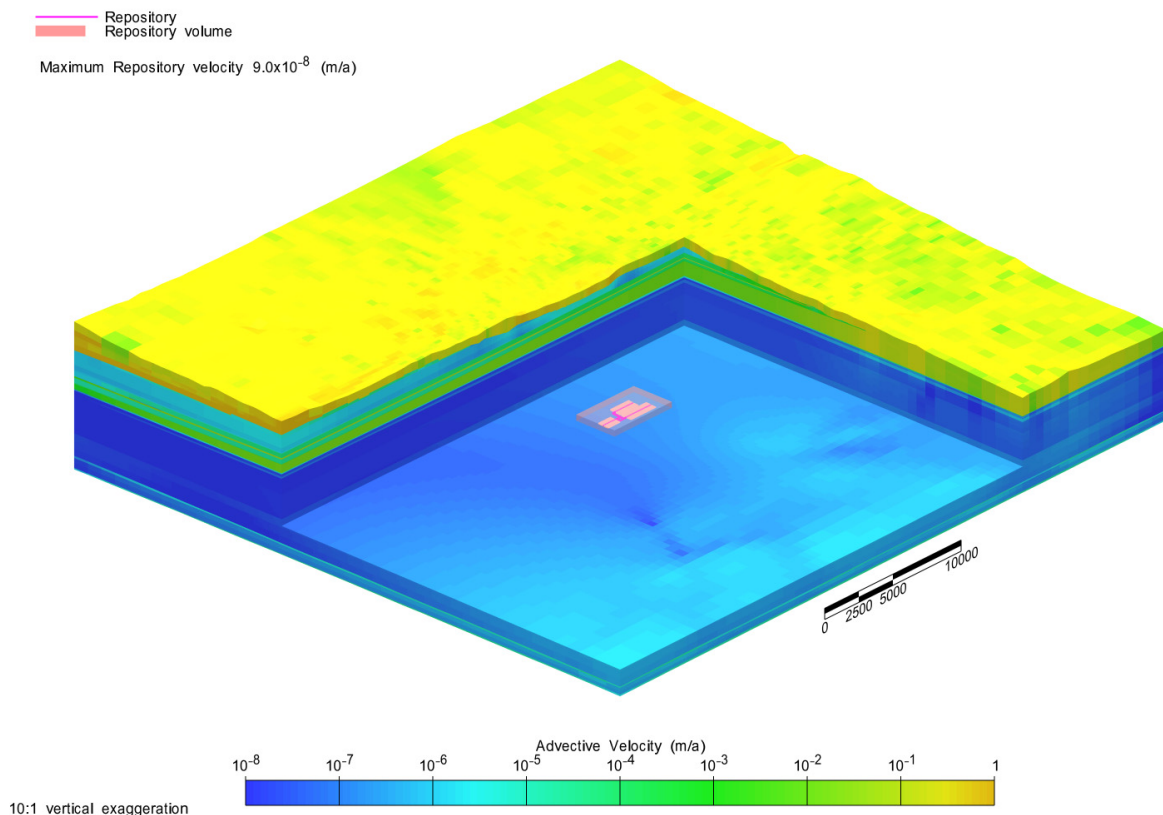
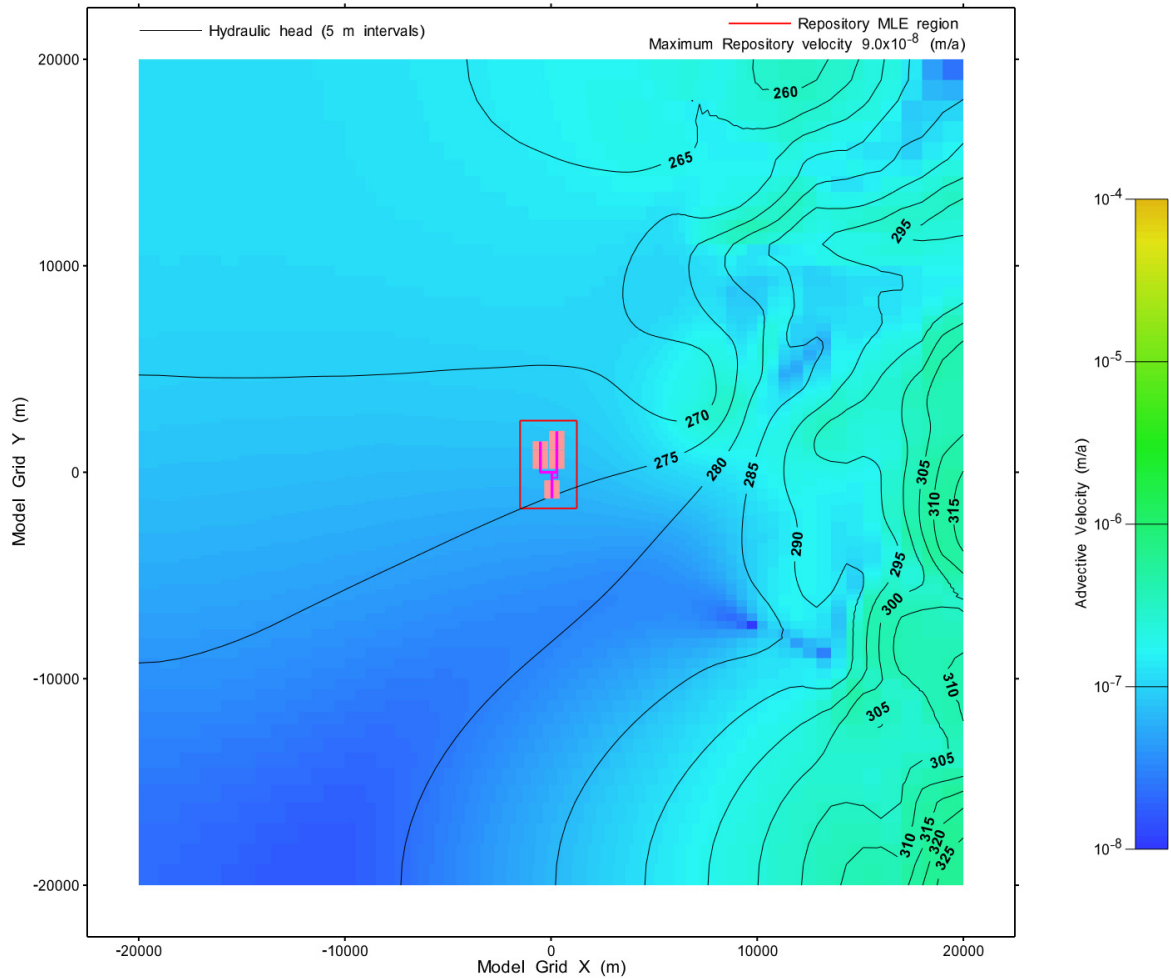


Figure 7-38: Subregional Flow Model: Base Case (No Well) - Advective Velocity

Velocities on plan sections through the Cobourg formations is shown in Figure 7-39.



31 Oct 2018
SubRegionalFlow.mxd

Figure 7-39: Subregional Flow Model: Base Case (No Well) - Advective Velocity and Hydraulic Head over a Horizontal Slice through the Cobourg Formation

Mean Life Expectancy (MLE) calculations account for advective, dispersive, and diffusive transport processes to provide an estimate of the mean travel time from any point in the model domain to exit from the model. For the Subregional Flow Model, all model boundaries except the upper surface are zero flow, meaning that MLE calculations are the mean time to surface discharge. MLE calculations on the Subregional Flow Model grid required fairly high dispersivity values for numeric stability. Low permeability formations were assigned a longitudinal dispersivity of 500 m, while formations with higher advective velocities were assigned 750 m and 1000 m. Results (Figure 7-40) show that the mean time to discharge from the repository volume exceeds 3.5×10^8 a.

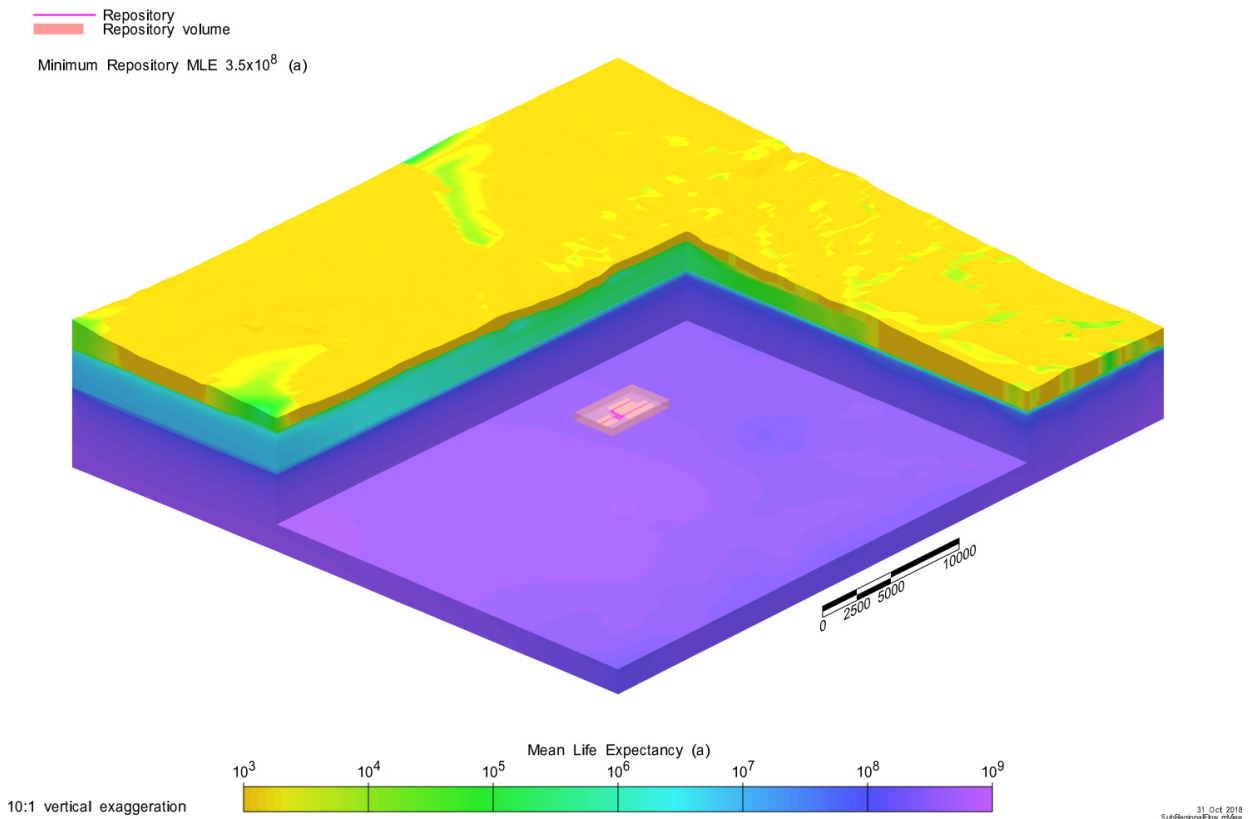


Figure 7-40: Subregional Flow Model: Base Case (No Well) - Mean Life Expectancy (a)

Mean Life Expectancy on a vertical slice (Figure 7-41) shows the sharp delineation between the low-permeability Ordovician system and the more permeable Guelph formation.

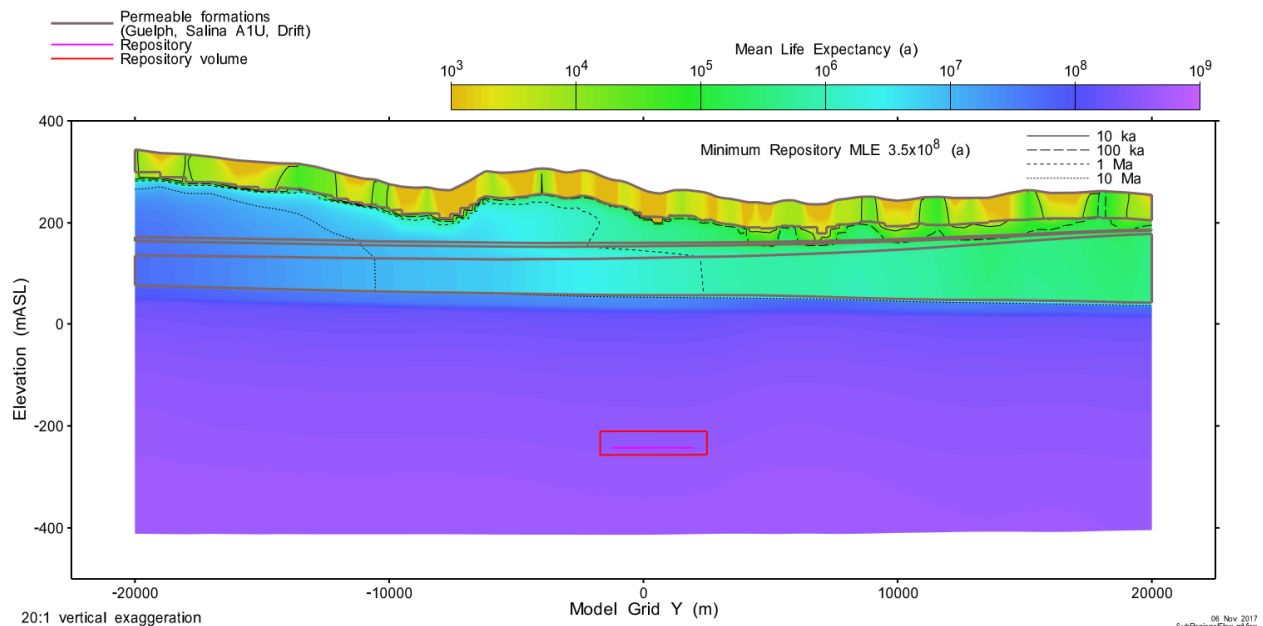


Figure 7-41: Subregional Flow Model: Base Case (No Well) - Mean Life Expectancy on a Vertical Slice through the Grid Origin

7.7.2.2 Main and Detailed Transport Models Flow Results

As described in Section 7.7.1.2, the Main Transport Model domain is an approximately 9.8 km x 19 km area that includes the repository and the portion of the subregional flow system into which groundwater flow from above the repository may travel and discharge to. The Main Transport Model includes a simplified description of the repository EDZ and EBS. In contrast, the Detailed Transport Model is limited to a 9.8 km x 9 km area that does not include the entire potential downgradient flow system discharge zones. The Detailed Transport Model incorporates a more detailed repository EDZ and EBS and is computationally much slower than the Main Transport Model.

The Main Transport Model is used to determine:

- Base Case flow results for simulations both with and without the well;
- High consequence well and container locations. These are the locations that result in the fastest and / or highest magnitude radionuclide transport to the well;
- Base Case and sensitivity case radionuclide transport results; and
- Advective transport pathway and tracer results for use in creating the System Model geosphere network.

The Detailed Transport Model is used for a more limited set of simulations:

- Base Case flow results for simulations both with and without the well;
- Base Case radionuclide transport results; and
- Boundary conditions for the Container Transport Models.

Main and Detailed Transport Model results are compared for identical cases to provide confidence in the results.

Radionuclide transport modelling for I-129, Cl-36, Cs-135, and U-238 is performed for the Base Case. Other cases typically consider only I-129 because, as will be seen later in Section 7.8.2.1, I-129 is the overwhelmingly dominant contributor to public dose.

Individual containers are not modelled at this scale of resolution.

Figures representing release time histories are shown with shading at times greater than one million years to emphasize that results at these times are illustrative and included only to indicate model behaviour.

7.7.2.2.1 Base Case – No Well Flow Results

Figure 7-42 shows a detailed view of the effect of repository features with a comparison of advective velocities between the Detailed Transport and Subregional Flow models. Velocities in tunnels are higher given the increased permeability of the tunnel backfill and EDZ compared to the intact rock. Velocities in the placement rooms to the north of the central services area are mostly slower, as the east-west oriented tunnels in the central services area are collecting flow and diverting it from the placement rooms to the access tunnels.

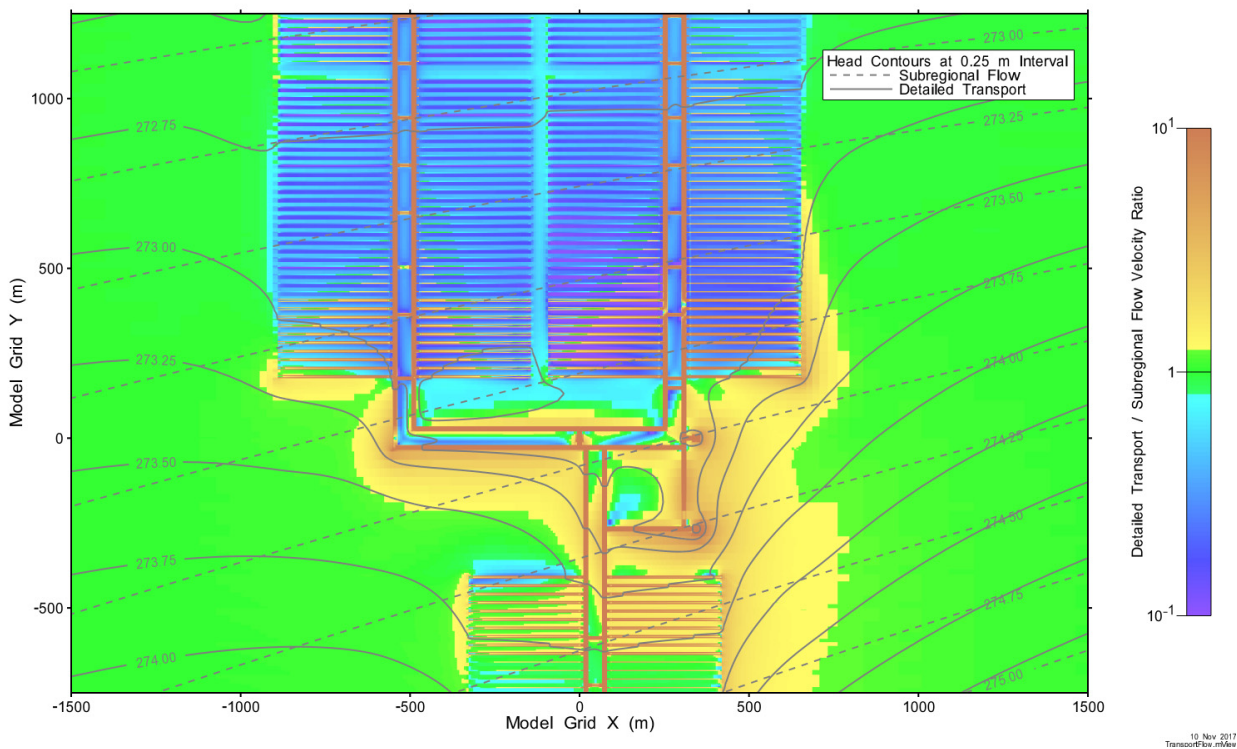


Figure 7-42: Detailed Transport Model: No Well Comparison of Hydraulic Heads and Advective Velocities With Subregional Flow Model at Repository Elevation

Differences between the Main and Detailed Transport Models are shown in Figure 7-43. Velocities are very similar throughout the footprint, except where the Detailed Transport Model has features (e.g., cross-tunnels, EDZ on the side of tunnels and rooms) that are not represented in the Main Transport Model.

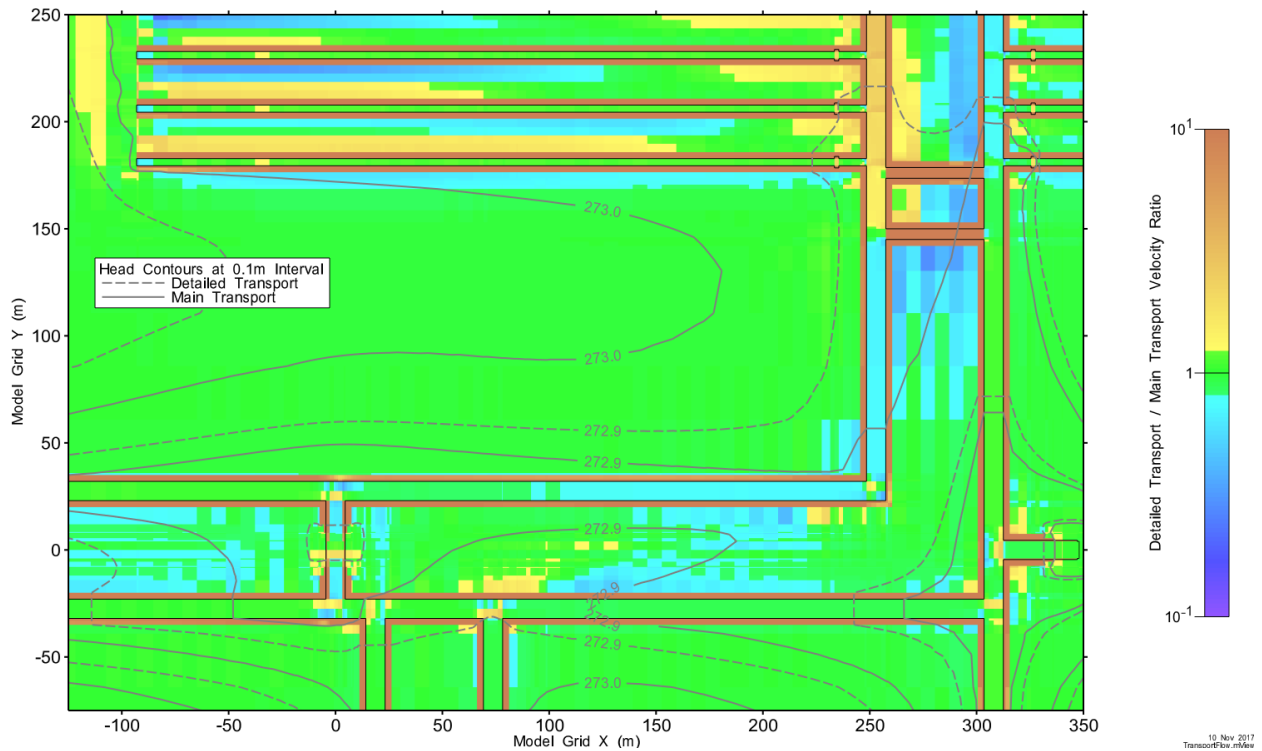


Figure 7-43: Main and Detailed Transport Models: No Well Comparison of Hydraulic Heads and Advective Velocities at Repository Elevation

Mean Life Expectancy for the Main Transport Model is compared to the Subregional Flow Model on a vertical slice along the Y axis in Figure 7-44. Results are similar in structure; however, the MLEs for the Main Transport Model are greater than for the Subregional Flow Model. This is due to differences in dispersivities between the models. Differences in grid size required larger dispersivities for numeric stability of the Subregional Flow Model. For example, dispersivities in the Guelph formation are 1000 m in the Subregional Flow Model and 100 m in the Main Transport Model. Larger dispersivities lead to larger dispersive flux and earlier discharge times.

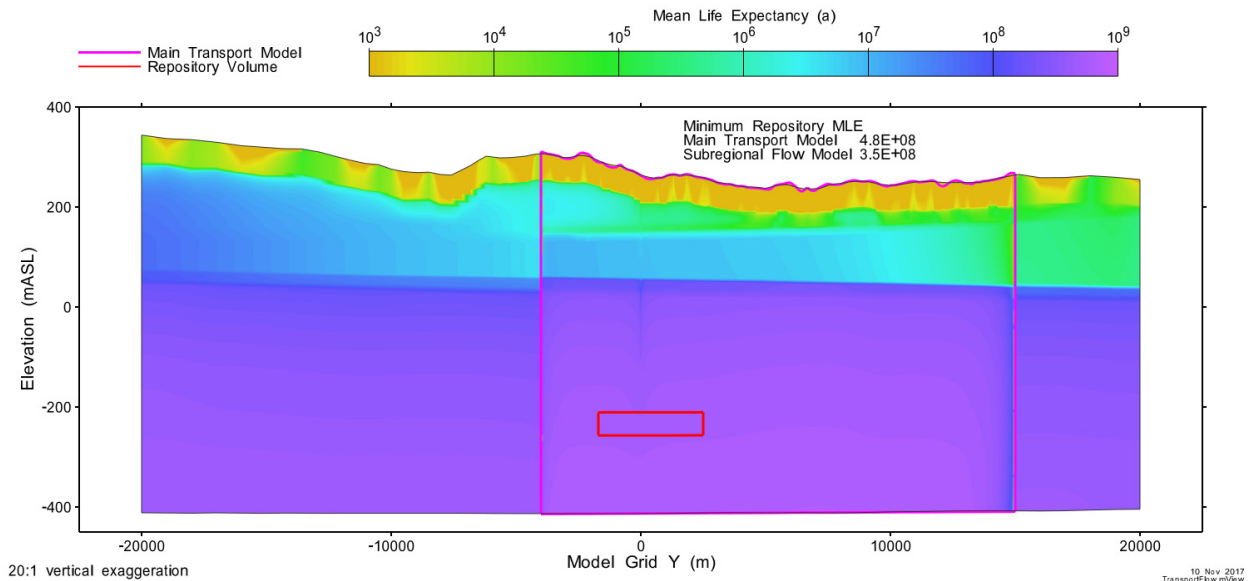


Figure 7-44: Subregional Flow and Main Transport Model: No Well Mean Life Expectancy on Vertical Slice through Repository

Surface discharge zones for the Main Transport model are based on Watersheds. This allows maximum surface water concentrations at watershed defining stream locations (pour points) to be calculated. The illustrative watershed and sub-watershed boundaries, based on the model surface topography, are shown in Figure 7-45. Watersheds C and D are sub-watersheds of the full watershed defined by the pour point for Watershed B. There is no mapping of repository rooms to surface discharge locations. The diffusion dominated transport within the Ordovician formations, when combined with significant advective travel distances within the Guelph formation, blends transport to the extent that different repository source locations have no perceptible impact on surface discharge.

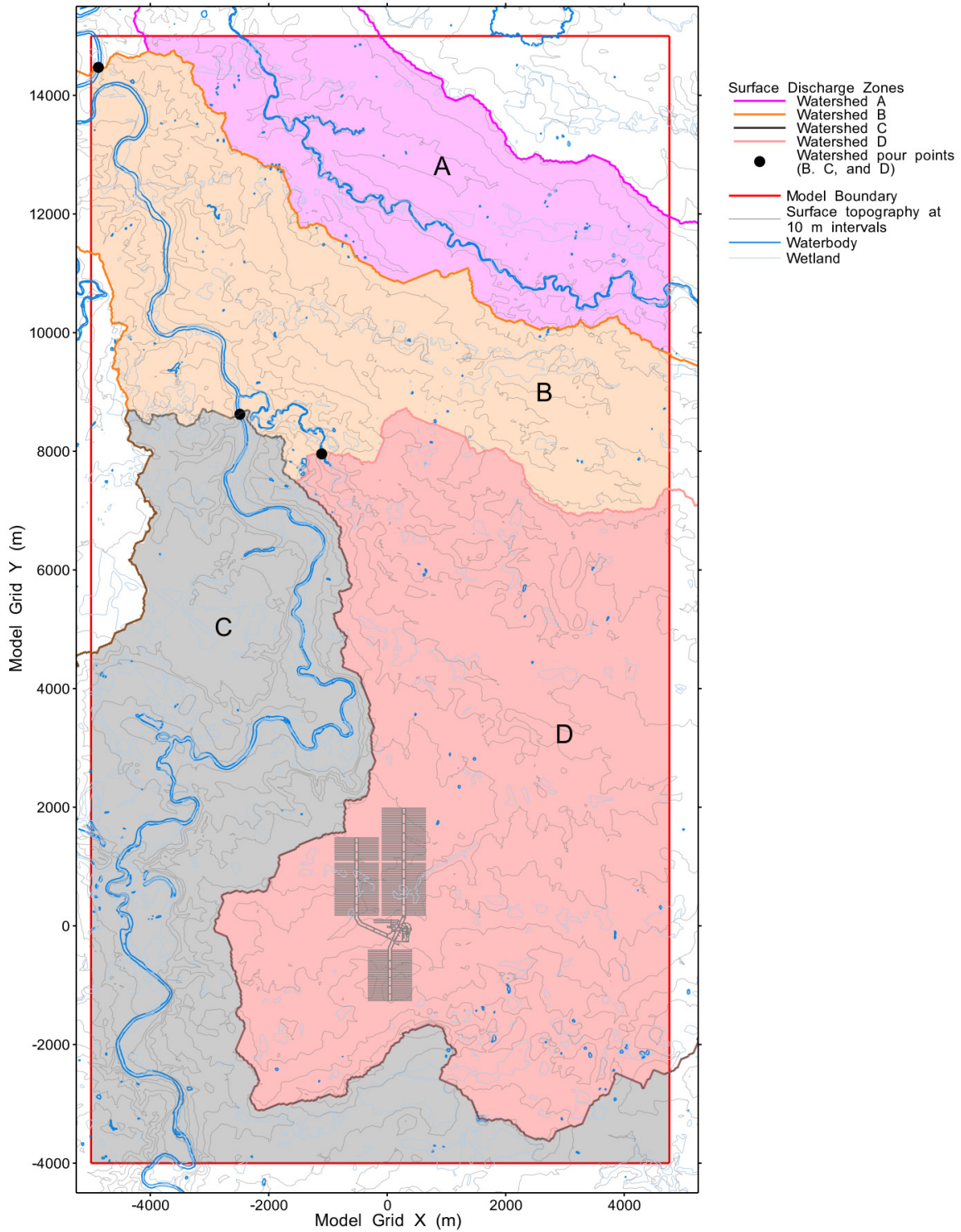


Figure 7-45: Main Transport Model: Watershed Boundaries

7.7.2.2.2 Base Case Flow Results

The well location for this discussion corresponds to the well location determined in Section 7.7.2.3.2. As will be shown later, this is the location that maximizes dose rate to the small farming family that is assumed to be unknowingly living on top of the repository.

When compared to Figure 7-44, Figure 7-46 shows the effect of the water supply well, with significantly reduced MLE in the Guelph Formation near the well. Slight changes in the MLE within the Ordovician formations near the shaft (at Model Grid Y = 0) are also apparent. However, the minimum Repository level MLE decrease, from 4.8×10^8 years to 4.1×10^8 a, is not significant in terms of overall system performance. It should also be noted that the steady-state flow regime induced by the well would likely take hundreds of thousand or even millions of years of continuous well operation to establish in the deeper low-permeability units.

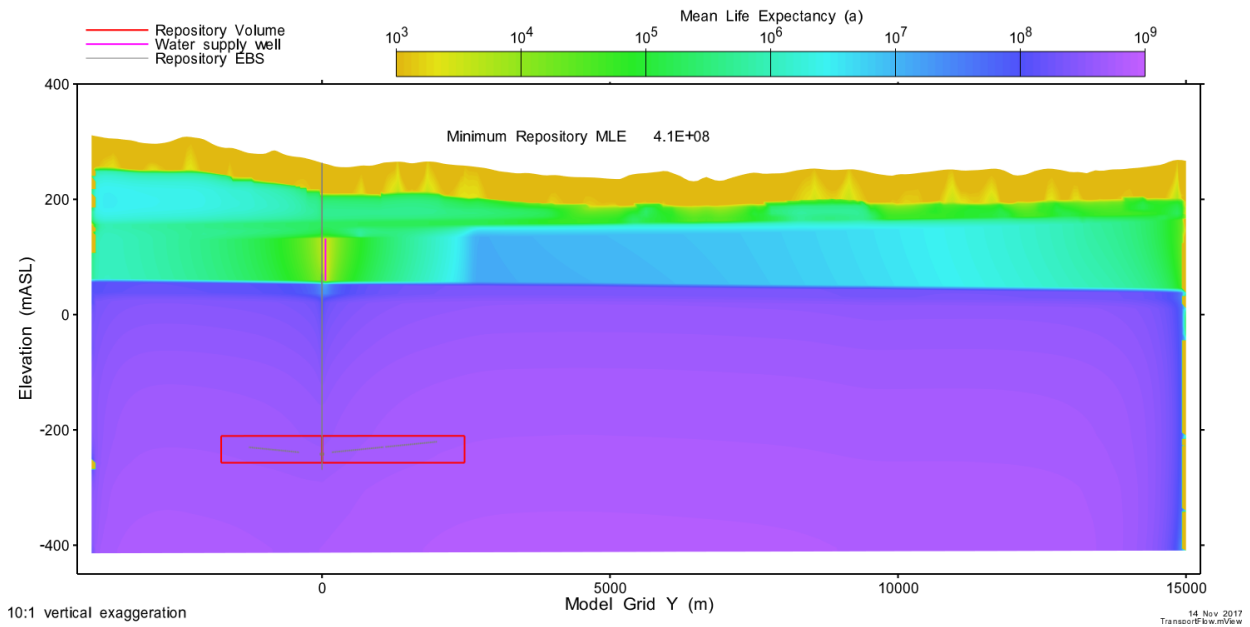


Figure 7-46: Main Transport Model: With Well Mean Life Expectancy on Vertical Slice through Repository

MLE ratio and hydraulic head comparisons of No Well and Base Case MLE (Figure 7-47 and Figure 7-48) confirm the extent of the impact. Note that the ratio scale varies between each figure with Figure 7-47 (which includes the Guelph Formation) showing much larger variation.

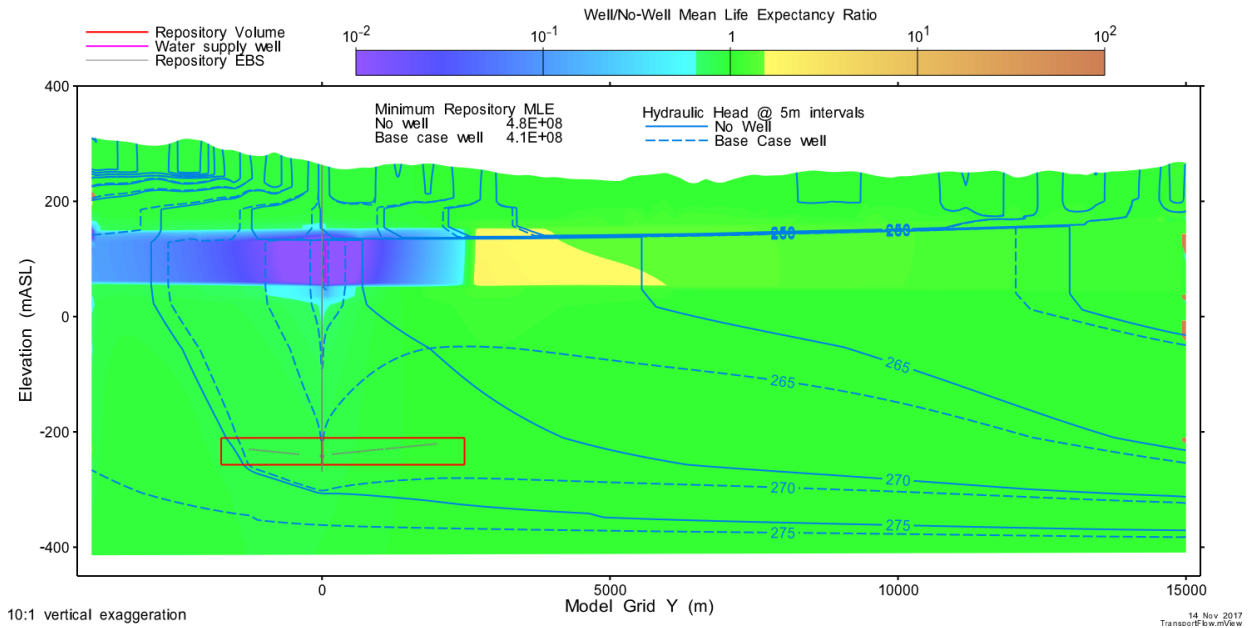


Figure 7-47: Main Transport Model: No Well and Base Case Hydraulic Head and Mean Life Expectancy Ratio on Vertical Slice through Repository

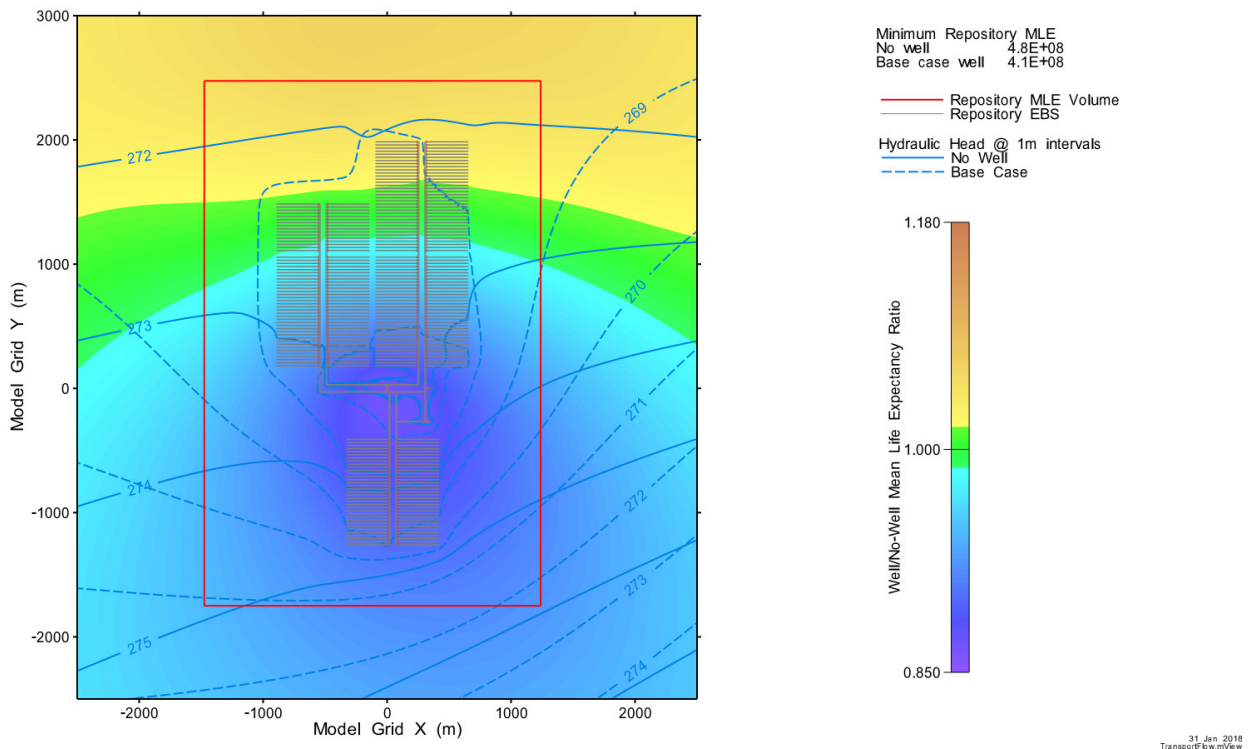


Figure 7-48: Main Transport Model: No Well and Base Case Hydraulic Head and Mean Life Expectancy Ratio on Plan through Repository

7.7.2.3 Main and Detailed Transport Model Radionuclide Transport Results

This section presents radionuclide transport results as determined using the Main and Detailed Transport Models. The following are described:

- A comparison of results from the Detailed Transport Model and the Main Transport Model. The effect of different container source terms is also examined.
- High consequence well and container locations. These are the locations that result in the fastest and / or highest magnitude radionuclide transport to the well.
- Base Case transport results;
- Base Case with no well transport results;
- Sensitivity case results illustrating the effect of deviations (Section 7.7.2) affecting the performance of the buffer, backfill and seals barrier and the geosphere barrier; and
- Sensitivity case results illustrating the effect of FRAC3DVS-OPG modelling parameters.

7.7.2.3.1 Comparison of Different Transport Models

As discussed in Section 7.5.1, two site scale models are used for transport simulations, the Main Transport Model and the computationally demanding Detailed Transport Model. In addition, there are two source term models that are used as input to these site scale models. In some cases, the Container Transport Model (Section 7.7.1.3) is used to provide a detailed source term input, while in other cases the container release rate summed over all defective containers is conservatively directly coupled with the site scale models, thereby bypassing the Container Transport Models and therefore also bypassing the EBS.

Figure 7-49 shows Base Case results for I-129 transport to the well for the various model and source term combinations are virtually identical. The Detailed Transport Model has marginally higher and earlier transport than the Main Transport Model, as does the Combined Source Term and Container Transport Model Source Term approach ("Container Source" in the figure). The differences are sufficiently small as to be insignificant, providing confidence in results from either model and source term for I-129 transport. Additional information concerning the Base Case results is provided in Section 7.7.2.3.3.

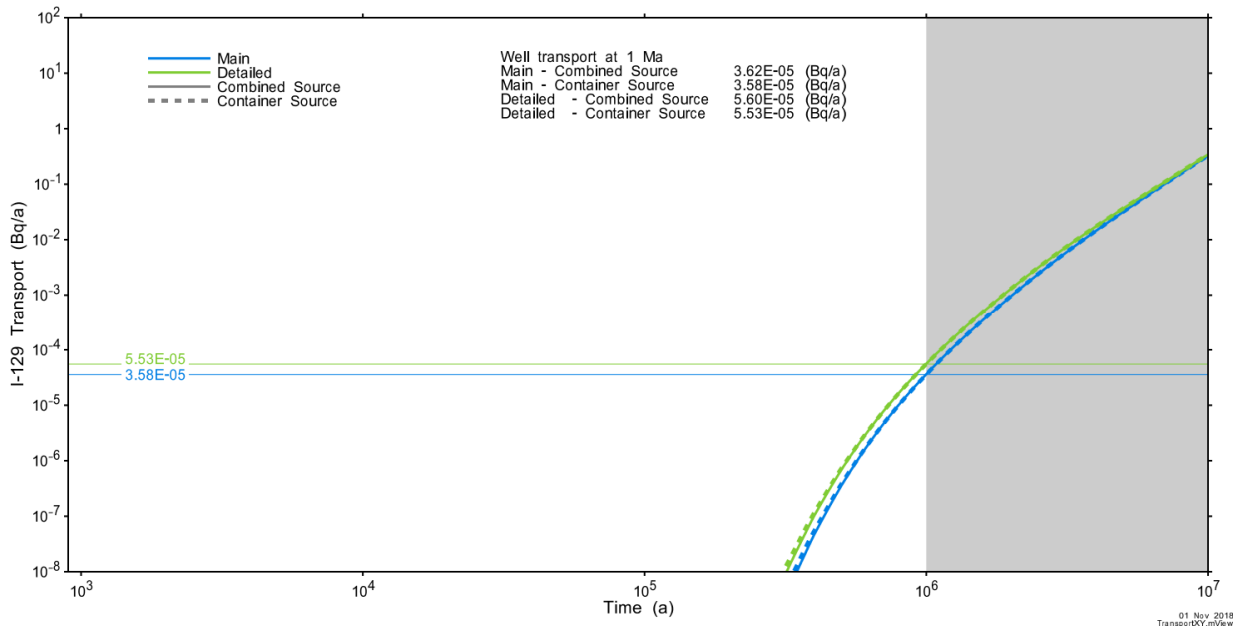


Figure 7-49: Main and Detailed Transport Models: Base Case Comparison of Container Source Term and the Combined Source Term for I-129 Transport to the Well

Note that this good agreement applies only to non-sorbing species (or to species with very low sorption coefficients). Contaminants which strongly sorb to EBS components show slightly different results between the Container Transport Model approach and the Combined Source Term, with the Combined Source term showing higher transport rates. However, I-129 is effectively the only species that reaches the well or surface discharge locations.

This is illustrated in Figure 7-50, which shows a comparison of transport through the top of the Cobourg formation into the Georgian Bay / Blue Mountain for Cs-135. The Detailed Model has faster and earlier transport, with the effect of the EBS on the source also apparent.

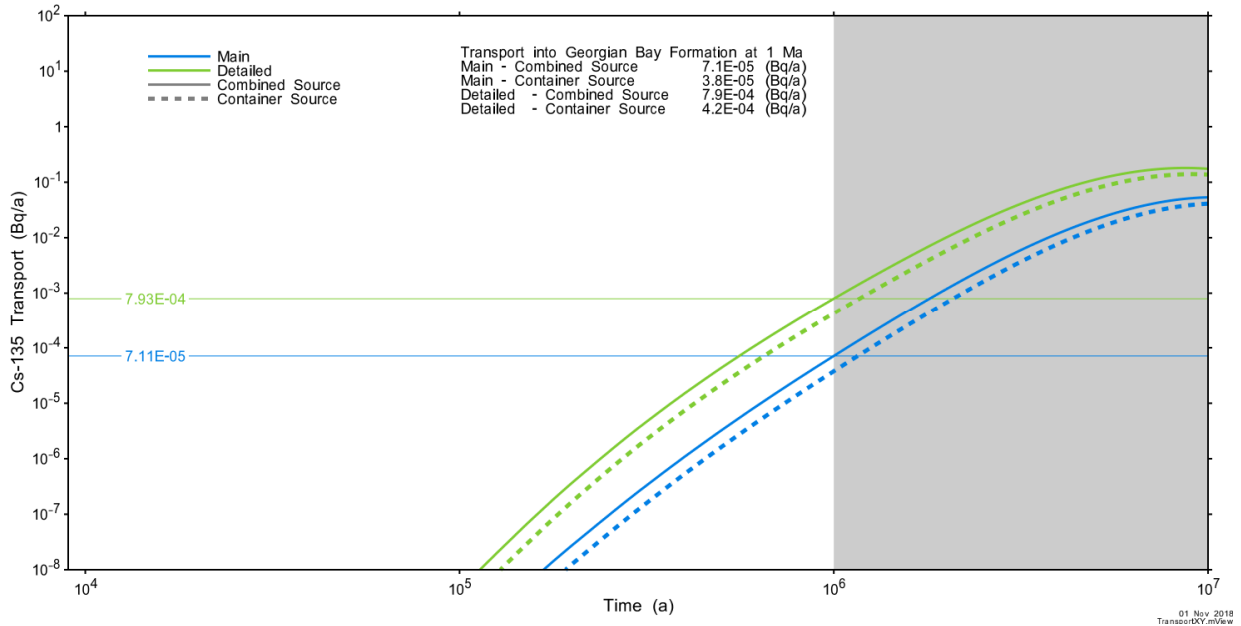


Figure 7-50: Main and Detailed Transport Models: Base Case Comparison of Container Source Term and the Combined Source Term for Cs-135 Transport into the Georgian Bay Formation

7.7.2.3.2 Location of the Well and Defective Containers

The location of the well and of assumed defective containers are important factors in dose results. In previous postclosure safety assessments, the most conservative location of the water supply well was determined through a combination of analytic assessments (i.e., transport pathways and mean life expectancy results), and from understanding the flow system. Provided the pathway to the surface from the repository location with the minimum MLE is relatively short, the location of a well that would intercept that pathway is usually obvious. However, this is not the case for the geosphere in the current study where transport is diffusion dominated with extremely long transport times. Repository MLE does not vary substantially over the repository footprint and advective travel paths are not relevant to actual transport. Preliminary scoping simulations also indicated the shaft EBS and EDZ form a preferential pathway for radionuclide transport due to significantly higher effective diffusion coefficients within the shaft (Figure 7-51).

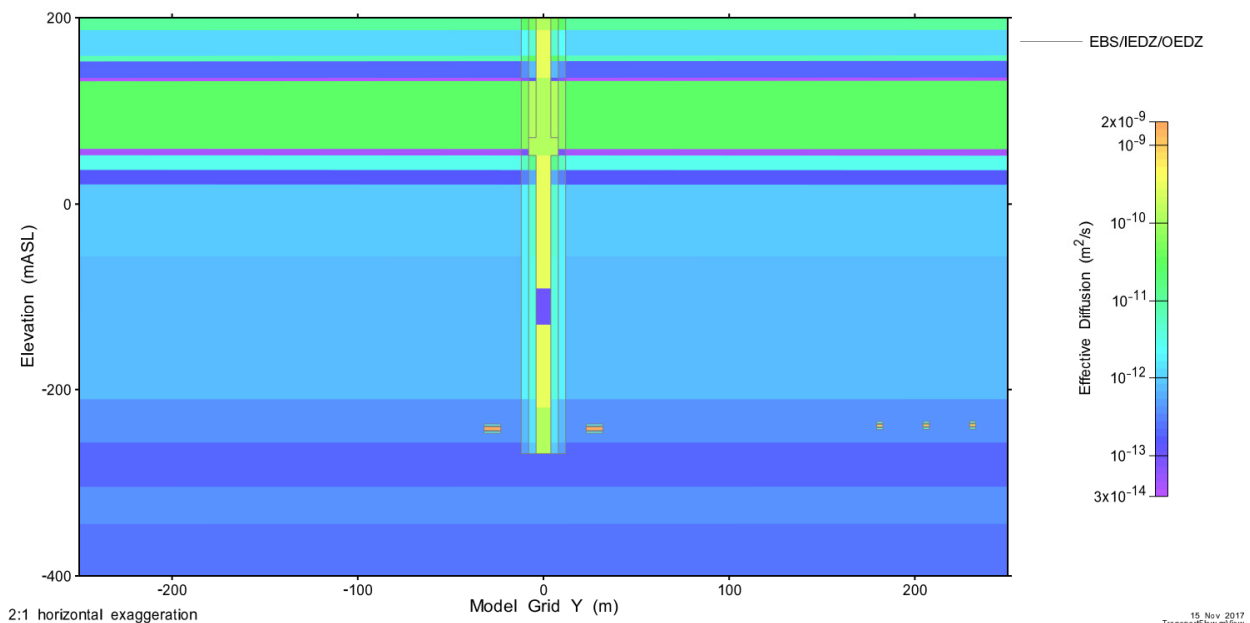
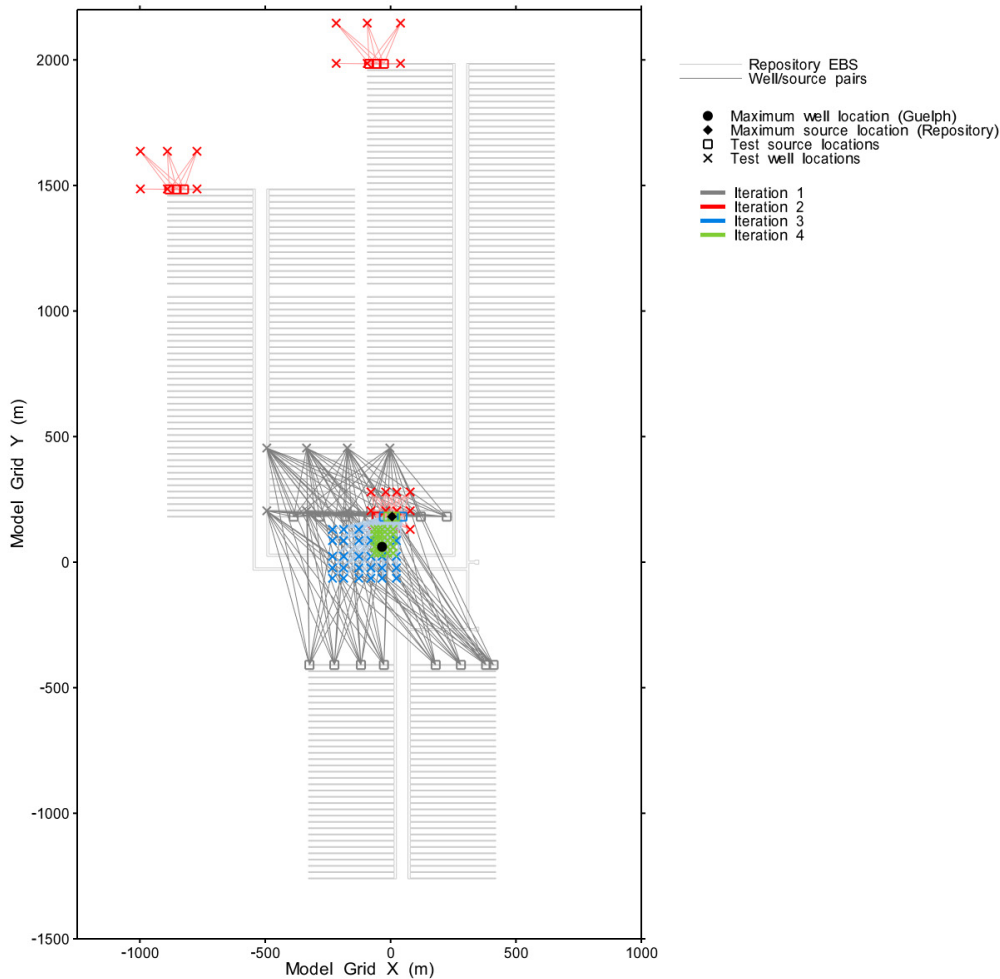


Figure 7-51: Main Transport Model: Effective Diffusion Coefficient on Vertical Slice through Repository

An alternative approach has therefore been adopted to address these issues. Potential well and defective container locations are initially selected with relatively wide spacing between locations, and transport simulations are performed for each combination of well and source using a simplified pulse source term. Well transport results are reviewed and the highest peak transport source / location pairs are selected. A new set of well and source locations is then generated at more refined spacing centred on the selected pair. The refinement approach is performed iteratively until a peak location pair is determined. For this assessment, four iterations of refined spacing were completed, resulting in the well / source location pairs shown in Figure 7-52.

Initial screening locations were concentrated around the main shaft and adjacent placement rooms. Locations at the north end of the repository were also evaluated to assess the possible

effect of reduced diffusion distance where the repository room ceilings are closer to the top of the Cobourg formation (see Figure 7-19). The final selected pair source location is in the room closest to the shaft with a well located very close to the shaft and downgradient.



31 Oct 2018
WellSourceLocation.mxd

Figure 7-52: Well / Source Location Pairs

The source term used is a short duration pulse, where 10^9 Bq of I-129 is released at each container location at a constant rate over a 1000 year period starting at $t = 0$. This is not the same as the I-129 source term from the defective containers, and has only been adopted in this part of the work to simplify the output information and reduce simulation times. Simulations are conducted for 10 Ma using the computationally more efficient Main Transport Model, with the Base Case well demand of $1261 \text{ m}^3/\text{a}$.

A total 360 well / source combinations were examined in the four iterations. Figure 7-53 shows well transport versus time results for all examined combinations.

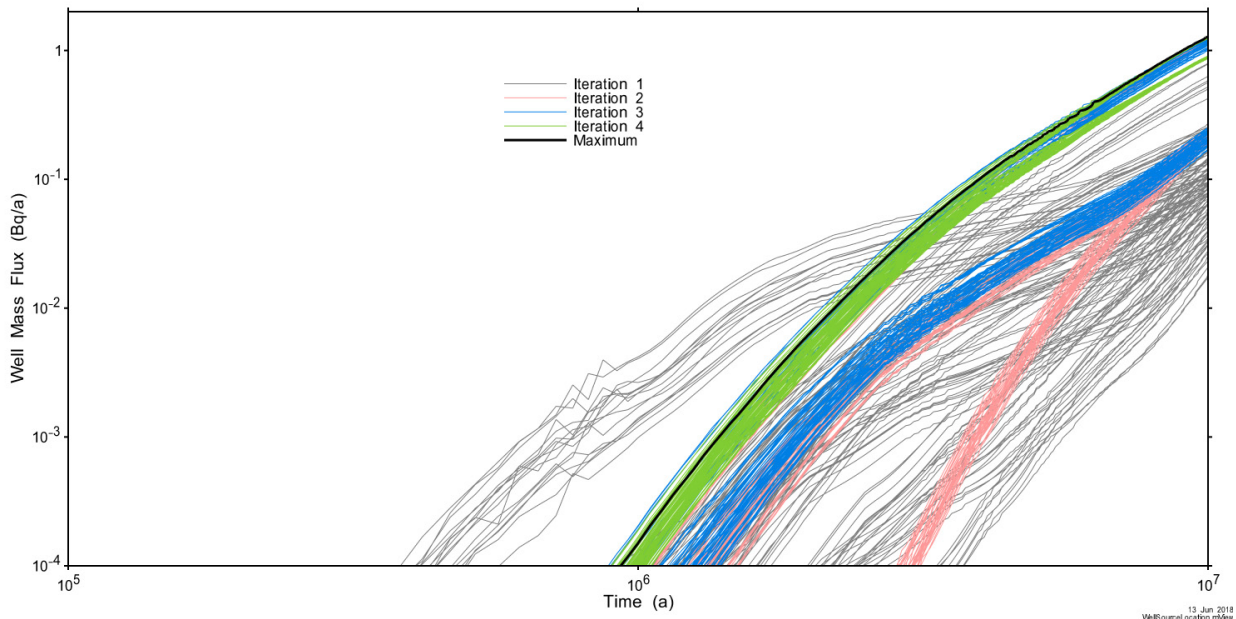


Figure 7-53: Main Transport Model: Well Transport for All Tested Well and Source Locations using Pulse Source Term

7.7.2.3.3 Base Case Results

The Base Case has 10 containers failing over the first one million years, with the first container failing at 1000 years and other containers failing at a rate of one container every 100,000 years.

As described in Section 7.7.2.3.2, the combination of well and defective container locations is selected to ensure contaminant transport to the well is maximized.

In the results presented below, transport from the near-field repository into the rock (at the Inner EDZ boundary) is calculated by the Container Transport Model and imposed as a source term on the Main Transport Model, where a time-varying radionuclide mass is injected into the model at nodes surrounding the container location (see Figure 7-27).

I-129 Transport to Well and Surface

Figure 7-54 shows I-129 transport to the well and surface locations over the 10 Ma simulation period. Surface discharge is essentially zero, as the well abstracts virtually all radionuclides transported into the Guelph formation.

I-129 is selected for this discussion because, as will be seen later in Section 7.8.2.1, essentially all of the dose consequence is due to I-129. No other radionuclides reach the well or surface discharge. Transport rates rise throughout the simulation period with well transport of 3.6×10^{-5} Bq/a at one million years.

As the results are still slowly increasing, it is of interest to extend the simulation until the peak value is obtained. Note that this extension is for illustrative and comparative purposes only, as it is likely that geological processes will have a significant effect on results at this time scale. In this case, the peak value of 3.3 Bq/a is reached at 31 million years.

The transport rate to the surface in one million years is off-scale low and is effectively zero.

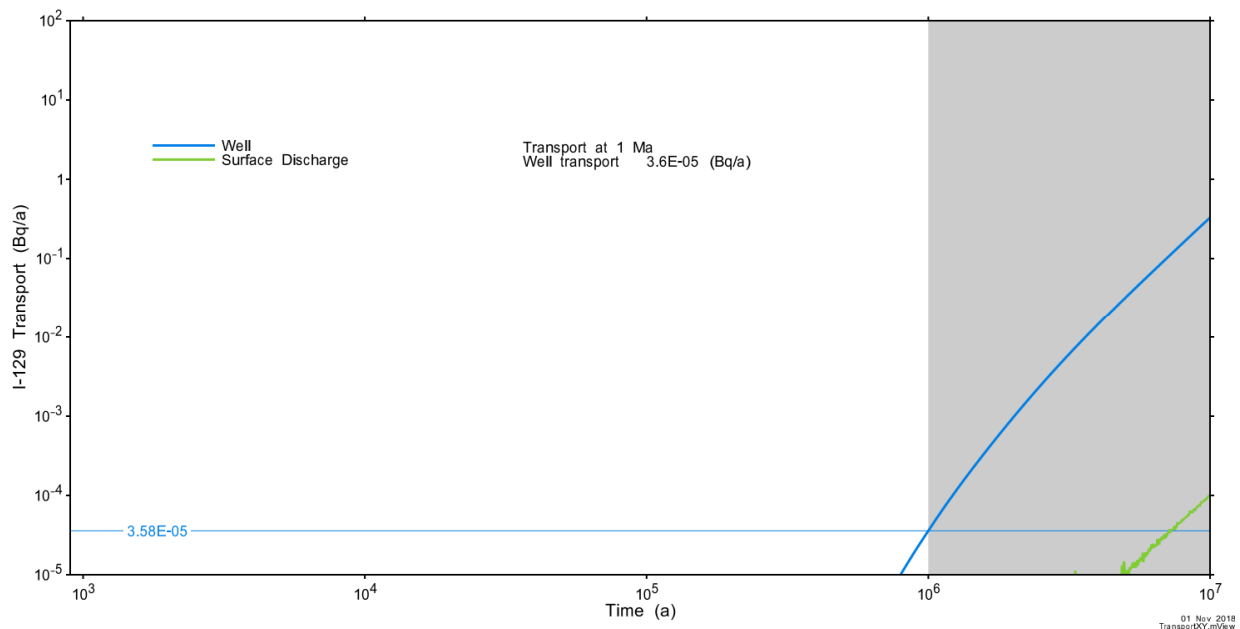


Figure 7-54: Main Transport Model: Base Case I-129 Transport to the Well and Surface

Overall capture by the well, defined as the integrated transport to the well over 10 Ma divided by the total mass injected into the model, is very small, at 0.032 % of the I-129 released from the defective containers. The breakdown of transport throughout the model domain over time is shown in Figure 7-55. Nearly all mass remains within the low-permeability Ordovician formations or the repository EBS over the 10 Ma simulation period.

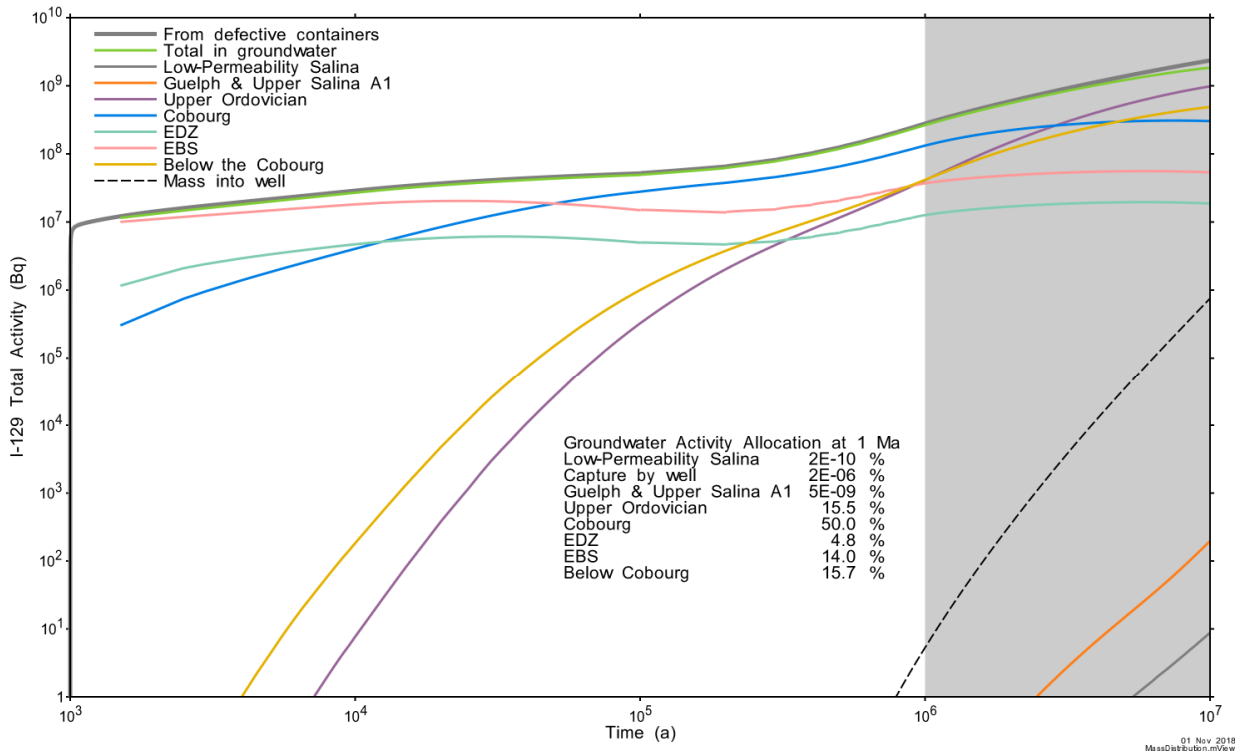


Figure 7-55: Main Transport Model: Base Case I-129 Integrated Activity Allocation

Figure 7-56 through Figure 7-58 illustrate the time dependent behaviour of the I-129 plume on a plan view at the repository elevation and on a vertical slice perpendicular to the placement room containing the defective containers and through the main shaft. The contour plots are on a logarithmic scale. The outer concentration contour, 1 Bq/m³, corresponds to an effective I-129 drinking water dose of about 0.1 μSv/a based on a water consumption of 1.08 m³/a per person. The color shaded concentrations, solid contours, and repository EBS are from the Detailed Model. The dashed contours are Main Transport Model results presented for comparison purposes.

The plume develops very slowly, with preferential transport along the relatively higher diffusion materials comprising the EBS. At 10,000 a the 10⁵ Bq/m³ contour has extended over 110 m of placement room, but only extends 10 m into the intact rock on either side of the room. By 100 ka, the edge of the plume has reached the main access tunnel and started to diffuse through the tunnel. At 1 Ma transport up through the shaft EBS is occurring and has reached the same elevation as within the intact geosphere.

Detailed and Main Transport Model results are very similar. The cross tunnels, present in the Detailed Model but not the Main Model, serve as additional pathways for diffusion, resulting in slightly wider (in the X direction) and shorter (in the Y direction) plume extents for the Detailed Transport Model.

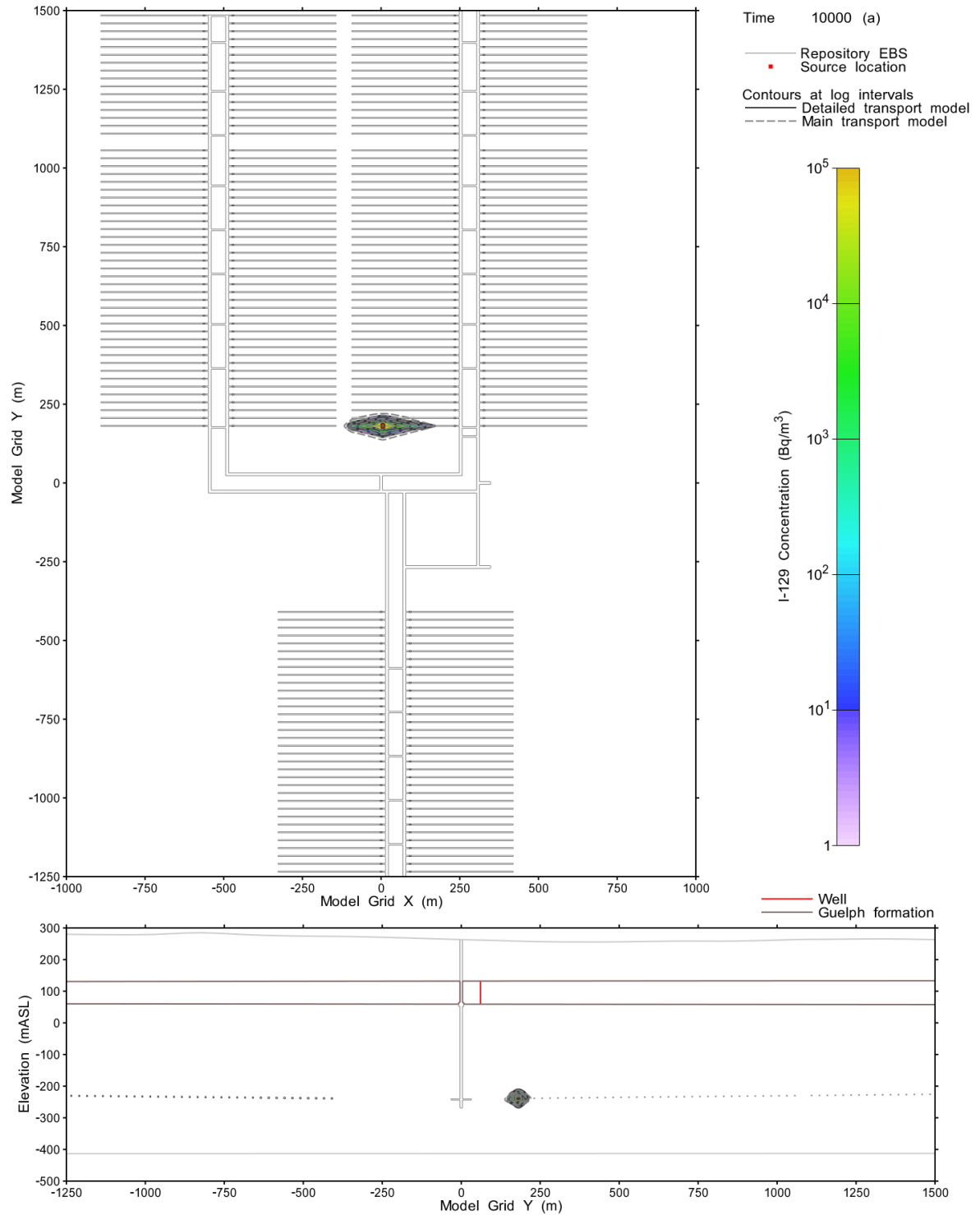


Figure 7-56: Detailed and Main Transport Model: Base Case I-129 Concentration at 10 k Years

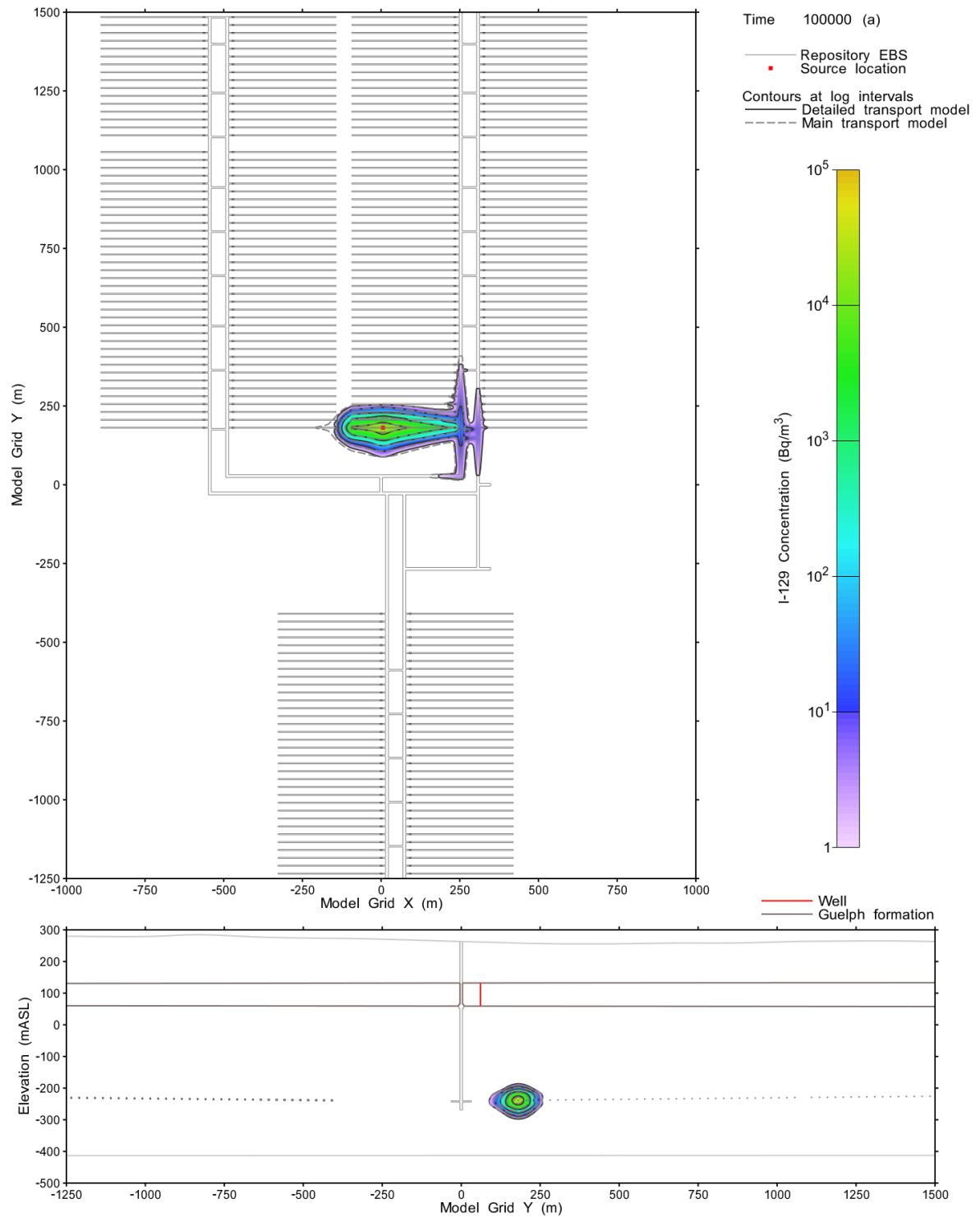


Figure 7-57: Detailed and Main Transport Model: Base Case I-129 Concentration at 100 k Years

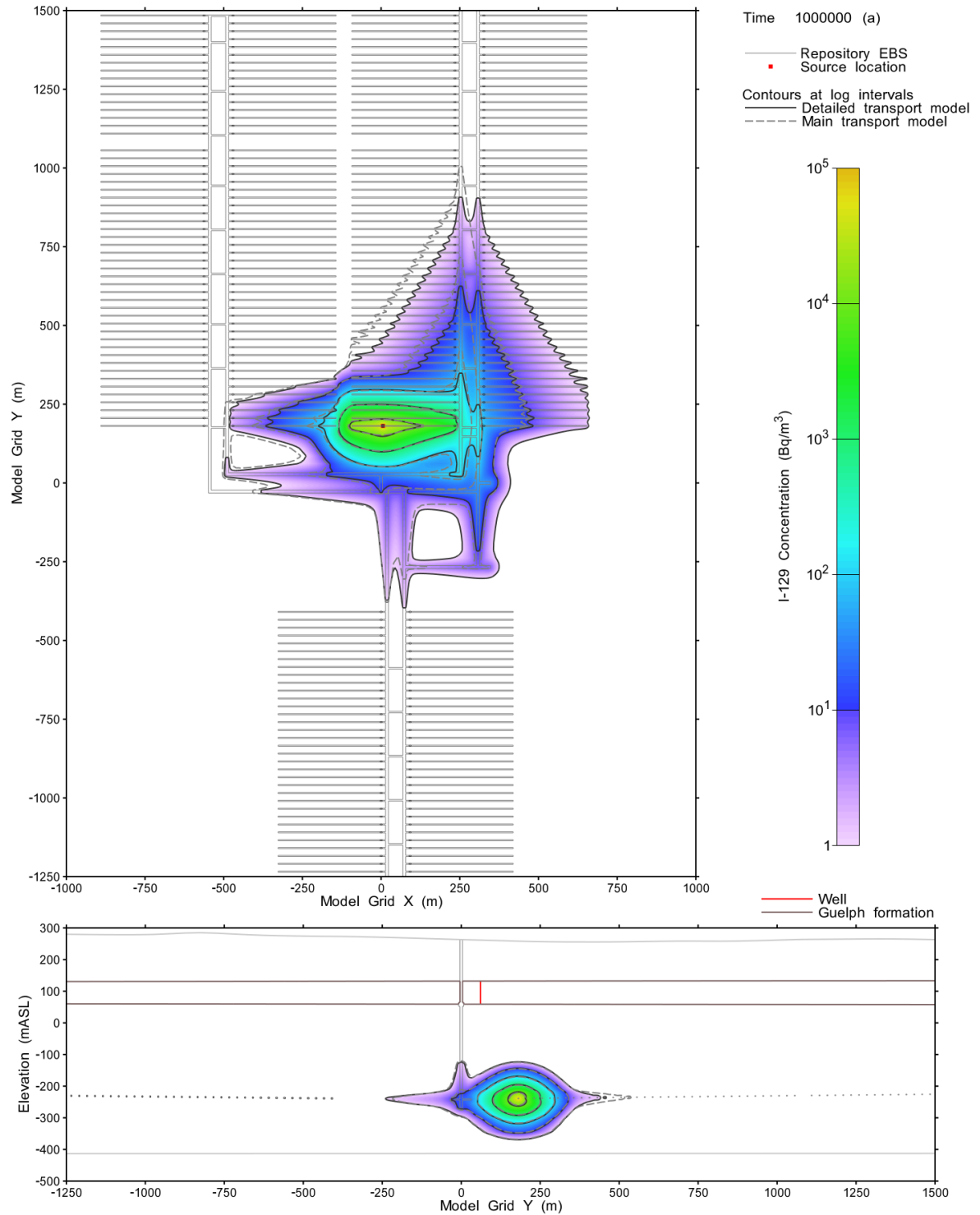


Figure 7-58: Detailed and Main Transport Model: Base Case I-129 Concentration at 1 Ma Years

Figure 7-59 is a 3D illustration of transport at 1 Ma. The figure shows two iso-volumes, with one corresponding to I-129 concentrations of 1 Bq/m³ and another to I-129 concentrations of 100 Bq/m³.

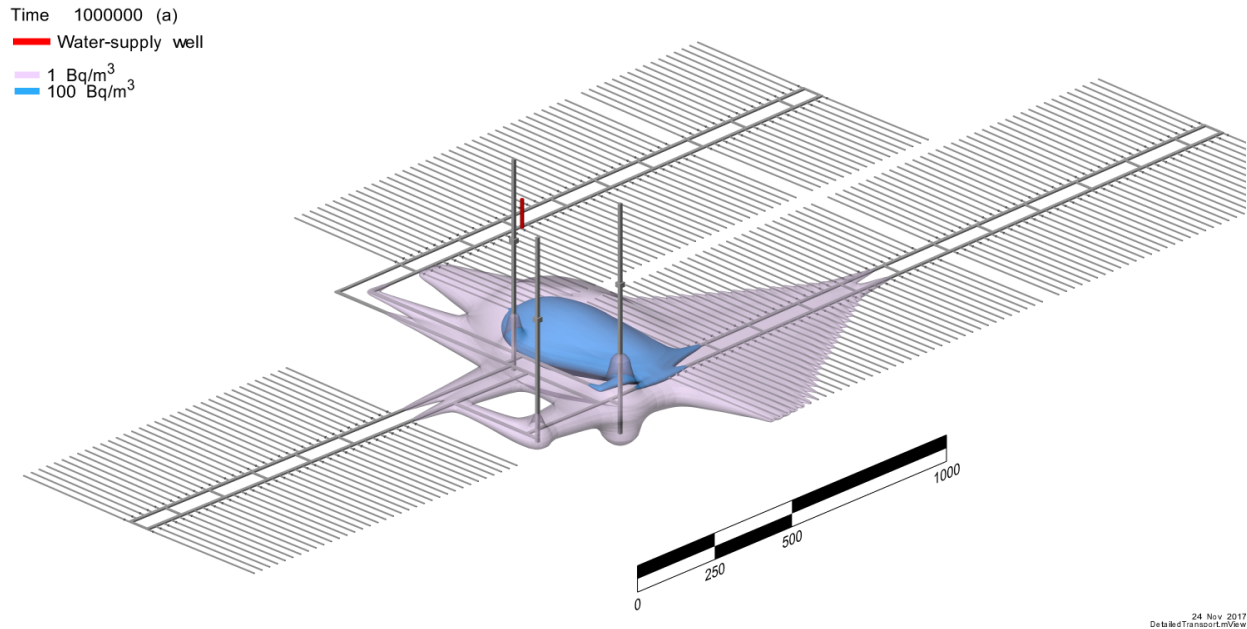


Figure 7-59: Detailed Transport Model: Base Case I-129 Concentration in 3D at 1 Ma

CI-36 Transport to Well and Surface

Figure 7-60 shows CI-36 transport to the well and surface locations over the 10 Ma simulation period using the Combined Source term. Compared to I-129, the relatively shorter half life (308 ka versus 15.7 Ma) and lower release rate results in very low transport to the well and essentially zero transport to surface. Peak well transport occurs at approximately 1.9 Ma, after which transport is reduced due to decay.

Figure 7-61 illustrates 3D transport results at 1 Ma.

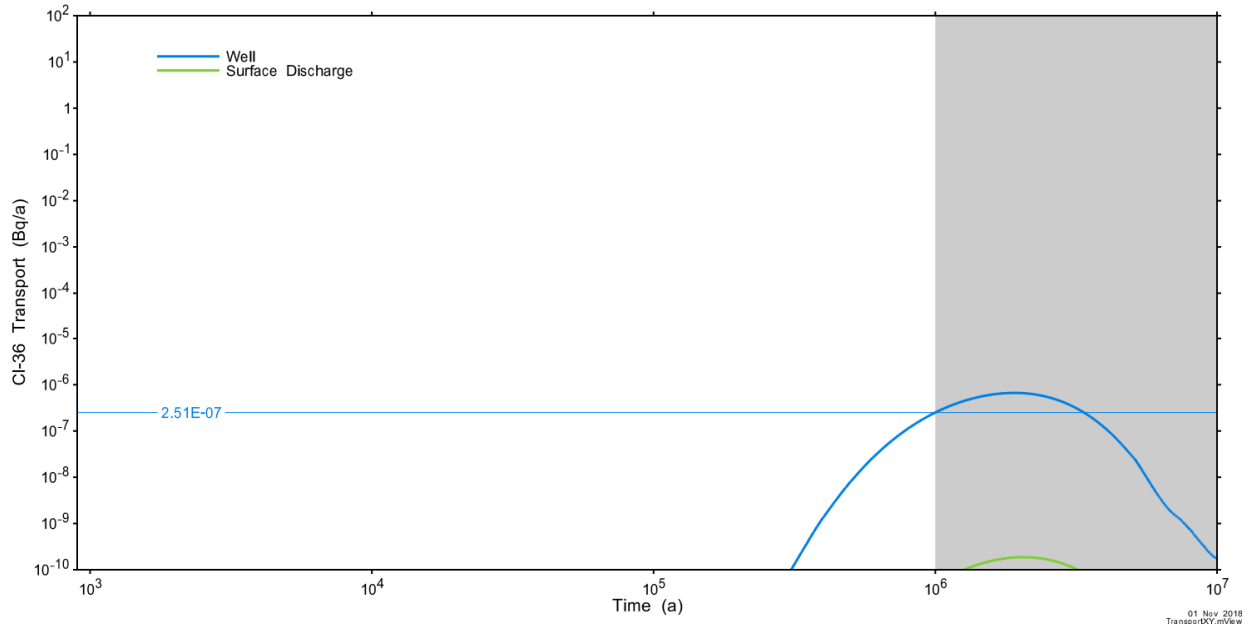


Figure 7-60: Main Transport Model: Base Case Cl-36 Transport to the Well and Surface

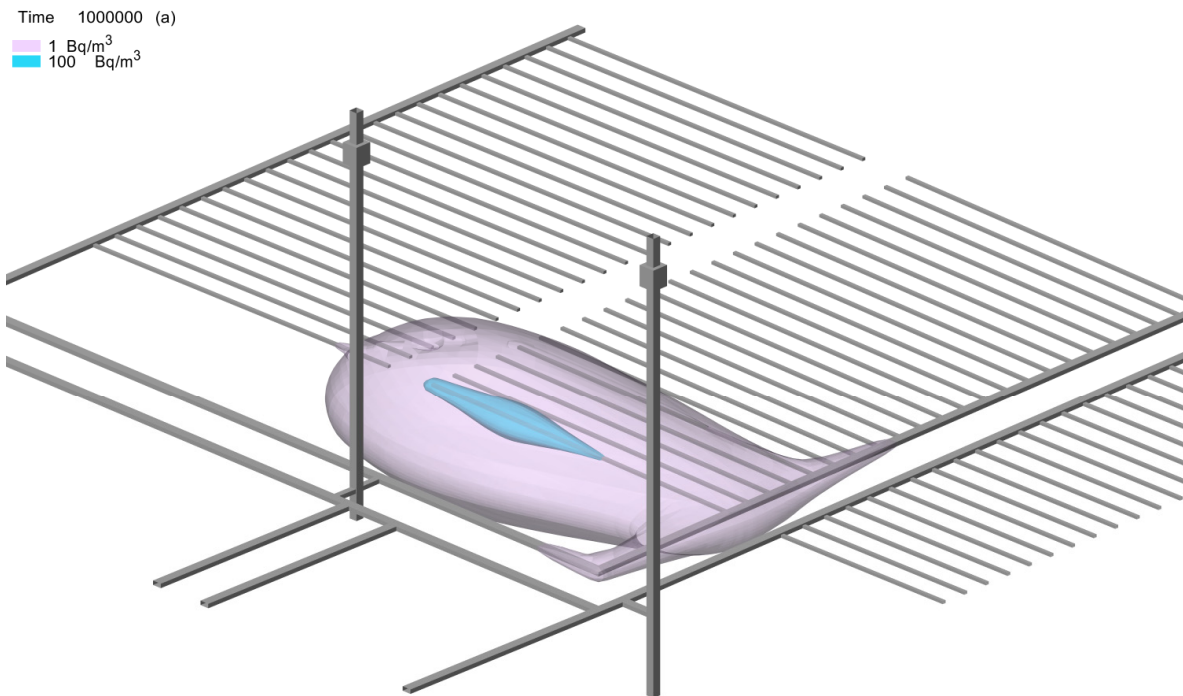


Figure 7-61: Main Transport Model: Base Case Cl-36 Concentration in 3D at 1 Ma

Cs-135 Transport to Well and Surface

Cs-135 transport results show no measurable transport at the well or to surface discharge locations. The breakdown of mass transport in groundwater throughout the model domain is shown in Figure 7-62. The relatively high sorption for Cs-135 results in nearly all mass being sorbed onto the geosphere and EBS. Of the small component of mass in groundwater nearly all (99.84%) remains within the Cobourg formation or the repository EBS over the 10 Ma simulation period.

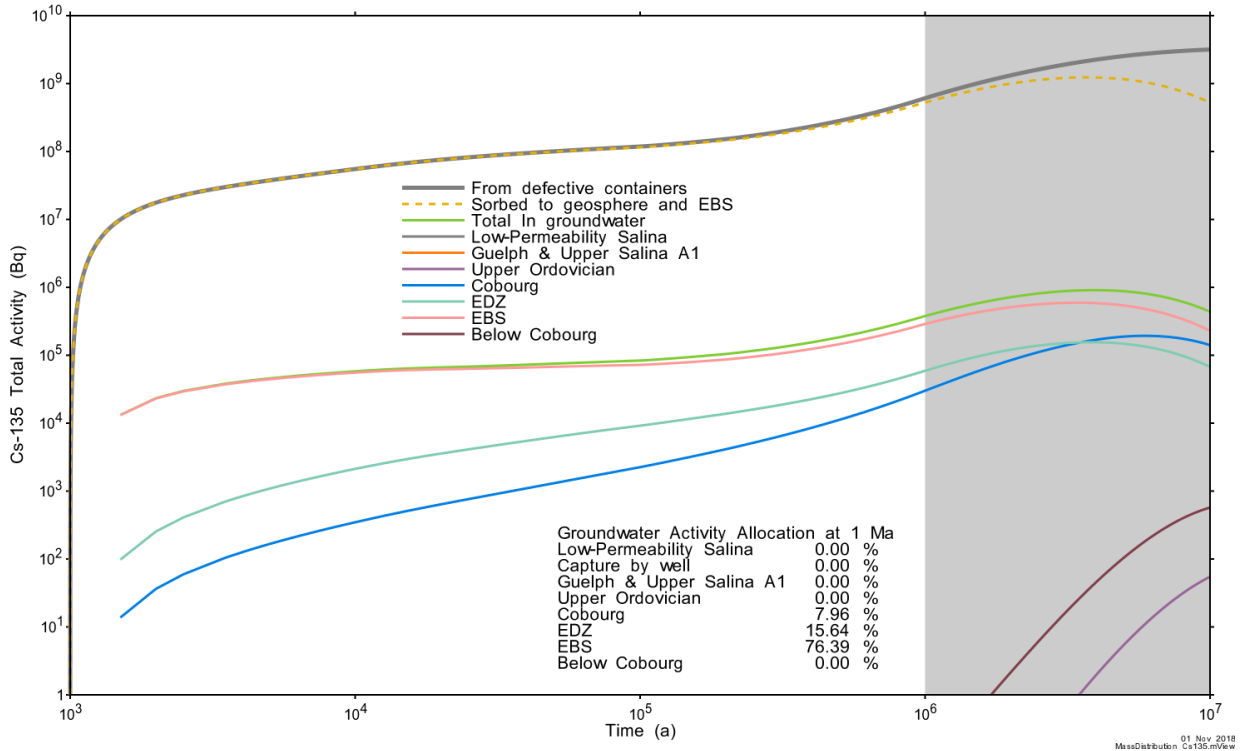


Figure 7-62: Main Transport Model: Base Case Cs-135 Integrated Activity Allocation

U-238 Transport to Well and Surface

U-238 is the most strongly sorbed of the simulated radionuclides and shows no measurable transport to the well or to surface discharge locations. The breakdown of mass transport in groundwater throughout the model domain over time is shown in Figure 7-63. All mass is retained within the repository and Cobourg formation, with most mass not leaving the EBS.

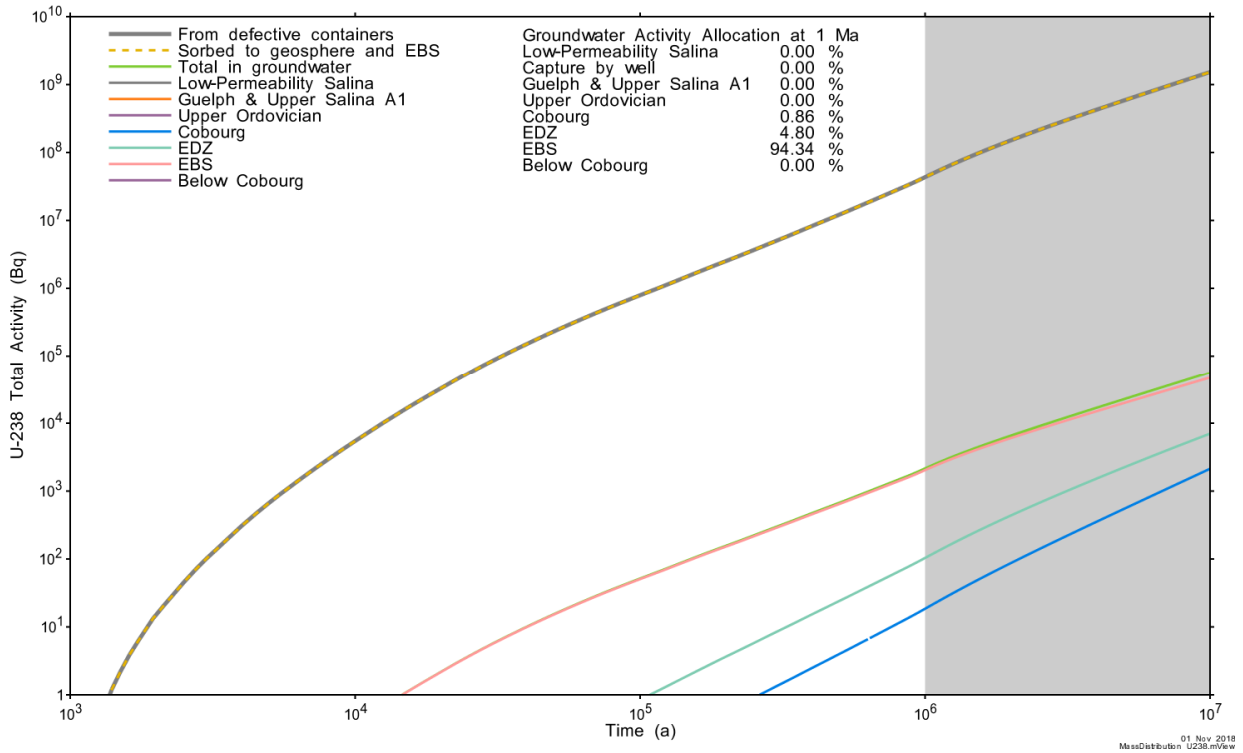


Figure 7-63: Main Transport Model: Base Case U-238 Integrated Activity Allocation

7.7.2.3.4 Well Assumption Sensitivity Cases

The System Model results in Section 7.8.2.1 show that the dose consequence for the Base Case is due entirely to I-129, with the I-129 dose due to the use of well water. In the System Model, well water is used for drinking, irrigation of food crops and for watering animals.

Given the importance of the well pathway, the following three sensitivity studies have been defined (Section 7.2.1.3) to illustrate the effect of the well on dose consequences:

- No well;
- Intermittent well operation; and
- Random well location.

Of these, the intermittent well case and the random well location case are examined with the 3D models.

The No Well case is simulated with the System Model and discussed in Section 7.8.2.2.

Intermittent Well Operation

The Base Case assumes the well is pumping continuously at a rate of 1261 m³/a. This sensitivity study assumes the well and defective containers are present in their bounding Base Case locations; however, the well is assumed to operate intermittently.

During periods of no well, the transport plume can accumulate within the Guelph formation. If a well is then established, there could initially be a greater mass of contaminant within the well capture zone than would otherwise be present under conditions of continuous well operation. After some time, the excess would be eliminated through well uptake and the transport processes would re-equilibrate.

This sensitivity case assumes the well operates for 5000 years starting at a postclosure time of 1 Ma.

Since the well operation is not constant over the simulation period, a transient flow simulation is required. The Main Transport Model is used with the Combined Source Term and with specific storage for all formations set to $1 \times 10^{-7} \text{ m}^{-1}$.

Figure 7-64 shows the results. There is a transient increase in transport rate for a period of time after the well starts. If turned on at 1 Ma, transport to the well rises to $3.3 \times 10^{-4} \text{ Bq/a}$, a factor of 9 times higher than the equivalent Base Case value. The increase depends on the well pumping rate, with higher rates causing increased dispersion and dilution therefore resulting in a reduced effect.

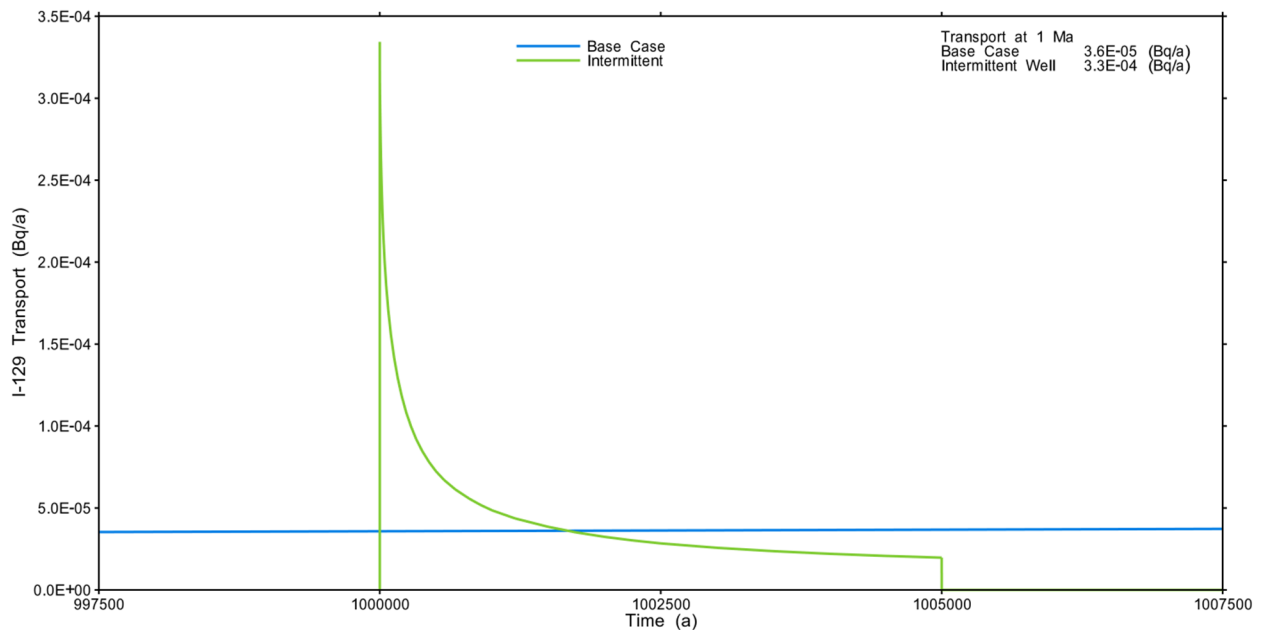


Figure 7-64: Rooms-Only Repository-Scale Model: Intermittent Well Sensitivity – I-129 Comparison to Base Case

Random Well Location

There are millions of combinations of potential well and defective container locations and it is not practical to test them all. Instead, this sensitivity case uses results generated in Section 7.7.2.3.2 for determining the position of the well.

Figure 7-52 shows the positions of 360 well and source locations that were examined to determine the limiting combination. Despite these positions not being truly random (i.e., they have been pre-selected as potential worst combinations), the results shown in Figure 7-53 indicate transport to the well can vary substantially. If more combinations are considered, it is expected that some would result in zero transport to the well with the transport plume eventually discharging to surface locations.

7.7.2.3.5 Barrier Sensitivity Cases

This section presents the subset of sensitivity cases identified in Section 7.7.2 that affect the barriers and have the potential to affect the groundwater flow distributions. The cases are:

- Hydraulic conductivities of the engineered barrier system (EBS), increased by a factor of 10;
- Hydraulic conductivities of the host rock increased by a factor of 10;
- Hydraulic conductivity in the excavation damaged zones (EDZ) increased by a factor of 10;
- 150 m overpressure in the Shadow Lake Formation; and
- 100 m of surface erosion.

These sensitivity cases are simulated using the Main Transport Model with the Combined Source Term for I-129 and described below, except for the erosion case.

No simulations have been performed for the 100 m of surface erosion sensitivity. With 100 m of erosion, the top of the Guelph formation would be about 40 m below grade (rather than 140 m below grade), but still capped with the very low permeability units of the Salina formation. Even if these units become more permeable due to their nearer surface exposure, the overall system would remain diffusion-dominant, with radioactivity reaching the Guelph on the same time-scale and proceeding from there to the well and biosphere with the same capture rate. No significant changes to the rate of radionuclide release to the biosphere would therefore result.

All other sensitivity cases are simulated using the Main Transport Model with the Combined Source Term for I-129.

Well Transport Results for Sensitivity Cases

Well transport results for all cases are presented in Figure 7-65 for a simulation time of 10 million years, with transport results at one million years indicated on the figure. Results are generally much greater than the Base Case; however, this is because the peak values have yet to be reached.

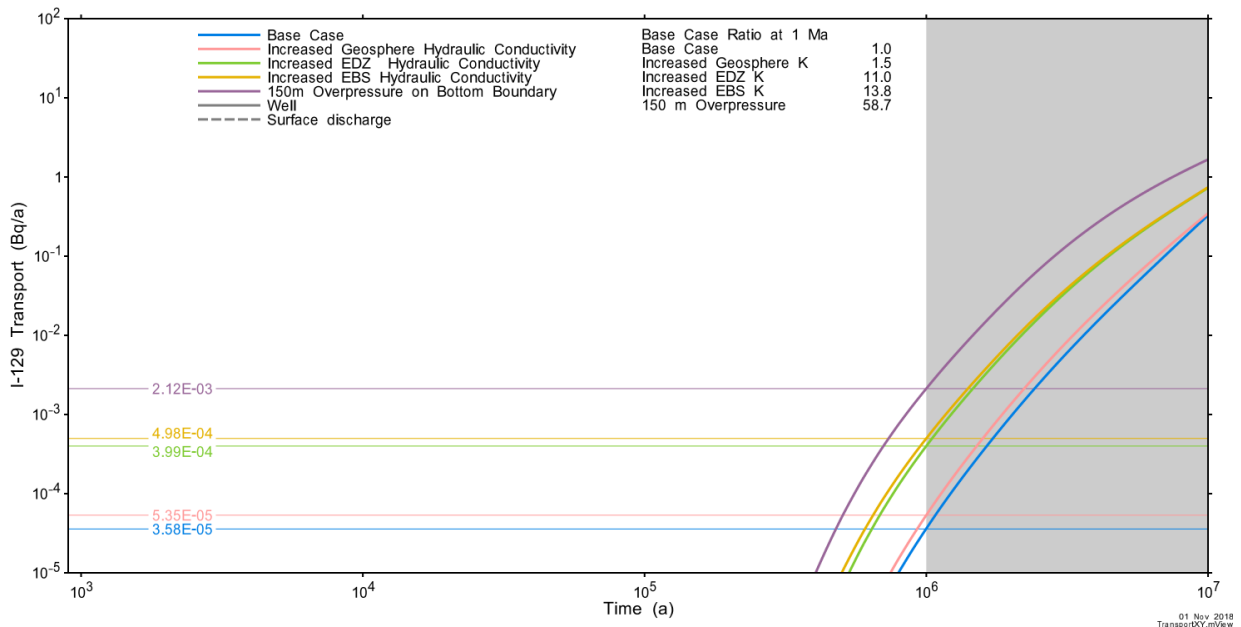


Figure 7-65: Main Transport Model: I-129 Transport to the Water-Supply Well for Geosphere Sensitivity Cases

7.7.2.3.6 Numeric Parameter Sensitivity Cases

This section presents results for sensitivity cases performed to illustrate the effect of FRAC3DVS-OPG numeric parameters on the Base Case results. The cases are:

- Increased spatial resolution to confirm convergence for the 3D groundwater flow and transport models; and
- Increased and decreased number of time steps to confirm model results are not sensitive to temporal resolution.

Increased Spatial Resolution

The effect of spatial resolution on simulation results can be examined by comparing results of the Main and Detailed Transport Models (Figure 7-56 through Figure 7-58). Although the Detailed Transport Model contains nearly three times the number of elements (37.9 million compared to 12.7 million), the very minor differences between the results can be ascribed to the slight differences in property assignment, as they are primarily due to the presence of the cross tunnels in the Detailed Model, and absence thereof in the Main Model. Figure 7-49 shows the models provide essentially the same results for I-129 transport to the well.

Based on this comparison, it can be concluded that the spatial discretization in both models is fit for purpose.

Temporal Resolution

The effect of time step size is determined by modifying control parameters in Main Transport Model simulations. Because the choice of source term and standard output times affects this analysis, the specified output times were reduced from 302 to three and the Container Transport Model generated source term was used. The sensitivity assessment consisted of three simulations:

- Increase maximum time step size to 100 ka and increase concentration control parameter to 0.05,
- Decrease maximum time step size to 10 ka and decrease concentration control parameter to 0.002, and
- Repeat the Base Case (maximum time step size of 25 ka and concentration control parameter of 0.01) but with the specified output times reduced to three. This corresponds to the “normal” time step in the absence of the target time feature and allows for a self-consistent comparison with the other two cases.

Figure 7-66 shows the number of time steps for the three sensitivity cases above together with those for the Base Case, with Figure 7-67 showing a comparison of I-129 transport to the well. Results at the well are very similar for all cases, with transport increasing by less than two percent despite a doubling in the number of timesteps. This indicates that that the temporal discretization used is fit for purpose.

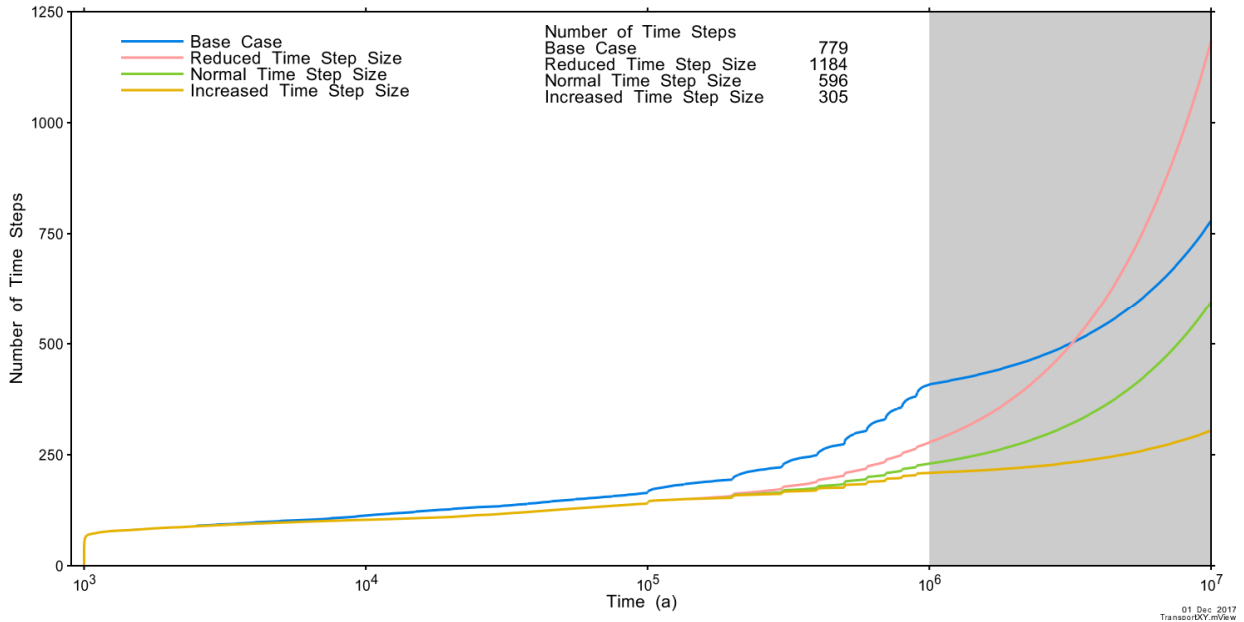


Figure 7-66: Main Transport Model: I-129 Time Step Sensitivity – Time Steps

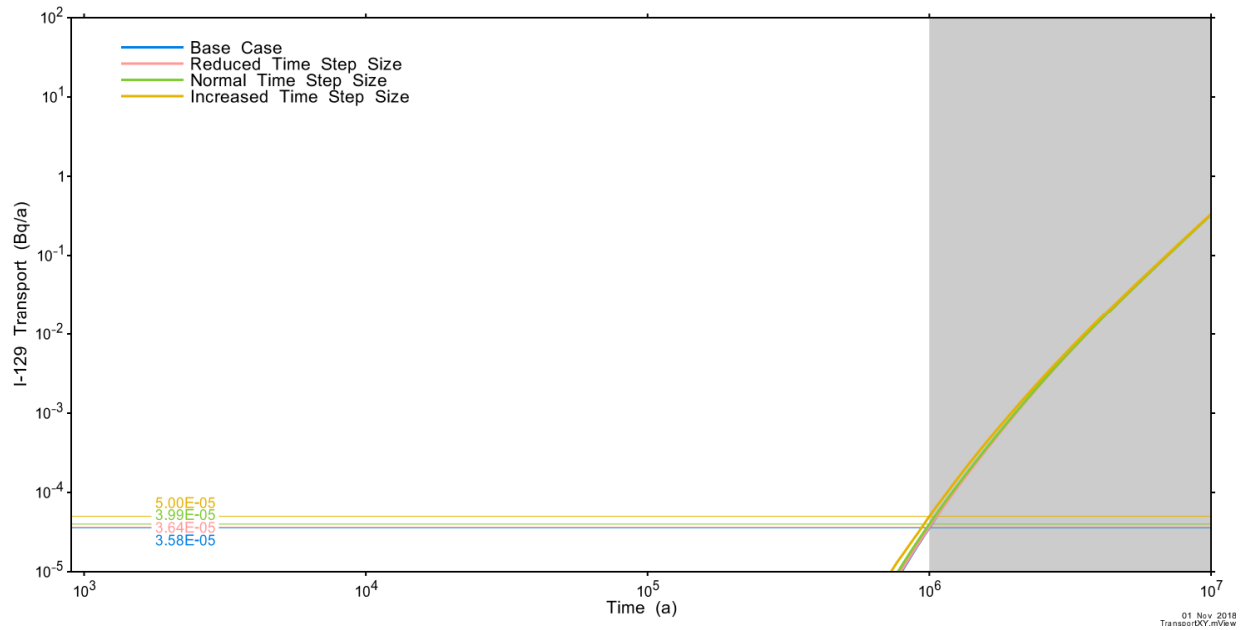


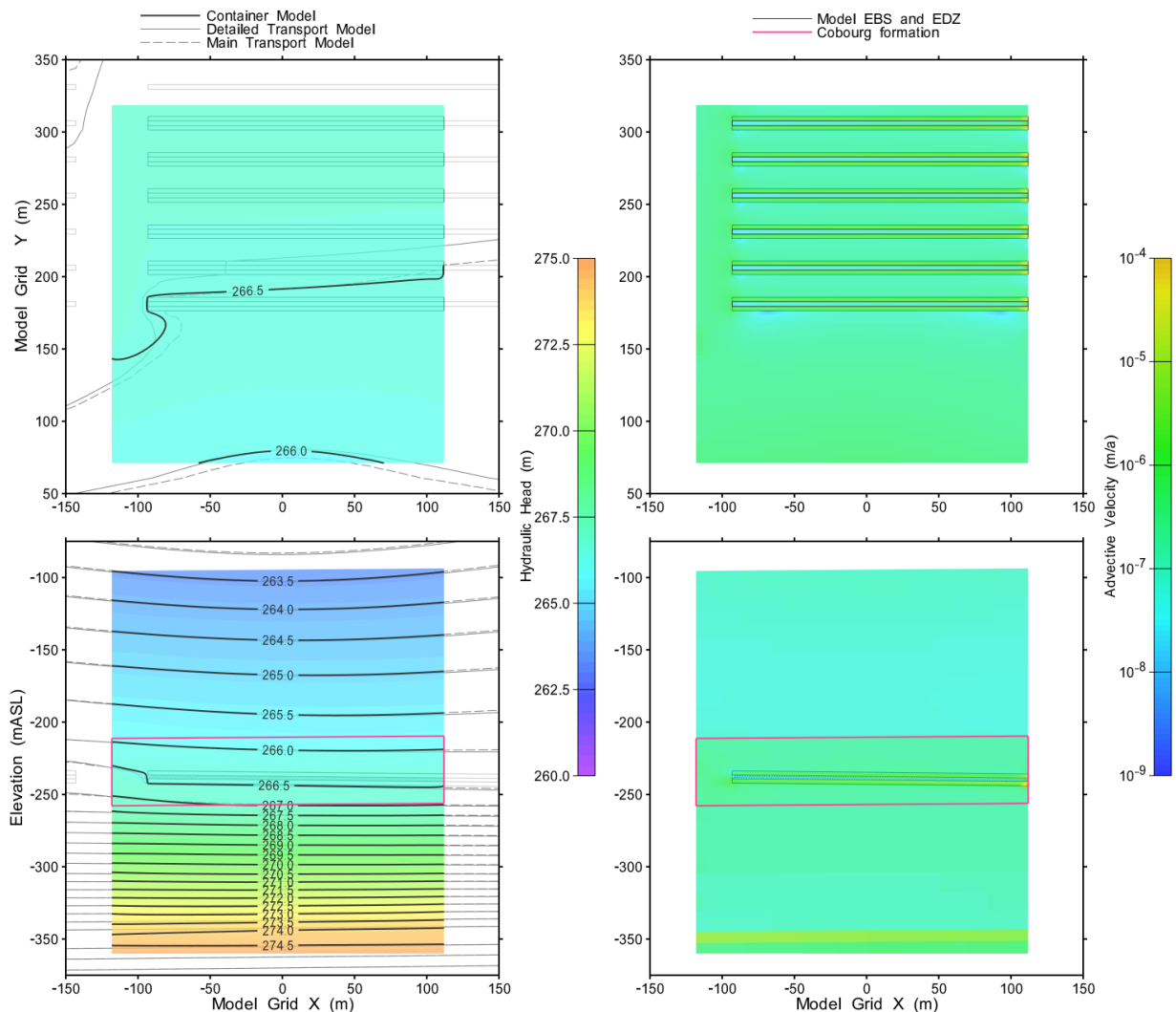
Figure 7-67: Main Transport Model: I-129 Time Step Sensitivity – Comparison of Well Transport

7.7.2.4 Container Transport Model Flow Results

The Container Transport Model represents a small section of the repository surrounding the defective containers and the adjacent geosphere. The model incorporates a high level of detail with individual containers represented. Base Case simulations are performed with the

Container Transport Model to generate source terms for the Main and Detailed Transport Models. Container Transport Model results are also used to provide a more detailed understanding of the behaviour of repository components.

Figure 7-68 shows hydraulic head and advective velocities on plan and vertical sections through the middle of the placement room. The Main and Detailed Transport Model hydraulic heads are also shown. The good agreement confirms correct implementation of the fixed head external boundary conditions. Velocity plots provide insight into the effectiveness of the barrier system in reducing flow rates within the repository system. Although velocities are slightly lower within the EBS and slightly increased in the EDZ, the magnitudes are all very low and the flow is essentially stagnant.



26 Nov 2017
ContainerResults.mxd

Figure 7-68: Container Model: Hydraulic Head and Advective Velocity on Horizontal Plane through Repository (top) and Vertical Plane through Source Room (bottom)

Figure 7-69 shows advective velocities in a three dimensional view through the EBS and EDZ materials. The cross-section is cut vertically through the centre of the room. The highest velocities are in the Inner EDZ, with lower velocities within the placement room.

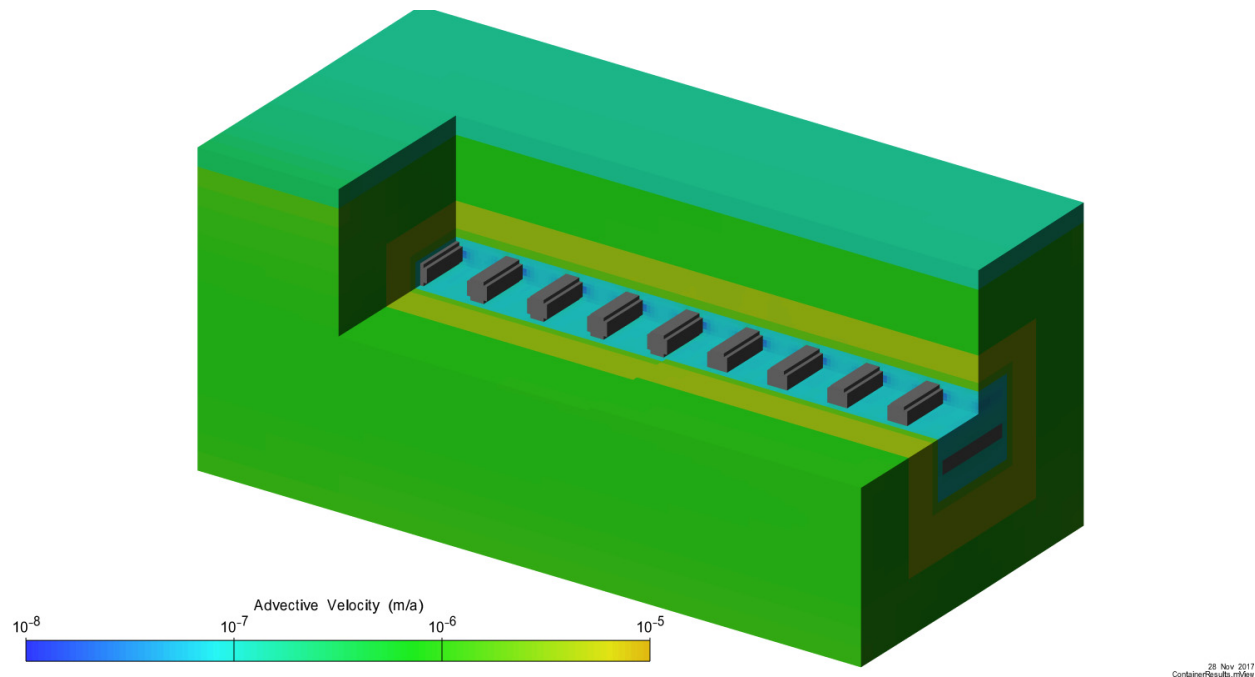


Figure 7-69: Container Model: 3D View of Advective Velocity Magnitudes in EBS and EDZ

7.7.2.5 Container Transport Model Radionuclide Transport Results

Base Case radionuclide transport modelling is performed for I-129, Cs-135 and U-238. The radionuclides are representative of the behaviours for non-sorbing, low sorbing, and very highly sorbing species.

I-129 Spatial Results

Figure 7-70 through Figure 7-72 illustrate the time dependent behaviour of the I-129 plume at repository level and on a vertical slice through the placement room. Contours of equivalent results from the Main and Detailed Transport Models are also overlaid for comparison. The results show a close correspondence between models, again providing confidence in the Transport Model results.

The outer concentration contour, 1 Bq/m^3 , corresponds to an effective I-129 drinking water dose of about $0.1 \mu\text{Sv/a}$ based on a water consumption of $1.08 \text{ m}^3/\text{a}$ per person.

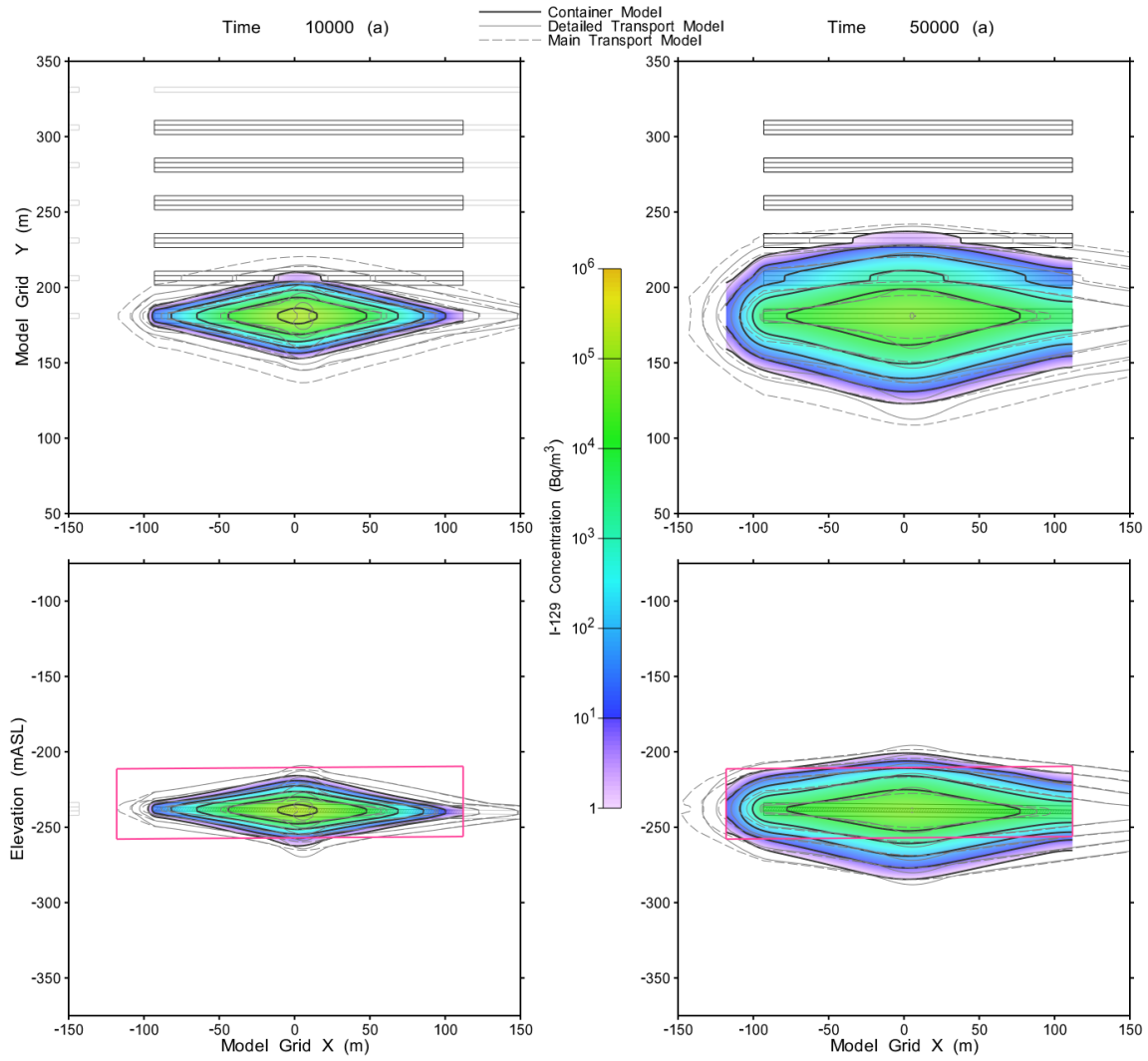
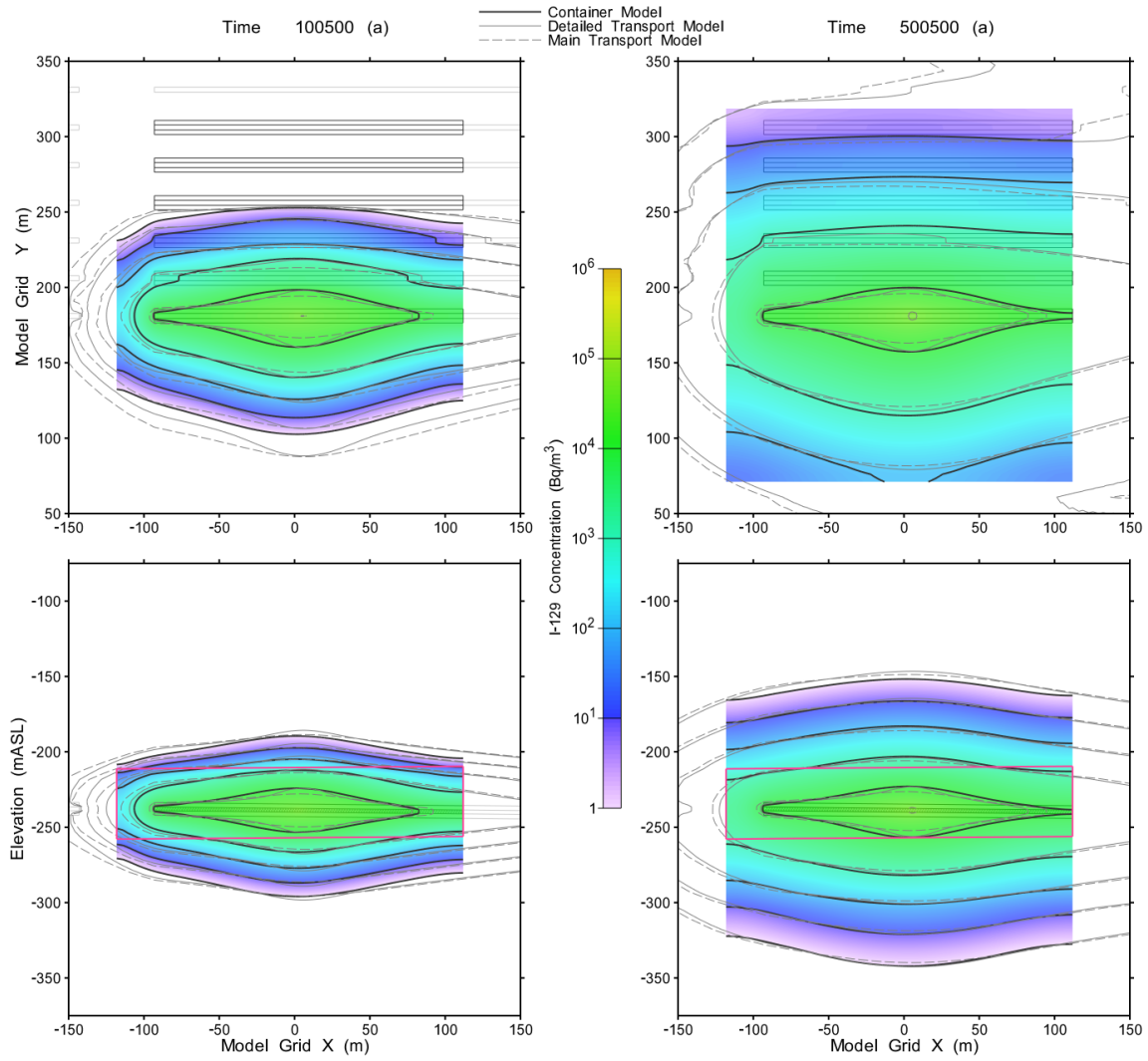
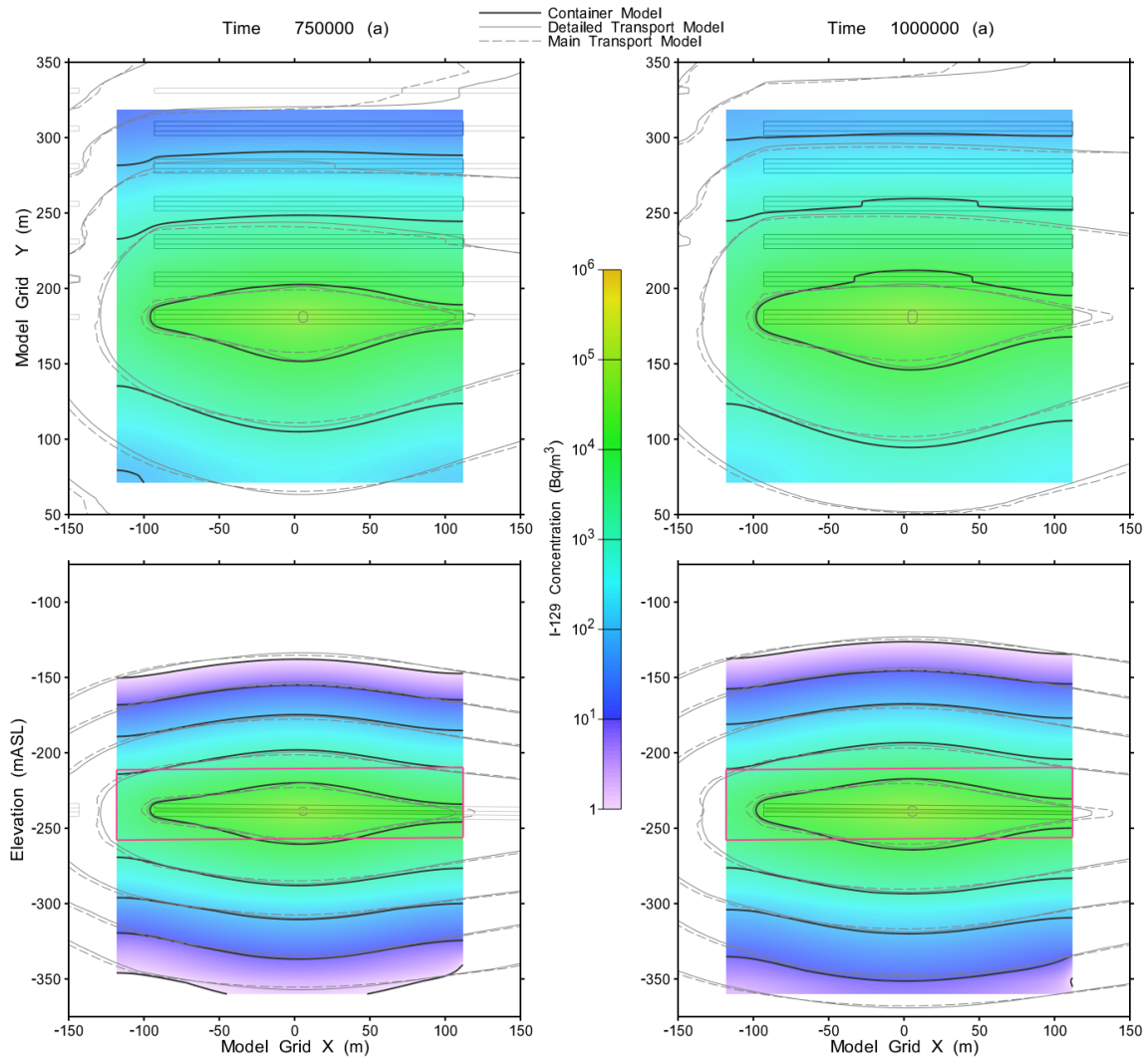


Figure 7-70: Container Transport Model: I-129 Concentration at 10 ka and 50 ka (top Horizontal, bottom Vertical)



28 Nov 2017
ContainerResults.mView

Figure 7-71: Container Transport Model: I-129 Concentration at 100.5 ka and 500.5 ka (top Horizontal, bottom Vertical)



31 Oct 2018
ContainerResults.mView

Figure 7-72: Container Transport Model: I-129 Concentration at 750 ka and 1 Ma (top Horizontal, bottom Vertical)

Changes in the three dimensional plume structure at various times are shown in Figure 7-73 through Figure 7-76.

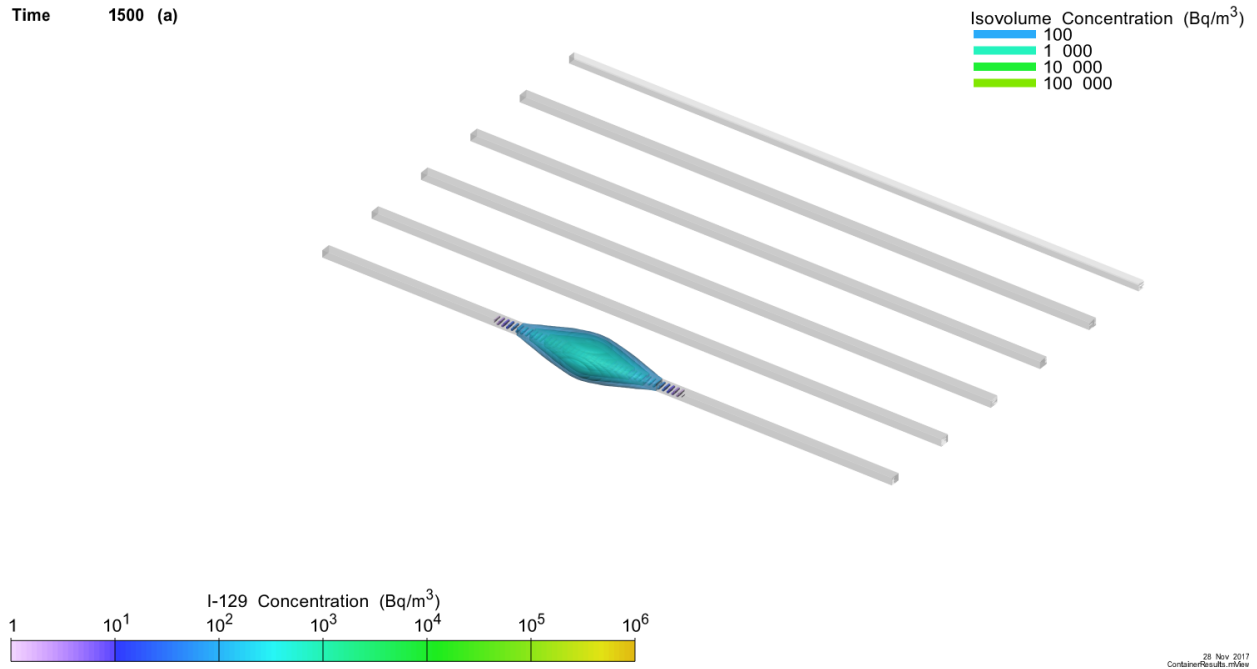


Figure 7-73: Container Transport Model: 3D View of I-129 Concentration at 1500 a

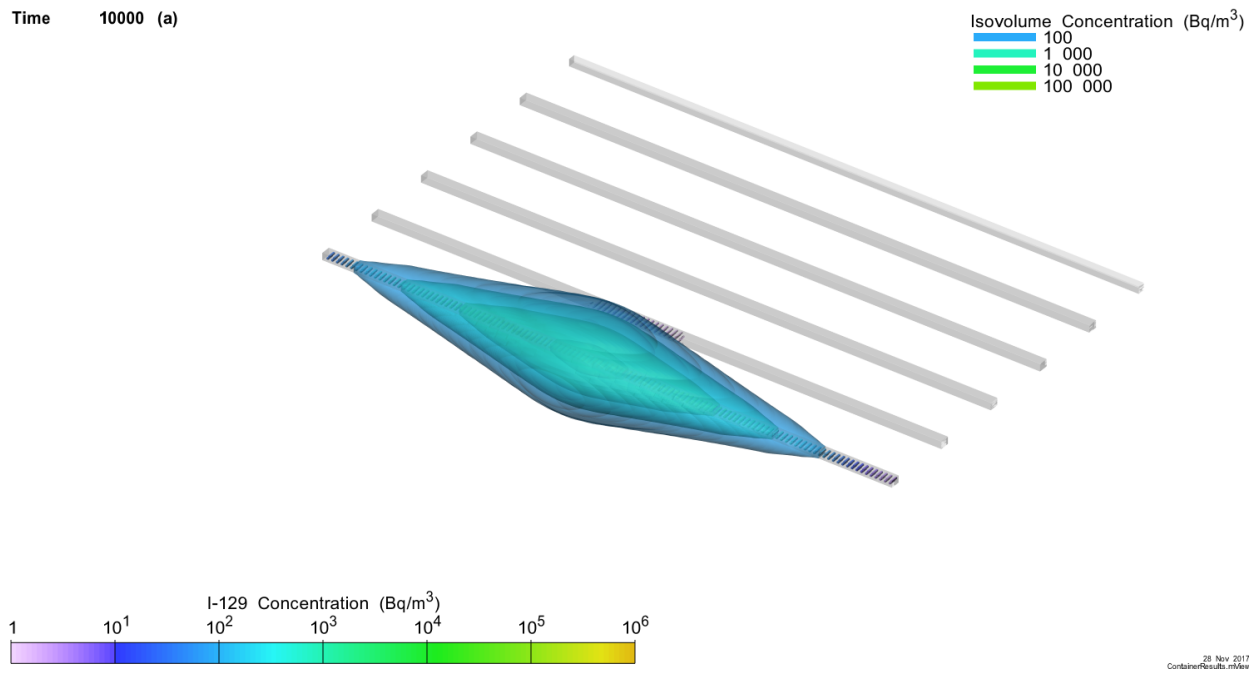


Figure 7-74: Container Transport Model: 3D View of I-129 Concentration at 10000 a

Time 500000 (a)

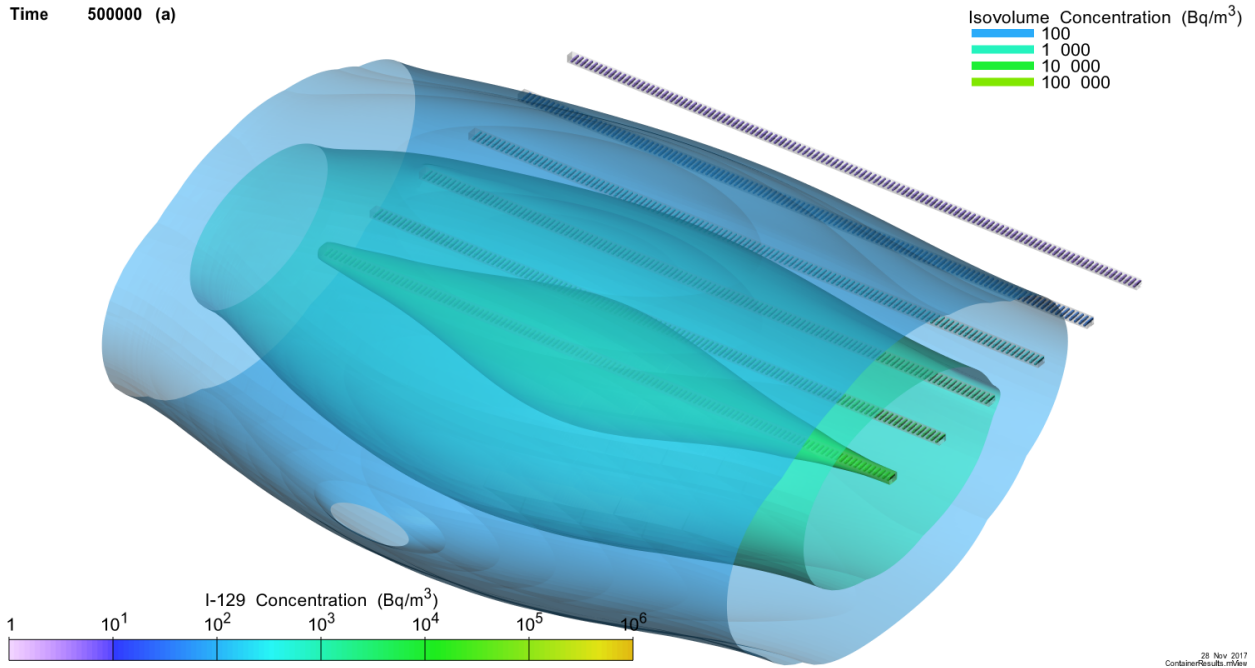


Figure 7-75: Main Container Transport Model: 3D View of I-129 Concentration at 500 ka

Time 1000000 (a)

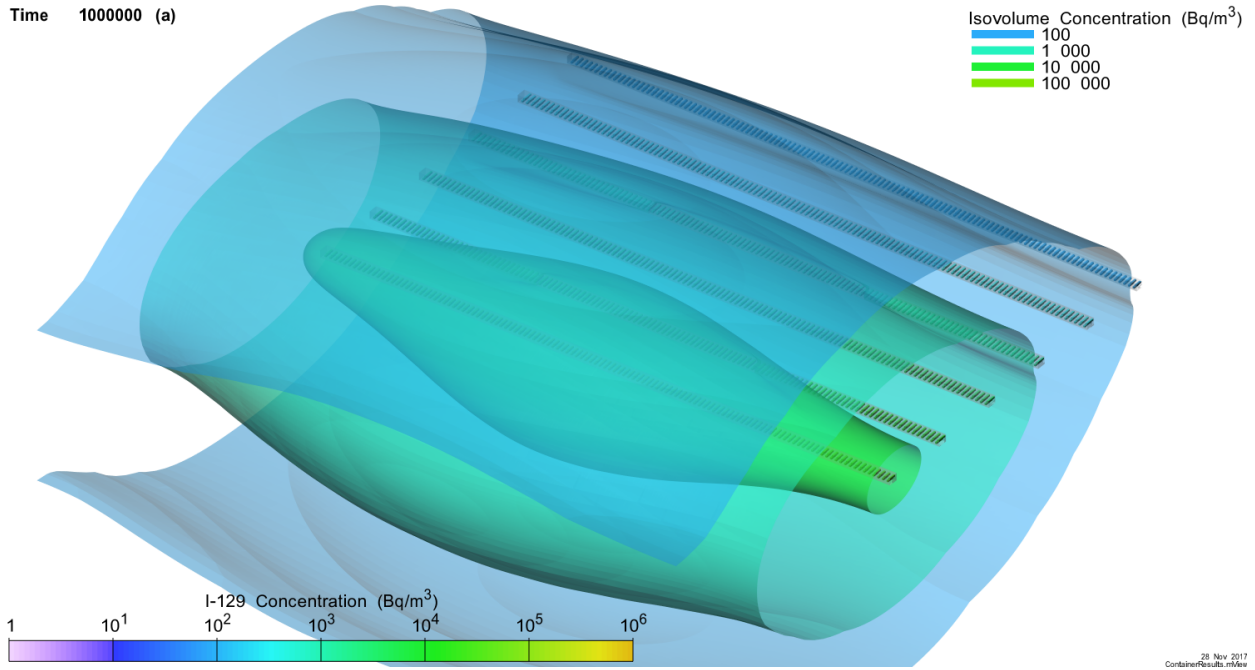
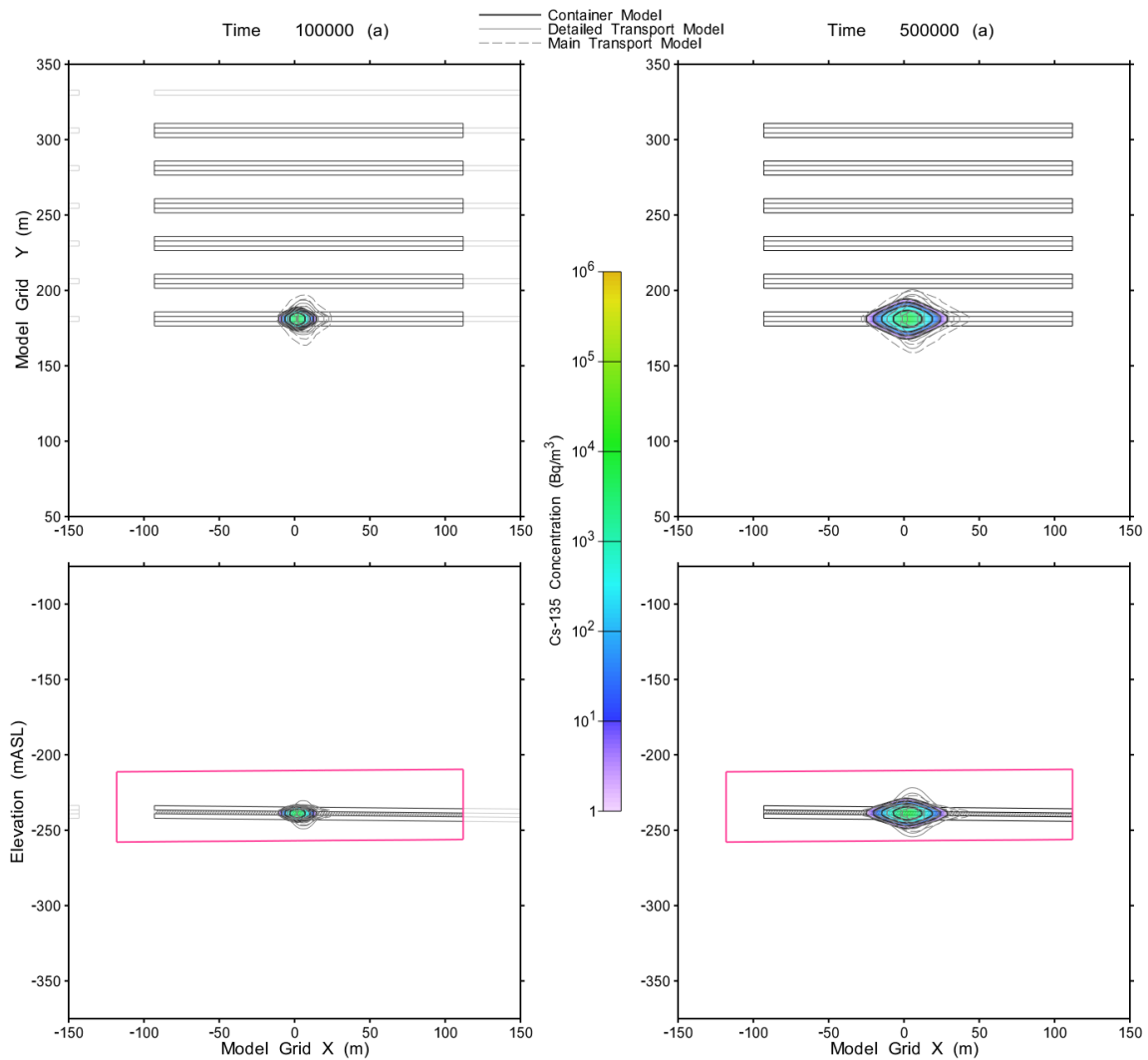


Figure 7-76: Container Transport Model: 3D View of I-129 Concentration at 1 Ma

Cs-135 Spatial Results

Unlike I-129, Cs-135 is sorbed onto the EBS and geosphere. Figure 7-77 and Figure 7-78 shows the Cs-135 plume at various times to 1 Ma. Figure 7-79 is a three-dimensional visualization of the Cs-135 concentration at 100 ka. The results show transport is largely confined to the vicinity of the source placement room. The 1 Bq/m³ contour line corresponds to a Cs-135 drinking water dose of about 0.002 μSv/a based on water consumption of 1.08 m³/a per person.



28 Nov 2017
ContainerResults Cs135.mView

Figure 7-77: Container Transport Model: Cs-135 Concentration at 100 and 500 ka

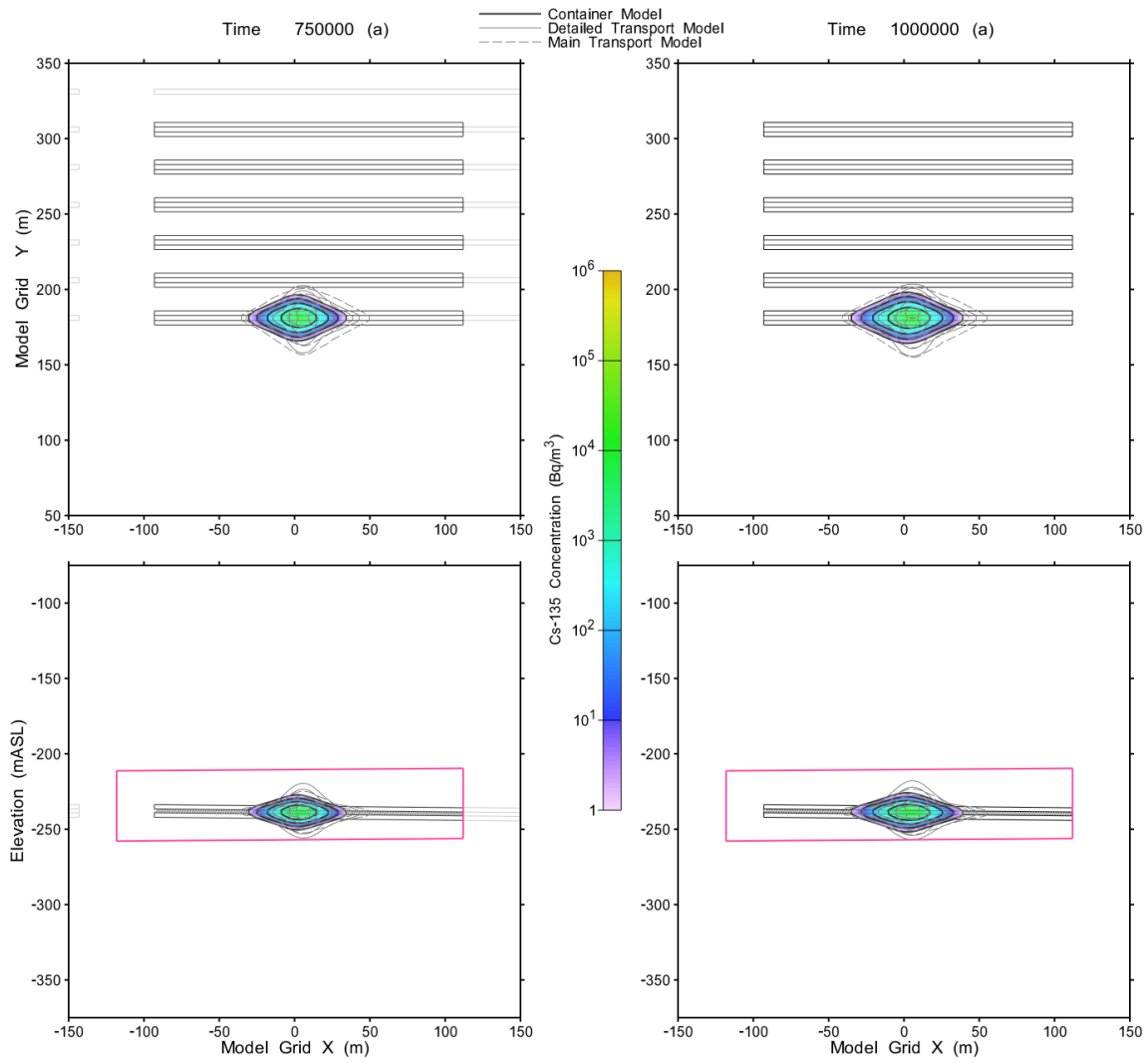


Figure 7-78: Container Transport Model: Cs-135 Concentration at 750 ka and 1 Ma

Time 1000000 (a)

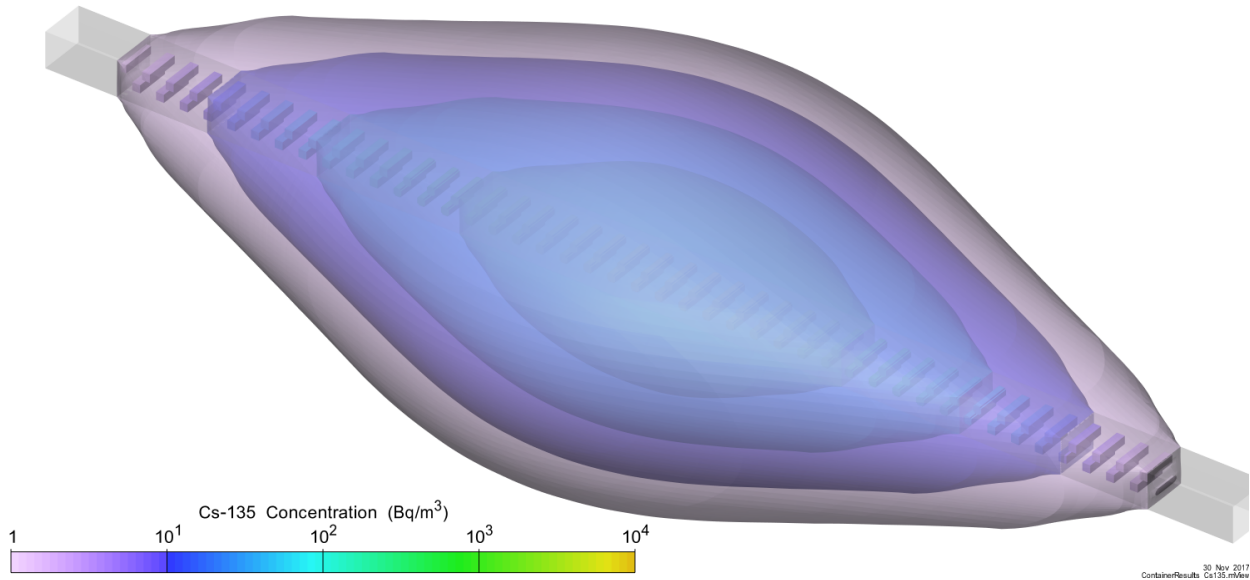
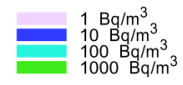


Figure 7-79: Main Container Transport Model: 3D View of Cs-135 Concentration at 1 Ma

U-238 Spatial Results

U-238 is very strongly sorbed onto sealing materials and the host rock. Consequently, transport of U-238 is limited to a small domain immediately surrounding the defective container. Figure 7-80 shows sectional views through the release plane and adjacent buffer after the tenth container failure. The contour plots are on a logarithmic scale. The 0.001 Bq/m³ concentration contour corresponds to an effective U-238 drinking water dose of about 0.00005 μ Sv/a (i.e., essentially zero) based on water consumption of 1.08 m³/a per person.

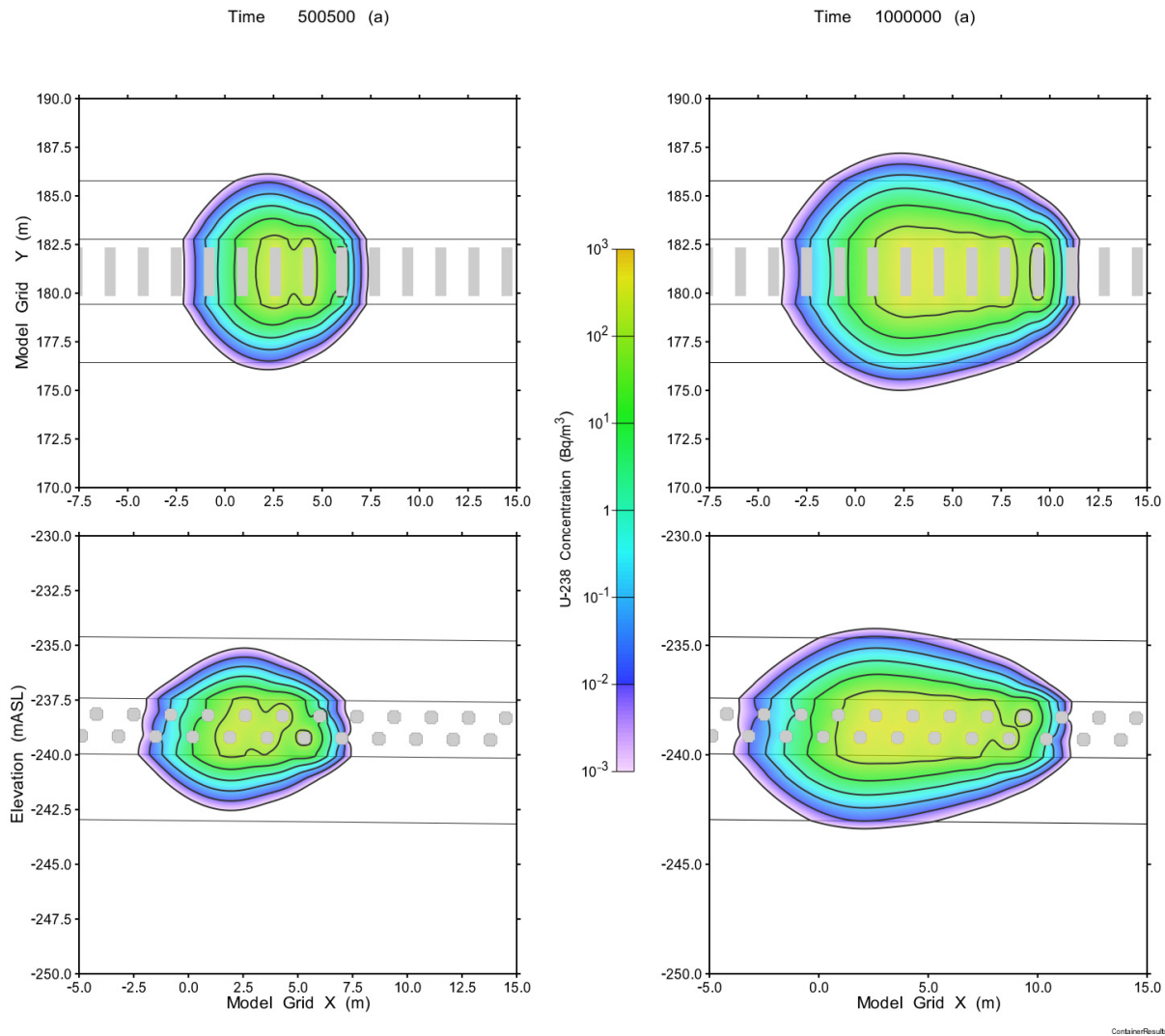


Figure 7-80: Container Transport Model: U-238 Concentration at 500.5 and 1 Ma

Figure 7-81 is a three-dimensional view of the U-238 plumes at 1 Ma (after failure of 10 containers). The limited extent of the plume expansion is evident.

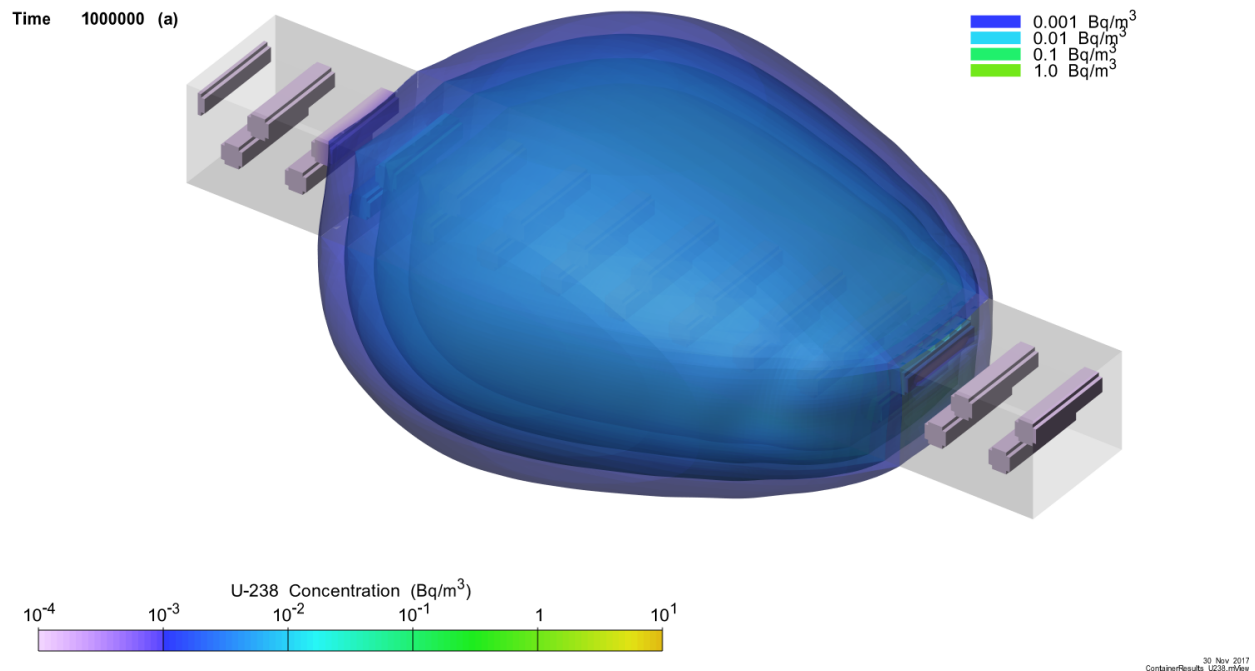


Figure 7-81: Main Container Transport Model: 3D View of U-238 Concentration at 1 Ma

7.7.2.6 Effect of Barriers on Radionuclide Transport

This section provides information to illustrate the effect of the various barriers on radionuclide transport for the Base Case. Results shown here are determined using the Main and Container Transport Models.

Figure 7-82 through Figure 7-84 show transport for I-129 (a non-sorbing radionuclide), Cs-135 (a low sorbing fission product), and U-238 (a highly sorbing solubility limited actinide) through the various barriers for the Base Case. The figures show the retarding effects of the various barriers on the transport of the different radionuclides.

Each figure shows:

- The release rate from the defective containers (labelled Container release in the figures).
- The release rate from the bentonite surrounding the defective containers (labelled Release from repository). This corresponds to transport through the gold hued surface in Figure 7-85.
- The release rate to the Cobourg formation. In this case transport from the Inner EDZ to Outer EDZ is determined. For the Container Transport Model, transport is subsequently out of the EDZ and into the immediately adjacent intact rock at the end of the room. This corresponds to the pink hued surface in Figure 7-85.
- The release rate to the Georgian Bay formation. Transport through the top of the Cobourg formation into the Georgian Bay/Blue Mountain formation.

- The release rate to the Queenston formation. Transport through the top of the Georgian Bay/Blue Mountain formation into the Queenston formation.
- The release rate to the Guelph formation. Transport from the top of the low-permeability system into the higher permeability Guelph formation.
- Capture by the well and surface discharge.

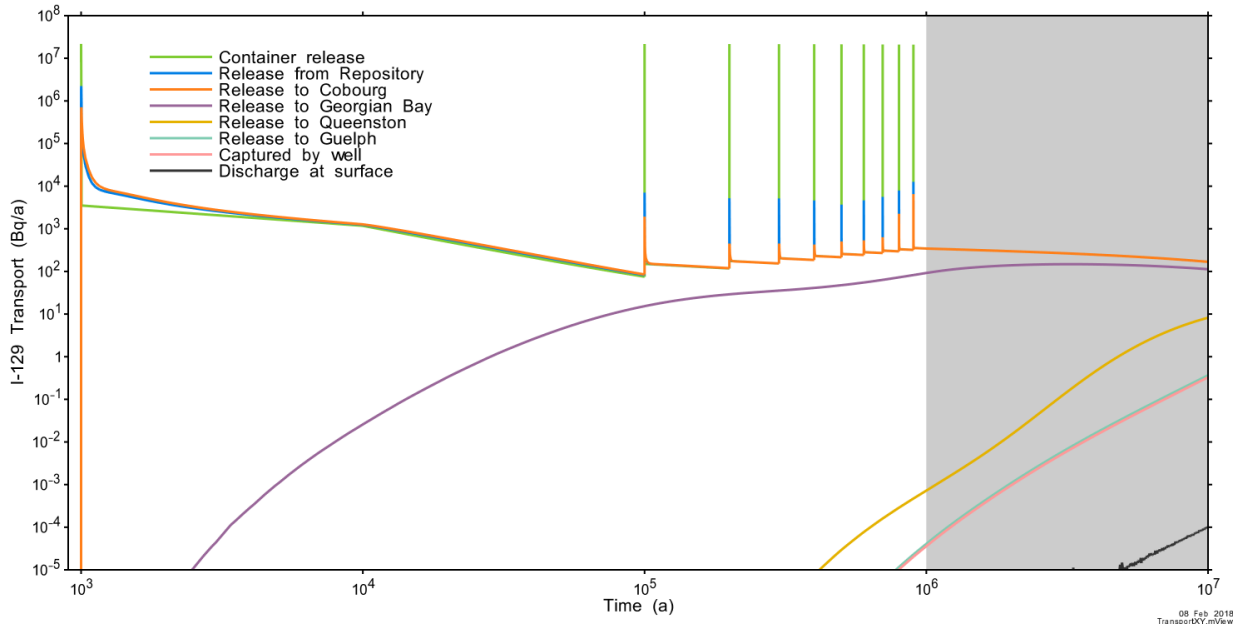


Figure 7-82: Main Transport and Container Models: Base Case I-129 Transport through Barriers

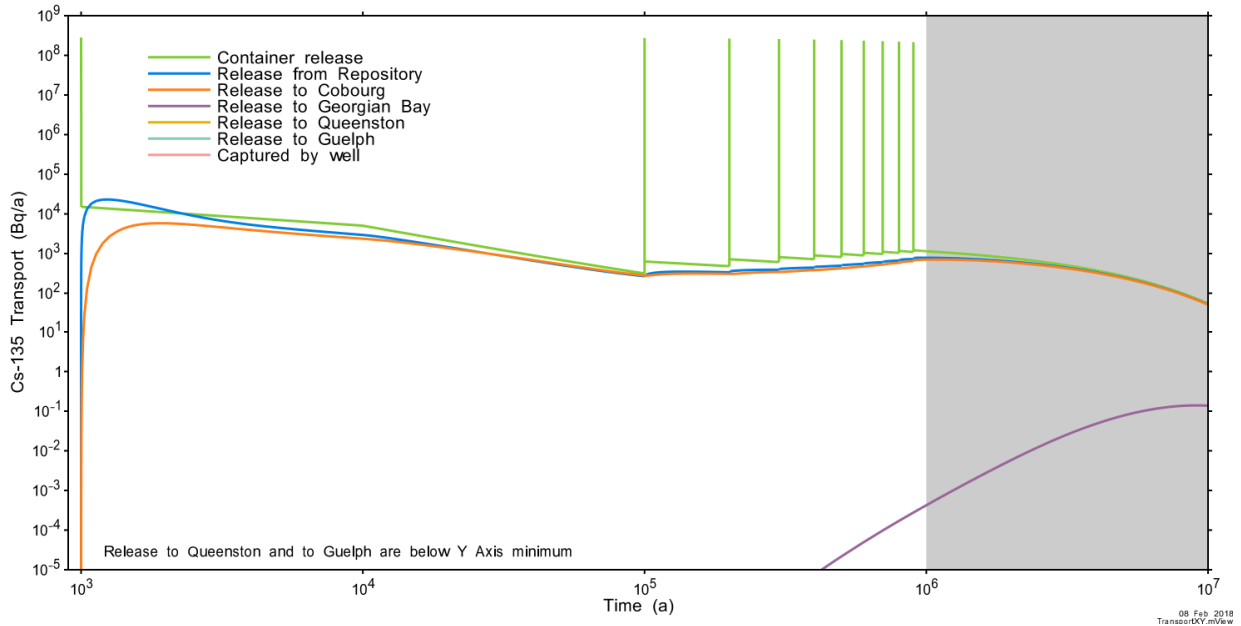


Figure 7-83: Main Transport and Container Transport Models: Base Case Cs-135 Transport through Barriers

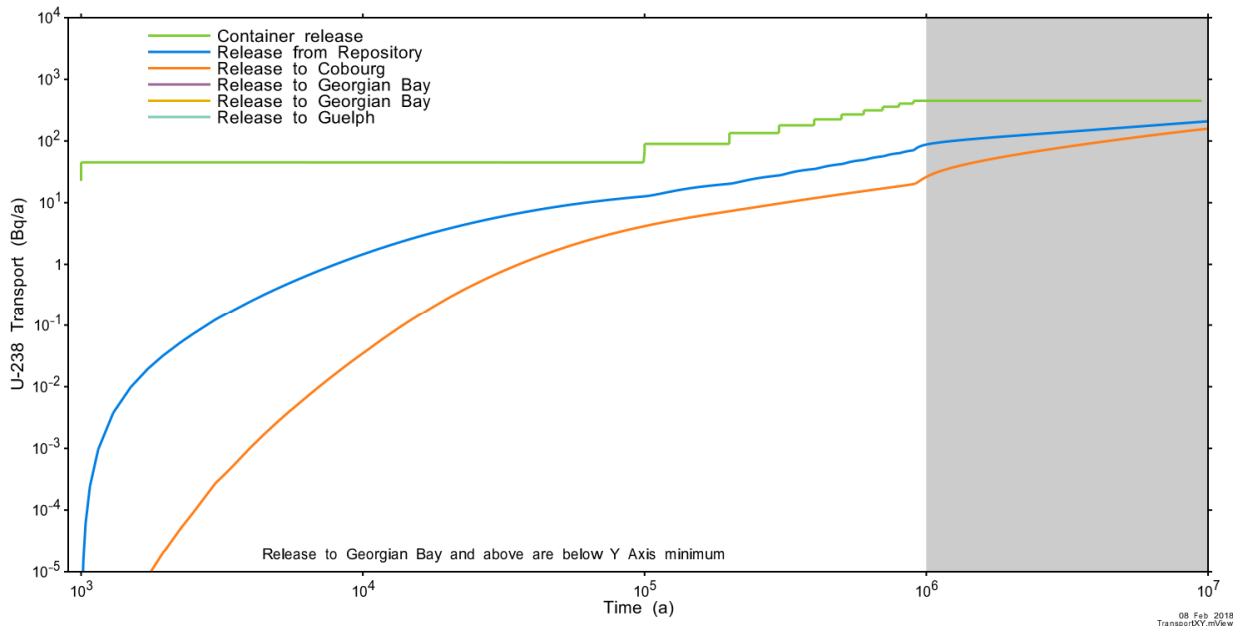
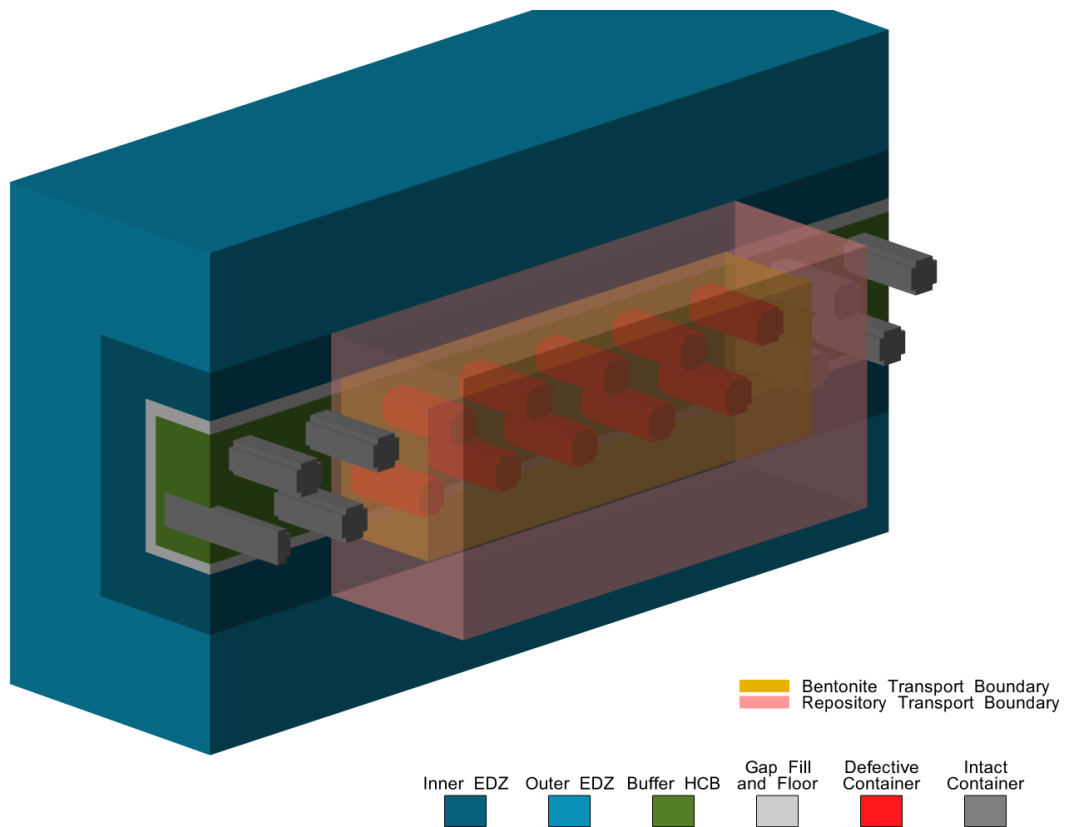


Figure 7-84: Main Transport and Container Transport Models: Base Case U-238 Transport through Barriers



Note: the pink hued surface is set at the boundary between the Inner and Outer EDZ

Figure 7-85: Container Transport Model: Transport Surface for the Bentonite and Repository Release

7.7.2.7 Summary of Results for 3D Modelling

Table 7-33 summarizes results for the sensitivity cases analyzed with the 3D Groundwater Flow and Transport Model in this Section 7.7.2. Modelling parameter sensitivity cases are not included. Only I-129 results are presented as this is essentially the only radionuclide released to the well.

Table 7-33: Summary of Results for I-129 3D Modelling

Case	1 Ma I-129 Transport to Well (Bq/a)	Ratio to Base Case⁽¹⁾
REFERENCE CASE	0	-
Base Case (Detailed Transport Model)	5.5×10^{-5}	-
Base Case (Main Transport Model)	3.6×10^{-5}	-
Base Case (Intermittent Well)	3.3×10^{-4}	-
Rock Hydraulic Conductivity Increased by a Factor of 10	5.4×10^{-5}	1.5
EDZ Hydraulic Conductivity Increased by a Factor of 10	4.0×10^{-4}	11
EBS Hydraulic Conductivity Increased by a Factor of 10	5.0×10^{-4}	14
100 m Erosion estimated same as Base Case	3.6×10^{-5}	1.0
150 m Overpressure in Shadow Lake Formation	2.1×10^{-3}	58

Notes: (1) Care should be taken when drawing conclusions through comparison of results because none of the comparisons are based on peak values, and much of the differences are due to transport time effects.

No simulation conducted for the 100 m Erosion case as noted in Section 7.7.2.6.

All other cases except Base Case (Detailed Transport Model) are simulated with the Main Transport Model.

The Well is in the most conservative locations for the Based Case and not repositioned for other cases. It is therefore possible the actual release could be higher.

7.8 Modelling and Results for the System Model

The System Model combines an idealized geometric description of the repository and a computationally efficient geosphere transport model with more detailed representations of releases from the used fuel and radionuclide transport in the biosphere to compute the radiological consequences. It is implemented in the SYVAC3-CC4 code.

Confidence in the model is provided through comparison with results obtained for selected radionuclides from the detailed 3D Groundwater Flow and Transport Model.

The description provided here applies to the situation in which the climate, biosphere and geosphere are constant throughout the simulation. The groundwater flow field is also constant.

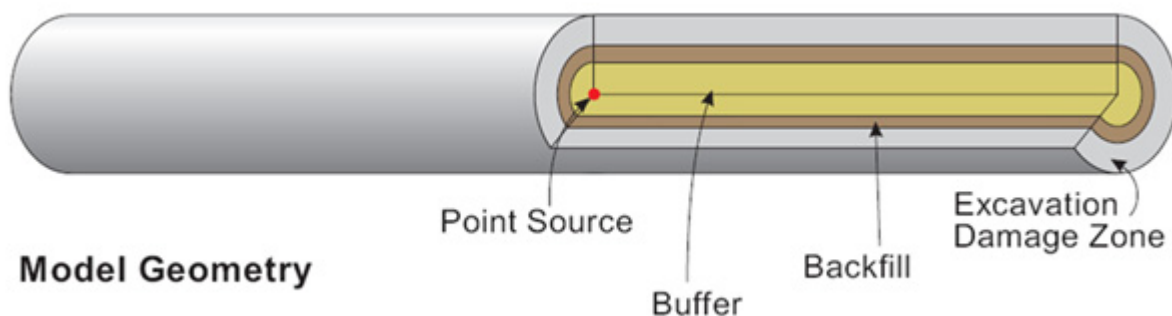
7.8.1 Methods

7.8.1.1 Repository Submodel

The System Model represents the placement rooms as a series of concentric cylinders of varying thicknesses (Figure 7-86) to approximate radionuclide transport through the buffer, backfill and excavation damaged zone. This simplification allows for the use of semi-analytical solutions which result in fast computation times suitable for use in probabilistic analyses.

Conceptually, the model represents one container within a placement room surrounded by concentric cylinders of buffer material, backfill material and EDZ. Input data for the concentric cylinders are specified such that only homogenized buffer and gap fill (~37 cm thick – corresponding to the minimum vertical distance between the container and placement room wall) and placement room Inner EDZ (1 m thick) are represented. The length of the concentric cylinder is about 342 m, corresponding to the length of the placement room. A semi-infinite boundary condition that maintains continuity of concentration and continuity of flux is established at the outer boundary.

The radionuclide release from the defective container is represented by a source that lies along the axis of the nested cylinder. The container is not physically represented.



Note: the backfill thickness is 0 cm in the repository model used in this study.

Figure 7-86: System Model, Repository Submodel

The repository submodel simulates the following processes:

- Container Failure – At a specified time some of the containers are assumed to fail.
- Instant Release – A fraction of soluble fission products, representing the radionuclide inventory present at the UO₂ fuel grain boundaries and cladding gap is instantaneously dissolved once the container is breached and water comes into contact with the used fuel. A fraction of the C-14 in the Zircaloy is also released instantaneously when water contacts the Zircaloy.
- Congruent Release – A slow long-term radionuclide release occurs, consistent with the long-term corrosion / dissolution of the ceramic fuel pellet and release of radionuclides trapped within the fuel matrix. Radionuclides are also released from the Zircaloy as it corrodes.
- Precipitation – The precipitation of elements whose concentration in the container exceeds the solubility of the element.
- Radioactive Decay and Ingrowth – Radioactive decay of radionuclides and progeny.
- Transport – The diffusive and advective transport of radionuclides through the engineered barrier system.

As discussed in Section 7.2.1.2, the defective containers are assumed to fill with water as soon as the steel vessel is breached, which itself is assumed to occur immediately upon full penetration of the copper coating. For the Base Case, this means the first container is entirely full of water at 1000 years.

7.8.1.2 Geosphere Submodel

The geosphere is represented as a network of 1D transport pathways. Each 1D pathway represents a path in which transport is primarily in one direction, with relatively uniform material properties. This network is defined to approximate the hydrogeological and geochemical features of the geosphere zones located between the repository and the surface biosphere. Transport in each segment is characterized using the 1D advection-diffusion equation, for which robust semi-analytical solutions are available.

The starting point for generation of the System Model geosphere network is a detailed 3D steady-state groundwater flow field determined with the 3D Groundwater Flow and Transport Model. However, because the hydraulic conductivity of the hypothetical geosphere is so low, contaminant transport is effectively entirely diffusive and advective flow trajectories have not been used. Instead, a series of diffusive transport pathways has been independently defined and the geosphere model created through execution of the following steps.

- Sector Selection – The repository is divided into sectors. A sector is typically defined so that its properties are uniform. For example, it has the same waste form type and room length, and it connects to a portion of the groundwater flow field whose properties are approximately uniform for the entire sector. Different sectors typically have different properties, and often the properties of the surrounding geosphere are the delineating factor.
- Selection of Representative Pathways – A representative pathway for each sector is generally chosen to give the shortest travel time to the surface. In areas of low flow velocity, diffusion towards fractures (if present) may be the shortest travel path. Pathways may

merge with pathways from other sectors and may diverge as portions of the plume are captured by the well or terrestrial discharge areas.

- Selection of Nodes along Pathways – Nodes are generally selected at material property boundaries so that the resulting segments have constant properties.
- Addition of Well and Near-surface Nodes – Additional nodes are required for the well - for example, upper and lower reference nodes define the range of positions for the well and drawdown nodes, which give a better representation of the drawdown cone in the vicinity of the well. Also, near-surface nodes are added to define an overburden and a sediment node for each discharge location, and possibly terrestrial and wetland nodes associated with aquatic discharges.
- Property Assignment – Data needed include the Cartesian coordinates of all the nodes, hydraulic heads and temperatures at the nodes, and hydraulic and chemical properties of the different geosphere units.
- Well Model – The effects of the well drawdown on adjacent node heads is accounted for via an analytical well model within the aquifer, and by a site-specific well-effects model outside the aquifer.

Sector Selection

Since all containers contain the same used fuel waste form and the placement room design is common across the repository there is no sectorization on this basis. Also, as transport in the near field is diffusion dominant, transport is largely uniform across the entire repository area. As a result, sectorization for this study is required solely to accommodate the different assumed container failure times. Ten sectors, each representing one container or a cluster of containers all failing at the same time, are included.

This 10 sector structure is used in the two representations described below:

- In the Base Case representation, each of the 10 defective containers is modelled as a separate sector to allow for input of specific container failure times. The containers are clustered in the location that results in the well capturing all contaminants entering the Guelph aquifer. No other containers are represented in this model. This model is used for the Normal Evolution Scenario and associated sensitivity studies, and for the probabilistic case in which the number of defective containers is fixed.
- In the Full Case representation, the entire population of containers in the repository is divided evenly across the 10 sectors. This is used for the All Containers Fail Disruptive Event Scenario and for the probabilistic case in which the number of defective containers varies.

Selection of Representative Pathways

For each sector, a representative transport pathway is selected to approximate the transport segment leading to the surface discharge point(s). These pathways may converge and combine on the way to the surface, or conversely may diverge and lead to different discharge points, depending on conditions such as the well demand rate.

In this study, the diffusive nature of transport results in two representative pathways from the repository to the surface. The first represents the bulk of the transport through the sedimentary rock mass, while the second represents the small fraction of slightly faster transport through the shaft materials. Despite diffusive transport being uniform in all directions, these two pathways are conservatively selected to represent the the shortest (straightline) pathways to the surface.

Selection of Nodes along Pathways

Representative transport pathways are broken up into shorter segments, with each representing either a stratigraphic layer of the sedimentary formation or a single component of the shaft seal design. Nodes define the boundaries of each of these layers allowing a given segment to represent a single material.

Addition of Well, Overburden and Sediment, and Other Features

Four additional nodes are associated with the well. A well discharge node is located at the ground surface immediately above the well aquifer node (the well depth is 219 m). A well capture algorithm determines how much of the contaminant plume is captured by the well.

For proper operation of the code, the surface water system is assumed to have both a terrestrial discharge node and an aquatic discharge node. The aquatic and terrestrial discharges have an overburden and associated sediment / soil node for a total of four additional nodes.

Property Assignment

Once the network is defined, physical and chemical properties are assigned to the various rock layers, shaft seal materials, overburden, and sediment nodes and segments.

Values for the hydraulic heads at each node location are obtained from 3D modelling results. Values for transport parameters such as porosity and hydraulic conductivity are supplied for each network segment. Advection is typically the dominant component of geosphere transport at shallow depths and in aquifers; however, diffusion and dispersion processes are dominant in instances of very low advective flow (e.g., in the deep geosphere). The model accounts for both advective and diffusive transport processes.

Finally, retardation due to sorption is calculated using the sorption coefficient (K_d) assigned to each network segment.

Well Model

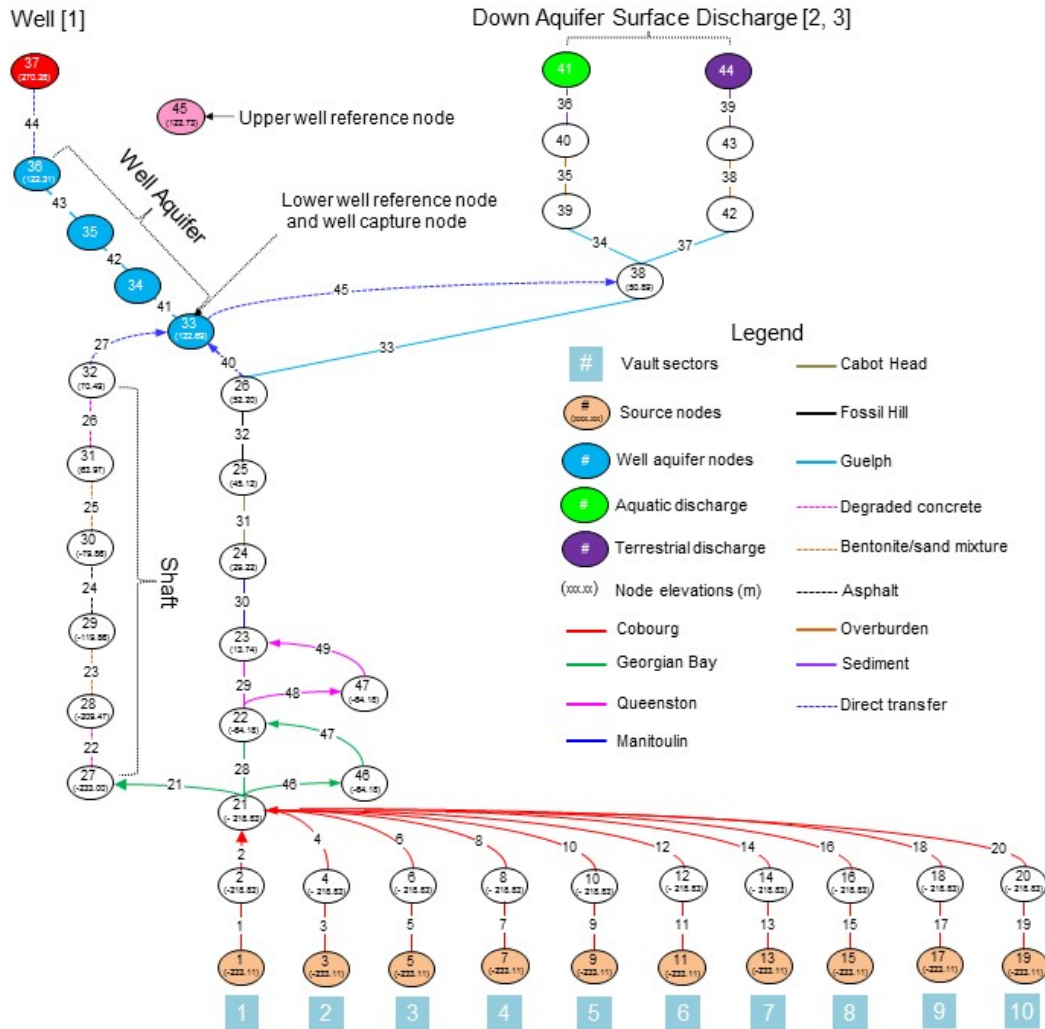
The well is located in an aquifer capable of supplying sufficient water.

The System Model uses an analytical solution to provide the hydraulic head drawdown at the nodes and the capture envelope for the groundwater flowing in the aquifer. The well model allows the assessment of well demands other than that in the Base Case, which is useful in assessing alternative lifestyles or critical groups, and in probabilistic calculations.

The effects of the well extend outside the well "aquifer". These cannot be calculated with the well model equations so 3D modelling results for different well demands are used to derive empirical relationships that describe these effects. These include: drawdown at nodes outside

the aquifer, plume fractionation towards the well at branching locations outside the well aquifer, and reduction factors for discharge areas due to capture of groundwater by the well.

The process described above has been applied to develop the Geosphere Submodel. The complete network for the Geosphere Submodel consists of 47 nodes. The network and its connectivity are shown in Figure 7-87.



Notes: Only nodes (ellipses) with a particular function are colour coded. The line segments, representing the 1D transport pathways, are colour coded (see legend) to indicate the geosphere zone through which they pass.

Figure 7-87: System Model, Geosphere Submodel: Transport Network Connectivity

Section 7.8.1.4 shows transport results generated with this model have good agreement when compared against similar results generated with the detailed 3D model.

7.8.1.3 Biosphere Submodel

Key elements of the model are discussed below. A detailed description of all input data used is available in Gobien et al. (2018).

The topography of the watershed area near the repository is relatively flat as shown in Figure 7-9. The local biosphere is assumed to have the characteristics of the Southern Ontario region and its properties are assumed constant during the simulation period. The normal present-day variation of climate and other biosphere parameters is included via the use of probabilistically sampled parameter values.

Surface Water

Radionuclides discharging from the geosphere can reach the surface through a well or through one or more topological low points.

It is conservatively assumed that radionuclides discharging to the well also simultaneously end up in one of the potential discharge areas. This allows local biosphere transfer processes such as runoff, recycling and atmospheric suspension and deposition to be treated very simply. The transport processes considered in the surface water submodel are:

- Discharge to surface water – direct discharge from the geosphere into rivers in the surrounding watershed area.
- Sedimentation – contamination of sediments by settling of particulates in the water.
- Biological Uptake – uptake of contaminants by plants and animals residing in the surface water bodies.
- Suspension and Volatilization – loss of contaminants from the surface water to the atmosphere.
- Outflow – flow of contaminated water further downstream. The impact of contaminant releases to the downstream environment is not assessed since they are bounded by the site impacts.
- Irrigation – well water or surface water can be used as the water source for irrigation of soil. In the current study well water is used for irrigation of gardens. The forage field is not irrigated.
- Domestic Use – human water use for drinking, cooking, bathing, laundry, and watering livestock.

A characteristic of this illustrative site with diffusion dominant transport at depth and a low permeability overlying rock formation is that discharge areas may be distant and involve multiple surface watersheds, and any corresponding discharge would be at very low concentrations. For this illustrative case study, surface discharge areas were estimated from transport modelling where the calculated cumulative discharge over 10 million years reached the background concentration of I-129 in Canadian water samples (i.e., 10^{-4} Bq/m³, Sheppard et al. 2011a). Table 7-34 provides the surface discharge areas, and the relative proportions of the discharge areas that are terrestrial or covered by water.

Table 7-34: System Model - Biosphere Submodel, Surface Water Discharge Areas

Watershed	Total Discharge Area ⁽¹⁾ (m ²)	Aquatic Discharge ⁽²⁾ (m ²)	Terrestrial Discharge ⁽³⁾ (m ²)
Watershed A	1.08x10 ⁶	5.27x10 ⁵	5.50x10 ⁵
Watershed B	1.34x10 ⁵	6.16x10 ⁴	7.26x10 ⁴
Watershed C	0	0	0
Watershed D	5.67x10 ⁶	2.32x10 ⁶	3.35x10 ⁶

Notes: (1) Discharge areas equal to 4.7%, 6.1%, 0% and 8.8% of the watershed area for watersheds A, B, C, and D, respectively.

(2) Aquatic fraction based on areas equal to 2.3%, 2.8%, 0%, and 3.6% of the watershed area for watersheds A, B, C and D, respectively.

(3) Terrestrial fraction set to total discharge area minus the aquatic discharge.

Soil

The soil model calculates the concentration of contaminants in the surface (rooting or cultivated) soil layer. This layer is assumed to be well-mixed due to, for example, plowing in an agricultural field or bioturbation. Two soil models are considered, one for upland soil and one for shallow soil. The upland soil model describes a typical soil layer, with the water table a reasonable distance below the surface soil layer. In the shallow soil model, the water table extends into the surface soil layer on a regular and extended basis (as in the case of marsh or swamp land). The distinction between these two soil types is important in determining how readily contaminated groundwater can reach the surface. In the upland soil model, it must be transported by processes such as capillary action while in the shallow soil model groundwater is discharged directly into the surface soil.

Areas of surface soils have specific designations including use as a vegetable garden, a forage field, and a woodlot. Some of the parameters describing the transport pathways in the soil model are dependent on the type of field (e.g., irrigation rate).

The transport processes considered in the soil model are:

- Irrigation – contaminated water from the well or surface water is added to the soil.
- Groundwater Discharge – direct discharge from a contaminated groundwater water source below the surface soil (shallow soil only).
- Capillary Rise – upwelling of contaminated groundwater from the water table (upland soil only).
- Leaching – contaminants in surface soil migrate to deeper soil layers as water percolates through the soil layer.
- Runoff – precipitation runoff from the watershed area entering the water body.

- Root Uptake – uptake of contaminants by plants and trees.
- Suspension and Volatilization – loss from the soil to the atmosphere due to soil resuspension (wind erosion) and volatilization.
- Deposition – deposition of contaminants from the atmosphere onto surface soils.

For context, some of the physical characteristics of the soil at the hypothetical site are described in Table 7-35 (Gobien et al. 2018). These reflect the values in CSA (2014) where available.

Table 7-35: System Model - Biosphere Submodel, Soil Properties

Parameter	Base Case Value	Comment
Soil types	Sandy	Using soil type from Western Ontario.
Surface soil bulk density	1500 kg dry soil/m ³ soil	Sandy Soil
Active surface soil depth	0.2 m	This is the active or root zone layer for which nuclide concentrations in the soil are determined (CSA 2014).
Soil Depth to water table	1.5 m	Normal PDF, 1.5 m mean, 0.5 m standard deviation, and bounds of 0.01 to 2.5 m.
Minimum soil depth to water table for upland soil model	0.5 m	This is the minimum depth-to-water-table at which the upland soil model is used. For smaller depths, a shallow soil model is used that allows for flooding of the surface soil by contaminated groundwater.
Upland soil leach rate fraction	0.55	Fraction of net precipitation (precipitation + irrigation – evapotranspiration) that infiltrates into soil. Uniform PDF from 0.1 to 1.

Note: Data taken from Gobien et al. (2018).

Atmosphere

The atmosphere model calculates radionuclide concentrations in air due to the following transport processes:

- Suspension and Volatilization – contamination of the air from particulate or gaseous releases from surface water (if present) and soil.
- Dispersion – reduction in the concentration of contaminants in the air by having them disperse over a larger area.
- Fire – release of contamination into the air from fires assumed to occur on-site. This includes fuel fires used by the critical group as well as natural fires such as a forest fire.

A list of parameters important to the concentration of airborne contaminants is given in Table 7-36 (Gobien et al. 2018). When calculating the concentrations in the atmosphere, all

contaminants are conservatively assumed to be located within a couple of metres of the land surface.

Table 7-36: System Model - Biosphere Submodel, Climate and Atmosphere Parameters

Parameter	Base Case Value	Comment
Annual total precipitation	1.02 m/a	Normal PDF with a SD of 0.16 and bounds of 0.3 and 3.0 m/a. Calculated using historical records between 1965 and 2006 in Owen Sound, which is assumed to be representative of a sedimentary site in Southern Ontario. The bounds represent half the minimum and twice the maximum recorded rainfall.
Annual surface average runoff	0.42 m/a	Average value for the region defined as "Great Lakes". Variation coefficient is 0.72, which is the ratio of the monthly mean to the standard deviation. Conservatively assume variation on an annual basis is the same; thus, standard deviation is 0.58. Bounds are taken as the range of Ontario runoff values, thus 0.1 to 0.8 m/a.
Average wind speed ⁽¹⁾	2.36 m/s	Normal PDF with mean of 2.36 m/s (8.5 km/h), standard deviation of 0.64 m/s, and bounds of 0.44 and 6 m/s.
Dry deposition velocity	0.0014 m/s	CSA (2014) dry deposition velocity for all radionuclides except for noble gases and N-13(0 m/s), Cl-36 (0.02 m/s), particular iodine (0.0036 m/s), elemental iodine (0.0075 m/s) and organic iodine (9.2×10^{-6} m/s). Geometric standard deviation of 2 is adopted.
Atmospheric dust load ⁽¹⁾	3.2×10^{-8} kg _{drysoil} /m ³ _{air}	Lognormal PDF with GM calculated from suspended particulate matter concentrations in ON, NB, QC and SK during years 1996 to 2002. GSD of 1.7 with bounds of 7.0×10^{-9} and 7.5×10^{-8} kg _{drysoil} /m ³ _{air} .
Atmospheric aerosol load ⁽¹⁾	2.9×10^{-10} m ³ _{water} /m ³ _{air}	Lognormal PDF with geometric mean of 2.9×10^{-10} m ³ _{water} /m ³ _{air} , and geometric standard deviation of 1.41. Based on estimate for sea salt aerosol over oceans.
Washout Ratio	5 500 000	Washout ratio for deposition to soil for all elements other than noble gases and iodine. This value is conservative for iodine. CSA (2014) recommends 160000 for elemental iodine and 74000 for organic iodine.

Note: (1) Values for these parameters not available in CSA (2014). See Gobien et al. (2018) for information.

Dose Calculations

The dose model uses the concentrations of radionuclides in the various biosphere compartments to calculate the annual dose to a member of the critical group.

To ensure that dose rates are not underestimated, conservative assumptions are made concerning the characteristics of the critical group. Specifically, it is assumed that the members of the critical group spend all their lives in the local biosphere and obtain all their food, water, fuel and building materials from the local biosphere. The water source for the critical group is a

well that intercepts the radionuclide plume. Their food includes plants grown in a garden, domesticated animals and fish. All plant and animal biota used as food are subject to contamination from surface water, soil and air. This lifestyle is consistent with but more self-sufficient than typical current habits and leads to an overestimate of the impact. Because of these characteristics, the hypothetical member of the critical group is referred to as a Self-Sufficient Farmer. The Self-Sufficient Farmer has been found in previous studies to be a good indicator of risk for a range of plausible lifestyles (Garisto et al. 2005).

Some critical group lifestyle characteristics are shown in Table 7-37 (Gobien et al. 2018).

Table 7-37: System Model - Biosphere Submodel, Human Lifestyle Data

Parameter	Reference Case Value	Comment
People per household	3	Piece-wise uniform PDF from 1 to 12 people.
Domestic water demand per person	100 m ³ /a	Lognormal PDF with geometric mean 100 m ³ /a, GSD of 46 and bounds of 7 and 690 m ³ /a.
Man's total energy need	17490 kJ/d	95 th percentile
Man's air inhalation rate	8400 m ³ /a	95 th percentile
Man's water ingestion rate	1080 L/a	95 th percentile
Man's meat ingestion rate	289 g _{fw} /d	95 th percentile intakes for male adult. The model only considers the consumption of beef meat, but the meat ingestion amount is set to the sum of all meat sources other than fish and chicken tracked in CSA (2014) (beef offal, veal, pork, lamb, deer, deer and rabbit).
Man's milk ingestion rate	516 g _{fw} /d	95 th percentile intakes for male adult. Defined as a constant PDF.
Man's plant ingestion rate	1824 g _{fw} /d	95 th percentile intakes for male adult. Sum of grain, fruits and berries, vegetables, mushrooms, potatoes, dulse and honey. Defined as a constant PDF.
Man's poultry ingestion rate	239 g _{fw} /d	95 th percentile intakes for male adult. Sum of poultry and egg. Defined as a constant PDF.
Man's fish ingestion rate	34 g _{fw} /d	95 th percentile intakes for male adult. Sum of fish and shellfish. Defined as a constant PDF.
Soil ingestion rate	0.12 kg/a	95 th percentile of incidental soil ingestion rate.
Annual energy consumption per household	1.2x10 ⁵ MJ/a	Normal PDF with GM of 1.2x10 ⁵ MJ/a, standard deviation of 8x10 ³ MJ/a and bounds of 10 ⁵ MJ/a and 1.3x10 ⁵ MJ/a
Building occupancy factor	0.8	Fixed value
Building air infiltration rate	0.35 /hr	Value is conservatively set to maximize entrainment.

7.8.1.4 Verification of the System Model

In this section, transport results for the System Model are compared against similar results obtained from the detailed 3D simulations. Comparisons for I-129, Cs-135, and Cl-36 are made, thereby providing a cross-verification of the SYVAC3-CC4 and the FRAC3DVS-OPG code implementations. U-238 is not included in this comparison because there is very little movement of U-238 within the repository and surrounding rock due to the highly sorbing nature of this radionuclide, as discussed in Section 7.7.2.3.3.

The Base Case representation of the Geosphere Submodel is compared against Base Case results, while the Full Case representation is compared against the All Containers Fail at 60,000 Years Disruptive Event Scenario.

The 3D transport results used in the comparison are described in Section 7.7.2.3.3 (Base Case) and Section 7.9.2 (All Containers Fail).

Transport Comparison for the Base Case

Comparisons of transport from the repository to the well for the Base Case are shown in Figure 7-88 for I-129, Figure 7-89 for Cs-135 and Figure 7-90 for Cl-36. For each radionuclide, transport is compared at the interface between the Cobourg and Georgian Bay formations (i.e., at the top of the Cobourg), at the interface between the Georgian Bay and Queenston formations (i.e., at the top of the Georgian Bay) and at the Well. For species other than I-129 transport beyond the Cobourg is off-scale low.

I-129 is mobile non-sorbing species with a long half-life (15.7 million year). The transport results compare relatively well at the top of the Cobourg, top of the Georgian Bay and the well. The maximum transport rate to the well for I-129 is within about 30% of the 3D model and occurs at 10 million years. The slightly higher transport seen in the I-129 transport to the well in Figure 7-88 is due to transport through the shaft pathway in the System Model.

Cs-135 is a moderately sorbing species with a long half-life (2.3 million year). Transport at the top of the Cobourg is greater than in the 3D model (and therefore conservative) with maximum transport being approximately 29 times higher in the System Model. This is due to the simplified (1D) pathways, whereas the 3D model has significant rock mass to move through and sorb onto. Transport through the subsequent sedimentary layers is off-scale low with transport to the well within the 10 million year simulation time being negligible.

Cl-36 is a non-sorbing species with a moderate half-life (3.01×10^5 year). Maximum transport through the top of the Cobourg is again conservative, reaching a value approximately 6.6 times higher in the System Model.

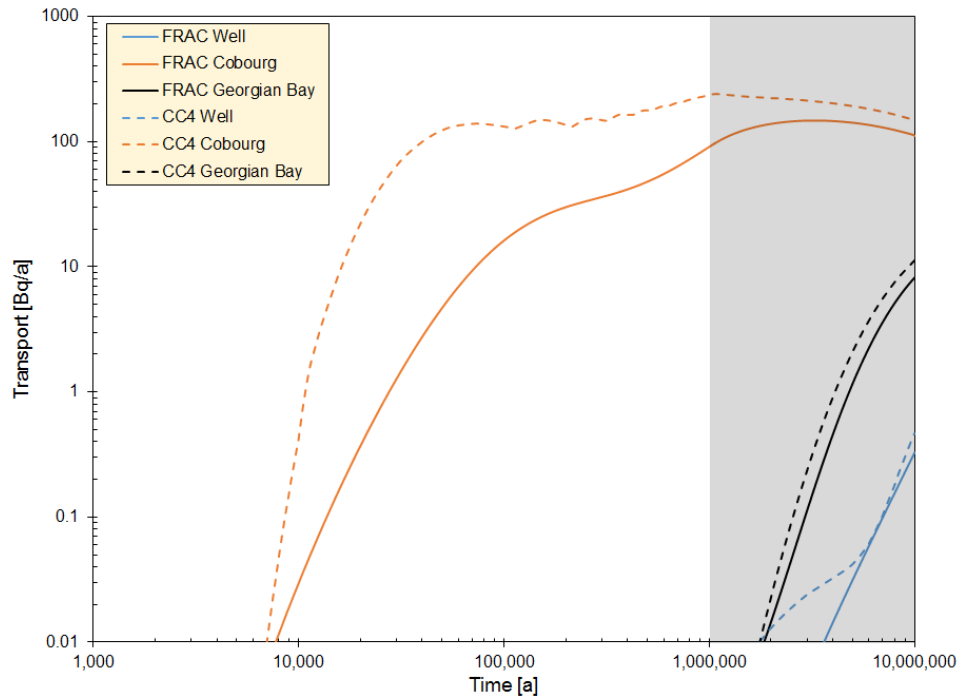
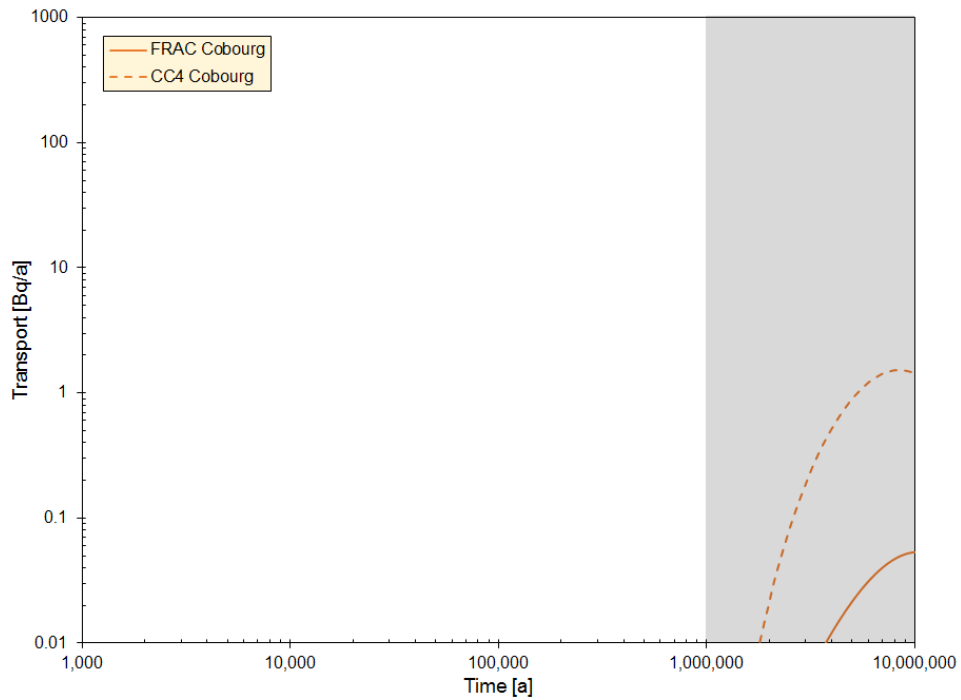


Figure 7-88: Transport Comparison for I-129 for the Base Case



Note: Transport beyond the Cobourg Layer is off-scale low

Figure 7-89: Transport Comparison for Cs-135 for the Base Case

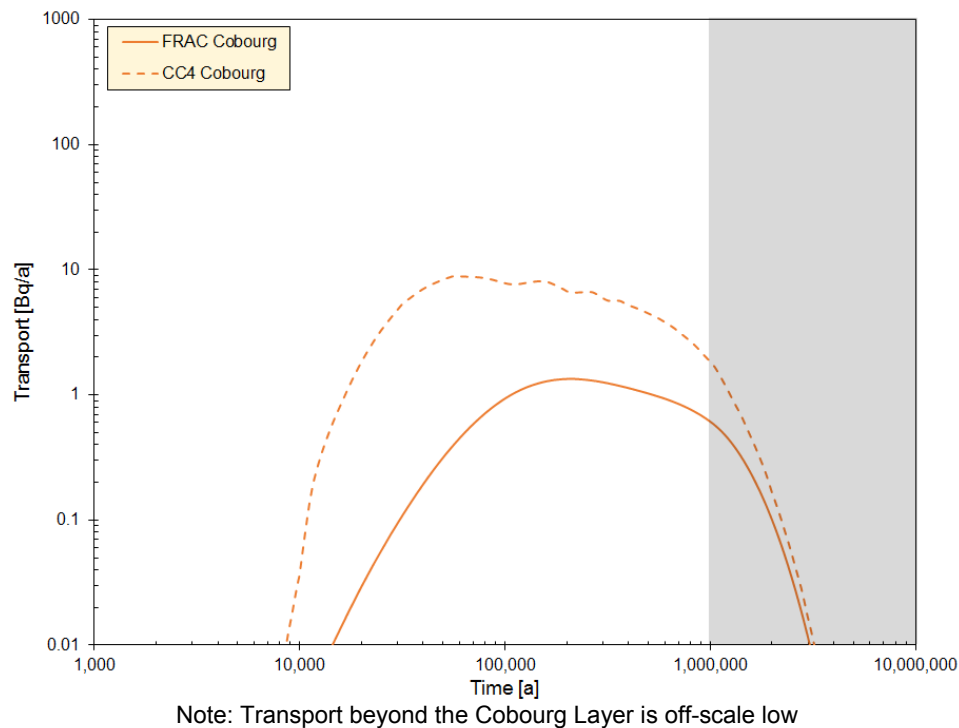


Figure 7-90: Transport Comparison for CI-36 for the Base Case

Transport Comparison for the All Containers Fail at 60,000 Years Case

Transport results are also compared for the All Containers Fail Disruptive Scenario. As in the Base Case comparison, transport is compared at the top of the Cobourg formation, the top of the Georgian Bay formation and to the Well. Similar to the Base Case, I-129 is the only species with non-negligible transport to the well. The sorbing species Cs-135 has effectively zero transport through the top of the Cobourg.

In the 3D model simulation, the location of the well is reoptimized to maximize capture using a similar approach to that described in Section 7.7.2.3.2. A total of 106 well locations were evaluated to ensure the location that maximizes the well uptake is determined. The final selected location is approximately 1150 m distant from the Base Case defective container well location. This change is required to account for the small advective flow in the Guelph unit (i.e., the unit intercepted by the well).

This change has no effect on the geosphere portion of the System Model (Section 7.8.1.2) as the manner in which the model is constructed ensures the System Model provides conservative results for both well locations. Figure 7-91, Figure 7-92 and Figure 7-93 show the transport comparison for the two models for I-129, Cs-135 and CI-36 respectively. In all cases, the System Model is conservative in that it results in higher overall transport than the 3D model.

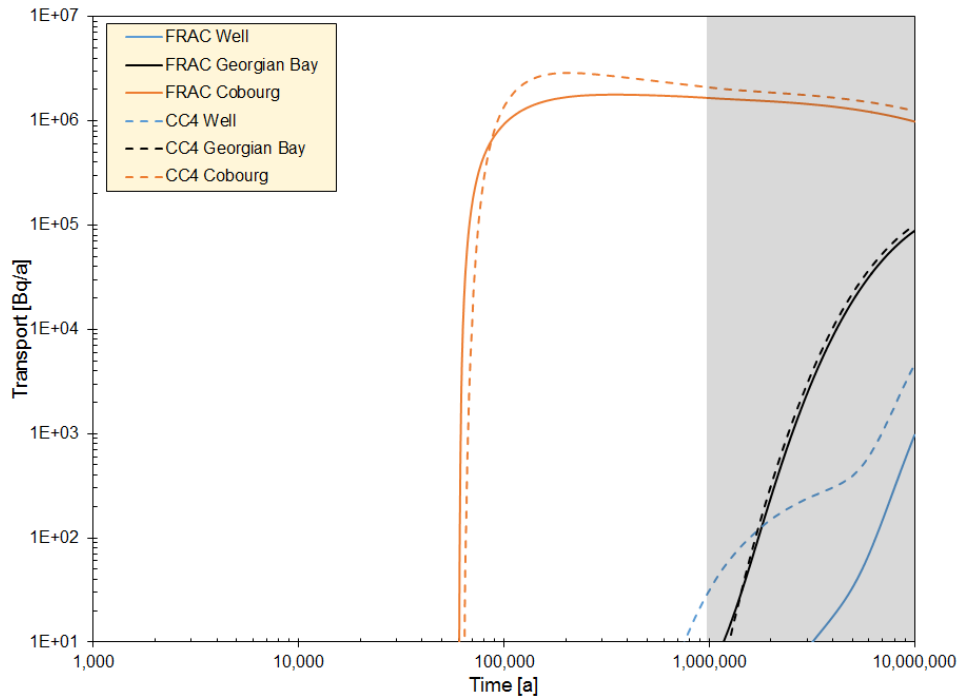
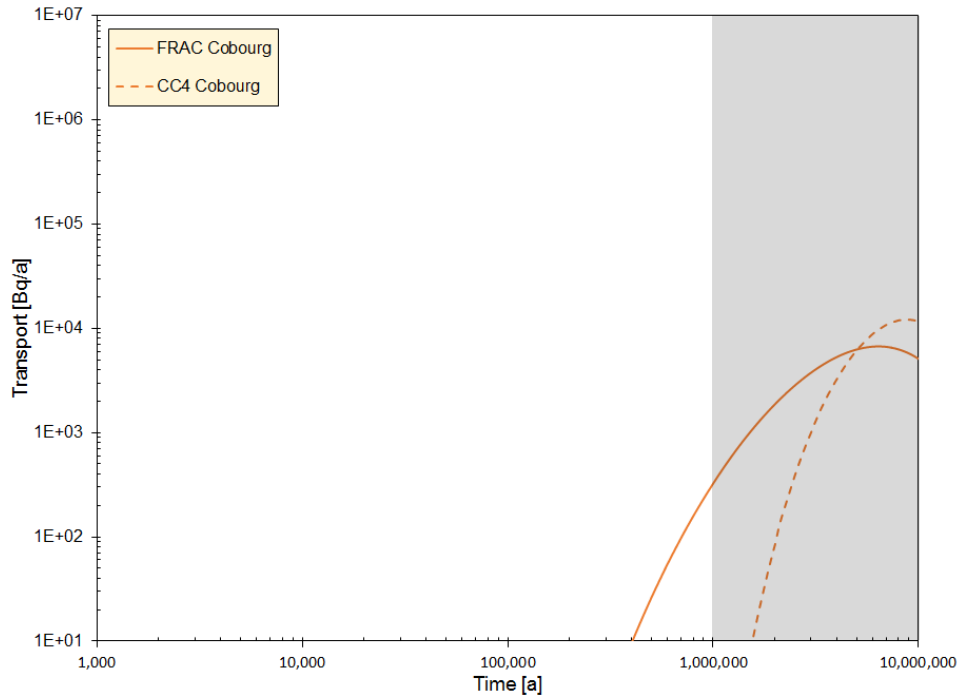
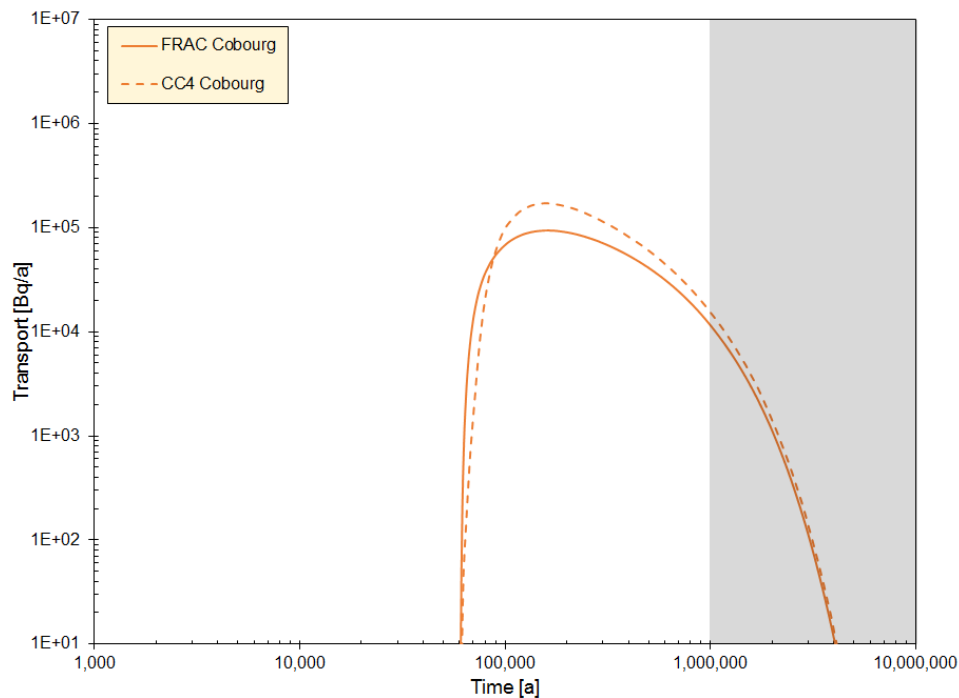


Figure 7-91: Transport Comparison for I-129 for the All Containers Fail Case



Note: Transport beyond the Cobourg Layer is off-scale low

Figure 7-92: Transport Comparison for Cs-135 for the All Containers Fail Case



Note: Transport beyond the Cobourg Layer is off-scale low

Figure 7-93: Transport Comparison for CI-36 for the All Containers Fail Case

Summary of Transport Comparison Cases

Transport results for I-129, Cs-135 and CI-36 from the System Model have been compared with similar results from the 3D model at three geosphere interfaces, these being the top of the Cobourg formation, the top of the Georgian Bay formation and at the Well.

The extremely slow transport through the sedimentary layers means that for any species with even moderate sorption and a half-life less than a few million years, transport beyond the Cobourg layer is negligible. For highly sorbing species transport through the Cobourg itself is effectively zero. I-129 is the only radionuclide that reaches the well in these comparisons.

I-129 transport to the well is conservative in the System Model for both the Base Case and the All Containers Fail at 60,000 Years Disruptive Scenario, with the peak transport being higher and the time of the peak occurring earlier. It is concluded that the System Model provides conservative results and is therefore fit for purpose.

7.8.2 Results

This section presents the results of deterministic and probabilistic analyses of the Base Case and a set of related sensitivity cases as determined using the System Model described in Section 7.8.1. As discussed in Section 7.8.1.4, transport computed using the System Model is conservative in comparison to transport computed using the detailed 3D models.

The purpose of the sensitivity cases is to illustrate the effect of deviations in barrier performance on the Base Case consequences.

For the Reference Case of the Normal Evolution Scenario, all repository components meet their design specification and function as anticipated. As such, the used fuel containers remain intact essentially indefinitely (see Chapter 5) and no contaminant releases occur in the one million year time period of interest to the safety assessment.

Section 7.2.1, Table 7-4 and Table 7-5 present the list of barrier and well sensitivity cases considered in this postclosure safety assessment. Of these, the following have the potential to affect the groundwater flow field and are not amenable to modelling with the System Model (i.e., because the System Model is based on the constant 3D groundwater flow field defined in the Base Case). Simulations of these cases are therefore performed with the 3D Groundwater Flow and Transport Model with results as described in Section 7.7.2.3 and associated subsections.

- Hydraulic conductivities of the engineered barrier system (EBS), increased by a factor of 10;
- Hydraulic conductivities of the host rock increased by a factor of 10;
- Hydraulic conductivity in the excavation damaged zones (EDZ) increased by a factor of 10;
- 100 m of surface erosion;
- 150 m overpressure in the Shadow Lake Formation;
- Intermittent well operation; and
- Random well operation.

The remaining barrier cases from Table 7-5 (i.e.; those that do not affect the groundwater flow field) are listed below. These cases are simulated with the System Model, as is the No Well sensitivity case.

Fuel Barrier:

- Fuel dissolution rate increased by a factor of 10; and
- Instant release fractions set to 0.10 for all contaminants (i.e., 10% of the entire inventory is instantly released).

Zircaloy Sheath Barrier:

No credit is taken in the postclosure safety assessment for the presence of the Zircaloy fuel sheath as a barrier to contaminant release from the fuel. However, because the sheath itself contains contaminants and because the screening analysis identifies some of these contaminants as potentially important, the following Zircaloy specific sensitivity cases are simulated:

- Zircaloy dissolution rate increased by a factor of 10; and
- Instant release fractions set to 0.10 for all contaminants.

Container Barrier:

- All 10 containers fail at 1000 years;
- 50 containers fail at 1000 years;
- 50 and 1000 containers fail at 10,000 years;
- Low sorption in the engineering barrier materials with coincident high solubility limits in the container; and
- No solubility limits in the container.

Buffer, Backfill and Seals Barrier:

- Low sorption in the engineered barrier materials with coincident high solubility limits in the container;
- Bentonite and geosphere diffusivities a factor of 10 and a factor of 100 higher; and
- No sorption in the engineered sealing materials.

Geosphere Barrier:

- Sorption parameters set to two standard deviations (low) values;
- Bentonite and geosphere diffusivities a factor of 10 and a factor of 100 higher; and
- I-129 sorption credited.

The effect of glaciation is also discussed quantitatively based on the analyses by Avis and Calder (2015) and Chen et al. (2017). The important features of these glaciation studies are described and their applicability to the current study is discussed in Section 7.8.2.4.

Two probabilistic cases are also simulated. These are:

- 1) Number, locations and failure times for the defective containers fixed at their Base Case values, with all other available parameters varied; and
- 2) All parameters with probability distributions varied, including the number, locations and failure times for the defective containers.

Figures in this section are shown with shading at times greater than one million years to emphasize that these results are illustrative and included only to indicate peak impacts. Shading for dose rates below 10^{-6} mSv/a indicates these values are negligible and are included to indicate trends.

Due to the very low hydraulic conductivity of the host rock and the dominance of diffusive transport, the dose rates arising in the one million year period of interest are below the 10^{-6} mSv/a threshold value for almost all cases. The peak dose rate is also not reached in this time frame. To provide a basis for comparison, one million year results are quoted. Additionally, select simulations are extended further to provide information on the peak. This is

for illustrative purposes only, as other factors not accounted for in the analysis may play a role at these lengthy time scales.

7.8.2.1 Base Case

Figure 7-94 shows the total dose rate for the Base Case. The total dose rate is the sum of the individual contributions from all radionuclides of potential interest and their progeny.

The dose rate at one million years is off-scale low (i.e. 5.9×10^{-10} mSv/a). This is so far below the average Canadian background dose rate of 1.8 mSv/a and the 0.3 mSv/a interim dose rate acceptance criterion established in Section 7.1.1 that it can be considered zero.

Beyond one million years, the uranium in the repository is similar to that in a naturally occurring uranium ore body.

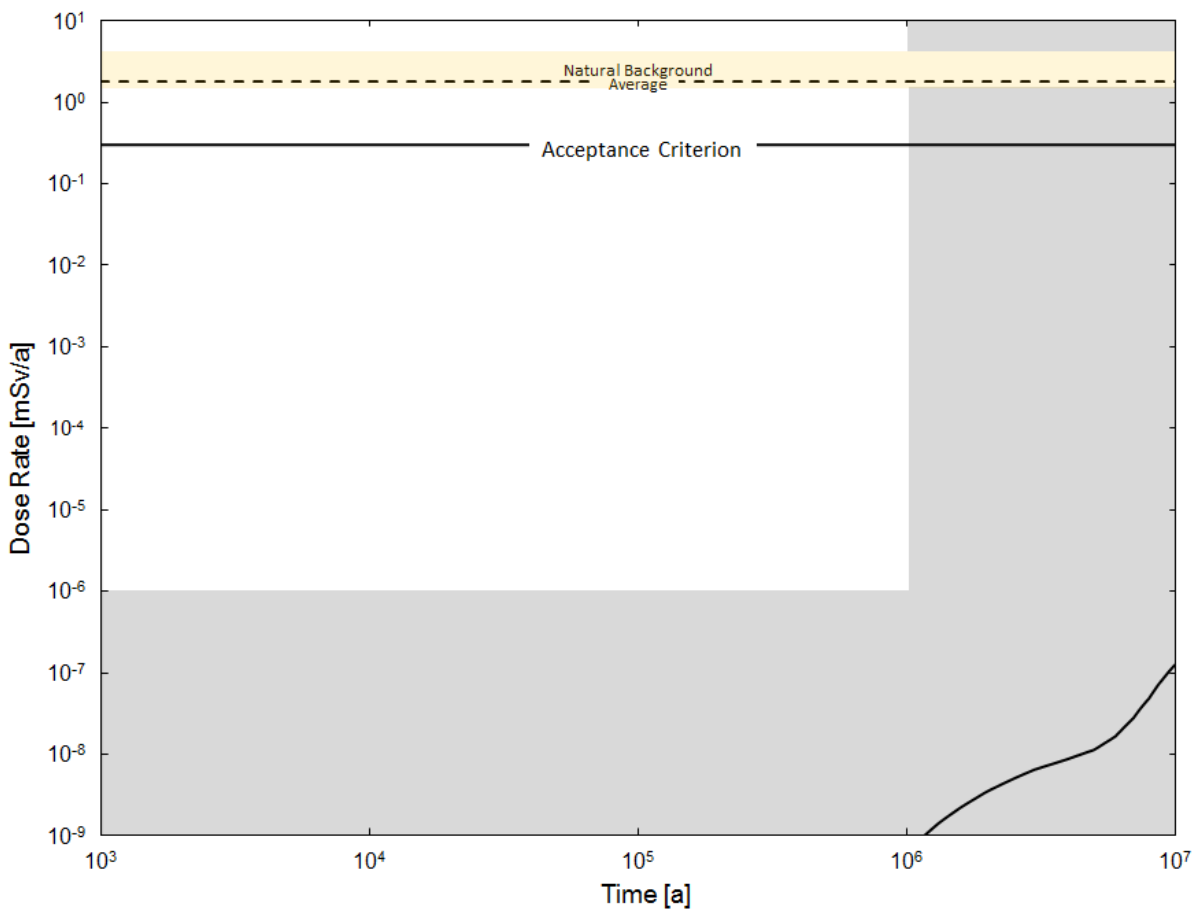


Figure 7-94: System Model: Base Case Total Dose Rate

I-129 is the only potential dose contributor. This is because I-129 has a sizeable initial inventory, a non-zero instant release fraction, a very long half-life, is not solubility limited, is non-sorbing in the buffer, backfill and geosphere and has a radiological impact on humans. Other

fission products and actinides either decay away, or are released very slowly as the fuel dissolves and are thereafter sorbed in the engineered barriers and geosphere.

Essentially all of the I-129 dose contribution is due to internal pathways, with drinking water and food ingestion being dominant. Drinking water is supplied by the well, and well water is used to irrigate crops used as food sources by the family.

7.8.2.2 Well Assumption Sensitivity Cases

The previous section shows that the dose consequence for the Base Case is entirely due to I-129, with the I-129 dose entirely due to the use of well water. In the System Model, well water is used for drinking, irrigation of food crops and for watering animals.

Due to the importance of the well pathway, much effort is made in Section 7.7.2.3.2 to identify the combination of well and defective container locations that maximize the dose consequence. The following three sensitivity studies have also been defined (Section 7.2.1.3) to further illustrate the effect of the well:

- No well;
- Intermittent well operation; and
- Random well location.

Of these, the intermittent well case and the random well case both have the potential to affect the groundwater flow field and are therefore examined with the 3D models in Section 7.7.2.3.4. The No Well case is examined with the System Model and described below.

No Well

In this sensitivity study, the location of the defective containers is assumed the same as in the Base Case. This simplification means that all 10 containers are clustered together at the location indicated by the black diamond in Figure 7-52. This is shown in closeup detail in Figure 7-31.

With no well, the dose rate at one million year simulation time is below the threshold for inclusion on a dose rate figure (i.e., 10^{-9} mSv/a) and as such, the dose rate can be considered zero.

7.8.2.3 Barrier Performance Sensitivity Cases

7.8.2.3.1 Fuel Barrier Sensitivity

Sensitivity cases illustrating the effect of deviations in the performance of the fuel barrier are:

- Fuel dissolution rate increased by a factor of 10; and
- Instant release fractions for fuel contaminants set to 0.10.

Figure 7-95 shows the total dose rate for the case with the fuel dissolution rate increased by a factor of 10. For this case, all fuel in the container dissolves within one million years, whereas in the Base Case, only about 21% of the fuel dissolves (see Figure 7-10).

In comparison to the Base Case result in Figure 7-94, the higher fuel dissolution rate has a small observable effect on the I-129 dose contribution; however, the dose rate at one million years still remains below 10^{-6} mSv/a. This is so far below the average Canadian background dose rate of 1.8 mSv/a and the 0.3 mSv/a interim dose rate acceptance criterion established in Section 7.1.1 that it can be considered zero.

Dose rates due to all other species are also effectively zero because they are either strongly sorbed in the buffer and geosphere or because their half-lives are such that the species decays prior to reaching the biosphere.

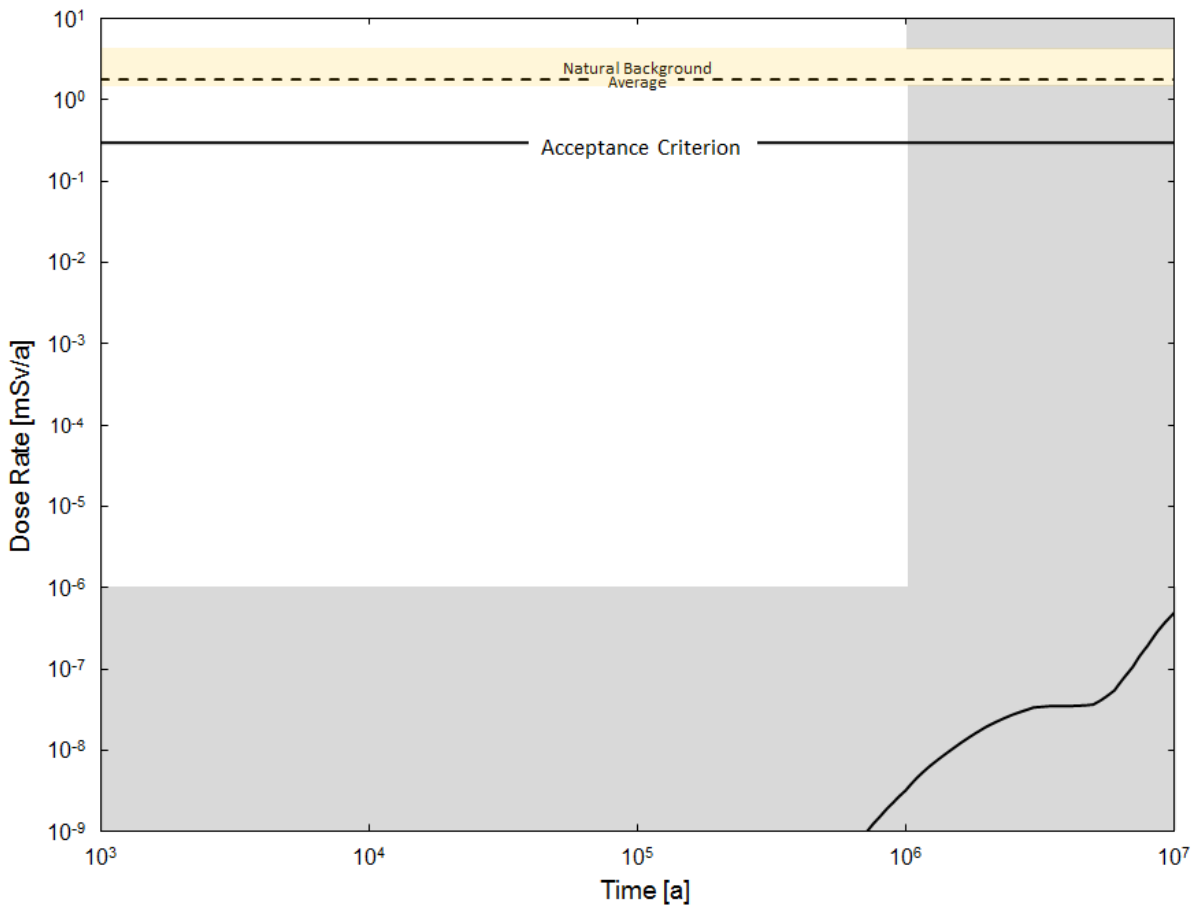


Figure 7-95: System Model: Sensitivity to a Factor of 10 Increase in Fuel Dissolution Rate

Figure 7-96 shows the total dose rate for the sensitivity case with the instant release fractions for all radionuclides set to 10%.

In comparison to the Base Case result in Figure 7-94, the higher instant release fractions have almost no effect the I-129 dose contribution and the dose rate at one million years still remains below 10^{-6} mSv/a. This is so far below below the average Canadian background dose rate of 1.8 mSv/a and the 0.3 mSv/a interim dose rate acceptance criterion established in Section 7.1.1 that it can be considered zero.

The effect is minor due to the combination of decay and the effects of dispersion and broadening of the contaminant plume as it travels through the clay barriers and geosphere.

Dose rates due to all other species are also effectively zero because they are either strongly sorbed in the buffer and geosphere or because their half-lives are such that the species decays prior to reaching the biosphere.

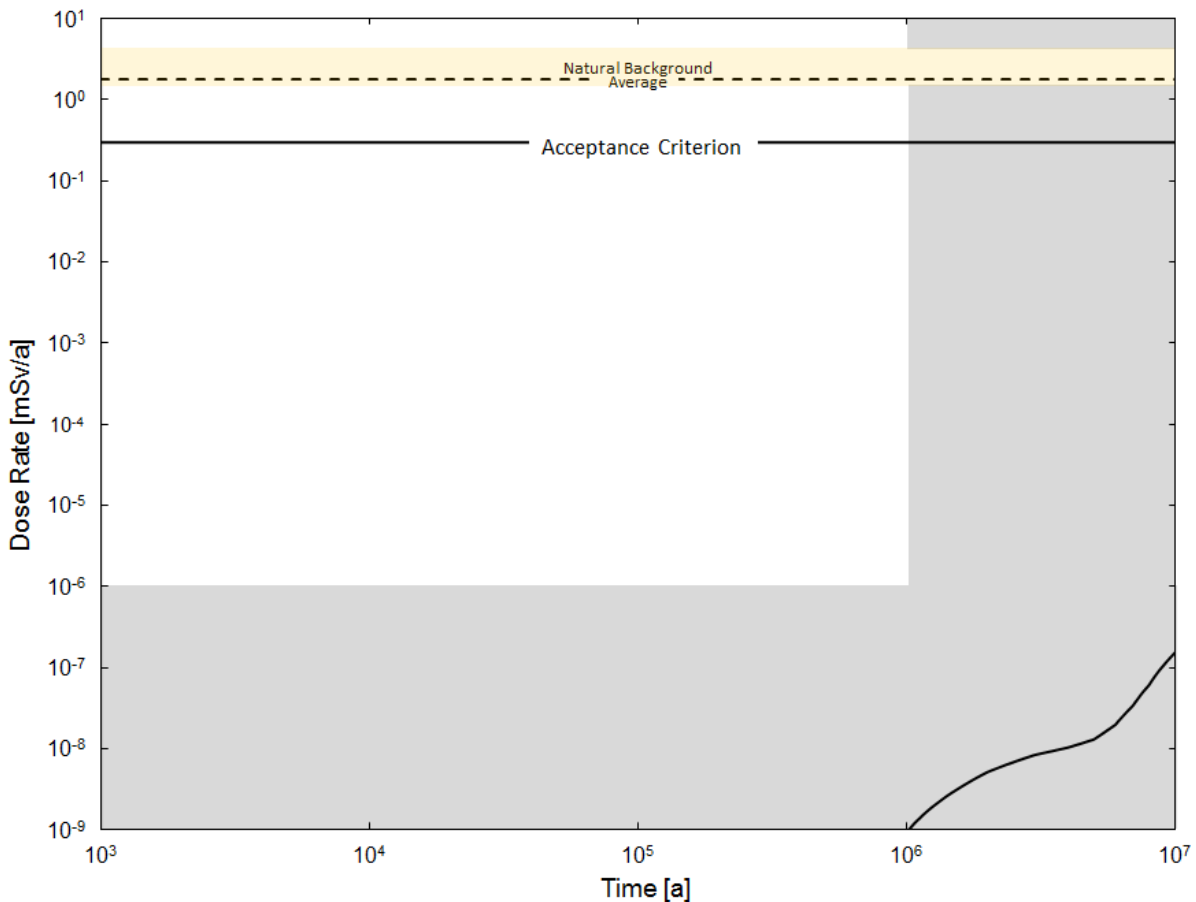


Figure 7-96: System Model: Sensitivity to Fuel Instant Release Fractions Set to 10%

7.8.2.3.2 Zircaloy Sheath Barrier Sensitivity

No credit is taken in the postclosure safety assessment for the presence of the Zircaloy fuel sheath as a barrier to contaminant release from the fuel. However, because the sheath itself contains contaminants and because the screening analysis identifies some of these contaminants as potentially important, the following Zircaloy specific sensitivity cases are simulated:

- Zircaloy dissolution rate increased by a factor of 10; and
- Instant release fractions for Zircaloy sheath contaminants set to 0.10.

Figure 7-97 shows the total dose rate from the for the sensitivity case with the Zircaloy dissolution rate increased by a factor of 10, and Figure 7-98 shows the total dose rate for the sensitivity case with the Zircaloy instant release fractions set to 10%.

In comparison to the Base Case in Figure 7-94, neither result has any observable effect on the I-129 dose contribution, and the dose rate at one million years remains below 10^{-6} mSv/a. This is so far below below the average Canadian background dose rate of 1.8 mSv/a and the 0.3 mSv/a interim dose rate acceptance criterion established in Section 7.1.1 that it can be considered zero.

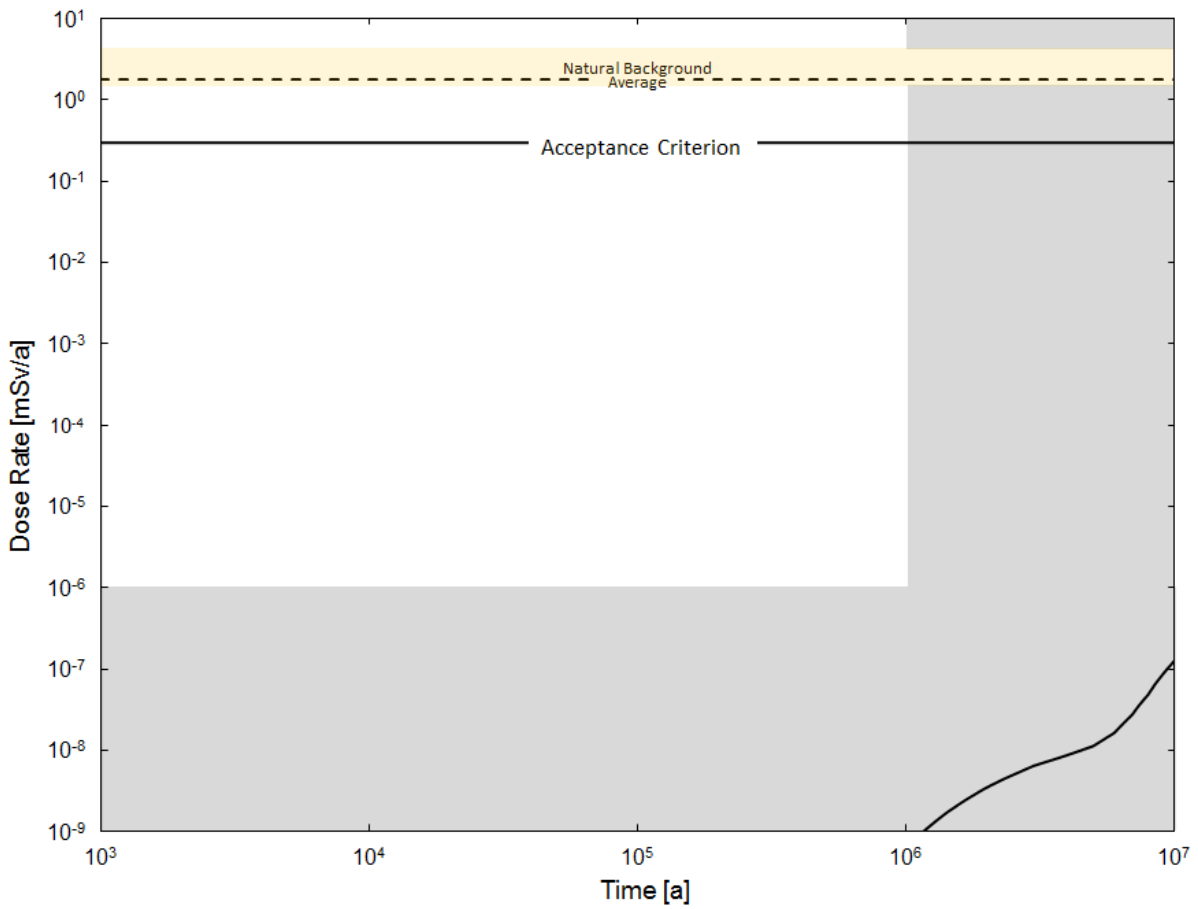


Figure 7-97: System Model: Sensitivity to a Factor of 10 Increase in Zircaloy Corrosion Rate

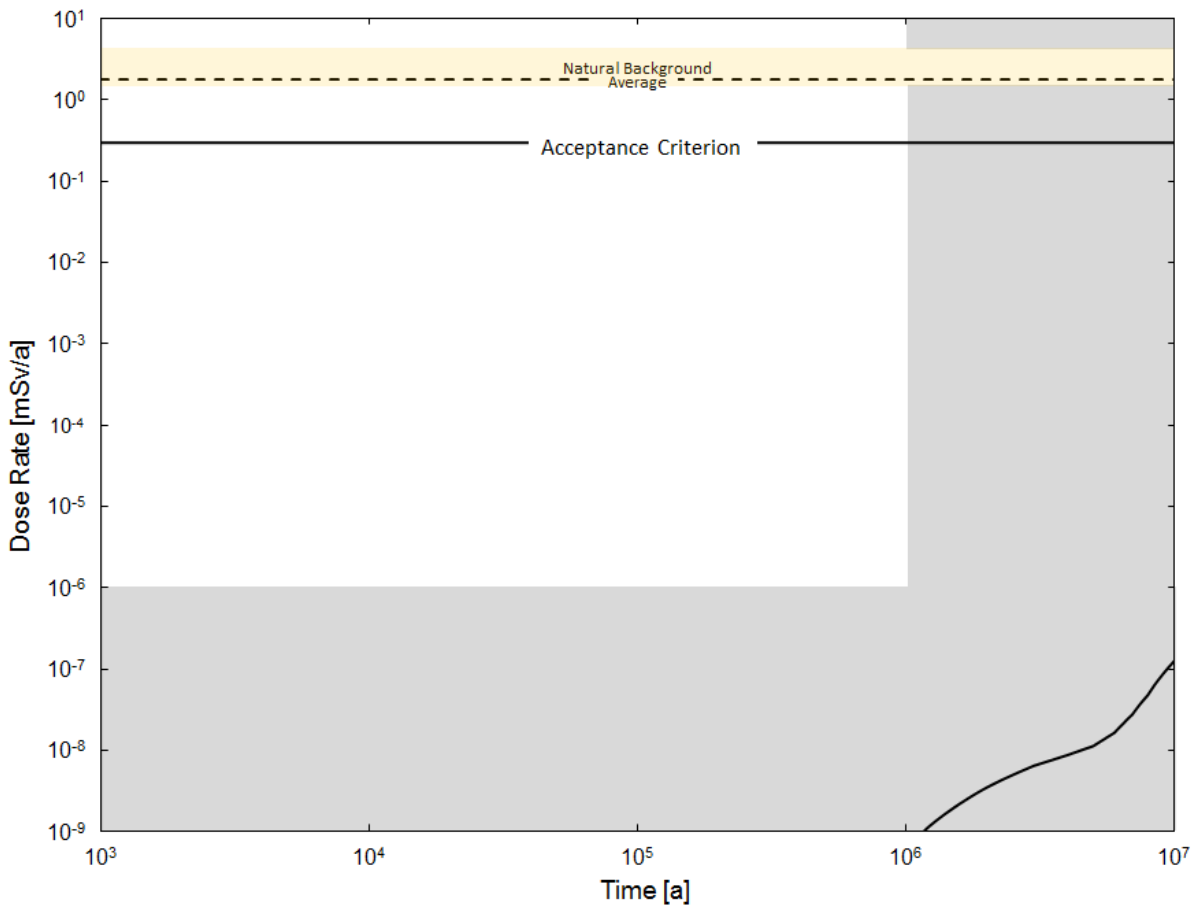


Figure 7-98: System Model: Sensitivity to Zircaloy Instant Release Fractions Set to 10%

7.8.2.3.3 Container Barrier Sensitivity

Sensitivity studies illustrating the effect of variations in the container barrier are:

- All 10 containers fail at 1000 years;
- 50 containers fail at 1000 years;
- 50 containers and 1000 containers fail at 10,000 years;
- Low sorption in the engineered barrier materials with coincident high solubility limits in the container; and
- No solubility limits in the container.

Figure 7-99 shows the individual contributions to the total dose rate from the most significant radionuclides for the sensitivity case in which all 10 containers fail at 1000 years. As noted in Table 7-3, the 1000 year failure time is very conservative compared to what might be expected in reality.

In comparison to the Base Case result (Figure 7-94), Figure 7-99 shows there is a small increase in the I-129 dose contribution; however, the dose rate at one million years remains below 10^{-6} mSv/a. This is more than 300,000 times less than the 0.3 mSv/a interim dose rate acceptance criterion established in Section 7.1.1 and can therefore be considered zero.

Dose rates due to all other species are also effectively zero because they are either strongly sorbed in the buffer and geosphere or because their half-lives are such that the species decays prior to reaching the biosphere.

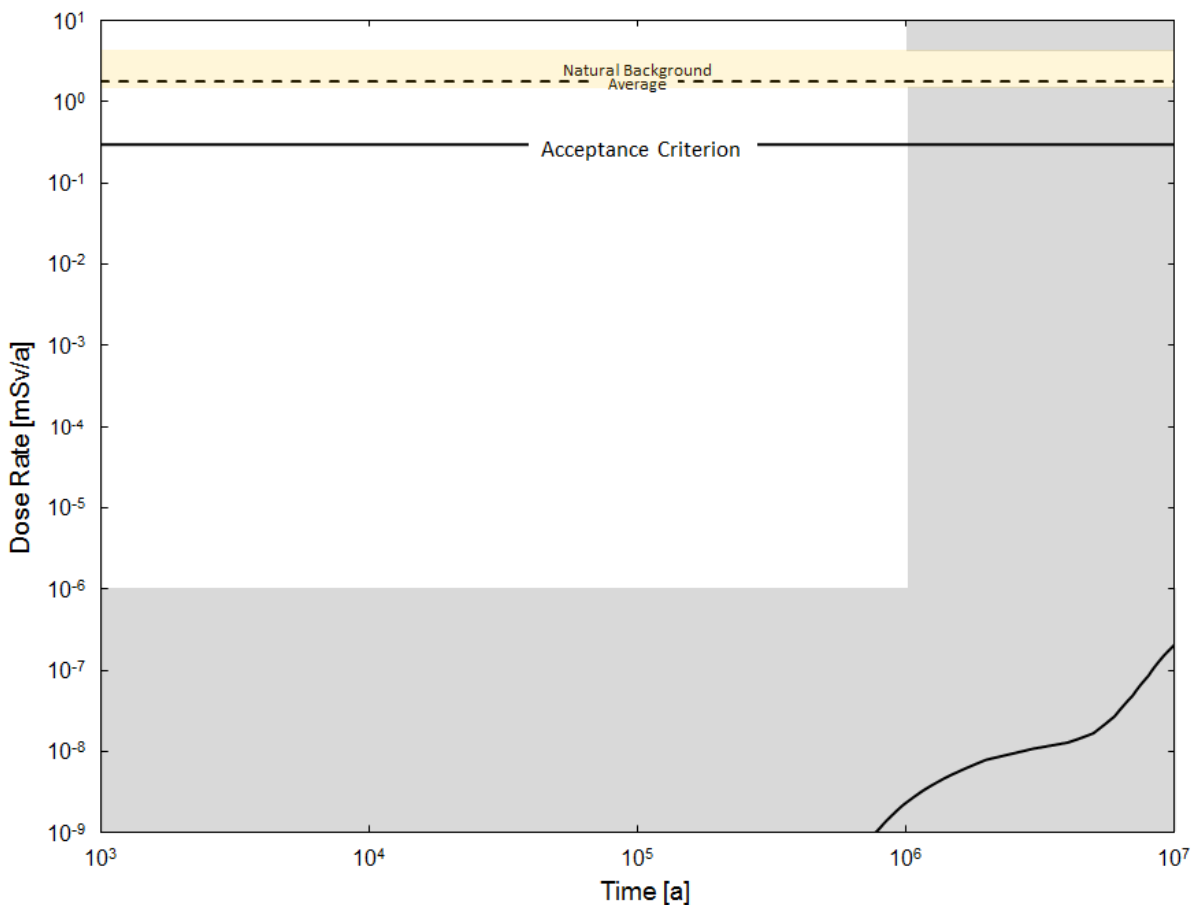


Figure 7-99: System Model: Sensitivity to 10 Containers Fail at 1000 years

The effect of a slightly larger number of container failures can be illustrated by scaling these results. For example, if 50 containers are assumed to fail early at 1000 years, and all of these containers are assumed clustered in the location that maximizes the dose consequence, an estimate of the dose rate in one million years is 1.2×10^{-8} mSv/a (i.e., five times the dose rate for 10 containers failing at 1000 years). This dose rate remains more than 300,000 times less than the interim dose rate criterion of 0.3 mSv/a and can therefore be considered zero.

To illustrate the effect of an even greater number of container failures, a different approach is used because it is not possible for large numbers of defective containers to all be simultaneously in the location that maximizes the dose consequence. Because there are millions of potential combinations of defective container locations, for this case the results of the All Containers Fail at 10,000 years Disruptive Event Scenario (discussed in Section 7.9.2) can be used for illustration. These results can be scaled based on the number of assumed defective containers to illustrate repository performance for a uniform distribution of defective containers, given that there are 108,833 containers for approximately 5.2 million bundles.

Applying the above approach for 1000 containers, the dose rate at one million years for a uniform distribution of defective containers failing at 10,000 years is 1.7×10^{-7} mSv/a. Similarly, the dose rate at one million years for a uniform distribution of 50 containers failing at 10,000 years is 8.7×10^{-9} mSv/a. These dose rates are more than 300,000 times less than the interim dose rate criterion of 0.3 mSv/a and can therefore be considered zero.

Figure 7-100 shows total dose rate for the sensitivity case with low sorption in the engineered barrier materials with coincident high solubility limits in the containers.

Results are identical to the Base Case. This is because I-129 is the dominant dose rate contributor, and I-129 is not solubility limited and is non-sorbing. Dose rates due to all other species are effectively zero because they are either strongly sorbed in the buffer and geosphere or because their half-lives are such that the species decays prior to reaching the biosphere.

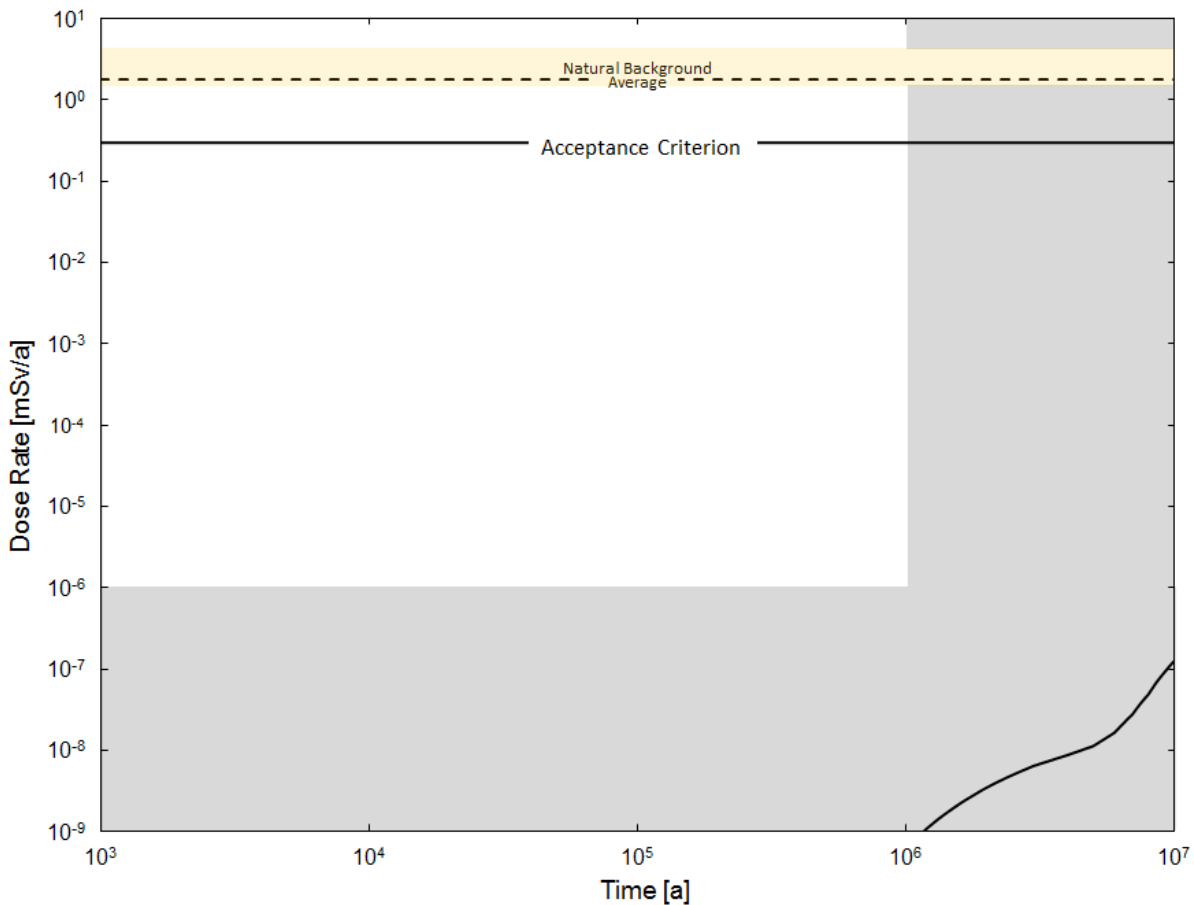


Figure 7-100: System Model: Sensitivity to Low Sorption in the EBS Materials with Coincident High Solubility Limits in the Container

Figure 7-101 shows the total dose rate for the sensitivity case with no solubility limits in the containers.

Results are again identical to the Base Case. This is because I-129 is the dominant dose rate contributor, and I-129 is not solubility limited and is non-sorbing. Dose rates due to all other species are effectively zero because they are either strongly sorbed in the geosphere or because their half-lives are such that the species decays prior to reaching the biosphere.

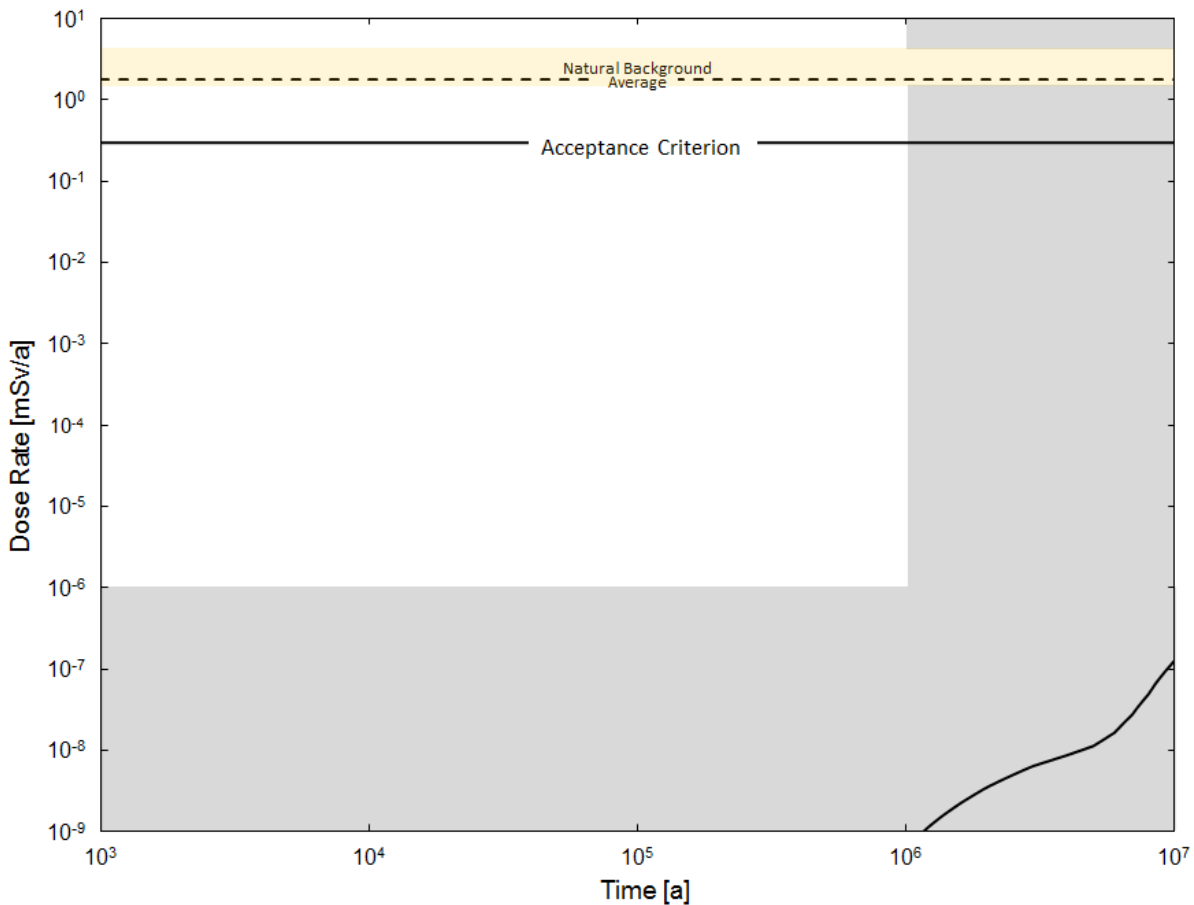


Figure 7-101: System Model: Sensitivity to No Solubility Limits

7.8.2.3.4 Buffer, Backfill, and Seals Barrier Sensitivity

Sensitivity studies illustrating the effect of variations in the buffer, backfill and seals barrier are:

- Low sorption in the engineered barrier materials with coincident high solubility limits in the container
- No sorption in the near field;
- Bentonite and geosphere diffusivities increased by a factor of 10 and by a factor of 100; and
- I-129 sorption credited in the bentonite and geosphere.

The sensitivity study with low sorption in the engineered barrier materials with coincident high solubility limits in the container is discussed with the container barrier sensitivity cases in Section 7.8.2.3.3. It is also included here because this case also assumes degraded barrier materials.

Figure 7-102 shows the total dose rate for the sensitivity case with no sorption in the near field.

Results are again identical to the Base Case. This is because I-129 is the dominant dose rate contributor, and I-129 is not solubility limited and is non-sorbing. Dose rates due to all other species are effectively zero because they are either strongly sorbed in the geosphere or because their half-lives are such that the species decays prior to reaching the biosphere.

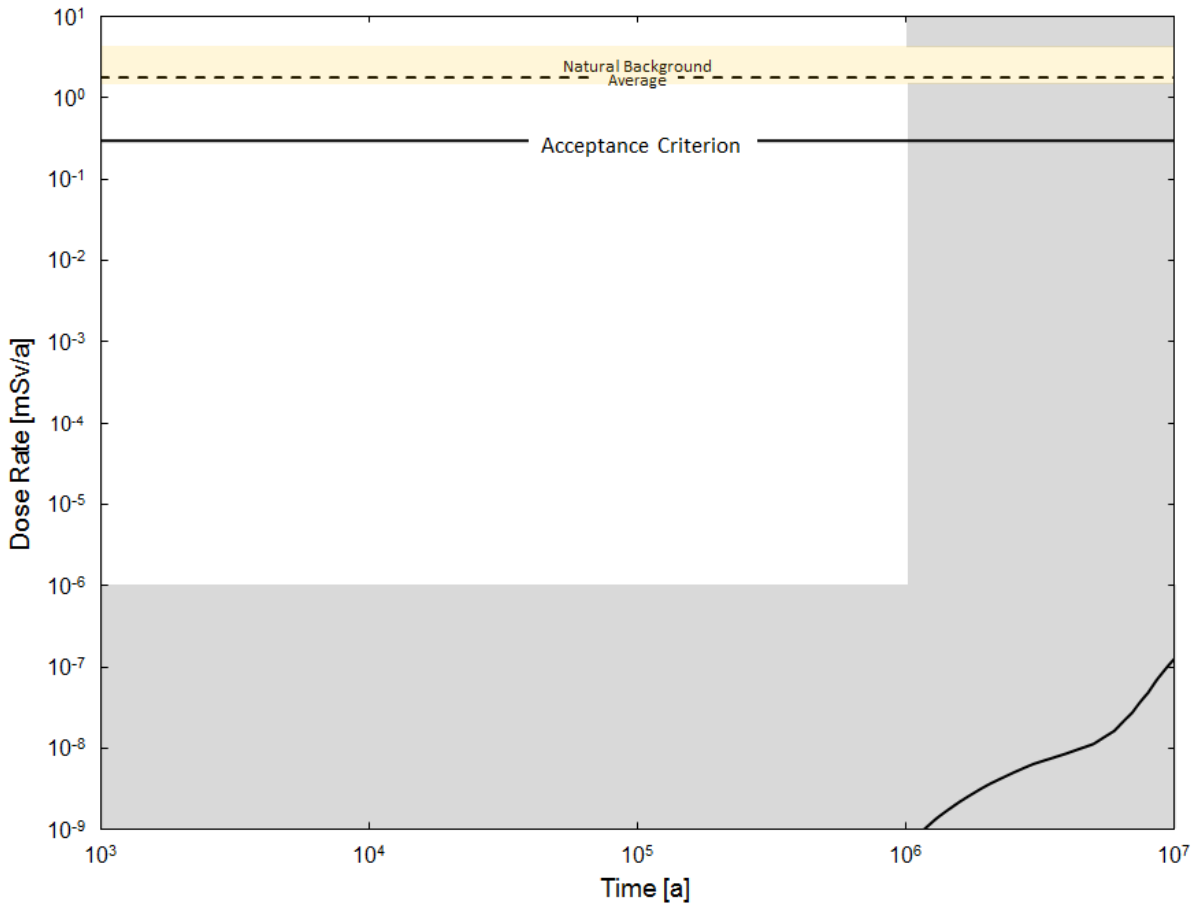


Figure 7-102: System Model: Sensitivity to No Sorption in the Near Field

Figure 7-103 shows the total dose rate for the case with bentonite and geosphere diffusivities increased by a factor of 10 and by a factor of 100. The factor of 100 increase represents an extreme case, but considers the importance of the diffusive rock barrier.

The one million year dose rate is 2.1×10^{-7} mSv/a for the 10 times diffusivity case and 4.0×10^{-5} mSv/a for the 100 times diffusivity case. In comparison to the Base Case (Figure 7-94), both cases result in higher values, although for the factor of 10 case, the dose rate remains more than 300,000 times less than the interim dose rate criterion of 0.3 mSv/a, and can therefore be considered zero.

As in the other cases, I-129 is the dominant dose contributor. This is because I-129 is not solubility limited and is non-sorbing. Dose rates due to all other species are effectively zero

because they are either sorbed despite the reduced geosphere sorption parameters or because their half-lives are such that the species decays prior to reaching the biosphere.

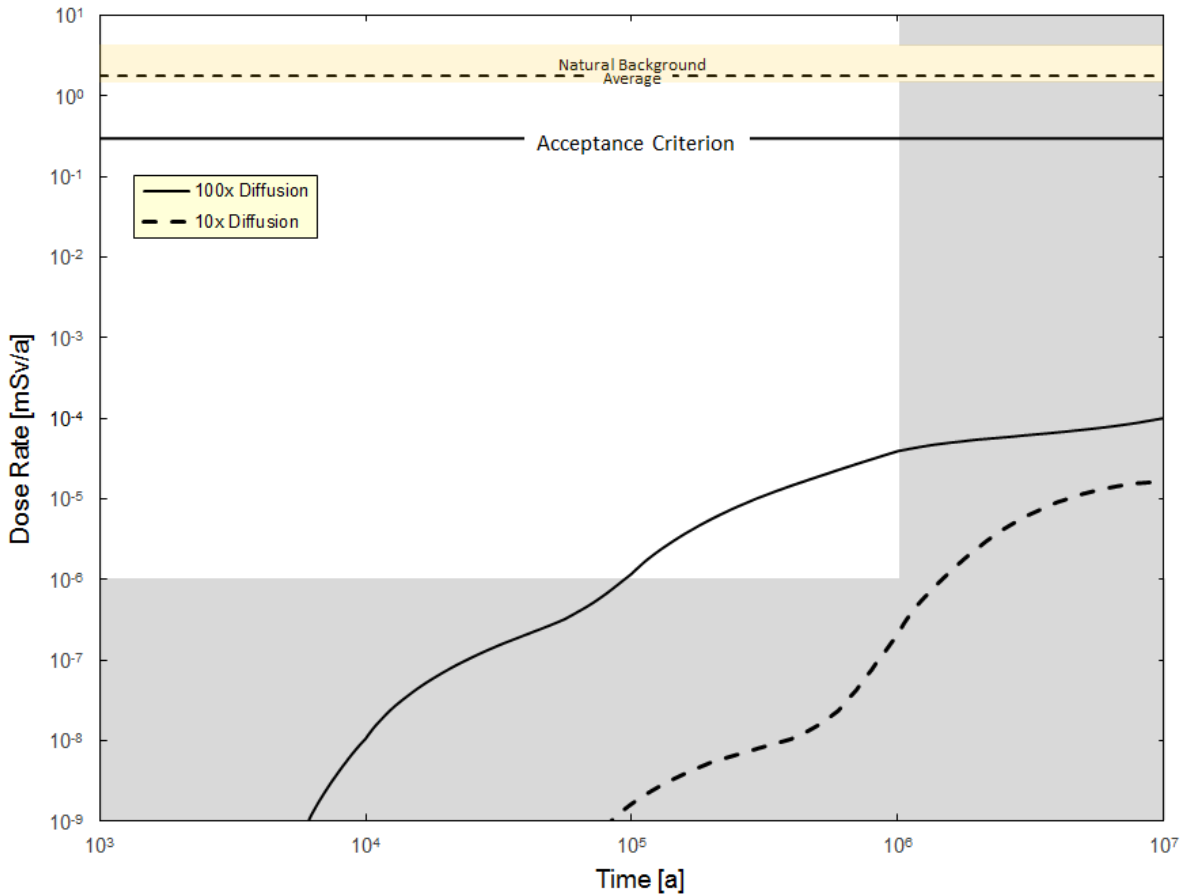


Figure 7-103: System Model: Sensitivity to 10 and 100 Time Higher Bentonite and Geosphere Diffusivity Coefficients

Figure 7-104 shows the total dose rate for the case with credit taken for I-129 sorption. The Base Case (with no I-129 sorption) is shown for comparison.

As expected the sorption credit reduces the dose rate at one million years, with the small reduction evident on the figure. As in the Base Case, the dose rate is more than 300,000 times less than the interim dose ratio criterion and can therefore be considered zero.

This decrease is not significant given the wide margins available to the interim acceptance criterion; however, decreases of this order may have more relative importance for a real site.

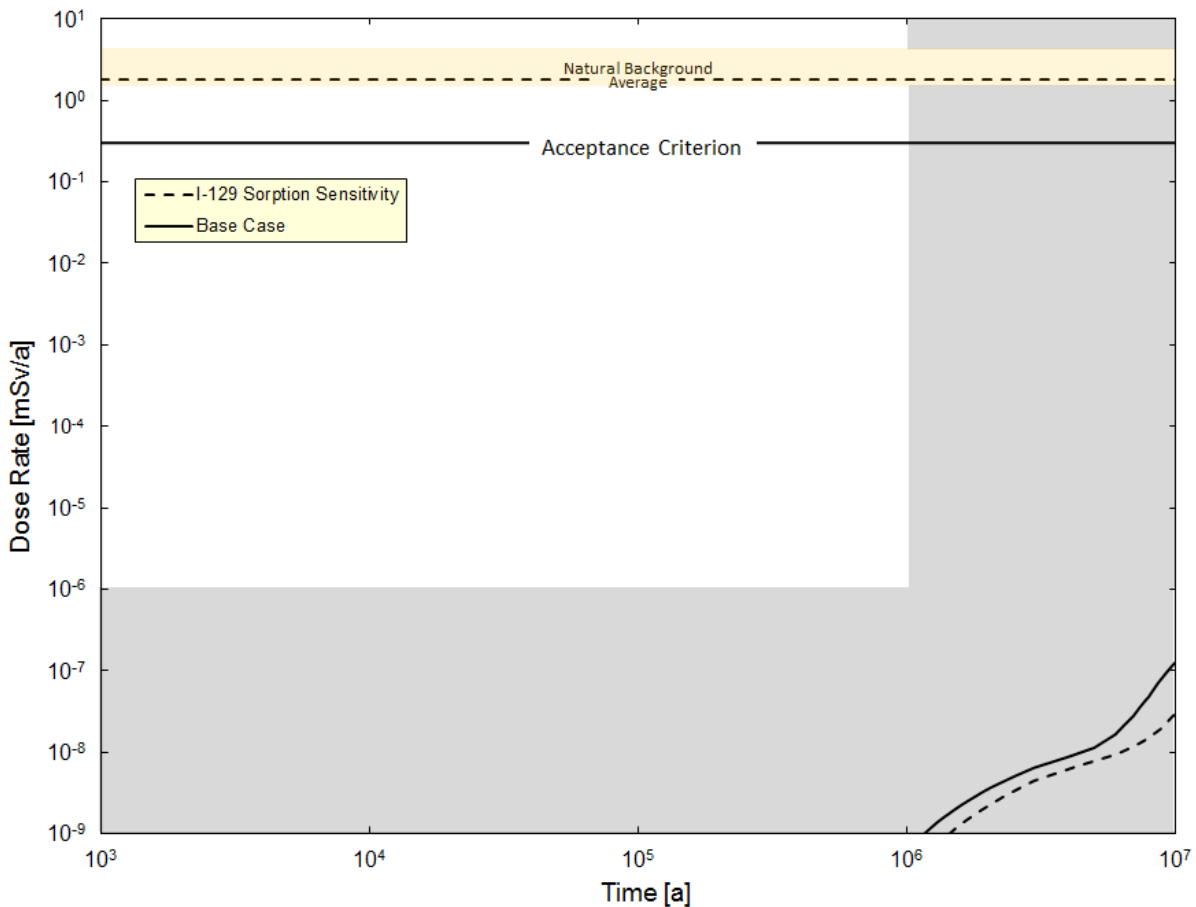


Figure 7-104: System Model: Sensitivity to I-129 Sorption

7.8.2.3.5 Geosphere Barrier Sensitivity

The sensitivity studies illustrating the effect of variations in the geosphere barrier are:

- Sorption parameters set to two standard deviation (low) values;
- Bentonite and geosphere diffusivities increased by a factor of 10 and a factor of 100; and
- I-129 sorption credited in the bentonite and geosphere.

Figure 7-105 shows the total dose rate for the low sorption sensitivity case.

Results are identical to the Base Case. This is because I-129 is the dominant dose rate contributor, and I-129 is not solubility limited and is non-sorbing. Dose rates due to all other species are effectively zero because they are either sorbed despite the reduced geosphere sorption parameters or because their half-lives are such that the species decays prior to reaching the biosphere.

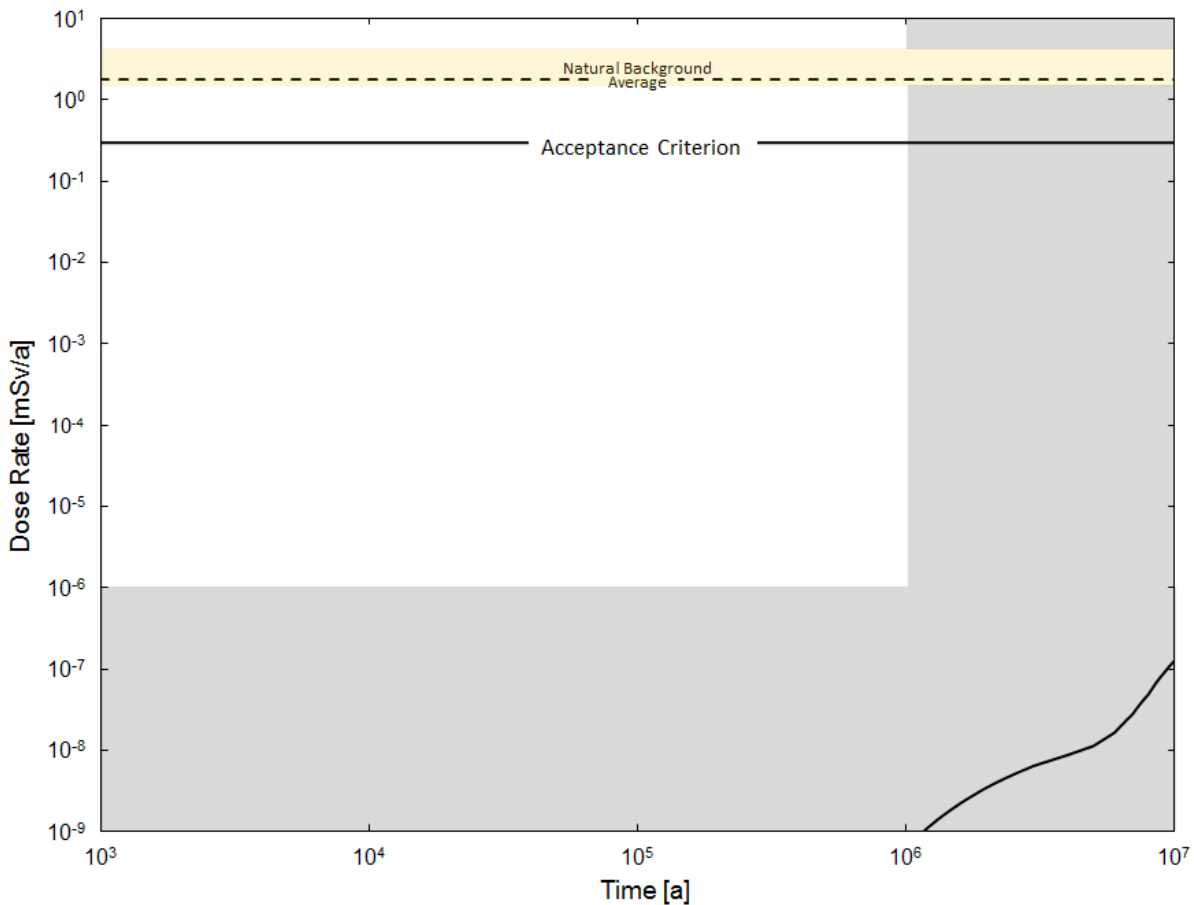


Figure 7-105: System Model: Sensitivity to Two Standard Deviations (Low) Sorption in the Geosphere

The sensitivity cases with bentonite and geosphere diffusivities increased by a factor of 10 and a factor of 100, and with I-129 sorption credited in the bentonite and geosphere are described in Section 7.8.2.3.4. They are both mentioned here because the geosphere parameters are also changed.

7.8.2.4 Glaciation Sensitivity

A discussion of the potential effects of glaciation on the deep groundwater system for the current study geosphere is provided in Chapter 2.

The effect of glaciation is discussed quantitatively based on analyses performed for the same hypothetical geosphere as in the current but with a different repository layout (Avis and Calder (2015), Chen et al. (2017)). The important features of these glaciation studies are described here together with a discussion of their applicability to the current study.

The glaciation modelling was performed using models implemented in the 3D Groundwater Flow and Transport code FRAC3DVS-OPG. The configuration includes the 1D

hydromechanical (HM) coupling module, which is based on the work of Neuzil (2003) and assumes purely vertical strain. Constant density water is assumed; this is likely conservative for groundwater flow as denser (saline) water at depth is generally viewed as stabilizing (Normani 2009).

7.8.2.4.1 Glacial Cycles

To explore the effects of glaciation, a representative future glacial cycle has been defined in terms of climate and surface boundary conditions using models of past glacial behaviour for the region.

Paleo-glacial data obtained with the University of Toronto (UofT) Glacial System Model (GSM) have been used. The glacial data are based on the nn9930 (warm-based) scenario (Peltier 2011). The GSM produces several outputs with a spatial resolution of 1.0° (longitude) by 0.5° (latitude) and a temporal resolution of 500 a, but only the ice thickness and permafrost depth outputs are applied to the paleo-hydrogeological simulations. Ice thickness is applied as both hydraulic and mechanical boundary conditions along the ground surface, and permafrost is applied as a permeability reduction (i.e., 5×10^{-11} m/s; McCauley et al., 2002) to the elements whose centroids are within the time-varying estimated depth of frozen ground. To avoid abrupt changes which may introduce numerical instabilities, both outputs are spatially and temporally interpolated. The dataset contains one full glacial cycle of glacial climate outputs, from 120 ka ago to present day.

UofT GSM (nn9930) simulated ice-sheet thickness and permafrost depth at the hypothetical repository site are shown in Figure 7-106.

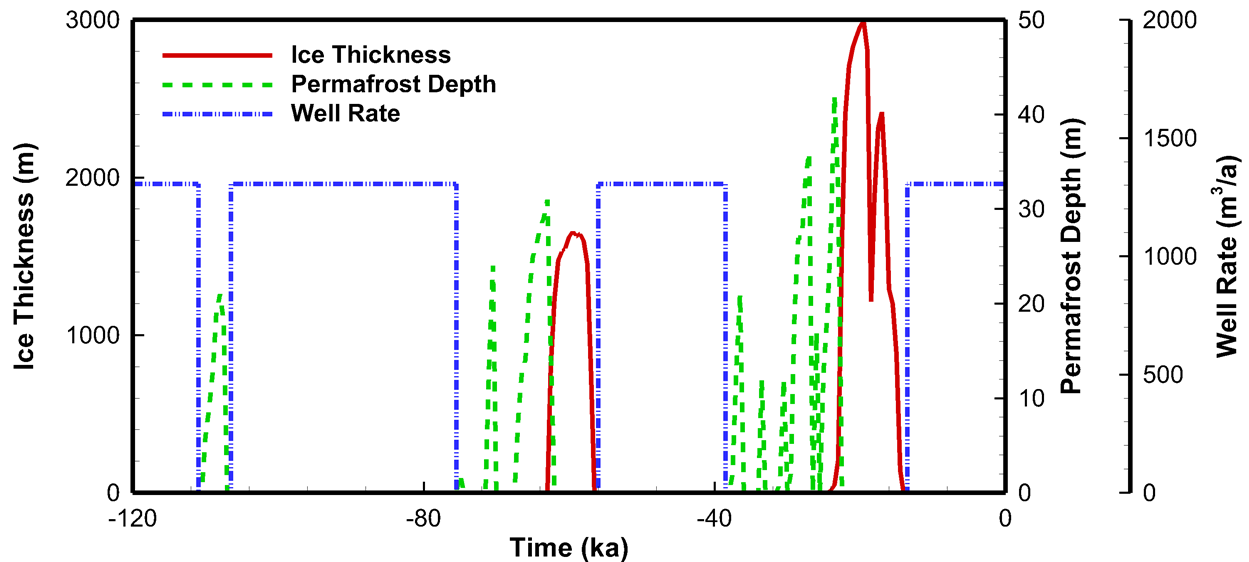


Figure 7-106: Simulated Ice Thickness, Permafrost Depth, and Well Operation at the Repository Site over One Full Glacial Cycle

7.8.2.4.2 Hydrogeological Modelling

In the glaciation study, the repository was positioned at the same depth in the same assumed sedimentary rock formation sequence as in the current assessment.

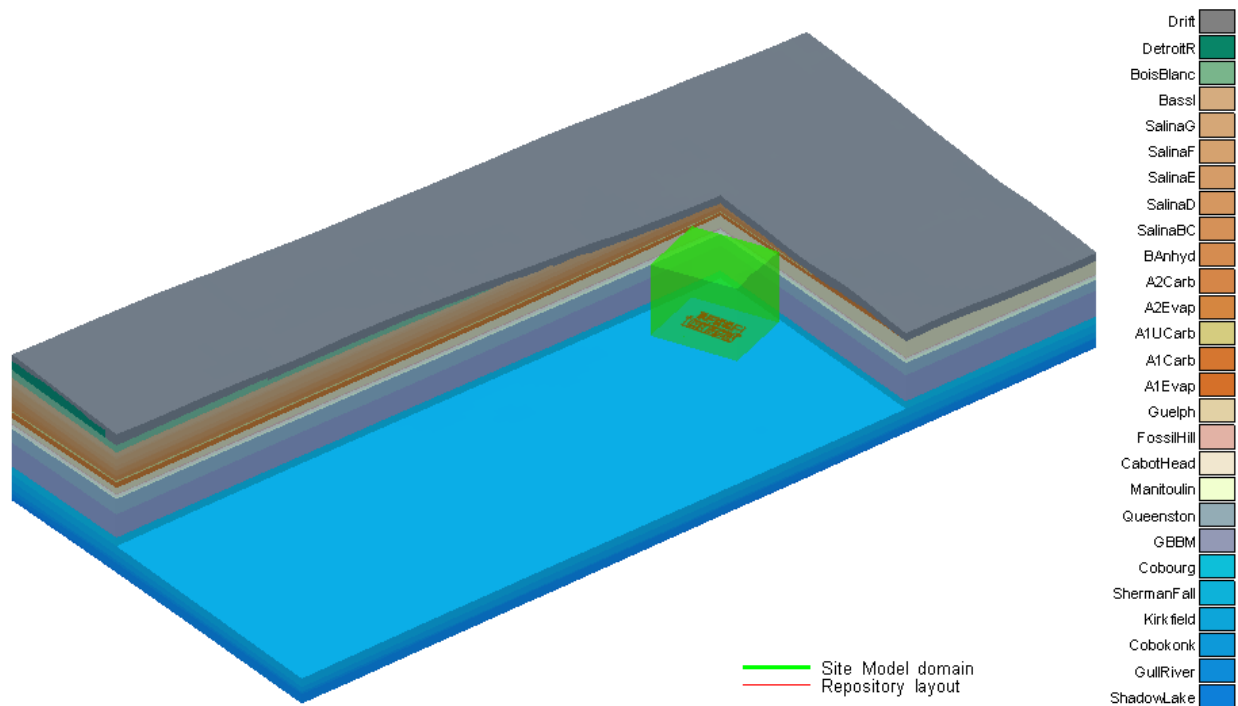
Topography of this region is relatively flat, with elevation generally ranging from 200 m - 400 m above sea level (mASL). At the hypothetical repository site, a 30 m thick layer of Quaternary-aged glacial drifts overlays an approximately 650 m thick sequence of Silurian and Ordovician-aged sedimentary rocks, underlain by the Precambrian-aged metamorphic basement rocks.

The Cobourg formation comprises fine-grained to argillaceous limestone, offering both mechanical strength and low permeability. Field studies suggest that fractures in this region are generally sparse and they are not expected to reach Ordovician-aged rocks. Detailed descriptions of the geosphere at the hypothetical site are provided in Chapter 2.

A Subregional Model was used to perform glaciation flow simulations. The Subregional Model has a rectangular domain of 25 km (west-east) by 50 km (north-south). This orientation was chosen based on the assumption that glaciers advance and retreat along the north-south direction. Horizontally, the domain is discretized into a 500 m square mesh, and vertically the model has 59 node layers, resulting in 303,909 nodes and 290,000 elements in total. Due to the coarse grid resolution, repository features are not represented in the Subregional Model.

The Subregional Model comprises 27 geological units, with drift at the top and the Shadow Lake formation at the bottom (Figure 7-107). A no-flow boundary defines the bottom of the model and the sides parallel to the direction of glacial advance and retreat. Transient hydraulic head and stress-loading boundary conditions calculated from ice thickness data are applied along the model top surface. Transient head boundary conditions are also applied at the north and south ends of the model to allow glacially driven flow into and out of the model domain for the more permeable units. Properties of elements whose centroids are within the time-varying permafrost depth are modified to reflect the presence or absence of permafrost.

The model assumes a water-supply well pumping from the bottom of the Guelph formation, as is also assumed in the current study (Section 7.2.1.2). The well pumps water when there is no glacier or permafrost at the repository site as illustrated in Figure 7-106. The Guelph formation has an assumed thickness of 73 m at the well location and is the first permeable formation that any hypothetical releases from the repository would encounter in transport towards surface discharge.



Note: Vertical exaggeration = 10.

Figure 7-107: Glaciation Subregional Model Property Assignments (after Avis and Calder, 2015)

After obtaining the present-day (i.e., constant-climate) steady-state solution as the initial condition, the Subregional Model is used to simulate eight glacial cycles, totaling 960 ka. Hydraulic head results for a few selected representative formations are presented in Figure 7-108. Hydraulic heads in all formations respond to glaciation events, increasing during the ice-sheet loading phases and decreasing during the unloading phases. Figure 7-109 presents hydraulic head profiles at the times of maximum well transport for each glacial cycle, revealing that there is a steady accumulation of glacial overpressure along the formations between Queenston and Shadow Lake.

The accumulation of glacial overpressure has little impact on either advective velocity results or contaminant transport. Figure 7-110 shows the advective velocity within a few selected formations – while loading and unloading of ice sheets increases groundwater velocity by factors of 10 to 100, groundwater velocity around the repository remains low due to the low permeability of the sedimentary formations.

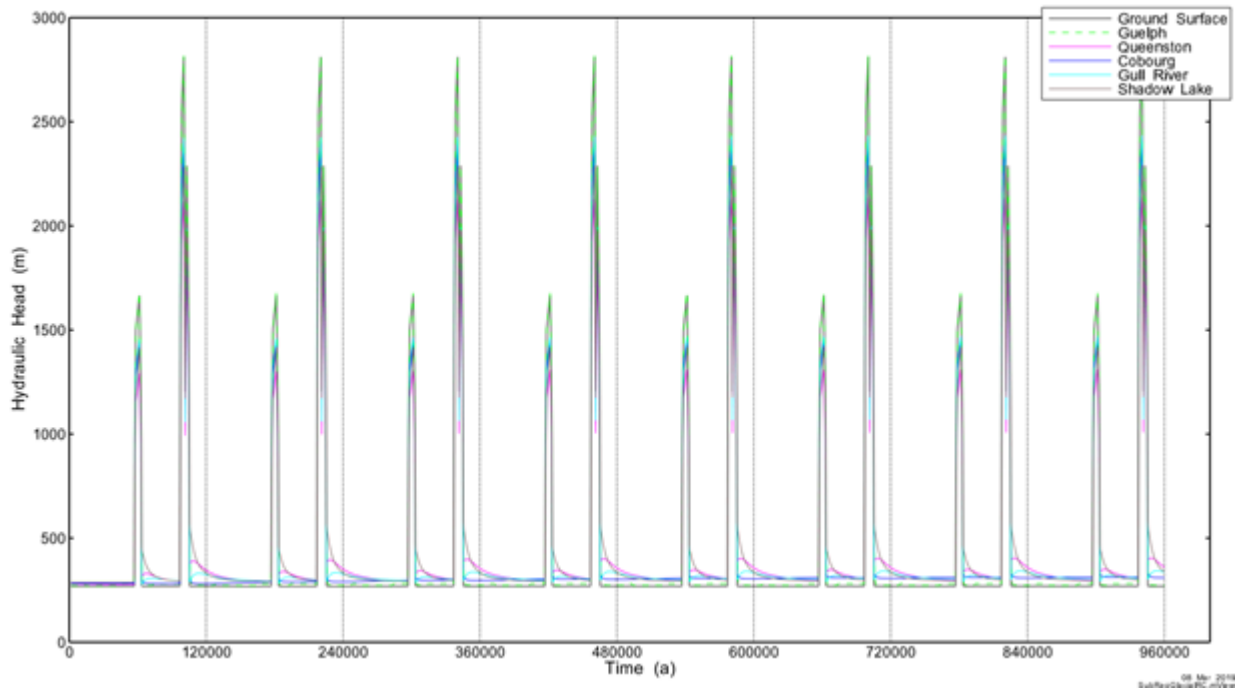


Figure 7-108: Glacial Cycle Simulations: Hydraulic Head at the Repository Location within Selected Formations (Avis and Calder, 2015)

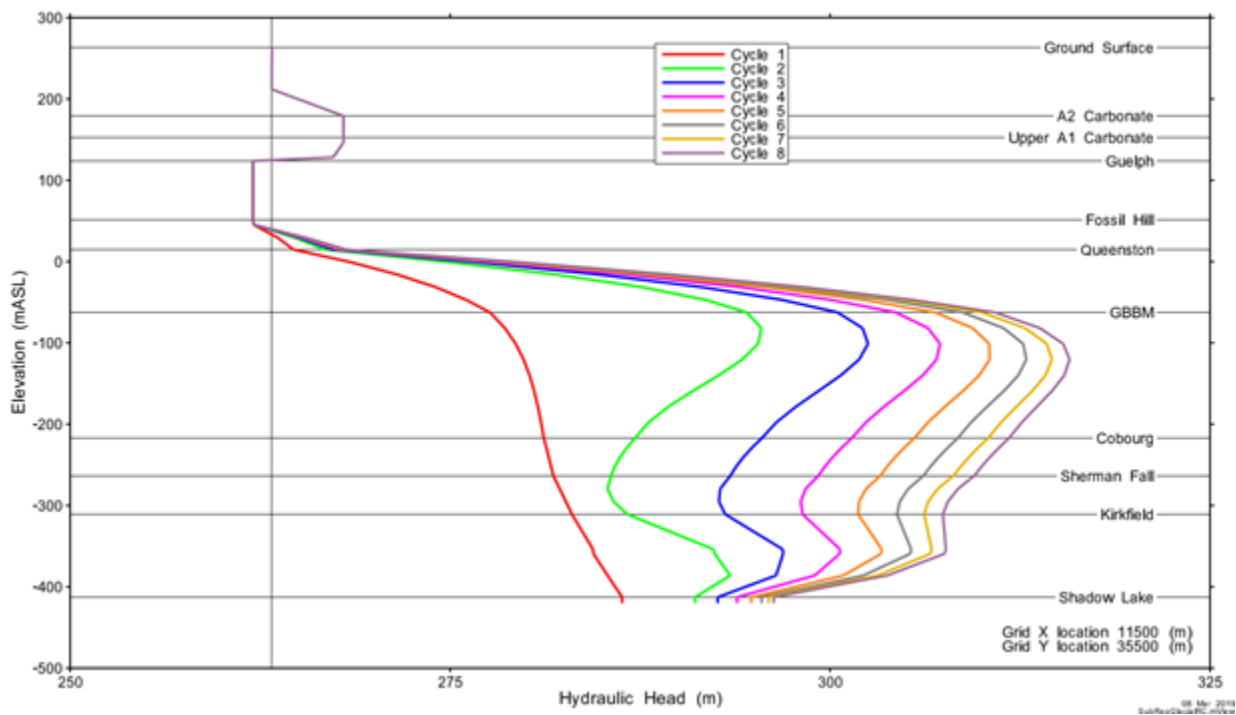


Figure 7-109: Glacial Cycle Simulations: Hydraulic Head at Times of Maximum Well Transport for Each Glacial Cycle (Avis and Calder, 2015)

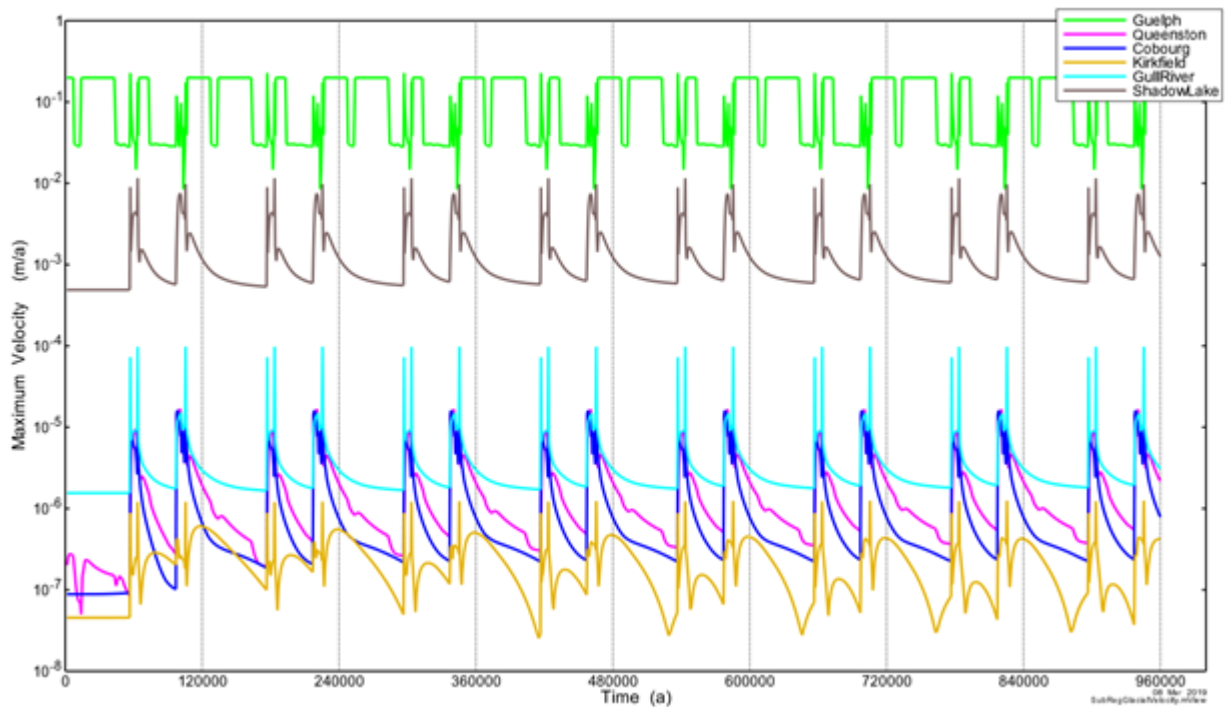


Figure 7-110: Glacial Cycle Simulations: Advective Velocity within Selected Formations (Avis and Calder, 2015)

7.8.2.4.3 Transport Modelling

The glaciation scenario study assumes hypothetical failures of used fuel containers occur at the most consequential location within the repository. I-129 is the modelled radionuclide, because simulations of contaminant transport in constant temperate conditions indicate this is the only radionuclide of consequence (see for example Section 7.8.2.1).

Figure 7-111 shows the assumed rate of release of I-129 due to hypothetical failure of used fuel containers. This is for a pinhole leak in three defective used fuel containers, with each container holding 360 used fuel bundles. The current study assumes 10 defective containers, with each container holding 48 used fuel bundles with no credit taken for any transport resistance provided by the container wall.

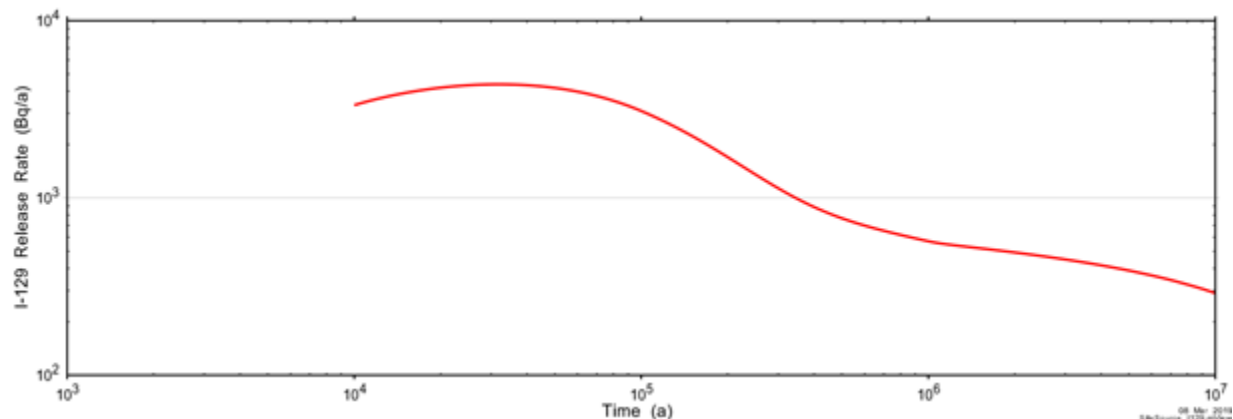


Figure 7-111: Glacial Cycle Simulations: Assumed Container Release of I-129

Glacial-cycle transport modelling is presented for two scenarios: the With-Well Scenario and the No-Well Scenario. The With-Well Scenario considers a water-supply well pumping from the bottom of the Guelph formation (see Section 7.2.1.2), while the No-Well Scenario has the water-supply well turned off. These scenarios are used to estimate transport of hypothetical contaminants from the repository.

With-Well Scenario

A high-resolution Site Model that explicitly represents major repository features is used for transport modelling. The Site Model covers a rectangular domain of approximately 4.0×5.2 km. Figure 7-107 (green box) shows the location of its domain with respect to the Subregional Model. Figure 7-112 shows the Site Model vertical discretization through the grid centre and Figure 7-113 shows the vertical property assignment through the main shaft. The vertical domain of the Site Model extends from the bottom of the Shadow Lake formation to the top of the Salina A2 Carbonate formation. Those formations above A2 Carbonate are omitted to reduce computational load. In total, the Site Model has 58 node layers, with 3.89 million nodes and 3.79 million elements. A no-flow boundary condition is assigned to the bottom of the Site Model and time-varying specified head boundary conditions are extracted from the Subregional Model for the remaining sides. In addition, the time-varying surface load is extracted from the Subregional Model and applied to the model to impose glacial loading and unloading.

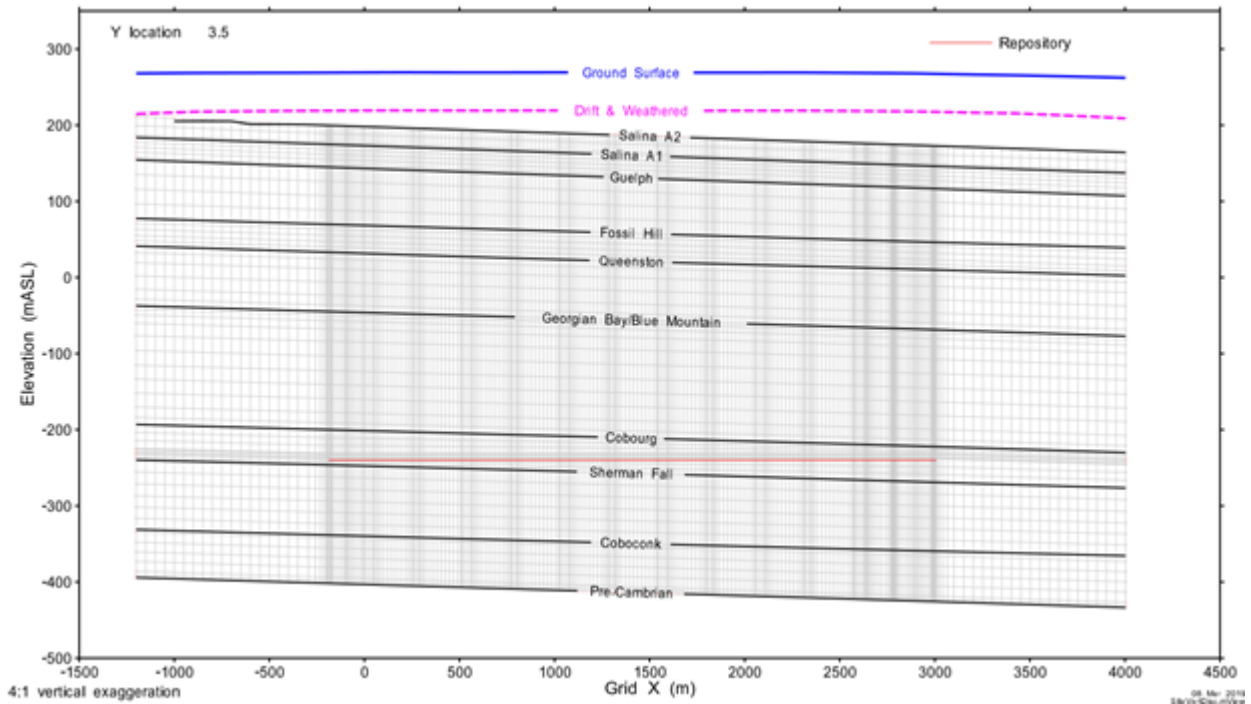


Figure 7-112: Glaciation Site Model: Vertical Discretization (Avis and Calder, 2015)

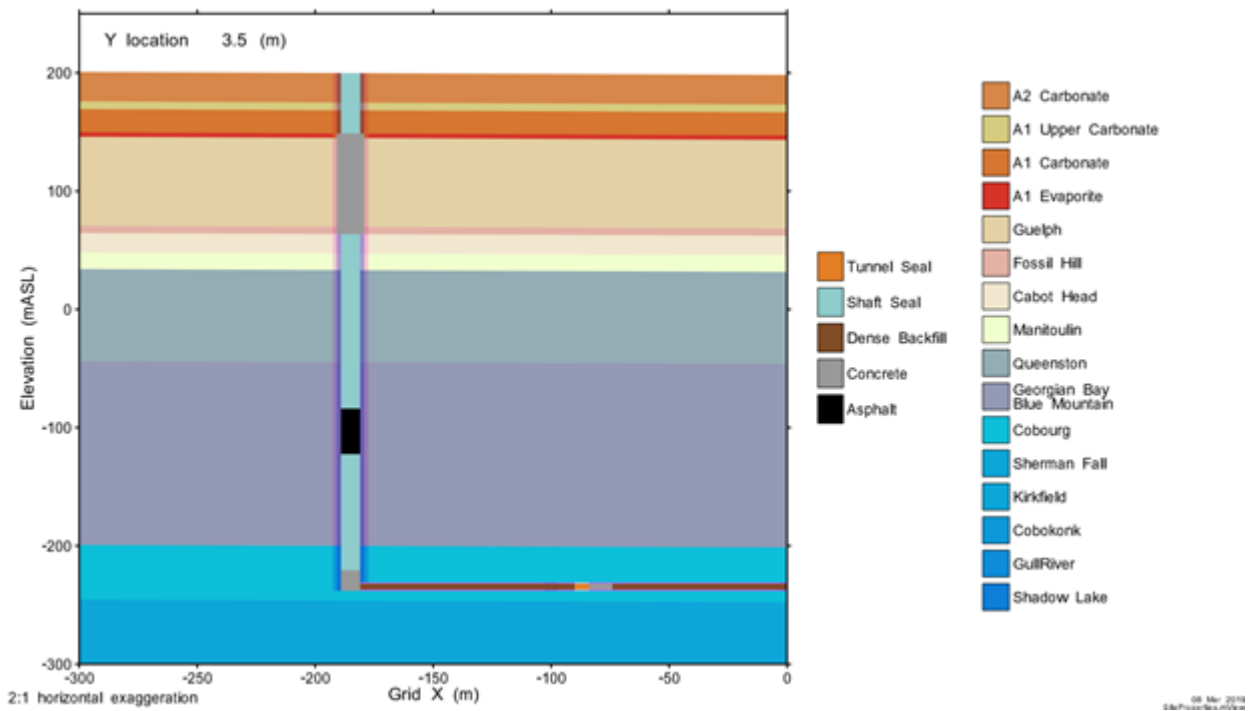


Figure 7-113: Glaciation Site Model: Vertical Property Assignment (Avis and Calder, 2015)

Two sub-cases are simulated, one for constant-climate conditions and another for glacial cycling, with comparisons of I-129 transport presented in Figure 7-114. After almost eight glacial cycles, the majority of I-129 remains within the vicinity of the repository. This is due to the low permeability of the sedimentary formations. In addition, there is essentially no difference between I-129 transport during glacial cycling compared to constant-climate conditions, further illustrating the diffusion-dominant nature of the repository system.

Figure 7-115 compares I-129 transport at various locations. Transport into the Queenston and Blue Mountain / Georgian Bay formations is virtually the same during glacial cycling compared with constant-climate conditions.

Glaciation cycles do have an effect on transport of I-129 into the Guelph formation and then to the water-supply well. When ice sheets or permafrost are present, the well is off and transport of I-129 to and through the Guelph decreases, allowing the concentration of I-129 to increase in some areas. Consequently, when the well is turned on, there is an initial, brief peak in transport of I-129 to the well of up to 100 times the value with a continuously pumping well, which then quickly reduces to constant-climate levels. This is the same type of behaviour illustrated in the Intermittent Well sensitivity case in the current study (Section 7.7.2.3.4).

Figure 7-115 also shows that essentially all I-129 entering the Guelph formation is captured by the water-supply well.

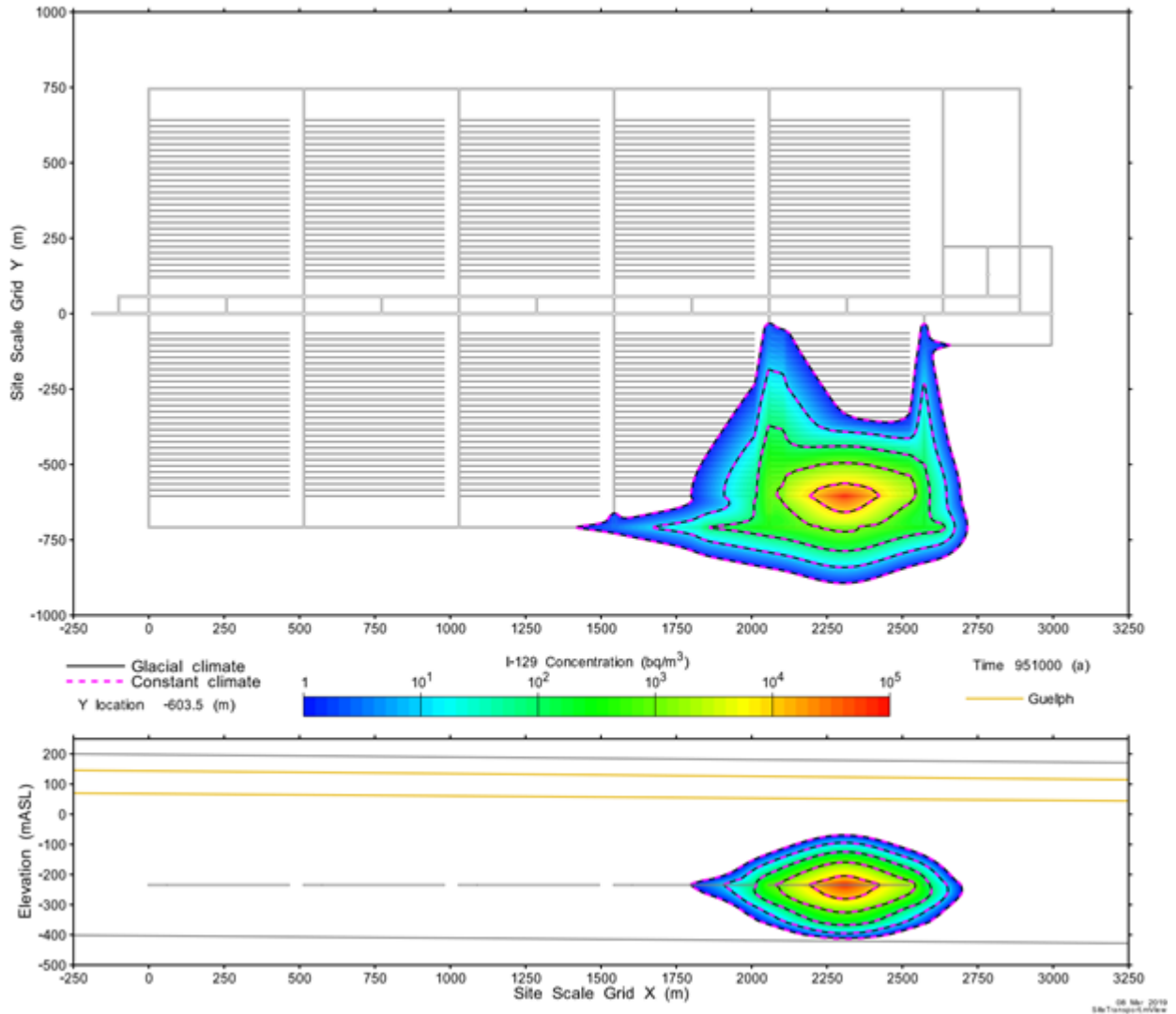


Figure 7-114: Comparison of I-129 Concentration between Glaciation and Constant Climates (Avis and Calder, 2015)

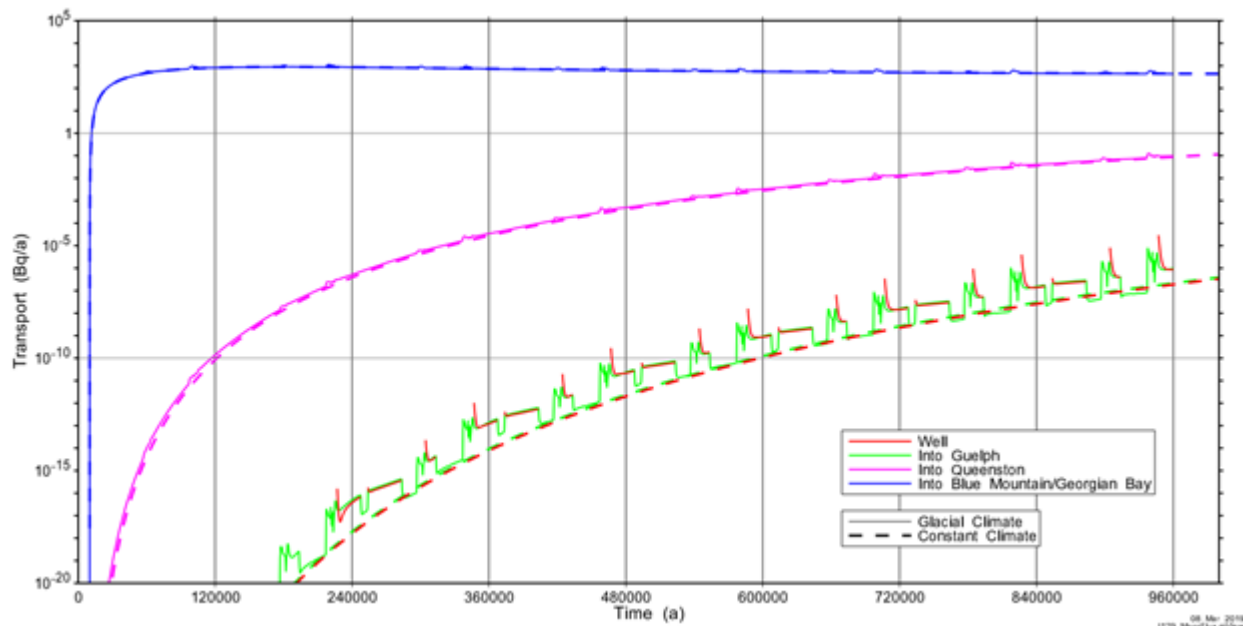


Figure 7-115: Transport of I-129 for Constant-Climature Conditions vs. Glacial Cycling (Avis and Calder, 2015)

No-Well Scenario

The No-Well Scenario estimates transport of I-129 in the absence of water-supply well. The Site Model is used to calculate I-129 transport entering the Guelph formation, then a Regional Model is used to calculate transport of I-129 beyond the Site Model boundaries.

To reduce computational load, all model layers above the bottom of the Guelph formation are removed from the Site Model. The resulting No-Well Site Model has 3.1 million nodes and 3.0 million elements.

The top of the Site Model is therefore the top of the Fossil Hill formation, conservatively defined as a zero-concentration boundary. Time-varying boundary conditions reflecting ice-sheet thickness are applied to the top of the model. Due to the low permeability of these formations, horizontal flow is assumed negligible and no-flow boundary conditions are applied to the bottom and four sides of the model. The Fossil Hill formation is well below the maximum permafrost depth, such that the entire Site Model is unaffected by permafrost.

Six sensitivity cases illustrate the impact of parameter uncertainties on I-129 transport:

- Reference: glacial cycling, using reference values for all system parameters;
- Control: constant-climate conditions, using reference values for all system parameters;
- All LE=1.0: all loading efficiencies (LE) are set to 1.0;
- All LE=0.0: all loading efficiencies are set to 0.0;
- Diffusion×2: the diffusion coefficient of I-129 is increased by a factor of two; and,
- Dispersivity×2: dispersivity throughout the Site Model is increased by a factor of two.

Transport results for all six sensitivity cases are presented in Figure 7-116. Results show that, as in the With-Well Scenario, cycling of glacial loading and unloading can lead to cycling of transport into the Guelph formation, although rates of transport remain very low overall.

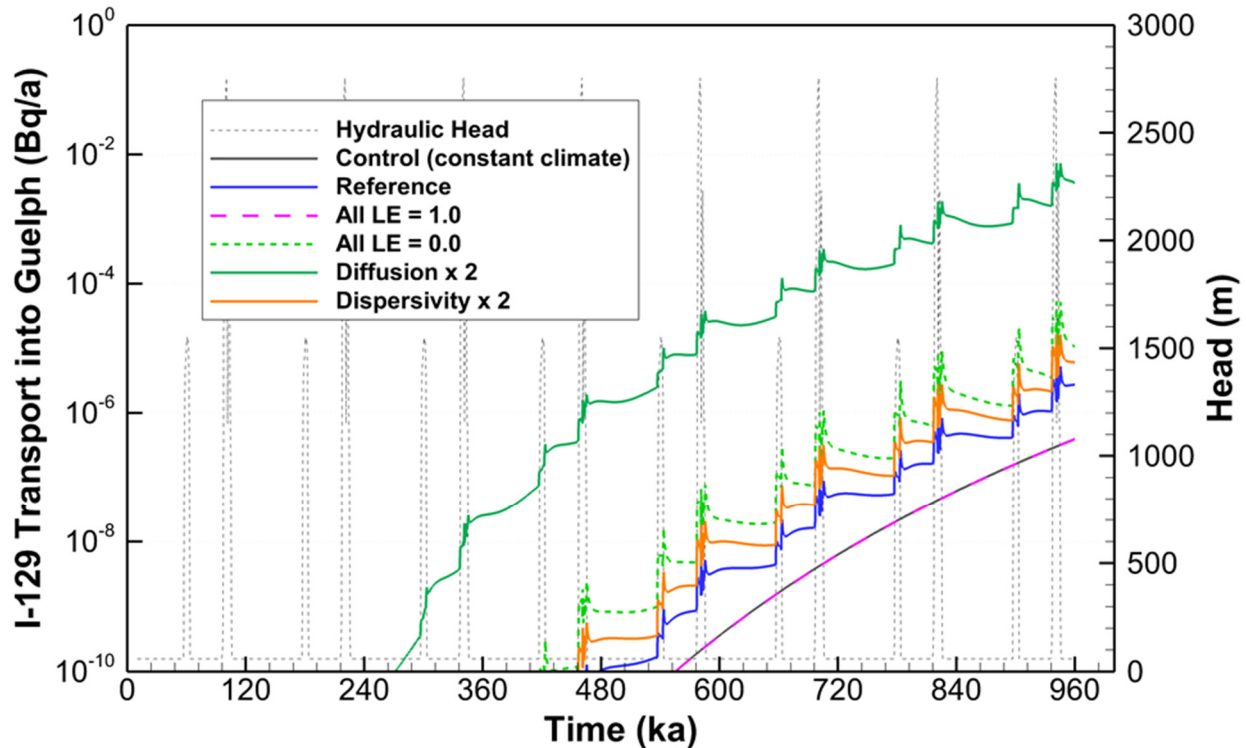


Figure 7-116: No-Well Site Glaciation Model: I-129 Transport into the Guelph Formation (Avis and Calder, 2015)

The diffusion coefficient has the greatest initial impact, substantially more than the other sensitivity cases. Doubling the diffusion coefficient for I-129 causes transport to the Guelph to increase by about two orders of magnitude in the time period examined; however, the effect on peak transport (not reached in the simulation time) is expected to be much less. This behaviour is largely a reflection of the very low I-129 concentrations near the top of the model – hardly any I-129 reaches the Guelph formation (the bulk of I-129 remains within close proximity to the repository), so small changes in system parameters can have relatively large effects. Transport through the reference geosphere is strongly diffusion-dominant, making transport especially sensitive to changes in the diffusion coefficient. Despite this, overall transport remains very low.

When dispersivities throughout the model are doubled, transport to the Guelph formation increases by roughly a factor of two to three in the time period examined. As with sensitivity to the diffusion coefficient, this response is largely due to very low I-129 concentrations near the top of the model, such that small changes in system parameters can have relatively large effects. Again, as with the diffusion coefficient, peak transport is not reached within the simulation time and therefore the maximum effect may be less than observed.

Transport results with all loading efficiencies set to 1.0 are essentially identical to the constant-climate case, indicating that glaciation would have little impact on transport if the glacial load was carried fully by the groundwater; conversely, results from setting all loading efficiencies to 0.0 show that, if the glacial load was carried fully by the rock, I-129 transport to the Guelph could increase by roughly a factor of 10. This latter case is a bounding but non-physical scenario, as loading efficiencies within the reference geosphere are typically well above 0.5 (Chapter 2).

7.8.2.4.4 Dose Results for Glaciation Scenario

During the temperate state between glacial periods, a Self-Sufficient Farmer household is the critical group. This group is assumed to spend their entire lives in the vicinity of the site and to obtain all their needs locally. All water needs (including irrigation and drinking) are met by the water-supply well.

The current study finds that dose consequences is entirely due to transport of I-129 to the well; accordingly, well transport of I-129 is used to estimate dose consequences for the glaciation studies. From the With-Well (glacial) Scenario, results presented in Figure 7-115 show I-129 transport to the water-supply well never exceeds 10^{-4} Bq/a in the approximate one million year simulation time. Using the System Model biosphere submodel, this translates to a dose consequence of 2.7×10^{-11} mSv/a. This is so low as to be considered zero.

7.8.2.4.5 Applicability to the Current Study

These glaciation scenario results are based on prior studies (Avis and Calder, 2015; Chen et al. 2017). Both these glaciation scenario studies consider repositories at the same hypothetical location as the repository considered in the current study; consequently, the climate would evolve similarly and the glacial cycles considered here would be representative of the future climate at the postclosure safety assessment site.

Notable differences between the two glaciation scenario studies and the current study are:

- The glaciation studies assume three defective used fuel containers, with each container holding 360 used fuel bundles. The current study assumes 10 defective containers, with each container holding 48 used fuel bundles.
- The three defective containers in the glaciation studies are assumed to fail at 10,000 years. In the current study, the first container fails after 1000 years and subsequent containers fail at a rate of one container every 100,000 years.
- The glaciation studies assume a pinhole failure in each defective container whereas the current study takes no credit for the container inhibiting the release of contaminants.
- The underground layout of the repository placement rooms and connecting access tunnels is different in the glaciation studies compared to the current study; also, the design of the engineered-barrier system is substantially different.

The differences outlined above are limited to the scale of the repository and, as such, can be expected to have relatively little impact on the glaciation conclusions presented here.

A discussion of the potential effects of glaciation on the deep groundwater system for the current study geosphere is provided in Chapter 2.

7.8.2.5 Probabilistic Analysis

In the previous sections, deterministic analyses are performed for the Base Case and a series of sensitivity studies to illustrate the effect of degraded barrier performance on radionuclide transport.

Many of the modelling parameters are uncertain or have a natural degree of variability, and are therefore more generally characterized by a range or distribution of values. Simultaneous accounting of these uncertainties is achieved by using the System Model in probabilistic mode.

Probabilistic mode uses a random sampling strategy that considers the full range of possible parameter values. The results presented here draw from 100,000 simulations in which parameter values are randomly sampled from their probability density functions. Each of these thousands of simulations produces a unique estimate of impact that is used to collectively generate a distribution that reflects the underlying uncertainty. An important caveat is that parameter values that could affect groundwater flow are not varied in these simulations.

Two probabilistic cases are simulated. These are:

- 1) Number, locations and failure times for the defective containers fixed at their Base Case values, with all other available parameters varied; and
- 2) All parameters with a probability distribution varied, including the number, locations and failure times of defective containers.

A detailed description of the probability distributions for all parameters is provided in Gobien et al. (2018). The well is fixed at its Base Case location in all simulations.

All simulation results are reported based on one million year simulations.

Container Assumptions

In the Base Case, 10 defective containers are assumed present in the repository.

For the first probabilistic case, this assumption is fixed.

For the probabilistic case in which the number of defective containers is varied (i.e., the second case noted above), the number of defective containers is described by a binomial distribution with the individual container failure probability selected such that the 95th percentile value results in at least 100 containers failing. This is an anticipated conservative representation of the extent to which defective containers may be present in the repository despite the careful manufacturing process and associated robust quality assurance program that will be established.

In the Base Case, the defective containers are all clustered in the location that maximizes contaminant uptake to the well. For the probabilistic case in which container locations are varied, defective containers can be in any of the 10 sectors of the Geosphere Submodel (see Section 7.8.1.2). Container failures in multiple sectors can also occur.

In the Base Case, the first defective container fails at 1000 years, with subsequent containers failing at a rate of one container for every additional 100,000 years. In the probabilistic case in which container failure times are varied, the failure times are defined using a uniform distribution ranging between 1 and 1,000,000 years. The model allows containers in different sectors to fail at different times; however all defective containers in a given sector must fail at the same time.

7.8.2.5.1 Results for Container Failure Assumptions Fixed

In this probabilistic case, the number, locations and failure times of the containers are fixed at their Base Case values, with all other available parameters varied.

This is simulated using the System Model described in Section 7.8.1.

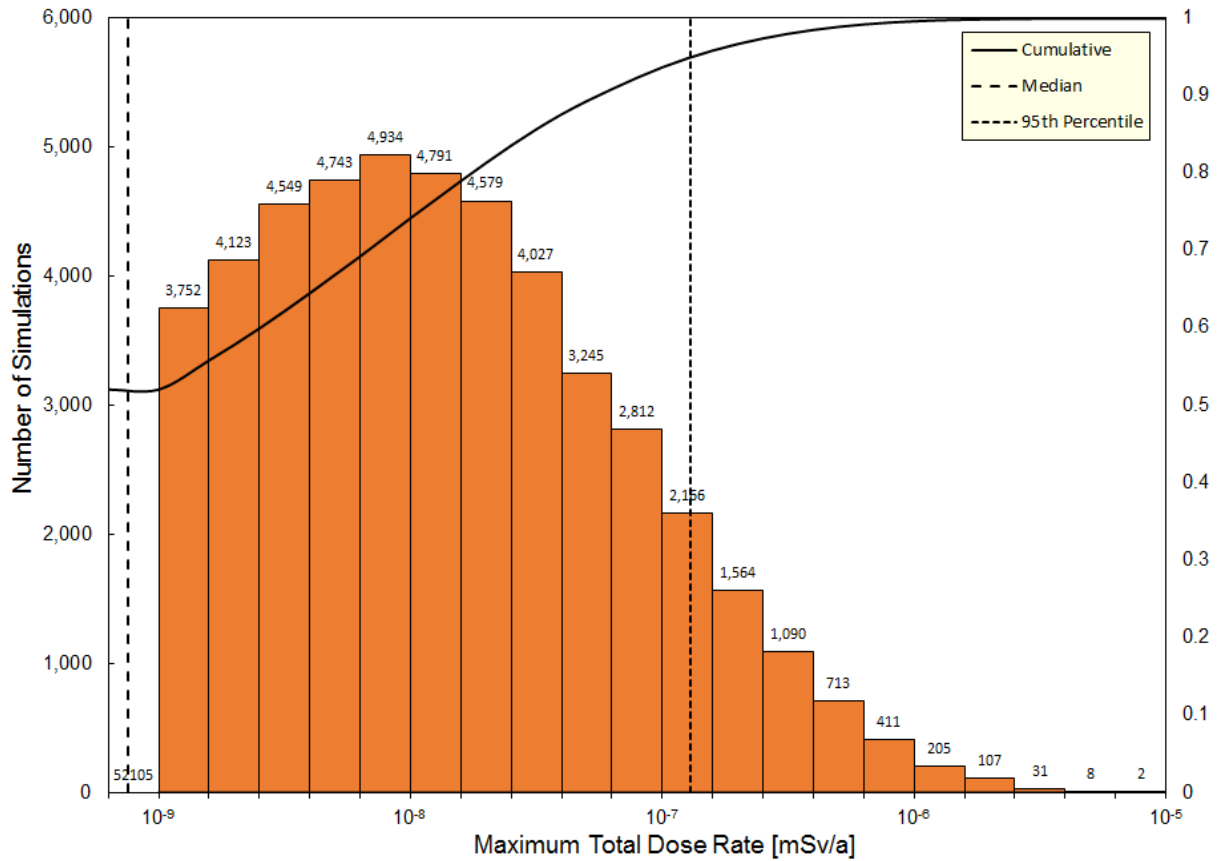
Dose Rate Results

Figure 7-117 presents a histogram of the 1 Ma dose rates obtained over 100,000 simulations, while

Table 7-38 presents a summary of the histogram statistics. The median, 95th percentile and 99th percentile values are 7.5×10^{-10} mSv/a, 1.3×10^{-7} mSv/a and 5.3×10^{-7} mSv/a. The median and 95th percentile values are marked on the figure. For comparison, the Base Case deterministically determined the 1 Ma dose rate is 5.9×10^{-10} mSv/a (Section 7.8.2.1). This is slightly greater than median value, suggesting that the Base Case parameters are slightly conservative.

There are some higher dose simulations on the right hand side of Figure 7-117, with the maximum of these having a dose rate of 7.3×10^{-6} mSv/a at 1Ma. These higher dose rate cases are discussed in a later part of this section.

All values are well below the interim dose rate acceptance criterion of 0.3 mSv/a established in Section 7.1.1.



Note: The leftmost bin at 10⁻⁹ mSv/a includes all simulations (52105) that resulted in a dose less than 10⁻⁹ mSv/a.

Figure 7-117: Probabilistic Assessment: 1 Ma Dose Rate Histogram with Container Assumptions Fixed

Table 7-38: Statistical Information for the 1Ma Dose Rate Histogram with Container Assumptions Fixed

Statistic	Value (mSv/a)	Bootstrap 95% Confidence Bounds ⁽¹⁾	
		Lower Bound (mSv/a)	Upper Bound (mSv/a)
Median	7.5x10 ⁻¹⁰	6.6x10 ⁻¹⁰	8.6x10 ⁻¹⁰
95th Percentile	1.3x10 ⁻⁷	1.2x10 ⁻⁷	1.4x10 ⁻⁷
99th Percentile	5.3x10 ⁻⁷	4.6x10 ⁻⁷	6.0x10 ⁻⁷

Note: (1) Based on 10 sets of 10,000 replicates of the dataset obtained using the bootstrap methodology. The confidence intervals are calculated using the bootstrap method (with replacement). Since the distribution of peak dose rates is skewed, the bootstrap BC_a methodology described by DiCiccio and Efron (1996) is used.

Table 7-39 shows the median, 95th percentile and 99th percentile values for those radionuclides that contribute more than 0.001% of the total dose rate. As in the Base Case, I-129 is the dominant dose contributor.

Table 7-39: Probabilistic Assessment: Individual Radionuclides Dose Contributions for Container Assumptions Fixed

Radionuclide	Median (mSv/a)	95 th Percentile (mSv/a)	99 th Percentile (mSv/a)
I-129	7.5×10^{-10}	1.3×10^{-7}	5.3×10^{-7}
Cl-36 (Zircaloy)	1.3×10^{-12}	1.7×10^{-10}	5.2×10^{-10}

Note: Only those radionuclides with values greater than 0.001% of the maximum column value are shown

Figure 7-118 shows the distribution of dose rates from all 100,000 simulations showing the time dependence of the dose bands for the 25th, 50th, 75th, 90th, 95th and 99th percentiles.

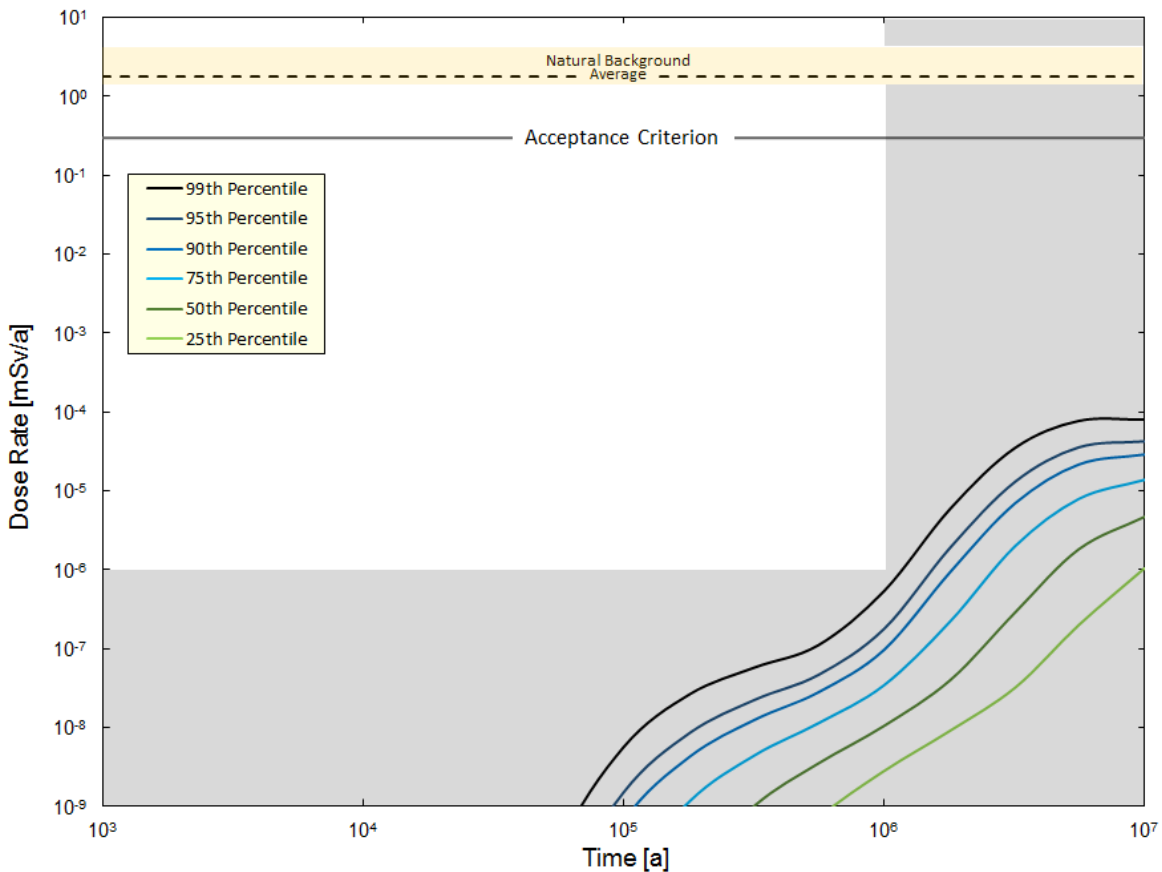


Figure 7-118: Probabilistic Assessment: Time Dependence of Percentile Values with Container Assumptions Fixed

Maximum Value Simulations

Figure 7-117 shows that there are a number of cases with dose rates higher than the 95th percentile value (1.3×10^{-7} mSv/a), with the maximum value reported over all 100,000 simulations as 7.3×10^{-6} mSv/a. Extending the simulation results in a peak value of 3.4×10^{-5} mSv/a, which is well below the interim dose rate criterion.

The cases with the five highest dose rates have been extracted and studied to identify the causal factors. Table 7-40 summarizes each of these five cases, showing the 1 Ma dose rates, the time of the peak, the dominant radionuclide, how much the dominant radionuclide contributes to the total, and the main exposure pathway.

Table 7-40: Probabilistic Assessment: Results for Top 5 High-Dose Simulations with Container Assumptions Fixed

Simulation	1 Ma Dose Rate (mSv/a)	Dominant Radionuclide	% of total dose from I-129	Dominant Pathway
20229	7.41×10^{-6}	I-129	100%	65% Food Ingestion 35% Water Ingestion
77205	6.64×10^{-6}	I-129	100%	84% Food Ingestion 16% Water Ingestion
35324	5.30×10^{-6}	I-129	100%	95% Food Ingestion 5% Food Ingestion
90464	4.88×10^{-6}	I-129	100%	18% Food Ingestion 82% Water Ingestion
27782	4.50×10^{-6}	I-129	100%	21% Food Ingestion 79% Water Ingestion

Table 7-40 shows that I-129 is the dominant dose contributor in these cases, with the dominant exposure pathway being uptake of food. All of these cases are controlled by ingestion of vegetables. The following observations can be made:

- The dominant dose pathways are ingestion of garden vegetables and drinking water. For each of the five cases the dominant pathways are generally consistent with those of the Base Case.
- Peak dose rates all occur prior to 10 million years. This suggests that the maximum dose cases are primarily caused by high I-129 diffusion coefficients. Table 7-41 shows the free water diffusion coefficients values for these simulations. The free water diffusion coefficients are used to calculate the effective diffusion coefficient through the sedimentary rock mass and values are many times greater than those of the Base Case.

Table 7-41: Probabilistic Assessment: I-129 Pathway

Simulation	I-129 Free Water Diffusion Coefficient (m ² /a)	Ratio to the Base Case Value ⁽¹⁾
20229	0.485	9.3
77205	0.485	9.3
35324	0.522	10.0
90464	0.484	9.2
27782	0.499	9.5

Note: (1) The Base Case assumes a free water diffusion coefficient for I-129 of 0.0524 m²/a. This parameter is loguniformly distributed with an upper bound 10 times higher.

In summary, none of these simulations exceed the dose rate criterion. The dominant radionuclides and dominant dose pathways are generally consistent with the Base Case and no anomalous data were found to be driving assessment results.

7.8.2.5.2 Results for All Parameters Varying

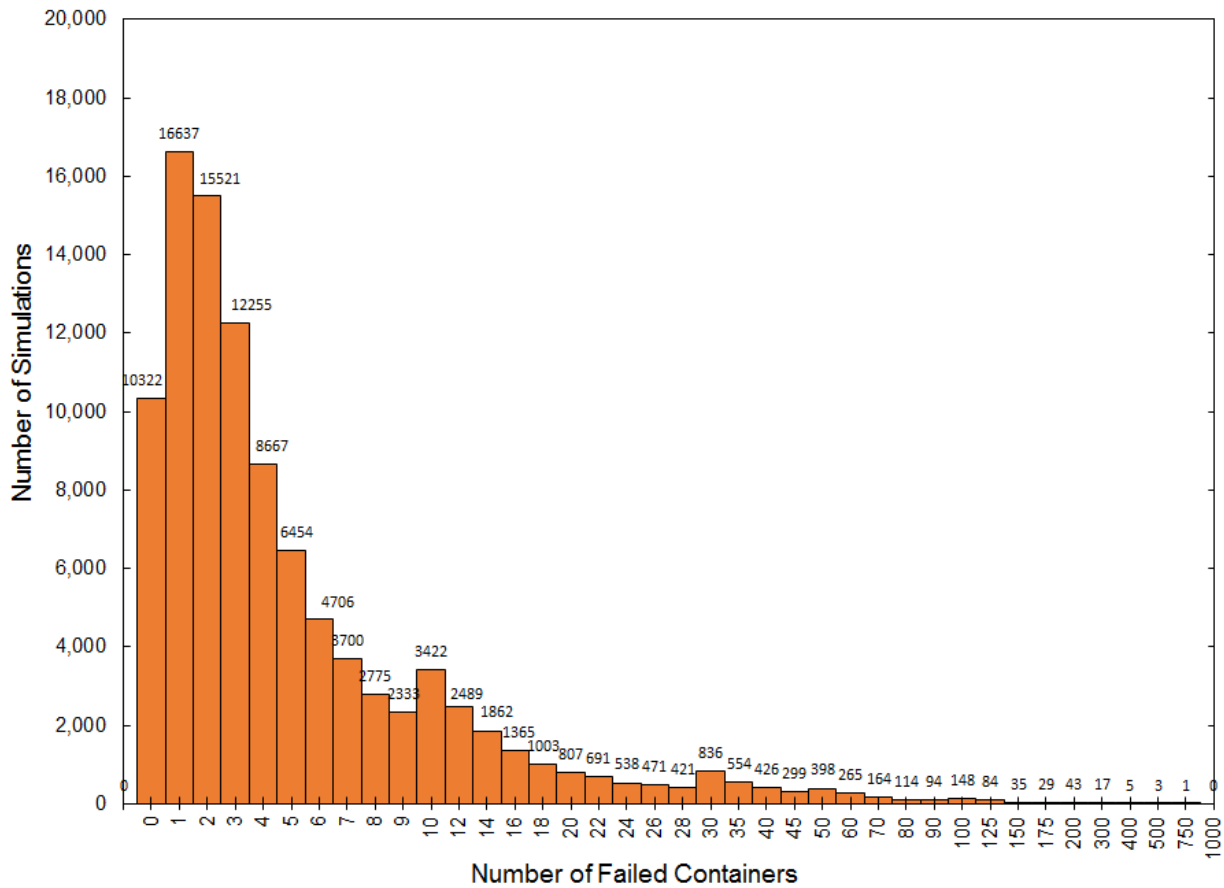
In this probabilistic case, all parameters with a probability distribution are varied, including the number, locations and failure times of defective containers.

This is again simulated using the System Model described in Section 7.8.1.

Number of Defective Containers

Figure 7-119 presents a histogram of the number of container failures over the 100,000 simulations. As noted earlier in Section 7.8.2.5, this is determined based on a binomial distribution with the individual container failure probability selected such that the 95th percentile value results in at least 100 containers failing.

The minimum number of failures is 0 (in 10322 simulations) and the maximum number is 868 (in one simulation). The median is 3, the 95th percentile is 23 and the 99th percentile is 60.



Note: Steps in the histogram binning increases at 10, 30, 50, 100, 200 and 500.

Figure 7-119: Probabilistic Assessment: Distribution of Container Failures with All Assumptions Varying

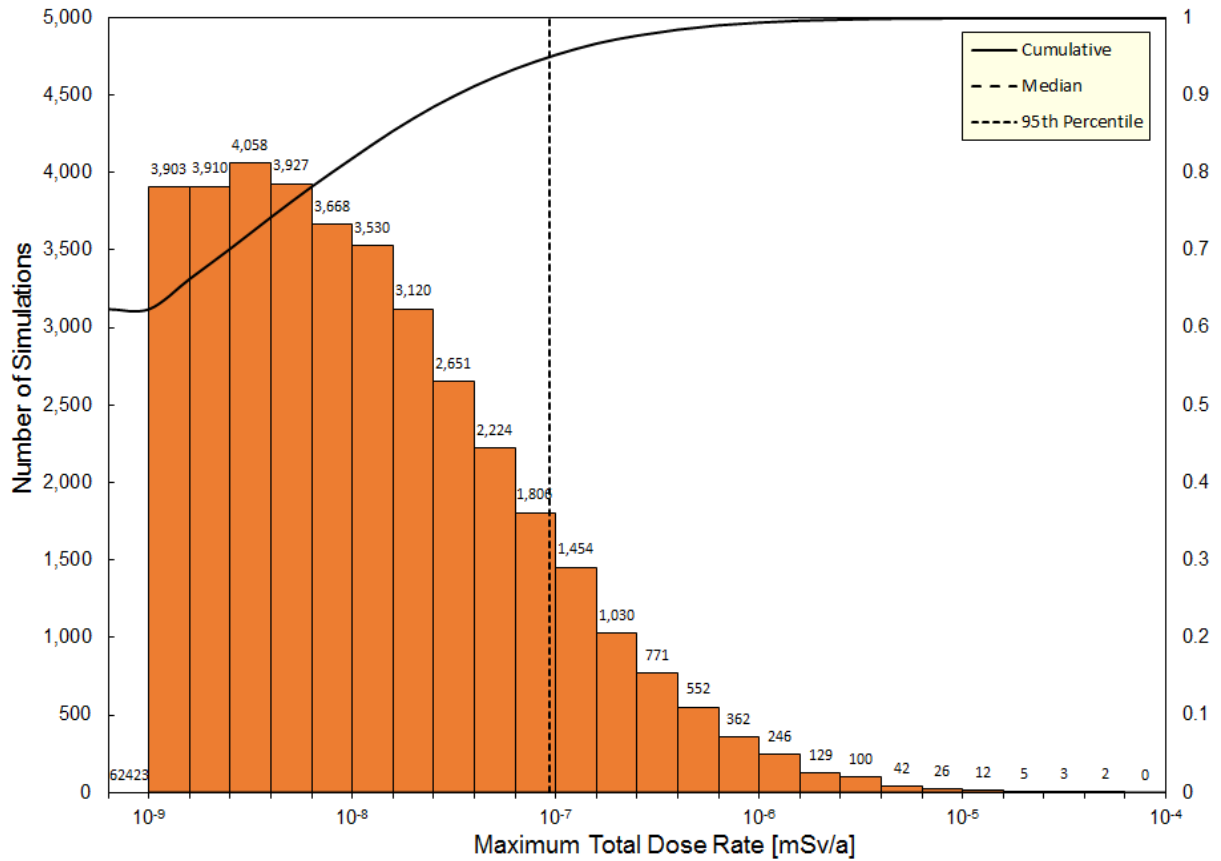
Dose Rate Results

Figure 7-120 presents a histogram of the 1 Ma dose rates obtained over the 100,000 simulations (excluding the zero dose results), while Table 7-42 presents a summary of the histogram statistics. The median, 95th percentile and 99th percentile values are 1.9×10^{-10} mSv/a, 9.3×10^{-8} mSv/a and 5.9×10^{-7} mSv/a. The median and 95th percentile values are marked on the figure. The maximum over all simulations 6.0×10^{-5} mSv/a. For comparison, the Base Case dose rate at 1 Ma is 5.9×10^{-10} mSv/a (Section 7.8.2.1). This is between the median and 95th percentile values.

Figure 7-120 is very similar in shape to the Container Assumptions Fixed probabilistic case discussed previously. This is because the sedimentary rock is diffusion dominant and the container location and failure times do not significantly affect the peak dose. The 1 Ma dose simulations have somewhat higher values than those in the other probabilistic case because of the larger number of failed containers.

The maximum dose rate is 6.0×10^{-5} mSv/a. This is discussed in a later part of this section.

All values are well below the interim dose rate acceptance criterion of 0.3 mSv/a established in Section 7.1.1.



Note: The leftmost bin at 10^{-9} mSv/a includes all simulations (62423) that resulted in a dose less than 10^{-9} mSv/a

Figure 7-120: Probabilistic Assessment: 1 Ma Dose Rate Histogram with All Assumptions Varying

Table 7-42: Statistical Information for the 1 Ma Dose Rate Histogram with All Assumptions Varying

Statistics ⁽¹⁾	Value (mSv/a)	Bootstrap 95% Confidence Bounds ⁽²⁾	
		Lower Bound (mSv/a)	Upper Bound (mSv/a)
Median	1.9x10 ⁻¹⁰	1.6x10 ⁻¹⁰	2.2x10 ⁻¹⁰
95 th Percentile	9.3x10 ⁻⁸	8.3x10 ⁻⁸	1.0x10 ⁻⁷
99 th Percentile	5.8x10 ⁻⁷	4.8x10 ⁻⁷	7.0x10 ⁻⁷

Notes: (1) These statistics are lower than the container assumptions fixed probabilistic case because they include ~10,000 simulations with zero dose consequence.

(2) Based on 10 sets of 10,000 replicates of the dataset obtained using the bootstrap methodology. The confidence intervals are calculated using the bootstrap method (with replacement). Since the distribution of 1 Ma dose rates is skewed, the bootstrap BC_a methodology described by DiCiccio and Efron (1996) is used.

Table 7-43 shows the median, 95th percentile and 99th percentile values for those radionuclides that contribute more than 0.001% of the total dose rate. As in the Base Case, I-129 is the dominant dose contributor.

Table 7-43: Individual Radionuclide Dose Rates with All Assumptions Varying

Radionuclide	Median (mSv/a)	95 th Percentile (mSv/a)	99 th Percentile (mSv/a)
I-129	1.9x10 ⁻¹⁰	9.3x10 ⁻⁸	5.9x10 ⁻⁷
Cl-36	1.2x10 ⁻¹³	1.1x10 ⁻¹⁰	6.3x10 ⁻¹⁰
Cl-36 (Zircaloy)	1.9x10 ⁻¹³	1.2x10 ⁻¹⁰	6.1x10 ⁻¹⁰

Note: Only those radionuclides with values greater than 0.001% of the maximum column value are shown.

Figure 7-121 shows the time dependence of the dose band for all 100,000 simulations for the 25th, 50th, 75th, 90th, 95th and 99th percentiles. The difference in shapes as compared to Figure 7-118 (i.e., for the probabilistic simulation with the number of failed containers fixed) occurs because of the uniform distribution adopted for the time of container failure (1 to 1,000,000 years), the varying number of failed containers, and because transport times to the well are generally longer due to the distribution of containers throughout the repository.

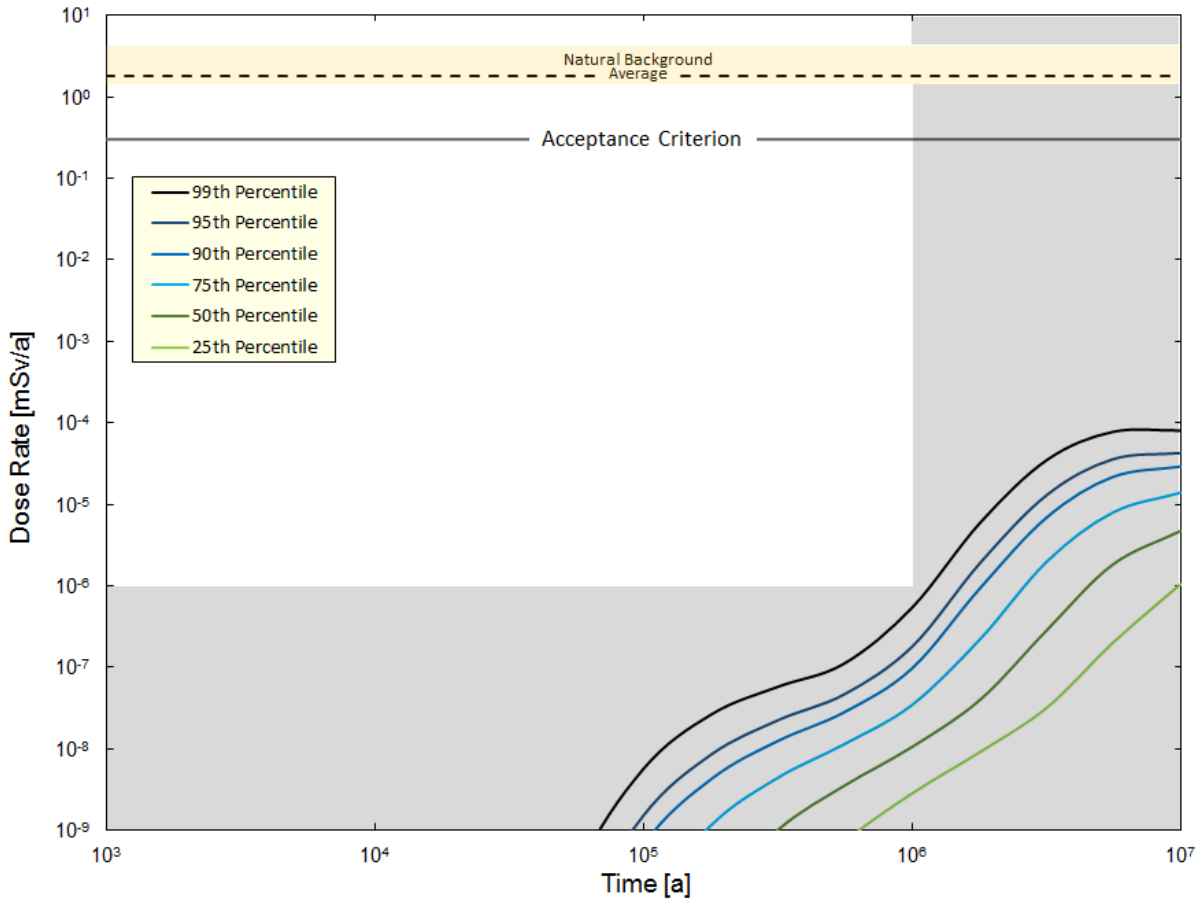


Figure 7-121: Probabilistic Assessment: Time Dependence of Percentile Values with All Assumptions Varying

Maximum Value Simulations

Figure 7-120 shows there are a number of cases with dose rates higher than the 95th percentile value (9.3×10^{-8} mSv/a), with the maximum value reported over all 100,000 simulations as 6.0×10^{-5} mSv/a. These results are investigated further below to develop an improved understanding of the simulations. Extending the simulation time beyond one million years, the peak value is 1.45×10^{-5} mSv/a, which is well below the interim dose rate criterion.

Table 7-44 presents results from the five simulations with the highest dose rates.

Table 7-44: Probabilistic Assessment: Results for Top 5 High Dose Simulations with All Assumptions Varying

Run ID	1 Ma Dose Rate (mSv/a)	Main Contributor	% of total from I-129	Number of Failed Containers	I-129 Free Water Diffusion Coefficient (m ² /a)
50091	6.0x10 ⁻⁵	I-129	100%	203	0.48
35324	4.2x10 ⁻⁵	I-129	100%	50	0.52
53732	3.3x10 ⁻⁵	I-129	100%	36	0.41
97055	3.1x10 ⁻⁵	I-129	100%	199	0.49
23105	2.8x10 ⁻⁵	I-129	100%	140	0.44

All of these cases have many containers failing across the 10 sectors of the System Model. While the containers in each sector fail at a different time, the long transport time in the geosphere means the individual failure times do not have a large effect on the dose results.

In summary, the maximum dose cases for the All Parameters Varying Probabilistic Assessment are driven by a combination of the number of failed containers and a high I-129 free water diffusion coefficient. All results are well below the interim dose rate criterion of 0.3 mSv/a established in Section 7.1.1.

7.8.2.6 Summary of Results for System Modelling

Table 7-45 summarizes results for all of the cases described in Section 7.8.2. The results illustrate the importance of the well and its assumed location, with the fuel dissolution rate and geosphere diffusion coefficients also having observable impacts.

A greater number of failed containers can also have a significant effect; however, the magnitude of the effect depends on where the additional defective containers are located within the repository with respect to the well.

Table 7-45: Summary of Dose Results for System Model

Case	1 Ma Dose Rate (mSv/a)	1 Ma Ratio to Base Case	Peak⁽¹⁾ Dose Rate (mSv/a)	Peak Ratio to Base Case
REFERENCE CASE	0	-	0	-
Sensitivity Cases				
Base Case	5.9x10 ⁻¹⁰	1.0	1.2x10 ⁻⁶	1.0
Base Case – No Well	0.0	0.0	6.6x10 ⁻¹⁰	0.0
Fuel Barrier Sensitivity⁽¹⁾				
Fuel Dissolution Rate Increased by a Factor of 10	3.3x10 ⁻⁹	5.6	1.6x10 ⁻⁶	1.3
Fuel Instant Release Fractions Set to 10%	9.5x10 ⁻¹⁰	1.6	1.3x10 ⁻⁶	1.1
Zircaloy Sheath Barrier Sensitivity				
Zircaloy Dissolution Rate Increased by a Factor of 10	5.9x10 ⁻¹⁰	1.0	1.2x10 ⁻⁶	1.0
Zircaloy Instant Release Fractions Set to 10%	5.9x10 ⁻¹⁰	1.0	1.2x10 ⁻⁶	1.0
Container Barrier Sensitivity				
All 10 Containers Fail at 1000 Years	2.4x10 ⁻⁹	4.1	1.3x10 ⁻⁶	1.1
50 Containers Fail at 1000 Years, all in worst location	1.2x10 ⁻⁸	20	6.5x10 ⁻⁶	5.4
50 Containers Fail at 10,000 Years, uniform distribution	8.7x10 ⁻⁹	14	4.6x10 ⁻⁶	3.8
1000 Containers Fail at 10,000 Years, uniform distribution	1.7x10 ⁻⁷	288	9.2x10 ⁻⁵	77
Low Sorption in the EBS With Coincident High Solubility Limits in the Container	5.9x10 ⁻¹⁰	1.0	1.2x10 ⁻⁶	1.0
No Solubility Limits in the Container	5.9x10 ⁻¹⁰	1.0	1.2x10 ⁻⁶	1.0
Buffer, Backfill and Seal Barrier Sensitivity				
Low Sorption in the EBS With Coincident High Solubility Limits in the Container	5.9x10 ⁻¹⁰	1.0	1.2x10 ⁻⁶	1.0
Ten Times Higher Bentonite and Geosphere Diffusivity Coefficients	2.1x10 ⁻⁷	356	1.7x10 ⁻⁵	14
I-129 Sorption Credited in Bentonite and Geosphere	2.3x10 ⁻¹⁰	0.39	6.7x10 ⁻⁷	0.54
No Sorption in the Near Field	5.9x10 ⁻¹⁰	1.0	1.2x10 ⁻⁶	1.0
Geosphere Barrier				
Two Sigma (Low) Sorption in the Geosphere	5.9x10 ⁻¹⁰	1.0	1.2x10 ⁻⁶	1.0
Ten Times Higher Bentonite and Geosphere Diffusivity Coefficients	2.1x10 ⁻⁷	356	1.7x10 ⁻⁵	14

Case	1 Ma Dose Rate (mSv/a)	1 Ma Ratio to Base Case	Peak ⁽¹⁾ Dose Rate (mSv/a)	Peak Ratio to Base Case
I-129 Sorption Credited in Bentonite and Geosphere	2.3x10 ⁻¹⁰	0.39	6.7x10 ⁻⁷	0.54
Glaciation Sensitivity				
Glaciation Case	Could be up to 100 times greater than temperate climate case when a deep well is established shortly after glacial retreat			
Probabilistic Sensitivity				
Containers Assumptions Fixed (95 th Percentile)	1.3x10 ⁻⁷			
All Assumptions Vary (95 th Percentile)	9.3x10 ⁻⁸			

Note: (1) The peak values are the highest values reached by extending the simulation time beyond one million years.

7.9 Modelling and Results for Disruptive Event Scenarios

Disruptive Event Scenarios postulate the occurrence of unlikely events leading to possible penetration of barriers and abnormal loss of containment. Chapter 6 describes how the Disruptive Event Scenarios are identified and concludes that the following are relevant to the hypothetical site and conceptual repository design:

- Inadvertent Human Intrusion;
- All Containers Fail;
- Repository Seals Failure;
- Undetected Fault;
- Severe Erosion;
- Poorly Sealed Borehole;
- Container Failure³; and
- Partially Sealed Repository.

As noted in Section 7.2, a reduced scope of work has been adopted in this illustrative postclosure safety assessment, and as such, only the first four scenarios are examined in detail. It is recognized that for an actual site, the full set of scenarios would need to be evaluated.

Section 7.2.2 and Table 7-7 contain a description of these four scenarios.

³ This considers delayed but substantive failure of a few containers due to unexpected in-situ conditions, and is different from the Normal Evolution Scenario which considers a small defect unknowingly present in some containers as the initiating event.

Regarding the excluded scenarios:

- For the Poorly Sealed Borehole Scenario, as long as the boreholes are sufficiently far from the repository footprint, they are unlikely to be important due to the small size of the borehole and the limits of transport in low permeability rock. Care would be taken to position the boreholes in locations that have minimal impact. The potential effects of the boreholes would be analyzed as part of a real site investigation, when the borehole distances are known.
- For the Container Failure Scenario, the peak dose arising from this event is anticipated to be similar to the Base Case of the Normal Evolution Scenario and significantly less than that arising from the All Containers Fail Scenario due to the much smaller number of affected containers.
- The Partially Sealed Repository scenario considers the consequences if the repository is abandoned and the shafts are not sealed, thereby implying a near-future loss-of-society. This is an unlikely scenario, and in any case likely better than the alternative where the used fuel is abandoned at surface

Analysis results and dose consequences for the first four Scenarios are discussed below.

7.9.1 Inadvertent Human Intrusion

The Inadvertent Human Intrusion Scenario considers the same evolution of the repository system as for the Normal Evolution Scenario, with the only difference being the occurrence of human intrusion sometime after institutional control of the site is no longer effective. In this scenario, an exploratory borehole is assumed to be drilled through the geosphere and into the repository.

In an exploratory borehole, the investigators would most likely collect samples or conduct measurements at the repository level, which would then lead to identification of any significant residual radioactivity (e.g., gamma logging is a standard borehole measurement). The investigators would then initiate precautions to prevent further exposure, including cleanup and appropriate disposal of any surface-released materials. The borehole would also be properly sealed, so that under normal drilling circumstances, there would be little impact.

Nevertheless, the Inadvertent Human Intrusion Scenario assumes that the presence of radioactivity is not immediately recognized and safety restrictions are therefore not imposed. It further assumes that the drill site is not managed according to current standards, and that material from the borehole is released onto the surface.

The assessment does not include the variant case in which the borehole is poorly sealed thereby providing a long-term pathway for contaminants to escape the repository. Such a case has been considered in SKB (2010a), which shows that the consequences are orders of magnitude less than the SKB acute exposure dose rate for the Inadvertent Human Intrusion Scenario. Although not calculated here, a similar conclusion is expected because there is little driving force to transport contaminated material up the (narrow) borehole, and any such release would be further diluted in the groundwater flowing in the upper geosphere.

7.9.1.1 Description

Figure 7-122 presents an event tree defining the possible outcomes associated with drilling in a repository location.

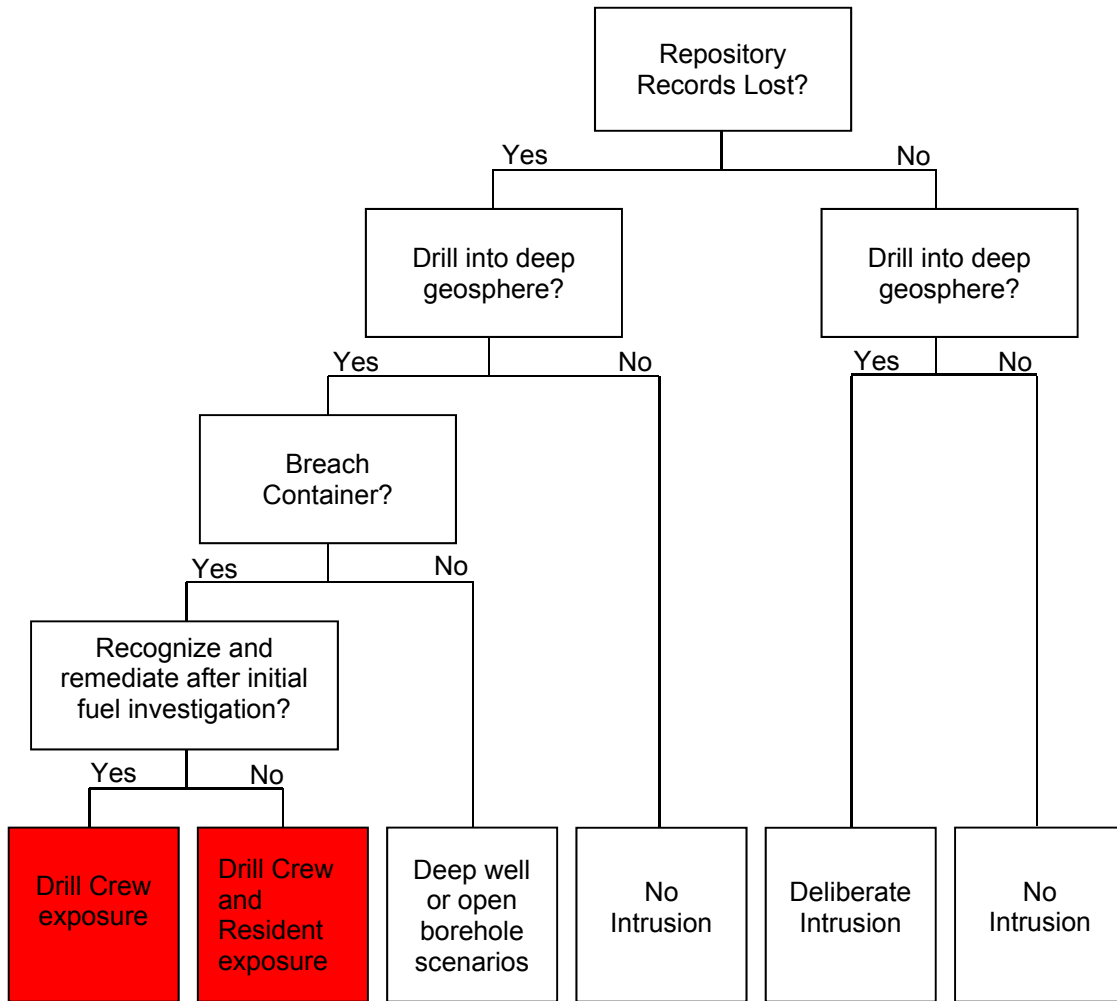


Figure 7-122: General Sequence of Events for Inadvertent Human Intrusion

Of interest to this discussion is the outcome in which:

- The repository records are lost;
- There is drilling into the deep geosphere; and
- The drilling breaches a used fuel container such that used fuel is inadvertently and unknowingly brought to the surface. Note that the early occurrence of such an event is unlikely given today’s technology because drilling through a container wall without detecting it on the surface is not thought possible.

This then leads to the potential exposure of the following two groups:

- The Drill Crew, exposed to a core section containing used fuel and contaminated drill slurry; and
- A Site Resident, exposed to soil contaminated by drill slurry⁴.

To provide context, Table 7-46 presents a summary of the exposure groups considered in recent national and international inadvertent human intrusion safety assessments.

Table 7-46: Human Intrusion Pathways Considered in Recent Safety Assessments

Assessment	Scenario / Exposure Cases Considered
Quintessa et al 2011 (Canada)	Drill crew exposed to extracted core and slurry spread around the drill rig. Resident living and growing crops on contaminated soil from drilling slurry ⁽¹⁾
Posiva Oy2014 (Finland)	Drill crew exposed while drilling into used fuel container ⁽¹⁾ Geologist exposed to used fuel core sample Drill crew exposed while drilling into buffer material Geologist exposed to buffer material sample Drill crew exposed while drilling into backfill material Geologist exposure to backfill material sample Resident exposed through use of deep borehole for drinking water Resident exposed through use of deep borehole for drinking water, irrigation of crops and watering of livestock.
SKB 2014 (Sweden)	Drill crew exposed while working at the drill site ⁽¹⁾ Construction worker exposed to the contaminated soil from drilling waste at the drill site after redevelopment of the land for commercial or residential construction. Residents exposed from growing a garden in soil contaminated by the drilling wastes.
DOE 2008 (USA)	Reasonable Maximally Exposed Individual (Resident) exposed as a result of direct pathway to the groundwater made accessible by the borehole.
Nagra 2002 (Switzerland)	Resident exposed as result of open borehole into buffer or waste creating pathway for radionuclide to reach aquifer
JNC 2000 (Japan)	Excavation workers (exposed externally to core sample and internally by inhalation)

Note: (1) Represents most limiting exposure case.

⁴ Note that current drilling standards would not permit drill slurry to be left at the drill site, but it is conservatively assumed here that such standards are not applied.

Intrusion Likelihood

Regulatory document REGDOC-2.11.1, Volume III (CNSC 2018) recognizes that inadvertent human intrusion events could result in dose rates that exceed the regulatory limit and it states that reasonable efforts should be made to limit the probability of such high consequence scenarios. The following repository characteristics are assumed present at this hypothetical site to minimize the likelihood of this event:

- A deep location;
- Site selection based on an absence of known groundwater resources at repository depth that could be used for drinking, agricultural or industrial purposes;
- Site selection based on an absence of economically exploitable natural resources; and
- The use of records and markers to preserve institutional memory to the extent practicable.

Furthermore, compartmentalizing the used fuel into containers is a design measure that mitigates the impact of intrusion. Another mitigating factor is the strength of the containers, which means inadvertent penetration is unlikely.

7.9.1.2 Model and Assumptions

Exposure Scenarios

The Human Intrusion model determines the dose consequences to both exposure groups from the pathways illustrated in Figure 7-123. It models the acute dose to the Drill Crew at the time the material is brought to the surface and the annual chronic dose to a Site Resident who are assumed to live nearby and grow crops on the site after the intrusion has occurred.

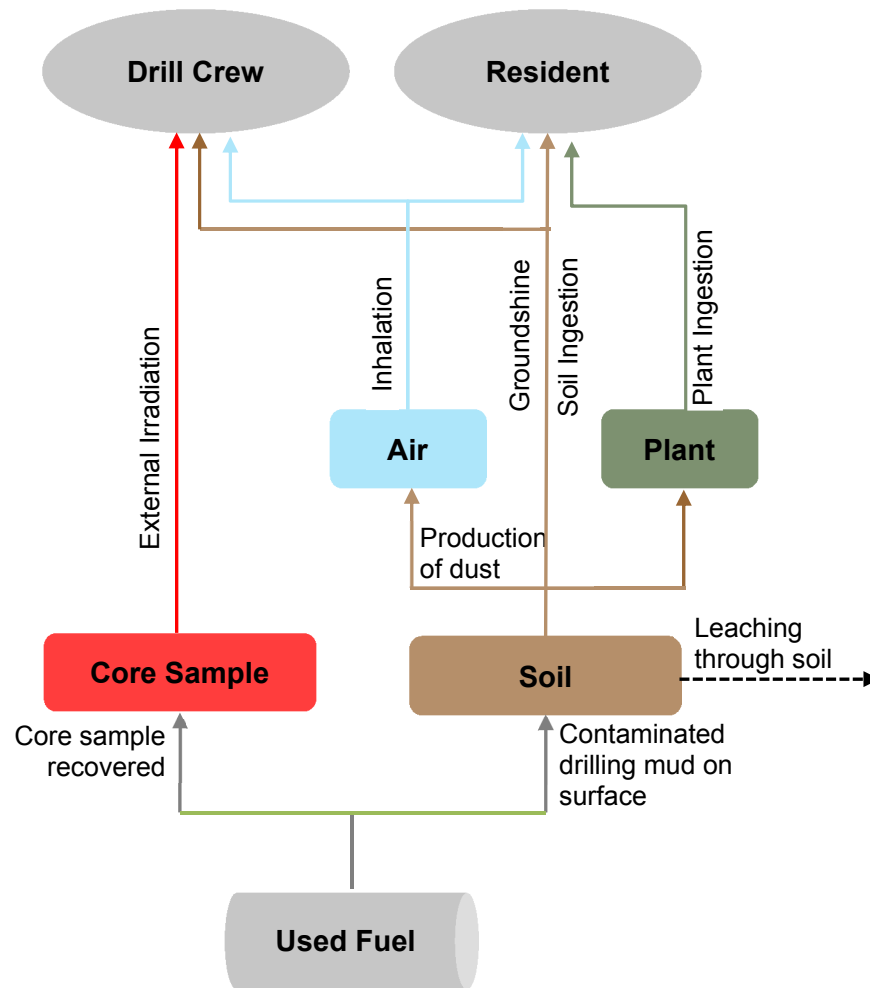


Figure 7-123: Inadvertent Human Intrusion - General Conceptual Model

Three different exposure scenarios are considered. The exposure scenarios are stylized; they include approximate representations of inhalation, ingestion and direct exposure pathways such that the overall dose estimates are indicative of potential doses.

In each scenario, used fuel is brought to the surface in the form of drill core and drill mud / slurry. Normal practice is for core to be logged and put into storage, and for drill slurry to be contained at the site and ultimately disposed according to regulatory requirements. However, in this assessment, the drill slurry is conservatively assumed to be dumped around the drill rig without containment. The contaminated slurry would become mixed with surface material, as well as with subsequent drilled material. The waste is assumed to be uniformly mixed through a small near-surface volume of soil around the rig. The Drill Crew member handles the core sample for an hour, leading to a direct external exposure. The Drill Crew member is also exposed to the waste through groundshine, inhalation of contaminated dust and ingestion of contaminated soil from the mixed volume of near-surface material. The Drill Crew member is assumed to not wear a mask.

The exposure scenarios are:

Scenario 1 (Hazard Identified / Site Remediated): Drilling operations take place for two days after the intrusion event (two 12-hour shifts), at which point the Drill Crew becomes aware of the hazard, immediately ceases operations and vacates the site.

The site is then completely remediated by qualified experts, and thus the Site Resident is unaffected by the incident. The dose to the remediation experts is not considered because they are assumed to take appropriate precautions.

Scenario 2 (No Detection / Substandard Drill Site / No Remediation): In Scenario 2, drilling operations continue for 14 workings days, at which point the Drill Crew vacates the site without identifying the hazard. Debris deposited on the surface around the drilling site remains in place without remediation, subject only to radioactive decay and leaching.

The Site Resident lives at the contaminated site immediately after the drill crew leave the site, and grows food on the contaminated soil. The Site Resident is exposed to contaminants through groundshine, dust inhalation and through ingestion of contaminated plants and soil. It is assumed that the contaminated land is limited in extent (and therefore has a higher concentration of contaminants), and so an allowance is made for the fraction of time that the Resident is exposed to the contaminated site on an annual basis.

Leaching considers the portion of precipitation that draws contaminants downward into the deeper soil where they become inaccessible. As a conservative estimate, the Site Resident exposure is assumed to begin in the first year after intrusion, before leaching has any significant effect on the soil contaminant levels. Leaching is therefore ignored in this case. However, the Site Resident's annual dose is also examined for an assumed arrival time of 100 years after the original intrusion, in which case the effect of leaching is included.

Scenario 3 (Higher Burnup Fuel): Scenario 3 is the same as Scenario 1, except that a higher fuel burnup is assumed (i.e., 280 MWh/kgU instead of 220 MWh/kgU). Table 3-1 in Chapter 3 shows that the 220 MWh/kgU value corresponds to roughly the 63rd to 93rd percentile value over all used CANDU fuel bundles (depending on the nuclear station), while the 280 MWh/kgU value similarly corresponds to the 95th to the 99.9th percentile value (again depending on the nuclear station).

Key Assumptions and Parameters

Key assumptions are:

- Institutional control is maintained for a minimum of 300 years after closure, at which point intrusion becomes possible;
- Decay and ingrowth calculations start at the time of placement, at which point the used fuel is 30 years old;
- There is a minimum period of 70 years of extended monitoring and 25 years of decommissioning and closure following placement, which means the fuel is 425 years old (i.e., 30 + 70 + 25 + 300) at the earliest time of intrusion. This is conservative in that the fuel will likely be older at a real site;
- The drill intercepts a container in the repository and brings used fuel debris to the surface, either mixed with the drill slurry or as a section of intact drill core; and

- The biosphere is unchanging; that is, radioactive material is not carried away by wind, by water erosion or other external forces and airborne material is not assumed to deposit on top of the contaminated soil.

Table 7-47 lists important parameters used in the assessment. Source references for these values can be found in Medri (2015a).

Table 7-47: Parameters for Human Intrusion Scenario

Parameter	Value
Parameters related to used fuel quantities	
Fraction of used fuel per container that is damaged by borehole	0.17
Mass of used fuel in a container (kg)	1150
Fraction of U intercepted brought to surface as core	0.4
Fraction of U intercepted brought to surface as slurry	0.3
Instant release fractions (selected radionuclides)	Table 7-13
Radionuclide Inventory (mol/kgU or mol/kgZr)	See Medri (2015a)
Parameters related to soil and air	
Soil type	Clay
Soil density (kg/m ³)	1400
Soil water content (m ³ /m ³)	0.3
Net infiltration rate of water through soil (m/a)	0.325
Depth of contaminated soil (m)	0.2
Contaminated soil fraction	0.1
Slurry area (m ²)	Drill Crew: 30 Resident: 80
Thickness of contaminated soil (m)	0.2
Dust loading in air (kg _{soil} /m ³)	Drill Crew: 1.0×10 ⁻⁷ Resident: 3.2×10 ⁻⁸
Soil distribution coefficients for clay (m ³ /kg)	See Medri (2015a)
Plant/Soil Concentration Ratios (kg _{drysoil} /kg _{wetsoil})	See Medri (2015a)
Parameters related to human behavior	
Air inhalation rate (m ³ /a)	8400
Plant ingestion (kg/a)	291
Resident annual soil ingestion (kg)	0.12
Drill Crew soil ingestion amount per intrusion event (g)	Scenario 1: 0.66 Scenario 2: 4.62 Scenario 3: 0.66
Contaminated food fraction	0.1
Exposure time of Drill Crew to core sample (hr)	1

Postclosure Safety Assessment of a Used Fuel Repository in Sedimentary Rock			
Document Number: NWMO-TR-2018-08	Revision: 000	Class: Public	Page: 533

Parameter	Value
Exposure time of Drill Crew to contaminated site (hr)	Scenario 1: 24 Scenario 2: 168 Scenario 3: 24
Exposure time for Resident each year (a)	0.1
Ingestion, Inhalation, groundshine and external dose coefficients (Sv/Bq or (Sv/a)/(Bq/kg))	See Medri (2015a)

Computer Code

The radiological consequences are determined using simple equations implemented in HIMv2.1 (Medri 2015a), a human intrusion computer model developed using the AMBER v5.7.1 platform.

Prior to the detailed assessment, screening calculations are done to identify the potentially radiologically significant radionuclides. In this screening, hypothetical doses are calculated for ingestion and inhalation of the radionuclides in an entire fuel bundle, and for a one-year groundshine exposure to the contents of a fuel bundle mixed into 1 kg of soil. For each type of exposure, all radionuclides whose dose contributions are within six orders of magnitude of the maximum dose contributor are screened in. The calculations are done for 30, 500, and 1,000,000 year old fuels with discharge burnups of 220 MWh/kgU. As a result, 79 radionuclides emerged from the screening and are tracked in the HIMv2.1 model. Short-lived radionuclides are included through the dose coefficients of their parents. Doses are obtained using inhalation, ingestion, groundshine and external dose coefficients.

A detailed description of the parameters and equations used in HIMv2.1 is available in Medri (2015a).

7.9.1.3 Dose Results

Scenario 1 (Hazard Identified / Site Remediated)

Scenario 1 is described in Section 7.9.1.2. Figure 7-124 shows the calculated acute dose to a Drill Crew member as a function of intrusion time after repository closure, showing a breakdown of contributing pathways. The maximum one-time dose to the Drill Crew, occurring at the earliest time of intrusion, is 90 mSv.

The Site Resident is unaffected by this scenario because the site is assumed to be completely remediated.

The total dose is dominated by Am-241 for the first 300 to 1000 years, by Pu-239 and Pu-240 from 10^3 to 10^5 years, and by the U-238 decay chain for longer times.

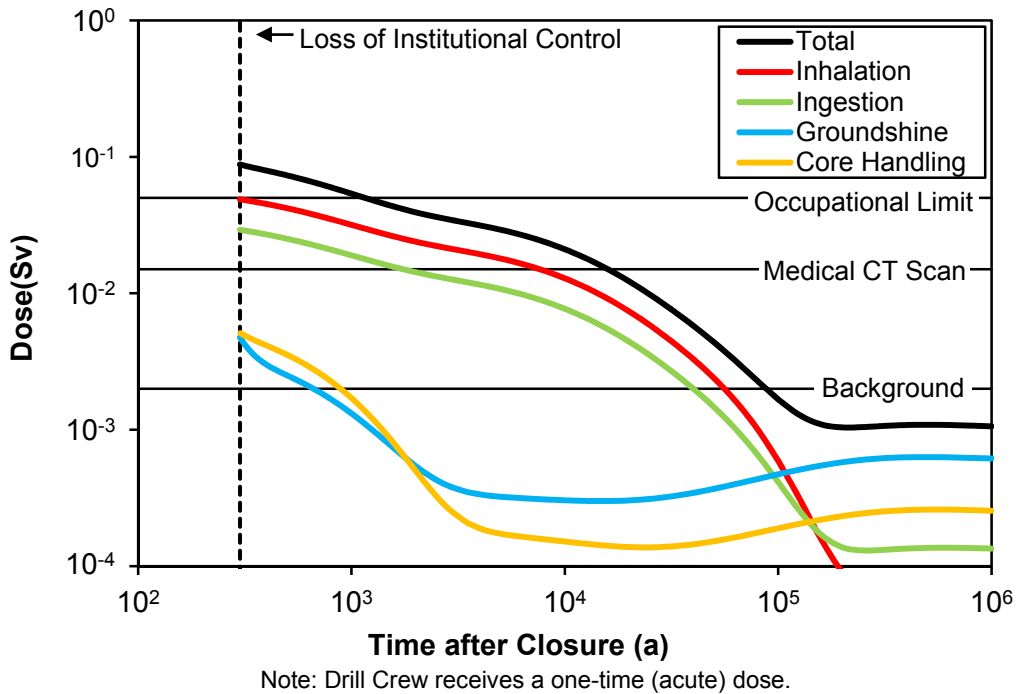
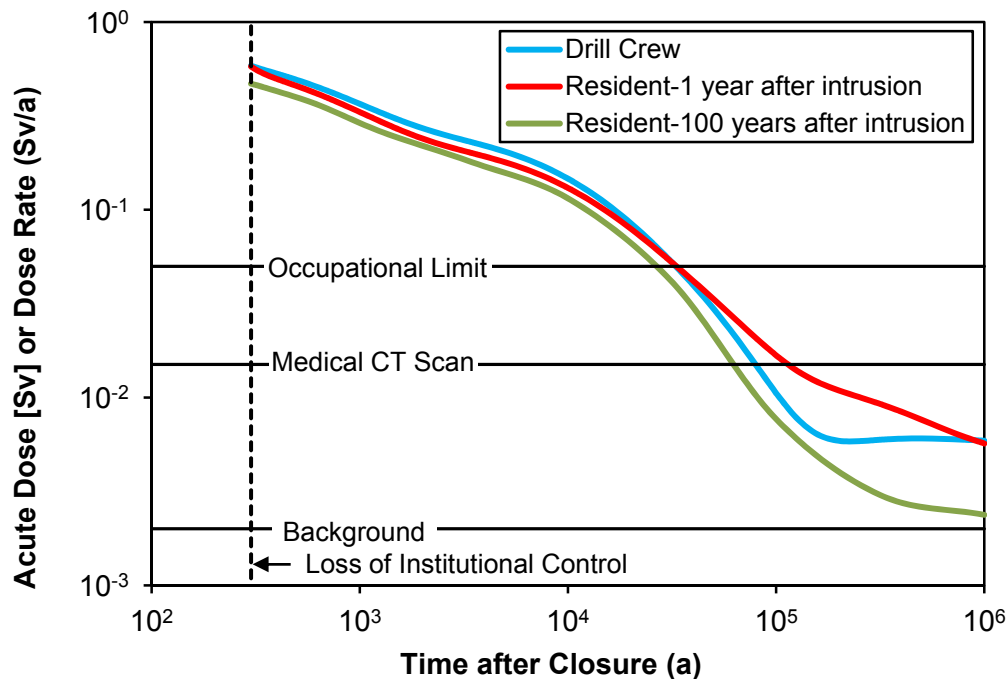


Figure 7-124: Inadvertent Human Intrusion: Exposure Pathways to the Drill Crew - Hazard Identified and Site Remediated

Scenario 2 (No Detection / Substandard Drill Site / No Remediation)

Scenario 2 is also described in Section 7.9.1.2. Figure 7-125 shows the calculated acute dose to the Drill Crew member and chronic dose rate to the Site Resident as a function of the assumed time of intrusion after repository closure. The Site Resident’s annual dose is also examined for an assumed arrival time of 100 years after intrusion, in which case the effect of leaching is included.



Note: The Drill Crew receives a one-time (acute) dose, while the Resident receives a (chronic) dose rate.

Figure 7-125: Inadvertent Human Intrusion: Summary of Exposures - Hazard Not Identified and No Remediation

The principal results are:

- The maximum one-time dose to the Drill Crew member is 590 mSv.
- The maximum annual chronic dose to the Site Resident is 580 mSv.
- After 100 years of leaching, the maximum annual dose to the Site Resident is 470 mSv.
- Doses decrease as a function of the assumed time of intrusion due to radioactive decay. Intrusion doses after about 100,000 years are in the range of 10-20 mSv.

The total dose for both groups tends to be dominated by Am-241 for the first 300 to 1000 years, by Pu-240 and Pu-239 from 1000 to 100,000 years, and by the U-238 and Pu-241 decay chains for longer times. After about 100,000 years, the consequences are similar to those that might result from similar inadvertent drilling into an equivalent amount of natural uranium.

The Site Resident's exposure could potentially occur much later after the used fuel is inadvertently brought to the surface, assuming that the site is not remediated in the meantime. In this case, the exposure would be lower due to radioactive decay and to leaching of contaminants from the near-surface. Figure 7-126 shows the dose rate to a Site Resident living near and growing crops on the contaminated site as a function of time following an intrusion that occurs 300 years after repository closure. Leaching is not a significant factor in reducing potential doses until after about 1000 years.

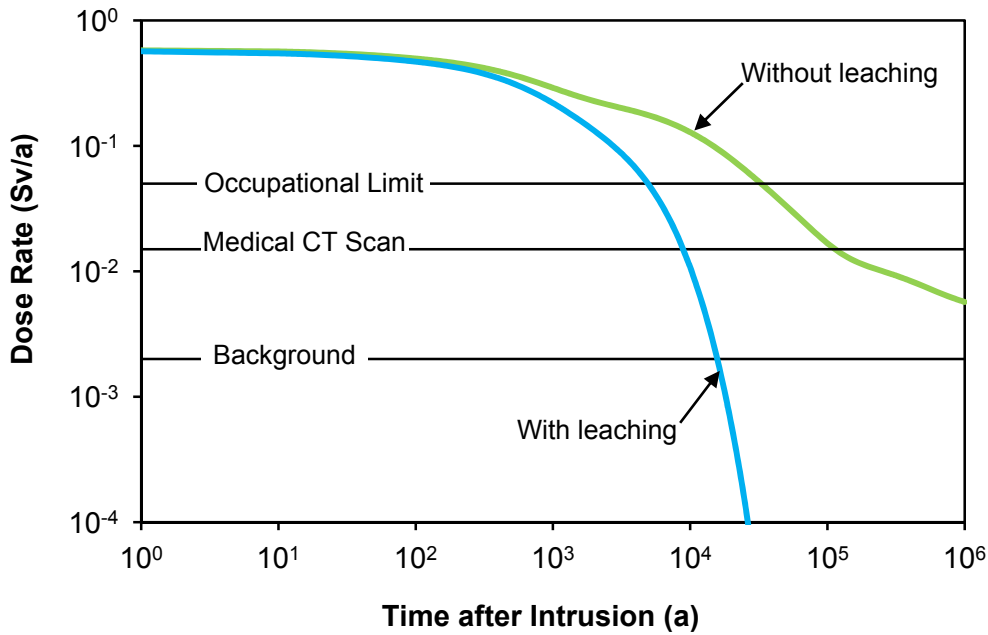
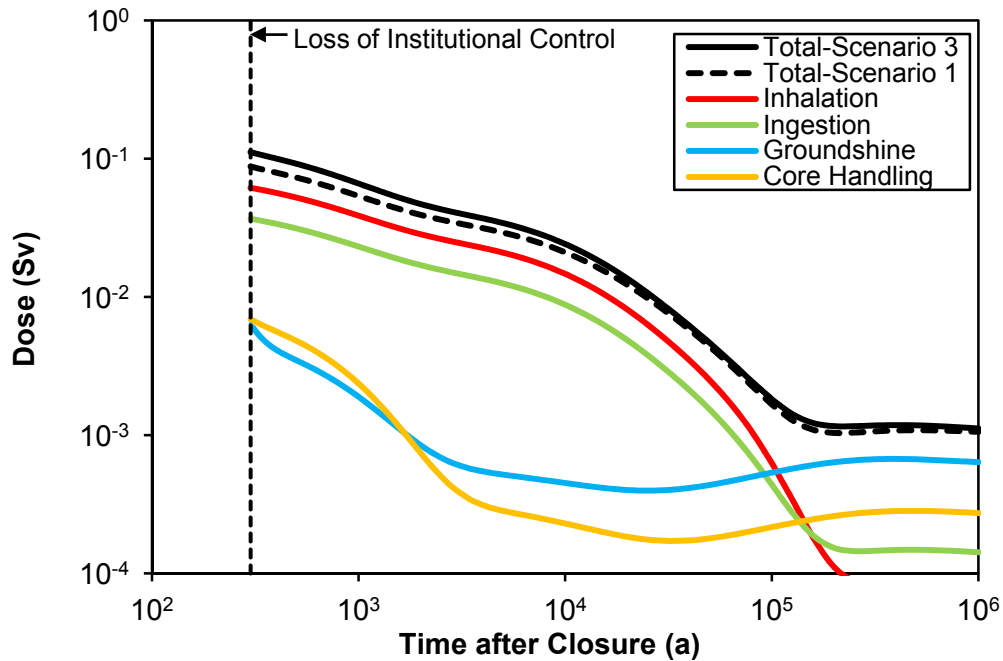


Figure 7-126: Inadvertent Human Intrusion: Effect of Leaching on Exposure to the Resident - Hazard Not Identified and No Remediation

Scenario 3 (Higher Burnup Fuel)

Scenario 3 is identical to Scenario 1, except that it considers the unlikely case of a container loaded entirely with 280 MWh/kgU burnup fuel. As shown in Figure 7-127, increasing the burnup increases the maximum one-time acute dose to the Drill Crew member from 90 mSv to 110 mSv. This is because the amount of actinides increases with burnup.

The increase in dose is due mainly to the higher initial inventory of Am-241, Pu-241 (which decays to Am-241) and Pu-240. The total dose rate to the Drill Crew member in Scenario 1 is included in Figure 7-127 for comparison.



Note: Drill Crew receives a one-time (acute) dose.

Figure 7-127: Inadvertent Human Intrusion: Pathways for Drill Crew Exposure - Hazard Identified and Site Remediated, Higher Burnup Fuel

Annual Risk

To provide context for the dose rates, the annual risk to the most exposed individual can be estimated.

The annual risk to the Drill Crew (R_{DC}) is determined via:

$$R_{DC} = Y \cdot H \cdot P \quad (7-2)$$

where: Y is the probability coefficient for stochastic effects per Sv or 0.057 according to ICRP (2007);
 H is the highest dose in the time period of concern; and
 P is the intrusion frequency.

While the intrusion frequency could in principle be estimated by assigning numerical values to each of the events in Figure 7-122, in practice these values are, to a large extent, non-quantifiable. Consequently, a more simplistic approach is adopted to illustrate the frequency with which an intrusion event may occur. This approach considers only the frequency of drilling.

Specifically, given that the area around the repository has no significant mineral resources, a deep drilling frequency to resurvey or update the geological information of about once every 100 years is assumed. Assuming each borehole characterizes an area of 10 km × 10 km, this

results in a drilling frequency of $10^{-10}/\text{m}^2\text{a}$. Since the repository consists of 318 rooms, with each room having a projected area of about 1087 m^2 , the frequency of inadvertent human intrusion into a room can be estimated as $3.5 \times 10^{-5}/\text{a}$. If only the container area is used, the intrusion frequency is estimated as $1.5 \times 10^{-5}/\text{a}$.

With $\Upsilon = 0.057/\text{Sv}$, $H = 0.59 \text{ Sv}$ and $P = 3.5 \times 10^{-5}/\text{a}$, the annual risk to the Drill Crew from an inadvertent human intrusion event is $1.2 \times 10^{-6}/\text{a}$. This is below the risk target of $10^{-5}/\text{a}$ for Disruptive Event Scenarios identified in Section 7.1.1.

The intrusion probability does not take into account the beneficial effect of institutional memory. Institutional memory could decrease with time, but at earlier times when high doses are more likely, ongoing institutional memory could significantly reduce the intrusion probability (and the risk) of such an event.

The repository might also be detected through surface geophysical measurements, but not recognized as a used fuel facility. In this case exploration drilling would specifically aim for the repository and the intrusion probability could be higher than the above random drilling frequency. But since the drilling program would be specifically designed to explore the anomaly, it is also more likely that the repository would be recognized before or shortly after the repository level was reached and the consequences would therefore be less than those estimated above.

At long times, the cumulative probability of intrusion increases, but the consequences also decrease until eventually they are similar to those for inadvertent intrusion into a uranium ore body.

7.9.2 All Containers Fail

The long-lived used fuel containers are an important feature of the multi-barrier concept. As discussed in Chapter 5, the containers are anticipated to remain intact for well in excess of one million years, based on consideration of the copper corrosion barrier, their sturdy mechanical design, and favourable site attributes. Nevertheless, the All Containers Fail Scenario considers the hypothetical case in which all the containers fail simultaneously and relatively early.

The scenario assumes failure at 60,000 years. This is correlated with the earliest possible timeframe for an ice sheet to cover the site, and it assumes that some unanticipated effect of the ice sheet causes failure. The sensitivity to earlier failure times is examined in a sensitivity case in which all containers are assumed to fail at 10,000 years.

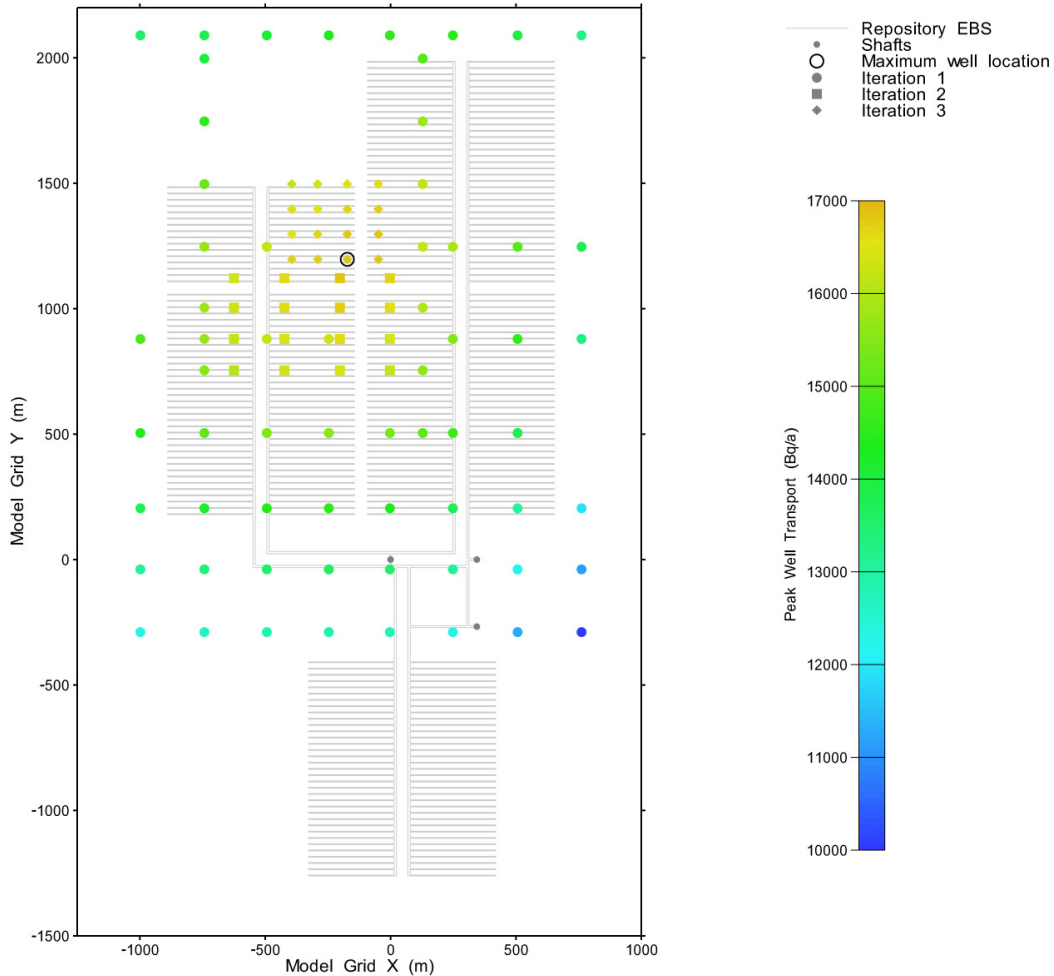
This scenario with failure at 60,000 years is simulated with both the 3D Main Transport Model and the System Model.

7.9.2.1 3D Model Methods and Results

The Main Transport Model (Section 7.7.1.2) is used to simulate the All Container Fail at 60,000 Years Disruptive Event Scenario for I-129, Cl-36, Cs-135, and U-238. The per-container specified release source term is scaled by the total number of containers (108,833) and then applied evenly to all 31336 placement room nodes.

The location of the water supply well is conservatively located to maximize capture using a similar approach to that used for the Base Case (described in Section 7.7.2.3.2). A total of three iterations were performed, evaluating 106 potential well locations.

Figure 7-128 shows the location and maximum transport for each tested well. The final selected location is approximately 1150 m distant from the Base Case well location.



03 Jan 2018
ACFWellLocation.mxd

Figure 7-128: 3D Model: All Containers Fail at 60,000 Years - Evaluated and Final Well Locations

Figure 7-129 show I-129 transport results. The I-129 transport rate to the well from All Containers Failing is about 0.2 Bq/a at one million years. However due to the low-permeability of the rock, the release rate is still increasing. Extending the simulation results in a peak rate of 22,700 Bq/a at 33 Ma.

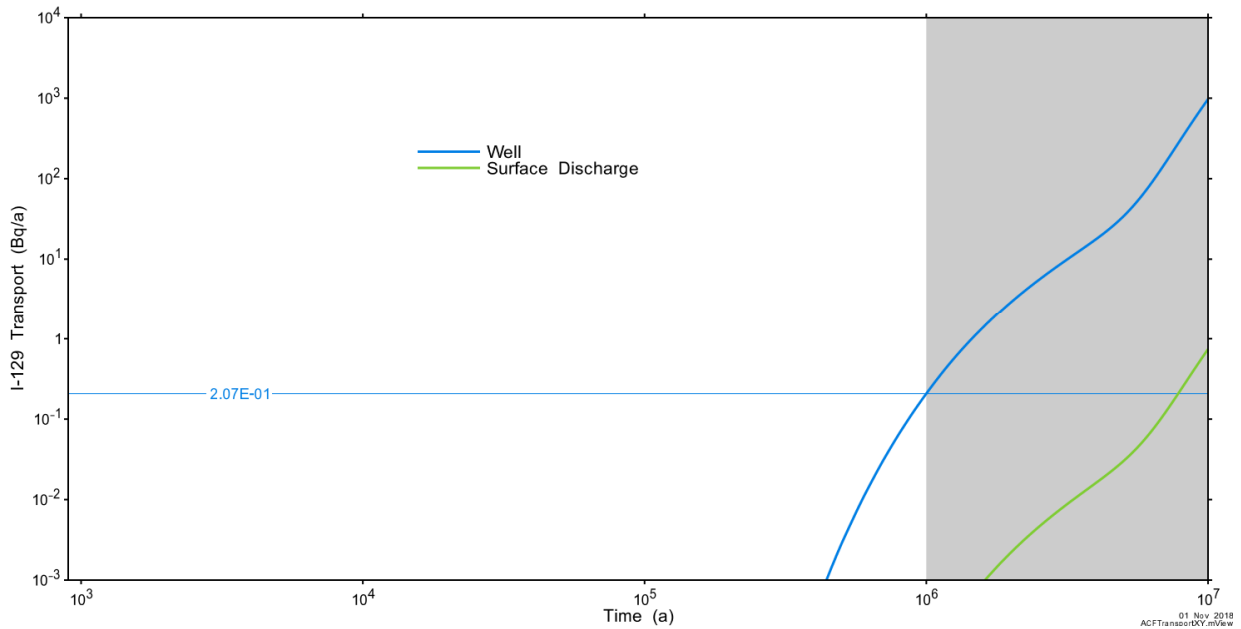


Figure 7-129: 3D Model: All Containers Fail at 60,000 Years - I-129 Transport

7.9.2.2 System Model Methods and Results

The dose assessment is performed using the System Model described in Section 7.8.1. All model parameters are identical to those in the Base Case except:

- All 108,833 containers fail simultaneously; and
- The potential presence of a few containers with small initial defects is not included. This modelling simplification does not affect the peak dose rate.

The behaviour of hydrogen gas generated through corrosion of the internal steel container is discussed in Chapter 8.

All Containers Fail at 60,000 Years

Figure 7-130 shows the dose rate for the case in which all containers fail at 60,000 years. Also included for comparison is the dose rate for the Base Case of the Normal Evolution Scenario.

The dose rate is 8.4×10^{-6} mSv/a at one million years. Extending the simulation results in a peak value of 0.01 mSv/a. While the peak dose rate is much higher than that of the Base Case (due to the greater number of failed containers), it remains a factor of about 100 times below the interim dose rate acceptance criterion of 1 mSv/a.

The dominant radionuclide is I-129, as in the Base Case.

Section 7.8.1.4 shows that the System Model produces conservative results compared to the 3D Model. Peak I-129 transport to the well in the 3D Model is 22,700 Bq/a while peak transport in the System Model is 39,400 Bq/a, a factor of 1.7 times higher. This conservatism could be removed by reducing the System Model dose rate by an equivalent amount; however, given the wide margin available to the interim dose rate criterion, this correction has not been made.

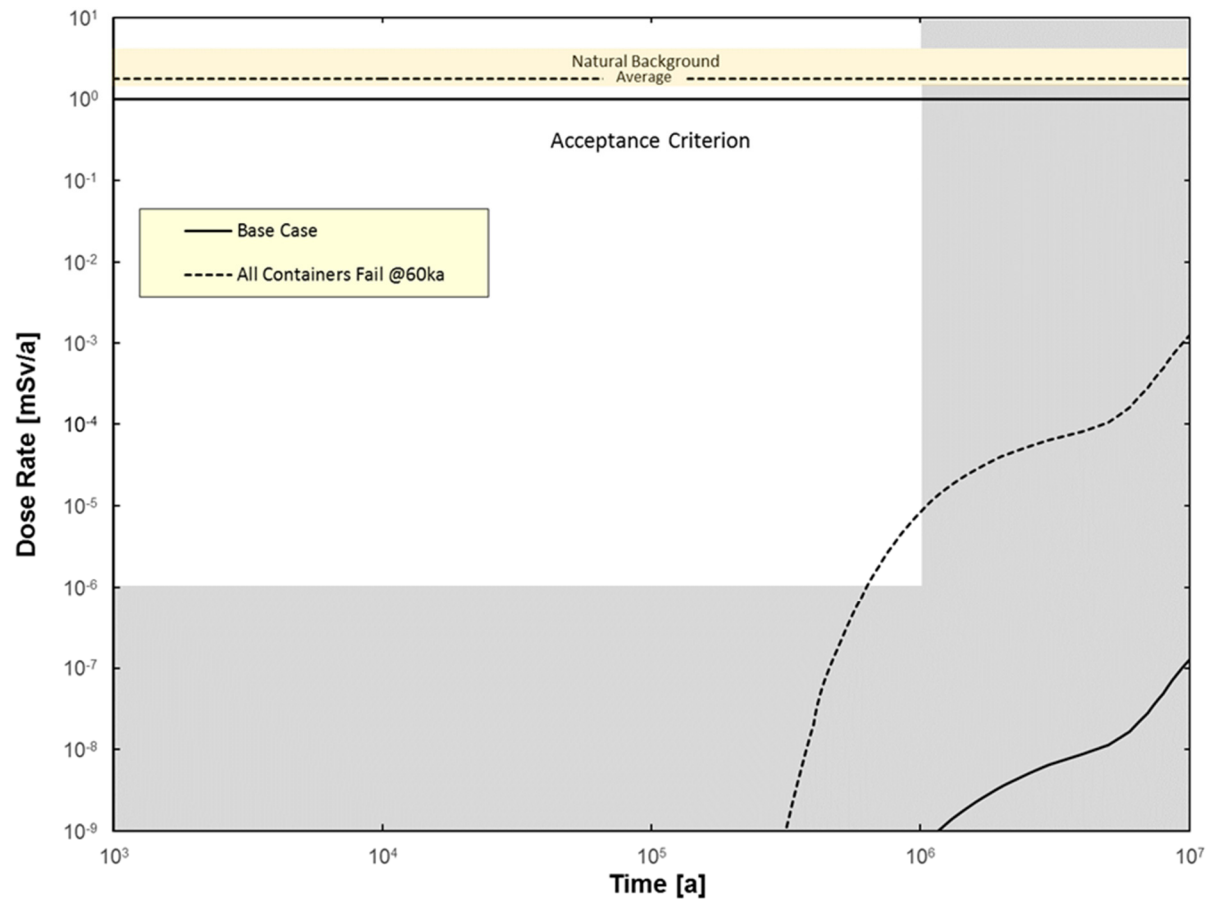


Figure 7-130: System Model: All Containers Fail at 60,000 Years: Dose Rate

All Containers Fail at 10,000 Years

Figure 7-131 compares the dose rate for the sensitivity case in which all containers fail at 10,000 years with that of the case with all containers failing at 60,000 years. The Base Case results are also shown for comparison purposes.

The results are not substantially different from the All Containers Fail at 60,000 years case, with a dose rate of 1.4×10^{-5} mSv/a at one million years. Extending the simulation results in a peak dose rate of 0.01 mSv/a. The peak result is essentially the same as the All Containers Fail at 60,000 years case because the peak occurs so long after the assumed time of container failure that the relatively small difference in assumed failure time is of no consequence.

As noted above, the System Model results are 1.7 times higher than the 3D Model results for the All Containers Fail at 60,000 Years case. No correction for this conservatism has been included here.

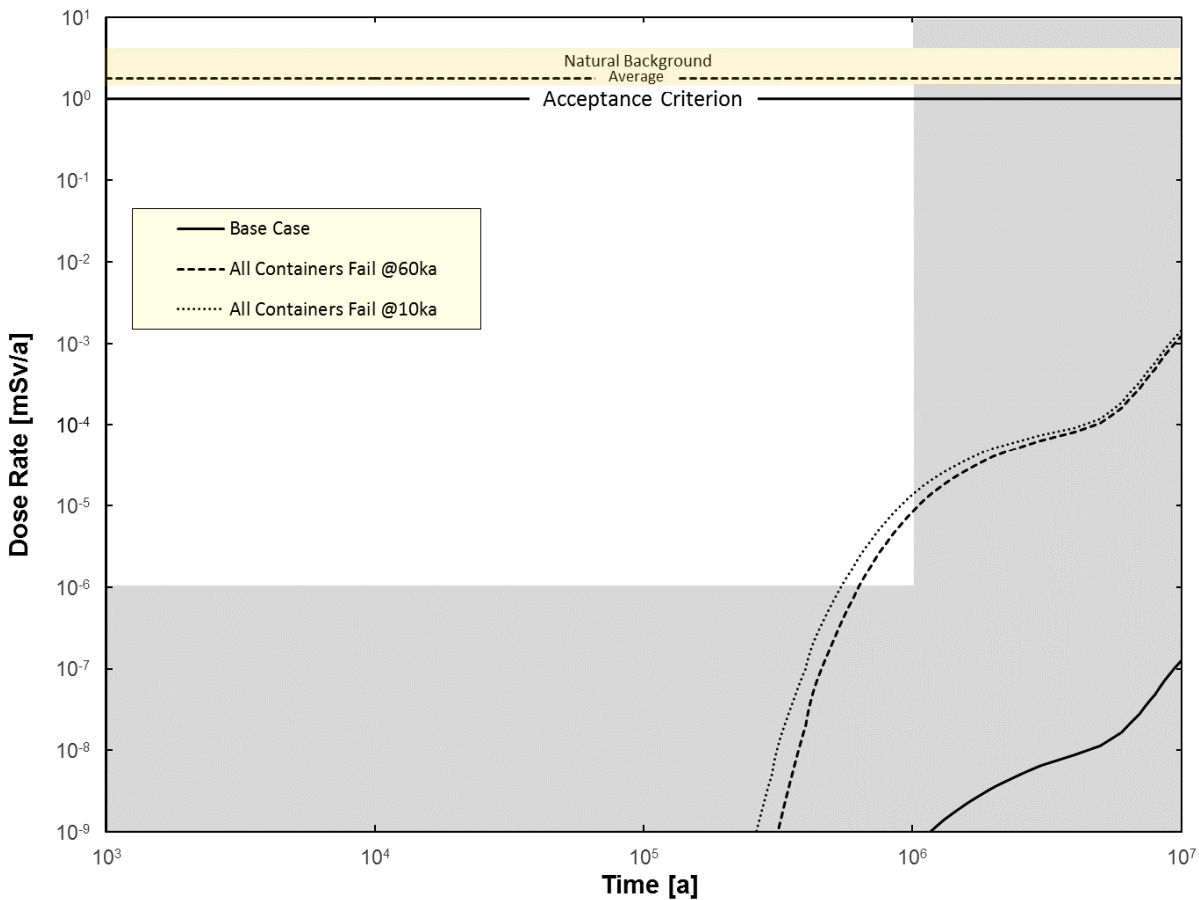


Figure 7-131: All Containers Fail at 10,000 Years: Sensitivity Case Dose Rate

7.9.3 Repository Seal Failure

The Normal Evolution Scenario considers the likely behaviour of the shaft and repository seals and their associated excavation damaged zones. The Repository Seal Failure Scenario considers the same evolution of the repository system and the same exposure pathways as in the Base Case of the Normal Evolution Scenario, except that rapid and extensive degradation of the repository seals is assumed. For conservatism, it is assumed that this degradation occurs at the time of repository closure.

Simulations are performed using the Main Transport Model with the Combined Source term described in Section 7.7.1.2. This model allows for changes in the groundwater flow field in the repository and vicinity due to the assumed seal degradation.

The Repository Seal Failure Scenario assumes that shaft seal components (i.e., bentonite / sand, asphalt, and concrete) in all shafts have a hydraulic conductivity of 1×10^{-7} m/s and a diffusivity of 3×10^{-10} m²/s. The shaft inner and outer EDZ hydraulic conductivities are also increased by a factor of 100 and 10 respectively. No other changes are made to the material properties in the model.

Due to the increase in shaft permeability, the location of the well / defective container combination has been revised to obtain the highest dose consequence. In this case, well locations in each of the Main, Service and Vent shafts are considered and potential source locations were selected in placement rooms according to three criteria:

1. Closest – the shortest distance from a placement room location to the shaft, located at the nearest room to the shaft, at a location where transport to the the shaft would be perpendicular to the room orientation.
2. Shortest tunnel distance – recognizing the preferential transport through the tunnels (i.e., due to higher hydraulic conductivity as compared to that of the surrounding host rock), these sources are located in the end of placement rooms closest to the tunnel with the shortest “along tunnel” distance to the shaft.
3. Mean Lifetime (MLE) location – the placement room location with the smallest MLE.

This resulted in four potential source locations for the Main Shaft, three potential source locations for the Vent shaft, and one potential source location for the Service shaft (i.e., for the Service Shaft, all criteria are met for the same location).

Figure 7-132 shows the results for I-129 transport to the well for all shaft / source combinations considered compared to the Base Case response. The maximum transport source for each well is labelled, while the multipliers on the Base Case (i.e., the one million year value) are listed for all cases. The maximum transport at one million years is 0.37 Bq/a to the Service shaft well from the single Service shaft source location. Extending the simulation establishes a peak transport value of 4.6 Bq/a at 15.2 Ma.

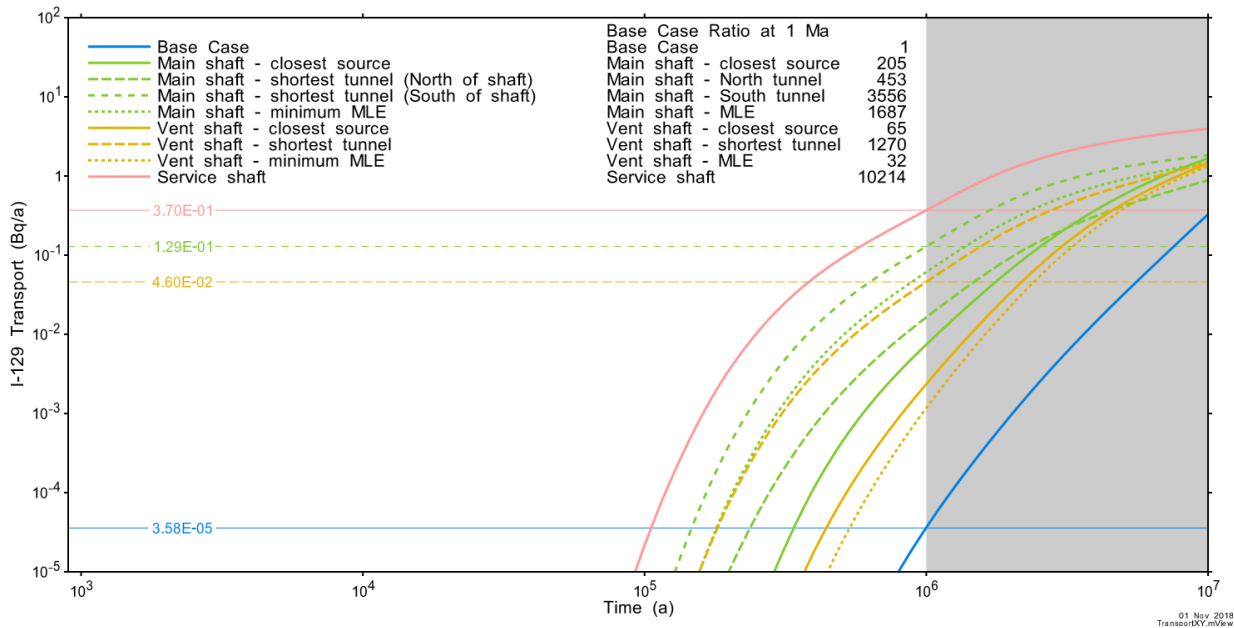


Figure 7-132: Main Transport Model: Repository Seal Failure - I-129 Transport to the Well for Each Well/Source Location

7.9.4 Undetected Fault

The Normal Evolution Scenario considers the likely behaviour of the repository in a geosphere with no major faults or fracture systems. This is consistent with available geoscience information describing the Ordovician formations near the hypothetical repository location. However, it is possible, although unlikely, that undetected vertical faults could be present near the repository. This scenario assumes that such a fault is present, and that it is located close enough to the repository to affect the flow system and / or intercept diffusive transport from the well.

7.9.4.1 Model and Assumptions

There are two geosphere sensitivity cases defined, differing only by fault and well location, with the fault assumed located approximately 100 m from the repository in the first case and at 500 m for the second case. In both cases the fault is defined as a 1 m thick enhanced permeability zone with a hydraulic conductivity of 10^{-8} m/s. Vertically, the fault extends from the bottom of the model, through the Ordovician formations, and terminates at the bottom of the Guelph unit. Laterally, the fault extends across the model domain starting and ending approximately 750 m from the model boundaries. The vertical fault thus provides a pathway of higher hydraulic conductivity for transport of radionuclides from the repository horizon. The well is positioned at locations where the fault intersects the Guelph formation, so as to have maximum impact on flow within the fault.

Figure 7-133 shows the vertical fault positions and extents.

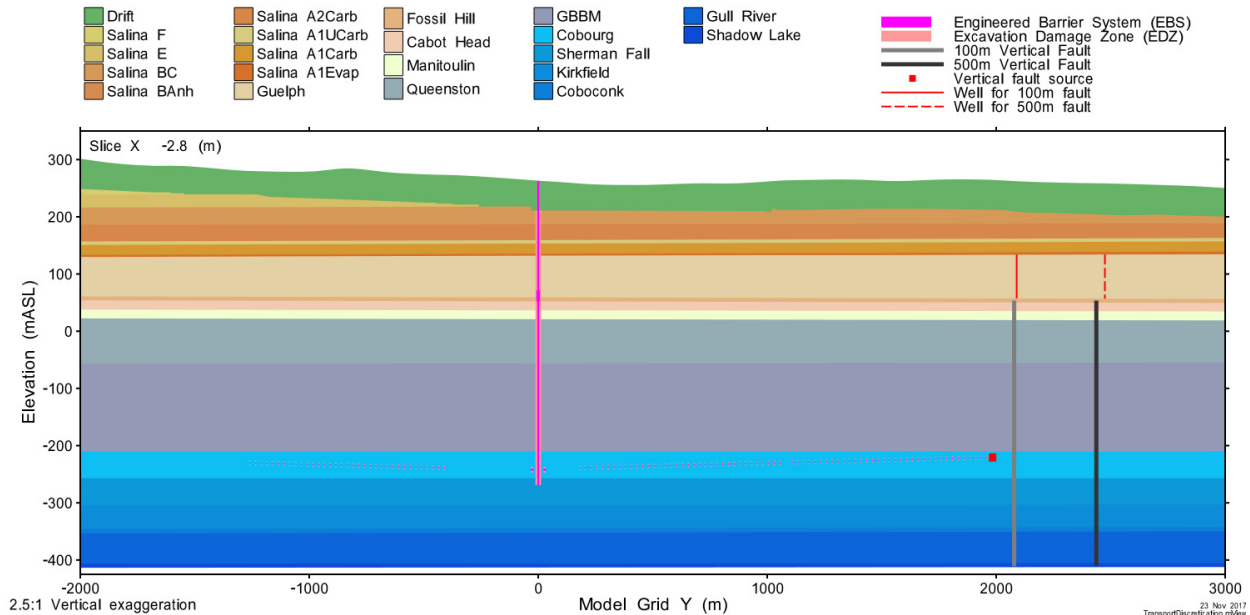


Figure 7-133: Main Transport Model: Assumed Vertical Fault Locations

Simulations are performed using the Main Transport Model with the Combined Source term described in Section 7.7.1.2. This model calculates changes to the groundwater flow field in the repository and vicinity due to the fault. To maximize transport, the defective container source term is located in the placement room closest to the assumed fault locations.

The faults are implemented using both equivalent porous media (EPM) and discrete fracture network (DFN) approaches. In the EPM approach, the 3D elements containing the fault are assigned conductivities and porosities reflective of blended material properties. For DFN, a 2D planar fault element is defined on the the 3D element face at the specified distance.

7.9.4.2 Transport Results

Figure 7-134 shows the results for I-129 transport to the well for the 100 m and 500 m fault offsets and for EPM and DFN modelling approaches. Both cases show significant increases when compared to the Base Case. Not surprisingly, the 100 m offset fault has significantly greater well transport than the 500 m offset, reflecting the additional 400 m of transport through the low permeability Ordovician formations. Well capture at the 100 m fault is the highest of any defective container case. EPM and DFN approaches compare well in terms of timing.

For the 100 m offset case, the one million year transport is 0.55 Bq/a for the DFN approach and 10 Bq/a for the EPM approach. Peak transport is 79 Bq/a for the DFN approach and 73 Bq/a for the EPM approach, occurring after about 8.2 million years.

For the 500 m offset case, the one million year transport results are below the threshold value of 1×10^{-5} Bq/a. These simulations have not been extended to establish the peak value.

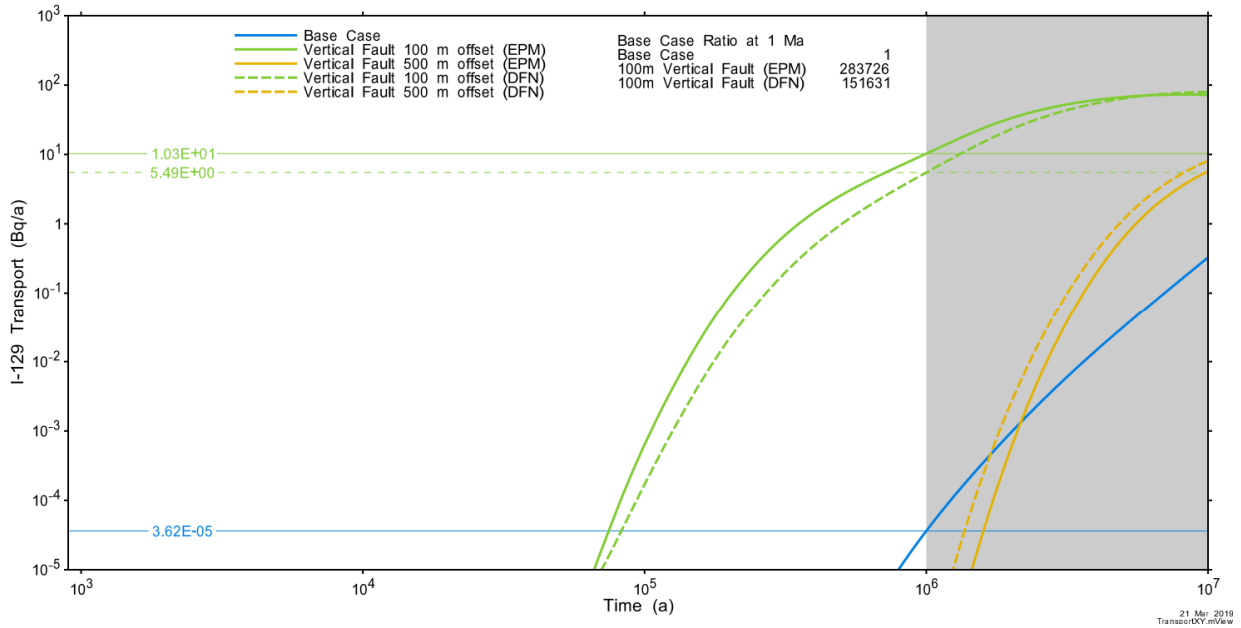


Figure 7-134: Main Transport Model: Vertical Fault Cases - I-129 Transport to the Well

Surface transport is shown in Figure 7-135. The transport rate is very low, indicating that the well is very effective at capturing contaminants that enter the Guelph formation.

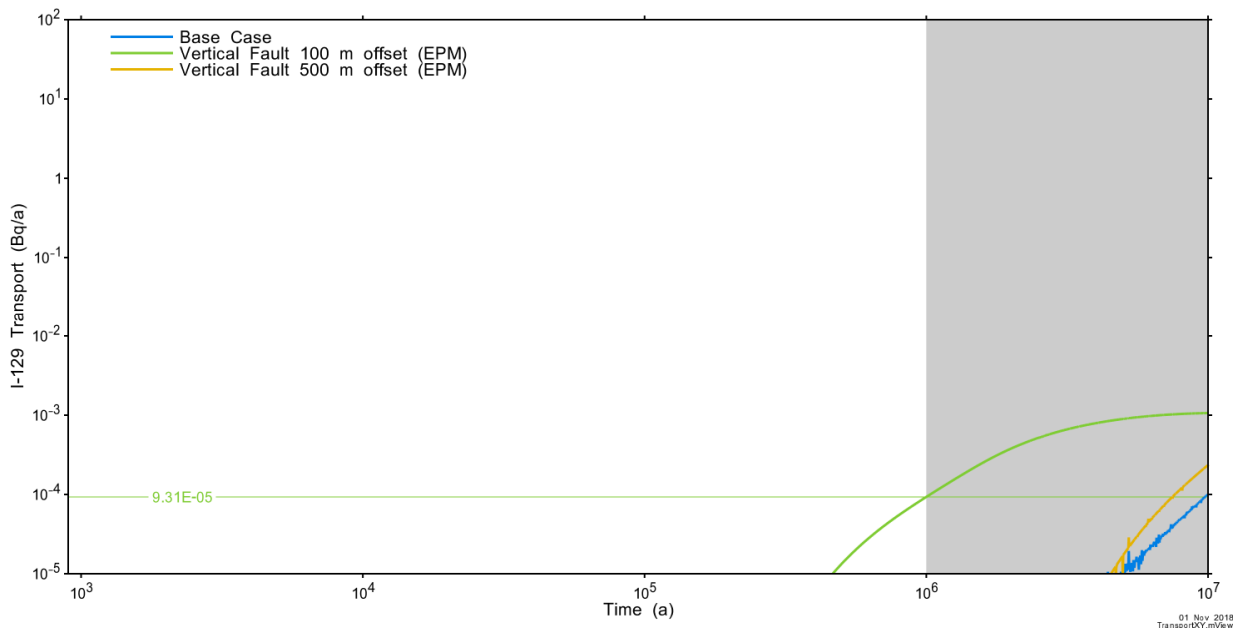


Figure 7-135: Main Transport Model: Vertical Fault Cases - I-129 Transport to Surface for Each Fracture Location

7.10 Modelling and Results for the Radiological Protection of the Environment

The results previously presented in Section 7.7 through Section 7.9 address the potential radiological effect of releases from the repository on persons. This section addresses the potential radiological effect on the environment.

For the Reference Case of the Normal Evolution Scenario, there is no effect because there are no releases.

The approach taken here is therefore to compare results obtained for the Base Case and for the All Containers Fail at 60,000 Years Disruptive Event Scenario against the interim acceptance criteria established in Section 7.1.3 for the radiological protection of the environment.

The All Containers Fail Scenario is the disruptive event which results in the greatest release of contaminants.

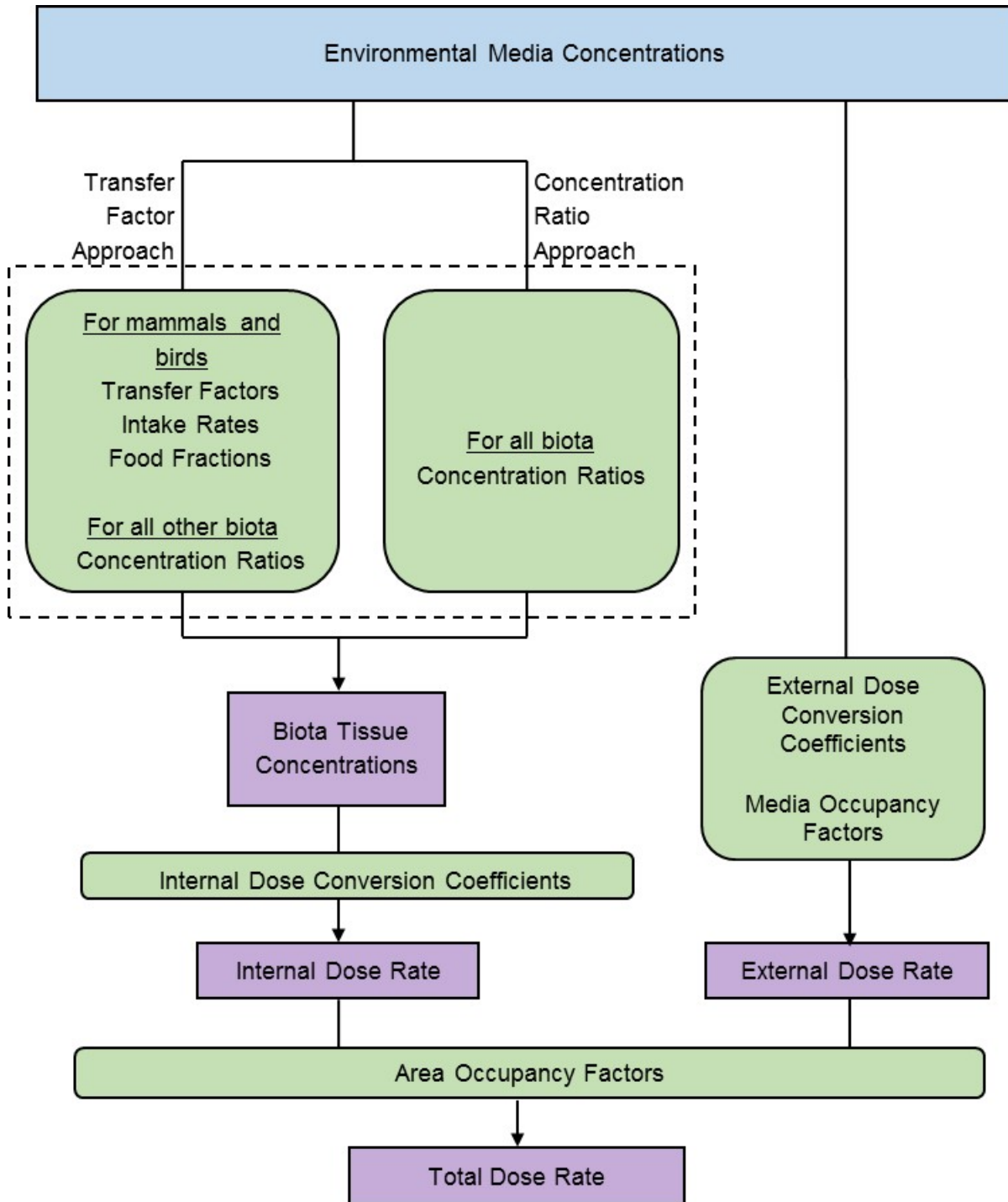
7.10.1 Method

The dose rates to non-human biota are assessed using the equations and data described in Medri and Bird (2015). The calculation method accounts for contamination by various radionuclides and pathways to different organisms, and considers two approaches to calculating the biota tissue radionuclide concentrations: the Concentration Ratio approach and the Transfer Factor approach.

Concentration Ratios estimate the radionuclide concentrations in all organisms based on the radionuclide concentrations in appropriate substrate media (soil, water, sediment or air). In Europe, calculation of dose consequences to non-human biota are largely performed using Concentration Ratios, often using the ERICA Tool (Brown et al. 2008).

Transfer Factors estimate the radionuclide concentration in mammals and birds based on the intake rate of food, soil, water and sediment. In previous work, the NWMO has used Transfer Factors to assess the radiological impact on mammals and birds and Concentration Ratios for all other biota (Garisto et al. 2008).

Figure 7-136 shows the dose calculation flow chart for the assessment. Input media concentrations are provided as a function of time by the System Model for the cases of interest.



Note: Purple boxes represent calculated quantities, green boxes represent model parameters and the blue box represents inputs

Figure 7-136: Non-Human Biota Dose Assessment Flow Chart

The assessment is carried out using using NHBv1.0 (see Table 7-12). Two different sets of dose rate estimates for mammals and birds are generated, corresponding to the two different

approaches (i.e., Transfer Factors and Concentration Ratios). The dose rates to all other non-human biota (i.e., reptiles, amphibians, plants, fish and invertebrates) are evaluated using Concentration Ratios.

Dose rate results are compared against the Interim Acceptance Criteria provided in Table 7-2 to judge whether the exposures are of radiological concern.

For the evaluation of potential future impacts, three representative ecosystems have been defined: the Southern Canadian Deciduous Forest, the Boreal Forest and the Inland Tundra (Garisto et al. 2008). These ecosystems are analysed through representative biota and simple biological exposure pathways. Selection of representative biota species for each of these ecosystems is detailed in Medri and Bird (2015).

The Southern Canadian Deciduous Forest ecosystem is most appropriate for the hypothetical site in Southern Ontario, while the two other ecosystems represent potential future ecosystems depending on possible climate change in the longer term. Environmental conditions appropriate to these other ecosystems have not been modelled in this postclosure safety assessment (i.e., a constant temperate climate is assumed); however, to explore potential future implications, dose consequences to biota in these ecosystems are also calculated using the same environmental media concentrations as for the Southern Canadian Deciduous Forest.

7.10.2 Results

Table 7-48 presents the dose rates over a one million year simulation time for the superset of representative biota across all three ecosystems.

Table 7-48: 1 Ma Dose Rates to Non-Human Biota

Scenario ⁽⁴⁾	Base Case ($\mu\text{Gy/h}$)		All Containers Fail ⁽³⁾ ($\mu\text{Gy/h}$)	
	CR ⁽¹⁾	TF ⁽²⁾	CR ⁽¹⁾	TF ⁽²⁾
Non-Human Biota				
Arctic Fox	2.2×10^{-13}	9.7×10^{-15}	3.2×10^{-9}	1.4×10^{-10}
Arctic Ground Squirrel	2.2×10^{-13}	2.2×10^{-14}	3.1×10^{-9}	3.1×10^{-10}
Arctic Hare	2.2×10^{-13}	9.8×10^{-15}	3.1×10^{-9}	1.4×10^{-10}
Arctic Wolf	1.1×10^{-13}	4.4×10^{-15}	1.6×10^{-9}	6.3×10^{-11}
Barren Ground Caribou	1.1×10^{-13}	5.0×10^{-15}	1.6×10^{-9}	7.1×10^{-11}
Beaver	1.1×10^{-13}	6.4×10^{-15}	1.6×10^{-9}	9.2×10^{-11}
Berries	1.3×10^{-14}	1.3×10^{-14}	1.9×10^{-10}	1.9×10^{-10}
Brown Lemming	2.1×10^{-13}	2.5×10^{-14}	3.0×10^{-9}	3.5×10^{-10}
Brush Wolf	5.5×10^{-14}	2.2×10^{-15}	7.9×10^{-10}	3.1×10^{-11}
Canada Goose	5.4×10^{-14}	1.4×10^{-14}	7.7×10^{-10}	2.1×10^{-10}
Chironomid Larvae	3.7×10^{-15}	3.7×10^{-15}	1.7×10^{-11}	1.7×10^{-11}
Common Garter Snake	2.1×10^{-13}	2.1×10^{-13}	2.9×10^{-9}	2.9×10^{-9}
Common Loon	1.3×10^{-16}	1.0×10^{-16}	7.9×10^{-12}	4.0×10^{-12}
Dwarf Arctic Willow	4.0×10^{-14}	4.0×10^{-14}	5.7×10^{-10}	5.7×10^{-10}
Earthworm	9.2×10^{-14}	9.2×10^{-14}	1.3×10^{-9}	1.3×10^{-9}

Postclosure Safety Assessment of a Used Fuel Repository in Sedimentary Rock

Document Number: NWMO-TR-2018-08

Revision: 000

Class: Public

Page: 551

Scenario ⁽⁴⁾	Base Case ($\mu\text{Gy/h}$)		All Containers Fail ⁽³⁾ ($\mu\text{Gy/h}$)	
	CR ⁽¹⁾	TF ⁽²⁾	CR ⁽¹⁾	TF ⁽²⁾
Eastern Cottontail Rabbit	2.1×10^{-13}	1.1×10^{-14}	3.0×10^{-9}	1.5×10^{-10}
Gray Wolf	5.5×10^{-14}	2.3×10^{-15}	7.9×10^{-10}	3.3×10^{-11}
Great Horned Owl	2.1×10^{-13}	2.1×10^{-14}	3.0×10^{-9}	2.9×10^{-10}
Groundhog	2.2×10^{-13}	1.7×10^{-14}	3.1×10^{-9}	2.5×10^{-10}
Lake Trout	4.4×10^{-16}	4.4×10^{-16}	1.5×10^{-11}	1.5×10^{-11}
Lake Whitefish	2.2×10^{-15}	2.2×10^{-15}	2.0×10^{-11}	2.0×10^{-11}
Lichen	1.7×10^{-13}	1.7×10^{-13}	2.4×10^{-9}	2.4×10^{-9}
Mallard	1.2×10^{-16}	1.4×10^{-16}	7.6×10^{-12}	4.9×10^{-12}
Meadow Vole	1.9×10^{-13}	1.4×10^{-14}	2.8×10^{-9}	1.9×10^{-10}
Mink	2.3×10^{-16}	1.3×10^{-16}	1.4×10^{-11}	2.4×10^{-12}
Moose	1.8×10^{-13}	1.4×10^{-14}	2.6×10^{-9}	2.0×10^{-10}
Muskrat	1.1×10^{-13}	6.6×10^{-15}	1.5×10^{-9}	9.5×10^{-11}
Northern Leopard Frog	2.2×10^{-15}	2.2×10^{-15}	5.1×10^{-11}	5.1×10^{-11}
Pondweeds	4.1×10^{-15}	4.1×10^{-15}	2.4×10^{-11}	2.4×10^{-11}
Red Fox	2.2×10^{-13}	1.0×10^{-14}	3.1×10^{-9}	1.5×10^{-10}
Red Throated Loon	1.3×10^{-16}	1.0×10^{-16}	7.9×10^{-12}	4.0×10^{-12}
Ruffed Grouse	2.1×10^{-13}	3.5×10^{-14}	2.9×10^{-9}	4.9×10^{-10}
Sedge Species	4.3×10^{-14}	4.3×10^{-14}	6.1×10^{-10}	6.1×10^{-10}
Snowshoe Hare	2.1×10^{-13}	1.1×10^{-14}	3.0×10^{-9}	1.5×10^{-10}
Water Sedge	4.0×10^{-15}	4.0×10^{-15}	2.4×10^{-11}	2.4×10^{-11}
White Cedar	3.8×10^{-14}	3.8×10^{-14}	5.4×10^{-10}	5.4×10^{-10}
White-Tailed Deer	2.3×10^{-13}	6.6×10^{-15}	3.3×10^{-9}	9.4×10^{-11}
Willow Ptarmigan	2.1×10^{-13}	3.6×10^{-14}	3.0×10^{-9}	5.2×10^{-10}

Notes: (1) Results using Concentration Ratios

(2) Results using Transfer Factors

(3) All Containers Fail at 60,000 Years Disruptive Event Scenario

(4) Results are maximum over a one million year simulation.

All dose rates are more than 9 orders of magnitude below the Tier 1 Interim Acceptance Criteria defined in Table 7-2 for both cases considered. It is therefore concluded that there is no concern about adverse impacts to non-human biota from the potential release of radioactive contaminants from the repository.

For added context, the Tier 1 Interim Acceptance Criteria can be used to determine a “Tier 1 Quotient”, where this is the ratio formed by dividing the dose rates in Table 7-48 by the appropriate Tier 1 Interim Acceptance Criteria. Figure 7-137 shows the resulting Tier 1 Quotients for all species for the All Containers Fail event.

The highest quotient value is 3.3×10^{-9} for the white tailed deer.

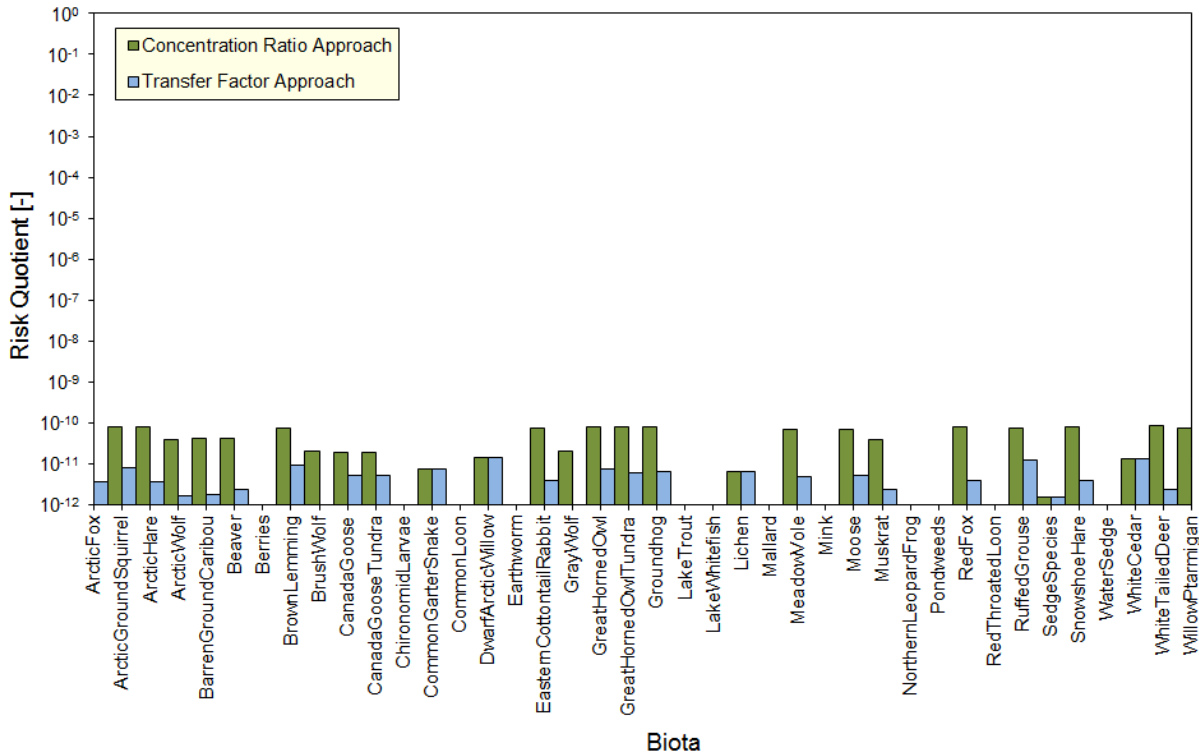


Figure 7-137: Tier 1 Quotients in the All Containers Fail Disruptive Event Scenario

7.11 Modelling and Results for the Protection of Persons and the Environment from Hazardous Substances

This section addresses the potential non-radiological consequences of contaminants arising from the used fuel bundles and from the container on the health and safety of persons and the environment.

The potentially significant chemically hazardous elements from the used fuel bundles considered in this study are Ag, Hg, Mo, Nd, Pd, Rh, and Ru, as identified in Section 7.6.2.

Potential chemical elements of concern from the copper containers are also considered. The the sealing materials are not considered because their components are natural clay materials, concrete and asphalt, which are widely used at surface.

Section 7.1.2 discusses the applicable interim acceptance criteria, and Table 7-1 presents these criteria for groundwater, surface water, sediment, soil and air.

The ratio determined by dividing an element concentration by its acceptance criterion is called the 'Concentration Quotient'. Concentration Quotients less than 1.0 indicate the interim acceptance criterion is not exceeded.

7.11.1 Used Fuel Chemical Hazard Assessment

There are no releases for the Reference Case of the Normal Evolution Scenario.

To illustrate the potential consequences of contaminant releases, the approach compares results obtained for the Base Case and for the All Containers Fail at 60,000 Disruptive Event Scenario against the interim acceptance criteria. The All Containers Fail scenario is selected because it is the disruptive event that results in the greatest contaminant release.

Surface water, sediment, soil and air concentrations in the System Model biosphere are compared to the corresponding acceptance criteria. Groundwater concentrations are taken to be those in the well.

In the Base Case, all contaminants enter the well and therefore sediment concentrations from groundwater discharge into surface water features are not calculated. Instead, Base Case sediment values are estimated by multiplying the surface water concentrations by sediment sorption coefficients taken from Gobien et al. (2018). As noted in Section 7.3.4, the System Model conservatively assumes all radionuclides in the well are simultaneously transferred to surface water features. Therefore, surface water concentrations are generated by the System Model even though there is no direct discharge to the surface water.

Table 7-49 shows the one million year Concentration Quotients for the Base Case. The single greatest value is 5.4×10^{-9} for Ru in soil. Wide margins are available to the interim acceptance criteria.

Table 7-50 shows the one million year Concentration Quotients for the All Containers Fail Disruptive Event Scenario. As expected, the quotients are higher than in the Base Case due to the significantly greater source term, with the single greatest value being 8.3×10^{-5} for Ru in soil.

The Table 7-49 and Table 7-50 results are also illustrated in Figure 7-138 to Figure 7-142.

If simulations are extended to peak, the highest overall peak concentration ratios for the Base Case and All Containers Fail cases are 6.85×10^{-5} and 0.74 respectively for Ru in soil.

Based on these results, it is concluded that the repository would not pose a non-radiological health and safety hazard to persons or to the environment for contaminants released from the used fuel bundles.

Table 7-49: System Model: Concentration Quotients for the Base Case

Element	Groundwater	Surface Water	Soil	Sediment ⁽¹⁾	Air
Ag	1.1x10 ⁻¹⁰	9.5x10 ⁻¹⁵	1.9x10 ⁻¹¹	1.8x10 ⁻¹³	2.9x10 ⁻¹³
Hg	4.6x10 ⁻¹¹	1.8x10 ⁻¹³	3.7x10 ⁻¹³	6.7x10 ⁻¹⁶	2.5x10 ⁻¹⁴
Mo	6.5x10 ⁻¹⁴	8.4x10 ⁻¹⁸	2.7x10 ⁻¹⁵	1.0x10 ⁻¹⁸	1.5x10 ⁻¹⁷
Nd	-	3.1x10 ⁻¹³	-	0.0	4.8x10 ⁻¹⁴
Pd	0.0	0.0	0.0	0.0	0.0
Rh	8.9x10 ⁻¹⁰	1.1x10 ⁻¹²	1.8x10 ⁻⁹	1.2x10 ⁻¹³	1.4x10 ⁻¹¹
Ru	3.2x10 ⁻⁹	6.3x10 ⁻¹³	5.4x10 ⁻⁹	5.1x10 ⁻¹²	1.6x10 ⁻¹²

Note: (1) Values are estimated using the surface water concentration as described in Section 7.11.3.

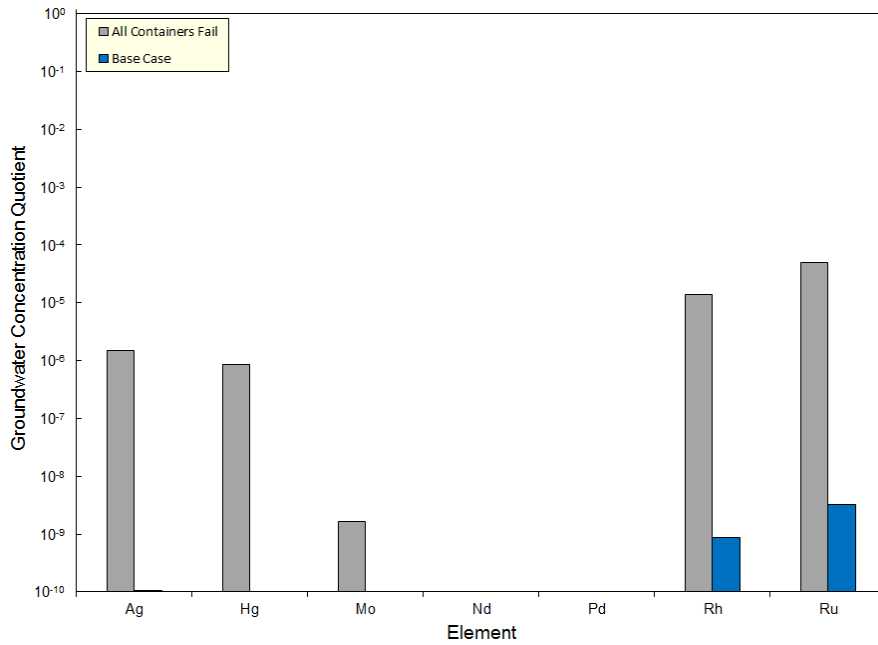
“-“ Indicates there is no acceptance criteria available for a given element in that media
Concentration Quotients below 1x10⁻¹⁵ are listed as zero

Table 7-50: System Model: Concentration Quotients for the All Containers Fail Case

Element	Groundwater	Surface Water	Soil	Sediment ⁽¹⁾	Air
Ag	1.5x10 ⁻⁶	1.3x10 ⁻¹⁰	2.6x10 ⁻⁷	2.5x10 ⁻⁹	4.0x10 ⁻⁹
Hg	8.5x10 ⁻⁷	3.3x10 ⁻⁹	6.8x10 ⁻⁹	1.2x10 ⁻¹¹	4.6x10 ⁻¹⁰
Mo	1.7x10 ⁻⁹	2.1x10 ⁻¹³	6.9x10 ⁻¹¹	2.6x10 ⁻¹⁴	3.7x10 ⁻¹³
Nd	-	4.3x10 ⁻⁹	-	0.0	6.6x10 ⁻¹⁰
Pd	0.0	0.0	0.0	0.0	0.0
Rh	1.4x10 ⁻⁵	1.7x10 ⁻⁸	2.8x10 ⁻⁵	1.8x10 ⁻⁹	2.1x10 ⁻⁷
Ru	4.9x10 ⁻⁵	9.7x10 ⁻⁹	8.3x10 ⁻⁵	7.8x10 ⁻⁸	2.5x10 ⁻⁸

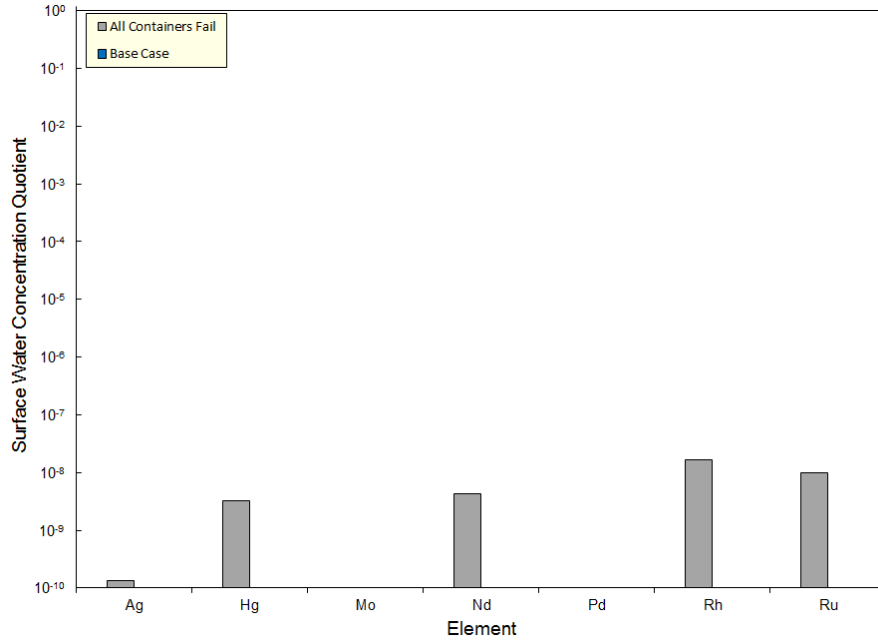
Notes: (1) Values are estimated using the surface water concentration as described in Section 7.11.3.

“-“ Indicates there is no acceptance criteria available for a given element in that media
Concentration Quotients below 1x10⁻¹⁵ are listed as zero



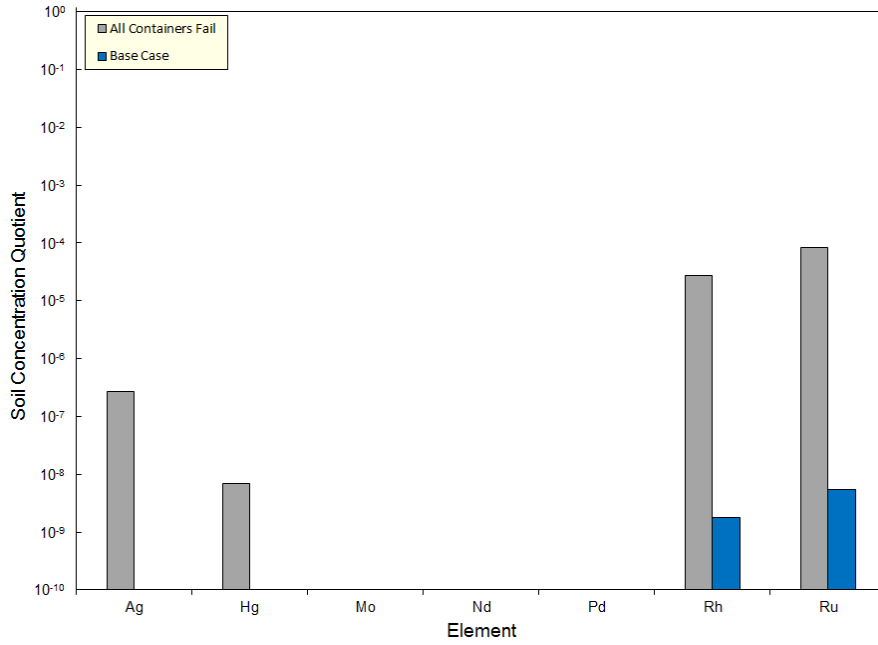
Note: Nd does not have acceptance criteria for groundwater, Pd results are off scale low

Figure 7-138: Non-Radiological Hazard: Base Case Groundwater Results



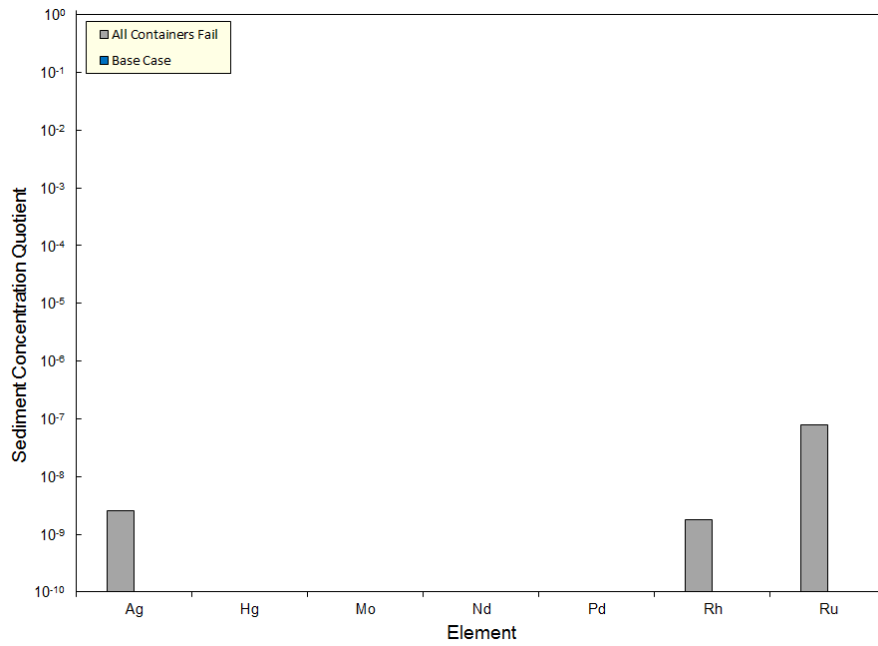
Note: Pd results are off scale low

Figure 7-139: Non-Radiological Hazard: Base Case Surface Water Results



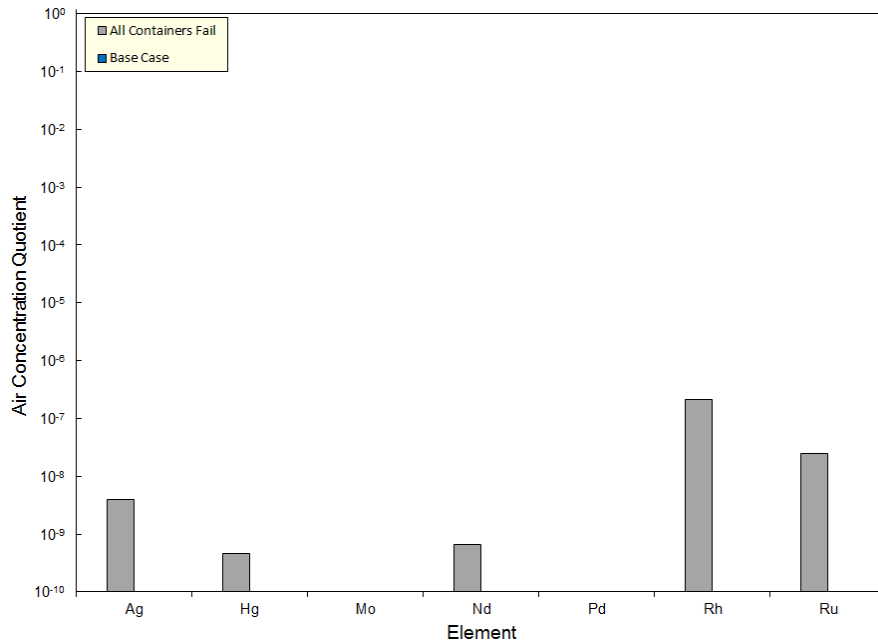
Note: Nd does not have acceptance criteria for soil, Pd results are off scale low

Figure 7-140: Non-Radiological Hazard: Base Case Soil Results



Note: Nd and Pd results are off scale low

Figure 7-141: Non-Radiological Hazard: Base Case Sediment Results



Note: Pd results are off scale low

Figure 7-142: Non-Radiological Hazard: Base Case Air Results

7.11.2 Copper Container Chemical Hazard Assessment

The release rate of contaminants from the copper metal depends on the copper corrosion or dissolution rate. As described in Chapter 5, this is expected to be very slow.

For this chemical hazard assessment, a solubility-limited dissolution model is used to determine the rate of copper release and the Main Transport Model (Section 7.7.1.2) is used to model transport to the biosphere. The transport of copper away from the container is simulated by applying a constant concentration boundary condition of 0.264 mol/m³ (Duro et al. 2010) at every grid node intersecting containers in the repository. This concentration corresponds to the measured copper solubility limit increased by a factor of 10 to account for uncertainties in temperature and chemical conditions near the container. This conservatively results in a continuous input of copper into the model. Simulations were performed for the “With-Well” and the “No-Well” Scenarios.

Copper transport to the well and to surface is shown in Figure 7-143.

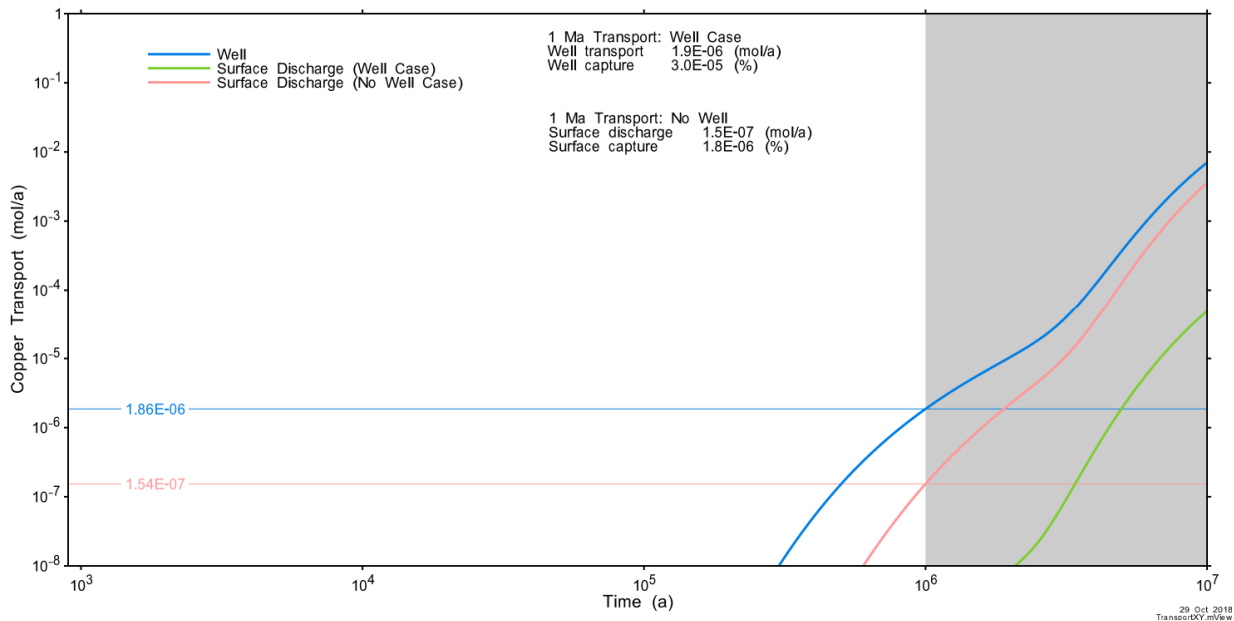


Figure 7-143: Main Transport Model: Copper Transport to the Well

To determine the groundwater Concentration Quotient, the maximum copper transport rate to the well at one million years (i.e., 1.86×10^{-6} mol/a) is assumed, with the well pumping at the reference rate of $1261 \text{ m}^3/\text{a}$. The resulting well water concentration is $1.48 \times 10^{-9} \text{ mol}/\text{m}^3$.

The surface water and groundwater concentrations are conservatively assumed to be the same as the well water concentration. The maximum soil and sediment concentrations are then determined by multiplying the well water concentration by the applicable sorption coefficients for soil ($0.11 \text{ m}^3/\text{kg}$) and sediment ($0.37 \text{ m}^3/\text{kg}$).

Chemical element impurities present in the copper are not currently known; however, given that the copper will be at least 99.9% pure, the contaminant levels will be very low. To allow for an assessment, impurity levels in Table 7-51 (SKB 1998 and SKB 2010b) are adopted. The calculation of impurity concentrations assumes the impurities are transported away at the same rate as the copper. Element specific K_d values for impurities in the buffer and geosphere may produce some variation in the transport times but because chemical species do not decay, peak impurity concentrations are largely independent of transport time.

Table 7-51 shows the computed surface water, groundwater, soil and sediment Concentration Quotients for copper and for the assumed impurity elements for a simulation time of one million years. As expected, the copper itself has the largest quotient value. However since these quotients are all orders of magnitude below 1.0, it is concluded that the components of the copper container itself would not pose a hazard to persons or to the environment.

Table 7-51: Concentration Impurity Levels in Copper and Estimated Element Concentration Quotients

Element	Impurity Level ⁽¹⁾ (mol/mol Cu)	Maximum Element Conc in Well Water (mol/m ³)	Surface Water Conc Quotient ⁽²⁾	Groundwater Conc Quotient ⁽³⁾	Soil Conc Quotient ⁽⁴⁾	Sediment Conc Quotient ⁽⁵⁾
Cu	balance	1.48x10 ⁻⁹	9.37x10 ⁻⁵	1.36x10 ⁻⁶	4.54x10 ⁻⁸	2.89x10 ⁻⁶
Ag	1.47x10 ⁻⁵	2.17x10 ⁻¹⁴	2.34x10 ⁻⁸	1.95x10 ⁻⁹	4.22x10 ⁻¹⁰	7.03x10 ⁻⁸
As	4.24x10 ⁻⁶	6.26x10 ⁻¹⁵	9.37x10 ⁻¹¹	4.69x10 ⁻¹¹	4.26x10 ⁻¹⁴	7.94x10 ⁻¹³
Bi	3.04x10 ⁻⁷	4.49x10 ⁻¹⁶	6.70x10 ⁻¹³	6.70x10 ⁻¹⁴	4.69x10 ⁻¹³	2.16x10 ⁻¹⁵
Cd	5.65x10 ⁻⁷	8.34x10 ⁻¹⁶	1.04x10 ⁻⁹	4.46x10 ⁻¹¹	7.50x10 ⁻¹²	1.25x10 ⁻¹⁰
Co	2.16x10 ⁻⁵	3.18x10 ⁻¹⁴	3.12x10 ⁻⁹	4.93x10 ⁻¹⁰	5.11x10 ⁻¹²	3.71x10 ⁻¹¹
Cr	1.83x10 ⁻⁵	2.70x10 ⁻¹⁴	1.41x10 ⁻⁹	2.87x10 ⁻¹⁰	1.43x10 ⁻¹⁰	1.46x10 ⁻¹¹
Fe	1.14x10 ⁻⁵	1.68x10 ⁻¹⁴	3.12x10 ⁻¹²	3.12x10 ⁻¹²	1.03x10 ⁻¹²	2.19x10 ⁻¹³
Hg	3.17x10 ⁻⁷	4.67x10 ⁻¹⁶	2.34x10 ⁻⁸	7.81x10 ⁻¹⁰	7.50x10 ⁻¹²	1.07x10 ⁻¹⁰
Mn	5.78x10 ⁻⁷	8.53x10 ⁻¹⁶	9.37x10 ⁻¹³	9.37x10 ⁻¹³	2.30x10 ⁻¹⁴	4.99x10 ⁻¹⁴
Ni	1.08x10 ⁻⁵	1.60x10 ⁻¹⁴	3.75x10 ⁻¹¹	9.37x10 ⁻¹²	1.01x10 ⁻¹¹	6.44x10 ⁻¹¹
P	2.05x10 ⁻⁴	3.03x10 ⁻¹³	2.34x10 ⁻⁹	-	-	-
Pb	1.53x10 ⁻⁶	2.26x10 ⁻¹⁵	1.56x10 ⁻¹¹	4.69x10 ⁻¹¹	2.81x10 ⁻¹²	3.68x10 ⁻¹⁰
S	2.97x10 ⁻⁵	4.38x10 ⁻¹⁴	7.40x10 ⁻¹⁰	2.81x10 ⁻¹¹	3.09x10 ⁻¹⁴	-
Sb	2.09x10 ⁻⁶	3.08x10 ⁻¹⁵	6.25x10 ⁻¹¹	6.25x10 ⁻¹¹	1.69x10 ⁻¹¹	6.75x10 ⁻¹¹
Se	2.41x10 ⁻⁶	3.56x10 ⁻¹⁵	2.81x10 ⁻¹⁰	2.81x10 ⁻¹¹	3.52x10 ⁻¹¹	5.62x10 ⁻¹⁰
Sn	1.07x10 ⁻⁶	1.58x10 ⁻¹⁵	2.57x10 ⁻¹²	-	4.87x10 ⁻¹²	-
Te	9.96x10 ⁻⁷	1.47x10 ⁻¹⁵	3.23x10 ⁻¹¹	3.23x10 ⁻¹²	9.37x10 ⁻¹⁴	1.15x10 ⁻¹¹
Zn	9.72x10 ⁻⁷	1.43x10 ⁻¹⁵	1.31x10 ⁻¹³	1.47x10 ⁻¹³	9.02x10 ⁻¹⁴	1.74x10 ⁻¹²

Notes: '-' indicates that there are no defined criteria for that element in the given medium.

(1) Impurity levels are maximum values taken from SKB (1998), P impurity level is taken from SKB (2010b). C, N, O, Si not included as these are common elements

(2) Surface water concentration quotients are estimates based on the maximum element concentration in the well compared against the surface water criteria from Table 7-1.

(3) Groundwater concentration quotients are estimates based on the maximum element concentration in the well compared against the groundwater criteria from Table 7-1.

(4) Soil concentration quotients are estimated using the maximum element concentration in the well, the soil Kd values from Gobien and Garisto (2012) and the soil acceptance criteria from Table 7-1.

(5) Sediment concentration quotients are estimated using the maximum element concentration in the well, the sediment Kd values from Gobien and Garisto (2012) and the sediment acceptance criteria from Table 7-1.

7.12 Modelling and Results for Complementary Indicators

An “indicator” is a characteristic or consequence of a repository which can be used to indicate the overall safety or performance of the system. The most widely used indicator is the peak radiological dose rate, which is calculated from the characteristics of the waste and repository, the properties of the geosphere and biosphere, and the characteristics of the critical group.

The relevance of the calculated dose rates as indicators of potential exposure tends to decrease with time, in part because of uncertainties in the models and data used to calculate them. In particular, assumptions concerning the biosphere (e.g., climate), human lifestyles (i.e., critical group characteristics) and water flows in the near-surface environment become increasingly uncertain. The purpose of complementary long-term indicators is to supplement the dose rate indicator using system characteristics that are much less sensitive to such assumptions.

The types of complementary indicators considered are:

- Concentrations in the biosphere; and
- Transport to the biosphere.

Indicators of the first type avoid assumptions about biosphere pathways but make assumptions about flow rates in surface water bodies (i.e., dilution rates). Indicators of the second type avoid assumptions about surface water flows. Concentration type indicators are useful on medium timeframes (about 10^4 to 10^5 years), while transport type indicators are useful for very long timeframes ($> 10^5$ years) when there is more uncertainty about surface conditions.

The specific complementary indicators considered for radiological contaminants have been selected based on the recommendations of the SPIN project (Becker et al. 2002). The indicators are:

- Radiotoxicity concentration in a water body, for medium time scales; and
- Radiotoxicity transport from the geosphere, for longer time scales.

Radiotoxicity concentration (in mSv/m^3) is the sum over all radionuclides of the activity concentrations in the water body (in Bq/m^3) multiplied by the corresponding radionuclide ingestion dose coefficient. Radiotoxicity transport from the geosphere (in mSv/a) is similarly defined.

Although these complementary indicators are expressed in units of mSv/m^3 or mSv/a , they do not represent a dose; rather, they are radiotoxicity-weighted concentration or transport indicators.

Results are shown for the Base Case and for the All Containers Fail at 60,000 Years Disruptive Event Scenario.

7.12.1 Reference Values

To make use of indicators, reference values are required for comparison purposes. These are derived below.

Radiotoxicity Concentration in a Water Body

A reference value for the radiotoxicity concentration in a water body can be derived using information on present-day natural background radionuclide concentrations in Canadian surface waters. Table 7-52 shows these concentrations for a variety of radionuclides. Data representative of Canadian surface waters are taken from Sheppard et al. (2011a) while Southern Ontario data are taken from a subset of samples in Sheppard and Sanipelli (2011b).

Table 7-52: Background Concentration of Radionuclides in Surface Waters

Radionuclide	Surface Water Concentration (Bq/L)		Ingestion DCF (Sv/Bq)	Radiotoxicity (Canadian) (mSv/m ³)
	Canadian	Southern Ontario		
H-3	3.2x10 ⁰	3.7x10 ⁰	1.8x10 ⁻¹¹	5.8x10 ⁻⁵
Cl-36	5.1x10 ⁻⁶	2.0x10 ⁻⁶	9.3x10 ⁻¹⁰	4.7x10 ⁻⁹
K-40	3.3x10 ⁻²	3.4x10 ⁻² (1)	6.2x10 ⁻⁹	2.0x10 ⁻⁴
Rb-87	2.6x10 ⁻⁴	1.1x10 ⁻³ (2)	1.5x10 ⁻⁹	3.9x10 ⁻⁷
I-129	1.0x10 ⁻⁷	8.7x10 ⁻⁸	1.1x10 ⁻⁷	1.1x10 ⁻⁸
Bi-210	6.4x10 ⁻³ (3)	2.0x10 ⁻² (3)	1.3x10 ⁻⁹	8.3x10 ⁻⁶
Pb-210	6.4x10 ⁻³	2.0x10 ⁻²	6.9x10 ⁻⁷	4.4x10 ⁻³
Po-210	7.1x10 ⁻³	2.0x10 ⁻² (3)	1.2x10 ⁻⁶	8.5x10 ⁻³
Rn-222	2.7x10 ⁻³ (4)	5.8x10 ⁻³ (4)	2.5x10 ⁻¹⁰	6.8x10 ⁻⁷
Ra-223	2.0x10 ⁻⁷ (6)	4.8x10 ⁻⁷ (6)	1.0x10 ⁻⁷	2.0x10 ⁻⁸
Ra-224	7.8x10 ⁻³ (8)	6.3x10 ⁻³ (8)	7.1x10 ⁻⁸	5.6x10 ⁻⁴
Ra-226	2.7x10 ⁻³	5.8x10 ⁻³	2.8x10 ⁻⁷	7.6x10 ⁻⁴
Ac-227	2.0x10 ⁻⁷ (6)	4.8x10 ⁻⁷ (6)	1.1x10 ⁻⁶	2.2x10 ⁻⁷
Th-227	2.0x10 ⁻⁷ (6)	4.8x10 ⁻⁷ (6)	8.8x10 ⁻⁹	1.8x10 ⁻⁹
Ra-228	2.9x10 ⁻⁴	3.1x10 ⁻⁴ (7)	6.9x10 ⁻⁷	2.0x10 ⁻⁴
Th-228	9.6x10 ⁻⁴	3.1x10 ⁻⁴ (7)	7.2x10 ⁻⁸	6.9x10 ⁻⁵
Th-230	1.9x10 ⁻³	5.1x10 ⁻³ (6)	2.1x10 ⁻⁷	4.0x10 ⁻⁴
Pa-231	2.0x10 ⁻⁷ (6)	4.8x10 ⁻⁷ (6)	7.1x10 ⁻⁷	1.4x10 ⁻⁷
Th-231	1.5x10 ⁻⁷	4.8x10 ⁻⁷ (6)	3.4x10 ⁻¹⁰	5.1x10 ⁻¹¹
Th-232	3.9x10 ⁻⁴	3.1x10 ⁻⁴	2.3x10 ⁻⁷	9.0x10 ⁻⁵
Th-234	3.3x10 ⁻³ (5)	5.1x10 ⁻³ (5)	3.4x10 ⁻⁹	1.1x10 ⁻⁵
U-234	7.3x10 ⁻³	5.1x10 ⁻³ (5)	4.9x10 ⁻⁸	3.6x10 ⁻⁴
U-235	9.3x10 ⁻⁵	2.4x10 ⁻⁴	4.7x10 ⁻⁸	4.4x10 ⁻⁶
U-238	3.3x10 ⁻³	5.1x10 ⁻³	4.5x10 ⁻⁸	1.5x10 ⁻⁴
			Total	1.6x10 ⁻²

- Notes: (1) Estimated using stable K concentration
 (2) Estimated using stable Rb concentration
 (3) Assumed to be in secular equilibrium with Pb-210
 (4) Assumed to be in secular equilibrium with Ra-226
 (5) Assumed to be in secular equilibrium with U-238
 (6) Values are 500 times lower than for U-235 in water, as recommended by Amiro (1992, 1993)
 (7) Assumed to be in secular equilibrium with Th-232
 (8) Values are 20 times higher than for Th-232 in water, as recommended by Amiro (1992, 1993)

Sheppard et al. (2011a) suggest that the background concentration of radioactive species in surface water remains fairly homogeneous across Canada. Data extracted specifically for Southern Ontario appears to verify this with most radionuclide concentrations within a factor of two of the Canadian values. The largest difference is for Rb-87, with the Canadian value 4.2 times lower than the Southern Ontario value. However, given the limited number of samples for

the Southern Ontario data and the error associated with measuring concentrations around the detection limit, it is likely that the variations between the Canadian values and Southern Ontario values are within the variability of the measurements. Consequently, Canadian surface water data have been selected as representative of the surface waters applicable to this hypothetical site.

Radiotoxicity concentration is determined by multiplying the surface water concentrations by the appropriate ingestion dose conversion factor (Gobien et al. 2018). The results are shown in the rightmost column of Table 7-52, with the total value of 1.6×10^{-2} mSv/m³ indicated at the bottom right. For comparison, use of data specific to Southern Ontario results in a higher radiotoxicity concentration of 4.2×10^{-2} mSv/m³. Thus, the selected reference value is conservative when used as a comparative baseline.

Dose impacts associated with these natural background levels are not of public concern so it follows that any dose impacts from the repository that are small in comparison should also not be of concern.

Radiotoxicity Transport from the Geosphere

Natural transport processes continuously carry small amounts of naturally occurring radioactivity from within the geosphere to the biosphere. The most important processes are groundwater flow and erosion (IAEA 2002). The natural radioactivity discharged to the biosphere with groundwater flow has been calculated in Garisto et al. (2004) from groundwater flow rates and radionuclide concentrations in groundwater. The result is a value of 7×10^5 mSv/a over a 100 km² subregional watershed area.

Alternatively, natural radiotoxicity transport to the surface can be calculated from the elemental composition of sedimentary rocks and their associated erosion rate over long time periods.

Table 7-53 presents elemental concentrations for naturally radioactive elements in rocks (Rudnick and Gao 2014). From this, the elemental concentrations of their associated radioactive progeny can be determined, assuming secular equilibrium, as noted in Table 7-54.

Table 7-53: Radioactive Element Concentrations in Rocks

Element	Rock Concentration (g/kg Rock)
U	0.0027
Th	0.0105
K	23.7
Rb	0.084

Table 7-54: Radiotoxicity Concentration in Rocks

Nuclide	Activity Concentration (Bq/kg)	Ingestion DCF ⁽²⁾ (Sv/Bq)	Radiotoxicity Concentration (mSv/kg)
U-238	33	4.50x10 ⁻⁸	1.50x10 ⁻³
Th-234 ⁽¹⁾	33	3.40x10 ⁻⁹	1.13x10 ⁻⁴
U-234 ⁽¹⁾	33	4.90x10 ⁻⁹	1.63x10 ⁻⁴
Th-230 ⁽¹⁾	33	2.10x10 ⁻⁷	7.00x10 ⁻³
Ra-226 ⁽¹⁾	33	2.80x10 ⁻⁷	9.33x10 ⁻³
Rn-222 ⁽¹⁾	33	2.50x10 ⁻¹⁰	8.33x10 ⁻⁶
Pb-210 ⁽¹⁾	33	6.90x10 ⁻⁷	2.30x10 ⁻²
Bi-210 ⁽¹⁾	33	1.30x10 ⁻⁹	4.33x10 ⁻⁵
Po-210 ⁽¹⁾	33	1.20x10 ⁻⁶	4.00x10 ⁻²
U-235	1.5	4.70x10 ⁻⁸	7.21x10 ⁻⁵
Th-231 ⁽¹⁾	1.5	3.40x10 ⁻¹⁰	5.22x10 ⁻⁷
Pa-231 ⁽¹⁾	1.5	7.10x10 ⁻⁷	1.09x10 ⁻³
Ac-227 ⁽¹⁾	1.5	1.10x10 ⁻⁶	1.69x10 ⁻³
Th-227 ⁽¹⁾	1.5	8.80x10 ⁻⁹	1.35x10 ⁻⁵
Ra-223 ⁽¹⁾	1.5	1.00x10 ⁻⁷	1.53x10 ⁻⁴
Th-232	43	2.30x10 ⁻⁷	9.80x10 ⁻³
Ra-228 ⁽¹⁾	43	6.90x10 ⁻⁷	2.94x10 ⁻²
Th-228 ⁽¹⁾	43	7.20x10 ⁻⁸	3.07x10 ⁻³
Ra-224 ⁽¹⁾	43	7.13x10 ⁻⁸	3.04x10 ⁻³
K-40	752	6.20x10 ⁻⁹	4.66x10 ⁻³
Rb-87	76	1.50x10 ⁻⁹	1.14x10 ⁻⁴
		Total	1.34x10 ⁻¹

Notes: (1) Assumed to be in secular equilibrium with parent radionuclide
 (2) DCFs from either Gobien et al. (2018)

By adopting the Section 7.6.1.2 values for erosion rate (1.0x10⁻⁴ m/a), assumed repository footprint area (5 km²) and rock density (2750 m³/kg), a total erosion rate of about 1.4x10⁶ kg/a can be estimated. By applying the ingestion dose conversion factors from Gobien et al. (2018) to the Table 7-54 values, a radiotoxicity transport value of about 1.85x10⁵ mSv/a for natural erosion can be determined.⁵

⁵ Erosion rates are expected to be lower during interglacial periods when people are present. However erosion is also occurring over the entire surface, and not just repository footprint. These effects counter each other so the nominal radiotoxicity value is a reasonable balance.

This value is four times less than the 7×10^5 mSv/a radiotoxicity groundwater transport value mentioned earlier, and is adopted as the reference value for the radiotoxicity transport indicator.

Reference Values:

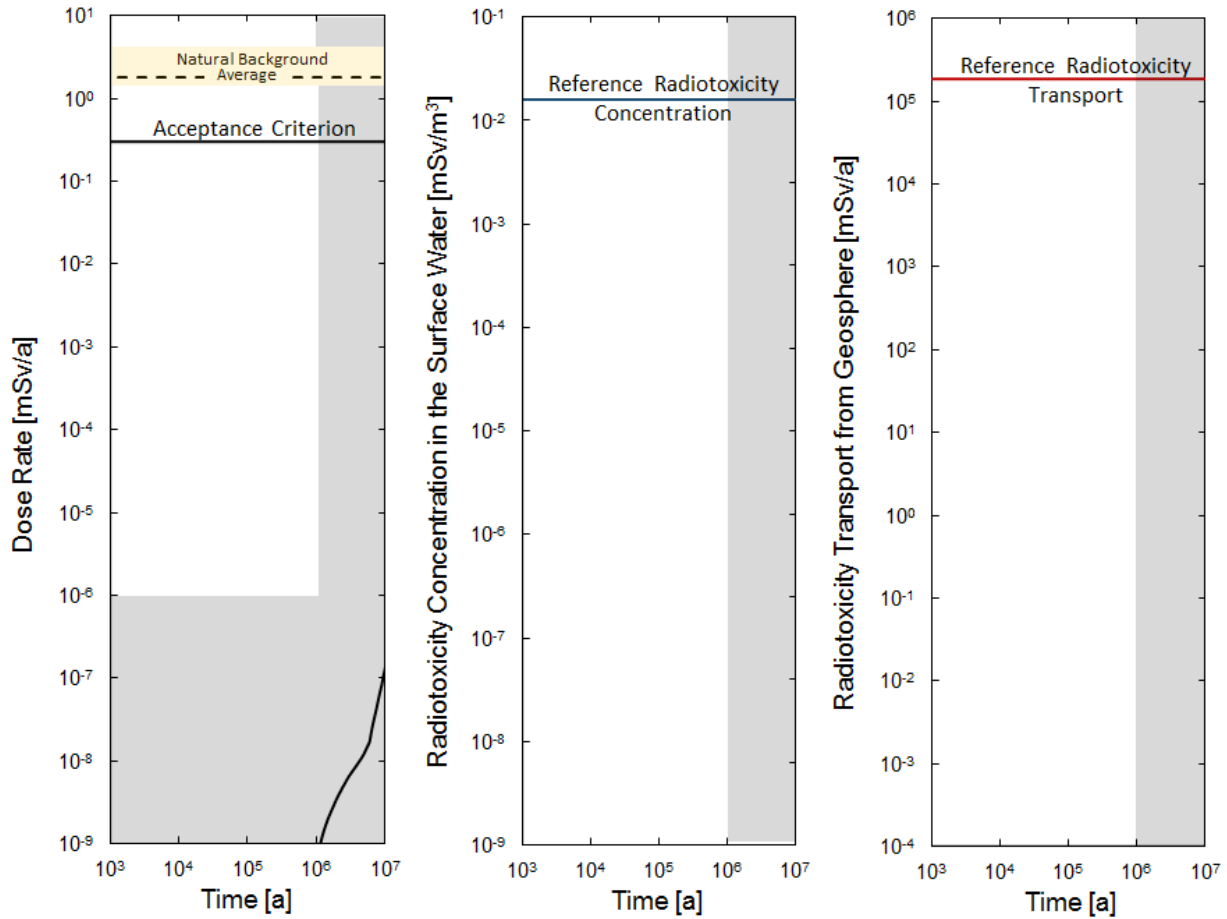
Table 7-55 summarizes the complementary long-term indicators developed for use in this study. The reference values proposed in the EC SPIN project (Becker et al. 2002) are also shown for comparison.

Table 7-55: Reference Values for Indicators

Indicator	Reference Value	
	Current Study	SPIN
Dose rate (mSv/a)	0.3	0.1 to 0.3
Radiotoxicity concentration in surface water (mSv/m ³)	1.6×10^{-2}	2×10^{-2}
Radiotoxicity transport from the geosphere (mSv/a)	1.85×10^5	6×10^4

7.12.2 Results for Complementary Indicators

Figure 7-144 shows the indicator values for the Base Case together with the dose rate indicator for comparison. The indicators for the Base Case are off-scale low due to the extremely low transport to the biosphere.



Note: Base Case results for Radiotoxicity Concentration in the Surface Water and Radiotoxicity Transport from the Geosphere are off-scale low

Figure 7-144: System Model: Base Case - Results for Indicators

Figure 7-145 shows the indicator values for the All Containers Fail at 60,000 Years Disruptive Event Scenario together with the dose rate indicator for comparison. The peak dose rate value is 6.16×10^{-3} mSv/a. The indicators have the same general shape because they both depend on radionuclide transport to the biosphere. The peak surface water radiotoxicity is 2.5×10^{-7} mSv/m³, and the peak radiotoxicity transport from the geosphere is 4.3 mSv/a, both values being well below their associated criteria for complementary indicators.

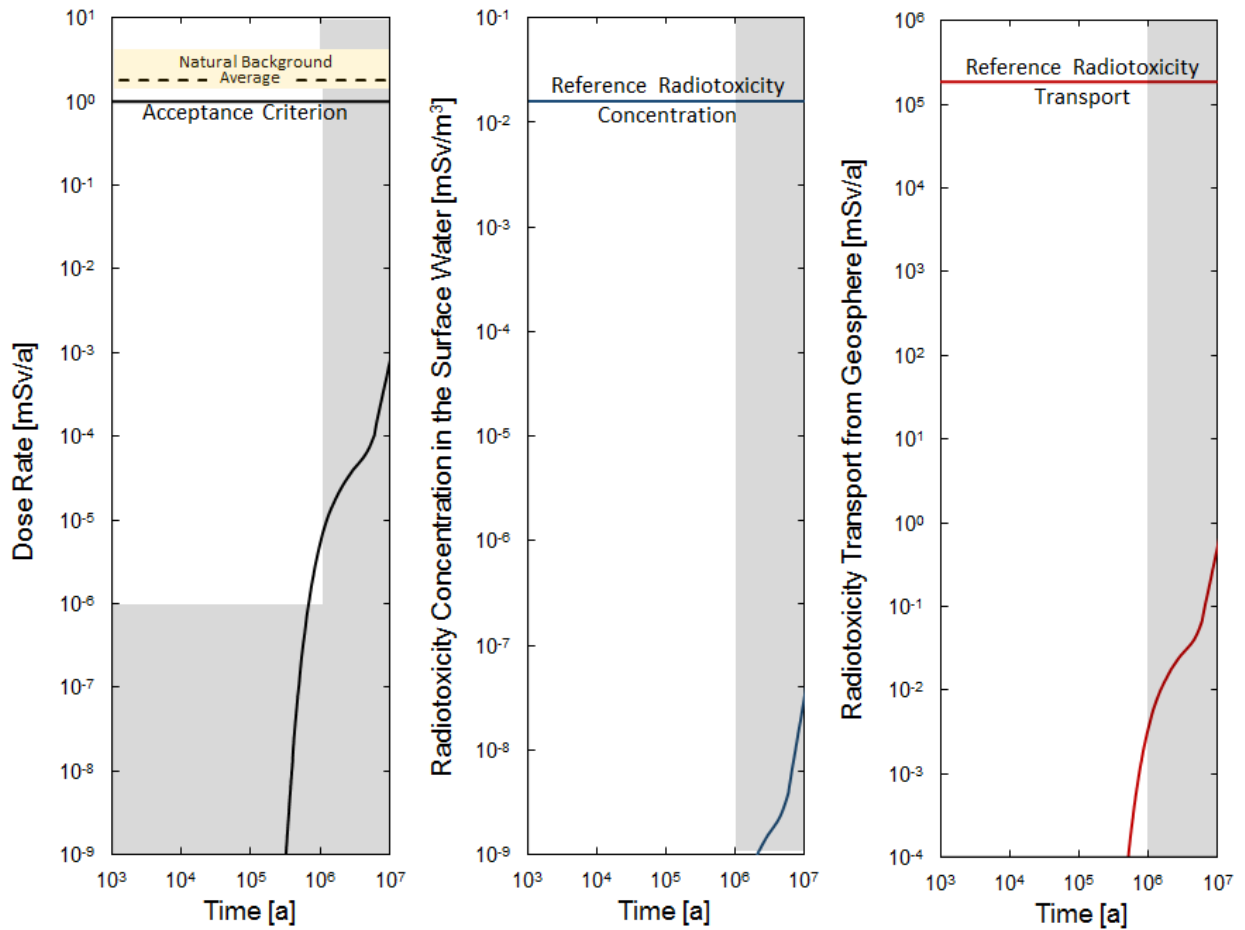


Figure 7-145: System Model: All Containers Fail at 60,000 Years - Results for Indicators

Table 7-56 summarizes the full suite of results for the two complementary indicators, based on simulations run to peak values. Since both indicators are well below their acceptance / reference values shown in Table 7-55, additional confidence is provided that at long times (i.e., when the dose rate indicator is more uncertain) the impacts of the repository are likely to be very small.

Table 7-56: Results for Complementary Indicators

Case	Value	Radiotoxicity Concentration in Surface Water (mSv/m ³)	Radiotoxicity Transport from Geosphere (mSv/a)
-	Reference Indicator Value⁽¹⁾	1.6x10 ⁻²	1.4x10 ⁵
Reference Case	-	0	0
Base Case	1 Ma Value	1.4x10 ⁻¹⁴	2.4x10 ⁻⁷
Probabilistic Container Assumptions Fixed	Median	1.3x10 ⁻¹⁴	3.4x10 ⁻⁷
	95 th Percentile	2.6x10 ⁻¹²	4.3x10 ⁻⁵
	99 th Percentile	1.1x10 ⁻¹¹	1.5x10 ⁻⁴
Probabilistic All Assumptions Varying	Median	3.6x10 ⁻¹⁵	7.3x10 ⁻⁸
	95 th Percentile	1.9x10 ⁻¹²	3.1x10 ⁻⁵
	99 th Percentile	1.2x10 ⁻¹¹	1.7x10 ⁻⁴
All Containers Fail at 60,000 Years	1 Ma Value	2.0x10 ⁻¹³	3.4x10 ⁻³
	Peak Value	2.5x10 ⁻⁷	4.3

Note: (1) from Table 7-55

7.13 Summary and Conclusions

This section summarizes the postclosure safety assessment for liquid-borne contaminant transport.

7.13.1 Scope Overview

The Normal Evolution Scenario represents the normal (or expected) evolution of the site and facility. Disruptive Event Scenarios consider the effects of unlikely events that lead to possible penetration of barriers and abnormal degradation and loss of containment.

Section 7.2 presents the detailed scope of the assessment. Both Normal Evolution and Disruptive Event Scenarios are considered. The cases considered are illustrated in Figure 7-1.

The Reference Case of the Normal Evolution Scenario represents the situation in which all repository components meet their design specification and function as anticipated. As such, the used fuel containers remain intact essentially indefinitely (see Chapter 5) and no contaminant releases occur in the one million year time period of interest to the safety assessment.

Sensitivity studies are performed on the Reference Case to illustrate repository performance for a range of reasonably foreseeable deviations from key assumptions. These deviations arise from components that are unknowingly placed in the repository that either (a) do not meet their design specification or (b) do not fully function as anticipated.

Both deterministic and probabilistic simulations are performed.

The “Base Case” sensitivity study assumes a small number of containers have been fabricated with sizeable defects in their copper coating, and that 10 of these off-specification containers escape detection by the quality assurance program and are unknowingly placed in the repository. The Base Case adopts a number of simplifying and bounding assumptions describing the container failure model, as described in Section 7.2.1.2.

Key assumptions in the Base Case are:

- Geosphere properties as per Chapter 2;
- Used fuel inventories as per Chapter 3;
- Repository design as per Chapter 4;
- 10 containers with large defects in the copper coating are present in the repository. The copper coating is penetrated in the first container at 1000 years, with one additional container failing every 100,000 years;
- No other container failures occur;
- Constant temperate climate and steady-state groundwater flow;
- A self-sufficient farming family is unknowingly living on top of the repository, growing crops and raising livestock;
- Drinking and irrigation water for the family is obtained from a 219 m deep well that penetrates the entire thickness of the Guelph formation. The well / defective container locations are such that contaminant release to the well is maximized;
- The well is pumped at a rate of 1261 m³/a. This is sufficient for drinking water and irrigation of household crops;
- Input parameters with uncertainty and variability represented by probability distributions are set to either the most probable value (when there is one) or to the median value otherwise.

Deterministic sensitivity studies are performed about the Base Case to illustrate the effect of well assumptions, the effect of deviations in barrier performance, the effect of various modelling parameter assumptions, and the effect of glaciation. The full suite of deterministic sensitivity cases is described below:

Cases Illustrating the Effect of Well Assumptions

- No well;
- Intermittent well operation; and
- Random well operation.

The well cases are described in Section 7.2.1.3 and Table 7-4.

Cases Illustrating the Effect of Deviations in Barrier Performance

Fuel Barrier:

- Fuel dissolution rate increased by a factor of 10; and

- Instant release fractions for fuel contaminants set to 0.10 for all contaminants (i.e., 10% of the entire inventory is instantly released).

Zircaloy Sheath Barrier:

No credit is taken in the postclosure safety assessment for the presence of the Zircaloy fuel sheath as a barrier to contaminant release from the fuel. However, because the sheath itself contains contaminants and because the screening analysis (Section 7.6) identifies some of these contaminants as potentially important, the following Zircaloy specific sensitivity cases are simulated:

- Zircaloy dissolution rate increased by a factor of 10; and
- Instant release fractions set to 0.10 for all contaminants.

Container Barrier:

- All 10 containers fail at 1000 years;
- 50 containers fail at 1000 years;
- 50 and 1000 containers fail at 10,000 years;
- Low sorption in the engineered barrier materials with coincident high solubility limits in the container; and
- No solubility limits in the container.

The cases with 50 and 1000 containers illustrate repository performance for a greater assumed number of failed containers. For the two 50 container cases, the first case assumes all containers are clustered in the location that maximizes dose consequence, while the second case assumes the containers are uniformly distributed across the repository. The 1000 container case also assumes the containers are uniformly distributed across the repository.

Buffer and Backfill and Seals Barrier:

- Hydraulic conductivities of all engineered barrier sealing materials in the repository and shaft increased by a factor of 10;
- Low sorption in the engineered barrier sealing materials with coincident high solubility limits in the container;
- Bentonite and geosphere diffusivities increased by a factor of 10 and by a factor of 100;
- I-129 sorption credited in the bentonite and geosphere; and
- No sorption in the engineered sealing materials.

Geosphere Barrier:

- Hydraulic conductivities increased by a factor of 10;
- Hydraulic conductivity in the excavation damaged zones (EDZ) increased by a factor of 10;
- Bentonite and geosphere diffusivities increased by a factor of 10 and by a factor of 100;
- 100 m of surface erosion in one million years;
- I-129 sorption credited in the bentonite and geosphere;

- 150 m overpressure in the Shadow Lake formation; and
- Sorption parameters set to two standard deviations below the mean.

These barrier sensitivity cases are described in Section 7.2.1.4 and Table 7-5.

The Effects of Glaciation

The effects of glaciation is discussed quantitatively based on the analyses by Avis and Calder (2015) and Chen et al. (2017). The glaciation study is described in Section 0.

Probabilistic Studies

For the probabilistic simulations, random sampling is used to simulate 100,000 realizations of the following two cases:

- Number, locations and failure times for defective containers fixed at their Base Case values, with all other available parameters varied; and
- All parameters with probability distributions varied, including the number, locations and failure times for the defective containers.

Parameter values that could affect the groundwater flow distribution are not varied in these simulations.

These cases are described in Section 7.2.1.4 and Table 7-5.

Disruptive Event Scenarios

The Disruptive Event Scenarios examined are described in Section 7.2.2 and Table 7-7. The cases considered are:

- Inadvertent Human Intrusion;
- All Containers Fail at 60,000 Years (with a sensitivity case that has the failure occurring at 10,000 years);
- Repository Seals Failure; and
- Undetected Fault.

Disruptive Event Scenarios are analysed with deterministic models.

Other Calculations

The main focus of the above is on the radiological protection of persons. The following are also addressed for the Base Case and for the All Containers Fail at 60,000 Years Disruptive Event Scenario:

- The radiological protection of the environment; and
- The protection of persons and the environment from hazardous substances.

Finally, results are also generated for two complementary indicators of radiological safety for the Base Case and for the All Containers Fail at 60,000 Years Disruptive Event Scenario.

The effects of gas generation and migration are discussed in Chapter 8.

7.13.2 Result Summary

7.13.2.1 Radiological Protection of Persons

7.13.2.1.1 Normal Evolution Scenario

Table 7-57 presents the result summary for the Normal Evolution Scenario. This table is an amalgam of results in Section 7.7.2 generated with the detailed 3D models (summarized in Table 7-33) and results in Section 7.8.2 generated with the System Model (summarized in Table 7-45). Cases with results in Bq/a have been simulated with the 3D models while cases with results in mSv/a have been simulated with the System Model. Three-dimensional modelling is used for cases that have the potential to affect the groundwater flow distribution because the System Model assumes the groundwater flow field is constant.

Results are shown for the Reference Case, the Base Case sensitivity study, the sensitivity studies performed on the Base Case to illustrate the effects of well assumptions, the sensitivity studies performed on the Base Case to illustrate the effect of deviations in barrier performance, and the sensitivity study performed to illustrate the effects of glaciation. The results at one million years and at peak, as well as the dose ratio (compared to the Base Case) are shown. The factor by which the dose rates are below the 0.3 mSv/a interim acceptance criterion are not shown; however, the Base Case peak result is 250,000 times smaller, and the individual variations for the other cases can be determined using this result. Both deterministic and probabilistic results are included in the table.

A brief discussion of the main results is provided following the table.

Table 7-57: Normal Evolution Result Summary

Case	1 Ma Impact		Peak Impact ⁽¹⁾		Peak Ratio to Base Case
	I-129 (Bq/a)	Dose Rate (mSv/a)	I-129 (Bq/a)	Dose Rate (mSv/a)	
REFERENCE CASE	0	0	0	0	-
Sensitivity Cases					
Base Case (3D Detailed Model) ⁽²⁾	5.5x10 ⁻⁵	-	-	-	-
Base Case (3D Main Model) ⁽²⁾	3.6x10 ⁻⁵	-	3.3	-	-
Base Case (System Model)	2.2x10 ⁻³	5.9x10 ⁻¹⁰	4.6	1.2x10 ⁻⁶	-
Sensitivity Cases for Well Model					
Base Case – No Well	-	0.0	-	6.6x10 ⁻¹⁰	1/1800
Base Case – Intermittent Well	With 5000 years of well operation beginning at one million years, the peak I-129 transport to the well is 3.3x10 ⁻⁴ Bq/a, which is 9 times the Base Case value (3.6x10 ⁻⁵ Bq/a)				
Base Case – Random Well	Could be many orders of magnitude less than the Base Case depending on the well location				
Sensitivity Cases Illustrating the Effect of Deviations in Barrier Performance on the Base Case					
Fuel Barrier Sensitivity					
Fuel Dissolution Rate Increased by a Factor of 10	-	3.3x10 ⁻⁹	-	1.6x10 ⁻⁶	1.3
Fuel Instant Release Fractions Set to 10%	-	9.5x10 ⁻¹⁰	-	1.3x10 ⁻⁶	1.1
Zircaloy Sheath Barrier Sensitivity⁽³⁾					
Zircaloy Dissolution Rate Increased by a Factor of 10	-	5.9x10 ⁻¹⁰	-	1.2x10 ⁻⁶	1.0
Zircaloy Instant Release Fractions Set to 10%	-	5.9x10 ⁻¹⁰	-	1.2x10 ⁻⁶	1.0
Container Barrier Sensitivity					
All 10 Containers Fail at 1000 Years	-	2.4x10 ⁻⁹	-	1.3x10 ⁻⁶	1.1
50 Containers Fail at 1000 Years, all in worst location	-	1.2x10 ⁻⁸	-	6.5x10 ⁻⁶	5.4
50 Containers Fail at 10,000 Years, uniform distribution	-	8.7x10 ⁻⁹	-	4.6x10 ⁻⁶	3.8
1000 Containers Fail at 10,000 Years, uniform distribution	-	1.7x10 ⁻⁷	-	9.2x10 ⁻⁵	77
Low Sorption in the EBS With Coincident High Solubility Limits in the Container	-	5.9x10 ⁻¹⁰	-	1.2x10 ⁻⁶	1.0

Postclosure Safety Assessment of a Used Fuel Repository in Sedimentary Rock

Document Number: NWMO-TR-2018-08

Revision: 000

Class: Public

Page: 573

Case	1 Ma Impact		Peak Impact ⁽¹⁾		Peak Ratio to Base Case
	I-129 (Bq/a)	Dose Rate (mSv/a)	I-129 (Bq/a)	Dose Rate (mSv/a)	
No Solubility Limits in the Container	-	5.9x10 ⁻¹⁰	-	1.2x10 ⁻⁶	1.0
Buffer, Backfill and Seal Barrier Sensitivity					
EBS Hydraulic Conductivity Increased by a Factor of 10	5.0x10 ⁻⁴	-	3.7	-	1.1
Low Sorption in the EBS With Coincident High Solubility Limits in the Container	-	5.9x10 ⁻¹⁰	-	1.2x10 ⁻⁶	1.0
Ten Times Higher Bentonite and Geosphere Diffusivity Coefficients	-	2.0x10 ⁻⁷	-	1.7x10 ⁻⁵	14
I-129 Sorption Credited in Bentonite and Geosphere	-	2.3x10 ⁻¹⁰	-	6.7x10 ⁻⁷	0.54
No Sorption in the Near Field	-	5.9x10 ⁻¹⁰	-	1.2x10 ⁻⁶	1.0
Geosphere Barrier					
Rock Hydraulic Conductivity Increased by a Factor of 10	5.4x10 ⁻⁵	-	2.2	-	0.67 ⁽⁴⁾
EDZ Hydraulic Conductivity Increased by a Factor of 10	4.0x10 ⁻⁴	-	3.7	-	1.1
100 m Erosion estimated same as Base Case	3.6x10 ⁻⁵	-	3.3	-	1.0
150 m Overpressure in Shadow Lake Formation	2.1x10 ⁻³	-	5.0	-	1.5
Two Sigma (Low) Sorption in the Geosphere	-	5.9x10 ⁻¹⁰	-	1.2x10 ⁻⁶	1.0
Ten Times Higher Bentonite and Geosphere Diffusivity Coefficients	-	2.0x10 ⁻⁷	-	1.7x10 ⁻⁵	14
I-129 Sorption Credited in Bentonite and Geosphere	-	2.3x10 ⁻¹⁰	-	8.1x10 ⁻⁷	0.68
Glaciation Sensitivity					
Glaciation Case	Could be up to 100 times greater than temperate climate case if a deep well is established after a glacial period				
Probabilistic Sensitivity					
Container Assumptions Fixed (95 th Percentile)	1.3x10 ⁻⁷				
All Assumptions Vary (95 th Percentile)	9.3x10 ⁻⁸				

Notes: (1) The 1 Ma and peak impacts are determined from simulations performed with either the 3D models or the System Model. The 3D models do not include biosphere and dose representations and therefore results are presented for I-129 transport to the well. This is a reasonable surrogate for dose because System Model

simulations show that I-129 transport to the well is effectively the only dose contributor. The peak values are the highest values reached by extending the simulation time beyond one million years.

(2) Two 3D repository scale models are used – the Detailed Transport Model and the Main Transport Model. The Detailed Model contains more detail but takes longer to run. Results from the two models compare well, with I-129 transport to the well being essentially the same.

(3) As discussed in Section 7.2.1.4, no credit is taken for the fuel sheath acting as a barrier to prevent the fuel from coming into contact with water.

(4) The well is in the same location as the Base Case. Repositioning the well would likely result in a greater consequence.

Deterministic Results

The dose rate is zero for the Reference Case.

For the other cases, the results show that I-129 is essentially the only dose contributor. This is because I-129 has a sizeable initial inventory, a non-zero instant release fraction, a very long half-life, no solubility limit, is non-sorbing in the buffer, backfill and geosphere and has a radiological impact on humans. All other fission products and actinides either decay away, or are released very slowly as the fuel dissolves and are thereafter sorbed in the engineered barriers and geosphere.

For the Base Case, the dose rate in one million years is 5.9×10^{-10} mSv/a. Due to the low permeability of the host rock, almost all the radionuclides remain confined within the repository and surrounding host rock. If the simulations are continued assuming constant geosphere, then the calculated peak dose rate is 1.2×10^{-6} mSv/a, occurring after one million years. This long time frame reflects the I-129 half-life. These results are far below the 0.3 mSv/a interim dose rate acceptance criterion established in Section 7.1.1 for the radiological protection of persons.

The sensitivity cases show that the well assumptions used in the Base Case are generally conservative. If no well is present or if the well happens to be located distant from the defective containers, then the dose rate could be many orders of magnitude lower.

These sensitivity cases also show that if the well is established at a much later time, the peak dose rate can be transiently higher than that with a continuously operating well. This increase occurs due to accumulation of the I-129 in the very slow moving Guelph aquifer, with the value decreasing if the well continues to operate as equilibrium conditions are established.

Of the remaining sensitivity cases illustrating the effect of deviations in barrier performance, only one has the potential of increasing the dose rate appreciably. This case (Ten Time Higher Bentonite and Geosphere Diffusivity Coefficients) increases the peak dose rate by a factor of 14 times as compared to the Base Case. This is not surprising given the dominance of diffusive transport in this geosphere.

On the other side, crediting a small amount of I-129 sorption causes the peak dose rate to decrease by a factor of 1.8.

For the cases with 50 and 1000 failed containers, the dose rate could be higher as would be expected because of the greater radionuclide source term; however, the actual dose would depend on where the failed containers are located in the repository with respect to the well, and whether or not a well is even present. For the 1000 failed container case considered here, an

increase of 77 times the dose rate of the Base Case resulted. This is a factor of about 3,300 times below the interim dose rate acceptance criterion.

The Glaciation Sensitivity shows the stability of the geosphere, with very little effect on contaminant movement in the host rock. The push and pull of transient ice sheet coverage does enhance release of small amounts from the host rock into the Guelph formation, such that a transient potential dose increase of about 100 times could occur. This is also caused by an effect similar to that examined in the Intermittent Well sensitivity case where contaminants accumulate within the slowly moving groundwater in the Guelph formation in the absence of a pumping well. In the glacial scenario, there is no well and no pumping during the period of ice sheet coverage, so there can be accumulation into the Guelph formation.

Probabilistic Results

The probabilistic cases examine the effect of simultaneous variation in multiple parameters.

The first case, in which the number, location and failure times of the defective containers are fixed at the same values as in the Base Case with all other available parameters varied, gives a measure of the overall uncertainty in the Base Case. The 95th percentile 1 Ma dose rate emerging from 100,000 simulations is 1.3×10^{-7} mSv/a or 2,300,000 times less than the interim dose rate criterion of 0.3 mSv/a. Extending the simulation time beyond one million years, the 95th percentile peak dose rate is 3.4×10^{-5} mSv/a, which is well below the interim dose rate criterion.

The second probabilistic case, in which all parameters represented by probability distributions are varied, including the number, location and failure times of defective containers results in a 95th percentile 1 Ma dose rate emerging from 100,000 simulations of 9.3×10^{-8} mSv/a, a value 3,200,000 times less the interim dose rate criterion. Extending the simulation time beyond one million years, the 95th percentile peak dose rate is 1.45×10^{-5} mSv/a, which is well below the interim dose rate criterion.

7.13.2.1.2 Disruptive Event Scenarios

Table 7-58 presents summary results from Section 7.9 for the All Containers Fail Disruptive Event Scenario, the Repository Seals Failure Disruptive Event Scenario, and the Undetected Fault Disruptive Event Scenario and compares them against the 1.0 mSv/a interim dose rate acceptance criterion for Disruptive Event Scenarios. Key features to note are:

- Both the All Containers Fail at 60,000 Years and the All Containers Fail at 10,000 Years cases result in a peak dose rate of 0.01 mSv/a. These results are below the interim dose rate acceptance criterion.
- The Repository Seals Failure Scenario has a small effect (increase of about 1.4 times) on the peak impact as compared to the Base Case, and would remain well below the interim dose rate criterion.
- The peak impact for the Undetected Fault Scenarios increases, with I-129 transport for the 100 m offset case being about 22 times higher than that for the Base Case. Even with this increase, the inferred dose rate would still be well below the interim dose rate acceptance criterion.

Table 7-58: Disruptive Event Scenarios Result Summary

Case	1 Ma Impact ⁽¹⁾		Peak Impact ⁽¹⁾	
	I-129 (Bq/a)	Dose Rate (mSv/a)	I-129 (Bq/a)	Dose Rate (mSv/a)
REFERENCE CASE	0	0	0	0
Base Case (3D Main Model)	3.6x10 ⁻⁵	-	3.3	
Base Case (System Model)	2.2x10 ⁻³	5.9x10 ⁻¹⁰	4.6	1.2x10 ⁻⁶
Disruptive Event Scenarios				
All Containers Fail at 60,000 Years (3D Model)	0.21	-	22,700	-
All Containers Fail at 60,000 Years (System Model)	31	8.4x10 ⁻⁶	39,400	0.01
All Containers Fail at 10,000 Years (System Model)	51	1.4x10 ⁻⁵	39,900	0.01
Repository Shaft Seals Failure	0.37	-	4.6	-
Undetected Fault (100 m offset) EPM	10	-	73	-
Undetected Fault (500 m offset)	-	-	-	-

Note: (1) The 1 Ma and peak impacts are determined from simulations performed with either the 3D models or the System Model. The 3D models do not include biosphere and dose representations and therefore results are presented for I-129 transport to the well. This is a reasonable surrogate for dose because System Model simulations show that I-129 transport to the well is effectively the only dose contributor.

The peak values are the highest values reached by extending the simulation time beyond one million years.

Section 7.9.1 presents a stylized analysis for the Inadvertent Human Intrusion Scenario. This scenario is not included in Table 7-58 because it is a special case, as recognized in CNSC REGDOC-2.11.1, Volume III (CNSC 2018). The assumed intrusion bypasses all barriers, and therefore dose consequence may exceed the regulatory limit.

The risk of inadvertent human intrusion is minimized by placing the used fuel deep underground in a location with no viable mineral resources and no potable groundwater resources, and by the use of markers and institutional controls.

Three illustrative human intrusion cases are considered, as follows:

Scenario 1: Drilling operations take place for two days after the intrusion event, at which point the Drill Crew becomes aware of the hazard (e.g. through borehole logging or evaluation of results), ceases operations and vacates the site. The site is then remediated. Any future person living at the site would be unaffected.

Scenario 2: Drilling operations continue for 14 working days, at which point the Drill Crew vacates the site without identifying the hazard. Drilling debris deposited on the surface around

the drill site (inconsistent with current regulations) remains in place without remediation. A Site Resident is assumed to live at the contaminated site immediately after the intrusion, and grows food on the contaminated soil.

Scenario 3: Scenario 3 is the same as Scenario 1, except that a higher fuel burnup is assumed (i.e., 280 MWh/kgU instead of 220 MWh/kgU).

The results are summarized in Table 7-59 for intrusion at 300 years. The values decrease over time.

The likelihood of this event occurring cannot be accurately determined; however, Section 7.9.1 shows that based on simple estimates of deep drilling rates, a risk to the Resident of about 10^{-6} per annum can be estimated. This is below the risk target of 10^{-5} per annum identified in Section 7.1.1.

Table 7-59: Inadvertent Human Intrusion Dose Summary for Intrusion at 300 years

Scenario Number	Maximum Dose to Drill Crew (mSv)	Maximum Dose Rate to Site Resident (mSv/a)
1	90	0
2	590	580
3	110	0

7.13.2.2 Radiological Protection of the Environment

Section 7.10 describes the modelling and results obtained for the assessment of the radiological protection of the environment. The results are compared against both the screening criterion and the interim acceptance criteria established in Section 7.1.3. The Normal Evolution Base Case and the All Containers Fail at 60,000 Years Disruptive Event Scenario are considered.

Table 7-48 shows the peak dose rates to non-human biota computed using both the Concentration Ratio approach and the Transfer Factor approach are all many orders of magnitude below the screening criterion of $10 \mu\text{Gy/h}$.

For added context, Figure 7-137 shows the “Tier 1 Quotients” for the All Containers Fail at 60,000 Years Disruptive Event Scenario, formed by dividing the dose rates in Table 7-48 by the appropriate Tier 1 Interim Acceptance Criteria. The highest quotient value is 3.3×10^{-9} for the white tailed deer.

Based on this, it can be concluded that there is no concern about adverse environment impacts associated with the potential release of radioactive contaminants from the repository.

7.13.2.3 Protection of Persons and the Environment from Hazardous Substances

Section 7.11 describes the modelling and results for the assessment of the non-radiological impact of the repository on persons and the environment. Copper is also assessed due to the amount of copper associated with the large number of containers in the repository. The results

are compared against the interim acceptance criteria established in Section 7.1.2 and Section 7.1.4.

The Section 7.11 results are expressed in terms of a “Concentration Quotient”, where this is the ratio formed by dividing the concentrations in specific environmental media by the applicable interim acceptance criterion.

Table 7-49 shows the 1 Ma Concentration Quotients for the Base Case. The single greatest value is 5.4×10^{-9} for Ru in soil. Wide margins are available to the interim acceptance criteria.

Table 7-50 shows the 1 Ma Concentration Quotients for the All Containers Fail Disruptive Event Scenario. As expected, the quotients are higher than in the Base Case due to the significantly greater source term, with the single greatest value being 8.3×10^{-5} for Ru in soil.

If simulations are extended to peak, the highest overall peak concentration ratios for the Base Case and All Containers Fail cases are 6.85×10^{-5} and 0.74 respectively for Ru in soil.

Based on these results, it is concluded that the repository would not pose a non-radiological health and safety hazard to persons or to the environment for contaminants released from the used fuel bundles.

7.13.2.4 Complementary Indicators

Section 7.12 presents the modelling and results for two complementary indicators.

These indicators (i.e., radiotoxicity concentration in a water body and radiotoxicity transport from the geosphere) supplement the dose rate indicator using system characteristics that are much less sensitive to assumptions regarding the biosphere and human behaviour.

Results for the Base Case are shown in Figure 7-144 and results for the All Containers Fail at 60,000 Years Disruptive Event Scenario are shown in Figure 7-145. Table 7-56 summarizes the full set of results, including the two probabilistic assessments of the indicators.

Both indicators are well below their acceptance / reference values (Table 7-55), thereby providing additional confidence that at long times (i.e., when the dose rate indicator is more uncertain) the impacts of the repository are likely to be very small.

7.13.3 Conclusion

This postclosure safety assessment shows, for the Normal Evolution Scenario (and associated sensitivity cases), as well as for the analysed Disruptive Event Scenarios (excluding Inadvertent Human Intrusion), that all radiological and non-radiological interim acceptance criteria are met during the postclosure period.

For the Inadvertent Human Intrusion Scenario, significant doses to the drill crew and significant dose rates to a site resident may occur. However the repository is sited and designed, and controls and markers initiated, to make the likelihood of this scenario very low. This meets the risk requirement identified for this special scenario.

Figure 7-146 shows the dose rates for the Reference Case, the Normal Evolution Base Case, and the All Containers Fail after 60,000 Years Disruptive Event Scenario.

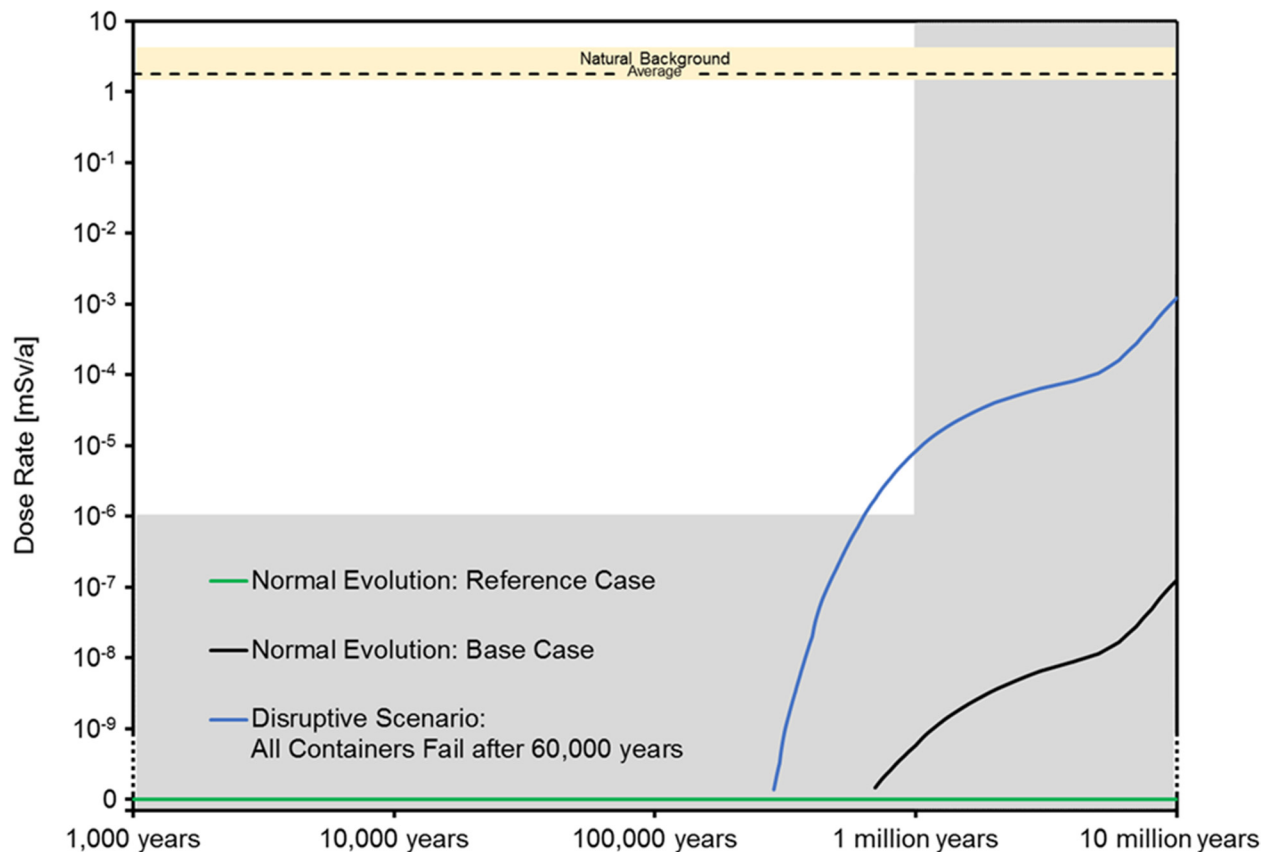


Figure 7-146: Dose Rate Result Summary

7.14 References for Chapter 7

Amiro, B.D. 1992. Baseline concentrations of nuclear fuel waste nuclides in the environment. Atomic Energy of Canada Limited, AECL10454, COG 91231. Pinawa, Canada.

Amiro, B.D. 1993. Protection of the environment from nuclear fuel waste radionuclides: a framework using environmental increments. *Science of the Total Environment* 128: 157-89.

Andersson, P., K. Beaugelin-Seiller, N.A. Beresford, D. Copplestone, C. Della Vedova, J. Garnier-Laplace, B. J. Howard, P. Howe, D.H. Oughton, C. Wells, P. Whitehouse. 2008. Deliverable 5: Numerical benchmarks for protecting biota from radiation in the environment: proposed levels, underlying reasoning and recommendations. PROTECT. Stockholm, Sweden.

- Avis, J. and N. Calder. 2015. Modelling of the Fifth Case Study Glaciation and Erosion Scenarios. Nuclear Waste Management Organization Report NWMO-TR-2015-14. Toronto, Canada.
- Becker, D.-A., D. Buhmann, R. Storck, J. Alonso, J.-L. Cormenzana, M. Hugi, F. van Gemert, P. O'Sullivan, A. Laciok, J. Marivoet, x. Sillen, H. Nordman, T. Vieno and M. Niemeyer. 2002. Testing of Safety and Performance Indicators (SPIN). European Commission Report FIKW-CT2000-00081. European Commission, Brussels, Belgium.
- Berger, A. and M.F. Loutre. 2002. An exceptionally long interglacial ahead? *Science* 297, 1287-1288.
- Brown, J.E., B. Alfonso, R. Avila, N.A. Beresford, D. Copplestone, G. Pröhl and A. Ulanovsky. 2008. The ERICA Tool. *J. Environ. Radioactivity* 99: 1371-1383.
- Carbol, P., J. Cobos-Sabate, J-P. Glatz, C. Ronchi, V. Rondinella, D.H. Wegen, T. Wiss, A. Loida, V. Metz, B. Kienzler, K. Spahiu, B. Grambow, J. Quinones, A. Martinez Esparza Valiente. 2005. The effect of dissolved hydrogen on the dissolution of ²³³U-doped UO₂ (s), high burn-up spent fuel and MOx fuel. Swedish Nuclear Fuel and Waste Management Company Technical Report TR-05-09. Stockholm, Sweden.
- Chen, J., J. Avis and N. Calder. 2017. Effects of glaciation on radionuclide transport in sedimentary rocks. Proc. Int. High-Level Radioactive Waste Management Conf, Charlotte, North Carolina, April 9 – 13, American Nuclear Society.
- CNSC. 2011. Setting Radiation Requirements on the Basis of Sound Science: The Role of Epidemiology. Canadian Nuclear Safety Commission, INFO-0812. Ottawa, Canada.
- CNSC. 2013. Linear-Non-Threshold Model Fact Sheet. Canadian Nuclear Safety Commission. Ottawa, Canada. Available online: <http://nuclearsafety.gc.ca/eng/pdfs/reading-room/healthstudies/Fact-Sheet-Linear-Non-Threshold-Model-2013.pdf>
- CNSC. 2018. Regulatory Document REGDOC-2.11.1 Volume III: Assessing the Long-Term Safety of Radioactive Waste Management. Canadian Nuclear Safety Commission. Ottawa, Canada.
- CSA. 2014. Guidelines for Calculating Derived Release Limits for Radioactive Material in Airborne and Liquid Effluents for Normal Operation of Nuclear Facilities. Canadian Standards Association N288.1-14. Toronto, Canada.
- Curti E. and P. Wersin. 2002. Assessment of Porewater Chemistry in the Bentonite Backfill for the Swiss SF/HLW Repository. Nagra Technical Report 02-09. Wetingen, Switzerland.
- DiCiccio, T.J. and B. Efron. 1996. Bootstrap Confidence Intervals. *Statistical Science* Volume 11(3), 189-228.
- DOE. 2008. Final Supplemental Environmental Impact Statement for a Geologic Repository for the Disposal of Spent Nuclear Fuel and High-Level Radioactive Waste at Yucca Mountain. US Department of Energy Report DOE/EIS-0250F-S1. Nevada, USA.

- Duro, L., V. Montoya, E. Colàs and D. García. 2010. Groundwater equilibration and radionuclide solubility calculations. Nuclear Waste Management Organization Report NWMO TR-2010-02. Toronto, Canada.
- Eckerman, K.F. and R.W. Leggett. 1996. DCFPAK: Dose coefficients data file package for Sandia National Laboratory. Oak Ridge National Laboratory report ORNL/TM-13347. Oak Ridge, USA.
- Ferry, C., J.-P. Piron, A. Poulesquen, and C. Poinssot. 2008. Radionuclides Release from the Spent Fuel under Disposal Conditions: Re-evaluation of the instant release fraction. Material Research Society Symposium Proceedings 1107, 447-454.
- Garisto, F. 1989. The Energy Spectrum of α -particles Emitted from Used CANDU Fuel, Annals of Nuclear Energy 16. 33-38.
- Garisto, F. 2001. Radionuclide Screening Model (RSM) Version 1.1 Verification and Validation. Ontario Power Generation Report 06819-REP-01300-10029-R00. Toronto, Canada.
- Garisto, F., J. Avis, N. Calder, A. D'Anrea, P. Gierszewski, C. Kitson, T. Melnyk, K. Wei and L. Wojciechowski. 2004. Third Case Study – Defective Container Scenario. Ontario Power Generation Report 06819-REP-01200-10126-R00. Toronto Canada.
- Garisto, F. and M. Gobien. 2013. SYVAC3-CC4 Verification and Validation Summary. Nuclear Waste Management Organization Report NWMO TR-2013-14. Toronto, Canada.
- Garisto, N.G., Z. Eslami and F. Bhesania. 2005. Alternative Exposure Groups, Characteristics and Data for the Post-Closure Safety Assessment of a Deep Geological Repository. Ontario Power Generation Report 06819-REP-01200-10150-R00. Toronto Canada.
- Garisto, N.G., F. Copper and S.L. Fernandes. 2008. Non-Effect Concentrations for Screening Assessment of Radiological Impacts on Non-Human Biota. Nuclear Waste Management Organization Report NWMO TR-2008-02. Toronto, Canada.
- Garnier-Laplace, J., R. Gilbin, A. Agüero, F. Alonzo, M. Björk, Ph. Ciffroy, D. Copplestone, M. Gilek, T. Hertel-Aas, A. Jaworska, C-M. Larsson, D. Oughton and I. Zinger. 2006. Deliverable 5: Derivation of Predicted-No-Effect-Dose-Rate values for ecosystems (and their sub-organisational levels) exposure to radioactive substances. ERICA.
- Gobien, M., and F. Garisto. 2012. Data for Radionuclide and Chemical Element Screening. Nuclear Waste Management Organization Report NWMO TR-2012-11. Toronto, Canada.
- Gobien, M., F. Garisto, E. Kremer and C. Medri. 2018. Seventh Case Study: Reference Data and Codes. Nuclear Waste Management Organization Report NWMO-TR-2018-10. Toronto, Canada.
- Goodwin, B.W., P. Gierszewski and F. Garisto. 2001. Radionuclide Screening Model (RSM) Version 1.1 - Theory. Ontario Power Generation Report 06819-REP-01200-10045-R00. Toronto, Canada.

- Grambow, B., J. Bruno, L. Duro, J. Merino, A. Tamayo, C. Martin, G. Pepin, S. Schumacher, O. Smidt, C. Ferry, C. Jegou, J. Quiñones, E. Iglesias, N. Rodriguez Villagra, J. M. Nieto, A. Martínez-Esparza, A. Loida, V. Metz, B. Kienzler, G. Bracke (GRS), D. Pellegrini, G. Mathieu, V. Wasselin-Trupin, C. Serres, D. Wegen, M. Jonsson, L. Johnson, K. Lemmens, J. Liu, K. Spahiu, E. Ekeroth, I. Casas, J. de Pablo, C. Watson, P. Robinson, and D. Hodgkinson. 2010. MICADO Model Uncertainty for the Mechanism of Dissolution of Spent Fuel in Nuclear Waste Repository. European Commission Report EUR 24597 EN. Brussels, Belgium.
- Gras, J.M. 2014. State of the art of ¹⁴C in Zircaloy and Zr alloys – ¹⁴C release from zirconium alloy hulls. Carbon-14 Source Term (CAST) Report CAST-2014-D.3.1.
- Grasty, R.L. and J.R. LaMarre. 2004. The Annual Effective Dose from Natural Sources of Ionising Radiation in Canada. Radiation Protection Dosimetry 108, No 3, 215-226.
- Guo, R. 2015. Thermal Modelling of a Mark II Container. Nuclear Waste Management Organization Report NWMO-TR-2015-06. Toronto, Canada.
- Guo, R. 2018. Thermal Response of a Conceptual Deep Geological Repository in Sedimentary Rock. Nuclear Waste Management Organization Report NWMO-TR-2018-09. Toronto, Canada.
- Hallet, B. 2011. Glacial Erosion Assessment. Nuclear Waste Management Organization Report NWMO DGR-TR-2011-18. Toronto, Canada.
- Health Canada. 2010. Part IV Guidance on Human Health Detailed Quantitative Radiological Risk Assessment. Ottawa, Canada.
- Hermann, O.W. and R.M. Westfall. 1995. ORIGEN-S - SCALE System Module to Calculate Fuel Depletion, Actinide Transmutation, Fission Product Buildup and Decay, and Associated Radiation Source Terms. In: SCALE: A Modular Code System for Performing Standardized Computer Analyses for Licensing Evaluations. Oak-Ridge National Laboratory NUREG/CR-0200, Rev.4 (ORNL/NUREG/CSD-2/R4) Volume II, Part I. Oak-Ridge, USA.
- IAEA. 2002. Safety Indicators for the Safety Assessment of Radioactive Waste Disposal. International Atomic Energy Agency TECDOC-1372. Vienna, Austria.
- IAEA. 2006. Safety Requirements: Geological Disposal of Radioactive Waste. International Atomic Energy Agency Safety Requirements WS-R-4. Vienna, Austria.
- ICRP. 1991. 1990 Recommendations of the International Commission on Radiological Protection. International Commission on Radiological Protection Publication 60, Annals of the ICRP 21(1-3). Vienna, Austria.
- ICRP. 1995. Age-dependent Doses to the Members of the Public from Intake of Radionuclides - Part 5 Compilation of Ingestion and Inhalation Coefficients. International Commission on Radiological Protection Publication 72, Annals of the ICRP 26(1). Vienna, Austria.

- ICRP. 2007. The 2007 Recommendations of the International Commission on Radiological Protection. International Commission on Radiological Protection Publication 103, Annals of the ICRP (W2-4). Vienna, Austria.
- ICRP. 2008. Environmental Protection: the Concept and Use of Reference Animals and Plants. ICRP Publication 108. Vienna, Austria.
- ICRP. 2013. Radiological Protection in Geological Disposal of Long-lived Solid Radioactive Waste. International Commission on Radiological Protection Publication 122, Annals of the ICRP 42(3). Vienna, Austria.
- Jackson, D, K. Smith and M.D. Wood. 2014. Demonstrating Compliance with Protection Objectives for Non-Human Biota within Post-closure Safety Cases for Radioactive Waste Repositories. J. Env. Rad. 133, 60-68.
- JNC. 2000. H12: Project to Establish the Scientific and Technical Basis for HLW in Japan. Supporting Report 3, Safety Assessment of the Geological Disposal System. Japan Nuclear Cycle Development Institute JNC TN1410 2000-004. Tokai, Japan.
- Kitson C.I., T.W. Melnyk, L.C. Wojciechowski, T. Chshyolkova. 2012. SYVAC3-CC4 User Manual, Version SCC409. Nuclear Waste Management Organization Report NWMO TR-2012-21. Toronto, Canada.
- Liu, N., L. Wu, Z. Qin and D.W. Shoesmith. 2016. Roles of radiolytic and externally generated H₂ in the corrosion of fractured spent nuclear fuel. Environ. Sci. Technol. 50 (22), 12348-12344.
- McCauley, C.A., D.M. White, M.R. Lilly and D.M. Nyman. 2002. A comparison of hydraulic conductivities, permeabilities and infiltration rates in frozen and unfrozen soils. Cold Regions Science and Technology 34(2), 117–125.
- Medri, C. 2015a. Human Intrusion Model for the Mark II Container in Crystalline and Sedimentary Rock Environments: HIMv2.1. Nuclear Waste Management Organization Report NWMO-TR-2015-04. Toronto, Canada.
- Medri, C. 2015b. Non-Radiological Interim Acceptance Criteria for the Protection of Persons and the Environment. Nuclear Waste Management Organization Report NWMO-TR-2015-03. Toronto, Canada.
- Medri, C. and G.Bird. 2015. Non-Human Biota Dose Assessment Equations and Data. Nuclear Waste Management Organization Report NWMO TR-2014-02 R001. Toronto, Canada.
- Muurinen, A. and J. Lehtikoinen. 1999. Porewater chemistry in compacted bentonite. Engineering Geology 54, 207-214.
- Nagra. 2002. Project Opalinus Clay: Safety Report, Demonstration of the Disposal Feasibility for Spent Fuel, Vitrified HLW and Long-lived ILW. Nagra Technical Report 02-05. Wettingen, Switzerland.

- Neuzil, C. 2003. Hydromechanical coupling in geological processes. *Hydrogeology Journal*, 11, 41-83.
- Normani, S.D. 2009. Paleoevolution of pore fluids in glaciated geologic settings. Ph.D. Thesis, University of Waterloo, Department of Civil Engineering. Waterloo, Canada.
- NRC. 2006. Health Risks from Exposure to Low Levels of Ionizing Radiation: BEIR VII Phase 2. Committee on the Biological Effects of Ionizing Radiations (BEIR). The National Academies Press, Washington, DC, USA.
- NWMO. 2012. SYVAC3-CC4 Theory, Version SCC409. Nuclear Waste Management Organization Report NWMO TR-2012-22. Toronto, Canada.
- Parkhurst, D.L. and C.A.J. Appelo. 1999. User's Guide to PHREEQC (Version 2) – A Computer Program for Speciation, Batch-Reaction, One-Dimensional Transport, and Inverse Geochemical Calculations. U.S Department of the Interior and U.S. Geological Survey Water-Resources Investigations Report 99-4259. Denver, USA.
- Peltier, W.R. 2011. Long-term Climate Change. Nuclear Waste Management Organization Report NWMO DGR-TR-2011-14. Toronto, Canada.
- Posiva Oy. 2014. Safety Case for the Disposal of Spent Nuclear Fuel at Olkiluoto Radionuclide Transport and Dose Assessment for Humans in the Biosphere Assessment BSA-2012. POSIVA 2012-31. Eurajoki, Finland.
- Quintessa, Geofirma and SENES. 2011. Postclosure Safety Assessment Report. Quintessa Ltd., Geofirma Engineering Ltd. and SENES Consultants Ltd. report for the Nuclear Waste Management Organization NWMO DGR-TR-2011-25. Toronto, Canada.
- Razdan, M. and D.W. Shoesmith. 2015. The influence of hydrogen peroxide and hydrogen on the corrosion of simulated nuclear fuel. *Faraday Discussions* 180, 283-299.
- Rollin, S., K. Spahiu and U.-B. Eklund. 2001. Determination of dissolution rates of spent fuel in carbonate solutions under different redox conditions with flow-through experiments. *J. Nucl. Mat.* 297, 231-243.
- Rudnick R.L. and S. Gao. 2014. Composition of the Continental Crust. *Treatise on Geochemistry* 2nd Edition. Volume 3, 1-64, Elsevier, New York. New York, USA.
- Sheppard, S.C., M.I. Sheppard and B. Sanipelli. 2011a. Review of Environmental Radioactivity in Canada. Nuclear Waste Management Organization Report NWMO TR-2011-17. Toronto, Canada.
- Sheppard, S.C. and B. Sanipelli. 2011b. Environmental Radioactivity in Canada - Measurements. Nuclear Waste Management Organization Report NWMO TR-2011-16. Toronto, Canada.
- Shoesmith, S. and D. Zagidulin. 2010. The Corrosion of Zirconium under Deep Geological Repository Conditions. Nuclear Waste Management Organization Report NWMO TR-2010-19. Toronto, Canada.

- SKB. 1998. Design Premises for Canister for Spent Nuclear Fuel. Swedish Nuclear and Waste Management Company Technical Report TR-98-08. Stockholm, Sweden.
- SKB. 2010a. Handling of future human actions in the safety assessment SR-Site. Swedish Nuclear and Waste Management Company Technical Report TR-10-53. Stockholm, Sweden.
- SKB. 2010b. Design, Production and Initial State of the Canister. Swedish Nuclear and Waste Management Company Technical Report TR-10-14. Stockholm, Sweden.
- Smith, H.D. and D.L. Baldwin. 1993. An investigation of thermal release of carbon-14 from PWR Zircaloy spent fuel cladding. J. Nucl. Mat. 200, 128-137.
- SKB. 2014. Handling of future human actions in the safety assessment SR-PSU. Swedish Nuclear Fuel and Waste Management Company Report SKB TR-14-08. Stockholm, Sweden.
- Tait, J.C., I.C. Gauld and A.H. Kerr. 1995. Validation of the ORIGEN-S Code for Predicting Radionuclide Inventories in Used CANDU Fuel. J. Nucl. Mat. 223, 109-121.
- Therrien, R., R.G. McLaren, E.A. Sudicky, S.M. Panday and V. Guvanase. 2010. FRAC3DVS-OPG: A Three-Dimensional Numerical Model Describing Subsurface Flow and Solute Transport. User's Guide, Groundwater Simulations Group, University of Waterloo. Waterloo, Canada.
- Vilks, P. and T. Yang. 2018. Sorption of Selected Radionuclides on Sedimentary Rocks in Saline Conditions – Updated Sorption Values. Nuclear Waste Management Organization Report NWMO-TR-2018-03. Toronto, Canada.
- Wu, L., N. Liu, Z. Qin and D.W. Shoesmith. 2014. Modeling the radiolytic corrosion of fractured nuclear fuel under permanent disposal conditions. J. Electrochem. Soc. 161, E3259-E3266
- Yamaguchi, I., S. Tanuma, I. Yasutomi, T. Nakayama, H. Tanabe, K. Katsurai, W. Kawamura, K. Maeda, H. Katao and M. Saigusa. 1999. A study on chemical forms and migration behaviour of radionuclides in hull wastes. In ICM'99 Conference Proceedings, Nagoya, Japan, Sept. 26-30. American Society of Mechanical Engineers. New York, USA.

THIS PAGE HAS BEEN LEFT BLANK INTENTIONALLY

8. POSTCLOSURE SAFETY ASSESSMENT – GAS GENERATION AND TRANSPORT

This chapter, together with Chapter 7, presents an illustrative postclosure safety assessment for a used fuel repository located in the sedimentary rock of Southern Ontario. The focus of this chapter is on gas generation and transport of volatile radionuclides. Chapter 7 addresses waterborne contaminant transport.

Exposure of the steel components of an engineered-barrier system (EBS) to groundwater will result in the generation of gas due to corrosion processes. Microbial processes, if present, may also generate (or consume) gas. The fate of this gas as it migrates through the repository, the excavation-damaged zone (EDZ) and the surrounding host rock can affect both the internal repository pressure and the transport of gaseous radionuclides.

The assessment is arranged as follows:

- Section 8.1 – Interim Acceptance Criteria;
- Section 8.2 – Scope, a detailed description of the analysis cases;
- Section 8.3 – Conceptual Model of the repository evolution;
- Section 8.4 – Computer Code;
- Section 8.5 – Overall Approach and Selected Data for Gas Transport and Migration;
- Section 8.6 – Analysis Methods and Key Assumptions;
- Section 8.7 – Results of Gas Generation and Transport Modelling;
- Section 8.8 – Dose Consequences; and
- Section 8.9 – Summary and Conclusions.

8.1 Interim Acceptance Criteria

For radiological consequences, the interim acceptance criteria are identical to those adopted for the waterborne contaminant transport assessment described in Chapter 7.

For pressure, the target acceptance criterion is that pressure in the intact host rock surrounding the repository should remain below 80% of lithostatic pressure. Geomechanical analysis indicates that lithostatic pressure must be exceeded before fracturing of the host rock can occur. If this criterion is met, the possibility that gas pressure build-up will lead to fracturing can be excluded.

This assessment assumes the repository host rock is the sedimentary Cobourg formation within the Michigan Basin. The vertical lithostatic stress is approximately 13 MPa at a depth of 500 mBGS (Itasca 2015); so, the target acceptance criterion is approximately 10 MPa.

8.2 Scope

This chapter considers the Base Case of the Normal Evolution Scenario and the Extreme Case of the All Containers Fail Disruptive Event Scenario. The Extreme Case is the bounding scenario, in that it has the largest potential for gas production and radiological impact from gas-borne radionuclides.

The Base Case assumes 10 containers are placed in the repository with undetected defects in their copper coatings, with the defects large enough to cause each of the 10 containers to fail within one million years. For conservatism, container failure assumes the copper coating has become fully ineffective across the entire container surface, leaving all of the container's steel surface exposed to groundwater.

As it is unlikely that 10 containers would all fail simultaneously, the failure times are assumed to be evenly spread over the one million year time period of interest, with the first failure occurring at 1000 years and subsequent failures occurring sequentially every 100,000 years (see Chapter 7, Section 7.2.1.2).

The Extreme Case of the All Containers Fail Disruptive Event Scenario assumes some unexpected common cause leading to failure of all containers at 10,000 years (see Chapter 7, Section 7.2.2).

Additional gas sources, notably from corrosion of rock bolts, degradation of trace organic materials in the backfill, and radiolysis of water, are neglected on the basis that the amount of gas produced by such processes is small, non-radioactive, dispersed, and subject to chemical or microbial consumption.

8.3 Conceptual Model

The generation and migration of gas is a coupled process, in which gas generation is dependent on the availability and transport of groundwater near the container. Gas can migrate through the repository by:

- Conventional two-phase flow, where gas pressure is sufficient to partially or completely displace water from the pore space of a material, allowing gas to travel through the connected porosity.
- Dissolving in groundwater, where dissolved gas can travel with groundwater flow or diffuse through groundwater.
- Dilational flow, where gas pressure exceeds the local confining stress and physically displaces material, with gas moving through the resultant open pathway. Pathways are typically small scale and are localized. They will generally propagate until sufficient pathway volume has been opened to reduce the pressure. Dilational flow paths are typically unstable and will close once the pressure is reduced below the confining stress.

The following sections describe the conceptual model for gas generation and transport applied in the analysis.

8.3.1 Gas Generation

In low-permeability sedimentary rock, saturation of the repository may take thousands of years. This leads to the definition of the following four phases in the evolution of the corrosion environment (Chapter 5):

Phase 1: This is an early aerobic period that occurs prior to the onset of aqueous corrosion, immediately following closure of the repository. In this phase, saturation of the materials surrounding the container has not yet occurred, no liquid water is available for corrosion, and the material immediately adjacent to the container remains unsaturated due to high temperatures. Oxygen is initially present in the unsaturated pore space. If relative humidity is also low, corrosion is limited to slow air oxidation. In this phase, gas (oxygen) is consumed.

Phase 2: This is an unsaturated aerobic phase that occurs following the condensation of liquid water on the steel surface. Steel corrosion is higher under these conditions. Gas (oxygen) is consumed.

Phase 3: This corresponds to an unsaturated anaerobic phase that occurs following the consumption of oxygen but prior to full saturation of the materials surrounding the container. Corrosion during this period is supported by the cathodic reduction of water accompanied by the evolution of hydrogen.

Phase 4: This is a saturated anaerobic phase that is entered once the materials surrounding the container have become fully saturated by groundwater. As with Phase 3, corrosion during Phase 4 is supported by the cathodic reduction of water accompanied by the evolution of hydrogen.

These four phases do not necessarily occur sequentially. Phases 1 and 2 both occur under aerobic conditions and the degree to which the Phase 1 and Phase 2 corrosion processes are active depends on the relative humidity. The Phase 3 and 4 corrosion processes proceed under anaerobic conditions after Phase 1 and Phase 2 and may occur concurrently. The Phase 3 process also depends on relative humidity.

There are a number of processes, such as methanogenesis, through which the quantity of gas in the repository may be reduced as discussed in Suckling et al. (2015). The gas modelling presented in this chapter takes no credit for these pressure mitigation processes.

Parameter values used in the corrosion calculations are discussed by Suckling et al. (2015) and by King (2013).

8.3.2 Gas Migration and Transport

Conventional two-phase flow and groundwater dissolution processes are considered sufficient for estimating gas migration through the repository for the most likely scenarios and associated sensitivity cases.

Two-phase flow gas migration modelling is based on the van Genuchten and Mualem-Luckner models for water retention (van Genuchten 1980, Mualem 1976, Luckner et al. 1989). The van Genuchten model describes the relationship between the water content of a porous matrix and the suction, or capillary pressure. Capillary pressure is the difference in pressure across the

interface between two immiscible fluids, and is defined here as the difference in pressure between the gas phase (non-wetting phase) and the water phase (wetting phase). The pressure difference is a function of the pore throat radius, with capillary pressure increasing as the wetting fluid is displaced into smaller and smaller pores. The Mualem-Luckner model describes the relationship between the water content of a porous matrix and the relative permeability through the porous matrix. The model parameters have been fitted to the measured behavior of bentonites and also low permeability limestone and shale rocks.

The van Genuchten equations for capillary pressure as a function of liquid saturation are as follows.

$$P_c = -\frac{1}{\alpha} [S_{ec}^{-1/m} - 1]^{1/n} \quad (8-1)$$

$$S_{ec} = \frac{S_l - S_{lrc}}{1 - S_{lrc}} \quad (8-2)$$

where:

- P_c is the capillary pressure, Pa;
- α is a van Genuchten fitting parameter, Pa⁻¹. The inverse of α is analogous to the air entry pressure, but is often larger than the actual air entry pressure;
- S_{ec} is the effective saturation for the capillary pressure relationship (volume ratio);
- S_l is the liquid saturation (volume ratio);
- S_{lrc} is the residual liquid saturation for capillary pressure (volume ratio), the liquid saturation below which liquid does not flow, and capillary pressure is confined;
- m is a van Genuchten fitting parameter (unitless); and
- n is a van Genuchten fitting parameter (unitless).

Mualem developed an equation for relative liquid permeability, and Luckner expanded the Mualem equation to consider relative gas permeability. The Mualem and Luckner equations for relative permeability are as follows:

$$k_{rl} = S_{ek}^{1/2} [1 - (1 - S_{ek}^{1/m})^m]^2 \quad (8-3)$$

$$k_{rg} = (1 - S_{ek})^{1/3} [1 - S_{ek}^{1/m}]^{2m} \quad (8-4)$$

$$S_{ek} = \frac{S_l - S_{lr}}{1 - S_{lr} - S_{gr}} \quad (8-5)$$

where:

- k_{rl} is the liquid phase relative permeability (ratio);
- k_{rg} is the gas phase relative permeability (ratio);
- S_{ek} is the effective saturation for the relative permeability relationship (volume ratio);
- S_{lr} is the residual liquid saturation (volume ratio), the liquid saturation below which liquid does not flow; and
- S_{gr} is the residual gas saturation (volume ratio), the gas saturation below which gas does not flow.

Table 8-1 shows the two-phase flow properties used for each geologic unit and EBS material.

Two-phase flow properties for the EDZ are identical to the associated geologic unit, except for the $1/\alpha$ parameter, which was scaled according to the permeability difference with the associated geologic unit, as per the Davies (1991) relationship:

$$\left(\frac{1}{\alpha}\right)_{EDZ} = \frac{1}{\alpha} \left(\frac{k_{EDZ}}{k}\right)^{-0.346} \quad (8-6)$$

where 'k' is the permeability (m^2). The calculated scaling factors are 1/11 for the repository inner EDZ, 1/5 for the repository outer EDZ, 1/5 for the shaft inner EDZ, and 1/2 for the shaft outer EDZ.

The two-phase flow relationship between gas and liquid is based on a capillary pressure function and a relative permeability function. Figure 8-1 to Figure 8-3 show the van Genuchten capillary pressure function and the Mualem-Luckner relative permeability for Placement Room Bentonite, Repository Inner EDZ, and the intact host rock of the Cobourg formation. These curves are formulated using the two-phase flow parameters associated with these materials.

Dissolution of gas in water is described by Henry's law, where the concentration of dissolved gas is proportional to the partial pressure of the gas. Salinity reduces the Henry's law coefficient; 4×10^{-11} mol fraction/Pa is used for hydrogen (Quintessa and Geofirma 2011).

8.4 Computer Code

The conceptual model is numerically represented in the T2GGM computer code (Suckling et al. 2015).

Figure 8-4 identifies the interrelationship with repository parameters. Information from engineering design and site characterization is used to develop a site-specific system description.

Table 8-1: Two-Phase Flow Properties

Material	1/α (MPa)	n	m	S_{lrc}	S_{lr}	S_{gr}
Unit B and C	0.31	4.22	0.35	0.55	0.56	0.00
Unit A-2 Carbonate	0.76	3.06	0.50	0.00	0.01	0.00
Unit A-1 Upper Carbonate	39	2.41	0.99	0.00	0.01	0.00
Unit A-1 Carbonate	39	2.41	0.99	0.00	0.01	0.00
Unit A-1 Evaporite	2.1	2.28	0.99	0.01	0.02	0.10
Unit A0	5.9	2.25	1.13	0.00	0.01	0.14
Guelph	0.04	4.89	0.15	0.25	0.26	0.00
Fossil Hill	28	6.11	0.68	0.03	0.04	0.00
Cabot Head	15	6.82	0.24	0.00	0.01	0.05
Manitoulin	41	3.65	1.31	0.11	0.12	0.05
Queenston	36	4.45	1.13	0.09	0.10	0.06
Georgian Bay/Blue Mountain	30	3.82	1.10	0.17	0.18	0.04
Cobourg	62	3.13	1.69	0.06	0.07	0.03
Sherman Fall	28	2.33	1.00	0.17	0.18	0.11
Kirkfield	173	2.17	7.22	0.00	0.01	0.15
Cobokonk	66	1.82	1.73	0.00	0.01	0.03
Gull River	40	4.06	0.78	0.21	0.22	0.11
Shadow Lake	0.23	1.20	0.58	0.04	0.05	0.00
Precambrian	0.23	1.20	0.58	0.04	0.05	0.00
Placement Room Bentonite (Homogenized Bentonite)	108	2.71	1.21	0.01	0.01	0.10
Tunnel Seal Bentonite	108	2.71	1.21	0.01	0.01	0.10
Placement Room	108	2.71	1.21	0.01	0.01	0.10
Gap Fill	108	2.71	1.21	0.01	0.01	0.10
Tunnel Dense Backfill	10	1.80	0.40	0.09	0.10	0.01
Concrete, degraded	1.0	2.00	0.50	0.19	0.20	0.10
Shaft Asphalt	-	-	-	-	0.00	0.00
Shaft Bentonite/Sand	285	1.94	4.80	0.00	0.01	0.12

Note: Data taken from Gobien et al. (2018)

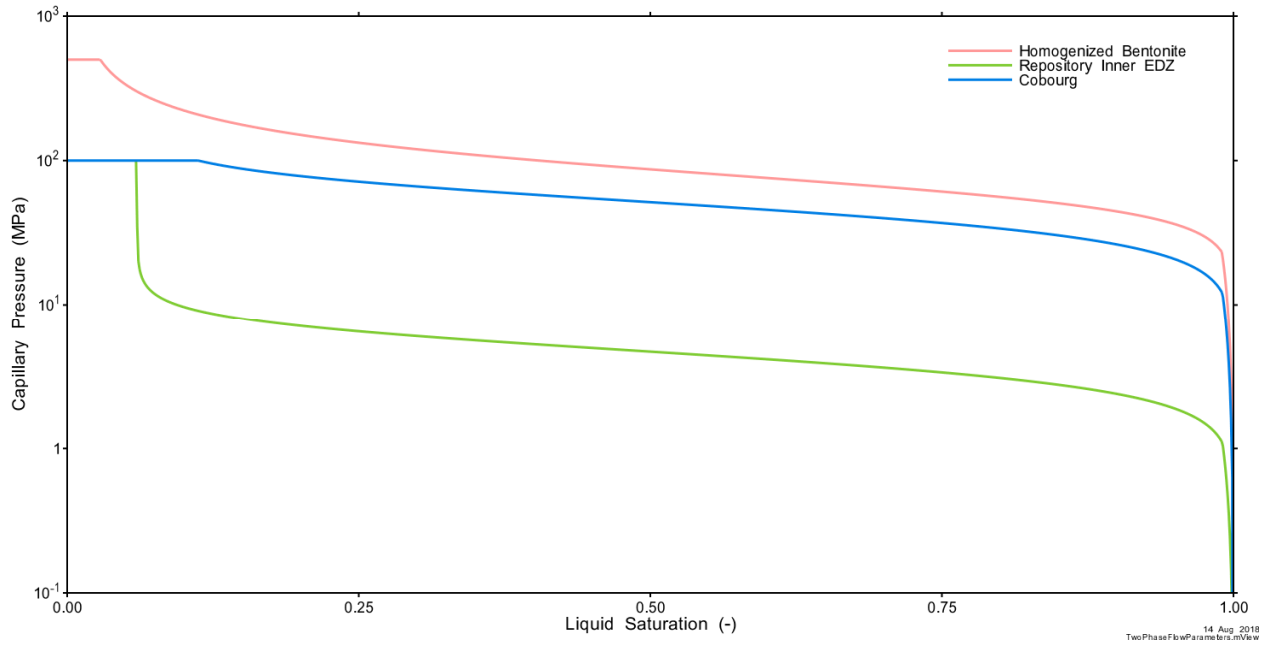


Figure 8-1: Capillary Pressure Curves for Placement Room Bentonite (Homogenized Bentonite), Repository Inner EDZ, and the Cobourg Formation

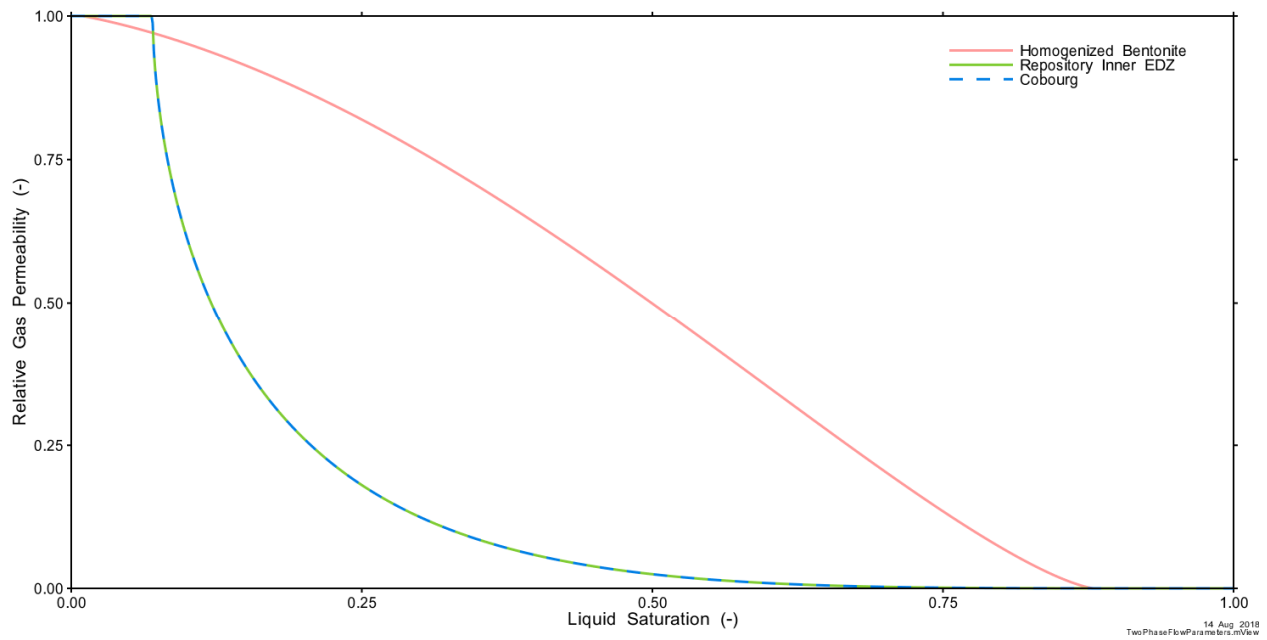


Figure 8-2: Relative Gas Permeability Curves for Placement Room Bentonite (Homogenized Bentonite), Repository Inner EDZ, and the Cobourg Formation

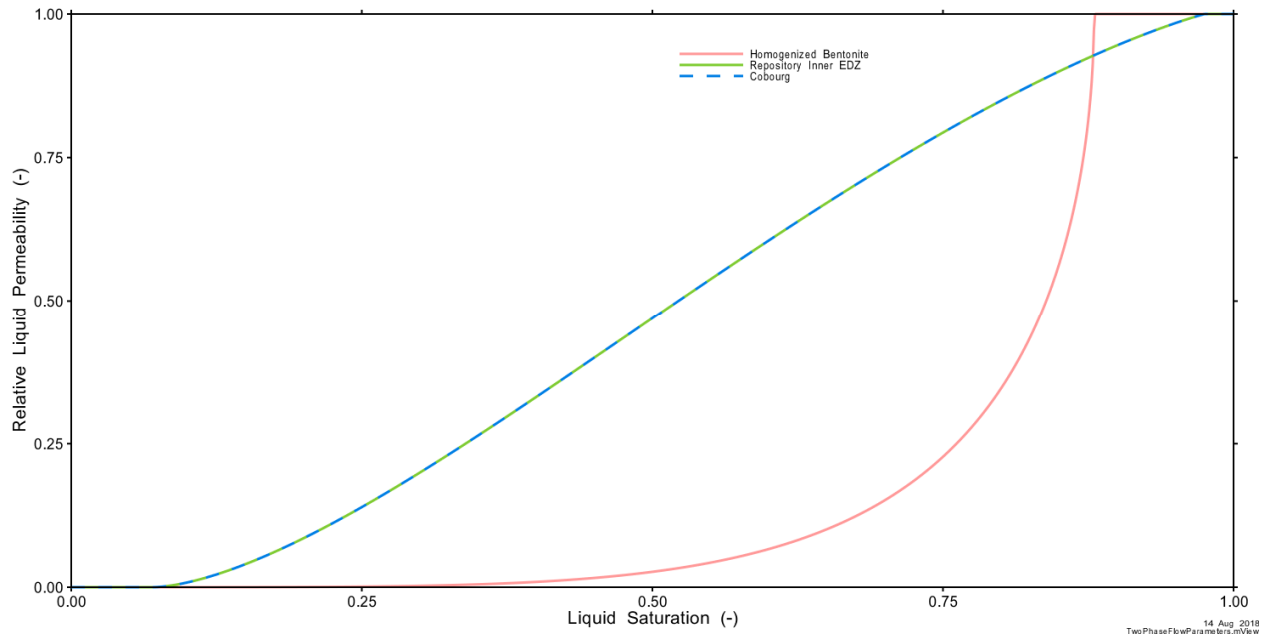


Figure 8-3: Relative Liquid Permeability Curves for Placement Room Bentonite (Homogenized Bentonite), Repository Inner EDZ, and the Cobourg Formation

T2GGM assesses the coupled behaviour between gas generation, temperature and the movement of gas and water by conventional two-phase flow and groundwater dissolution processes (see Section 8.3.2); the code does not provide dilational flow calculations for this assessment.¹

T2GGM is composed of two coupled models: the Gas Generation Model (GGM) used to describe the generation of gas due to corrosion of steel components, and the TOUGH2 model (Pruess et al. 1999) used to describe gas and water transport from the repository and within the geosphere. Key outputs are estimates of the repository pressure, repository saturation, and gas flow rates within the geosphere and repository system.

T2GGM has been used for gas modelling in support of the postclosure safety assessment for the Low and Intermediate Level Waste DGR proposed by Ontario Power Generation (Geofirma and Quintessa 2011). T2GGM was used to calculate the generation and build-up of gas in the repository, the exchange of gas and groundwater between the repository and the surrounding rock, and between the rock and the surface environment. T2GGM was also used to perform similar calculations for another used fuel repository design (NWMO 2013). The two coupled models are described below.

Table 8-2 provides more information on T2GGM.

¹ T2GGM can estimate dilational flow (Suckling et al. 2015); however, calculations for the systems represented in this assessment require very long processing times, rendering these simulations intractable.

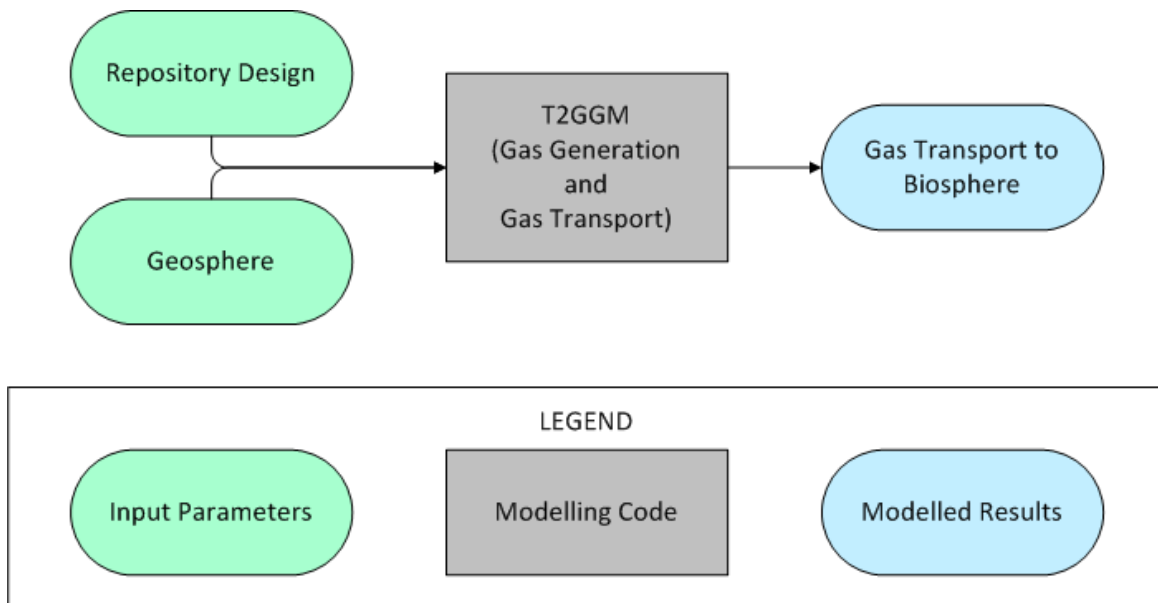


Figure 8-4: Main Computer Code

TOUGH2:

The TOUGH2 gas transport model is a widely used code for two-phase flow and gas transport in geological media, including for deep geological repositories (e.g., Talandier et al. 2006, Nagra 2008, FORGE 2010, Bate et al. 2012).

TOUGH2 is a multi-phase flow and heat transport program for fluid mixtures. T2GGM Version 3.2.1 includes TOUGH2 Version 2.0 with the EOS3 V1.01 equation-of-state module (ideal gas – air and water) (Pruess et al. 1999). The EOS3 module defines two-phase flow of water and air, or single-phase flow of water or air. Thermophysical properties of water are represented by steam-table equations, while the air is treated as an ideal gas. Dissolution of air in water is modelled with Henry's law. An option is provided to represent the gas phase by an alternative gas, such as H₂.

GGM:

GGM is a gas generation model developed for the NWMO (Suckling et al. 2015). It is implemented as a FORTRAN module that is used by TOUGH2 to incorporate gas generation due to corrosion and degradation processes. GGM includes a kinetic description of the various microbial and corrosion processes that lead to the generation and consumption of various gases. GGM can also be used to assess the effect of different gas-mitigation methods and other processes that can lead to the consumption of gas in the repository.

The GGM gas generation model is consistent with general literature and with approaches adopted in other waste management organizations for similar models.

Table 8-2: T2GGM Version 3.2.1

Parameter	Comments
Components:	
TOUGH2	Core Code Version 2.0
EOS3	TOUGH2 Equation of State Module 3 Version 1.01
GGM	Gas Generation Component of T2GGM Version 3.2.1
Main Documents	T2GGM Version 3.2: Gas Generation and Transport Code (Suckling et al. 2015) TOUGH2 User Guide (Pruess et al. 1999)
Main Features:	<ul style="list-style-type: none"> - Temperature-dependent corrosion product and hydrogen gas generation from corrosion of steel and other alloys under aerobic and anaerobic conditions in the presence of a bentonite buffer - CO₂-enhanced corrosion of carbon steel and passive alloys - CO₂ and CH₄ gas generation from degradation of organic materials under aerobic and anaerobic conditions - H₂ gas reactions, including methanogenesis with CO₂ - Limitation of both microbial and corrosion reactions by the availability of water - Carbon, iron and water are mass balanced within repository reactions - Exchange of gas and water between the repository and the surrounding geosphere - Calculation of the generation and build-up of gas in each repository volume - Two-phase flow of water and gas within the geosphere with gas dissolution according to Henry's law - Heat flow coupled to two-phase flow of water and gas - 1D hydro-mechanical model to assess the effects of a uniformly applied glacial stress - Time-variable permeability, allowing the permeability properties of certain materials, such as engineered materials or EDZ, to evolve or degrade with time - Time-variable Dirichlet boundary conditions - The ability to stop and restart the simulations - Automatically restart simulations with modified convergence parameters when incipient failure is detected - Link and simultaneously solve two different models at identified boundary junction points. This approach prevents incongruent boundary conditions in nested models

8.5 Overall Approach and Selected Data for Gas Transport and Migration

Gas generation and transport are investigated using models at two different scales of resolution, Room-Scale and Repository-Scale. The models are linked such that the Repository-Scale Model provides boundary conditions to the end of the Room-Scale Model, and the Room-Scale Model provides scaled hydrogen and water inputs to the Repository-Scale Model.

The Room-Scale Model considers hydrogen gas generation from corrosion processes and two-phase flow with a simplified EBS geometry within a single placement room. Gas transport results are used as input² to the Repository-Scale Model. Thermal effects from the used fuel containers on groundwater flow and gas flow are accounted for.

The Repository-Scale Model includes a simplified representation of the repository tunnels. It also includes a single shaft representing the combined cross-sectional areas of the three planned shafts. The model considers the transport of gas and water along the main drifts and shaft of the repository to estimate the amount of gas reaching the Guelph formation. Hydrogen and water transport data are distributed within the model at locations where the rooms intersect the main access tunnels.

Both models use the geosphere and repository material properties described in Chapter 7. Within the host rock and the various engineered sealing materials, interactions between gas and liquid are modelled using the van Genuchten equations for water retention described in Section 8.3.2.

During setup, the models are initially run for a sufficient period of time to allow the pre-construction conditions to equilibrate. Thereafter, simulations are conducted in three consecutive segments to account for the evolution of repository conditions. These are:

1. Preclosure – once constructed, the engineered facilities are open to atmospheric pressure and are fully saturated with gas.³ Placement rooms will be open for approximately seven years prior to sealing and closure. Prior to decommissioning and closure of the repository, the access tunnels and shafts will be open for the operational period of 40 years or more, plus an extended monitoring period of several decades, nominally 70 years. Desaturation of the neighbouring rock is modelled and used to initialize the postclosure period. For simplicity, the preclosure periods for both models are simulated for seven years. This is conservative, insofar as reduced time for desaturation allows for earlier resaturation; even so, modelling results were found to be largely insensitive to the length of the preclosure period.

² For the Extreme Case of the All Containers Fail Disruptive Event Scenario, gas transport results are scaled to represent the entire repository.

³ Although the actual gas present in the pre-closure period is air, hydrogen is used in the simulations for consistency with the post-failure stage where hydrogen gas is generated. The main implication of assuming hydrogen is slower dissolution of hydrogen into water compared to air, which will have negligible impacts during the operational period.

2. Postclosure / pre-failure – the EBS is placed with specified gas saturations⁴ at atmospheric pressure within the room and cross-cut drift (Room-Scale Model) or main tunnels and shaft (Repository-Scale Model) as the system is sealed. The system resaturates and repressurizes initially with no gas generation taking place.
3. Post-failure – carbon steel containers that have lost their copper corrosion barrier are exposed to the surrounding EBS and gas generation commences. Gas generation processes and rates are calculated as described in Section 8.3.1.

Pressure, gas saturation, and dissolved gas content are continuous within the geosphere from one segment to the next.

8.6 Analysis Methods and Key Assumptions

This section describes the Room-Scale and Repository-Scale Models. Although they are linked within a single simulation, the models are described separately for clarity.

8.6.1 Room-Scale Model

The Room-Scale Model uses a simplified EBS geometry.

The domain consists of a full single room, and includes containers, the concrete and bentonite seals, and dense backfill at the end of the room intersecting with the tunnels. Containers are abstracted into a single “container”, representing the average 342 containers in each room. The average number of containers is calculated as the total number of containers to be placed in the repository (108,833), divided by the number of rooms (318). Horizontal symmetry is assumed and only one-half of the cross-section is modelled, including host rock horizontally adjacent to the room. The plan section domain of 366.6 m × 12.5 m represents the full length of a single room located in the middle of the repository and one-half the intact rock separating the room from adjacent rooms. The vertical extent of the model is from 2000 m below the repository⁵ to the top of the Salina Unit B and C formations (i.e., the bottom of the Guelph formation).

The volume of the single “container” is equivalent to the volume of 342 containers, and consequently, the amount of bentonite is the same as in the actual system. Figure 8-5 illustrates the model.

Figure 8-6 shows the end of the room adjoining the tunnels. The Room-Scale Model is linked to the Repository-Scale Model at a single node in the dense backfill, shown in Figure 8-6. This single linked node is specified as a boundary condition, with the pressure, gas saturation and temperature fixed to a value calculated from the Repository-Scale Model.

⁴ Gas saturation is the volumetric fraction of a material's porosity that is filled with free-phase gas. Similarly, liquid saturation is the fraction of porosity filled with liquid. Within a pore volume, the sum of the gas and liquid saturations is unity. As above, though the actual gas present during the pre-failure period is air, the model assumes it is hydrogen. Again, the main implication of assuming hydrogen is slower dissolution of hydrogen into water as compared to air – the modelled repository resaturates more slowly with hydrogen than it would with air.

⁵ The extensive vertical depth is selected to minimize boundary condition effects for thermal transport.

The portion of the room bentonite seal that cuts into the Inner EDZ is simplified by a rectangular cut-out, with permeabilities adjusted to account for the triangular shape of the bentonite cut-out and the thin EDZ formed by the cut-out. A plan view of a portion of the room is shown in Figure 8-7 and a cross-section through the container is shown in Figure 8-8. The discretization contains 84 layers and 14,978 nodes.

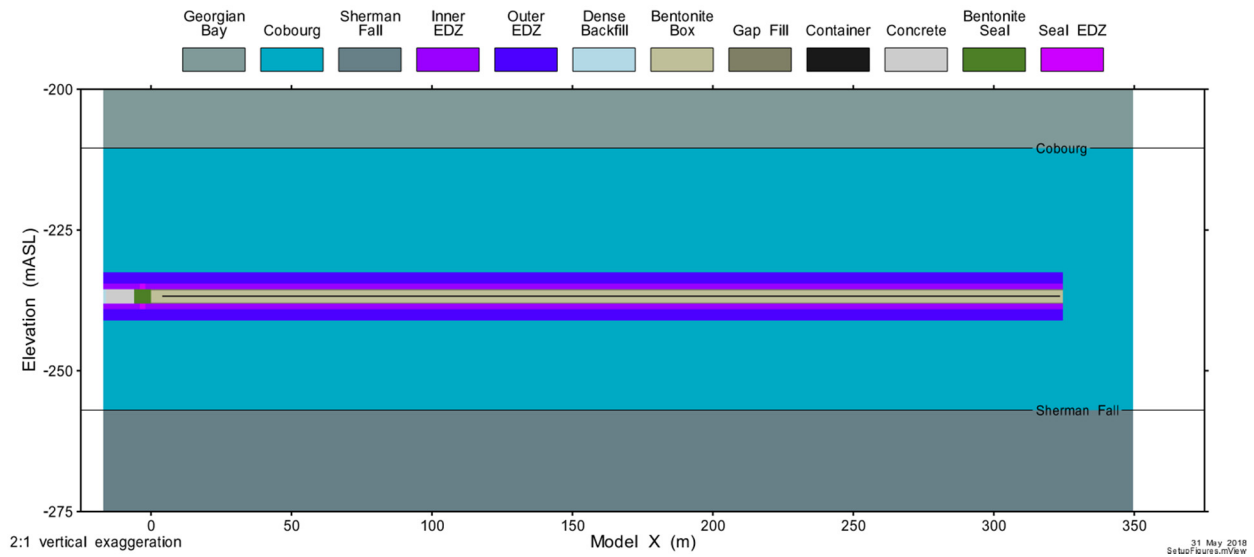


Figure 8-5: Room-Scale Model: Illustration

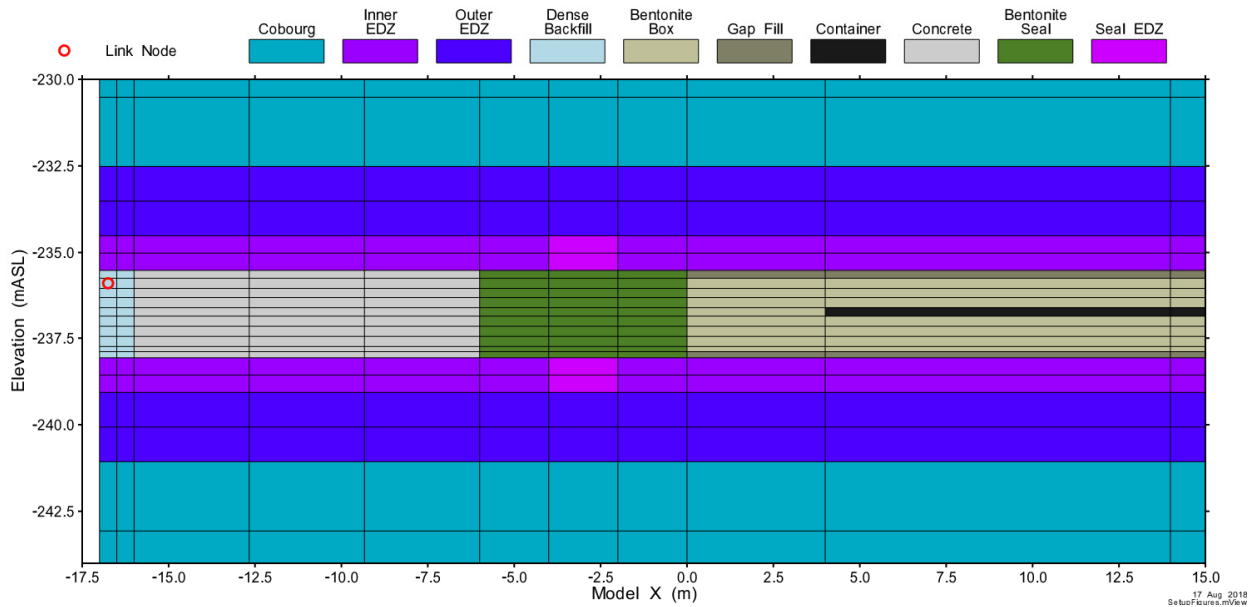


Figure 8-6: Room-Scale Model: Tunnel End of Room

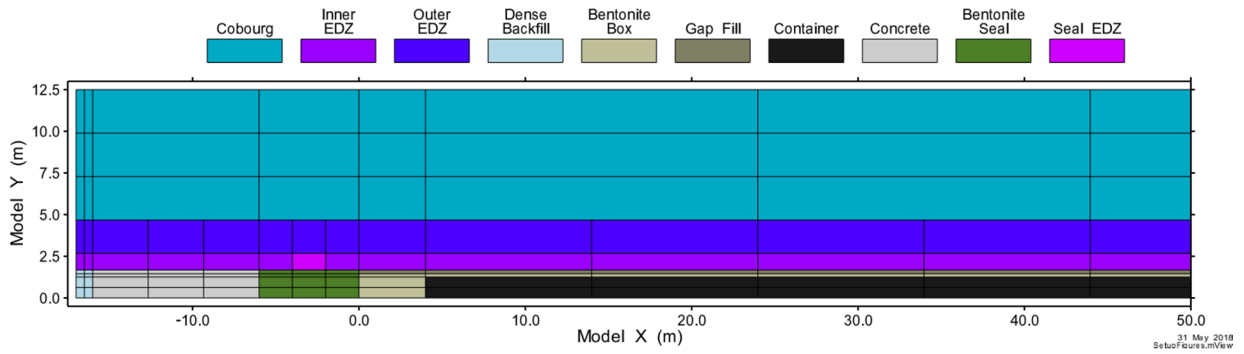


Figure 8-7: Room-Scale Model: Plan-Section through Middle of Placement Room

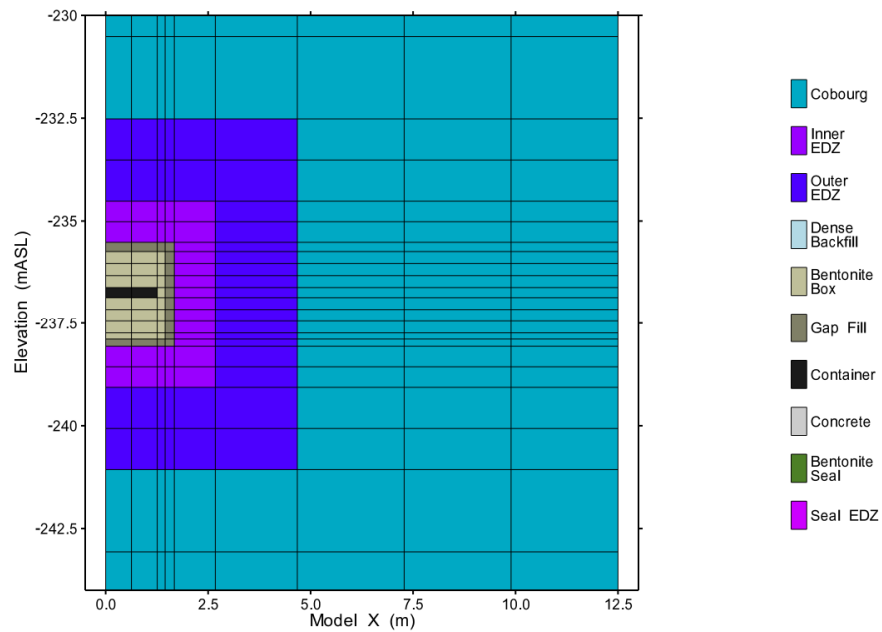


Figure 8-8: Room-Scale Model: Cross-Section through Container

Boundary and Initial Conditions:

Pressure boundary conditions at the top and bottom of the model (i.e., the Salina Units B and C formations and 2000 m below the repository) are set to simulate a system at hydrostatic equilibrium. Initial pressures for all intact rock nodes are set to freshwater hydrostatic⁶.

At the start of the post-closure phase, highly compacted bentonite is assigned an initial liquid saturation of 67% as per the installed material properties. The highly compacted bentonite around the containers is surrounded by gap fill at 6% initial liquid saturation. Concrete and dense backfill are assigned liquid saturations of 50% and 80%. Liquid saturations in the EDZ and rock are obtained from results of the pre-closure phase simulation.

A temperature of 10°C was specified at the top of the model (ground surface). A temperature at the bottom of the model (2000 m below the repository) was defined based on a thermal gradient of 12°C/km. The thermal gradient will not be constant in the model, due to different thermal properties of the stratigraphic units. With these boundary conditions, the steady-state thermal conditions in the geosphere, without a repository, results in temperatures of approximately 17°C at the repository horizon. Figure 8-9 illustrates the geothermal gradient in the geosphere. For comparison, Figure 8-9 includes measured temperature profiles reported from deep boreholes in other locations in southern Ontario.

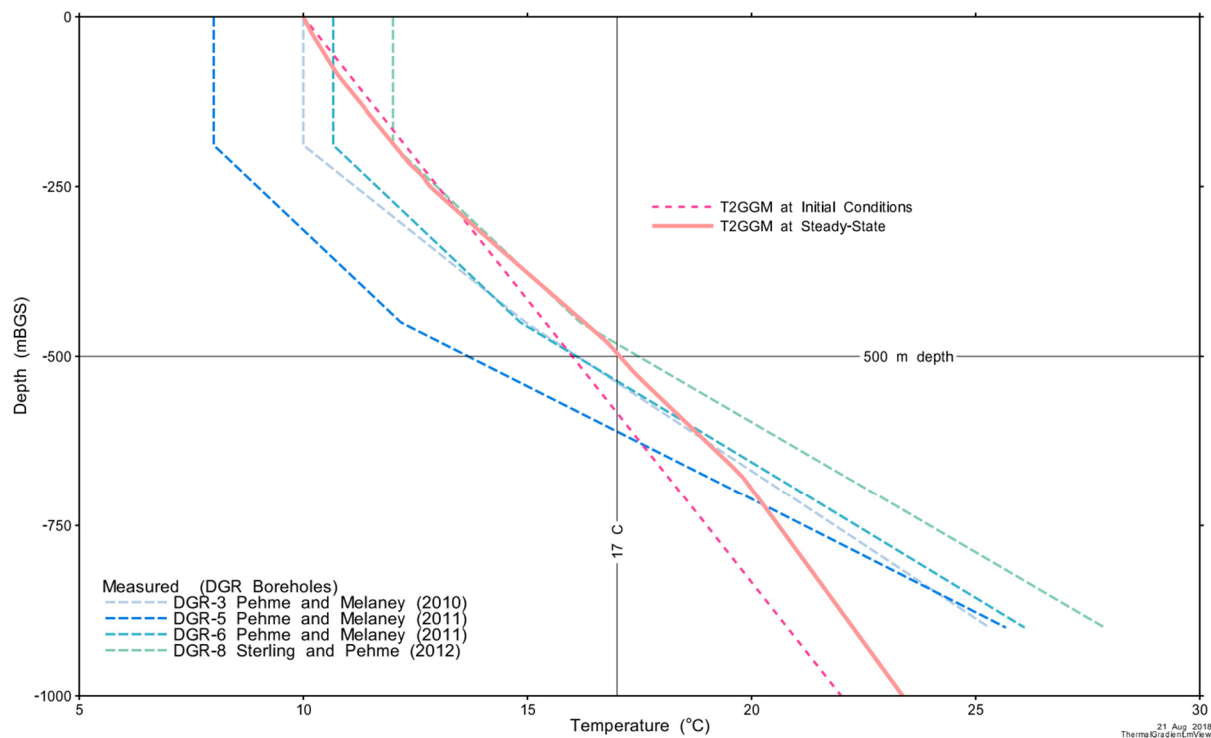


Figure 8-9: Geothermal Gradient

⁶ Variations in fluid density will have negligible impact on the simulations, where pressures and flows are largely driven by processes occurring within the placement room. T2GGM has the ability to scale water density to simulate saline water; however, this feature was not used.

The thermal source term for heat released as a result of radioactive decay is provided in Guo (2018). Only heat generated by radioactive decay is considered. Although aerobic corrosion of steel is exothermic, the total heat generated would be negligible compared to the decay heat. Anaerobic corrosion of steel is endothermic.

The watt-per-container values provided in Guo (2018) are multiplied by 342 to account for the 342 containers in the room and then divided by two to reflect the half-room geometry. The resulting thermal source term is uniformly distributed among the nodes representing the containers.

The pressure, gas saturation and temperature of the single linked node in the Room-Scale model is based on results from the Repository-Scale Model.

GGM Implementation:

Scoping simulations indicated that the thermal state and resaturation profile did not vary significantly over the length of the room. Consequently, a single GGM compartment is used to simulate corrosion-generated gas from all affected containers. The Base Case uses a single homogenized bentonite node, located adjacent to the room seal, as shown in Figure 8-10. The steel mass and area available for corrosion is adjusted at each prescribed failure time.

For the All Containers Fail Scenario, the GGM compartment consists of all homogenized bentonite nodes that are directly connected to a container node, as shown in Figure 8-11, with the source term mass and surface areas specified to be consistent with 342 containers (divided by two to reflect the half-room geometry). The surface area and mass of steel available for corrosion is adjusted as the process evolves.

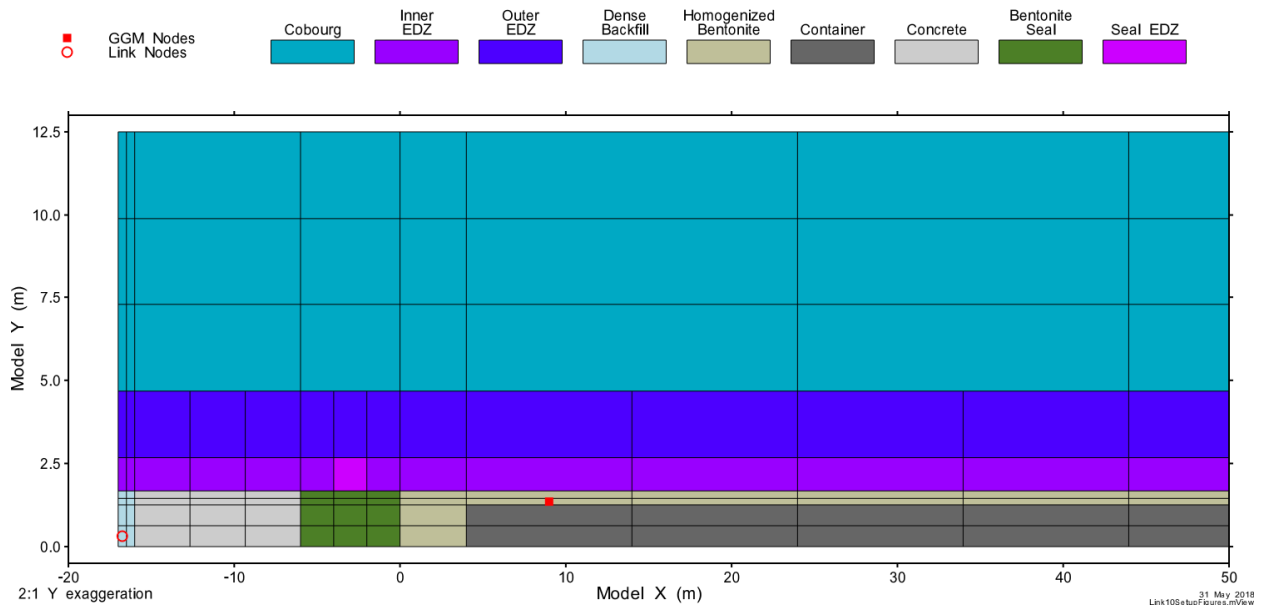


Figure 8-10: Room-Scale Model: Plan-Section View showing GGM Node for the Base Case

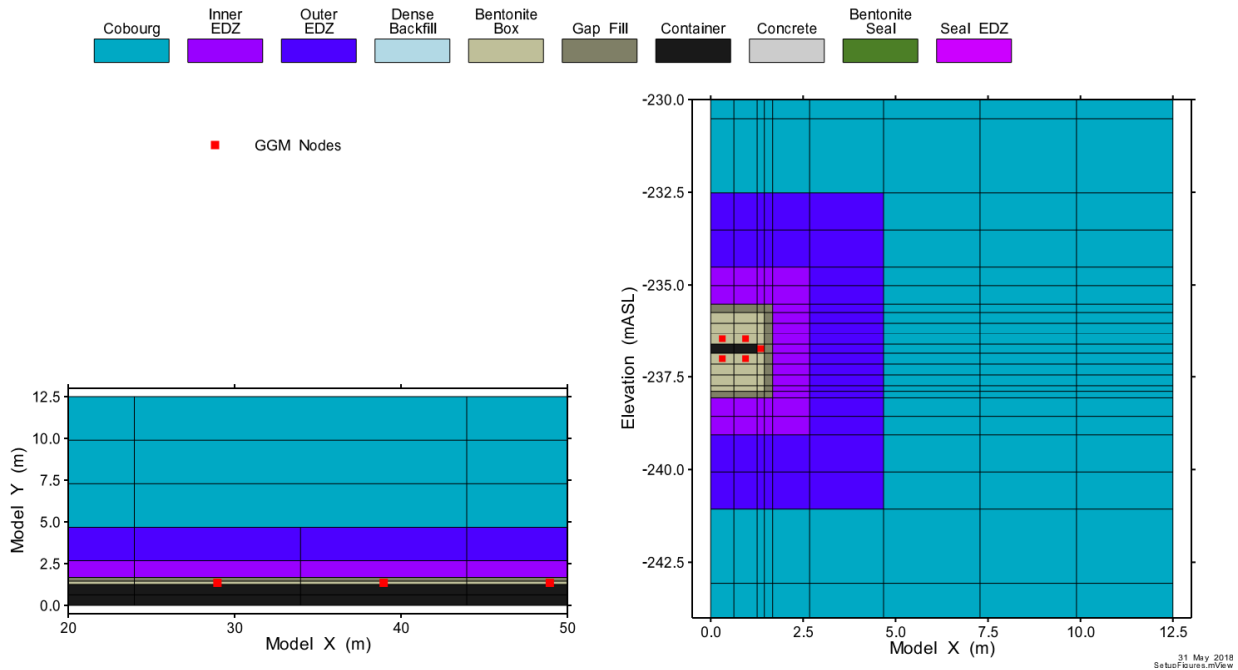


Figure 8-11: Room-Scale Model: Plan- and Cross-Section View showing GGM Nodes for the All Containers Fail Scenario

8.6.2 Repository-Scale Model

The Repository-Scale Model considers the transport of gas and water along the main tunnels and shaft of the repository, with results from the Room-Scale Model used to determine the amount of gas reaching the tunnels. The model ignores potential transport to other placement rooms.

The model domain consists of three main tunnels and a single shaft. Tunnels are simplified to rectangular dimensions. The shaft dimensions are scaled to the equivalent cross-sectional area of the three shafts: main, ventilation and service shafts. The model only extends vertically and horizontally into the host rock approximately 50 m from the tunnels and shaft. The limited extents of the model are based on previous gas transport modelling of a repository in this sedimentary geosphere which showed gas transport in the geosphere would be limited to the immediate vicinity of the repository features. The top of the model ends at the bottom of the Guelph formation. Figure 8-12 illustrates the repository domain in plan and cross-section view.

The single link node location, where hydrogen and water from the Room-Scale Model are injected into the Repository-Scale Model, is shown in Figure 8-13 for the Base Case. Figure 8-14 shows the location of the link nodes in the Repository-Scale Model for the All Containers Fail Scenario, along with plan discretization. Discretization is identical for both the Base Case and All Containers Fail Scenario. The average pressure, gas saturation and temperature at the link nodes provide the boundary condition values for the link node in the associated Room-Scale Model.

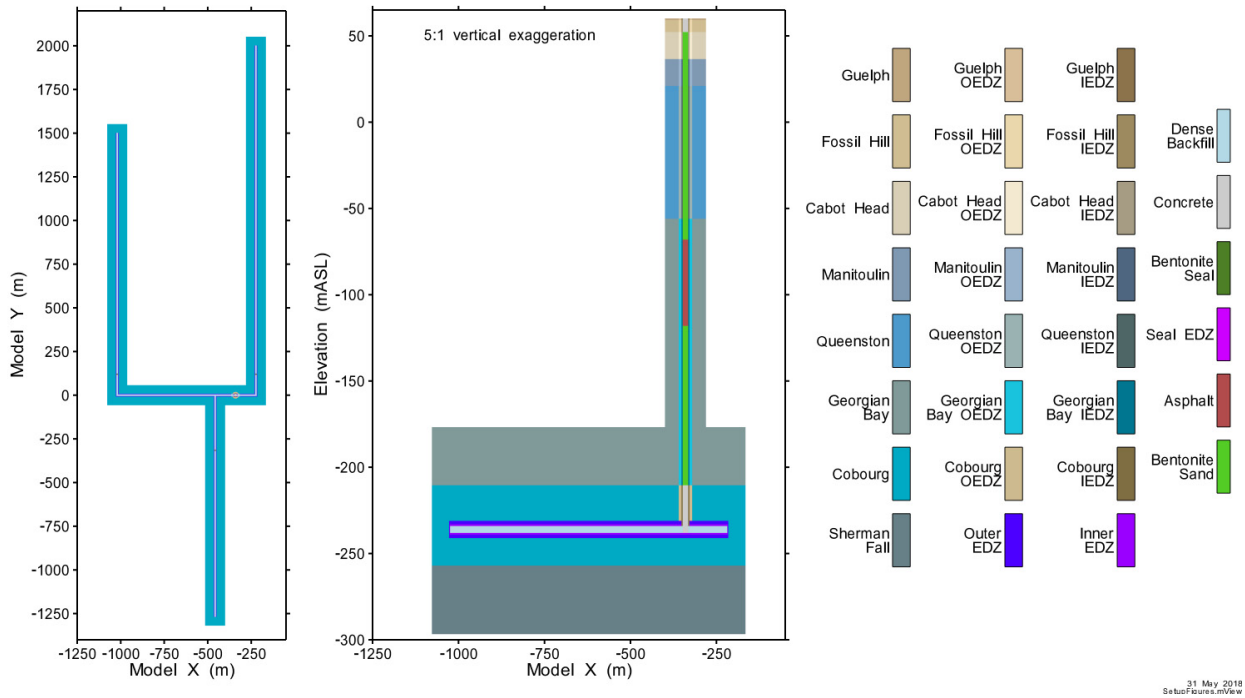


Figure 8-12: Repository-Scale Model: Illustration

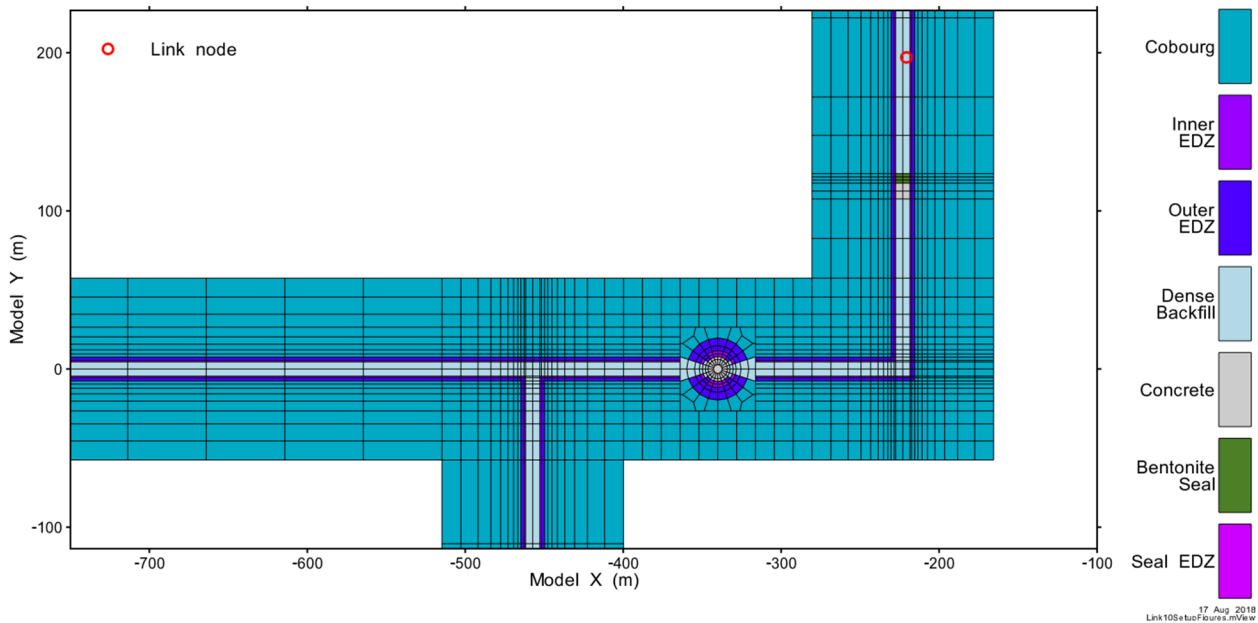
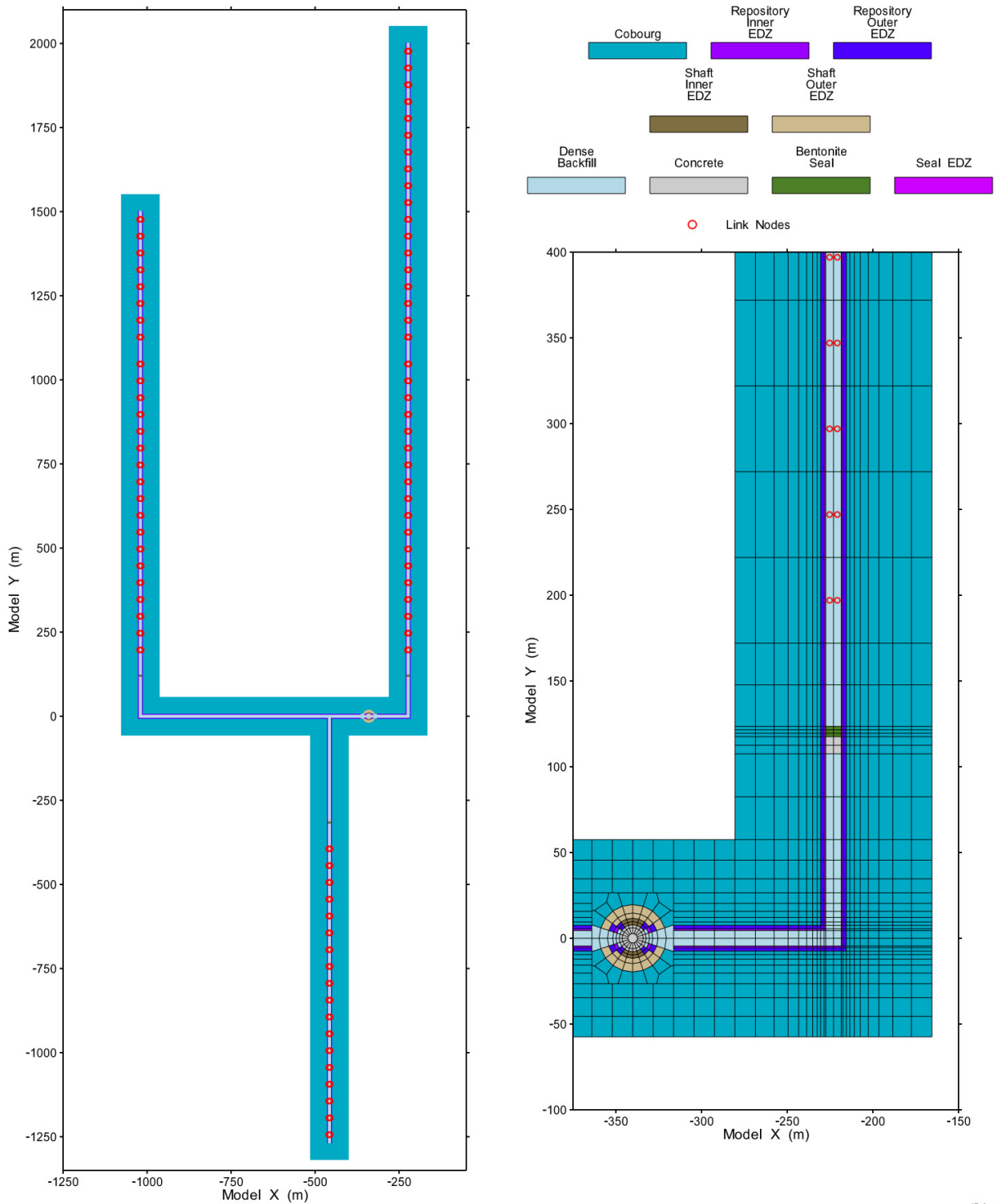


Figure 8-13: Repository-Scale Model: Plan-Section View showing the Link Node for the Base Case



17 Aug 2018
SetupFigure.mView

Figure 8-14: Repository-Scale Model: Plan-Section View showing the Link Nodes for the All Containers Fail Scenario

Figure 8-15 shows the XZ section intersecting the shaft. The Repository-Scale Model discretization contains 37 layers and 103,641 nodes.

The domains of the linked Repository-Scale and Room-Scale Models are shown in Figure 8-16, showing their relative size and extent.

Boundary and Initial Conditions:

Hydraulic pressure boundary conditions on all sides of the Repository-Scale Model are extracted from the 3D Main Transport Model described in Chapter 7. These boundary conditions are assumed fully water saturated with a temperature consistent with the geothermal gradient described for the Room-Scale model.

At the start of the post-closure phase, EBS materials have 80% liquid saturation in the dense backfill, 50% in the concrete, 67% in the tunnel bentonite seals, 73% in the bentonite-sand and 100% in the asphalt seal. Liquid saturations in the EDZ and rock are obtained from results of the pre-closure phase simulation.

Hydrogen and water released from the rooms are injected into the repository model at link node locations within the tunnel. The Room-Scale Model results are extracted at a link node that connects to the Repository-Scale Model. The Base Case takes the Room-Scale Model result and applies this at a single link node in the Repository-Scale Model. The All Containers Fail Scenario takes the Room-Scale Model result, and duplicates this at link nodes for all 318 rooms in the repository.

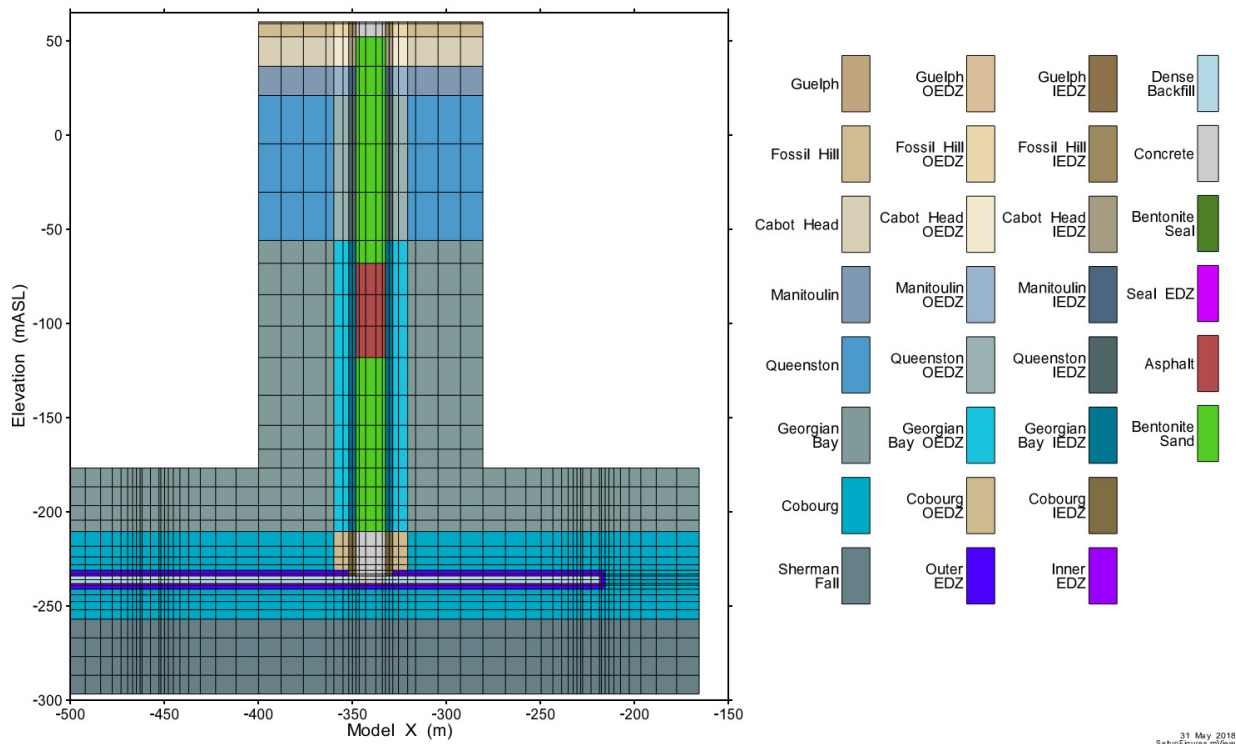
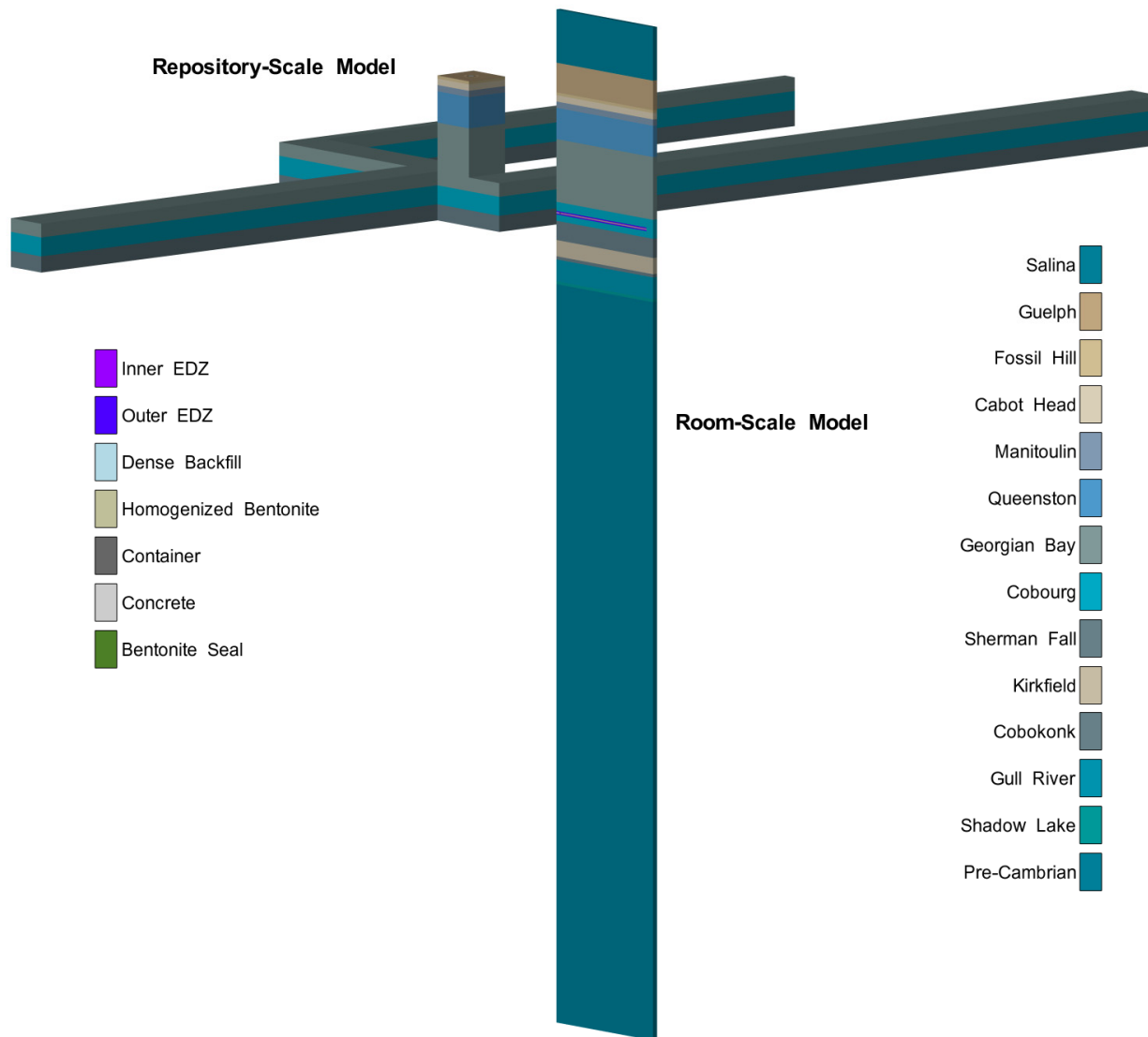


Figure 8-15: Repository-Scale Model: Cross-Section Discretization



22 Aug 2018
Link108a to Figure 8-16.mView

Figure 8-16: Repository-Scale and Room-Scale Model: 3D Relationship of Linked Model Domains

8.7 Results of Gas Generation and Transport Modelling

Upon container failure, the copper coating is conservatively assumed to have completely disappeared, leaving the entire exterior surface of steel available for corrosion. The exterior surface area is available until the thinner hemispherical ends of the containers are consumed; then, the interior of the container cylinder becomes available for corrosion, too, as well as the entire surface area of the thin steel baskets holding the multiple fuel bundles. The steel baskets are consumed in a relatively short time period, after which only the interior and exterior of the container cylinder walls remain. Corrosion continues until the walls are completely consumed.

Although the Room-Scale Model and Repository-Scale Model run simultaneously, the results for temperature, saturation, and pressure are presented separately for clarity. Results for gas flows and gas mass allocation from both models are presented together (Section 8.7.3).

8.7.1 Room-Scale Model

Time-series results for temperature, gas saturation and pressure are reported for nodes that are adjacent to containers and that are along the horizontal plane defined by Z=0, as shown in Figure 8-17.

For reporting purposes, the model is divided into the following components:

- Container nodes correspond to the modelled containers. Their function is essentially limited to acting as thermal sources. Temperatures are the only plotted container results.
- Bentonite Box nodes are within the placement room and surround the containers. They are present until placement rooms resaturate.
- Gap Fill nodes are between the bentonite box and the placement room walls. As with the Bentonite Box nodes, Gap Fill nodes are present until placement rooms resaturate.
- Homogenized bentonite nodes are assigned the averaged properties of the Bentonite Box and Gap Fill nodes once placement rooms resaturate. Homogenized bentonite nodes are implemented for the gas generation period of the Base Case and All Containers Fail Scenario (i.e., for the period following container failure, after 1,000 years for the Base Case and after 10,000 years for the All Containers Fail scenario).
- Inner EDZ nodes correspond to the inner EDZ of the placement rooms.
- Outer EDZ nodes correspond to the outer EDZ of the placement rooms.
- Intact rock nodes are adjacent to and beyond the outer EDZ of placement rooms.
- Intact rock nodes at the model boundary are reported separately as “Intact Rock, 11 m”.

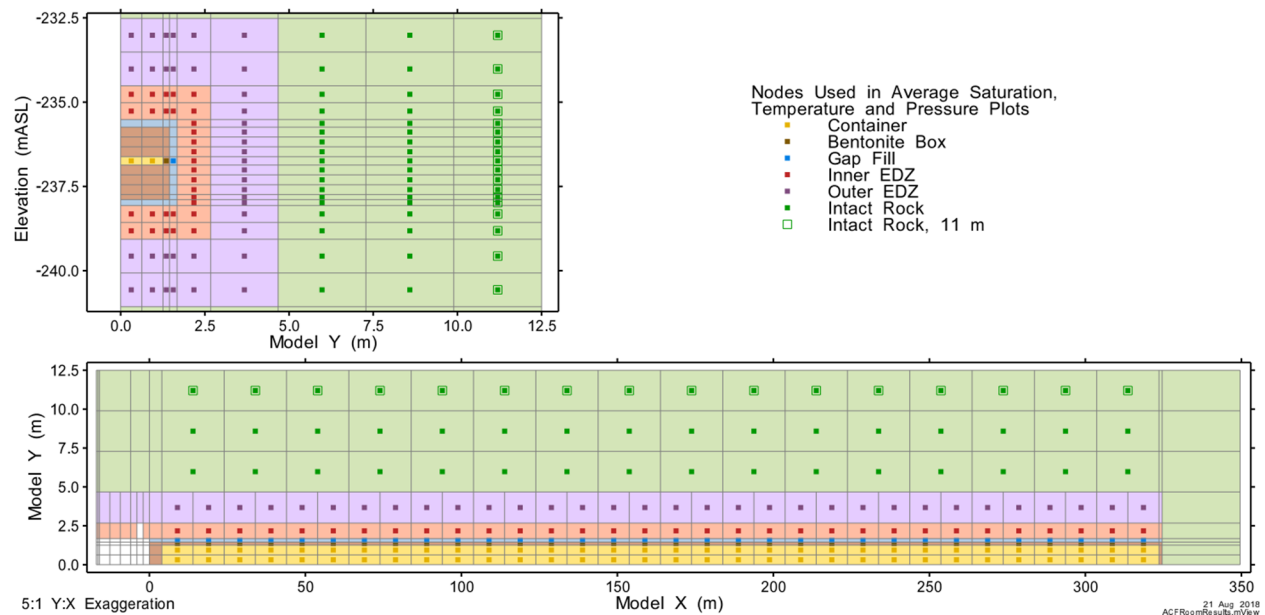


Figure 8-17: Room-Scale Model: Locations of Time-Series Plot Points

In time-series plots, the thin, lighter-coloured lines represent individual nodal values while the thicker, darker-coloured lines are the average of all nodes within one component.

8.7.1.1 Resaturation Period

Initial conditions for the post-closure period are shown in Figure 8-18. The EBS is at initial specified saturations and atmospheric pressure, while inner and outer EDZ reflect drainage and gas transport during the repository operating period.

Figure 8-19 and Figure 8-20 show time-series results for the first 10,000 years with no container failures.

Figure 8-19 shows that the peak temperatures occur at approximately 35 years, with the container reaching a maximum temperature of 82°C.⁷ The figure also shows that placement room bentonite materials are fully water saturated by 400 years (with the exception of a small amount of residual gas that slowly dissolves into the water), and the EDZ is more than 99% water saturated by 10,000 years. Very little gas enters the intact rock. Bentonite saturates more rapidly than the EDZ due to the high suction potential of the bentonite compared to the EDZ.

Figure 8-20 presents the pore pressures⁸ within the EBS and EDZ (upper panel) separately from the pore pressures within the intact rock (lower panel), as pressures within the intact rock are to be compared with the lithostatic pressure. The negative pore pressures in the EBS materials are due to the strongly negative capillary pressures in the bentonite and represent suction pressures. Pressures in the intact rock at 11 m decrease in the 10 to 100 year period as fluid drains from the host rock formation into the room during the resaturation process.

8.7.1.2 Base Case

The first container failure, at 1000 years, occurs when the room has only partially resaturated (Figure 8-21) and is still relatively warm (66-72°C within the EBS).

As discussed previously, the corrosion rate is conservatively assessed taking no credit for the presence of the copper barrier. Metal inventory and corrosion rates for the first container failure are shown in Figure 8-22.

⁷ These results can be compared with separate thermal modelling completed for the same conceptual repository within the same host geosphere (Guo 2018). Modelling by Guo discounts the impact of resaturation on thermal conductivity and heat transport, choosing instead to adopt conservative thermal conductivities and then assuming those conductivities remain constant for the duration of the simulation. These conservatisms lead to a calculated maximum container temperature of 93°C after 47 years. Modelling by Guo was completed using the COMSOL code.

⁸ Pore pressure is calculated as the saturation-weighted average of gas and liquid pressures. The fluid volumetric saturations are used as a proxy for fluid surface areas on the contact surface. The resultant fluid pressure on the contact surface can be taken as a weighted average of the pressures in each of the two fluid phases (water and gas).

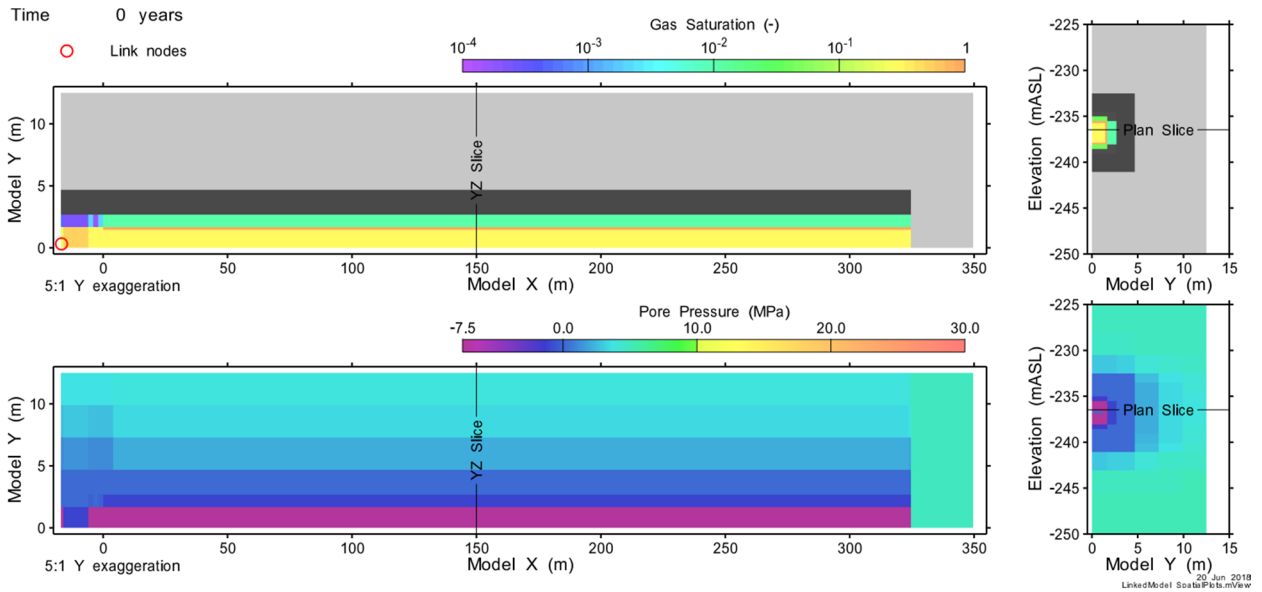


Figure 8-18: Room-Scale Model: Gas Saturation and Pore Pressure at Closure (0 Years)
(Grey / black colouring represents zero gas saturation.)

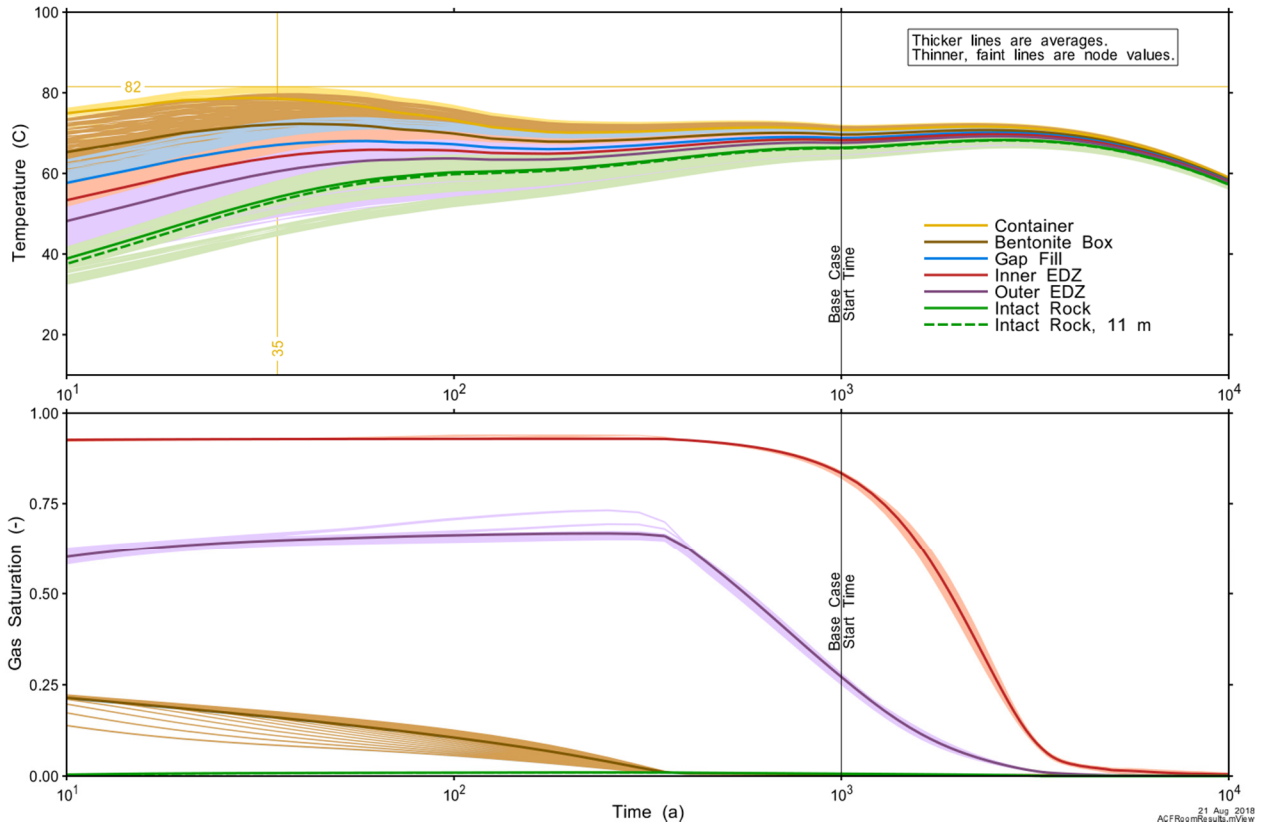


Figure 8-19: Room-Scale Model: Temperature and Gas Saturation Conditions prior to Container Failures

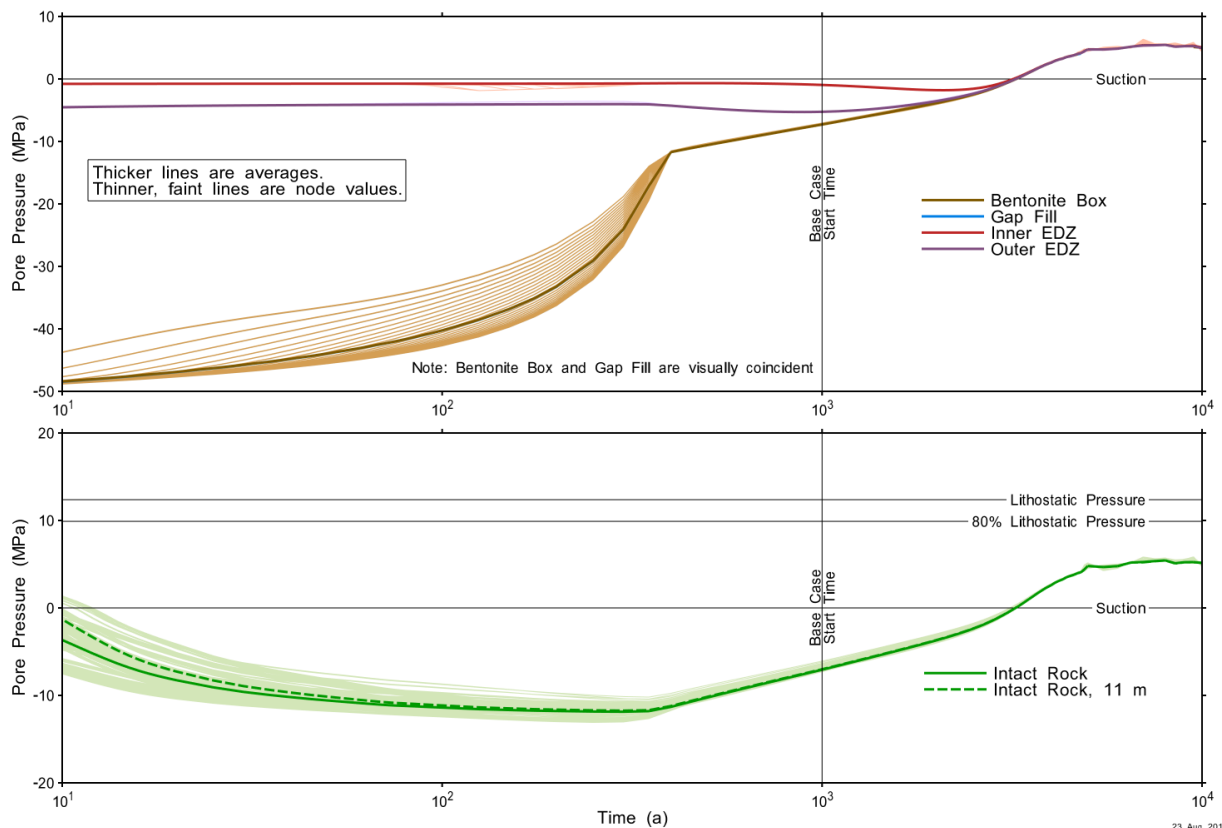


Figure 8-20: Room-Scale Model: Nodal and Average Pore Pressure prior to Container Failures

The hemispherical heads of the container are thinner than the vessel body and will fully corrode earlier. Once the hemispherical heads have fully corroded, approximately 72% of the steel vessel mass has been consumed. At that point, the mass of steel and surface area available for corrosion increases to include the steel baskets within the container and the interior of the container cylinder. This surface area is maintained until the mass of the baskets has been corroded, at which point the corroding surface area is reduced to only the inner and outer surface area of the remaining container cylinder.

Phase 4 corrosion dominates; this, alongside relatively high temperatures, translates into high corrosion rates. The steel in the first container is entirely consumed within 6400 years of container failure. The effect of the additional corrosion area available when the hemispherical heads fully corrode is apparent with the increase in corrosion rates and consequent faster reduction in inventory.

Time series results for the first container failure up to 100,000 years are shown in Figure 8-23 and Figure 8-24. The plots show data on a vertical slice through the node containing the defective container. Temperatures are relatively uniform over the immediate vicinity of the room, peaking at 69°C at 2450 years. Gas saturations in the intact rock diffuse out, with minor amounts present in the homogenized bentonite due to gas generation.

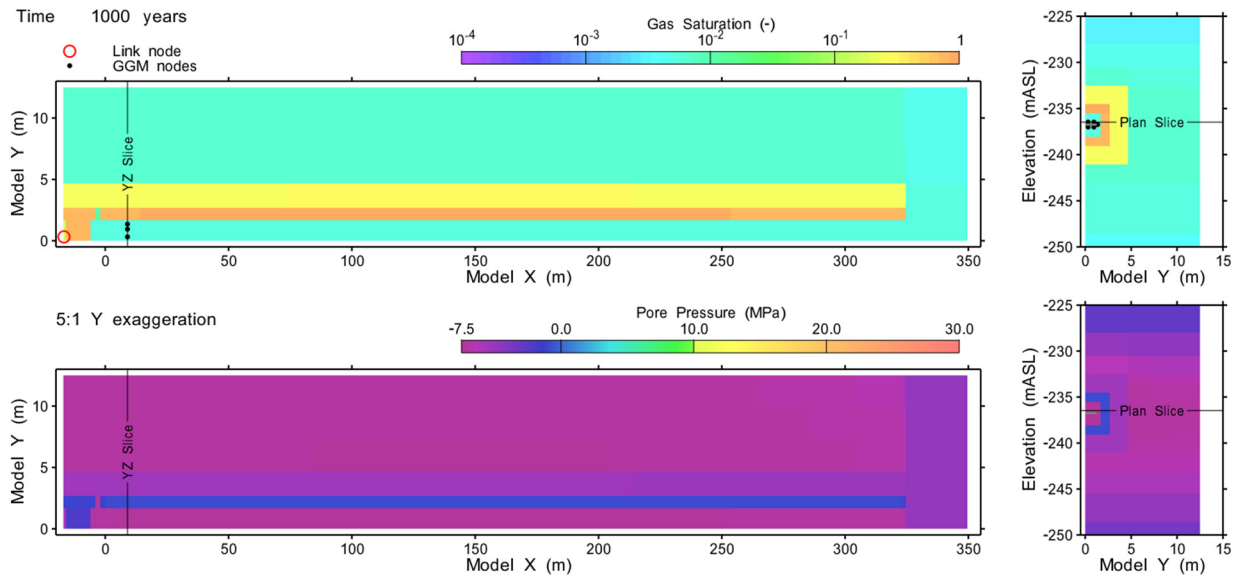


Figure 8-21: Room-Scale Model: Base Case - Gas Saturation and Pore Pressure at 1000 Years

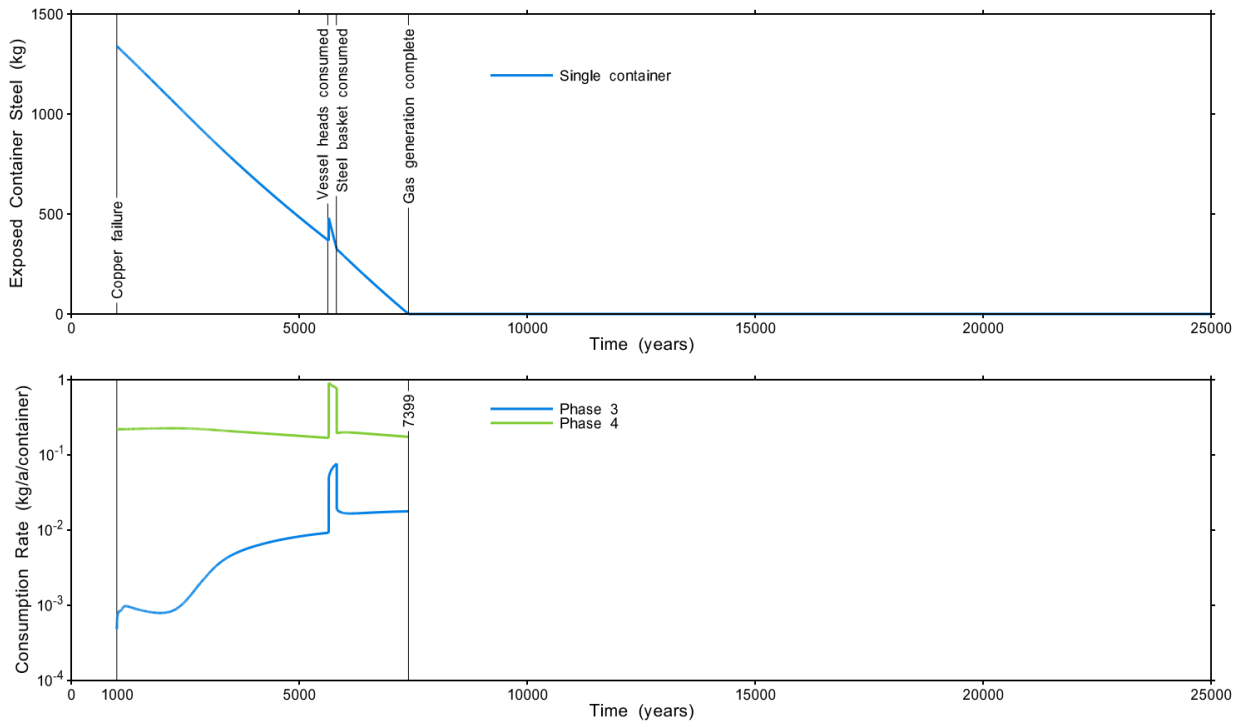


Figure 8-22: Room-Scale Model: Base Case - Steel Consumption and Corrosion Processes for First Container Failure

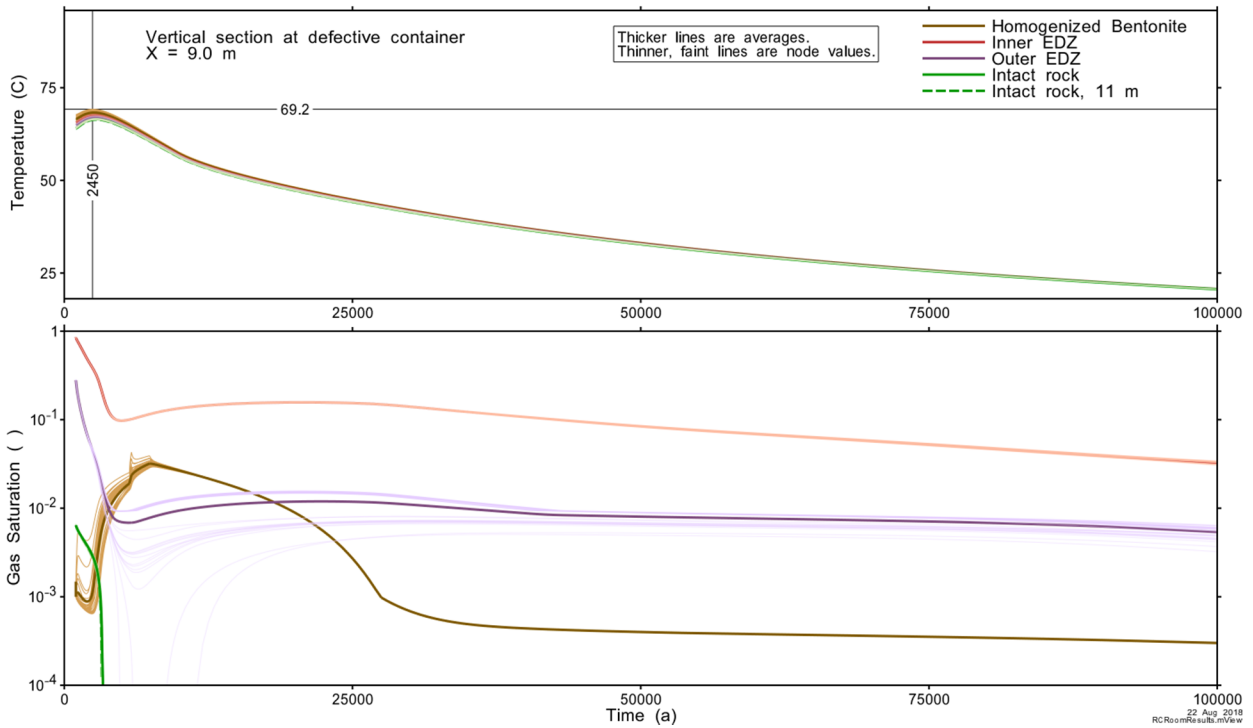


Figure 8-23: Room-Scale Model: Base Case - Nodal and Average Temperature and Gas Saturation Conditions after First Container Failure

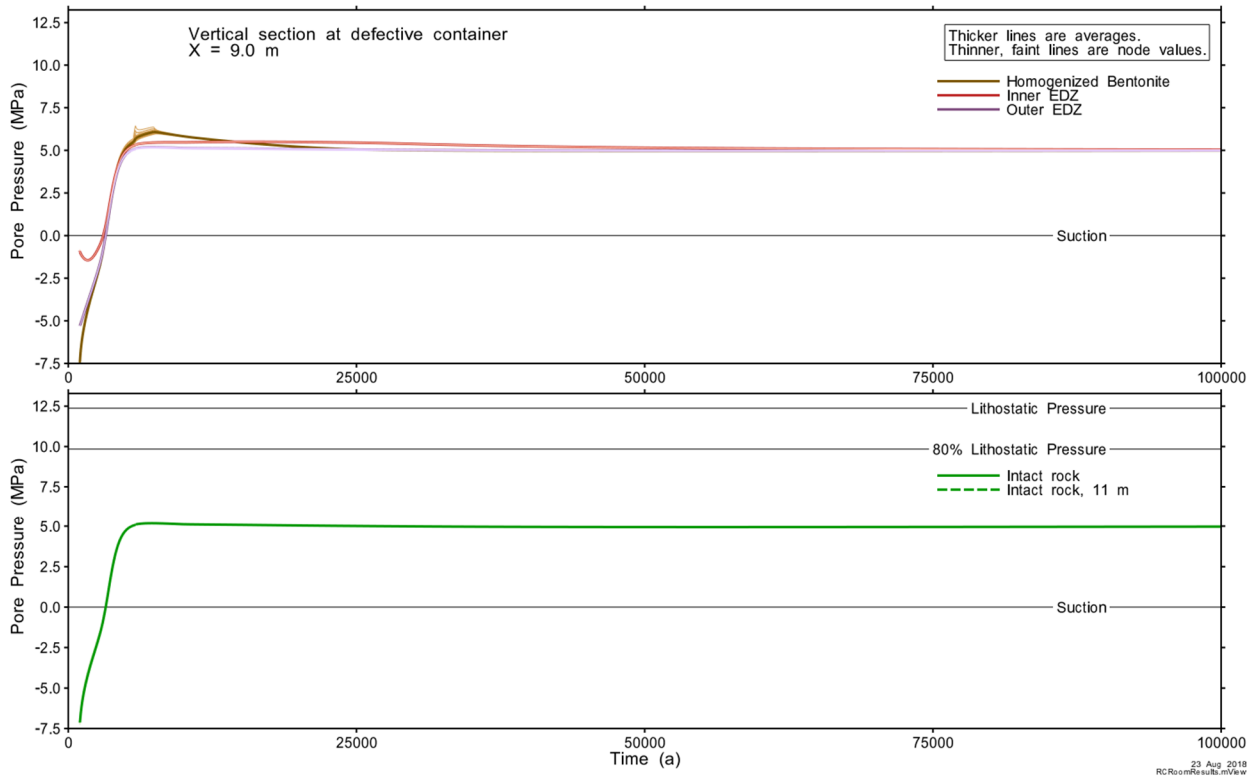


Figure 8-24: Room-Scale Model: Base Case - Nodal and Average Pore Pressure after First Container Failure

Maximum pore pressure of 6.2 MPa at 7400 years is well below 80% of lithostatic (10 MPa).

Gas generation impacts are very limited in domain, being largely restricted to the immediate vicinity of the defective container. The spatial distribution of gas saturation and pressures at the time of peak gas pressure are shown in Figure 8-25.

Excess gas saturations have nearly entirely dissipated by 100,000 years (Figure 8-26).

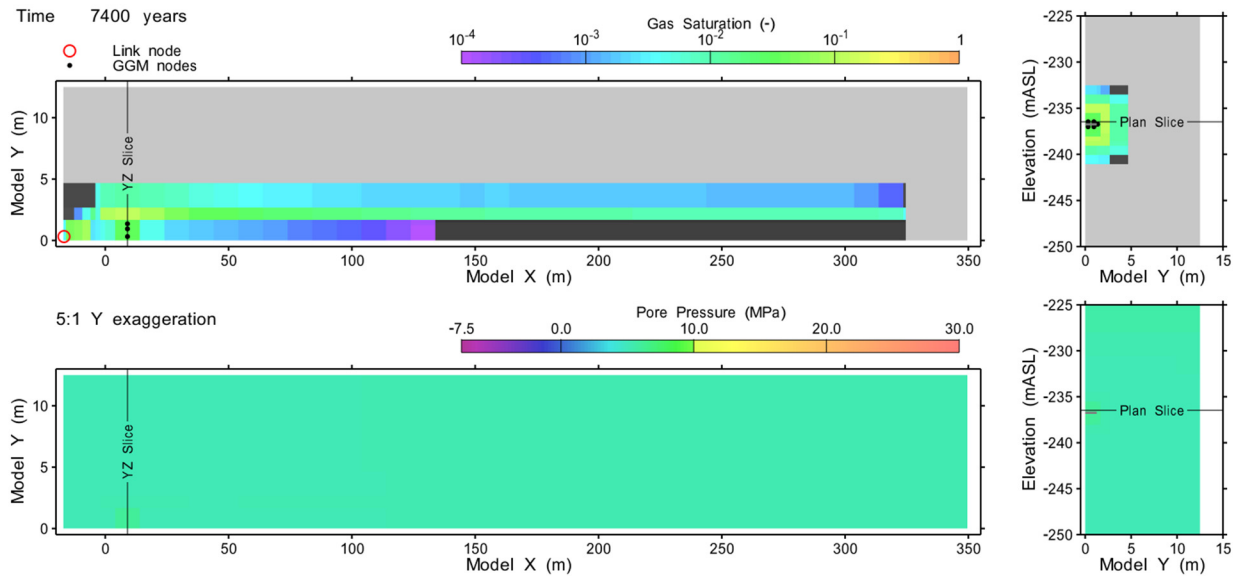


Figure 8-25: Room-Scale Model: Base Case - Gas Saturation and Pore Pressure at Time of Peak Pressure after First Container Failure (7400 Years)

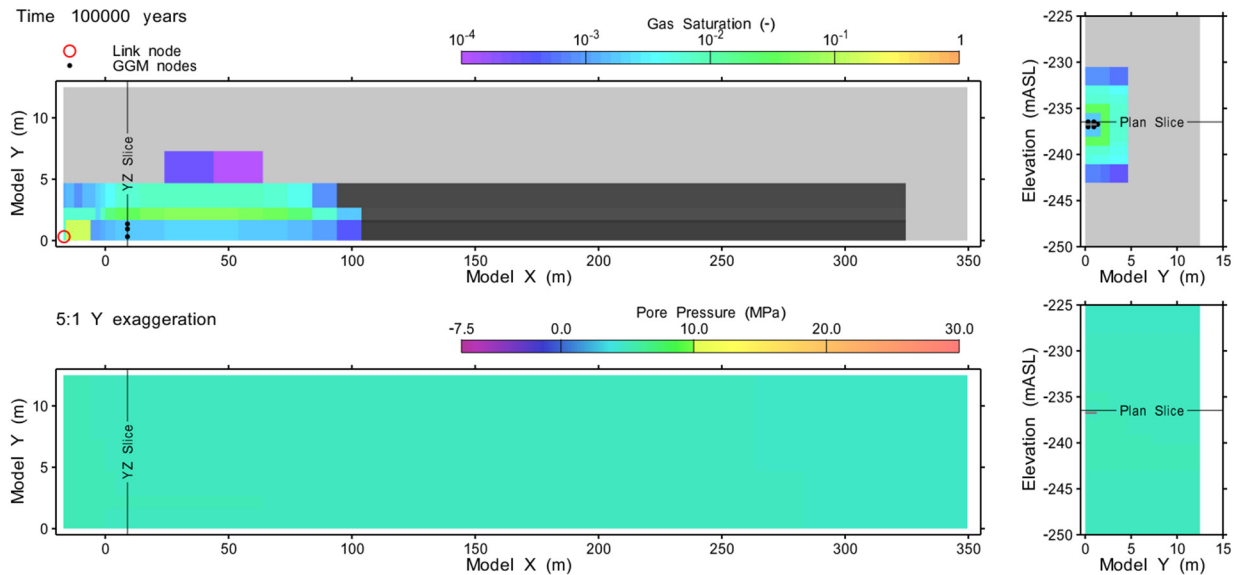


Figure 8-26: Room-Scale Model: Base Case - Gas Saturation and Pore Pressure at Time of Second Container Failure (100,000 Years)

The much reduced temperatures at 100,000 years lead to reduced corrosion rates for the second container failure (Figure 8-27). Compared to the first container, the second container takes about three times as long (20,500 a) to be completely consumed. Phase 4 corrosion continues to dominate, albeit at lower rates than for the first container failure.

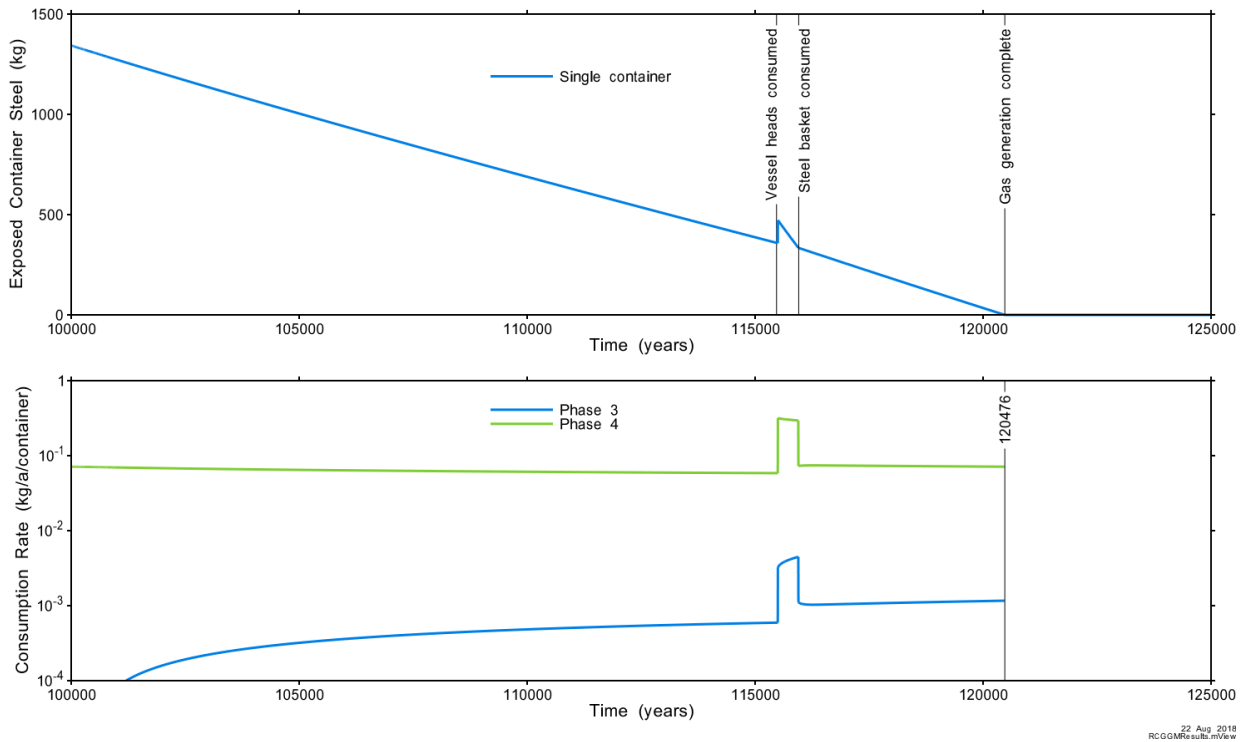


Figure 8-27: Room-Scale Model: Base Case - Steel Consumption and Corrosion Processes for Second Container Failure

Peak pore pressures are only slightly above hydrostatic, as shown in Figure 8-28. The spatial impact of the container failure is more limited than the first container, with excess gas pressures only present in the first 100 m of the room entrance (Figure 8-29).

Subsequent failures of containers 3 through 10 are similar in character to the second container failure, except that gas saturations within the intact rock reaches approximate steady-state conditions, as shown in Figure 8-30 for containers 2 through 4. As well, gas saturations at the peak pressure time after the third container failure (Figure 8-31) have extended well into the intact rock. A similar response is seen after container failures 4 through 10.

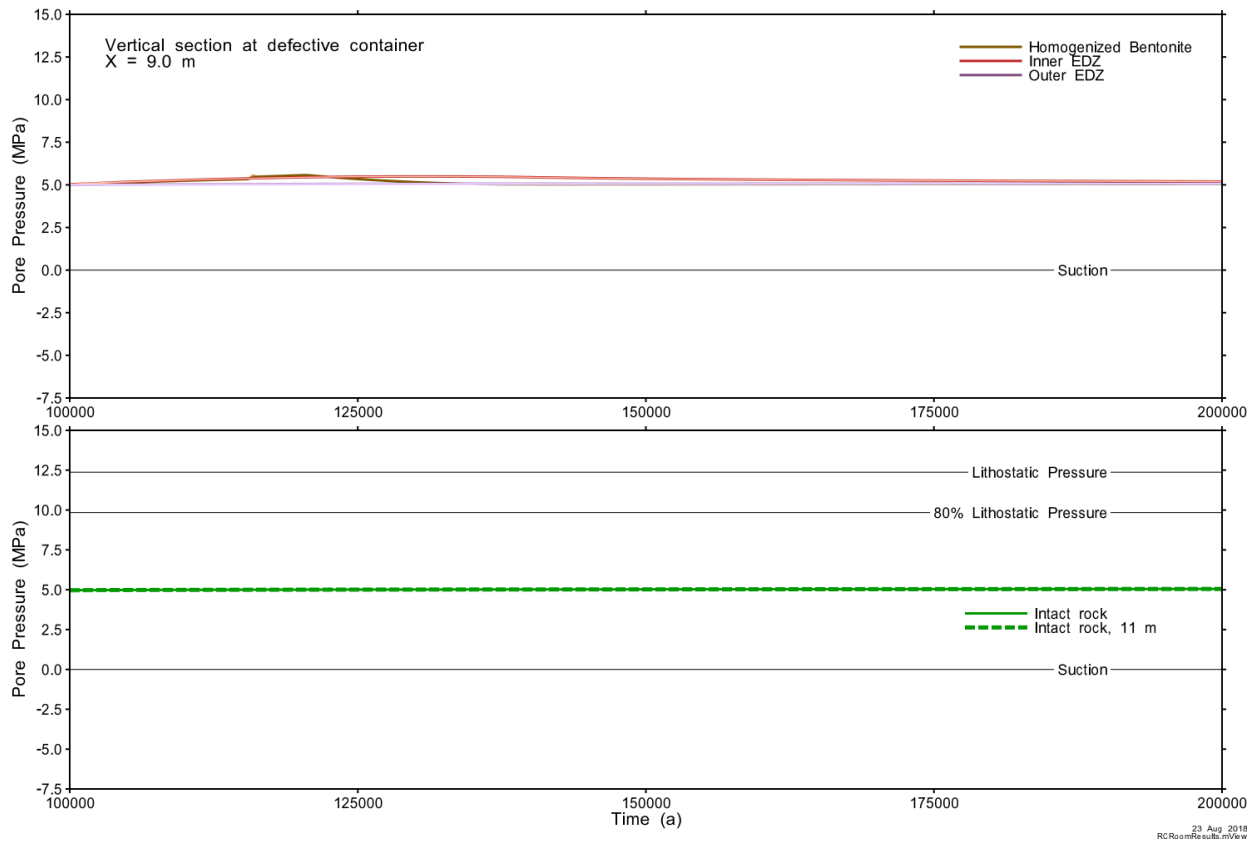


Figure 8-28: Room-Scale Model: Base Case - Nodal and Average Pore Pressure after Second Container Failure

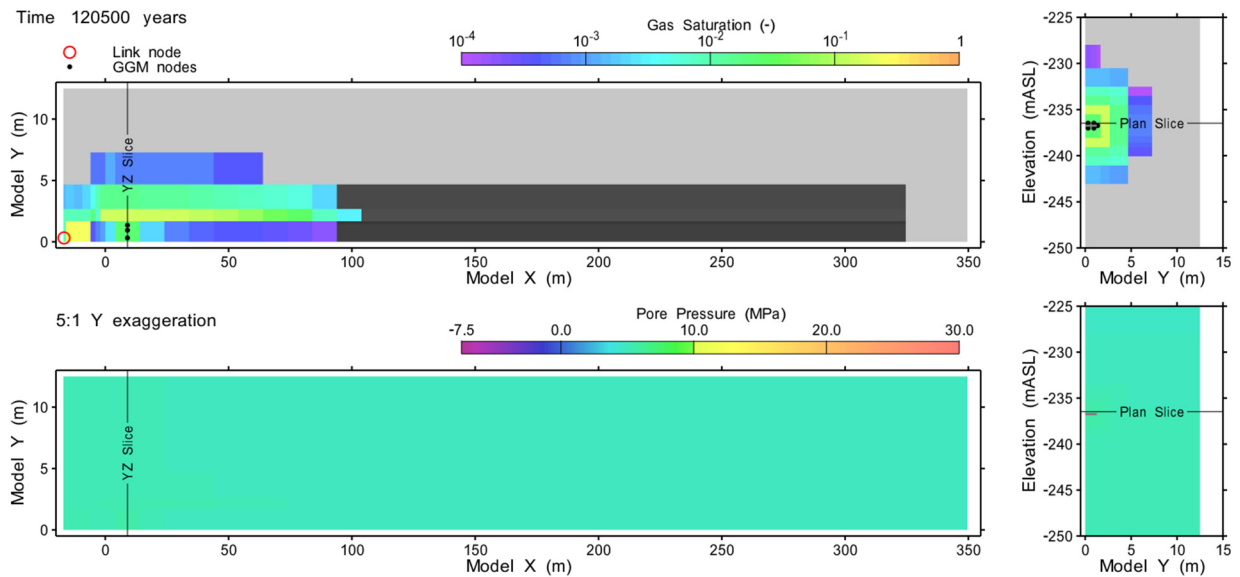


Figure 8-29: Room-Scale Model: Base Case - Gas Saturation and Pore Pressure at Time of Peak Pore Pressure for Second Container Failure (120,500 Years)

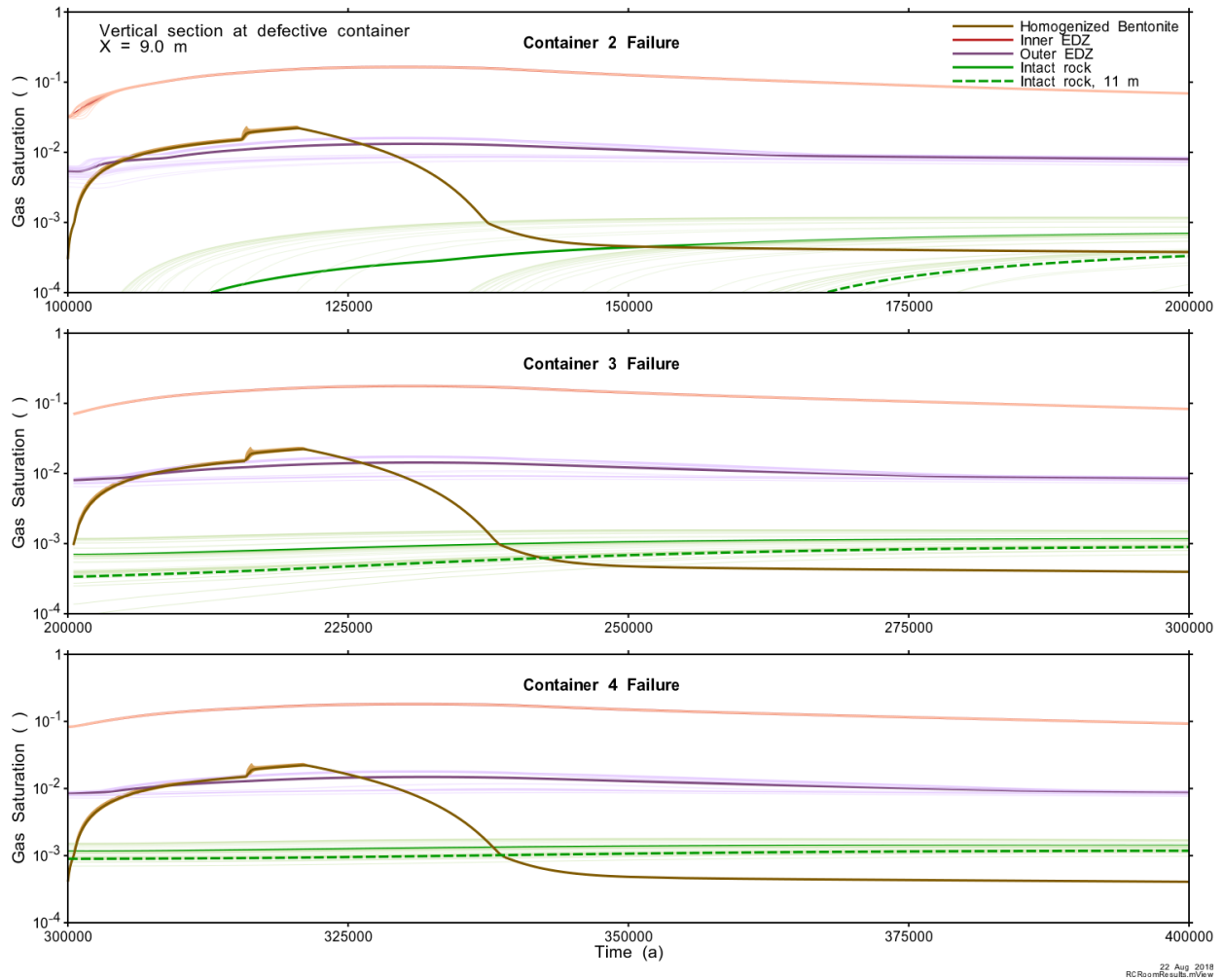


Figure 8-30: Room-Scale Model: Base Case - Comparison of Gas Saturation Profiles for Container 2, 3, and 4 Failures

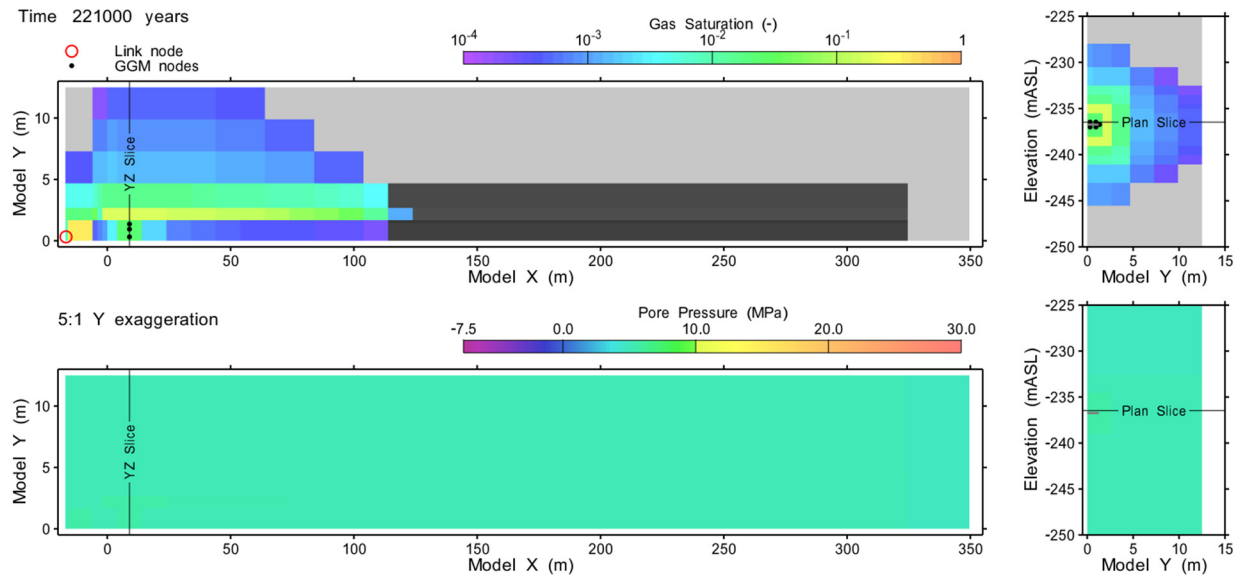


Figure 8-31: Room-Scale Model: Base Case - Gas Saturation and Pore Pressure at Time of Peak Pore Pressure for Third Container Failure (221,000 Years)

8.7.1.3 All Containers Fail Disruptive Event Scenario

In this scenario, all the containers fail simultaneously at 10,000 years. Just prior to the failure, at 10,000 years, the bentonite has homogenized and is almost completely water saturated, with minor amounts of gas remaining in the inner EDZ (Figure 8-32). Pore pressure has largely returned to hydrostatic.

At 10,000 years, all containers are assumed to fail as described in Section 8.2. Figure 8-33 shows corrosion results in terms of container mass remaining (per container) and corrosion rates by process. Initially, Phase 4 corrosion dominates due to the high average liquid saturation (>99.9%) within the EBS at the time of assumed failure. Soon afterwards, both Phase 3 and 4 corrosion occur, reflecting the partially saturated nature of the bentonite immediately surrounding the container. The thinner hemispherical ends of the containers are consumed at approximately 20,000 years, with an associated increase in both Phase 4 and Phase 3 corrosion due to the additional surface area of the basket and the interior of the container cylinder. The basket is consumed fairly quickly (in approximately 1000 years), after which only the exterior and interior of the container cylinder are available for corrosion. Phase 3 and Phase 4 corrosion rates change with available area, with Phase 4 decreasing as gas saturation in the EBS increases. The total amount of steel mass is exhausted by approximately 32,300 years, or less than 25,000 years after initial container failure.

Temperature and gas saturation results shown in Figure 8-34 indicate that the thermal profile is uniform across the room, EDZ and intact rock, and that temperature declines to a near-steady state by approximately 100,000 years. Gas saturations in the Inner EDZ reach 93% as generated gas moves from the EBS to the EDZ and porewater flows from the EDZ to the EBS due to the capillary pressure gradient. At a gas saturation of 93%, the amount of liquid

remaining in the Inner EDZ is equivalent to the residual liquid saturation and, as such, liquid ceases to move by conventional two-phase flow except by evaporation and diffusion. Gas saturation within the EBS remains below the residual gas saturation of the EBS and, as such, conventional two-phase flow of gas through the EBS only occurs by dissolution and diffusion. Gas saturations in the intact rock are essentially zero, with some small amounts of gas entering the rock adjacent to the EDZ at approximately 16,000 years.

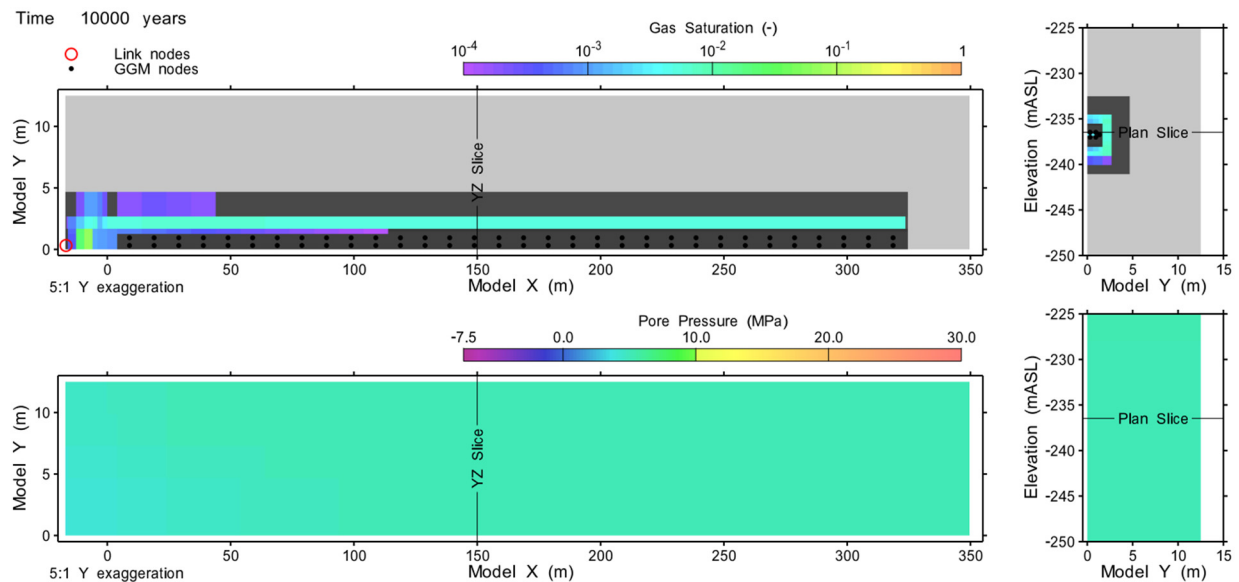


Figure 8-32: Room-Scale Model – All Containers Fail Scenario – Gas Saturation and Pore Pressure at 10,000 Years

Gas generation and transport are modelled by conventional two-phase flow and groundwater dissolution processes (see Section 8.3.2); however, the high corrosion rates presented in Figure 8-33 indicate high rates of gas generation which, considering the placement rooms are near fully saturated, will result in dilational flow of gas through the bentonite-based sealing materials. As the T2GGM code does not provide dilational flow calculations (see Section 8.4), the potential for high gas pressures is addressed qualitatively (note that hypothetical gas-borne dose consequences are estimated through bounding calculations; see Section 8.7.3.3).

For pressure, the target acceptance criterion is that pressure in the intact host rock surrounding the repository should remain below 80% of lithostatic pressure (i.e., below 10 MPa; see Section 8.1). While not providing dilational flow calculations, modelling results do illustrate whether pressures within the intact host rock can exceed the acceptance criterion before dilational flow allows dissipation of gas through the placement room.

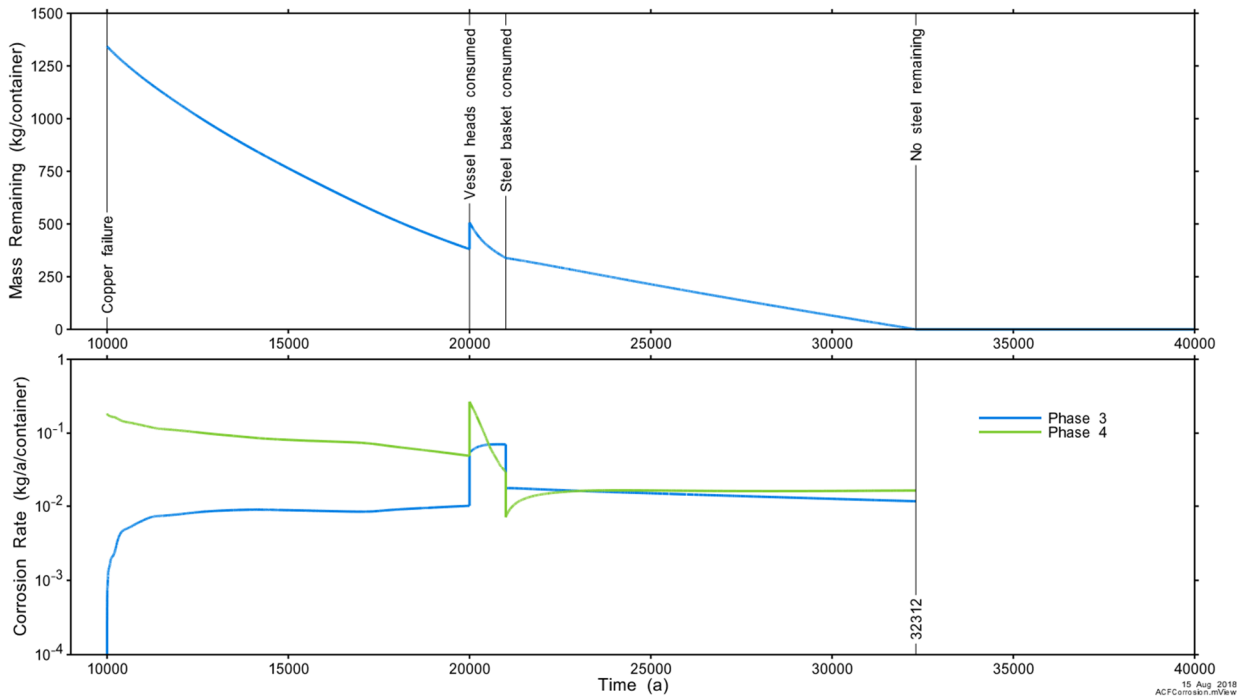


Figure 8-33: Room-Scale Model: All Containers Fail Scenario - Steel Consumption and Corrosion Processes

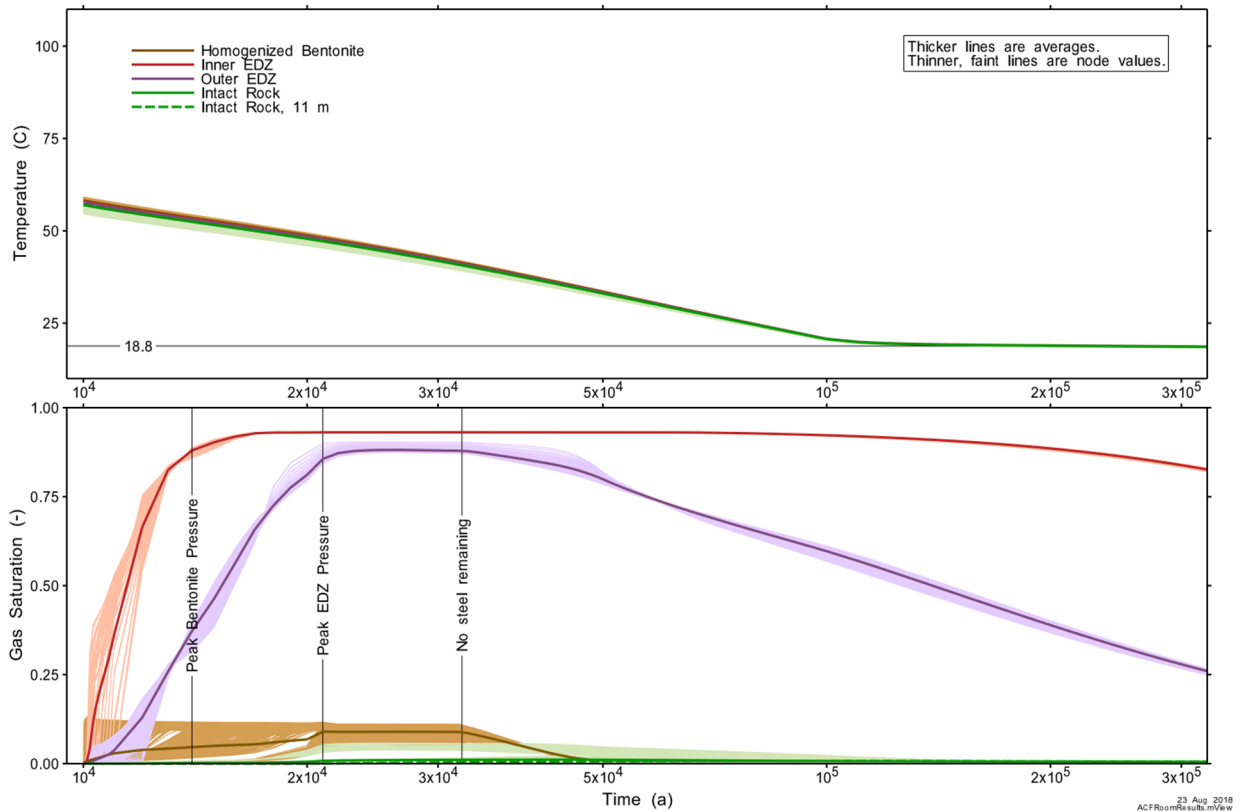


Figure 8-34: Room-Scale Model: All Containers Fail Scenario - Nodal and Average Temperature and Gas Saturation Conditions after Container Failures

When fully saturated, gas flow through bentonite-based sealing materials by two-phase flow processes is limited; instead, when increasing pressure exceeds the local confining stress (the sum of the swelling pressure and the local hydrostatic pressure), saturated bentonite will consolidate, leading to dilation of small-scale pathways and gas intrusion (Birgersson et al. 2008). Dilational flow of gas will continue until the pressure decreases below the local confining stress (Senger and Marschall, 2008; Cuss et al. 2011).

The bentonite sealing materials in the placement rooms (made from 100% bentonite) are expected to reach a maximum swelling pressure of approximately 1 MPa (Gobien et al. 2018). The local hydrostatic pressure is just above 5 MPa; as such, the local confining stress of the bentonite could be as much as approximately 6 MPa, but no greater.

Figure 8-35 shows gas saturations and pore pressures through the middle of the room at 10,500 years. By this time, there are a few locations where pressures within the bentonite have significantly exceeded the confining stress, indicating gas transport will proceed via dilational flow rather than conventional two-phase flow. Gas generation impacts are very limited in domain, being largely restricted to the immediate vicinity of the containers; the figure illustrates essentially no propagation of gas into the intact rock, with pore pressures well below 80% of lithostatic pressure.

Given that dilational flow will be the dominant gas transport process, pore pressures within the intact rock can be expected to remain well below 80% of lithostatic pressure and the possibility that gas pressure build-up will lead to fracturing can be excluded.

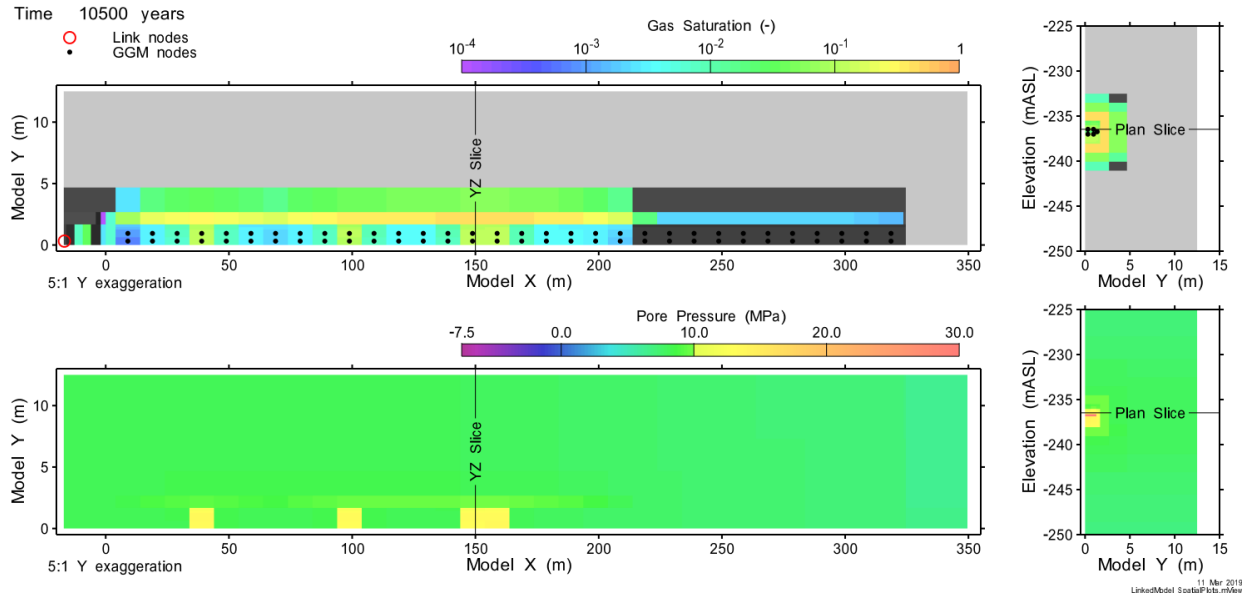


Figure 8-35: Room-Scale Model: All Containers Fail Scenario - Gas Saturation and Pore Pressure at 10,500 Years

8.7.2 Repository-Scale Model

Time-series results of temperature, gas saturation and pressure are reported for nodes in the Repository-Scale Model tunnels, as shown in Figure 8-36, and for nodes in the Repository-Scale Model shafts, as shown in Figure 8-37.

For reporting purposes, the model is divided into the following components:

- EBS nodes include dense backfill, bentonite seals, concrete, bentonite-sand, and asphalt.
- Inner EDZ nodes correspond to the inner EDZ of placement rooms.
- Outer EDZ nodes correspond to the outer EDZ of placement rooms.
- Intact rock nodes are adjacent to and beyond the outer EDZ of placement rooms.
- Intact rock nodes at the model boundaries are reported separately as “Intact Rock Boundaries”. For the Repository-Scale Model, these nodes have fixed pressures, saturations, and temperatures.

Time-series results are presented separately for the tunnel and shaft nodes. In time-series plots, the thin, lighter-coloured lines represent individual nodal values while the thicker, darker-coloured lines are the average of all nodes considered. Tunnel results for the pre-failure re-saturation period (Section 8.7.2.1) and the All Containers Fail Scenario (Section 8.7.2.3) use all the model nodes in each category, while the Base Case results (Section 8.7.2.2) use a limited subset of nodes in the vicinity of the connected Room-Scale Model and the shaft.

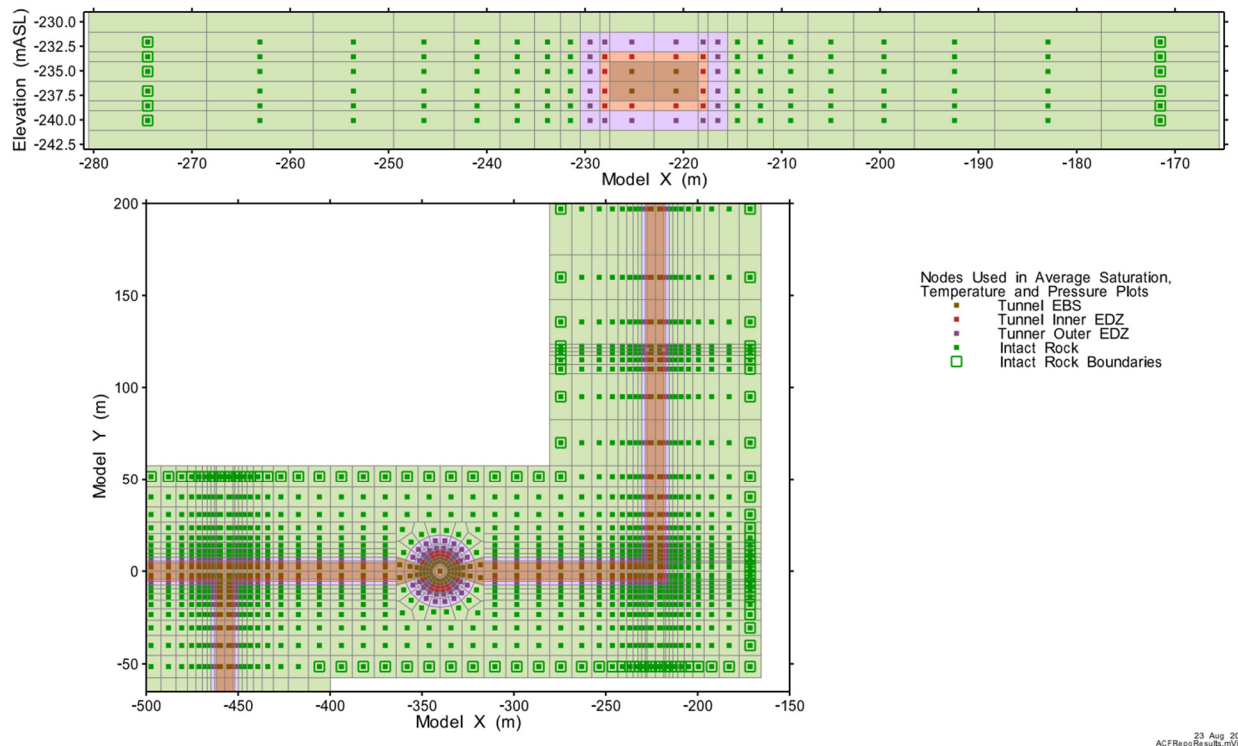


Figure 8-36: Repository-Scale Model: Locations of Time-Series Plot Points in the Tunnels

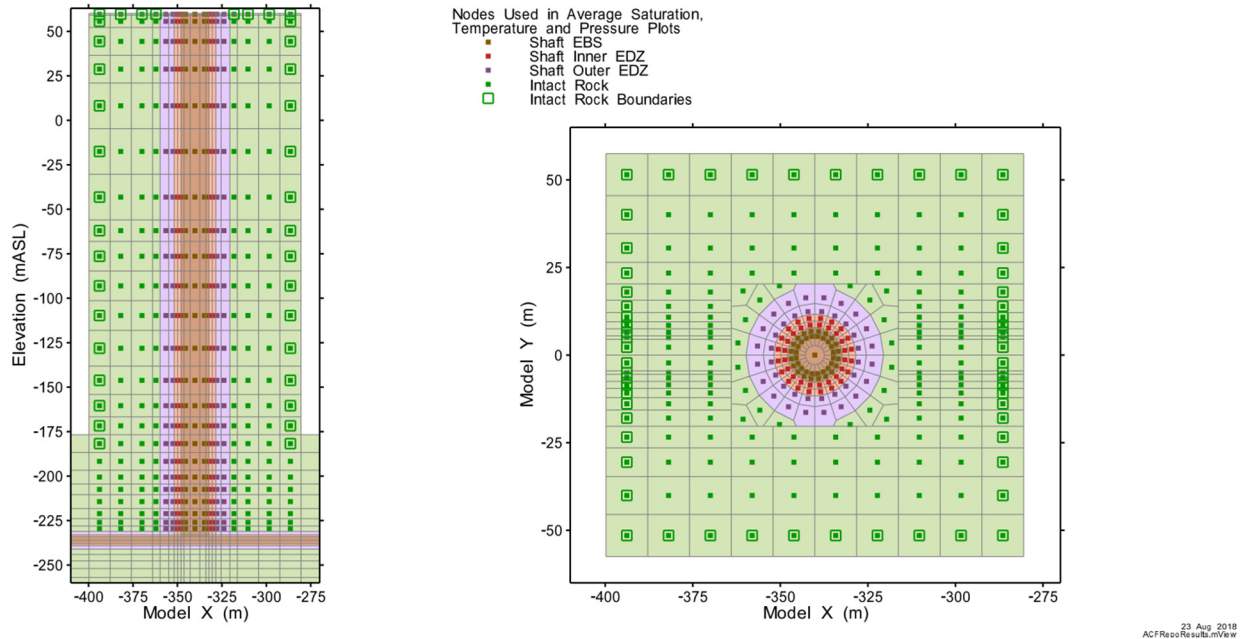


Figure 8-37: Repository-Scale Model: Locations of Time-Series Plot Points in the Model Shaft

8.7.2.1 Resaturation Period

Figure 8-38, Figure 8-39 and Figure 8-40 show saturation and pressure results for the first 10,000 years, the period of time prior to the assumed container failure for the All Containers Fail Scenario. Resaturation for the Base Case progresses until 1000 years only, as indicated on the figures. Temperatures are not shown as these model domains are sufficiently far from containers that temperatures vary little from the initial temperatures over the course of the simulation.

Figure 8-38 shows that the system becomes almost fully water saturated by 3600 years (with the exception of a small amount of residual gas that slowly dissolves into the water). There are also a few nodes, near the asphalt seal, that show an increase of gas saturation after the asphalt seal nodes saturate with water. The large variation in EBS saturation is a result of the different initial liquid saturations of the EBS materials. Very little gas enters the intact rock – saturations for the intact rock remain at or near zero.

Figure 8-39 and Figure 8-40 show pore pressures for the tunnels and shaft, respectively. Oscillations in the pressures are due to minor instabilities in the linked flows between the Room-Scale Model and Repository-Scale Model. The oscillations are local to the linked nodes and not observed in the pressures in the shaft.

The spatial distributions of pressures and saturations in the tunnels and shaft at the time of the first Base Case container failure are shown in Figure 8-41 and Figure 8-42. Pressures are still in a suction state (i.e., below 0 MPa) within the EBS and EDZ. By 10,000 years, gas has largely dissolved out of the tunnels with very low levels of remaining gas within the shafts (Figure 8-43 and Figure 8-44). Pressures in both are at hydrostatic.

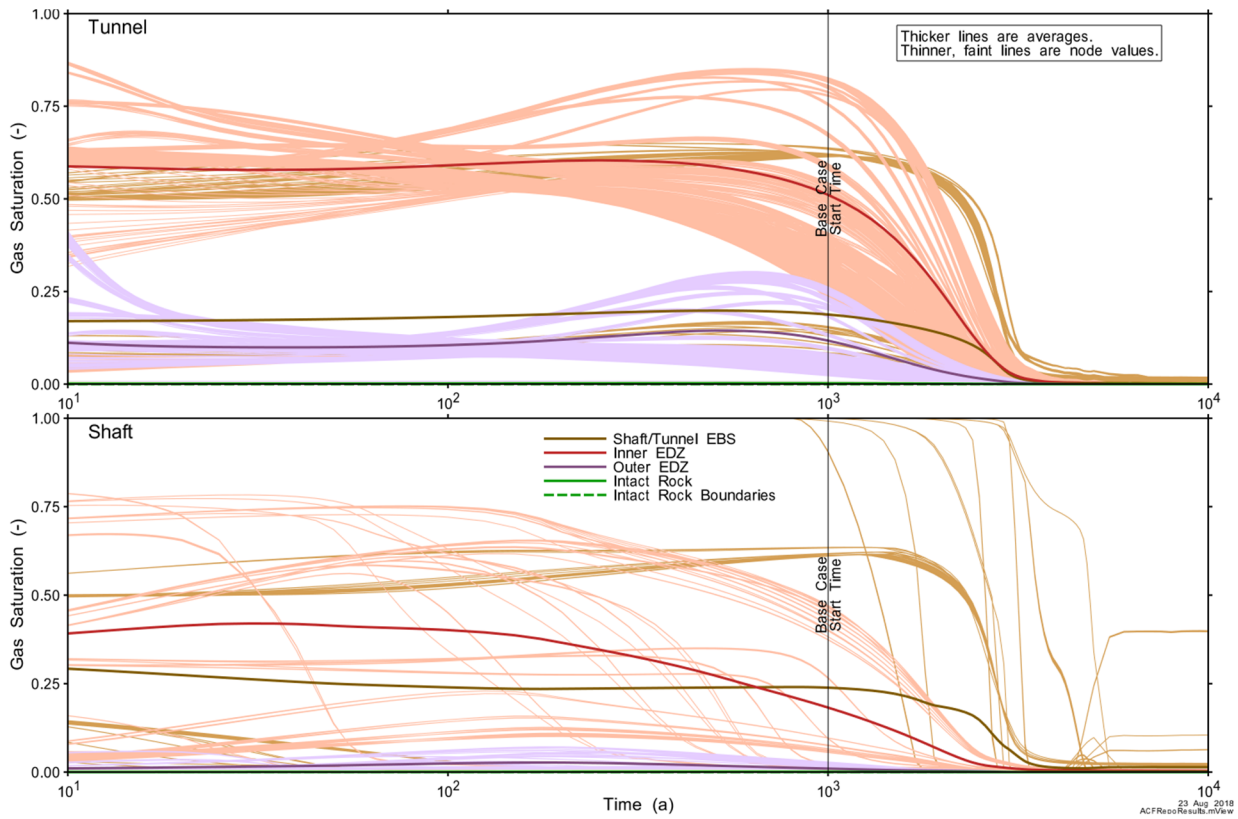


Figure 8-38: Repository-Scale Model: Gas Saturation prior to Container Failures

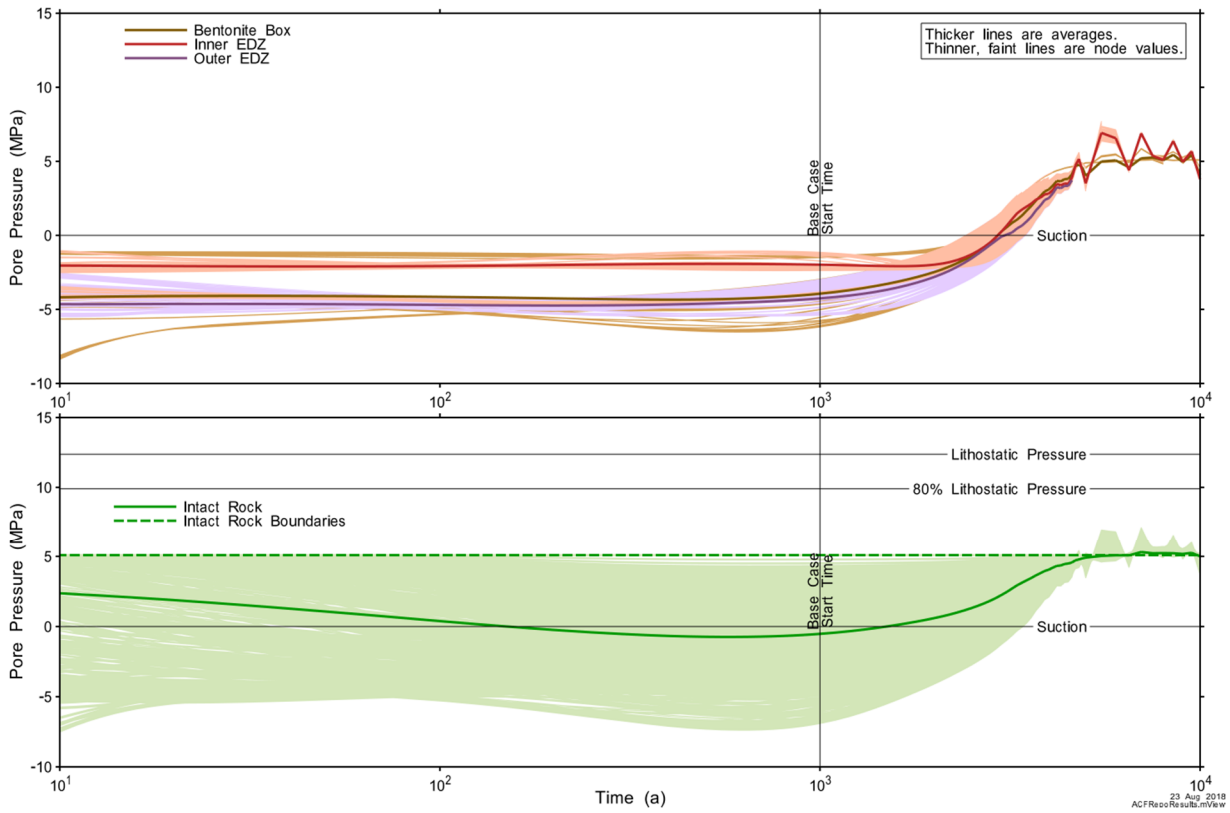


Figure 8-39: Repository-Scale Model: Tunnel Pore Pressure prior to Container Failures

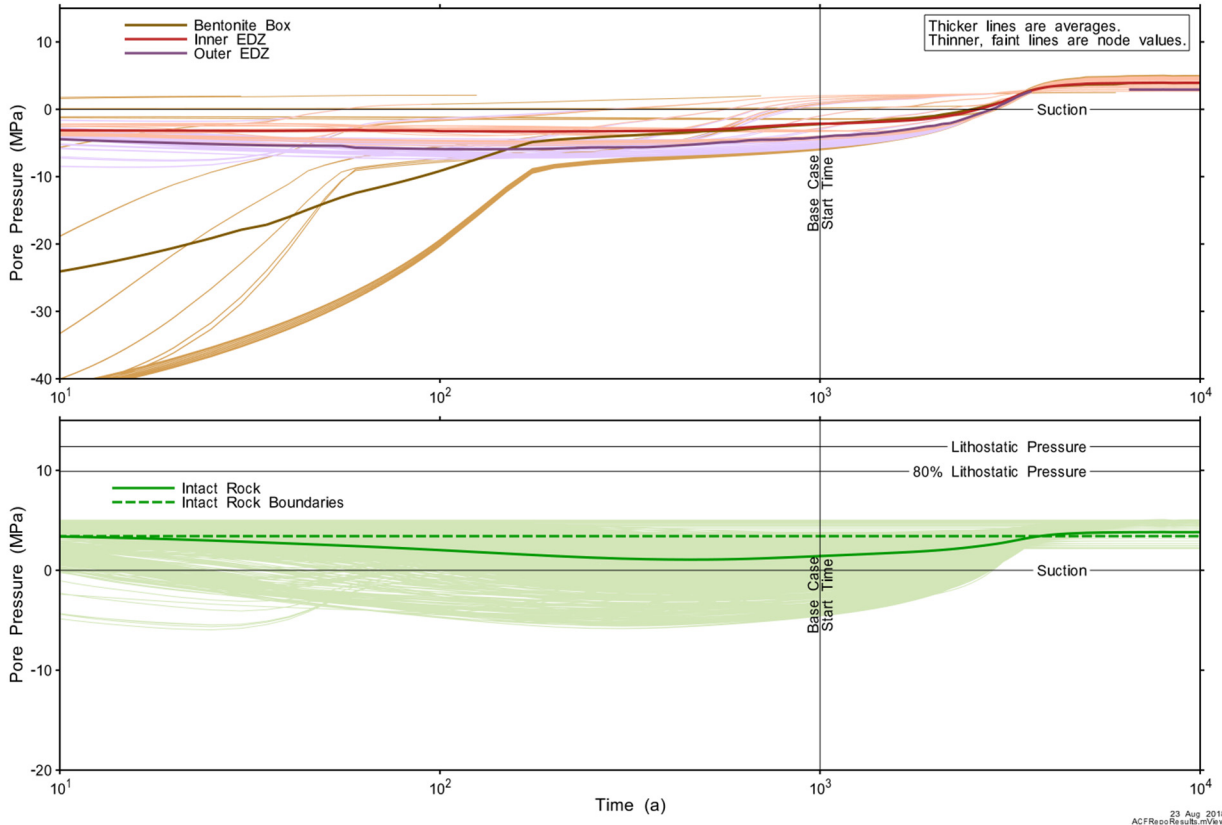


Figure 8-40: Repository-Scale Model: Nodal and Average Shaft Pore Pressure prior to Container Failures

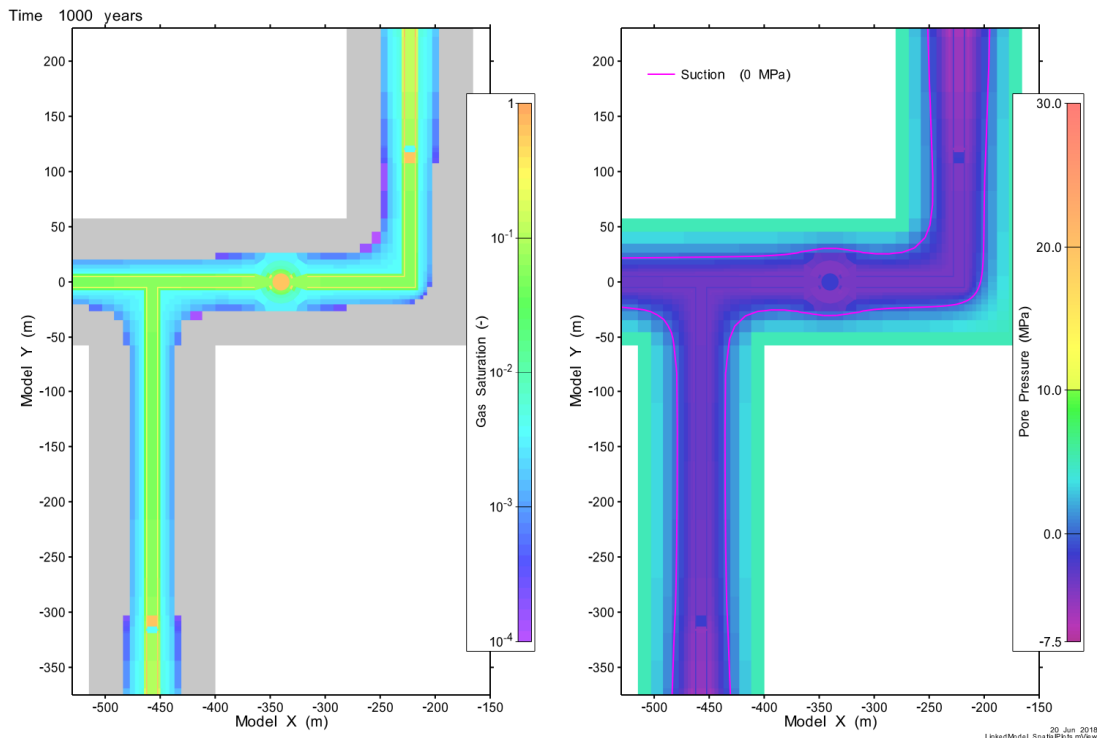


Figure 8-41: Repository-Scale Model: Gas Saturation and Pore Pressure in the Repository Tunnels at 1000 Years

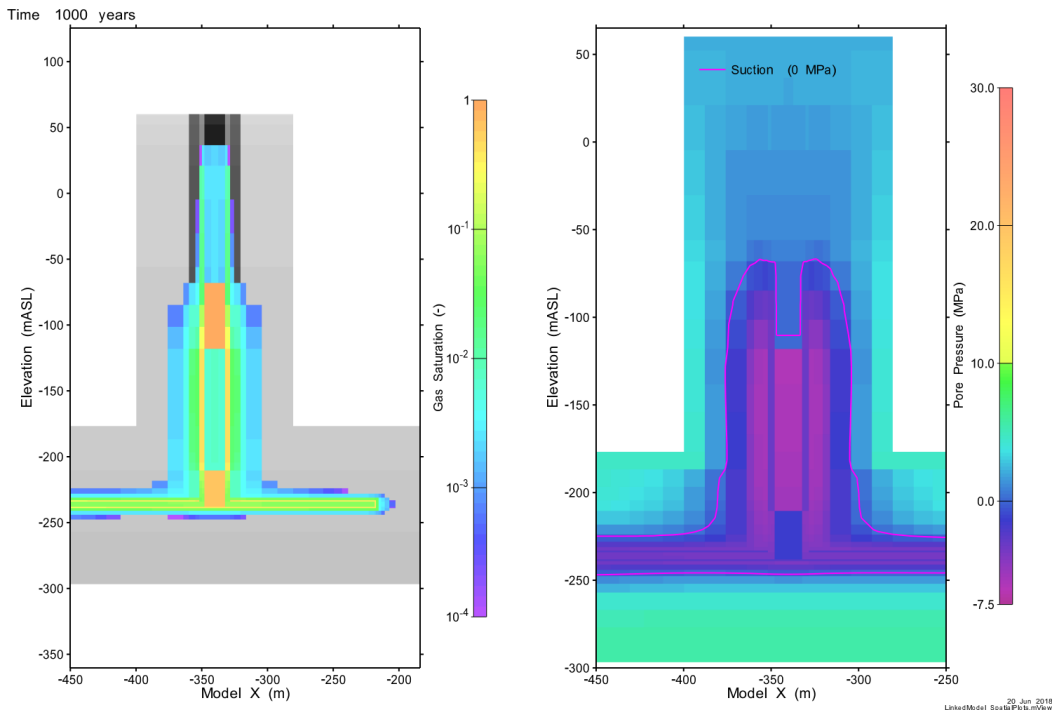


Figure 8-42: Repository-Scale Model: Gas Saturation and Pore Pressure in the Repository Shaft at 1000 Years

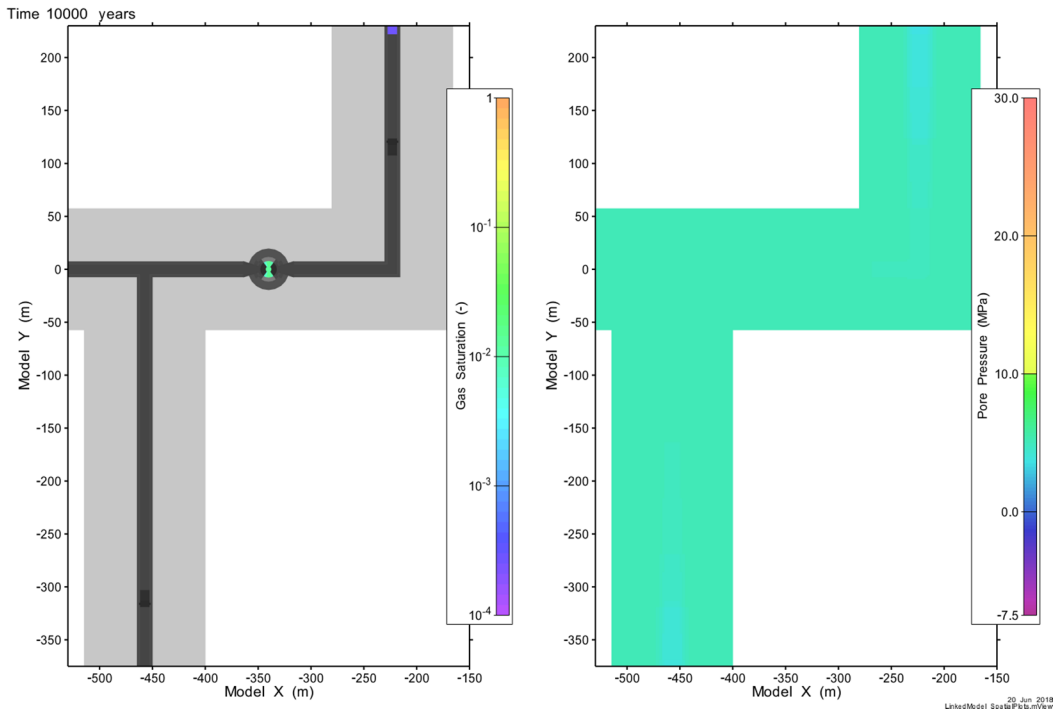


Figure 8-43: Repository-Scale Model: Gas Saturation and Pore Pressure in the Repository Tunnels at 10,000 Years

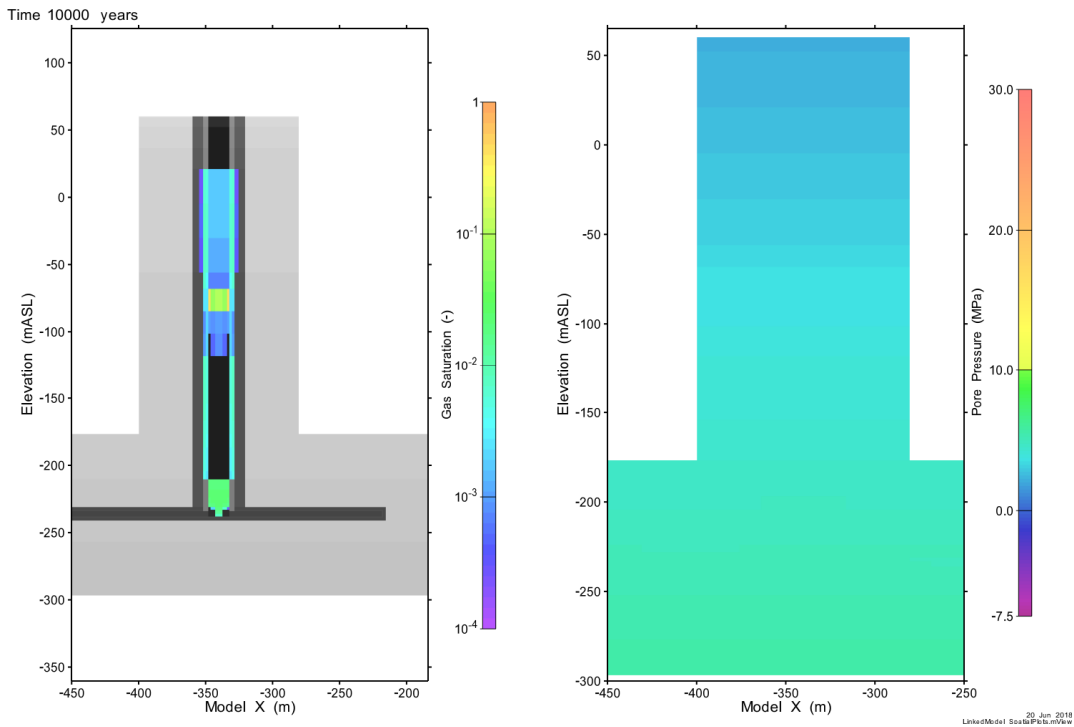


Figure 8-44: Repository-Scale Model: Gas Saturation and Pore Pressure in the Repository Shaft at 10,000 Years

8.7.2.2 Base Case

In general, gas generation from the Base Case container failures has almost no impact on the Repository-Scale Model; consequently, behaviour in the tunnels and shaft mostly follows the resaturation profile from 1000 years to 10,000 years described in Section 8.7.2.1. This is not unexpected as the gas generation for a single container is very small. Also, as shown with Room-Scale results in Section 0, the 100,000 year interval between failures minimizes cumulative effects, as gas generated from a previous failure has almost entirely dissipated before the next failure.

Tunnel gas saturations and pressures are plotted for the subset of repository nodes as shown in Figure 8-45. Shaft results are plotted for the repository nodes as shown previously in Figure 8-37.

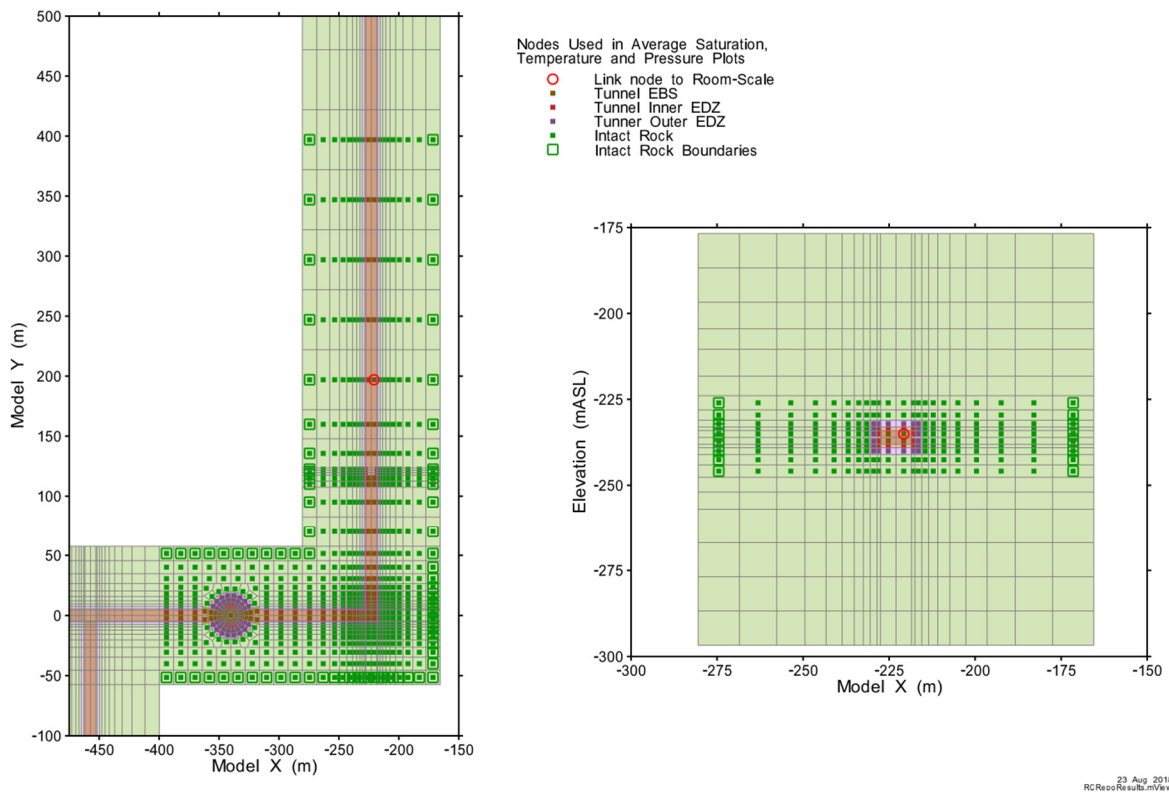


Figure 8-45: Repository-Scale Model: Locations of Time-Series Plot Points in the Model Tunnels for the Base Case

Figure 8-46 shows gas saturations in the tunnels and shaft from the time of failure of the first container until the time immediately prior to the failure of the fifth container. Comparing saturations shown in Figure 8-46 to the shaft and tunnel gas saturations during resaturation shown in Figure 8-38 confirms there are no significant impacts of the single container failure. Note that the wide variations in shaft EBS saturation are due to the differences in behaviour of bentonite/sand and the asphalt seal, with the asphalt responsible for the higher gas saturations.

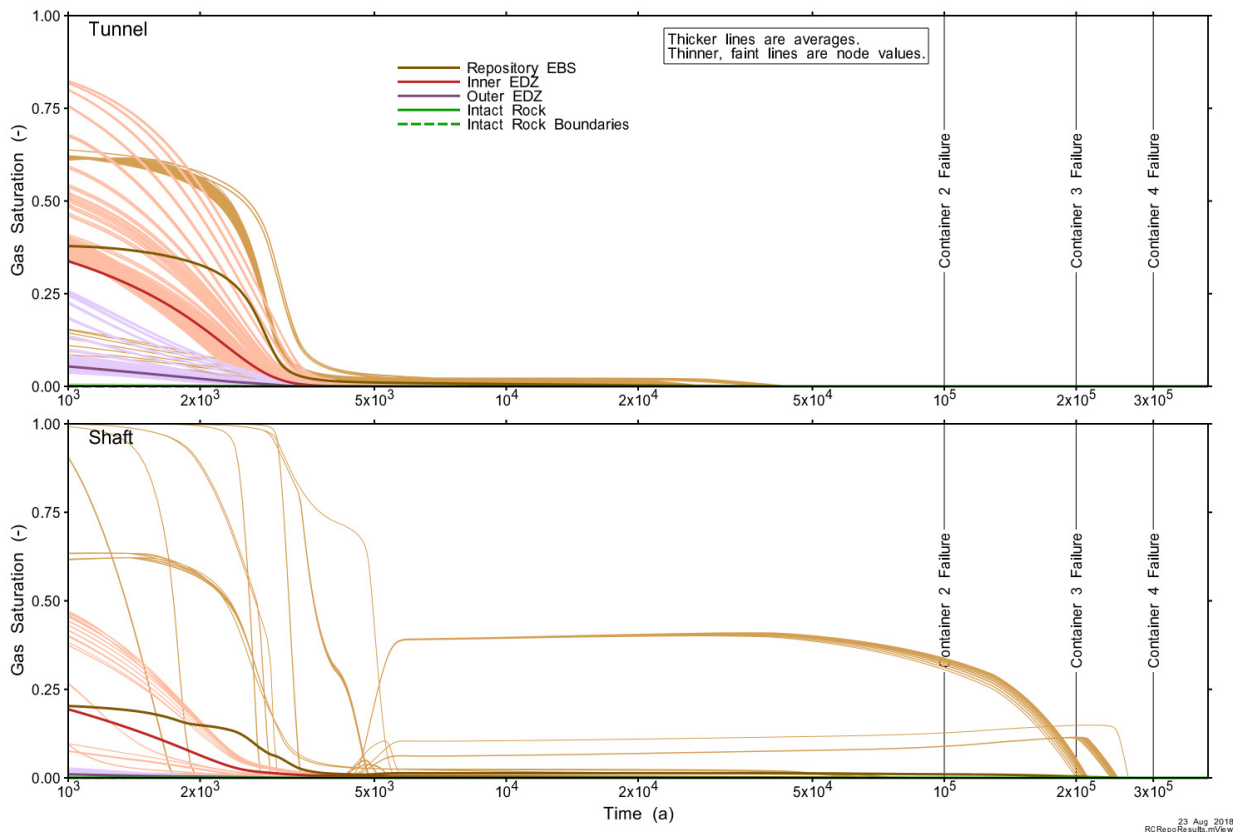


Figure 8-46: Repository-Scale Model: Base Case - Gas Saturation in the Tunnels and Shaft

Gas saturations and pore pressures in a vertical section through the tunnel location coincident with the link node are shown in Figure 8-47 through Figure 8-50, for 1000 years (initial conditions) and then for the times associated with peak pressures in the rooms following container failures 1 through 3. There are no visually discernable impacts of room gas migration into the tunnel.

Figure 8-51 and Figure 8-52 show pore pressures for the tunnel and shaft materials. All initially present gas dissolves and pressures equilibrate to hydrostatic. There is no indication of any impact due to the container failures.

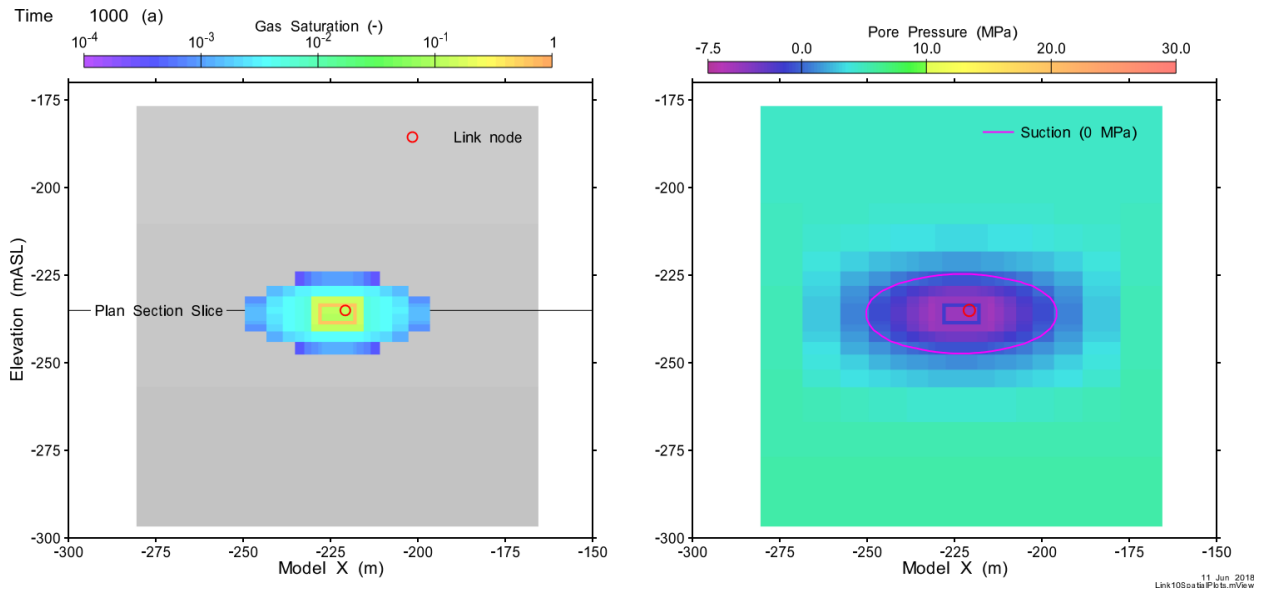


Figure 8-47: Repository-Scale Model: Base Case - Gas Saturation and Pore Pressure in a Vertical Section through the Tunnel at the Room-Scale/Repository-Scale Linking Point at 1000 Years

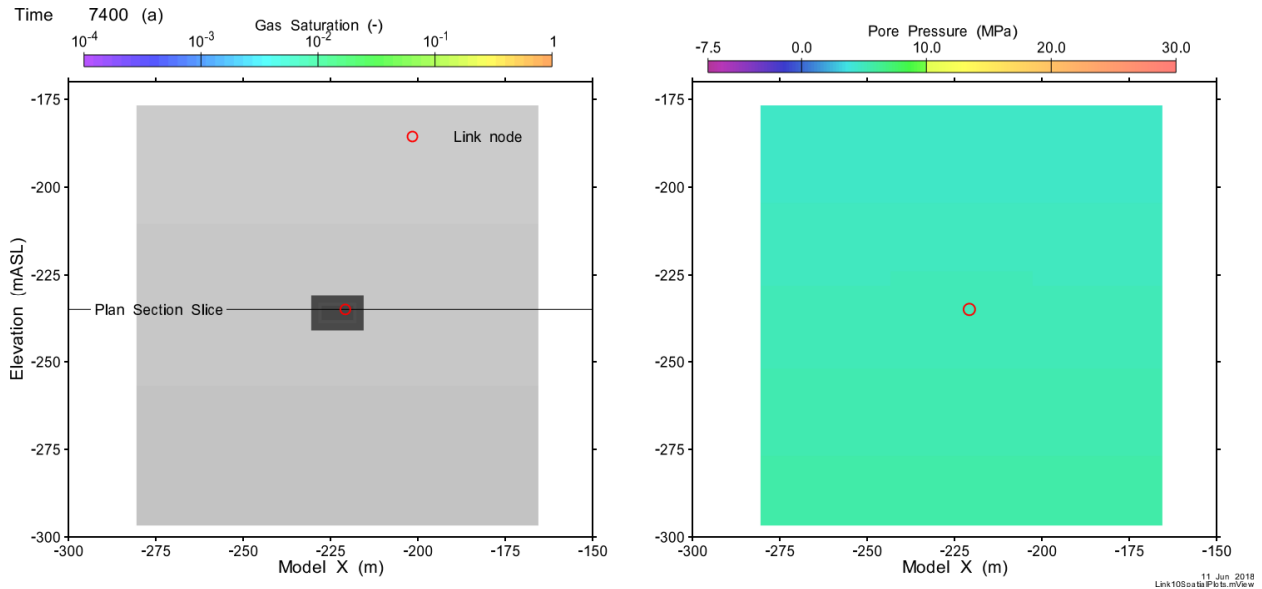


Figure 8-48: Repository-Scale Model: Base Case - Gas Saturation and Pore Pressure in a Vertical Section through the Tunnel at the Room-Scale/Repository-Scale Linking Point at the Time of Peak Room Pressure after First Container Failure (7400 Years)

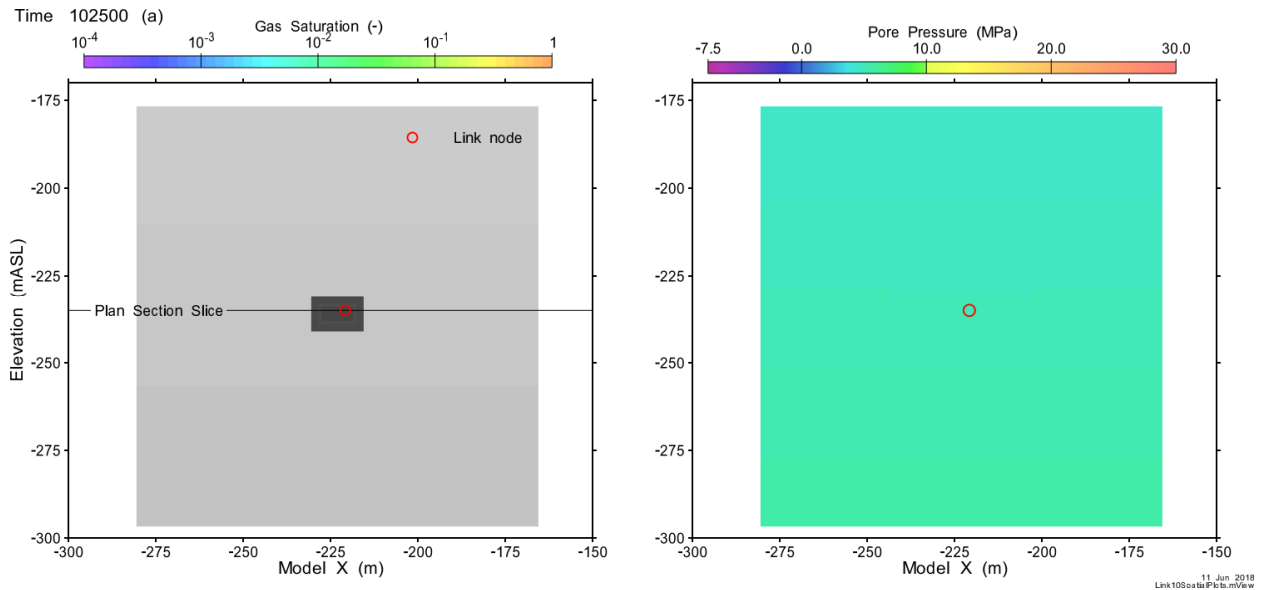


Figure 8-49: Repository-Scale Model: Base Case - Gas Saturation and Pore Pressure in a Vertical Section through the Tunnel at the Room-Scale/Repository-Scale Linking Point at the Time of Peak Room Pressure after Second Container Failure (120,500 Years)

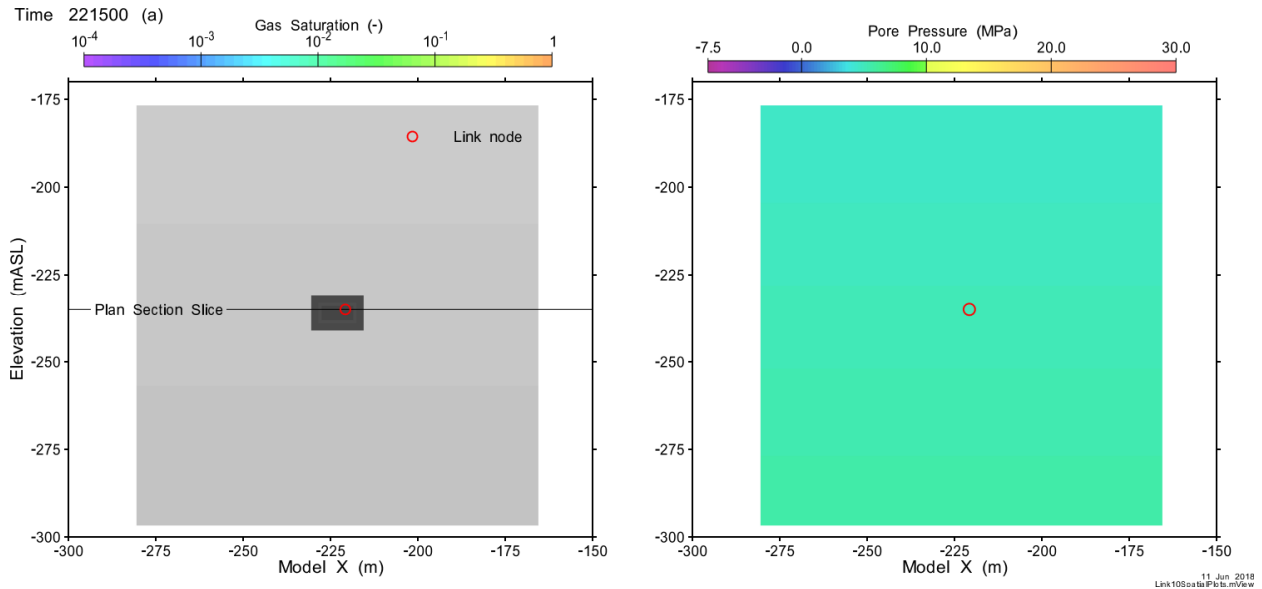


Figure 8-50: Repository-Scale Model: Base Case - Gas Saturation and Pore Pressure in a Vertical Section through the Tunnel at the Room-Scale/Repository-Scale Linking Point at the Time of Peak Room Pressure after Third Container Failure (221,500 Years)

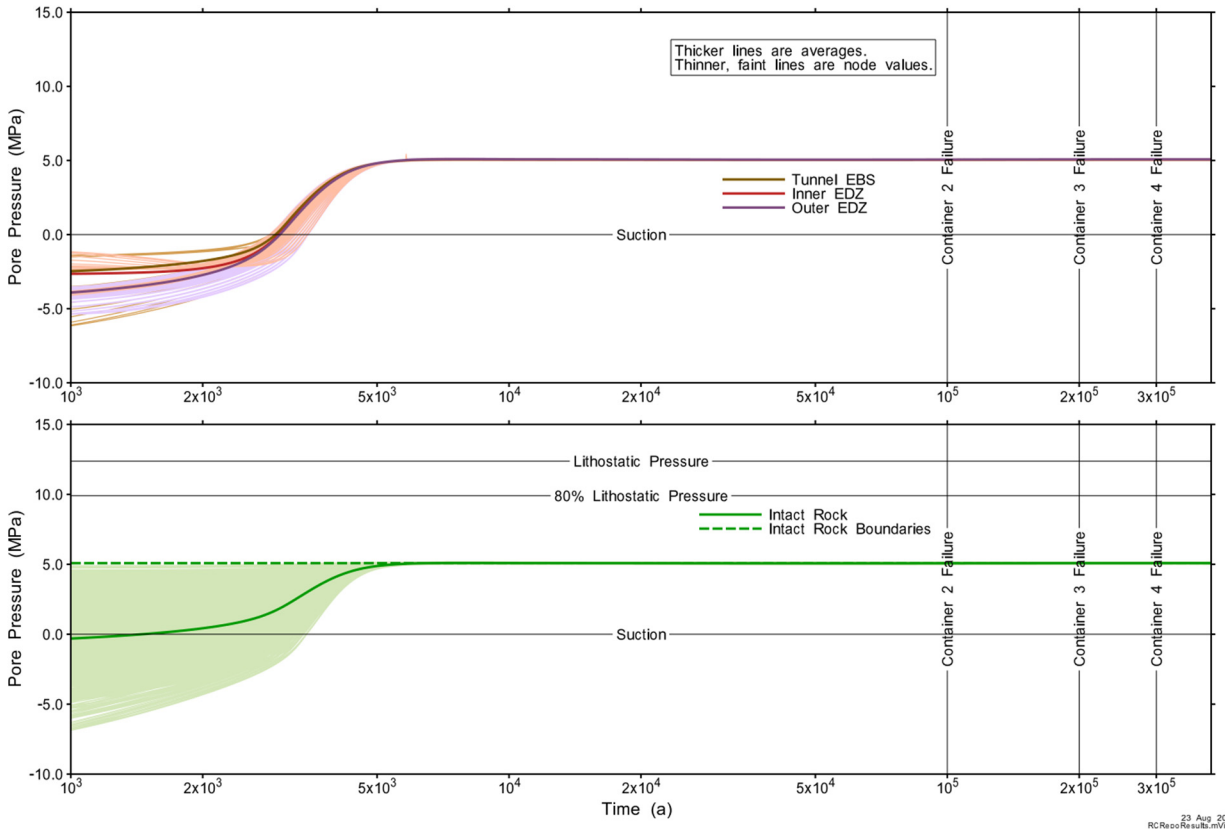


Figure 8-51: Repository-Scale Model: Base Case - Nodal and Average Tunnel Pore Pressure after Container Failures

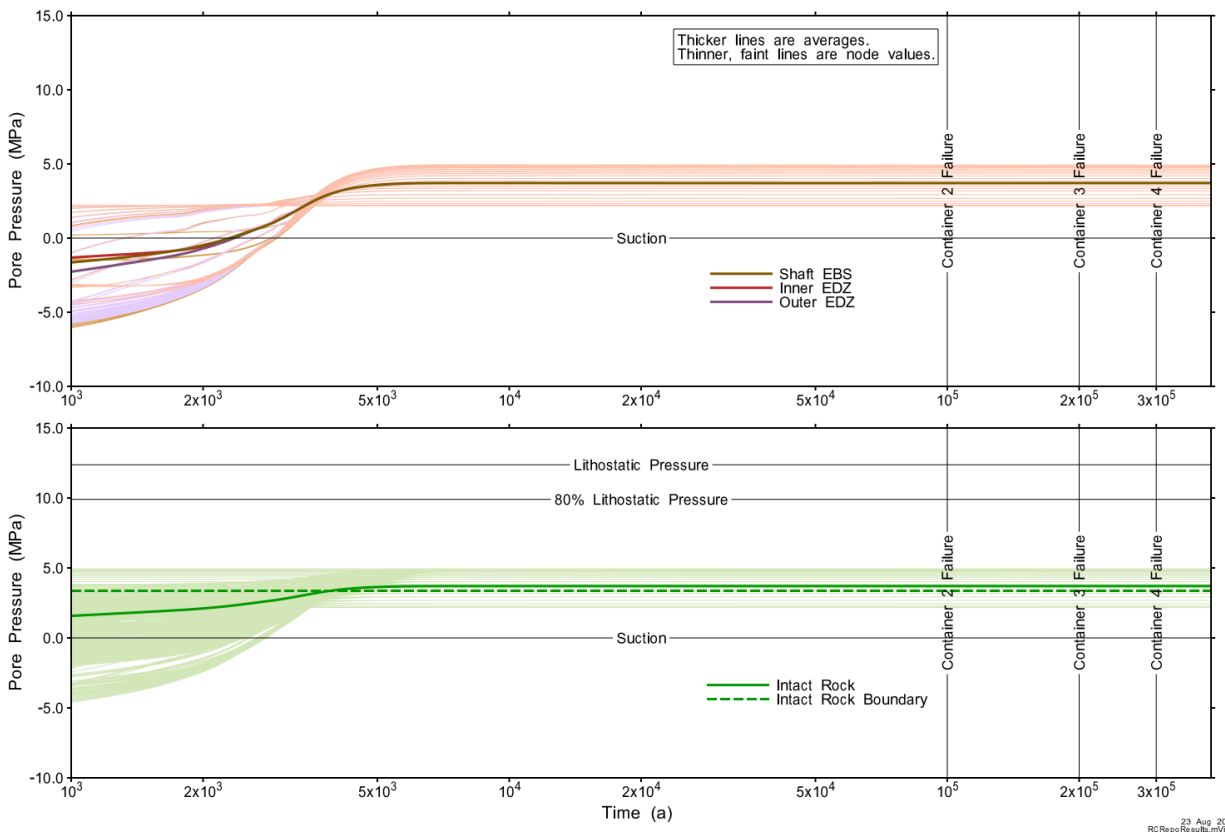


Figure 8-52: Repository-Scale Model: Base Case - Nodal and Average Shaft Pore Pressure after Container Failures

8.7.2.3 All Containers Fail Disruptive Event Scenario

Figure 8-53 shows gas saturations within the tunnels and shaft after 10,000 years, the period of time after the assumed container failures. Temperatures are not shown as these model domains are sufficiently far from containers that temperatures vary little from initial temperatures over the course of the simulation⁹.

As described for the Room-Scale Model (see Section 8.7.1.3), the T2GGM code does not provide dilational flow calculations. The potential for high gas pressures in the All Containers Fail scenario is addressed qualitatively (note that hypothetical gas-borne dose consequences are estimated through bounding calculations; see Section 8.7.3.3).

For pressure, the target acceptance criterion is that pressure in the intact host rock surrounding the repository should remain below 80% of lithostatic pressure (see Section 8.1). While not

⁹ There is no thermal conduction connection from the intact rock in the Room-Scale Model to the Repository-Scale Model; however, thermal fluxes are included in the model linking.

providing dilational flow calculations, modelling results do illustrate whether pressures within the intact host rock can exceed the acceptance criterion before dilational flow allows dissipation of gas through the repository access tunnels and shaft.

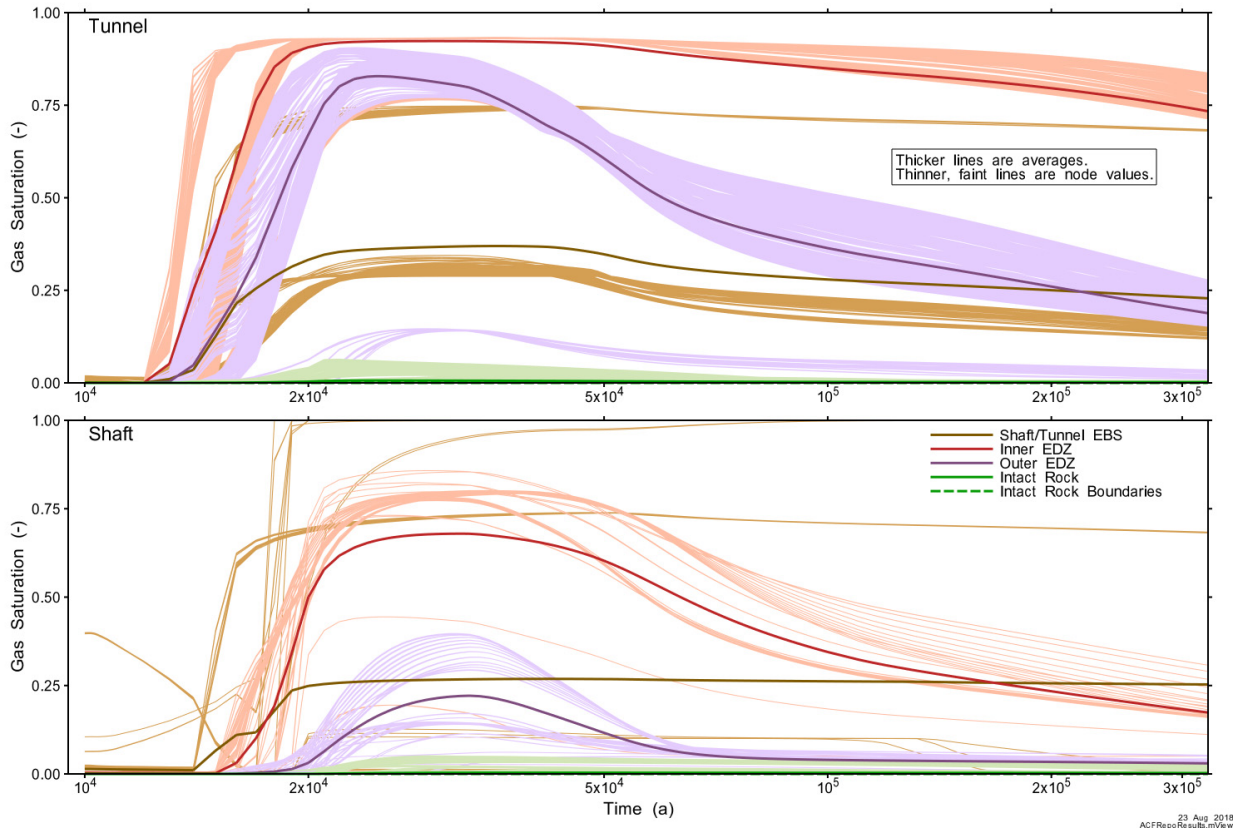


Figure 8-53: Repository-Scale Mode: All Containers Fail Scenario - Gas Saturation in the Tunnels and Shaft after Container Failures

When fully saturated, gas flow through bentonite-based sealing materials by two-phase flow processes is limited; instead, when increasing pressure exceeds the local confining stress (the sum of the swelling pressure and the local hydrostatic pressure), saturated bentonite will consolidate, leading to dilation of small-scale pathways and gas intrusion (Birgersson et al. 2008). Dilational flow of gas will continue until the pressure decreases below the local confining stress (Senger and Marschall, 2008; Cuss et al. 2011).

As described in Section 8.7.1.3, the bentonite-based sealing materials in the placement rooms (made from 100% bentonite) are expected to reach a maximum swelling pressure of approximately 1 MPa (Gobien et al. 2018). The local hydrostatic pressure at repository depth is just above 5 MPa; as such, the local confining stress of the bentonite could be as much as

approximately 6 MPa, but no greater. For conservatism, the same local confining stress will be assumed for bentonite-based sealing materials throughout the repository¹⁰.

Figure 8-54 and Figure 8-55 show gas saturations and pore pressures within the tunnels at 10,500 years. Gas is entering the EBS and EDZ from the rooms. Note that the light grey shown within the figures represents intact rock with no gas present; very little gas enters the intact rock. By this time, pressures within the bentonite-based sealing materials have already reached or exceeded the confining stress, indicating gas transport will proceed via dilational flow rather than conventional two-phase flow.

Figure 8-56 shows gas saturations and pore pressures within the shaft at 14,000 years. There are a few nodes near the asphalt seal that show an increase in gas saturation. Very little gas enters the intact rock – saturations for the intact rock remain at or near zero. Here, too, pressures within the bentonite-based sealing materials have reached or exceeded the confining stress, indicating gas transport will proceed via dilational flow rather than conventional two-phase flow.

There are no visually discernable impacts of room gas migration into the tunnel. Gas generation impacts are very limited in domain with essentially no propagation of gas into the intact rock and pore pressures remaining near hydrostatic. Given that dilational flow will be the dominant gas transport process, pore pressures within the intact rock can be expected to remain well below 80% of lithostatic pressure and the possibility that gas pressure build-up will lead to fracturing can be excluded.

¹⁰ Gap-fill pellets (made from 100% bentonite) in repository tunnels and bentonite-sand shaft seals (made from 70% bentonite) both have expected maximum swelling pressures of only 300 kPa.

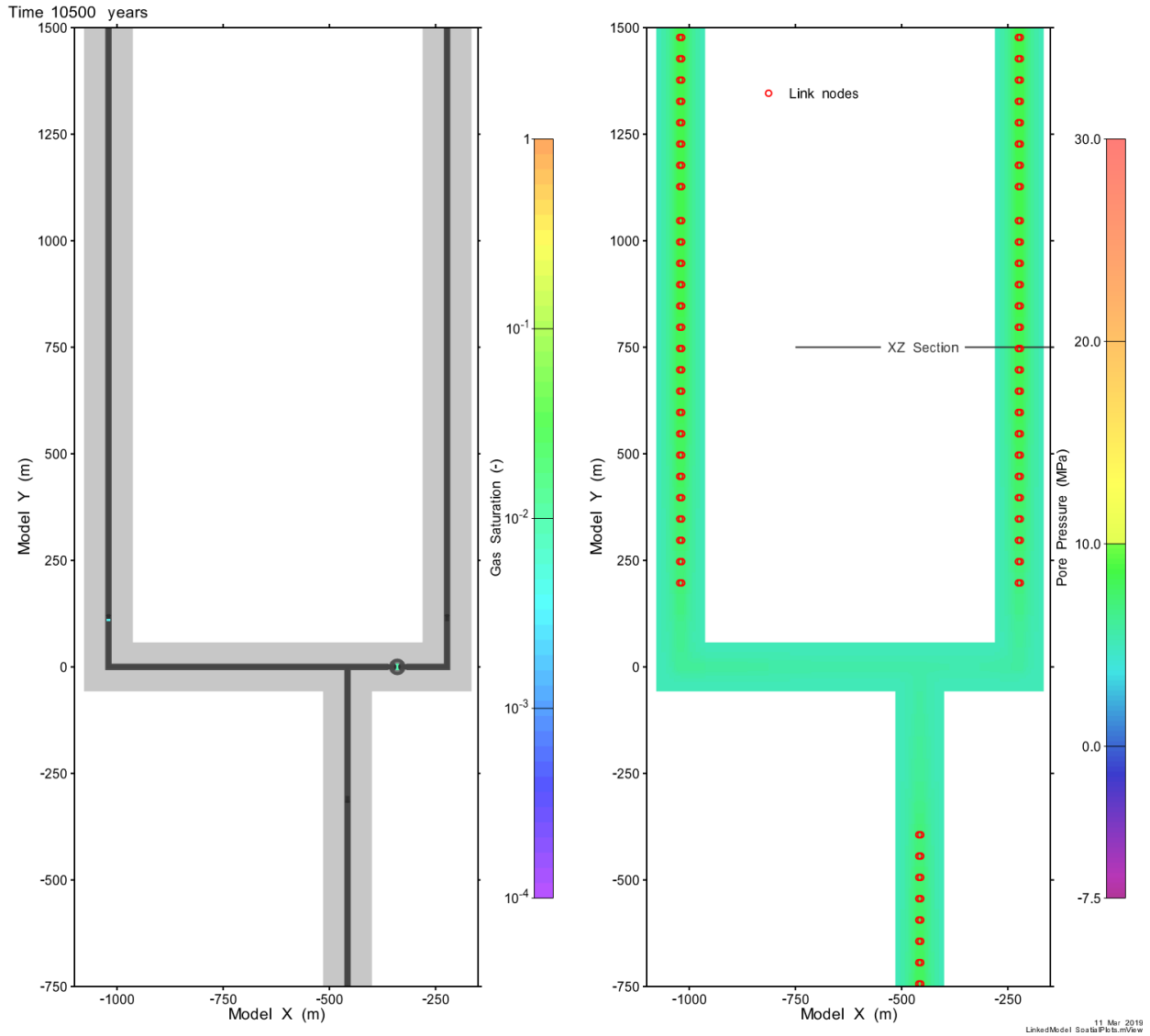


Figure 8-54: Repository-Scale Model: All Containers Fail Scenario - Gas Saturation and Pore Pressure on a Plan Section in the Tunnels at 10,500 Years

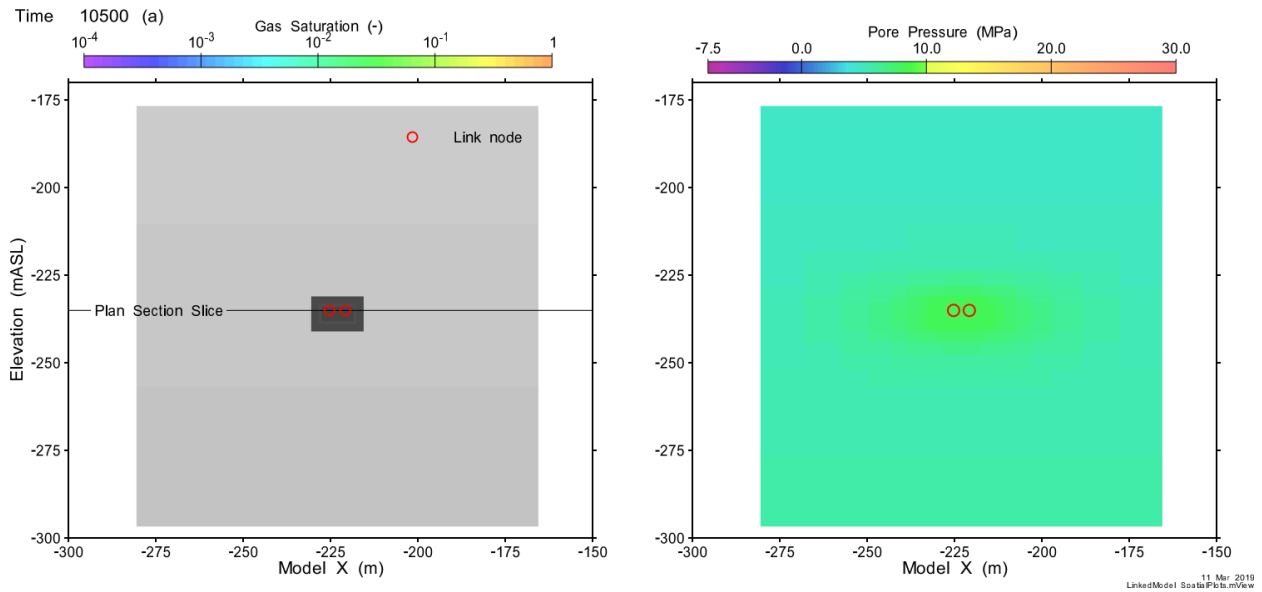


Figure 8-55: Repository-Scale Model: All Containers Fail Scenario - Gas Saturation and Pore Pressure on a Vertical Section in a Single Tunnel at 10,500 Years

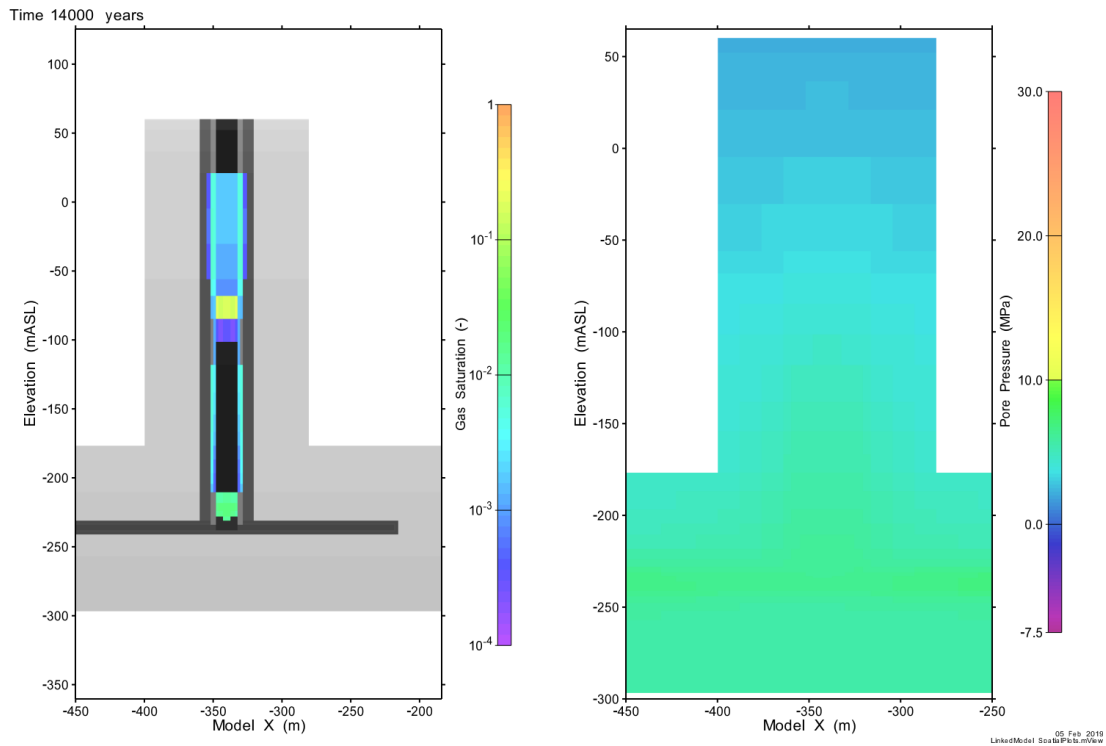


Figure 8-56: Repository-Scale Model: All Containers Fail Scenario - Gas Saturation and Pore Pressure in the Shaft at 14,000 Years

8.7.3 Gas Flow and Gas Mass Allocation

Gas allocations describe the distribution of gas throughout the simulation in terms of gas flow (kg/a) and gas mass (kg). Data are presented for the gas phase present in different material types and for the total gas present overall. Results for gas dissolved in the liquid phase are also provided.

8.7.3.1 Resaturation Period

Figure 8-57 presents the allocation of gas mass during the resaturation period before container failure. The upper figure shows the distribution of gas within the 318 placement rooms, while the lower figure shows the distribution within the repository tunnels and shaft. The bulk of the gas is located within the Room-Scale Model. Note that while the gas during the pre-failure period is initially air, the model assumes hydrogen for consistency with post-failure simulations. The total amount of gas remains relatively constant and, after approximately 3700 years, most of the gas is dissolved; otherwise, gas is mostly within the EDZ of the Room-Scale Model.

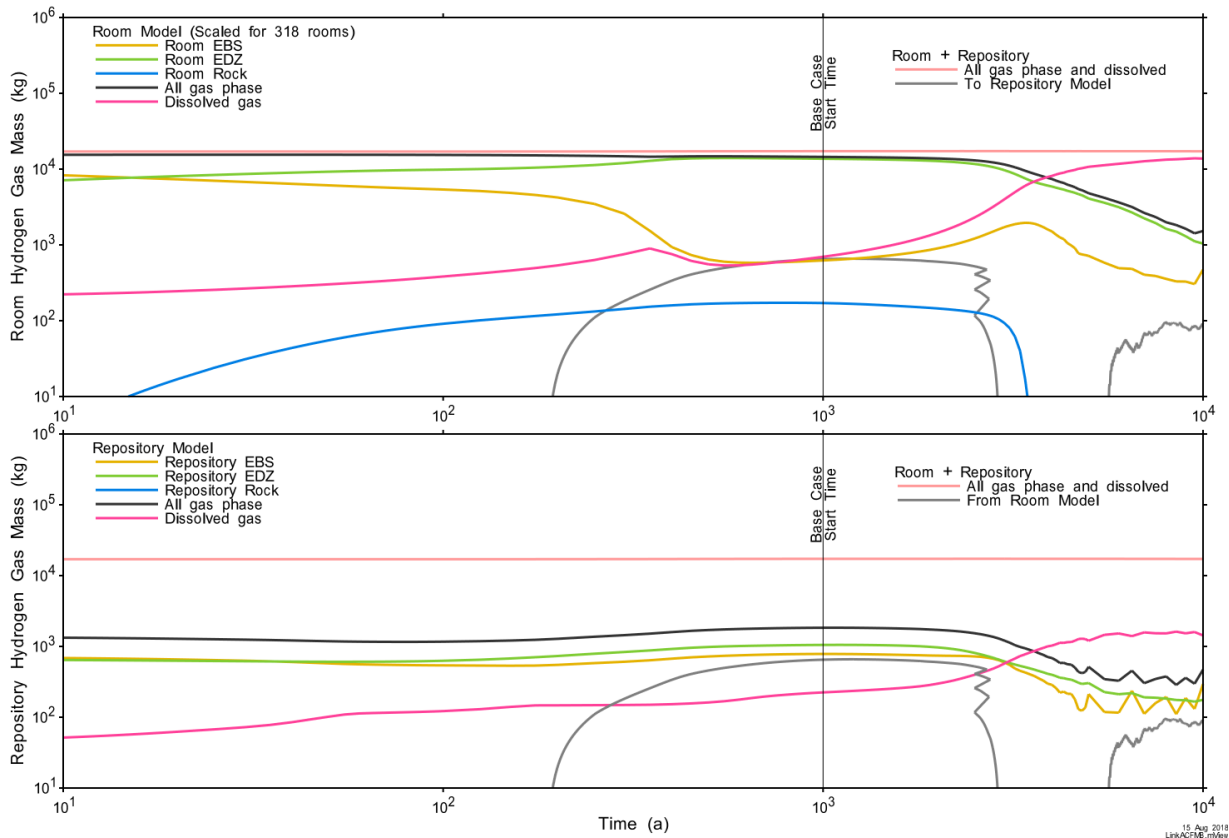


Figure 8-57: Gas Mass in Room and Repository prior to Container Failures

8.7.3.2 Base Case

Base Case results show the initial gas within the repository (lower panel of Figure 8-58) dominates the gas allocations over the entire one million year assessment period, with gas generation from defective containers having no significant impact.

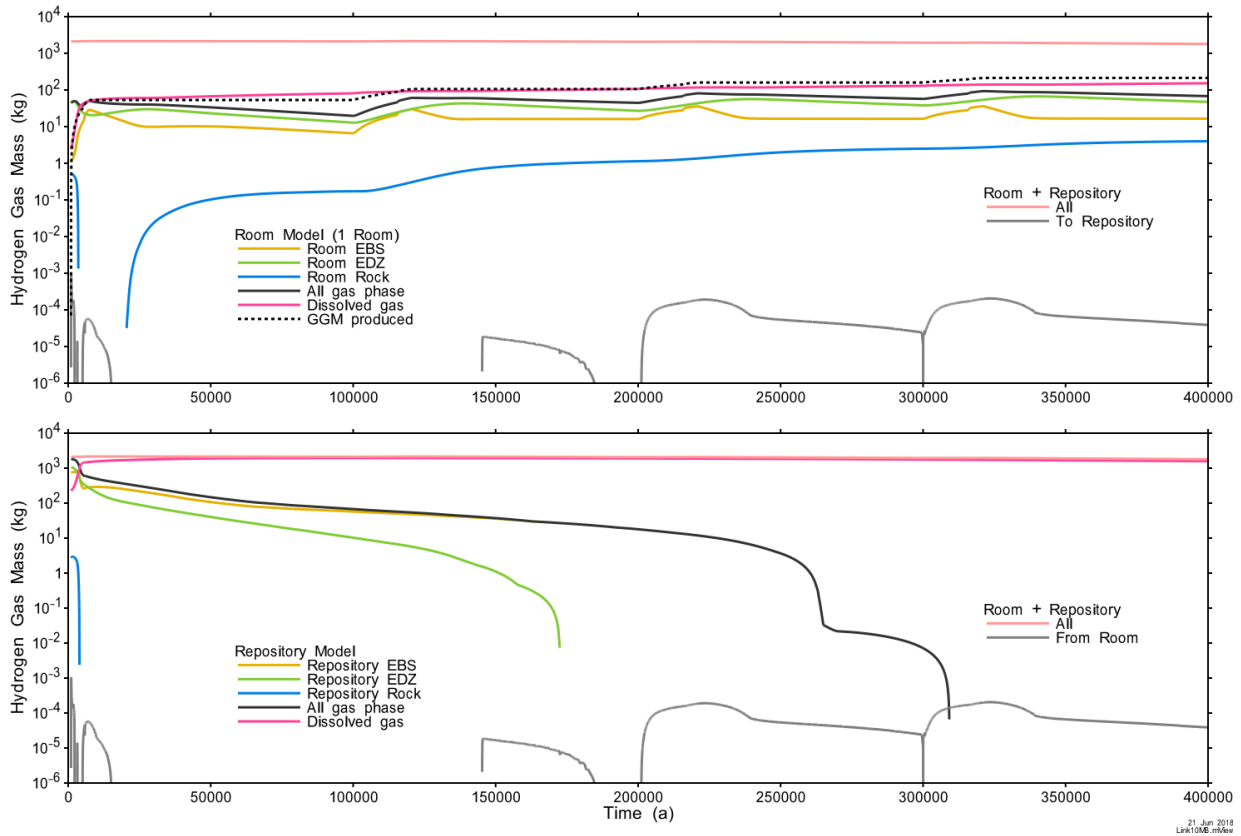


Figure 8-58: Base Case: Gas Mass Distribution after Container Failures

Figure 8-59 and Figure 8-60 show that there is no flow of gas leaving the model into the Guelph formation.

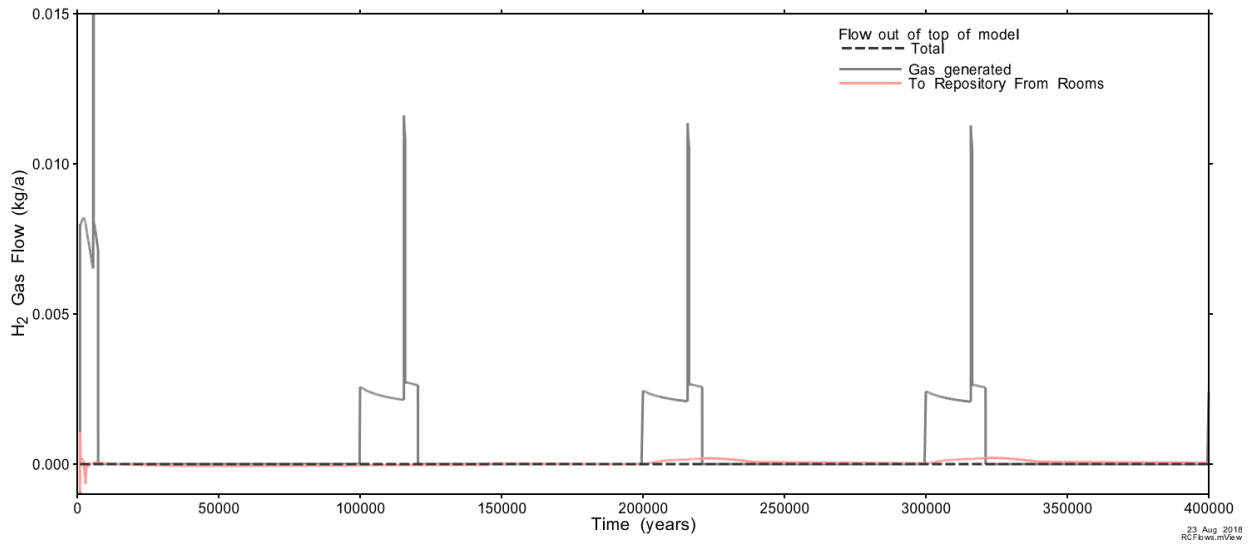


Figure 8-59: Base Case: Gas Flow out the Top of the Model

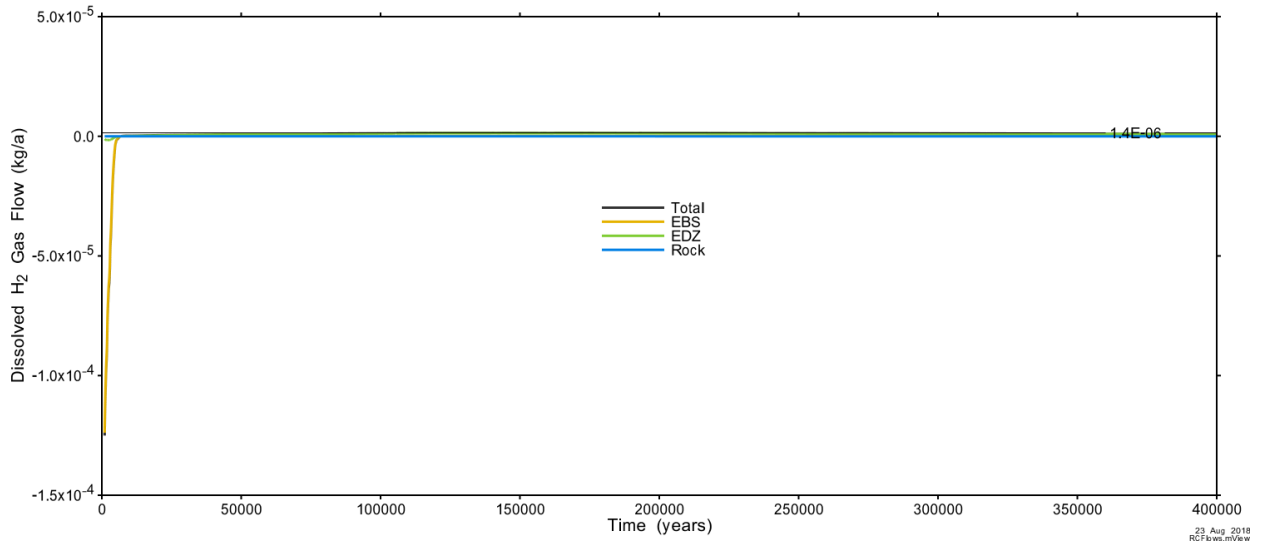


Figure 8-60: Base Case: Dissolved Gas Flow out the Top of the Model

8.7.3.3 All Containers Fail Disruptive Event Scenario

The Extreme Case of the All Containers Fail Disruptive Event Scenario assumes some unexpected common cause leading to failure of all containers at 10,000 years (see Chapter 7, Section 7.2.2). For conservatism, container failure assumes the copper coating has become fully ineffective across the entire container surface, leaving all of the container's steel surface exposed to groundwater.

Conventional two-phase flow and groundwater dissolution processes are considered sufficient for estimating gas migration through the repository for the most likely scenarios and associated sensitivity cases. As described in Section 8.7.1.3 and Section 8.7.2.3, the postulated rates at which corrosion-generated gas would be produced from this hypothetical Disruptive Event would result in dilational flow of gas through the bentonite-based sealing materials.

The T2GGM code does not provide dilational flow calculations for this assessment; the code models gas generation and transport using conventional two-phase flow and groundwater dissolution processes (see Section 8.3.2).

The potential for high gas pressures in the All Containers Fail scenario is addressed qualitatively (see Sections 8.7.1.3 and 8.7.2.3).

Although dilational flow is substantially different, conventional two-phase flow results generated by T2GGM are presented here in support of estimating hypothetical gas-borne dose calculations. Using these flow results, hypothetical gas-borne dose consequences are estimated in Section 8.8 through bounding calculations.

After the containers are assumed to fail at 10,000 years, nearly all gas generated within the Room-Scale Model migrates from the container source, through the EBS and into the EDZ. About 85% of the gas then migrates along the room EDZ to the room entry, where it is linked into the Repository-Scale Model tunnel EBS. This is indicated in the upper panel of Figure 8-61, where gas to the Repository-Scale Model (solid grey line) approaches the GGM produced line (dashed black line). Mass remaining in gas phase within the Room-Scale Model at 300 ka is retained primarily within the EDZ, while a much smaller amount is dissolved. The dissolved gas mass increases with time as the gas within the EDZ dissolves.

The lower panel of the figure illustrates the distribution of gas within the Repository-Scale Model. Approximately 70% of the gas mass from the Room-Scale Model (solid grey line) migrates through the tunnel and shaft EDZ and leaves the model through the shaft (dashed black line).

Figure 8-62 shows the gas generation rate within the placement room (grey line), the gas flow rate out of the placement rooms and into the tunnels (pink line), and the gas flow rates out the top of the model (entering the Guelph formation – the black line is the total gas flow, the gold, green, and blue lines are components of the total gas flow). Early oscillations in the gas flow rates out of the placement rooms (pink line) are due to model instabilities near the point of model linking and have minimal impact on the overall results. Gas does not flow out of the top of the model until approximately 19,000 years. Gas generated prior to that time is contained within the placement rooms, tunnels and shaft. Gas travels up the shaft mainly through the EDZ, with some gas travelling up through the EBS. Little-to-no gas reaches the top of the model through

the rock. The Phase 4 corrosion period conservatively assumes that there is sufficient carbonate available to allow the reaction to proceed unabated (otherwise corrosion and gas generation would continue but at a slower rate). Gas flow peaks at 141 kg/a at 25,000 years and then declines from that point on, with the rate of decline increasing at 32,000 years when the metal inventory is exhausted.

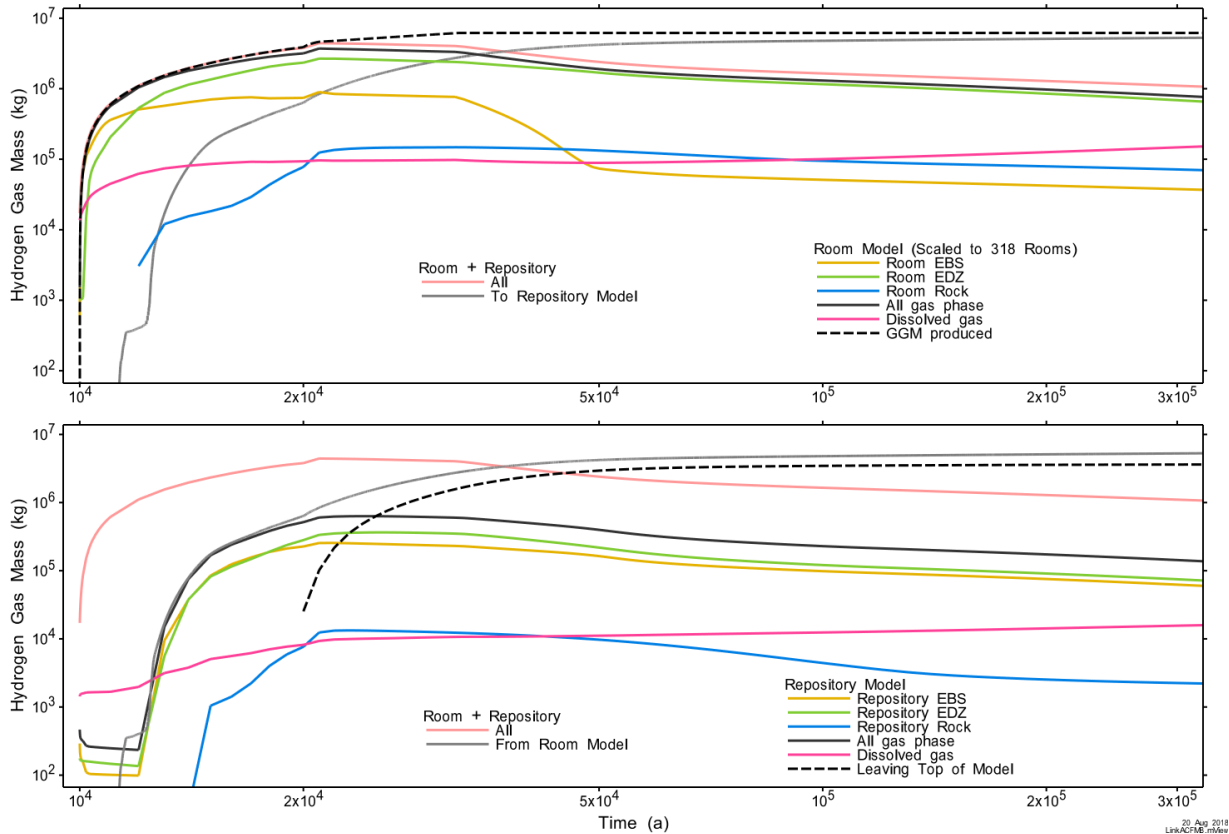


Figure 8-61: All Containers Fail Scenario: Gas Mass Distribution after Container Failures

Because the Guelph formation has a much lower gas entry pressure than does the concrete seal and the bentonite / sand seal above the concrete, the gas reaching the top of the model is expected to exit the shafts, remain within the EDZ and enter the Guelph formation.

Figure 8-63 illustrates the amount of dissolved gas leaving the top of the model. Comparison of Figure 8-62 and Figure 8-63 shows that gas is moving primarily in gas-phase, with dissolved gas accounting for approximately 0.02% of overall transport.

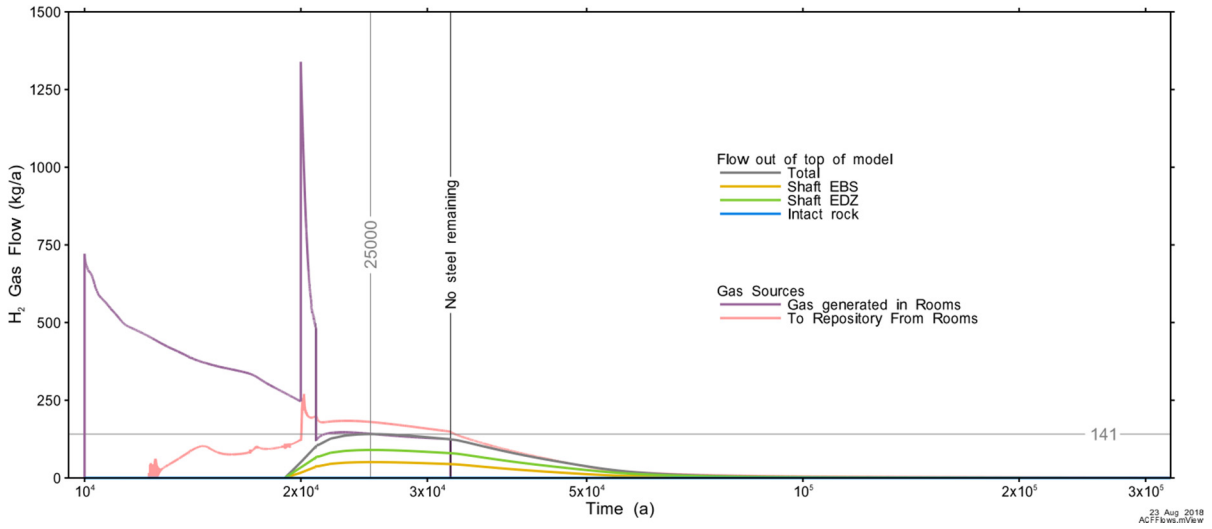


Figure 8-62: All Containers Fail Scenario: Gas Flow out the Top of the Model

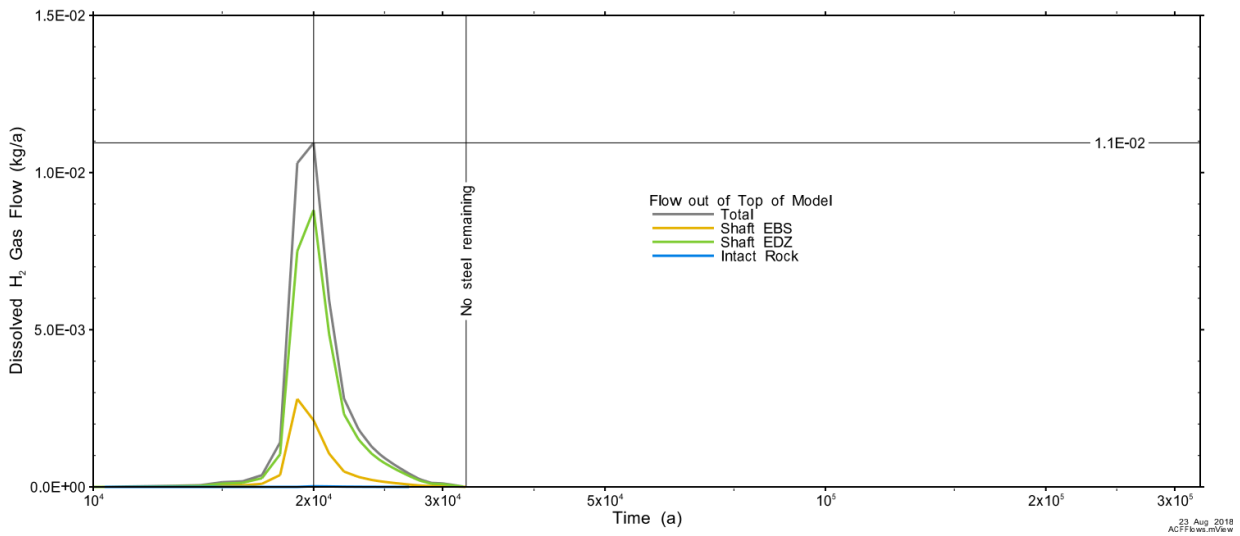


Figure 8-63: All Containers Fail Scenario: Dissolved Gas Flow out the Top of the Model

8.8 Dose Consequences

Gas generation and transport results are presented in Section 8.7 for both the Base Case of the Normal Evolution Scenario and the Extreme Case of the All Containers Fail Disruptive Event Scenario. For the Base Case, all gas remains within the repository. Only the All Containers Fail Scenario results in gas transport out of the repository and into the Guelph formation – accordingly, the potential for gas-borne dose consequences is assessed for the All Containers Fail Scenario.

Of the radionuclide species present within the used fuel, very few are volatile or semi-volatile under repository conditions. Of these, only C-14, Cl-36, Se-79, and I-129 have half-lives sufficiently long to be of potential concern (Quintessa and Geofirma 2011, Gobien et al. 2018).

As presented in Section 8.7.1.3, the thinner hemispherical ends of the containers are consumed at approximately 20,000 years, resulting in full container failure, and therefore this is the timeframe of most interest. Table 8-3 shows the 20,000-year source term for each radionuclide together with their inhalation dose coefficients and Henry’s law constants. The products of these three values allow a comparison of the relative hazard. Because the product for C-14 is over 300 times greater than the others, only C-14 is considered further in the dose calculations.

Table 8-3: Comparison of Volatile, Long-Lived Radionuclides

Nuclide	Half-Life (a)	Source term, 20,000 years (Bq/kgU)	Inhalation Dose Coefficient (Sv/Bq)	Henry’s Law Constant (C_{gas}/C_{aq})	Product (Sv/kgU)
C-14	5700	3.0×10^4	6.2×10^{-12}	10^2	1.8×10^{-5}
Cl-36	301,000	1.4×10^4	7.3×10^{-9}	10^{-6}	1.0×10^{-10}
Se-79	295,000	4.5×10^3	6.8×10^{-9}	10^{-4}	3.1×10^{-9}
I-129	15,700,000	1.4×10^4	3.6×10^{-8}	10^{-4}	5.1×10^{-8}

Notes:

The source term includes instant releases from both the fuel and the Zircaloy.

Henry’s Law Constants are taken from Quintessa and Geofirma (2011) and from Suckling et al. (2015). The C-14 dose coefficient is taken from Eckerman et al. (2012); the C-14 value is for CO₂. Other data are taken or derived from Gobien et al. (2018).

As described in Section 8.7.1.3 and Section 8.7.2.3, the postulated rates at which corrosion-generated gas would be produced from this hypothetical Disruptive Event would result in dilational flow of gas through the bentonite-based sealing materials. Although dilational flow is substantially different, conventional two-phase flow results generated by T2GGM are used in Section 8.8.1 in support of estimating hypothetical gas-borne dose consequences; dilational flow is considered in Section 8.8.2.

8.8.1 Conventional Two-Phase Flow

The Repository-Scale Model results presented in Figure 8-61 and Figure 8-62 provide data needed to estimate the rate at which C-14 activity leaves the repository. Figure 8-61 shows the

total amount of hydrogen gas in the repository while Figure 8-62 shows the rate at which hydrogen moves up the shafts.

As noted in Section 8.7.3.3, because the Guelph formation has a much lower air-entry pressure than the concrete seal and the bentonite / sand seal above the concrete, the rising hydrogen gas will exit the shafts and enter the more permeable Guelph formation. Once in the Guelph layer, the gas will most likely disperse and dilute laterally underground so there is no significant vertical flux upwards and no dose consequence to the critical group. Figure 8-64 shows the rate at which C-14 activity would enter the Guelph formation, taking into account radioactive decay of C-14.

For conventional two-phase flow, the bounding hypothetical gas-borne dose consequence can be estimated by assuming the gas is not dispersed in the Guelph formation and the critical group is exposed. This is done by assuming that all C-14 exits the repository via a single shaft, and that all C-14 in the shaft remains in the shaft until it reaches the surface. After reaching the surface, the C-14 then enters a house that is built directly on top of the shaft, exposing the occupants to an inhalation hazard. Under these assumptions, the rate information in Figure 8-64 also represents the rate at which C-14 activity enters the house. The maximum value is 8.3 kBq/hr.

The peak inhalation dose rate to the occupant is determined using data in Gobien et al. (2018). For a house volume of 226 m³, an air exchange rate equivalent to a volume fractional turnover rate of 0.35 per hour (i.e., 6.9×10⁵ m³/a), a dweller inhalation rate of 8400 m³/a, an occupancy factor of 0.8, and an adult inhalation dose coefficient for C-14 (as CO₂) of 6.2×10⁻¹² Sv/Bq (Eckerman et al. 2012), the peak dose rate is 4.4 µSv/a, occurring at 22,000 years. Even with the extreme conservatism of assuming simultaneous failure of all containers at 10,000 years, this remains more than a factor of 100 below the interim Disruptive Event acceptance criterion of 1 mSv/a.

8.8.2 Dilational Flow

The postulated rates at which corrosion-generated gas would be produced from this hypothetical Disruptive Event would result in dilational flow of gas through the bentonite-based sealing materials (see Section 8.7.3.3). As the T2GGM code does not provide dilational flow calculations (see Section 8.4), the potential for high gas pressures is addressed qualitatively (see Section 8.7.1.3 and Section 8.7.2.3); similarly, very conservative assumptions for dilational flow can be used to estimate the bounding hypothetical gas-borne dose consequence.

Conventional two-phase flow calculations determine that, for this Disruptive Event, approximately 85% of the corrosion-generated gas travels from the placement rooms into the tunnels, and then approximately 70% travels up through the shafts (Section 8.7.3.3). Gas does not begin to flow out of the shafts until after approximately 19,000 years, at which point well over 3,000 tonnes of gas is distributed across the entire repository (see Figure 8-61); by 22,000 years, this has increased to well over 4,000 tonnes.

By 10,500 years, calculated pressures within the bentonite in the placement rooms have significantly exceeded the confining stress (see Section 8.7.1.3). Given dilational flow will be the dominant gas transport process, it is very conservative to assume the following:

- As of 10,500 years, small-scale dilational pathways extending through all bentonite-based sealing materials connect all placement rooms to a house built directly on top of the shaft;
- From this time forward, the amount of corrosion-generated gas distributed across the entire repository ceases to increase and remains constant at 300 tonnes (see Figure 8-61);
- All corrosion-generated gas travels through these small-scale pathways directly to the house;
- With all containers failing, the full amount of available C-14 (see Table 8-3) mixes instantly with all gas across the entire repository and thereby enters the house at the peak flow rate of 1300 kg/a (see Figure 8-62).

Using these very conservative assumptions, adding to those described in Section 8.8.1 for conventional two-phase flow, the peak dose rate is estimated to be 0.78 mSv/a, occurring at 20,000 years. Even with these added substantial conservatisms for dilational flow, the bounding hypothetical gas-borne dose consequence does not reach or exceed the interim Disruptive Event acceptance criterion of 1 mSv/a.

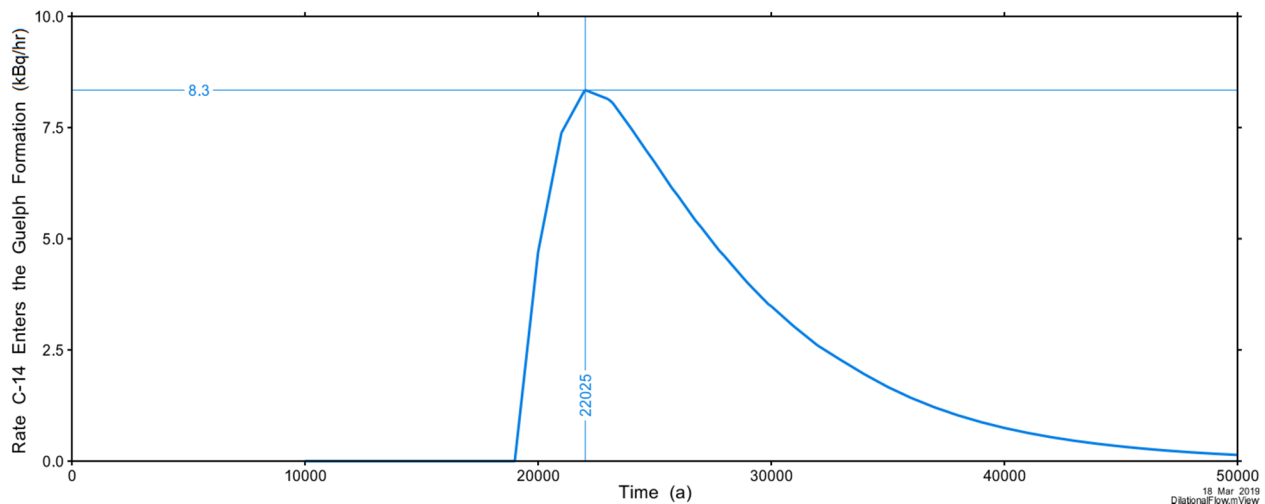


Figure 8-64: Rate at which C-14 enters the Guelph Formation

8.9 Summary and Conclusions

Exposure of the steel components of an engineered barrier system (EBS) to groundwater will result in the generation of gas due to corrosion processes. This gas can affect both the internal repository pressure and the transport of gaseous radionuclides.

For the Base Case, gas is not important because the rate of gas generation from the defective containers is small and all gas remains within the repository. Additionally, the half-life of C-14 is 5700 years, which implies that C-14 has substantively decayed away after about 60,000 years (i.e., 10 half-lives).

Model calculations for the Base Case determine that pore pressure within the host rock remains well below 80% of lithostatic pressure over the full 1 million year simulation period.

For the Extreme Case of the All Containers Fail Disruptive Event Scenario in which the container failures are all assumed to occur at 10,000 years, the postulated rates at which corrosion-generated gas would be produced would result in dilational flow of gas through the bentonite-based sealing materials. As the T2GGM code does not provide dilational flow calculations, the potential for high gas pressures is addressed qualitatively. Given that dilational flow will be the dominant gas transport process, pore pressure within the intact rock can be expected to remain well below 80% of lithostatic pressure and the possibility that gas pressure build-up will lead to fracturing can be excluded.

This Disruptive Event also provides a conservative assessment of the hypothetical gas-borne dose consequences:

- For conventional two-phase flow, using very conservative assumptions, the bounding hypothetical gas-borne dose consequence is estimated to be 4.4 $\mu\text{Sv/a}$, occurring at 22,000 years.
- Using an extended set of very conservative assumptions for dilational flow, adding substantially to the level of conservatism overall, the bounding hypothetical gas-borne dose consequence is estimated to be 0.78 mSv/a ¹¹, occurring at 20,000 years.

Even with these extreme conservatisms, the bounding hypothetical gas-borne dose consequence does not reach or exceed the interim Disruptive Event acceptance criterion of 1 mSv/a .

8.10 References for Chapter 8

Bate, F., D. Roberts, A. R. Hoch, and C.P. Jackson. 2012. Gas migration calculations on the vault scale. Serco Assurance report SA/ENV-0924 Issue 3.1. Oxfordshire, UK (available at http://www.nda.gov.uk/documents/biblio/upload/Gas-Migration-calculations-on-the-vault-scale-report_I3_1.pdf).

Birgersson, M., Åkesson, M. and Hökmark, H. 2008. Gas intrusion in saturated bentonite – A thermodynamic approach. *Physics and Chemistry of the Earth, parts A/B/C*, 33, S248-S251.

Cuss, R., Harrington, J., Noy, D.J., Wikman, A. and Sellin, P. 2011. Large Scale Gas Injection Test (LASGIT): Results from Two Gas Injection Tests. *Physics and Chemistry of the Earth Vol 36*, p. 1729-1742.

¹¹ For comparison, if the copper containers all fail on time scales associated with the next glaciation or later, hypothetical dose consequences would be at least 100 times further reduced due to decay of C-14.

- Davies, P.B. 1991. Evaluation of the Role of Threshold Pressure in Controlling Flow of Waste-Generated Gas into Bedded Salt at the Waste Isolation Pilot Plant (WIPP). Sandia Report SAND 90-3246. Albuquerque, USA.
- Eckerman, K., J. Harrison, H.G. Menzel and C.H. Clement. 2012. ICRP Publication 119: Compendium of Dose Coefficients based on ICRP Publication 60. Annals of the ICRP, 41, 1-130.
- FORGE. 2010. FORGE Milestone M15: Summary of Gas Generation and Migration. Current State-of-the-Art. Euratom 7th Framework Project, FORGE 2010. Deliverable D1.2-R.
- Geofirma and Quintessa. 2011. Postclosure Safety Assessment: Gas Modelling. Geofirma Engineering Ltd. and Quintessa Ltd. report for the Nuclear Waste Management Organization NWMO DGR-TR-2011-31. Toronto, Canada.
- Gobien, M., F. Garisto, E. Kremer and C. Medri. 2018. Seventh Case Study: Reference Data and Codes. Nuclear Waste Management Organization Report NWMO-TR-2018-10. Toronto, Canada.
- Guo, R. 2018. Thermal Response of a Conceptual Deep Geological Repository in Sedimentary Rock. Nuclear Waste Management Organization Report NWMO-TR-2018-09.
- Itasca Consulting Group. 2015. Long-term Stability Analysis of APM Mark II Conceptual Design in Sedimentary and Crystalline Rocks. Nuclear Waste Management Organization Report NWMO TR-2015-27. Toronto, Canada.
- King, F. 2013. Consequences of the General Corrosion of Carbon Steel Used Fuel Containers for Gas Generation in a DGR. Nuclear Waste Management Organization Report NWMO TR-2013-16. Toronto, Canada.
- Luckner, L., M.T. Van Genuchten and D.R. Nielsen. 1989. A consistent set of parametric models for the two-phase flow of immiscible fluids in the subsurface. Water Resources Research 25(10), 2187-2193.
- Mualem, Y. 1976. A New Model for Predicting the Hydraulic Conductivity of Unsaturated Porous Media. Water Resources Research 12(3), 513 – 522.
- Nagra. 2008. Effects of post-disposal gas generation in a repository for low- and intermediate-level waste sited in the Opalinus Clay of Northern Switzerland. Nagra Technical Report 08-07. Wettingen, Switzerland.
- NWMO. 2013. Postclosure Safety Assessment of a Used Fuel Repository in Sedimentary Rock: Pre-Project Report. Nuclear Waste Management Organization Report NWMO TR-2013-07. Toronto, Canada.
- Pehme, P. and M. Melaney. 2010. Borehole Geophysical Logging in DGR-3 and DGR-4. Intera Engineering Ltd. Report TR-08-15 Rev.1. Ottawa, Canada.
- Pehme, P. and M. Melaney. 2011. Borehole Geophysical Logging of DGR-5 and DGR-6. Intera Engineering Ltd. Report TR-09-03 Rev.0. Ottawa, Canada.

Pruess, K., C. Oldenburg and G. Moridis. 1999. TOUGH2 User's Guide, Version 2.0. Lawrence Berkeley National Laboratory Report LBNL-43134. Berkeley, USA.

Quintessa and Geofirma. 2011. Postclosure Safety Assessment: Data. Quintessa Ltd. and Geofirma Engineering Ltd. Report for the Nuclear Waste Management Organization. NWMO DGR TR-2011-32.

Senger, R.K. and Marschall, P. 2008. Task Force on EBS/Gas Transport in Buffer Material. NAGRA NAB 08-24. Wetingen, Switzerland.

Sterling, S. and P. Pehme. 2012. Borehole Geophysical Logging in DGR-7 and DGR-8. Geofirma Engineering Ltd. Report TR-11-04 Rev.0. Ottawa, Canada.

Suckling, P., J. Avis, N. Calder, O. Nasir, P. Humphreys, F. King and R. Walsh. 2015. T2GGM Version 3.2: Gas Generation and Transport Code. Quintessa Ltd. and Geofirma Engineering Ltd. Report for the Nuclear Waste Management Organization NWMO TR-2015-13. Toronto, Canada.

Talandier, J., G. Mayer and J. Croisé. 2006. Simulations of the Hydrogen Migration out of Intermediate-Level Radioactive Waste Disposal Drifts using TOUGH2. Proceedings, TOUGH Symposium 2006, Lawrence Berkeley National Laboratory. Berkeley, USA.

Van Genuchten, M. T. 1980. A Closed-Form Equation for Predicting the Hydraulic Conductivity of Unsaturated Soils. Soil Science Society of America Journal, 44(5), 892-898.

9. TREATMENT OF UNCERTAINTIES

All analysis calculations have an associated uncertainty. Regulatory document REGDOC-2.11.1, Volume III (CNSC 2018) expects that uncertainty will be taken into account.

9.1 Approach

Many organizations use the following three broad categories¹ to structure the analysis of uncertainties in postclosure safety assessments (e.g., Marivoet et al. 2008):

- **Scenario Uncertainty:** Arises from uncertainty in the evolution of the repository system and human behaviour over the time scales of interest.
- **Model Uncertainty:** Associated with uncertainty in the conceptual, mathematical and computer models used to simulate the behaviour of the repository system (i.e., due to approximations used to represent the system).
- **Data Uncertainty:** Arises from uncertainty in the data and parameters used as input in the models (e.g., due to incomplete site-specific data or due to parameter estimation errors from interpretation of test results).

The following briefly discusses the approach adopted for uncertainties in this assessment report.

Scenario Uncertainty

Uncertainty in the future evolution of the site is addressed by assessing a range of scenarios that describe the potential evolution of the system. The scenario identification process, described in Chapter 6, ensures that key uncertainties are identified and scenarios are defined to explore their consequences.

The scenarios defined include the Normal Evolution Scenario (which describes the expected evolution of the repository) and a series of Disruptive Event Scenarios that postulate the occurrence of unlikely events leading to possible penetration of barriers and abnormal loss of containment.

To estimate potential future impacts, a stylized representation² of the biosphere and human receptors is adopted. A stylized representation is used rather than a detailed assessment based on current conditions because:

- Human behaviour may change over the time scale of relevance to the repository system,

¹ The boundaries between these categories can overlap. Depending upon how models are formulated, an uncertainty may be classed as a model or a data uncertainty.

² A stylized representation of the biosphere and human behaviour is a representation that has been simplified to reduce natural complexity to a level consistent with the objectives of the analysis; that is, using assumptions that are plausible and internally consistent but that tend to overestimate health impacts on people and the environment living in the vicinity of the repository.

- The surface and near-surface environment are likely to change as a result of natural causes such as ice ages and / or as a result of future human actions, and
- Societal and technological changes are unpredictable over such timescales.

In the stylized representation, while the exposure models are more general, it is assumed that future humans are generally similar to present-day humans with behaviors consistent with current or past human practice. People are assumed to live on the repository site in the future in a manner that maximizes their potential dose from exposure to releases from the repository.

Since assumptions concerning the biosphere (e.g., climate), human lifestyles (e.g., critical group characteristics) and water flows in the near-surface environment become increasingly uncertain with time, two complementary long-term indicators are also used to supplement the dose rate indicator using system characteristics that are much less sensitive to such assumptions.

Model Uncertainty

Conceptual and mathematical model uncertainties are identified in the model development process. Key uncertainties are addressed by using alternative conceptual representations of the system. This is facilitated by the use of different computer codes (e.g., FRAC3DVS-OPG for Groundwater Flow and Transport modelling and SYVAC3-CC4 as the System Model) that provide different conceptualizations and mathematical descriptions.

Some conceptual and mathematical model uncertainties are amenable to representation with parameter values, and these are investigated using the methods applied to data uncertainties. For example, uncertainties in the representation of sorption are treated by considering extreme bounding cases in which the sorption parameters are set to either zero or minimal values.

Data Uncertainty

Data uncertainties are identified in Gobien et al. (2018). These are accounted for through:

- Deterministic Calculations – alternative specific sets of parameter values. In particular, the sensitivity cases are defined in Chapter 7 to explore the effect of variations in key parameters affecting the performance of the multi-barrier system.
- Results are compared to the Base Case of the Normal Evolution Scenario. This approach provides clear information on the effects of specific parameter variations. A limitation of this approach is that there is often no systematic or complete coverage of the uncertainty space in parameter values.
- Probabilistic Calculations – parameters are assigned probability distribution functions that describe their inherent uncertainty. The model is evaluated 100,000 times, with each case using input values randomly selected from the distribution functions. The model output is a distribution of results. The strength of the probabilistic approach lies in its ability to better explore the parameter space of the phenomena considered. Its weakness is the need to make use of simplified models.

Conservatism

Throughout the assessment process, it is necessary to make various assumptions relating to scenarios, models or data. Assumptions are often categorized as 'realistic' or 'conservative' (IAEA 2012), although care needs to be taken when using such terms. The key is to ensure that each major assumption used in the assessment is considered and documented, and that potential implications are understood.

To define the Base Case, a number of bounding assumptions are made to account for uncertainties affecting case definition. A "bounding assumption" is an assumption that results in a greater consequence than the entire range of uncertainty, usually at the expense of realism. To illustrate, a bounding assumption is created if the uncertainty associated with the location and lifestyle of people unknowingly living in the vicinity of the repository in the future is replaced by an assumption that instead has people unknowingly living on top of the repository and obtaining all of their drinking and crop irrigation water from a deep well, with the well positioned in the location that maximizes the uptake of any potential contaminant release.

The adoption of bounding assumptions is a common technique in safety assessment. It allows for complex problems to be reduced to much simpler ones, with the downside being that the resulting case is no longer the most realistic. While this is acceptable from a licensing viewpoint (provided results meet acceptance criteria), it can make repository performance appear to be much worse than it really is.

To illustrate the degree to which conservatism (and departure from reality) is incorporated in the Base Case, Table 7-3 in Chapter 7 (reproduced below as Table 9-1) compares key Base Case assumptions with what might actually occur in reality. For simplicity, the table is focussed on only the 10 defective containers, with separate sections shown for defect, container and dose related assumptions. A discussion of the key parameters in each section is included in Chapter 7 below Table 7-3.

Table 9-1: Base Case Sensitivity Study Assumptions

Parameter	Realistic Assumption	Base Case Assumption
When can contaminants escape the container?	After the container is breached and large amounts of water contact the fuel	After the container is breached
Defect Parameters		
What is the defect of concern?	Undetected defect in the copper corrosion barrier	Undetected defect in the copper corrosion barrier
What is smallest size of defect that can be reliably detected?	0.8 mm (Detection Threshold)	0.8 mm (Detection Threshold)
How large is the defect in the copper corrosion barrier?	Random sizes below the Detection Threshold	Large enough to cause container failure at the assumed times (>>0.8 mm depth)
Where is the defect located?	Random location <ul style="list-style-type: none"> • < 1% chance over 8 mm weld • ~5% chance over weld area (8-30 mm steel) • ~25% chance over container head (30 mm steel) • ~70% chance over container body (46 mm steel) 	Not applicable Complete container failure occurs at the assumed times independent of defect location
How long does a copper barrier with a defect remain effective?	> 74 million years for defects below the 0.8 mm Detection Threshold (see Chapter 5) <i>Based on an assumed groundwater sulphide concentration of 1 µM</i>	1000 years for the first container One additional container fails every 100,000 years
How many containers are breached prior to one million years?	0	10
Container Parameters		
Once the copper barrier is penetrated, how long before the steel inner shell is penetrated due to corrosion?	140,000 years for 8 mm 1,300,000 years for 30 mm 2,000,000 years for 46 mm <i>Based on 1 mm diameter hole in the copper barrier</i> <i>It is anticipated that there will be insufficient amounts of carbonate to promote siderite-</i>	0 years

Postclosure Safety Assessment of a Used Fuel Repository in Sedimentary Rock

Document Number: NWMO-TR-2018-08

Revision: 000

Class: Public

Page: 655

Parameter	Realistic Assumption	Base Case Assumption
	<i>producing corrosion reactions (see Chapter 5)</i>	
Once the steel barrier is penetrated, how long before large amounts of water enter the container?	It could take many tens of thousands of years for the container to fill with water	0 years
Do the Zr fuel sheaths prevent water from contacting fuel elements?	Possibly Some fuel sheaths may still be intact when water enters the container	No
For fuel elements that are contacted by water, how large is the instant release source term?	Depends on the power experienced while in the reactor and on the physical condition of each fuel pellet	Conservative Value
Does H ₂ released during steel corrosion and radiolysis inhibit the fuel dissolution rate (and thereby inhibit the contaminant release rate)?	Most likely Yes	No
Do corrosion products accumulate in the defect and obstruct the migration of contaminants?	Yes	No
After the steel barrier is penetrated, how long before the container wall corrodes away and no longer presents any resistance to contaminant release	120,000 years for 8 mm 460,000 years for 30 mm 710,000 years for 46 mm <i>It is anticipated that there will be insufficient amounts of carbonate to promote siderite-producing corrosion reactions (see Chapter 5)</i>	0 years
Dose Parameters		
Are people living close to the facility?	Unknown The repository footprint is small and the location may be far from populated areas	Yes Living on top of the repository
Are the nearby people using a deep well to obtain their drinking water?	Unlikely Surface water sources or a shallow well are more likely	Yes A 219 m deep well is assumed
If used, where is the well located in relation to the defective containers?	Random	Worst location The location that maximizes contaminant uptake
Where are the hypothetical defective containers located in the repository?	Random	Clustered In the location that maximizes uptake to the well

9.2 Key Uncertainties

The postclosure safety assessment discussed in Chapter 7 and Chapter 8 indicates that the deep geological repository in geologic settings similar to the assumed site could tolerate large changes in the properties of key barrier parameters without challenging any of the interim criteria established for the protection of people and the environment from radiological and non-radiological hazards.

The key uncertainties in terms of their importance to modify potential impacts are:

- **Chemical Reactions:** Under the highly saline conditions of the deep geosphere, several aspects of the chemistry in the repository are uncertain due to the limited database. These include the sorption of contaminants on seal materials and host rocks, as well as mineral precipitation / dissolution reactions. These uncertainties have been addressed through the adoption of conservative values, the analysis of various sensitivity cases, and the identification of appropriate disruptive scenarios such as the Container Failure Scenario.
- **Gas Pressure and Repository Saturation:** The presence of robust copper containers ensures gas generated from potential corrosion of the steel inner containers is not a significant issue for the Normal Evolution Scenario. However, gas behaviour becomes increasingly important when large number of containers are assumed to fail, such as in the All Containers Fail Disruptive Event Scenario. This report includes a detailed study of the expected gas evolution for this event.
- **Glaciation Effects:** Although geological evidence at a real site is expected to indicate the deep geosphere has not been affected by past glaciation events and that the deep groundwater system has remained stagnant, glaciation will have a major effect on the surface and near-surface environment that is not entirely predictable. However, glaciation is not likely to occur before 60,000 to 100,000 years, and by that time there would have been significant radionuclide decay. The likely effects of glaciation are discussed in Chapter 7 based on existing analysis performed for a different conceptual repository located at the same site.
- **Fracture Characterization:** For a real site, there will be some uncertainty in the nearby fracture network. However, in principle a sedimentary rock site may have features that provide high confidence that there are no significant fractures nearby. These uncertainties can be reduced through site selection and repository location and depth, and any residual uncertainties can be handled through the adoption of conservative assumptions and / or Disruptive Event Scenarios (such as the Undetected Fault Scenario) within the postclosure analysis.
- **Number of Container Failures:** The Base Case assumes 10 containers fail relatively early due to undetected defects in their copper coating. There is uncertainty in this number, and work is ongoing to better quantify the likelihood of a defect escaping the rigorous quality inspection program that will be implemented. In the meantime, additional sensitivity studies in which greater numbers of container failures are assumed are considered in Chapter 7.

9.3 References for Chapter 9

CNSC. 2018. Regulatory Document REGDOC-2.11.1 Volume III: Assessing the Long Term Safety of Radioactive Waste Management. Canadian Nuclear Safety Commission. Ottawa, Canada.

Gobien, M., E. Kremer and C. Medri. 2018. Seventh Case Study: Reference Data and Codes. Nuclear Waste Management Organization Report NWMO-TR-2018-10. Toronto, Canada.

IAEA. 2012. IAEA Safety Standards: The Safety Case and Safety Assessment for the Disposal of Radioactive Waste. International Atomic Energy Agency. Specific Safety Guide IAEA SSG-23. Vienna, Austria.

Marivoet, J., T. Beuth, J. Alonso and D.A. Becker. 2008. Safety Functions, Definition and Assessment of Scenarios, Uncertainty Management and Uncertainty Analysis, Safety Indicators and Performance/Function Indicators. PAMINA Deliverable D-No. 1.1.1, European Commission. Brussels, Belgium.

THIS PAGE HAS BEEN LEFT BLANK INTENTIONALLY

10. NATURAL ANALOGUES

Natural analogues are natural features (materials or processes) that are similar to those expected in some part of a deep geological repository. Natural analogues can include both natural and anthropogenic materials, provided the processes that affect them are natural. They provide understanding or demonstration of how a repository may behave over time scales ranging up to many millions of years. Analogues exist for most features of the repository system, including the used fuel, engineered and natural containment systems, and key processes such as transport of contaminants.

The use of natural analogues in supporting key assumptions in safety assessment and adding credibility to its findings is recommended in IAEA (2011) and in REGDOC-2.11.1, Volume III (CNSC 2018). REGDOC-2.11.1 states: "*Natural analogue information should be used to build confidence that the system will perform as predicted by demonstrating that natural processes will limit the long-term release of contaminants to the biosphere to levels well below target criteria.*"

The present summary focusses on the engineered barriers; the use of geosphere analogues would be described in the Geosynthesis that would be prepared as part of the analysis of a real site.

10.1 Analogues for Used Nuclear Fuel

10.1.1 Natural Uranium Deposits

Natural uranium is present at about 2.7 wppm average concentration in the earth's crust (Rudnick and Gao 2014). Like all other elements, it is cycled through biological and geological systems and tends to concentrate in some locations by natural processes. Uranium will slowly dissolve under oxidizing conditions and precipitate under reducing conditions. Most uranium ore bodies form by this process. Uranium ore bodies that are being mined today were formed hundreds of millions of years ago. The stability of these uranium ores provides information on the stability of used fuel.

Used fuel consists predominantly of uranium dioxide, with about 2% being fission products and activation products resulting from the nuclear reactions occurring in the fuel during power production. Natural uranium minerals are comparable in that many also consist of uranium dioxide along with uranium decay products.

One gram of natural uranium, as it is extracted from the earth in equilibrium with its progeny, contains approximately 10^5 Bq of radioactivity. In comparison, 30 years after discharge from a reactor, used fuel has an inventory of 2.1×10^9 Bq per gram of uranium, principally in the form of fission and activation products (Tait et al. 2000), and is therefore considerably more radioactive than the original uranium ore. Due to the decay of most of the fission product isotopes present in used fuel, its radioactivity decreases to 2.4×10^7 Bq per gram after 1000 years, while radioactivity decreases to a level similar to that in natural uranium after approximately one million years.

The Cigar Lake uranium deposit found in the Athabasca Basin in northern Saskatchewan provides a Canadian example of an analogue for geological placement of used nuclear fuel

(Figure 10-1). The Cigar Lake deposit is an operating uranium mine. The ore body formed about 1.3 billion years ago, and has been studied as a natural analogue (Cramer and Smellie 1994; Miller et al. 2000).

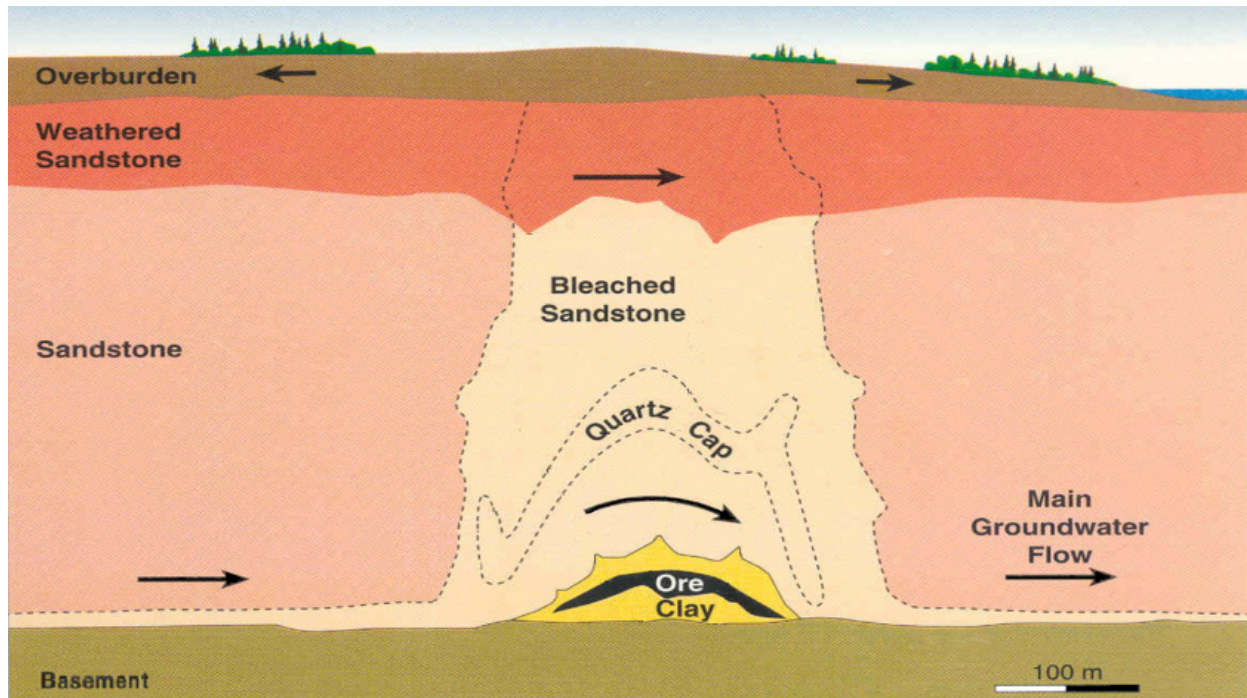


Figure 10-1: Cigar Lake Ore Deposit

The Cigar Lake uranium deposit is located about 430 m below surface, similar in depth to the repository considered in this study (i.e., 500 m underground). The ore body is primarily uraninite, co-precipitated with arsenides and sulfides. Uraninite is mostly uranium dioxide, so is similar to used fuel composition. The ore is also very rich in uranium, with much of the ore body at around 20% uranium and portions even higher. The total amount of uranium is roughly comparable to that to be placed in a Canadian repository. Also, the ore is surrounded by a clay envelope somewhat similar to the clay buffer specified in the repository design. It can be considered analogous to a “worst case” repository simulation, as it lacks any used fuel containers and also the host rock above the ore body is a permeable sandstone.

Natural radionuclide migration around Cigar Lake has not been sufficient to produce detectable concentration anomalies in the soil, surface water, lake sediments, and waters overlying the ore body. Environmental and geological exploration in the area has shown no surface expression of the ore body – it was discovered by geophysical techniques. Indeed, on a map of surface radioactivity in Canada, the area of the Saskatchewan deposits generally shows up as having below-average surface radioactivity (McKee and Lush 2004).

Based on studies of the Cigar Lake ore body (Cramer and Smellie 1994), it was concluded that:

- uranium dioxide will remain stable over 100 million year time scales under the chemically-reducing conditions found adjacent to the Cigar Lake ore body, with very little uranium migrating from the deposit;
- the natural clay surrounding the ore has provided an effective long-term seal, preventing migration of radionuclides from the deposit;
- dissolved organic matter in groundwater migrating past the ore has not played a significant role in mobilizing radionuclides from the deposit; and
- natural hydrologic barriers and appropriate geochemical conditions found at the site are effective in preventing significant radionuclide migration from the deposit.

Experimental and theoretical evidence shows that the dissolution rate of used nuclear fuel drops by several orders of magnitude in the presence of even modest pressures of hydrogen gas (see Chapter 5 and Chapter 7). Bruno and Spahiu (2014) concluded that the presence of dissolved hydrogen in the groundwater contacting the Cigar Lake ore body is a major factor in its stability; specifically, that hydrogen is activated on the surface of the Cigar Lake uraninites by alpha radiation, consuming the generated radiolytic oxidants.

A different type of uranium ore body found in permeable rocks is the roll-front type of ore body, named because they are slowly but continuously migrating or “rolling” through the permeable host rock. The front of the ore body is in a reduced state, while the rear of the ore body is in a more oxidized state as a consequence of oxidizing groundwaters that are slowly driving the ore body through the rock formation. This creates a condition at the rear of the ore body in which the uranium becomes soluble and migrates to the front of the ore body where it again precipitates. Although used fuel would not be located in a permeable rock formation, these ore bodies are further indication of the importance of redox conditions to the long-term stability of uranium underground.

A well-studied example of a roll-front uranium deposit is the Osamu Utsumi mine in Brazil; Hofmann (1999) reported that migration of uranium, along with palladium and selenium, was strongly inhibited at a redox front, causing immobilization. Results indicated that reducing conditions inhibit transport of these elements under most natural low-temperature conditions.

Roll-front uranium deposits illustrate how migration of uranium and many elements through locally oxidizing conditions in the container (assuming groundwater infiltration of used fuel containers and subsequent radiolysis of this water near the used fuel) would be effectively suppressed by the reducing conditions of the placement rooms and repository host rock.

10.1.2 Natural Fissioned Uranium

Nuclear fission occurred naturally on Earth over two billion years ago. In Gabon, Africa, there are 15 deposits of uranium ore that have acted as natural nuclear reactors (Miller et al. 2000), sometimes referred to as the Oklo fossil reactors (Figure 10-2). These remnants of natural uranium fission provide a close natural analogue for used nuclear fuel over long time periods in a geological environment.

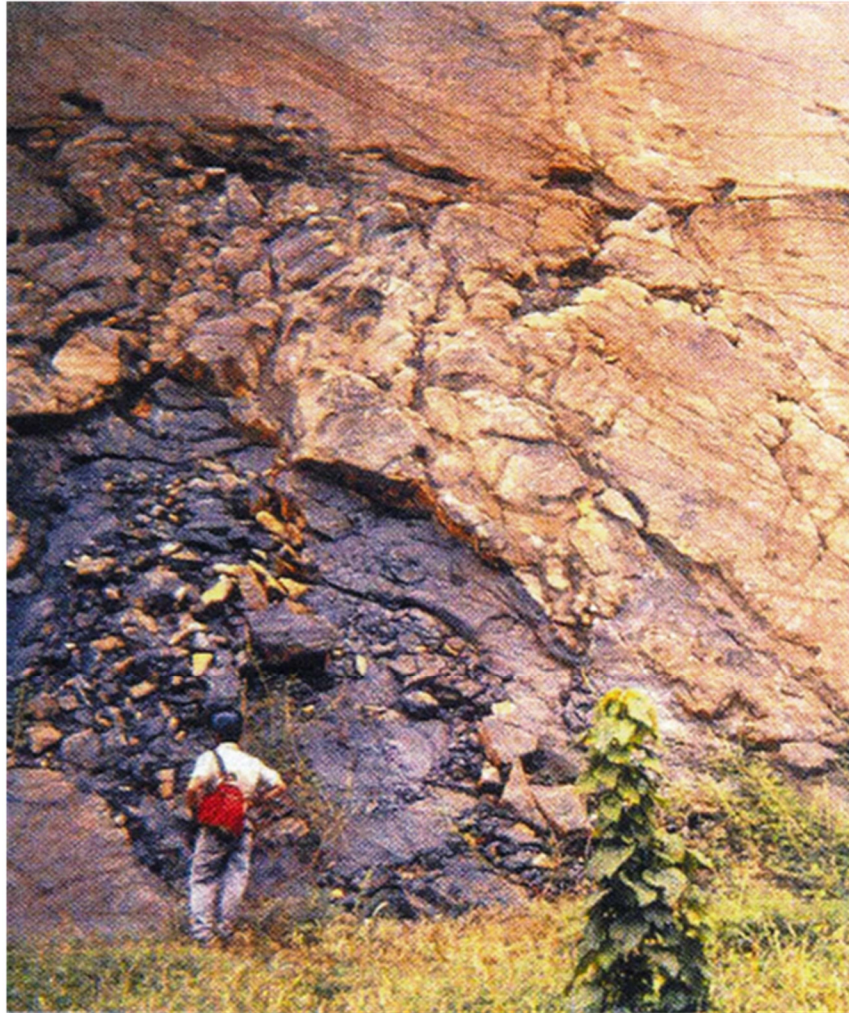
Approximately two billion years ago, when the Oklo ore bodies formed, the fraction of U-235 present in natural uranium was about 5%, much greater than the current value of about 0.7%

(due to natural decay over time). With this level of U-235, and under the groundwater and pressure conditions in the Oklo ore bodies, sustained nuclear chain reactions occurred. The Oklo reactors operated at low power over about one million years. Approximately 6 to 12 tonnes of U-235 underwent fission, producing fission products, plutonium and other actinides, and generating temperatures in the natural reactors of up to 350°C.

Oklo reactor studies provide data regarding the stability of uranium dioxide in the presence of fission products, and on the transport of radionuclides within the surrounding geology. These studies indicate that more than 90% of the uranium “fuel” present in the reactors two billion years ago has remained in place. The transuranic elements, most of the fission products and their decay products were trapped in the uranium ore or the surrounding clay; the plutonium moved less than 3 m. This is in absence of any analogues for the engineered barriers incorporated into a geological repository; containment and isolation of the Oklo reactors was achieved by the ore body and the surrounding sandstone and sedimentary formations. The rock has proved to be a well-sealed vault.

The stability of the Oklo used fuel has lasted through two billion years of continental drift and groundwater movement. This is particularly impressive considering the present day near-surface location of these natural reactors.

Studies of the Oklo reactors also illustrate the abilities of geochemical models (Duro and Bruno 2012). Gurban et al. (2003) modelled the hydrogeological and hydrochemical data from the Oklo sites to validate the models with in-situ data to better understand the geochemical behaviour of radionuclides in the natural system, and to identify and select processes and parameters for repository performance assessment calculations and modelling exercises.



Notes: In Oklo, Gabon, the remains of an ancient natural nuclear reactor indicate the resulting plutonium has moved less than 3 m over two billion years (from Miller et al. 2000).

Figure 10-2: Naturally Occurring Fission Reactor

The Oklo fossil reactors provide a snapshot in time of the condition of a natural used fuel repository two billion years after decommissioning. Information is obtained through indirect evidence such as the quantity and location of fission products and their decay products, and the actinides that can still be found in association with these natural reactors. This evidence indicates that careful selection of the host rock formation for a used fuel deep geological repository can render many fission products and actinides largely immobile.

10.1.3 Fractured Uranium Deposits

The Tono uranium deposit, located near Tokyo, has been the subject of analogue studies relating to transport of uranium (Miller et al. 2000). The uranium deposit, formed approximately 10 million years ago, lies between underlying crystalline bedrock and overlying sedimentary formations. The area is tectonically active and between 5 and 10 million years ago, the deposit was split by a fault. This displaced a portion of the ore body 30 m upward. Despite this large

fault, many other nearby faults, and the occurrence of frequent tremors, Yoshida (1994) found that no significant uranium transport has occurred along the fault. Detailed examination of the host rock found substantial matrix diffusion, providing a very large surface area for sorption of radionuclides. Consequently, no substantial remobilisation of the uranium has occurred, despite the faulting history of the area.

The preferred location for a used fuel repository will include a minimum distance separating the repository from significant fracture zones, because large faults are considered the most consequential pathway for transport of any hypothetical release of radioactivity from the repository to the surface. Nonetheless, it is important to note that the Tono uranium deposit was split by a large fault and no significant fracture-based transport has occurred.

10.2 Analogues for Barriers

The repository design uses multiple barriers, including materials such as iron, copper, clays, concrete and asphalt to inhibit or prevent movement of radioactive elements and other materials from the facility into the surrounding environment.

In particular, the used fuel will be sealed inside a container made from steel and covered in copper, and surrounded by a clay-based buffer layer. Placement rooms, underground tunnels and the shafts will be sealed with a combination of clay, concrete and asphalt-based materials.

10.2.1 Copper

Copper is one of the relatively few metals that naturally occur in their metallic state, indicating that it is stable under geological conditions. Solid pieces of native copper have been found containing more than 99% copper.

Copper “plates” found in the mudstones from South Devon in England (Figure 10-3) provide a natural analogue for the corrosion of used fuel containers placed in a clay backfill. These copper plates are up to 4 mm thick, comprising stacks of thin copper sheets that are between a few tens of microns to a couple of millimetres in thickness. The plates were formed 200 million years ago and show little corrosion since that time, due in part to the protection of the clay-rich mudstone (Milodowski et al. 2000). Data from these natural coppers help bound long-term copper corrosion rates for both reducing and oxidizing environments, which are useful in assessing the longevity of the used fuel containers.



Note: From Milodowski et al. (2000).

Figure 10-3: Copper Plate and Mudstone Covering

The largest known deposit of metallic copper is in the Keweenaw Peninsula of Michigan (Crisman and Jacobs 1982), where large pieces of almost pure copper were either mined or found in glacial outwash. Indigenous societies have explored the copper deposits around the Great Lakes over 5000 years ago (Emerson et al. 2000), building substantial local, traditional knowledge.

10.2.2 Iron

There are both archaeological and natural analogues for the long-term behavior of iron underground. These provide information on the corrosion rate of iron that can be expected over long time frames underground, as well as on the role of iron in maintaining favorable reducing conditions.

Recorded use of iron dates to Egypt in 1900 BCE (Miller et al. 2000). Johnson and Francis (1980) studied the corrosion of artifacts under a wide range of environmental conditions. From this work they have reported annual corrosion ranging from 0.1 to 10 microns, lasting over timescales of several thousand years.

The large amounts of iron (carbon steel) in the used fuel containers may buffer redox conditions in the repository, preventing oxidizing conditions near the used fuel. The Inchtuthil Roman nails found in Scotland provide an interesting analogue for this. At a Roman fortress that was abandoned in 87 CE (Angus et al. 1962; Pitts and St. Joseph 1985), over one million nails were buried in a 5-m deep pit under 3 m of earth. When the nails were unearthed in the 1950s, the nails on the outside of the mass were found to have corroded and formed a solid crust of iron oxides (rust) around the remaining mass of nails. The outside layer of nails formed a sacrificial redox sink, consuming oxygen before it could penetrate to the interior of the mass of nails. The physical expansion of the rust also served to self-seal the remaining nails from intruding

groundwater and water vapour. As a result, the nails inside the rusty barrier experienced minimal-to-no corrosion over nearly 2,000 years.

In Greenland, on Disko Island, magmatic conditions within a crystalline rock formation (basalt) promoted deposition of native iron over a period of volcanism spanning from about 63 to 30 million years ago. An estimated 10 million tons of iron were deposited. Mass transport limitations (low diffusivity of reactants combined with high redox capacity) favoured preservation of the native iron. Native iron has survived millions of years in the rock matrix (Hellmuth 1991).

The natural redox buffering capacity of the clay and rock surrounding the Cigar Lake ore body is due mainly to ferrous compounds in the mafic mineral phases (Smellie and Karlsson 1996). These reducing conditions have suppressed transport of uranium and other oxidising species. The combination of slow groundwater flow and reducing conditions resulted in a very stable ore body.

10.2.3 Clays

Sealing capacity

The primary sealing material within the engineered containment system is bentonite clay. Bentonite (Figure 10-4) is a type of naturally occurring clay, containing a swelling component referred to as smectite or, more specifically, montmorillonite. Bentonite swells when exposed to water, minimizing water seepage and making an excellent sealing material when physically confined. It also has a high chemical sorption capacity, able to bind many elements to its crystalline surfaces, which greatly slows the migration of radionuclides. Bentonite is also very stable, typically formed millions to hundreds of millions of years ago. Clay materials can act as a very robust physical and chemical barrier, as illustrated in the discussion above of Cigar Lake where naturally formed clays acted as a protective barrier for geological time periods. Laine and Karttunen (2010) produced a wide-ranging review of natural analogues for bentonite.



Figure 10-4: Bentonite Clay

The Dunarobba Forest in Italy (Figure 10-5) provides a natural analogue of the effectiveness of clays in minimizing groundwater movement (Benvegnú et al. 1988; Ambrosetti et al. 1992). The sequoia-like Dunarobba trees were buried in clay for 1.5 million years. The clay minimized the flow of water to the trees and prevented oxygen from reaching the wood. This maintained reducing conditions around the wood, protecting the wood from bacterial or fungal decay or chemical oxidation. As a result, the trees did not decay. They also did not fossilize - they are still made of wood.

Similar analogues have been found in the Canadian Arctic on Axel Heiberg Island (Greenwood and Basinger 1994) and at the Strathcona Fiord on Ellesmere Island (Francis 1988), where shale deposits over 40 million years old were found to contain preserved specimens of redwood, walnut, elm, birch and alder; also, ginkgo and katsura, now native to eastern Asia. The shale, which is consolidated clay, provided an effective barrier to oxygen and preserved the wood such that the wood grain and bark are preserved without chemical alteration – the cellular structure and most of its molecular structure remain intact.



Note: Retrieved Nov 23 2015 from <http://it.wikipedia.org/wiki/File:Dunarobba.jpg>.

Figure 10-5: 1.5 Ma Sequoia-like Tree Stumps at Dunarobba, Italy

Sensitivity to Temperature

Thermal alteration of bentonite has been studied, with a focus on higher temperatures of relevance to the near field. These studies indicate little reaction or degradation of bentonite physical properties below 150°C (Wersin et al. 2007). This compares well with repository temperatures (see Chapter 5), where the temperature at the surface of the container is predicted to peak at less than 100°C approximately 47 years after closure, then steadily decrease to 81°C after 600 years and ultimately return to ambient temperature by approximately 200,000 years.

For example, the bentonite beds at Kinnekulle in Southern Sweden were exposed to temperatures of 140-160°C over a period of about 1000 years as a result of a basaltic intrusion (Pusch et al. 1998). For this bentonite, 350 million years after the intrusion event, the measured swelling pressures are still substantial and hydraulic conductivities are reasonably low, indicating that the sealing properties of the bentonite remain favourable.

Laine and Karttunen (2010) report on the Ishirini bentonite body in Libya. Some of the bentonite formations were crosscut by basaltic intrusions about 20 million years ago, causing local thermal alteration near the intrusions. Kolaříková and Hanus (2008) found that the minimum

temperature experienced by the bentonite during the intrusions was probably higher than 190°C. The impact of raised temperatures, however, appears minimal: while some local cementation occurred, the majority of the bentonite remains unaltered.

Sensitivity to Salinity

The effects of potential saline groundwaters have been studied. High salinity, such as is likely to occur in the sedimentary rocks of Southern Ontario (not likely in crystalline rocks), is expected to affect the swelling properties of the bentonite; however, it is not expected to alter the mineral stability of the bentonite.

For example, Alexander and Milodowski (2014) observe that the Perapedhi bentonites studied under the Cyprus Natural Analogue Project likely remained in a marine, saline environment for nearly 90 million years. Figure 10-6 compares the swelling pressure of the Cyprus bentonite with a range of industrial bentonites, showing that the swelling behavior is about what would be expected for a bentonite material of this nature (with an inherent low amount of montmorillonite). This indicates that exposure of this bentonite to marine saline conditions for nearly 90 million years had no significant impact on its swelling capacity. This analogue is at lower salinity than could be seen in sedimentary rock repository settings; however the exposure was also for a very long period of time and yet there was no significant impact.

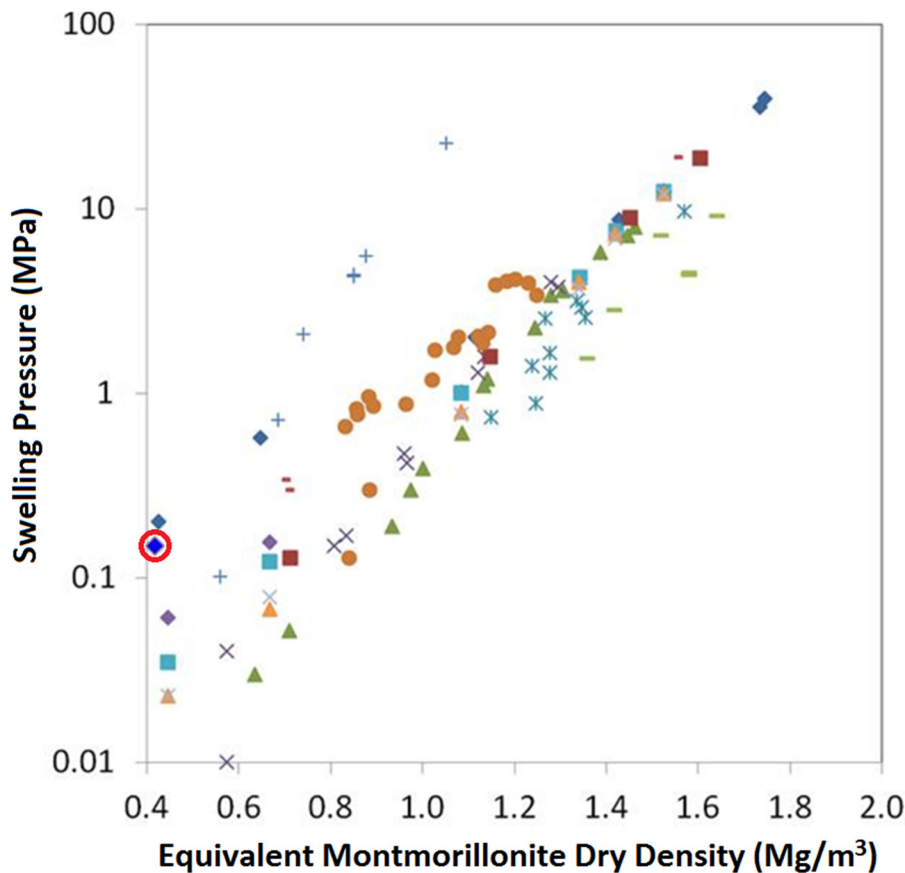


Figure 10-6: Swelling Performance of Various Bentonites (Cyprus is circled in red)

Sensitivity to Alkalinity

Bentonite, particularly the swelling clay component (smectite), is unstable under high pH conditions. In the repository, concrete may produce alkaline conditions locally, affecting adjacent bentonite. However, as the low-heat high-performance concrete leachates will have a lower pH (10 - 11) than Ordinary Portland Cement, it is expected that any reaction with the bentonite will be local. Furthermore, the concrete plugs are placed at a distance from the bentonite buffer around the containers.

Significant degradation of smectite has been observed in conditions with large amounts of alkaline groundwater; however, in natural analogue systems with limited groundwater flow, the reaction is limited. For example, results from the International Philippines Natural Analogue Project (Fujii et al. 2010) show that reaction with alkaline water (pH ~11) in the bentonite is restricted to the contact interface, with the width of the reaction zone a maximum of 5 cm. In another example, at the Cyprus Natural Analogue Project (Alexander and Milodowski 2014), the groundwater (9 < pH < 11) appears to have been circulating under the bentonite for approximately 500,000 to 800,000 years. In this time, less than 1% of the smectite in the bentonite has reacted, indicating very slow reaction times. The authors note that sufficient swelling pressure remains in the reacted bentonite to minimize further reaction due to pore throat reduction (see also Wilson et al. 2011).

10.2.4 Concrete

Low-heat, high-performance concrete may be used to close container placement rooms. The concrete bulkheads will counteract the swelling pressure of the bentonite components and maintain the tunnel backfill materials in their intended position. Concrete bulkheads could also be used to provide structural support and confinement to the column of shaft sealing materials. Low-heat high-performance concrete is designed to minimize effects on the adjacent clay.

Analogue studies of natural cements suggest that, within tectonically stable systems, the material is durable, with the oldest reported cements at Maqarin in north Jordan being some two million years old (Alexander 1992). Milodowski et al. (1989) also reported the presence of unreacted natural cements from the Scawt Hill and Carneal Plug sites in Northern Ireland. These cements were produced during the thermal metamorphism of the host limestone and are estimated to be some 58 million years old. In both examples, the natural cements are effectively impermeable and remain unchanged until accessed by groundwaters (through tectonic damage, for example). If damaged, the tendency is for these systems to reseal, either with secondary calcium silicate hydrate phases (Linklater 1998) or carbonates (Clark et al. 1994).

Of the natural analogue studies reported to date on cements, it is important to note that the natural cements examined are more akin to Ordinary Portland Cement, not low-heat high-performance cement (Gray and Shenton 1998). Low-heat high-performance cement is essentially the same as the pozzolanic cements developed by the Romans in the 3rd century BCE, or perhaps in Tiryns and Mycenae a millennium earlier (Middleton 1888). Recent studies of Roman cements exposed to marine salinities for about 2000 years tend to suggest little degradation of the cement (Oleson et al. 2004; Vola et al. 2011).

10.2.5 Asphalt

Bitumens are meltable substances distilled from fossil fuels while asphalts are solid bitumens containing various mineral materials¹. The shaft seal design concept includes a layer of asphalt, providing a redundant low-permeability seal.

Natural asphalts and bitumens have been used as glue or mastic for water-proofing for many thousands of years. In almost all cases where archaeological artifacts have been found coated in asphalt, they have been well preserved when mechanical disruption of the bitumen has not occurred: one example is provided by Babylonian buildings from 1300 BCE, where asphalt was used to coat floors and as a building material in river banks and piers (Hellmuth 1989); another comes from remains within the caves of Lascaux in France, approximately 15,000 years old (Nagra 1988).

Natural asphalts are found in a number of geological environments and in all climatic zones. Examples include the asphalt lakes of Trinidad and Guanoco, Venezuela, impregnated sandstones and limestones in Athabasca (Canada), Utah (USA), Val de Travers (Switzerland), and Hannover (Germany), and hydrothermal veins in Derbyshire (England).

The Athabasca oil sands located in the McMurray Formation in Athabasca are the largest known reservoir of crude bitumen in the world. The host formation is of early Cretaceous age and composed of numerous lenses of unconsolidated oil-bearing sand. Isotopic studies show the oil deposits to be about 112 million years old (Selby and Creaser 2005). The study by Longstaffe (1993) indicates that the bitumen has remained stable for over 10 million years.

The bitumen deposits in sandstone rocks in the Uinta Basin in Utah are believed to be from the late Cretaceous to Eocene period, 70 to 30 million years ago (Schamel 2009), formed under basin waters that were likely comparable to marine salinity. This natural analogue provides another example of the long-term stability of bitumen under likely saline conditions.

Also within the Uinta Basin in Utah, extensive veins of another natural asphalt called gilsonite were formed by hydrothermal fluids during the Eocene period, 56 to 34 million years ago, and have subsequently remained little altered for several tens of millions of years (Boden and Tripp 2012).

Drake et al. (2006) report natural asphalt (asphaltite) in open and closed fractures at the Forsmark site in Sweden. This asphalt was exposed to saline water (45 g/L at present) for at least several million years, suggesting very long-term stability of asphalt under saline conditions.

10.3 Analogue for Geosphere

Natural analogues for the behavior of the geosphere are also available. The site itself is an important analogue for the future behaviour of the geosphere at the site. In particular, geoscientific evidence of the past history of the site provides a direct analogue for future behaviour. This will be gathered for a real site as part of the site characterization, and presented

¹ Local preference may reverse this terminology (e.g., United Kingdom vs. United States); similarly, common usage may not align with preferred geological terminology.

in the geosynthesis. While this is not available for this hypothetical site, Southern Ontario in general has low seismicity and no volcanism, with evidence that oxygen does not penetrate to any great depth during glaciation.

10.4 Natural Analogue Summary

Performance of repositories cannot be verified by experiment for time scales relevant to their long-term safety. Natural analogues provide qualitative and quantitative illustrations of long-term behaviour. While they do not prove that the performance of the various repository components will continue indefinitely, as they are not repository replicates, natural analogues provide support for key model assumptions and for the identification of processes that need to be represented and those that can be excluded. The natural analogues identified here provide additional understanding of the materials and processes that influence the behaviour of radionuclides in a deep geological repository. They provide supporting arguments and increase confidence in the long-term performance of the repository.

10.5 References for Chapter 10

Alexander, W.R. and A.E. Milodowski (eds). 2014. Cyprus Natural Analogue Project (CNAP) Phase IV Final Report. Posiva Working Report 2014-02. Posiva, Eurajoki, Finland.

Ambrosetti, P., G. Basilici, S. Gentili, E. Biondi, Z. Cerquaglia and O. Girotti. 1992. La Foresta Fossile di Dunarobba. Ediart, Todi, Italy.

Angus, N.S., G.T. Brown and H.F. Cleere. 1962. The Iron Nails from the Roman Legionary Fortress at Inchtuthil, Perthshire. *Journal of Iron and Steel Institute* 200, 956-968.

Benvegnú, F., A. Brondi and C. Polizzano. 1988. Natural Analogues and Evidence of Long-term Isolation Capacity of Clays Occurring in Italy: Contribution to the Demonstration of Geological Disposal Reliability of Long-lived Wastes in Clay. CEC Nuclear Science and Technology Report EUR 11896. Luxembourg.

Boden, T. and B.T. Tripp. 2012. Gilsonite veins of the Uinta Basin, Utah. Utah Geological Survey, Special Study 141. Utah Dept. of Natural Resources, Salt Lake City, USA.

Bruno, J. and K. Spahiu. 2014. The long-term effect of hydrogen on the UO₂ spent fuel stability under anoxic conditions: Findings from the Cigar Lake Natural Analogue study. *Applied Geochemistry* 49, 178-183.

Clark, I.D., R. Dayal and H.N. Khoury. 1994. The Maqarin (Jordan) natural analogue for ¹⁴C attenuation in cementitious barriers. *Waste Management* 14, 467-477.

CNSC. 2018. Regulatory Document REGDOC-2.11.1, Waste Management, Volume III: Assessing the Long-Term Safety of Radioactive Waste Management. Canadian Nuclear Safety Commission. Ottawa, Canada.

Cramer, J.J. and J.A.T. Smellie. 1994. Final Report for the AECL/SKB Cigar Lake Analog Study. Atomic Energy of Canada Limited Report AECL-10851, COG-93-00147, SKB-TR-94-04. Pinawa, Canada.

- Crisman, D. and G Jacobs. 1982. Native Copper Deposits of the Portage Lake Volcanics, Michigan: Their Implications with Respect to Canister Stability for Nuclear Waste Isolation in Columbia River Basalts beneath the Hanford Site, Washington. Rockwell Hanford Operations Technical Report RHO-BW-ST- 26P. Hanford, USA.
- Drake, H., B. Sandström and E-L. Tullborg. 2006. Mineralogy and geochemistry of rocks and fracture fillings from Forsmark and Oskarshamn: Compilation of data for SR-Can. SKB R-06-109. SKB, Stockholm, Sweden.
- Duro, L. and J. Bruno. 2012. Natural analogues of nuclear waste repositories: studies and their implications for the development of radionuclide migration models. In Radionuclide Behaviour in the Natural Environment (pp. 411-445).
- Emerson, T.E., D.L. McElrath and A.C. Fortier (Eds.). 2000. Late Woodland Societies: Tradition and Transformation across the Midcontinent. U of Nebraska Press.
- Francis, J.E. 1988. A 50-million-year-old fossil forest from Strathcona Fiord, Ellesmere Island, Arctic Canada: evidence for a warm polar climate. *Arctic* 41, 314-318.
- Fujii, N., C.A. Arcilla, M. Yamakawa, C. Pascua, K. Namiki, T. Sato, N. Shikazono and W.R. Alexander. 2010. Natural analogue studies of bentonite reaction under hyperalkaline conditions: overview of ongoing work at the Zambales Ophiolite, Philippines. Proc. ICM 2010 Conference, ASME, Washington, USA.
- Gray, M.N. and B.S. Shenton. 1998. For better concrete, take out some of the cement. In Proc. 6th ACI/CANMET Symposium on the Durability of Concrete, Bangkok, Thailand.
- Greenwood, D.R. and J.F. Basinger. 1994. The paleoecology of high latitude Eocene swamp forests from Axel Heiberg Island, Canadian High Arctic. *Review of Palaeobotany and Palynology* 81, 83-97.
- Gurban, I., M. Laaksoharju, B. Madé and E. Ledoux. 2003. Uranium transport around the reactor zone at Bangombé and Okélobondo (Oklo): examples of hydrogeological and geochemical model integration and data evaluation. *Journal of contaminant hydrology* 61(1-4), 247-264.
- Hellmuth, K-H. 1989. Natural Analogues of Bitumen and Bitumenized Radioactive Waste. Finnish Centre for Radiation and Nuclear Safety, STUK-B-VALO 58, Helsinki, Finland.
- Hellmuth, K-H. 1991. The Existence of Native Iron – Implications for Nuclear Waste Management. Part II: Evidence from Investigation of Samples of Native Iron. Helsinki, Finland: Finnish Centre for Radiation and Nuclear Safety. Report STUK-B-VALO 68.
- Hofmann, B.A. 1999. Geochemistry of Natural Redox Fronts – A Review. Nagra Technical Report NTB 99-05. Wettingen, Switzerland.
- IAEA. 2011. Disposal of Radioactive Waste, Specific Safety Requirements SSR-5, International Atomic Energy Agency. Vienna, Austria.

- Johnson, A.B. and B. Francis. 1980. Durability of Metals from Archaeological Objects, Metal Meteorites, and Native Metals. Battelle Pacific Northwest Laboratory PNL-3198. Hanford, USA.
- Kolaříková, I. and R. Hanus. 2008. Geochemistry and mineralogy of bentonites from Ishirini (Libya). *Chemie der Erde-Geochemistry* 68(1), 61-68.
- Laine, H. and P. Karttunen. 2010. Long-Term Stability of Bentonite: A Literature Review. Posiva Working Report 2010-53, Posiva, Eurajoki, Finland.
- Linklater, C.M. (ed). 1998. Nirex Safety Assessment Research Programme. A Natural Analogue Study of Cement-Buffered, Hyperalkaline Groundwaters and their Interaction with a Repository Host Rock (No. NIREX-SR-S-98/003). UK Nirex Ltd.
- Longstaffe, F. 1993. Meteoric Water and Sandstone Diagenesis in the Western Canada Sedimentary Basin, in SG36: Diagenesis and Basin Hydrodynamics. American Association of Professional Geologists AAPG Special Volume. Tulsa, USA.
- McKee, P. and D. Lush. 2004. Natural and Anthropogenic Analogues – Insights for Management of Spent Fuel. Nuclear Waste Management Organization Technical Report APM-REF-06110-24105. Toronto, Canada.
- Middleton, J.H. 1888. On the chief methods of construction used in ancient Rome. *Archaeologia* 51, 41-60.
- Miller, W., R. Alexander, N. Chapman, I McKinley and J. Smellie. 2000. Geologic Disposal of Radioactive Wastes & Natural Analogues Volume 2. Elsevier/ Pergamon Press. Oxford, UK.
- Milodowski, A.E., P.H.A. Nancarrow and B. Spiro. 1989. A Mineralogical and Stable Isotope Study of Natural Analogues of Ordinary Portland Cement (OPC) and CaO–SiO₂–H₂O (CSH) Compounds. United Kingdom Nirex Safety Studies Report, NSS/R240, NDA, Moor Row, UK.
- Milodowski, A.E., M.T. Styles, M.S.A. Horstwood and S.J. Kemp. (2002). Alteration of Uraniferous and Native Copper Concretions in the Permian Mudrocks of South Devon, United Kingdom. SKB Technical Report TR-02-09. Stockholm, Sweden.
- Nagra. 1988. Solidification of Swiss Radioactive Waste with Bitumen. National Cooperative for the Disposal of Radioactive Waste (Nagra). NTB 85-28. Baden, Switzerland (in German).
- Nagra. 1992. A Natural Analogue Study of the Maqarin Hyperalkaline Groundwaters I: Source Term Description and Thermodynamic Database Testing. Nagra Technical Report Series NTB 91-10. Nagra, Wettingen, Switzerland.
- Oleson, J.P., C. Brandon, S.M. Cramer, R. Cucitore, E. Gotti and R.L. Hohlfelder. 2004. The ROMACONS Project: a contribution to the historical and engineering analysis of

hydraulic concrete in Roman maritime structures. *International Journal of Nautical Archaeology* 33.2, 199–229. doi: 10.1111/j.1095-9270.2004.00020.x

Pitts, L. and J.K. Sr. Joseph. 1985. *Inchtuthil: Roman Legionary Fortress Excavations, 1952-1965*. Society for the Promotion of Roman Studies. *Britannia Monographs Series 6*. London, England.

Pusch, R., H. Takase and S. Benbow. 1998. Chemical processes causing cementation in heat-affected smectite – the Kinnekulle bentonite. SKB Technical Report TR-98-25, Stockholm, Sweden.

Rudnick R.L. and S. Gao. 2014. *Composition of the Continental Crust*. Treatise on Geochemistry 2nd Edition. Volume 3, 1-64, Elsevier, New York, New York, USA.

Schamel, S. 2009. *Strategies for In Situ Recovery of Utah's Heavy Oil and Bitumen Resources*. Utah Geological Survey, Open File Report 551. Salt Lake City, USA.

Selby D. and R.A. Creaser. 2005. Direct radiometric dating of hydrocarbon deposits using rhenium-osmium isotopes. *Science* 308, 1293-1295.

Smellie, J.A.T. and F. Karlsson. 1996. *A Reappraisal of Some Cigar Lake Issues of Importance to Performance Assessment*. SKB Technical Report TR 96-08, SKB, Stockholm, Sweden.

Tait, J.C., H. Roman and C.A. Morrison. 2000. *Characteristics and Radionuclide Inventories of Used Fuel from OPG Nuclear Generating Stations Volumes 1 and 2*. Ontario Power Generation Report 06819-REP-01200-10029-R00. Toronto, Canada.

Vola, G., E. Gotti, C. Brandon, J.P. Oleson and R.L. Hohlfelder. 2011. Chemical, mineralogical and petrographic characterization of Roman ancient hydraulic concretes cores from Santa Liberata, Italy, and Caesarea Palestinae, Israel. *Periodico di Mineralogia* 80, 317–338.

Wersin, P., L.H. Johnson and I.G. McKinley. 2007. Performance of the bentonite barrier at temperatures beyond 100°C: A critical review. *Physics and Chemistry of the Earth, Parts A/B/C* 32, 780-788.

Wilson, J., D. Savage, A. Bond, S. Watson, R. Pusch and D. Bennett. 2011. *Bentonite: a review of key properties, processes and issues for consideration in the UK context*. Quintessa Report QRS-1378ZG-1.1 for the NDA-RWMD, Quintessa, Henley-on-Thames, UK.

Yoshida, H. 1994. Relation between U-series nuclide migration and microstructural properties of sedimentary rocks. *Applied Geochemistry*, 9 (5), 479-490.

THIS PAGE HAS BEEN LEFT BLANK INTENTIONALLY

11. QUALITY ASSURANCE

11.1 Introduction

This chapter describes how project activities important to safety in this postclosure safety assessment were conducted under an appropriate quality assurance framework.

11.2 APM Safety Case Project Quality Plan

The APM Design and Technical Project Quality Plan (PQP) APM-PLAN-01913-0222-R000 (NWMO 2016) was prepared by the NWMO Director, Quality Assurance and approved by the responsible Vice President for use during the preparation of the Used Fuel Repository Conceptual Design and Postclosure Safety in Sedimentary Rock. This APM Design and Technical PQP meets the requirements of both CSA N286-12 and ISO 9001:2008/2015.

The quality program applies to all organizational units with responsibilities for the preparation of the Used Fuel Repository Conceptual Design and Postclosure Safety in Sedimentary Rock project. The following processes implement the program:

- A managed system consisting of governing documents that prescribe controls and responsibilities to ensure activities are carried out in a quality assured, effective manner by qualified personnel;
- Individual accountability for implementing and adhering to the managed system elements;
- A specific APM Safety Case Work Plan identifying project scope, work breakdown, responsibilities and controls, and
- Evaluation and enhancement of the program elements through continuous improvement processes.

Selected vendors and suppliers are required to be qualified to appropriate quality assurance standards defined by the NWMO. Each of these vendors and suppliers selected is required to have an appropriate management system for quality assurance (e.g. ISO 9001, CSA N286-12) and submit a detailed quality assurance and verification/inspection plan for review and approval.

The quality program includes provisions for planned audits and assessments designed to provide a comprehensive, critical and independent evaluation of project activities. These audits and assessments cover the overall quality program, sub-tier programs, and interfaces between programs. The audits and assessments monitor compliance with governing procedures, standards and technical requirements, and confirm that quality program requirements are being effectively implemented. Audit and assessment results are documented, reported to and evaluated by a level of management having sufficient breadth of responsibility to assure actions are taken to address the findings.

Additional oversight of activities is provided through regular project monitoring and reporting, self-assessment and the non-conformance and corrective action program. In particular, the corrective action program assures that non-conformance conditions are identified, documented, reported, evaluated and corrected in a timely manner.

The APM Design and Technical PQP is supported by NWMO governance that establishes expectations for engineering and design, safety assessment, procurement, occupational health

and safety, environmental protection, product and services approval, document control and record keeping.

The following are key elements of the APM Design and Technical PQP:

- Project specific quality objectives are established.
- Each person working on the project is responsible for achieving and maintaining quality and management is responsible for providing adequate resources and evaluating the quality of the work.
- APM project work is performed in accordance with applicable NWMO governing documents and established processes and procedures.
- Specific requirements for design, safety assessment and technical studies involving computer modeling are described.
- All work is conducted by qualified individuals.
- When work within the scope of the APM project is performed by another organization, the consultant/contractor performs work in compliance with ISO 9001:2008/2015 or CSA N286-12 as appropriate and in compliance with a reviewed and approved work specific quality plan and APM project-specific governing documents. Typically contractor's ISO 9001, management systems are augmented to ensure CSA N286-12 requirements such as safety, competency, verification and change management are integrated. When a consultant/contractor provides a specialized technical service, and their quality management system is not based on a recognized system, their quality management system with appropriate augmentation may be accepted, if it meets internal quality objectives and requirements.
- APM work is verified via verification processes and procedures. Furthermore for work conducted by contractors, project quality plans are reviewed and approved and include appropriate verification procedures for deliverables including verification process documentation.
- Experience from related industries is obtained through planned activities including information exchanges with other nuclear waste management organizations, participation in technical conferences, contracting with organizations and obtaining independent expert review and input.
- NWMO APM project personnel have access to observe and verify consultants/contractors' quality processes and examine quality assurance documentation.
- Documents considered to be quality assurance records as per APM-LIST-08133-0001, Quality Assurance Documents (NWMO 2014), are transmitted into NWMO records.
- Targeted periodic assessments of work are performed on the APM project. Work performed by NWMO project personnel is assessed for compliance with the APM PQP and applicable procedures. Work performed by consultants/contractors and their subcontractors are assessed to confirm that it is being performed in compliance with their work specific quality plans.

11.3 Examples of Peer Review and Quality Assurance

Experienced contractors worked with NWMO to carry out the illustrative postclosure safety assessments for the APM project under approved project specific quality plans. The contractors committed to provide high quality work through effective application of a quality system that fostered best practice and included processes for continual improvement. Safety assessments

were conducted consistent with NWMO's governance, NWMO-PROC-EN-0003 Safety Assessment Procedure (NWMO 2015). For this illustrative safety case formally accepted data clearance forms were used between the geoscience, engineering and safety assessment teams. Software and reference datasets were procured, developed and maintained consistent with NWMO's governance, NWMO-PROC-EN-0002 Technical Computer Software Procedure (NWMO 2017). The confidence in the software models used for this illustrative safety assessment is obtained through verifications which include consistency in terms of nuclide transport observed between the simple and complex models as described in Section 7.8.1.4 and the consistency between the deterministic and probabilistic results.

NWMO and independent peer review of key results and conclusions in the illustrative postclosure safety assessment was planned by the NWMO and completed. The comments and suggested improvements provided by the independent reviewers have been addressed and incorporated as appropriate into this illustrative safety assessment.

11.4 Future Safety Case Quality Assurance

Once an actual repository site is selected, on-site work will commence to characterize the site in terms of its geophysical and environmental properties. Simultaneously, the conceptual design will progress towards the detailed design required for licensing and ultimately container manufacture and facilities construction. The project quality assurance plan will necessarily expand in scope to ensure that the site characterization, detailed design, associated preclosure and postclosure safety assessment and environmental assessment are prepared under a comprehensive and robust quality assurance regime. At an appropriate time in the future, specific quality assurance plans will be prepared and implemented for the manufacturing and qualification of containers and the construction and commissioning of the used fuel transfer facility and the repository.

11.5 References for Chapter 11

CSA. 2017. Management System Requirements for Nuclear Facilities. Canadian Standards Association N286-12 (R2017). Toronto, Canada.

ISO. 2008. Quality Management Systems - Requirements. International Organization for Standardization ISO 9001: 2008. Geneva, Switzerland.

ISO. 2015. Quality Management System - Requirements. International Organization for Standardization ISO 9001: 2015. Geneva, Switzerland.

NWMO. 2014. APM Deep Geological Repository Project Quality Assurance Documents. Nuclear Waste Management Organization List APM-LIST-08133-0001. Toronto, Canada.

NWMO. 2015. Safety Assessment Procedure. Nuclear Waste Management Organization Procedure NWMO-PROC-EN-0003-R003. Toronto, Canada.

NWMO. 2016. APM Design and Technical Project Quality Plan. Nuclear Waste Management Organization Plan APM-PLAN-01913-0222-R000. Toronto, Canada.

Postclosure Safety Assessment of a Used Fuel Repository in Sedimentary Rock

Document Number: NWMO-TR-2018-08

Revision: 000

Class: Public

Page: 680

NWMO. 2017. Technical Computing Software Procedure. Nuclear Waste Management Organization Procedure NWMO-PROC-EN-0002-R005. Toronto, Canada.

12. SUMMARY AND CONCLUSIONS

12.1 Safety Case

This report presents an illustrative postclosure safety assessment for a conceptual deep geological repository located at a hypothetical site in the sedimentary rock of the Southern Ontario. The postclosure safety assessment forms part of the overall safety case that would be provided in support of a licence application.

The safety case is supported by a set of arguments or attributes that collectively define the basis for repository safety. Table 12-1 summarizes the safety attributes or arguments addressed in the current study, and where further information on these is presented.

One important objective for this work is to illustrate how expectations, documented in CNSC Regulatory Document REGDOC-2.11.1 Volume III *Assessing the Long-Term Safety of Radioactive Waste Management* (CNSC 2018), are satisfied. Table 1-4 provides links between REGDOC-2.11.1 Volume III and sections of this report. Relevant aspects of REGDOC-2.11.1 Volume III are extracted and included in grey 'text' boxes throughout this chapter.

Developing a Long-Term Safety Case, REGDOC-2.11.1 Volume III, Section 5:

Demonstrating long-term safety consists of providing reasonable assurance that waste management will be conducted in a manner that protects human health and the environment. This is achieved through the development of a safety case, which includes a safety assessment complemented by various additional arguments...

This summary chapter highlights the means by which a safety assessment methodology has been developed and applied to evaluate the safety and associated uncertainty of a deep geological repository for used nuclear fuel. The strategy adopted is based, in part, on a defence-in-depth approach consistent with current international practice. The results of the illustrative safety assessment provide confidence that, from a technical perspective, a suitable repository could be a suitable repository could be designed, sited and constructed in the sedimentary rock of the Southern Ontario.

Table 12-1: Summary of Key Safety Attributes

Safety Attribute	Section
1. The geologic setting provides isolation and containment.	
1.1. The repository depth isolates the waste and repository components from surface changes created by human activities or natural events.	Design basis, Section 1.6.3.1
1.2. The repository is enclosed by stable, competent and low permeability rock.	Assumed, Section 1.6.3.1; also Section 2.2
1.3. The hydrogeologic setting that encloses the repository restricts groundwater and radionuclide movement.	Section 2.3
1.4. The mineralogy of the host rock, and the composition of the ground/porewater, are compatible with the engineered barriers.	Section 5.2
1.5. The host rock mineralogy and the composition of the ground/porewater are favourable for mitigating radionuclide movement.	Section 7.5.2
1.6. Natural resource potential is low within the repository geologic setting.	Assumed, Section 1.6.3.1
1.7. Seismic hazard is low.	Assumed, Section 1.6.3.1
1.8. The host rock is predictable and amenable to characterization.	Assumed, Section 1.6.3.1
2. The site geology has long-term stability.	
2.1. The hydrogeologic conditions at repository depth are stable and resilient to internal and external perturbations, including glaciation.	Section 2.3 and Section 5.1
2.2. The host rock is capable of withstanding thermal and mechanical stresses induced by internal and external perturbations, including glaciation.	Section 5.2
2.3. The repository conditions including chemistry and physical condition important for safety are not influenced by internal and external perturbations, including glaciation.	Section 5.2 and Section 5.5
2.4. Rate of erosion is low.	Section 5.1.2.3
2.5. Repository safety is not influenced by strong ground motions associated with rare earthquakes.	Section 5.1.1 and Section 5.2.6.3
3. The site supports robust construction and operation.	
3.1. Repository host rock conditions allow safe construction and operation.	Not covered in this study
3.2. Safe transportation route to site.	Not covered in this study
3.3. Frequency of severe natural events at site during construction and operation is low.	Not covered in this study
3.4. Robust facility design for safe construction and operation.	Not covered in this study
3.5. The site is not located in a sensitive ecological environment.	Not covered in this study

4. The used fuel wasteform is a barrier which contributes to the containment of radionuclides.

- | | |
|---|---------------------------------|
| 4.1. Most radionuclides are immobile within the uranium oxide grains of the used CANDU fuel. | Section 5.3.3 |
| 4.2. The used CANDU fuel grains are mechanically durable and not materially impacted by radiation damage or helium gas buildup. | Section 5.3.3 and Section 5.3.5 |
| 4.3. The used fuel has low solubility under conditions of a failed container with contact with ground/porewater. | Section 5.4.4.7 |
| 4.4. The Zircaloy cladding provides a barrier to contact between ground/porewater and used fuel in a failed container. | Section 5.3.4 |
| 4.5. The Zircaloy cladding corrodes slowly under conditions of a failed container in contact with ground/porewater. | Section 5.4.4.6 |

5. Container and sealing systems are barriers which contribute to the isolation and containment of radionuclides.

- | | |
|--|--------------------------------------|
| 5.1. The container is designed for the underground conditions at timeframes relevant to repository safety. | Section 4.3.1 and Section 5.4 |
| 5.2. Inspection methods would ensure the container is built consistent with design specifications. | Not covered in this study |
| 5.3. The in-room buffer system holds and protects the containers. | Section 4.3.2, 4.8.2 and Section 5.5 |
| 5.4. Engineered seals isolate the placement rooms from the access tunnels. | Section 4.3.2, 4.8.2 |
| 5.5. Shaft backfill and seals isolate the repository from the surface. | Section 4.3.2, 4.12 |

6. Repository construction, operation and closure supports the long term repository performance objective.

- | | |
|---|-------------------------------|
| 6.1. Repository layout and spacing are designed for long-term structural stability. | Section 4.8 and Section 5.2.6 |
| 6.2. Repository design and construction methods minimize the excavation damaged zone. | Section 5.2.5 |
| 6.3. Materials used in repository construction and operation will not compromise long-term performance. | Section 5.2.4 |
| 6.4. Institutional controls and monitoring will verify performance. | Section 1.3.5 |

7. The repository is robust to accidents and unexpected events.

- | | |
|---|-------------------------------|
| 7.1. Credible accident during operations would have low effects on public and environment. | Not covered in this study |
| 7.2. Postclosure analyses show low effect from normal or expected scenarios, with large safety margin to regulatory criteria. | Section 7.13 and Section 7.14 |
| 7.3. Postclosure analyses show risk from disruptive scenarios to be acceptable. | Section 7.13 and Section 7.14 |

12.2 Repository System

Design optimization, REGDOC-2.11.1 Volume III, Section 4.3.2:

The design of a nuclear facility should be optimized to exceed all applicable requirements. In particular, a radioactive waste management facility should more than meet the regulatory limits, remaining below those limits by a margin that provides assurance of safety for the long term.

This report describes a deep geological repository design in a sedimentary rock setting. The deep geological repository system is described in Chapters 2 through 5 of this report where:

- Chapter 2 describes the hypothetical geosphere setting;
- Chapter 3 describes the characteristics of the used nuclear fuel;
- Chapter 4 describes the repository design concept; and
- Chapter 5 describes how key components of the system will interact with each other and with the environment in the long term.

The key points from these chapters are summarized in this section along with parameters identified in the safety assessment as being influential to repository performance.

12.2.1 Geologic Description of the Hypothetical Site

Information on the geologic characteristics of the site relevant to this illustrative safety assessment is presented in Chapters 1 and 2. Site-specific characterization activities at a candidate site would be used to develop a Descriptive Geosphere Site Model and Geosynthesis, to document the site and support a repository safety case.

For the purpose of this illustrative case study in a hypothetical site, several key attributes have been assumed for the site as listed in Chapter 1 (Section 1.6.3.1).

Such attributes that normally would be confirmed through site-specific investigation include:

- The repository is positioned at a depth of 500 m below ground surface in a sufficient volume of competent, low-permeability rock;
- The repository is located in an area of low seismic hazard;
- The repository location is not associated with potable groundwater resources;
- The repository location is not associated with economically viable natural resources;
- The groundwater system at repository depth is electrochemically reducing;
- The host rock formation can withstand transient thermal and mechanical stresses; and
- The rates of site uplift and erosion are sufficiently small so as not to influence repository safety.

Specific site characteristics for the postclosure safety assessment are described in Chapter 2. In particular, this chapter describes the structural, physical, geochemical, hydrogeologic, and geomechanical properties of the host rock. The selection of these properties has been informed

by historic work conducted within the Canadian Nuclear Fuel Waste Management Program and through the OPG proposed Deep Geologic Repository for Low & Intermediate Level Waste.

The information presented in Chapter 2 outlines the properties and long-term behaviour of the groundwater system for the hypothetical site.

12.2.2 Used Fuel

The characteristics of the used fuel are described in Chapter 3. The durability and distribution of radionuclides within the fuel form an important part of the multi-barrier system.

12.2.3 Design Concept

The repository design concept is presented in Chapter 4. The design concept includes the following features relevant to long-term safety:

- The repository is positioned at a depth of 500 m to provide isolation from surface processes, and a stable, chemically reducing environment;
- The primary waste form is used CANDU fuel bundles;
- A long-lived container with a 3-mm copper corrosion barrier;
- Low-permeability dense bentonite encloses the containers;
- Placement room and container spacing such that the peak container temperature (and also the bentonite temperature) remains below 100°C;
- Placement rooms selected to minimize intersection with fractures, and excavated to control the production of EDZ;
- Rooms plugs to seal rooms from access tunnels;
- Access tunnels backfilled to provide support and minimize groundwater flow;
- Placement rooms laid out in panels that are designed to fit within blocks of competent rock;
- Shafts located in a central service area to avoid creation of flow-through paths; and
- Shafts backfilled with low-permeability sealing material, including bentonite.

Chapter 5 describes the repository system, and how key components of the system will interact with each other and the environment in the long term.

The influence of design features and their properties on repository performance is explored through the safety assessment summarized in Section 7.13. The long-term safety assessment provides information that can be used to support and inform future decision making.

12.3 Safety Assessment

A structured approach is used in the postclosure safety assessment where two classes of scenarios are assessed, consistent with Sections 5 and 7 of REGDOC-2.11.1 Volume III. More specifically, the expectation to demonstrate understanding of the system through a well-structured, transparent, and traceable methodology is described.

Performing Long-Term Assessments, REGDOC-2.11.1 Volume III, Section 7:

The CNSC expects the applicant to use a structured approach to assess the long-term performance of a waste management system. Although long-term assessments are done with different levels of detail and rigour for different purposes, the overall methodology for performing them should include the following elements:

- 1. Selection of appropriate methodology;*
- 2. Assessment context;*
- 3. System description;*
- 4. Timeframes;*
- 5. Assessment scenarios; and*
- 6. Development of assessment models.*

Chapter 6 describes a systematic scenario identification process that acknowledges the timeframes of interest and that identifies the features, events, and processes which could have an effect on the repository's safety features. The different assessment strategies, including key assumptions and rationale are described in Chapter 7 and summarized in this section.

The **Normal Evolution Scenario** is based on a reasoned extrapolation of the hypothetical site and repository features, events and processes. The Reference Case assumes all repository components are correctly fabricated, correctly installed, and function as expected, leading to zero releases of radionuclides in the one million year timeframe of interest.

The computer models and key assumptions are discussed in Chapter 7 and analyses of impacts are also presented for a Base Case (see below) in which a number of container failures are assumed. This case is extended through a range of variant cases in which the effects of imperfect barrier performance is also examined.

Disruptive Event Scenarios examine the occurrence of unlikely events leading to the unexpected circumvention of barriers and loss of confinement. Chapter 7 presents the methods, assumptions and results associated with the analysis of disruptive events.

Criteria for protection of persons and the environment, REGDOC-2.11.1 Volume III, Section 6.2:

The regulatory requirements for protection of persons and the environment from both radiological and non-radiological hazards of radioactive wastes lead to four distinguishable sets of acceptance criteria for a long-term assessment:

- 1. Radiological protection of persons;*
- 2. Protection of persons from hazardous substances;*
- 3. Radiological protection of the environment; and*
- 4. Protection of the environment from hazardous substances.*

Analysis results from the Normal Evolution Scenario and from Disruptive Event Scenarios are compared against interim acceptance criteria in Chapter 7. Interim acceptance criteria selected to meet the expectations in Section 6 of the regulatory document are proposed in Section 7.1 for each of the following categories:

- Radiological protection of persons;
- Protection of persons from hazardous substances;
- Radiological protection of the environment; and
- Protection of the environment from hazardous substances.

12.3.1 Assessment Strategies

Use of different assessment strategies, REGDOC-2.11.1 Volume III, Section 5.2:

The strategy used to demonstrate long-term safety may include a number of approaches, including, without being limited to:

1. *Scoping assessments to illustrate the factors that are important to long term safety;*
2. *Bounding assessments to show the limits of potential impact;*
3. *Calculations that give a realistic best estimate of the performance of the waste management system, or conservative calculations that intentionally over-estimate potential impact; and*
4. *Deterministic or probabilistic calculations, appropriate for the purpose of the assessment, to reflect data uncertainty.*

Any combination of these or other appropriate assessment strategies can be used in a complementary manner to increase confidence in the demonstration of long-term safety.

Key elements included in the Chapter 7 approach are:

- Performing a screening exercise to identify potentially significant dose contributing radionuclides and hazardous substances so that subsequent steps can focus solely on these.
- Conducting 3-dimensional hydrogeological modelling of the groundwater system(s) hosting the repository.
- Presenting a best estimate of performance in the Reference Case of the Normal Evolution Scenario (i.e., containers remain intact with zero release).
- Performing deterministic and probabilistic calculations of contaminant transport from the fuel to surface for scenarios in which containers are assumed to fail. This includes analysis of both Normal and Disruptive Event Scenarios accompanied by sensitivity cases and bounding assessments.
- Estimating dose consequences for a critical group assumed to be farming on the surface biosphere directly above the repository and obtaining all their drinking and crop irrigation water from a deep well situated in the location that maximizes contaminant capture.

12.3.2 Modelling Tools and Computer Codes

As discussed in Sections 7.3 and 7.4, computer codes are applied to assess key aspects of the repository's components and specific scenarios.

The main computer codes are FRAC3DVS-OPG v1.3 for 3D groundwater and transport analysis and SYVAC3-CC4 v4.09.3 for system modelling. These codes and associated datasets are

maintained under a NWMO software quality assurance system. They have been in use for Canadian repository safety assessments for many years.

Developing assessment models, REGDOC-2.11.1 Volume III, Section 7.6.1:

An assessment model should be consistent with the site description, waste properties, and receptor characteristics, and with the quality and quantity of data available to characterize the site, waste, exposure pathways, and receptors. A systematic process should be used to ensure that the set of data used for developing the assessment model is accurate and representative. Complex models should not be developed if there is not sufficient data to support them. The use of generic or default data in place of site-specific data in developing the conceptual and computer models may be acceptable when there is no site-specific data available, such as in early stages of development; however, with the acquisition of as-built information and operational data, and increased understanding of site characteristics throughout the facility lifecycle, site-specific data should be used.

Confidence in assessment models, REGDOC-2.11.1 Volume III, Section 7.6.3:

Confidence in the assessment model can be enhanced through a number of activities, including (without being limited to):

- 1. performing independent predictions using entirely different assessment strategies and computing tools;*
- 2. demonstrating consistency between the results of the long term assessment model and complementary scoping and bounding assessments;*
- 3. applying the assessment model to an analog of the waste management system;*
- 4. performing model comparison studies of benchmark problems;*
- 5. scientific peer review by publication in open literature; and*
- 6. widespread use by the scientific and technical community.*

The codes are used in a complementary manner, with FRAC3DVS-OPG providing detailed 3D results for a limited number of cases, and SYVAC3-CC4 extending the results to a broad range of contaminants and sensitivity cases. The SYVAC-CC4 model is derived from detailed FRAC3DVS-OPG transport results for I-129, and then verified for other specific radionuclides that represent a range of decay and transport parameters (i.e., Cs-135 and Cl-36).

To explore uncertainties arising from variability in the data used in the assessment predictions, SYVAC3-CC4 is also used to carry out probabilistic safety assessments of the repository system. Over 100,000 simulations are performed in which hundreds of input variables are simultaneously varied according to defined parameter distributions.

12.3.2.1 Key Assumptions and Conservatism in Modelling

Realistic best estimates vs. conservative overestimates, REGDOC-2.11.1 Volume III, Section 5.2.2:

Conservative calculations intentionally overestimate future consequences to provide an additional margin of safety for situations where assessment results cannot be considered accurate predictions, but merely indicators of safety. A conservative approach should be used when developing computer codes and models, and assumptions and simplifications of processes to make them more amenable for inclusion in computer models should not result in underestimation of the potential risks or impacts.

Chapter 7 describes the key attributes for the Base Case of the Normal Evolution Scenario. The illustrative assessment presented in this report uses different strategies consistent with expectations in REGDOC-2.11.1 Volume III. The assessment of the Base Case includes the following conservatisms, as described in Chapter 7, Table 7-3:

- Containers with undetected defects are assumed present, with the defects existing from the time of container placement;
- Upon breaching of the copper barrier, no credit is taken for the additional time to corrode the steel barrier. Similarly, no credit is taken for the time required to fill the container with water once the steel barrier is breached. Instead, the containers are assumed to fill with water immediately upon penetration of the copper barrier;
- No credit is taken for the presence of the fuel sheath in maintaining fuel integrity and in preventing water from contacting the fuel matrix;
- No credit is taken for the effect of hydrogen gas (H₂) produced by corrosion of the container on the dissolution rate of the uranium oxide fuel (UO₂) fuel;
- No credit is taken for the effect of corrosion deposits (produced by corrosion of the container) in reducing the container internal void volume and providing a high surface area for adsorption of some of the radionuclides released from the fuel;
- No credit is taken for the likely filling of the defect with bentonite and/or corrosion products which could significantly increase the transport resistance;
- The defective containers are assumed positioned in the repository location that, in combination with the well location, maximizes the dose consequence;
- A 219 m deep well is included in the assessment. The well is positioned in the location that, in combination with the defective container locations, maximizes the dose consequence; and
- Conservative properties are assigned to the critical group (e.g., daily energy need, obtaining all food, fuel, water and building material locally, all drinking and irrigation water taken from the well, etc.).

Since the Base Case assumes a constant temperate climate, Section 7.8.2.4 also discusses the anticipated effects of glaciation on the assessment.

Analyzing uncertainties, REGDOC-2.11.1 Volume III, Section 8.2:

A formal uncertainty analysis of the predictions should be performed to identify the sources of uncertainty. This analysis should distinguish between uncertainties arising from:

- 1. Input data;*
- 2. Scenario assumptions;*
- 3. The mathematics of the assessment model; and*
- 4. The conceptual models.*

These conservatisms are further described as part of the approach to assess uncertainties in Chapter 9. The division of uncertainties into scenario, model and data uncertainties is consistent with the guidance of REGDOC-2.11.1 Volume III.

12.3.3 Normal Evolution Scenario

Normal evolution scenario, REGDOC-2.11.1 Volume III, Section 7.5.1:

A normal evolution scenario should be based on reasonable extrapolation of present day site features and receptor lifestyles. It should include expected evolution of the site and degradation of the waste disposal system (gradual or total loss of barrier function) as it ages.

Depending on site-specific conditions and the timeframe for the assessment, a normal evolution scenario may need to include extreme conditions such as climate shifts or the onset of glaciations.

In this report, the Normal Evolution Scenario is described in terms of a “Reference Case”, a “Base Case” sensitivity study and a series of additional sensitivity studies around the Base Case.

Reference Case

The Reference Case represents the situation in which all repository components meet their design specification and function as anticipated. As such, the used fuel containers remain intact essentially indefinitely and no contaminant releases occur in the one million year time period of interest. Radiological doses to the public and the environment are therefore zero.

Base Case

Sensitivity studies are used to illustrate repository performance for a range of reasonably foreseeable deviations from key Reference Case assumptions. These deviations arise as a result of components placed in the repository that either (a) do not meet their design specification or (b) do not fully function as anticipated.

The likelihood of such deviations will be very low and much care is being taken to design, develop and test a robust fabrication and placement technology which will ultimately be

implemented under a comprehensive quality assurance program. However, given the large number of containers, it is not unreasonable to anticipate that some failures may occur.

To illustrate repository performance in the presence of failed containers, the “Base Case” sensitivity study assumes a small number of containers are fabricated with sizeable defects in their copper coating, and that a smaller number of these off-specification containers escape detection by the quality assurance program and are unknowingly placed in the repository. The defects are assumed sufficiently large to cause each of 10 containers to fail within one million years. The failure times are assumed to be evenly spread over the one million year time period of interest, with the first failure occurring at 1000 years and subsequent failures occurring every 100,000 years.

The Base Case results are described in Section 7.7.2 and Section 7.8.2.1.

The dose results at one million years are essentially zero (i.e., below 10^{-9} mSv). This is because transport rates are extremely low due to the very low hydraulic conductivity of the host rock, the absence of fractures, and the dominance of diffusive transport. Results are therefore also quoted in the main body of the report at 10 million years and are still very low; however, this is for illustrative purposes only because long-term geological processes not accounted for in the assessment may be important at this time-scale. Due to the extremely low transport, peak dose rates for most cases are still not reached and the calculations have been extended further to reach peak values. Peak values are useful for case-to-case comparisons; however, again these are only illustrative.

The resulting peak dose rate is 1.2×10^{-6} mSv/a. This is well below the average Canadian background dose rate of 1.8 mSv/a and is a factor of 250,000 times less than the 0.3 mSv/a interim dose rate acceptance criterion established in this report for the radiological protection of persons. The actual dose rate could be even lower, depending on the location of the defective containers, whether or not a well is present, and where that well is located with respect to the defective containers. Results indicating this are presented in Chapter 7.

Results show I-129 is the only dose contributor (through the use of a deep well). This is because I-129 has a sizeable initial inventory, a non-zero instant release fraction, a very long half-life, no solubility limit, and is non-sorbing in the buffer, backfill and geosphere. All other fission products and actinides either decay away, or are released very slowly as the fuel dissolves and are thereafter sorbed in the engineered barriers and geosphere.

12.3.3.1 Results from Sensitivity Analyses and Bounding Assessments

Deterministic and probabilistic calculations, REGDOC-2.11.1 Volume III, Section 5.2.3:

The mathematical approach to analyzing the scenarios in the safety case is guided by the purpose of the long term assessment. A deterministic model uses single-valued input data to calculate a single-valued result that will be compared to an acceptance criterion. Variations in input data values are taken into account in these calculations. To account for data variability, individual deterministic calculations must be done using different values of input parameters.

This is the approach used for performing sensitivity analyses (determining the response of model predictions to variations in input data) and importance analyses (calculating the range of predicted values that corresponds to the range of input values) of deterministic models.

To account for the variation in key input data used in the Base Case, a number of sensitivity analyses are completed for key parameters as described in Section 7.2.1 and illustrated in Figure 7-1 (shown as Figure 12-1 in this chapter). Some parameters are also pushed beyond the reasonable range of variations by setting their values to zero or by removing limits and running a set of bounding assessments, where a specific parameter is completely ignored. The identified parameters, the variation in their values and the rationale for selecting these cases are summarized in Chapter 7, Table 7-5.

The impacts are determined from simulations performed with either the FRAC3DVS-OPG or the SYVAC3-CC4 code. The FRAC3DVS-OPG code does not have a biosphere model and therefore its results are presented in terms of I-129 transport to the surface. This provides a reasonable estimate of potential impacts by comparison with I-129 transport to surface for the Normal Evolution Scenario, since I-129 dominates the dose consequence.

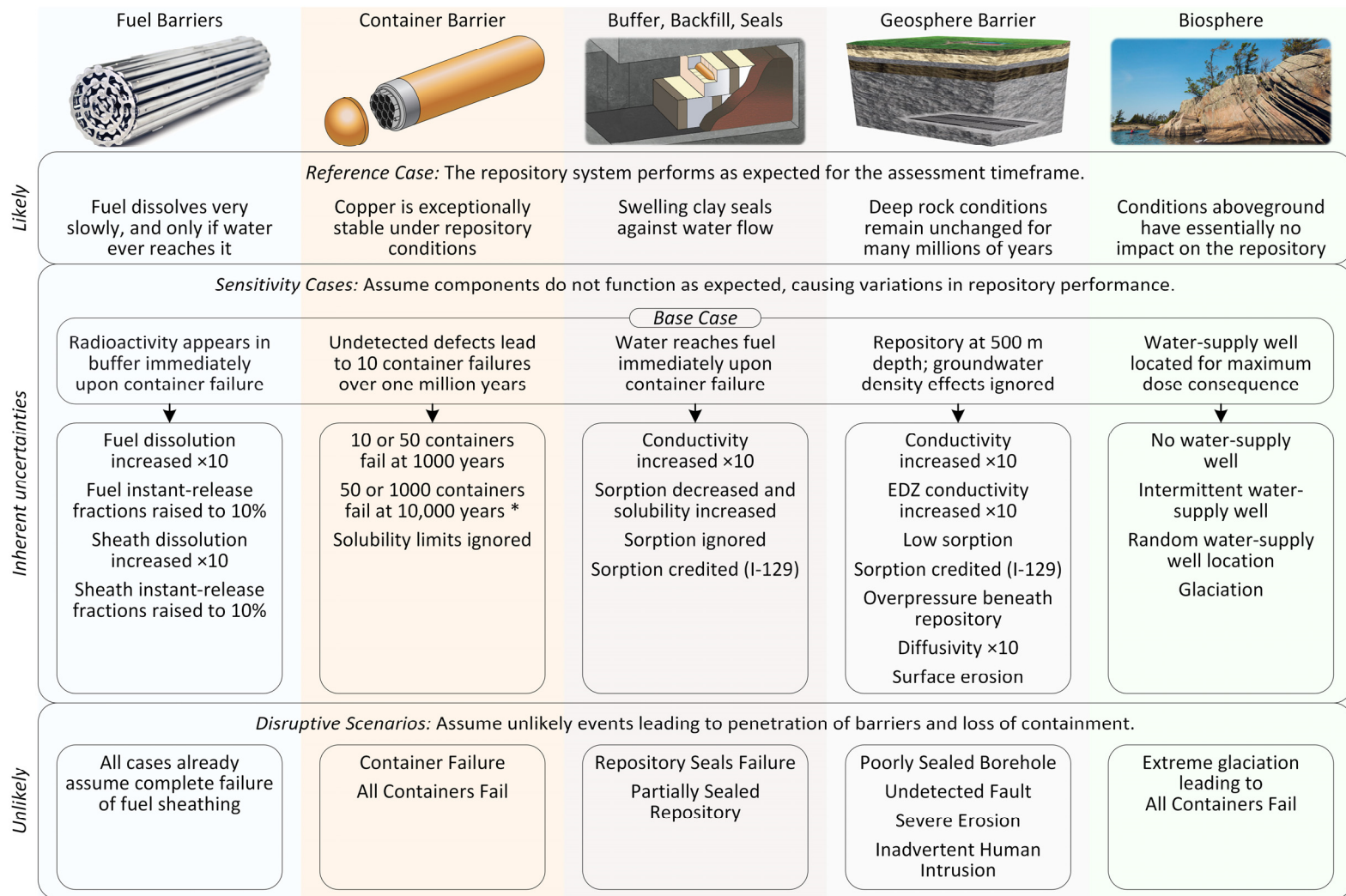
Postclosure Safety Assessment of a Used Fuel Repository in Sedimentary Rock

Document Number: NWMO-TR-2018-08

Revision: 000

Class: Public

Page: 693



Note: Hypothetical container failures all occur in the one location that would yield the largest dose consequence. The case marked '*' is an exception, where hypothetical container failures are equally likely to occur at all locations across the repository.

Figure 12-1: Illustration Showing Normal Evolution Scenario, Sensitivity Studies, and Disruptive Event Scenarios

A summary of the key cases, a comparison against the interim acceptance criterion and the key findings are presented in Chapter 7, Table 7-57 and illustrated in Figure 12-2. The comparison of assessment results with interim acceptance criteria is consistent with the guidance in Section 8 of REGDOC-2.11.1, Volume III.

The sensitivity analyses show that the impact on dose remains acceptable when key parameters are varied. The sensitivity cases with the most significant impact on dose occur when more containers fail early, the diffusion coefficients of the bentonite and host rock are increased and when glaciation occurs. The peak dose consequence is 5 times greater than the Base Case when 50 containers fail early and 14 times greater when the diffusion coefficients are increased by a factor of 10.

Some sensitivity cases are found to have a minimal to no impact on dose as shown in Chapter 7, Table 7-57.

12.3.3.2 Results from the Probabilistic Analysis

Deterministic and probabilistic calculations, REGDOC-2.11.1 Volume III, Section 5.2.3:

Probabilistic models can explicitly account for uncertainty arising from variability in the data used in assessment predictions. Such models may also be structured to take account of different scenarios (as long as they are not mutually exclusive) or uncertainty within scenarios. Probabilistic models typically perform repeated deterministic calculations based on input values sampled from parameter distributions, with the set of results expressed as a frequency distribution of calculated consequences. Frequency multiplied by consequence is interpreted as the overall potential risk of harm from the waste management system.

Results from two probabilistic cases are presented in Chapter 7, consistent with the expectations of REGDOC-2.11.1, Volume III in Section 5.2. In this study, relevant parameters for contaminant release and transport were varied whereas parameters associated with groundwater flow were not.

The first probabilistic case, in which the number, location and failure times of the 10 defective containers are fixed at the same values as in the Base Case with all other available parameters varied, gives a measure of the overall uncertainty in the Base Case. The 95th percentile 1 Ma dose rate emerging from 100,000 Monte Carlo simulations is 1.3×10^{-7} mSv/a, which is a factor of 2,300,000 times less than the interim dose rate criterion of 0.3 mSv/a. Extending the simulation time beyond one million years, the 95th percentile peak dose rate is 3.4×10^{-5} mSv/a, which is well below the interim dose rate criterion.

The second probabilistic case, in which all parameters are varied including the number, location and failure times of the defective containers, has a 95th percentile 1 Ma dose rate of 9.3×10^{-8} mSv/a, which is a factor of 3,200,000 times less than the interim dose rate criterion. The dose consequence is lower than the previous case because there is a large number of probabilistic cases in which zero container failures occur. Extending the simulation time beyond one million years, the 95th percentile peak dose rate is 1.45×10^{-5} mSv/a, which is well below the interim dose rate criterion.

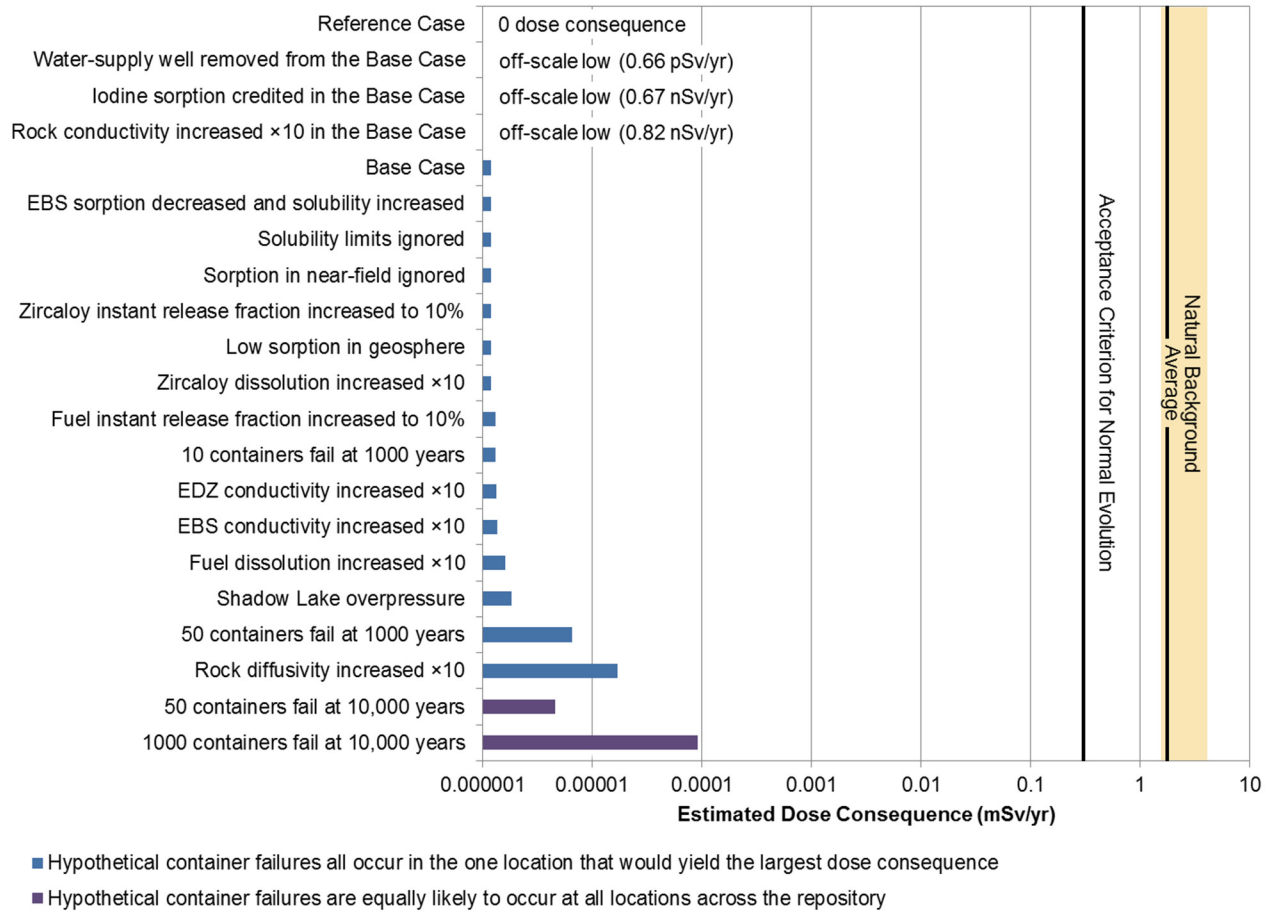


Figure 12-2: Key Results from Sensitivity Analyses and Bounding Assessments

12.3.3.3 Results from Complementary Indicators

Use of complementary indicators of safety, REGDOC-2.11.1 Volume III, Section 5.4:

Several other safety indicators, such as those that reflect containment barrier effectiveness of site-specific characteristics that can be directly related to contaminant release and transport phenomena, can also be presented to illustrate the long-term performance of a waste management system. Some examples of additional parameters include:

- 1. container corrosion rates;*
- 2. waste dissolution rates;*
- 3. groundwater age and travel time;*
- 4. fluxes of contaminants from a waste management facility;*
- 5. concentrations of contaminants in specific environmental media (for example, concentration of radium in groundwater); or*
- 6. changes in toxicity of the waste.*

Two complementary indicators other than dose to an assumed human group are described in Section 7.12. The indicators are:

- Radiotoxicity concentration in a water body, for medium time scales; and
- Radiotoxicity transport from the geosphere, for longer time scales.

The results presented in Chapter 7 show that the indicators are well below reference values based on natural concentrations and fluxes. Other factors have also been evaluated in the safety assessment but not specifically defined as “complementary indicators.”

12.3.4 Disruptive Event Scenarios

Disruptive event scenarios, including human intrusion, REGDOC-2.11.1 Volume III, Section 7.5.2:

Disruptive event scenarios postulate the occurrence of unlikely events leading to possible penetration of barriers and abnormal loss of containment.

Disruptive Event Scenarios involve cases in which barriers are assumed to degrade / fail, as described in Section 6.2 of this report and consistent with Section 7.5 of REGDOC-2.11.1 Volume III.

Chapter 6 includes a review of the Disruptive Event Scenarios considered in safety assessments of deep geological repositories in other countries. The results, summarized in Table 6-6, show that most assessments have identified a limited number of additional scenarios that consider the degradation / failure of engineered and natural barriers by natural processes (e.g., earthquakes, climate change) and human actions (e.g., drilling, poor quality control).

Although some scenarios are identified that are not considered in the current study, these are either not relevant to the Southern Ontario site or relevant but not included in the scope of this study.

The summary results for all Disruptive Event Scenarios considered in this study are presented in Table 7-58. Key features arising from the analysis of the All Containers Fail, the Repository Seals Failure and the Undetected Fault Disruptive Event Scenarios are:

- Both the All Containers Fail at 60,000 Years and the All Containers Fail at 10,000 Years cases result in a peak dose rate of 0.01 mSv/a. These results are below the interim dose rate acceptance criterion.
- The Repository Seals Failure scenario has a small effect (increase of about 1.4 times) on the peak impact for I-129 transport as compared to the Base Case, and the inferred dose consequence would remain well below the interim dose rate criterion.
- The peak impact for the Undetected Fault Scenarios increases, with I-129 transport for the 100 m offset case being about 22 times higher than that for the Base Case. Even with this increase, the inferred dose consequence would still be well below the interim dose rate acceptance criterion. In reality, this would depend on the location of the fault with respect to the well (if any) and the number and location of the defective containers (if any).

Disruptive event scenarios, including human intrusion, REGDOC-2.11.1 Volume III, Section 7.5.2:

Scenarios assessing the risk from inadvertent intrusion should be case-specific, based on the type of waste and the design of the facility, and should consider both the probability of intrusion and its associated consequences. Surface and near-surface facilities (e.g., tailings sites) are more likely to experience intrusion than deep geological facilities.

Scenarios concerning inadvertent human intrusion into a waste facility could predict doses that are greater than the regulatory limit. Such results should be interpreted in light of the degree of uncertainty associated with the assessment, the conservatism in the dose limit, and the likelihood of the intrusion. Both the likelihood and the risk from the intrusion should therefore be reported.

Chapter 7, Section 7.9.1 presents a stylized analysis for the Inadvertent Human Intrusion Scenario. This scenario is a special case, as recognized in Section 7.5.2 of REGDOC-2.11.1 Volume III, because it bypasses all barriers, thereby creating potential for the associated dose consequences to exceed the regulatory limit.

The results from the human intrusion assessment show a potential maximum dose to the drill crew of about 590 mSv, and to a site resident (i.e., someone farming on the site) of about 580 mSv, assuming early intrusion and improper management of the drill site.

This scenario is addressed through making it very unlikely, through placing the used fuel deep underground in a geologic setting with low mineral resource potential and poor prospects for potable groundwater resources, and by the use of institutional controls.

The likelihood of inadvertent intrusion is roughly estimated as 3.5×10^{-5} per year, based on current deep drilling rates, which implies a risk of serious health effects of 1.2×10^{-6} per year (or less). This is below the risk target of $10^{-5}/a$ for Disruptive Event Scenarios identified in Section 7.1.1.

12.4 Future Work

The conceptual design and illustrative postclosure assessment presented in this report for a hypothetical site represents a single case study in sedimentary rock. Other design concepts and other site conditions have been explored in other Canadian and international case studies.

Since this report is prepared for a hypothetical site and thus is not a full safety case, a number of aspects are not covered in detail. These are noted in Chapter 1. Also, the postclosure safety assessment illustrates the method and approach, but does not assess all scenarios or aspects of relevance for a full safety case (see Section 7.2.3).

There is ongoing work at NWMO to support siting activities, design development and other research. As new information emerges from these studies, the analysis methods and assumptions will be updated accordingly.

12.5 Conclusion

The current case study work, done at an early stage in the APM Project, provides confidence that, from a technical perspective, a suitable repository could be designed, sited and constructed in the sedimentary rock of the Southern Ontario.

12.6 References for Chapter 12

CNSC. 2018. Regulatory Document REGDOC-2.11.1 Volume III: Assessing the Long-Term Safety of Radioactive Waste Management. Canadian Nuclear Safety Commission. Ottawa, Canada.

13. SPECIAL TERMS

13.1 Units

a	annum
Bq	becquerel
°C	degree Celsius
cm	centimetre
d	day
g	gram
Gy	gray
GPa	gigapascal
h	hour
K	Kelvin
kg	kilogram
kgU	kilogram of Uranium
kgw	kilogram water
kJ	kilojoule
km	kilometre
kW	kilowatt
L	litre
m	metre
Ma	million years
mASL	metres above sea level
mBGS	metres below ground surface
mg	milligram
Mg	megagram
MJ	megajoule
mm	millimetre
mol	mole
MPa	megapascal
mSv	millisievert
mV	millivolt
mW	milliwatt

MW	megawatt
n	neutron (associated with neutron fluence)
nm	nanometre
nSv	nanosievert
Pa	pascal
ppm	parts per million
s	second
Sv	sievert
W	watt
wt%	mass percentage
µg	microgram
µm	micrometre
µSv	microsieverts

13.2 Abbreviations and Acronyms

1D	One-Dimensional
2D	Two-Dimensional
3D	Three-Dimensional
3DGF	Three-Dimensional Geologic Framework
AECL	Atomic Energy of Canada
ALARA	As Low as Reasonably Achievable
APM	Adaptive Phased Management
AQ or (aq)	Aqueous
BCE	Before Common Era
BSB	Bentonite-Sand Buffer
CANDU	CANada Deuterium Uranium
CANLUB	Thin graphite coating between the fuel pellet and the fuel sheath
CC4	Canadian Concept Generation 4
CC	Constant Climate
CCME	Canadian Council of the Environment
CCM-UC	Copper Corrosion Model for Uniform Corrosion
CE	Common Era

CEAA	Canadian Environmental Assessment Act
CFU	Colony Forming Units
CNSC	Canadian Nuclear Safety Commission
CSA	Canadian Standards Association
DDW	Dry Density Weight
DEM	Digital Elevation Model
DFN	Discrete Fracture Network
DGR	Deep Geological Repository
DGSM	Descriptive Geosphere Site Model
EA	Environmental Assessment
EBS	Engineered Barrier System
E_{CORR}	Corrosion Potential
EDZ	Excavation Damage Zone
EIS	Environmental Impact Statement
EMDD	Effective Montmorillonite Dry Density
EPM	Equivalent Porous Media
ERICA	Environmental Risks from Ionising Contaminants Assessment
FEPs	Features, Events and Processes
FP	Fission Product
GGM	Gas Generation Model
GM	Geometric Mean
GSD	Geometric Standard Deviation
GSM	Glacial Systems Model
HCB	Highly-Compacted Bentonite
HEPA	High-Efficiency Particulate Air
HGS	HydroGeoSphere
HIM	Human Intrusion Model
HM	Hydromechanical
IAEA	International Atomic Energy Agency
ICRP	International Commission on Radiological Protection
ID	Inner Diameter

Imp	Impurity
ISO	International Organization for Standardization
LHHPC	Low-Heat, High-Performance Concrete
LVRF	Low Void Reactivity Fuel
MIC	Microbiologically Influenced Corrosion
MLE	Mean Life Expectancy
NDE	Non-Destructive Examination
NEA	Nuclear Energy Agency
NOAA	National Oceanic and Atmospheric Administration
NSCA	Nuclear Safety and Control Act
NTS	National Topographic System
NWMO	Nuclear Waste Management Organization
NSCA	Nuclear Safety and Control Act
OD	Outer Diameter
OHSA	Ontario Occupational Health and Safety Act
O/M	Oxygen/Metal
OPG	Ontario Power Generation
PDF	Probability Density Function
PPT	Precipitate
PQP	Project Quality Plan
PSHA	Probabilistic Seismic Hazard Analysis
PWR	Pressurized Water Reactor
RH	Relative Humidity
RSM	Radionuclide Screening Model
SCC	Stress Corrosion Cracking
SKB	Swedish Nuclear Fuel and Waste Management Company (Svensk Kärnbränslehantering AB)
SRTM	Shuttle Radar Topography Mission
SR-270	Sedimentary rock with a total dissolved solids of approximately 270 g/L)
SSM	Swedish Radiation Safety Authority
STP	Standard Temperature and Pressure
SYVAC3	System Variable Analysis Code
TDS	Total Dissolved Solids

THM	Thermal-hydraulic-mechanical
UCS	Uniaxial Compressive Strength
UDF	Underground Demonstration Facility
UFC	Used Fuel Container
UFPP	Used Fuel Packaging Plant
UFTP	Used Fuel Transportation Package
UofT GSM	University of Toronto Glacial Systems Model
URL	Underground Research Lab
WIP	Work In Progress
WRA	Whiteshell Research Area

THIS PAGE HAS BEEN LEFT BLANK INTENTIONALLY